WOODHEAD PUBLISHING SERIES IN CIVIL AND STRUCTURAL ENGINEERING

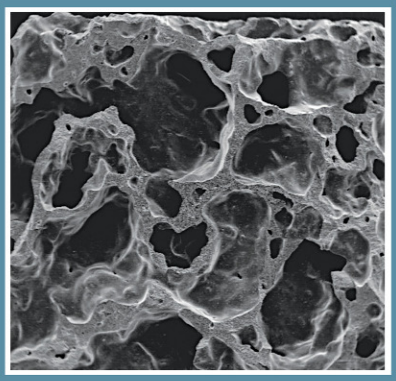

Handbook of Alkali-activated Cements, Mortars and Concretes

Edited by F. Pacheco-Torgal, J. A. Labrincha, C. Leonelli, A. Palomo and P. Chindaprasirt

WP
WOODHEAD PUBLISHING

Handbook of Alkali-activated Cements, Mortars and Concretes

Related titles

Understanding the rheology of concrete
(ISBN 978-0-85709-028-7)

Sustainability of construction materials
(ISBN 978-1-84569-349-7)

Eco-efficient concrete
(ISBN 978-0-85709-424-7)

Woodhead Publishing Series in Civil and Structural Engineering: Number 54

Handbook of Alkali-activated Cements, Mortars and Concretes

Edited by

F. Pacheco-Torgal, J. A. Labrincha, C. Leonelli, A. Palomo and P. Chindaprasirt

AMSTERDAM • BOSTON • CAMBRIDGE • HEIDELBERG
LONDON • NEW YORK • OXFORD • PARIS • SAN DIEGO
SAN FRANCISCO • SINGAPORE • SYDNEY • TOKYO
Woodhead Publishing is an imprint of Elsevier

Woodhead Publishing is an imprint of Elsevier
80 High Street, Sawston, Cambridge, CB22 3HJ, UK
225 Wyman Street, Waltham, MA 02451, USA
Langford Lane, Kidlington, OX5 1GB, UK

British Library Cataloguing-in-Publication Data
A catalogue record for this book is available from the British Library

Library of Congress Control Number: 2014944427

ISBN 978-1-78242-276-1 (print)
ISBN 978-1-78242-288-4 (online)

For information on all Woodhead Publishing publications visit our website at http://store.elsevier.com/

Typeset by Replika Press Pvt Ltd, India
Printed and bound in the United Kingdom

Contents

List of contributors

S. Ahmari Cornerstone Engineering Inc., Louisville, KY, USA

A. Allahverdi Iran University of Science and Technology, Tehran, Iran; Ryerson University, Toronto, ON, Canada

M. M. Alonso Instituto Eduardo Torroja (IETcc-CSIC), Madrid, Spain

S. Baklouti University of Sfax, Sfax, Tunisia

E. Balomenos National Technical University of Athens, Athens, Greece

L. Barbieri Università degli Studi di Modena e Reggio Emilia, Modena, Italy

J. Barroso de Aguiar University of Minho, Guimarães, Portugal

Z. Baščarević University of Belgrade, Belgrade, Serbia

S. A. Bernal University of Sheffield, Sheffield, UK

M. V. Borrachero Universitat Politècnica de València, València, Spain

T. Cao Surface Design Consulting Pty Ltd, Sydney, NSW, Australia

A. Cevik Gaziantep University, Gaziantep, Turkey

P. Chindaprasirt Khon Kaen University, Khon Kaen, Thailand

M. Criado Instituto de Ciencia de Materiales de Madrid (CSIC), Madrid, Spain

M. Cyr Université de Toulouse, Toulouse, France

Y. Ding Dalian University of Technology, Dalian, China

A. Fernández-Jiménez Instituto Eduardo Torroja (IETcc-CSIC), Madrid, Spain

I. Garcia-Lodeiro Instituto Eduardo Torroja (IETcc-CSIC), Madrid, Spain

G. Habert Swiss Federal Institute of Technology Zurich (ETH Zurich), Zurich, Switzerland

D. Hardjito Petra Christian University, Surabaya, Indonesia

K. M. A. Hossain Ryerson University, Toronto, ON, Canada

E. Joussein National School of Industrial Ceramics, Limoges, France

L. Kang Xi'an University of Architecture and Technology, Xi'an, China

M. Komljenović University of Belgrade, Belgrade, Serbia

M. Lachemi Ryerson University, Toronto, ON, Canada

I. Lancellotti Università degli Studi di Modena e Reggio Emilia, Modena, Italy

C. Leonelli Università degli Studi di Modena e Reggio Emilia, Modena, Italy

L. C. Liu Xi'an University of Architecture and Technology, Xi'an, China

K. J. D. MacKenzie MacDiarmid Institute for Advanced Materials and Nanotechnology, Wellington, New Zealand

J. Monzó Universitat Politècnica de València, València, Spain

E. Najafi Kani Semnan University, Semnan, Iran

A. Nazari Swinburne University of Technology, Hawthorn, VIC, Australia

C. Ouellet-Plamondon Swiss Federal Institute of Technology Zurich (ETH Zurich), Zurich, Switzerland

F. Pacheco-Torgal University of Minho, Guimarães, Portugal

A. Palomo Instituto Eduardo Torroja (IETcc-CSIC), Madrid, Spain

D. Panias National Technical University of Athens, Athens, Greece

J. Payá Universitat Politècnica de València, València, Spain

R. Pouhet Université de Toulouse, Toulouse, France

E. Prud'homme National School of Industrial Ceramics, Limoges, France

F. Puertas Instituto Eduardo Torroja (IETcc-CSIC), Madrid, Spain

M. Romagnoli Università degli Studi di Modena e Reggio Emilia, Modena, Italy

S. Rossignol National School of Industrial Ceramics, Limoges, France

K. Sakkas National Technical University of Athens, Athens, Greece

J. G. Sanjayan Swinburne University of Technology, Hawthorn, VIC, Australia

P. Sargent AECOM, Newcastle upon Tyne, UK

W. Tahri University of Sfax, Sfax, Tunisia

M. M. Tashima UNESP – Univ. Estadual Paulista, Ilha Solteira, Brazil

M. Torres-Carrasco Instituto Eduardo Torroja (IETcc-CSIC), Madrid, Spain

S. E. Wallah Sam Ratulangi University, Manado, Indonesia

H. Wang University of Southern Queensland, Toowoomba, QLD, Australia

L. Zhang University of Arizona, Tucson, AZ, USA

Y. J. Zhang Xi'an University of Architecture and Technology, Xi'an, China

Z. Zhang University of Southern Queensland, Toowoomba, QLD, Australia

Woodhead Publishing Series in Civil and Structural Engineering

1 **Finite element techniques in structural mechanics**
C. T. F. Ross
2 **Finite element programs in structural engineering and continuum mechanics**
C. T. F. Ross
3 **Macro-engineering**
F. P. Davidson, E. G. Frankl and C. L. Meador
4 **Macro-engineering and the earth**
U. W. Kitzinger and E. G. Frankel
5 **Strengthening of reinforced concrete structures**
Edited by L. C. Hollaway and M. Leeming
6 **Analysis of engineering structures**
B. Bedenik and C. B. Besant
7 **Mechanics of solids**
C. T. F. Ross
8 **Plasticity for engineers**
C. R. Calladine
9 **Elastic beams and frames**
J. D. Renton
10 **Introduction to structures**
W. R. Spillers
11 **Applied elasticity**
J. D. Renton
12 **Durability of engineering structures**
J. Bijen
13 **Advanced polymer composites for structural applications in construction**
Edited by L. C. Hollaway
14 **Corrosion in reinforced concrete structures**
Edited by H. Böhni
15 **The deformation and processing of structural materials**
Edited by Z. X. Guo
16 **Inspection and monitoring techniques for bridges and civil structure**
Edited by G. Fu
17 **Advanced civil infrastructure materials**
Edited by H. Wu
18 **Analysis and design of plated structures Volume 1: Stability**
Edited by E. Shanmugam and C. M. Wang
19 **Analysis and design of plated structures Volume 2: Dynamics**
Edited by E. Shanmugam and C. M. Wang
20 **Multiscale materials modelling**
Edited by Z. X. Guo
21 **Durability of concrete and cement composites**
Edited by C. L. Page and M. M. Page
22 **Durability of composites for civil structural applications**
Edited by V. M. Karbhari
23 **Design and optimization of metal structures**
J. Farkas and K. Jarmai

24 **Developments in the formulation and reinforcement of concrete**
Edited by S. Mindess
25 **Strengthening and rehabilitation of civil infrastructures using fibre-reinforced polymer (FRP) composites**
Edited by L. C. Hollaway and J. C. Teng
26 **Condition assessment of aged structures**
Edited by J. K. Paik and R. M. Melchers
27 **Sustainability of construction materials**
J. Khatib
28 **Structural dynamics of earthquake engineering**
S. Rajasekaran
29 **Geopolymers: Structures, processing, properties and industrial applications**
Edited by J. L. Provis and J. S. J. van Deventer
30 **Structural health monitoring of civil infrastructure systems**
Edited by V. M. Karbhari and F. Ansari
31 **Architectural glass to resist seismic and extreme climatic events**
Edited by R. A. Behr
32 **Failure, distress and repair of concrete structures**
Edited by N. Delatte
33 **Blast protection of civil infrastructures and vehicles using composites**
Edited by N. Uddin
34 **Non-destructive evaluation of reinforced concrete structures Volume 1: Deterioration processes**
Edited by C. Maierhofer, H.-W. Reinhardt and G. Dobmann
35 **Non-destructive evaluation of reinforced concrete structures Volume 2: Non-destructive testing methods**
Edited by C. Maierhofer, H.-W. Reinhardt and G. Dobmann
36 **Service life estimation and extension of civil engineering structures**
Edited by V. M. Karbhari and L. S. Lee
37 **Building decorative materials**
Edited by Y. Li and S. Ren
38 **Building materials in civil engineering**
Edited by H. Zhang
39 **Polymer modified bitumen**
Edited by T. McNally
40 **Understanding the rheology of concrete**
Edited by N. Roussel
41 **Toxicity of building materials**
Edited by F. Pacheco-Torgal, S. Jalali and A. Fucic
42 **Eco-efficient concrete**
Edited by F. Pacheco-Torgal, S. Jalali, J. Labrincha and V. M. John
43 **Nanotechnology in eco-efficient construction**
Edited by F. Pacheco-Torgal, M. V. Diamanti, A. Nazari and C. Goran-Granqvist
44 **Handbook of seismic risk analysis and management of civil infrastructure systems**
Edited by F. Tesfamariam and K. Goda
45 **Developments in fiber-reinforced polymer (FRP) composites for civil engineering**
Edited by N. Uddin
46 **Advanced fibre-reinforced polymer (FRP) composites for structural applications**
Edited by J. Bai
47 **Handbook of recycled concrete and demolition waste**
Edited by F. Pacheco-Torgal, V. W. Y. Tam, J. A. Labrincha, Y. Ding and J. de Brito
48 **Understanding the tensile properties of concrete**
Edited by J. Weerheijm

49 **Eco-efficient construction and building materials: Life cycle assessment (LCA), eco-labelling and case studies**
Edited by F. Pacheco-Torgal, L. F. Cabeza, J. Labrincha and A. de Magalhães
50 **Advanced composites in bridge construction and repair**
Edited by Y. J. Kim
51 **Rehabilitation of metallic civil infrastructure using fiber-reinforced polymer (FRP) composites**
Edited by V. Karbhari
52 **Rehabilitation of pipelines using fiber-reinforced polymer (FRP) composites**
Edited by V. Karbhari
53 **Transport properties of concrete: Measurement and applications**
P. A. Claisse
54 **Handbook of alkali-activated cements, mortars and concretes**
Edited by F. Pacheco-Torgal, J. A. Labrincha, C. Leonelli, A. Palomo and P. Chindaprasirt
55 **Eco-efficient masonry bricks and blocks: Design, properties and durability**
Edited by F. Pacheco-Torgal, P. B. Lourenço, J. A. Labrincha, S. Kumar and P. Chindaprasirt

This page intentionally left blank

Foreword

My tryst with alkali-activated slag (AAS) cement dates back to the 1960s when I was doing my doctoral research at the Baikov Institute of Metallurgy and Moscow State University in the then Soviet Union. One of the earliest publications on the subject I had come across then was by A.O. Purdon (*J. Soc. Chem. Ind.* Vol. 59, 1940, pp. 191–202). The principle of alkali activation therefore has been in the realm of scientific investigation for more than seven decades now. However, a more comprehensive and systematic research on AAS, to the best of my knowledge, was initiated by V.D. Glukhovskii and his team in Kiev, the capital of Ukraine, in the late 1950s. In fact his patent on the binder, possibly the first in the world, was applied for in 1958, although the patent seems to have been formally listed much later (USSR 449894, Pub. No. 42, 1974). In the 1970s and 1980s Glukhovskii took the initiative of publishing at least four books devoted exclusively to AAS binders and concretes covering the theory, properties and use of these materials. All these publications were in the Russian language and in the absence of English translations, the dissemination of knowledge was highly localized.

In the same tradition, at least two national conferences were organized in Kiev, one in 1979 and another in 1984 on AAS-based products and their applications. In the second conference in particular 235 papers from all regions of the then Soviet Union were presented on alkali-activated slag cements, concretes and constructions, reflecting by then about three decades of experience in the field (*Proceedings of the 2nd National Conference on 'Alkali-Activated Cements, Concretes and Constructions'*, Kiev, KISI, 1984). In 1988 a book was published by R.L. Serykh and V.A. Pakhomov, entitled *Constructions from Alkali-Activated Slag Concretes* (Stroiizdat Publishers, Moscow).

It is relevant to mention here that in a span of about three decades the concept of AAS turned into a diverse field of practices. Large water pipelines were manufactured, building elements of different types were cast, road slabs were laid, air-field runways were placed. From all published data these structures proved to be highly durable. The success of AAS concretes in sanitary engineering was observed to be particularly phenomenal. The comprehensive strength of specimens taken from waste water sewers after 10–15 years was reported to be 120–150% higher. Massive breakwater blocks on sea shores reportedly showed a 250% gain in strength.

For obvious reasons the technology of alkali-activated binders spread quite rapidly to the East European countries. In Romania pavement stones, curbs and other precast elements were found to be in excellent condition after 15–20 years. Many road and highway sections, based on AAS formulations, some of them placed with roller compaction, were in visibly good condition in Eastern Europe and in France for 10–25 years. Several publications in the 7th International Congress on Cement Chemistry (ICCC) held in Paris in 1980 as well in the 8th ICCC held in Rio de Janeiro in 1986 bear testimony to the rising and widening interest of the global

community in successful development and application of alkali-activated binder technologies throughout the course of the 1980s.

Notwithstanding such a prolonged period of development and successful application of alkali-activated binders and concretes, to me it appears that there was a perceptible slow-down in dealing with this range of products in the 1990s. The reasons were many, and for brevity, cannot be deliberated on here and now. However, with the advent of the new millennium with renewed emphasis on carbon dioxide emission reduction and sustainable green construction, a revival of the alkali-activated binder technology was clearly perceptible. The repositioning of 'geopolymer concretes' by J. Davidovits, extensive knowledge dissemination through several publications by B.V. Rangan, formulation of Recommended Practice Note on Geopolymer Concrete by the Concrete Institute of Australia, significant investment in geopolymer research by various countries all point towards the likely re-emergence of AAS and associated technologies.

With this backdrop the publication of *Handbook of Alkali-Activated Cements, Mortars and Concretes* edited by Dr F. Pacheco-Torgal and Professor João Labrincha of Portugal, Professor Cristina Leonelli of Italy, Professor Angel Palomo of Spain and Professor Prinya Chindaprasit of Thailand provides a great impetus for an accelerated commercialization of an eco-friendly alternative binder technology with more in-depth understanding of its strengths, weaknesses, opportunities and threats. We must bear in mind that Portland cement has a history of 190 years and yet it is evolving. Compared to that, the alkali-activated binder technology has a history of only 70 years, much of the past of which has got buried in history, compelling 'reinvention of wheel' in many cases.

This Handbook, therefore, will go a long way to fulfil the essential requirements of transferring the technology from the laboratory to the field. But before I conclude, I want all of you to believe that –

'Knowing is not enough
We must apply
Willing is not enough
We must do'

Then only the challenges, perspectives and social dimensions of the emerging technology can be appreciated and squarely encountered.

Dr Anjan K. Chatterjee
Fellow of Indian National Academy of Engineering
Chairman, Conmat Technologies Pvt Ltd, Kolkata, India
Director, Dr Fixit Institute of Structural Protection & Rehabilitation, Mumbai, India
Former Wholetime Director, ACC Limited, Mumbai, India

Introduction to *Handbook of Alkali-activated Cements, Mortars and Concretes*

1

F. Pacheco-Torgal
University of Minho, Guimarães, Portugal

1.1 Brief overview on alkali-activated cement-based binders (AACB)

According to Provis and van Deventer (2009) Purdon was the first to demonstrate in 1940 the synthesis of construction materials by alkaline activation of high-calcium blast furnace slags. Shi *et al*. (2011) gives credit for this achievement to the work of German cement chemist and engineer Kuhl in 1930. More recently a 1908 patent of Kuhl was recognized as the first use of the alkali activation of aluminosilicate precursors in order to obtain an ordinary Portland cement (OPC) alternative material (Provis and van Deventer, 2013; Provis, 2014).

In the next decades the field of alkali activation was almost non-existent, the only exception being the work of Glukhovsky (Table 1.1).

Relevant changes took place in the 1970s with the findings of the French scientist and engineer Joseph Davidovits who coined the term 'geopolymer' in 1979 having patented several aluminosilicate formulations. The 1980s and 1990s saw other relevant investigations in the field of alkali activation. Still it is only in the last few years that the production of scientific AACB-related papers has 'exploded'. Figure 1.1 shows that only in the twenty-first century has the accumulated number of papers exceeded 100. As a comparison, since 1993 almost 8,000 articles/reviews related to Portland cement were published in Scopus journals. The search also shows that the term 'geopolymer' has been much more popular than the term 'alkali-activated materials'.

The University of Melbourne was the affiliation with the highest number of 'geopolymer'-related papers while the Instituto de Ciencias de la Construcción Eduardo Torroja was responsible for the major part of 'alkali-activated' papers. Another interesting fact was that two Elsevier BV journals published the majority of AACB related papers. *Construction and Building Materials* has the highest number of 'geopolymer' papers while *Cement and Concrete Research* was the lead journal for alkali-activated papers.

At this stage it is important to mention that notes on the various terminologies used for categorizing AACB are deemed redundant in this chapter just because too much has already been written about it. Section 1.2 of the introductory chapter of the 2009 book by Provis and van Deventer (2009) provides a clear and up-to-date

Handbook of Alkali-activated Cements, Mortars and Concretes. http://dx.doi.org/10.1533/9781782422884.1

Table 1.1 Bibliographic listing of some important events in the history of AACB

Author	Year	Significance
Feret	1939	Slags used for cement
Purdon	1940	Alkali-slag combinations
Glukhovsky	1959	Theoretical basis and development of alkaline cements
Glukhovsky	1965	First called 'alkaline cements'
Davidovits	1979	'Geopolimer' term
Malinowski	1979	Ancient aqueducts characterized
Forss	1983	F-cement (slag-alkali-superplasticizer)
Langton and Roy	1984	Ancient building materials characterized
Davidovits and Sawyer	1985	Patent of 'Pyrament' cement
Krivenko	1986	DSc Thesis, $R_2O - RO - SiO_2 - H_2O$
Malolepsy and Petri	1986	Activation of synthectic melilite slags
Malek *et al.*	1986	Slag cement-low level radioactive wastes forms
Davidovits	1987	Ancient and modern concretes compared
Deja and Malolepsy	1989	Resistance to chlorides shown
Kaushal *et al.*	1989	Adiabatic cured nuclear wastes forms from alkaline mixtures
Roy and Langton	1989	Ancient concretes analogs
Majundar *et al.*	1989	$C_{12}A_7$ – slag activation
Talling and Brandstetr	1989	Alkali-activated slag
Wu *et al.*	1990	Activation of slag cement
Roy *et al.*	1991	Rapid setting alkali-activated cements
Roy and Silsbee	1992	Alkali-activated cements: an overview
Palomo and Glasser	1992	CBC with metakaolin
Roy and Malek	1993	Slag cement
Glukhovsky	1994	Ancient, modern and future concretes
Krivenko	1994	Alkaline cements
Wang and Scrivener	1995	Slag and alkali-activated microstructure
Shi	1996	Strength, pore structure and permeability of alkali-activated slag
Fernández-Jiménez and Puertas	1997	Kinetic studies of alkali-activated slag cements
Katz	1998	Microstructure of alkali-activated fly ash
Davidovits	1999	Chemistry of geopolymeric systems, technology

Table 1.1 (Continued)

Author	Year	Significance
Roy	1999	Opportunities and challenges of alkali-activated cements
Palomo	1999	Alkali-activated fly ash – a cement for the future
Gong and Yang	2000	Alkali-activated red mud–slag cement
Puertas	2000	Alkali-activated fly ash/slag cement
Bakharev	2001–2002	Alkali-activated slag concrete
Palomo and Palacios	2003	Immobilization of hazardous wastes
Grutzeck	2004	Zeolite formation
Sun	2006	Sialite technology
Duxson	2007	Geopolymer technology: the current state of the art
Hajimohammadi *et al.*	2008	One-part geopolymer
Provis and van Deventer	2009	Geopolymers: structure, processing, properties and industrial applications

Notes: According to Provis (2010), this table forgot to list the 'extremely valuable 2006 book of Shi *et al.* (2006)'. Moreover, Li *et al.* (2010) should have credited the 'one-part geopolymer' concept to Kolousek *et al.* (2007) because their paper was submitted to review process on March 19, 2007 and published online on 27 July, 2007, before the paper of Hajimohammadi *et al.* was submitted to review process on April 28, 2008 and accepted on September 23 and published only on October 29, 2008.
Source: Reprinted from Li *et al.* (2010). Copyright © 2010, with permission from Elsevier. Based on the previous table of Roy (1999).

overview on that issue. One fact, however, deserves to be emphasized: the several names used by different authors (e.g., geopolymers, mineral polymers, inorganic polymers, inorganic polymer glasses, alkali-bonded ceramics, alkali ash material, soil cements, hydroceramics, zeocements, zeoceramics, among others) have made it more difficult for AACB to become an alternative to OPC. This reflects the concern to find the most scientific name but at the same time also reflects the lack of commercial good sense of the scientific community.

Although the exponential increase of articles on AACB makes it very difficult to choose the most relevant ones in order to update Table 1.1, this author thinks that three of them merit that distinction: Shi *et al.* (2011), van Deventer *et al.* (2012) and Provis (2014). This is not only because the first two have been widely cited and the author of the third won the RILEM Robert L'Ermite medal, but most importantly because they contain very important insights on the future of AACB research. Also it was not until the twenty-first century that the first Technical Committee in the area of alkali activation was formed. The RILEM Technical Committee on Alkali-activated Materials (TC 224-AAM) was initiated in 2007 and concluded its work in 2012 and the state-of-the-art report was published recently (Provis and van Deventer, 2013).

Fortunately the participants had the good sense to embrace the alkali-activated terminology even though some had published the majority of their research on geopolymers (low calcium alkali-activated systems).

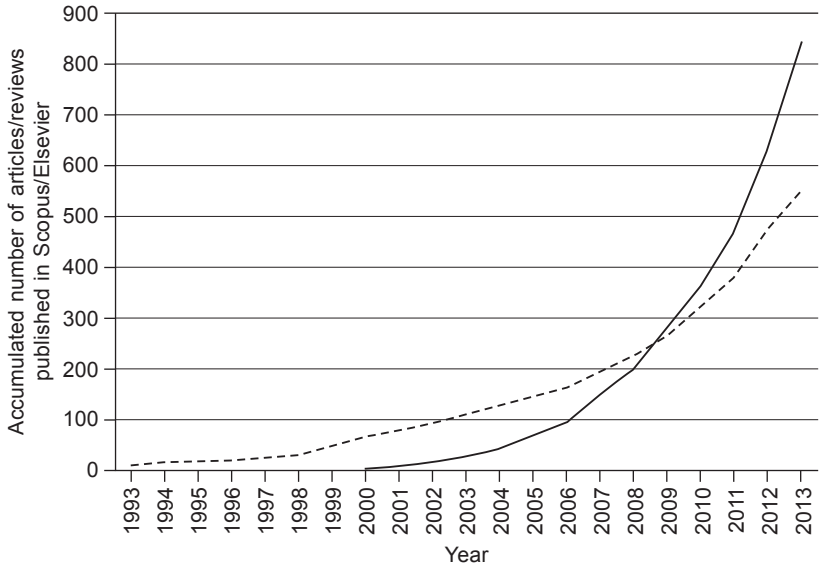

Figure 1.1 Evolution of the accumulated number of articles/reviews published in Scopus/Elsevier journals by the keyword 'alkali-activated' (dotted line); and the keyword 'geopolymer' (solid line) searched in the sections title, abstract or keywords.

The TC 224 constitutes an important landmark for AACB in tackling the lack of uniformly accepted standards which are 'critical to the acceptance of alkali-activated materials in the industrialized world'. In their 2012 insightful paper, van Deventer *et al*. had already emphasized the importance of the development of new standards as pivotal to the commercialization of these materials.

A subsequent Technical Committee (247 DTA) was initiated in 2012 with a five-year work plan focusing on 'Durability testing on alkali-activated materials'. The aim of this TC is to provide recommendations regarding appropriate test methodologies and protocols for the analysis of AACB. This is a relevant issue because the durability of AACB is still a subject of some controversy (Pacheco-Torgal *et al*., 2012a).

Duxson *et al*. (2007) recognized that durability is the most important issue in determining the success of these new materials. On the other side Juenger *et al*. (2011) argue that '*The key unsolved question in the development and application of alkali activation technology is the issue of durability*' and more recently van Deventer *et al*. (2012) stated that '*whether geopolymer concretes are durable remains the major obstacle to recognition in standards for structural concrete*'. The importance of the durability of AACB (as well as the importance of alkali-activation technology itself) can be seen by the fact that recently the European Research Council approved a Starting Grant for a research project entitled 'Durability of geopolymers as 21st century concretes'. This project which is coordinated by John Provis was initiated in September 2013 and goes up to September 2018.

Another relevant issue regarding AACB concerns their CO_2 emissions. According to Davidovits *et al*. (1990) geopolymers generate just 0.184 tons of CO_2 per ton of

binder. It is important to remember that this alleged extraordinary environmental performance over OPC fueled the growing interest in AACB that took place in the following decades. The majority of AACB-related papers used to make very impressive statements on the role of the activation technology in contributing to greatly reduced overall CO_2 emissions of the binder industry. Unfortunately the astonishing numbers of Davidovits were not confirmed by other authors.

Duxson *et al*. (2007) stated that although the CO_2 emissions generated during the production of Na_2O are very high, still the production of AACB is associated to a level of CO_2 emissions lower than the emissions generated in the production of OPC. An independent study made by Zeobond Pty Ltd concluded that the latter had 80% lower CO_2 emissions (Duxson and van Deventer, 2009).

Weil *et al*. (2009) compared OPC concrete and AACB concrete with similar durability reporting that the latter have 70% lower CO_2 emissions. McLellan *et al*. (2011) reported a 44–64% reduction in greenhouse gas emissions of Australian AACB when compared to OPC. However, the information on the performance of AACB is scarce and it is not easy to comprehend why sodium silicate-free mixtures did not show the lowest emissions.

Habert *et al*. (2011) confirmed that they have a lower impact on global warming than OPC but on the other hand they have a higher environmental impact regarding other impact categories. More recently, Turner and Collins (2013) showed that the CO_2 footprint of a 40 MPa AACB concrete was approximately just 9% less than comparable concrete containing 100% OPC binder (328 kg/m^3), the major part being due to sodium silicate.

The OPC concrete mixture used in this study could even have a much lower carbon footprint (below the geopolymer concrete) if fly ash had been used as partial replacement of Portland cement. A similar 40 MPa 28 days compressive strength could easily be achieved with a mixture of just 200 kg/m^3 Portland cement type II 42.5 plus 300 kg/m^3 fly ash (Azevedo *et al*., 2012). These results confirm that in some situations AACB can show 'an emissions profile worse than that of Portland cement-based concretes' (Provis, 2014) constituting a crucial argument for the search for AACB that are sodium silicate free. Of course current two-part low calcium silicate-based AACB technology will continue to play an important role in the construction industry for niche applications, especially fire resistant ones and also in other innovative applications.

Unfortunately, although hundreds of papers have been published on AACB with low CO_2 emissions, (low cost) alkaline activators were not at the heart of the investigators' concerns. One exception is the recent paper by Kim *et al*. (2013) which shows promising results on the use of CaO as a low cost alternative to classic alkali activators (sodium hydroxide and sodium silicate) leading to mixtures with around 42 MP compressive strength after 28 days curing. Still further investigations regarding durability and environmental performance are needed to confirm the viability of this activator. Instead the majority of the published investigations deal with interesting but low commercial relevance scientific aspects. That is why the comments in the introductory chapter of the 2009 book by Provis and van Deventer are worth

remembering '*a material that is well characterized but not used in the real world is in effect useless*'.

The efflorescences problem is another example of the misguided priorities of the AACB scientific community. As Zheng *et al*. (2007) rightly put it, since 'the alkaline and/or soluble silicates cannot be totally consumed during geopolymerization … this causes severe efflorescence … and high permeability and water absorption due to the movement of alkali together with water to the geopolymer surfaces'. However, in the several hundred AACB-related papers published on Scopus/Elsevier journals, only less than ten addressed in some way the efflorescence problem and of those only three focus directly on that problem.

The most interesting efflorescence-related article is the one by Škvára *et al*. (2012) who state that Na,K is bound only weakly in the nanostructure of the (N,K)–A–S–H gel and is leachable almost completely. This lack of research effort is even more odd considering that almost 7 years ago some authors (Zheng *et al*., 2007) have already acknowledged the fact that AACB were prone to severe efflorescence. These unresolved issues help us to understand why AACB are still far from being able to compete commercially against OPC.

Interestingly, and not without some irony, some authors (Shi *et al*., 2011) have recently admitted that the global replacement of Portland cement by any kind of binder (AACB included) is virtually impossible. As a consequence they suggested that a future trend in the field of binder materials could encompass the dilution of Portland cement in high volumes of SCMs in hybrid Portland cement–alkali-activated aluminosilicate. More recently relevant publications address this new trend (Garcia-Lodeiro *et al*., 2013a, 2013b).

Since the high strength of these new mixtures is only attainable if sodium silicate is used, it remains to be seen if these formulations are more competitive than OPC ones concerning eco-efficiency and cost-efficiency. Besides, this trend may raise some concerns regarding the chemical durability (alkali-silica reaction) just because the same research team recognized that the guarantee for the absence of expansive products by ASR is precisely a low calcium content (Fernandez-Jimenez and Palomo, 2009).

A 2007 international patent by Zeobond Research PTY Ltd (WO 109862 A1) on a dry-mix cement composition already recommended the use of as much as 30% Portland cement (Zheng *et al*., 2007). This fact and the statement by van Deventer *et al*. (2012) that calcium is pivotal for the strength and durability of geopolymers do not anticipate a bright future in the cement industry for low calcium alkali-activated systems. The patented new formulation (WO 109862 A1) attempts to overcome the problems of 'two-part' mix AACB, namely the difficulty of handling caustic solutions, poor workability, quality control and 'most important' the problem of efflorescence.

van Deventer *et al*. (2012) cite an updated US patent on this dry-mix cement composition (van Deventer *et al*., 2010). This new formulation commercially termed E-CRETE^{TM}, is allegedly associated with very low CO_2 emissions (Figure 1.2).

The commercial LCA conducted by NetBalance Foundation reported 60–80% reduction in CO_2 emissions. However, no LCA studies have been published in major

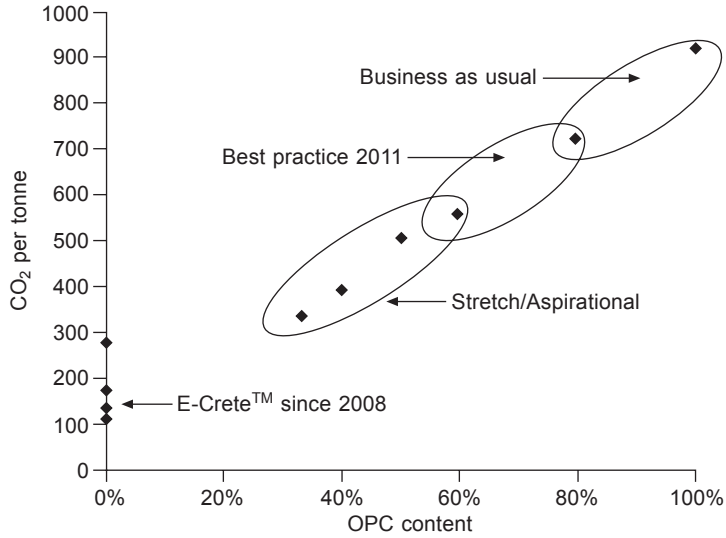

Figure 1.2 CO_2 emissions of various cement binders as a function of OPC content (reprinted from van Deventer *et al.*, 2012. Copyright © 2012, with permission from Elsevier).

journals that confirm that statement and could help to understand which compositions were evaluated.

1.2 Potential contributions of AACB for sustainable development and eco-efficient construction

1.2.1 AACB with lower CO_2 emissions

Climate change is one of the most important environmental problems faced by Planet Earth (IPCC, 2007; Schellnhuber, 2008; Rockström *et al.*, 2009). This is due to the increase of carbon dioxide (CO_{2eq}) in the atmosphere for which the built environment is a significant contributor. In the early eighteenth century, the concentration level of atmospheric CO_{2eq} was 280 parts per million (ppm). At present it is already 450 ppm. Keeping the current level of emissions (which is unlikely given the high economic growth of less developed countries with consequent increases in emission rates) will imply a dramatic increase in CO_{2eq} concentration to as much as 731 ppm by the year 2130 leading to a 3.7°C global warming above pre-industrial temperatures (Valero *et al.*, 2011).

Global warming will lead to a rise in the sea level caused by thermal expansion of the water. If the sea level rises above 0.40 m it will submerge 11% of the area of Bangladesh and as a result almost 10 million people will be rendered homeless (IPCC, 2007). Another consequence of global warming is the occurrence of increasingly extreme atmospheric events. Global warming may also be responsible

for the thawing of the permafrost (permanently frozen ground), where approximately 1×10^6 million tons (1000 $GtCO_{2eq}$) are still retained. This astonishing figure is equivalent to the current worldwide production (34 $GtCO_{2eq}$) during 30 years. Even if all the greenhouse gas emissions suddenly ceased, the inertia associated to climatic systems would mean that the rise in the sea level, ocean acidification and extreme atmospheric events will continue at least for the next 100 years.

To make things worse, in the coming years the construction industry will keep on growing at a fast pace. China alone will need 40 billion square meters of combined residential and commercial floor space over the next 20 years, equivalent to adding one New York City every two years (Pacheco-Torgal and Jalali, 2011).

A recent forecast estimates that by 2030, urban land cover will increase by 1.2 million km^2 (equivalent to an area about the size of South Africa). This will be concomitant with an enormous infrastructure boom in road construction, water and sanitation, energy and transport, and buildings (Seto *et al.*, 2012).

The latest findings on silicate-based AACB do not confirm their carbon footprint advantage over OPC. Therefore the contribution of these materials to reduce the overall CO_2 emissions of the binder industry, thus ameliorating climate change, is not at all clear. However, it is hoped that in the next few years investigators in this field could be able to find low CO_2 emissions (low cost) alkaline activators that may permit such goal.

1.2.2 AACB for building energy efficiency

According to the *World Energy Outlook 2012* energy efficiency improvements show the greatest potential of any single strategy to abate global GHG emissions from the energy sector (IEA, 2012).

The building sector is the largest energy user responsible for about 40% of the EU's total final energy consumption (Lechtenbohmer and Schuring, 2011).

According to the *Energy Road Map 2050* (European Commission, 2011a) higher energy efficiency in new and existing buildings is key for the transformation of the EU's energy system. Of the several areas related to the built environment, energy efficiency and renewable energies are the only ones that will be funded under the HORIZON 2020 EU framework program (Pacheco-Torgal, 2014).

The European Energy Performance of Buildings Directive 2002/91/EC (EPBD) has been recast in the form of Directive 2010/31/EU by the European Parliament on 19 May 2010. One of the new aspects of the EPBD is the introduction of the concept of nearly zero-energy building (Pacheco-Torgal *et al.*, 2013a).

The use of thermal insulation materials constitutes the most effective way of reducing heat losses in buildings, thus reducing heat energy needs. These materials have a thermal conductivity factor, k (W/m.K) lower than 0.065 and a thermal resistance higher than 0.30 $(m^2.K)/W$. Current commercial insulation materials (expanded polystyrene, extruded polystyrene, rigid foam of poly-isocyanurate or polyurethane) are associated with negative impacts in terms of toxicity.

Polystyrene, for example, contains anti-oxidant additives and ignition retardants.

Additionally, its production involves the generation of benzene and chlorofluorocarbons. On the other hand, polyurethane is obtained from isocyanates, which are widely known for their tragic association with the Bhopal disaster. Besides, it releases toxic fumes when subjected to fire (Pacheco-Torgal *et al.*, 2012b).

The information regarding hazardous substances is a crucial aspect in the new Construction Products Regulation (CPR) fully enforced since 1 July 2013. CPR links this subject to EC Regulation No. 1907/2006 (Registration, Evaluation, Authorisation and Restriction of Chemicals – REACH Regulation). Investigations into the development of thermal insulators based on AACB could constitute a lower toxicity alternative to some of the current commercial insulators.

1.2.3 AACB capable of reusing a high waste content

According to the Waste Management Acts 1996 and 2001, wastes can be defined as 'any substance or object belonging to a category of waste which the holder discards or intends or is required to discard, and anything which is discarded or otherwise dealt with as if it were waste shall be presumed to be waste until the contrary is proved'. The milestone related to the recycling of other kinds of waste can be found in the *Roadmap to a Resource Efficient Europe*: '*By 2020, waste is managed as a resource. Waste generated per capita is in absolute decline. Recycling and re-use of waste are economically attractive options for public and private actors due to widespread separate collection and the development of functional markets for secondary raw materials. More materials, including materials having a significant impact on the environment and critical raw materials, are recycled. Waste legislation is fully implemented. Illegal shipments of waste have been eradicated. Energy recovery is limited to non-recyclable materials, landfilling is virtually eliminated and high quality recycling is ensured.*' Improving the reuse of raw materials through greater 'industrial symbiosis' across the EU could save €1.4bn a year and generate €1.6bn in sales (European Commission, 2011b).

Construction and demolition wastes (CDW) deserve special attention in eco-efficient construction because the high volume of CDW constitutes a serious problem to be dealt with. CDW in the US is estimated at around 140 million metric tonnes (Yuan *et al.*, 2012). Eurostat estimates the total for Europe to be 970 million tonnes/year, representing an average value of almost 2.0 tonne per capita (Sonigo *et al.*, 2010).

Recycling of CDW is of paramount importance because it reduces environmental pressure. It prevents an increase of the area needed for waste disposal and also avoids the exploitation of non-renewable raw materials. Currently, the average recycling rate for EU-27 is just 47%. The need to recycle at least 70% of non-hazardous construction and demolition waste by 2020, expressed in *Roadmap to a Resource Efficient Europe* (European Commission, 2011b), was set by the Revised Waste Framework Directive 2008/98/EC (European Parliament, 2008) and does not include naturally occurring material defined in category 170504 (soil and stones not containing dangerous substances) in the European Waste Catalogue.

Eurostat estimates the total for Europe to be 970 million tonnes/year, representing

an average value of almost 2.0 tonne/per capita. As the current average recycling rate of CDW for the EU-27 is only 47%, achieving the 2020 target in just a decade seems an ambitious goal, further stressing the need for new and more effective recycling methods (Pacheco-Torgal *et al.*, 2013b). Moreover, in the next decades waste recycling will be increasingly challenging as a result of the zero waste scenario (Zaman and Lehmann, 2013).

Mining and quarrying wastes represent another worrying waste (more than 700 million tonnes/year just in Europe) that can be reused in construction materials. Mineral waste can be defined as the 'residues, tailings or other non-valuable material produced after the extraction and processing of material to form mineral products' (Harrison *et al.*, 2002).

In the recent past the failures of the Aznalcollar mine in Spain (1998), which contaminated 2656 ha of Donana Nature Park with pyrite sludge, and the Baia Mare mine (2000) in Romania clearly show that in the short term mine wastes represent a clear and present environmental danger (Pacheco-Torgal and Labrincha, 2013).

Given that most mining wastes have toxic substances, research efforts to find construction materials capable of immobilizing these wastes are needed. A recent COST action termed NORM4Building materials (in which the author participated in the initial proposal) was approved on 15 May 2013. NORM4Building intends to stimulate research on the reuse of industrial residues containing enhanced concentrations of natural radionuclides (NORM) in tailor-made building materials. Investigations on AACB are considered an emerging field under that COST action, which is why waste reuse is the subject of three chapters in this book.

1.3 Outline of the book

This handbook provides an updated state-of-the-art of the field of alkali-activated materials.

The first part encompasses an overview on the chemistry, mix design and manufacture of alkali-activated binders (Chapters 2–4).

Chapter 2 concerns the chemistry of the different types of alkali-activated binders. It reviews the physical-chemical principles governing alkali-activation processes in both high- and low-CaO aluminosilicate materials. It addresses factors such as starting material composition, reaction mechanisms, and the nature, composition and structure of the reaction products.

Chapter 3 discusses the most prominent characteristics and properties of the two-part component of alkali-activated materials, i.e, solid aluminosilicates and alkaline activators. It includes the $[CaO]/[SiO_2]$ and $[SiO_2]/[Al_2O_3]$ ratios in the cementitious materials; the best activator for each solid precursor; and the effect of anions (OH^- (pH), silicates, carbonates and sulfates) and cations (Na^+ or K^+).

Chapter 4 analyses a case study related to the synthesis of a new activator like waterglass from waste glass reuse through processes of solubility. The feasibility

of using this solution as a potential alkaline activator for blast furnace slag cement pastes is also analysed.

The properties of AACB are the subject of Part Two (Chapters 5–10).

Chapter 5 is concerned with setting time, segregation and bleeding of alkali-activated binders. Setting time for three different precursors is analysed (ground granulated blast furnace slag, metakaolin and fly ash). Comments on the segregation and bleeding of alkali-activated binders are made.

Chapter 6 looks at rheology parameters of alkali-activated binders. The chapter is divided into three parts: the first relates to forming techniques, the second concerns scientific rheology aspects, and the third presents the results of rheological studies on different alkali-activated systems.

Chapter 7 covers the mechanical strength and Young's modulus of alkali-activated binders. The influence of the type of aluminosilicate precursors and synthesis conditions on compressive and flexural strength is discussed. Comments on tensile strength are given. Analyses of Young's modulus of alkali-activated binder (AAB) gels, paste, mortars and concretes are made. The mechanical performance of fibre reinforced AAB is also analysed.

Chapter 8 analyses a case study related to the prediction of the compressive strength of alkali-activated binders by neuro-fuzzy modelling. The model was constructed by 395 experimental data collected from the literature and divided into 80% and 20% for training and testing phases, respectively. Absolute fraction of variance, absolute percentage error and root mean square error of 0.94, 11.52 and 14.48, respectively in the training phase and 0.92, 15.89 and 23.69, respectively in the testing phase of the model were achieved, showing the relatively high accuracy of the proposed neuro-fuzzy model.

Chapter 9 analyses the pore structure of alkali-activated metakaolin and alkali-activated slag. Water permeability, absorption and chloride iron diffusion of AACB are also examined

Chapter 10 addresses shrinkage and creep of alkali-activated binders. It includes a discussion of the importance of shrinkage and creep as well as of the factors that affect these two parameters. An example of shrinkage and creep prediction is also included.

Part Three (Chapters 11–17) deals with the durability of AACB.

Chapter 11 reviews freezing and thawing resistance of alkali-activated binders. It describes frost damage mechanisms and significant parameters of frost action.

Chapter 12 analyses the resistance to carbonation of alkali-activated binders**.** The protocols followed to assess the carbonation susceptibility are presented. A critical overview of the role of testing conditions and chemistry of the binding phases on the results acquired from those tests is included.

Chapter 13 is concerned with the corrosion behaviour of reinforced steel embedded in alkali-activated mortar. A discussion on the influence between the passivating capacity and the nature and dosage of binder on the type of activator used and on the environmental conditions is presented. New palliative methods (inhibitors and stainless steel) to prevent reinforced concrete corrosion are presented.

Chapter 14 is concerned with resistance to chemical attack of alkali-activated

binders. Three cases merit the author's attention. Acid resistance of alkali-activated slags, acid resistance of alkali-activated pozzolan (ash, metakaolin, mine waste) and acid resistance of a hybrid Portland cement–alkali-activated aluminosilicate system. The decalcification resistance of alkali-activated granulated blast furnace slag and the resistance to alkaline solutions are also presented.

Chapter 15 is related to the resistance to alkali-aggregate reaction (AAR) of alkali-activated binders. The chapter starts with an overview on the visual and microscopic manifestations as well as on the mechanisms of ASR in Portland cement concrete. Analyses of AAR in alkali-activated slag, alkali-activated fly ash and alkali-activated metakaolin are included.

Chapter 16 analyses the resistance to fire of alkali-activated binders. The introduction reviews the risks arising from fires in construction; the principles of passive fire protection; the definition of the fire resistance of materials; the standard temperature–time fire curves used for the simulation of several fire incidents; and the potential of alkali-activated binders as fire resistant materials. A discussion on the theoretical principles governing the fire performance of alkali-activated binders is included as well as a review on fire resistant alkali-activated binders.

Chapter 17 closes Part Three with a closer look at the efflorescence control of alkali-activated binders. It starts with comments on general features, definitions, effects and consequences, types of efflorescence and formation mechanism. Methods to reduce efflorescence are described, including careful adjustment of chemical composition, curing conditions and utilization of special additives.

Part Four (Chapters 18–24) concerns current applications of AACB.

Chapter 18 examines the reuse of aluminosilicate industrial wastes in alkali-activated binders. It includes residues from industrial activities related to energy, metallurgy, mining, ceramics, construction and demolition, chemical and petrochemical industries and agro-industry. Mechanical and microstructural properties of paste, mortar or concrete prepared by alkali activation of these residues are presented.

Chapter 19 covers the reuse of recycled aggregates in alkali-activated concretes. A brief discussion on recycled aggregates is included. The properties of alkali-activated recycled aggregate concrete are discussed, including normal strength, lightweight and pervious alkali-activated concrete. The performance of alkali-activated concrete containing recycled aggregates from other sources is also reviewed.

Chapter 20 looks at the use of alkali-activated binders for toxic waste immobilization. A discussion on the nature of the waste, in terms of mineralogy, alumina and silica contents, particle size, surface area and morphology and its influence on the reactivity of the waste is carried out.

Chapter 21 deals with alkali-activated mixtures for foil stabilization. The basic mechanisms of chemical soil stabilization are presented. Current materials and techniques for stabilization are reviewed. Recent results on the development of alkali-activated binders for soil stabilization are discussed.

Chapter 22 covers alkali-activated cements for OPC concrete coating. The properties (setting time and bond strength) and durability of metakaolin-based AACB used as inorganic coating for OPC concrete in the marine environment are presented. The

results of on-site trials over OPC concrete accropodes along the Shanghai Jinshan coast are also presented.

Chapter 23 looks at the performance of alkali-activated mortars for OPC concrete repair and strengthening. It provides a literature overview on concrete repair materials, highlighting current problems faced by them. The potential of alkali-activated mortars to overcome those limitations is analysed. Two specific cases are addressed: the case of concrete patch repair and the strengthening of concrete structures with fibre sheets.

Chapter 24 closes Part Four and covers the properties and durability of alkali-activated masonry units. Physical, mechanical properties and durability of alkali-activated binders based on different types of wastes are discussed.

Finally, Part Five concerns life cycle analysis (LCA) and novel applications of AACB (Chapters 25–28).

Chapter 25 looks at the LCA of alkali-activated cements and concretes. A revision of the theory on the compressive strength of concrete to define a functional unit that also includes the volume of the cement paste in the concrete to compare mixes was carried out. A new method to recalculate the cement equivalent of an alkali-activated concrete is presented. The global warming potential (GWP) of the mixes in the published LCA was calculated and compared to the current concrete alternative and the best available technology. Simulations on GWP of hybrid alkali-activated cements and one-part geopolymers are included.

Chapter 26 is concerned with the use of alkali-activated binders as inorganic thermal insulator materials. The chapter starts with an overview on general aspects and thermal phenomena in porous materials. It then reviews the various ways to prepare foam-based AACB, and analyses the influence of blowing agent and alkaline elements on the foam network, microstructure, porosity and thermal properties.

Chapter 27 addresses the photocatalytic degradation of water pollutants with alkali-activated cements.

Chapter 28 closes Part Five with important insights on innovative applications of low calcium alkali-activated binders (geopolymers). These include: potential for fast ion conductor applications, to act as photocatalysts for the photodegradation of pollutants, biological applications, to be used as solid-state humidity indicator, as chromatography media for separating mixtures of organic compounds, as low temperature ceramics, as carbothermal reduction and nitridation (CRN) precursors for wear-resistant engineering components, as stable host material for luminescent systems, as catalyst for organic reactions, and as solid-state hydrogen storage material.

References

Azevedo, F., Pacheco-Torgal, F., Jesus, C. and Barroso de Aguiar, J.L. (2012) Properties and durability of HPC with tyre rubber waste. *Construction and Building Materials* 34, 186–191.

Davidovits, J., Comrie, D., Paterson, J. and Ritcey, D. (1990) Geopolymeric concretes for environmental protection. *ACI Concrete International*12, 30–40.

Duxson, P. and van Deventer, J.S.J. (2009) Commercialization of geopolymers for construction – opportunities and obstacles. In *Geopolymers: Structure, Processing, Properties and Industrial Applications* (J. Provis and J. van Deventer, eds). Woodhead Publishing Limited, Cambridge, pp. 379–400.

Duxson, P., Provis, J., Luckey, G. and van Deventer, J.S.J. (2007) The role of inorganic polymer technology in the development of 'Green Concrete'. *Cement and Concrete Research* 37, 1590–1597.

European Commission (2011a) *Energy Roadmap 2050*. COM(2011) 885/.EC, Brussels.

European Commission (2011b) *Roadmap to a Resource Efficient Europe*. COM(2011) 571. EC, Brussels.

European Parliament (2008) Directive 2008/98/EC – Revised Waste Framework. *Official Journal of the European Union*, European Parliament, Brussels.

Fernandez-Jimenez, A. and Palomo, A. (2009) Chemical durability of geopolymers. In *Geopolymers: Structures, Processing, Properties and Industrial Applications* (J. Provis and J. van Deventer, eds). Woodhead Publishing Limited, Cambridge, pp. 167–193.

Garcia-Lodeiro, I., Fernandez-Jimenez, A. and Palomo, A. (2013a) Variation in hybrid cements over time: alkaline activation of fly ash–Portland cement blends. *Cement and Concrete Research* 52, 112–122.

Garcia-Lodeiro, I., Fernandez-Jimenez, A. and Palomo, A. (2013b) Alkali-activated based concrete. In *Eco-efficient Concrete* (F.) Pacheco-Torgal, S. Jalali, J. Labrincha and V.M. John, eds). Woodhead Publishing Limited, Cambridge, pp. 439–487.

Habert, G., de Lacaillerie, J. and Roussel, N. (2011) An environmental evaluation of geopolymer based concrete production: reviewing current research trends. *Journal of Cleaner Production*11, 1229–1238.

Harrison, D.J., Bloodworth, A.J., Eyre, J.M., Macfarlane, M., Mitchell, C.J., Scott, P.W. and Steadman, E.J. (2002) Utilisation of mineral waste: cases studies. BGS Commissioned Report CR/02/227 N.

IEA (2012) *World Energy Outlook 2012*, OECD/IEA, Paris.

IPCC (Intergovernmental Panel on Climate Change) (2007) *Climate Change 2007: Synthesis Report*, IPCC, Geneva.

Juenger, M., Winnefeld, F., Provis, J. and Ideker, J. (2011) Advances in alternative cementitious binders. *Cement and Concrete Research* 41, 1232–1243.

Kim, M.-S., Jun, Y., Lee, C. and Oh, J.-E. (2013) Use of CaO as an activator for producing a price-competitive non-cement structural binder using ground granulated blast furnace slag. *Cement and Concrete Research* 54, 208–214.

Kolousek, D., Brus, J., Urbanova, M., Andertova, J., Hulinsky, V. and Vorel, J. (2007) Preparation, structure and hydrothermal stability of alternative (sodium silicate-free) geopolymers. *Journal of Materials Science* 42, 9267–9275.

Lechtenbohmer S and Schuring A (2011) The potential for large-scale savings from insulating residential buildings in the EU. *Energy Efficiency* 4, 257–270.

Li, C., Sun, H. and Li, L. (2010) A review: The comparison between alkali-activated slag (Si+Ca) and metakaolin (Si+Al) cements. *Cement and Concrete Research* 40, 1341–1349.

McLellan, B., Williams, R., Lay, J., van Riessen, A. and Corder, G. (2011) Costs and carbon emissions for geopolymer pastes in comparison to ordinary Portland cement. *Journal of Cleaner Production* 19, 1080–1090.

Pacheco-Torgal, F. (2014) Eco-efficient construction and building materials research under the EU Framework Programme Horizon 2020. *Construction and Building Materials* 51, 151–162.

Pacheco-Torgal, F. and Jalali, S. (2011) *Eco-efficient Construction and Building Materials*. Springer Verlag, London.

Pacheco-Torgal, F. and Labrincha, J. (2013) The future of construction materials research and the seventh UN Millennium Development Goal: a few insights. *Construction and Building Materials* 40, 729–737.

Pacheco-Torgal, F., Abdollahnejad, Z., Camões, A.F., Jamshidi, M. and Ding, Y. (2012a) Durability of alkali-activated binders: a clear advantage over Portland cement or an unproven issue? *Construction and Building Materials* 30, 400–405.

Pacheco-Torgal, F., Fucic, A. and Jalali, S. (eds) (2012b) *Toxicity of Building Materials*. Woodhead Publishing Limited, Cambridge.

Pacheco-Torgal, F., Cabeza, L., Mistretta, M., Kaklauskas, A. and Granqvist, C.G. (2013a) *Nearly Zero Energy Building Refurbishment. A Multidisciplinary Approach*. Springer Verlag, London.

Pacheco-Torgal, F., Tam, V.W.Y., Labrincha, J.A., Ding, Y. and de Brito, J. (eds) (2013b) *Handbook of Recycled Concrete and Other Demolition Waste*. Woodhead Publishing Limited, Cambridge.

Provis, J.L. (2010) Discussion of C. Li *et al*., A review: The comparison between alkali-activated slag (Si + Ca) and metakaolin (Si + Al) cements. *Cement and Concrete Research* 40, 1766–1767.

Provis, J.L. (2014) Geopolymers and other alkali activated materials: why, how, and what? *Materials and Structures* 47, 11–25.

Provis, J.L. and van Deventer, J.S.J. (eds) (2009) *Geopolymers: Structures, Processing, Properties and Industrial Applications*. Woodhead Publishing, Cambridge.

Provis, J.L. and van Deventer, J.S.J. (eds) (2013) Alkali-activated materials: State-of-the-Art Report, RILEM TC 224-AAM. Springer/RILEM, Berlin.

Rockström, J., Steffen, W., Noone, K., Persson, Å., Chapin, III, F.S., Lambin, E., Lenton, T.M., Scheffer, M., Folke, C., Schellnhuber, H., Nykvist, B., De Wit, C.A., Hughes, T., van der Leeuw, S., Rodhe, H., Sörlin, S., Snyder, P.K., Costanza, R., Svedin, U., Falkenmark, M., Karlberg, L., Corell, R.W., Fabry, V.J., Hansen, J., Walker, B., Liverman, D., Richardson, K., Crutzen, P. and Foley, J. (2009) Planetary boundaries: exploring the safe operating space for humanity. *Ecology and Society* 14, 32. http://www.ecologyandsociety.org/vol14/iss2/art32/

Roy, D.M. (1999) Alkali-activated cements – opportunities and challenges. *Cement Concrete Research*, 29, 249–254.

Schellnhuber, H. (2008) Global warming. Stop worrying, start panicking? *Proceedings of the National Academy of Sciences of the United States of America* 105, 14239–14240.

Seto, K.C., Güneralp, B. and Hutyra, L.R. (2012) Global forecasts of urban expansion to 2030 and impacts on biodiversity and carbon pools. *Proceedings of the National Academy of Sciences of the United States of America* 109, 16083–16088.

Shi, C., Krivenko, P.V. and Roy, D.M. (2006) *Alkali-Activated Cements and Concretes*. Taylor & Francis, Abingdon.

Shi, C., Fernandez-Jimenez, A. and Palomo, A. (2011) New cements for the 21st century: the pursuit of an alternative to Portland cement. *Cement and Concrete Research* 41, 750–763.

Škvára, F., Šmilauer, V., Hlaváček, P., Kopecký, L. and C'lová, Z. (2012) A weak alkali bond in (N, K)–A–S–H gels: evidence from leaching and modelling. *Ceramics – Silikáty* 56, 374–382.

Sonigo, P., Hestin, M. and Mimid, S. (2010) Management of construction and demolition waste in Europe. Stakeholders Workshop, Brussels.

Turner, L. and Collins, F. (2013) Carbon dioxide equivalent (CO2-e) emissions: a comparison between geopolymer and OPC cement concrete. *Construction and Building Materials* 43, 125–130.

Valero, A., Agudelo, A. and Valero, A. (2011) The crepuscular planet: a model for the exhausted atmosphere and hydrosphere. *Energy* 36, 3745–3753.

van Deventer, J.S.J., Feng, D. and Duxson, P. (2010) Dry Mix Cement Composition, Methods and Systems Involving Same. US Patent 7691,198 B2.

van Deventer, J.S.J., Provis, J. and Duxson, P. (2012) Technical and commercial progress in the adoption of geopolymer cement. *Minerals Engineering* 29, 89–104.

Weil, M., Dombrowski, K. and Buchawald, A. (2009) Life-cycle analysis of geopolymers. In *Geopolymers, Structure, Processing, Properties and Industrial Applications* (J. Provis and J. van Deventer, eds). Woodhead Publishing Limited, Cambridge, pp. 194–210.

Yuan, H., Chini, A., Lu, Y. and Shen, L. (2012) A dynamic model for accessing the effects of management strategies on the reduction of construction and demolition waste. *Waste Management* 32, 521–531.

Zaman, A.U. and Lehmann, S. (2013) The zero waste index: a performance measurement tool for waste management systems in a 'zero waste city'. *Journal of Cleaner Production* 50, 123–132.

Zheng, D., van Deventer, J.S.L. and Duxson, P. (2007) The dry mix cement composition, methods and systems involving same. International Patent WO 2007/109862 A1.

Part One

Chemistry, mix design and manufacture of alkali-activated, cement-based concrete binders

This page intentionally left blank

An overview of the chemistry of alkali-activated cement-based binders

2

I. Garcia-Lodeiro, A. Palomo, A. Fernández-Jiménez
Instituto Eduardo Torroja (IETcc-CSIC), Madrid, Spain

2.1 Introduction: alkaline cements

Portland cement is the construction material par excellence. Its manufacture, however, is energy-intensive (requiring kiln temperatures of 1450–1550°C) and has other significant environmental consequences (Taylor, 1990; Habert, 2103). Generating nearly one tonne of CO_2 for each tonne of Portland cement produced, this binder is one of the primary causes of global warming (accounting for 7% of worldwide CO_2 emissions). Moreover, Portland cement consumption has grown nearly exponentially in the last 20 years; by 2020 overall demand is estimated to reach 3.6×10^9 tonnes, which will translate into an unsustainable flow of CO_2 emissions. Portland cement manufacture also entails significant over-exploitation of natural resources, particularly limestone quarries. It takes over 3.0 billion tonnes of raw materials (70% of which are limestone) to produce the world's 2.0 billion tonne Portland cement output.

All these factors encourage the study and development of new alternative binders with lower energy and environmental costs (lower CO_2 emissions, reuse of industrial by-products) and performance as high or higher than ordinary Portland cement (OPC). A series of binders generically known as alkaline cements constitute one such category of materials (Wu *et al*., 1983; Glukhovsky, 1994; Wang *et al*., 1995; Palomo *et al*., 1999; Fernández-Jiménez, 2000; Shi *et al*., 2006; Duxson *et al*., 2007a; Provis and van Deventer, 2009).

Many a study on alkaline activation has been conducted since the main components of alkaline binders were discovered by Glukhovsky in 1967. A very wide range of natural raw materials, industrial by-products and recycled aluminosilicates can be used as alkaline cement components: metakaolin, pozzolans, blast furnace slag, phosphorous slag, fly ash, glass waste and combinations of two or more of these materials. Although the characteristics of the materials used and their alkaline activators play a significant role in the hydration and microstructural development of the binders obtained, with the concomitant variations in their mechanical strength, suitably alkali-activated cements and concretes can exhibit even higher performance than Portland cement concretes.

Alkaline cements are cementitious materials formed as the result of an alkaline attack on the amorphous or vitreous aluminosilicates. When mixed with alkaline

Handbook of Alkali-activated Cements, Mortars and Concretes. http://dx.doi.org/10.1533/9781782422884.1.19

activators, these materials set and harden, yielding a material with good binding properties.

One of the most prominent features of alkaline activation technology is that both natural materials (such as clay or feldspars) and industrial by-products (such as slag, fly ash and paper sludge) can be used as prime materials. This chapter explores the role of all the constituents of these cements in depth.

A wide variety of alkali-activated cements has been developed in the last few decades. Based on the nature of their cementitious components (CaO-SiO_2-Al_2O_3 system), alkaline cements may be grouped under two main categories: (1) high calcium and (2) low calcium cements. The activation pattern differs in each.

- ***(Na,K)$_2$O-CaO-Al$_2$O$_3$-SiO$_2$-H$_2$O system, Model 1*:** in this model calcium- and silicon-rich materials such as blast furnace slag (SiO_2 + CaO > 70%) are activated under relatively moderate alkaline conditions (Bakharev *et al*., 2000; Fernández-Jiménez, 2000; Shi *et al*., 2006). In this case the main reaction product is a C-A-S-H (calcium silicate hydrate) gel, similar to the gel obtained during Portland cement hydration, which takes up Al in its structure.
- ***(Na,K)$_2$O-Al$_2$O$_3$-SiO$_2$-H$_2$O system, Model 2:*** in this model the materials activated comprise primarily *aluminium* and *silicon*. The materials used in this second alkali activation procedure such as metakaolin or type F fly ash (from coal-fired steam power plants) have low CaO contents. In this case more aggressive working conditions are required to kick-start the reactions (highly alkaline media and curing temperatures of 60–200°C). The main reaction product formed in this case is a three-dimensional inorganic alkaline polymer, a ***N-A-S-H*** (or alkaline aluminosilicate hydrate) gel that can be regarded as a zeolite precursor (Palomo *et al*., 1999, 2004; Duxson *et al*., 2007a; Provis and van Deventer, 2009). This gel also goes by the names of *geo- or inorganic polymer* among others.

Today, a third alkaline activation model, a combination of the preceding two, can also be described. Here the product would be a new type of binder known as a *blended or hybrid alkaline cement*, formed as the result of the alkaline activation of materials with CaO, SiO_2 and Al_2O_3 contents > 20% (Alonso and Palomo, 2001; Yip *et al*., 2005; Palomo *et al*., 2007; García-Lodeiro *et al*., 2013a, 2013b). These materials can be divided into two groups. *Group A* includes materials having a low Portland cement clinker content and a high proportion (over 70%) of mineral additions (Palomo *et al*., 2007). Examples are cement + slag, cement + fly ash, cement + slag + fly ash. *Group B* comprises blends containing no Portland cement: blast furnace slag + fly ash, phosphorous slag + blast furnace slag + fly ash and similar.

The reaction products precipitating in this third group (hybrid cements) are very complex, comprising a mix of cementitious gels, including C-A-S-H (which takes sodium into its composition) and (N,C)-A-S-H (high calcium content N-A-S-H gels) gels (Garcia-Lodeiro *et al*., 2010a, 2010b).

The following is a description of the most significant features and the chemistry governing the activation reactions in each of the aforementioned models.

2.2 Alkaline activation of high-calcium systems: $(Na,K)_2O$-CaO-Al_2O_3-SiO_2-H_2O

2.2.1 Composition of starting materials

The material most commonly used to prepare calcium-rich alkaline cements and concretes is blast furnace slag. This vitreous steel industry waste is formed when the acid oxides (SiO_2 and Al_2O_3) from the mix of acid clay gangue present in iron ore and sulfur ash in coke combine with the basic oxides (CaO and MgO) present in the limestone or dolomite used as fluxes during high temperature (1600°C) smelting followed by abrupt cooling to temperatures of >800°C (Fernández-Jiménez, 2000; Shi *et al.*, 2006).

The majority components in slag (Provis and van Deventer, 2009) are CaO (35–40%), SiO_2 (25–35%), MgO (5–10%) and Al_2O_3 (5–15%), while its minority constituents include S, Fe_2O_3, MnO and K_2O (with percentages of under 1%). In other words, slag contains both network-forming anions $(SiO_4)^{4-}$, $(AlO_4)^{5-}$ and $(MgO_4)^{6-}$ and network-modifying cations, Ca^{2+} and Al^{3+} and Mg^{2+}.

On average, 90–95% of slag is vitreous (a depolymerised calcium silicate) and the rest is a solid solution of minority crystalline phases: gehlenite ($2CaO.Al_2O_3.SiO_2$) and akermanite ($2CaO.MgO.2SiO_2$), tetragonal lattice, melilite family crystals (Fernández-Jiménez, 2000; Shi *et al.*, 2006).

Slag reactivity in alkaline activation processes depends largely (Swamy and Bouikni, 1990; Mostafa *et al.*, 2001; Li *et al.*, 2002) on the vitreous phase content, for which values of over 90% are recommended. Nonetheless, Pal *et al.* (2003) noted that slag with low vitreous phase contents (30–65%) could also deliver good results. The degree of depolymerisation (DP), a parameter whose value normally ranges from 1.3 to 1.5, apparently bears a direct relationship to slag reactivity (Pal *et al.*, 2003; Provis and van Deventer, 2009; Li *et al.*, 2010). It is calculated from the following equation:

$$DP = n(CaO) - 2n(MgO) - n(Al_2O_3) - n(SO_3)/n(SiO_2)$$
$$- 2n(MgO) - 0.5n(Al_2O_3)$$

According to most of the literature, the main properties required of slag to be apt for use in activated slag cement are as listed below (Fernández-Jiménez, 2000; Shi *et al.*, 2006; Provis and van Deventer, 2009).

- It must be granulated or pelletised and have a vitreous phase content of >85–95%.
- It must exhibit structural disorder, for the lower the degree of polymerisation in the glass, the higher is its hydraulic activity: the degree of polymerisation depends on the (SiO_4) tetrahedra and Al and Mg coordination in the vitreous phase of the slag.
- It must be pH-basic, i.e., have a CaO + MgO/SiO_2 ratio of >1. Basic slag has a higher hydraulic potential, for the lime content in the slag controls its activation. That notwithstanding, acid slag may also be alkali-activated.
- It must be ground to a specific surface of 400–600 m^2/kg. Specific surface plays an important role in the rate and intensity of the activation reaction.

2.2.2 Reaction mechanisms

Glukhovsky and Krivenko (Glukhovsky, 1967, 1994; Krivenko, 1994) proposed a model that would explain the alkaline activation of silica- and lime-rich materials such as blast furnace slag by means of the series of reactions summarised below:

$$\equiv Si\text{-}O^- + R^+ = \equiv Si\text{-}O\text{-}R$$

$$\equiv Si\text{-}O\text{-}R + OH^- = \equiv Si\text{-}O\text{-}R\text{-}OH^-$$

$$\equiv Si\text{-}O\text{-}R\text{-}OH^- + Ca^{2+} = \equiv Si\text{-}O\text{-}Ca\text{-}OH + R^+$$

The alkaline cation (R^+) acts as a mere catalyser in the initial phases of hydration, via cationic exchange with the Ca^{2+} ions. These same authors believed that as the reactions advance, the alkaline cations are taken up into the structure.

Fernández-Jiménez (2000) and Fernández-Jiménez *et al*. (2003) reported that the nature of the anion in the solution also plays an instrumental role in activation, especially at early ages and in particular with regard to paste setting. One of the models that describes the reaction mechanisms (based on a model proposed by Glasser in 1990) is depicted in Figure 2.1.

Slag alkaline activation forms part of a complex process that takes place by stages, in which slag destruction is followed by polycondensation of the reaction products (Li *et al*., 2010).

2.2.3 Reaction products

The majority reaction product formed in Portland cement hydration is a C-S-H-type gel to which the material primarily owes its mechanical properties. The secondary products include portlandite, ettringite and calcium monosulfoaluminate (Taylor, 1990). The process is similar in alkaline cements. The main reaction product, a gel (whose composition and structure vary with respect to the standard C-S-H generated in OPC hydration), forms along with a series of secondary products. The type of secondary product generated depends on starting material composition, activator type and concentration, curing conditions and pH, among others (LaRosa *et al*., 1992; Cheng *et al*., 1992; Roy *et al*., 1994; Wang *et al*., 1995; Puertas. 1995; Fernández-

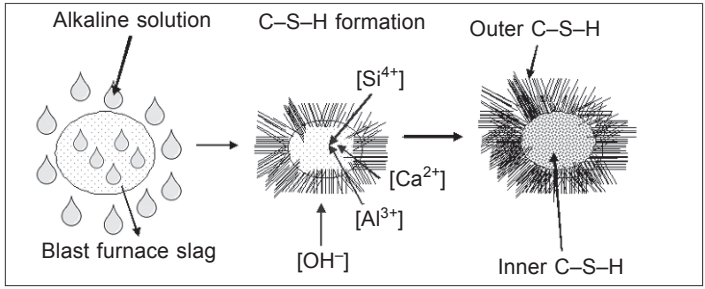

Figure 2.1 Theoretical model for the reaction mechanism in alkali-activated slag.

Jiménez *et al*., 1996; Palomo *et al.,* 1999; Fernández-Jiménez, 2000; Shi *et al*., 2006; Duxson *et al*., 2007a; Duxson and Provis, 2008; Provis and van Deventer, 2009).

Table 2.1 compares the most common reaction products forming in normal Portland cement hydration to the products of (high- and low-calcium) alkaline cement activation (Taylor, 1990; LaRosa *et al*., 1992; Cheng *et al*., 1992; Roy *et al*., 1994; Wang *et al*., 1995; Puertas, 1995; Fernández-Jiménez *et al*., 1996; Palomo *et al*., 1999; Fernández-Jiménez, 2000; Shi *et al*., 2006; Duxson *et al*., 2007a; Duxson and Provis, 2008; Provis and van Deventer, 2009).

Broadly speaking, the nature and composition of the reaction products forming during the alkaline activation of materials are among the most controversial aspects of this field of research and the areas most in need of continued study. Nonetheless, most authors agree to the following assertions.

- The main hydration product is a calcium silicate hydrate with aluminium in its composition (C-A-S-H gel). This gel differs slightly from the gel forming in Portland cement paste, in that it has a lower C/S ratio (C/S = 0.9–1.2).
- The structure and composition of C-A-S-H gel and the presence of other secondary phases or compounds depend on the type and amount of activator used, slag structure and composition and the curing conditions in which the material hardens.

The minority phases whose formation during the alkaline activation of slag has marshalled the widest consensus are listed below.

- A phase known as hydrotalcite ($Mg_6Al_2CO_3(OH)_{16}{\cdot}4HO$) has been detected in slag activated with NaOH (Fernández-Jiménez, 2000; Ben Haha *et al*., 2011, 2012) and waterglass (Cheng *et al*., 1992; Wang and Scrivener, 1995). Hydrotalcite is a natural mineral whose structure consists of layers of brucite ($Mg(OH)_2$) with interstitial water molecules and CO_3^{2-} ions. These (often sub-microscopic) crystals are scattered throughout the C-A-S-H gel. Phases of this type have also been found in cement + slag blends.
- C_4AH_{13}-type phases have been detected in slag activated with NaOH. These phases form platelets 0.1–0.2 μm thick and approximately 1.5 μm in diameter (LaRosa *et al*., 1992; Wang *et al*., 1995). Other authors (Cheng *et al*., 1992) have observed carbonated phases such as C_4AcH_{11} and $C_8Ac_2H_{24}$ in slag pastes activated with NaOH and $Ca(OH)_2$.

Table 2.1 Products precipitating in different types of binders

Binder type		**OPC**	**Alkaline cement**	
			(Na,K)$_2$O-CaO-Al$_2$O$_3$-SiO$_2$-H$_2$O	***(Na,K)$_2$O-Al$_2$O$_3$-SiO$_2$-H$_2$O***
Reaction product	**Primary**	**C-S-H**	**C-A-S-H**	**N-A-S-H**
	Secondary	$Ca(OH)_2$ AF_m AF_t	Hydrotalcite $[Mg_6Al_2CO_3(OH)_{16}{\cdot}4H_2O]$ C_4AH_{13} $CASH_8$ C_4AcH_{11} $C_8Ac_2H_{24}$	Zeolites: hydroxysodalite, zeolite P, Na-chabazite, zeolite Y, faujasite
C = CaO, S = SiO$_2$, A = Al$_2$O$_3$, N = Na$_2$O, H = H$_2$O, c = CO$_2$				

2.2.4 Micro- and nanostructure of the gel formed: C-A-S-H-type gels

The alkaline activation of blast furnace slag may vary slightly with the chemical and mineralogical composition of the slag, as well as with activator type and composition. Sodium hydroxide and waterglass are the two activators most commonly used. Wang *et al*. (1995) studied the effect of these two activators on early and later age gel microstructure, as determined by SEM/EDX analysis. In the early stages of activation, the hydration products precipitated in the inter-particle voids initially occupied by the alkaline solution, an indication that they formed as a result of dissolution followed by precipitation. For pastes activated with waterglass, the gels were uniformly amorphous. When a NaOH solution was used as the activator, however, platelets 0.1–0.2 μm thick and 15 μm in diameter could be distinguished. As activation progressed (5–7 days), 0.5–1 μm dark rings appeared around lighter-coloured and thinner slag rings. EDX microanalysis confirmed that regardless of the type of activator, the majority product was always a C-S-H gel with a low Ca/Si ratio containing small amounts of Na, Mg, Al and S. When NaOH was the activator, a semi-crystalline C-S-H gel (I) was visible in the early stages of the reaction, while with waterglass, crystallinity remained very low even after a full year of hydration.

Fernández-Jiménez *et al*. (2003) also used different microscopic techniques to study these materials. Figure 2.2 contains a series of transmission electron micrographs (TEM) of the initial slag and the products resulting from its activation with NaOH and waterglass. An analysis of the electron diffraction patterns (EDX) confirmed the presence of a leaf-shaped, semi-crystalline calcium silicate hydrate as the main reaction product. EDX microanalysis of the 7-day materials revealed that the pastes made with waterglass had lower Ca/Si ratios (0.6–0.7) than the NaOH pastes (0.9–1.0). Aluminium and some sodium were identified in the composition of all the pastes. A magnesium- and aluminium-rich secondary phase, attributed to hydrotalcite, was also detected.

The nanostructure of cementitious gels cannot be readily determined due to their amorphous nature. Nonetheless, the information reported in recent years as a result of the application of a number of characterisation techniques, most prominently nuclear magnetic resonance (NMR) (Engelhardt and Michel, 1987), has proven to be very helpful for developing models to ascertain and describe the structure of the various gels formed.

Based on ^{29}Si and ^{27}Al MAS NMR studies, Schilling *et al*. (1994) proposed that Al is taken up in the C-S-H gels generated in alkali-activated slag pastes, in which aluminium tetrahedra replace silicon tetrahedra in bridging positions to give rise to Q^1, Q^2 and $Q^2(1Al)$ units. The aluminium uptake was shown to depend on the concentration of alkalis and to be greater at high temperature and humidity. Richardson *et al*. (1994), Richardson and Groves (1997) and Richardson and Cabrera (2000) also explored Al uptake in C-(A)-S-H gels in tetrahedral bridging positions and proposed a series of equations to calculate mean silicon chain length and the Si/Al ratio in the gel formed from NMR data.

This model was subsequently ratified by Fernández-Jiménez *et al*. (Fernández-

(a)

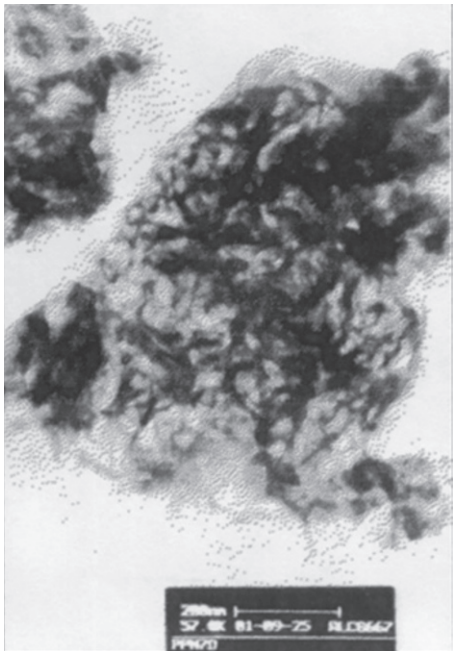

(b)

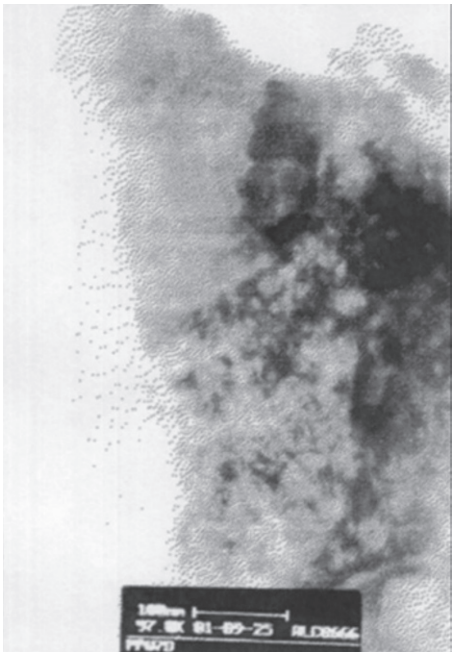

(c)

Figure 2.2 TEM micrographs of (a) anhydrous slag (Ca/Si=1.21, Ca/Al= 2.63, Si/Al= 2.13); (b) slag hydrated with NaOH for 7 days (Ca/Si=0.93, Ca/Al=1.35, Si/Al=1.45): (c) slag hydrated with waterglass for 7 days (Ca/Si= 0.64, Ca/Al = 1.49, Si/Al= 2.32) (Fernández-Jiménez *et al*., 2003).

Jiménez, 2000; Fernández-Jiménez *et al.*, 2003). They showed that the presence of Al gives rise to gels with longer linear chains as well as to the possible existence of sporadic inter-chain, Si-O-Al bonds and consequently two-dimensional (Q^3(*n*Al) unit, cross-linked) structures. Under those conditions, the C-S-H gels would become C-(A)-S-H gels (see Figure 2.3). These same authors established that the type of activator has a direct effect on the degree of silicate species condensation in the gel structure; when the activator used was waterglass, highly condensed structures formed. Consequently, a substantial number of Q^2(1Al) and Q^3(nAl) units were observed, along with Q^1(0Al) and Q^2(0Al) units, favouring the formation of two-dimensional, cross-linked structures. When NaOH was the activator, however, the C-S-H gel generated had a significant number of Q^2(1Al) units, but no Q^3 units (Fernández-Jiménez *et al.*, 2003).

Many papers can now be found in the literature that confirm the presence of Q^3(*n*Al) units in the C-A-S-H gels forming during slag alkaline activation (Fernández-Jiménez *et al.*, 2003; Puertas *et al.*, 2011). One prominent article, authored by Puertas *et al.* (2011) reported that in C-A-S-H gels forming in slag activated with a NaOH solution, the existence of tetrahedral Al in bridging positions in the silicate chains goes hand-in-hand with a considerable increase in the number of Q^2(1Al) units, as well as with a small amount of Q^3(*n*Al) units. When waterglass was used as an activator, the C-A-S-H gels forming had a higher aluminium content in tetrahedral bridging positions, favouring chain cross-linking and raising the percentage of Q^3(*n*Al) units significantly and with it the formation of layered structures in certain regions.

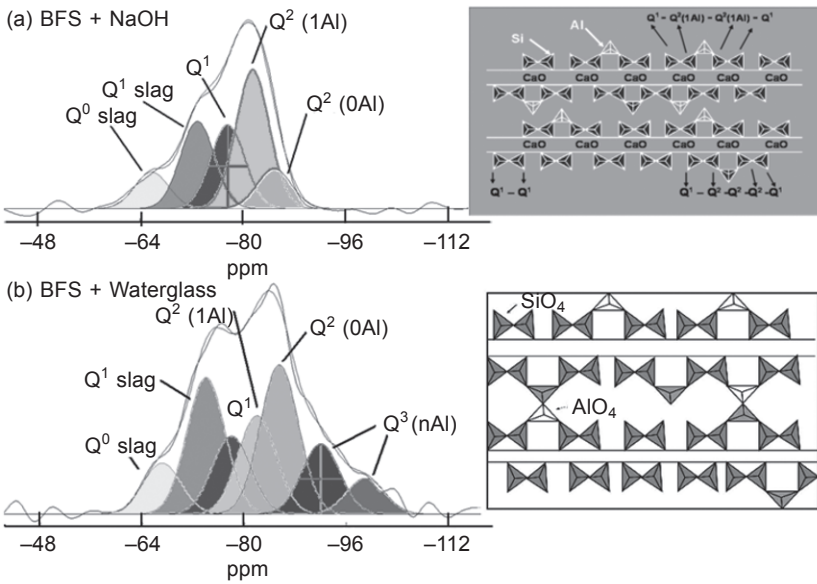

Figure 2.3 Structural model for an Al-containing C S H gel (Fernández-Jiménez, 2000); (a) linear chains; (b) linear chains with occasional cross-linking, forming planes.

This gel was also observed to contain a small amount of alkalis (normally Na), that neutralised the charge imbalance created when a Si is replaced by an Al tetrahedron. In fact, these are calcium-sodium aluminosilicate hydrate [C-(N)-A-S-H] gels. Hannus *et al*. (1999), Barbosa *et al*. (2000), Bernal *et al*. (2013) and Myers *et al*. (2013) proposed a model to describe this gel as a mix of cross-linked and non-cross-linked tobermorite-based structures (the cross-linked substituted tobermorite model, CSTM).

2.3 Alkaline activation of low-calcium systems: $(N,K)_2O$-Al_2O_3-SiO_2-H_2O

2.3.1 Composition of starting materials

Fly ash and metakaolin are the low-calcium materials most commonly deployed in alkaline cement and concrete manufacture, although the higher cost of metakaolin constrains its use.

Metakaolin is a pozzolanic material generated as a result of kaolinite clay calcination at temperatures ranging from 650 to 850°C, depending on the purity and crystallinity of the precursor clays (see Eq. 2.1) (Ambroise *et al*., 1985; Calderon and Burg, 1994; Granizo and Blanco, 1998; Pera, 2001; Granizo *et al*., 2002, 2007; Provis and van Deventer, 2009; Li *et al*., 2010).

$$XSiO_2.YAl_2O_3.ZH_2O \rightarrow XSiO_2.YAl_2O_3 + z\ H_2O \quad (2.1)$$

Generally speaking, metakaolin is structured around a series of alternating layers of silicates and aluminates, in which the silicon has a coordination number of 4 (tetrahedral), while the numbers for aluminium are 4, 5 and 6. The usability of metakaolin as a source of aluminosilicates in alkaline activation depends heavily on the particle size, purity and crystallinity of the initial kaolinite. As a rule, the MK particles should be under 5 μm, with an intrinsic clay grain size on the order of 20 nm (Li *et al*., 2010).

Fly ash morphology, in turn, is characterised by hollow spheres that may or may not house other smaller spheres. It consists essentially of a vitreous phase and a few minority crystalline phases such as quartz (5–13%), mullite (8–14%) and magnetite (3–10%) (Fernández-Jiménez and Palomo, 2003). Fly ash composition may nonetheless vary depending on the type of coal used and the incineration process in place at the power plant. After an exhaustive study of a large number of types of ash, Fernández-Jiménez and Palomo (2003) concluded that for a type F fly ash to be suitable for use in the manufacture of alkaline cements, it must meet the following requirements (Fernández-Jiménez and Palomo, 2003; Fernández-Jiménez *et al*., 2006):

- unburnt percentage < 5%
- $[Fe_2O_3] \leq 10\%$;
- $[CaO] \leq 10\%$;

- reactive $[SiO_2] > 40\%$;
- 80–90% particles < 45 μm
- vitreous phase content > 50%
- a $[SiO_2]_{reactive} / [Al_2O_3]_{reactive}$ ratio > 1.5

2.3.2 Reaction mechanisms

The alkaline activation of silica- and alumina-rich materials is less thoroughly understood than slag activation because it is a relatively recent line of research. Glukhovsky (1994) proposed a general mechanism for the activation reactions in these materials, consisting of three stages: (a) destruction-coagulation; (b) coagulation-condensation; and (c) condensation-crystallisation.

In the first (see Eq. 2.2), the reaction begins when the OH^- ions in the alkaline activator break the Si-O-Si bonds. The ions redistribute their electronic density around the silicon atoms, weakening the Si-O-Si bonds and making them more liable to rupture. This attack yields silanol (–Si-OH) and sialate ($–Si-O^-$) species. The presence of the alkaline cation neutralises the resulting negative charge, while the formation of $Si-O^-Na^+$ bonds hinders the reversion to siloxane (Si-O-Si).

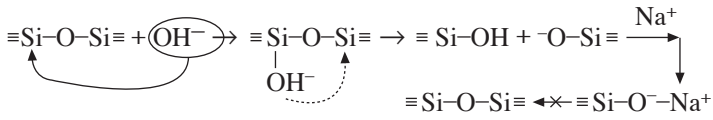

(2.2)

The OH^- groups impact the Si-O-Al bonds (see Eq. 2.3) in the same way: dissolved aluminium species form complex species, predominantly $Al(OH)_4^-$ anions.

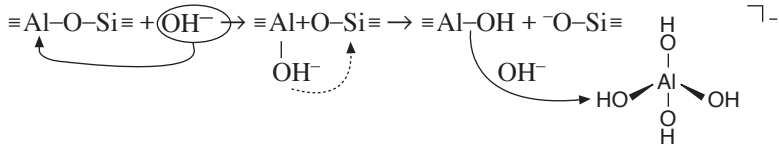

(2.3)

In the second stage, coagulation-condensation, the accumulation of ionic species favours the contact between the disaggregated products and polycondensation begins, giving rise to coagulated structures. The silica monomers inter-react to form dimers (forming Si-O-Si bonds), which in turn react with other monomers to build polymers (see Eq. 2.4). This stage is catalysed by the OH^- ions. The clusters formed as a result of the polymerisation of the silicic acid begin to grow in all directions, generating colloids. The aluminates also participate in polymerisation, isomorphically replacing the silicon tetrahedra. While the alkaline metal catalyses the reaction in the first stage, in the second it acts as a structural component.

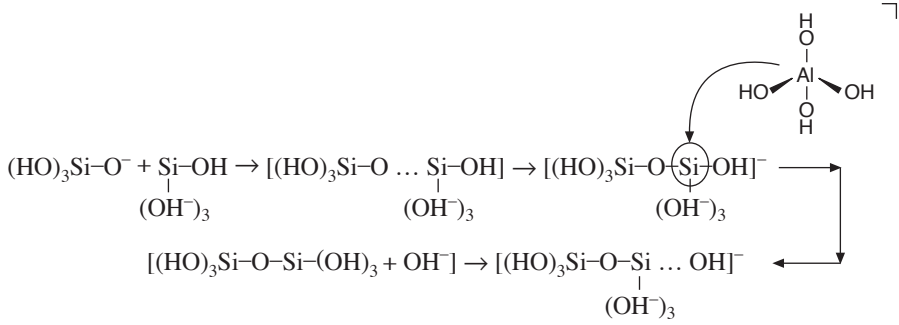

(2.4)

Lastly, in the third stage, condensation-crystallisation, the presence of particles in the initial solid phase furthers reaction product precipitation. The composition of these products depends on the mineralogy and chemical composition of the prime materials, the alkaline activator used and the curing conditions.

The mechanisms involved in the alkaline activation of metakaolin and fly ash, while generally conforming to the stages described above, vary as discussed below.

Palomo *et al*. (2005) proposed a model to describe the alkaline activation of fly ash based on zeolite synthesis. Under this model, the process consists of two stages: (a) nucleation, with the dissolution of the aluminates present in the ash and the formation, via polymerisation, of complex ionic species (a stage highly dependent upon thermodynamic and kinetic parameters, which would cover the first two stages proposed by Glukhovsky); and (b) growth, when the nuclei reach a critical size and the crystal begins to grow. This stage is very slow due to experimental conditions. The final result of the alkaline activation of fly ash is an amorphous matrix with cementitious properties whose main component is an aluminosilicate gel known as N-A-S-H gel or 'zeolite precursor'. Hypothetically, this gel would eventually evolve into a zeolite.

This model was subsequently revised by various authors (Palomo *et al*., 2005; Fernández-Jiménez *et al*., 2005b; Duxson *et al*., 2007b; Shi *et al*., 2011). According to the new model (see Figure 2.4), N-A-S-H gel formation would include a series of stages that can be summarised as follows. When the source of aluminosilicate comes into contact with the alkaline solution, it dissolves into several species, primarily silica and alumina monomers. These monomers interact to form dimers, which in

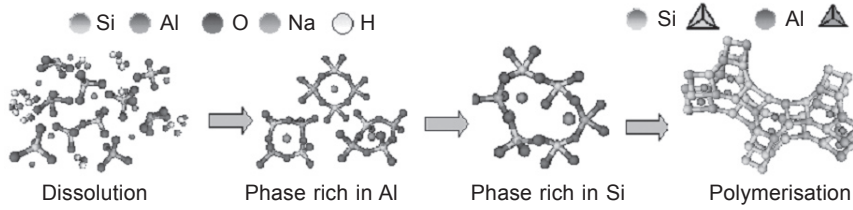

Figure 2.4 Model proposed for N-A-S-H gel formation (Fernández-Jiménez *et al*., 2005b; Shi *et al*., 2011).

turn react with other monomers to form trimers, tetramers and so on. When the solution reaches saturation an aluminosilicate gel, N-A-S-H gel, precipitates. This gel is initially Al-rich (called Gel 1, a metastable intermediate reaction product) (Fernández-Jimenez *et al*., 2006). Its formation can be explained by the high Al^{3+} ion content in the alkaline medium in the early stages of the reaction (from the first few minutes through the first few hours), for reactive aluminium dissolves more quickly than silicon because Al-O bonds are weaker than Si-O bonds. As the reaction progresses, more Si-O groups in the original source of aluminosilicate dissolve, raising the silicon concentration in the reaction medium and its proportion in the N-A-S-H gel in the medium (Gel 2).

This structural reorganisation determines the final composition of the polymer, as well as pore microstructure and distribution in the material, which are instrumental in the development of many physical properties of the resulting cement.

2.3.3 Reaction products

The main reaction product generated in the alkaline activation of silica- and alumina-rich materials such as fly ash and metakaolin is an amorphous alkaline aluminosilicate hydrate (M_n-(SiO_2)-$(AlO_2)_n$.wH_2O) known as N-A-S-H gel (Palomo *et al*., 2005) (see Figure 2.5). This product also goes by the name AIP, alkaline inorganic polymer. Its silicon and aluminium tetrahedra are distributed at random, forming a three-dimensional skeleton (Palomo *et al*., 2004; Fernández-Jiménez *et al*., 2003, 2006; Provis and van Deventer, 2009).

The secondary reaction products in this type of systems are zeolites such as hydroxysodalite, zeolite P, Na-chabazite, zeolite Y and faujasite (Palomo *et al*., 1999; Fernández-Jiménez *et al*., 2003, 2006; Duxson *et al*., 2007a).

Studies conducted by a number of authors (Palomo *et al*., 2005; Bakharev, 2005; Criado *et al*., 2005) showed that both the curing temperature and type of activator

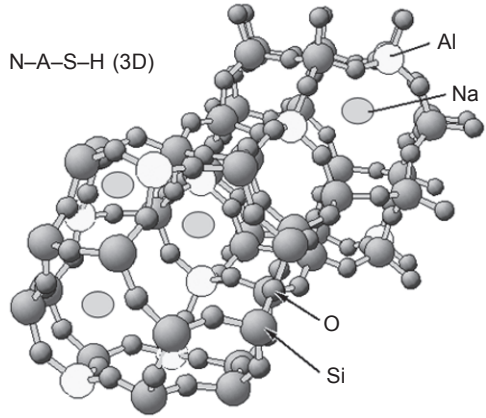

Figure 2.5 Plan view projection of the three-dimensional structure of a N-A-S-H gel.

impact reaction kinetics, with the degree of reaction rising with the former. The nature of the products generated (N-A-S-H gel-like and zeolite precipitates) in aluminosilicate activation also varies with curing time and temperature. Long curing times give rise to the formation of silica-rich products, favouring the development of mechanical strength in the material.

Moreover, the raw material is not the sole origin of the silicon forming part of the N-A-S-H gel generated as the main product; rather, part may also be present in the activator (waterglass) (Duxson *et al*., 2007a; Criado *et al*., 2007). In fact, the silica in the sodium silicate normally used as an alkaline activator is highly soluble and consequently readily taken up into the N-A-S-H gel. The degree of polymerisation in such sodium silicate, which depends directly on its SiO_2/Na_2O ratio, conditions the structure of the gels precipitating in the various stages involved in N-A-S-H gel formation.

Criado *et al*. (2007) studied the effect of different degrees of activator polymerisation (SiO_2/Na_2O ratios of 0.17, 0.60 and 1.90) on the intermediate reaction products generated in the alkaline activation of fly ash. They observed that this parameter played an instrumental role in the kinetics, structure and composition of the initial gel formed. The addition of soluble silica affected the intermediate but not the end reaction products. They noted that the Si/Al ratio does not rise indefinitely in N-A-S-H gel and found that the optimal value appears to be 2, toward which the system tends irrespective of the initial conditions, perhaps for reasons of thermodynamic stability. These authors further proposed that the effect of highly polymerised silica on N-A-S-H gel formation kinetics would involve retarding ash reaction and zeolite crystallisation.

2.3.4 Micro- and nanostructure of the gel formed: N-A-S-H-type gels

2.3.4.1 Microstructure of N-A-S-H gels generated in the alkaline activation of metakaolin and fly ash

The microstructure generated in the alkaline activation of metakaolin has been analysed in detail (Criado *et al*., 2007). Broadly speaking, the reaction products generated exhibit very uniform microstructures.

Fernández-Jiménez *et al*. (2005a) proposed a model to describe alkaline activation in fly ash based on scanning electron microscopic data (see Figure 2.6). The process would begin with a chemical attack on the ash surface (Figure 2.6(a)) whose outcome would be the formation of small cavities in the particle walls, exposing the smaller grains inside to the action of the alkalis. In this stage of the reaction the alkalis would attack from inside and outside the particles (Figure 2.6(b)). The ash would continue to dissolve and the reaction products generated inside and outside the ash crust would precipitate (Figure 2.6(c)), covering the smaller unreacted spheres and hindering their contact with the alkaline solution (Figure 2.6(d)). Thereafter, alkaline activation would continue slowly since the ash particles covered by the reaction products could only be attacked by alkalis through diffusion mechanisms. This would

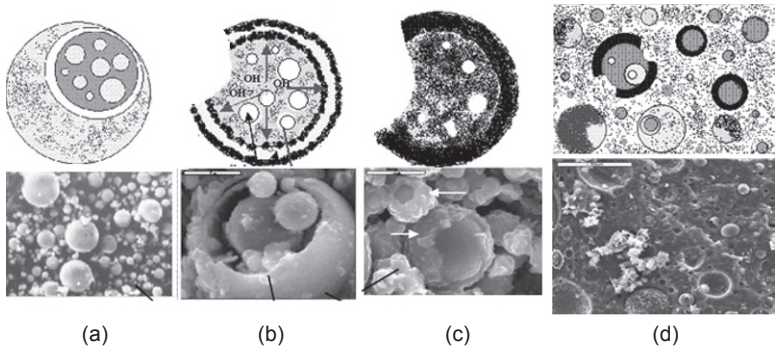

Figure 2.6 (a–d) Model for the alkaline activation of fly ash over time (Fernández-Jiménez *et al.*, 2005a).

lead to a final situation in which different morphologies may co-exist in the same paste (unreacted ash particles, particles under alkaline attack and reaction products (N-A-S-H gel, zeolites, etc.) (see Figure 2.6(d)).

2.3.4.2 N-A-S-H gel nanostructure

In 1988, Davidovits pioneered the use of NMR techniques to explore the nanostructure of the N-A-S-H and K-A-S-H gels generated in metakaolin alkaline activation. A full understanding of the structure of these gels was not possible until many years later, however, due to the low spectral resolution available at the time. Today's equipment is fortunately much more powerful and sophisticated, delivering much higher resolution spectra.

These N-A-S-H gels are characterised by a three-dimensional (3D) structure in which the Si is found in a variety of environments, with a predominance of $Q^4(n\text{Al})$ (n = 0, 1, 2, 3 or 4) units. The Si^{4+} and Al^{3+} cations are tetrahedrally coordinated and joined by oxygen bonds. The negative charge on the AlO^{4-} group is neutralised by the presence of alkaline cations (typically Na^+ or K^+). Nonetheless, significant variations may be detected in the gel structure depending on the degree of reaction, curing temperature and particularly the presence of soluble silica in the activator.

Provis and van Deventer (2009) described the nanostructural characteristics of the N-A-S-H gels generated during metakaolin alkaline activation as summarised below.

- The gel, with a charge-balanced aluminosilicate structure, is characterised by local order strongly resembling the order observed in zeolites and related aluminosilicate materials.
- The Si/Al ratio and nature of the alkaline cation present determine the details of the local structure.
- The negative charge generated by the substitution of aluminium for silicon tetrahedra is neutralised by alkaline metal cations. Each alkaline cation is directly associated not with an aluminium atom, but with one or more (depending on steric factors) of the negatively charged oxygen atoms that surround the aluminium.

- The gel forming in suitably cured stoichiometric metakaolins ($M^+/Al = 1$ where M is the alkaline metal) has a fully connected nanostructure, with few oxygen atoms outside bridging positions. In the presence of excess alkalis or in improperly cured gels, a certain number of non-bridging oxygen atoms appear in the network, bonded to silicon atoms. If these oxygen atoms are not protonated, the excess negative charge is neutralised by alkaline cations.
- The water present is normally found in the pore structure of the gel, which consists of a series of nano- and macro-pores whose respective proportions depend on the chemistry and thermal history of the sample. This is one of the major differences between the N-A-S-H gel generated during aluminosilicate alkaline activation and the C-S-H gel generated in normal Portland cement hydration: in the former the water is not chemically bonded to the structure of the matrix.
- Thermodynamic, steric and other factors hinder the formation of Al(IV)-O-Al(IV) bonds in the N-A-S-H gel nanostructure. Tetrahedral aluminium tends to be surrounded by four silicon tetrahedra, fully integrated in the network.

Fernandez Jimenez *et al*. (2006) studied the variations in gel nanostructure (^{29}Si MAS NMR) during the early stages of fly ash activation with 8-M NaOH at 85°C (see Figure 2.7). The ^{29}Si MAS NMR spectrum for the anhydrous ash (A) differed substantially from the post-activation spectra (B, C, D, E and F) for 2- to 20-hour through 7-day materials. The most prominent changes occurred during the early reaction stages (from 2 to 8 hours). The most intense signal, located at around –87 ppm, was associated with the formation of an aluminium-rich N-A-S-H gel with a predominance of Q^4(4Al) environments. The signals detected at higher shift values (around –80, –77 and –72 ppm), whose intensity declined as the reaction progressed, were attributed to the presence of less condensed units (monomers and dimers).

As the reaction progressed (24 h and 7 d) the spectra changed substantially. Five signals were clearly visible at around –110, –104, –98, –93 and –88 ppm, respectively attributed to the presence of silicon tetrahedra surround by zero Q^4(0Al), one Q^4(1Al), two Q^4(2Al) or four Q^4 (4Al) aluminium tetrahedra, indicative of a N-A-S-H gel with a higher silicon content (Gel 2).

Studies conducted by a number of authors (Krivenko, 1992; Palomo *et al*., 2004; Bakharev, 2005; Fernández-Jiménez and Palomo, 2005; Criado *et al*., 2005, 2007; Bernal *et al*., 2013) showed that both curing temperature and the nature of the activator play a significant role in reaction kinetics. Degree of reaction has been shown to rise with curing temperature. Different reaction products can be obtained by varying the reaction time and curing temperature: with time, N-A-S-H gel becomes silicon-richer, forming higher strength matrices.

Fernández-Jiménez *et al*. (2006) also studied the role of aluminium in the structure of the gels formed. When silica and alumina species come into contact, they interact to form a N-A-S-H-type gel, which precipitates (alkaline silicates, metastable at high and moderate pH values, are unable to alone form a chemically stable hardened material). In alkaline aluminosilicates, condensation reactions are induced by aluminium. Determining the amount of aluminium available in the reactive system is consequently crucial for the formulation of alkaline mineral polymers.

In anhydrous ash (see Figure 2.7(b)) two signals are found, at +53 and +2.5

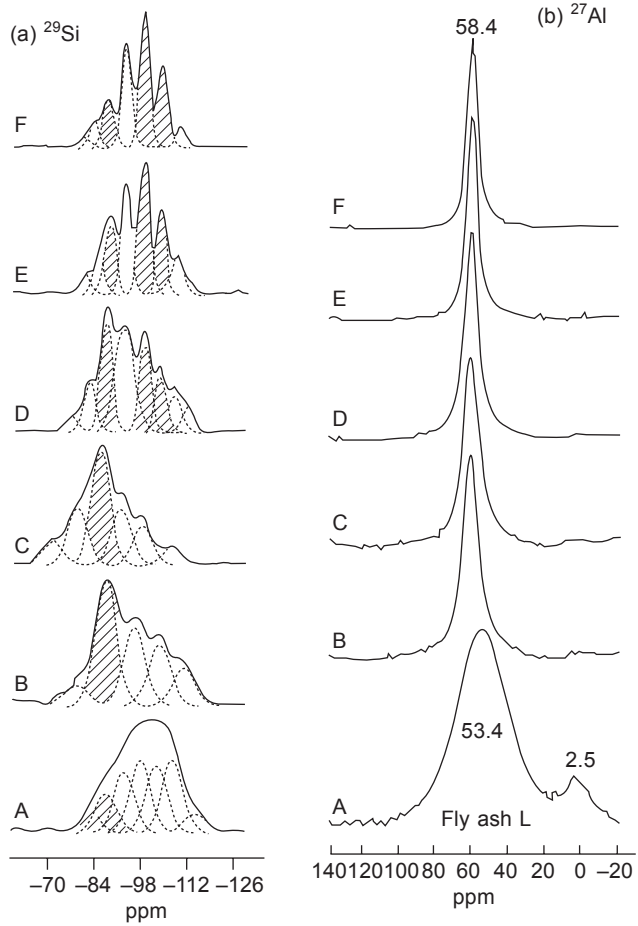

Figure 2.7 (a) 8-M ^{29}Si MAS NMR spectra and (b) ^{27}Al MAS NMR spectra for (A) anhydrous fly ash; and ash alkali-activated with 8-M NaOH at 85°C for (B) 2 hours; (C) 5 hours; (D) 8 hours; (E) 20 hours and (F) 7 days (Fernández -Jiménez *et al*., 2006).

ppm, respectively attributed to tetrahedral (Al_T: ash) and octahedral (Al_o: mullite) aluminium. The signal at 53 ppm is the more intense. When the ash is stirred into the alkaline solution, the signal associated with tetrahedral aluminium grows narrower (because the aluminium available is quickly taken up to form N-A-S-H gel) and less intense with time, while a new signal appearing at around +58/+59 ppm is attributed to Al_T integrated in the N-A-S-H gel.

While the role of the alkalis in the alkaline aluminosilicate hydrate structure is assumed to be to neutralise the excess negative charge generated by the replacement of silica tetrahedra with AlO_4 species during gel formation, scant information is available on this question.

Duxson *et al*. (2005), analysing the ^{23}Na spectra generated in gels formed in the alkaline activation of metakaolin, concluded from the two signals observed, at around

–4 and 0 ppm, that sodium can neutralise the excess negative charge in two ways. The –4 ppm signal was attributed to sodium associated with aluminium in the gel structure (offsetting the excess negative charge). The signal at 0 ppm, which only appeared in spectra for alkaline aluminosilicate gels with Si/Al ratios of under 1.4, was associated with the sodium present in the pore solution, which neutralises the negative charge in $Al(OH)_4^-$ groups.

Later, Criado *et al.* (2008), studied the position of sodium in the N-A-S-H gel structure, detecting a single signal between –6.6 and –10 ppm. This signal was associated with partially protonated sodium, which neutralised the loss of charge prompted by the replacement of silicon by aluminium. Rises in water content in the system shifted the signal to less negative values. Garcia-Lodeiro *et al.* (2010a,b) also studying the ^{23}Na MAS NMR spectra generated by synthetic N-A-S-H gels, confirmed the presence of a sole signal located at around –10 ppm, likewise attributed to partially hydrated sodium ($Na(H_2O)_x^+$).

2.4 Alkaline activation of hybrid cements

2.4.1 Introduction to hybrid cements

Various alternatives to traditional Portland cement have been explored throughout this chapter, including products generated by alkali-activating high-calcium (blast furnace slag) and low-calcium (metakaolin and particularly fly ash) materials. The growing interest in both the scientific community and the industry around a third type of cements, however, heralds their role as the binders of the future. These materials are known as hybrid or blended cements (Garcia-Lodeiro *et al.*, 2012, 2013c; Palomo *et al.*, 2013; Fernández-Jiménez *et al.*, 2013).

In these complex cementitious blends the type of product formed depends largely on the reaction conditions, including the chemical composition of the prime materials, alkaline activator type and concentration and curing temperature. Most of the wide spectrum of hybrid cements in place include small amounts of Portland cement or clinker. (While differences exist between using Portland clinker or cement, in these new cements such differences have a greater effect on workability than on the composition and structure of the gels generated: consequently the conclusions drawn in this section are valid for both.)

The hybrid cementitious systems most frequently studied include the following blends:

- Portland cement + blast furnace slag
- Portland cement + phosphorous slag
- Portland cement + fly ash
- Portland cement + steel mill and blast furnace slag
- Portland cement + fly ash + blast furnace slag
- Multi-constituents.

In the systems containing Portland clinker (clinker + blast furnace, phosphorous or steel mill slag, clinker + fly ash, clinker + slag + fly ash), C-S-H gel normally prevails as the main reaction product in slightly alkaline media (i.e., 2 M NaOH), whereas N-A-S-H gel prevails in highly basic environments (10 M NaOH) (Alonso and Palomo, 2001).

2.4.2 Co-precipitation of cementitious gels: C-A-S-H + N-A-S-H

Hybrid alkaline cements are complex cementitious blends with initial CaO, SiO_2 and Al_2O_3 contents of over 20% (Garcia-Lodeiro *et al*., 2012, 2013c; Palomo *et al*., 2013; Fernández-Jiménez *et al*., 2013); their reaction products are intricate mixes of different gels (the type of product formed depends largely on the reaction conditions).

The reaction products forming during the alkaline activation of cement and ash blends is an area of keen scientific and technological interest and the compatibility between the main cementitious gels, N-A-S-H and C-S-H, precipitating in the two systems is the object of considerable research today (Garcia-Lodeiro *et al*., 2009, 2010a, 2010b, 2011).

Prior studies have shown that the co-precipitation of these two gels in hybrid cements is possible (Alonso and Palomo, 2001; Yip *et al*., 2005; Palomo *et al*., 2007), although recent research has revealed that the two products do not develop singly as two separate gels, but that they interact, undergoing structural and compositional change in the process (García-Lodeiro *et al*., 2011).

Garcia-Lodeiro *et al*. (2009, 2010a, 2010b, 2011) conducted a number of studies on synthetic gels to explore the compatibility of the two gels at different pH values and the effect of adding Al and Na to C-S-H-type gels and Ca to N-A-S-H-type gels. Their studies showed that: (i) high pH values and the presence of aluminium species in the aqueous phase had a substantial effect on C-S-H gel structure and composition, for the aluminium was taken up into the gel structure; (ii) the presence of dissolved calcium modified N-A-S-H-type gels, with partial replacement of sodium by calcium and the formation of (N,C)-A-S-H-type gels; and (iii) these replacement processes depended heavily on the pH value (García-Lodeiro *et al*., 2011). In the presence of sufficient calcium and pH values of over 12, C-A-S-H gel is favoured over N-A-S-H gel formation (see Figure 2.8). Be it said, however, that the experiments yielding these findings were conducted in equilibrium conditions, which are not normally in place during binder hydration, particularly in the early stages of the reaction.

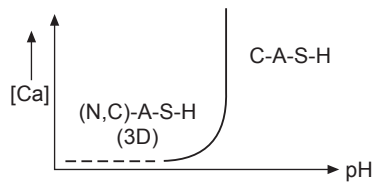

Figure 2.8 Model proposed to define N-A-S-H gel stability in terms of pH and calcium content.

In 2005, Yip *et al*. studied the co-existence of the two gels, C-S-H and the geopolymer, in the alkaline activation slag + metakaolin blends. Using scanning electron microscope (SEM) techniques, these authors proved that the co-precipitation of the two gels was possible, albeit highly conditioned by system alkalinity. The two gels only co-precipitated at low pH values. In the presence of high (7.5 M) NaOH concentrations, the geopolymer predominated and took up small amounts of calcium. Moreover, the two phases were only observed to co-exist where a sufficient source of reactive calcium was present.

Some years later, Palomo *et al*. (2007) studied both the mechanical behaviour of, and the reaction products generated in, hybrid systems containing minority (30%) proportions of Portland cement clinker and high (70%) fly ash contents. The cementitious material was mixed with deionised water (W) and two alkaline solutions (N8-NaOH and SS-waterglass) and cured at ambient temperature. The mechanical development attained by the cementitious systems varied greatly with the hydration liquids used. Pastes made with water and NaOH exhibited similar 28-day values of around 24–28 MPa, whereas the 28-day material activated with sodium silicate attained values of 37 MPa, i.e., higher than required by European standard EN 197-1:2000 for 32.5-type cement.

These results confirmed that Portland cement hydration is affected by the alkaline content (OH^- concentration) and the presence of soluble silica. In addition, fly ash activation at ambient temperature was accelerated by the presence of Portland cement clinker. This beneficial effect can be explained by the heat released during cement hydration, the energy from which would favour the chemical reactions that induce ash dissolution, setting and hardening.

The micro- and nanostructural characterisation of the pastes generated in the aforementioned systems showed that a complex mix of amorphous gels (C-A-S-H + (N,C)-A-S-H) precipitates in activated systems (see Figure 2.9). Co-precipitation of the two gels (C-S-H + N-A-S-H) was observed only at early ages (28 days at most) (Alonso and Palomo, 2001; Yip *et al*., 2005; Palomo *et al*., 2007). Recent research conducted by Garcia-Lodeiro *et al*. (2013) on these same systems (alkali-activated blends of 70% fly ash and 30% OPC) over long reaction times (1 year), revealed the presence of different, mostly C-A-S-H-type gels (see Figure 2.9(a)). These authors also observed that (N,C)-A-S-H gels evolved into compositions with a higher calcium and a lower aluminium content (see Figure 2.9(b)). These findings, which would appear to support the hypothesis that the formation of C-A-S-H-type gels is favoured over time, are consistent with reports in the literature on the compatibility of N-A-S-H and C-A-S-H gels in equilibrium conditions (García-Lodeiro *et al*., 2011).

2.4.3 Activation models

The research conducted on hybrid cements appears to clearly show that the type and characteristics of the gel/s formed are significantly impacted by the working pH and the calcium concentration in the system; a high calcium content and pH level favour C-A-S-H over N-A-S-H gel formation. Nonetheless, little is known about

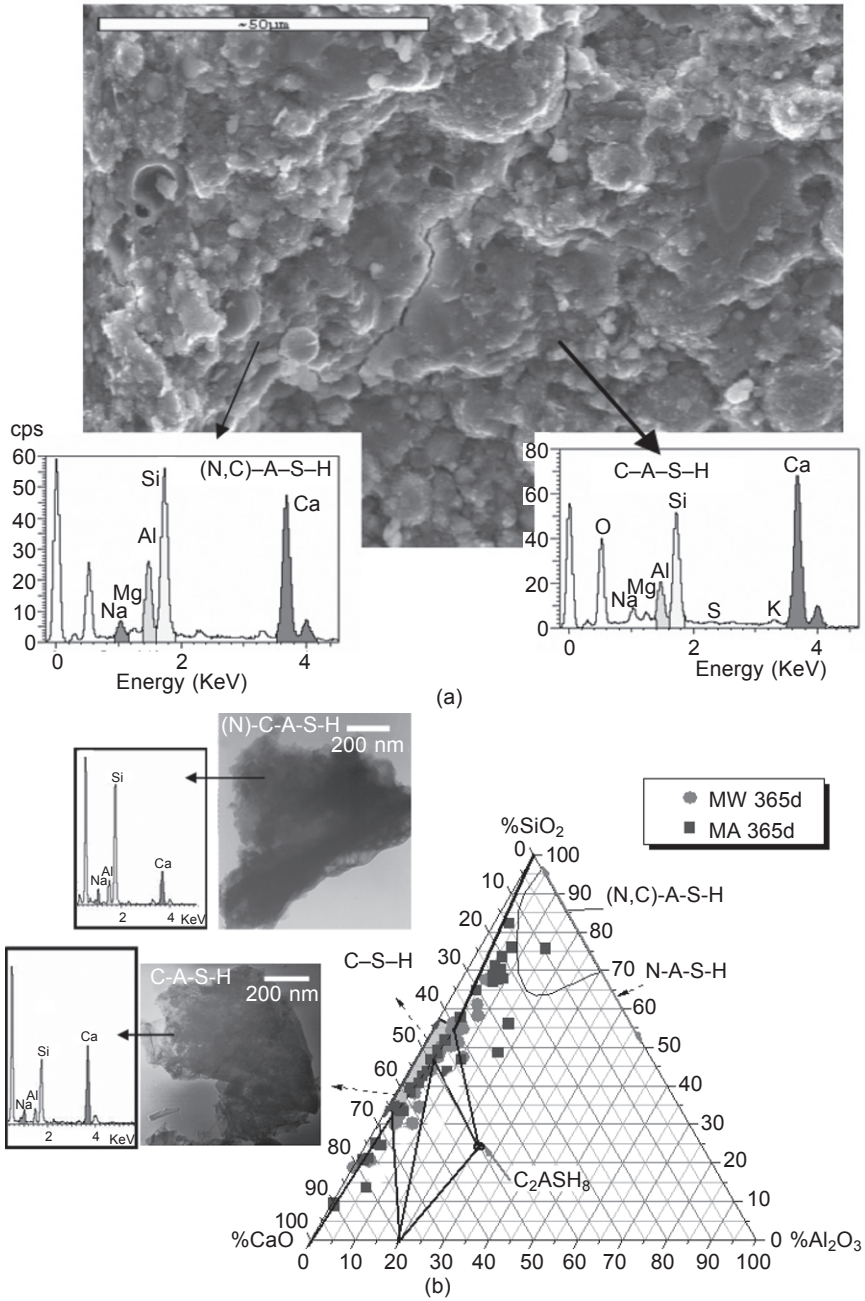

Figure 2.9 (a) SEM/EDX micrograph of a 1-year blend of 70% FA + 30% OPC activated with NaOH+ Wg at Tamb in a climatic chamber; (b) EDX analysis (with TEM micrographs) projected onto the SiO_2-Al_2O_3-CaO ternary diagram for the gels detected in 70% FA + 30% OPC systems activated with the alkaline solution (MA) and hydrated with water (MW); after 1 year most of the EDX analyses (squares) were located inside the C-A-S-H-type gel composition range (Garcia-Lodeiro *et al.*, 2013a).

the kinetics of the reactions taking place during the alkaline activation of this type of hybrid systems, particularly in the early stages.

Garcia-Lodeiro *et al*. (2013b) used isothermal conduction calorimetry in an initial study on early age (72-hour) reaction kinetics in a hybrid cement consisting of 30% OPC and 70% fly ash. To that end, they used two activating solutions: Na_2CO_3 and a mix of NaOH + Na_2SiO_3. Further to the data from several analytical techniques (BSEM, FTIR, DTA/TG, etc.), they concluded that hydration kinetics were substantially modified by the type of alkaline activator, particularly with respect to the secondary phases generated. The main reaction products, however, a mix of C-A-S-H and (N,C)-A-S-H gels, were unaffected by the activator. These findings were used to develop an activation kinetics model describing the possible product formation reactions taking place in the earliest activation stages (see Figure 2.10).

While the type of alkaline activator impacted reaction kinetics and the formation of secondary reaction products (carbonates, AF_m phases, etc.) significantly, it did not appear to have any material effect on the main cementitious gels formed ((N,C)-A-S-H /C-A-S-H). The thermodynamically stable majority product was a mix of cementitious gels that formed irrespective of the activator used. The use of Na_2CO_3 as an alkaline activator retarded gel precipitation, favouring the formation of secondary phases such as gaylussite and AF_m-type species. Nonetheless, a larger proportion of gel phase appeared to precipitate than in the system activated with the solution containing NaOH + Wg.

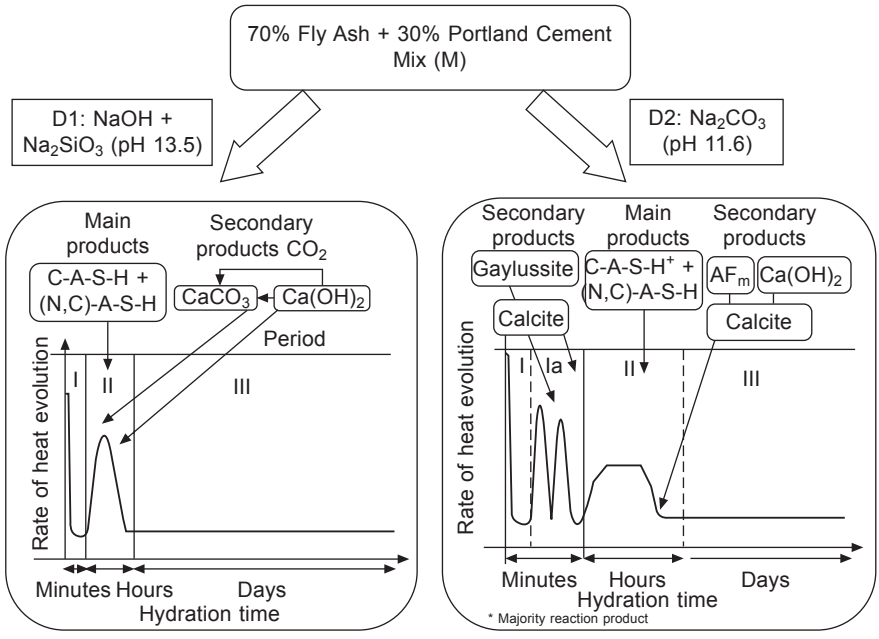

Figure 2.10 Activation kinetics models for hybrid cements (70% FA + 30% OPC) activated with NaOH + Wg (D1) and a Na_2CO_3 solution (D_2) (Garcia-Lodeiro *et al*., 2013b).

Based on their own experience in the analysis of the compatibility of the two synthetic gels (Garcia-Lodeiro *et al*., 2009, 2010a, 2010b, 2011) and real cementitious blends (70% FA + 30% OPC activated with NaOH + Wg) (Garcia-Lodeiro *et al*., 2013a) and on data drawn from the literature on hybrid systems (Alonso and Palomo, 2001; Yip *et al*., 2005; Palomo *et al*., 2007), García-Lodeiro *et al*. (2013a) also proposed a conceptual model describing the activation stages of high-silica and alumina and fairly low-calcium cementitious blends from the first few hours up to a full year (see Figure 2.11).

According to that model, the process begins with the dissolution of the sources of calcium and aluminosilicates in the alkaline solution via rupture of the T-O-T bonds (T: Si or Al) in the ash and the Ca-O and Si-O bonds in the cement, leading to a wide variety of dissolved species (Stage A). When the solution reaches saturation, N-A-S-H, an aluminosilicate gel, precipitates (Stage B). This gel initially adopts a compositionally metastable form with a high aluminium content (Fernández-Jiménez *et al*., 2006). Analogously, the Ca^{2+} and silicon species resulting from the dissolution of Portland cement react to form a C-S-H-type gel. As the reaction progresses, more Si-O groups dissolve from both the original aluminosilicate (fly ash) and from the calcium silicate in the cement, raising the silicon concentration in the reaction medium and with it the silicon uptake in both gels. Hence, the N-A-S-H gel would change from a type 1 gel (Gel 1, Si/Al ratio $\approx$ 1) to a type 2 gel (Gel 2, Si/Al ratio $\approx$ 2) (Fernández-Jiménez *et al*., 2006). In the C-S-H gel, in turn, Si uptake would enhance gel polymerisation (from chains comprising three silica tetrahedra to chains with five or more links, i.e., gels with a higher percentage of Q^2 than of Q^1 units) (Stage C). Stages B and C may take place at a fairly quick pace in these hybrid systems, and lead directly to the following stage, described below.

As the reactions progress, the Ca and Al ions present in the aqueous solution begin to diffuse across the cementitious matrix formed. A small number of Ca ions (not participating in the C-S-H gel) interact with the N-A-S-H gel to form a (N,C)-A-S-H gel. Given the similar ionic radius and electronegative potential in sodium and calcium ions, calcium replaces the sodium ions via ion exchange reminiscent of the mechanisms observed in clay and zeolites (Engelhardt and Michel, 1987), maintaining the three-dimensional structure of the (N,C)-A-S-H-type gel (García-Lodeiro *et al*., 2010b). Similarly, the C-S-H gel forming from the silicates in cement takes aluminium into its composition (preferably) in bridge positions (Sun *et al*., 2006), yielding C-(A)-S-H $\rightarrow$ C-A-S-H gels as the aluminium content rises. The presence of tetrahedral aluminium in the bridge position may favour chain cross-linking, generating two-dimensional structures. This is the situation prevailing in 28-day hybrid cements (Stage D).

Where a sufficient store of calcium is available, it continues to diffuse into the pores in the matrix and interact with the (N,C)-A-S-H gel. The polarising effect of the Ca^{2+} (to form Si-O-Ca bonds) distorts the Si-O-Al bonds, inducing stress and ultimately rupture. As the N-A-S-H gel releases aluminium, less polymerised structures such as C-A-S-H gels form. At the same time, the C-A-S-H gel that formed in preceding stages is able to take up more silicon and aluminium ions in bridge

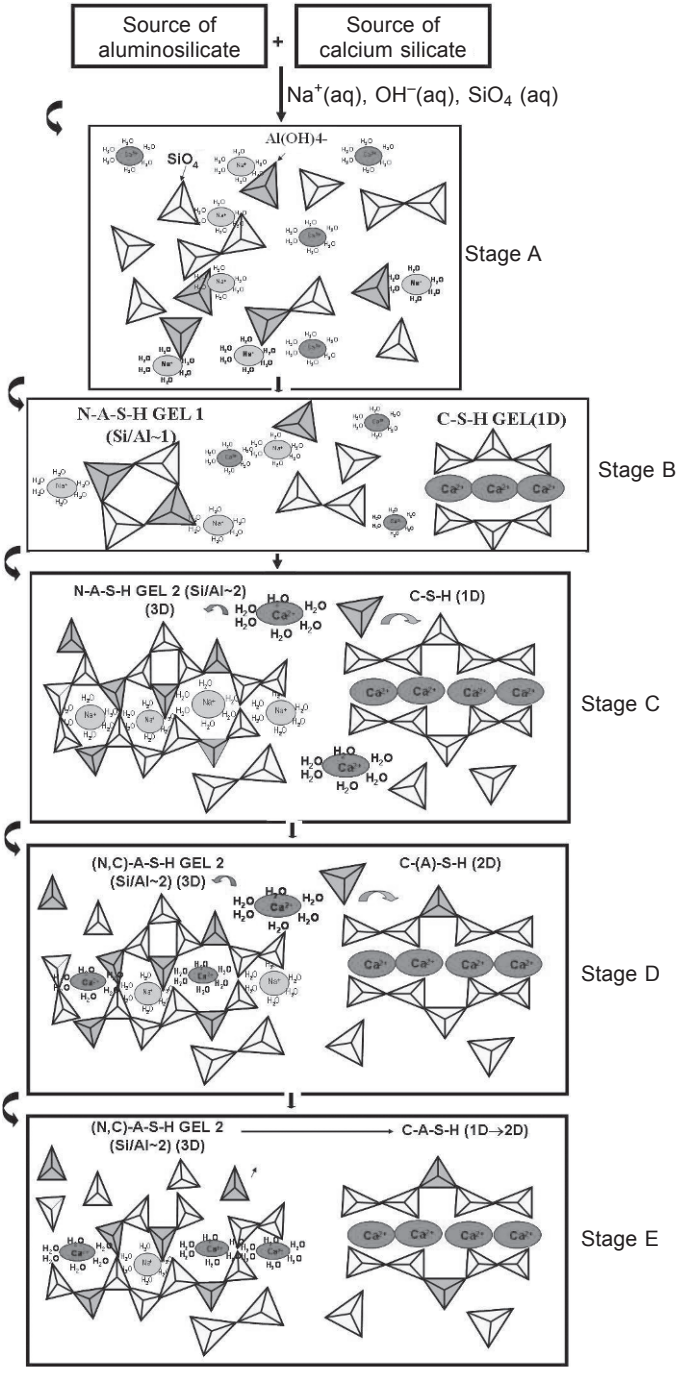

Figure 2.11 Alkaline activation model for cement blends with high silica and alumina and low calcium contents (70% FA + 30% OPC; activator: NaOH + Wg) (García-Lodeiro *et al*. 2013a).

positions (Richardson *et al.*, 1994). The 1-year hybrid cements studied here would be in this stage of the reaction (Stage E).

Lastly, in the hypothetical stage in which hydration finalises (which may take years), the system would evolve, given sufficient time and the necessary experimental conditions (suitable calcium concentration and pH (García-Lodeiro *et al.*, 2011)), toward the most thermodynamically stable gel, a C-A-S-H-type gel.

In any event, sight should not be lost of the fact that the system studied was nearly but not wholly in equilibrium. After one year of hydration, unreacted ash and cement particles co-existed in the cementitious matrix with secondary phases such as AF_m or alumina-type gels, along with a (N,C)-A-S-H and C-A-S-H gel mix which, over time, would evolve toward a single C-A-S-H gel.

By way of summary, the co-precipitation of C-S-H/N-A-S-H gels is visible in activated ash/cement blends, although these gels do not precipitate as pure products, but are affected by the presence of the species dissolved in the medium. In the presence of calcium and as the reaction progresses, N-A-S-H gel degenerates (losing aluminium) and tends toward more depolymerised structures. Nonetheless, the compositional and structural changes observed in N-A-S-H gels apparently have no impact on the strength of the material.

2.5 Future trends

Elementary information has been provided throughout this chapter on the chemistry surrounding the alkaline activation of aluminosilicates with varying calcium contents.

Extensive literature is in place on blast furnace slag-based alkaline cements, ranging from the alkaline activation fundamentals of these specific systems to the latest research on the nanostructural models that describe C-A-S-H gel formation.

One of the limitations that constrains or inhibits the worldwide introduction of alkaline cements is the local unavailability and non-uniformity of the raw materials required to manufacture these binders, in particular type F fly ash cements, i.e., silica- and alumina-based binders. This chapter has discussed the enormous dependence of the physical and chemical properties of alkaline cements on the nature of the raw materials used: hence the need to control the quality and origin of such materials. Future research should consequently focus on the pursuit of alternative materials with which to develop competitively priced binders with good cementitious properties, long durability and no irreversible environmental impact. Objectives along these lines are pursued by research on the alkaline activation of hybrid cements (Alonso and Palomo, 2001; Yip *et al.*, 2005; Palomo *et al.*, 2007), the activation of natural aluminosilicates such as common clay and feldspars (Buchwald *et al.*, 2009; Ruiz-Santaquiteria *et al.*, 2013) and the alkaline activation of glass or synthetic aluminosilicates (Buchwald *et al.*, 2009; Garcia-Lodeiro *et al.*, 2014).

References

Alonso S. and Palomo A. (2001), 'Alkaline activation of metakaolin-calcium hydroxide solid mixtures: influence of temperature, activator concentration and metakaolin/$Ca(OH)_2$ ratio', *Materials Letters* 47, 55–62.

Ambroise J., Murat M. and Pera J. (1985), 'Hydration reaction and hardening of calcined clays and related minerals: V. Extension of the research and general conclusions', *Cem. Concr. Res.* 15, 261–268.

Barbosa V.F.F., Mackenzie K.J.D. and Thaumaturgo C. (2000), 'Synthesis and characterization of materials based on inorganic polymers of alumina and silica: sodium polysialate polymers', *Int. J. Inorganic Mat.* 2, 209–317.

Bakharev T. (2005), 'Geopolymeric materials prepared using Class F fly ash and elevated temperature curing', *Cem. Concr. Res.* 35, 1224–1232.

Bakharev T., Sanjayan J.G. and Cheng Y.B. (2000), 'Effect of admixtures on properties of alkali-activated slag concrete', *Cem. Concr. Res.* 30, 1367–1374.

Ben Haha M., Lothenbach B., Le Saout G and Winnefeld F. (2011), 'Influence of slag chemistry on the hydration of alkali-activated blast-furnace slag – Part I. Effect of MgO', *Cem. Concr. Res.* 41, 955–963.

Ben Haha M., Lothenbach B., Le Saout G. and Winnefeld F. (2012), 'Influence of slag chemistry on the hydration of alkali-activated blast furnace slag – Part II. Effect of Al_2O_3', *Cem. Concr. Res.* 42, 74–83.

Bernal S.A., Provis J.L., Walkley B., San Nicolas R., Gehman J.D., Brice D.G., Kilcullen A.R., Duxson P. and van Deventer J.S.J. (2013), 'Gel nanostructure in alkali-activated binders based on slag and fly ash, and effects of accelerated carbonation', *Cem. Concr. Res.* 53, 127–144.

Buchwald A., Hohmann M., Posern K. and Brendler E. (2009), 'The suitability of thermally activated illite/smectite clay as raw material for geopolymer binders', *Applied Clay Science* 46, 300–304.

Calderon A.A. and Burg R.G. (1994), 'High-reactivity metakaolin: a new generation mineral', *Concr. Int.* 11, 37–40.

Cheng Q.H., Tagnit-Hamou A. and Sarkar S.L. (1992), 'Strength and microstructural properties of water glass activated slag'. *Mater. Res. Soc. Symp. Proc.* 245, 49–54.

Criado M., Palomo A. and Fernández-Jimenez A. (2005), 'Alkali activation of fly ashes. Part I. Effect of curing conditions on the carbonation of reaction products', *Fuel* 84, 2048–2054.

Criado M., Fernández-Jimenez A., de la Torre A.G., Aranda M.A.G. and Palomo A. (2007), 'An XRD study of the effect of SiO_2/Na_2O ratio on the alkali activation of fly ash', *Cem. Concr. Res.* 37, 671–679.

Criado M., Fernández-Jimenez A., Palomo A., Sobrados I. and Sanz J. (2008), 'Effect of the SiO_2/Na_2O ratio on the alkali activation of fly ash. Part II: ^{29}Si MAS NMR Survey', *Microporous and Mesop. Mat.* 109, 525–534.

Davidovits J. (1988), 'Geopolymer properties and chemistry', 1st European Conference on Soft Mineralurgy, Geopolymer 88, Compiegne, France, 25–48.

Duxson P. and Provis J.L. (2008), 'Designing precursors for geopolymer cements', *J. Am. Ceram. Soc.* 91, 3864–3869.

Duxson P., Lukey G.C., Separovic F. and van Deventer J.S.J. (2005), 'Effect of alkali cations on aluminium incorporation in geopolymeric gels', *Ind. Eng. Chem. Res.* 44, 832–839.

Duxson P., Fernández-Jiménez A., Provis J.L., Lukey G.C., Palomo A. and van Deventer J.S.J. (2007a), 'Geopolymer technology: the current state of the art', *J. Mater. Sci.* 42, 2917–2933.

Duxson P., Mallicoat S.W., Lukey G.C., Kriven W.M. and van Deventer J.S.J. (2007b), 'The effect of alkali and Si/Al ratio on the development of mechanical properties of metakaolin based geopolymers', *Colloids and Surfaces A: Physicochemical and Engineering Aspects* 292, 8–20.

Engelhardt G. and Michel D. (1987), *High Resolution Solid State RMN of Silicates and Zeolites*, John Wiley & Sons, New Delhi.

Fernández-Jiménez A. (2000), 'Cementos de escorias activadas alcalinamante: influencia de las variables y modelización del proceso', Ph.D. Thesis, Universidad Autónoma de Madrid.

Fernandez-Jiménez A. and Palomo A. (2003), 'Characterization of fly ashes: potential reactivity as alkaline cements', *Fuel,* 82, 2259–2265.

Fernández-Jiménez A., and Palomo A. (2005), 'Composition and microstructure of alkali activated fly ash binder: effect of activator', *Cem. Concr. Res.* 35, 1985–1992.

Fernández-Jiménez A., Puertas F. and Fernández-Carrasco L. (1996), 'Procesos de Activación Alcalino-Sulfaticos de una Escoria Española de Alto Horno'. *Materiales de Construcción* 46, 23–37.

Fernández-Jiménez A., Puertas F., Sobrados I. and Sanz, J. (2003), 'Structure of calcium silicate hydrate formed in alkaline activated slag: influence of the type of alkaline activator', *J. Am. Ceram. Soc.* 86, 1389–1394.

Fernandez-Jimenez A., Palomo A. and Criado M. (2005a), 'Microstructure development of alkali-activated fly ash cement: a descriptive model', *Cem. Concr. Res.* 35, 1204–1209.

Fernández-Jiménez, A. Palomo A. and Alonso M.M. (2005b), 'Alkali activation of fly ashes: mechanisms of reaction', in *Congress of Non-Traditional Cement and Concrete II*, Ed. V. Bilek and Z. Kersner, Brno University of Technology, 1–12.

Fernández-Jiménez A., Palomo A., Sobrados I. and Sanz J. (2006), 'The role played by the reactive alumina content in the alkaline activation of fly ashes', *Microporous and Mesoporous Materials* 91, 111–119.

Fernández-Jiménez A., Flores E., Maltseva O., Garcia Lodeiro I. and Palomo A. (2013), 'Hybrid alkaline cements: Part III. Durability and industrial applications', *Romanian Journal of Materials*, 43 68–73.

García-Lodeiro I., Macphee D.E., Palomo A. and Fernández-Jiménez A. (2009), 'Effect of alkalis on fresh C-S-H gels: FTIR analysis', *Cem. Concr. Res.* 39, 147–153.

García-Lodeiro I., Fernández-Jimenez A., Palomo A. and Macphee D.E. (2010a), 'Effect on fresh C-S-H gels of the simultaneous addition of alkali and aluminium', *Cem. Concr. Res.* 40, 27–32.

Garcia-Lodeiro I., Fernández-Jiménez A., Palomo A. and Macphee D.E. (2010b), 'Effect of calcium additions on N–A–S–H cementitious gels', *J. Am. Ceram. Soc.* 93, 1934–1940.

Garcia-Lodeiro I., Palomo A., Fernández-Jiménez A. and Macphee D.E (2011), 'Compatibility studies between N-A-S-H and C-A-S-H gels: study in the ternary diagram Na_2O-CaO-Al_2O_3-SiO_2-H_2O', *Cem. Concr. Res.* 41, 923–931.

Garcia-Lodeiro, I., Maltseva O., Palomo A. and Fernández-Jimenez A. (2012), 'Hybrid alkaline cements: Part I. Fundamentals', *Romanian Journal of Materials* 42, 330–335.

Garcia-Lodeiro I., Fernández-Jiménez A. and Palomo A. (2013a), 'Variation in hybrid cements

over time: alkaline activation of fly ash–Portland cement blends', *Cem. Concr. Res.* 52, 112–122.

Garcia-Lodeiro I., Fernández-Jiménez A. and Palomo A. (2013b), 'Hydration kinetics in hybrid binders: early reaction stages', *Cem. Concr. Compos.* 39, 82–92.

Garcia-Lodeiro I., Fernández-Jimenez A. and Palomo A. (2013c), 'Alkali-activated based concrete', in *Eco-efficient Concrete*, Ed. F. Pacheco-Torgal, S. Jalali, L. Labrincha and V.M. John, Woodhead Publishing Limited, Cambridge, pp. 439–487.

Garcia-Lodeiro I., Fernández-Jiménez A., Pena P. and Palomo A. (2014), 'Alkali activation of synthetic aluminosilicate glasses', *Ceramic International* 40, 5547–5558.

Glasser F.P. (1990), 'Cements from micro to macrostructure', *Br. Ceram. Trans. J.* 89, 192–202.

Glukhovsky V.D. (1967), *Soil Silicate Articles and Structure (Gruntosilikatnye vyroby I konstruktsii)*, Ed. Budivelnyk Publisher, Kiev.

Glukhovsky V. (1994), 'Ancient, modern and future concretes', First Inter. Conf. Alkaline Cements and Concretes, Kiev, Ukraine, 1, 1–8.

Granizo M.L. and Blanco M.T. (1998), 'Alkaline activation of metakaolin – an isothermal conduction calorimetry styudy', *J. Thermal Analysis* 52, 957–965.

Granizo M.L., Alonso S., Blanco-Varela M.T. and Palomo A. (2002), 'Alkaline activation of metakaolin: effect of calcium hydroxide in the products of reaction', *J. Am. Ceram. Soc.* 85, 225–231.

Granizo M.L., Blanco M.T. and Martinez Ramirez S. (2007), 'Alkaline activation of metakaolins: parameters affecting mechanical, structural and microstructural properties', *J. Mater. Sci.* 42, 2934–2943.

Habert G. (2013), 'Enviromental impact of Portland cement production', in *Eco-efficient Concrete*, Ed F. Pacheco-Torgal, S. Jalali, J. Labrincha and V.M. John, Woodhead Publishing, Cambridge, pp. 3–25.

Hannus I., Kiricsi I., Lentz P. and Nagy J.B. (1999), 'Characterization of alkali ions in the Y-type zeolites by multi MAS NMR studies', *Colloids and Surfaces A.* 158, 29–34.

Krivenko P.V. (1992), 'Fly-ash alkaline cements and concretes', Proceedings of the Fourth CANMET-ACI International Conference of Fly Ash, Silica Fume, Slag and Natural Pozzolans in Concrete (Supplementary Volume), Istanbul, Turkey, 721–734.

Krivenko P.V. (1994), 'Alkaline cements', First Int. Conf. Alkaline Cements and Concretes, Kiev, Ukraine, 1, 12–129.

LaRosa J.L., Kwan S. and Grutzeck M.W. (1992), 'Zeolite formation in Class F fly ash blended cement pastes', *J. Am. Ceram. Soc.* 75, 1574–1578.

Li C., Sun H. and Li L. (2010), 'A review: The comparison between alkali-activated slag (Si+Ca) and metakaolin (Si+Al) cements', *Cem. Concr. Res.* 40, 1341–1349.

Li D., Xu Z., Luo, Z., Pan Z. and Lin C. (2002), 'The activation and hydration of glassy cementitious materials', *Cem. Concr. Res.* 32, 1145–1152.

Mostafa N.Y., El-Hemaly S.A.S., Al-Wakeel E.I., El-Korashy S.A. and Brown P.W. (2001), 'Characterization and evaluation of the hydraulic activity of water-cooled slag and air-cooled slag', *Cem. Concr. Res.* 31, 899–904.

Myers R.J., Bernal S.A., San Nicolas R. and Provis J.L. (2013), 'Generalized structural description of calcium–sodium aluminosilicate hydrate gels: the cross-linked substituted tobermorite model', *Langmuir*, 29, 5294–5306.

Pal S.C., Mukherjee A. and Pathak S.R. (2003), 'Investigation of hydraulic activity of ground granulated blast furnace slag in concrete', *Cem. Concr. Res* 33, 1481–1486.

Palomo A., Grutzeck M.W. and Blanco M.T. (1999), 'Alkali-activated fly ashes – a cement for the future', *Cem. Concr. Res.* 29, 1323–1329.

Palomo A., Alonso S., Fernández-Jiménez A., Sobrados I. and Sanz J. (2004), 'Alkaline activation of fly ashes: a NMR study of the reaction products', *J. Am. Ceram. Soc.* 87, 1141–1145.

Palomo A., Fernández-Jimenez A. and Kovalchuck G. (2005), 'Some key factors affecting the alkali activation of fly ash', *2nd International Symposium of Non-Traditional Cement and Concrete*, Brno, Czech Republic.

Palomo A., Fernández-Jiménez A., Kovalchuk G., Ordoñez L.M. and Naranjo M.C. (2007), 'OPC-fly ash cementitious system: study of the gel binders produced during alkaline hydration', *J. Mater. Sci.* 42, 2958–2966.

Palomo A., Maltseva O., Garcia Lodeiro I. and Fernández-Jimenez A. (2013), 'Hybrid alkaline cements: Part II. Clinker factor', *Romanian Journal of Materials*, 43, 74–79.

Pera J. (2001), 'Metakaolin and calcined clays as pozzolnas for concrete: a review', *Cem. Concr. Compos.* 23, 441–454.

Provis J. and van Deventer J.S.J. (eds) (2009), *Geopolymers: Structure, Processing, Properties and Industrial Aplications*, Woodhead Publishing Limited, Cambridge.

Puertas F. (1995), 'Cementos de escorias activadas alcalinamente: situación actual y perspectivas de futuro', *Materiales de la Construcción* 45, 53–64.

Puertas F., Fernández-Jiménez A. and Blanco-Varela M.T. (2004), 'Pore solution in alkali activated slag cement pastes: relation to the composition and structure of calcium silicate hydrate', *Cem. Concr. Res.* 34, 195–206.

Puertas F., Palacios M., Manzano H., Dolado J.S., Rico A. and Rodríguez J. (2011), 'A model for the C-A-S-H gel formed in alkali-activated slag cements', *J. Eur. Ceram. Soc.* 31, 2043–2056.

Richardson I.G. and Cabrera, J.G. (2000), 'The nature of C-S-H in model slag cements', *Cem. Concr. Compos.* 22, 259–266.

Richardson I. and Groves G.W. (1997), 'The structure of the calcium silicate hydrate phases present in hardened pastes of white Portland cement/blast-furnace slag blends', *J. Mater. Sci.* 32, 4793–4802.

Richardson I.G., Brough A.R., Groves G.W. and Dobson C.M. (1994), 'The characterisation of hardened alkali-activated blast-furnace slag pastes and the nature of the calcium silicate hydrate (C-S-H)', *Cem. Concr. Res.* 5, 813–829.

Roy A., Schilling P.J. and Eaton H.C. (1994), 'Activation of ground blast-furnace slag by alkali-metal and alkaline-earth hydroxides', *J. Am. Ceram. Soc.* 75, 3233–3240.

Ruiz-Santaquiteria C., Fernádez-Jiménez A., Skibsted J. and Palomo A. (2013), 'Clay reactivity: production of alkali activated cements', *Applied Clay Science* 73, 11–16.

Schilling P.J., Butler L.G., Roy A. and Eaton H.C. (1994), '^{29}Si and ^{27}Al MAS-NMR of NaOH activated blast furnace slag', *J. Am. Ceram. Soc.* 77, 2363–2368.

Schneider, M., Cincotto A. and Panepucci H (2001), '^{29}Si and ^{27}Al high-resolution NMR characterization of calcium silicate hydrate phases in activated blast furnace slag pastes', *Cem. Concr. Res.* 31, 993–1001.

Shi C., Krivenko P.V. and Roy D. (2006), *Alkali-activated Cements and Concretes*, Taylor & Francis, London.

Shi C., Fernández-Jiménez A. and Palomo A. (2011), 'New cements for the 21st century: the pursuit of an alternative to Portland cement', *Cem. Concr. Res.* 41, 750–763.

Sun G.K., Young J.F. and Kirkpatrick, R.J. (2006), 'The role of Al in CñSñH: NMR, XRD, and compositional results for precipitated samples', *Cem. Con. Res.* 36, 18–29.

Swamy R.N. and Bouikni A. (1990), 'Some engineering properties of slag concrete as influenced by mix proportioning and curing', *ACI Mater. J.* 87, 210–220.

Taylor H.F.W. (1990), '*Cement Chemistry*', Academic Press, London.

Wang S.D. and Scrivener K.L. (1995), 'Hydration products of alkali activated slag cement', *Cem. Concr. Res.* 25, 561–571.

Wang S.D., Pu X.C., Scrivener K.L. and Pratt P.L. (1995), 'Alkali-activated slag: a review of properties and problems', *Cem. Concr. Res.* l7, 93–102.

Wu X., Roy D.M. and Langton C.A. (1983), 'Early stage hydration of slag-cement', *Cem. Concr. Res.* 13, 277–286.

Yip C.K., Lukey G.C. and Deventer J.S.J. (2005), 'The coexistence of geopolymeric and calcium silicate hydrate at the early stage of alkaline activation', *Cem. Concr. Res.* 35, 1688–1697.

This page intentionally left blank

Crucial insights on the mix design of alkali-activated cement-based binders

3

I. Garcia-Lodeiro, A. Palomo, A. Fernández-Jiménez
Instituto Eduardo Torroja (IETcc-CSIC), Madrid, Spain

3.1 Introduction

Alkaline cements are essentially the result of an alkaline attack on amorphous or vitreous natural materials or industrial by-products. When mixed with alkaline activators, these substances set and harden, yielding a good binder. Figure 3.1 highlights the two main components of these cementitious systems: a cementitious constituent and an alkaline activator.

The alkaline activators normally used are alkaline salts or caustic solutions. Glukhovsky classified activators by their chemical composition, identifying six groups (Glukhovsky, 1967, 1994):

1. caustic solutions: MOH
2. slightly acid, non-siliceous salts: M_2CO_3, M_2SO_3, M_3PO_4, MF;
3. silicates: $M_2O.nSiO_2$;

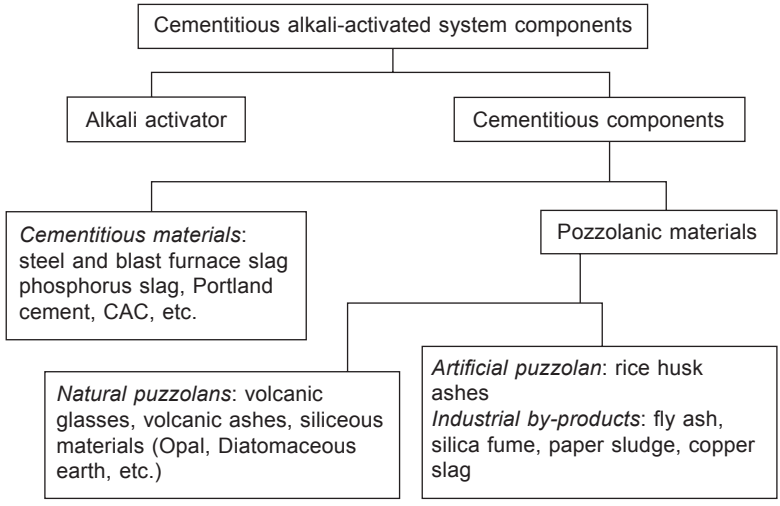

Figure 3.1 Alkali-activated system components.

Handbook of Alkali-activated Cements, Mortars and Concretes. http://dx.doi.org/10.1533/9781782422884.1.49

4. aluminates: $M_2O.nAl_2O_3$;
5. aluminosilicates: $M_2O.Al_2O_3.SiO_2$;
6. non-siliceous, highly acid salts: M_2SO_4.

The cementitious components used to manufacture alkali-activated cements may be cementitious materials with intrinsic hydraulicity (slag, OPC) or pozzolanic materials (see Figure 3.1). One of the most prominent features of alkaline activation technology is that both natural materials (such as clay or feldspars) and industrial by-products (such as slag, fly ash and paper sludge) can be used as prime materials. This chapter explores the role of the constituents of these cements in depth.

3.2 Cementitious materials

The raw materials most commonly used for alkaline cement-related research are slag (primarily blast furnace slag), fly ash from coal combustion and burnt clay (mostly metakaolin). The $CaO\text{-}SiO_2\text{-}Al_2O_3$ ternary diagrams in Figure 3.2 show the typical composition ranges for these materials.

Geopolymers have also been synthesised with other types of materials (Hos *et al.*, 2002; Gordon *et al.*, 2005; Garcia Lodeiro *et al.*, 2010), based essentially on synthetic precursors (laboratory reagents). Nonetheless, as they have been used less extensively than the aforementioned materials, they are limited to laboratory procedures and still a long way from being industrially applicable.

The main characteristics of these key materials are described below.

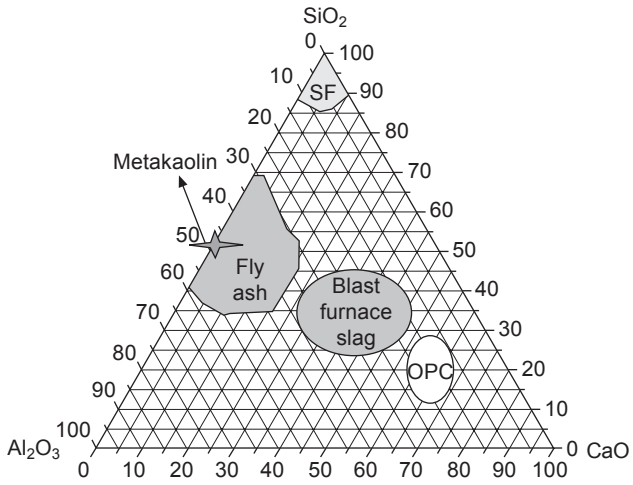

Figure 3.2 Usual range of compositions of the raw materials used to manufacture alkaline cements on a $CaO\text{-}SiO_2\text{-}Al_2O_3$ diagram.

3.2.1 Blast furnace slag and other slags

A number of studies (e.g., Fernández-Jiménez, 2000; Shi *et al.*, 2006; Bakharev *et al.*, 1999; Duran Atiş *et al.*, 2009) have shown that slag of different origins and nature can be alkali-activated to yield adhesive and cementitious hydration products. Slag comes in different varieties: phosphorous, steel and blast furnace slag, to name a few. Granulated blast furnace slag (known as BFS) is the type preferably used as a raw material in alkaline activation.

Blast furnace or steel slag forms when the 'clayey' acid gangue in iron ore and (likewise acid) coke sulfur ash combine with lime and magnesium, basic components of the more or less dolomitic limestone used as fluxes (Fernández-Jiménez, 2000; Shi *et al.*, 2006).

Acid (SiO_2 and Al_2O_3) and basic (CaO and MgO) oxides, as well as the slag constituents, form by high temperature (1600°C) fusion and subsequent cooling of the fluid magma from 1400°C to ambient temperature. When liquid slag cools abruptly to temperatures of under 800°C, crystals have no time to form and the solidified material acquires a vitreous structure. This is the slag normally used in alkaline activation (Fernández-Jiménez, 2000; Shi *et al.*, 2006; Provis and van Deventer, 2009).

The chemical composition of slag depends primarily on the steel-making process applied and type of steel manufactured. The most common composition ranges for the main constituent oxides are listed in Table 3.1.

Mineralogically speaking, BFS is normally described as a mix of scantly crystallised phases in the interval ranging from gehlenite ($2CaO.Al_2O_3.SiO_2$) to akermanite ($2CaO.MgO.2SiO_2$), plus a vitreous phase consisting of a network of depolymerised calcium silicates. The latter contains the hydraulically active component of slag, while the crystalline phase may be regarded as practically inert. Nonetheless, some authors (e.g., Smolcyk, 1980) contend that the presence of small amounts of crystals may raise slag reactivity, given the disorderly structure formed early in crystallisation.

BFS is characterised by latent or potential hydraulicity. In other words, when finely ground and mixed with water, it can set and harden, yielding hydration products similar to the products found in Portland cement pastes, albeit at fairly long reaction times. Slag hydraulicity develops slowly, with its cementitious products and consequently mechanical strength appearing much later than in Portland cement. When activated by any of several methods and activating agents, however, slag hydrates quickly and en masse, forming adherent and cementitious products. Research by Wang and

Table 3.1 Mean chemical composition of blast furnace slag

SiO_2	CaO	Al_2O_3	MgO	Fe_2O_3	S	Cr_2O_3	Na_2O+K_2O	MnO_2	P_2O_5	TiO_2
27–40%	30–50%	5–33%	1–2.1%	<1%	<3%	0.003–0.007%	1–3%	< 2%	0.02–0.09%	<3%

* Cl_2 (0.19–0.26%) and F_2 (0.09–0.23%) may also appear.

Scrivener (1995) and Wang *et al*. (1995) has shown that alkaline compounds are the activating agents that enhance slag hydraulicity most effectively.

Slag reactivity is also known to depend on its particle size. Slag with particle sizes of over 20 microns react very slowly, while those with sizes of under 2 microns react fully within 24 hours of mixing with alkaline activators (Wang *et al*., 2005).

The main requirements for slag to be usable as cement are listed below (Fernández-Jiménez, 2000; Shi *et al*., 2006; Provis and van Deventer, 2009).

- It must be granulated or pelletised and have a vitreous phase of 85–95%.
- It must have a highly disorganised structure, for the higher the degree of glass polymerisation, the lower is its hydraulicity.
- It must be basic, i.e., have a $CaO+MgO/SiO_2$ ratio of > 1. Basic slag has a higher hydraulic potential, for its lime content apparently controls its activation. That notwithstanding, acid slag may also be alkali-activated.
- It must be ground to a specific surface of 400–600 m^2/kg. As discussed later, specific surface plays an important role in the rate and intensity of the activation reaction.

As established in Chapter 2, the main product generated in blast furnace slag activation is a C-A-S-H gel, similar to the gel generated in normal Portland cement hydration (C-(A)-S-H gel), but with lower C/S ratios (normally ranging from 0.9 to 1.2) (Wang and Scrivener, 1995; Wang *et al*., 1995; Fernández-Jiménez *et al*., 2003, Puertas *et al*., 2011; Myers *et al*., 2013). The secondary reaction product usually generated is hydrotalcite ($Mg_6Al_2CO_3(OH)_{16}{\cdot}4HO$), which may precipitate with C_4AH_{13}, C_4AcH_{11}– and $C_8A_2cH_{24}$-type phases.

Other types of slag besides BFS can be used to prepare alkaline cements (Shi *et al*., 2006; Provis and van Deventer, 2014), including various types of steel mill slag: electric arc furnace (EAF), basic oxygen furnace (BOF), ladle and converter slag.

The main mineral phases detected in steel slag generally include olivine, merwinite, and C_3S-, β-C_2S-, and γ-C_2S-type calcium silicates, as well as C_4AF and a phase known as 'RO' (a CaO-FeO-MnO-MgO solid solution) (Shi, 2004). This type of slag, duly mixed with the proper activators, may exhibit good cementitious properties (Li and Wu, 1992; Shi *et al*., 1993).

Another type of slag potentially usable to prepare alkaline cements is phosphorous slag, composed mainly of SiO_2 and CaO. The minor components in phosphorus slag, which depend on the nature of the phosphate ores used, are Al_2O_3 (0.2–2.5%), Fe_2O_3 (0.2–2.5%), MgO (0.5–3*f*%), P_2O_5 (1–5%) and F (0–2.5%) (Shi *et al*., 2006).

The earliest studies on the alkaline activation of phosphorus slag date from the 1980s (Shi, 1988, 1989). The use of suitable activators, primarily sodium silicate, yields cementitious materials with good workability and acceptable mechanical strength. The use of other activators such as NaOH furthers the development of mechanical strength, especially in the early stages of the reaction, while the use of silicate-type activators favours the development of mechanical strength at older ages (Shi and Qian, 2000).

3.2.2 Fly ash (types F and C)

Fly ash is an industrial by-product deriving from coal combustion. It is the solid waste collected by electrostatic precipitation or mechanical capture of the particles present in the combustion gas emitted by furnaces in pulverised coal-fired steam power plants. Prior to combustion, the coal is milled to a powder. It is subsequently blown into a furnace in a current of hot air flowing at high speed, with or without secondary fuels. This suspension is then heated to a temperature of 1500 ± 200°C, which is above the melting point of most of the minerals present. As the inorganic particles are not fully combusted in this process, however, ash is released.

Power generation in coal-fired steam power plants (normally using pulverised anthracite or other bituminous coal) produces essentially two types of waste: fly ash, the main subject of this section, and bottom ash or slag. The difference between the two lies mainly in their particle size. The finer particles (fly ash) are collected by mechanical or electrostatic precipitation out of the combustion gas, while the coarser bottom ash or slag falls to the bottom of the furnace and is removed to provisional storage silos, usually with a wet discharge. The percentages of these two types of waste depend on steam plant configuration, boiler type and combustion conditions, although fly ash accounts on average for 80% of the total and bottom ash for the remaining 20%.

The chemical composition of fly ash varies widely, depending on coal composition. The percentages of ash components vary from ash to ash, although in most the main constituents are silica (SiO_2), alumina (Al_2O_3), iron oxides (Fe_2O_3), lime (CaO) and unburnt coal, while smaller amounts (generally under 5 wt.%) of magnesia (MgO), sulfur oxide (SO_3), alkalis (Na_2O and K_2O) as well as traces of titanium, vanadium, manganese, phosphorus, germanium and gallium are also present.

Fly ash is classified into two types depending on its lime content (ASTM C618-08a):

- Type F fly ash: with a CaO content of under 10%. The result of anthracite or bituminous coal calcination, it is the most abundant ash and the type most frequently re-used. The majority oxides in this type of ash are SiO_2, Al_2O_3 and iron oxides. Its pH is normally basic and may be over 10. This is the type generally used as a raw material in silica- and alumina-based alkaline cements (see Chapter 2).
- Type C fly ash: with a high CaO content (higher than 10%, usually from 15 to 30%). Produced during the calcination of sub-bituminous coal or lignite, this ash exhibits pozzolanic and cementitious properties.

Table 3.2 lists the average percentages of the compounds contained in high- and low-calcium fly ash. The chemical composition of bottom ash resembles the composition of fly ash and depends essentially on the type of coal used. It is classified as siliceous if its majority compound is SiO_2 or calcareous if the main component is CaO.

Fly ash particles, which are normally spherical, may be hollow or house smaller spheres. They are not uniform, however, but include both vitreous and crystalline phases (normally mullite and quartz and iron oxides) (see Figure 3.3(a)). Its particle size distribution covers a broad spectrum. As a rule, 50% of the particles have an

Table 3.2 Average percentage (wt.%) of the compounds in high- and low-calcium ash

Component	Type C fly ash: with a high CaO content	Type F fly ash: with a low CaO content
SiO_2	34.1	42.6–59.8
Al_2O_3	14.2	21.8–34.5
Fe_2O_3	7.2	6.3–18.1
CaO	38.0	2.8–7.0
SO_3	4.2	0.19–1.9
MgO	1.5	1.2–2.6
K_2O	1.4	0.38–6.0
Na_2O	0.44	0.15–0.94
Reactive silica	30.9	0.94
Free lime	17.1	Very low 0.74

equivalent diameter of under 30–40 μm. Ash specific surface ranges from 2500 to 5000 cm^2/g and its density from 2.2 to 2.8 g/cm^3. Such a lack of uniformity means that particular care must be taken when working with this ash to ensure that the product obtained is of constant quality (Fernández-Jiménez *et al.*, 2003). Bottom ash or slag, on the contrary, consists of angular particles with a very porous and rough surface texture (see Figure 3.3(b)). The particle size of bottom ash ranges from fine gravel to fine sand, with a low percentage of fines. Its density depends on its chemical composition: it declines with rising coal content, with typical values ranging from 2.1 to 2.7 g/cm^3.

Fly ash quality varies with coal type and combustion furnace. Its composition may also vary very significantly depending on the origin. These changes in composition may affect both the nature and the properties of the alkaline cements obtained. In this regard, Fernández-Jiménez and Palomo (2003) defined the requirements to be met by fly ash to produce good binders, namely:

- less than 5% unburnt material
- Fe_2O_3 content under 10%
- low CaO content
- 40–50% reactive silica content
- 80–90% particles with a size of under 45 μm
- high vitreous content.

As noted, (primarily type F) fly ash is the raw material most commonly used to prepare alkaline cements. The alkaline activation of this type of high-silica, high-alumina and low-calcium materials induces the precipitation of an amorphous alkaline aluminosilicate hydrate (M_n-$(SiO_2)_z$-$(AlO_2)_n$.wH_2O) known as N-A-S-H gel (Fernandez-Jiménez and Palomo, 2005; Duxson *et al.*, 2005a; Criado *et al.*, 2007, Duxson *et al.*, 2007a), which differs widely from the gel generated in slag alkaline activation (see Chapter 2). Here the secondary reaction products are zeolites such as hydroxysodalite, zeolite P, Na-chabazite, zeolite Y and faujasite.

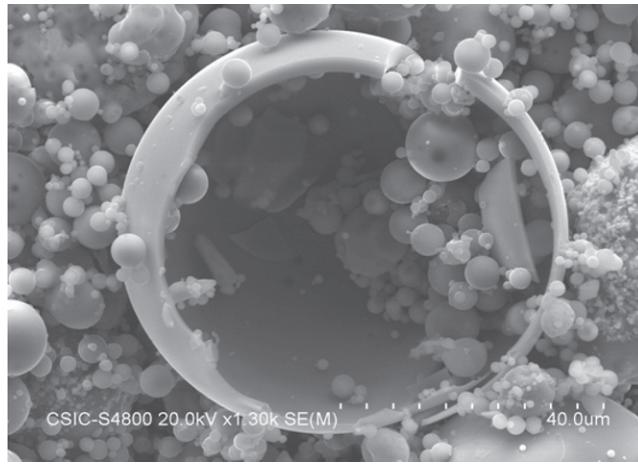

(a)

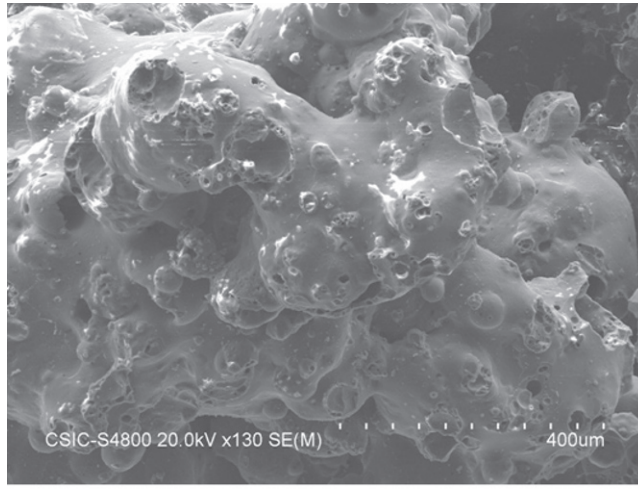

(b)

Figure 3.3 SEM images of (a) fly ash and (b) bottom ash.

3.2.3 Metakaolin and other kaolinite clays

Kaolin is a white or light coloured rock with normally over 15 wt.% of (essentially kaolinitic) clay material. Kaolin is the product of water and atmospheric CO_2-induced feldspar decomposition. Kaolinite is obtained by processing kaolin. Kaolinite is a clay mineral family phyllosilicate whose composition is $Al_2Si_2O_5(OH_4)$. Its structure consists of alternating sheets of SiO_4 tetrahedra (layer T) and alumina octahedra (layer O) joined by apical oxygen atoms (atoms not shared by SiO_4 tetrahedra) in the T layer (see Figure 3.4(a)).

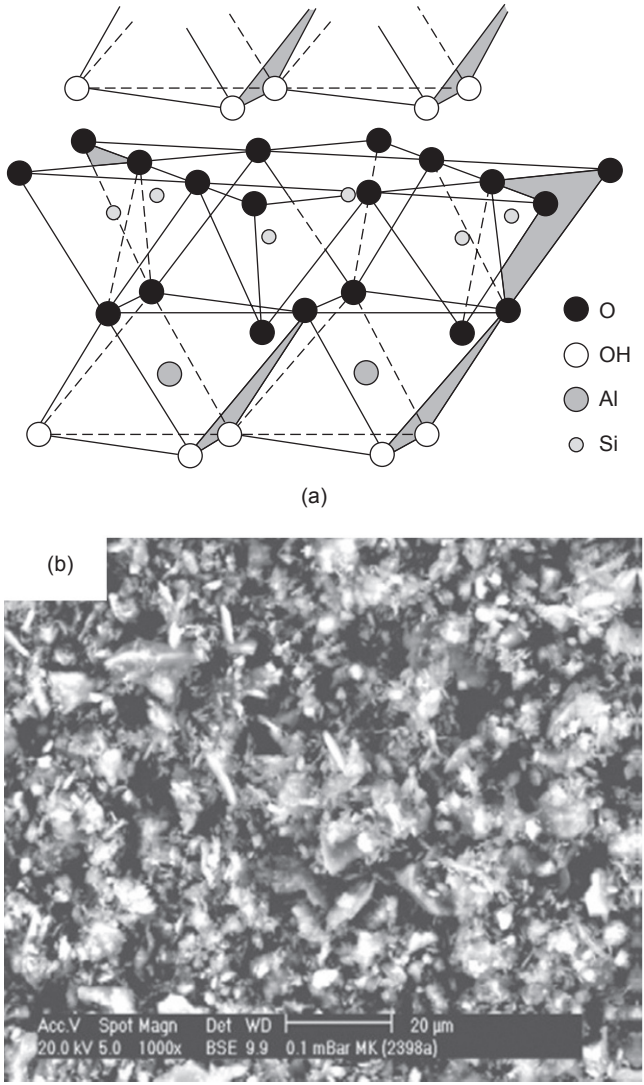

Figure 3.4 (a) Structure of one sheet of kaolinite (Ruiz Santaquiteria, 2013); (b) SEM micrograph of metakaolin (Criado *et al.*, 2007).

Clay minerals may be heated to enhance their reactivity. The concomitant loss of water (hydroxyl groups in the O layer) causes the structure to collapse and a new amorphous phase to form. The post-heating amorphous phase deriving from kaolinite is known as metakaolinite (see Figure 3.4(b)). Equation 3.1 describes a model for the conversion of kaolinite to metakaolinite when the temperature is raised.

$$\Delta \sim 550°C$$

$$Al_2Si_2O_5(OH)_4 \rightarrow Al_2Si_2O_7 + 2H_2O \quad (3.1)$$

When a kaolinitic clay is fired, its physical and chemical properties change. From 100 to 250°C, inter-layer water or moisture is lost; dehydration begins at 300–400°C and is accelerated at 500–600°C, temperatures at which the clay becomes fully dehydrated and its atomic structure is destroyed. The resulting metakaolin is pozzolanic, although both the temperature and the time required to complete the process depend on the type of clay mineral. Alumina (Al_2O_3), a scantly grindable, low activity product, forms at 950°C. Temperature control, then, plays a key role in artificial pozzolan manufacture (Acuña, 2006).

Metakaolin is an amorphous, highly reactive aluminosilicate whose chemical composition is heavily impacted by the chemical and mineralogical composition of the starting kaolinite. Generally speaking, its majority oxides include SiO_2 (40–70%) and Al_2O_3 (20–35%), with lower proportions of Fe_2O_3 and TiO_2 (<1%) and other alkaline oxides (Na_2O, K_2O). Heating kaolinite may yield crystalline compounds such as quartz or illite, in addition to metakaolin.

The use of metakaolin in alkaline cement production has been essentially limited to ceramic-type applications and small-scale laboratory tests, in light of the high temperatures needed and associated costs, as well as the high hydration liquid demand involved in producing a workable paste (Provis *et al*., 2010). Nonetheless, concrete based on alkali-activated metakaolin has been successfully produced with fairly low liquid/solid ratios (Marín-López *et al*., 2009).

As in the alkaline activation of fly ash, in the alkaline activation of metakaolin the main reaction product is a N-A-S-H gel, an amorphous alkaline aluminosilicate hydrate, from which the system derives its mechanical strength. Here also, the secondary reaction products are zeolites, whose precipitation depends heavily on the curing conditions (temperature and humidity) and activator type (see Chapter 2) (Shi, 1989; Kovalchuk *et al*., 2007; Criado *et al*., 2010; Najafi Kani and Allahverdi, 2009).

The possibility of alkali-activating common clays or natural aluminosilicates has also been addressed in the literature (Xu and van Deventer, 2000, 2002, 2003; Buchwald *et al*., 2007, 2009; Fernández-Jiménez *et al*., 2007, Ruiz-Santaquiteria *et al*., 2013), although these materials have been studied much less thoroughly than metakaolin, fly ash or blast furnace slag.

Buchwald *et al*. (2007, 2009) conducted several studies on the susceptibility of smectite- and smectite/illite-type clays to alkaline activation. They concluded that these materials, after proper thermal activation, dissolve partially in a basic medium (6 M NaOH), yielding a material able to harden after moderate heating (60°C). The reactivity (amount of silica and alumina dissolved) of these clays in a basic medium and the final properties of the cement obtained appear to be affected by the prior thermal treatment applied.

Xu and van Deventer (2000), in turn, examined the possible use of 16 natural aluminosilicate minerals with different structures and compositions (illite, sillimanite, andalusite and others) as potential sources of silicon and aluminium in alkaline activation. They concluded that all dissolved to a greater or lesser degree in a basic medium (more effectively in NaOH than KOH as a rule). After curing at 35°C for 72 hours, they developed mechanical strength ranging from approximately 2.5 to

19 MPa, depending on factors such as the composition and structure of the mineral, its solubility in a basic medium and the alkaline cation in the activator.

More recently, alkaline thermal pre-treatment of minerals has been put forward as a means of valorising high-volume mineral wastes. Pacheco-Torgal and Jalali (2010) attempted to burn clay-rich tungsten mining waste with Na_2CO_3, the product obtained exhibited severe efflorescence due to its high alkali content. In 2013 Ruiz Santaquiteria *et al.* assessed the reactivity of a number of dehydroxylated clays for use as raw materials in alkaline cements. Their results showed that activated dehydroxylated clays or activated blends of dehydroxylated clays and fly ash reached compressive strengths of up to 15 MPa (25 MPa in the blends with ash).

The mechanical performance of alkaline cements obtained with common clay and feldspar is lower as a rule than found in alkaline cements made with fly ash or metakaolin.

3.2.4 Other aluminosilicate materials

Volcanic ash and certain natural pozzolans are other aluminosilicate materials susceptible to alkaline activation.

Volcanic ash, the origin of natural pozzolans, was initially used by the Romans to make concrete. This ash consists of small particles of pulverised volcanic rock and glass. As a result of rapid post-eruption cooling, volcanic ash exhibits high chemical reactivity. That, together with its large proportion of vitreous phase and high silica and alumina content make it a promising raw material for alkaline activation (Provis and van Devanter, 2014; Leonelli *et al.*, 2007; Kamseu *et al.*, 2009).

Volcanic ash is normally characterised by high SiO_2, Al_2O_3, Fe_2O_3 and CaO contents, along with smaller proportions of other oxides including MgO, Na_2O, K_2O and TiO_2, as well as traces of many other elements. In addition to a high vitreous phase content, it contains mineral phases such as plagioclases, olivines and pyroxenes (Provis and van Deventer, 2014).

Natural pozzolans have proven to date to be another raw material with high alkaline activation potential (Allahverdi *et al.*, 2008; Najafi Kani and Allahverdi, 2009; Bondar *et al.*, 2011a). In natural pozzolans with a low lime content and pozzolans with sodium-rich zeolites and a high soluble silica content, the optimal SiO_2/Al_2O_3 molar ratio is low but higher than in CaO-rich or pre-calcined pozzolans (Bondar *et al.*, 2011a). High temperature curing has also been shown to improve the mechanical strength of these materials considerably (Najafi Kani and Allahverdi, 2009; Bondar *et al.*, 2011b; Najafi Kani *et al.*, 2012) and lower the risk of efflorescence (Najafi Kani and Allahverdi, 2009).

3.2.5 Effect of the $([CaO]/[SiO_2])_{reactive}$ ratio

The chemical composition of the original raw material and its mineralogical characteristics (primarily its amorphous or vitreous phase content and the presence of minority crystalline phases) are determinants in the formation of the main reaction

products comprising alkaline cements: C-A-S-H gels (alkaline activation of high-silica, high-calcium materials such as slag) and N-A-S-H gels (alkaline activation of high-silica, high-alumina materials such as fly ash and metakaolin). Gel composition largely conditions system mechanical strength and durability.

The characteristics of the gel formed can be evaluated and system performance predicted *a priori* by measuring two parameters: in BFS, the $[CaO]/[SiO_2]_{reactive}$ ratio, and in aluminosilicate materials, especially fly ash, the $[SiO_2]/[Al_2O_3]_{reactive}$ ratio. These parameters are discussed below.

Blast furnace slag is characterised by a very high vitreous phase content (from 90 to 95%) and a chemical composition based essentially on CaO, SiO_2 and Al_2O_3 (Puertas, 1993). Slag dissolution after addition of the activator generates a series of dissolved Si^{4+}, Al^{3+} and Ca^{2+} species that are immediately available to form C-A-S-H gel. Consequently, nearly all the CaO and SiO_2 present in the original slag ($([CaO]/[SiO_2])_{reactive}$) participate in gel formation.

The main reaction product forming in slag-based alkaline cements, to which such systems owe their strength and durability, is an aluminium-containing calcium silicate hydrate (C-A-S-H gel). This gel is similar to the product generated in normal Portland cement hydration, although its C/S ratio is lower than in the latter. C-A-S-H gel ratios usually range from 0.9 to 1.2. It has a dreierkette structure (see Chapter 2) in which the parallel chains of silicates are arranged around a central sheet of CaO and the aluminium atoms usually replace bridge position silicon atoms, favouring inter-chain cross-linking.

The silica content of gels conditions their polymerisation: the higher the silica content (lowering the C/S ratio) the longer the silicate chains (Taylor, 1990). The standard method of modifying the CaO/SiO_2 ratio in these systems is by adding soluble silica to the system along with the alkaline activator (sodium silicate), as discussed more fully in a later section of this chapter. Many papers have been published on the effect of the presence of soluble silica in the activator on C-A-S-H gel composition and structure. A rise in the silica content leads to more densely packed, more polymerised gels (presence of Q^3(nAl) units) with excellent mechanical properties (> 80 MPa at 28 days, Fernández-Jiménez *et al.*, 2003; Puertas *et al.*, 2011).

3.2.6 Effect of the $([SiO_2]/[Al_2O_3])_{reactive}$ ratio

In aluminosilicate (fly ash and metakaolin) alkaline activation, the silica and alumina content of the raw material unquestionably plays an essential role in the degree of reaction as well as in the composition and structure of the products. In these materials, however, particularly fly ash, not all the silica and alumina comprising the raw material take part in the formation of cementitious gel. Their vitreous component co-exists with a series of minority crystals (such as quartz and mullite) which, while containing SiO_2 and Al_2O_3, are practically unaltered by the activator.

Hence the importance of defining their $([SiO_2]/[Al_2O_3])_{reactive}$ ratio, for this value is closely related to their degree of reaction, to the composition and structure of the

N-A-S-H gel formed and consequently to the mechanical strength and durability of the end product, the alkaline cement. This ratio can be reliably calculated for fly ash, metakaolin and even some kaolinitic clays by means of a selective attack with 1% HF (Arjuman *et al.*; 1997; Ruiz-Santaquiteria *et al.*, 2011). The percentages of insoluble waste (undissolved after the attack) are associated with non-reactive phases, i.e., phases unaffected by activation. The post-attack SiO_2 and Al_2O_3 contents are determined very simply with ICP analysis of the liquid phase or leachate and in turn used to find the $(SiO_2/Al_2O_3)_{reactive}$ ratio.

According to the literature, the best binders, the ones exhibiting the highest mechanical strength, are obtained with materials whose starting $([SiO_2]/[Al_2O_3])_{reactive}$ ratios range from 2 to 4 (Duxson *et al.*, 2005a; Fletcher *et al.*, 2005; Kovalchuk *et al.*, 2008; Criado *et al.*, 2010; Pimraksa *et al.*, 2011; Chindaprasirt *et al.*, 2012; Garcia-Lodeiro *et al.*, 2014).

Another critical parameter in inorganic polymer (geopolymer) formation is the amount of silicon and aluminium present. Fernández-Jiménez *et al.* (2006b) reported that a minimum content of around 20% of reactive aluminium is needed in fly ash to ensure good mechanical development. The aluminium present in the solution initially favours the early formation of Al-O-Si bonds and hence of a metastable, high-aluminium gel. Denominated Gel 1, over time this product evolves into a high-silicon gel (Gel 2, see Figure 3.5), which is what drives system mechanical development (Fernández-Jiménez *et al.*, 2006b). The absence of a sufficient amount of reactive aluminium retards the conversion of Gel 1 into Gel 2, affecting the mechanical strength of the material.

Nonetheless, an excess of reactive aluminium may also be detrimental, as reported by Silva *et al.* (2007). An overly high aluminium concentration accelerates the aluminate and silicate condensation rate considerably, shortening setting time and raising the crystallinity of the reaction products (more zeolites and less gel). The result is lower mechanical strength. The N-A-S-H gel structures generated under these circumstances tend to be granular (more crystalline and with more aluminium and sodium).

The degree of aluminium dissolution (out of the precursor material) during geopolymer formation was analysed by Hajimohammadi *et al.* (2010). A high rate

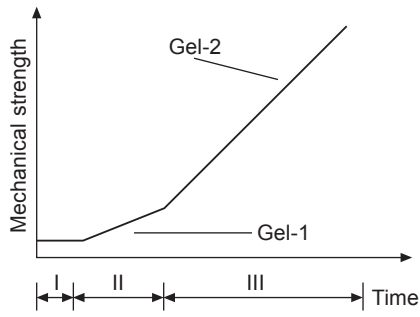

Figure 3.5 Variation in Gel 1 and Gel 2 mechanical strength over time (Fernández-Jiménez *et al.*, 2006b).

of aluminium release from the precursor raises the number of available aluminate species in the solution, favouring speedy formation of high-alumina N-A-S-H gel. That in turn enhances the intermixture of the gels generated and hence more uniform compositions. Nonetheless, the ready availability of aluminium species in the early stages of the reaction may also hinder silica dissolution due to the partial adsorption of the dissolved alumina onto the silica particles; a paucity of silica species available in the solution hampers silicon enrichment of the gel and consequently future mechanical development in the system.

3.3 Alkaline activators: choosing the best activator for each solid precursor

Alkaline activators are the second essential component in alkaline cement design and development. Broadly speaking, the activators used in aluminosilicate (such as fly ash or metakaolin) based alkaline cements (M_2O-SiO_2-Al_2O_3-H_2O system) are alkaline hydroxides, alkaline silicates or blends of the two, to generate high alkalinity. In contrast, as more moderate alkalinity is needed in the high-CaO alkaline cements (M_2O-CaO-SiO_2-Al_2O_3-H_2O) made from slag, weak acid salts such as R_2CO_3, R_2S or RF (where R = alkaline or alkaline-earth ion such as Na, K, Li or Ca) or strong acid salts such as Na_2SO_4 or $CaSO_4.2H_2O$ may be used in addition to the aforementioned products.

Cations and anions play distinctly different roles in alkaline activation. The most commonly researched activators are described briefly below. For a full review of the general chemistry governing each activator, see Shi *et al*. (2006) and Provis and van Deventer (2009).

The anion in the activating solution plays an important role in the reactions taking place in the systems and consequently in the mineralogical and microstructural characteristics of the materials synthesised. The anions that are normally mixed with the raw materials used to prepare alkaline cements are hydroxides, silicates, carbonates and, to a lesser extent, sulfates. The effect of the each type of anion is analysed below.

3.3.1 Effect of OH^- (pH)

OH^- ions catalyse the dissolution of Si^{4+} and Al^{3+}cations (Glukhovsky, 1967) by inducing the hydrolysis of Si-O-Si and Si-O-Al bonds, among others, after which the various species are released into the dissolution (see activation mechanisms in Chapter 2).

The presence of OH^- ions not only catalyses the hydrolytic reactions involved in the various stages of alkaline activation, but also raises the pH to the values required for initial precursor dissolution and the subsequent condensation reactions.

Figure 3.6 plots the percentage of soluble silica in slag versus pH; for pH values

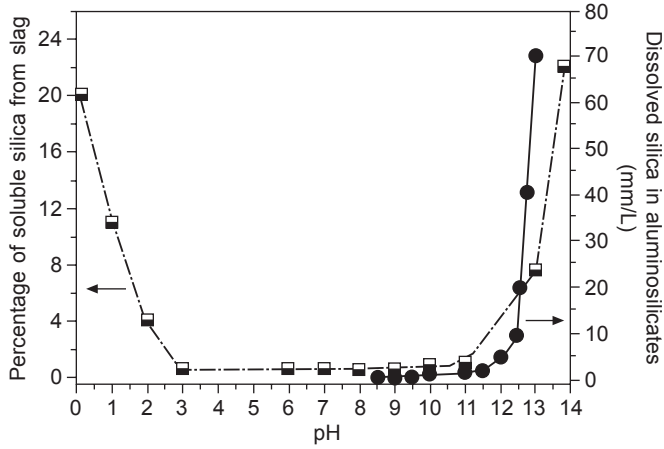

Figure 3.6 Solubility of soluble silica in slag versus pH and amount of dissolved silica in aluminosilicates versus pH (Fernandez Jimenez, 2000; Tang and Su-Fen, 1980).

of 3 to 11 silica solubility is low, but rises steeply at values of under 3 and over 11 (Puertas, 1993; Fernández-Jiménez, 2000). While slag solubility rises in acid media, the hydrates formed are unstable and form no consistent structures. Basic pH on the contrary not only favours slag dissolution but also the formation of stable hydrates, gradually raising the cementitious properties of the material. Similar findings are observed in connection with silica dissolution in aluminosilicates such as fly ash or metakaolin. Hydrolysis in these aluminosilicates rises with the pH of the solution used (see Figure 3.6), although only up to a 'point of diminishing returns' after which raising the OH^- ion concentration does not materially increase the amount of material dissolved (Alonso and Palomo, 2001; Granizo *et al.*, 2002).

Aluminium follows a similar pattern. As shown by the plot in Figure 3.7 of aluminium hydroxide solubility versus pH, solubility increases at both acid and basic pH values, with a trough at a pH of around 6.3. The cation Al^{3+} prevails in acid media, although it co-exists with others, such as $Al(OH)^{2+}$ and $Al(OH)_2^+$ (see Figure 3.7), while at basic pH $Al(OH)_4^-$-type species may form. These are the species that react with the silica likewise dissolved in the medium, favouring polymerisation and the formation of N-A-S-H- or C-A-S-H-type gels, further to the mechanisms described in detail in Chapter 2.

Very high OH^- concentrations are not favourable when slag is the raw material, however, for unlike silica and alumina, calcium becomes less soluble with rising pH. Consequently, the concentration of the alkaline solutions used to activate high-calcium blast furnace slag is much lower than required to activate low-calcium aluminosilicates (fly ash and metakaolin).

Alkaline hydroxides (primarily NaOH) are effective granulated blast furnace slag activators, as are soluble alkaline salts whose anion or anion group (such as silicates, carbonates or sulfates) can react with the Ca^{2+} ions in the slag to form

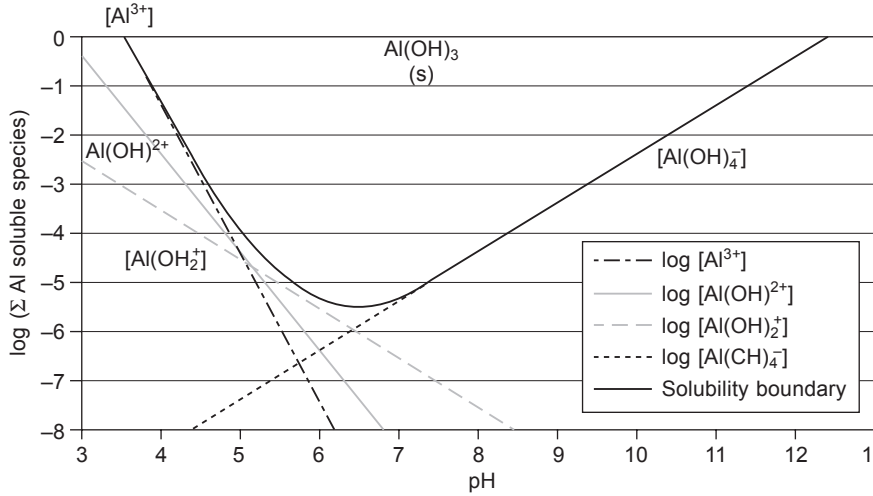

Figure 3.7 Solubility diagram for aluminium hydroxide ($Al(OH)_3$) (mononuclear species of Al only) (source: Holt *et al*., 2002).

calcium compounds that are less soluble than $Ca(OH)_2$ (Fernández-Jiménez, 2000). Concentrations on the order of 2–4 M are needed to prepare slag-based cements. Despite the extensive literature on the subject, no consensus has been reached on the optimal concentration, which depends heavily on activator type (Fernández-Jiménez, 2000). In slag alkaline activation, activators with high Na_2O concentrations (higher than 5% slag weight) fail to raise strength significantly. Moreover, such high doses of alkalis may be detrimental, increasing efflorescence and rendering the material more brittle. Economic factors should also be borne in mind, for the higher the dosage, the higher the cost.

The activators traditionally used to prepare metakaolin- or fly ash-based alkaline cements include concentrated alkaline hydroxides, primarily NaOH, for reasons of price, availability and low viscosity. System performance in aluminosilicate alkaline activation is optimal when its pH is similar to the value generated by an 8 M solution of sodium hydroxide (Duxson *et al*., 2005b, 2007a; Fernández-Jiménez and Palomo, 2005). Lower alkalinity than generated by that solution adversely affects the mechanical properties of the cements obtained because the ionic strength generated in the binder-activating solution system is not high enough to satisfactorily hydrolyse the silicon and aluminium present in the starting materials.

Palomo *et al*. (2004) analysed the matrices generated when type F fly ash was activated with different concentrations (from 8 to 18 M) of hydroxyl solutions. Their findings revealed the intense effect of concentration on microstructure: at a higher activator concentration, the matrix becomes denser, favouring the formation of a quasi-vitreous material. They also reported a rise in the alkali content fixed by the geopolymer at higher activator alkaline concentrations.

3.3.2 Effect of silicates: degree of soluble silicate polymerisation

Silicate solutions, especially sodium silicate, are the second most commonly used agents in the alkaline activation of slag and aluminosilicates (fly ash and metakaolin). The availability of soluble silica is of cardinal importance in these systems, for it affects workability, setting, and mechanical strength development and modifies both gel composition and the microstructure of the material formed.

The general formula for these soluble silicates is: $xSiO_2/R_2O$, where R = Na, K or Li and x = molar ratio. Of the three possibilities, the one most frequently used in alkaline activation is sodium silicate. Silicate solutions can be modified by dilution in deionised water or by adding extra alkalis to change the molar ratio. Two very important factors must be borne in mind when soluble silica is added: (i) the silica concentration and (ii) the SiO_2/Me_2O molar ratio. A solution with a low molar ratio (1/1) consists primarily of monomers (SiO_4^{4-}) and dimers ($Si_2O_5^{2-}$), while a solution with a high molar ratio (3.3/1) has a higher proportion of polymeric species. Solution pH depends on its SiO_2/R_2O molar ratio. At values of pH lower than 10, the solution begins to gel. The method most commonly deployed to control the SiO_2/Na_2O ratio and raise the solution pH is to add alkalis, normally in the form of an NaOH solution. The result is known as waterglass ($xSiO_3$. $yNa_2O.nH_2O$).

In slag activation, waterglass is believed to make a dual contribution to strength development: as an alkaline activator and an inducer of the formation of a high-silica primary gel. This gel forms when soluble silicates react with the Ca^{2+} ions in the slag to form a C-S-H/C-A-S-H-type, silica-rich, calcium silicate hydrate. The reaction products formed often exhibit high strength, significant drying shrinkage (Wang *et al.*, 1995; Fernández-Jiménez *et al.*, 1999; Palacios and Puertas, 2004), and short setting times, while the formation of Q^3(nAl) units in their structure is also favoured (Fernández-Jiménez, 2000; Fernández-Jiménez *et al.*, 2003; Puertas *et al.*, 2011; Myers *et al.*, 2013). Depending on slag nature and fineness and curing conditions, the optimal Na_2O content is regarded to be around 4% of slag weight and the optimal SiO_2/Na_2O molar ratio on the order of 0.75–1.25 for acid slag, 0.9–1.3 for neutral slag and 1.0–1.5 for basic slag (Smolcyk, 1980; Wang and Scrivener, 1995, Wang *et al.*, 1995).

In the waterglass activation of aluminosilicates, the soluble silica induces the development of a microstructure that resembles many types of glass (absence of pores and a uniform and compact microstructure). Furthermore, higher soluble silica content in the starting system induces a rise in the silicon content in the structure of these cements (Palomo *et al.*, 2004). Likewise in systems with a higher silica content, the formation of zeolite-like species (minority products) appears to be slower (Fernández-Jiménez and Palomo, 2005; Criado *et al.*, 2007, 2008). Nonetheless, a very high concentration of silica in the activating solution lowers pH and raises solution viscosity, inducing a decline in the degree of reaction in the raw material (Duxson *et al.*, 2005b).

The ^{29}Si MAS-NMR spectra for waterglass solutions reproduced in Figure 3.8 reflect the effect of the SiO_2/Na_2O ratio on the amount of sodium silicate taken

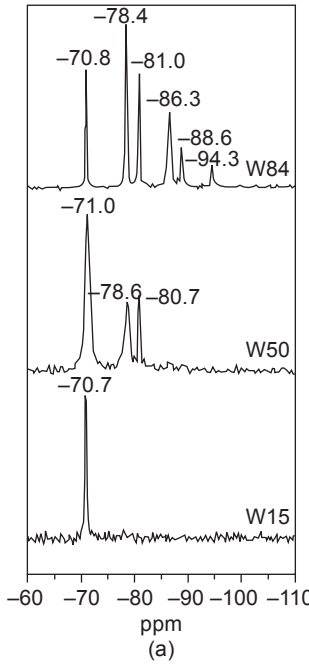

Solution	–δ ppm	Area (%)	Q^n site	Structure	Silicate species
W84	–70.8	14.5	Q^0	●	Monomer
	–78.4	(23.7)*	Q^1	●—●	Dimer
	–78.4	(23.7)*	Q^1	●—●—●	Linear trimer
	–88.6	8.5	Q^2		
	–81.0	24.6	C^2_{cyc}	△	Cyclic trimer
	–86.3	24.3	Q^2_{cyc}	□	Bridged cyclic tetramer
	–94.3	4.4	Q^3_{cyc}		
W50	–71.0	59.2	Q^0	●	Monomer
	–78.6	25.3	Q^1	●—●	Dimer
	–81.43	15.5	C^2_{cyc}	△	Cyclic trimer
W15	–70.7	100	Q^0	●	Monomer

* Overlapping signal

(b)

Figure 3.8 (a) ^{29}Si MAS-NMR spectra of alkaline solutions; (b) ^{29}Si chemical shift, δ, of the silicate anion in silicate solutions, identified in accordance with the literature (Criado *et al.*, 2008).

up and its degree of polymerisation. The Na_2O concentration was ≈8% in all the solutions, although SiO_2/Na_2O ratios differed (0.19, 0.69 and 1.17 for W15, W50 and W84, respectively). The solution W15 spectrum has a single peak at –70.7 ppm, associated with the presence of Q^0 units (monomers). The solution W50 spectrum has three, one more intense at –71 ppm and the other two at –78.6 and –80.7 ppm; these signals may be respectively assigned to Q^0, Q^1 (dimer) and $Q_{cy}{}^2$ (cyclic trimer) units. The six peaks observed on the solution W84 spectrum, at positions –70.8, –78.4, –81.0, –86.3, –88.6 and –94.3 ppm, are indicative of more intense polymerisation of the Si tetrahedra (Criado *et al.*, 2008). In the literature on sodium silicates, these signals are attributed to the presence of monomers, dimers, linear trimers and bridged cyclic tetramers (see Figure 3.8(b)). These data show that increasing the silicate ion concentration in solutions with similar concentrations of Na_2O (≈8%) induces greater silicate unit polymerisation.

The greater or lesser degree of polymerisation has a triple effect on reaction kinetics and the nature of the N-A-S-H gel initially formed. The presence of monomeric and, to a lesser extent, dimeric (i.e., scantly polymerised) silica shortens the time needed for the gel to start to precipitate. A rise in the amount of dimeric silica accelerates gel precipitation even more, but the gel formed under these conditions is less stable. Lastly, the presence of cyclical trimers induces the formation of initially more

stable gels but which retard reaction progress. Consequently, the optimal value for aluminosilicate alkaline activation is around 1–1.5 (Duxson *et al*., 2005b; Criado *et al*., 2008; van Deventer *et al*., 2007).

3.3.3 Effect of carbonates

The use of carbonates in the alkali activation of both slag and aluminosilicates has also been researched (Fernández-Jiménez and Palomo, 2005; Criado *et al*., 2005, Shi *et al*., 2006; Provis and van deventer, 2014). The reason for the interest in these compounds is that their production has a lower environmental impact than hydroxide or silicate solution production. This activator induces a lower pH than found in many alkali-activated binder systems, a potentially beneficial effect in terms of occupational health and safety. Carbonate-activated binders have attracted less attention from academia and the industry than other systems, however, because they generally harden and develop strength much more slowly than NaOH- or sodium silicate-activated cements. Nonetheless, sodium carbonate-activated BFS has been used in demonstration projects as well as in buildings and civil infrastructure for over 50 years in eastern and central Europe (Krivenko, 1994; Shi *et al*., 2006).

In the early stages of BFS activation with Na_2CO_3, calcium carbonates and sodium/calcium carbonate blends form double salts as a result of the interaction between the CO_3^{2-} present in the activator and the Ca^{2+} released from the BFS. The formation of these carbonates, together with the lower solution pH, lengthen the induction period and intensify plasticity loss in the paste, which nonetheless fails to set and harden. In extreme cases, setting times extend to over 3 days (Fernández-Jiménez and Puertas, 2001). The result is lower initial strength than when NaOH or waterglass is the activator, although at later ages strength may be higher than in NaOH-activated materials.

At later curing times, an Al-containing C-S-H-type gel forms, favouring paste hardening (Fernández-Jiménez and Puertas, 2001). The C-A-S-H gel formed in Na_2CO_3-activated BFS has a highly cross-linked structure with Q^3 sites, and forms precipitates along with carbonate salts such as gaylussite ($Na_2Ca(CO_3)_2{\cdot}5H_2O$) (Fernández-Jiménez *et al*., 2003). Xu *et al*. (2008) assessed older BFS concretes activated with Na_2CO_3 and Na_2CO_3/NaOH blends that had been gaining strength for years or decades. They identified the main reaction product in these materials as a highly cross-linked C-S-H-type phase with a relatively low Ca/Si ratio as the outer gel, and a carbonate anion-bearing inner gel. Xu *et al*. (2008) submitted that in Na_2CO_3-activated BFS binders, the long-term activation reaction is a cyclic hydration process in which the Na_2CO_3 would create a buffered alkaline environment. The level of CO_3^{2-} available in the system would be maintained by the gradual dissolution of $CaCO_3$, in which the Ca released would react with the dissolved silicate from the BFS. No detailed evidence has yet been forthcoming, however, on what this mechanism might entail in the first few months of reaction in Na_2CO_3-activated binders.

The use of carbonates has also been studied in low-calcium aluminosilicates. The

presence of carbonate ions leads to the formation of alkaline (trona- and nahcolite-type) carbonates/bicarbonates that acidify the medium, lowering the degree of reaction. The greater porosity and less compact structure, in conjunction with the presence of carbonates, yield mortars whose strength is lower than in NaOH- or waterglass-activated materials (Fernández-Jiménez and Palomo, 2005; Criado *et al.*, 2005).

3.3.4 Effect of sulfates

While sulfates are less commonly applied as activators, a few papers have been published on their use in (primarily) slag activation (Fernández-Jiménez, 2000; Shi *et al.*, 2006). Sulfate ions induce a less basic alkaline medium, lowering the amount of soluble silica released by the slag (Fernández-Jiménez, 2000; Shi *et al.*, 2006). A slag produced in India activated with hemihydrate ($CaSO_4.1/2H_2O$) was nonetheless found to set more quickly (Shi *et al.*, 2006).

Slag can be activated with a saturated Na_2SO_4 solution with a relatively low pH (≈ 7), although the process is slow. As when gypsum is the activator, a sufficient source of hydroxyl ions is needed to accelerate activation. At a sufficiently high pH, bonds are broken in the slag structure and the ettringite formed stabilises. Activation with a combination of gypsum and NaOH yields Na_2SO_4. While this procedure calls for five times more activator than needed in calcium activation, it yields double the amount of hydration product.

3.3.5 Effect of cations (Me = Na, K, Li, etc.)

The cations present in the activator also play a significant role in alkaline activation, for they may be taken up in the system, maintaining the pH values of the aqueous phase or forming part of the gel structure, where they neutralise the electrical charge produced when a SiO_4 tetrahedron is replaced by an AlO_4^- tetrahedron. The Me/Al ratios would logically be expected to be approximately 1. As the aluminium uptake in the gels rises, then, the fixed alkaline content also rises and is clearly greater in N-A-S-H than in C-A-S-H gels.

In high-CaO materials (BFS), using a NaOH solution as the activator has been shown to favour the dissolution of the Ca and Mg ions present in slag and the formation of a honeycombed C-S-H-type gel with a low C/S ratio (≈ 0.7–0.9). When KOH is the activator, less Mg dissolves out of the slag. Under these conditions the reaction product is a plate-like C-S-H-type gel with a higher C/S ratio (≈ 1.4), which forms along with a residual layer of high-Mg hydrates (Rajaokarivony-Andriambololona *et al.*, 1990; Roy *et al.*, 1994).

The effect of cations has also been analysed in high-aluminium and -silicon (low-calcium) metakaolin and fly ash activation. Here the type of cation involved in the activation reaction affects system microstructure as well as the Si/Al ratio in the pre-zeolite gel formed. Research has shown that Na^+ is more prone to form zeolite (Fernández-Jiménez *et al.*, 2006a, 2007), possibly because it is smaller than the K^+ cation and consequently able to flow more effectively through the gel, or perhaps also

due to its lower charge density. This is consistent with the greater tendency of Na^+ than other alkaline cations such as K^+, Rb^+ or Cs^+ to form zeolites in hydrothermal synthesis (Barrer and White, 1952, 1953; Barrer and Baynham, 1956). Na^+ is even more prone to zeolite formation than Li^+, a smaller but more readily hydrated ion, whose greater post-hydration volume fails to stimulate zeolite growth (Barrer and McCallum, 1951).

Given that the first stage of the reaction is controlled by the rate at which the alkaline compound dissolves the solid network of aluminosilicates to form small, reactive aluminate and silicate species, the more alkaline potassium hydroxides might reasonably be thought to induce a greater degree of dissolution than the less alkaline sodium hydroxides. Nonetheless, empirical studies have shown that sodium releases silicate and aluminate monomers more effectively than potassium (van Jaarsveld and van Deventer 1999; Xu and van deventer, 2003; Duxson *et al*., 2005a; Duxson *et al*., 2007b).

In 'conventional' geopolymer systems, the cations are typically Na^+ or K^+ (Macphee and Garcia-Lodeiro, 2011; Fernández-Jiménez *et al*., 2013). These ions are of particular interest because they determine differential coagulation in silica sols (Depasse and Watillon, 1970), due essentially to differences in their ionic size and, consequently, to their hydration tendencies. In aqueous environments, the positive charge on cations becomes associated with the partial negative charges on the oxygen atoms in the surrounding water molecules. This configuration is a result of the Lewis acidity of the cation, in which the oxide ion (in water) is the Lewis base. The relatively high charge density of Li^+ and Na^+ ensures that these ions remain hydrated, even at high pH values, whereas less intensely hydrated K^+ and larger alkali metal ions shed hydration water and associate with negatively charged silicate surface sites. The less negative $\Delta Hhydn$ indicates less tightly bound water. Li^+ and Na^+ are believed to further gelling because this 'structural' water coordinates hydrogen bonding between silicates (Depasse, 1997), which the weakly hydrated K^+ and larger alkali metal cations are unable to do.

3.4 Conclusions and future trends

In alkaline cement design, both the raw material and the activator used must be chosen carefully. An initial assessment of cement system performance can be obtained with a thorough analysis of the chemical composition and physical-chemical properties of the raw material. One of the limitations faced today is the lack of raw material (BF and phosphorous slag, F fly ash). Future research is focusing on the pursuit of new, uniform cementitious materials.

As the present discussion has shown, activators play an essential role in alkaline activation. The hazards involved in handling the corrosive solutions normally used (which contain soluble silicates or hydroxides) have driven the scientific community to seek solid activators able to deliver ready-mix geopolymers.

One of the challenges outstanding in connection with alkaline activation technology

is, therefore, the use of solid activators, i.e., the development of binders with built-in solid alkaline activators (such as finely ground sodium silicate or alkaline salts) to which only water would have to be added (Kolousek *et al*., 2007; Yang *et al*., 2008).

The result would be an activator-containing solid binder that could be mixed with aggregate and potable water in much the same way as in commercial concrete production. Moreover, the heat of hydration released by some solid activators may enhance the reactivity of certain mineral components. This may or may not be desirable, depending on the mix design, specimen geometry and intended application. The use of warm water or some other practical approach may be suggested as a source of heat where required to dissolve low solubility activators in a reasonable amount of time (Provis and van Deventer, 2014).

References

Acuña L. (2006), 'Tratamiento térmico del caolín y su influencia en las propiedades físicas y mecánicas de los hormigones', CONAMET/SAM.

Allahverdi A., Mehrpour K. and Najafi Kani E. (2008), 'Investigating the possibility of utilizing pumice-type natural pozzolan in production of geopolymer cement', *Ceram.-Silik.* 52 (1), 16–23.

Alonso S. and Palomo A. (2001), 'Alkaline activation of metakaolin and calcium hydroxide mixtures: influence of temperature, activator concentration and solids ratio', *Mat. Lett.* 47, 55–62.

Arjuman P., Silbee M.R. and Roy D.M. (1997), 'Quantitative determination of the crystalline and amorphous phases in low calcium fly ash', in *Proc. 10th Int. Congr. Chem. Cem.*, ed. H. Justnes, Gothenburg, Sweden.

Bakharev T., Sanjayan J.G. and Cheng, Y.-B. (1999), 'Alkali activation of Australian slag cements', *Cem. Concr. Res.* 29(1), 113–120.

Barrer R.M. and Baynham J.W. (1956), 'The hydrothermal chemistry of the silicates. Part VII. Synthetic potassium aluminosilicates', *J. Chem. Soc.* 1956, 2882–2891.

Barrer R.M. and McCallum N. (1951), 'The hydrothermal chemistry of silicates. Part I. Synthetic lithium aluminosilicates', *J. Chem. Soc.* 1951, 1267–1278.

Barrer R.M. and White E.A.D. (1952), 'The hydrothermal chemistry of silicates. Part II. Synthetic crystalline sodium aluminosilicates', *J. Chem. Soc.*, 1952, 1561–1571.

Barrer R.M. and White E.A.D. (1953), 'Hydrothermal chemistry of silicates. Part IV. Rubidium and cesium aluminosilicates', *J. Chem. Soc.* 1953, 4029–4035.

Bondar D., Lynsdale C.J., Milestone N.B., Hassani N. and Ramezanianpour, A.A. (2011a), 'Effect of type, form, and dosage of activators on strength of alkali-activated natural pozzolans', *Cem. Concr. Compos.* 33(2), 251–260.

Bondar D., Lynsdale C.J., Milestone N.B., Hassani N. and Ramezanianpour, A.A. (2011b), 'Engineering properties of alkali-activated natural pozzolan concrete', *ACI Mater. J.* 108(1), 64–72.

Buchwald A., Hohmann M. and Kaps Ch. (2007), 'The suitability of different clay resources in respect to form geopolymeric binders', *Proceedings of International Conference on Alkali Activated Materials: Research, Production and Utilization*, Prague, 137–148.

Buchwald A., Hohmann M., Posern K. and Brendler E. (2009), 'The suitability of thermally activated illite/smectite clay as raw material for geopolymer binders', *Appl. Clay Sci.* 46, 300–304.

Chindaprasirt P., De Silva P., Sagoe-Crentsil K. and Hanjitsuwan S. (2012), 'Effect of SiO_2 and Al_2O_3 on the settings and hardening of high calcium fly ash-based geopolymer systems', *J. Mat. Sci.* 47, 4876–4883.

Criado M., Palomo A. and Fernández-Jiménez A. (2005), 'Alkali activation of fly ashes. Part 1: Effect of curing conditions on the carbonation of the reaction products', *Fuel* 84, 2048–2054.

Criado M., Fernández-Jiménez A., de la Torre A.G., Aranda M.A.G. and Palomo A. (2007), 'An XRD study of the effect of the SiO_2/Na_2O ratio on the alkali activation of fly ash', *Cem. Concr. Res.* 37, 671–679.

Criado M., Fernández-Jiménez A., Palomo A., Sobrados I. and Sanz J. (2008), 'Effect of the SiO_2/Na_2O ratio on the alkali activation of fly ash. Part II: ^{29}Si MAS-NMR Survey', *Microporous Mesoporous Mat.* 109, 525–534.

Criado M., Fernández-Jiménez A. and Palomo A. (2010), 'Alkali activation of fly ash. Part 3: Effect of curing conditions on reaction and its graphical description', *Fuel* 89, 3185–3192.

Depasse J. (1997), 'Coagulation of colloidal silica by alkaline cations: surface dehydration or interparticle bridging', *J. Colloid. Interface Science*. 194, 260–262.

Depasse J. and Watillon A. (1970), 'The stability of amorphous colloidal silica', *J. Colloid. interface Science* 33(3), 430–438.

Duran Atiş C., Bilim C., Çelik Ö. and Karahan, O. (2009), 'Influence of activator on the strength and drying shrinkage of alkali-activated slag mortar', *Constr. Build. Mater.* 23(1), 548–555.

Duxson P., Lukey G.C., Separovic F. and van Deventer J.S.J. (2005a), 'Effect of alkali cations on aluminum incorporation in geopolymeric gels', *Ind. Eng. Chem. Res.* 44, 832–839.

Duxson P., Provis J., Grant L., Mallicoat S., Kriven W. and van Deventer J.S.J. (2005b), 'Understanding the relationship between geopolymer composition, microstructure and mechanical properties', *Colloids. Surf.* 269, 47–58.

Duxson P., Fernández-Jiménez A., Provis J.L., Lukey G.C., Palomo A. and van Deventer J.S.J. (2007a), 'Geopolymer technology: the current state of the art', *J. Mater. Sci.* 42, 2917–2933.

Duxson P., Mallicoat S.W., Lukey G.C., Kriven W.M. and van Deventer J.S.J. and (2007b), 'The effect of alkali and Si/Al ratio on the development of mechanical properties of metakaolin-based geopolymers', *Colloids and Surfaces A: Physicochem. Eng. Aspects* 292, 8–20.

Fernández-Jiménez A. (2000), 'Cementos de escorias activadas alcalinamante: influencia de las variables y modelización del proceso', PhD Thesis, Universidad Autónoma de Madrid, Spain.

Fernández-Jiménez A. and Palomo A. (2003), 'Characterisation of fly ashes: potential reactivity as alkaline cements', *Fuel* 82, 2259–2265.

Fernández-Jiménez A. and Palomo A. (2005), 'Composition and microstructure of alkali activated fly ash binder: effect of the activator', *Cem. Concr. Res.* 35, 1984–1992.

Fernández-Jiménez A. and Puertas F. (2001), 'Setting of alkali-activated slag cement: influence of activator nature', *Adv. Cem. Res.* 13(3), 115–121.

Fernández-Jiménez A., Palomo J.G. and Puertas F. (1999), 'Alkali-activated slag mortars: mechanical strength behaviour', Cem. Concr. Res. 29(8), 1313–1321.

Fernández-Jiménez A., Puertas F., Sobrados I. and Sanz J. (2003), 'Structure of calcium silicate

hydrates formed in alkaline-activated slag: influence of the type of alkaline activator', *J. Am. Ceram. Soc.* 86(8), 1389–1394.

Fernández-Jiménez A., Palomo A. and Criado M. (2006a), 'Alkali activated fly ash binders: a comparative study between sodium and potassium activators', *Mater. Construcc.* 56, 51–65.

Fernández-Jiménez A., Palomo A., Sobrados I. and Sanz J. (2006b), 'The role played by reactive alumina content in the alkaline activation of fly ashes', *Microp. Mesopor. Mater.* 91, 111–119.

Fernández-Jiménez A., Monzó M., Vicent M., Barba A. and Palomo A. (2007), 'Ceramic industry materials as potential alkaline binders', *Proceedings of International Conference on Alkali Activated Materials: Research, Production and Utilization*, Prague, 217–236.

Fernández- Jiménez A., Zibouche F., Boudissa N., Garcia-Lodeiro I., Tahar Abadlia M. and Palomo A. (2013), 'Metakaolin-slag-clinker blends: the role of Na^+ or K^+ as alkaline activators of theses ternary blends', *J. Am. Ceram. Soc.* 96, 1991–1998.

Fletcher R.A., Mackenzie K.J.D., Nicholson C.L. and Shimada S. (2005), 'The composition range of alumino silicate geopolymers', *J. Eur. Ceram. Soc.* 25, 1471–1177.

Garcia-Lodeiro I., Fernández-Jiménez A. and Palomo A. and Macphee D.E. (2010), 'Effect of calcium additions on N–A–S–H cementitious gels', *J. Am. Ceram. Soc.* 93, 1934–1940.

Garcia-Lodeiro I., Fernádez-Jiménez A., Pena P. and Palomo A. (2014), 'Alkali activation of synthetic aluminosilicate glasses', *Ceramic International* 40, 5547–5558.

Glukhovsky V.D. (1967), *Soil Silicate Articles and Structure (Gruntosilikatnye vyroby I konstruktsii)*, Ed. Budivelnyk Publisher, Kiev.

Glukhovsky V. (1994), 'Ancient, modern and future concretes', *First Int. Conf. Alkaline Cements and Concretes*, Kiev, Ukraine, 1, 1–8.

Gordon M., Bell J.L. and Kriven W.M. (2005), 'Comparasion of naturally and synthetically derived potassium-based geopolymers', *Ceram. Trans.* 165, 95–106.

Granizo M.L., Alonso S., Blanco-Varela M.T. and Palomo A. (2002), 'Alkaline activation of metakaolin: effect of calcium hydroxide in the products of reaction', *J. Am. Ceram. Soc.* 85(1), 225–231.

Hajimohammadi A. Provis J.L. and van Deventer J.S.J. (2010), 'Effect of alumina release rate on the mechanism of geopolymer gel formation', *Chem. Mater.* 22, 5199–5208.

Holt P.K., Barton G.W., Wark M. and Mitchell C.A. (2002) 'A quantitative comparison between chemical dosing and electrocoagulation', *Colloids and Surfaces A: Physicochem. Eng. Aspects* 211, 233–248.

Hos J.P., McCormick P.G. and Byrne L.T. (2002), 'Investigation of synthetic aluminosilicate polymer', *J. Mater. Sci.* 37, 2311–2316.

Kamseu E., Leonelli C., Perera D.S., Melo U.C. and Lemougna P.N. (2009), 'Investigation of volcanic ash based geopolymers as potential building materials', *Interceram* 58(2–3), 136–140.

Kolousek D., Brus J., Urbanova M., Andertova J., Hulinsky V. and Vorel J. (2007), 'Preparation, structure and hydrothermal stability of alternatice (sodium silicate-free) geopolymers', *J. Mater. Sci.* 42, 9267–9275.

Kovalchuk G., Palomo A. and Fernández-Jiménez A. (2007), 'Alkali activated fly ashes: effect of thermal curing conditions on mechanical and microstructural development – Part II', *Fuel* 86, 315–322.

Kovalchuk G., Palomo A and Fernández-Jiménez A. (2008), 'Activación alcalina de cenizas volantes. Relación entre el desarrollo mecánico resistente y la composición química de la ceniza', *Materiales de la Construcción* 58, 35–52.

Krivenko P.V. (1994), 'Alkaline cements', First Int. Conf. Alkaline cements and concretes, Kiev, Ukraine, 1, 12–129.

Leonelli C., Kamseu E., Boccaccini D.N., Melo U.C., Rizzuti A., Billong N. and Piselli, P. (2007), 'Volcanic ash as alternative raw materials for traditional vitrified ceramic products', *Adv. Appl. Ceram.* 106(3), 141–148.

Li. D. and Wu. X. (1992), 'Improvement of early strength of steel slag cement', *Jiangsu Build. Mater.* 4, 24–27.

Macphee D.E. and Garcia-Lodeiro I. (2011), 'Activation of aluminosilicates – some chemical considerations', *Proceedings of the Second International Slags Valorisation Symposium*, Leuven, Belgium.

Marín-López C., Reyes Araiza J., Manzano-Ramírez A., Rubio Avalos J., Perez-Bueno J., Muñiz-Villareal M., Ventura-Ramos E. and Vorobiev, Y. (2009), 'Synthesis and characterization of a concrete based on metakaolin geopolymer', *Inorg. Mater.* 45(12), 1429–1432.

Myers R.J., Bernal S.A., San Nicolas R. and Provis J.L. (2013), 'Generalized structural description of calcium–sodium aluminosilicate hydrate gels: the cross-linked substituted tobermorite model', *Langmuir*, 29, 5294–5306.

Najafi Kani E. and Allahverdi A. (2009), 'Effects of curing time and temperature on strength development of inorganic polymeric binder based on natural pozzolan', *J. Mater. Sci.* 44, 3088–3097.

Najafi Kani E. Allahverdi A. and Provis, J.L. (2012), 'Efflorescence control in geopolymer binders based on natural pozzolan', *Cem. Concr. Compos.* 34 (1), 25–33.

Pacheco-Torgal F. and Jalali S. (2010), 'Influence of sodium carbonate addition on the thermal reactivity of tungsten mine waste mud based binders', *Constr. Build. Mater.* 24(1), 56–60.

Palacios M. and Puertas, F. (2004), 'Effect of superplasticizer and shrinkage-reducing admixtures on alkali-activated slag pastes and mortars', *Cem. Concr. Res.* 35(7), 1358–1367.

Palomo A., Fernández-Jiménez A. and Criado M. (2004), 'Geopolymers: same basic chemistry, different microstructures', *Mater. Construcc.* 54, 77–91.

Pimraksa K., Chindaprasirt P., Rungchet A., Sagoe-Crentsil K. and Sato T. (2011), 'Lightweight geopolymer made of highly porous siliceous materials with various Na_2O/Al_2O_3 and SiO_2/Al_2O_3 ratios', *Mater. Sci. Eng. A* 528, 6616–6623.

Provis J. and van Deventer J.S.J. (eds) (2009), *Geopolymers: Structure, Processing, Properties and Industrial Applications*, Woodhead Publishing Limited. Cambridge.

Provis J.L. and van Deventer J.S.J (2014), 'Alkali-activated materials', State-of-the-art Report, RILEM TC 224-AMM.

Provis J.L., Duxson. P. and van Deventer J.S.J. (2010), 'The role of particle technology in developing sustainable construction materials', *Adv. Powder Technol.* 21(1), 2–7.

Puertas F. (1993), 'Escorias de alto horno: composicion y comportamiento hidráulico', *Materiales de Construccion* 43(229), 37–48.

Puertas F., Palacios M., Manzano H., Dolado J.S., Rico A. and Rodríguez J. (2011), 'A model for the C-A-S-H gel formed in alkali-activated slag cements', *J. Eur. Ceram. Soc.* 31(12), 2043–2056.

Rajaokarivony-Andriambololona Z., Thomassin J.H, Baillif P. and Touray J.C. (1990), 'Experimental hydration of two synthethic glassy blast furnace slags in water and alkaline solution (NaOH and KOH 0.1N) at 40°C: structure, composition and origin of the hydrated layer', *J. Mater. Sci.* 25, 2399–2410.

Roy A., Schilling P.J. and Eaton H.C. (1994), 'Activation of ground blast-furnace slags by alkali-metal and alkaline-earth hydroxides', *J. Am. Ceram. Soc.* 75(12), 3233–3240.

Ruiz-Santaquiteria C. (2013), 'Materials primas alternativas para el desarrollo de nuevos cementos: activación alcalina de vidrio silicoaluminosos', PhD Thesis, Universidad Autónoma de Madrid, Spain.

Ruiz-Santaquiteria C., Fernández-Jiménez A. and Palomo A. (2011), 'Quantitative determination of reactive SiO_2 and Al_2O_3 in aluminosilicate materials', *XIII International Congress of Cement Chemistry*, Madrid, Spain.

Ruiz-Santaquiteria C., Fernádez-Jiménez A. and Skibsted J and Palomo A. (2013), 'Clay reactivity: production of alkali activated cements', *Applied Clay Science* 73(1), 11–16.

Shi C. (1988), 'Study on alkali activated phosphorous slag cement', *J. Nanjing Inst. Chem. Technol.* 10(2), 110–116.

Shi C. (1989), 'Influence of temperature on hydration of alkali activated phosphorous slag', *J. Nanjing Inst. Chem. Technol.* 11(1), 94–99.

Shi C. (2004), 'Steel slag – its production, processing, characteristics and cementitious properties', *J. Mater. Civil Eng.* 16(3), 230–236.

Shi C. and Qian J. (2000), 'High performance cementing materials from industrial slags – a review', *Resourc. Conserv. Recyc.* 29, 195–207.

Shi C., Wu X. and Tang M. (1993), 'Research on alkali-activated cementitious systems in China', *Adv. Cem. Res.* 5(17), 1–7.

Shi C., Krivenko P.V. and Roy D. (2006), *Alkali-activated Cements and Concretes*, Taylor & Francis, London.

Silva P.D., Sagoe-Crenstil K. and Sirivivatnanon V. (2007), 'Kinetics of geopolymerization: role of Al_2O_3 and SiO_2', *Cem. Concr. Res.* 37, 512–518.

Smolcyk H.G. (1980), 'Structure et characterisation des laitiers', *7th International Congress of the Chemistry of Cement*, Paris, vol. 1, 1–16.

Tang M.S. and Su-Fen H. (1980), 'Effect of $Ca(OH)_2$ on alkali-silica reaction', *Proceedings of the Eight International Congress of Cement Chemistry*, Paris, France, Vol. 2, pp. 94–99.

Taylor H.F.W. (1990), *Cement Chemistry*, Academic Press, London.

van Deventer J.S., Provis J.L., Rees C.A., Yong C.Z., Duxson P. and Lukey G.C. (2007), International Conference, *Alkali Activated Materials, Research, Production and Utilization*, Prague.

van Jaarsveld J.G.S. and van Deventer J.S.J. (1999), 'Effect of the alkali metal activator on the properties of fly ash-based geopolymers', *Ind. Eng. Chem. Res.* 38, 3932–3941.

Wang S.D. and Scrivener K.L. (1995), 'Hydration products of alkali activated slag cement', *Cem. Concr. Res.* 25(3), 561–571.

Wang S.D., Pu X.C., Scrivener K.L. and Pratt P.L. (1995), 'Alkali-activated slag: a review of properties and problems', *Cem. Concr. Res.* l7(27), 93–102.

Wang F.S., Rui-Lian S. and Ying-Jing C. (2005), 'Study on modification of the high-strength slag cement material', *Cement and Concrete Research* 35, 1344–1348.

Xu H. and van Deventer J.S.J. (2000), 'The geopolymerisation of alumino-silicate minerals', *Int. J. Miner. Process.* 59(3), 247–266.

Xu H. and van Deventer J.S.J. (2002), 'Geopolymerisation of multiple minerals', *Miner. Eng.* 15(12), 1131–1139.

Xu H. and van Deventer J.S.J. (2003), 'The effect of alkali metals on the formation of geopolymeric gels from alkali-feldspars', *Colloids and Surfaces A: Physicochem. Eng. Aspects* 216, 27–44.

Xu H., Provis J.L., van Deventer J.S.J. and Krivenko P.V. (2008), 'Characterization of aged slag concretes', *ACI Mater. J.* 105(2), 131–139.

Yang K.H, Song J.K., Ashour A.F. and Lee E.T. (2008), 'Properties of cementless mortars activated by sodium silicate', *Construction and Building Materials* 22, 1981–1989.

This page intentionally left blank

Reuse of urban and industrial waste glass as a novel activator for alkali-activated slag cement pastes: a case study

4

F. Puertas, M. Torres-Carrasco, M. M. Alonso
Instituto Eduardo Torroja (IETcc-CSIC), Madrid, Spain

4.1 Introduction

The amount of urban and industrial waste has increased the world over in the last few decades. In the late twentieth century, urban waste was treated primarily in incineration plants, a technology that raised serious environmental problems, primarily associated with the emission of carbon dioxide and toxic particles. This situation led to the implementation of waste management and sorting policies in most highly developed countries. Hence the importance attached to recycling and valorisation of all manner of industrial waste and by-products, to enhance environmental protection.

Waste glass collection and management are increasingly common elements of environmental policy in the developed world. In 1994, approximately 9.2 million metric tonnes of post-consumer glass was discharged in the municipal waste stream in the United States. Approximately 8.1 million metric tonnes or 80% of this waste glass was container glass (Chesner *et al.*, 1997; Shi and Zheng, 2007). In Hong Kong, there are 44,000 t of waste glass generated from domestic sources per year. In addition, there are 20,000 t of waste glass annually generated from commercial sources. Of the total 64,000 t of waste glass, only about 8000 t is recycled and reused, although about 50,000 t of waste glass are technically recoverable (Chen *et al.*, 2002). In Spain, a total of 712 t of glass containers or 15.1 kg of glass waste per inhabitant were deposited in street-side bins in 2010 (Ecovidrio, 2012). This statistic is encouraging, bearing in mind that glass container consumption has declined by 5.7% in recent years. In that same year, a further 2240 kg were taken from sorting plants, the second source of glass waste after street-side bins (Ecovidrio, 2012). Moreover, many of these waste glasses are currently disposed of in landfill sites which are being filled much faster than expected. If the current trend of waste generation and disposal continues, our landfills will be exhausted by 2015.

Glass comes in many shapes: as bottles, flasks or glazing for windows; flat or round; coloured or clear; and with or without ceramic or metal coating. Since its service life is nearly always very short despite its shape, it is typically reused or recycled. Glass waste must meet a series of requirements for reuse in the manufacture of other glass articles, however. The tendency is to collect and sort urban and industrial glass

Handbook of Alkali-activated Cements, Mortars and Concretes. http://dx.doi.org/10.1533/9781782422884.1.75

waste by type. Even so, the wide variety of materials and chemical compositions involved renders its reuse by conventional technological processes highly complex. As a result, between 10 and 30% of glass waste is not recyclable for these purposes and alternative valorisation pathways must be sought. All the existing technologies for recycling mixed glass waste involve crushing. The fragments obtained (1–8 mm fraction), blended in the form of powder (scarcely reusable in glass manufacture), can be reused in construction in the following applications:

1. as pozzolanic additions to prepare Portland cements (Shi *et al.*, 2005);
2. in the preparation of vitroceramic composites together with other industrial waste or by-products, such as fly ash, slag and ceramic discards (Andreola *et al.*, 2008; Luz and Riberio, 2007);
3. in the preparation of composites with a polymer matrix (vehicle and pedestrian pavements) (Chesner, 1992);
4. as the main component in the production of foam glass for thermal insulating materials (Gorokhovski *et al.*, 2005);
5. as a prime material for synthesising solid sodium silicates or purified silica.

The fifth application, addressed here, has scarcely been studied. Very recent research by the authors (Torres *et al.*, 2009; Torres-Carrasco *et al.*, 2012) has shown that sodium silicate-based urban glass waste may serve as an active component in the preparation of alkali-activated slag or fly ash cements. Moreover, the construction industry is presently very keen on developing new cements and construction materials, whose manufacture would be less energy-intensive and entail the emission of less polluting gas (primarily CO_2) than conventional Portland cement manufacture. These cements are obtained by mixing amorphous silico-aluminates such as blast furnace slag, fly ash, metakaolin or volcanic rock, or blends of two or three of these materials, with highly alkaline solutions (NaOH, Na_2CO_3 or alkaline silicate hydrates) (Puertas, 1995; Shi *et al.*, 2006; Puertas *et al.*, 2000, 2004; Puertas and Fernández-Jiménez, 2003; Sánchez *et al.*, 2011; Mejía *et al.*, 2013). Inorganic polymer binders provide an alternative to traditional cements up to 80% less CO_2 emissions, and are derived from industrial waste materials (Van Deventer *et al.*, 2010, 2012).

Prior studies (Fernández-Jiménez *et al.*, 1999) showed that the predominant factor in the strength of these alkaline cements was the nature of the alkaline activator. Sodium silicate hydrate (waterglass) proved to be most effective. Bearing in mind that urban glass waste is an amorphous material whose chemical composition includes SiO_2 (65–75%), CaO (6–12%), Na_2O (12–15%), Al_2O_3 (0.5–5%) and Fe_2O_3 (0.1–3%), it may be regarded as a potential (waterglass family) alkaline activator for blast furnace slag, fly ash or other aluminosilicates. Soluble sodium silicates have been used in industry for a wide variety of applications. The raw materials for sodium silicate manufacture are soda ash and sand. Heated to 1100–1200°C, the materials fuse and a glass forms upon cooling. This glass is sold as anhydrous powder or dissolved in water at the manufacturing plant. The resulting solution, also known as 'waterglass', may be sold as it is, or it may be causticised to form more alkaline solutions (Larosa-Thomson *et al.*, 1997). Therefore, the process of synthesis of waterglass is costly and entails negative environmental

effects because it is necessary to reach high temperatures in the decarbonation of Na_2CO_3.

In regard to the chemistry of silica, there are numerous studies concerning the solubility of silico-aluminous materials, polymerisation, colloidal and surface properties, etc. (Iler, 1979). Key features of the glass, along with transparency, are the high chemical resistance. Due to its good qualities, interaction almost always takes place between the glass and chemicals. Glasses are attacked in both aqueous acid and alkaline solutions, although the mechanisms of attack and the degree of corrosion are different in each case (Fernández Navarro, 2003). Apparently, the solubility of these glass materials is high when the pH values are high (El-Shamy and Panteno, 1977; El Shamy *et al*., 1972; Paul, 1977). From pH 9 to 10.7, there is an apparent increase in the solubility of amorphous silica, owing to the formation of silicate ion in addition to the monomer which is in equilibrium with the solid phase. Above pH 10.7, all the solid phase of amorphous silica dissolves to form soluble silicate, since at higher pH the concentration of $Si(OH)_4$ is greatly lowered by conversion to ionic species, so that no amorphous solid can remain in equilibrium. Moreover, the effect of temperature was also studied on the solubility of glass (Paul, 1977; Goto, 1955), where an increase in the temperature favours the dissolution of the waste glass.

The main objective of this study is to know the possibility to generate solutions of sodium silicates (as potential waterglass solutions) by the solubility of different types of waste glass. Three different dissolution processes have been applied: at room temperature (22°C ± 2°C), at 80° ± 2°C and by mechano-chemical means. The final goal is to establish the optimal solubility conditions in order to investigate in further studies the feasibility of the use of waste glass as potential alkaline activators of materials such as slag or fly ash and to study the behaviour of AAS materials with a new type of activator. The uses of these dissolutions from the waste glass in the preparation of AAS systems will be discussed in the next sections.

4.2 Chemistry and structural characteristics of glasses

Based on the major compositions, glasses can be classified into the following categories: vitreous silica, alkali silicates, soda-lime glasses, borosilicate glasses, lead glasses, barium glasses, and aluminosilicate glasses. Small amounts of additives are often added during the production of glasses to give glasses different colours or to improve specific properties. Soda-lime glasses are most widely used to manufacture containers, float and sheets. Soda-lime glasses represent over 80% by weight in waste glass. On a colour basis, 63% are clear, 25% are amber, 10% are green and 2% are blue or other colors. The main composition of these glasses is the same except small amounts of additives are used for colouring purpose. The typical compositions of different types for different applications are listed in Table 4.1. Soda-lime glasses consist of approximately 73% SiO_2, 13% Na_2O and 10% CaO. Thus, based on their chemical composition, soda-lime glasses will be pozzolanic-cementitious materials and a potential alkaline activator waterglass family.

Table 4.1 Chemical composition of selected commercial glasses

Glasses and uses	SiO_2	Al_2O_3	B_2O_3	Na_2O	K_2O	MgO	CaO	BaO	PbO	Others
Soda–lime glasses										
Containers	66–75	0.7–7		16–12	0.1–3	0.1–5	6–12			
Float	73–74	0.5–1.5		13.5–15	0.2	3.6–3.8	8.7–8.9			
Sheet	71–73	1		12–15		1.5–3.5	8–10			
Light bulbs	73	1.5		17		4	5			
Tempered ovenware	75			14			9.5			
Borosilicate										
Chemical apparatus	81	2	13	4						
Pharmaceutical	72	6	11	7	1					
Tungsten sealing	74	1	15	4						
Lead glasses										
Colour TV funnel	54	2		4	9				23	
Neon tubing	63	1		8	6				22	
Electronic parts	56	2		4	9				29	
Optical dense flint	32			1	2				65	
Barium glasses										
Colour TV panel	65	2		7	9	2	2	2	2	10% SrO
Optical dense barium crown	36	4	10						41	9% ZnO
Aluminosilicate glasses										
Combustion tubes	62	17	5	1		7	8			
Fiberglass	64.5	24.5		0.5		10.5				
Resistor substrates	57	16	4			7	10	6		

Source: McLellan and Shand, 1984.

The XRD mineralogical characterisation (see Figure 4.2a) shows the glass to be an amorphous material, with low range structural order. No peaks attributed to any crystallised compound can be identified except a broad diffraction halo, which is attributed to the glassy phase. The position of the diffraction halo is related to the lime content and sodium content in the glass (Diamond, 1983; McCarthy *et al*., 1988; Van Roode *et al*., 1987; Shi and Zheng, 2007).

The structure of a glass can be described using a two-dimensional framework of SiO_4 tetrahedra represented schematically in Figure 4.1. According to the network

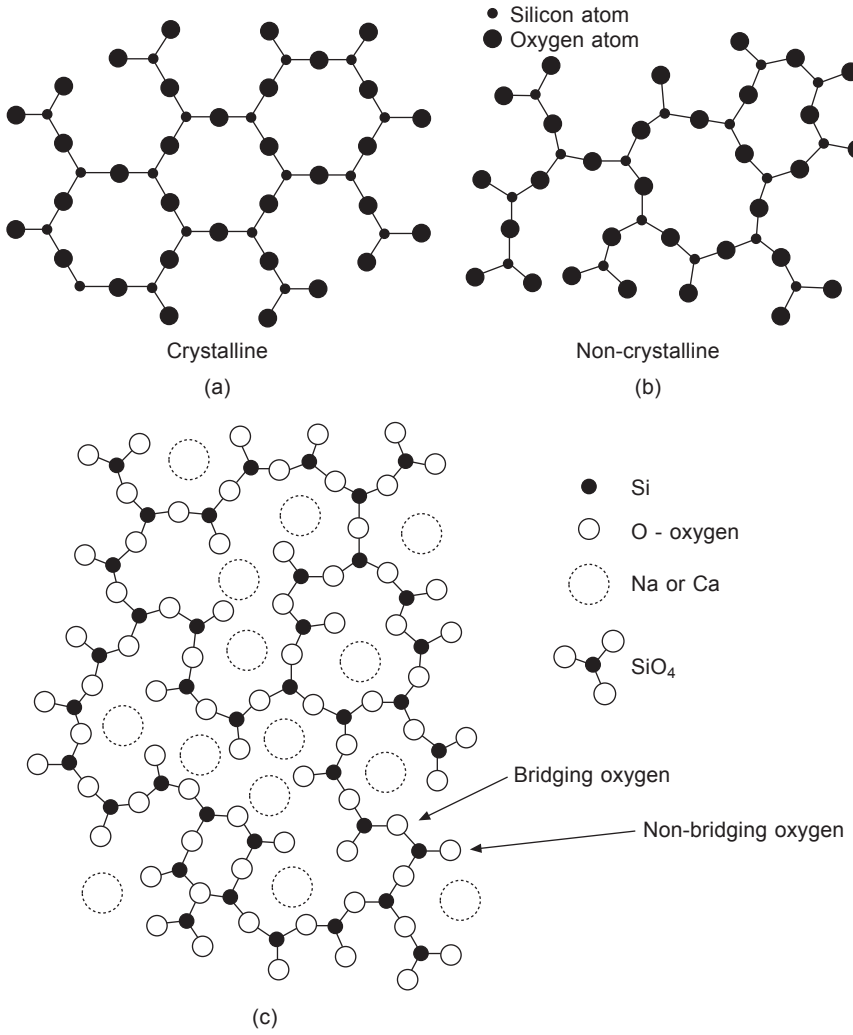

Figure 4.1 (a–c) Structure of quartz, silica glass and Na-Ca silicate glass (adapted from Partyka *et al*., 2014).

theory proposed by Zachariasen (1932), the components of a glass can be classified into three groups:

1. network formers;
2. network modifiers; and
3. intermediates.

Network formers are characterised by small ionic ratio, the highest possible ionic valences, and are surrounded by four oxygen atoms. Together with oxygen atoms,

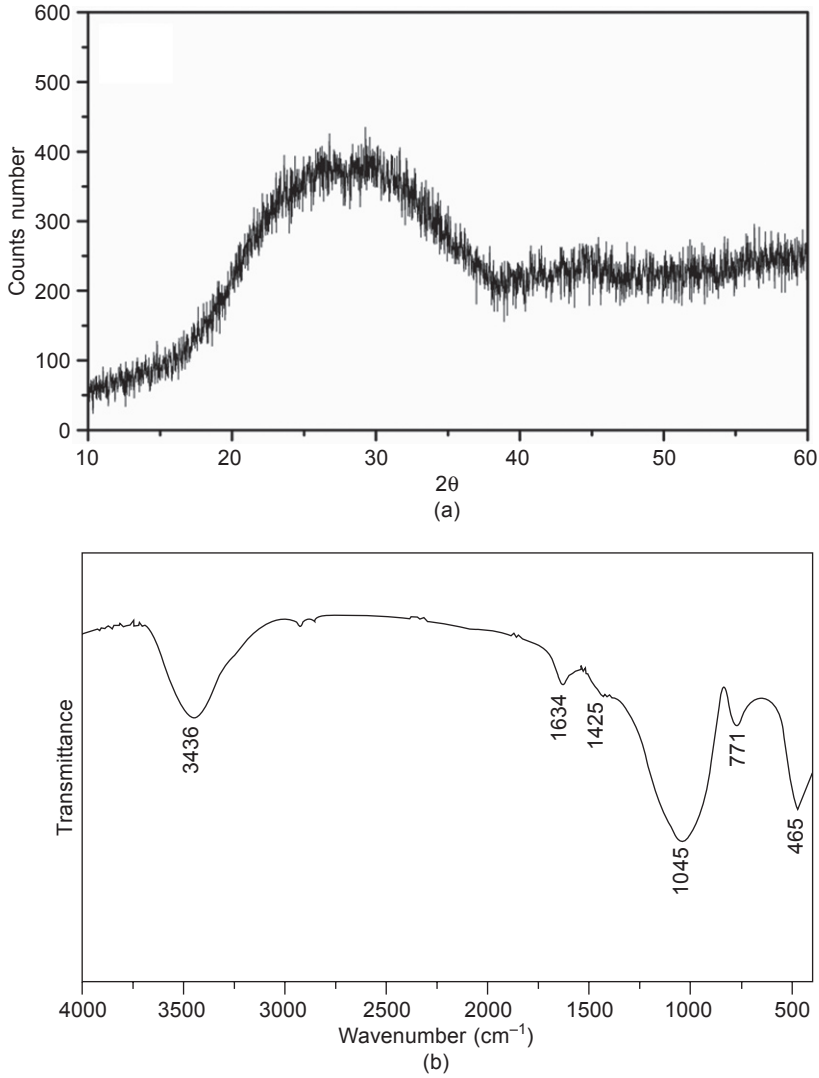

Figure 4.2 (a) XRD pattern and (b) FTIR spectrum for waste glass (soda-lime glasses) (Torres-Carrasco *et al*., 2014).

they form a more or less disordered three-dimensional network through tetrahedral. The bond energies between these network formers and oxygen atoms are usually higher than 335 KJ/mol. Si and P are typical network formers in vitreous blast furnace slag. The higher content the network formers are, the higher is the condensation degree of the glass.

Network modifiers have coordination number of 6 or 8, and have large ionic ratio. The presence of network modifiers disorders and depolymerises the network. The bond energies between the network modifiers and oxygen atoms are usually less than 210 KJ/mol. Na, K, Ca are typical network modifiers in vitreous blast furnace slag.

Intermediates can act as both network formers and modifiers. Their coordination number is 4 when they act as network formers and 6 as network modifiers. Their bond energies with oxygen atoms range from 210 to 335 KJ/mol. From the bond energies of network formers and network modifiers, it can be anticipated that the greater the content of network formers, the less reactive the glass is.

The IR spectra for these glass waste (Figure 4.2) contained a wide and intense band at 900–1100 cm^{-1} associated with the Si-O (ν_3 (Si-O)) asymmetric stretching vibrations in the SiO_4 tetrahedral groups present in the silicates, and another at 450–470 cm^{-1} due to the ν_4 (O-Si-O) bending vibrations in the SiO_4 groups, likewise in the silicates. The XRD and FTIR findings were practically identical in soda-lime glasses (see Figure 4.2).

4.3 Waste glass solubility trials in highly alkaline media

The process of solubility of waste glasses in aqueous, acid and alkali media has been studied and depends on numerous factors such as the nature of solution, the particle size of waste, the temperature of solubility, the stirring time, etc. (Torres-Carrasco *et al*., 2014). Therefore, it is necessary to know under what conditions the higher solubility of silicon oxide from waste glass arises, then try to use this as an activating solution of silicoaluminous materials such as slag to produce AAMs.

Glass solubility was determined by Torres-Carrasco *et al*. (2014) in the following three processes:

- at ambient temperature (22 ± 2°C)
- at high temperature (80 ± 2°C)
- by a mechano-chemical process (in a ball grinder) at ambient temperature (22 ± 2°C).

The chemical process consists of magnetic stirring at ambient temperature (22 ± 2°C) and a constant speed, where the solid:liquid ratio is 1g of glass material per 100 mL of solution (1:100). Besides these, there are other conditions such as three particle sizes (<45 μm, 45–90 μm and >125 μm), the stirring times of 10 min, 2, 4 and 6 hours to determine the effect of time on glass dissolution and, finally, the use of three different solutions: distilled water (pH = 7) as the reference, a NaOH solution (pH = 13.8) and a 1:1 NaOH/Na_2CO_3 solution – 50% mix of NaOH and

Na_2CO_3 in molar (pH = 13.6), where the concentration of the two alkaline solutions was 5% of Na_2O. The results of the behaviour of the solubility using these conditions are discussed in Section 4.3.1.

Based on the findings for the chemical process at ambient temperature, Torres-Carrasco *et al*. decided to work with high temperature to see the solubility of these materials. All the other conditions remained unchanged: stirring times, glass particle size and the activating solutions (NaOH and NaOH/Na_2CO_3 at the same concentration as in chemical process at ambient temperature). Solution temperature was held steady at 80 ± 2°C. The results of the behaviour of the solubility using these conditions are discussed in Section 4.3.2.

Lastly, in the mechano-chemical process trials, the glass was ground in a steel ball grinder. In such procedures, the relationship between the size and number of balls and the solid:liquid ratio had an important effect on the solubility process. The best grinding performance was found for 5 g of solid in 500 ml of solution and 1 kg of balls (with a size distribution of approximately 2.5% of balls 20 mm in diameter; and 12.3% measuring 15 mm, 29.3%, 9 mm and 56%, 5 mm in diameter). As in the case of the other processes, all conditions were the same. The results of the behaviour of the solubility using these conditions are discussed in Section 4.3.3.

All the solutions obtained were gravity filtered and brought to a known volume for subsequent ICP-AES laboratory analysis of elements Si, Al, Ca and Mg. The analyses were conducted in a VARIAN 725-ES inductively coupled plasma atomic emission spectrometer.

4.3.1 Chemical process at ambient temperature (22 ± 2°C)

In most cases where glass is exposed to chemical attack, the medium is aqueous. The mechanism governing glass–water interaction must consequently be the first question addressed. Contact with the aqueous medium induces an exchange of sodium and hydrogen ions. Since the latter are present in water in equilibrium with OH^- ions, this exchange governs dissolution (Fernández Navarro, 2003). As Figure 4.3 shows, the solubility of the silicon oxide present in the glass rose with stirring time, irrespective of particle size. Nonetheless, solubility was highest when the glass particle size was under 45 microns, for the smaller the particle size the greater the specific surface and consequently the more intense the contact between the solution and the glass. The result is higher solubility.

Highly alkaline attacks are governed by a different mechanism, in which the OH^- groups are predominant, further to the following reactions (Fernández Navarro, 2003):

$$\equiv Si\text{-}O\text{-}Si\equiv + OH^- \rightarrow \equiv Si\text{-}OH + \equiv Si\text{-}O^- \quad (4.1)$$

Unsaturated $\equiv Si\text{-}O^-$ groups may react with water molecules and form new silanol groups and more OH^- groups:

$$\equiv Si\text{-}O^- + H_2O \rightarrow \equiv Si\text{-}OH + OH^- \quad (4.2)$$

The reaction between the glass and the OH^- groups always hydrolyses oxygen bridges,

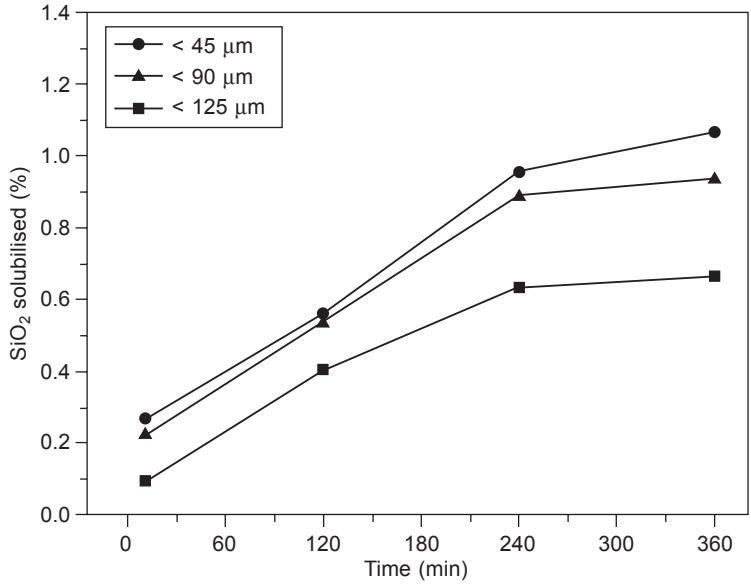

Figure 4.3 Percentage of SiO_2 solubilised in waste glass in water: effect of glass particle size (Torres-Carrasco *et al.*, 2014).

partially destroying the network. For that reason, glass is much less resistant to alkaline than acidic media. In alkaline media, glass may be said to be depolymerised, resulting in total destruction of its network and gradual solubilisation.

Figure 4.4 shows the solubility of different types of glasses in the two alkaline media (NaOH and NaOH/Na_2CO_3) for glass particle sizes of under 45 µm. These findings confirmed the greater solubility of SiO_2 and Al_2O_3 (forming oxides) in alkaline media than in water. In NaOH, solubility was 16–43% higher than in water, depending on the type of glass. When the solution pH was raised (using NaOH/Na_2CO_3 or NaOH), the amount of SiO_2 and Al_2O_3 extracted rose substantially, due to network destruction after the Si-O-Si and Al-O-Al bonds were broken. The differences between the two solutions were significant: SiO_2 solubility was 12–53% higher and Al_2O_3 solubility 17–54% higher with NaOH/Na_2CO_3 than with NaOH. However, the difference between both pH values was not very remarkable, but in this case it is possible that other determining factors, such as the presence of a common ion (Na^+) or the presence of carbonates contributed to dissolving a higher amount of glass (Ruiz-Santaquiteria *et al.*, 2013).

As Figure 4.4 shows, the Mg and Ca oxides, regarded as network modifiers on the grounds of their electronegative potential values (Stanworth, 1950), failed to exhibit very high solubility over time. Because of their higher solubility (lower Ca-O and Mg-O bond energy than in Al-O and Si-O), they dissolved from the time of initial contact between the alkaline solution and the glass.

Another interesting finding at ambient temperature was that glass solubility was very low and similar for the four types of glass studied (Figure 4.4), so that the nature of waste glass in this case is not important in their solubilisation.

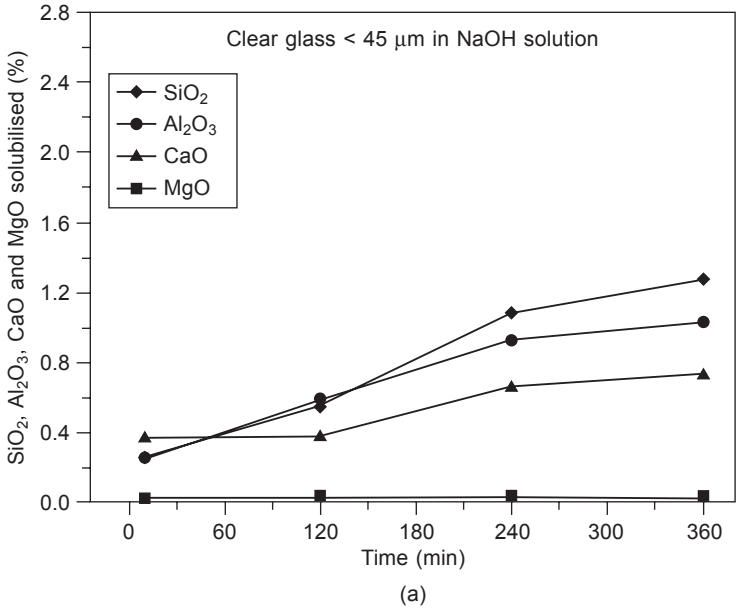

(a)

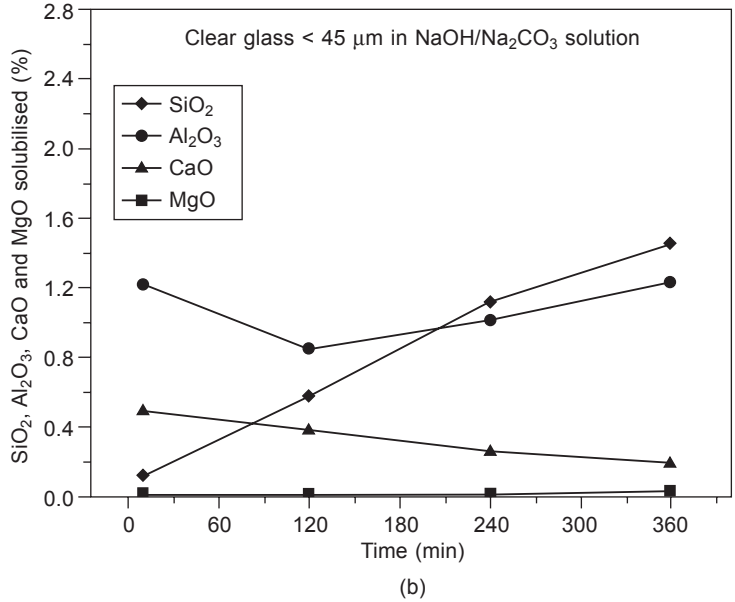

(b)

Figure 4.4 (a–h) Chemical process at ambient temperature. Solubility of Si, Al, Ca and Mg oxides present in different types of glasses in alkaline media (NaOH and NaOH/Na_2CO_3) (Torres-Carrasco *et al*., 2014).

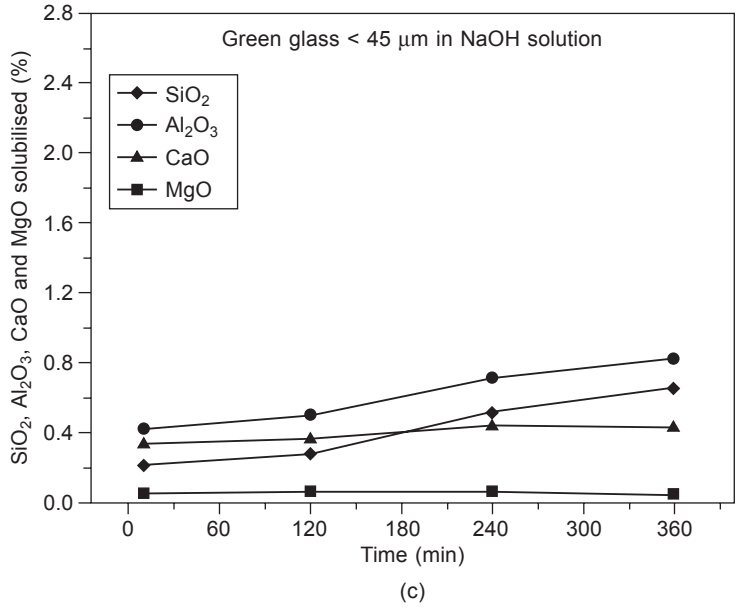

(c)

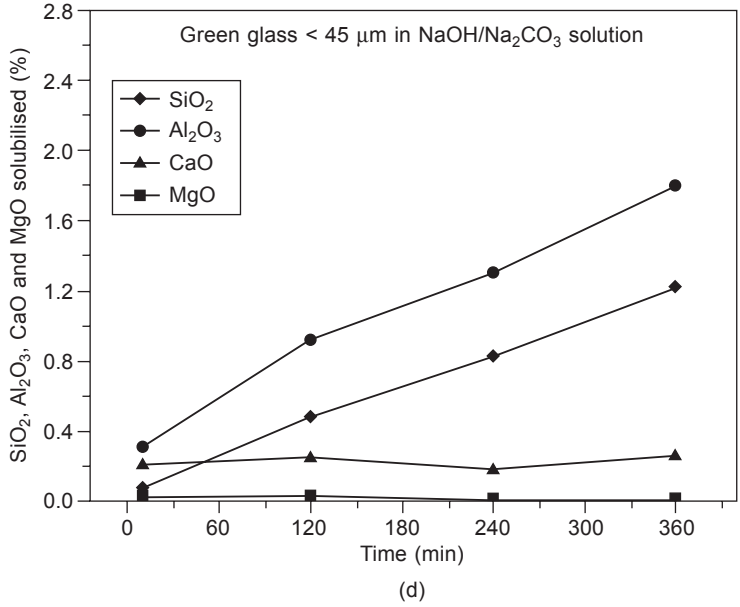

(d)

Figure 4.4 Continued

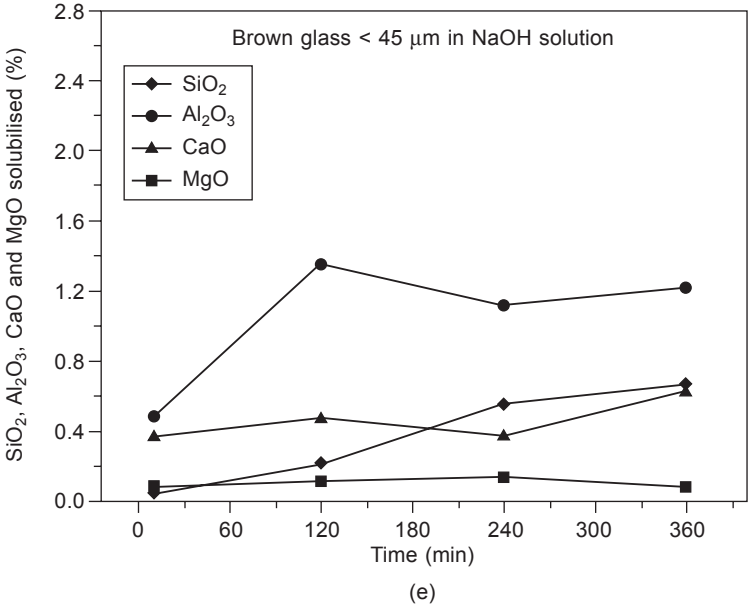

(e)

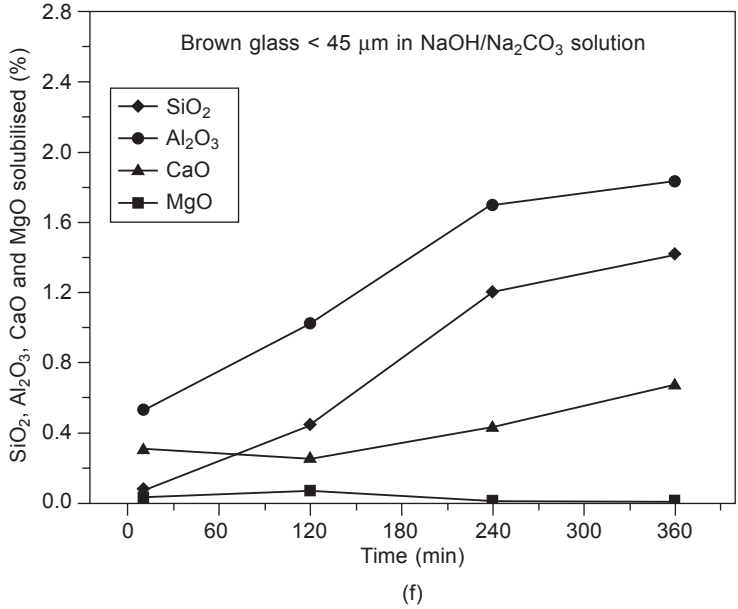

(f)

Figure 4.4 Continued

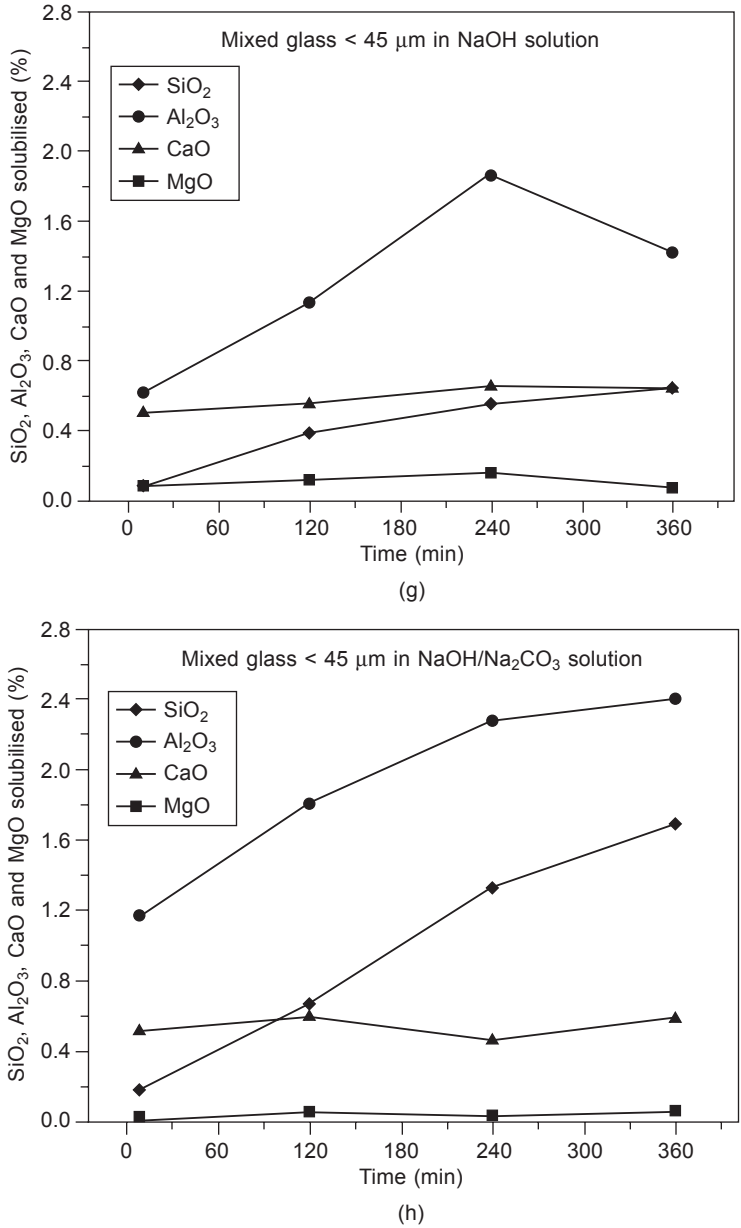

Figure 4.4 Continued

4.3.2 Chemical process at 80 ± 2°C

Figure 4.5 shows the percentage of solubilised Si, Al, Ca and Mg oxides in two types of waste glass after chemical process at 80 ± 2°C. As with chemical process at

ambient temperature, glass particle sizes was a key factor in the solubility of silicon oxide, where the higher solubility was reached for particle sizes lower than 45 μm. Moreover, unlike what occurred at ambient temperature, the effect of temperature

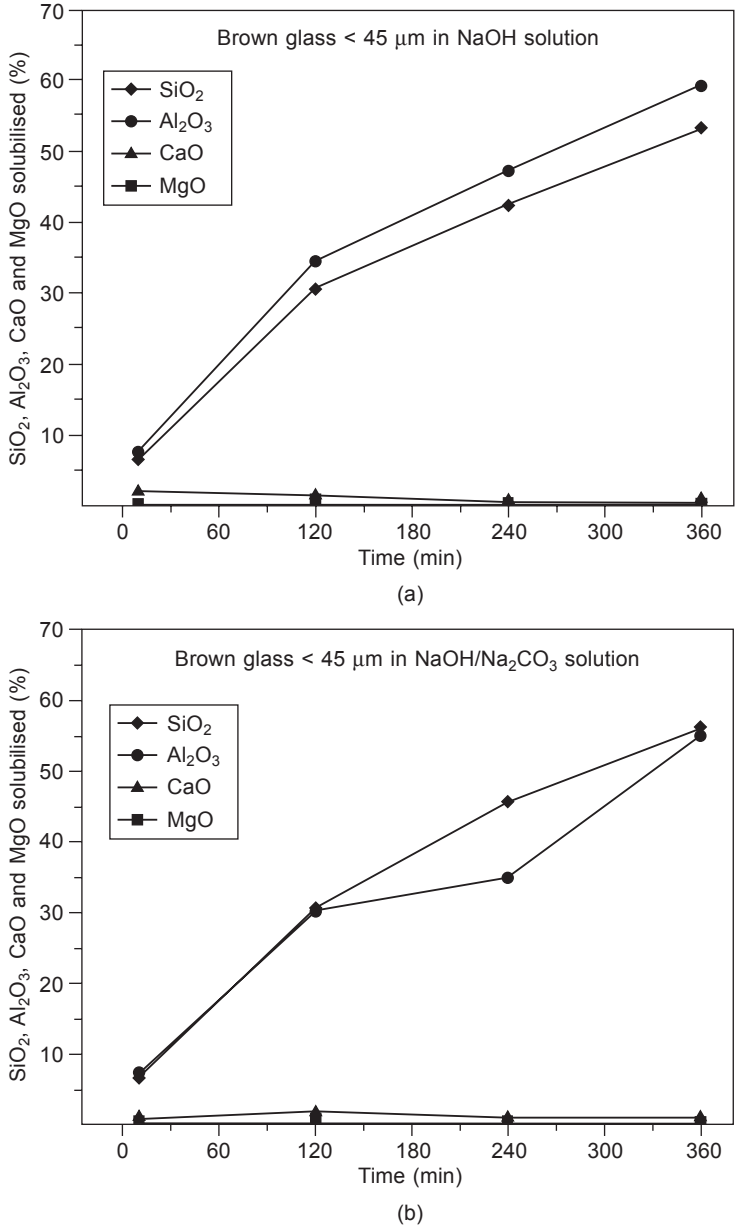

Figure 4.5 (a–d) Chemical process at 80 ± 2°C: Si, Al, Ca and Mg oxide solubility in alkaline solutions (Torres-Carrasco *et al*., 2014).

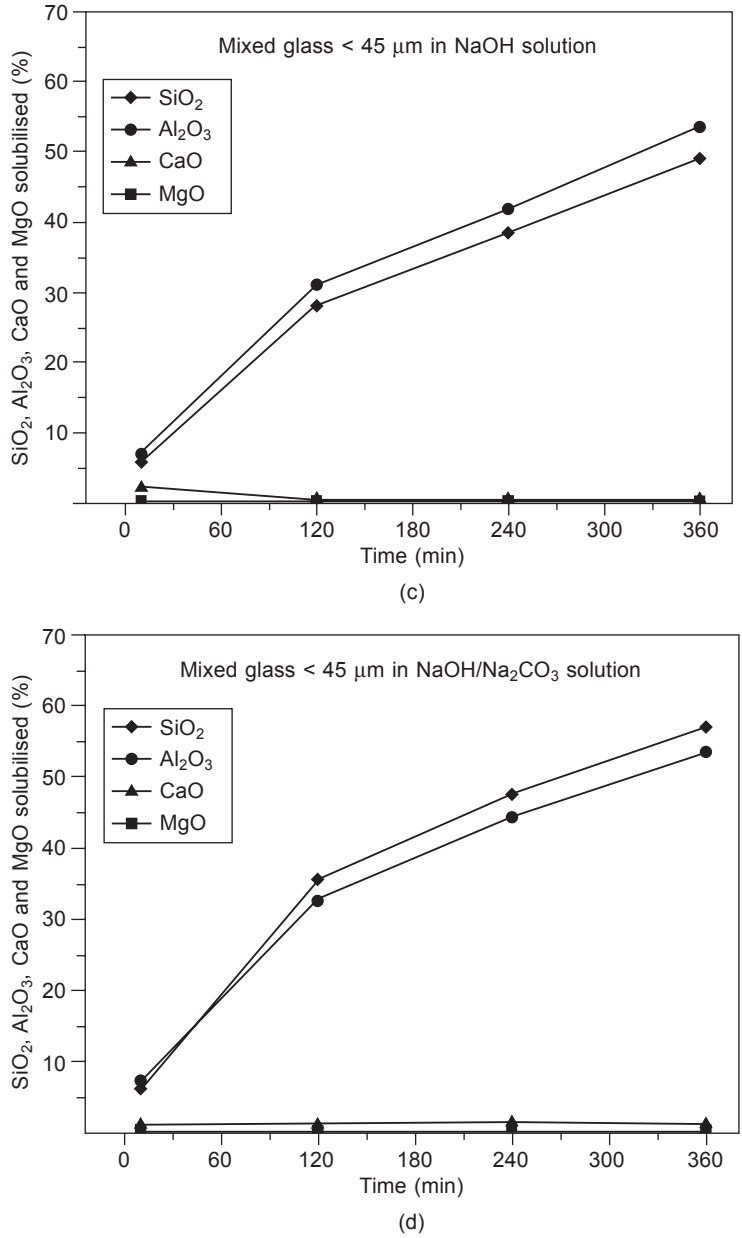

Figure 4.5 Continued

causes the particle size to be significant for Al_2O_3 and CaO. By contrast, the type of alkaline activator appeared to have a smaller impact at 80 ± 2°C than at ambient temperature. In the high temperature trial, the solubilisation percentages were on the order of 60% for SiO_2 and 55% for Al_2O_3 in all types of glass (see Figure

4.5) and the amount of SiO_2 dissolved similarly in the two types of glass for both alkaline solutions. Nonetheless, the $NaOH/Na_2CO_3$ solution exhibited slightly better performance, dissolving 14% more of the SiO_2 present in the glass. Given the higher solubility of the Ca and Mg oxides, the percentages dissolved were similar to the values found at ambient temperature. The findings for this type of process showed that temperature is a key variable in glass solubilisation.

4.3.3 Mechano-chemical process at ambient temperature (22 ± 2°C)

The solubility values obtained for the different oxides in this process were very similar to those reported in the chemical process at room temperature. Figure 4.6 shows a comparative representation of the three methods, confirming that the chemical process at room temperature and the mechano-chemical process dissolve the glass very similarly, while the chemical method at 80 ± 2°C is the most effective from the viewpoint of solubility of the glass.

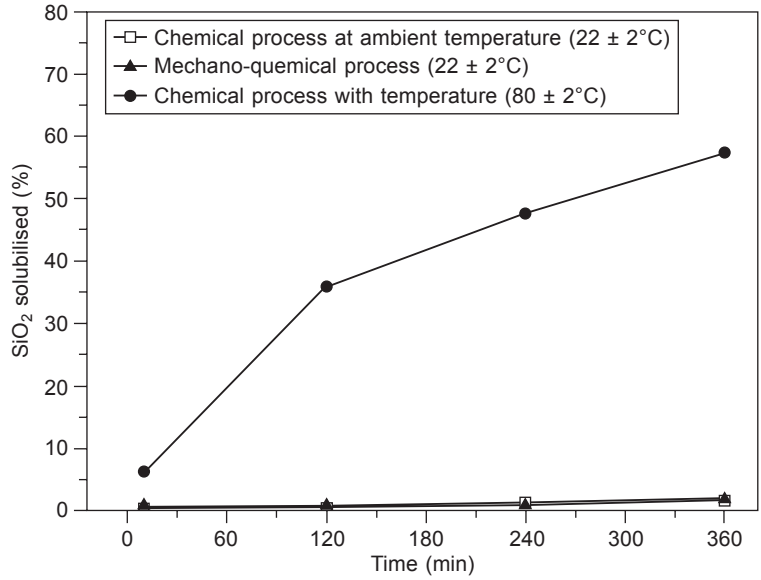

Figure 4.6 SiO_2 solubility in waste glasses: comparison of chemical and mechano-chemical process at ambient temperature and chemical process at 80 ± 2°C (Torres-Carrasco *et al.*, 2014).

4.4 Formation of sodium silicate solution from waste glasses dissolution: study by ^{29}Si NMR

From the previous analytical findings regarding the solubility of waste glasses, it is necessary to know and quantify the SiO_2 contents dissolved from waste glasses

because the main objective of this work is to generate solutions of sodium silicate (as potential waterglass solution) from the different solubilisation processes (Torres-Carrasco *et al.*, 2014; Puertas and Torres-Carrasco, 2014). Figure 4.7, in turn, reproduces the ^{29}Si NMR spectrum for the original waste glass (mixed glass) and the spectrum for the liquid obtained after treating the waste glass with NaOH/Na_2CO_3 at 80 ± 2°C for 2, 4 and 6 hours. The spectrum for the waste glass contains a single signal at around –93 ppm, indicative of the presence of the Q^4 Si units that characterise silica glass. The spectrum for the post treatment liquid, even after a short time, exhibits a single signal at around –71 ppm, associated with the presence of Q^0 units, i.e., dissolved Si monomers. This is important because, according to the literature (Engelhardt and Michel, 1987; Criado *et al.*, 2008; Palomo *et al.*, 2004), the effectiveness of Si in waterglass systems rises with declining condensation and polymerisation of the molecule in the medium.

The next step is to demonstrate that these sodium silicate solutions formed from waste glasses can be used as an alkaline activator of the waterglass family in the preparation of alkali-activated materials (AAMs).

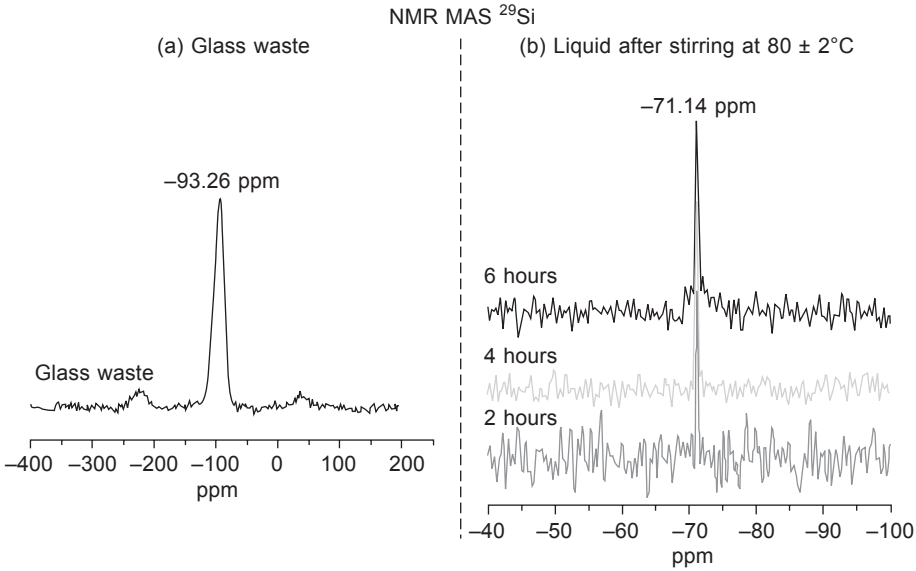

Figure 4.7 ^{29}Si MAS NMR spectra for (a) untreated solid waste glass and (b) liquid obtained after stirring waste in a NaOH/Na_2CO_3 solution for 2, 4 and 6 hours at 80 ± 2°C (reprinted from Puertas and Torres-Carrasco, 2014, Copyright © 2014, with permission from Elsevier).

4.5 Use of waste glasses as an activator in the preparation of alkali-activated slag cement pastes

Prior studies determined the solubility of different types of waste glasses in highly alkaline media (Brykov and Korneev, 2008; Torres-Carrasco *et al.*, 2012, 2014).

This waste has been found to dissolve most effectively (highest amounts of dissolved SiO_2 and Al_2O_3) with a $NaOH/Na_2CO_3$ solution (5% Na_2O) heated at 80 ± 2°C for 6 hours (Puertas *et al*., 2012). The question that must now be addressed is whether the solutions resulting from the treatment of waste glasses can replace traditional waterglass in the preparation of alkaline cements. Consequently, the primary objective of the present research is to explore the feasibility of using urban and industrial waste glasses as a potential alkaline activator for blast furnace slag, evaluating the rheology and workability of these systems (see Section 4.5.1), its mechanical-resistant behaviour (see Section 4.5.2) and microstructural characterisation (see Section 4.5.3).

In studies carried out by Rodríguez-Puertas *et al*. (2014) and Puertas and Torres-Carrasco (2014) the rheology, mechanical behaviour and porosity as well as the characterisation of the main reaction products obtained were studied when a blast furnace slag was activated with different activator solutions, including a solution obtained through the process of solubility previously described.

The following activating solutions, all at a constant 5% Na_2O by slag mass were used:

- 50% mix of NaOH and Na_2CO_3 in molar with a pH of 13.6
- Commercial waterglass (27% SiO_2; 8% Na_2O and 65% H_2O by weight) with a SiO_2/Na_2O ratio of 1.2
- 50% mix of NaOH and Na_2CO_3 in molar with different amounts of dissolved waste glass (from 1 to 25 g per 100 mL of solution).

The last group was prepared by adding 1, 10, 15, 20 and 25 g of waste glass (with a particle size under 45 μm) to the sodium hydroxide/sodium carbonate solution, stirring at 80 ± 2°C for 6 h and subsequent filtering (Torres-Carrasco *et al*., 2014). Table 4.2 lists the weight of oxides dissolving out of the glass and into the activating solution (g/100 mL).

Paste specimens measuring 1 × 1 × 6 cm were prepared to the compositions given in Table 4.3. The liquid/solid (L/S) ratio was 0.4 or 0.44, depending on the type of activator, to ensure that plasticity was as recommended in European standard EN 196-3 in all cases. However, for rheological measurements, the L/S ratio was increased to 0.55 due to rotational viscosimeter requirements. The pastes were chamber-cured

Table 4.2 SiO_2, Al_2O_3, CaO and MgO (g) from the glass waste dissolved after treatment in 100 ml of 50% mix $NaOH/Na_2CO_3$

Glass waste	SiO_2 (g/100 ml)	Al_2O_3 (g/100 ml)	CaO (g/100 ml)	MgO (g/100 ml)
1 g	0.42	0.05	1.2 E^{-03}	1.5 E^{-05}
10 g	2.82	0.13	5.3 E^{-04}	3.0 E^{-05}
15 g	3.34	0.16	6.1 E^{-04}	4.3 E^{-05}
20 g	4.49	0.19	6.9 E^{-04}	7.2 E^{-05}
25 g	4.54	0.25	8.2 E^{-04}	2.0 E^{-04}

Source: Reprinted from Puertas and Torres-Carrasco, 2014, Copyright © 2014, with permission from Elsevier.

Table 4.3 Pastes prepared and activation conditions

Sample name	Activator type	L/S	Glass content	SiO_2/Na_2O	pH
AAS N/C[a]	$NaOH/Na_2CO_3$	0.4	–	0	13.60
AAS WG[b]	Waterglass	0.44	–	1.2	13.76
AAS N/C-1[c]	$NaOH/Na_2CO_3$	0.4	1 g	0.08	13.79
AAS N/C-10	$NaOH/Na_2CO_3$	0.4	10 g	0.54	13.70
AAS N/C-15	$NaOH/Na_2CO_3$	0.4	15 g	0.63	13.63
AAS N/C-20	$NaOH/Na_2CO_3$	0.4	20 g	0.85	13.60
AAS N/C-25	$NaOH/Na_2CO_3$	0.4	25 g	0.86	13.48

[a]AAS N/C = slag alkali-activated with $NaOH/Na_2CO_3$.
[b]AAS WG = slag alkali-activated with waterglass.
[c]AAS N/C-(1-25) = slag alkali-activated with $NaOH/Na_2CO_3$ and from 1 to 25 g of glass waste.
Source: Reprinted from Puertas and Torres-Carrasco, 2014, Copyright © 2014, with permission from Elsevier.

(99% relative humidity, 20 ± 2°C) for 1, 2, 7 or 28 days and the prismatic specimens tested for mechanical strength.

The total porosity and pore size distribution were determined on pastes AAS N/C-25, AAS N/C and AAS WG at all ages. All other characterisation trials were conducted on the same pastes, but only on the 7-day specimens. After the mechanical tests, the pastes were immersed in acetone/ethanol to delay the hydration/activation process. The tests conducted on these pastes were Hg intrusion porosimetry, FTIR, XRD, ^{29}Si and ^{27}Al MAS NMR and BSEM/EDX.

4.5.1 Rheology and workability

An understanding of paste rheology is a pre-requisite for understanding the rheology of their respective mortars and concretes, which may determine the mechanical strength and durability of these materials. However, the rheology of alkali-activated slags is still not fully understood. Palacios *et al*. (2008) studied the rheology of AAS pastes and mortars activated with waterglass and NaOH and demonstrated that paste rheology depended on the nature of the activator used. Moreover, there is no information regarding the rheology of AAS systems with activators containing waste glasses.

Figure 4.8 shows the variations in shear stress at a constant shear rate in AAS WG and AAS N/C-25 with the same SiO_2/Na_2O ratio of 0.8 (Rodriguez-Puertas *et al.*, 2014). This figure shows that in AAS WG pastes after an initial decline, shear stress values reach a maximum after around 6 min. This signal is attributed to the initial formation of a primary C-S-H gel produced by the reaction between silicate ions in the activator (WG) and the Ca^{2+} ions from the slag (Palacios *et al.*, 2006; Varga *et al.*, 2013). At a constant shear rate, this primary gel is broken down, producing the decline in shear stress values. Palacios *et al*. (2008) and Palacios and Puertas (2011) showed that formation of this C-S-H gel determines the early setting times found for AAS WG materials, and that setting times could be controlled, lengthening the mixing times.

However, AAS N/C-25 pastes behave very differently, as after initial decline of

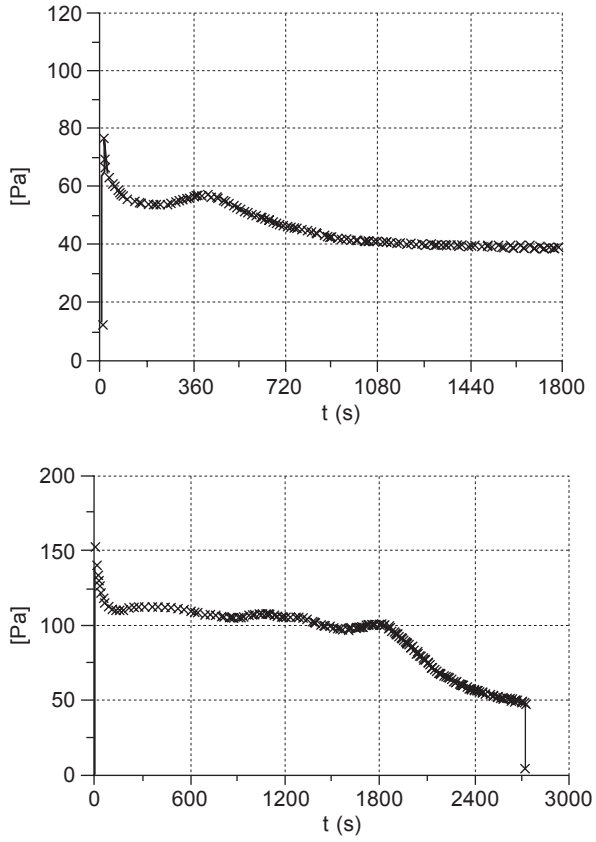

Figure 4.8 Shear stress versus time in AAS WG and AAS N/C-25 pastes tested at a constant shear rate of 100 s^{-1} (Rodríguez-Puertas *et al*., 2014).

shear stress values, no significant changes were observed until a maximum peak after around 30 min, indicating that the activating solution from the vitreous waste generates primary C-S-H gel at a significantly longer time than in the case of AAS WG.

Fluidity values of AAS WG and AAS N/C-25 pastes, found using the Minislump test, are illustrated in Figure 4.9 (Rodríguez-Puertas, 2014).

The Minislump test shows that AAS WG pastes lose their flowability after 7 min of testing, due to the formation of the primary C-S-H gel. In this static test, contrary to that found for dynamic rheological tests (Figure 4.8), the absence of mixing produced hardening and setting of pastes as primary C-S-H gel flocs are not dispersed (Varga *et al*., 2013). In AAS N/C-25, pastes are more fluid, and the decrease in flowability values occurs between 15 and 30 min.

These results show that AAS N/C-25 pastes have an adequate rheological behaviour. Therefore, the viability of the use of urban glass waste as potential alkaline activators, from the rheological and fluidity behaviour, is demonstrated, with the additional

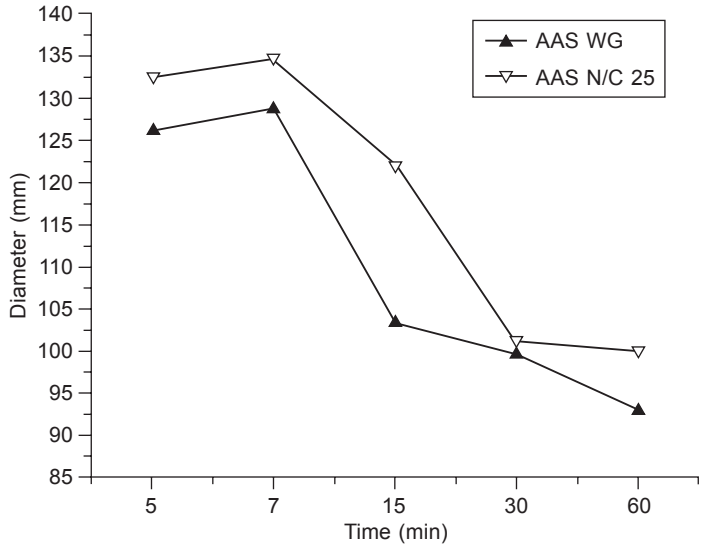

Figure 4.9 Minislump values for AAS WG and AAS N/C-25 pastes (Rodríguez-Puertas, 2014).

advantage of AAS N/C-25 pastes to maintain fluidity for longer times with respect to AAS WG pastes.

4.5.2 Mechanical strength and porosity

The mechanical performance of the pastes studied is reflected in Figure 4.10. The figure shows that compressive strength rose with curing time in all the pastes. The lowest strength values were recorded, at all ages, for paste AAS N/C, i.e., the paste prepared with $NaOH/Na_2CO_3$ as the activator, and the highest for paste AAS WG, prepared with waterglass. The graph also shows that the higher the waste glass content in the activating solution in the AAS N/C family of pastes, the higher was their mechanical strength, although none was as strong as paste AAS WG.

The total porosity and pore size distribution (in the 100–0.01 μm range) for the pastes are respectively given in Figure 4.11, where the porosity values are shown as a percentage of the total sample volume. According to the figure, total porosity was greatest in paste AAS N/C at all ages, ranging from 18 to 24%. In the pastes prepared with Si-containing activators, total porosity was significantly lower: 4–9% in AAS WG and 7–9% in paste AAS N/C-25.

Pore size distribution followed a similar pattern (Figure 4.11), with a greater proportion of micro- and mesopores in the pastes prepared with the activators containing silicon. The paste prepared with 25 g/100 mL glass waste had a larger fraction of pores smaller than 0.01 μm. These total porosity and pore size distribution findings are consistent with the compressive strength found for the materials tested (Figure 4.10).

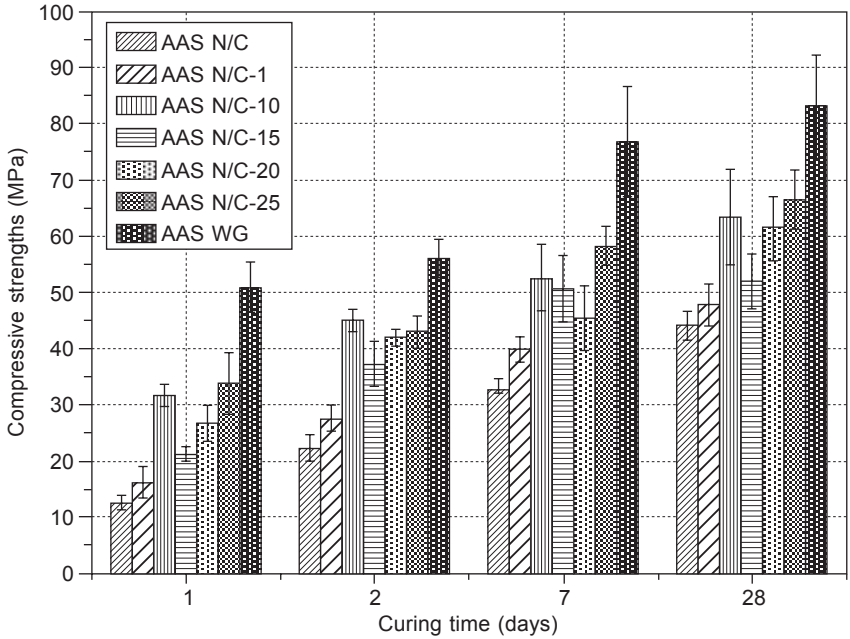

Figure 4.10 Compressive strength of AAS pastes prepared with different alkaline activators (reprinted from Puertas and Torres-Carrasco, 2014, Copyright © 2014, with permission from Elsevier).

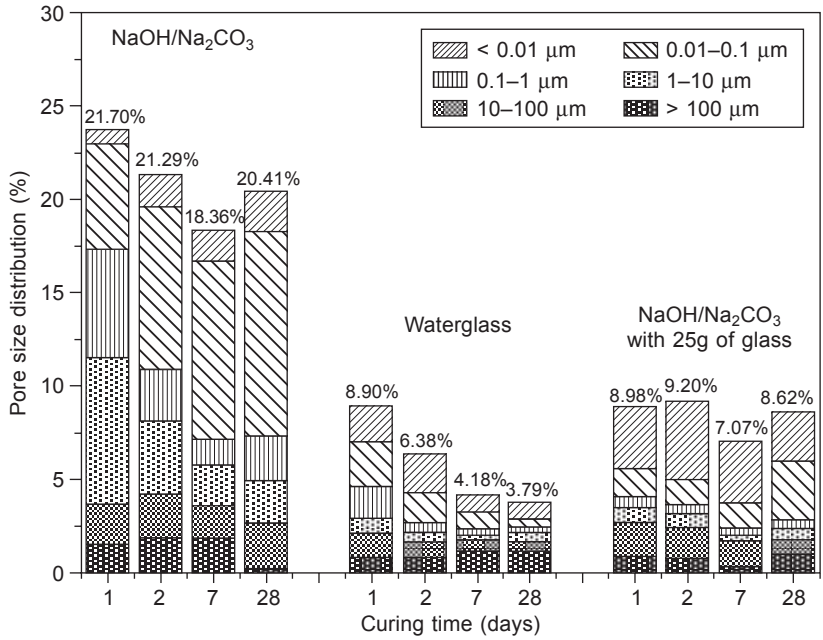

Figure 4.11 Pore size distribution in pastes AAS N/C, AAS WG and AAS N/C-25 (reprinted from Puertas and Torres-Carrasco, 2014, Copyright © 2014, with permission from Elsevier).

The strength values found for paste AAS N/C-25 were observed to lie in between the strength developed by pastes AAS NC and AAS WG, although closer to the latter. The 28-day compressive strength in paste AAS N/C was 44 MPa, in paste AAS WG 83 MPa, and in paste AAS N/C-25 66 MPa. That behaviour is consistent with the known facts that the nature of the alkaline activator is a determinant in alkali-activated slag pastes, mortars and concretes (Palacios and Puertas, 2007; Fernández-Jiménez and Palomo, 2005; Fernández-Jiménez and Puertas, 2003; Wang *et al.*, 1994), and that waterglass-activated materials develop the highest strength. Another determinant in the strength of these materials is the SiO_2/Na_2O ratio in the waterglass solution, whose optimal value stands at around 1.0–1.5 (Wang *et al.*, 1994). According to the solubility data recorded (see Table 4.2), treating 25 g of glass waste in a $NaOH/Na_2CO_3$ solution yielded a solubility of 4.53 g/100 mL, from which the silica ratio in the solution used to prepare paste AAS N/C-25 was calculated to be 0.86. The ratio in paste AAS WG was 1.2. Figure 4.12 shows the relationship between the compressive strength of pastes after 28 days of curing and the modulus of SiO_2/Na_2O in the activators with and without waste glasses. As the modulus of SiO_2/Na_2O increases, the mechanical strength also increases (Wang *et al.*, 1994).

The Hg porosimetry findings concurred with the data reported in the literature (Puertas *et al.*, 2006; Colling and Sanjayan, 2000; Palacios and Puertas, 2007), according to which AAS mortars and concretes prepared with waterglass have

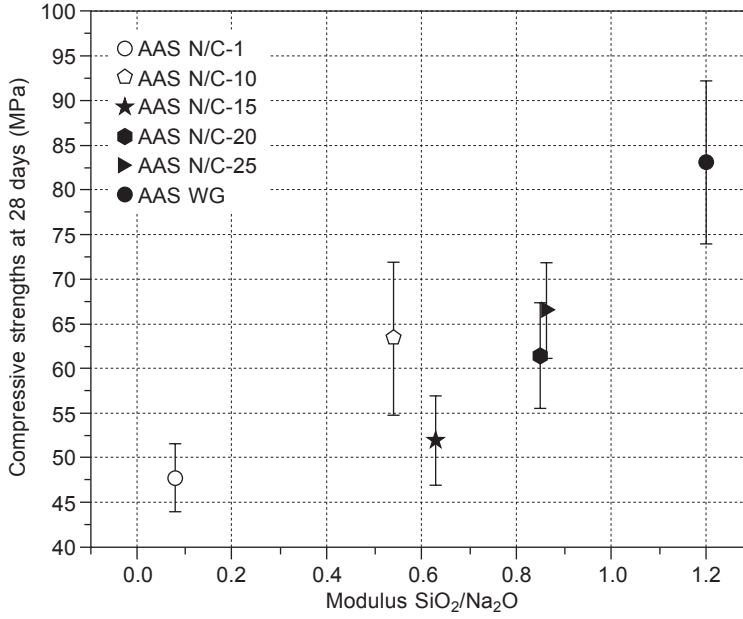

Figure 4.12 Relationship between compressive strength at 28 days of curing and the modulus of SiO_2/Na_2O of activators with and without waste glasses (reprinted from Puertas and Torres-Carrasco, 2014, Copyright © 2014, with permission from Elsevier).

lower total porosity values and greater microporosity than materials prepared with other activators, such as NaOH or $NaOH/Na_2CO_3$. The AAS N/C-25 pastes had total porosity and pore size distribution values closer to the values observed in paste AAS WG than in paste AAS N/C. There is a relationship between porosity and compressive strength values that can be observed in Figure 4.13, whereas the

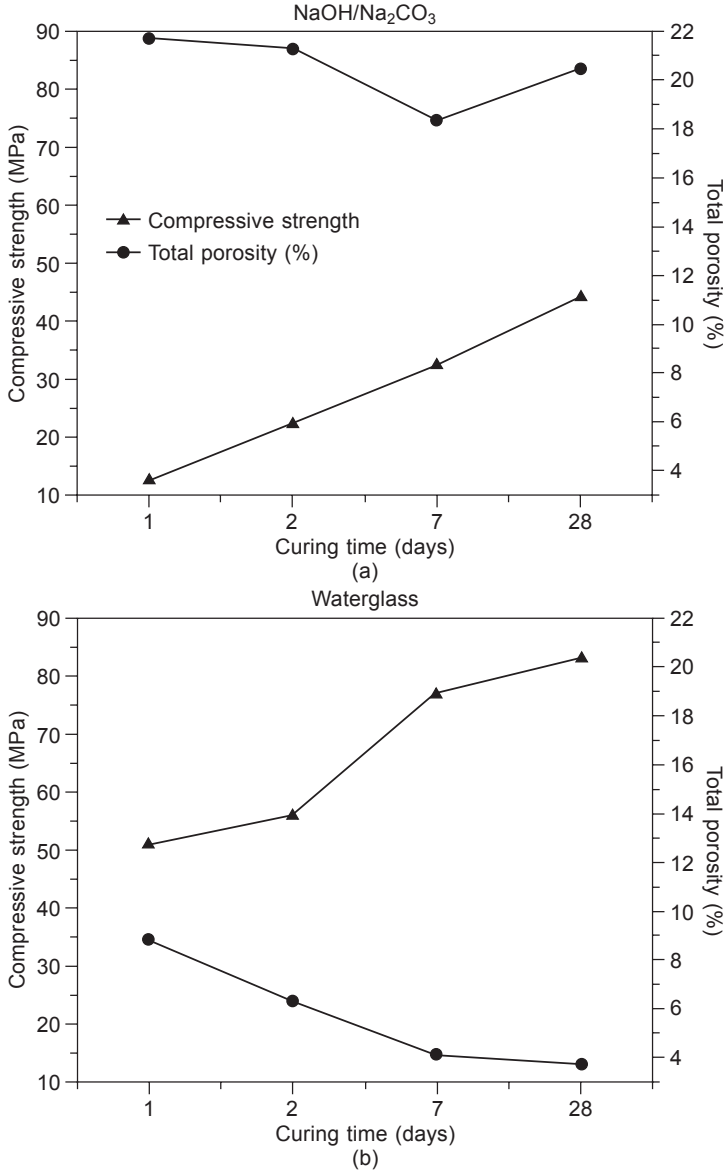

Figure 4.13 (a–c) Relationship between the compressive strength and the total porosity in AAS N/C, AAS WG and AAS N/C-25 (reprinted from Puertas and Torres-Carrasco, 2014, Copyright © 2014, with permission from Elsevier).

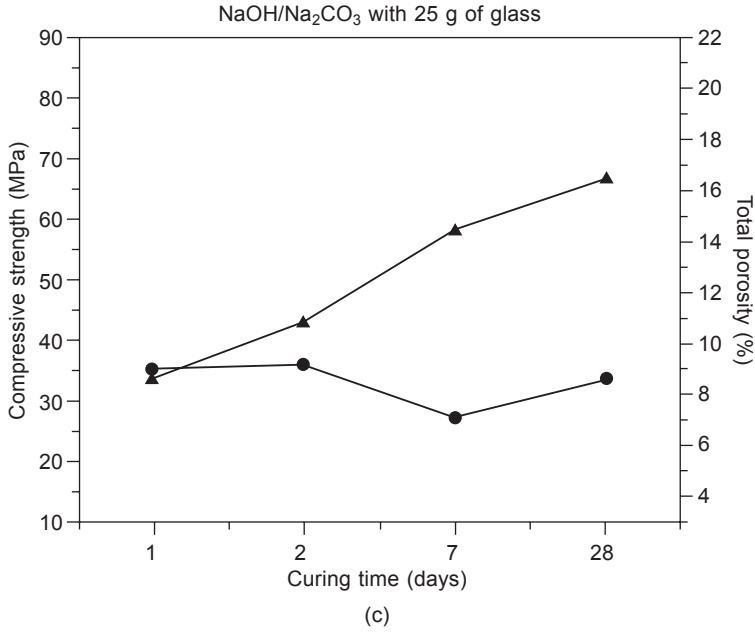

Figure 4.13 Continued

curing time increases the total porosity decrease regardless of the type of solution used (Wang *et al.*, 1994). This behaviour is similar to Portland cement systems.

4.5.3 Characterisation of reaction products: FTIR, XRD, ^{29}Si and ^{27}Al NMR MAS, BSEM/EDX

The characterisation techniques used in this study (FTIR and XRD) confirmed that the main reaction product in paste AAS N/C-25 was a C-A-S-H gel. Various calcium and calcium-sodium carbonates were identified in the pastes prepared with activators having Na_2CO_3 as a component.

The FTIR spectra for the anhydrous slag and the 7-day alkali-activated pastes are shown in Figure 4.14(a). An analysis of these spectra confirmed that reaction products formed as a result of the alkaline activation of the slag. The FTIR spectra for the pastes showed that the Si-O vibration band generated by the SiO_4 groups in the anhydrous slag shifted from 996 cm^{-1} to 961–969 cm^{-1} due to the formation of a calcium aluminosilicate hydrate, a C-A-S-H-type gel (Fernández-Jiménez *et al.*, 2003; Puertas *et al.*, 2004, 2011). The band at around 460 cm^{-1} was attributed to v_4(Si-O-Si) bond vibrations, while the signal at around 669 cm^{-1} was due to the stretching vibrations generated by the Al-O bonds in the AlO_4 groups. The band at 1625 cm^{-1} was the result of the bending vibrations generated by the OH groups in the water. The spectra also contained signals at 1420 cm^{-1} attributed to $v_3(CO_3^{2-})$, while the vibration bands detected between 875 and 711 cm^{-1} were

associated with $\nu_2(CO_3^{2-})$ and $\nu_4(CO_3^{2-})$, respectively, confirming paste carbonation or weathering.

The bands in IR spectra for pastes AAS WG and AAS N/C-25, especially for the Al-O and Si-O vibrations, exhibited similar positions, widths and intensities. The 1300–1500 cm^{-1} range on the IR spectrum for AAS N/C-25 contained absorption characteristics of carbonate groups, which were also identified on the IR spectrum for paste AAS N/C. These bands were attributed to the presence of calcium and calcium-sodium carbonates in the samples (Fernández-Jiménez and Puertas, 2001).

That finding was confirmed by XRD (see Figure 4.14(b)), along with the formation of a C-S-H-type gel (JCPDS 34-0002) and the formation of calcium carbonates (JCPDS 24-27) according to the reflection lines visible on the diffractograms for all the samples. The hydrotalcite ($Mg_6Al_2(CO_3(OH))_{16}{\cdot}4H_2O$) (JCPDS 22-0700) phase was also identified on the XRD patterns for all the pastes at $2\theta = 11.27°$ (Palacios and Puertas, 2011). These XRD findings afforded further proof of the similarity between pastes AAS WG and AAS N/C-25.

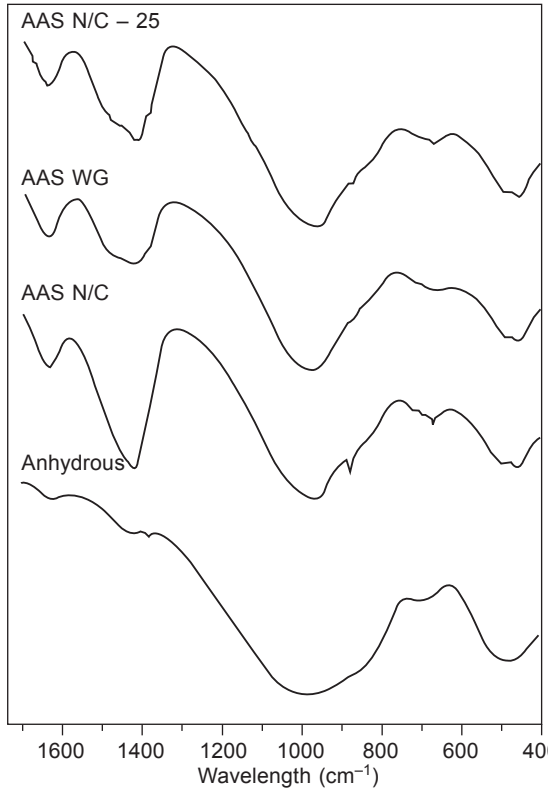

Figure 4.14 (a) FTIR spectra for the anhydrous slag and 7 day pastes; (b) XRD patterns for the anhydrous slag and 7-day pastes (reprinted from Puertas and Torres-Carrasco, 2014, Copyright © 2014, with permission from Elsevier).

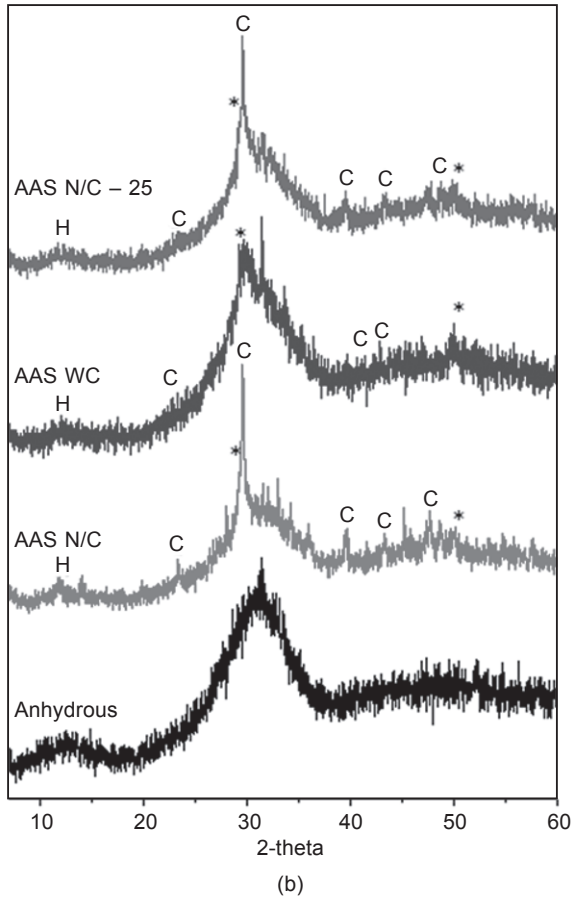

Figure 4.14 Continued

Figure 4.15 shows the ^{29}Si and ^{27}Al MAS NMR spectra for the anhydrous slag and the three 7-day AAS pastes. The identification of the components on the ^{29}Si NMR spectra was based on prior aluminosilicate studies (Schilling *et al*., 1994; Richardson *et al*., 1994; Richardson and Cabrera, 2000; Engelhardt and Michel, 1987). The spectrum deconvolution data are listed in Table 4.4.

The ^{29}Si NMR spectrum for the anhydrous slag exhibited a wide signal at around –75.50 ppm. According to Richardson and Groves (1997), that signal is associated with Q^0 units around –69 ppm, and to Schilling *et al*. (1994), to Q^1 units around –73 ppm. Attributing the signal to Q^1 units would be a sign that the silicate groups present in the slag were organised primarily as dimers. The ^{27}Al MAS NMR spectrum for the anhydrous slag, in turn, had a signal centred on +59.38 ppm associated with the presence of tetrahedrally coordinated aluminium (Al_T = 65.33%). Two smaller signals at around +33.00 and +10.50 ppm, were respectively attributed to pentahedrally (Al_P = 23.19%) and octahedrally (Al_O = 10.98%) coordinated Al (Puertas *et al*., 2011).

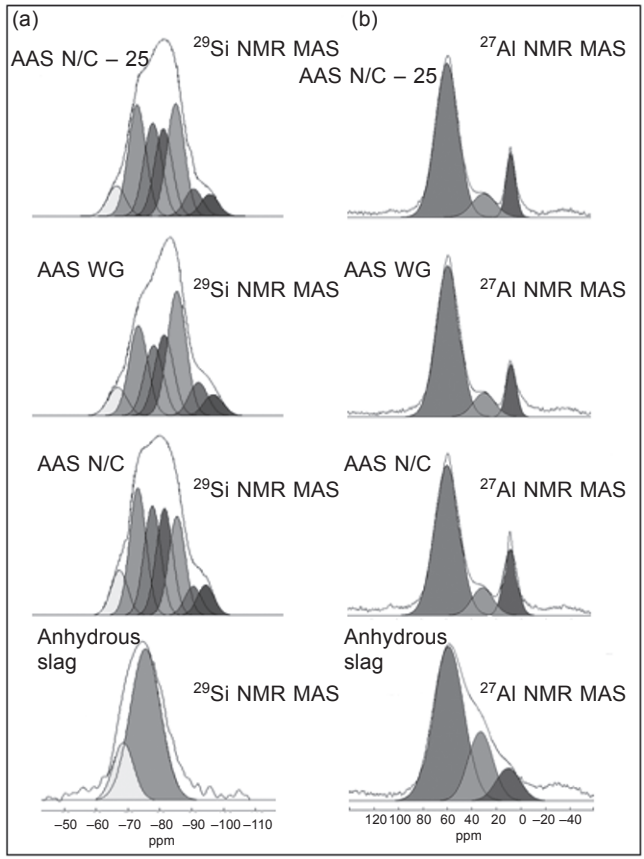

Figure 4.15 (a) ^{29}Si and (b) ^{27}Al MAS NMR spectra for the anhydrous slag and the 7-day alkali-activated pastes (reprinted from Puertas and Torres-Carrasco, 2014, Copyright © 2014, with permission from Elsevier).

The ^{29}Si MAS NMR spectrum for paste AAS N/C contained a wide signal with several peaks (Figure 4.15(a)). Its deconvolution revealed the presence of unreacted Q^0 and Q^1 units from the anhydrous slag. In addition, other signals were detected and attributed to Q^1 (end of chain), Q^2 (1Al), (0Al), Q^3 (1Al) and Q^3(0Al) units (Fernández-Jiménez *et al.*, 2003; Kirkpatrick and Cong, 1994). These units were associated with the formation of C-A-S-H gel, the main reaction product in slag alkali activation (Fernández-Jiménez *et al.*, 2003; Puertas *et al.*, 2011). The same signals were visible on the ^{29}Si MAS NMR spectrum for paste AAS WG, although clearly shifted toward more negative values. Lastly, the shape and deconvolution data for the paste AAS N/C-25 ^{29}Si MAS NMR spectrum were intermediate to the characteristics of the other two pastes.

The ^{27}Al MAS NMR spectra for anhydrous slag and the three pastes (Figure 4.15(b)) exhibited three clearly identified signals. Two were located in a wide, intense and asymmetrical band at around 60 ppm: one centred on around 59 ppm

Table 4.4 Deconvolution data for ^{29}Si and ^{27}Al MAS NMR spectra by the nature of the activator (anhydrous slag and 7-day pastes)

Sample		Q^0 (slag)	Q^0/Q^1 (slag)	Q^1 (end of chain)	Q^2 (1Al)	Q^2 (0Al)	Q^3 (1Al)	Q^3 (0Al)
Slag	Pos. (ppm)	–68.60	–75.50					
	Width	7.62	7.62					
	Integral (%)	20.54	79.46					
AAS N/C	Pos. (ppm)	–67.52	–73.40	–78.05	–81.90	–85.91	–91.07	–95.07
	Width	6.22	6.22	6.22	6.22	6.22	6.22	6.22
	Integral (%)	8.23	23.32	19.98	19.56	18.09	5.27	5.55
AAS WG	Pos. (ppm)	–66.92	–73.59	–78.47	–81.82	–85.86	–92.76	–97.47
	Width	7.05	7.05	7.05	7.05	7.05	7.05	7.05
	Integral (%)	6.26	20.08	15.69	18.05	27.80	7.41	4.71
AAS N/C–25	Pos. (ppm)	–66.59	–73.14	–78.17	–81.56	–85.50	–91.20	–96.30
	Width	6.65	6.65	6.65	6.65	6.65	6.65	6.65
	Integral (%)	6.22	23.06	19.25	18.10	23.30	5.59	4.48

and associated with tetrahedral aluminium (Al_T) and a smaller signal at around 31 ppm due to the presence of pentahedral aluminium (Al_P). A third, less intense but narrower signal, indicating the presence of octahedral aluminium (Al_O), appeared at 8 ppm (Fernández-Jiménez *et al*., 2003; Kirkpatrick and Cong, 1994; Cincotto *et al*., 2003). The Al_T signal at 59 ppm was narrower on the spectra for the AAS WG and AAS N/C-25 pastes than on paste AAS N/C. That, together with the greater intensity of the signal, was an indication that part of the Al_T had been taken up into the structure of the C-A-S-H gel.

The BSEM/EDX study (see Figure 4.16) revealed microstructural differences in the pastes depending on the activator used in their preparation. Further to its micrograph, paste AAS N/C contained substantial quantities of anhydrous slag particles (see Figure 4.16(a)), as well as an open and scantly compact structure. Less anhydrous slag and a more compact and uniform C-A-S-H gel were observed in the paste AAS WG micrograph (see Figure 4.16(b)). The microcracks characteristic of the intense drying shrinkage associated with these pastes were likewise visible (Palacios and Puertas, 2007). The AAS N/C-25 microstructure (Figure 4.16(c)) exhibited intermediate features, with smaller amounts of anhydrous slag than paste AAS N/C but a less uniform morphology than AAS WG. Table 4.5 gives the results of local analyses in different zones of the C-A-S-H gel to determine their Ca/Si ratios, which were found to be around 1 or less.

Further to the present knowledge of the micro- and nanostructure of AAS pastes, the interaction between activating solution and vitreous slag yields C-A-S-H-type gels, whose composition and structure depend on the nature of the alkaline activator (Fernández-Jiménez *et al*., 2003; Puertas *et al*., 2011). When the activator is waterglass or similar, such as the activator prepared here with glass waste, the gel formed has a more condensed structure (longer mean chain length, more aluminium in its composition, more cross-linked or Q^3 units), which is the reason for the greater

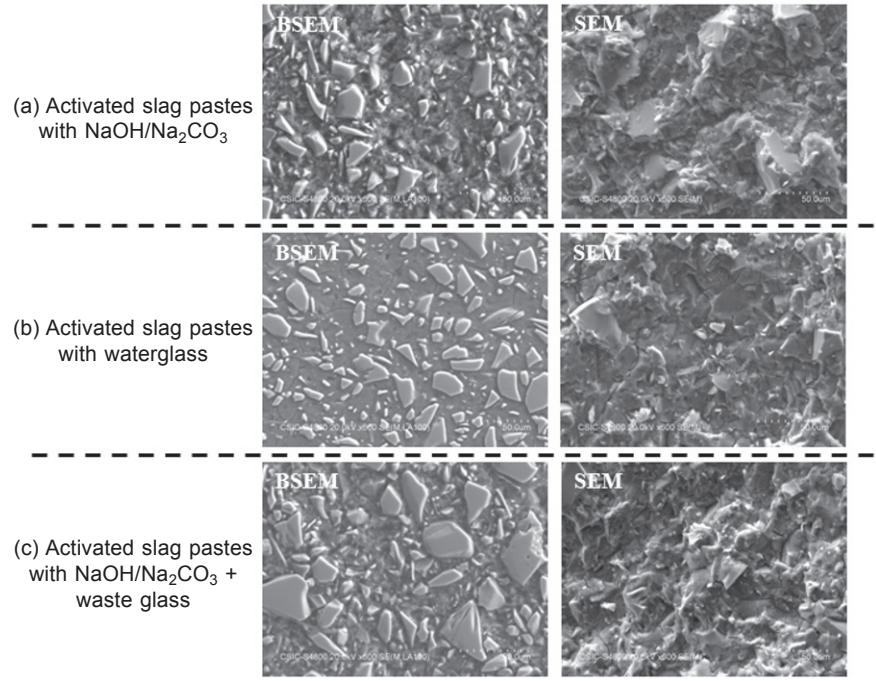

Figure 4.16 BSEM and SEM images of activated slag pastes with: (a) $NaOH/Na_2CO_3$, (b) Waterglass and (c) $NaOH/Na_2CO_3$ + waste glass.

Table 4.5 EDX determination of atomic ratio

Sample	Zone	Number of analyses	Ca/Si	Al/Ca	Al/Si
AAS N/C	C-A-S-H gel	20	1.06 ± 0.07	0.35 ± 0.04	0.37 ± 0.05
AAS WG	C-A-S-H gel	20	0.80 ± 0.05	0.30 ± 0.03	0.24 ± 0.02
AAS N/C-25	C-A-S-H gel	20	0.94 ± 0.07	0.34 ± 0.04	0.31 ± 0.02

microporosity and consequently lower porosity and higher mechanical strength of these systems. In the present study, in terms of composition and structure, the C-A-S-H gel formed in paste AAS N/C-25 was observed to resemble the gel formed in paste AAS WG more closely than the gel in paste AAS N/C. The different SiO_2/Na_2O ratio in the AAS WG and AAS N/C-25 pastes explains the differences observed in the reactivity, structure and composition of the C-A-S-H gels formed (see Tables 4.4 and 4.5).

An analysis of the deconvoluted ^{29}Si and ^{27}Al MAS NMR spectra and the microstructural studies revealed structural and compositional differences among the calcium silicate hydrates formed with the three activators. These differences can be gleaned from Table 4.6, which gives data for the 7-day ^{29}SI MAS NMR spectra. The calcium aluminosilicate hydrate formed in paste AAS WG had a lower $Q^1/\Sigma Q^2$

Table 4.6 ^{29}Si and ^{27}Al MAS NMR parameters in activated pastes, by the activator used

Parameters (%)	AAS N/C	AAS WG	AAS N/C-25
$\alpha = Q^0 + Q_{slag}$ [a]	68.45	73.34	70.72
$\Sigma Q^2/Q_{Total}$ [b]	0.55	0.62	0.58
Q^2 (0Al)/Q^2 (1Al)	0.92	1.54	1.28
$Q^1/\Sigma Q^2$	0.53	0.34	0.46
$\Sigma Q^3/Q^1 + \Sigma Q^2$	0.18	0.20	0.16
MCL (main chain length)	6.74	9.00	7.24

[a]$Q_{slag} = Q^0/Q^1$slag. [b]$Q_{Total} = \Sigma Q^n$ where Q^n stands for Q^1, Q^2 and Q^3 units.

ratio than the same product in the other two pastes. In other words, the former had a greater proportion of Q^2 units and consequently longer tetrahedral silicate chains (around nine tetrahedra, see Table 4.5). Paste AAS WG also had a higher percentage of Q^3 units, denoting more intense inter-chain cross-linking and the formation of layered structures in some areas (Puertas *et al.*, 2011). The ^{27}Al MAS NMR spectra, in turn, revealed a higher Al_T content in this gel. More polymerised C-A-S-H gel structures have low Ca/Si ratios, such as obtained in this study (paste AAS WG had a Ca/Si ratio of around 0.9).

The mean chain lengths of the C-A-S-H gels, found with the Richardson method (Richadrson *et al.*, 1994; Richardson and Cabrera, 2000; Richardson and Groves, 1993; Richardson, 1999) (Table 4.6), were shown to follow the pattern:

AAS Wg < AAS N/C-25 < AAS N/C

The silicon present in the activator has been shown to contribute to the formation of calcium aluminosilicate hydrate in AAS WG paste (Puertas *et al.*, 2004, 2011). The findings for all the trials conducted here showed that the silicon present in glass waste (AAS N/C-25) also favoured the formation of a silicon-rich C-A-S-H gel. The ^{29}Si and ^{27}Al MAS NMR spectra confirmed greater reactivity in these pastes than in paste AAS N/C (from 73.34% to 70.72%, see Table 4.6), as well as more densely polymerised structures with higher $Q^1/\Sigma Q^2$ ratios, a larger proportion of Q^3-type cross-linked units and more Al_T in the gel structure, as deduced from smaller Ca/Si ratios (see Table 4.5).

Again, the differences between the AAS WG and AAS N/C-25 gel structure and composition were due to the difference in the activator SiO_2/Na_2O ratio.

4.6 Conclusions

The analytical findings shown in this work indicate that silicon from waste glasses dissolved in $NaOH/Na_2CO_3$ solutions can induce much the same effects as the silicon in waterglass, so these waste glasses can be used as activators in alkali-activated systems (AAS).

The best conditions of solubility for these waste glasses were when the solution was $NaOH/Na_2CO_3$ (pH = 13.6). Chemical activation at 80 ± 2°C for 6 hours under stirring, delivered the highest SiO_2 and Al_2O_3 solubility, dissolving around 60% of the respective oxides and favoured the partial dissolution of the Si in the glass into its most reactive monomeric form.

The solutions resulting from the treatment of waste glasses acted as alkaline activators, partially dissolving vitreous blast furnace slag and generating compounds and microstructures similar to the products observed in waterglass-AAS pastes. Rheological and fluidity behaviour of these pastes is better than AAS WG ones, whereas the behaviour of these pastes in terms of strength and microstructural development was comparable to the performance observed in AAS pastes prepared with conventional activators.

The present findings show that the composition and structure of the C-A-S-H gels formed in two AAS pastes, one prepared with waterglass and the other with activators containing waste glasses, were similar. The differences observed between their reactivity, mechanical strength and gel nano and microstructure were due to the difference in the activator SiO_2/Na_2O ratios.

Acknowledgements

This work has been funded by the Spanish Ministry of the Economy and Competitiveness under project BIA2010-15516. Thanks to C. Carrillo for her assistance with the ICP analyses and P. Rivilla for her aid with the laboratory trials. Also thanks to C. Rodríguez-Puertas for his rheological trials.

References

Andreola, F., Barbieri, L., Karamanova, E., Lancellotti, I. and Pelino, M. (2008). Recycling of CRT panel glass as fluxing agent in the porcelain stoneware tile production. *Ceramics International* 34, 1289–1295.

Brykov, A.S. and Korneev, V.I. (2008). Production and usage of powdered alkali metal silicate hydrates. *Metallurgist* 52, 11–12.

Chen, G., Lee, H., Young, K.L., Yue, P.L., Wong, A., Tao, T. and Choi, K.K. (2002). Glass recycling in cement production – an innovative approach. *Waste Management,* 22, 747–753.

Chesner, W.H. (1992). Waste glass and sludge frit use in asphalt pavement. In Proceedings of Conference on Utilization of Waste Materials in Civil Engineering Construction, 296–307.

Chesner, W.H., Collins, R.J. and MacKay, M.H. (1997). User Guidelines for Waste and By-product Materials in Pavement Construction, US Department of Transportation, Federal Highway Administration, Publication. FHWA-RD-97-148.

Cincotto, M.A., Melo, A.A. and Repette, W.L. (2003). Effect of different activator types and dosages and relation to autogenous shrinkage of activated blast furnace slag cement.

Proceedings of the 11th International Congress on the Chemistry of Cement. Durban, South Africa, 1878–1888.

Colling, F. and Sanjayan, J.G. (2000). Effect of pore size distribution on drying shrinkage of alkali-activated slag concrete. *Cem. Concr. Res.* 30 (9), 1401–1406.

Criado, M., Fernández-Jiménez, A., Palomo, A., Sobrados, I. and Sanz, J. (2008). Effect of the SiO_2/Na_2O ratio on the alkali activation of fly ash. Part II: ^{29}Si MAS-NMR, Survey. *Microporous and Mesoporous Materials* 109 (1–3), 525–534.

Diamond, S. (1983). On the glass present in low-calcium and high-calcium fly ashes. *Cem. Concr. Res.* 13 (3), 459–463.

Ecovidrio 2012. http://www.ecovidrio.es/

El-Shamy, T.M. and Panteno, C.G. (1977). Decomposition of silicate glasses in alkaline solutions. *Nature*, 266, 704–706.

El-Shamy, T.M., Lewis, J. and Douglas, R.W. (1972). The dependence on the pH of the decomposition of glasses by aqueous solutions. *Glass Technology*, 13, 81–87.

Engelhardt, G. and Michel, D. (1987). *High Resolution Solid State NMR of Silicates and Zeolites*. Wiley, Chichester, UK.

Fernández-Jiménez, A. and Palomo, A. (2005). Composition and microstructure of alkali activated fly ash binder: effect of the activator. *Cem. Concr. Res.* 35, 1984–1992.

Fernández-Jiménez, A., Puertas, F. (2001). Setting of alkali-activated slag cement: influence of activator nature. *Adv. Cem. Res.* 13 (3), 115–121.

Fernández-Jiménez, A. and Puertas, F. (2003). Effect of activator mix on the hydration and strength behavior of alkali-activated slag cements. *Adv. Cem. Res.* 15 (3), 129–136.

Fernández-Jiménez, A., Puertas, F. and Palomo, J.G. (1999). Alkali-activated slag mortars: mechanical strength behavior. *Cem. Concr. Res.* 29, 593–604.

Fernández-Jiménez, A., Puertas, F., Sobrados, I. and Sanz, J. (2003). Structure of calcium silicate hydrates formed in alkaline-activated slag: influence of the type of alkaline activator. *J. Am. Ceram. Soc.* 86 (8), 1389–1394.

Fernández Navarro, J.M. (2003). El vidrio. Consejo Superior de Investigaciones Científicas. Sociedad Española de Cerámica y Vidrio. Madrid.

Gorokhovski, A.V., Escalante-García, J.I., Gashnikova Yu., Nikulina, L.P. and Artemenko, S.E. (2005). Composite materials based on wastes of flat glass processing. *Waste Management*, 25, 733–736.

Goto, J.K. (1955). States of silica in aqueous solution II. Solubility of amorphous silica. *Chem. Soc. Jap. Pure Chem Sect*, 76, 1364–1366.

Iler, R.K. (1979). The Chemistry of Silica. Solubility, Polymerization, Colloid and Surface Properties and Biochemistry. New York: John Wiley & Sons.

Kirkpatrick, R.J. and Cong, X. (1994). An introduction to ^{27}Al and ^{29}Si NMR spectroscopy of cements and concretes. In P. Colombet and A. Grimmer (eds), *Application of NMR Spectroscopy to Cement Science*. Amsterdam: Gordon and Breach Science Publishers, 55–76.

Larosa-Thomson, J., Gill, P., Scheetz, B.E. and Silsbee, M.R. (1997). Sodium silicate applications for cement and concrete. *Proc. 10th Int. Congr. on the Chemistry of Cement*, Gothenburg, 3.3.

Luz, A.P. and Riberio, S. (2007). Use of glass waste as a raw material in porcelain stoneware tile mixtures. *Ceramics International*, 33, 761–765.

McCarthy, G.J., Swanson, K.D. and Steinw and, S.J. (1988). X-ray diffraction analysis of fly ash. *Adv X-Ray Anal.* 31, 331–342.

McLellan, G.W. and Shand, E.B. (1984). *Glass Engineering Handbook*. New York: McGraw-Hill.

Mejía, J.M., Mejía de Gutiérrez, R. and Puertas, F. (2013). Rice husk ash as silica source in fly ash and ground blast furnace slag cementitious alkali activated systems. *Mater. Construcc*, 63, 311.

Palacios, M. and Puertas, F. (2007). Effect of shrinkage-reducing admixtures on the properties of alkali-activated slag mortars and pastes. *Cem. Concr. Res.* 37 (5), 691–702.

Palacios, M. and Puertas, F. (2011). Effectiveness of mixing time on hardened properties of waterglass-activated slag pastes and mortars. *ACI Materials Journal* 108 (1), 73–78.

Palacios, M., Puertas, F., and Banfill, P.F.G. (2006). Effect of organic admixtures on the activation process, rheological and mechanical properties and durability of alkali-activated slag pastes and mortars. In V.M. Malhotra (ed.), *Eighth CANMET/ACI International Conference on Superplasticizers and Other Chemical Admixtures in Concrete*. 345–356.

Palacios, M.; Banfill, P.F.G. and Puertas, F. (2008). Rheology and setting behavior of alkali-activated slag pastes and mortars: effect of organic admixture. *ACI Materials Journal* 105 (2), 140–148.

Palomo, A., Fernández-Jiménez, A. and Criado, M. (2004). Geopolimeros: una única base química y diferentes microestructuras. *Mater. Construcc*. 54, 275.

Partyka, J., Gajek, M. and Gasek, K. (2014). Effects of quartz grain size distribution on the structure of porcelain glaze. *Ceramics International*, http://dx.doi.org/10.1016/j.ceramint.2014.04.044.

Paul, A. (1977). Chemical durability of glasses; a thermodynamic approach. *Journal of Materials Science* 12, 2246–2268.

Puertas, F. (1995). Cementos de escorias activadas alcalinamente: Situación actual y perspectivas de futuro. *Mater. Construcc*. 45 (239), 53–66.

Puertas, F. and Fernández-Jiménez, A. (2003). Mineralogical and microstructural characterization of alkali-activated fly ash/slag pastes. *Cem. Concr. Comp*. 23, 287–293.

Puertas, F. and Torres-Carrasco, M. (2014). Use of glass waste as an activator in the preparation of alkali-activated slag: mechanical strength and paste characterisation. *Cem. Concr. Res*. 57, 95–104.

Puertas, F., Martínez-Ramirez, S., Alonso, S. and Vázquez, T. (2000). Alkali-activated fly ash/slag cement: strength behaviour and hydration products. *Cem. Concr. Res*. 30, 1625–1632.

Puertas, F., Fernández-Jiménez, A. and Blanco-Varela, M.T. (2004). Pore solution in alkali-activated slag cement pastes: relation to the composition and structure of calcium silicate hydrate. *Cem. Concr. Res*. 34, 139–148.

Puertas, F., Palacios, M. and Vázquez, T. (2006). Carbonation process of alkali-activated slag mortars. *J. Mater. Sci*. 41, 3071–3082.

Puertas, F., Palacios, M., Manzano, H., Dolado, J.S., Rico, A. and Rodríguez, J. (2011). A model for the C-A-S-H gel formed in alkali-activated slag cements. *J. Eur. Cer. Soc*. 31, 2043–2056.

Puertas, F., Torres, J.J., Varga, C. and Torres-Carrasco, M. (2012). Spanish patent: Procedimiento para la fabricación de cementos alcalinos a partir de residuos vítreos urbanos e industriales. PCT/ES2012/070408.

Richardson, I.G. (1999). The nature of C-S-H in hardened cements. *Cem. Concr. Res*. 29, 1131–1147.

Richardson, I.G. and Cabrera, J.G. (2000). The nature of C-S-H in model slag-cements. *Cem. Concr. Compos*. 20, 259–266.

Richardson, I.G. and Groves, G.W. (1997). The structure of the calcium silicate hydrate phases present in the hardened pastes of white Portland cement/blast furnace slag blends. *J. Mater. Sci*. 32, 4793–4802.

Richardson, I.G., Brough, A.R., Groves, G.W. and Dobson, C.M. (1994). The characterisation of hardened alkali-activated blast furnace-slag pastes and the nature of the calcium silicate hydrate (C-S-H) phase. *Cem. Concr. Res.* 24 (5), 813–829.

Rodríguez-Puertas, C. (2014). Comportamiento reológico y mecánico de pastas y morteros de cementos eco-eficientes. reutilización de residuos vítreos. Proyecto Fin de Carrera. UPM. Escuela de Ing. Industriales.

Rodríguez-Puertas, C., Torres-Carrasco, M., Alonso, M.M. (2014). Comportamiento reológico, mecánico y microestructural de pastas y morteros de cementos ecoeficientes. XIII Congreso Nacional de Materiales, Barcelona.

Ruiz-Santaquiteria, C., Torres-Carrasco, M., Alonso, M.M. and Puertas, F. (2013). Valorización de residuos vítreos en la elaboración de morteros alcalinos. Workshop on Environmental Impact of Building Construction, Universidad Politécnica de Madrid.

Sánchez, R., Palacios, M. and Puertas, F. (2011). Cementos petroleros con adición de escoria de horno alto: características y propiedades. *Mater. Construcc.* 61 (302), 185–211.

Schilling, P.J., Butler, L.G., Roy, A. and Heaton, H.C. (1994). ^{29}Si and ^{27}Al MAS-NMR of NaOH activated blast-furnace slag. *J. Am. Ceram. Soc.* 77 (9), 2363–2368.

Shi, C. and Zheng, K. (2007). A review on the use of waste glasses in the production of cement and concrete. *Resources Conservation and Recycling*, 52, 234–247.

Shi, C., Wu, Y., Riefler, C. and Wang, H. (2005). Characteristics and pozzolanic reactivity of glass powders. *Cem. Concr. Res.* 35 (5), 987–993.

Shi, C., Kryvenko, P.V. and Roy D. (2006). *Alkali-activated cements and concretes*. Abingdon: Taylor & Francis.

Stanworth, J.E. (1950). Physikalische Eigenschaften und Struktur von Gläsern. *Glastech* 23, 297–304.

Torres, J.J., Palacios, M., Hellouin, M. and Puertas, F. (2009). Alkaline chemical activation of urban glass to produce cementitiuous materials. *1ª Conferencia sobre Reciclado de Materiales y Eco-Energía (RECIMAT 09),* 110–114.

Torres-Carrasco, M., Puertas, F. and Blanco-Varela, M.T. (2012). Preparación de cementos alcalinos a partir de residuos vítreos. Solubilidad de residuos vítreos en medios fuertemente básicos. *XII Congreso Nacional de Materiales*, Alicante.

Torres-Carrasco, M., Palomo, J.G. and Puertas, F. (2014). Sodium silicate solutions from dissolution of glass wastes: statistical analysis. *Mater. Construc.* 64, 314.

Van Deventer, J.S.J., Provis, J.L., Duxson, P. and Bride, D.G. (2010). Chemical research and climate changes as drivers in the commercial adoption of alkali activated materials. *Waste Biomass Valor.* 1, 145–155.

Van Deventer, J.S.J., Provis, J.L. and Duxon, P. (2012). Technical and commercial progress in the adoption of geopolymer cement. *Minerals Engineering*, 29, 89–104.

Van Roode, M., Douglas, E. and Hemmings, R.T. (1987). X-ray diffraction measurement of glass content in fly ashes and slags. *Cem. Concr. Res.* 17 (2), 183–197.

Varga, C., Alonso, M.M. and Puertas, F. (2013). Alkali-activated cement paste rheology: effect of superplasticisers. *7th RILEM Conference on Self-Compacting Concrete*, Paris.

Wang, S.D., Scrivener, K.L. and Pratt, P.L. (1994). Factors affecting the strength of alkali-activated slag. *Cem. Concr. Res.* 24 (6), 1033–1043.

Zachariasen, W.H. (1932). The atomic arrangement in glass. *J. Am. Chem. Soc.* 54, 3841–3851.

This page intentionally left blank

Part Two

The properties of alkali-activated cement, mortar and concrete binders

This page intentionally left blank

Setting, segregation and bleeding of alkali-activated cement, mortar and concrete binders

5

P. Chindaprasirt[1], *T. Cao*[2]
[1]Khon Kaen University, Khon Kaen, Thailand; [2]Surface Design Consulting Pty Ltd, Sydney, NSW, Australia

5.1 Introduction

Alkali-activated cements/binders (Wang, 1991; Shi *et al*., 2006; Pacheco-Torgal *et al*., 2008) consist of two components: cementitious components (starting materials) and alkaline activators. The cementitious components are aluminosilicate materials and are either natural or artificial pozzolans. Artificial pozzolans include 'industrial by-products' such as granulated blast furnace slag, granulated phosphorus slag, steel slag, coal fly ash, silica fume and non-ferrous slags, and 'burnt materials' such as metakaolin and rice husk ash. Natural pozzolans include volcanic glasses such as volcanic ash and pumice; volcanic tuffs such as zeolites; and siliceous pozzolans such as opal and diatomaceous earth.

Commonly used supplementary cementitious materials (Pacheco-Torgal *et al*., 2008; Siddique and Khan, 2011) such as ground granulated blast furnace slag, metakaolin and fly ash are the most popular cementitious components in alkali-activated cement systems for various reasons, including the favourable mechanical properties achievable with these starting materials.

Ground granulated blast furnace slag (GGBFS) is a pozzolanic material generated from the by-product of the blast furnaces used to make iron. Molten slag, one of the two products produced when iron ore, coke and limestone melt in the blast furnace, comprises mostly silicates and alumina. The molten slag is tapped from the blast furnace and rapidly quenched through high pressure water jets. This forms granular particles generally smaller than 5 mm diameter comprising approximately 95% non-crystalline calcium-aluminosilicates (National Slag Association, 2013). The granulated slag is then dried and ground to a very fine powder. Basic requirements and classification of GGBFS for use in concrete are prescribed in ASTM C989/C989M-12a (2012).

Metakaolin is a dehydroxylated form of kaolinitic clay obtained by calcination at a temperature between 500°C and 800°C (Siddique and Khan, 2011). When appropriately treated at this temperature, kaolinite becomes metakaolin which has two-dimensional order in crystal structure. Physically, metakaolin is an off-white

Handbook of Alkali-activated Cements, Mortars and Concretes. http://dx.doi.org/10.1533/9781782422884.2.113

powder with extremely small particle size. The average particle size is usually in the range of about 3–5 μm. Chemically, metakaolin consists of SiO_2 and Al_2O_3 with smaller amounts of other elements such as iron oxides, calcium oxides, magnesium oxide and potassium oxide. The relevant standard providing the requirements for metakaolin for use in concrete is ASTM C618-12a (2012).

Fly ash is produced from burning of pulverized coal in an electric power generating plant. During combustion of the coal, other mineral constituents such as clay, feldspar, quartz and shale fuse and while in the suspension state with exhaust gas escape the combustion chamber. The fused particles cool and solidify into spherical particles and are trapped by bag filters or electrostatic precipitators. Fly ash particle size is primarily dependent upon the type of dust collection equipment. The chemical composition of fly ash is determined by the source and make-up of the coal(s) being burned. Generally, fly ash contains a substantial amount of SiO_2 in both amorphous and crystalline forms, aluminium oxide and calcium oxide. Basic requirements and classification of fly ash for use in concrete are prescribed in ASTM C618-12a (2012).

There are a wide range of alkaline activators used in alkali-activated cement systems. They have been classified into six groups (Glukhovsky *et al.*, 1980) as shown below where M is an alkali ion:

1. alkalis, MOH
2. weak acid salts, M_2CO_3, M_2SO_3, M_3PO_4, MF
3. silicates, $M_2O.nSiO_3$
4. aluminates, $M_2O.nAl_2O_3$
5. aluminosilicates, $M_2O.Al_2O_3.(2\text{-}6)\ SiO_3$, and
6. strong acid salts, M_2SO_4.

The most commonly used alkaline activators are mixtures of sodium or potassium hydroxide (NaOH, KOH) with sodium waterglass ($nSiO_2.Na_2O$) or potassium waterglass ($nSiO_2.K_2O$) with relatively high SiO_2-to-M_2O ratio.

Alkali-activated cements can be classified into five main categories (Shi *et al.*, 2011) using the main cementitious components as a criterion as follows:

1. alkali-activated slag-based cements
2. alkali-activated pozzolan cements (including alkali-activated fly ash cement, alkali-activated metakaolin cement)
3. alkali-activated lime-pozzolan/slag cements
4. alkali-activated calcium aluminate blended cements, and
5. alkali-activated Portland blended cements (hybrid cements).

Brief descriptions of the main characteristics of these alkali-activated cements can readily be found in the literature (Roy, 1999; Pacheco-Torgal *et al.*, 2008; Davidovits, 2011).

5.2 Setting times of cementitious materials and alkali-activated binder systems

Setting times of cementitious materials and alkali-activated binder systems are usually given as initial setting time and final setting time. Initial setting time is of practical importance since it is an indicator of the time available for transit, placing, compacting (if required) and finishing. Setting times are defined as times when the material will just withstand a prescribed pressure or resist penetration to a prescribed depth. Setting times of cement paste are usually determined using the Vicat needle method specified in ASTM C191-08 (2008) or equivalent standards. Setting times of mortars and concrete are commonly determined using methods specified in ASTM C807-08 (2008) and ASTM C403/C403M-08 (2008), respectively.

Similar to the case of Portland cement and blended cements, setting characteristics of alkali-activated materials depend strongly on the characteristics and the composition/formulation of the systems. The setting characteristics of alkali-activated binders based on slag, metakaolin and fly ash are significantly different from each other. This is also applicable when the alkali-activated binders are made from the same type of starting materials but from different sources. This is a result of the connection between setting time and the nature of the reaction products formed between the starting material and the alkaline activator(s) used (Fernández-Jiménez and Puertas, 2001). In this section, setting characteristics of some alkali-activated cements are discussed.

5.2.1 Alkali-activated GGBFS cements

Calorimetric studies of early hydration of alkali slag cements (Shi and Day, 1995; Fernández-Jiménez and Puertas, 1997) indicate that there are three classes/patterns of heat evolution curves as shown in Figure 5.1.

1. Type I curves show one early initial small heat evolution peak with no other peaks detected in the first 3 days. This pattern is observed for mixtures of slag and Na_2HPO_4 solution at 25 and 50°C. When observed, the mixture is either very slow to set or does not set at all.
2. Type II heat evolution curves of alkali slag cements are very similar in pattern to that of Portland cement including one initial peak followed by an induction period and one accelerated hydration peak after that. This pattern is commonly observed for NaOH-activated slag cement or with activators with high pH values.
3. Type III heat evolution curves have three peaks with two peaks occurring before the induction period. This pattern is commonly observed with slag activated by Na_2SiO_3. The first peak is attributed to the wetting and initial dissolution of the slag particle. The second initial peak is attributed to the reaction between dissolved Ca^{2+} from slag and anions/anion groups from activators including the initial formation of calcium silicate hydrate (C-S-H) due to Ca from slag and silicate anions from the activator (Brough and Atkinson, 2002). This reaction and the corresponding reaction products are the key elements affecting the setting times of this group of alkali-activated slag cements (Fernández-Jiménez and Puertas, 2003), particularly the initial setting time of the mix. The timing of the last peak-hydration peak of slag is related primarily to the final setting time.

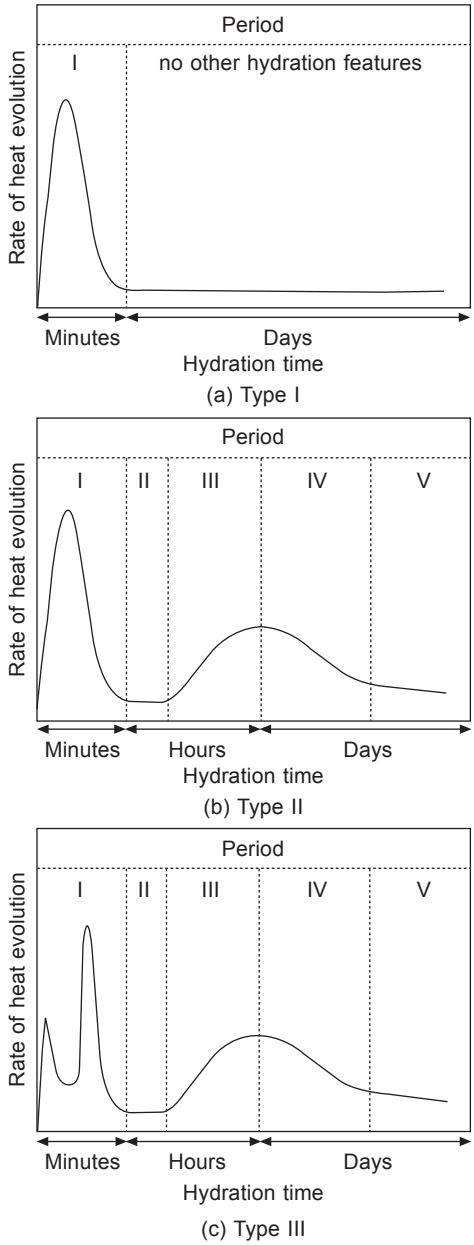

Figure 5.1 (a–c) Hydration models of alkali-slag cements (reprinted from Shi and Day, 1995, Copyright © 1995), with permission from Elsevier).

Initial and final setting times of alkali-activated slag cement pastes (using activators with 3% of Na_2O by mass of the slag) were reported as 2h 20min and 4h 45min for waterglass activator; 3h 40min and 4h 40 min for sodium hydroxide activator;

and greater than 3 days for sodium carbonate activator (Andersson and Gram, 1987). The Blaine fineness of the slag does not appear to affect the setting times of alkali-activated slag cement greatly in the range of 350–530 m^2/kg (Andersson and Gram, 1987). However, a very sharp reduction in setting times is noted when the slag fineness is increased from 530 to 670 m^2/kg and tested with various activators, namely, 6% $Na_2O.0.9SiO_2$ and $Na_2O.3.35SiO_2$; 5% Na_2CO_3; and 5% NaOH. Setting time of alkali-activated slag is also influenced by the basicity [(CaO+MgO)/SiO_2] of the slag. Higher basicity will likely result in shorter setting times regardless of the nature of activators used (Krivenko, 1992).

As indicated earlier, $Na_2O.nSiO_2$-activated slag cements tend to exhibit shorter setting time than either NaOH- or Na_2CO_3-activated slag cements, noting that setting times usually decrease with increased activator dosage as shown in Figure 5.2 (Chang, 2003). Increase in the modulus of liquid sodium silicate (Bakharev *et al.*, 1999) commonly results in decrease in initial and final setting times. When solid sodium silicate is used, the trend is somewhat reversed (Peng, 1982, cited in Shi *et al.*, 2006). This has been attributed to the decreased dissolution rate and solubility of sodium silicate glass with increased modulus.

The combination of two or more activators can drastically change the setting characteristics of alkali-activated slag. For example, the addition of 1.3% K_2SO_4 to 4% NaOH-activated slag cement can lead to an increase in initial setting time of 34 min to about 100 min (Chen and Liao, 1992). The setting times of liquid waterglass-

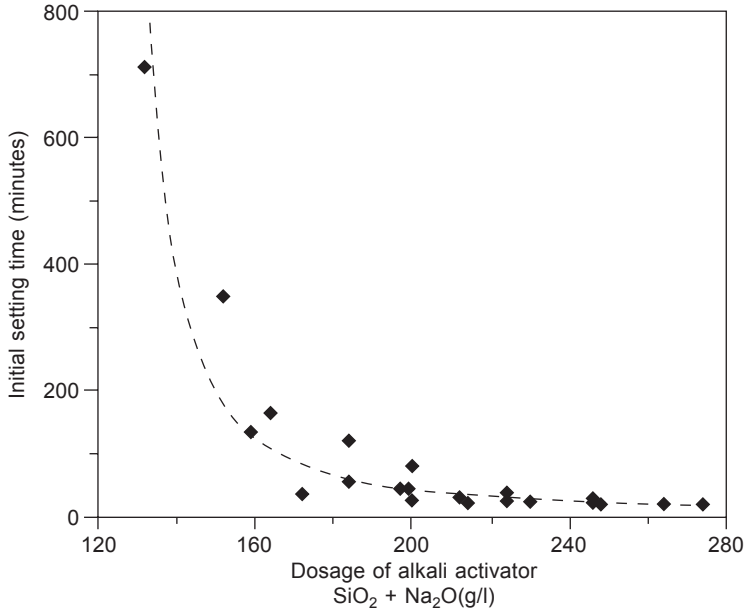

Figure 5.2 Influence of sodium silicate-based alkali activator dosage on initial setting time of alkali-activated slag cements (reprinted from Chang, 2003, Copyright © 2003, with permission from Elsevier).

activated slag can also be increased by addition of K_2CO_3 (Gu, 1991, cited in Shi *et al.*, 2006). Similar observations have been made when phosphoric acid is used at a dosage greater than 0.84 M in the mixing water of sodium silicate-activated slag cement (Chang, 2003). For the retarding effect, several additives have also been investigated as set retarders for alkali-activated slag cements. They include potassium sodium tartrate, molasses (Wu *et al.*, 1993, cited in Shi *et al.*, 2006) and malic acid (Brough *et al.*, 2000).

5.2.2 Alkali-activated metakaolin

Metakaolin is different from GGBFS in many respects (Duxson *et al.*, 2007; Duxson and Provis, 2008; Provis and van Deventer, 2009; Li *et al.*, 2010; Rashad, 2013); the notable ones are as follows.

1. The glassy phase of GGBFS is formed by melting and rapid cooling. In the case of metakaolin, the crystalline structure is broken down to form amorphous phase by calcinations at a temperature lower than that necessary to generate liquid phase and produce glass on cooling.
2. The major components of GGBFS (ACI 233R-03, 2003; ASA, 2011) are CaO (32–45%), SiO_2 (32–42%), Al_2O_3 (7–16%) and MgO (5–15%), while the main components of metakaolin (Ambroise *et al.*, 1994; Wild *et al.*, 1996; Tafraoui *et al.*, 2009) are SiO_2 (51–58%), and Al_2O_3 (35–41%) with CaO usually about 1% or less.
3. The reaction mechanism of alkali activation of metakaolin is different from that of alkali activation of GGBFS due to the high content of CaO in the glass structure and its influence in the hydration process. The reaction of metakaolin/sodium activator mixture system involves the formation of sodium aluminate silicate hydrate (N-A-S-H) gel (De Silva and Sagoe-Crentsil, 2008).

Activators commonly used for activation of metakaolin are a mixture of sodium hydroxide and (liquid) sodium silicate solution since this can produce materials with higher mechanical strength than that activated with either sodium hydroxide or sodium silicate only (Blanco-Varela *et al.*, 2007). The mixture is commonly selected and formulated for better mechanical properties with SiO_2/Al_2O_3 in the range of 3.0–3.8 and Na_2O/Al_2O_3 of approximately 1.0 (Rowles and O'Connor, 2003).

It has been indicated that alkaline activation of metakaolin for use as cementitious material is an exothermic process having three steps: an initial and fast step of dissolution followed by an induction period and finally an exothermic step (Granizo *et al.*, 2000) of precipitation of cementitious materials/polycondensation of hydrolysed aluminate and silicate species (Davidovits, 1994; Weng *et al.*, 2002). Similarly to alkali-activated slag, the material is in a plastic state for most if not all of the induction period. After the final exothermic step, the material is hardened.

Published results of isothermal calorimetry studies shown in Figure 5.3 (Muñiz-Villarreal *et al.*, 2011) indicate that the setting times of metakaolin activated with NaOH and waterglass are extended at temperatures below 30°C. At temperatures above 30°C, the setting times of alkali-activated metakaolin are 'compatible' to that of normal cement when the SiO_2/Al_2O_3 molar ratio of 3.8 (or slightly higher)

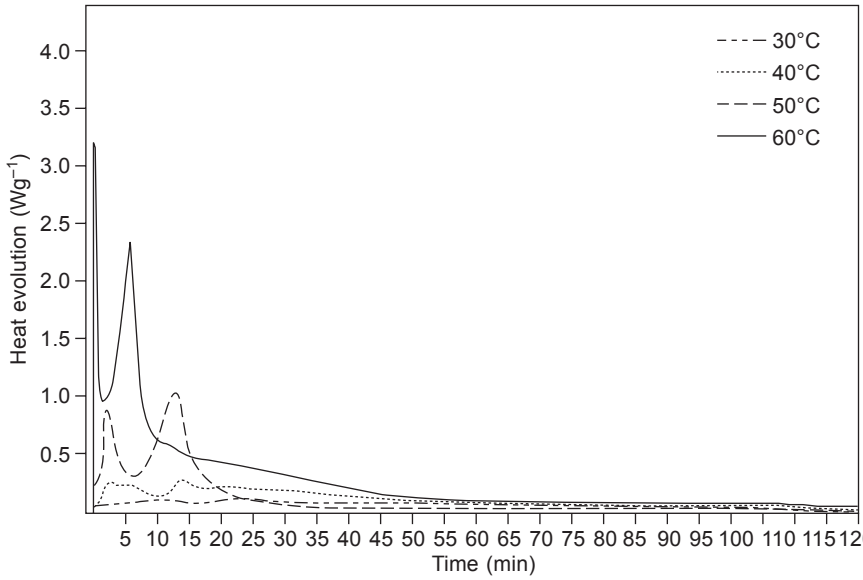

Figure 5.3 Iso-thermal heat evolution curves for a metakaolin activated with NaOH and waterglass at different temperatures (reprinted from Muñiz-Villarreal *et al.*, 2011, Copyright © 2011, with permission from Elsevier).

is maintained in the mix and the optimum strength development is obtained with SiO_2/Al_2O_3 molar ratio of 3.4–3.8 (De Silva and Sagoe-Crentsil, 2008). At the range of SiO_2/Al_2O_3 molar ratio of 2.5–5.0, the setting time increases with the increasing SiO_2/Al_2O_3 ratio. The same authors suggested that the Al appears to play a major role in controlling the setting characteristics of metakaolin/NaOH/sodium silicate systems as the rate of condensation between silicate species is slower than that between aluminate and silicate species, therefore setting occurs later with increasing Si content.

These results suggest strongly that by formulating an appropriate mixture of alkali-activated metakaolin, desirable strength and setting time of the mix can be achieved under the selected curing regime/temperature. The optimum curing temperature of alkali-activated metakaolin was found to be approximately 60°C which gave the best geo-polymerization process (Muñiz-Villarreal *et al.*, 2011). However, it was also found that treatment of fresh mixture at high temperature accelerated setting and strength development but also led to lower 28-day mechanical properties and increases in pore size and pore volume of the paste (Rovnaník, 2010). Setting times (and compressive strengths) are also affected by the specific surface area of metakaolin activated by NaOH/sodium silicate. The higher the specific surface area of metakaolin, the quicker is the setting time (Weng *et al.*, 2005). Activated lime-metakaolin cements had also been studied (De Silva and Glasser, 1992a, 1992b). Studies of setting times of lime-metakaolin cement with different activators (Jiang,

1997) indicated that Na_2SO_4-activated lime-metakaolin cement showed much longer setting times than those of NaOH- and Na_2CO_3-activated cements.

5.2.3 Alkali-activated fly ash

Both Class F (Palomo *et al.*, 1999; Hardjito *et al.*, 2004; Duxson *et al.*, 2007) and Class C fly ashes (Chindaprasirt *et al.*, 2007; Guo *et al.*, 2010; Chindaprasirt *et al.*, 2011) as per ASTM C618-12a (2012) can be used as cementing materials in alkali-activated cements. Class F fly ash is required to have a high content of SiO_2 + Al_2O_3 + Fe_2O_3 of 70% minimum and is generally low in CaO (usually around 3–5%). Class F fly ash has pozzolanic properties. Class C fly ash is a fly ash with a lower requirement of SiO_2 + Al_2O_3 + Fe_2O_3 content and usually contains a relatively high CaO content. Class C fly ash has some cementitious properties in addition to pozzolanic properties.

According to the literature (Diaz *et al.*, 2010; Diaz-Loya *et al.*, 2011), factors such as particle size distribution, degree of vitrification and location of the glass diffraction maximum (which is related to the analytical CaO content) strongly affect both fresh and hardened properties of the resulting alkali-activated cements/geopolymers. Setting times of fly ash-based geopolymers appear to be significantly quickened with increased CaO content (Temuujin *et al.*, 2009; Diaz *et al.*, 2010) as shown in Figure 5.4. For Class F fly ash, particularly coarse size fly ashes, the setting times of the alkali-activated cement at temperatures lower than 30°C are extended and can be longer than 1 day. Curing of alkali-activated Class F fly ash is therefore commonly carried out at high temperatures within the range of 40–90°C. At normal temperature, fresh Class F fly ash can be handled (placed, compacted and

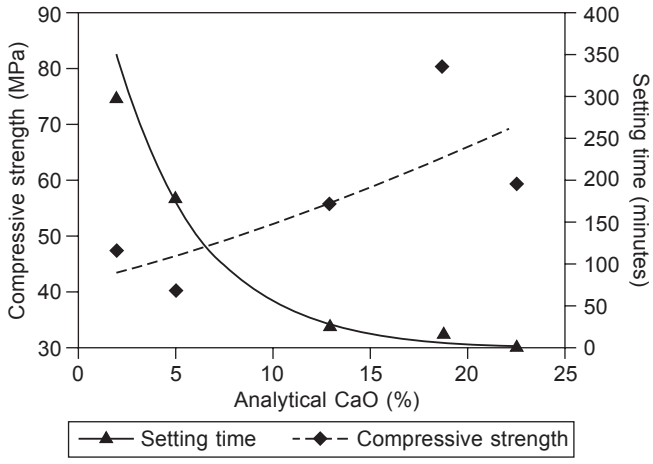

Figure 5.4 Influence of CaO content of fly ash on the setting time and compressive strength of fly ash-based geopolymer (reprinted from Diaz *et al.*, 2010, Copyright 2010, with permission from Elsevier).

finished) up to two hours without indication of setting or evidence of degradation in the compressive strength (Hardjito, 2005).

The curing temperature has a significant effect on the activation kinetics of Class F fly ash-based alkali-activated cements (Chithiraputhiran and Neithalath, 2013). At room temperature, the main reaction product of alkali-activated fly ash is an amorphous aluminosilicate gel with a 3D structure but it is short range ordered. As temperature increases, a metastable intermediate Al-rich phase is formed at an early stage which then evolves into a more stable Si-rich phase – zeolite precursor with time (Palomo *et al.*, 2004). Zeolite crystallization may happen in the long term as the final stage of alkali-activated fly ash. The typical molar ratios of hydration products of Class F fly ash are approximately Si/Al = 1.5 and Na/Al = 0.48; and Si/Al = 2.8 and Na/Al= 0.46 for NaOH activator and NaOH/sodium silicate activator, respectively. A summary of hydration products of alkali-activated fly ashes (Class F) under different curing conditions can be found in the literature (Krivenko and Kovalchuk, 2002).

When Class C fly ash is used, calcium silicate hydrate (C-S-H) (Chindaprasirt *et al.*, 2012; Somna *et al.*, 2011), calcium aluminate silicate hydrate (C-A-S-H) (Garcia-Lodeiro *et al.*, 2011) and traces of calcium alumino silicate zeolite (Guo *et al.*, 2010) can be found. The rapid formation of C-S-H has been attributed to the rapid setting characteristics of the alkali-activated Class C fly ash cement (Rattanasak *et al.*, 2011) which can be 1–2 hours at room temperature. Recent research (Garcia-Lodeiro *et al.*, 2011; Chindaprasirt *et al.*, 2012) indicates that in addition to the calcium content, the SiO_2/Al_2O_3 has a critical influence on the setting characteristics, and the initial precipitation of C-A-S-H may be another key factor regulating the setting time. In the Class C fly ash/NaOH/sodium silicate system, the increases in both SiO_2 and Al_2O_3 shortens setting time as shown in Figure 5.5 due to the involvement of Ca^{2+} in the setting time with formation of C-A-S-H gel. The C-A-S-H gel is stable at high pH (over 12) environments and is, therefore, dominant in the setting process, whereas N-A-S-H gel formation is possible at lower pH (9–12) and is secondary in this system (Chindaprasirt *et al.*, 2012). The strength of the class C fly ash/NaOH/sodium silicate system is also related to the amount of SiO_2 and Al_2O_3.

With regard to setting characteristics, the issues facing alkali-activated Class C fly ash is short setting times (when rapid setting is not required), whereas extended setting time is a concern for alkali-activated Class F fly ash at room temperature. This can be resolved in practice by blending with other pozzolans such as ground GGBFS and selecting suitable activators. To adjust the setting characteristic of alkali-activated fly ash, the use of accelerator and retarder is also practised. Lee and and Deventer (2002) examined the incorporation of inorganic salt addition on the setting characteristics of KOH/sodium silicate-activated Class F fly ash pastes. Setting was accelerated by Ca and Mg salts through solid dissolution. The authors also found that potassium salts delayed setting only when the initial activated solution was low in soluble silicate. Furthermore, the right composition of Cl, CO_3 and NO_3 salts could retard setting. For Class C fly ash, some of the normal accelerators and retarders are applicable. Addition of the proper amount of sucrose efficiently delays the setting time of alkali-activated high calcium fly ash paste with no adverse effect

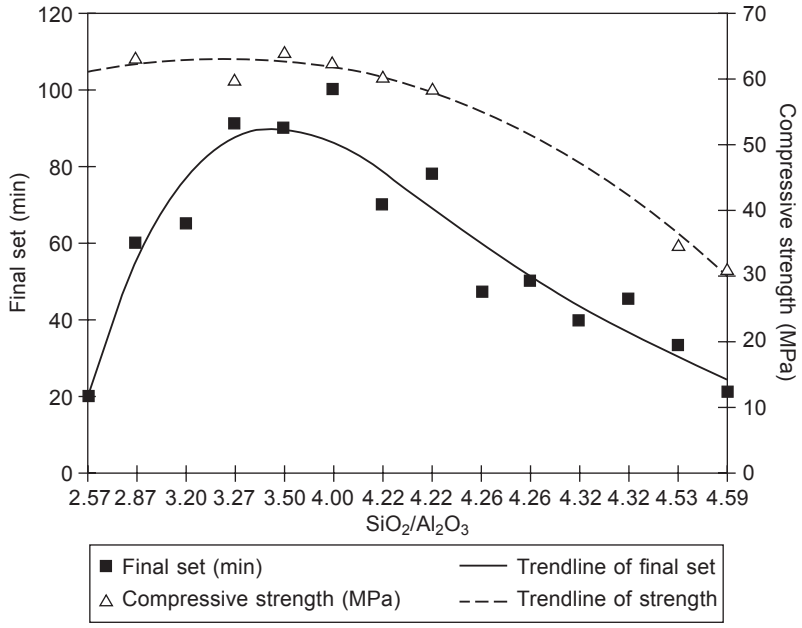

Figure 5.5 Final set and strength of Class C fly ash/NaOH/sodium silicate cement with various SiO_2/Al_2O_3 ratios (reprinted from Chindaprasirt *et al.*, 2012, with kind permission from Springer Science and Business Media).

on strength. Addition of 1 and 2% sucrose could delay final setting time from 130 min to 210 and 230 min, respectively (Rattanasak *et al.*, 2011). On the other hand, addition of 1 and 2% $CaCl_2$ in the system could accelerate the setting with reduction of final setting times from 130 min to 60 and 45 min, respectively.

5.3 Bleeding phenomena in concrete

Bleeds of concrete are commonly evaluated by:

1. monitoring reduction in height of a sample of undisturbed concrete,
2. measuring the amount of bleed water rising to the surface of an undisturbed sample; this is measured after drawing off with a pipette as per ASTM C232/C232M-12 (2012), and
3. observing the mix under test such as ASTM C1611/C1611M-09be1 (2009) for visual stability index.

These methods could be applied in the case of alkali-activated binder as well.

Alkali-activated paste, mortar and concrete are multiphase mixtures of components of varying densities. With such a mixture, gravity is an enemy of homogeneity. For cementitious materials, gravity-induced homogeneities are commonly divided into two categories depending on the phase that is migrating: bleeding and segregation

(Kovler and Roussel, 2011). Bleeding is concerned with water migration, whereas segregation is concerned with the movement of the coarsest particles. Both are induced by density difference segregation (Kovler and Roussel, 2011). It should be noted that for cementitious materials, bleeding is not strictly the settlement of cement grains but is a consolidation process, i.e. the upward movement of water or solution through a dense network of interacting cementing material grains (Tan *et al*., 1987; Josserand *et al*., 2006). The key factors influencing bleeding are therefore the interactions between cement grains, permeability of the fresh cement paste and the viscous nature of the fluid. In practical terms, bleeding exhibits as an accumulation of water at the surface of paste, mortar and concrete.

For alkali-activated cements, there have not been any reports indicating that concretes made with this type of cements are prone to excessive bleed under handling, compaction and vibration. For alkali-activated slag, it is known that the slag pastes show higher apparent viscosity and yield stress than those without alkaline activators (Jiang, 1997). In addition to this, the slump loss of alkali-activated slag paste is generally higher than that of Portland cement (Jolicoeur *et al*., 1992) (except when solid sodium silicate is used) suggesting the viscosity and yield stress of the alkali-activated slag cement increase with time more prominently than those of conventional cement paste. The overall picture is that since the alkali-activated slag pastes are generally cohesive/sticky, the susceptibility of the alkali-activated slag cement concrete to excessive bleed should not be a concern for well-designed concrete mixes in comparison to Portland cement concrete mixes. This has been experimentally confirmed and reported (Collins and Sanjayan, 1999). It should be noted that the lack of bleed of alkali-activated slag cement concrete (in conjunction with drying shrinkage (Chi *et al*., 2012) may contribute to the occurrence of cracking/microcracking (Collins and Sanjayan, 2001; Puertas *et al*., 2003) observed on the surface when there is lack of moist curing. This is an issue to be considered for practical application of the alkali-activated slag cement concrete. Workability of alkali-activated slag cement concrete is strongly dependent on the activator modulus (Law *et al*., 2012). Higher activator modulus results in sticky concrete mix with lower slump. Lower activator modulus results in higher slump concrete with an increased rate of bleeding. The use of set retarding admixture in the mix would also lead to increased bleed (Collins and Sanjayan, 1998).

Alkali-activated Class F fly ash concretes normally show cohesive characteristics. However, when the concretes are subjected to prolonged mixing time, mixtures with high water content show bleed and segregation followed by exhibition of low compressive strength (Hardjito, 2005; Hardjito and Rangan, 2005). This however, can be minimized by premixing sodium silicate and sodium hydroxide together at least one day before introduction to solid constituents. The increase in rate of bleeding noted previously for alkali-activated slag cement with low modulus activators is also applicable for alkali-activated Class F fly ash cement (Adam, 2009). In the case of self-compacting alkali-activated Class F fly ash cement concrete, it has been observed that when the water exceeds a certain level (increased water/geopolymer solids ratio), bleeding and segregation will result (Ahmed *et al*., 2011) noting that the total mass of water is the sum of the mass of water contained in sodium silicate

solution and sodium hydroxide solution, and the mass of extra water. The use of plasticizers to obtain workability of the mix may result in excessive bleeding when the mix is not appropriately designed and tested. Some helpful guidance on the design of geopolymer concrete mixtures can be found in the literature (Rangan, 2008).

Numerous studies (Chindaprasirt *et al.*, 2007; Topark-Ngarm *et al.*, 2011; Chindaprasirt *et al.*, 2011) have also been carried out on the properties and behaviours of alkali-activated Class C fly ash cements. The general consensus is that the alkali-activated Class C fly ash cements are more cohesive and show less susceptibility to bleed. This is also applicable to alkali-activated metakaolin cement, noting that the properties of alkali-activated metakaolin cement are more consistent than that of fly ash-based geopolymer due to a more consistent starting material.

5.4 Segregation and cohesion in concrete

ASTM C125-13 (2013) states that segregation is the unintentional separation of the constituents of concrete or particles of an aggregate, causing a lack of uniformity in their distribution. The property that describes the ability of concrete to resist segregation is conventionally known as cohesion (Binns, 2003; Domone, 2003). Currently there is no specific test for determining this quality in fresh concrete. Viscosity of the plastic concrete is arguably a measure of the cohesiveness of the concrete. Cohesive concrete mixes are known to be more stable and more resistant to segregation and bleeding.

It was mentioned previously that apparent viscosity (and yield stress) of alkali-activated slag cement paste is generally higher than that of Portland cement paste. It has also been observed that both the static and dynamic viscosity of low calcium fly ash-based geopolymer concrete are larger than that of normal Portland cement concrete (Škvára *et al.*, 2006). This is also applicable for fly ash-based geopolymer and metakaolin-based geopolymer concretes (Chindaprasirt *et al.*, 2007; Wu and Sun, 2007; Poulesquen *et al.*, 2011; Lizcano *et al.*, 2012; Chotetanorm *et al.*, 2013). The general trend is that alkali-activated cement concrete will be less susceptible to segregation in comparison to Portland cement concretes and this characteristic can be attributed to the higher cohesiveness of alkali-activated cement concrete. However, segregation can also occur in alkali-activated cement concrete, particularly for mixes using low modulus activators or NaOH activators of low molarities or mixes with high water-to-geopolymer solids ratios. It should be noted further that segregation is also dependent on factors other than the concrete mixes such as the extent and method of compaction; transportation and casting method. For example, over-vibration can cause segregation in a concrete mix which normally does not show segregation.

For mortar, segregation is often found in a mixture with high paste content. If too little paste is used, the mixture is too harsh and does not possess cohesiveness. Mortar containing a low amount of activator solution does not have sufficient cohesiveness. Rostami and Brendley (2003, cited by Brooks *et al.*, 2010) show that about 8–18%

chemical activator is required to produce mortar with the required cohesiveness, but more than 18% of activating chemical may result in heavy segregation and adversely affect the strength of mortar.

For concrete, it is also important to use proper paste content and good aggregate gradation. Hardjito and Rangan (2005) suggest the good coherent alkali-activated mixture can be obtained using aggregate contents of 75–80% similar to normal cement concrete. Marín-López *et al*. (2009) also suggested the ratio of geopolymer paste to aggregate ratio of approximately 0.33 (which corresponds to 75% aggregate content) to obtain a good homogeneous distribution of the aggregate particles to avoid segregation. Using this aggregate content, high workability fresh geopolymer concrete with a slump of 240 mm without segregation is obtained (Hardjito *et al*., 2004).

Since the risk of segregation would be more prevalent with high flowing concrete, there are test methods to assess the likelihood of segregation for high flowing concrete such as self-compacting concrete. These test methods include ASTM C1610/C1610M-10 (2010); ASTM C1611/C1611M-09be1 (2009) and the sieve stability test. ASTM C1611/C1611M-09be1 (2009) can be adapted for most concrete while the sieve stability test is more suitable for high flow concrete. The visual stability index (VSI) obtained from ASTM C1610 / C1610M-10 (2010) is suitable for self-compacting concrete. However, these procedures can be adapted to obtain some quantitative comparison between concrete mixes tested by flow table test (BS EN 12350-5, 2009). For example, the VSI is used successfully to gauge the stability of alkali-activated Class C fly ash concrete with NaOH and sodium silicate as activators (Topark-Ngarm *et al*., 2011). The stability of concretes was better with low liquid to ash ratio and high sodium silicate content. The high sodium silicate/NaOH ratios gave better stability mixes due to the increased viscosity of mixes.

5.5 Future trends

The increase in usage of alkali-activated paste, mortar and concrete in the future is evident. A variety of properties of fresh paste, mortar and concrete are therefore needed in order to serve the specific requirements of various usages and also for special applications. For example in the repair of concrete (Pacheco-Torgal *et al*., 2012), the quick setting types may be required to reduce the time of repair; and self-compacting concrete is required for highly workable mixes to ensure proper placing (Hardjito *et al*., 2004; Topark-Ngarm *et al*., 2011; Ahmed *et al*., 2011). Furthermore, various blends of starting materials will be used to produce alkali-activated concrete with specific properties both in the fresh and hardened states. The alkali-activated Portland blended cements (hybrid cements) are also a good alternative. Portland cement is used as an additive in controlling the setting and to enhance the strength development of the mixes at room temperature (Pangdaeng *et al*., 2014; Phoo-ngernkham *et al*, 2013). This is attractive and may set the future trend as the hybrid alkali-activated fly ash–Portland cement can obtain good strengths under normal

curing (Pangdaeng *et al.*, 2014) without resorting to temperature curing, which thus can save labour and energy costs.

5.6 Sources of further information and advice

The literature supports that setting, bleeding and segregation of alkali-activated paste, mortar and concrete are important properties. Setting, in particular, can be regulated with adjustment of starting materials and activators (Fernández-Jiménez and Puertas, 2001; De Silva and Sagoe-Crentsil, 2008; Chindaprasirt *et al.*, 2012) as well as mixing condition and speed (Chindaprasirt *et al.*, 2014). The related phenomenon of flash setting is not yet well documented. The literature only reveals a few reported cases of flash setting of alkali-activated binders. The overdosage of strong alkali activators, namely, NaOH, $Ca(OH)_2$ and KOH (at high concentration) (Lim *et al.*, 2012) and low water content (Slabbert, 2008) can lead to flash setting. In his thesis, Slabbert (2008) also discussed other possible causes for flash setting. Care should be taken to avoid this mishap; it is not common but it can happen.

References

ACI 233R-03 (2003), *Slag cement in concrete and mortar*, ACI Committee 233, American Concrete Institute, Farmington Hills, MI.

Adam A. A. (2009), 'Strength and durability properties of alkali-activated slag and fly ash based geopolymer concrete', PhD thesis, School of Civil, Environmental and Chemical Engineering, RMIT University, Melbourne, Australia.

Ahmed M. F., Nuruddin M. F. and Shafiq N. (2011), 'Compressive strength and workability characteristics of low-calcium fly ash-based self-compacting geopolymer concrete', *World Acad Sci Eng Tech,* 50, 8–14.

Ambroise J., Maximilien S. and Pera J. (1994), 'Properties of metakaolin blended cements', *Adv Cem Based Mater*, 1, 161–168.

Andersson R. and Gram H-E. (1987), 'Properties of alkali-activated slag concrete', *Nordic Concr Res*, 6, 7–18.

ASA (2011), *Reference data sheet 2-2011, Blast furnace slag aggregates, properties, characteristics and applications*, Australasian (Iron & Steel) Slag Association, Wollongong, Australia.

ASTM C125-13 (2013), *Standard terminology relating to concrete and concrete aggregates*, American Society for Testing and Materials, Book of Standards Vol. 04.02, West Conshohocken, PA.

ASTM C191-08 (2008), *Standard test methods for time of setting of hydraulic cement by Vicat needle*, American Society for Testing and Materials, Book of Standards Vol. 04.01, West Conshohocken, PA.

ASTM C232/C232M-12 (2012), *Standard test methods for bleeding of concrete*, American Society for Testing and Materials, Book of Standards Vol. 04.02, West Conshohocken, PA.

ASTM C403/C403M-08 (2008), *Standard test method for time of setting of concrete mixtures by penetration resistance*, American Society for Testing and Materials, Book of Standards Vol. 04–02, West Conshohocken, PA.

ASTM C618-12a (2012), *Standard specification for coal fly ash and raw or calcined natural pozzolan for use in concrete*, American Society for Testing and Materials, Book of Standards Vol. 04.02, West Conshohocken, PA.

ASTM C807-08 (2008), *Standard test method for time of setting of hydraulic cement mortar by modified Vicat needle*, American Society for Testing and Materials, Book of Standards Vol. 04.01, West Conshohocken, PA.

ASTM C989/C989M-12a (2012), *Standard specification for slag cement for use in concrete and mortars*, American Society for Testing and Materials, Book of Standards Vol. 04.02, West Conshohocken, PA.

ASTM C1610/C1610M-10 (2010), *Standard test method for static segregation of self-consolidating concrete using column technique*, American Society for Testing and Materials, Book of Standards Vol. 04.02, West Conshohocken, PA.

ASTM C1611/C1611M-09be1 (2009), *Standard test method for slump flow of self-consolidating concrete*, American Society for Testing and Materials, Book of Standards Vol. 04.02, West Conshohocken, PA.

Bakharev T., Sanjayan J. G. and Cheng Y-B. (1999), 'Alkali activation of Australian slag cements', *Cem Concr Res*, 29, 113–120.

Binns T. (2003), 'Pumped concrete', in Newman, J. and Choo B. S. (eds), *Advanced Concrete Technology: Processes*, Butterworth-Heinemann, Oxford.

Blanco-Varela M. T., Granizo M. L. and Martínez-Ramírez S. (2007), 'Alkali activation of metakaolins: parameters affecting mechanical, structural and microstructural properties', *J Mater Sci*, 42, 2934–2943.

Brooks R., Bahadory M., Tovia F. and Rostami H. (2010), 'Properties of alkali-activated fly ash: high performance to lightweight', *Int J Sustain Eng*, 3(3), 211–218.

Brough A. R. and Atkinson A. (2002), 'Sodium silicate-based, alkali-activated slag mortars: Part I. Strength, hydration and microstructure', *Cem Concr Res*, 32, 865–879.

Brough A. R., Holloway M., Sykes J. and Atkinson A. (2000), 'Sodium silicate-based alkali-activated slag mortars: Part II. The retarding effect of additions of sodium chloride or malic acid', *Cem Concr Res*, 30, 1375–1379.

BS EN 12350-5 (2009), *Testing fresh concrete, flow table test*, British Standard Institution, London.

Chang J. J. (2003), 'A study on the setting characteristics of sodium silicate-activated slag pastes', *Cem Concr Res*, 33, 1005–1011.

Chen Z. Z. and Liao X. (1992), 'The selection of stimulation agents for alkali-slag cement', *9th International Congress on the Chemistry of Cement*, New Delhi, India.

Chi M. C., Chang J. J. and Huang R. (2012), 'Strength and drying shrinkage of alkali-activated slag paste and mortar', *Adv Civ Eng*, 2012, Article ID 579732.

Chindaprasirt P., Chareerat T. and Sirivivatnanon V. (2007), 'Workability and strength of coarse high calcium fly ash geopolymer', *Cem Concr Res*, 29, 224–229.

Chindaprasirt P., Chareerat T., Hatanaka S. and Cao T. (2011), 'High-strength geopolymer using fine high-calcium fly ash', *J Mater Civ Eng*, 23, 264–270.

Chindaprasirt P., De Silva P., Sagoe-Crentsil K. and Hanjitsuwan S. (2012), 'Effect of SiO_2 and Al_2O_3 on the setting and hardening of high calcium fly ash-based geopolymer systems', *J Mater Sci*, 47, 4876–4883.

Chindaprasirt P., Hanjitsuwan S. and De Silva P. (2014), 'Influence of mixing on properties of high calcium fly ash geopolymer', *Arab J Sci and Eng,* 39, 6001–6007.

Chithiraputhiran S. and Neithalath N. (2013), 'Isothermal reaction kinetics and temperature dependence of alkali activation of slag, fly ash and their blends', *Const Build Mater*, 45, 233–242.

Chotetanorm C., Chindaprasirt P., Sata V., Rukzon S. and Sathonsaowaphak A. (2013), 'High-calcium bottom ash geopolymer: sorptivity, pore size, and resistance to sodium sulfate attack', *J Mater Civ Eng*, 25, 105–111.

Collins F. and Sanjayan J. G. (1998), 'Early age strength and workability of slag pastes activated by NaOH and Na_2CO_3', *Cem Concr Res*, 28, 655–664.

Collins F. and Sanjayan J. G. (1999), 'Workability and mechanical properties of alkali-activated slag concrete', *Cem Concr Res*, 29, 455–458.

Collins F. and Sanjayan J. G. (2001), 'Microcracking and strength development of alkali-activated slag concrete', *Cem Concr Res*, 23, 345–352.

Davidovits J. (1994), 'Alkaline cement and concretes, properties of geopolymer cements', *Proceedings of the 1st International Conference on Alkaline Cements and Concretes*, Kiev, Ukraine**,** 131–149.

Davidovits J. (2011), *Geopolymer Chemistry and Applications*, 3rd edn, Institut Géopolymère, Saint-Quentin, France.

De Silva P. S. and Glasser F. P. (1992a), 'The hydration behavior of metakaolin-$Ca(OH)_2$-sulphate binder', *9th International Congress on the Chemistry of Cement*, New Delhi, India.

De Silva P. S. and Glasser F. P. (1992b), 'Pozzolanic activation of metakaolin', *Adv Cem Res*, 4, 167–178.

De Silva P. and Sagoe-Crentsil K. (2008), 'The effect of Al_2O_3 and SiO_2 on setting and hardening of Na_2O-Al_2O_3-SiO_2-H_2O geopolymer systems', *J Aust Ceram Soc*, 41, 39–46.

Diaz E. I., Allouche E. N. and Eklund S. (2010), 'Factors affecting the suitability of fly ash as source material for geopolymers', *Fuel*, 89, 992–996.

Diaz-Loya E. I., Allouche E. N. and Vaidya S. (2011), 'Mechanical properties of fly ash based geopolymer concrete', *ACI Mater J*, 108, 300–306.

Domone P. L. (2003), 'Fresh concrete', in Newman, J. and Choo, B. S. (eds), *Advanced Concrete Technology: Concrete Properties*, Butterworth-Heinemann, Oxford.

Duxson P. and Provis J. L. (2008), 'Designing precursors for geopolymer cements', *J Am Ceram Soc*, 91, 3864–3869.

Duxson P., Fernández-Jiménez A., Provis J. L., Lukey G. C., Palomo A. and Van Deventer J. S. J. (2007), 'Geopolymer technology: the current state of the art', *J Mater Sci*, 42, 2917–2933.

Fernández-Jiménez A. and Puertas F. (1997), 'Alkali-activated slag cements: kinetic studies', *Cem Concr Res*, 27, 359–368.

Fernández-Jiménez A. and Puertas F. (2001), 'Setting of alkali-activated slag cement. influence of activator nature', *Adv Cem Res*, 13, 115–121.

Fernández-Jiménez A. and Puertas F. (2003), 'Effect of activator mix on the hydration and strength behaviour of alkali-activated slag cements', *Adv Cem Res*, 15, 129–136.

Garcia-Lodeiro I., Palomo A., Fernández-Jiménez A. and Macphee D. E. (2011), 'Compatibility studies between N-A-S-H and C-A-S-H gels: study in the ternary diagram Na_2O–CaO–Al_2O_3–SiO_2–H_2O', *Cem Concr Res*, 41, 923–931.

Glukhovsky V. D., Rostovskaja G. S. and Rumyna G. V. (1980), 'High strength slag alkaline cements', *Proceedings of the 7th International Congress on the Chemistry of Cement*, Paris.

Granizo M. L., Blanco-Varela M. T. and Palomo A. (2000), 'Influence of the starting kaolin

on alkali-activated materials based on metakaolin: study of the reaction parameters by isothermal conduction calorimetry', *J Mater Sci*, 35, 6309–6315.

Gu, J. (1991), 'Hydration mechanism, properties and application of alkali-slag cement', *Cement and Concrete Product (in Chinese)*, 5, 8–11.

Guo X., Shi H. and Dick W. A. (2010), 'Compressive strength and microstructural characteristics of class C fly ash geopolymer', *Cem Concr Compos*, 32, 142–147.

Hardjito D. (2005), 'Studies on fly ash based geopolymer concrete', PhD. Thesis, Department of Civil Engineering, Faculty of Engineering and Computing, Curtin University of Technology, Perth, Australia.

Hardjito D. and Rangan B. V. (2005), 'Development and properties of low-calcium fly ash based geopolymer concrete', Research report GC1, Faculty of Engineering, Curtin University of Technology, Perth, Australia.

Hardjito D., Wallah S. E., Sumajouw D. M. J. and Rangan B. V. (2004), 'On the development of fly ash-based geopolymer concrete', *ACI Mater J*, 101, 467–472.

Jiang W. (1997), 'Alkali-activated cementitious materials: mechanisms, microstructure and properties', PhD. Thesis, The Pennsylvania State University, Pennsylvania, USA.

Jolicoeur C., Simard M.A., Sharman J., Zamojska R., Dupuis M., Spiratos N., Douglas E., and Malhotra, V. M. (1992), 'Chemical activation of blast furnace slag: an overview and systematic experimental investigation', in Malhotra, V. M. (ed.), *Advances in Concrete Technology*, Ministry of Supply and Services, Ottawa, Canada, 471–502.

Josserand L., Coussy O. and De Larrard F. (2006), 'Bleeding of concrete as an ageing consolidation process', *Cem Concr Res*, 36, 1603–1608.

Kovler K. and Roussel N. (2011), 'Properties of fresh and hardened concrete', *Cem Concr Res*, 41, 775–792.

Krivenko P. V. (1992), 'Alkaline cements', *9th International Congress on the Chemistry of Cement*, New Delhi, India.

Krivenko, P. V. and Kovalchuk, G. Y. (2002), 'Heat-resistant fly ash based geocements', in Lukey, G. C. (ed), *Proceedings of the Geopolymers 200: Turn Potential into Profit*, Siloxo Pty. Ltd., CD-ROM, Melbourne, Australia.

Law D., Adam A., Molyneaux T. and Patnaikuni I. (2012), 'Durability assessment of alkali-activated slag (AAS) concrete', *Mater Struct*, 45, 1425–1437.

Lee W. K. W. and Van Deventer J. S. J. (2002), 'The effect of ionic contaminants on the early-age properties of alkali-activated fly ash-based cements', *Cem Concr Res*, 32, 577–584.

Li C., Sun H. and Li L. (2010), 'A review: the comparison between alkali-activated slag (Si + Ca) and metakaolin (Si + Al) cements', *Cem Concr Res*, 40, 1341–1349.

Lim N.G., Jeong S.W., Her J.W. and Ann K.Y. (2012), 'Properties of cement-free concrete cast by finely grained nanoslag with the NaOH-based alkali activator', *Const Build Mater*, 35, 557–563

Lizcano M., Kim H., Basu S. and Radovic M. (2012), 'Mechanical properties of sodium and potassium activated metakaolin-based geopolymers', *J Mater Sci*, 47, 2607–2616.

Marín-López C., Reyes Araiza J. L., Manzano-Ram'rez A., Rubio Avalos J. C., Perez-Bueno J. J., Muñiz-Villareal M. S., Ventura-Ramos E. and Vorobiev Y. (2009), 'Synthesis and characterization of a concrete based on metakaolin geopolymer', *Inorg Mater*, 45, 1429–1432.

Muñiz-Villarreal M. S., Manzano-Ramírez A., Sampieri-Bulbarela S., Gasca-Tirado J. R., Reyes-Araiza J. L., Rubio-Ávalos J. C., Pérez-Bueno J. J., Apatiga L. M., Zaldivar-Cadena A. and Amigó-Borrás V. (2011), 'The effect of temperature on the geopolymerization process of a metakaolin-based geopolymer', *Mater Lett*, 65, 995–998.

National Slag Association (2013), Product, blast furnace slag. Available from: http://www.nationalslag.org/blast-furnace-slag (accessed 10 October 2013).

Pacheco-Torgal F., Castro-Gomes J. and Jalali S. (2008), 'Alkali-activated binders: a review: Part 1. Historical background, terminology, reaction mechanisms and hydration products', *Const Build Mater*, 22, 1305–1314.

Pacheco-Torgal F., Abdollahnejad Z., Miraldo S., Baklouti S. and Ding Y. (2012), 'An overview on the potential of geopolymers for concrete infrastructure rehabilitation (review)', *Const Build Mater*, 36, 1053–1058.

Pangdaeng S., Phoo-ngernkham T, Sata V. and Chindaprasirt P (2014), 'Influence of curing condition on the properties of high calcium fly ash geopolymer containing Portland cement as additive', *Mater Des*, 53, 269–274.

Palomo A., Grutzeck M. W. and Blanco M. T. (1999), 'Alkali-activated fly ashes: a cement for the future', *Cem Concr Res*, 29, 1323–1329.

Palomo A., Alonso S., Fernandez-Jimenez A., Sobrados I. and Sanz J. (2004), 'Alkaline activation of fly ashes: NMR study of the reaction products', *J Am Ceram Soc*, 87 (6), 1141–1145.

Peng J. (1982), 'New solid water glass-slag cements', *Cem Eng (in Chinese)*, 6, 6–10.

Phoo-ngernkham T., Chindaprasirt P., Sata V., Pangdaeng S. and Sinsiri T. (2013), 'Properties of high calcium fly ash geopolymer pastes with Portland cement as an additive', *Int J Miner Metal Mater*, 20(2) 214–219.

Poulesquen A., Frizon F. and Lambertin D. (2011), 'Rheological behavior of alkali-activated metakaolin during geopolymerization', *J Non-Cryst Solids*, 357, 3565–3571.

Provis J. and van Deventer J. (2009), *Geopolymers: Structure, Processing, Properties and Industrial Applications*, Woodhead Publishing, Cambridge.

Puertas F., Amat T., Fernandez-Jimenez A. and Vazquez T. (2003), 'Mechanical and durable behavior of alkaline cement mortars reinforced with polypropylene fibres', *Cem Concr Res*, 33, 2031–2036.

Rangan B. V. (2008), 'Low calcium fly ash based geopolymer concrete', in Nawy, E. G. (ed.), *Concrete Construction Engineering Handbook*, 2nd edn, CRC Press, Boca Raton, FL.

Rashad A. M. (2013), 'Alkali-activated metakaolin: a short guide for civil engineer – an overview', *Const Build Mater*, 41, 751–765.

Rattanasak U., Pankhet K. and Chindaprasirt P. (2011), 'Effect of chemical admixtures on properties of high-calcium fly ash geopolymer', *Int J Miner Metall Mater*, 18, 364–369.

Rostami H. and Brendley W. (2003), 'Alkali ash material: a novel fly ash-based cement', *Envi Sci Techno*, 37(15), 3454–3457.

Rovnaník P. (2010), 'Effect of curing temperature on the development of hard structure of metakaolin-based geopolymer', *Const Build Mater*, 24, 1176–1183.

Rowles M. and O'Connor B. (2003), 'Chemical optimisation of the compressive strength of aluminosilicate geopolymers synthesised by sodium silicate activation of metakaolinite', *J Mater Chem*, 13, 1161–1165.

Roy D. M. (1999), 'Alkali-activated cement: opportunities and challenges', *Cem Concr Res*, 29, 249–254.

Shi C. and Day R. L. (1995), 'A calorimetric study of early hydration of alkali-slag cements', *Cem Concr Res*, 25, 1333–1346.

Shi C., Roy D. and Krivenko P. (2006), *Alkali-Activated Cements and Concretes*, Taylor and Francis, London.

Shi C., Jiménez A. F. and Palomo A. (2011), 'New cements for the 21st century: the pursuit of an alternative to Portland cement', *Cem Concr Res*, 41, 750–763.

Siddique R. and Khan M. I. (2011), *Supplementary Cementing Materials*, Springer, Berlin.

Škvára F., Svoboda P., Doležal J., Kopecký L., Pawlasová S., Myšková L., Lucuk M., Dvo Rácek K., Beksa M. and Šulc R. (2006), 'Concrete based on fly ash geopolymer', *10th East Asia-Pacific Conference on Structural Engineering and Construction*, Bangkok, Thailand.

Slabbert M. C. (2008), 'Utilising waste products from Kwinana industries to manufacture low specification geopolymer concrete', Master of Engineering thesis, Department of Civil Engineering, Curtin University of Technology, Australia, p. 167.

Somna K., Jaturapitakkul C., Kajitvichyanukul P. and Chindaprasirt P. (2011), 'NaOH-activated ground fly ash geopolymer cured at ambient temperature', *Fuel*, 90, 2118–2124.

Tafraoui A., Escadeillas G., Lebaili S. and Vidal T. (2009), 'Metakaolin in the formulation of UHPC', *Const Build Mater*, 23, 669–674.

Tan T. S., Wee T. H., Tan S. A., Tam C. T. and Lee S. L. (1987), 'A consolidation model for bleeding of cement paste', *Adv Cem Res*, 1, 18–26.

Temuujin J., Van Riessen A. and Williams R. (2009), 'Influence of calcium compounds on the mechanical properties of fly ash geopolymer pastes', *J Hazard Mater*, 167 82–88.

Topark-Ngarm P., Sata V. and Chindaprasirt P. (2011), 'Workability and strength of high calcium geopolymer concrete cured at room temperature', *Proceedings of the 7th Annual Concrete Conference of Thailand,* Thai Concrete Association, Thailand, MAT-120 - MAT-125.

Wang S-D. (1991), 'Review of recent research on alkali-activated concrete in China', *Mater Sci Eng*, 43, 29–35.

Weng L., Sagoe–Crentsil K. and Brown T. (2002), 'Speciation and hydrolysis kinetics of aluminates in inorganic polymer systems', *Geopolymer 2002 International Conference*, Melbourne, Australia.

Weng L., Sagoe-Crentsil K., Brown T. and Song S. (2005), 'Effects of aluminates on the formation of geopolymers', *Mater Sci Eng B*, 117, 163–168.

Wild S., Khatib J. M. and Jones A. (1996), 'Relative strength, pozzolanic activity and cement hydration in superplasticised metakaolin concrete', *Cem Concr Res*, 26, 1537–1544.

Wu C., Zhang Y. and Hu Z. (1993), 'Properties and application of alkali-activated slag cement', *J Chin Ceram Soc*, 21(2), 176–181.

Wu H.-C. and Sun P. (2007), 'New building materials from fly ash-based lightweight inorganic polymer', *Const Build Mater*, 21, 211–217.

This page intentionally left blank

Rheology parameters of alkali-activated geopolymeric concrete binders

6

C. Leonelli, M. Romagnoli
Università degli Studi di Modena e Reggio Emilia, Modena, Italy

6.1 Introduction: main forming techniques

Industrially, a material has a practical interest if a shape, however complex, can be produced quickly and at low cost. Given the characteristics of the geopolymeric fresh pastes, colloidal dispersions featuring temporary structural stability prior to the polymerization process, some forming methods are eligible as best suitable for this purpose. Unfortunately, the scientific and technical literature is not very rich in examples on this topic in relation to geopolymeric systems. For this reason, in this section we briefly describe not only the most commonly used forming methods, but also those of potential application that have received only a limited and quick reference: casting, extrusion, double-diaphragm forming, compression molding, injection molding, hand lay-up, rotational molding, and shaping by 3D printer. In some cases it has been possible to trace only a brief reference about the experimentation without any additional information on the actual efficiency of the forming technique. Nevertheless, the techniques presented in the following are all potentially usable depending on the characteristics of the geopolymer paste before consolidation which have to match the parameters requested by each single forming process.

6.1.1 Casting

Casting, also known as 'slip casting', is a technique most widely used in the field of geopolymers. It is used for the production of complex shapes from a suspension poured into a mold. The suspension is made of raw materials in powder form, dispersed in a liquid which, in the case of geopolymers, is water. To complete the formulation other reagents and additives are added to generate the chemical reactions necessary for consolidation and for the correct rheological behavior for the forming process. The suspension is very concentrated in solid content but it is more fluid than a paste. It appears therefore easily deformable, even simply under the action of its own weight. It is obtained by mixing and it is homogenized by forced dispersion of the various components. Finally the suspension must possess the appropriate rheological characteristics suitable for casting, i.e. to be poured into a mold with the negative shape of the desired item inside.

Handbook of Alkali-activated Cements, Mortars and Concretes. http://dx.doi.org/10.1533/9781782422884.2.133

Traditional casting is divided into drain and solid casting. In the former the slip is poured into the mold and as the slip hardens against the inside of the mold, reaching the desired wall thickness for the piece, the mold is inverted and the excess slip is drained away. Afterwards the piece is left to dry in the mold until it is stiff and then removed for the subsequent steps (Singer and Singer, 1979). Solid casting is used for thick pieces such as sanitary ware, chemical stoneware and refractory blocks. The slip is again poured into a mold which is surrounded by plaster on all sides with a reservoir for slip, and is removed when the solid piece is held within.

Often, especially in complex forms, drain and solid casting are present simultaneously and this requires maximum attention because, in the areas of contact between these parts a small difference in the density may occur and lead to severe damage. Traditionally, the method is used to produce both complex and large objects, such as sanitary ware, and small, but equally complex, items, such as tableware (cups, teapots etc.). In the construction industry casting is reported for the pouring of the hydraulic binder, currently concrete but in the future geopolymer, in the presence or absence of steel reinforcements.

Casting, and in particular solid casting, is the most diffused method of forming geopolymers. The presence of a significant quantity of water in the starting formulation makes possible the preparation of a suspension with the required rheological characteristics. Unlike traditional ceramic systems, for geopolymer forming the mold is not required to possess a water absorption capacity, so there is greater freedom of choice of materials to be shaped for the mold. The materials of the mold should not show any reactions at the high pH of the geopolymer, so the most common are plastics such as polyethylene (PE) at different densities or poly(propene) PP. In the filling operations, the rheological behavior of the suspension phase is of great importance, as it must present as low viscosity as possible in order to allow a rapid and complete filling of the mold even in the smallest details, or in the most distant parts of the mold from the entry points of the suspension. Indeed a fluid system even in conditions of slow motion, or low shear rate, allows a more efficient filling compared to a higher viscosity. A small yield stress, but not zero, is preferable to reduce the phenomenon of sedimentation of particles in the stages of storage or during the initial moments of the consolidation. In general, shear thinning and thixotropic rheological behavior are the properties required for a correct casting.

Tape casting is similar to slip casting and is used to form sheets with large surface area and thin cross section. It was developed more than 50 years ago for the production of ceramic capacitors used in the emerging microelectronics industry. Also in this case, a suspension of geopolymer is obtained by mixing together its different components. Slurries are milled and then mixed in a pressure vessel where viscosity and temperature are controlled, and vacuum de-airing is performed prior to casting. Good slip preparation practices are essential to making high-quality finished products. Inconsistent, non-uniform mixtures are often the cause of tape defects. The slip is then cast onto a flat surface, commonly a polymeric films of Mylar, by doctor blade to a carrier film. After the slip has been doctor bladed to a carrier, the wet tape is dried to remove the liquid phase.

It is possible to have two different tape casting machines which are either

stationary doctor blade/moving carrier film or moving doctor blade/stationary carrier film machines (Mistler, 1991). In Figure 6.1(a) an example of geopolymer sheet obtained with this technique is presented. In Figure 6.1(b) a sketch of the doctor blade is shown: the suspension (A) is put into the doctor blade. It is then moved in the direction of the arrows. The slip passes below the gap controlled by the blade (C) which is adjustable by means of two micrometre screws (D).

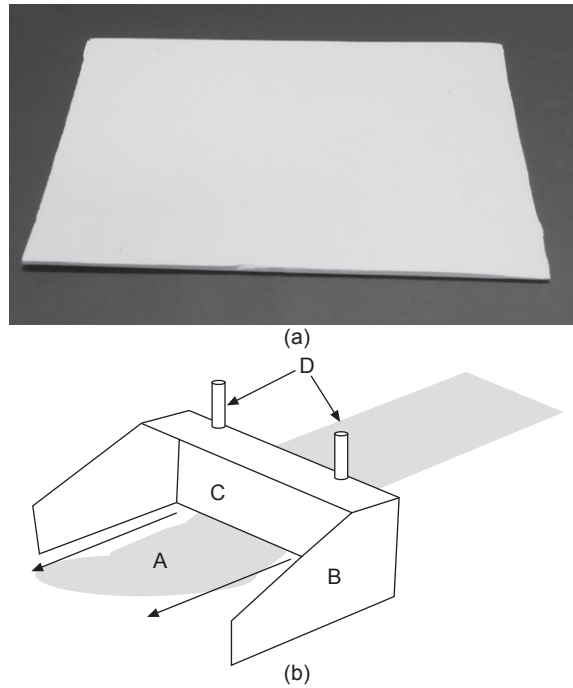

Figure 6.1 (a) Tape cast geopolymer sheet (0.1 mm thick) (courtesy M. Romagnoli); (b) sketch of doctor blade.

6.1.2 Extrusion

Extrusion is a forming process used to create products with a constant cross-section such as pipes, bricks, profiles, etc. It is very common in the field of ceramics, metal processing, food industry, and plastic materials, just to mention the most important.

The material to be extruded must possess a plastic behavior and deform irreversibly, but must keep the shape once the applied force for the deformation ceases and finally has to sustain its own weight. The viscosity of the paste used in extrusion is therefore much higher than in the case of casting and is obtained through a smaller amount of liquid phase. The elastic behavior must be maintained at a low level, preferably zero to avoid phenomena of die swelling, a partial recovery or 'swell' back to the former shape and volume of the materials after exiting the die, or to surface irregularities known as shark skin. The optimal characteristics are obtained with either a correct

formulation of the paste, and with the possible use of chemical additives, and with the most suitable choice of process variables and the geometry of the extruder. The viscoelastic behavior of a system depends on the intrinsic properties of the material in relation to those of the process. From a rheological point of view this is expressed through the Deborah number (See Section 6.2.5).

The system for continuous and direct extrusion, the most widely used in industrial production, is shown in Figure 6.2(a). With this system the shape is given by entering the material in the extruder through a hopper. The paste is forced to pass through a

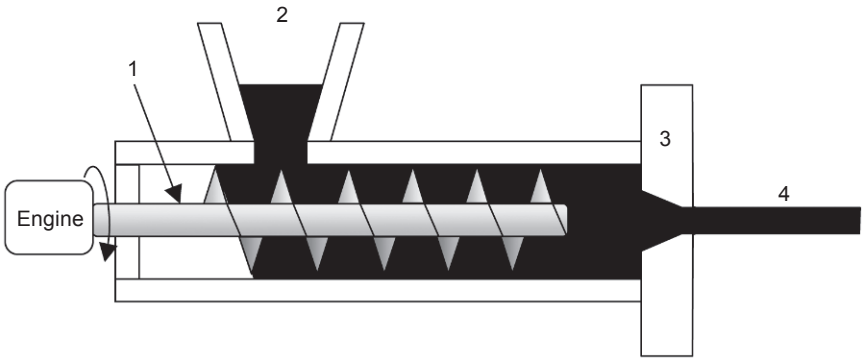

(a)

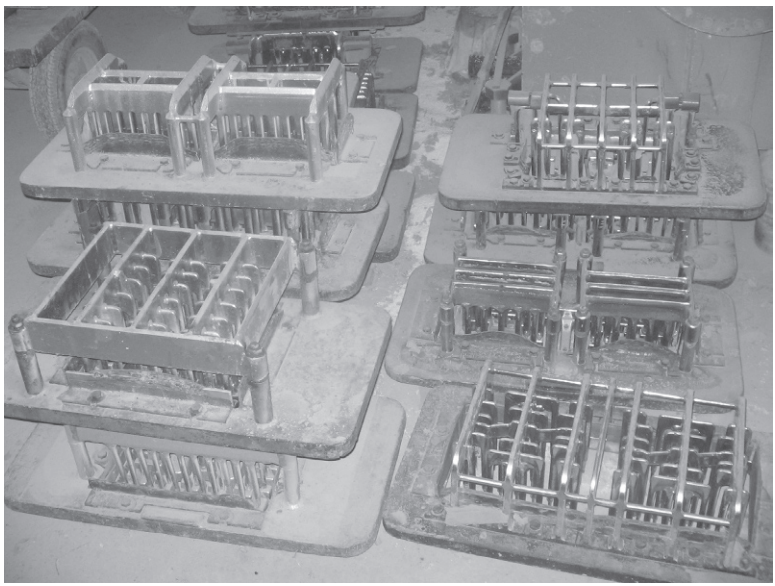

(b)

Figure 6.2 (a) Scheme of a continuous and direct extruder: 1. extrusion auger; 2. hopper; 3. die; 4. extruded material. (b) Extrusion dies used in the brick industry to produce porotherm-style clay block brick (courtesy of M. Romagnoli).

shaped opening, called a 'die' or 'extrusion die', which deforms under the pressure of a piston or an extrusion auger. Often the hopper is preceded by a depression zone in order to reduce entrained air from mixing. This treatment allows the porosity of the extruded material and some of the eventual flaws to be reduced.

An example of extrusion dies for the production of bricks is shown in Figure 6.2(b). The products obtained with this technique can have a complex shape and well-finished surface, provided that the material to be extruded has the rheological characteristics required.

The extrusion technique can be divided into some variants.

1. In *direct extrusion*, represented schematically in Figure 6.3(a), the material is compressed by the piston toward the chain, in the case of a batch system, a screw in the case of a continuous process. The example in the figure falls into the first category.
2. In *inverse extrusion*, represented schematically in Figure 6.3(b), the chain is moving, connected to a piston, which has a central cavity in order to allow the exit of the extruded product. The method is discontinuous, but allows for a reduction of friction between the extruder and the material.
3. *Hydrostatic extrusion* is similar to direct extrusion, but in this case there is a fluid in contact with the material to be extruded, thus acting as a transfer system pressure. The main benefit of using this method is the reduction of friction, generally considerable between the walls of the extruder and the material.
4. *Impact extrusion* is used to make hollow shapes, and is obtained by impact of a shaped punch on the material placed inside a container which is also suitably shaped.

Direct extrusion is the most used technique in the ceramic field, especially because it can be operated in a continuous way, particularly advantageous in the case of industrial production.

Several factors can influence the extrusion process, especially the rheology of the material under the process conditions. Such behavior can be adjusted through proper formulation of the paste, the use of suitable additives, the adjustment of

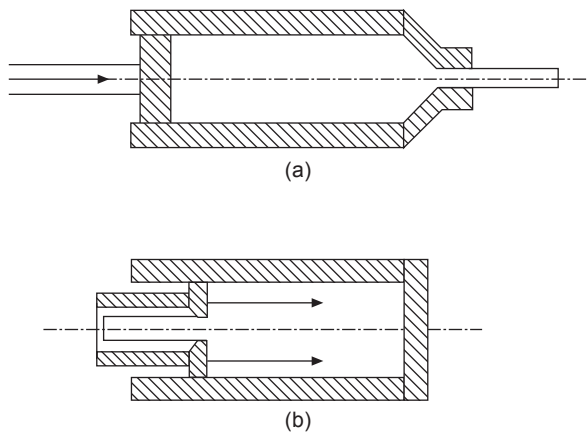

Figure 6.3 Sketch of (a) direct and (b) indirect extrusion.

process variables such as the extrusion pressure, the adjustment of the dies, etc. The optimal behavior in fact must always consider the geometrical characteristics of the extruder, the complexity of the die and the extrusion speed, which should be sustained.

The main defects typical of the forming process by extrusion are as follows.

- *Fractures and extrusion streaks* visible immediately after the exit from the die. These defects may be due to low plasticity of the material or the presence of impurities such as coarse particles of solid.
- *Presence of internal fractures*. This defect is particularly present in direct extrusion using a screw and is due to a lack of plasticity of the material, which is unable to reconstruct the cuts produced by the internal motion of the screw soon before the extrusion die.
- *Deformations* at the exit of the die. At the exit of the extruder it may occur that the shaped material undergoes unwanted curvatures. This defect is caused by a gradient in the extrusion rate of different parts of the paste. An adjustment of the braking plates present on the die eliminates this defect. Deformations from die swelling (Figure 6.4) and shark skin are instead due to improper viscoelasticity of the paste. In these cases the solution is a correction of the paste composition, the speed of extrusion or the geometry of the extruder.
- *Excessively rapid drying* of the extruded material. The drying step must be slow enough not to cause crack formation due to uneven shrinkage. Generally this defect is controlled by correcting the velocity or geometry by swirling jets of hot air.

In traditional ceramics mixtures, water is added in order to obtain a material sufficiently plastic to allow extrusion, the amount varying between 15 and 20–22%

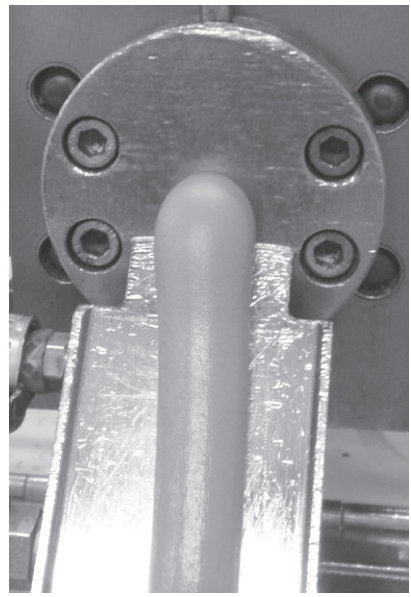

Figure 6.4 Example of die swelling in organic polymers (source: https://commons.wikimedia.org/wiki/File:Powder_Coating_after_Extrusion.JPG).

by weight. This quantity may be subject to change due to the particular characteristics of raw materials. It must be underlined that if this water quantity is compatible with that required for the geopolymerization, then extrusion can be used provided that the extruder is constructed with materials that can withstand the conditions of mechanical and chemical stress generated by the geopolymer paste (Reed, 1995; Langan *et al*., 2011).

6.1.3 Double-diaphragm forming

Double-diaphragm forming is a technique in which a foil of a thermoplastic substance is placed between two deformable layers indicated as diaphragms. The sandwich material is then heated and formed by hydrostatic pressing (Figure 6.5). This method allows composite materials containing reinforcing fibers to be produced, but generally requires a relatively long molding time.

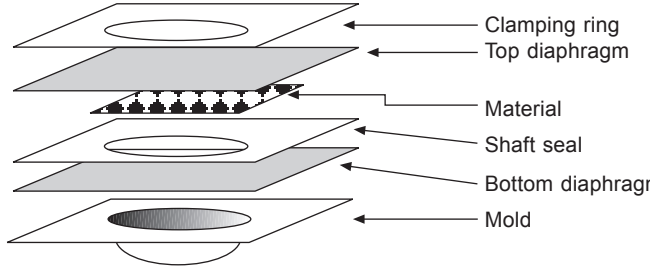

Figure 6.5 Sketch of double-diaphragm forming technique.

6.1.4 Compression molding

Compression molding is typically used for advanced composite materials where the sample is preheated and then placed inside a mold. Once closed, a force is applied onto the mold to form the material. The consolidation is obtained following a subsequent heating within the mold (Figure 6.6). The artefact is then extracted after appropriate

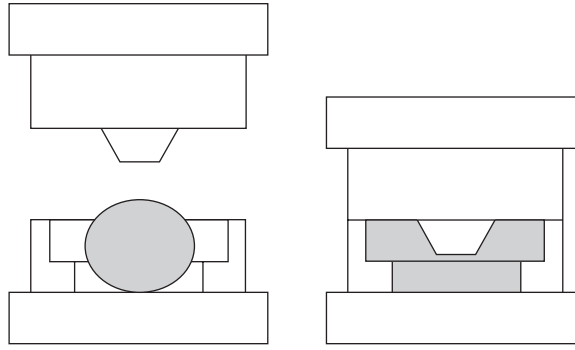

Figure 6.6 Sketch of compression molding.

cooling. The technique is widely used in the automotive field. In the case of a geopolymer with a consistency similar to pulp, the method can be used effectively even if in the literature it was possible to find only a single reference (Davidovits, 2008) poorly detailed relative to an experiment conducted at the industrial level.

6.1.5 Injection molding

In injection molding the ceramic material and/or polymer in the form of a suspension or fluid paste is injected into the cavity of a mold by means of an extruder with a screw (Figure 6.7(a)). After consolidation, the product size can be extracted from the mold. Forming with this method is generally used to manufacture small pieces of complex form.

6.1.6 Hand lay-up

Hand lay-up is an open forming method for the manufacture of composite materials. It is the simplest and oldest method and can be considered within the lamination methods suited especially for large components. A reinforcing material such as glass, polymeric or carbon fibers are placed manually into the open mold after having poured a resin which, in this case, may be a suspension of geopolymer. Manually, using a trowel or roller, the suspension is spread all over the mold, soaking the fibers

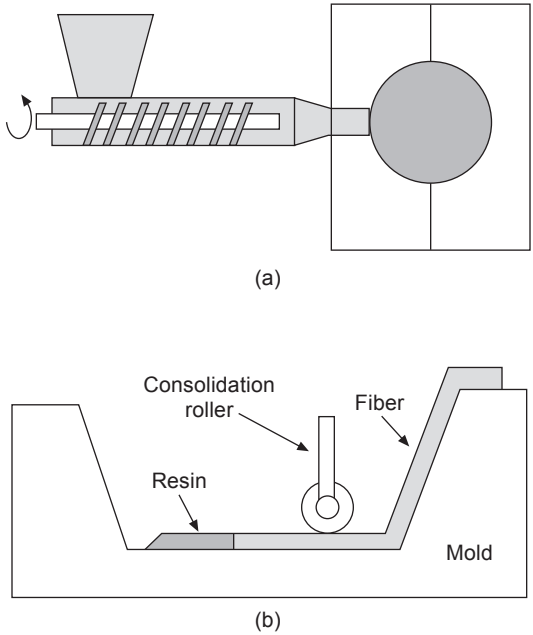

Figure 6.7 Sketches of (a) injection molding and (b) hand lay-up.

(Figure 6.7(b)). The hardening step follows before demolding. For a geopolymer in the form of suspension there is only one report on experimentation at industrial level (Davidovits, 2008).

6.1.7 Rotational molding

This is a particular molding technique used to create hollow objects of large dimensions. It is much used for the forming of objects in plastic material, but there are also examples of attempts in ceramic materials (Figure 6.8) (Calamai, 2006). The method consists in placing the material in the form of suspension within a hollow mold that rotates (generally along two axes) so as to adhere the suspension to its walls in a homogeneous layer. The latter can be heated thus allowing a geopolymeric object to harden more rapidly. Once a sufficient consolidation is reached, the mold may be cooled and opened in order to extract the product.

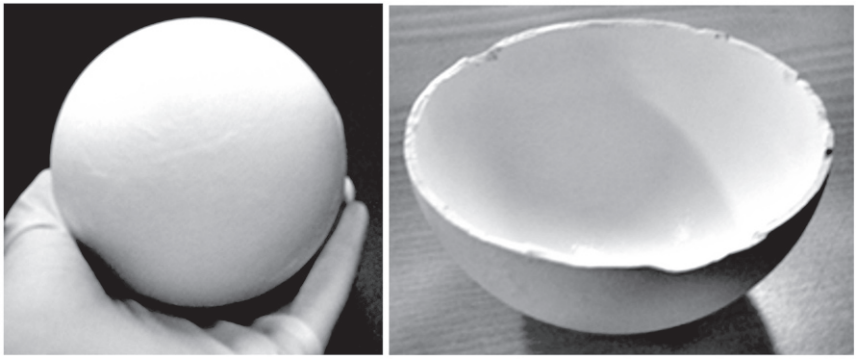

Figure 6.8 Example of a hollow sphere in alumina obtained by rotational molding (Calamai, 2006).

6.1.8 Shaping by 3D printer

The three-dimensional printing technique creates a 1:1 or different scale copy of an object designed with 3D modeling software. It is based on the addition of successive layers of materials up to the final product. There are examples of experiments for the cement which, depending on its characteristics, is also potentially applicable to geopolymers (Figure 6.9).

6.2 Rheology of suspensions

In the case of forming methods that require geopolymeric systems in the form of suspension or paste, the shape is given by applying forces with directions, intensity and duration that would generate extensional and shear deformations. Knowing the

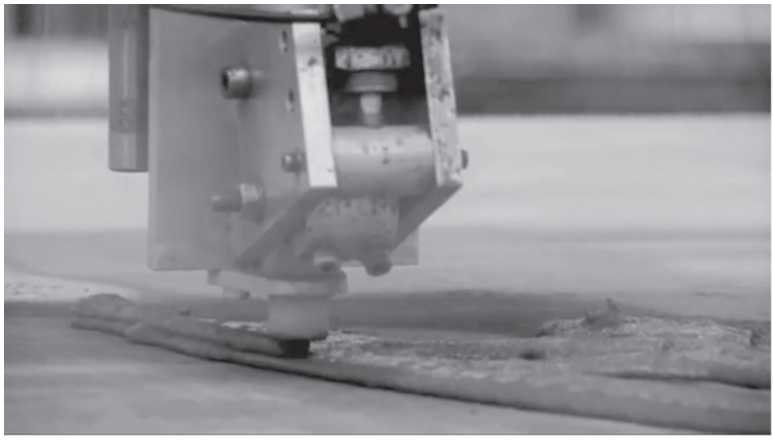

Figure 6.9 Use of binders in 3D printer (Buswell and Austin, 2010).

behavior of the system under the action of these forces is crucial to obtain products with the desired shape, free from defects and with the use of cheap techniques. Rheology, or the science that studies the deformation and flow of a system subjected to external forces, then becomes an indispensable tool to control the forming process.

Rheology has long found a prominent role both in the scientific and in the technology field for its usefulness in the understanding and control of production processes. Knowledge of the rheological behavior is of paramount importance in industrial fields such as plastics, paints, food, lubricants, cement and ceramic materials just to name a few.

Rheology is a multidisciplinary science because it requires knowledge of physics, mathematics, and also of materials science because the rheological behavior is a direct consequence of the characteristics of the material.

In this section, we do not have the ambition to present a comprehensive presentation of rheological science, which would require much more space, as well as falling outside the scope of this book. We want, instead, to give a brief description of some rheological variables that have a great importance in the study and control of the forming of geopolymeric systems. The aim is to provide an overview to act as a starting point for all those who are interested in gaining further insights.

6.2.1 Basic rheological concepts

In materials science the systems are divided into solids and fluids. When an external force is applied on the former, they store the energy by deforming. When the applied stress is removed, they return to their undeformed state. On the contrary, the latter dissipate the energy producing an irreversible deformation. This means that when the external stress is removed, a fluid does not return to its initial shape. Among the fluids we have liquids and gases. Energy is dissipated both to change the shape and produce heat (Mezger, 2006).

The reality, however, presents us with systems that do not belong exclusively to one of these two extremes, but they are placed in the middle and may modify their aggregation state as a function of the applied force, the environmental conditions and the characteristics of the material. Real systems behave in a viscoelastic manner, that is to say that their deformation is partly reversible and partly irreversible. This evidence makes the rheological approach more complex and, at the same time, essential to the industrial process.

6.2.2 Viscosity

Dynamic viscosity, denoted by the Greek letter η, is certainly the most well known of the rheological variables. It measures the resistance with which a material deforms irreversibly when deformed by an external force. This behavior is due to internal frictions in the material that are generated during the deformation. The greater the viscosity of a material, the lower its deformation per time unit under equal applied force. In rheology, a classic definition of viscosity is given by using the Two-Plates-Model (Figure 6.10). According to this description, the sample is placed between two surfaces ideally perfectly parallel and placed at distance h from each other. It is also assumed that the sample has a perfect adhesion onto the two surfaces. Then a force $\vec{F}$ is applied in parallel to the upper surface in order to avoid to exerting a pressure on the material.

Shear stress σ (or in some cases τ) is defined as the force F applied per unit area A:

$$\sigma = \frac{F}{A} \text{ (Pa)} \tag{6.1}$$

It is expressed in Pascals (Pa) in the International System of units, similarly to pressure, although it is not really a pressure as commonly understood. In this condition we can assess the movement of the upper surface which, in an initial phase, accelerates until reaching a constant speed v_{max} when the internal friction forces inside the sample balance the external applied force. If under these conditions the system enters a regime of laminar motion, i.e. when the motion of the fluid occurs with sliding of infinitesimal layers on each other without any kind of mixing of fluid even on a

Figure 6.10 Two-Plates-Model of viscosity.

microscopic scale, then it is possible to define the shear rate $\dot{\gamma}$ (s^{-1}) and the strain γ (dimensionless). In the condition in which the speed of each sheet of fluid decreases linearly from a maximum, in contact with the upper plate, to zero, in contact with the lower, the velocity gradient is calculated as the ratio between the speed v_{max} reached by the surface in motion (the upper) and the distance h between the two plates.

$$\dot{\gamma} = \frac{v_{max}}{h} (s^{-1}) \tag{6.2}$$

The shear rate is related to the flow velocity of the material: high values of $\dot{\gamma}$ correspond to a flow with high speed and vice versa. These two quantities are related to each other through a third one known as dynamic viscosity. It is expressed as the ratio between the shear stress σ (Pa) and the shear rate $\dot{\gamma}$ (s^{-1}).

$$\eta = \frac{\sigma}{\dot{\gamma}} \text{ (Pas)} \tag{6.3}$$

The unit of measure of dynamic viscosity in the SI system is the Pascal × seconds (Pa·s). The most commonly used submultiple is the milliPascal × second (mPa·s). Still surviving in common use is the historical unit centiPoise (cP) in the CGS system, which is equivalent to mPa·s. As a multiple there is the Poise (P). In good practice, these units should be abandoned (Barnes *et al.*, 2000; Mezger, 2006).

The strain γ is defined as the ratio between the deformation of the body ξ as a result of shear stress and the distance h between the two plates.

$$\gamma = \frac{\xi}{h} \tag{6.4}$$

The viscosity is not necessarily a constant property for a material, and in fact it very rarely is since in most cases viscosity changes under the effect of different parameters. An easy and common classification of materials sees materials divided into 'Newtonian' and 'non-Newtonian' fluids. The first group collects materials whose viscosity does not change with the change of shear rate, assuming constant all the other variables that could affect the material. This clarification is necessary because phenomena such as temperature variation, sedimentation of any solid phases present, evaporation of the liquid phase, reactions within the material, etc., can change the state of the system. The non-Newtonian fluids have a change in viscosity due only to a change of the shear rate, keeping constant all the other variables. Systems with non-Newtonian behavior are further divided as follows:

- *shear thinning*: their viscosity decreases with increasing shear rate
- *shear thickening*: their viscosity increases with increasing shear rate.

Since viscosity is not constant for these materials it is defined as '*apparent viscosity*'. Typically the systems consisting of solid powder dispersed in a liquid phase in a medium–high concentration show a non-Newtonian behavior. The variation of viscosity with shear rate is attributed to a reorganization of the dispersed phase within the continuous phase, which restructures favoring or hindering the flow. In the presence

of superficially charged solid particles, the phenomenon of variation of viscosity is due to rupture of the electrostatic interactions between particles.

In Figure 6.11(a) the rheological behavior is presented as apparent viscosity vs the shear rate of two aqueous suspensions of a metakaolin geopolymer. The two samples show a different solid content while all the other variables of the composition remain the same. Both show a non-Newtonian behavior, less pronounced in the system with a lower concentration. The effect of the higher solid content produces a higher apparent viscosity which increases with time as a consequence of the consolidation reaction. These results are also confirmed by other studies (Criado *et al.*, 2009), which have shown that the behavior of geopolymeric suspensions often, but not always, follows the Bingham model (Bingham, 1916) reported below:

$$\sigma = \sigma_0 + K\dot{\gamma} \tag{6.5}$$

where σ_0 is the yield stress, K is a coefficient known as 'plastic viscosity' and $\dot{\gamma}$ is the velocity gradient.

The effect of viscosity increase due to the increase of the solid content is well known in the field of suspensions similar to the geopolymeric ones. A model often

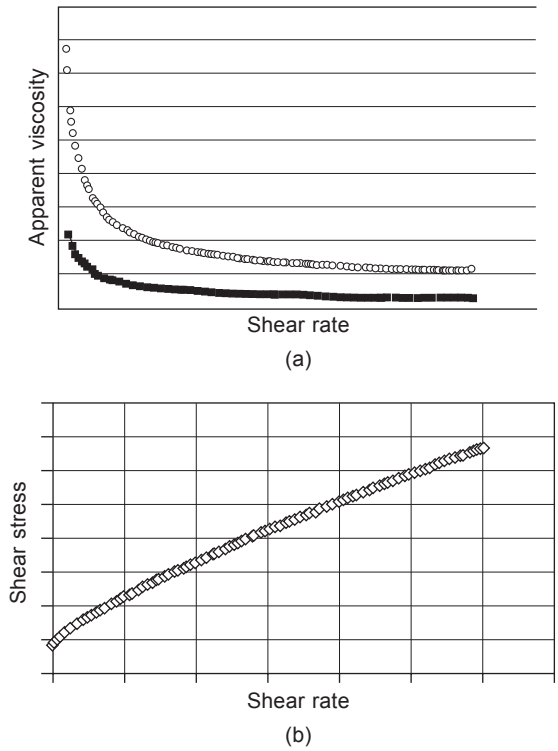

Figure 6.11 (a) Viscosity vs shear rate of metakaolin geopolymers at two different solid content: at lower concentration (■) and higher concentration (❍). (b) Shear stress vs.shear rate in a geopolymer suspension with yield stress (Romagnoli *et al.*, 2012).

used to describe this behavior is the Krieger-Dougherty model (Krieger and Dougherty, 1959):

$$\eta = \eta_s \left(1 - \frac{\Phi}{\Phi_m}\right)^{-|\eta|\Phi_m} \tag{6.6}$$

where Φ is the volume fraction of solid contained in the suspension; Φ_m is the maximum volume fraction of solid the suspension can contain corresponding to the content at which the viscosity becomes infinite (this condition is usually ascribed to the attainment of a close-packed structure); η_s is the viscosity of the liquid phase; and $|\eta|$ the intrinsic viscosity.

6.2.3 Yield stress

For practical purposes it is important to introduce the concept of yield stress or yield point σ_0, defined as the minimum value of the shear stress necessary to produce a flow of the system. Although in the field of rheology, after a thorough analysis, the conclusion was reached that in fact such a limit does not exist and that its manifestation is only a problem related to the reaction time of the system to the stress, the use of the concept of yield stress in the application area persists because it is useful for practical purposes.

Figure 6.11(b) is a graph of shear stress vs shear rate for a geopolymeric system in aqueous phase. It can be observed as the experimental points intersect the ordinate axis, at $\dot{\gamma} = 0$, to a value of non-zero shear stress. This can be seen – at the macroscopic level – as presenting a certain difficulty in starting the flow when the applied forces are near to but lower than this value.

As a general summary, some typical behaviors of rheological systems are presented in Figure 6.12. The first is Newtonian behavior ①, characterized by a constant

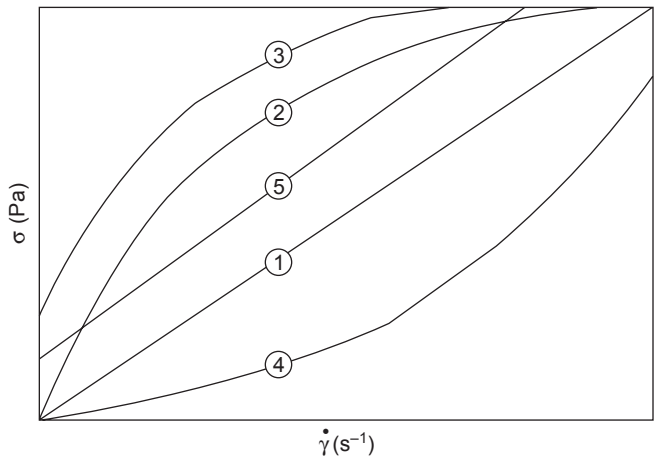

Figure 6.12 Typical shear dependent rheological behaviors: ① Newtonian; ② pseudoplastic; ③ plastic; ④ dilatant or shear thickening; ⑤ Bingham.

viscosity that in the plot of shear stress/shear rate is represented with a straight line at a constant slope. The second ② is shear thinning (also called pseudoplastic) behavior without yield stress, while the third ③ behavior is shear thinning with yield stress (also called plastic), which differs from the previous one for yield stress. Both ② and ③ behaviors show a less than linear dependence of the shear stress with increasing shear rate which means a reduction in viscosity with increasing of $\dot{\gamma}$. The fourth ④ is the dilatant fluid characterized by a greater than linear increase of the shear stress which corresponds to an increase in viscosity with shear rate. Finally, the fifth ⑤ and last behavior is Bingham fluid, which is similar to Newtonian, but with a yield stress.

Please bear in mind that these are just the model behaviors and that a real system may present different behaviors. For example, it is possible that the sample shows different behaviors from those listed in different ranges of shear rate.

6.2.4 Time-dependence

Many systems have a behavior referred to as 'time-dependent' which manifests itself as a change in viscosity over time at constant shear rate or shear stress. The phenomenon is thus different from that seen in Sections 6.2.2 and 6.2.3 where, in the case of non-Newtonian, the viscosity is changed, but due to the variation of the flow regime.

Also in this case we can have two opposite behaviors, one known as 'anti-thixotropy' (also called rheopexy), and the second as 'thixotropy'. Both phenomena are special types of time–dependent behaviors; in fact they present the additional feature of being reversible. The term 'time-dependence' can be better explained by looking at the example in Figure 6.13. The material is first subjected to a deformation at constant shear rate until time t_1, then the system rests until time t_2, and finally is again deformed at the same shear rate value of the previous speed. The graph represents this rheological behavior with the dotted line. The behavior of the two samples, both time-dependent, are shown in thicker black lines. If they are subjected

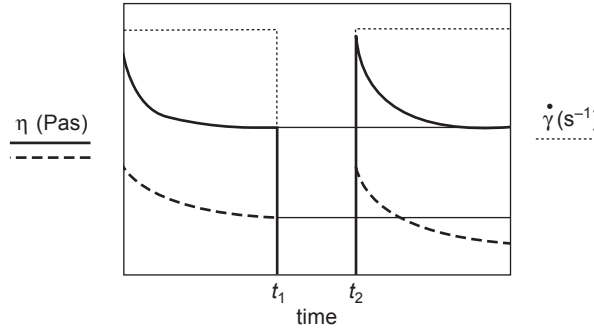

Figure 6.13 On-off procedure (dotted line) on a time-dependent thixotropic material (solid line) and one only time-dependent (dashed line).

to cycles of shear rates for a time sufficiently long to permit the achievement of a stable viscosity value, they may show the following trends of viscosity: (i) the sample represented by the solid line is time-dependent and in particular it is thixotropic, (ii) the other (dashed line) is simply time-dependent. Their difference lies in the fact that both curves, passing from a state of no-flow to one of motion, exhibit a viscosity that decreases over time. The first sample, however, always reaches the same equilibrium viscosity value while the second does not always reach the same equilibrium viscosity, rather presenting a decrease with time. The anti-thixotropic fluid behaves in the opposite way or shows an increase in viscosity when flowing at constant shear rate.

The time-dependent phenomena are due to a variation in microstructure of the suspension which passes from one microstructure to another following the change of the shear rate. A geopolymeric system, due to its reactivity and occurrence of sedimentation and evaporation phenomena, hardly shows behaviors closely resembling thixotropic or anti-thixotropic. Geopolymer rheological behavior can rather be defined as generally time-dependent.

6.2.5 Viscoelasticity

As mentioned above, viscoelastic systems have characteristics intermediate between the two limiting cases of ideal solid and ideal fluid. Such behaviors may have some importance both during the molding as well as in the first stages of consolidation. It is clear to expect that, during the consolidation process, the elastic component should increase with respect to the viscous one. In these cases, the rheological measurement techniques are very sensitive in detecting changes that occur in the material at the microstructural level, especially in the early stages.

In actual systems, macroscopic viscoelastic phenomena such as the one known as the 'Weissenberg effect' are observed. If a fluid system with an important viscoelastic behavior is mixed in a container by means of a vertical rotating shaft, an ascent movement of the paste along the rod may be observed, contrary to fluid with a minimum of viscoelasticity which instead is pushed towards the walls by centrifugal forces. This behavior can have a practical effect in the mixing phase of the suspension or during the pouring of the suspension into the mold. Another typical phenomenon is the 'Barus effect', also known as 'die swelling' that occurs when a viscoelastic system is forced to escape from an orifice, as in the case of a system formed by extrusion. In these conditions, the material shows an increase in cross-sectional area at the exit of the extrusion die with a consequent change of its size. In the worst cases there is even the appearance of superficial fractures and severe deformations of the extruded material.

In the field of rheology particular attention has been devoted to the study of linear viscoelasticity which considers small deformations of the sample. This limitation, which allows a treatment less complex than that in the non-linear field, allows useful information to be obtained on the behavior of the material. While not entering into a complex discussion of this issue, which is beyond the scope of this book, however, it

is useful to present some important concepts. One of these is the 'Deborah number'. The distinction between solid and fluid is no longer so clear since the system can show either behavior depending on its characteristics and the type of stress to which it is subjected. The problem has been resolved by introducing the concept of Deborah number (D_e), which is defined as the ratio between the characteristic relaxation time of the material τ and the time of observation of the phenomenon, T (Reiner, 1964).

$$D_e = \frac{\tau}{T} \tag{6.7}$$

The Deborah number is dimensionless since it is defined as the ratio of two times. High values of D_e are characteristic of solid-like behaviors while for small values, less than one, the behavior is liquid-like. From this it follows that a system with a certain value τ can behave like a fluid if the observation time T is greater than the characteristic relaxation time (D_e low) or as a solid if, vice versa, the time of observation is smaller (D_e high). It must be added that the characteristic time of a system changes to vary its microstructure and its temperature, therefore it cannot be considered a constant of the material regardless of its chemical condition, physical and microstructural properties at the time of stress.

The viscoelasticity of a material is often defined on the basis of two variables G′ (storage modulus) and G″ (loss modulus), which respectively measure the elastic and viscous component of the sample. If the measurement is performed with a rheometer using a measurement system in coaxial cylinders, cone-plate or plate-plate (see Section 6.3.3), the applied stress is varied according to a sinusoidal model like the one shown in Figure 6.14. The deformation of the sample must be small and should not exceed the limit of the linear viscoelasticity which depends on the characteristics

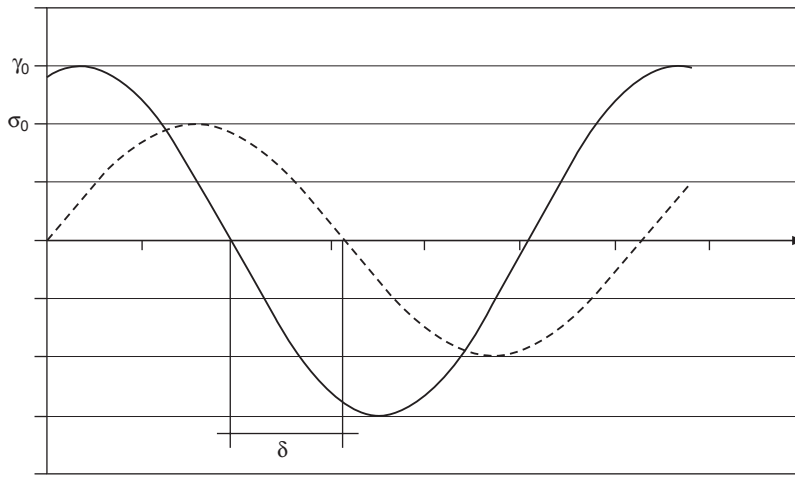

Figure 6.14 Test in oscillatory condition. Variation of shear stress (dashed line) and corresponding strain (solid line).

of the material and, as we shall see later, the oscillation frequency of the measuring system.

In the graph, when the stress is positive, the measurement system applies a force on the sample by turning it in one direction, when it is negative in the opposite direction. The instrument then measures the deformation γ produced in the sample represented by the solid line. As you can see, there is a phase shift between the two curves indicated with the letter δ. In these conditions, we have that:

$$G'(\omega) = \frac{\sigma_0}{\gamma_0} \cos\delta \text{ (Pa)} \tag{6.8}$$

$$G''(\omega) = \frac{\sigma_0}{\gamma_0} \sin\delta \text{ (Pa)} \tag{6.9}$$

where σ_0 is the maximum shear stress applied on the material in a test; γ_0 is the maximum deformation reached; ω is the frequency used or the number of sinusoidal cycles completed per second; and δ is the phase shift between the applied stress σ and deformation γ (Mezger, 2006).

$$\tan(\delta) = \frac{G''}{G'} \tag{6.10}$$

The tangent of phase shift or phase angle tanδ is defined as the ratio between G″ and G′ (Steffe, 1996). It is used as a measure of the prevalence of the elastic contribution when tan $\delta < 1$ or that in the case in which it is viscous tan $\delta > 1$ in the viscoelastic behavior of a sample.

6.2.6 Extensional viscosity

Extensional viscosity is generally encountered less than a material subjected to shear deformation. In spite of this, elongational deformations are often encountered when a fluid system is forced to exit from a container due to the application of a pressure on the container itself. Classic examples are toothpaste or cream coming out from a tube under the influence of an external force. More generally, an extensional deformation is present when a fluid is moving inside a pipe that changes its diameter. If a diameter restriction occurs, a portion of fluid will be forced to deform and stretch going from a larger diameter to a smaller one. The type of motion is different from in shear and therefore it defines an extensional viscosity, η_e, which can also differ greatly from the shear viscosity.

Typically extensional deformations are present in such forming methods as casting, extrusion and injection molding.

In the case of the simplest extensional flows, the uniaxial one, it is possible to define an extensional stress σ_e (also called the tension) and an elongational rate $\dot{\varepsilon}$. Figure 6.15 shows the reference model relative to a uniaxial stretching. This introduces an element of material bound to one side while the other acts as a force which determines an extension which, under equilibrium conditions, is characterized by a velocity V. Based on this simple model, σ_e is equal to the ratio between the

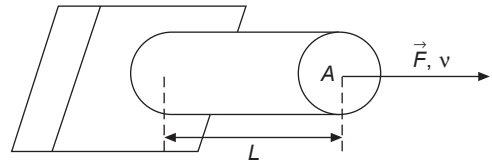

Figure 6.15 Model of extensional uniaxial flow when a force *F* is applied on a sample.

applied force and the surface *A* perpendicular to the force. The elongational rate is, under some conditions, calculated as the ratio between the speed of elongation *V* and the length *L*.

In a similar way to the definition of the viscosity for a shear motion, the extensional viscosity is defined as:

$$\eta_e = \frac{\sigma_e}{\dot{\varepsilon}} \text{ (Pa.s)} \tag{6.11}$$

In conditions of low shear rate, the following mathematical relationship exists between the two viscosities for Newtonian fluids (Barnes *et al.*, 2000):

$$\eta_e = 3\eta \tag{6.12}$$

In general, however, the behavior of a material under shear or extensional flow is different. Interesting is the difference in the case of fluids in which elongated particles or fibers are present in the system. In the case of a shear flow, increasing the shear rate, the particles or fibers will be gradually oriented in the direction of the deformation, so the opposition to the movement decreases until reaching a minimum when they are perfectly aligned with the flow direction of the fluid. Conversely, in an extensional motion, the same rotation in the direction of motion produces an increase in viscosity as the particles or the fibers resist the stretching induced in the material. The difference between the two viscosities depends very heavily on morphological characteristics of the solid phase dispersed (Barnes *et al.*, 2000).

6.3 Rheometry

To define the rheological behavior of a material, the procedures and tools used are not secondary variables. Given the importance of these aspects, a specific field of rheology called ‘Rheometry’ has been developed. In this section the most important and diffused instruments and procedures used in the rheological characterization of materials are briefly presented.

6.3.1 Main measuring instruments

There are several examples of instruments for measuring the rheological characteristics of fluid systems. Some are defined as ‘absolute’ and are based on the measurement

of physical quantities such as absolute forces, torques, strains and speeds. The flow conditions which occur in the material are the closest possible to those required for a proper assessment of the rheological behavior of the samples. The flow is as simple and as laminar as possible; the speeds and forces are known. Instruments with these characteristics are called 'rheometers'. The results that are obtained can be expressed in absolute units, such as the Pascal per second as regards viscosity. They may be considered the top level instruments in the rheological characterization of a fluid system.

Other tools widely used industrially for their simplicity and low cost are defined as 'relative' viscosimeters. Using them the flow conditions of the samples are not so known for an accurate rheological definition as the previous ones. In fact the flow of the fluids is not often well defined and controlled. The flow is non-laminar, the shear rates are not always constant but often complex and not well defined, the shear stresses are not well known nor controlled in any point of the sample. For all these reasons, the results obtained on non-Newtonian fluids with this class of instruments should be considered relative, good for qualitative comparisons between samples, but not expressible in absolute units.

6.3.2 Relative instruments

In this category, the most common for use with fluids such as geopolymers are: the Ford cup, the Gallenkamp viscosimeter and the rotational 'Brookfield' viscometer. On the basis of analogies with cements, also methods such as the slump test must be considered.

The Ford cup (Figure 6.16) is essentially a funnel with an orifice located at the bottom, of a defined and known diameter, from which the material is poured

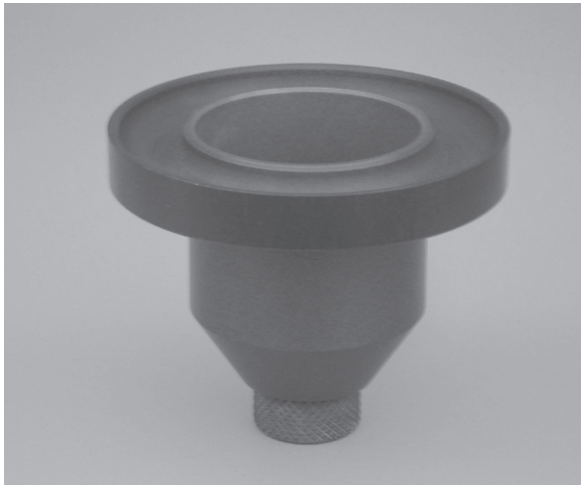

Figure 6.16 Ford cup.

out by gravity. The measurement is performed by filling the funnel with a known volume and measuring the time it takes to empty: the greater is the efflux time, the greater the viscosity of the fluid. It is possible either to change the diameter of the orifice (in order to extend the range of measurable viscosity) or to perform the measurements to have an idea of the sample time-dependence. The regime of motion of the material is a mixture of shear and extensional flow with large variability of its characteristics.

The Gallenkamp viscometer (Figure 6.17(a)) is formed by a measuring steel rotor, generally cylindrical in shape, hanging from a cable of harmonic steel. The cylinder is immersed in the sample and then rotated 360° so as to put the metal wire in torsion. When left free, the torsion of the wire generates a restoring force that allows the rotor to turn toward the starting position while the suspension opposes the motion because of its viscosity. The cylinder then slows down to a stop at a certain angle with respect to the initial position. From the measurement of this angle the viscosity of the sample is derived. The condition of motion that is generated within the suspension during the test is neither constant nor simple to model. Also in this

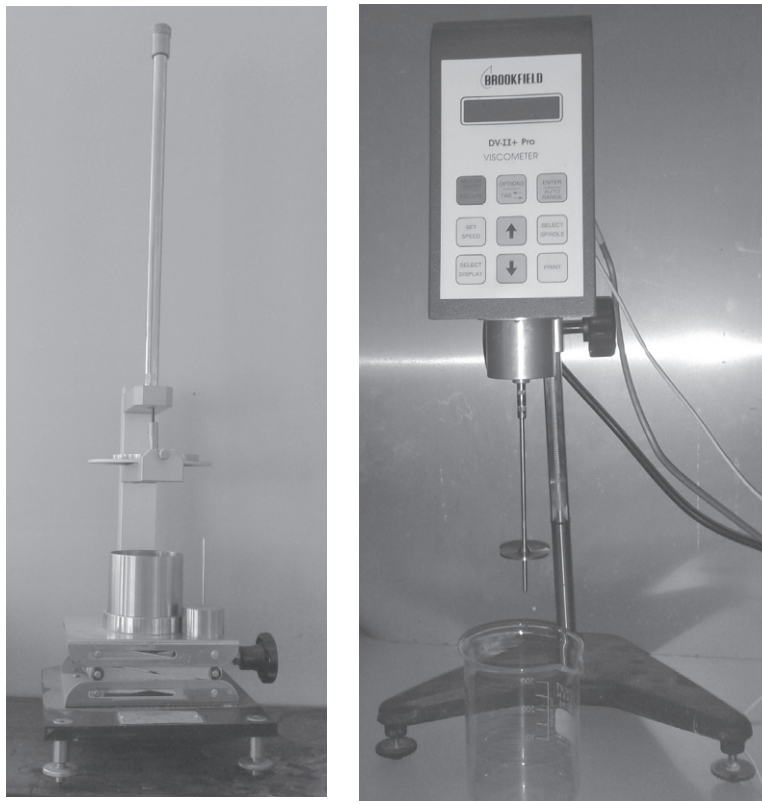

(a) (b)

Figure 6.17 (a) Gallenkamp and (b) Brookfield viscosimeters.

case it is possible to perform measurements so as to have an idea of the sample time-dependence.

The 'Brookfield' viscometer (Figure 6.17(b)) is an electrical rotational instrumentation so used that the brand name has become the synonym for this model. It is based on the measurement of the torque required to turn a rotor immersed in a fluid at a constant rotation speed. As the rotor is indented, a variously shaped tool is immersed in the sample and connected to the electric engine of the instrument. The most common ones have the form of flat discs, called 'spindles', connected to the viscometer through a vertical shaft. There are others of cylindrical shape or in the form of a small palette. The spindles can rotate at different speeds.

All the instruments described can be usefully employed for measuring the viscosity of Newtonian samples, but for the non-Newtonian ones there are strong limits and therefore they can only be used for relative measures and careful analysis of the results is still required. The same considerations are valid for the instruments described below.

The slump test is probably the most widely used method for determining the fluidity of fresh concrete and hence similarly for fresh geopolymers. The test, normed by EN 12350-2 (Figure 6.18), owes part of its diffusion to its simplicity, low cost of the equipment used, the easy interpretation of results, and the fact that it can be performed both on site and in the laboratory. It is based on the evaluation of the deformation that a slurry, in the shape of a truncated cone, called an Abrams cone, by means of a suitable container, undergoes the effect of its own weight. The test takes place before moistening the mold, then putting it on a rigid, smooth, moist, non-absorbent horizontal surface. The cone is then filled up quickly so as to eliminate any air pockets that may be present in accordance with written procedures. After the cone is filled, the paste surface is smoothed and the mold is removed, in a period of between 5 and 10 seconds, lifting it with care in the vertical direction. Immediately after the removal of the Abrams cone, the slump S is measured as the difference between the nominal height of the cone (hm = 300 mm) and the highest point of the sample.

Based on the result of the slump test, five classes of consistency are identified ranging from a moist texture (slump from 10 to 40 mm) to a superfluid behavior (slump ≥ 220 mm). From the data of the slump test, we can get a measurement of yield stress. Among the proposed equations, the following is one of the most used (Ferraris and de Larrard, 1998):

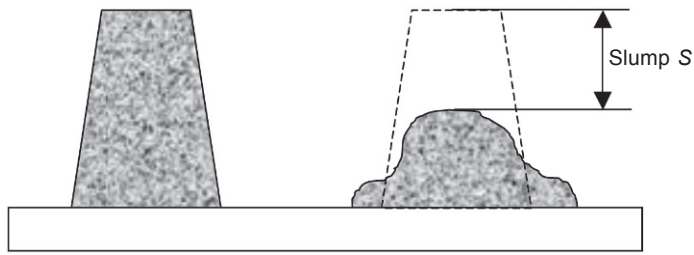

Figure 6.18 Slump test.

$$\sigma_o = \frac{\rho}{347}(300 - s) + 212 \tag{6.13}$$

where σ_0 is the yield stress in Pa, s is the slump in mm and σ the density in kg/m^3.

Slightly different versions of the method are the following:

1. The *mini-slump test* is a variation of the slump test with reduced size. In fact the cone is smaller than the Abrams cone (h = 57 mm). The cone is placed at the centre of a square of glass or other similar material on which are depicted diagonals and medians. Once the cone is filled and lifted, after a minute the average enlargement of the sample along the diagonals and medians is measured. High average values correspond to high fluidities and vice versa.
2. The *mini-flow test* is a variant of the mini-slump test (see ASTM C230) where, once raised, the mold taper is placed on a plastic surface, which is raised and lowered 15 times in 15 seconds favoring the spreading of the sample. The measurement is performed by determining the diameter or area of the sample on the surface. Also in this case, high average values correspond to high fluidities and vice versa.

The data obtained using these methods have been used by some researchers in practical applications, but provide less rich information than rotational methods (Criado *et al.*, 2009). The method also allows the effect of time on the characteristics of the suspension to be measured. In fact, the viscosity increases with time and this is measured by a decrease in the area of spreading of the sample after the lifting of the cone. The use of mini-slump tests allows the effect of additives such as Na_2O on the rheology of geopolymers based on foundry slag to be highlighted (Qing-Hua and Sarkar, 1994) and also on high calcium fly ash (Chaimoon *et al.*, 2012). In the work it is reported that the viscosity increases with the increasing of sodium silicate in the formulation. The surface of the geopolymer after the lifting of the cone decreases with respect to the suspension without silicate. The same effect, qualitatively speaking, is observed by adding calcium hydroxide to the suspension. In general, however, the mini-flow test method is judged more suitable for Portland cement rather than for geopolymers as good correlations have not been found with the results of methods described in the next section (Tattersall and Banfill, 1983; Beaupré and Mindess, 1998).

6.3.3 Instruments for absolute measurements

These tools can be divided into two types: searle and couette. In the first case the sample is placed on a surface or inside a cylindrical container, then the measuring system is placed in contact with the material. During the measurement, the cylindrical container is put in rotation. In the second case, it is vice versa: the sample is a cup that rotates while the bob, immersed into the sample, remains stationary.

The measurement systems have different shapes: cylindrical, conical and flat. The former are combined with cylindrical containers while others require that the samples are placed on a flat surface. They are schematically presented in Figure 6.19. The

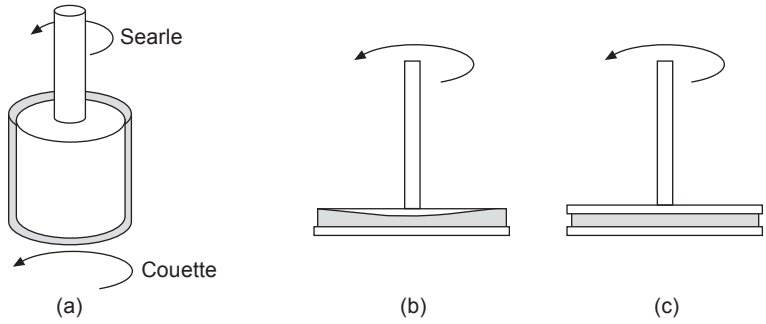

Figure 6.19 Most common measuring system tools used in rotational rheometers: (a) searle and couette in coaxial cylinders; (b) cone-plate and (c) plate-plate.

measurements can be made in two ways: (a) controlled stress and (b) controlled shear rate. In the former, the shear stress is imposed on the sample and the resulting shear rate is measured (rheometer works in control stress mode or CS). In the latter the shear rate is imposed and the necessary shear stress is measured (rheometer works in control rate mode or CR).

6.3.4 Procedures for measurement and analysis of results

The instrumentation described in the previous sections must be used according to procedures adapted to measure the rheological properties of interest. The sample in fact responds according to how it is solicited during the test. In the field of rheometry some 'standard' procedures were developed and below some of the most used are reported. The first, represented in Figure 6.20(a) and called a 'loop test' consists of increasing the shear rate (or shear stress) from a minimum to a maximum value in a linear manner and then decreasing it back down to the starting value. The cycle can be repeated several times, generally two or three times. The results, shown in Figure 6.20(b), allow the following information to be obtained: whether the system is Newtonian, the viscosity at different shear rates, the presence of time-dependence, and yield stress. The time-dependence is more properly evaluated with procedures such as those shown in Figure 6.21. The first is an example of an on-off procedure (Figure 6.21(a)). It consists of a succession of periods in which the sample is subjected to constant shear rates (or shear stress) for a defined time and by periods of rest to increasing times.

In addition to time-dependence, the measurement obtained allows evaluation of the kinetics of the microstructure's reconstruction of the sample. The second standard procedure, known as the steps procedure (Figure 6.21(b)), consists of subjecting the sample to shear rates (or shear stresses), gradually increasing each one for a time sufficient to achieve a situation of equilibrium. Once the maximum value of shear rate is reached, the sample goes back down the curve to the lower limit. The resulting viscosity allows estimation of the time-dependence in different flow regimes and at the same time the viscosities at different shear rates.

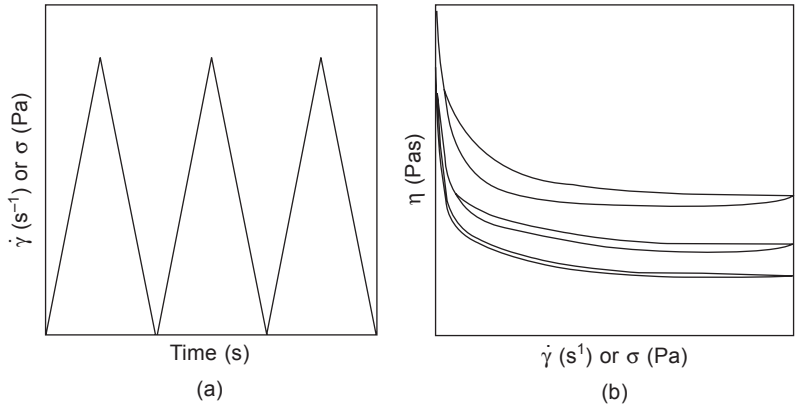

Figure 6.20 (a) Loop test and (b) example of results for a non-Newtonian and time-dependent sample.

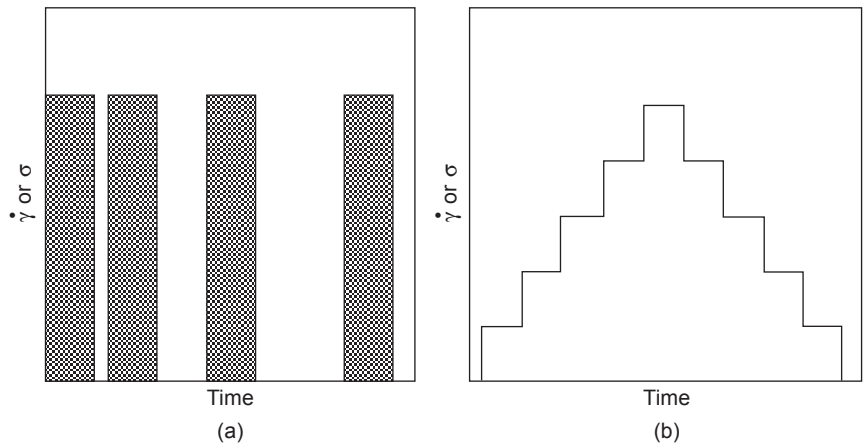

Figure 6.21 (a) On-off and (b) steps procedures.

The measurement of the viscoelastic properties is achieved using mainly two types of measure: the 'creep and recovery' and the 'oscillatory' measurements. The first consists in applying a constant shear stress on the material and to record the deformation of the sample over time (creep). Over a short time, elastic behavior is more pronounced while at long times the viscous behavior is more in evidence. The stage of creep can follow the stage of recovery where the shear stress is cancelled, and the deformation is observed in the reverse direction due to the elastic component.

The procedure of oscillatory measurement, as already seen in Section 6.2.5, consists in applying to the material a shear stress or a deformation that varies sinusoidally in intensity and direction according to an imposed frequency ω. This induces a deformation in the material which is partly elastic and partly viscous. With tools like absolute rheometers it is possible to differentiate the two contributions by measuring

them through parameters such as G′ and G″. However, there are also other valid procedures for measuring these and other rheological properties. For more details, refer to the recommended readings at the end of the chapter.

6.4 Examples of rheological behaviors of geopolymers

Up to the present, few scientific papers have studied deeply the rheology of geopolymeric suspensions and pastes. The results found in the scientific and technological literature show that geopolymeric suspensions with formulations suitable for casting, or aqueous suspensions with a medium–high solid content, show a trend ranging from Bingham to shear thinning.

If an aqueous suspension of a metakaolinitic geopolymer with a solid content around 60 wt.% is considered, it presents a non-null yield stress. In general, it is possible to observe that it is quite difficult to measure geopolymers because of the peculiar characteristics of these systems. In effect, they show sedimentation, evaporation as well as chemical reactivity. An approximate value can be calculated more easily, with all the limits of the method, by fitting the data obtained experimentally using classical rheological models. Values of yield stress between 7 and 25 Pa have been reported for samples with different solid contents, temperatures and additives (Romagnoli *et al.*, 2012).

The experimental data may be fitted using, for example, the Herschel–Bulkley model:

$$\sigma = \sigma_o + K\dot{\gamma}^n \tag{6.14}$$

where: σ is the shear stress, σ_0 is the yield stress, $\dot{\gamma}$ the shear stress, and K and n are two constants used to fit the data. In particular, the latter provides a reference parameter to determine if the rheological behavior of the system is Newtonian, shear thinning or shear thickening. In particular, if $n = 1$, Eq. (6.12) becomes the Bingham model (6.4); if $n = 1$ and $\sigma_0 = 0$, the behavior is Newtonian; with $n > 1$ the suspension is shear thickening; while with $n < 1$ and $\sigma_0 > 0$ the suspension has a shear thinning behavior with yield stress and without yield stress if $\sigma_0 = 0$.

Some authors consider the Bingham model as the better one to describe the experimental data (Palomo *et al.*, 2005). However, such a model is not always satisfactory (Romagnoli *et al.*, 2012). In some cases the Herschel–Bulkley model is able to better fit the experimental data because its three parameters give it more flexibility.

In Figure 6.22 the 3D plots show the effect of the solid content and temperature on the *n* parameter of Herschel–Bulkley model. Figure 6.22(a) refers to freshly prepared suspensions, and Figure 6.22(b) shows the same suspensions but after 90 min of aging at constant temperature in a flask hermetically closed to prevent evaporation of the liquid phase. The additive used, a water soluble sodium polyacrylate with low molecular weight, has shown a null effect in the concentration used so it was not considered here.

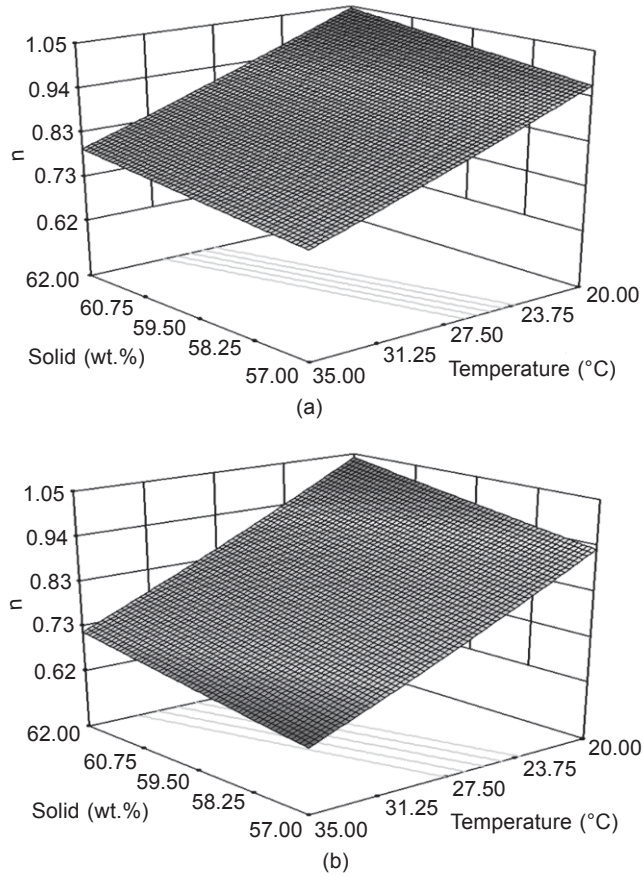

Figure 6.22 3D plot for *n* coefficient of Herschel–Bulkley model for aqueous suspension of metakaolin-based geopolymers, as function of solid content and temperature, for (a) fresh samples and (b) after 90 minutes with the addition of 0.10 wt.% of additive (Romagnoli *et al.*, 2012).

The two graphs show that the *n* values are close or lower than 1. This means that the geopolymers have a shear thinning or at most Binghamian behavior (in fact all the samples have yield stress). After 90 minutes, the surface of the 3D plot is steeper and slightly lower than the surfaces for the just prepared suspensions. This may be due to the geopolymerization reactions that take place within the samples. The effect of temperature is more pronounced and inverse with respect to the solid content: as the temperature decreases the parameter *n* increases but the converse happens for the solid percentage.

In Figure 6.23 it is possible to observe the effect of the solid and additive content on the yield stress in samples of metakaolin-based geopolymers just prepared and after 90 minutes of curing at constant temperature in a plastic bottle hermetically closed. In general, no null values are observed. The variations depend only on the

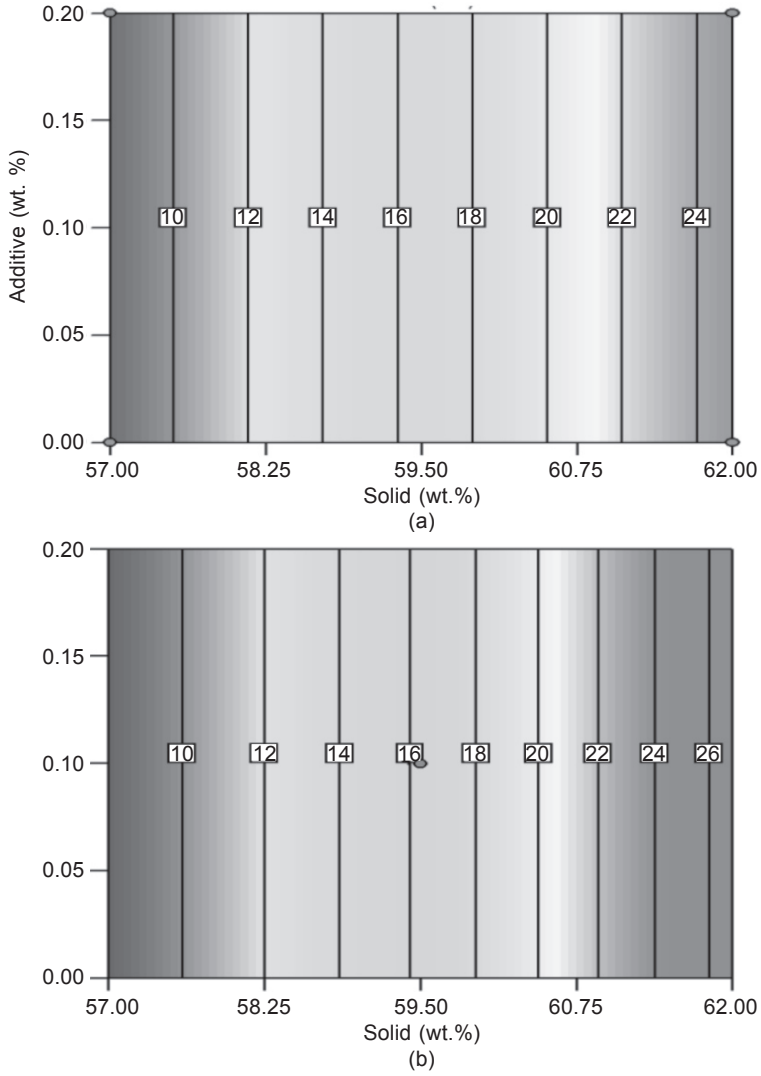

Figure 6.23 Countor plot for yield stress of metakaolin-based geopolymer aqueous suspensions vs percentage of additive and solid content, for (a) fresh samples and (b) after 90 minutes at 27.5°C. The data are obtained using the Herschel–Bulkley model (Romagnoli *et al*., 2012).

solid content rather than the additive and the temperature, in the range 20–35°C. With respect to temperature, the result should not be understood as evidence of the limited effect of this variable on the yield stress, but rather as its small influence on the considered range. In the case of the additive, it also appears ineffective in the explored interval of concentration.

The yield stress increases as the solid content increases (Romagnoli *et al*., 2012; Phair *et al*., 2003). As shown in Figure 6.24, after 90 minutes the effect of additive and solid percentage remains the same as seen previously.

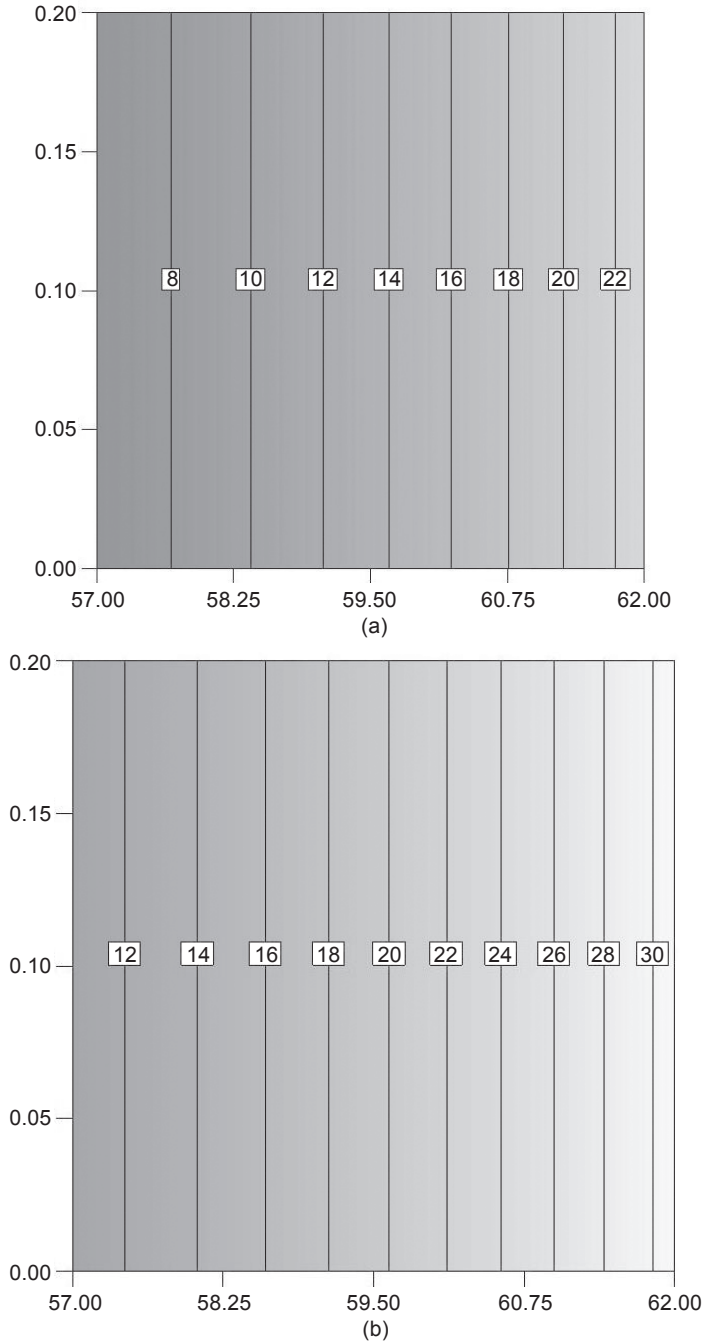

Figura 6.24 Countor plot for yield stress (in Pa) of metakaolin-based geopolymers aqueous suspensions vs percentage of additive and solid content, for samples after 90 minutes of aging at (a) 20°C and (b) 35°C. The data are obtained using the Herschel–Bulkley model (Romagnoli *et al.*, 2012).

However, at 20°C the yield stress is generally lower than in the freshly prepared samples and measured at the same temperature. On the contrary, the samples maintained at 35°C, after 90 minutes, always have a yield stress higher than the samples measured at the same temperature immediately after their preparation. These differences may be due to the polymerization reactions that are accelerated with the increasing of temperature.

Not all the additives have shown scarce effect on the rheology of these systems. In the case of fly ash-based geopolymer, additives normally used for OPC, such as purified lignosulphonate, modified polycarboxylic ethers, and melamine-derived synthetic polymers, have shown the effectiveness to change viscosity and yield stress. Figure 6.25 shows their effect measured with a flow table spread (Spanish standard UNE 80-116-86) (Criado *et al.*, 2009).

Regarding the viscosity at low shear rates, it is observable that the solid content is the main parameter that determines the value of viscosity both in the freshly made suspension (Figure 6.26(a)) and after an aging of 90 min (Figure 6.26(b)). However in the latter, the increasing of the viscosity with the solid content is more evident.

Moreover, in the time range of aging observed in the paper by Romagnoli *et al.* (2012), the temperature works in the opposite way with respect to the well-known effect of this parameter on the rheology of a suspension. In fact, if generally an increase of temperature determines a decrease of viscosity, in the metakaolin-based geopolymer samples, an increase of temperature can determine an increase of viscosity. This reverse trend could be assumed to have the same explanation seen for the increase of yield stress with temperature.

As expected on the basis of the shear thinning behavior of the samples, with the increasing of the shear rate the viscosity decreases as observed in Figure 6.27, where the viscosity is measured at 300 s^{-1} versus solid content and additive percentage in freshly and aged samples, in comparison with Figure 6.26, where the viscosity is

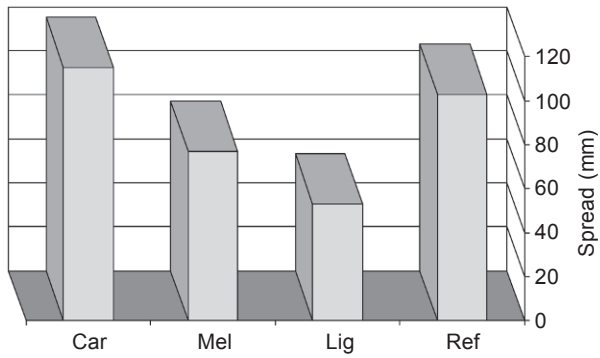

Figure 6.25 Flow table spread in fly-ash mortar (Ref) with respect to the same fly-ash mortar with some commercial additives (Car = modified polycarboxylic ethers; Mel = melamine-derived synthetic polymers; Lig = purified lignosulphonate) (elaborated data from Criado *et al.*, 2009).

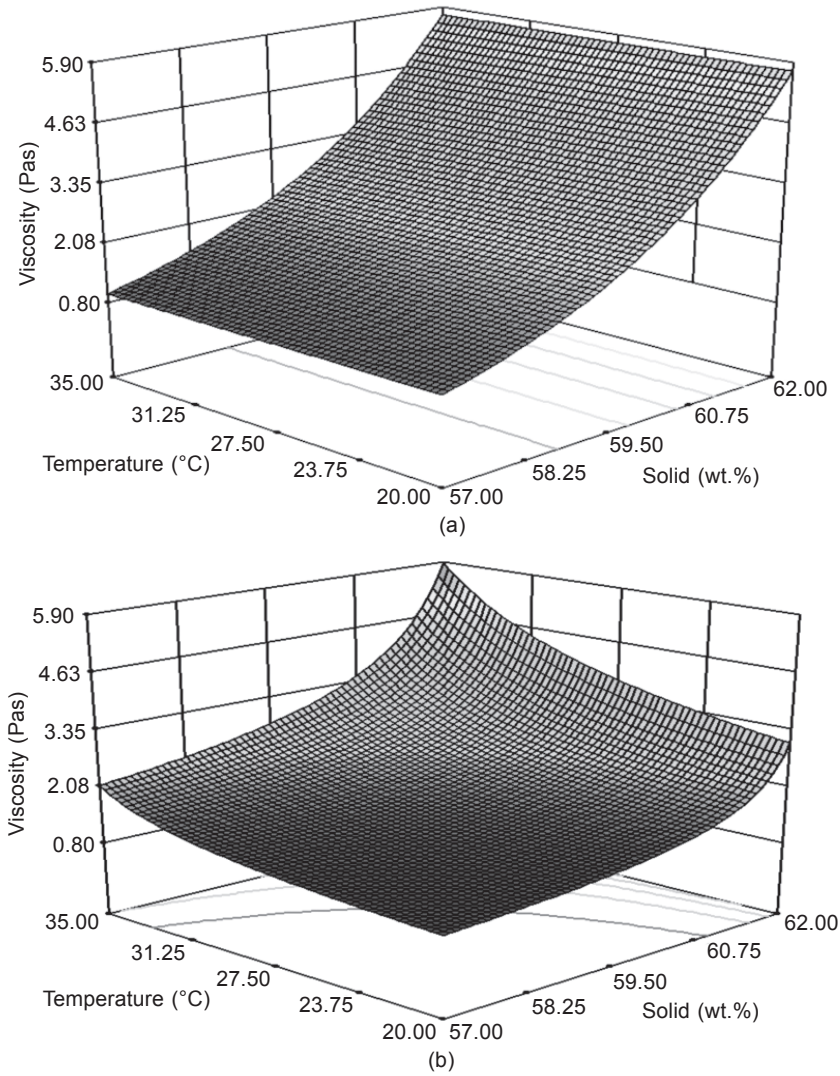

Figura 6.26 3D plot for viscosity at 10 s^{-1} for aqueous suspension of metakaolin-based geopolymers, as a function of solid content and temperature, for (a) fresh samples and (b) after 90 minutes with the addition of 0.10 wt.% of additive (Romagnoli *et al.,* 2012).

measured at 10 s^{-1}. The effect of solid content is still the main parameter while the effect of additive is very poor.

Therefore the viscosity, measured with a rotational rheometer permits control of the progress of the reactions inside the geopolymeric suspensions (Palomo *et al.*, 2005). On the contrary the yield stress does not always seem to be an efficient rheological parameter for following the kinetics of geopolymerization.

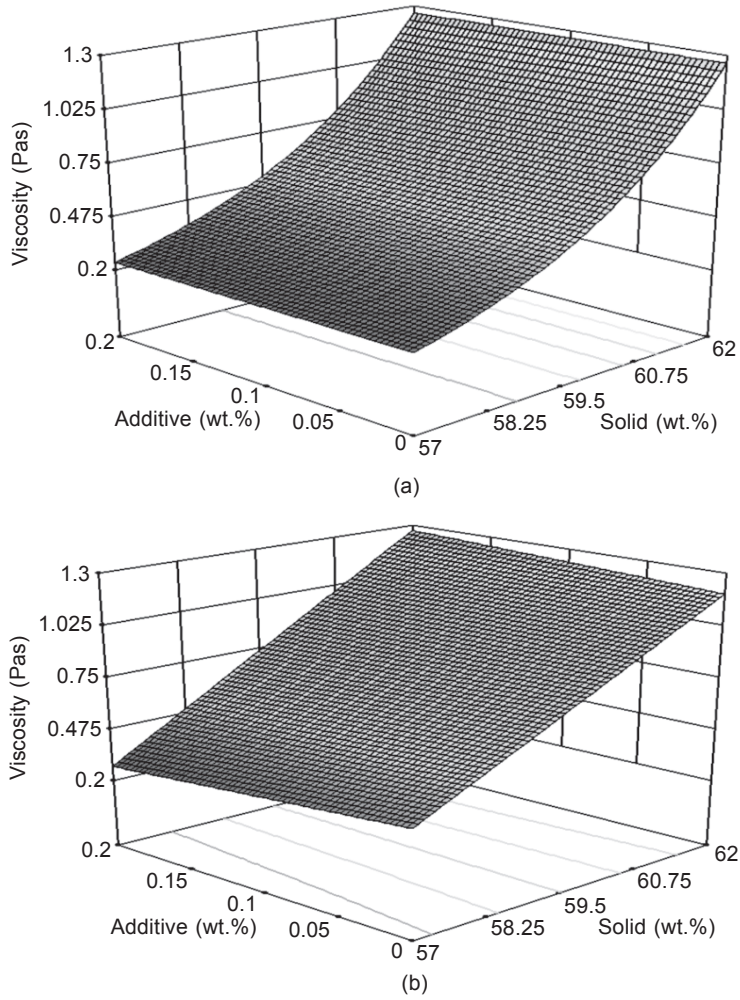

Figure 6.27 3D plot for viscosity at 300 s^{-1} for aqueous suspension of metakaolin-based geopolymers, as a function of solid content and temperature, for (a) fresh samples and (b) after 90 minutes with the addition of 0.10 wt.% of additive (Romagnoli *et al.,* 2012).

6.4.1 Viscoelastic behavior

Oscillatory measurements allow even better analysis of the trend of geopolymerization from the very early minutes after the mixing of the components. In effect, when conducted in the range of linear viscoelasticity, the oscillations produce only little stress on the material that does not substantially alter the three-dimensional structure formed during the reactions. Moreover, they are very sensitive to microstructural changes in the sample during the geopolymerization reaction.

In general, for samples obtained with metakaolin, the storage modulus G′ exceeds the loss modulus G″ after the mixing of the components (Figure 6.28). In the G′ curve

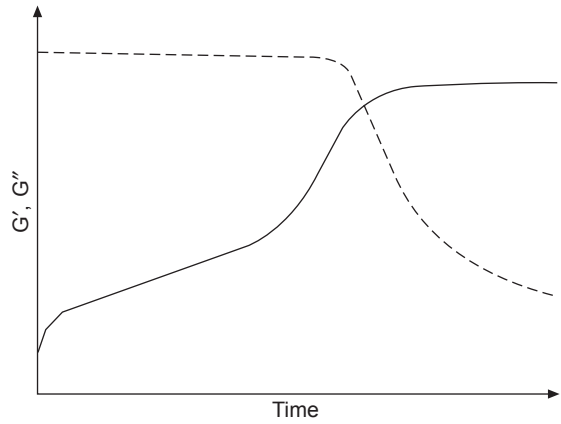

Figure 6.28 Qualitative trend of storage modulus G′ (solid line) and loss modulus G″ (dashed line) versus aging time for a geopolymer during curing (elaborated data from Poulesquen *et al.*, 2011).

it is possible to observe the effect of the dissolution of the aluminosilicates. As a consequence, the store modulus increases due to the formation of oligomers into the suspensions. The oscillatory measurements also permit differentiation of the effect of the alkaline base used: NaOH or KOH. The G′ and G″ curves crossing may be due to the formation of links among the monomers produced by the dissolution of the metakaolin to form stronger structures. The predominance of the elastic properties is reached, therefore, very early in the geopolymeric system. On the contrary G″ is initially constant and after falls to zero.

Measurements in oscillatory mode are very sensitive to temperature and alkaline activators.

With increasing sodium hydroxide, an increase of the slope of G′ and a more rapid consolidation of the material was observed. Substituting sodium hydroxide with potassium hydroxide meant a longer time was required for the elastic modulus to grow, so predominantly viscous modulus was observed (Poulesquen *et al.*, 2011).

6.4.2 Workability tests of geopolymers compared to OPC

Alkali-activated slag (AAS) concrete has been found to have some superior properties as compared to OPC concrete, namely, low heat of hydration, high early strength, and excellent durability in aggressive environments (Roy and Idorn, 1982; Pu *et al.*, 1988; Bakharev *et al.*, 1999). Nevertheless, there are some workability problems that impede its practical application (Collins and Sanjayan, 1999).

An interesting paper by Bakharev *et al.* (2000) tried to rationalize the study of workability of concrete that incorporated alkali-activated slag as the only binder. The activators were liquid sodium silicates (4 ± 7% Na, mass of slag) and a multi-compound activator (NaOH + Na_2CO_3) (8% Na, mass of slag). To ameliorate

the workability, measured by the slump loss test, different additives have been proposed: superplasticizer based on modified naphthalene formaldehyde polymers (S), air-entraining agent (AEA), water-reducing (WRRE), shrinkage-reducing (SHR) admixtures at dosages of 6 ± 10 ml/kg, and gypsum (G) (6% of slag weight). Concrete activated by liquid sodium silicate had the best mechanical properties. AEA, SHR, and G significantly reduced its shrinkage but only AEA improved also workability and had no negative effect on compressive strength (Figure 6.29) (Bakharev *et al*., 2000; Jang *et al*., 2014).

Alkali-activated slag and Portland cement (OPC) mortars were also compared in term of workability with mini-slump tests (truncated conical mold $19 \times 38.1 \times 57.2$ cm^3) (Palacios and Puertas 2005). Mortars were prepared with quartz as aggregate to binder ratio of 2:1 and with 0.5 liquid to solid (l/s) ratio. An important effect of the two types of alkaline solutions used to activate the blast furnace slag mortars was found. NaOH and waterglass both in two different concentrations of Na_2O were used, 4% and 5% by mass of slag.

As shown in Figure 6.30 the waterglass (WG) addition to blast furnace-activated geopolymer decreases the flowability with respect to NaOH, OPC still maintaining the highest values of slump.

In Figure 6.31 the initial and final setting times of the activated slag pastes are reported in comparison to the Portland cement paste. It can be observed that the setting time of the geopolymers were much shorter than for OPC. NaOH-activated slag pastes with 4% and 5% of Na_2O were observed to have very similar setting times, although compared to the WG-activated pastes, the initial times were slightly longer and the final times shorter in most cases. However, the setting times for the pastes could be extended significantly by adding naphthalene-based superplasticizer (1% of additive by mass of binder) (Palacios and Puertas, 2005).

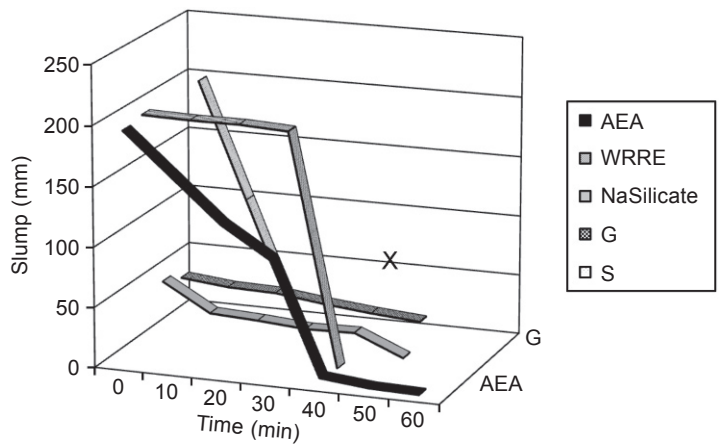

Figure 6.29 Effect of admixtures on slump loss for AAS concrete samples with sodium silicate activator (data elaborated from Bakharev *et al*., 2000).

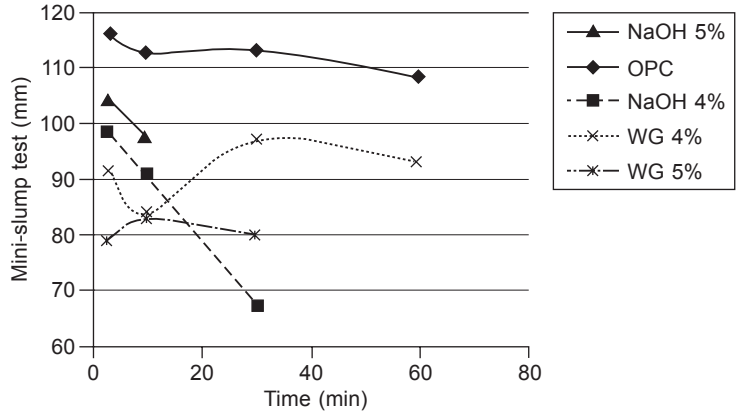

Figure 6.30 Development in time of the slump of the alkali-activated slag and Portland cement pastes (data elaborated from Palacios and Puertas, 2005).

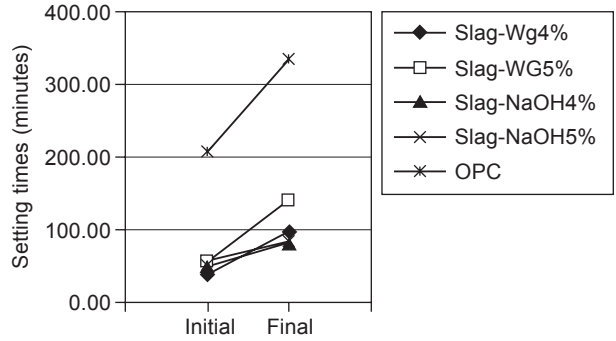

Figure 6.31 Setting times of alkali-activated slag and cement Portland pastes. The initial and final setting times were determined according to European standard EN 196-3 (data elaborated from Palacios and Puertas, 2005).

6.4.3 Defect related to rheological behavior

Examples of defects associated with unsuitable rheological behavior can be very numreous. Below we report a short list of the most important.

1. In the case of slip casting, the incomplete filling of the mold in all its parts may depend on: too high a viscosity; too high value of yield stress or an excessive time-dependence of the suspension. In particular, a high kinetic of rebuilding of viscosity is highly dangerous.
2. In the case of extrusion or inject molding, a high viscosity produces overheating of the paste and extruder. In these conditions, the process can become irregular with the onset of deformation or fracture in the extruded materials. Acceleration of the process of geopolymerization is also possible due to the rise of temperature as seen in Section 6.4.
3. Again in extrusion, too high a viscosity can produce a strong friction between the material and the internal surfaces of the extruder and screw. As a result, pollution is observable in the material jointly with an accelerated wear of the extruder.

4. Too high a viscoelasticity of the paste may produce superficial defect such as the well-known shark skin (a regular ridged surface distortion, with the ridges running perpendicular to the extrusion direction).
5. An excessive viscosity produces the incorporation into the paste of air bubbles during the mixing phase. The air that is not eliminated may produce excessive porosity, reduction of mechanical strength, and low surface bulk quality.

6.5 Future trends

The scientific and technical works on the rheology of geopolymers are very few despite the importance of the topic. Among the future trends in geopolymer investigations, rheology has to be pursued to increase the knowledge of rheological behavior and in particular the effect of various parameters such as the following.

1. The temperature at which the consolidation of the geopolymer occurs. This physical parameter has an important effect on the reaction kinetics.
2. The effect of the geopolymer composition and the degree of amorphicity in the raw materials. These two aspects determine a different dissolution kinetics of the raw materials which have an effect on the rheological behavior.
3. The effect of cations and anions present in the water used to prepare the mixture. In the industrial field distilled water or water at controlled and constant composition often cannot be used. The variation of cations and anions may have an important effect on the rheological parameters such as viscosity, yield stress and the time-dependence.
4. To find additives capable of reducing or, more generally, correcting the viscosity of the geopolymeric suspensions thus allowing the viscosity to be reduced and the solid content to be increased. This produces more resistant geopolymer from the mechanical point of view.

References

Bakharev, T., Sanjayan, J.G. and Cheng, Y.-B. (1999), 'Alkali activation of Australian slag cements', *Cem Concr Res*, 29, 113–120.

Bakharev, T., Sanjayan, J.G. and Cheng, Y.-B. (2000), 'Effect of admixtures on properties of alkali-activated slag concrete', *Cem Concr Res*, 30, 1367–1374.

Barnes, H.A., Hutton, J.F. and Walters, K. (2000), *A Handbook of Elementary Rheology*, Cardiff: University of Wales Institute of Non-Newtonian Fluid Mechanics.

Beaupré, D. and Mindess, S. (1998), 'Rheology of fresh concrete: principles, measurement, and applications', in Skalny, J. (ed.), *Materials Science of Concrete*, *vol. V* Westerville, OH: American Ceramic Society, 149.

Bingham, E.C. (1916), 'An investigation of the laws of plastic flow', *U.S. Bureau of Standards Bulletin*, 13, 309–353.

Buswell R. and Austin S. (2010), Frame from the documentary '3D concrete printing', Loughborough University. Available from: http://www.youtube.com/watch?v=EfbhdZKPHro (accessed 14 January 2014).

Calamai, L. (2006), 'Rheology of ceramic suspensions for gelcasting in rotational molding', Masters thesis in Materials Engineering (in Italian), Università degli studi di Modena e Reggio Emilia, Italy.

Chaimoon, K., Pantura, S., Homwuttiwong, S., Wongkvanklom, A. and Chindaprasirt, P. (2012), 'Factors affecting the workability and strength of alkali-activated high calcium fly ash concrete', *Env Eng Manag J*, 11, 1425–1432.

Collins, F.G. and Sanjayan, J.G. (1999), 'Workability and mechanical properties of alkali activated slag concrete', *Cem Concr Res*, 29, 607–610.

Criado, M., Palomo, A., Fernández-Jiménez, A. and Banfill, P.F.G. (2009), 'Alkali activated fly ash: effect of admixtures on paste rheology', *Rheol Acta*, 48, 447–455.

Davidovits, J. (2008), *Geopolymer Chemistry and Applications*, Institut Géopolymère, Saint-Quentin, France.

Ferraris, C.F. and de Larrard, F. (1998), 'Modified slump test to measure rheological parameters of fresh concrete', *Cem Conc Aggreg*, 20(2), 241–247.

Jang, J.G., Lee, N.K. and Lee, H.K. (2014), 'Fresh and hardened properties of alkali-activated fly ash/slag pastes with superplasticizers', *Constr Build Matls*, 50, 169–176.

Krieger, I.M. and Dougherty, T.J. (1959), 'A mechanism for non-Newtonien flow in suspensions of rigid spheres', *Trans Soc Rheol*, 3, 137.

Langan, M., Reid, M. and Sheppard, P. (2011), 'Extruded geopolymer frame profiles for windows or doors'. United States Patent Application 20110056161.

Mezger, T.G. (2006), *The Rheology Handbook*, 3rd edn, Hannover: Vincentz Network.

Mistler, R.E. (1991), 'Tape casting', in *Ceramic and Glasses*, *Engineered Materials Handbook*, *vol. IV*, Materials Park, OH: ASM International.

Palacios, M. and Puertas, F. (2005), 'Effect of superplasticizer and shrinkage-reducing admixtures on alkali-activated slag pastes and mortars', *Cem Concr Res*, 35, 1358–1367.

Palomo, A., Banfill, P.F.G., Fernandez-Jimenez A. and Swift, D.S. (2005), 'Properties of alkali-activated fly ashes determined from rheological measurements', *Adv Cem Res*, 17, 143–151.

Phair, J.W., Smith, J.D. and Van Deventer, J.S.J. (2003), 'Characteristics of aluminosilicate hydrogels related to commercial "Geopolymers"', *Matls Lett*, 57, 4356–4367.

Poulesquen, A., Frizon, F. and Lambertin, D. (2011), 'Rheological behavior of alkali-activated metakaolin during geopolymerization', *J Non-Cryst Sol*, 357, 3565–3571.

Pu, X.C., Gan, C.C., Wang, S.D. and Yang, C.H. (1988), *Summary Reports of Research on Alkali-Activated Slag Cement and Concrete, Vols. 1–6*, Chongqing, China: Chongqing Institute of Architecture and Engineering.

Qing-Hua, C. and Sarkar, S.L. (1994), 'A study of rheological and mechanical properties of mixed alkali activated slag pastes', *Advn Cem Bas Mat*, 1, 178–184.

Reed, J.S. (1995), *Principles of Ceramics Processing*, 2nd edn. New York: John Wiley & Sons.

Reiner, M. (1964), 'The Deborah number', *Phys Today*, January, 62.

Romagnoli, M., Leonelli, C., Kamseu, E. and Lassinantti Gualtieri, M. (2012), 'Rheology of geopolymer by DOE approach', *Constr Build Matls*, 36, 251–258.

Roy, D.M. and Idorn, G.M. (1982), 'Hydration, structure, and properties of blast furnace slag cements, mortars, and concrete', *ACI J*, 79, 444–457.

Singer, F. and Singer, S.S. (1979), *Industrial Ceramics*, London: Chapman and Hall.

Steffe, J.F. (1996), *Rheological Methods in Food Process Engineering*, 2nd edn, East Lansing: Freeman Press.

Tattersall, G.H. and Banfill, P.F.G. (1983), *The Rheology of Fresh Concrete*, London: Pitman.

This page intentionally left blank

Mechanical strength and Young's modulus of alkali-activated cement-based binders

7

M. Komljenović
University of Belgrade, Belgrade, Serbia

7.1 Introduction

The majority of published studies on alkali-activated binders (AAB) have focused on the compressive and flexural strength as the most important mechanical properties. Compressive strength testing, due to its simplicity and availability is commonly used as a basic measure of usability of different materials in the synthesis of AAB. For some materials, such as concrete, the compressive strength is one of the most important material properties used by engineers when designing and building structures. Compressive strength testing also represents a valuable tool by which the synthesis-structure-properties relationship of AAB may be analyzed. Understanding this relationship is of crucial importance for practical applications.

Tensile testing is a fundamental mechanical test used to determine the Young's modulus of elasticity and other tensile properties. Elastic properties of materials under applied force are of particular importance for construction applications. Generally AAB, like cement-based systems, exhibit poor tensile and flexural properties. The standardized correlations for the prediction of elastic modulus of Portland cement concrete as a function of compressive strength are commonly used in practice. However, the use of existing empirical equations for the prediction of elastic properties of AAB leads to errors due to significant differences in properties of these two systems. New correlations between elastic modulus and compressive strength should be established for the AAB concrete. The incorporation of fibers is a plausible solution for overcoming this deficiency as it changes AAB brittle behavior with significant improvement in tensile properties.

7.2 Types of prime materials – solid precursors

Most common types of prime materials used for AAB production are metallurgical slags, thermally activated (calcined) clays, and coal combustion-based fly ashes. Ground granulated blast furnace slag (BFS) is the most widely used metallurgical slag for the production of AAB (Shi *et al*., 2006; Ben Haha *et al*., 2011a; Rashad, 2013b). On the other hand, calcined clays (metakaolin) and fly ash (ASTM C 618

Handbook of Alkali-activated Cements, Mortars and Concretes. http://dx.doi.org/10.1533/9781782422884.2.171

Class F and Class C) are the most frequently used aluminosilicate prime materials in geopolymer synthesis (Duxson *et al.*, 2007a; Komnitsas and Zaharaki, 2007; Davidovits, 2008; Provis and van Deventer, 2009; Blissett and Rowson, 2012; Rashad, 2013a; Shaikh, 2013). The strength of AAB depends on the type of the prime materials. AAB produced from calcined prime materials, such as slag, metakaolin and fly ash most commonly achieve higher strength than AAB from non-calcined prime materials (Xu and van Deventer, 2002). Calcined materials are mostly amorphous since the calcination process activates materials by changing their crystalline into amorphous structure, which provides extra energy storage and activity increase.

The basic types of prime materials differ markedly in physical, chemical and mineralogical properties. Each of these factors is important, which means that a simple specific procedure for the production of AAB from different types of prime materials is highly unlikely to exist. The great value of metakaolin-based AAB or geopolymers, due to its chemical simplicity, is that it may serve as a basic model system for studying more complex alkali-activated systems, such as fly ash-based geopolymers (van Deventer *et al.*, 2007). Davidovits (1989, 1991) was the first to coin the term 'geopolymer' by combining two distinct properties of AAB: similarity to natural geological systems and its polymeric structure.

AAB are most commonly based on BFS, metakaolin and/or fly ash. Despite the fact that other prime materials have been used to a limited extent, it is worth mentioning such materials as their use represents alternative routes for the production of AAB. Ladle slag (Natali Murri *et al.*, 2013; Bignozzi *et al.*, 2013), phosphorus slag (Shi *et al.*, 2006), ferronickel slag (Komnitsas *et al.*, 2009, 2013), non-ferrous metallurgy slags (Pontikes *et al.*, 2013), red mud (Pan *et al.*, 2003; Kumar, A. and Kumar, S. 2013), waste ceramic (Sun *et al.*, 2013), tungsten mine waste (Pacheco-Torgal *et al.*, 2008a, 2010; Pacheco-Torgal and Jalali, 2010), copper mine tailings (Ahmari and Zhang, 2013), fluid catalytic cracking catalyst residue (Tashima *et al.*, 2012; Rodríguez *et al.*, 2013), air pollution control residues glass (Kourti *et al.*, 2011), cement-rich fraction of construction and demolition waste (Shui *et al.*, 2011; Payá *et al.*, 2012), municipal solid waste incineration ash (Lancellotti *et al.*, 2010; Zheng *et al.*, 2011), palm oil fuel ash (Mijarsh *et al.*, 2014; Yusuf *et al.*, 2014), rice husk and bark ash (Songpiriyakij *et al.*, 2010; Wongpa *et al.*, 2010), volcanic ash (Lemougna *et al.*, 2011, 2014; Tchakoute *et al.*, 2013), kaolinitic clay (Slaty *et al.*, 2013), natural zeolite (Villa *et al.*, 2010) and natural pozzolans (Bondar *et al.*, 2011, 2013) have been used among others.

7.3 Compressive and flexural strength of alkali-activated binders

During the alkali activation process, the vitreous phase of prime materials dissolves, forming calciumsilicate or aluminosilicate gel afterwards (Li *et al.*, 2010). This reaction depends on a whole series of parameters such as: particle size distribution, chemical composition, amount of vitreous phase in prime materials, as well as the

nature, concentration, and pH of activators (Davidovits, 1991, 2008; Shi and Qian, 2000; Shi *et al.*, 2006, 2011; Khale and Chaudhary, 2007; Provis and van Deventer, 2009; Juenger *et al.*, 2011; Lyu *et al.*, 2013). Conditions of the reaction, i.e. the curing conditions (temperature, relative humidity, curing time), also show a great influence on the development of microstructure, and thereafter on the mechanical properties of AAB.

7.3.1 Chemical properties of prime materials

Slowly cooled slags tend to be crystalline and non-reactive. However, many rapidly cooled (granulated or pelletized) slags can contain crystalline inclusions. The chemical composition and highly amorphous nature of BFS favor the development of high strength of alkali-activated BFS. The strength also depends on the basicity (CaO/SiO_2 or $CaO + MgO/SiO_2 + Al_2O_3$ ratio) of the slag. Under the same reaction conditions basic slag develops much higher strength compared to acid and neutral slag (Wang *et al.*, 1994).

Higher MgO content of the slag resulted in a faster reaction and higher paste compressive strengths (50–80% increase after 28 days) of silicate-activated BFS, but in the case of hydroxide-activated BFS the strength increase was quite limited (Ben Haha *et al.*, 2011b). Mortar strength testing showed less distinct effects than observed for the pastes. Higher Al_2O_3 content of the slag resulted in a slower reaction and a lower compressive strength during the first days. At 28 days and longer, no significant effects of slag Al_2O_3 content on the compressive strengths were observed (Ben Haha *et al.*, 2012). On the other hand, small addition of Al_2O_3 powder to sodium silicate-activated slag concrete resulted in significant compressive strength increase (Sakulich *et al.*, 2010). After 28 days of curing at room temperature the strength of alkali-activated slag (AAS) concrete was ~65 MPa, compared to ~45 MPa for concrete without Al_2O_3 addition.

The purity of metakaolin is the dominant factor affecting geopolymer strength (San Nicolas *et al.*, 2013; Autef *et al.*, 2013a, 2013b; Arellano-Aguilar *et al.*, 2014). Strength of geopolymers increases with purity of metakaolin. Calcination temperature of kaolin also has great influence on the environment of aluminum atoms in the metakaolin and consequently on the structure and mechanical properties of metakaolin-based geopolymers (Wang *et al.*, 2010). Commercially produced metakaolin usually has high levels of purity as well as consistent chemical composition and properties (Kuenzel *et al.*, 2013). Thermal pre-treatment of common clays in reducing atmosphere provides better performance of clay-based geopolymeric binders than treatment of clays in oxidizing atmosphere at the same temperature (Seiffarth *et al.*, 2013).

The availability of aluminum for the reaction is one of the most important factors that influence the geopolymer strength (Weng *et al.*, 2005; Steveson and Sagoe-Crentsil, 2005a; Duxson *et al.*, 2007a). Maximum compressive strength of metakaolin-based geopolymers was usually achieved when the Si/Al and Na/Al ratios were 1.9–2.5 and 1.0–1.3, respectively (Rowles and O'Connor, 2003; Duxson *et al.*, 2007b). On the other hand, Burciaga-Díaz and Escalante-García (2012) reported maximum

compressive strength (~80 MPa) of metakaolin-based geopolymer at SiO_2/Al_2O_3 = 3.0 and Na_2O/Al_2O_3 = 0.7 molar ratios. Ruiz-Santaquiteria *et al*. (2013) studied the suitability of three common clays for use as prime materials in the production of alkaline cements. Red, white and ball clay, dehydroxylated at 750°C for 5 h, were activated with sodium hydroxide and cured at 85°C and 90% relative humidity (RH) for 20 h. It was observed that when the reactive phase content was above 50%, the reactive SiO_2/Al_2O_3 ratio in the starting materials had a larger impact than the amount of reactive phase on the developed strength.

Coal-fired fly ashes are relatively cheap and readily available industrial by-products. However, fly ashes are highly heterogeneous prime materials with variable chemical and physical properties not only from source to source, but from batch to batch (van Deventer *et al*., 2007; Vassilev and Vassileva, 2009; Komljenović *et al*., 2009; Diaz *et al*., 2010). Vassilev and Vassileva (2007) have developed a new approach for the classification system of coal fly ashes (FAs) based on their origin, phase-mineral and chemical composition, properties and behavior (Figure 7.1). Medium and high acid fly ashes have the highest amount of glassy phase, highest pozzolanic activity, and most likely high potential for alkali activation. Valcke *et al*. (2013) proposed a new method for screening coal combustion fly ashes for application in geopolymers

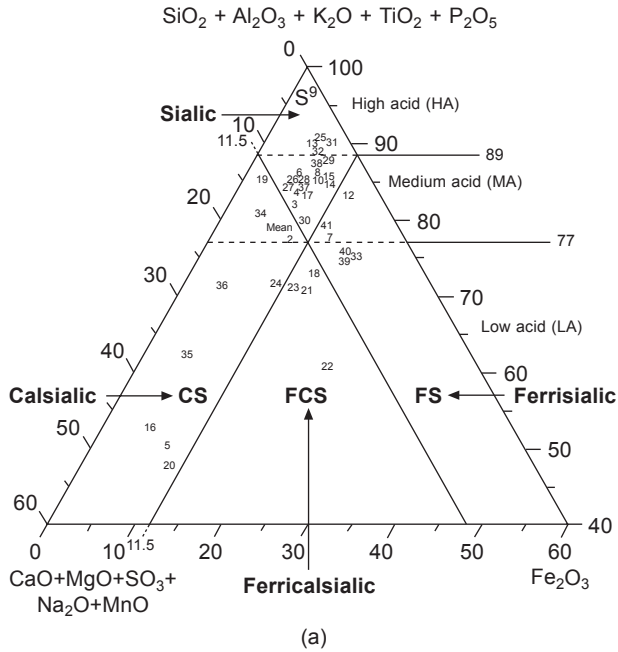

Figure 7.1 Classification system of 41 fly ashes from 37 coal-fired thermo-electric power stations in Spain, Bulgaria, The Netherlands, Italy, Turkey, and Greece (wt.%): (a) chemical classification; (b) phase-mineral classification (P: pozzolanic; I: inert; A: active; M: mixed) (reprinted from Vassilev and Vassileva, 2007, Copyright © 2007, with permission from Elsevier).

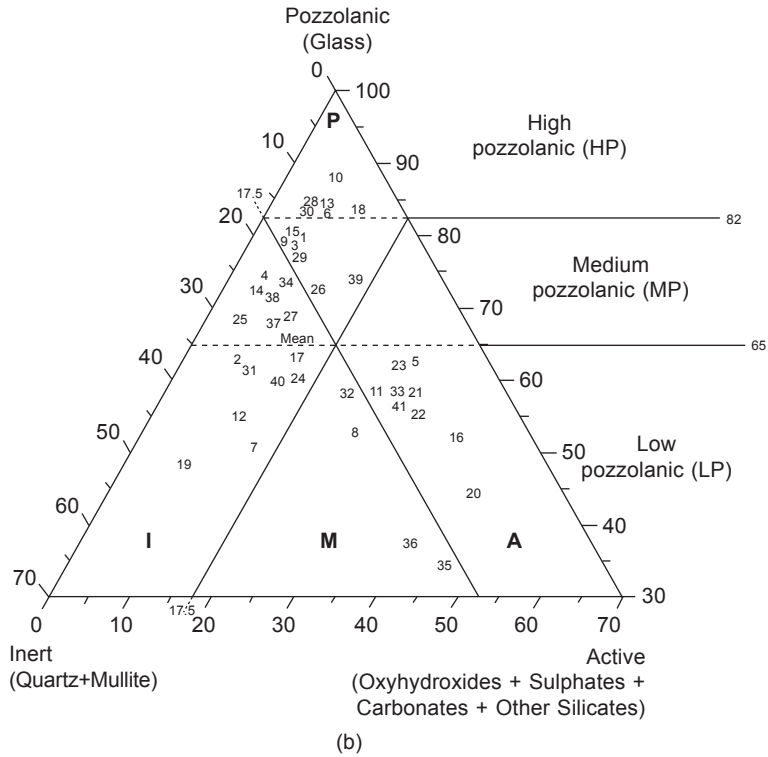

Figure 7.1 Continued

based on electron microscope feature sizing and chemical typing (FS&CT). Inter-particle variations in chemistry and size can be quantitatively measured and related to the reactivity of the fly ash.

The amount of reactive silicon and aluminum of fly ash also plays an important role in the strength development of alkali-activated fly ashes (Steveson and Sagoe-Crentsil, 2005b; Chindaprasirt *et al*., 2009). Fernández-Jiménez *et al*. (2006a) studied properties of sodium hydroxide activated Class F fly ashes. Very high mortar strength (70-80 MPa) was achieved after 7 days of reaction at 85°C under relative humidity >95%. It was concluded that the best performing fly ashes under alkaline activation are ashes with high reactive SiO_2 and Al_2O_3 contents and '$(Si/Al)_{reactive}$' ratios below 2. In some cases the effective aluminum in fly ashes is insufficient for geopolymerization, and additional Al-source materials, such as metakaolin, are required to provide VI-coordinated aluminum to meet the effective SiO_2/Al_2O_3 ratio requirement (Wu and Sun, 2010).

Besides the high content of vitreous phase, low calcium content of fly ashes is another important factor which determines the reactivity and properties of fly ash-based geopolymers (Winnefeld *et al*., 2010). High calcium (ASTM Class C) fly ashes provided much lower geopolymer strength than low calcium fly ashes, due to the lower alkali aluminate silicate hydrate contents, and a much more porous

microstructure formed. On the other hand, adding small amounts of calcium hydroxide (8%) to low calcium fly ash resulted in a remarkable increase in strength of sodium hydroxide activated fly ash (Dombrowski *et al*., 2007). However, high calcium fly ash-based geopolymer can also achieve high strength by providing optimal design and procedure (Chindaprasirt *et al*., 2007; Guo *et al*., 2010; Diaz-Loya *et al*., 2011). Furthermore, 100% Class C fly ash concrete can develop high strength even without chemical activator (Berry *et al*., 2011). Finally, it can be concluded that calcium content is an oversimplified criterion for estimating the quality of fly ashes as prime sources for AAB production.

7.3.2 Physical properties of prime materials

Particle size or fineness is a key physical factor influencing the mechanical properties of AAB. Reactivity of prime materials increases as fineness increases (particle size decreases). However, increase of fineness over a certain threshold value may have an adverse effect on strength due to the higher water demand. Higher (mortar or paste) compressive strength can be achieved by increasing fineness of BFS, especially at early ages (Brough and Atkinson, 2002; Križan *et al*. 2005). Wang *et al*. (1994) suggested the optimal fineness of BFS in the range between 400 and 550 m^2/kg. However, the BFS fineness increasing can cause significant shortening of setting time of alkali-activated BFS (Križan, 2005). On the other hand, partial replacement of slag with ultra-fine slag (~1500 m^2/kg) showed significantly greater strength than AAS at ages greater than 1 day, with minimal loss of concrete workability (Collins and Sanjayan, 1999a). BFS fineness can be significantly increased either by classification (extraction of the fine fraction), for example by the cyclone segregation method (Lim *et al*., 2012), or by mechanical activation (Kumar *et al*., 2005, 2008), resulting in the increased reactivity of BFS as well. Reactivity of other types of slag, such as silico-manganese slag, was also successfully improved by mechanical activation in eccentric vibratory mill (Kumar *et al*., 2013). Very high compressive strength (~100 MPa after 28 days of curing) of AAS paste was obtained.

Weng *et al*. (2005) studied properties of geopolymers based on sodium silicate-activated metakaolin of different SSA, and cured for 2 h at 85°C. It was found that higher specific surface area of metakaolin powders provided higher compressive strength of metakaolin-based geopolymers, which was, as in the case of alkali-activated BFS, accompanied by shorter setting time. Granizo *et al*. (2007) have also found that flexural strength of sodium silicate-activated metakaolin was directly impacted by the specific surface of metakaolin. Commercially available metakaolin usually contains very small particles, whereby the mean particle size (d_{50}) is only a few μm (Duxson *et al*., 2005; Kuenzel *et al*., 2013). Mechanical activation of commercial raw kaolin was found to reduce its particle size and increase its specific surface area (Hounsi *et al*., 2013). Consequently, geopolymer strength of mechanically and sodium silicate-activated kaolin was improved by 76% with respect to the solely chemically activated kaolin and under same curing conditions. The addition of 1%

of nano-SiO_2 particles with the average particle size of 10 nm improved the strength of metakaolin-based geopolymer (Gao *et al*., 2013).

The particle size of fly ash plays an important role in the process of alkali activation. In order to determine potential reactivity of fly ash as alkaline cement, Fernández-Jiménez and Palomo (2003) have characterized groups of Spanish fly ashes, alkali-activated by sodium hydroxide. The mechanical strength of fly ash-based geopolymers mortars, containing only fly ash particles lower than 45 μm, exceeded 60 MPa after 1 day of curing at 85°C. High strength was also connected to the high reactive silica content present. The importance of fly ash particle size distribution was also later confirmed. Komljenović *et al*. (2010) studied a group of Serbian fly ashes activated by different alkali and alkaline earth activators. Regardless of the nature and concentration of the activator used, the geopolymer based on fly ash with the highest content of fine particles (<43 μm) showed the highest compressive strength in all cases. Chindaprasirt *et al*. (2011) also studied the effect of fineness of fly ash on geopolymer properties (setting time, workability, strength development, and drying shrinkage) made from air-classified high-calcium fly ash. The strength of mortars was improved using fine fly ash, but the setting time of paste decreased with an increase in fly ash fineness. High 28-day geopolymer mortar compressive strength of 86.0 MPa was obtained. Fineness of lignite bottom ash was also crucial for geopolymer strength development (Sata *et al*., 2012).

In order to improve fly ash homogeneity and reactivity, van Riessen and Chen-Tan (2013) studied the beneficiation of fly ash conducted in a three-stage procedure using sieving, milling and magnetic separation. At each stage of beneficiation the proportion of reactive amorphous material increased resulting in increased reactivity and strength of geopolymer paste produced. Compressive strength of all samples after 7 days of curing (24 h at 70°C) was 100 MPa or more with sieving producing a 32% increase in strength. Mechanical activation also proved to be successful in the case of fly ash (Kumar *et al*., 2007a, 2007b; Kumar, S. and Kumar, R., 2011). Vibratory milling was much more successful than attrition milling, giving up to a 50% improvement in strength of geopolymer pastes, and reaching up to 120 MPa after 24 h curing at 60°C (Figure 7.2). On the other hand, attrition milling (in a planetary ball mill) of several Class F fly ashes proved to be quite successful resulting in the remarkable strength increase (more than 30 times) of fly ash-based geopolymer mortars, exceeding a strength of 70 MPa after only 4 hours of curing at 95°C (Marjanović *et al*., 2014) (Figure 7.3). Curing at room temperature (~90% RH) developed geopolymer mortar compressive strength of 30 MPa after 1 day, and 57 MPa after 28 days (Nikolić *et al*., 2014). However, in both cases geopolymer setting time was very short.

Particle shape significantly affects water demand and rheological properties, and consequently strength of AAB (Provis *et al*., 2010). Characteristic angular particles of BFS, spherical (solid or hollow) and irregular particles of fly ash, and angular layered (platy) particles of metakaolin have different properties showing different effects in each of these areas. More spherical particles present in the system means lower water demand and better workability.

The use of metakaolin in geopolymers is relatively problematic due to the high

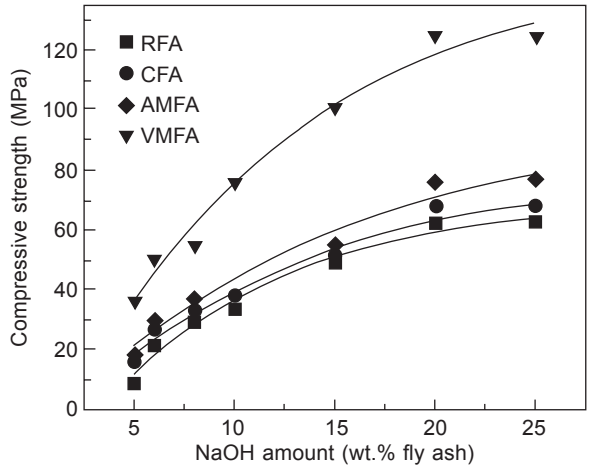

Figure 7.2 Strength of geopolymers based on raw fly ash (RFA), classified fly ash (CFA) and mechanically activated fly ash using vibratory mill (VMFA), and attrition mill (AMFA) versus amount of NaOH (reprinted from Kumar *et al.*, 2007b, Copyright © 2007, with permission from Elsevier).

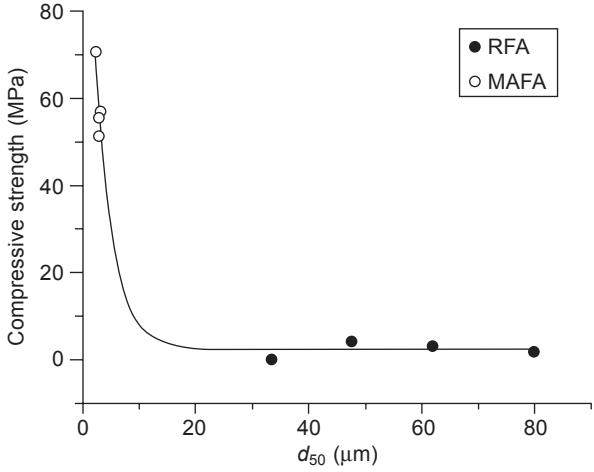

Figure 7.3 Correlation of geopolymer compressive strength and fly ash particle size (d_{50}). Four different raw fly ashes (RFA) and mechanically activated fly ashes (MAFA). Adapted from Marjanović *et al.* (2014), with permission from Elsevier.

water demand experienced, while the use of fly ashes enhances the rheology and strength development (Provis *et al.*, 2010; Rashad, 2013a; Zhang *et al.*, 2014). Metakaolin obtained from industrial flash calciner contains more spherical particles and possesses lower specific surface area compared to metakaolin from traditional rotary kiln (San Nicolas *et al.*, 2013). This higher circularity, associated with the lower specific surface area, provides better workability. However, the negative influence of

metakaolin on mortar workability, as well as the decrease of geopolymer compressive strength between 7 and 28 days of curing still remains (Duxson *et al*., 2007b; Rüscher *et al*., 2010; Pelisser *et al*., 2013; San Nicolas *et al*., 2013) (Figure 7.4).

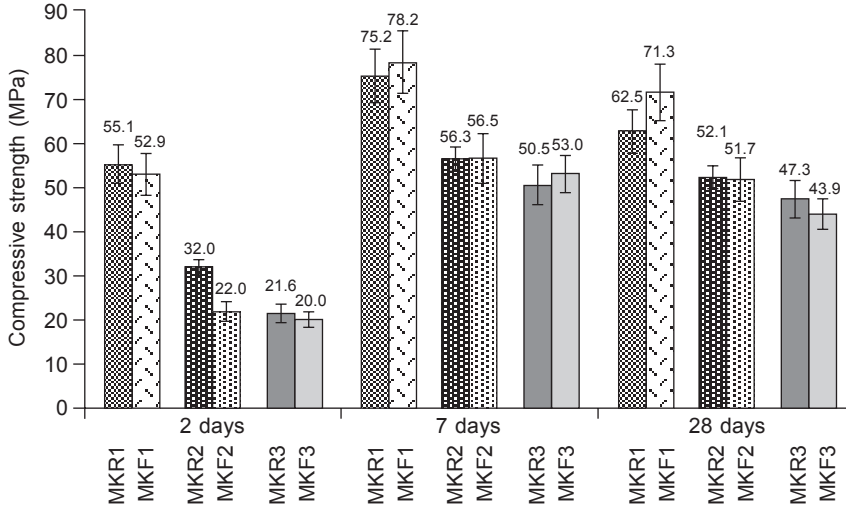

Figure 7.4 Compressive strength of geopolymer mortars with six metakaolins (MKF: flash-calcined metakaolin; MKR: rotary kiln calcined metakaolin; three kaolins with different levels of purity) (reprinted from San Nicolas *et al*., 2013, Copyright © 2013, with permission from Elsevier).

7.3.3 Synthesis conditions

Fernández-Jiménez *et al*. (1999) studied the joint influence of a series of factors (specific surface of slag, curing temperature, activator concentration, and nature of alkaline activator) on the strength development of alkaline-activated BFS mortars up to 180 days. The most significant influencing factor was the alkaline activator nature, followed by the activator concentration, curing temperature, and, finally, the specific surface of the slag. The importance of influencing factors can also be extended to other alkali-activated systems.

7.3.3.1 Activator type and concentration

Although BFS does react with water (without any chemical activator), the rate of hydration is very slow (Song and Jennings, 1999). Mixing BFS with water will only provide hardened material if the reaction lasts for a very long period of time (Taylor *et al*., 2010). Therefore, the main purpose of alkali activator is to accelerate the hardening process.

The strength of alkali-activated BFS is highly affected by the activator type (nature) and concentration (Wang *et al*., 1994). BFS is usually more reactive than metakaolin

or fly ash, so BFS can be successfully activated not only by alkali hydroxides and silicates, but by alkali sulfates and carbonates as well (Shi, 1996; Bakharev *et al*., 1999a; Živica, 2007; Xu *et al*., 2008; Pacheco-Torgal *et al*., 2008b; Rashad *et al*., 2012, 2013). Activator dosage has a significant effect on strength of AAS cements, and there is an optimum dosage in most cases. However, the optimum dosage varies with the nature of the slag and alkali activators used, and the curing conditions (Shi and Day, 1996).

The activation of BFS using NaOH results in high early (1 day) strength, but strength at 7 days and longer is lower than for the sodium silicate (waterglass) systems (Ben Haha *et al*., 2011a). Sodium silicate-activated BFS most commonly develops the highest strength (Fernández-Jiménez *et al*., 1999; Bakharev *et al*., 1999a; Burciaga-Díaz and Escalante-García, 2013), unfortunately usually accompanied by undesirable side effects, such as fast setting and/or high drying shrinkage (Wang *et al*., 1995; Bakharev *et al*., 1999b; Križan and Živanović, 2002; Živica, 2007; Komljenović *et al*., 2012; Bilim *et al*., 2013). Activation of BFS with KOH gave higher early (1 day) strength than for sodium silicate activation, but the subsequent strength development and strengths at later ages were much lower for the KOH system (Brough and Atkinson, 2002). Sodium carbonate activation of BFS provides significantly lower strength. However, setting time and drying shrinkage are more similar to the PC system (Atiş *et al*., 2009). The problem of undesirably short setting times for waterglass-activated slag mortars and concretes could also be overcome by extending mixing time (Palacios *et al*., 2008). Extended mixing time to up to 30 min improved strength and reduced drying shrinkage as well (Palacios and Puertas, 2011).

Both compressive and flexural strength of alkali-activated metakaolin-based mortars increases with increase of sodium hydroxide concentration (Pacheco-Torgal *et al*., 2011). However, increase of sodium hydroxide concentration reduces the workability of mortars. The flexural strength of metakaolin activated by sodium silicate and cured for 2 h at 85°C was greater than the strength of its analogue activated by NaOH alone (Granizo *et al*., 2007). Rowles and O'Connor (2003) studied the compressive strengths of sodium silicate activated metakaolin pastes with Si/Al molar ratios of 1.0–3.0 and Na/Al molar ratios of 0.5–2.0. The polymers were cured at 75°C for 24 h and their compressive strengths measured after aging for 7 days. The strength was found to depend systematically on the relative amounts of Si, Al, and Na, with the maximum being 64 ± 3 MPa for a Si/Al molar ratio of 2.5, and Na/Al molar ratio of 1.3. Increasing Si/Al and Na/Al molar ratios beyond the mentioned values led to a strength decrease. Duxson *et al*. (2005) also studied the relationship between sodium silicate-activated metakaolin-based geopolymer composition (Si/Al ratio between 1.15 and 2.15, and fixed Al_2O_3/Na_2O ratio of 1), and mechanical properties of pastes. The geopolymers were cured at 40°C for 20 h. There was a rapid increase in the compressive strength of geopolymers with increasing Si/Al ratio. However, it was found that the optimal Si/Al ratio was 1.90, where maximum geopolymer strength (>70 MPa) was observed. At the highest Si/Al ratio of 2.15, the strength was reduced (Figure 7.5).

Zhang *et al*. (2008) studied the influence of different parameters (SiO_2/Al_2O_3,

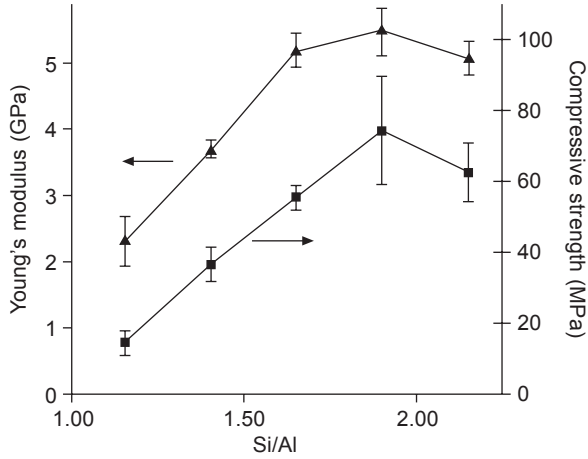

Figure 7.5 Young's modulus and ultimate compressive strength versus Si/Al ratio of geopolymers. Error bars indicate the average deviation from the mean over the six samples measured (reprinted from Duxson *et al*., 2005, Copyright © 2005, with permission from Elsevier).

K_2O/Al_2O_3, and H_2O/K_2O molar ratios) on mechanical properties of metakaolin activated with potassium silicate and cured at 20°C and 95% RH for 28 days. SiO_2/Al_2O_3 molar ratio had the most significant effect on geopolymer compressive strength and the highest compressive strength (34.8 MPa) was achieved when SiO_2/Al_2O_3 = 4.5, K_2O/Al_2O_3 = 0.8, and H_2O/K_2O = 5.0. The highest compressive strength (34.9 MPa) of metakaolin activated with sodium silicate was achieved at higher molar ratios: SiO_2/Al_2O_3 = 5.5, Na_2O/Al_2O_3 = 1.0, and H_2O/Na_2O = 7.0 (Zhang *et al*., 2010). Duxson *et al*. (2007b) studied the influence of mixed alkalis (sodium and potassium) ratio, and Si/Al ratio on mechanical properties of silicate-activated metakaolin-based geopolymer. The geopolymer pastes were cured at 40°C for 20 h, and thereafter at ambient temperature and pressure until testing at the age of 7 and 28 days. Regardless of the type of alkali and their ratio, maximum strength was again observed at an Si/Al ratio of 1.9. Minimal change in compressive strength of specimens was generally observed in specimens of different alkali or between 7 and 28 days of aging. However, mixed-alkali specimens with high Si/Al ratio exhibited significant increases in strength, while pure alkali specimens displayed decreased strength.

The nature of activator is one of the most dominant parameters in the alkali activation of fly ash. Komljenović *et al*. (2010) studied the influence of various activators and concentration on fly ash-based geopolymer mortar strength. Regardless of the fly ash properties, activation by sodium silicate provided the highest strength, due to dissolved and partially polymerized silicon. Concentration of activator can also considerably influence the mechanical characteristics of mortars based on alkali-activated fly ash (AAFA). The increase of activator concentration led to the compressive strength increase. Activation potential of the activators investigated

(taking into account equal concentrations of 10% Na_2O in relation to the mass of fly ash) was represented by the following pattern:

$$KOH < NaOH + Na_2CO_3 < NaOH < Na_2O{\cdot}nSiO_2$$

$$\text{min} \rightarrow \text{activation potential} \rightarrow \text{max}$$

The modulus of waterglass is also critical for the strength development of AAB. Wang *et al*. (2005) have found that the compressive strength of metakaolin-based geopolymers activated by a mixture of sodium silicate and sodium hydroxide, cured in an oven at 65°C for 10 h, increased along with the increase of NaOH concentration. Provis *et al*. (2009) studied the mechanical properties of geopolymer mortars synthesized from a single fly ash source using different sodium silicate modulus and liquid/solid ratios. Samples were cured sealed into plastic bags at 40°C for 3 days. A maximum in compressive strength (50–60 MPa) was found in the region of activator SiO_2/Na_2O mole ratio of 1–1.5, and liquid/ash mass ratio of 0.5–0.8.

Sodium aluminate, especially as an industrial waste source, showed significant potential in the process of alkali activation. Phair and van Deventer (2002) investigated various fly ash-based geopolymeric matrices activated with alkali silicate or alkali aluminate solutions. In some cases aluminate-activated geopolymers provided higher strength than traditional silicate-activated geopolymers. Van Riessen *et al*. (2013) explored a synergy between the alumina and geopolymer industries by using Bayer process liquors as a primary source of caustic sodium aluminate and by adding locally available fly ash as a source of reactive silica and additional alumina. Use of processed plant liquor resulted in the geopolymer compressive strength of 43 MPa. Ogundirana *et al*. (2013) explored the use of a spent aluminum etching solution (AES), which contains sodium aluminate, as an alkali activator. Fly ash/BFS slag mixture was activated with AES solution. Compressive strength of ~80 MPa was obtained after 28 days of curing at room temperature. However, the adverse effects of use of sodium aluminate were also reported. The incorporation of sodium aluminate into Class C fly ash alkali-activated by 10 M NaOH solution reduced the compressive strength (Oh *et al*., 2012).

7.3.3.2 Mixing conditions

Water plays an important role in the whole process of AAB synthesis. Water is a transporting medium for dissolved substances, but it does not take part in the chemical reaction, as in the case of Portland cement. Nevertheless, if the appropriate conditions for the reaction of alkali activation would be achieved, then the amount of water present in the system becomes an important factor for AAB workability and consequently for AAB strength.

Yang *et al*. (2009) examined the influence of water/binder ratio on flow and compressive strength of sodium silicate-activated slag and fly ash. Alkali-activated slag mortars exhibited much higher compressive strength but slightly less flow than fly ash-based mortars for the same mixing condition. The highest mortar strength was achieved with the lowest water/binder ratio of 0.3. High liquid/solid ratio

could accelerate the dissolution of raw materials and the hydrolysis of Si^{4+} and Al^{3+} compounds but hinder the polycondensation when OH^- concentration is high enough (Zuhua *et al*., 2009). Kobera *et al*. (2011) have shown that small changes in the mixing procedure may dramatically affect mechanical properties of metakaolin-based geopolymer. They have examined two different methods of required water addition: (A) mixing water with alkali activated metakaolin (AAMK), when initial gel was already formed, or (B) Mixing water with activator solution, before alkali activation itself. Curing of AAMK at room temperature for 7 days provided similar compressive strength of (65–67 ± 5 MPa) of both geopolymer systems. However, additional accelerated aging (at 140°C for 14 days) caused significant differences in mechanical behavior. While system A exhibited unaltered compressive strength of about 69 ± 5 MPa, the compressive strength of system B was markedly reduced to ~55% of the original value (37 ± 5 MPa), which was explained by extensive crystallization (zeolitization). It was also concluded that the mechanical strength of prepared geopolymers was affected by the extent of hydration, i.e. the strength of binding water into the inorganic framework.

7.3.4 Curing conditions

Curing conditions prior to testing have an extremely significant impact on the mechanical properties of AAB, as the provision of proper curing is essential for high strength development (Kuenzel *et al*., 2012). Although the majority of standard procedures for Portland cement mechanical properties testing are applicable to AAB testing, the most desirable curing condition for Portland cement, such as curing in water, is not applicable, as it would lead to premature leaching and unavoidable loss of strength (Kirschner and Harmuth, 2004; Sajedi and Razak, 2010). Curing in a humid chamber (RH > 90%) at room temperature represents a more appropriate option (Rodríguez *et al*., 2008; Baščarević *et al*., 2013; Komljenović *et al*., 2013). If the reaction of alkali activation at room temperature is relatively slow then heat or steam curing would be required. However, it might lead to a halt in strength development or even to strength loss, if the water present in the system and required for the reaction continuance is irreversibly lost.

There is a strong influence of curing temperature on strength development of alkali-activated BFS mortar, with significant retardation at 5°C and significant acceleration at 40°C, as compared with the strength development while curing at 20°C (Brough and Atkinson, 2002). Curing at 80°C developed strength very rapidly, over 70 MPa after 12 hours, quite similar to the strength achieved after 28 days at room temperature. Aydın and Baradan (2012) studied the effects of heat (steam and autoclave) curing on the mechanical properties and microstructure of AAS mortars. A compressive strength of 70 MPa has been reached by incorporation of 2% Na_2O under autoclave curing. Steam curing presented similar mechanical performance with autoclave curing for AAS mortar activated by the solutions with high modulus. Both curing methods were significantly effective in terms of reducing drying shrinkage of AAS mortars.

Heat treatment (closed curing) was found to be very effective in promoting high early strength of alkali-activated BFS concrete (AASC), and reducing drying shrinkage as well (Bakharev *et al.*, 1999b). However, due to inhomogeneity of the microstructure and coarse pore structure, the strength of AASC at later ages was significantly reduced compared with AASC cured at room temperature. Collins and Sanjayan (1999b, 2001) studied the strength development and shrinkage of AASC cured at room temperature and different humidity ('bath' curing in lime-saturated water, 'exposed' curing at 50% RH, and 'sealed' curing in two polyethylene bags and a sealed container). Bath curing provided the highest strength, followed by sealed and exposed curing. Besides the lowest strength, exposed curing also showed 17% strength loss of AASC between 28 and 365 days, due to the loss of water, microcrack formation, and high drying shrinkage during this process. Obviously, if being used for construction purposes, it is imperative for the AASC to be properly cured.

A process technology at ambient temperature may be less feasible for the production of building materials due to delayed setting and strength evolution. Kirschner and Harmuth (2004) investigated the effects of different curing conditions on the strength development of metakaolin-based geopolymers. Curing in water at ambient temperature deteriorated geopolymer strength in all cases, but the formation of cracks was suppressed. Curing at elevated temperature provided almost 50% lower strength than curing at ambient temperature, but also without crack formation. A heat treatment at 75°C for 4 h yielded desirable properties like water resistivity, limited shrinkage and sufficient strength values.

Rovnanik (2010) has also analyzed the effects of different curing regimes on the compressive and flexural strength development of alkali-activated metakaolin. Curing at elevated temperature accelerated geopolymer strength development, but after 28 days the strength was lower compared with the strength of geopolymers obtained at room or slightly decreased temperature. Curing at 80°C for 1 h, as well as at 40°C for 4 h produced relatively high early (1 day) strength, and the highest 28 days strength. The increase of curing temperature and time caused an increase of pore size and cumulative pore volume, which deteriorated mechanical properties. Temperature of 10°C retarded the setting and hardening of geopolymer mixture to 4 days, but it had no negative effect on the quality and properties of hardened product at the age of 28 days.

An interesting two-phase geopolymerization was reported by Alshaaer (2013). Immersion of kaolinite-based geopolymers in an alkali solution at 80°C for 1 h, as a second-phase geopolymerization, was investigated. The geopolymers produced exhibited an increase in compressive strength from 46 to 59 MPa, and from 22 to 27 MPa after drying and water immersion, respectively.

Curing conditions determine the water available during AAFA matrix hardening, and they play an essential role in the strength development. Palomo *et al.* (2004) studied the strength evolution of the sodium hydroxide-activated fly ash pastes as a function of temperature and time of activation. Higher reaction temperature and prolonged curing time developed higher strength, and the temperature was more influential than time. However, there was a temperature-dependent threshold for strength evolution, above which the increase in strength was markedly slower.

The influence of hydrothermal (closed heat) curing on geopolymer strength development, based on Class F fly ash activated by sodium silicate and sodium hydroxide solutions, was studied by Bakharev (2005). The effect of storage at room temperature (pre-curing) before the application of heat on strength development was also studied. Long pre-curing at room temperature was beneficial for strength development as it allowed shortening of time of heat treatment for high strength achievement. Shorter (6 h) heat curing was more beneficial for the strength development of fly ash activated by sodium silicate than longer (24 h) heat treatment. Geopolymer formed with sodium hydroxide had more stable strength properties than samples formed with sodium silicate. The changes which occurred after 24 h of heat treatment were reversible in the case of sodium silicate activator, as up to 20% loss of strength was observed afterwards for samples cured in water and in air. The strength retrogression of sodium silicate-activated fly ash is quite similar to the phenomenon noticed by Collins and Sanjayan (2001) in sodium silicate-activated BFS. Chindaprasirt *et al*. (2011) also studied the effect of the delay time (pre-curing at room temperature) before heat curing on the strength development of high-calcium fly ash-based geopolymer. The delay time had a positive impact on the strength development, but the effects of the delay time on the strength development of geopolymer mortars depended on the fineness of the fly ash as well.

Closed heat curing (at 85°C up to 7 days, RH > 90%) provided much higher strength with respect to open heat curing, where lower relative humidity (RH < 50%) was present and carbonation was not prevented (Criado *et al*., 2005). Curing procedures favoring carbonation negatively affected the strength development. The initial carbonation of the system involved the reduction of the pH levels, and therefore, the ash activation rate and the strength development were notably slowed down. Kovalchuk *et al*. (2007) have examined the effects of different curing regimes on Class F fly ash activated by sodium silicate. Sealed curing in molds at 95°C, dry curing at 150°C and steam curing at 95°C of demoulded samples were applied. Curing in covered molds can be successfully used with any type of AAFA mix, since it provides strength up to 102 MPa after 8 h of curing (Table 7.1). Dry curing was recommended only for NaOH-based systems (i.e., systems with a low SiO_2/Al_2O_3 ratio), since sodium silicate-based mixes tend to retard reaction kinetics. Izquierdo *et al*. (2010) studied geopolymers based on co-fired fly ash and BFS, synthesized

Table 7.1 Compressive strength (MPa) of alkali-activated fly ash paste versus mix composition and curing condition

	Molar ratio		Compressive strength after		
	SiO_2/Al_2O_3	Na_2O/Al_2O_3	Curing in covered moulds (CCM)	Dry curing (DC)	Steam curing (SC)
S4N1	4	1	102.1	31.8	71.0
S3N1	3	1	88.9	57.1	55.5
S4N0	4	0.5	64.1	27.6	76.0
S3N0	3	0.5	50.4	45.6	36.4

Source: Reprinted from Kovalchuk *et al*., 2007, Copyright © 2007, with permission from Elsevier.

at room temperature in open and closed curing conditions. Open curing conditions produced geopolymers characterized by high porosity and low compressive strength (16–26 MPa at 28 days), while closed curing promoted less porous systems and higher strength (49–52 MPa at 28 days).

Curing of bottom ash-based geopolymer mortar under controlled conditions (at room temperature 23 ± 2°C, and 50% RH) up to 1 year caused fluctuation of strength between 28 and 360 days, and even reduction of strength in the case of lower fineness of bottom ash (Sata *et al*., 2012). The need for the proper curing after hardening was confirmed by Baščarević *et al*. (2013). They studied the strength development of several Class F fly ashes alkali-activated by sodium silicate at 95°C for 24 h, and cured afterwards at room temperature in a humid chamber (RH > 90%) for up to 540 days. Minor fluctuation of strength but no significant strength reduction was noticed, probably due to high relative humidity present while curing at room temperature, and possible carbonation which was not prevented. The strength fluctuation also depended on the properties of the fly ash itself.

Unconventional curing by ultrasound or microwaves was also reported. The use of ultrasonication during geopolymerization increased compressive strength of metakaolin and fly ash-based geopolymers (Feng *et al*., 2004). Microwave curing of fly ash-based geopolymers accelerated the geopolymerization process and produced faster mortar strength development and high strength comparable to the conventional heat curing (Somaratna *et al*., 2010; Chindaprasirt *et al*., 2013) (Figure 7.6).

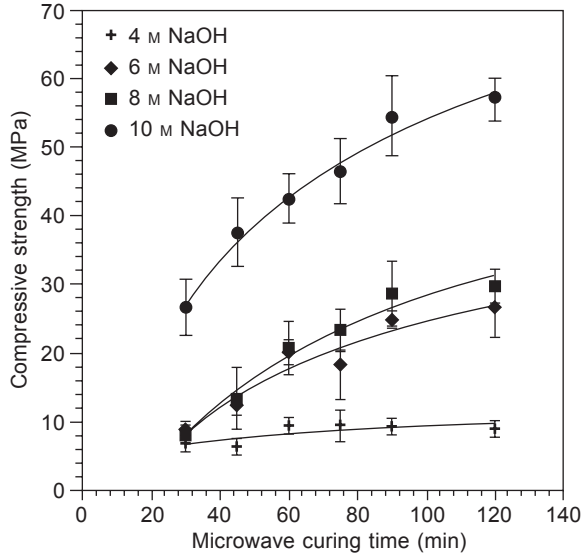

(a)

Figure 7.6 Response of alkali-activated fly ash mortars to microwave curing. Error bars indicate one standard deviation from the mean compressive strength of three companion specimens. (a) Compressive strength versus microwave curing time and NaOH solution concentration. (b) Comparison of compressive strengths of heat cured (48 h at 75°C) and microwave cured mortars (reprinted from Somaratna *et al*., 2010, Copyright © 2010, with permission from Elsevier).

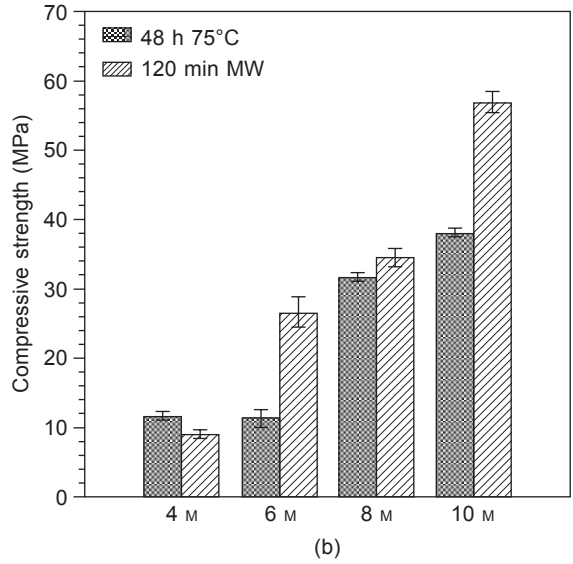

Figure 7.6 Continued

7.4 Tensile strength of alkali-activated binders

Alkali-activated slag concrete (AASC) showed greater tensile strain capacity than OPC concrete due to the greater creep, lower elastic modulus and higher tensile strength of AASC (Collins and Sanjayan, 1999b; Chi, 2012). Alkali-activated fly ash concrete (AAFAC) generally shows higher splitting tensile strength than the OPC concrete of similar compressive strength. Olivia and Nikraz (2012) optimized synthesis condition properties of AAFAC by using the Taguchi method. A compressive strength of 55 MPa of AAFAC at 28 days of curing was achieved. AAFAC showed higher splitting tensile and flexural strength, lower modulus of elasticity, and less drying shrinkage in respect to the OPC concrete of similar compressive strength (Table 7.2).

Ryu *et al*. (2013) investigated compressive and splitting tensile strength of AAFAC. The ratio of splitting tensile strength of AAFAC to its compressive strength was in the range from 7.8 to 8.2%, similar to that of OPC concrete. A new empirical formula was proposed for the relationship between compressive and splitting tensile strength. Sarker (2011) investigated the bond and tensile strength of AAFAC with reinforcing steel. AAFAC showed higher bond strength and higher splitting tensile strength than the reference OPC concrete of similar compressive strength. Heat-cured AAFAC needed a higher stress for the formation of cracks, and the failure modes were generally more brittle than those of the OPC concrete of similar compressive strength, due to the denser interfacial transition zone, higher bond and tensile strength of AAFAC (Sarker *et al*., 2013). Jing *et al*. (2006) activated fly ash with a mixture of calcium hydroxide and sodium hydroxide, compacted in a mold at 20–50 MPa, and then hydrothermally cured in an autoclave at 150–250°C for 15–60 h. The tensile strength determined by the Brazilian test reached more than 10 MPa.

Table 7.2 Mechanical properties of alkali-activated fly ash concrete (T) and OPC control concrete versus time

	Compressive strength (MPa)		Flexural strength (MPa)		Splitting strength (MPa)		Modulus of elasticity (GPa)		Poisson's ratio	
	28 days	91 days	28 days	91 days	28 days	91 days	28 days	91 days	28 days	91 days
OPC (control)	56.22	65.15	7.33	7.02	3.97	4.25	34.16	37.64	0.14	0.15
T7	56.49	56.51	7.39	9.21	4.13	4.18	25.33	27.18	0.15	0.17
T4	56.24	58.85	8.99	9.36	3.96	4.10	26.95	28.03	0.13	0.15
T10	60.20	63.29	8.38	9.85	4.29	4.79	29.05	26.80	0.15	0.15

Source: Reprinted from Olivia and Nikraz, 2012, Copyright © 2012, with permission from Elsevier.

Tho-in *et al*. (2012) evaluated the properties of pervious geopolymer concrete (PGC) made of high-calcium fly ash, activated with sodium silicate and cured at 60°C for 48 h. A compressive strength between 5.4 and 11.4 MPa and splitting tensile strength between 0.7 and 1.4 MPa were obtained. PGC showed mechanical properties similar to those of conventional pervious concrete. Properties of PGC made of high-calcium fly ash geopolymer binder and recycled aggregates (crushed structural concrete member and crushed clay brick) were further analyzed by Sata *et al*. (2013). The results of compressive strength, splitting tensile strength, total void ratio, and water permeability coefficient of the PGCs indicated that both investigated types of recycled aggregates can be used for making PGC with acceptable properties.

7.5 Young's modulus of alkali-activated binders

The fundamental properties of cement and/or concrete are affected by the material properties at the nanoscale. In order to improve the macroscale properties, it is necessary to first understand the nanoscale properties.

7.5.1 Alkali-activated binder gels

Recently published nanoindentation studies identified the elastic properties of basic structural units (gels) of AAB. Puertas *et al*. (2011) studied mechanical performance of C-S-H gels formed as a result of Portland cement hydration and of alkali activation of slag. C-S-H gel in OPC, and both (sodium hydroxide- and sodium silicate-activated) C-A-S-H gel in AAS, had distinct Young's modulus of elasticity and hardness. The C-A-S-H in AAS, like the C-S-H gel in OPCs, can be found in three different mechanical states. After 28 days of curing in a humid chamber (98%

RH, 20 ± 2°C) Young's modulus of C-S-H gel in OPC was in the overall range from 16 to 44 GPa, and hardness in the range 0.40–1.40 GPa. At the same time NaOH-AAS showed modulus of 12–43 GPa, and hardness 0.30–1.32, while sodium silicate-AAS showed 28–47 GPa, and 0.84–1.53. The nanoindentation measurements reflected porosity-related effects, i.e. dependence of Young's modulus on packing efficiency. The C-A-S-H gel formed in sodium silicate-AAS had a very densely packed structure and the highest modulus of elasticity, followed by NaOH-AAS. The C-S-H gel formed in hydrated Portland cement had the lowest packing density and the lowest modulus of elasticity (Figure 7.7). Oh *et al*. (2011) studied the influence of Al substitution for Si on mechanical properties of C-S-H(I) by using high-pressure synchrotron X-ray diffraction analysis. The reaction product of alkali-activated slag

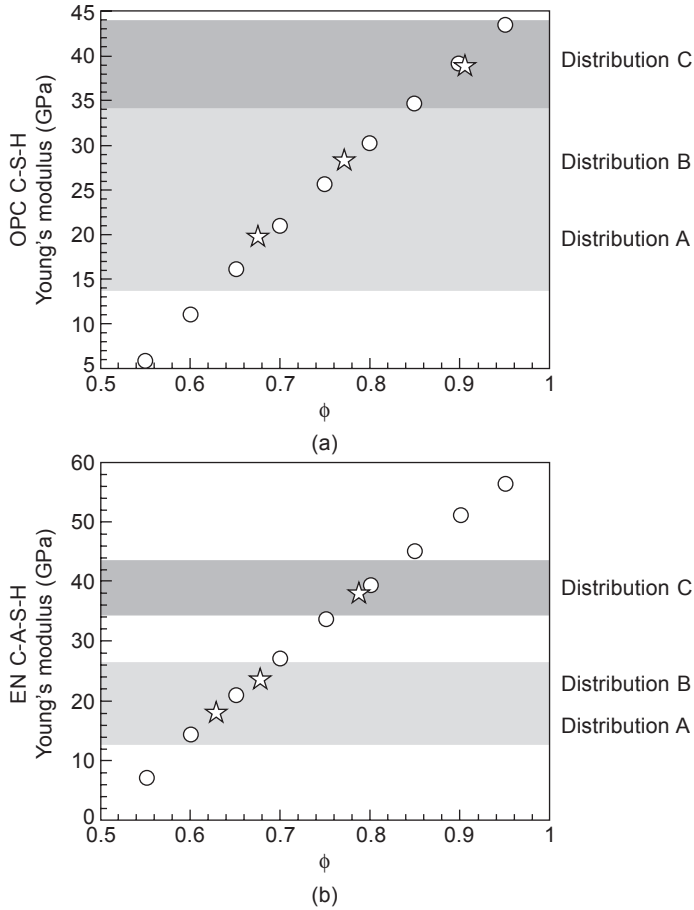

Figure 7.7 Young's modulus versus porosity for Portland cement (OPC) C-S-H, NaOH-activated (EN) C-A-S-H, and waterglass-activated (EW) C-A-S-H (reprinted from Puertas *et al*., 2011, Copyright © 2011, with permission from Elsevier).

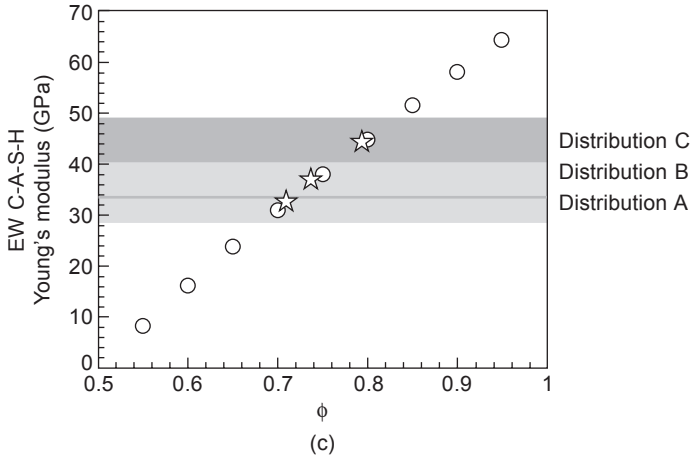

Figure 7.7 Continued

and synthetic C-S-H(I) were compared and it was found that, regardless of the Al substitution, different C-S-H(I) possessed similar mechanical properties.

Němeček *et al*. (2011) studied elastic properties of the main reaction product (N-A-S-H gel) of alkali-activated aluminosilicate materials. Low calcium ground fly ash and metakaolin were activated with sodium silicate solution and cured under ambient (at ~22°C for 6 months) and heat conditions (at 80°C for 12 h). The mature N-A-S-H gel had almost constant intrinsic Young's modulus of approximately 17–18 GPa, independent of the precursor material (fly ash or metakaolin) and curing conditions (ambient or heat cured) for a given mixture composition. The determined value of Young's modulus was similar to the typical value of 17.8 GPa for the low-density C-S-H gel found in cement paste. Da Silva *et al*. (2014) have recently proposed a new methodology for nanoindentation-assisted prediction of macroscale elastic properties, which allows a reliable advanced prediction of elastic properties of cementitious composites (Figure 7.8).

7.5.2 Alkali-activated binder paste

Young's modulus is influenced rather by the alkali-activated metakaolin microstructure than by its chemical composition (Duxson *et al*., 2007b). The development of Young's modulus was observed to be dependent on both Si/Al ratio and alkali (sodium and potassium), which may be related to the two different microstructures observed to form in the same specimens. The mixed-alkali (Na/K = 1/3) specimen with Si/Al = 2.15 exhibited maximum Young's modulus of ~6 GPa after 28 days of aging (Figure 7.9).

The effects of Si/Al ratios (in the 1.25–2.5 range), alkaline activator (K or Na), and curing time on the structure and mechanical properties (compressive strength, Young's modulus, hardness, and fracture toughness) of geopolymers were also

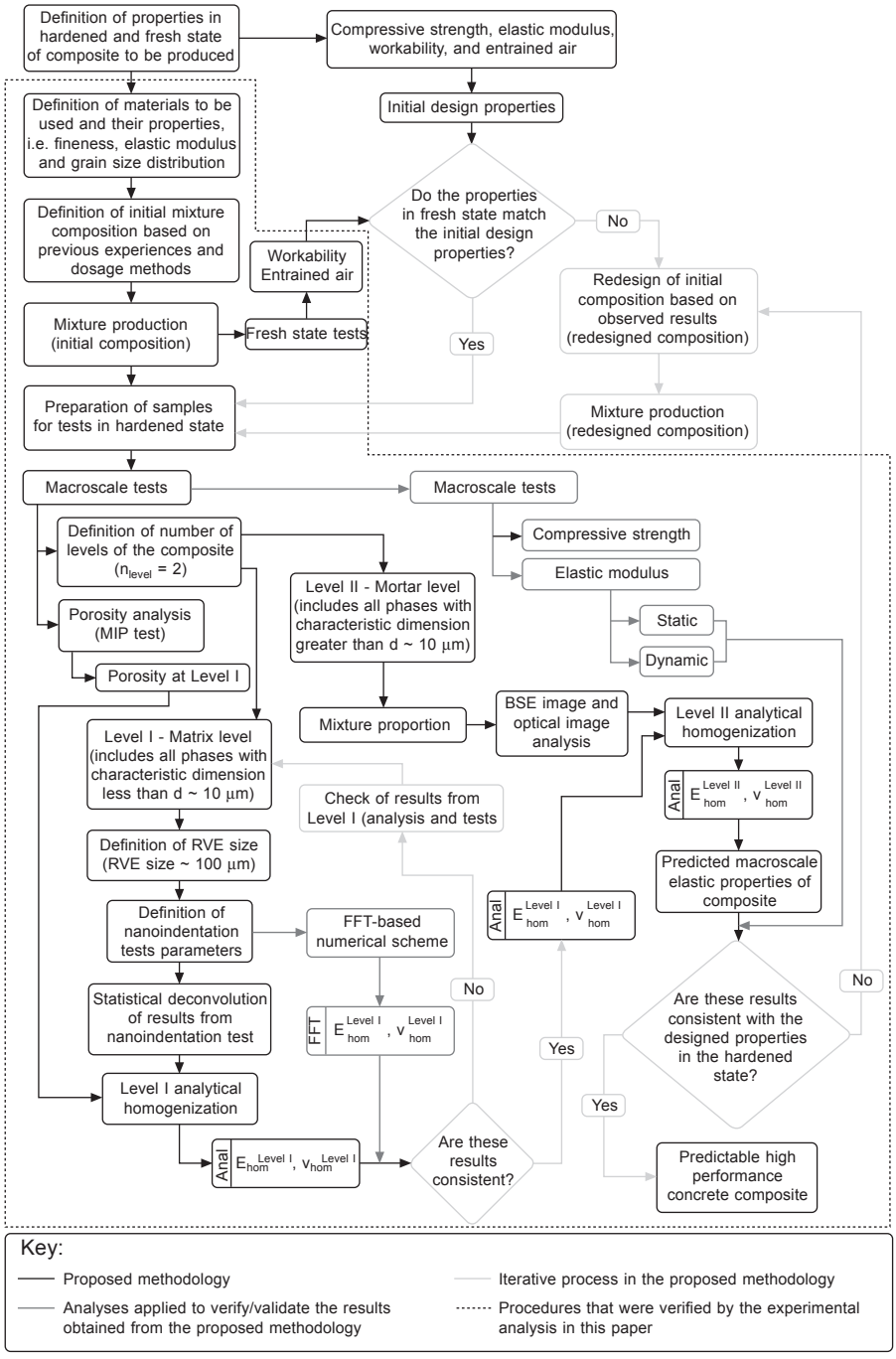

Figure 7.8 Flowchart of the nanoindentation-assisted methodology for prediction of macroscale elastic properties of high performance cementitious composites (reprinted from da Silva *et al.*, 2014, Copyright © 2014, with permission from Elsevier).

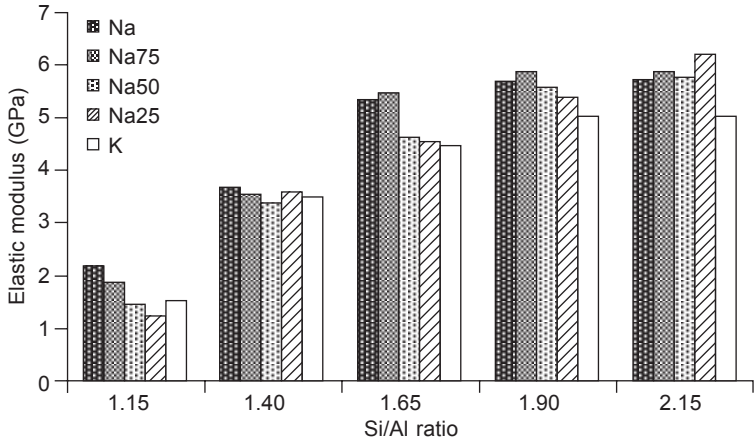

Figure 7.9 Elastic modulus (after 28 days) of metakaolin-based geopolymer pastes versus Si/Al molar ratio and Na/(Na + K) ratio (reprinted from Duxson *et al*., 2007b, Copyright © 2007, with permission from Elsevier).

studied by Lizcano *et al*. (2012). Metakaolin and SiO_2 mixture were alkali-activated (NaOH or KOH) and cured at 80°C for 24 and 48 h. The density of the geopolymers increased with increasing Si/Al ratios for both alkali activators, with significant effect on improvement of mechanical properties. The Young's moduli of both Na- and K-based geopolymers increased with increasing Si/Al ratio up to Si/Al = 2.0. At higher ratios of Si/Al, all mechanical properties decreased regardless of increasing density. Potassium-activated geopolymer with Si/Al = 2.0 exhibited the highest Young's modulus of ~5.5 GPa after 24 h of curing at 80°C. The trends shown, as well as measured values of Young's modulus are quite similar to the results obtained by Duxson *et al*. (2007b). Kamseu *et al*. (2013) investigated the effects of bulk composition and microstructure on strengthening mechanisms and fracture resistance of metakaolin-based geopolymers. Geopolymers with variable Si/Al molar ratio (1.15–2.19) were obtained by alkali activation (sodium hydroxide, potassium hydroxide, and sodium silicate) of mixtures of two different types of metakaolin (Al-rich and Si-rich). Flexural strength, Young's modulus, and impact toughness increased with increasing Si/Al molar ratio due to the formation of more polymerized phases and the presence of incompletely dissolved silica particles which contributed to the porosity reduction.

Kirschner and Harmuth (2004) investigated the effects of curing conditions and degree of reaction on Young's modulus of geopolymer binders, based on a commercial metakaolin activated with sodium silicate. The geopolymers were cured at 75°C for 2 or 4 h, and then cured either at ambient conditions or under water for 28 days. The initial modulus of elasticity was much higher after 4 h of curing at 75°C (9.20 GPa) than after 2 h of curing (4.82 GPa) confirming modulus of elasticity dependence of the degree of reaction. Further curing also had an impact on modulus of elasticity. After 28 days of curing at ambient conditions both geopolymers had similar modulus of ~7 GPa, while curing under water did not significantly affect the initial modulus

of elasticity. Geopolymer modulus of elasticity dependence of the degree of reaction was confirmed by Williams *et al*. (2011). Metakaolin was activated with sodium silicate solution, and then cured in sealed containers at 70°C for 24 h. Variable elemental Si/Al ratio (1.55–3.08) of the bulk geopolymer samples caused different degree of reaction of metakaolin and different mechanical properties. The fraction of reacted metakaolin varied with only small changes in bulk chemistry from 10 to 75% for geopolymers with compressive strengths varying from 3.1 to 67 MPa, and Young's modulus from 0.24 to 2.0 GPa.

He *et al*. (2012) studied the effects of source materials on mechanical properties by comparing two geopolymers derived from metakaolin and red mud–fly ash admixture. The stress–strain curves of the two geopolymers cured at room temperature at different durations exhibited a well-defined elastic regime, but the yielding was poorly defined. The metakaolin-based geopolymer exhibited higher compressive strength and greater stiffness or Young's modulus than the red mud–fly ash-based one. Williams and van Riessen (2010) determined accurately the composition of the amorphous part of three different types of fly ash and synthesized geopolymers accordingly. The average geopolymer paste compressive strength was from 9.5 to 48 MPa, while Young's modulus was from 1 to 2 GPa, respectively. The metakaolin geopolymer made with the same nominal composition was found to have a compressive strength of 32 MPa with a Young's modulus of 1.73 GPa. Van Riessen and Chen-Tan (2013) studied the beneficiation of fly ash conducted in a three-stage procedure using sieving, milling, and magnetic separation. Despite a 20–30% increase of geopolymer paste compressive strength, Young's modulus stayed within a very narrow range (3.10–3.58 GPa), and at low values in comparison to the high strength cement (>20 GPa). The lower than expected improvement of geopolymer mechanical properties was attributed to the changes in formulation required to maintain workability.

7.5.3 Alkali-activated binder mortar

Pelisser *et al*. (2013) characterized the mechanical and micro-nanomechanical properties of metakaolin-based geopolymer pastes and mortars. After 28 days of curing, geopolymer paste showed 64 MPa compressive strength, 17.6 MPa flexural strength, and elastic modulus of about 10 GPa. An excellent ratio between the flexural and compressive strength (27%) indicated good geopolymer resistance to cracking while under stress. Geopolymer mortar (sand/binder ratio = 3) compressive strength and elastic modulus were 59 MPa and 24.4 GPa, respectively. An increase of sand/binder ratio up to 5 also increased elastic modulus up to 31.3 GPa. The micro-nanomechanical properties of the geopolymer were very similar to those obtained for Portland cement. However, the geopolymer achieved greater deformation capacity and tensile strength than Portland cement.

Latella *et al*. (2008) determined the mechanical properties of different types of geopolymer mortar, but of the same composition (Na/Al ≈ 1, Si/Al ≈ 2 molar ratio). Four different combinations of different precursors and activators (metakaolin and sodium aluminate and sodium silicate; metakaolin and fumed silica and sodium

hydroxide; metakaolin and colloidal SiO_2 and sodium hydroxide; metakaolin and sodium silicate) were used. The water content was dependent on the precursor used. Sealed curing in an oven at 60°C for 24 h was performed. The average geopolymer mortar compressive strength with 40% of sand was from 16 to 70 MPa, while Young's modulus was from 5.5 to 14 GPa, respectively. Corresponding geopolymer pastes exhibited up to 20% higher compressive strength, but much lower Young's modulus (up to 50%). The porosity level dictated the mechanical properties and Young's modulus of the geopolymers irrespective of precursor type or composition. The removal of large macropores (defects) and minimization of the overall porosity is a requisite for improved strength and toughness. The mechanical properties of the geopolymers investigated are generally lower than those of ordinary Portland cement.

Temuujin *et al*. (2010) examined mechanical properties of fly ash-based geopolymer mortars with varying levels of sand aggregate (from 9 to 1). Compressive strength and Young's modulus of the geopolymer paste were 60 MPa and 2.27 GPa. Increase of the sand aggregate amount up to 50 wt.% did not affect either geopolymer mortar strength or modulus significantly. Geopolymer binder exhibited strong bonding to the sand aggregate as the amount of alkaline activator remained constant, while the increase in sand content resulted in a decreasing level of geopolymerization within the binder system. Steinerova (2011) also examined mechanical properties of metakaolin-based geopolymer mortars with varying levels of quartz sand aggregate (from 0 to 93%). The optimal content of the quartz sand aggregates was in the range of 75–78 wt.%, reaching compressive strength of 70 MPa, flexural strength of 11.7 MPa, and Young's modulus of 19 GPa. Such properties were the result of the strengthening effect of sand, strong interface, and a lack of large voids due to packing.

7.5.4 Alkali-activated binder concrete

Yang and Song (2012) provided a data bank and comprehensible design equations for the mechanical properties of calcium hydroxide-based alkali-activated BFS concrete. A total of 34 concrete mixtures were prepared. As the mechanical properties of AAS concrete mostly disagreed with predictions obtained from the equations specified in Code provisions, such as ACI 318-08, CEB-FIP, and EC2 for OPC concrete, new equations were proposed. The mechanical properties, including moduli of elasticity and rupture, splitting and direct tensile strengths, shear strength, and bond strength were proposed as a power function of the 28-day compressive strength (f'_c) (Figure 7.10).

Hardjito (2005) studied mechanical properties of AAFAC based on Class F fly ash activated with sodium silicate. Naphthalene-based superplasticizer was used to improve the workability of concrete. The majority of the coarse aggregate fraction was of granite type. Curing at elevated temperatures (30–90°C) was performed in two different ways, i.e. dry curing (covered, wrapped) in a laboratory oven or steam curing in a chamber. Mean concrete compressive strength was in the range from 44 to 89 MPa. The elastic properties of hardened fly ash-based geopolymer concrete,

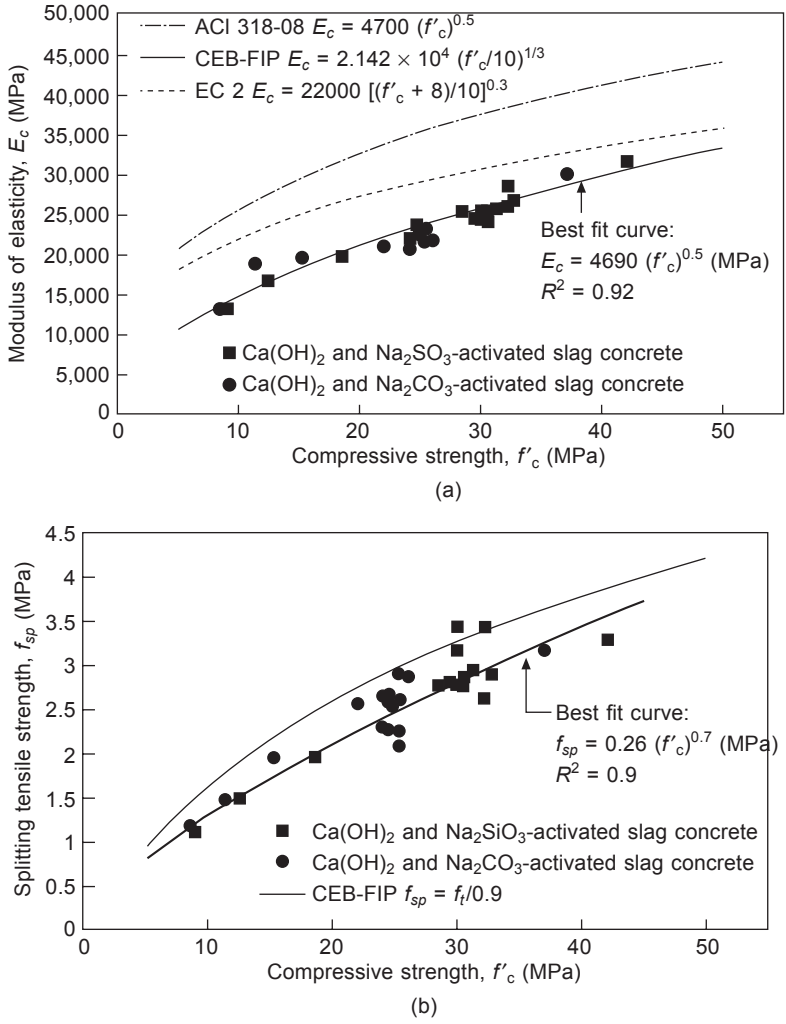

Figure 7.10 Empirical equations for mechanical properties of $Ca(OH)_2$-based alkali-activated slag (AAS) concrete: (a) modulus of elasticity versus compressive strength; (b) splitting tensile strength versus compressive strength (Yang and Song, 2012).

i.e. the Young's modulus (23–30.8 GPa), the Poisson's ratio (0.13–0.16), and the indirect tensile strength (4.43–7.43 MPa), respectively, were similar to those of ordinary Portland cement (OPC) concrete. The measured stress–strain relations of geopolymer concrete also fitted well with equations developed originally for Portland cement concrete. The suitability of using the existing stress–strain models originally proposed for OPC concrete for the analysis of fly ash-based geopolymer concrete was also confirmed by Sarker (2009) and Yost *et al*. (2013).

Fernández-Jiménez *et al*. (2006b) also investigated engineering properties of

AAFAC. After the first 24 h concrete compressive strength of ~45 MPa was achieved for sodium hydroxide, and ~50 MPa for the sodium silicate system. Besides high strength developing in a short period of time, AAFAC showed lower modulus of elasticity, better bond to reinforcing steel, and much less shrinkage than OPC concrete. Sofi *et al*. (2007) reported that the splitting tensile and flexural strength of AAFAC was comparable with the models presented by the standards for OPC-based concretes. However, elastic modulus of AAFAC was lower than predicted for OPC systems of similar compressive strength. Diaz-Loya *et al*. (2011) studied mechanical properties (static elastic modulus, Poisson's ratio, compressive strength, and flexural strength) of AAFAC made from 25 fly ash stockpiles (both Class F and C) from different sources. The highest compressive strength (~80 MPa), modulus of elasticity (~43 GPa), and Poisson's ratio (0.22) were achieved with Class C fly ash. The average values of the mentioned properties were also higher in the case of Class C fly ash. The mechanical behavior of AAFAC was similar to that of OPC concrete. Flexural to compressive strength ratio of AAFAC was generally higher than predicted by the ACI 318 equation, and this was more pronounced in the case of Class F fly ash. On the other hand, the elastic modulus was generally lower than the ACI 318 prediction (Figure 7.11). Yost *et al*. (2013) fabricated full-scale steel reinforced concrete beams to study the structural behavior of AAFAC. The strength gain at elevated temperature was very rapid and the compressive strength at 1 day ranged between 47 and 53 MPa. The average 28-day compressive strength of AAFAC ranged from 52.2 to 57 MPa. AAFAC is a brittle material with an approximately linear stress–strain response, and an elastic modulus slightly less than that predicted by ACI 318.

Lee and Lee (2013) investigated the mechanical properties of alkali-activated fly ash/BFS concrete manufactured at room temperature. The splitting tensile strength and modulus of elasticity of the alkali-activated fly ash/slag concrete were slightly lower than those of ordinary concrete as predicted by the ACI code and Eurocode 2. High shrinkage of alkali-activated fly ash/slag concrete due to the increased number of small pores caused microcrack formation, and consequently decreased elastic modulus and long-term compressive strength. Wongpa *et al*. (2010) studied properties of inorganic polymer concrete (IPC) based on fly ash and rice husk–bark ash, activated with sodium silicate and cured under ambient conditions. The solution/ash (S/A) ratio was the major parameter controlling compressive strength, modulus of elasticity, and water permeability of IPCs. Paste/aggregate ratio also affected investigated properties of IPCs, but the influence was less expressed. The compressive strength had much lower influence on the modulus of elasticity of IPCs than in the case of conventional Portland cement concrete (Figure 7.12). The compressive strength of IPCs at the age of 28 days (18–35 MPa) had the highest value compared to 7 days and 90 days. However, the modulus of elasticity reached a maximum value after 7 days (10.4–16.9 GPa). After 90 days, modulus of elasticity was much lower (5.6–14.3) due to high shrinkage and very fast crack development, as confirmed by water permeability coefficient increase during the same period.

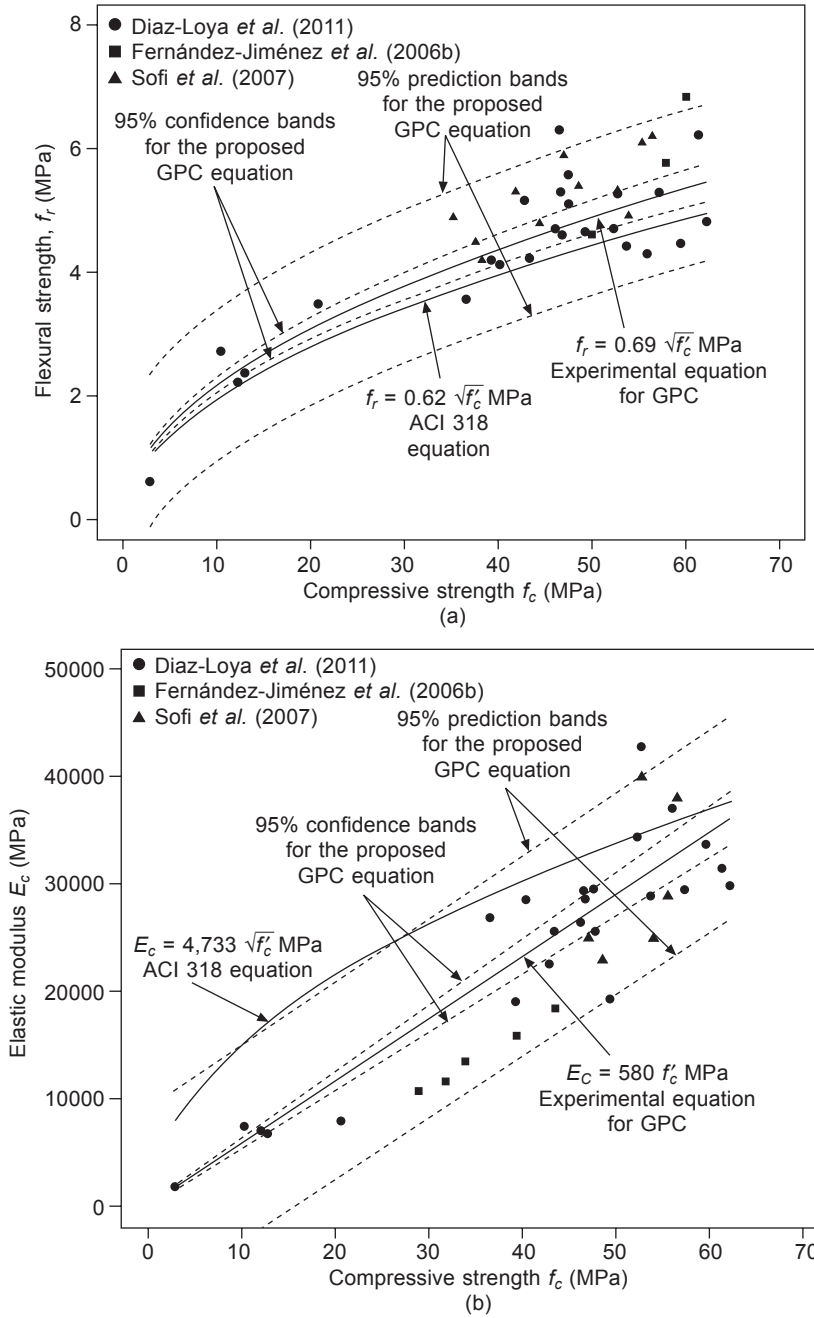

Figure 7.11 Regression models of fly ash-based geopolymer concrete: (a) flexural strength versus compressive strength; (b) elastic modulus versus compressive strength (Diaz-Loya *et al.*, 2011). Data reported by Fernández-Jiménez *et al.* (2006b) and Sofi *et al.* (2007) were also included.

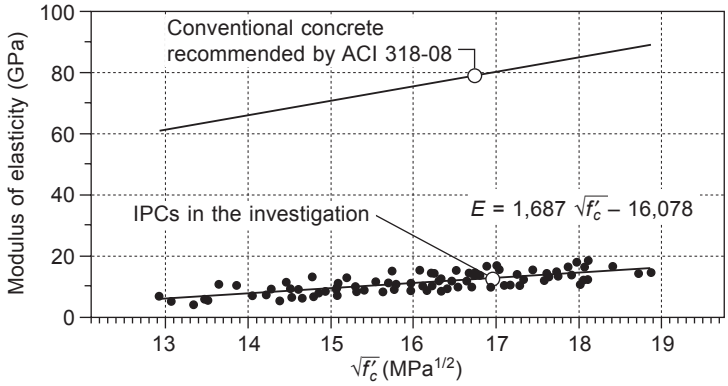

Figure 7.12 Relationship between modulus of elasticity and compressive strength of inorganic polymer concretes (IPCs) (reprinted from Wongpa *et al.*, 2010, Copyright © 2010, with permission from Elsevier).

7.6 Fiber-reinforced alkali-activated binders

The elastic properties of AAB under applied force are of particular importance for construction applications. These properties can be improved by introducing fiber reinforcement, such as short fibers or unidirectional long fibers into the AAB matrix. Incorporation of 0.5% polypropylene fibers (by volume of mortar) had some minor positive effect on mechanical properties of alkali-activated BFS, fly ash or BFS/fly ash (50/50%) mixture, while incorporation of 1.0% polypropylene fibers decreased modulus of elasticity of all investigated binders (Puertas *et al.*, 2003). At the same time the modulus of elasticity of its cement-based counterpart was increased. The inclusion of alkali-resistant glass fibers at a dosage of up to 0.22% in AAS prisms led, as in the OPC specimens, to flexural strength enhancement and 20% reduction of drying shrinkage, but did not influence compressive strength (Puertas *et al.*, 2006). Incorporation of carbon fibers also showed negative impact on mechanical properties of AAS (Alcaide *et al.*, 2007). Both compressive and flexural strength of AAS and reference cement mortar decreased with an increase in carbon fiber content. However, the inclusion of carbon fibers had some positive impact on AAS properties i.e. reduced drying shrinkage by about 50%.

Despite the high brittleness of the AAS mortar itself, strain-hardening and high tensile ductility in polyvinyl alcohol (PVA) fiber reinforced AAS mortar was achieved (Lee *et al.*, 2012). Bernal *et al.* (2010) investigated mechanical properties of AASC reinforced with steel fibers. Splitting tensile and flexural strength was significantly improved with increasing fiber content. However, with increasing fiber content the compressive strength was reduced, both in AASC and OPC type I-based reference concrete. Aydın and Baradan (2013a, 2013b) studied properties of a new type of ultra-high-strength composite material based on alkali-activated slag/silica fume (AAS/SF). This new type of high-performance composite material was developed as an alternative construction material to cement-based reactive powder concrete (CRPC),

with a compressive strength over 200 MPa. In contrast to Portland cement-based systems, the addition of silica fume had a positive effect on reducing water demand and shrinkage in alkali-activated systems. BFS/SF-quartz sand (four different size fractions, 3 mm maximum size) mixture was activated with sodium silicate (M_s = 1.2, 4% Na_2O by weight of binder). Water-to-binder ratio of all mixtures was 0.17. Autoclave curing resulted in lower mechanical properties with respect to the steam curing. In their first paper Aydın and Baradan (2013a) reported the effects of high strength brass-coated steel fiber reinforcement on the properties of AAS/SF mortars. Very high strength of the initial AAS/SF mortars improved dramatically with an increase of fiber volume fraction (0–2.0%) and length (6–13 mm). Compressive strength increased from 132 MPa without fibers to 192 MPa (6 mm fibers) and 223 MPa (13 mm fibers) with 1.5% fiber reinforcement. Further increase of fiber volume fraction (up to 2.0%) had small impact on compressive strength. At the same time flexural strength of mortars increased from 12 MPa without fibers to 25.2 MPa (6 mm fibers) and 48.4 MPa (13 mm fibers) with 2.0% fiber reinforcement. Longer fibers also resulted in better toughness of AAS/SF mortars. Regardless of the fiber length, the increase in fiber content reduced the drying shrinkage of AAS/SF mortars. In the second paper (Aydın and Baradan, 2013b), remarkable engineering properties of this new composite material (ARPC), reinforced with 1.5% high-strength brass-coated steel fibers (13 mm), were reported and compared with a conventional CRPC (Table 7.3).

Incorporation of fibers increases tensile strength of geopolymers and changes fracture behavior from a brittle to a more ductile pattern. MacKenzie and Bolton (2009) investigated mechanical properties of alkali-activated (potassium or sodium

Table 7.3 Mechanical properties of steam-cured and standard-cured alkali-activated (ARPC) and conventional CRPC

	Steam-cured (12 h at 100°C)		Standard-cured (28 days in water at 20°C)	
	ARPC	CRPC	ARPC	CRPC
Compressive strength (MPa)	215.9	214.6	147.5	176.1
Splitting tensile strength (MPa)	19.5	19.2	15.6	15.8
Modulus of elasticity (GPa)	84.1	114.0	46.0	69.2
Poisson's ratio	0.22	0.21	0.21	0.21
Fracture energy (N/m)	16,016	14,200	12,777	15,799
Flexural strength (MPa)	41.5	34.7	25.0	29.6

Source: Aydın and Baradan, 2013b.

silicate) dehydroxylated halloysite clay, reinforced with single-wall carbon nanotubes or graphite. No significant difference between the tensile strengths (~2 MPa) of carbon nanotubes and graphite-containing potassium-based geopolymer composites was noticed, while sodium-based geopolymers performed greater tensile strengths of both composites. Maximum tensile strength (~8 MPa) was obtained at carbon nanotube contents of 0.25 wt.%. The significant difference in tensile strength between investigated composites was explained by the necessity for less processing water in the synthesis of the sodium samples. The use of natural protein-based fibers as long-fiber reinforcement of a geopolymer matrix was reported by Alzeer and MacKenzie (2012). Dehydroxylated kaolinite-type halloysite clay was activated with sodium silicate and reinforced with carpet (crossbred) or Merino wool fibers. The geopolymer composites showed an approximately 40% improvement of flexural strength in respect to the initial matrix, and unlike the initial matrix that displayed ceramic-like brittle fracture, wool-based composites showed graceful failure. Graceful failure of geopolymer composites was also achieved by natural cellulose-based fiber reinforcement (Alzeer and MacKenzie, 2013). The mechanical properties of fiber-reinforced composites improved with increasing fiber content, achieving ultimate flexural strengths of ~70 MPa and modulus of elasticity of ~10 GPa at 10 vol.% fiber content.

An innovative process involving chemical activation with sodium hydroxide, hydrothermal curing (heat and moisture), and hot-pressing of fly ash (both Class F and Class C) was proposed by Sun and Wu (2009). Class C fly ash composite showed greater splitting tensile strength (5.4 MPa) than Class F fly ash under the same hydrothermal hot-pressing conditions. The addition of short PVA fibers significantly improved the ductility of both Class C and Class F fly ash composites (Sun and Wu, 2008). However, the first crack strength and the ultimate tensile strength of Class F fly ash composites were lower than those of Class C fly ash produced under the same conditions.

Li *et al.* (2005) studied mechanical properties of short PVA fiber reinforced metakaolin–fly ash geopolymer composites manufactured by extrusion. Metakaolin replacement by small amounts of fly ash provided higher geopolymer flexural strengths and smaller deflections. The addition of PVA fibers largely increased the ductility of geopolymer and changed the failure modes from a brittle pattern to a ductile one. The addition of PVA fibers also resulted in a great increase in geopolymer impact toughness, while the addition of small amounts of fly ash further improved impact toughness and impact stiffness (Zhang *et al.*, 2006). Larger amounts of added fly ash significantly reduced impact strength, impact toughness, and impact stiffness. Natali *et al.* (2011) investigated alkali-activated metakaolin/ladle-slag reinforced with different types of dispersed short fibers (1 wt.%): HT-carbon fibers, commercial E-glass fibers, PVA fibers, and PVC fibers. Significant flexural strength enhancement (30–70%) of geopolymer composites was achieved by all types of fiber investigated. Maximum values were found for the carbon fiber reinforced sample. Furthermore, the toughness of the investigated geopolymer composites was also increased, exhibiting a switch from a brittle failure mode to a more ductile one.

The effects of steel fiber reinforcement on the engineering properties (compressive strength, splitting tensile strength, modulus of rupture, modulus of elasticity, and Poisson's ratio) of Class F fly ash-based geopolymer concrete was investigated by Ganesan *et al*. (2013). Concrete workability was improved by using a naphthalene-based superplasticizer, and curing was performed for 24 h at a temperature of 60°C. The addition of 1% (by volume) of steel fibers increased compressive strength (49.23 MPa, 8.51% increase), splitting tensile strength (4.17 MPa, 61.63%), modulus of rupture (6.2 MPa, 24%), modulus of elasticity (35.5 GPa, 64.92%), and Poisson's ratio (0.21, 50%).

The fact that short carbon fibers have a great strengthening and toughening effect was proved by Lin *et al*. (2008, 2009). They studied the effects of fiber content on mechanical properties and fracture behavior of short carbon fiber reinforced geopolymer matrix composites. Geopolymer matrix composites based on potassium silicate-activated metakaolin reinforced with different volume fractions of short carbon fibers were prepared. Geopolymer impregnated 20–50 layers of sheet-like short carbon fiber preform were laid together one by one to create a stack. Composites were cured in a vacuum bag at 80°C for 24 h, taken out of the bag and dried for an additional 24 h at 120°C. In order to obtain the final thickness of 5 mm for preform laminates, at the early stage of curing a pressure of 0, 0.2, 1.2, or 2.0 MPa was loaded. A remarkable flexural strength of >90 MPa and Young's modulus of ~12 GPa was achieved at 4.5% of carbon fiber volume fraction (Figure 7.13). Increase of fiber volume fraction up to 6% reduced flexural strength by ~10%, but simultaneously Young's modulus was increased by 65%, up to ~20 GPa. Further increase of fiber volume fraction decreased the investigated properties. The property improvements

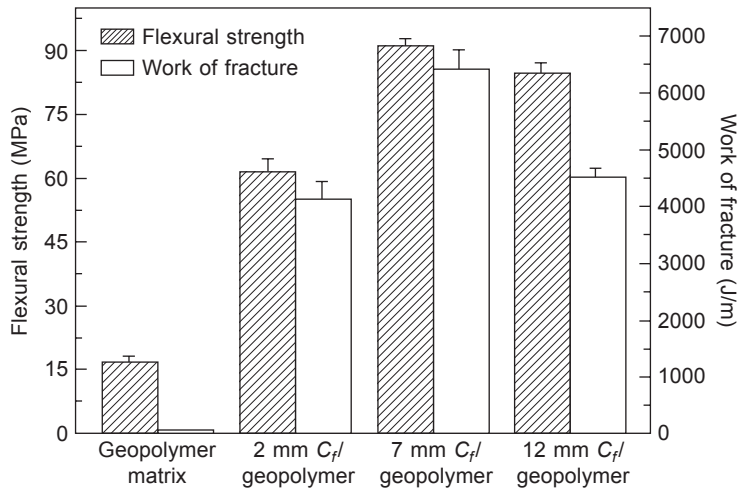

Figure 7.13 Variation of flexural strength and work of fracture of geopolymer matrix and short carbon fiber (C_f) geopolymer composites versus starting fiber length (reprinted from Lin *et al*., 2008, Copyright © 2008, with permission from Elsevier).

were primarily based on the network structure of short carbon fiber preform, and the predominant strengthening and toughening mechanisms were attributed to the apparent fiber bridging and pulling-out effect.

Lin and Jia (2009) studied electroless Ni-plated short carbon fiber reinforced geopolymer matrix composites with various carbon fiber/matrix interface coating thicknesses. Metakaolin was alkali-activated with potassium silicate, reinforced with short carbon fibers and prepared as in Lin *et al*. (2009). The flexural strength and Young's modulus of the investigated geopolymer composites increased as the average fiber coating thickness increased, and exhibited maximums of 55 MPa and 5.4 GPa at 0.15 μm coating thickness. However, the work of fracture showed immediate and sharp decrease, and the fracture manner changed from ductile to brittle. This was attributed mainly to the fact that carbon fibers favor breakage rather than pulling-out during loading because of the higher interface bonding strength of fiber/matrix. Furthermore, pliability of the carbon fibers decreases with the increase of the coating thickness.

High-temperature heat treatment is an efficient method to improve the mechanical properties of carbon fiber reinforced geopolymer composites as demonstrated by He *et al*. (2010). Metakaolin was alkali-activated with potassium silicate and reinforced with unidirectional continuous carbon fiber preform. A green geopolymer composite with 16 layers was prepared by the ultrasonic vibration treatment and degassed at 80°C for 24 h by using a vacuum-bag technique. High-temperature heat treatment (1100–1300°C) significantly improved the mechanical properties of the green geopolymer composites. Flexural strength of the initial geopolymer matrix (~12 MPa) was greatly increased by carbon fiber reinforcement (~133 MPa), and further by high-temperature heat treatment at 1100°C, reaching an amazing ~234 MPa. At the same time the values of Young's modulus were ~10 GPa, ~36 GPa and ~64 GPa, respectively. The amazing improvement in mechanical properties was attributed to the densified and crystallized matrix, and the enhanced fiber/matrix interface bonding based on the fine integrity of the carbon fibers. In contrast, the mechanical properties of geopolymer composites heat treated at 1400°C, were substantially lower followed by a very brittle fracture manner.

Geopolymers tend to be more brittle than OPC and thus less suitable for concrete structures due to safety concerns. On the other hand, geopolymers can also be used as self-sensing materials capable of detecting their own structural damage due to improved electrical properties. Saafi *et al*. (2013) investigated the effects of multiwalled carbon nanotubes on the mechanical and electrical properties of fly ash-based geopolymer composites. Low calcium fly ash was activated with sodium silicate, reinforced with carbon nanotubes (0–1.0% by weight) and cured in an oven at 60°C for 24 h. The addition of carbon nanotubes significantly increased the flexural strength (160%), Young's modulus (109%), flexural toughness (275%), fracture energy and electrical conductivity (both by 194%). It was concluded that geopolymer nanocomposites exhibited a piezoresistive response with high sensitivity to micro-crack propagation.

7.7 Conclusions and future trends

AAB are most commonly based on blast furnace slag, metakaolin (calcined clays), and/or coal fly ash as prime materials. Other industrial waste and natural materials have been used to a limited extent. However, it is worth mentioning such materials, as their use represents alternative routes for the development of AAB. Steel (ladle) slag, phosphorus slag, ferronickel slag, non-ferrous metallurgy slags, red mud, waste ceramic, tungsten mine waste, copper mine tailings, fluid catalytic cracking catalyst residue, air pollution control residue glass, cement-rich fraction of construction and demolition waste, municipal solid waste incineration ash, palm oil fuel ash, rice husk and bark ash, volcanic ash, kaolinitic clay, natural zeolites, and natural pozzolans, have been used among others. The list of potential prime materials is growing as the interest in the development of more 'green' and sustainable materials in the environmentally conscious age also grows.

Combined mechanical and chemical (alkali) activation provides a plausible solution for the use of lower quality prime materials in terms of their homogeneity, particle size, and reactivity. The quest for an inexpensive and abundant alkali activator is still in progress. Sodium aluminate, especially as an industrial waste source, showed respectable potential in the process of alkali activation. Little attention was paid to the mixing procedures during AAB preparation, as they may significantly affect the mechanical properties of AAB. More attention should be paid to such alternatives in the future.

Excess of water needed for the proper workability achievement still remains a limiting factor. Standard water reducing admixtures developed for the Portland cement systems do not work properly under high alkaline conditions present during the alkali activation process. The development of such admixtures would provide significant impact to the mechanical properties and durability improvement, and consequently to wider structural and non-structural applications of AAB.

Despite being the basic mechanical properties of AAB, comparing the results of mechanical strength and modulus of elasticity is not a simple task due to numerous differences in experimental conditions. Lack of standard testing procedures developed for AAB systems is widely recognized. Very high compressive strength of AAB can be obtained, even at room temperature. The flexural/compressive strength ratio of AAB is equal or better than its OPC counterpart. However, high sensitivity of AAB to environmental conditions, especially to relative humidity at early age, still exists. Therefore, appropriate curing to full maturity of AAB is one of the most important factors which should be controlled. Unconventional curing by ultrasound or microwaves was also recognized as a plausible improvement. Other routes for accelerated curing, especially those based on low energy consumption, should also be explored.

The majority of the results of mechanical properties presented here have been achieved more by trial and error than by an in-depth understanding of what is happening at the micro- or nanoscale. Nanoindentation of the constituent phases of AAB provides new means of correlating mechanical properties at the nanoscale to macroscale properties of AAB and possible applications.

Generally AAB, like cement-based systems, exhibit relatively poor tensile and flexural properties. The incorporation of different types of inorganic or organic fibers (steel, E-glass, wool, PVA, PVC, carbon) increases flexural strength, splitting tensile strength, and ductility of AAB. It also changes fracture behavior from brittle to a more ductile pattern. The addition of fibers represents the major route for improvement of AAB elastic properties.

High-temperature heat treatment of carbon fiber reinforced geopolymer composites produced ceramic material with outstanding mechanical properties, i.e. flexural strength of ~234 MPa and Young's modulus of ~64 GPa. Multiwalled carbon nanotube reinforced geopolymers are proposed as self-sensing materials capable of detecting their own structural damage. Such new types of materials based on AAB can contribute to the expansion of AAB fields of application.

7.8 Sources of further information and advice

Related titles:

Shi, C., Krivenko, P.V. and Roy, D.M. (2006) *Alkali-Activated Cements and Concretes*, Taylor & Francis, Abingdon. ISBN10: 0–415–70004–3 (Print Edition). ISBN13: 978–0–415–70004–7.

Davidovits, J. (2008) *Geopolymer Chemistry and Applications*, 2nd edn, Institut Géopolymère, Saint-Quentin, France. ISBN: 2-9514820-1-9. EAN: 9782951482012.

Provis, J.L. and van Deventer, J.S.J. (eds.) (2009) *Geopolymers: Structures, Processing, Properties and Industrial Applications*, Woodhead Publishing, Cambridge. Woodhead Publishing ISBN 978-1-84569-449-4 (book). Woodhead Publishing ISBN 978-1-84569-638-2 (e-book). CRC Press ISBN 978-1-4398-0970-9.

References

Ahmari, S. and Zhang, L. (2013) 'Durability and leaching behavior of mine tailings-based geopolymer bricks', *Constr Build Mater*, 44, 743–750.

Alcaide, J.S., Alcocel, E.G., Puertas, F., Lapuente, R. and Garcés, P. (2007) 'Carbon fibre-reinforced, alkali-activated slag mortars', *Mater Constr*, 57(288), 33–48.

Alshaaer, M. (2013) 'Two-phase geopolymerization of kaolinite-based geopolymers', *Appl Clay Sci*, 86, 162–168.

Alzeer, M. and MacKenzie, K.J.D. (2012) 'Synthesis and mechanical properties of new fibre-reinforced composites of inorganic polymers with natural wool fibres', *J Mater Sci*, 47, 6958–6965.

Alzeer, M. and MacKenzie, K. (2013) 'Synthesis and mechanical properties of novel composites of inorganic polymers (geopolymers) with unidirectional natural flax fibres (*Phormium tenax*)', *Appl Clay Sci*, 75–76, 148–152.

Arellano-Aguilar, R., Burciaga-Díaz, O., Gorokhovsky, A. and Escalante-García, J.I. (2014)

'Geopolymer mortars based on a low grade metakaolin: effects of the chemical composition, temperature and aggregate:binder ratio', *Constr Build Mater*, 50, 642–648.

Atiş, C.D., Bilim, C., Çelik, Ö. and Karahan, O. (2009) 'Influence of activator on the strength and drying shrinkage of alkali-activated slag mortar', *Constr Build Mater*, 23(1), 548–555.

Autef, A., Joussein, E., Poulesquen, A., Gasgnier, G., Pronier, S., Sobrados, I., Sanz, J. and Rossignol, S. (2013a) 'Influence of metakaolin purities on potassium geopolymer formulation: the existence of several networks', *J Colloid Interf Sci*, 408, 43–53.

Autef, A., Joussein, E., Gasgnier, G., Pronier, S., Sobrados, I., Sanz, J. and Rossignol, S. (2013b) 'Role of metakaolin dehydroxylation in geopolymer synthesis', *Powder Technol,* 250, 33–39.

Aydın, S. and Baradan, B. (2012) 'Mechanical and microstructural properties of heat cured alkali-activated slag mortars', *Mater Des,* 35, 374–383.

Aydın, S. and Baradan, B. (2013a) 'The effect of fiber properties on high performance alkali-activated slag/silica fume mortars', *Compos Part B*, 45, 63–69.

Aydin, S. and Baradan, B. (2013b) 'Engineering properties of reactive powder concrete without Portland cement', *ACI Mater J*, 110(6), 619–628.

Bakharev, T. (2005) 'Geopolymeric materials prepared using Class F fly ash and elevated temperature curing', *Cem Concr Res,* 35, 1224–1232.

Bakharev, T., Sanjayan, J. and Cheng, Y-B. (1999a) 'Alkali activation of Australian slag cements', *Cem Concr Res*, 29, 113–120.

Bakharev, T., Sanjayan, J.G. and Cheng, Y.-B. (1999b) 'Effect of elevated temperature curing on properties of alkali-activated slag concrete', *Cem Concr Res*, 29, 1619–1625.

Baščarević, Z., Komljenović, M., Miladinović, Z., Nikolić, V., Marjanović, N., Žujović, Z. and Petrović, R. (2013) 'Effects of the concentrated NH_4NO_3 solution on mechanical properties and structure of the fly ash based geopolymers', *Constr Build Mater*, 41, 570–579.

Ben Haha, M., Le Saout, G., Winnefeld, F. and Lothenbach, B. (2011a) 'Influence of activator type on hydration kinetics, hydrate assemblage and microstructural development of alkali activated blast-furnace slags', *Cem Concr Res*, 41(3), 301–310.

Ben Haha, M., Lothenbach, B., Le Saout, G. and Winnefeld, F. (2011b) 'Influence of slag chemistry on the hydration of alkali-activated blast-furnace slag – Part I: Effect of MgO', *Cem Concr Res*, 41(9), 955–963.

Ben Haha, M., Lothenbach, B., Le Saout, G. and Winnefeld, F. (2012) 'Influence of slag chemistry on the hydration of alkali-activated blast-furnace slag – Part II: Effect of Al_2O_3', *Cem Concr Res*, 42(1), 74–83.

Bernal, S., De Gutierrez, R., Delvasto, S. and Rodriguez, E. (2010) 'Performance of an alkali-activated slag concrete reinforced with steel fibers', *Constr Build Mater*, 24, 208–214.

Berry, M., Stephens, J. and Cross, D. (2011) 'Performance of 100% fly ash concrete with recycled glass aggregate', *ACI Mater J*, 108(4), 378–384.

Bignozzi, M.C., Manzi, S., Lancellotti, I., Kamseu, E., Barbieri, L. and Leonelli, C. (2013) 'Mix-design and characterization of alkali activated materials based on metakaolin and ladle slag', *Appl Clay Sci*, 73, 78–85.

Bilim, C., Karahan, O., Atiş, C.D. and Ilkentapar, S. (2013) 'Influence of admixtures on the properties of alkali-activated slag mortars subjected to different curing conditions', *Mater Des*, 44, 540–547.

Blissett, R.S. and Rowson, N.A. (2012) 'A review of the multi-component utilisation of coal fly ash', *Fuel*, 97, 1–23.

Bondar, D., Lynsdale, C.J., Milestone, N.B., Hassani, N. and Ramezanianpour A.A. (2011) 'Engineering properties of alkali-activated natural pozzolan concrete', *ACI Mater J*, 108(1), 64–72.

Bondar, D., Lynsdale, C.J. and Milestone, N.B. (2013) 'Alkali-activated natural pozzolan concrete as new construction material', *ACI Mater J*, 110(3), 331–338.

Brough, A.R. and Atkinson, A. (2002) 'Sodium silicate-based, alkali-activated slag mortars. Part I. Strength, hydration and microstructure', *Cem Concr Res*, 32, 865–879.

Burciaga-Díaz, O. and Escalante-García, J.I. (2012) 'Strength and durability in acid media of alkali silicate-activated metakaolin geopolymers', *J Am Ceram Soc*, 95(7), 2307–2313.

Burciaga-Díaz, O. and Escalante-García, J.I. (2013) 'Structure, mechanisms of reaction, and strength of an alkali-activated blast-furnace slag', *J Am Ceram Soc*, 96(12), 3939–3948.

Chi, M. (2012) 'Effects of dosage of alkali-activated solution and curing conditions on the properties and durability of alkali-activated slag concrete', *Constr Build Mater*, 35, 240–245.

Chindaprasirt, P., Chareerat, T. and Sirivivananon, V. (2007) 'Workability and strength of coarse high calcium fly ash geopolymer', *Cem Concr Comp*, 29, 224–229.

Chindaprasirt, P., Jaturapitakkul, C., Chalee, W. and Rattanasak, U. (2009) 'Comparative study on the characteristics of fly ash and bottom ash geopolymers', *Waste Manag*, 29(2), 539–543.

Chindaprasirt, P., Chareerat, T., Hatanaka, S. and Cao, T. (2011) 'High-strength geopolymer using fine high-calcium fly ash', *J Mater Civ Eng*, 23(3), 264–270.

Chindaprasirt, P., Rattanasak, U. and Taebuanhuad, S. (2013) 'Role of microwave radiation in curing the fly ash geopolymer', *Adv Powder Technol,* 24, 703–707.

Collins, F. and Sanjayan, J.G. (1999a) 'Effects of ultra-fine materials on workability and strength of concrete containing alkali-activated slag as the binder', *Cem Concr Res*, 29(3), 459–462

Collins, F. and Sanjayan, J.G. (1999b) 'Strength and shrinkage properties of alkali-activated slag concrete placed into a large column', *Cem Concr Res*, 29(5), 659–666.

Collins, F. and Sanjayan, J.G. (2001) 'Microcracking and strength development of alkali activated slag concrete', *Cem Concr Compos*, 23(4–5), 345–352.

Criado, M., Palomo, A. and Fernández-Jiménez, A. (2005) 'Alkali activation of fly ashes. Part I: Effect of curing conditions on the carbonation of the reaction products', *Fuel*, 84, 2048–2054.

da Silva, W.R.L., Němeček, J. and Štemberk, P. (2014) 'Methodology for nanoindentation-assisted prediction of macroscale elastic properties of high performance cementitious composites', *Cem Concr Comp*, 45, 57–68.

Davidovits, J. (1989) 'Geopolymers and geopolymeric materials', *J Therm Anal*, 35(2), 429–441.

Davidovits, J. (1991) 'Geopolymers – inorganic polymeric new materials', *J Therm Anal*, 37(8), 1633–1656.

Davidovits, J. (2008) *Geopolymer Chemistry and Applications*, 2nd edn, Institut Géopolymère, Saint-Quentin, France.

Diaz, E.I., Allouche, E.N. and Eklund, S. (2010) 'Factors affecting the suitability of fly ash as source material for geopolymers', *Fuel*, 89, 992–996.

Diaz-Loya, E.I., Allouche, E.N. and Vaidya, S. (2011) 'Mechanical properties of fly-ash-based geopolymer concrete', *ACI Mater J*, 108(3), 300–306.

Dombrowski, K., Buchwald, A. and Weil, M. (2007) 'The influence of calcium content on the structure and thermal performance of fly ash based geopolymers', *J Mater Sci*, 42, 3033–3043.

Duxson, P., Provis, J.L., Lukey, G.C., Mallicoat, S.W., Kriven, W.M. and van Deventer, J.S.J. (2005) 'Understanding the relationship between geopolymer composition, microstructure and mechanical properties', *Colloids Surf A*, 269, 47–58.

Duxson, P., Fernández–Jiménez, A., Provis, J.L., Lukey, G.C., Palomo, A. and van Deventer, J.S.J. (2007a) 'Geopolymer technology: the current state of the art', *J Mat Sci*, 42(9), 2917–2933.

Duxson, P., Mallicoat, S.W., Lukey, G.C., Kriven, W.M. and van Deventer, J.S.J. (2007b) 'The effect of alkali and Si/Al ratio on the development of mechanical properties of metakaolin–based geopolymers', *Colloids Surf A*, 292(1), 8–20.

Feng, D., Tan, H. and van Deventer, J.S.J. (2004) 'Ultrasound enhanced geopolymerisation', *J Mater Sci*, 39, 571–580.

Fernández-Jiménez, A. and Palomo, A. (2003) 'Characterisation of fly ashes: potential reactivity as alkaline cements', *Fuel*, 82, 2259–2265.

Fernández–Jiménez, A., Palomo, J.G. and Puertas, F. (1999) 'Alkali-activated slag mortars: mechanical strength behaviour', *Cem Concr Res*, 29, 1313–1321.

Fernández-Jiménez, A., Palomo, A., Sobrados, I. and Sanz, J. (2006a) 'The role played by the reactive alumina content in the alkaline activation of fly ashes', *Micropor Mesopor Mater*, 91, 111–119.

Fernández-Jiménez, A., Palomo, A. and López-Hombrados, C. (2006b) 'Engineering properties of alkali-activated fly ash concrete', *ACI Mater J*, 103(2), 106–112.

Ganesan, N., Indira, P.V. and Santhakumar, A. (2013) 'Engineering properties of steel fibre reinforced geopolymer concrete', *Adv Concr Constr*, 1(4), 305–318.

Gao, K., Lin, K.L., Wang, D.Y., Hwang, C.L., Tuan, B.L.A., Shiu, H.S. and Cheng, T.W. (2013) 'Effect of nano-SiO_2 on the alkali-activated characteristics of metakaolin-based geopolymers', *Constr Build Mater*, 48, 441–447.

Granizo, M.L., Blanco-Varela, M.T. and Mart'nez-Ram'rez, S. (2007) 'Alkali activation of metakaolins: parameters affecting mechanical, structural and microstructural properties', *J Mater Sci*, 42, 2934–2943.

Guo, X., Shi, H. and Dick, W.A. (2010) 'Compressive strength and microstructural characteristics of class C fly ash geopolymer', *Cem Concr Comp*, 32, 142–147.

Hardjito, D. (2005) 'Studies on fly ash-based geopolymer concrete', PhD thesis, Faculty of Engineering and Computing, Department of Civil Engineering, Curtin University of Technology, Perth, Australia.

He, P., Jia, D., Lin, T., Wang, M. and Zhou, Y. (2010) 'Effects of high-temperature heat treatment on the mechanical properties of unidirectional carbon fiber reinforced geopolymer composites', *Ceram Int*, 36, 1447–1453.

He, J., Zhang, J., Yu, Y. and Zhang, G. (2012) 'The strength and microstructure of two geopolymers derived from metakaolin and red mud-fly ash admixture: a comparative study', *Constr Build Mater*, 30, 80–91.

Hounsi, A.D., Lecomte-Nana, G.L., Djétéli, G. and Blanchart, P. (2013) 'Kaolin-based geopolymers: effect of mechanical activation and curing process', *Constr Build Mater*, 42, 105–113.

Izquierdo, M., Querol, X., Phillipart, C., Antenucci, D. and Towler, M. (2010) 'The role of open and closed curing conditions on the leaching properties of fly ash-slag-based geopolymers', *J Hazard Mater*, 176, 623–628.

Jing, Z., Matsuoka, N., Jin, F., Yamasaki, N., Suzuki, K. and Hashida, T. (2006) 'Solidification of coal fly ash using hydrothermal processing method', *J Mater Sci*, 41, 1579–1584.

Juenger, M.C.G., Winnefeld, F., Provis, J.L. and Ideker, J. (2011) 'Advances in alternative cementitious binders', *Cem Concr Res*, 41(12), 1232–1243.

Kamseu, E., Bignozzi, M.C., Melo, U.C., Leonelli, C. and Sglavo, V.M. (2013) 'Design of inorganic polymer cements: effects of matrix strengthening on microstructure', *Constr Build Mater*, 38, 1135–1145.

Khale, D. and Chaudhary, R. (2007) 'Mechanism of geopolymerization and factors influencing its development: a review', *J Mater Sci*, 42, 729–746.

Kirschner, A. and Harmuth, H. (2004) 'Investigation of geopolymer binders with respect to their application for building materials', *Ceram-Silik*, 48(3), 117–120.

Kobera, L., Slavik, R., Kolouöek, D., Urbanová, M., Kotek, J. and Brus, J. (2011) 'Structural stability of aluminosilicate inorganic polymers: influence of the preparation procedure', *Ceram-Silik*, 55(4), 343–354.

Komljenović, M., Petrašinović-Stojkanović, Lj., Baščarević, Z., Jovanović, N. and Rosić, A. (2009) 'Fly ash as the potential raw mixture component for Portland cement clinker synthesis', *J Therm Anal Calorim*, 96(2), 363–368.

Komljenović, M., Baščarević, Z. and Bradić, V. (2010) 'Mechanical and microstructural properties of alkali-activated fly ash geopolymers', *J Hazard Mater*, 181(1–3), 35–42.

Komljenović, M., Baščarević, Z., Marjanović, N. and Nikolić, V. (2012) 'Decalcification resistance of alkali-activated slag', *J Hazard Mater*, 233–234, 112–121.

Komljenović, M., Baščarević, Z., Marjanović, N. and Nikolić, V. (2013) 'External sulfate attack on alkali-activated slag', *Constr Build Mater*, 49, 31–39.

Komnitsas, K. and Zaharaki, D. (2007) 'Geopolymerisation: a review and prospects for the minerals industry', *Miner Eng*, 20, 1261–1277.

Komnitsas, K., Zaharaki, D. and Perdikatsis, V. (2009) 'Effect of synthesis parameters on the compressive strength of low-calcium ferronickel slag inorganic polymers', *J Hazard Mater*, 161, 760–768.

Komnitsas, K., Zaharaki, D. and Bartzas, G. (2013) 'Effect of sulphate and nitrate anions on heavy metal immobilisation in ferronickel slag geopolymers', *Appl Clay Sci*, 73, 103–109.

Kourti, I., Devaraj, A.R., Bustos, A.G., Deegan, D., Boccaccini, A.R. and Cheeseman, C.R. (2011) 'Geopolymers prepared from DC plasma treated air pollution control (APC) residues glass: properties and characterisation of the binder phase', *J Hazard Mater*, 196, 86– 92.

Kovalchuk, G., Fernández-Jiménez, A. and Palomo, A. (2007) 'Alkali-activated fly ash: effect of thermal curing conditions on mechanical and microstructural development – Part II', *Fuel*, 86, 315–322.

Križan, D.M. (2005) 'Study of the synthesis process and hydration of binder based on alkali-activated blast-furnace slag', PhD Thesis, Faculty of Technology and Metallurgy, University of Belgrade, Serbia (in Serbian).

Križan, D. and Živanović, B. (2002) 'Effects of dosage and modulus of water glass on early hydration of alkali–slag cements', *Cem Concr Res*, 32(8), 1181–1188.

Križan, D., Komljenović, M.M. and Živanović, B. (2005) 'The influence of different parameters on the hydration process of binders based on alkali activated slag', *J Serb Chem Soc*, 70(1), 97–105.

Kuenzel, C., Vandeperre, L.J., Donatello, S., Boccaccini, A.R. and Cheeseman, C. (2012) 'Ambient temperature drying shrinkage and cracking in metakaolin-based geopolymers', *J Am Ceram Soc*, 95(10), 3270–3277.

Kuenzel, C., Neville, T.P., Donatello, S., Vandeperre, L., Boccaccini, A.R. and Cheeseman, C.R. (2013) 'Influence of metakaolin characteristics on the mechanical properties of geopolymers', *Appl Clay Sci*, 83–84, 308–314.

Kumar, S. and Kumar, R. (2011) 'Mechanical activation of fly ash: effect on reaction, structure and properties of resulting geopolymer', *Ceram Int,* 37, 533–541.

Kumar, A. and Kumar, S. (2013) 'Development of paving blocks from synergistic use of red mud and fly ash using geopolymerization', *Constr Build Mater*, 38, 865–871.

Kumar, R., Kumar, S., Badjena, S. and Mehrotra, S.P. (2005) 'Hydration of mechanically activated granulated blast furnace slag', *Metall Mater Trans B*, 36(6), 873–883.

Kumar, S., Kumar, R., Alex, T.C., Bandopadhyay, A. and Mehrotra, S.P. (2007a) 'Influence of reactivity of fly ash on geopolymerisation', *Adv Appl Ceram*, 106(3), 120–127.

Kumar, R., Kumar, S. and Mehrotra, S.P. (2007b) 'Towards sustainable solutions for fly ash through mechanical activation', *Resourc Conserv Recyc*, 52, 157–179.

Kumar, S., Kumar, R., Bandopadhyay, A., Alex, T.C., Ravi Kumar, B., Das, S.K. and Mehrotra, S.P. (2008) 'Mechanical activation of granulated blast furnace slag and its effect on the Properties and structure of Portland slag cement', *Cem Concr Comp,* 8, 679–685.

Kumar, S., García-Triñanes, P., Teixeira-Pinto, A. and Bao, M. (2013) 'Development of alkali activated cement from mechanically activated silico-manganese (SiMn) slag', *Cem Concr Comp,* 40, 7–13.

Lancellotti, I., Kamseu, E., Michelazzi, M., Barbieri, L., Corradi, A. and Leonelli, C. (2010) 'Chemical stability of geopolymers containing municipal solid waste incinerator fly ash', *Waste Manag*, 30, 673–679.

Latella, B.A., Perera, D.S., Durce, D., Mehrtens, E.G. and Davis, J. (2008) 'Mechanical properties of metakaolin-based geopolymers with molar ratios of Si/Al ≈ 2 and Na/Al ≈ 1', *J Mater Sci*, 43, 2693–2699.

Lee, B.Y., Cho, C.-G., Lim, H.-J., Song, J.-K., Yang, K.-H. and Li, V.C. (2012) 'Strain hardening fiber reinforced alkali-activated mortar – a feasibility study', *Constr Build Mater*, 37, 15–20.

Lee, N.K. and Lee, H.K. (2013) 'Setting and mechanical properties of alkali-activated fly ash/slag concrete manufactured at room temperature', *Constr Build Mater*, 47, 1201–1209.

Lemougna, P.N., MacKenzie, K.J.D. and Chinje Melo, U.F. (2011) 'Synthesis and thermal properties of inorganic polymers (geopolymers) for structural and refractory applications from volcanic ash', *Ceram Int*, 37, 3011–3018.

Lemougna, P.N., Chinje Melo, U.F., Delplancke, M.-P. and Rahier, H. (2014) 'Influence of the chemical and mineralogical composition on the reactivity of volcanic ashes during alkali activation', *Ceram Int*, 40, 811–820.

Li, C., Sun, H. and Li, L. (2010) 'A review: the comparison between alkali-activated slag (Si+Ca) and metakaolin (Si+Al) cements', *Cem Concr Res*, 40(9), 1341–1349.

Li, Z., Zhang, Y. and Zhou, X. (2005) 'Short fibre reinforced geopolymer composites manufactured by extrusion', *J Mater Civ Eng*, 17(6), 624–631.

Lim, N.G., Jeong, S.W., Her, J.W. and Ann, K.Y. (2012) 'Properties of cement-free concrete cast by finely grained nanoslag with the NaOH-based alkali activator', *Constr Build Mater*, 35, 557–563.

Lin, T. and Jia, D. (2009) 'Mechanical properties and fracture behavior of electroless Ni-plated short carbon fiber reinforced geopolymer matrix composites', *Int J Modern Phys B*, 23(6–7), 1371–1376.

Lin, T., Jia, D., He, P., Wang, M. and Liang, D. (2008) 'Effects of fiber length on mechanical properties and fracture behavior of short carbon fiber reinforced geopolymer matrix composites', *Mater Sci Eng A*, 497, 181–185.

Lin, T., Jia, D., Wang, M., He, P. and Liang, D. (2009) 'Effects of fibre content on mechanical properties and fracture behaviour of short carbon fibre reinforced geopolymer matrix composites', *Bull Mater Sci*, 32(1), 77–81.

Lizcano, M., Kim, H.S., Basu, S. and Radovic, M. (2012) 'Mechanical properties of sodium and potassium activated metakaolin-based geopolymers', *J Mater Sci*, 47, 2607–2616.

Lyu, S.-J., Wang, T.-T., Cheng, T.-W. and Ueng, T.-H. (2013) 'Main factors affecting mechanical characteristics of geopolymer revealed by experimental design and associated statistical analysis', *Constr Build Mater,* 43, 589–597.

MacKenzie, K.J.D. and Bolton, M.J. (2009) 'Electrical and mechanical properties of aluminosilicate inorganic polymer composites with carbon nanotubes', *J Mater Sci*, 44, 2851–2857.

Marjanović, N., Komljenović, M., Baščarević, Z. and Nikolić, V. (2014) 'Improving reactivity of fly ash and properties of ensuing geopolymers through mechanical activation', *Constr Build Mater*, 57, 151–162.

Mijarsh, M.J.A., Megat Johari, M.A. and Ahmad, Z.A. (2014) 'Synthesis of geopolymer from large amounts of treated palm oil fuel ash: application of the Taguchi method in investigating the main parameters affecting compressive strength', *Constr Build Mater*, 52, 473–481.

Natali, A., Manzi, S. and Bignozzi, M.C. (2011) 'Novel fiber-reinforced composite materials based on sustainable geopolymer matrix', *Proc Eng*, 21, 1124–1131.

Natali Murri, A., Rickard, W.D.A., Bignozzi, M.C. and van Riessen, A. (2013) 'High temperature behaviour of ambient cured alkali-activated materials based on ladle slag', *Cem Concr Res*, 43, 51–61.

Němeček, J., Šmilauer, V. and Kopecký, L. (2011) 'Nanoindentation characteristics of alkali-activated aluminosilicate materials', *Cem Concr Comp*, 33, 163–170.

Nikolić, V., Komljenović, M., Marjanović, N., Baščarević, Z. and Petrović, R. (2014) 'Lead immobilization by geopolymers based on mechanically activated fly ash', *Ceram Int*, 40, 8479–8488.

Ogundirana, M.B., Nugterena, H.W. and Witkamp, G.J. (2013) 'Immobilisation of lead smelting slag within spent aluminate–fly ash based geopolymers', *J Hazard Mater*, 248–249, 29–36.

Oh, J.E., Clark, S.M. and Monteiro, P.J.M. (2011) 'Does the Al substitution in C–S–H(I) change its mechanical property?' *Cem Concr Res*, 41, 102–106.

Oh, J.E., Moon, J., Oh, S.G., Clark, S.M. and Monteiro, P.J.M. (2012) 'Microstructural and compositional change of NaOH-activated high calcium fly ash by incorporating Na-aluminate and co-existence of geopolymeric gel and C–S–H(I)', *Cem Concr Res*, 42, 673–685.

Olivia, M. and Nikraz, H. (2012) 'Properties of fly ash geopolymer concrete designed by Taguchi method', *Mater Des*, 36, 191–198.

Pacheco-Torgal, F. and Jalali, S. (2010) 'Influence of sodium carbonate addition on the thermal reactivity of tungsten mine waste mud based binders', *Constr Build Mater*, 24(1), 56–60.

Pacheco-Torgal, F., Castro-Gomes, J. and Jalali, S. (2008a) 'Properties of tungsten mine waste geopolymeric binder', *Constr Build Mater*, 22, 1201–1211.

Pacheco-Torgal, F., Castro-Gomes, J. and Jalali, S. (2008b) 'Alkali-activated binders: a review. Part 2. About materials and binders manufacture', *Constr Build Mater*, 22, 1315–1322.

Pacheco-Torgal, F., Castro-Gomes, J. and Jalali, S. (2010) 'Durability and environmental performance of alkali-activated tungsten mine waste mud mortars', *J Mater Civil Eng*, 22(9), 897–904.

Pacheco-Torgal, F., Moura, D., Ding, Y. and Jalali, S. (2011) 'Composition, strength and workability of alkali-activated metakaolin based mortars', *Constr Build Mater*, 25, 3732–3745.

Palacios, M. and Puertas, F. (2011) 'Effectiveness of mixing time on hardened properties of waterglass-activated slag pastes and mortars', *ACI Mater J*, 108(1), 73–78.

Palacios, M., Banfill, P.F.G. and Puertas, F. (2008) 'Rheology and setting of alkali-activated slag pastes and mortars: effect of organic admixture', *ACI Mater J*, 105(2), 140–148.

Palomo, A., Alonso, S., Fernández-Jiménez, A., Sobrados, I. and Sanz, J. (2004) 'Alkali activation of fly ashes: a NMR study of the reaction products', *J Am Ceram Soc*, 87, 1141–1145.

Pan, Z., Li, D., Yu, J. and Yang, N. (2003) 'Properties and microstructure of the hardened alkali-activated red mud-slag cementitious material', *Cem Concr Res*, 33(9), 1437–1441.

Payá, J., Borrachero, M.V., Monzó, J., Soriano, L. and Tashima, M.M. (2012) 'A new geopolymeric binder from hydrated-carbonated cement', *Mater Lett*, 74, 223–225.

Pelisser, F., Guerrino, E.L., Menger, M., Michel, M.D. and Labrincha, J.A. (2013) 'Micromechanical characterization of metakaolin-based geopolymers', *Constr Build Mater,* 49, 547–553.

Phair, J.W. and van Deventer, J.S.J. (2002) 'Characterization of fly-ash-based geopolymeric binders activated with sodium aluminate', *Ind Eng Chem Res*, 41(17), 4242–4251.

Pontikes, Y., Machiels, L., Onisei, S., Pandelaers, L., Geysen, D., Jones, P.T. and Blanpain, B. (2013) 'Slags with a high Al and Fe content as precursors for inorganic polymers', *Appl Clay Sci*, 73, 93–102.

Provis, J.L. and van Deventer, J.S.J. (eds.) (2009) *Geopolymers: Structures, Processing, Properties and Industrial Applications*, Woodhead Publishing, Cambridge.

Provis, J.L., Yong, C.Z., Duxson, P. and van Deventer, J.S.J. (2009) 'Correlating mechanical and thermal properties of sodium silicate-fly ash geopolymers', *Colloids Surf A*, 336, 57–63.

Provis, J.L., Duxson, P. and van Deventer, J.S.J. (2010) 'The role of particle technology in developing sustainable construction materials', *Adv Powder Technol*, 21(1), 2–7.

Puertas, F., Amat, T., Fernández-Jiménez, A. and Vázquez, T. (2003) 'Mechanical and durable behaviour of alkaline cement mortars reinforced with polypropylene fibres', *Cem Concr Res*, 33, 2031–2036.

Puertas, F., Gil-Maroto, A., Palacios, M. and Amat, T. (2006) 'Alkali-activated slag mortars reinforced with a glassfibre: performance and properties', *Mater Constr*, 56(283), 79–90.

Puertas, F., Palacios, M., Manzano, H., Dolado, J.S., Rico, A. and Rodríguez, J. (2011) 'A model for the C-A-S-H gel formed in alkali-activated slag cements', *J Eur Ceram Soc*, 31, 2043–2056.

Rashad, A.M. (2013a) 'Alkali-activated metakaolin: a short guide for civil engineer – An overview', *Constr Build Mater,* 41, 751–765.

Rashad, A.M. (2013b) 'A comprehensive overview about the influence of different additives on the properties of alkali-activated slag – a guide for civil engineer', *Constr Build Mater,* 47, 29–55.

Rashad, A.M., Bai, Y., Basheer, P.A.M., Collier, N.C. and Milestone, N.B. (2012) 'Chemical and mechanical stability of sodium sulfate activated slag after exposure to elevated temperature', *Cem Concr Res*, 42, 333–343.

Rashad, A.M., Bai, Y., Basheer, P.A.M., Milestone, N.B. and Collier, N.C. (2013) 'Hydration and properties of sodium sulfate activated slag', *Cem Concr Comp*, 37, 20–29.

Rodríguez, E., Bernal, S., Mejía de Gutiérrez, R. and Puertas, F. (2008) 'Alternative concrete based on alkali-activated slag', *Mater Constr*, 58(291), 53–67.

Rodríguez, E.D., Bernal, S.A., Provis, J.L., Gehman, J.D., Monzó, J.M., Payá, J. and Borrachero, M.V. (2013) 'Geopolymers based on spent catalyst residue from a fluid catalytic cracking (FCC) process', *Fuel*, 109, 493–502.

Rovnanik, P. (2010) 'Effect of curing temperature on the development of hard structure of metakaolin-based geopolymer', *Constr Build Mater,* 24, 1176–1183.

Rowles, M. and O'Connor, B. (2003) 'Chemical optimisation of the compressive strength of

aluminosilicate geopolymers synthesised by sodium silicate activation of metakaolinite', *J Mater Chem*, 13(5), 1161–1165.

Ruiz-Santaquiteria, C., Fernández-Jiménez, A., Skibsted, J. and Palomo, A. (2013) 'Clay reactivity: production of alkali activated cements', *Appl Clay Sci*, 73, 11–16.

Rüscher, C.H., Mielcarek, E., Lutz, W., Ritzmann, A. and Kriven, W.M. (2010) 'Weakening of alkali-activated metakaolin during aging investigated by the molybdate method and infrared absorption spectroscopy', *J Am Ceram Soc*, 93(9), 2585–2590.

Ryu, G.S., Lee, Y.B., Koh, K.T. and Chung, Y.S. (2013) 'The mechanical properties of fly ash-based geopolymer concrete with alkaline activators', *Constr Build Mater,* 47, 409–418.

Saafi, M., Andrew, K., Tang, P.L., McGhon, D., Taylor, S., Rahman, M., Yang, S. and Zhou, X. (2013) 'Multifunctional properties of carbon nanotube/fly ash geopolymeric nanocomposites', *Constr Build Mater*, 49, 46–55.

Sajedi, F. and Razak, H.A. (2010) 'The effect of chemical activators on early strength of ordinary Portland cement-slag mortars', *Constr Build Mater*, 24, 1944–1951.

Sakulich, A.R., Anderson, E., Schauer, C.L. and Barsoum, M.W. (2010) 'Influence of Si:Al ratio on the microstructural and mechanical properties of a fine-limestone aggregate alkali-activated slag concrete', *Mater Struct*, 43, 1025–1035.

San Nicolas, R., Cyr, M. and Escadeillas, G. (2013) 'Characteristics and applications of flash metakaolins', *Appl Clay Sci*, 83–84, 253–262.

Sarker, P.K. (2009) 'Analysis of geopolymer concrete columns', *Mater Struct*, 42(6), 715–724.

Sarker, P.K. (2011) 'Bond strength of reinforcing steel embedded in fly ash-based geopolymer concrete', *Mater Struct*, 44, 1021–1030.

Sarker, P.K., Haque, R. and Ramgolam, K.V. (2013) 'Fracture behaviour of heat cured fly ash based geopolymer concrete', *Mater Des*, 44, 580–586.

Sata, V., Sathonsaowaphak, A. and Chindaprasirt, P. (2012) 'Resistance of lignite bottom ash geopolymer mortar to sulfate and sulfuric acid attack', *Cem Concr Comp*, 34, 700–708.

Sata, V., Wongsa, A. and Chindaprasirt, P. (2013) 'Properties of pervious geopolymer concrete using recycled aggregates', *Constr Build Mater*, 42, 33–39.

Seiffarth, T., Hohmann, M., Posern, K. and Kaps, Ch. (2013) 'Effect of thermal pre-treatment conditions of common clays on the performance of clay-based geopolymeric binders', *Appl Clay Sci*, 73, 35–41.

Shaikh, F.U.A. (2013) 'Review of mechanical properties of short fibre reinforced geopolymer composites', *Constr Build Mater*, 43, 37–49.

Shi, C. (1996) 'Strength, pore structure and permeability of alkali-activated slag mortars', *Cem Concr Res*, 26(12), 1789–1799.

Shi, C. and Day, R.L. (1996) 'Some factors affecting early hydration of alkali-slag cements', *Cem Concr Res*, 26(3), 439–447.

Shi, C. and Qian J. (2000) 'High performance cementing materials from industrial slags – a review', *Resour Conserv Recycl,* 29, 195–207.

Shi, C., Krivenko, P.V. and Roy, D.M. (2006) '*Alkali-Activated Cements and Concretes*', Taylor & Francis, Abingdon.

Shi, C., Fernández-Jiménez, A. and Palomo, A. (2011) 'New cements for the 21st century: the pursuit of an alternative to Portland cement', *Cem Concr Res*, 41(7), 750–763.

Shui, Z., Yu, R. and Dong, J. (2011) 'Activation of fly ash with dehydrated cement paste', *ACI Mater J*, 108(2), 204–208.

Slaty, F., Khoury, H., Wastiels, J. and Rahier, H. (2013) 'Characterization of alkali activated kaolinitic clay', *Appl Clay Sci*, 75–76, 120–125.

Sofi, M., van Deventer, J.S.J., Mendis, P.A. and Lukey, G.C. (2007) 'Engineering properties of inorganic polymer concretes (IPCs)', *Cem Concr Res*, 37, 251–257.

Somaratna, J., Ravikumar, D. and Neithalath, N. (2010) 'Response of alkali activated fly ash mortars to microwave curing', *Cem Concr Res*, 40(12), 1688–1696.

Song, S. and Jennings, H.M. (1999) 'Pore solution chemistry of alkali-activated ground granulated blast-furnace slag', *Cem Concr Res*, 29, 159–170.

Songpiriyakij, S., Kubprasit, T., Jaturapitakkul, C. and Chindaprasirt, P. (2010) 'Compressive strength and degree of reaction of biomass- and fly ash-based geopolymer', *Constr Build Mater*, 24, 236–240.

Steinerova, M. (2011) 'Mechanical properties of geopolymer mortars in relation to their porous structure', *Ceram-Silik*, 55(4), 362–372.

Steveson M. and Sagoe-Crentsil, K. (2005a) 'Relationships between composition, structure and strength of inorganic polymers. Part 1. Metakaolin-derived inorganic polymers', *J Mater Sci*, 40, 2023–2036.

Steveson M. and Sagoe-Crentsil, K. (2005b) 'Relationships between composition, structure and strength of inorganic polymers. Part 2. Fly ash-derived inorganic polymers', *J Mater Sci*, 40, 4247–4259.

Sun, P. and Wu, H.-C. (2008) 'Transition from brittle to ductile behavior of fly ash using PVA fibers', *Cem Concr Comp*, 30, 29–36.

Sun, P. and Wu, H.-C. (2009) 'Splitting tensile strength of fly ash activated by hydrothermal hot-pressing process', *J Mater Civ Eng*, 21(8), 356–361.

Sun, Z., Cui, H., An, H., Tao, D., Xu, Y., Zhai, J. and Li, Q. (2013) 'Synthesis and thermal behavior of geopolymer-type material from waste ceramic', *Constr Build Mater*, 49, 281–287.

Tashima, M.M., Akasaki, J.L., Castaldelli, V.N., Soriano, L., Monzó, J., Payá, J. and Borrachero, M.V. (2012) 'New geopolymeric binder based on fluid catalytic cracking catalyst residue (FCC)', *Mater Lett*, 80, 50–52.

Taylor, R., Richardson, I.G. and Brydson, R.M.D. (2010) 'Composition and microstructure of 20-year-old ordinary Portland cement-ground granulated blastfurnace slag blends containing 0 to 100% slag', *Cem Concr Res*, 40(7), 971–983.

Tchakoute, H.K., Elimbi, A., Yanne, E. and Djangang, C.N. (2013) 'Utilization of volcanic ashes for the production of geopolymers cured at ambient temperature', *Cem Concr Comp*, 38, 75–81.

Temuujin, J., van Riessen, A. and MacKenzie, K.J.D. (2010) 'Preparation and characterisation of fly ash based geopolymer mortars', *Constr Build Mater*, 24, 1906–1910.

Tho-in, T., Sata, V., Chindaprasirt, P. and Jaturapitakkul, C. (2012) 'Pervious high-calcium fly ash geopolymer concrete', *Constr Build Mater*, 30, 366–371.

Valcke, S.L.A., Sarabèr, A.J., Pipilikaki, P., Fischer, H.R. and Nugteren, H.W. (2013) 'Screening coal combustion fly ashes for application in geopolymers', *Fuel*, 106, 490–497.

van Deventer, J.S.J., Provis, J.L., Duxson, P. and Lukey, G.C. (2007) 'Reaction mechanisms in the geopolymeric conversion of inorganic waste to useful products', *J Hazard Mater*, A139, 506–513.

van Riessen, A. and Chen-Tan, N. (2013) 'Beneficiation of Collie fly ash for synthesis of geopolymer. Part 2 – Geopolymers', *Fuel*, 111, 829–835.

van Riessen, A., Jamieson, E., Kealley, C.S., Hart, R.D. and Williams, R.P. (2013) 'Bayer-geopolymers: an exploration of synergy between the alumina and geopolymer industries', *Cem Concr Comp*, 41, 29–33.

Vassilev, S.V. and Vassileva, C.G. (2007) 'A new approach for the classification of coal fly ashes based on their origin, composition, properties, and behaviour', *Fuel*, 86, 1490–1512.

Vassilev, S.V. and Vassileva, C.G. (2009) 'A new approach for the combined chemical and mineral classification of the inorganic matter in coal. 1. Chemical and mineral classification systems', *Fuel*, 88, 235–245.

Villa, C., Pecina, E.T., Torres, R. and Gómez, L. (2010) 'Geopolymer synthesis using alkaline activation of natural zeolite', *Constr Build Mater*, 24, 2084–2090.

Wang, H., Li, H. and Yan, F. (2005) 'Synthesis and mechanical properties of metakaolinite-based geopolymer', *Colloids Surf A*, 268, 1–6.

Wang, M.R., Jia, D.C., He, P.G. and Zhou, Y. (2010) 'Influence of calcination temperature of kaolin on the structure and properties of final geopolymer', *Mater Lett*, 64, 2551–2554.

Wang, S.D., Scrivener, K.L. and Pratt, P.L. (1994) 'Factors affecting the strength of alkali-activated slag', *Cem Concr Res*, 24(6), 1033–1043.

Wang, S.-D., Pu, X.-C., Scrivener, K.L. and Pratt, P.L. (1995) 'Alkali-activated slag cement and concrete: a review of properties and problems', *Adv Cem Res*, 7(27), 93–102.

Weng, L., Sagoe-Crentsil, K., Brown, T. and Song, S. (2005) 'Effects of aluminates on the formation of geopolymers', *Mater Sci Eng B*, 117, 163–168.

Williams, R.P. and van Riessen, A. (2010) 'Determination of the reactive component of fly ashes for geopolymer production using XRF and XRD', *Fuel*, 89, 3683–3692.

Williams, R.P., Hart, R.D. and van Riessen, A. (2011) 'Quantification of the extent of reaction of metakaolin-based geopolymers using X-ray diffraction, scanning electron microscopy, and energy-dispersive spectroscopy', *J Am Ceram Soc*, 94(8), 2663–2670.

Winnefeld, F., Leemann, A., Lucuk, M., Svoboda, P. and Neuroth, M. (2010) 'Assessment of phase formation in alkali activated low and high calcium fly ashes in building materials', *Constr Build Mater*, 24, 1086–1093.

Wongpa, J., Kiattikomol, K., Jaturapitakkul, C. and Chindaprasirt, P. (2010) 'Compressive strength, modulus of elasticity, and water permeability of inorganic polymer concrete', *Mater Des*, 31, 4748–4754.

Wu, H.C. and Sun, P. (2010) 'Effect of mixture compositions on workability and strength of fly ash-based inorganic polymer mortar', *ACI Mater J*, 107(6), 554–562.

Xu, H. and van Deventer, J.S.J. (2002) 'Geopolymerisation of multiple minerals', *Miner Eng*, 15, 1131–1139.

Xu, H., Provis, J.L., van Deventer, J.S.J. and Krivenko, P.V. (2008) 'Characterization of aged slag concretes', *ACI Mater J*, 105(2), 131–139.

Yang, K.H. and Song, J.K. (2012) 'Empirical equations for mechanical properties of $Ca(OH)_2$-based alkali-activated slag concrete', *ACI Mater J*, 109(4) 431–440.

Yang, K.H., Song, J.K., Lee, K.S. and Ashour, A.F. (2009) 'Flow and compressive strength of alkali-activated mortars', *ACI Mater J*, 106(1), 50–58.

Yost, J.R., Radlińska, A., Ernst, S. and Salera, M. (2013) 'Structural behavior of alkali activated fly ash concrete. Part 1: mixture design, material properties and sample fabrication', *Mater Struct*, 46, 435–447.

Yusuf, M.O., Megat Johari, M.A., Ahmad, Z.A. and Maslehuddin, M. (2014) 'Strength and microstructure of alkali-activated binary blended binder containing palm oil fuel ash and ground blast-furnace slag', *Constr Build Mater*, 52, 504–510.

Zhang, Y., Sun, W. and Li, Z. (2006) 'Impact behavior and microstructural characteristics of PVA fibers reinforced fly ash-geopolymer boards prepared by extrusion technique', *J Mater Sci*, 41, 2787–2794.

Zhang, Y., Sun, W. and Li, Z. (2008) 'Synthesis and microstructural characterization of

fully-reacted potassium-poly(sialate-siloxo) geopolymeric cement matrix', *ACI Mater J*, 105(2), 156–164.

Zhang, Y., Sun, W. and Li, Z. (2010) 'Composition design and microstructural characterization of calcined kaolin-based geopolymer cement', *Appl Clay Sci*, 47, 271–275.

Zhang, Z., Wang, H., Zhu, Y., Reid, A., Provis, J.L. and Bullen, F. (2014) 'Using fly ash to partially substitute metakaolin in geopolymer synthesis', *Appl Clay Sci*, 88–89, 194–201.

Zheng, L., Wang, C., Wang, W., Shi, Y. and Gao, X. (2011) 'Immobilization of MSWI fly ash through geopolymerization: effects of water-wash', *Waste Manag,* 31, 311–317.

Zuhua, Z., Xiao, Y., Huajun, Z. and Yue, C. (2009) 'Role of water in the synthesis of calcined kaolin-based geopolymer', *Appl Clay Sci*, 43, 218–223.

Živica, V. (2007) 'Effects of type and dosage of alkaline activator and temperature on the properties of alkali-activated slag mixtures', *Constr Build Mater*, 21(7), 1463–1469.

This page intentionally left blank

Prediction of the compressive strength of alkali-activated geopolymeric concrete binders by neuro-fuzzy modeling: a case study

8

A. Nazari[1], *F. Pacheco-Torgal*[2], *A, Cevik*[3], *J. G. Sanjayan*[1]
[1]Swinburne University of Technology, Hawthorn, VIC, Australia; [2]University of Minho, Guimarães, Portugal; [3]Gaziantep University, Gaziantep, Turkey

8.1 Introduction

Low calcium alkali-activated binders (also know as geopolymers), a class of inorganic polymers having an amorphous structure consisting of $[SiO_4]^{4-}$ and $[AlO_4]^{5-}$ tetrahedrals which share all of their corners with each other through oxygen atoms, are generally produced through the reaction of 'an aluminosilicate normally supplied in powder form as an industrial by-product or other inexpensive material with an alkaline activator, which is usually a concentrated aqueous solution of alkali hydroxide, silicate, carbonate or sulphate' (Provis, 2014).

On account of their reduced carbon dioxide emissions during production, geopolymers are one of the primary replacements for ordinary Portland cement (OPC), whose production requires large amounts of energy and emits much anthropogenic CO_2 (Shi *et al.*, 2011; Provis and van Deventer, 2013). Various aluminosilicate sources have been used to date in the production of environmentally friendly geopolymers. Kaolin and metakaolin (Pacheco-Torgal *et al.*, 2011; Heah *et al.*, 2012; Rajamma *et al.*, 2012; Kouamo *et al.*, 2012, 2013), fly ash (Vargas *et al.*, 2011; Nazari *et al.*, 2011; Rickard *et al.*, 2012; Onisei *et al.*, 2012; Sarker *et al.*, 2013) and different types of slags and waste muds (Pacheco-Torgal *et al.*, 2007; Kumar *et al.*, 2010; Yang *et al.*, 2012; El-Didamony *et al.*, 2012) are among the most used aluminosilicate sources for geopolymerization.

Although such soft-computing techniques as artificial neural networks (ANNs), genetic programming (GP) and adaptive neuro-fuzzy interfacial systems (ANFIS) have been successfully applied to a wide range of civil engineering problems so far (Cevik, 2011; Tanyildizi and Cevik, 2010; Cevik *et al.*, 2010; Sobhani and Ramezanianpour, 2011; Nazari and Riahi, 2012a; Ahmadi-Nedushan, 2012; Amani and Moeini, 2012; Dantas *et al.*, 2013; Boğa *et al.*, 2013; Garzón-Roca *et al.*, 2013), their application in the geopolymers field is very limited as this is a new type of high performance construction material and there are few previous works (Nazari and Riahi, 2012b;

Handbook of Alkali-activated Cements, Mortars and Concretes. http://dx.doi.org/10.1533/9781782422884.2.217

Nazari and Safarnejad, 2013; Nazari and Pacheco-Torgal, 2013). In the previous work (Nazari and Pacheco-Torgal, 2013), compressive strength of geopolymers with different aluminosilicate sources was modeled by ANNs. It was reported that ANNs are able to predict the compressive strength of geopolymers with reasonable accuracy. In the present study, ANFIS has been utilized to predict the compressive strength of the previously modeled geopolymers. Through using fuzzy sets and a linguistic model incorporating a set of IF–THEN fuzzy rules, ANFIS integrates the human-like reasoning approach of fuzzy systems. Besides the ability to petition for interpretable IF–THEN rules, being universal approximators is the main strength of ANFIS approximations (Jang, 1993). To construct the ANFIS model in the present study, curing time (days), $Ca(OH)_2$ content (wt.%), NaOH concentration, mold type, aluminosilicate source and H_2O/Na_2O molar ratio were considered as independent input parameters and the compressive strength of the investigated geopolymers as independent target value. The experimental databases were divided into training (80%) and testing (20%) sets and modeled by the proposed ANFIS model which was constructed using a total of 128 rules.

8.2 Data collection to predict the compressive strength of geopolymer binders by neuro-fuzzy approach

The collected data were the same as those used in the previous work (Nazari and Pacheco-Torgal, 2013). Three main series of geopolymers each made from a certain aluminosilicate source were considered in this study as in the previous work:

1. The first series of samples were the compressive specimens made from tungsten mine wastes. Tungsten mine waste mud, which was subjected to a thermal treatment, the fine aggregate which was crushed sand from the same mine, distilled water, the sodium hydroxide flakes, sodium silicate solution and calcium hydroxide were the materials used to produce geopolymeric compressive specimens using $50 \times 50 \times 50$ mm^3 cubic molds, according to ASTM C109. The complete preparation method of the considered geopolymers is given in Pacheco-Torgal *et al*. (2008).
2. Metakaolin-based geopolymers made from metakaolin, calcium hydroxide, sodium hydroxide, sodium silicate solution, superplasticizer, sand and distilled water were used to dissolve the sodium hydroxide flakes (Sarker *et al*., 2013). Alkali-activated mortars were a mixture of aggregates, metakaolin, calcium hydroxide and alkaline silicate solution were poured into $160 \times 40 \times 40$ mm^3 cubic specimens according to EN 1015-11. The preparation method for compressive strength tests is presented in Pacheco-Torgal *et al*. (2011).
3. The third group of geopolymers made by tungsten waste mud consisted of aggregates, waste mud, calcium hydroxide, alkaline silicate solution and water in a similar way to the method described above for the data gathered from Pacheco-Torgal *et al*. (2008).

8.3 Fuzzy logic: basic concepts and rules

A wide range of applications, covering engineering, process control, image processing, pattern recognition and classification, management, economics and decision making, has been considered over the last decade by fuzzy logic, an interesting method invented in 1965 (Zadeh, 1965; Rutkowski, 2004). Fuzzy systems can be defined as rule-based systems that are constructed from a collection of linguistic rules which can represent any system with accuracy, i.e., they work as universal approximators. The rule-based system of the fuzzy logic theory uses linguistic variables as its antecedents and consequents, where antecedents express an inference or the inequality which should be satisfied, and consequents are what we can infer, and is the output if the antecedent inequality is satisfied. The fuzzy rule-based system is actually an IF–THEN rule-based system, given by, IF antecedent, THEN consequent (Sivanandam *et al.*, 2007). Fuzzy logic (FL) operations are based on fuzzy sets where the input data may be defined as fuzzy sets or a single element with a membership value of unity. The membership values (μ_1 and μ_2) are found from the intersections of the data sets with the fuzzy sets as shown in Figure 8.1, which illustrates the graphical method of finding membership values in the case of a single input (Haris, 2006).

A fuzzy set contains elements which have varying degrees of membership in the set, unlike the classical or crisp sets where a member either belongs to that set or does not (0 or 1). However, a fuzzy set allows a member to have a varying degree of membership which can be mapped into a function or a universe of membership values (Bai *et al.*, 2006). The implementation of fuzzy logic to real applications considers the following steps (Bai *et al.*, 2006):

1. Fuzzification which requires conversion of classical data or crisp data into fuzzy data or membership functions (MFs).
2. Fuzzy inference process which connects membership functions with the fuzzy rules to derive the fuzzy output.
3. Defuzzification which computes each associated output.

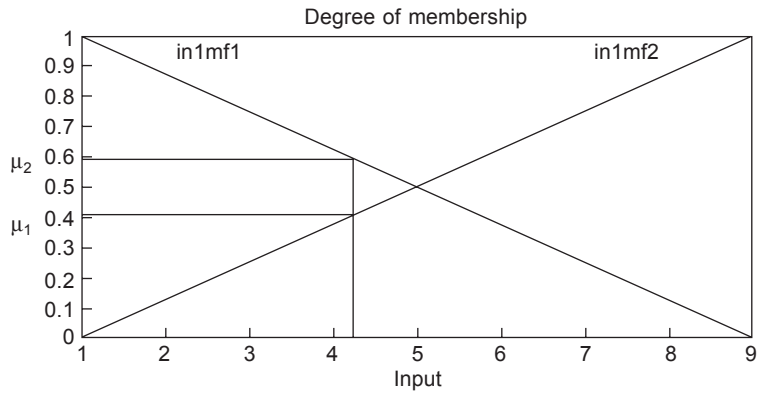

Figure 8.1 Input data membership values (Sivanandam *et al.*, 2007).

8.3.1 Neuro-fuzzy systems: basics and rules

Fuzzy systems can also be connected with neural networks to form neuro-fuzzy systems which exhibit advantages of both approaches. Neuro-fuzzy systems combine the natural language description of fuzzy systems and the learning properties of neural networks. Various neuro-fuzzy systems have been developed that are known in the literature under short names. The adaptive neuro-fuzzy inference system (ANFIS), developed by Jang *et al*. (1997), is one of these neuro-fuzzy systems which allow the fuzzy systems to learn the parameters using an adaptive back propagation learning algorithm (Rutkowski, 2004). Mainly three types of fuzzy inference systems (FIS) have been widely employed in various applications: Mamdani, Sugeno, and Tsukamoto fuzzy models. The differences between these three fuzzy inference systems arise as a result of their fuzzy rules, as well as their aggregation and defuzzification procedures which differ accordingly (Jang *et al*., 1997). In this study, the Sugeno FIS is used where each rule is defined as a linear combination of input variables. The corresponding final output of the fuzzy model is simply the weighted average of each rule's output. A Sugeno FIS consisting of two input variables x and y, for example, a one output variable f will lead to two fuzzy rules:

- Rule 1: If x is A_1, y is B_1 then $f_1 = p_1x + q_1y + r_1$
- Rule 2: If x is A_2, y is B_2 then $f_2 = p_2x + q_2y + r_2$

where p_i, q_i, and r_i are the consequent parameters of it h rule. A_i, B_i and C_i are the linguistic labels which are represented by fuzzy sets shown in Figure 8.2 (Jang *et al*., 1997).

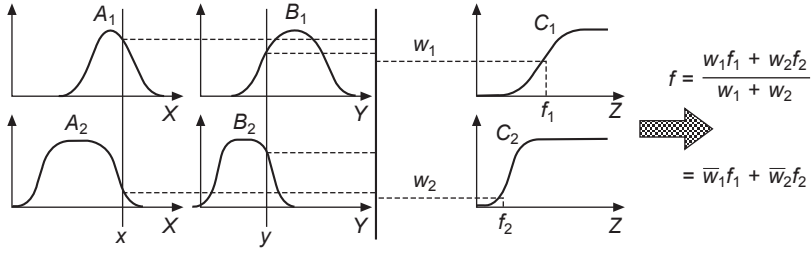

Figure 8.2 The Sugeno fuzzy model (Jang *et al*., 1997).

8.3.2 Solving a simple problem with adaptive neuro-fuzzy interfacial systems (ANFIS)

To illustrate how ANFIS works for function approximation, let us suppose one is given a sampling of the numerical values from the simple function below (Sonebi and Cevik, 2009):

$$y_i = a^3 + b^2 \tag{8.1}$$

where a and b are independent variables chosen over random points in the real interval [1,9]. In this case, a sample of data in the form of 17 pairs (a,b,y_i) is given where x_i

is the value of the independent variable in the given interval [1,9] and y_i is the output of the function given in Eq. (8.1) and presented in Table 8.1 on page 223.

The aim is to construct the ANFIS model fitting those values within minimum error for Eq. (8.1) by using the simplest ANFIS model that is available where the number of rules is two for each variable and the type of output membership function is constant. Initial and final membership values of rules for each input are given in Figures 8.3 and 8.4, respectively. Suppose one finds the output for input values of 1 and 9. The inference diagram of the proposed ANFIS model is given in Figure 8.5 for input values of 1 and 9 with corresponding values of output membership which is chosen as constant. For the first input which is 1, the value of the membership

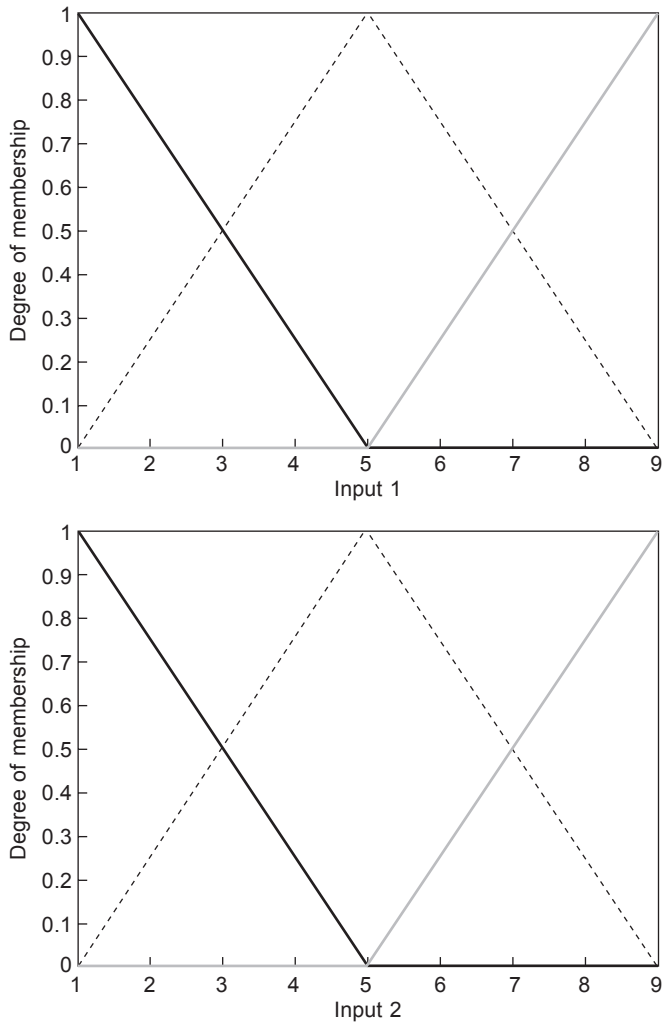

Figure 8.3 Initial membership functions (Sonebi and Cevik, 2009).

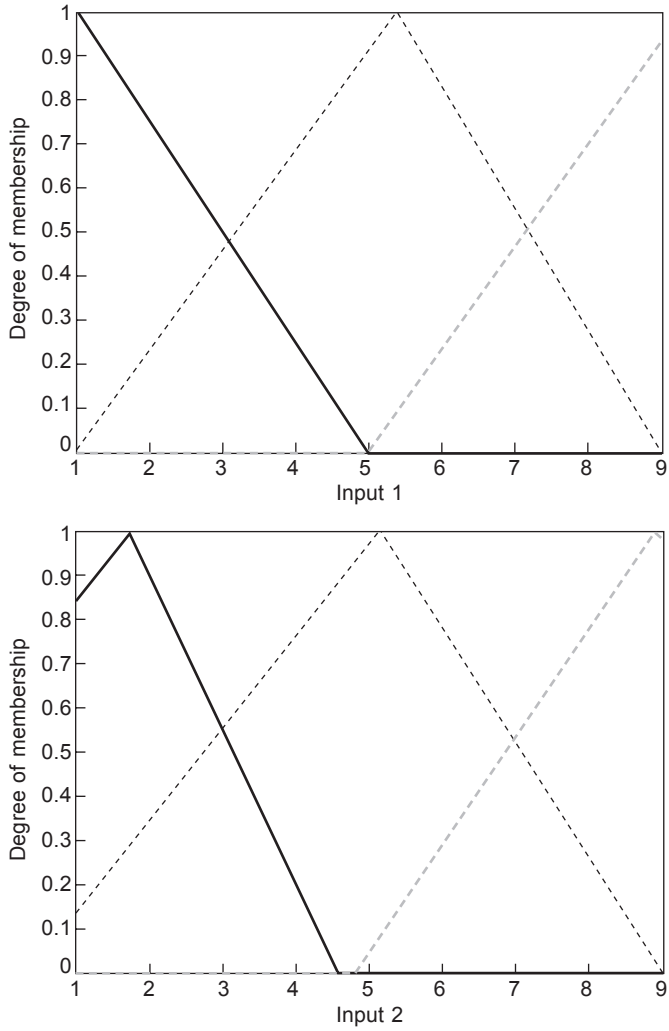

Figure 8.4 Final membership functions (Sonebi and Cevik, 2009).

function is observed to be 1 shown on left side of Figure 8.7 on page 225. For the second input which is 9, the value of the membership function is observed to be 1, again shown on left side of Figure 8.7. Thus the final output will be $82 \times 1 = 82$. The exact result for $a = 1$ and $b = 9$ from Eq. (8.1) will be $y = 1^3 + 9^2 = 82$.

The main aim of this study is the neuro-fuzzy modeling of compressive strength of geopolymers produced by different aluminosilicate sources based on an experimental database. Compressive strength of geopolymers will be obtained as a function of curing time (days), $Ca(OH)_2$ content (wt.%), NaOH concentration (M), mold type, aluminosilicate source and H_2O/Na_2O molar ratio. The experimental database was divided into training (80%) and testing (20%) sets. The ANFIS model is constructed

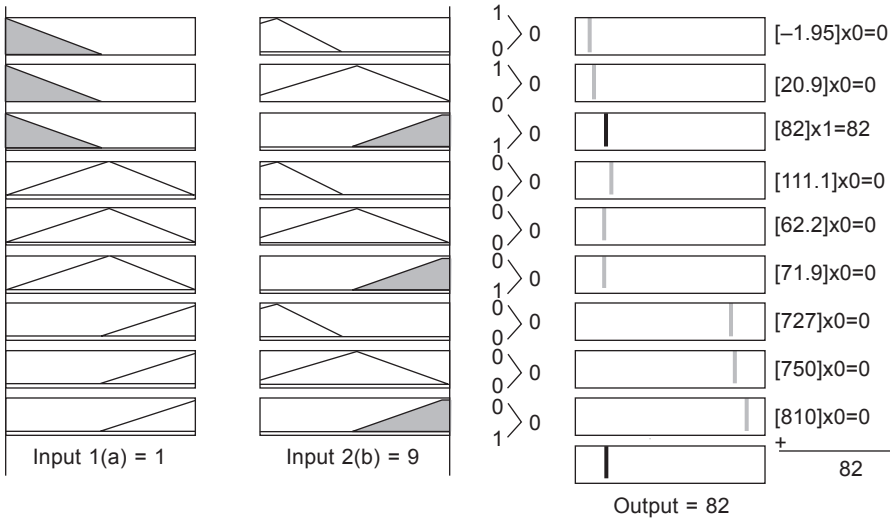

Figure 8.5 Fuzzy inference diagram (Sonebi and Cevik, 2009).

with training sets and the accuracy is verified by testing sets which the ANFIS model faces for the first time.

The proposed ANFIS model uses a Gaussian membership function with two rules. The output membership function is chosen as constant. Features of the proposed ANFIS model are given in Table 8.1. Statistical parameters of testing and training sets and overall results of the ANFIS model are presented in Table 8.2. The overall correlation of the ANFIS model can be seen in Figure 8.6. ANFIS results are observed to be very close to actual results. The initial and final membership functions of

Table 8.1 Features of the proposed ANFIS model

Type	Sugeno
Aggregation method	Maximum
Defuzzification method	Weighted average
Input membership function type	Gaussian
Output membership function type	Constant

Table 8.2 Statistical parameters of testing and training sets and overall results of ANFIS model for compressive strength

	Training set	Testing set	Total set
MSE	14.48	23.69	16.32
MAPE	11.52	15.89	12.40
R^2	0.94	0.92	0.94
Mean	1.00	1.03	1.00
Cov	0.17	0.23	0.19

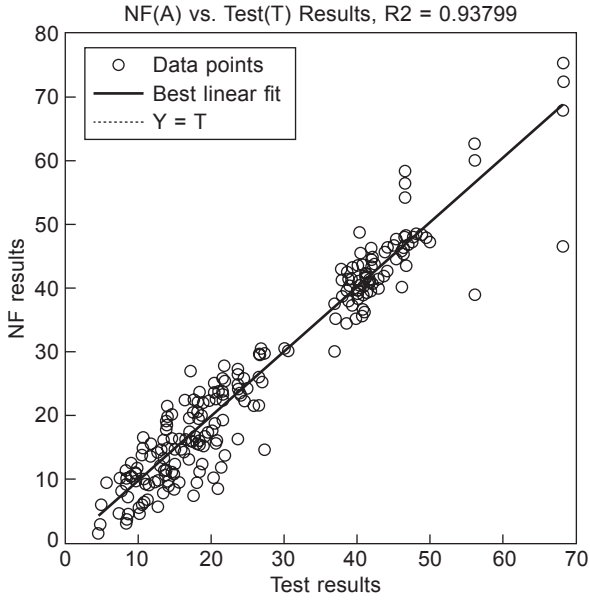

Figure 8.6 Performance of ANFIS model with respect to experimental results for compressive strength.

inputs for compressive strength are presented in Figures 8.7 and 8.8, respectively. The fuzzy inference diagram is presented in Figure 8.9 with a total of 128 rules.

8.4 Results and discussion of the use of neuro-fuzzy modeling to predict the compressive strength of geopolymer binders

Absolute fraction of variance (R^2), the absolute percentage error (MAPE) and the root mean square error (MSE) were used in this study to represent the error that arose during the training and testing of the proposed ANFIS model, and they were calculated by Eqs (8.2), (8.3) and (8.4), respectively (Guzelbey *et al.*, 2006):

$$R^2 = 1 - \left(\frac{\sum_i (t_i - o_i)^2}{\sum_i (o_i)^2} \right) \tag{8.2}$$

$$\text{MAPE} = \frac{1}{n} \sum_i \left| \frac{t_i - o_i}{t_i} \right| \times 100 \tag{8.3}$$

$$\text{MSE} = \frac{1}{n} \sum_i (t_i - o_i)^2 \tag{8.4}$$

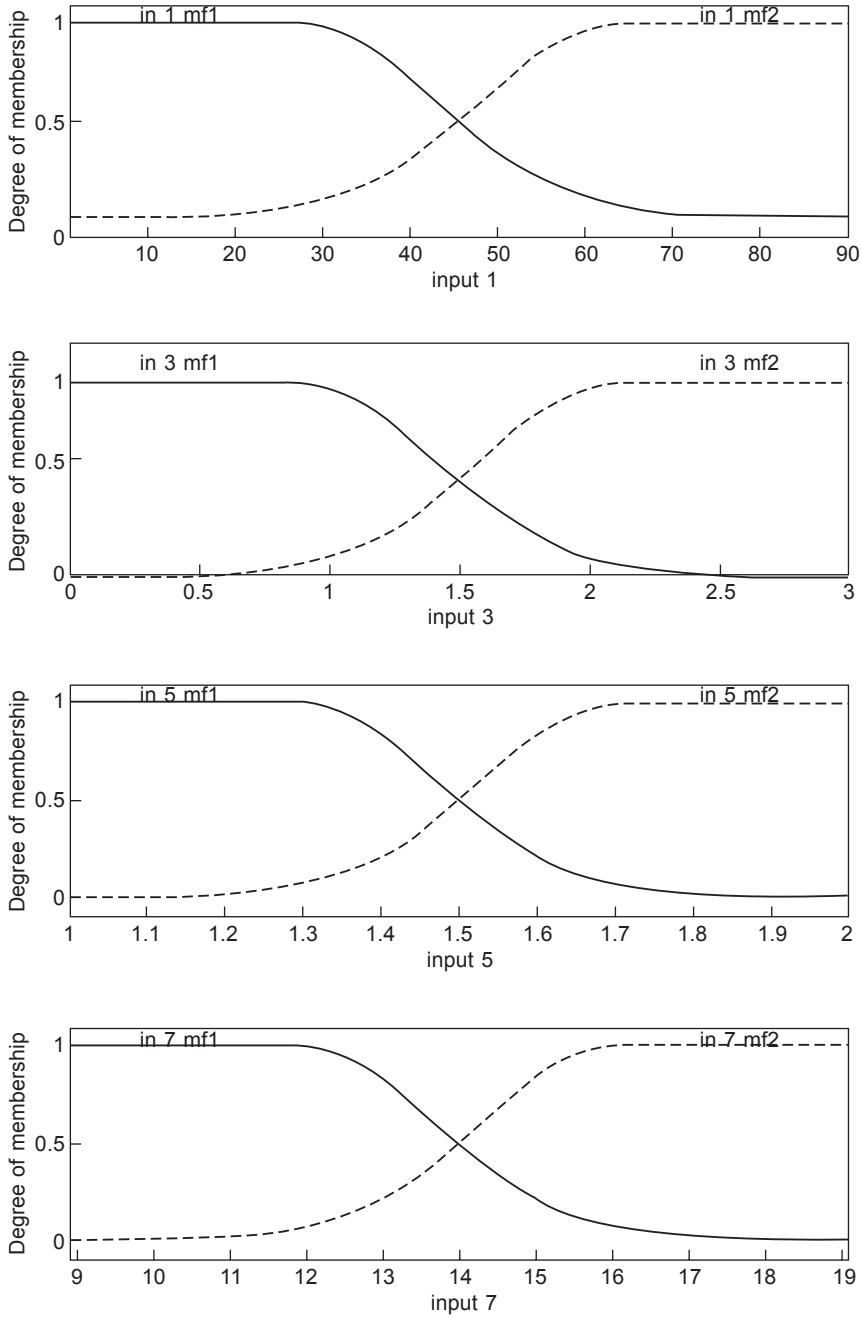

Figure 8.7 Initial membership functions for compressive strength (input1 = curing time (days); input2 = $Ca(OH)_2$ content (wt.%); input3 = the amount of superplasticizer (wt.%); input4 = NaOH concentration (M); input5 = mold type; input6 = aluminosilicate source; and input7 = H_2O/Na_2O molar ratio).

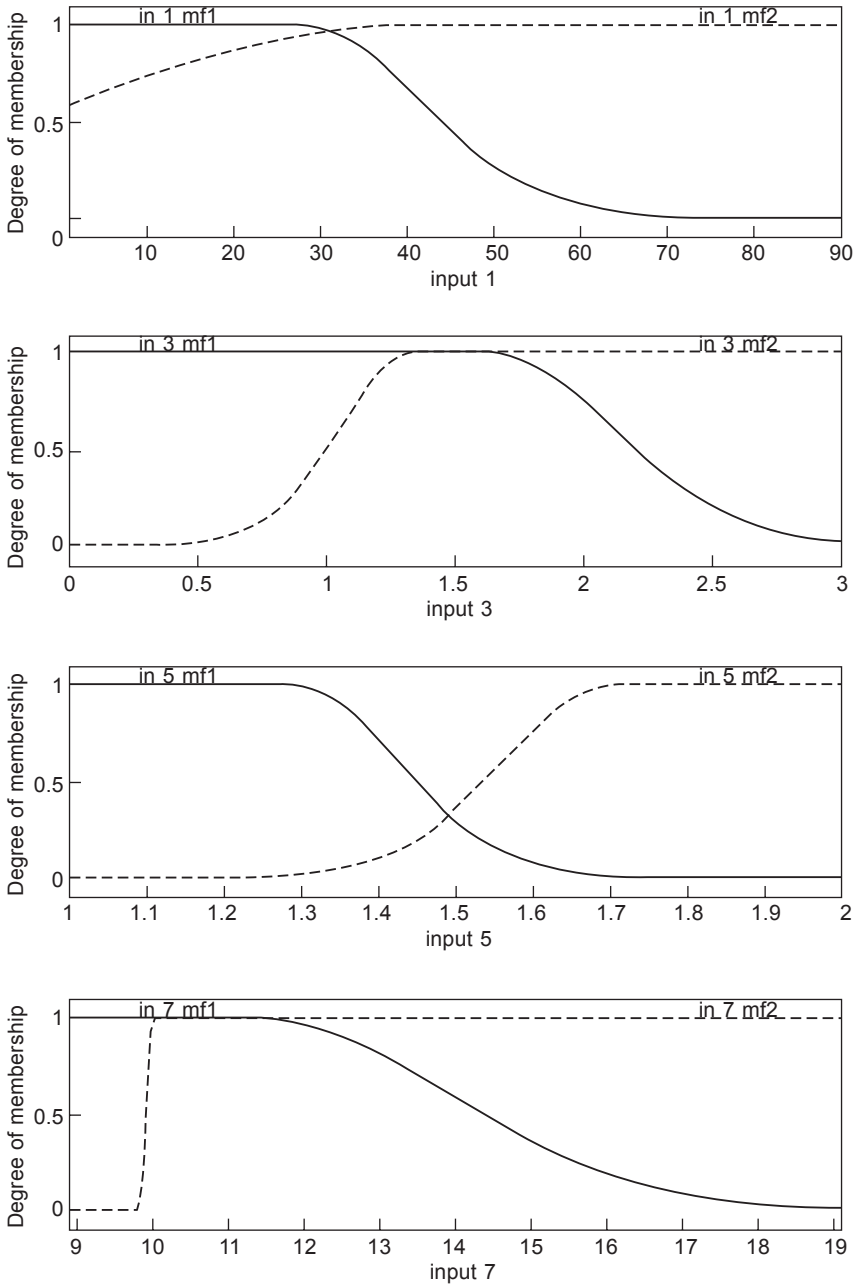

Figure 8.8 Final membership functions for compressive strength (input1 = curing time (days); input2 = $Ca(OH)_2$ content (wt.%); input3 = the amount of superplasticizer (wt.%); input4 = NaOH concentration (M); input5 = mold type; input6 = aluminosilicate source; and input7 = H_2O/Na_2O molar ratio).

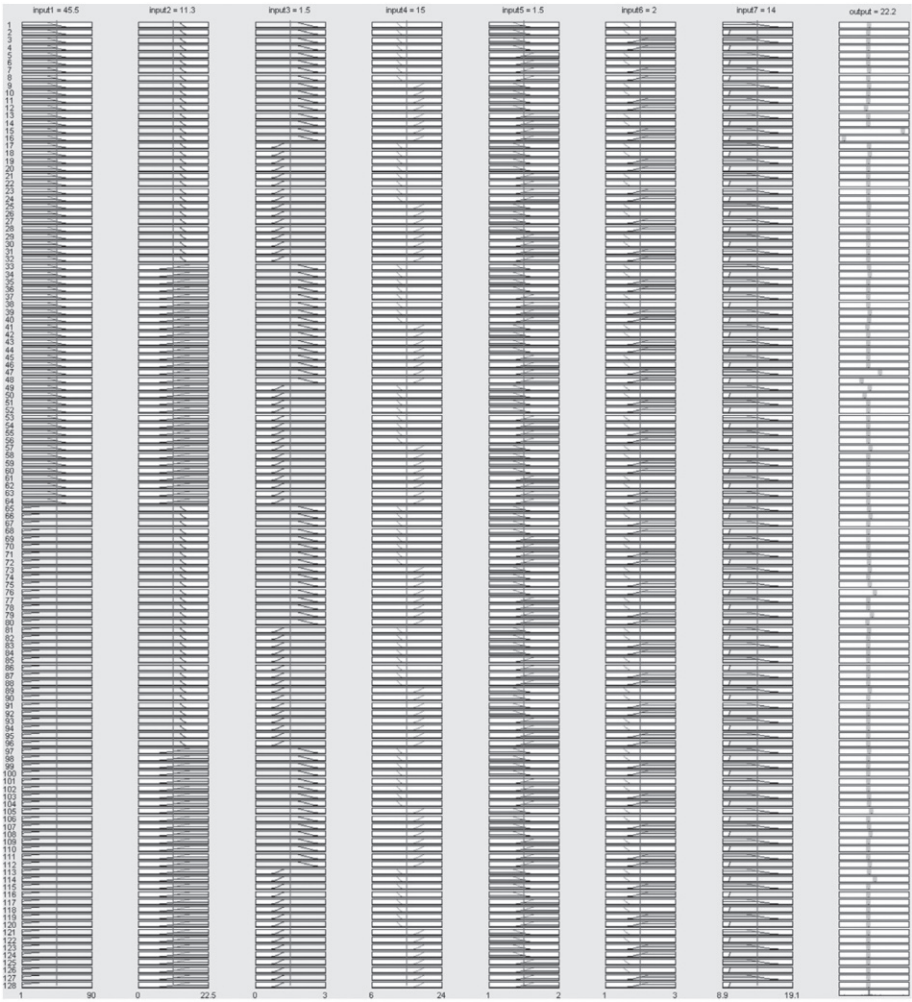

Figure 8.9 Fuzzy inference diagram for compressive strength.

where t, o and n are the target value, the output value and the number of data sets in each training and testing phase. The calculated performance values for the proposed ANFIS model have been presented in Table 8.1. The values of R^2, MAPE and MSE in the training phase of the model are 0.94, 11.52 and 14.48, respectively while these values in the testing phase are 0.92, 15.89 and 23.69, respectively. These values together with the results illustrated in Figure 8.6 show that the proposed ANFIS models could predict the compressive strength of the considered geopolymers appropriately. However, the predicted compressive strength for two geopolymeric mixtures with compressive strengths of about 56 and 68 MPa have the most deviation in the model. Although, some deviation is observed for some of the other data, the values predicted by the model have an accuracy of more than 90% and one may propose the

presented model as suitable for predicting the compressive strength of the considered geopolymers. A comparison between the predicted results by the proposed ANFIS model in this study and that of the previous work (Nazari and Pacheco-Torgal, 2013) shows that both ANNs and ANFIS models could predict the compressive strength of the evaluated geopolymers well. Since the presented soft-computing techniques are limited to those presented in the previous works (Nazari and Riahi, 2012a; Nazari and Pacheco-Torgal, 2013; Nazari and Safarnejad, 2013), it is not possible to present a comprehensive evaluation with different geopolymeric specimens. However, all of the proposed models in the previous work and that presented in this work show that such soft-computing methods as ANFIS, ANNs and GP could be suitably adopted for predicting the properties of geopolymeric specimens. The 3D interaction graph between some of selected variables generated by the proposed model can be seen in Figure 8.10. Figure 8.10(a) shows the interaction between H_2O/Na_2O ratio and NaOH concentration on compressive strength of the considered geopolymers. The results show that the highest strength has been achieved in higher concentrations of NaOH and lower H_2O/Na_2O ratio. This is in agreement with the previous work (Nazari and Pacheco-Torgal, 2013).

The strength of a geopolymeric mixture depends on several factors of which NaOH concentration has a significant effect. However, the effect of NaOH concentration on compressive strength of geopolymers is the complete opposite. While some reported an increased strength with high NaOH concentration (Zuhua *et al.*, 2009; Wongpa *et al.*, 2010; Nazari *et al.*, 2011), others (Chindaprasirt *et al.*, 2007; Somna *et al.*, 2011) showed a negative impact of high NaOH concentration. An investigation of the proposed NaOH concentration for production geopolymers with higher strength shows that this depends mainly on the aluminosilicate source (Nazari *et al.*, 2011).

This is very evident in Figure 8.10(b) where for type 1 aluminosilicate source, even at low NaOH concentration, the strength is high and in some cases for this source type, the strength has been decreased by the increased NaOH concentration. However, the results of the three sources in this work show that the strength and NaOH increments behave in a parallel manner. Figure 8.10(c) shows the interaction between NaOH concentration and the amount of superplasticizer. The figure shows that a higher amount of superplasticizer at all NaOH concentrations results in higher strengths. This is in agreement with the previous work (Nazari and Pacheco-Torgal, 2013), where higher content of superplasticizer usage led to a reduction in water required and hence increased strength. This is completely established for concrete specimens and since the nature of these constructional materials is similar, one may anticipate that geopolymers behave in the same manner. One of the most interesting findings from the proposed ANFIS model is illustrated in Figure 8.10(d) where the interaction between $Ca(OH)_2$ content and NaOH concentration is presented. The figure shows that for all of NaOH concentrations and high $Ca(OH)_2$ content, the compressive strength is very low. The highest strengths have been achieved at intermediate NaOH concentrations and up to 10% of $Ca(OH)_2$. The findings show that even at high NaOH concentration, excessive $Ca(OH)_2$ content may lead to decreased strength. This is in agreement with Nazari *et al.* (2012) where geopolymers were produced by ordinary Portland cement (OPC) and high content of lime. Relatively

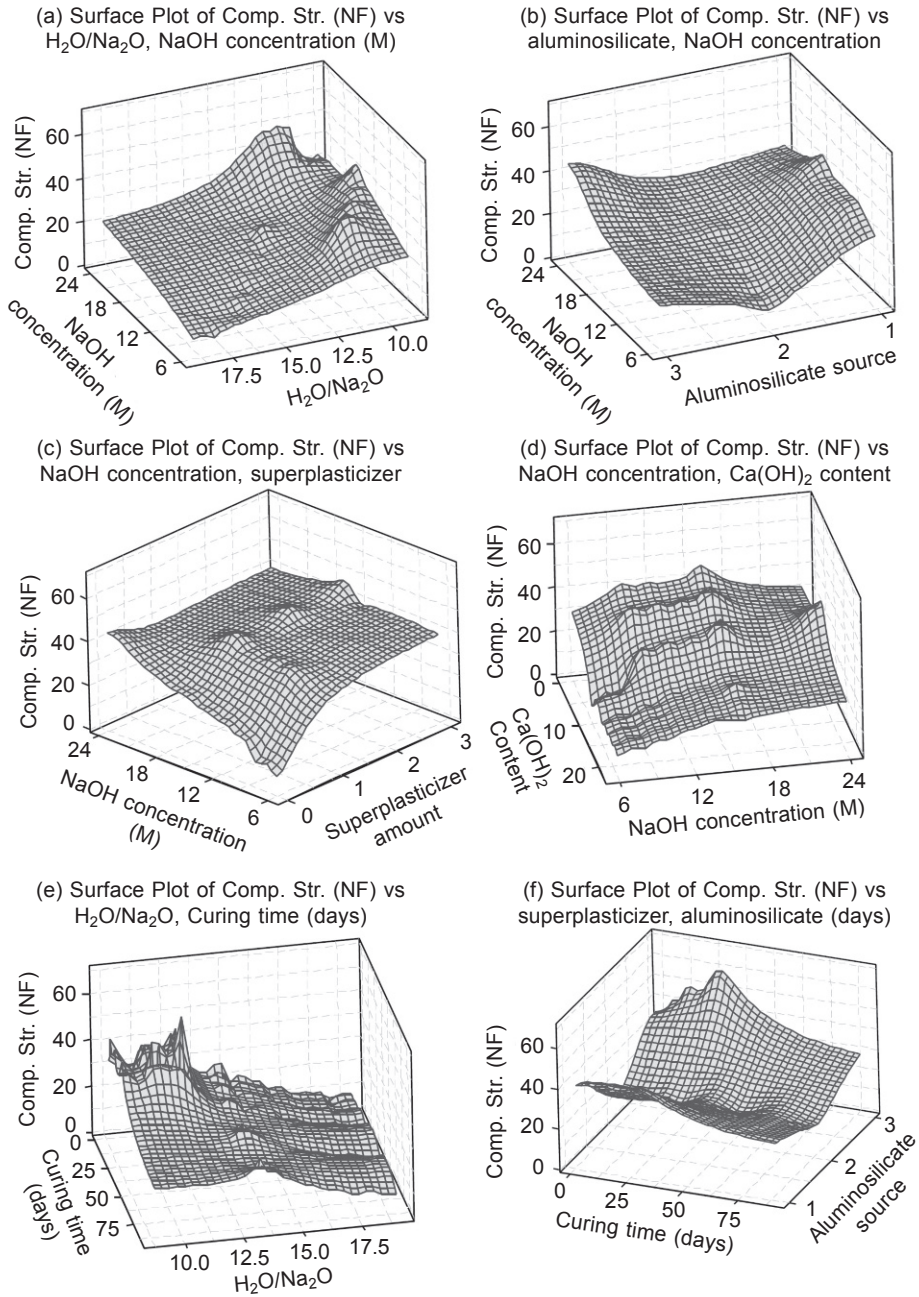

Figure 8.10 The 3D interaction graph between some selected variables generated by the proposed ANFIS model: (a) NaOH concentration and H_2O/Na_2O; (b) NaOH concentration and aluminosilicate source; (c) NaOH concentration and superplasticizer amount; (d) NaOH concentration and $Ca(OH)_2$ content; (e) curing time and H_2O/Na_2O; (f) curing time and aluminosilicate source; (g) curing time and NaOH concentration; (h) curing time and superplasticizer amount; and (i) curing time and $Ca(OH)_2$ content.

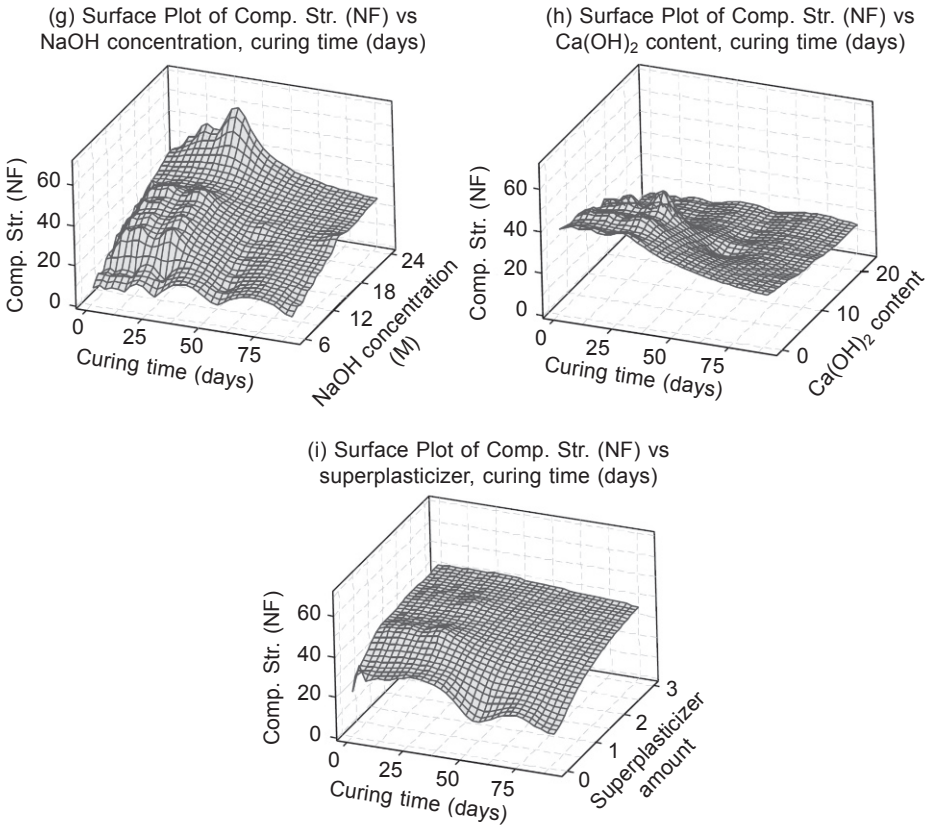

Figure 8.10 Continued

low compressive strength of those geopolymers shows the possible formation of $Ca(OH)_2$ during incomplete geopolymerization. Finally, Figure 8.10(e)–(i) shows the interaction between curing time and the other parameters. In all cases, it has been predicted that the compressive strength of the considered geopolymers increased up to 28 days and then will decrease. This is in agreement with the previous work (Nazari and Pacheco-Torgal, 2013). Although works conducted on the post-28-day compressive strength of geopolymers are limited, some of them have reported a decreased strength after 28 days of curing (Wongpa *et al*. 2010). However, conversely, some have reported an increased strength after 28 days of curing (Somna *et al*., 2011). This may be related to the production method and aluminosilicate source and requires further investigations.

8.5 Conclusions

Application of neuro-fuzzy approaches for the prediction of compressive strength of the considered geopolymers is very scarce. This paper presents a pioneer work

on the neuro-fuzzy approach in this field. The proposed ANFIS model is a unified rule-based model based on experimental data. The proposed ANFIS model shows very good agreement with experimental results. The values of R^2, MAPE and MSE in the training phase of the model were acquired as 0.94, 11.52 and 14.48, respectively and 0.92, 15.89 and 23.69, respectively, in the testing phase. The predicted results by the proposed ANFIS model showed that the effect of NaOH concentration as a main factor depends on the other factors. However, by considering the effect of all of the factors, the strength is decreased after 28 days of curing. As a conclusion of this study, the neuro-fuzzy approach may serve as an effective alternative tool for the modeling of compressive strength of geopolymers in the future.

References

Ahmadi-Nedushan B (2012) 'Prediction of elastic modulus of normal and high strength concrete using ANFIS and optimal nonlinear regression models', *Constr. Build. Mater.* 36, 665–673.

Amani J and Moeini R (2012) 'Prediction of shear strength of reinforced concrete beams using adaptive neuro-fuzzy inference system and artificial neural network', *Sci. Iran.* 19 (2), 242–248.

Bai Y, Zhuang H and Wang D (2006) *Advanced Fuzzy Logic Technologies in Industrial Applications*, Springer, London

Boğa A, Öztürk M and Topçu IB (2013) 'Using ANN and ANFIS to predict the mechanical and chloride permeability properties of concrete containing GGBFS and CNI', *Compos. Part B: Eng.* 45 (1), 688–696.

Cevik A (2011) 'Modeling strength enhancement of FRP confined concrete cylinders using soft computing', *Expert Syst. Appl.* 28 (5), 5662–5673.

Cevik A, Göğüş MT, Güzelbey IH and Filiz H (2010) 'Soft computing based formulation for strength enhancement of CFRP confined concrete cylinders', *Ad. Eng. Softw.* 41 (4), 527–536.

Chindaprasirt P, Chareerat T and Sircicatnanon V (2007) 'Workability and strength of coarse high calcium fly ash geopolymer', *Cem. Concr. Compos.* 29, 224–229.

Dantas AT, Leite MB and Nagahama KJ (2013) 'Prediction of compressive strength of concrete containing construction and demolition waste using artificial neural networks', *Constr. Build. Mater.* 38, 717–722.

El-Didamony H, Amer AA and Ela-ziz HA (2012) 'Properties and durability of alkali-activated slag pastes immersed in sea water', *Ceram. Int.* 38, 3773–3780.

Garzón-Roca J, Marco CO and Adam JM (2013) 'Compressive strength of masonry made of clay bricks and cement mortar: estimation based on neural networks and fuzzy logic', *Eng. Struct.* 48, 21–27.

Guzelbey IH, Cevik A and Erklig A (2006) 'Prediction of web crippling strength of cold-formed steel sheetings using neural networks', *J. Constr. Steel Res.* 62, 962–973.

Haris J (2006) *Fuzzy Logic Applications in Engineering Science*, Springer, London.

Heah CY, Kamarudin H, Al Bakri AMM, Bnhussain M, Luqman M, Nizar IK, Ruzaidi CM and Liew YM (2012) 'Study on solids-to-liquid and alkaline activator ratios on kaolin-based geopolymers', *Constr. Build. Mater.* 35, 912–922.

Jang JSR (1993) 'ANFIS: adaptive-network-based fuzzy inference system', *IEEE Trans. Syst. Man Cyber.* 23 (3), 665–685.

Jang JSR, Sun CT and Mizutani E (1997) *Neuro-Fuzzy and Soft Computing: A Computational Approach to Learning and Machine Intelligence*, Prentice Hall, Englewood Cliffs, NJ.

Kouamo HT, Elimbi A, Mbey JA, Ngally Sabouang CJ and Njopwouo D (2012) 'The effect of adding alumina-oxide to metakaolin and volcanic ash on geopolymer products: a comparative study', *Constr. Build. Mater.* 35, 960–969.

Kouamo HT, Mbey JA, Elimbi A, Kenne Diffo BB and Njopwouo D (2013) 'Synthesis of volcanic ash-based geopolymer mortars by fusion method: effects of adding metakaolin to fused volcanic ash', *Ceram. Int.* 39 (2), 269–276.

Kumar S, Kumar R and Mehrotra SP (2010) 'Influence of granulated blast furnace slag on the reaction, structure and properties of fly ash based geopolymer', *J. Mater. Sci.* 45, 607–615.

Nazari A and Pacheco-Torgal, F (2013) 'Predicting compressive strength of different geopolymers by artificial neural networks', *Ceram. Int.* 39 (3), 2247–2257.

Nazari A and Riahi S (2012a) 'Computer-aided prediction of the ZrO_2 nanoparticles' effects on tensile strength and percentage of water absorption of concrete specimens', *J. Mater. Sci. Technol.* 28 (1), 83–96.

Nazari A and Riahi S (2012b) 'Experimental investigations and ANFIS prediction of water absorption of geopolymers produced by waste ashes', *J. Non-Cryst. Solids* 358 (1), 40–46.

Nazari A and Safarnejad MG (2013) 'Prediction early age compressive strength of OPC-based geopolymers with different alkali activators and seashell powder by gene expression programming', *Ceram. Int.* 39 (2), 1433–1442.

Nazari A, Bagheri A and Riahi S (2011) 'Properties of geopolymer with seeded fly ash and rice husk bark ash', *Mater. Sci. Eng. A* 528, 7395–7401.

Nazari A, Khanmohammadi H, Amini M, Hajiallahyari H and Rahimi A (2012) 'Production geopolymers by Portland cement: designing the main parameters' effects on compressive strength by Taguchi method', *Mater. Des.* 41, 43–49.

Onisei S, Pontikes Y, Van Gerven T, Angelopoulos GN, Velea T, Predica V and Moldovan P (2012) 'Synthesis of inorganic polymers using fly ash and primary lead slag', *J. Hazard. Mater.* 205–206, 101–110.

Pacheco-Torgal F, Castro-Gomes J and Jalali S (2007) 'Investigations about the effect of aggregates on strength and microstructure of geopolymeric mine waste mud binders', *Cem. Concr. Res.* 37, 933–941.

Pacheco-Torgal F, Castro-Gomes J and Jalali S (2008) 'Investigations on mix design of tungsten mine waste geopolymeric binders', *Constr. Build. Mater.* 22, 1939–1949.

Pacheco-Torgal F, Moura D, Ding Y and Jalali S (2011) 'Composition, strength and workability of alkali-activated metakaolin based mortars', *Constr. Build. Mater.* 25, 3732–3745.

Provis JL (2014) 'Geopolymers and other alkali activated materials: why, how, and what?' *Materials and Structures* 47, 11–25.

Provis JL and van Deventer JSJ (eds) (2013) *Alkali-Activated Materials: State-of-the-Art Report*, RILEM TC 224-AAM. Springer/RILEM, Berlin

Rajamma R, Labrincha JA and Ferreira VM (2012) 'Alkali activation of biomass fly ash–metakaolin blends', *Fuel* 98, 265–271.

Rickard WDA, Temuujin J and Van Riessen A (2012) 'Thermal analysis of geopolymer pastes synthesised from five fly ashes of variable composition', *J. Non-Cryst.Solids* 35, 1830–1839.

Rutkowski L (2004) *Flexible Neuro-Fuzzy Systems: Structures, Learning and Performance Evaluation*, Springer, London.

Sarker PK, Haque R and Ramgolam KV (2013) 'Fracture behaviour of heat cured fly ash based geopolymer concrete', *Mater. Des.* 44, 580–586.

Shi C, Fernandez-Jimenez A and Palomo A (2011) 'New cements for the 21st century: the pursuit of an alternative to Portland cement', *Cem. Concr. Res.* 41, 750–763.

Sivanandam SN, Sumathi S and Deepa SN (2007) *Introduction to Fuzzy Logic using MATLAB*, Springer, London.

Sobhani J and Ramezanianpour AA (2011) 'Service life of the reinforced concrete bridge deck in corrosive environments: a soft computing system', *Appl. Soft Comput.* 11 (4), 3333–3346.

Somna K, Jaturapitakkul C, Kajitvichyanukul P and Chindaprasirt P (2011) 'NaOH-activated ground fly ash geopolymer cured at ambient temperature', *Fuel* 90 (6), 2118–2124.

Sonebi M and Cevik A (2009) 'Prediction of fresh and hardened properties of self-consolidating concrete using neurofuzzy approach', *J. Mater. Civil Eng.* 21 (11), 672–679.

Tanyildizi H and Cevik A (2010) 'Modeling mechanical performance of lightweight concrete containing silica fume exposed to high temperature using genetic programming', *Constr. Build. Mater.* 24 (12), 2612–2618.

Vargas AS, Dal Molin DCC, Vilela ACF, da Silva FJ, Pavão B and Veit H (2011) 'The effects of Na_2O/SiO_2 molar ratio, curing temperature and age on compressive strength, morphology and microstructure of alkali-activated fly ash-based geopolymers', *Cem. Concr. Compos.* 33, 653–660.

Wongpa J, Kiattikomol K, Jaturapitakkul C and Chindaprasirt P (2010) 'Compressive strength, modulus of elasticity, and water permeability of inorganic polymer concrete', *Mater. Des.* 31, 4748–4754.

Yang K-H, Cho A-R and Song J-K (2012) 'Effect of water–binder ratio on the mechanical properties of calcium hydroxide-based alkali-activated slag concrete', *Constr. Build. Mater.* 29, 504–511.

Zadeh AL (1965) 'Fuzzy set', *Inform. Control* 8, 338–353.

Zuhua Z, Xiao Y, Huajun Z and Yue C (2009) 'Role of water in the synthesis of calcined kaolin-based geopolymer', *Appl. Clay Sci.* 43 (2), 218–223.

This page intentionally left blank

Analysing the relation between pore structure and permeability of alkali-activated concrete binders

9

Z. Zhang, H. Wang
University of Southern Queensland, Toowoomba, QLD, Australia

9.1 Introduction

Hardened Portland cement binders have complex pore structure, including gel pores, capillary pores and air voids. The pore features (pore size, volume, shape and connectivity) are critical microstructure characteristics because they determine the fluid transport properties of concretes. Gel pores are nanopores, usually from 0.5 nm to 2.5 nm and are too small for water molecules to penetrate. Capillary pores are from several nanometres to several micrometres, which have a large effect on the permeability of water and other liquids (Shi *et al.*, 2006). The binder permeability in concrete is very important because it determines the ingress of surrounding fluids to a large extent. The aggressive species, such as carbonate, chloride and sulphate ions, intrude in concrete through pore transportation. As a result, they neutralize the alkalinity of concrete and reduce the protection of steel reinforcement in concrete structures.

Similar to Portland cement-based binders, alkali-activated binders also have very complex pore structure. To date, there is limited research on their pore structures and the effect on the permeability of on site alkali-activated concretes; however, laboratory research has identified some issues regarding the chloride diffusion, carbonation and strength loss of binders under aggressive conditions. These issues are closely related to the pore structure.

This chapter examines the pore structure in alkali-activated metakaolin (AAM), alkali-activated fly ash (AAFA) and alkali-activated slag (AAS) binders that are reported in the literature. The pore structure of different binders was mostly examined by mercury intrusion porosimetry (MIP), although the differences between porosimetric techniques in characterizing pores are acknowledged (Bernal *et al.*, 2014). The permeability of the binders is discussed based on the water absorption and permeability, and chloride diffusion. The aim of this chapter is to analyse the relation between pore structure and permeability of alkali-activated binders. This relation is useful for understanding the durability of alkali-activated binder products, such as mortars and concretes, and also for designing and manufacturing of such materials in industry.

Handbook of Alkali-activated Cements, Mortars and Concretes. http://dx.doi.org/10.1533/9781782422884.2.235

9.2 Alkali-activated metakaolin (AAM) binders

9.2.1 Pore structure of AAM binders

The pore structure of AAM binders depends on many factors. Firstly, it largely depends on the activator type (Zhang *et al.*, 2012b, 2013). Figure 9.1 shows the

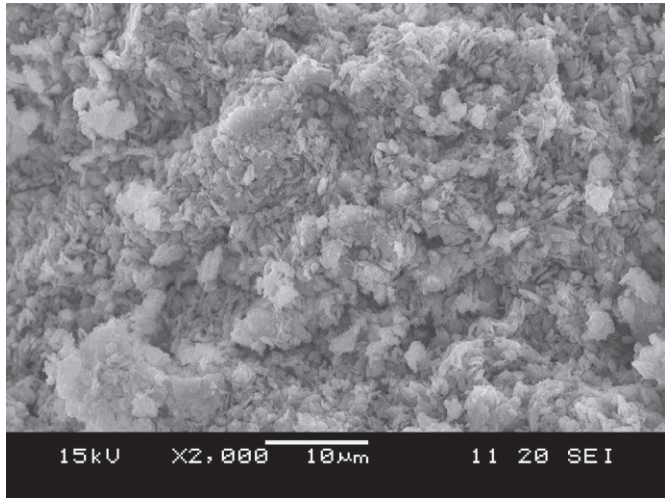

(a)

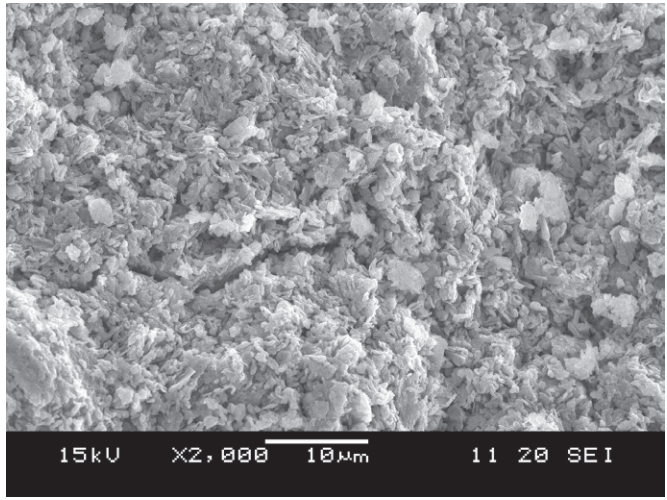

(b)

Figure 9.1 Representative SEM images of AAM binders: (a) 8 M NaOH; (b) 12 M NaOH; (c) $Na_2O{\cdot}1.0SiO_2$; (d) $Na_2O{\cdot}1.6SiO_2$. The metakaolin has D_{50} of 5.9 μm and specific surface area of 14.1 m^2/g. The liquid-to-solid ratio is 1.0 in NaOH activation systems, while it is 0.8 in sodium silicate activation systems. The reaction takes place at 30°C, normal pressure at a closed chamber for >72 h.

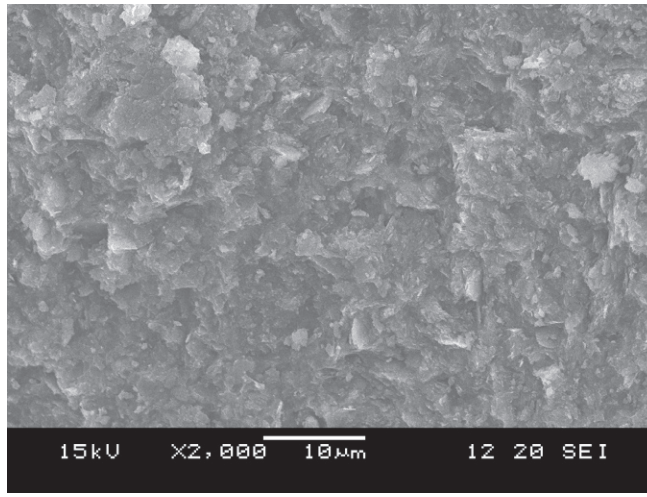

(c)

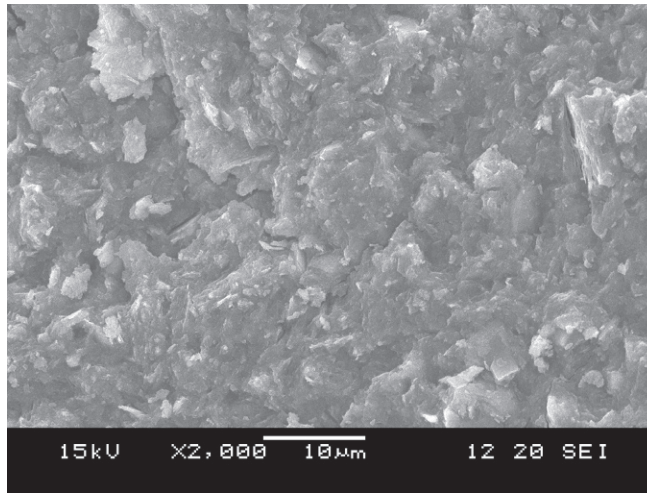

(d)

Figure 9.1 Continued

microstructure of AAM binders by sodium hydroxide and sodium silicate solutions. The pores in NaOH-AAMs appear much larger than in $Na_2O{\cdot}nSiO_2$-AAMs.

Generally, after reaction with highly concentrated NaOH solutions, metakaolin particles are converted into a porous, particulate gel, and are bound to each other on the surfaces, but also maintain their plate-like morphology to some extent. The observed porous gel morphology in NaOH-AAMs is similar to the previously published images of metakaolin geopolymers with low Si/Al ratios (Duxson *et al.*, 2005), and also those that resemble the precursor gels formed in some hydrothermal zeolite synthesis systems at very early stages (Chandrasekhar and Pramada, 2008).

Figure 9.2 shows the porosity and pore distribution of two NaOH-AAMs (Zhang *et al*., 2008). The porosity decreases with the increase of NaOH concentration. The pore size shifts towards smaller regions, from mainly 60–1000 nm to 100–1400 nm. Such a porous structure should be highly permeable. In comparison, $Na_2O{\cdot}nSiO_2$-AAMs are much more compact. The pore size distribution is usually in a range of 5–50 nm (Zhang *et al*., 2010a; Kamseu *et al*., 2012). This is because the soluble silicate itself is a binding material, becoming part of the gels. As metakaolin particles dissolve Al and Si in the activator solution, Na-Al-Si-OH gels form and bind the residual particles into a strong product.

The pore structure of AAM binders is affected by the nature of the metakaolin. Kamseu *et al*. (2012) examined the pore size distribution in AAMs that were derived from an Al-rich (51.59 wt.% of Al_2O_3) metakaolin M and a Si-rich (70.11 wt.% of SiO_2) metakaolin T by activation with a mixture of sodium hydroxide, potassium hydroxide and sodium silicate solutions. The pore structural features are summarized in Table 9.1. At a constant solid/liquid ratio, the AAM that synthesized using Al-rich metakaolin has higher porosity and larger pore size than that synthesized from Si-rich metakaolin. It seems that not only soluble Si in activator but also the Si present in metakaolin is beneficial in obtaining a compact structure.

The pore structure of AAM binder also depends on the liquid/solid ratio (Zhang *et al*., 2010a). This is somewhat similar to OPC binders, which have higher porosity and larger pores when the water/cement ratio is increased. The difference is that alkali activators contain solutes and the water is only consumed at a small proportion in geopolymerization (presented as hydroxyl bonds, absorbed water and pore solution).

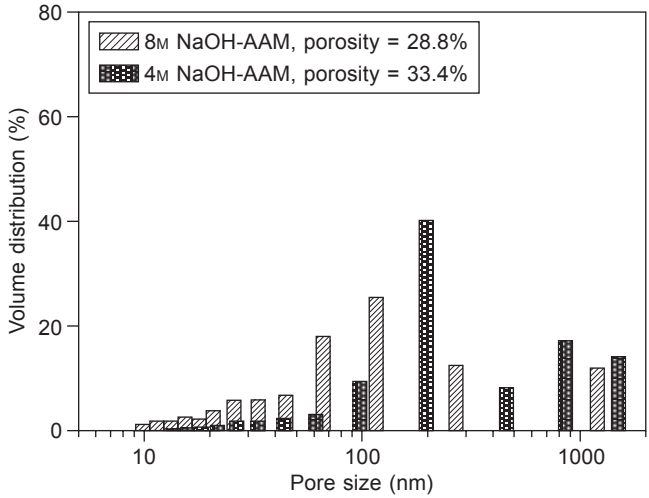

Figure 9.2 Pore size distribution of NaOH-AAMs. The metakaolin powder has a specific surface area of 10 m^2/g. The liquid/solid ratio is around 0.8 for both systems with 4 M and 8 M NaOH solutions, respectively. Samples are synthesized at 25 ± 2°C, relatively humidity (RH) = 95% for 24 h and followed by 6 days of steam curing at 80°C (data from Zhang *et al*., 2008).

Table 9.1 Pore structure for the AAMs by a mixture of sodium hydroxide, potassium hydroxide and sodium silicate solutions

Samples	Si/Al	Na/Al	Bulk density (g/cm^3)	Cumulative pore volume (mm^3/g)	Average pore size (μm)
M	1.23	0.83	1.32	0.318	0.031
75M	1.50	0.89	1.34	0.302	0.026
MT	1.79	0.96	1.34	0.308	0.024
25M	2.00	1.05	1.35	0.271	0.018
T	2.42	1.16	1.37	0.244	0.013

Note: The data have been reorganized according to the experimental conditions.
Source: Kamseu *et al*. (2012), with kind permission from Springer Science and Business Media.

Figure 9.3 shows the effects of liquid/solid ratio on slag containing AAMs. The porosity increases as the liquid/solid ratio increases, as summarized in Table 9.2. Most of the pores determined by MIP are below 20 nm, which are much smaller

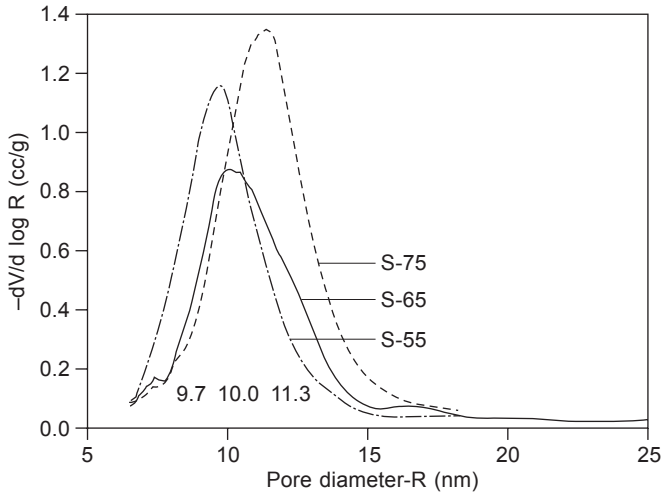

Figure 9.3 Effects of liquid/solid ratio on pore size distribution in AAMs. The AAM was prepared by sodium silicate solution activation of a metakaolin/slag (90/10) blend at 20°C. Systems S-55, S-65 and S-75 have liquid/solid ratios of 0.55, 0.65 and 0.75, respectively. More sample preparation details can be found in Zhang *et al*. (2010a).

Table 9.2 Pore size distribution and porosity for the AAMs as shown in Figure 9.3

System	Pore size distribution by volume ratio (%)				Porosity (%)
	<10 nm	<20 nm	<50 nm	>50 nm	
S–55	36.7	88.2	92.7	7.3	19.4
S–65	55.0	90.8	94.4	5.6	23.8
S–75	24.2	90.7	94.8	5.2	27.2

than in NaOH-AAMs (Chandrasekhar and Pramada, 2008) and also smaller than in hydrated cement binder (Zhang *et al*., 2010a). The binder S-55 has a higher volume of large pores (>50 nm) than S-65 and S-75, although the total volume of open porosity is the lowest (Table 9.2). This unexpected result is likely caused by the high viscosity of the geopolymer slurry, which makes the elimination of entrapped air bubbles difficult.

As one of the most important parameters, curing temperature also plays a significant role in affecting the pore structure of AAM binders (Rovnaník, 2010). As shown in Figure 9.4, the pore volume slightly increases with the increasing of curing temperature. Curing at higher temperatures also results in larger pores, whereas low temperature curing increases the bulk density (Rovnaník, 2010). As Rovnaník (2010) claimed, 'cumulative pore volume of geopolymer is generally twice as high in comparison with materials based on Portland cement or alkali activated slag'. This pore structural feature is attributed to the 'higher permeability and absorption capacity of water and aqueous solutions' as reported in the literature (Okada *et al*., 2009).

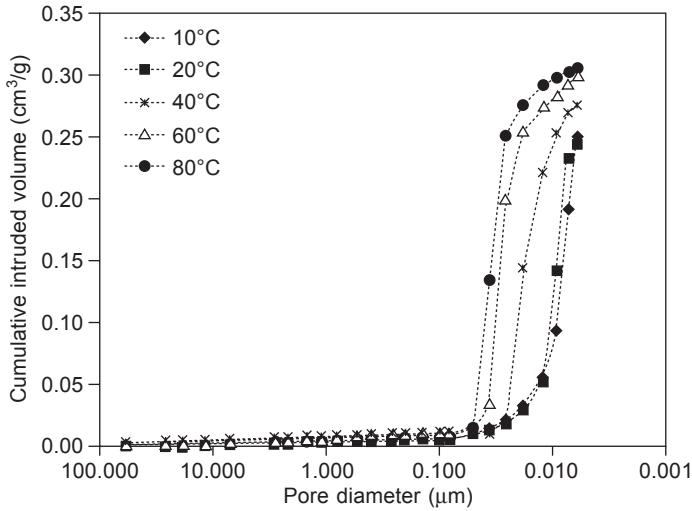

Figure 9.4 Effects of curing temperature on the pore size distribution and porosity of AAMs. Curing at 40, 60 and 80°C was carried out for the first 4 h (reprinted from Rovnaník, 2010, Copyright © 2010, with permission from Elsevier).

9.2.2 Permeability of AAM binders

Permeability is the ability for a material to allow liquid to pass through under a certain pressure gradient, such as when a binder is under hydrostatic pressure. AAM binders are known to have extremely low permeability, even under high pressure, because of their complex pore structures.

Given the nature of low permeability and high strength, Zhang *et al*. (2010b) used the Darcy method to measure the permeability. They developed a testing system as

shown in Figure 9.5. This method is usually used to test the well cores (hardened oil cement binders) in oil well cementing engineering (API recommended practice). The surrounding pressure, usually called confining pressure, is 3 MPa higher than the driven pressure to avoid liquid bypass along the surface of sample. After the permeation was steady, the permeated water over a period of time is recorded and the permeability can be calculated according to the following equation:

$$k = 10^5 \cdot Q \cdot \mu \cdot L/(A \cdot \Delta p) \tag{9.1}$$

where k is permeability coefficient (μm^2); Q is velocity of permeated liquid (mL/s); μ is viscosity of permeated liquid (Pa·s); L is length of sample; A is sample cross-section area; and Δp is the driving pressure of liquid.

It should be noted that the sample to be measured in the high pressure cabin should have gained a high enough strength against the liquid pressure. Otherwise, the sample will be damaged by the pressurized liquid and confining pressure. A single micro-crack can cause a large error in measurement. In their research, the samples were well cured for 3 days and achieved a compressive strength around 60 MPa, which was about three times over the confining pressure. Theoretically, under steady state, the liquid pressure should have very limited effect on the permeability of AAM binders. Figure 9.6 shows that in the testing pressure range, the water permeability decreases slightly with the increase in liquid pressure for the samples prepared at a liquid/solid ratio of 0.6. For the samples at a liquid/solid ratio of 0.7, this might not be the case. When the liquid pressure increases, the pore connectivity may be increased due to the intrusion of high pressure water, causing more open channels. However, as the confining pressure is also increased (confining pressure should always be higher than liquid pressure), the deformation of the sample due to the high pressure may decrease the pore connectivity. In general, from Figure 9.6, the effect of liquid pressure is very limited.

Zhang *et al*. (2010b) studied the effects of liquid/solid ratio on permeability of AAM binders under liquid pressure of 20.1 MPa. As expected, the permeability coefficient k increased along with the increase in liquid/solid ratio from 0.55 to 0.65 (Figure

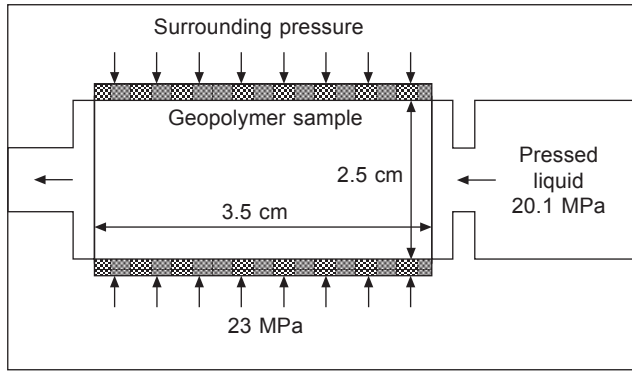

Figure 9.5 Testing of permeability of AAM binders by Darcy method (reprinted from Zhang *et al*., 2010b, Copyright © 2010, with permission from Elsevier).

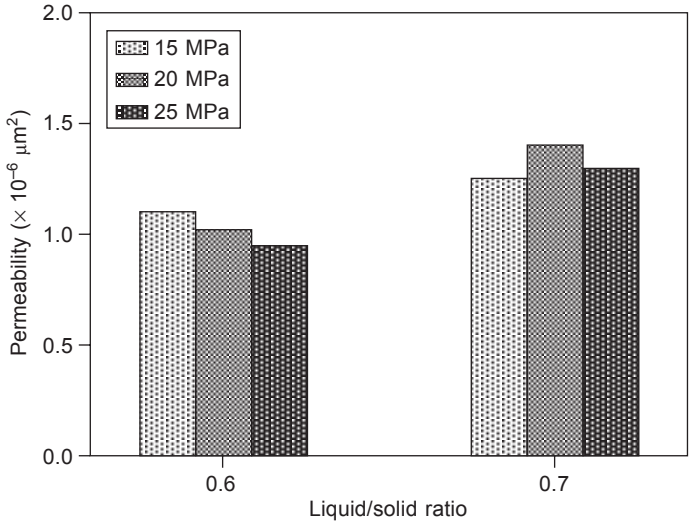

Figure 9.6 Effects of liquid pressure on the permeability of AAMs as determined by the Darcy method.

9.7). It suggested that more connected pores were formed in the geopolymer matrix prepared at higher liquid/solid ratios. This was because the polymerization process emitted excessive water during the polymerization stage, and the evaporation of water left open channels. When the liquid/solid ratio was higher than 0.65, it seemed the water permeability remained constant (or slightly decreased). This unexpected

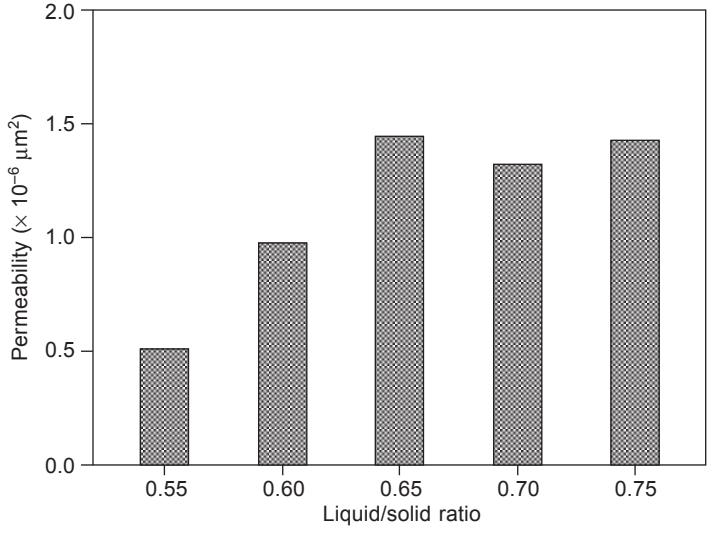

Figure 9.7 Effect of liquid/solid ratio on permeability of AAM binders (reprinted from Zhang *et al.*, 2010b, Copyright © 2010, with permission from Elsevier).

result was probably because of the decreased compressive elastic modulus of the samples at such high liquid/solid ratios. As discussed earlier, the shrinkage of pore volume of low modulus samples under high confining pressure may decrease the connectivity of pores and consequently reduce their permeability.

The permeability coefficient of AAM binder at liquid/solid ratio of 0.60 was 1.0×10^{-6} μm^2, almost twice that at 0.55. Under the same test conditions, a cement paste sample prepared with a water/solid ratio of 0.45 had an average permeability coefficient of 1.0×10^{-4} to 1.0×10^{-5} μm^2 (Zhang *et al.*, 2010a). Apparently, AAM binders have much lower water permeability, only 1/100 to 1/10 of that of cement paste. This is because of their dense structure and much smaller pore structure. Table 9.3 shows the comparison of pore size distribution of AAM binder and cement paste. The two materials have similar total pore volumes but with significantly different pore size. Most pores in the AAM binder are <50 nm while most of the pores in the cement paste are >50 nm. The volume of pores larger and smaller than 50 nm seems critical not only to mechanical properties but also to permeability.

Hardened cement pastes for oil well casing usually have water permeability of 1.0×10^{-4} to 1.0×10^{-1} μm^2, strongly depending on the slurry composition, quantity and type of additives, curing (setting) conditions and driven pressure of water (Goode, 1962; Backe *et al.*, 1999; Zhang, 2010). The utilization of reactive silicates, such as metakaolin and silica fume, can effectively reduce the water permeability of cement pastes (Zhang, 2010). It is reported that by using 1–2% nano-silica powder, the permeability of oil well cement paste that synthesized in accordance with API specification can be reduced to 1.0×10^{-6} to 2.0×10^{-5} μm^2 (Ershadi *et al.*, 2011), which is 20 times smaller than the permeability of AAM binders (Zhang *et al.*, 2010b). The porosity of the oil well cement paste was 28.5–30% (Ershadi *et al.*, 2011), which is not much higher than AAM binders. It suggests that other pore features, such as pore size, size distribution and pore shape, are probably more important than the total pore volume in determining the water permeability of AAM binders.

Zhang *et al.* (2010b) investigated the effects of curing condition on water permeability of AAMs, as shown in Figure 9.8. The binders by air curing conditions, seawater curing conditions and fresh water curing at 20°C had permeability of around 1.0×10^{-6} μm^2. Seawater curing slightly reduced permeability, which was believed to be due to the crystallization of the supersaturated salt liquid in the pores

Table 9.3 Pore size distribution of AAM binder and cement paste as determined by the MIP method

Binder	Pore size (nm)				Porosity (%)
	<10	<20	<50	>50	
AAM	61.5	90.9	95.9	4.1	24.1
Cement	2.4	8.0	26.3	73.7	29.5

Note: The AAM was activated by sodium silicate solution at liquid/solid ratio of 0.60 and the cement paste was prepared with Grade-52.5 ordinary Portland cement at water/solid ratio of 0.45.
Source: Reprinted from Zhang *et al.* (2010a), Copyright © 2010, with permission from Elsevier.

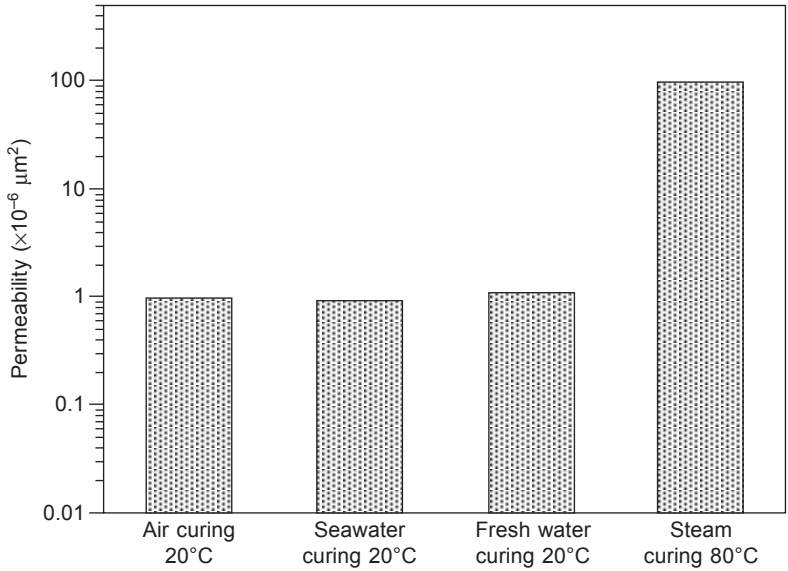

Figure 9.8 Effects of curing conditions on permeability of AAM binders prepared at liquid/solid ratio of 0.60 ml/g. The data for air curing, seawater curing and fresh water curing at 20°C were reported in Zhang *et al.*, 2010b. The data for steam curing at 80°C are not yet published.

on the sample surface. The crystals, possibly $Mg(OH)_2$ and $MgSO_4$, blocked the channels for water permeation. However, when the binder was subjected to 80°C steam curing, the permeability increased by 10 to 100 times that of low temperature cured samples. The much higher permeability is due to larger pore size distribution (Rovnaník, 2010; Lloyd, 2009), even micro-cracks (Zhang *et al.*, 2009a), in gels compared to the low temperature cured AAMs. As can be seen in Figure 9.4, the 20°C cured sample had a porosity of 25% and most of pores were smaller than 20 nm. In comparison, the 80°C cured sample had a porosity of 30% with pore size larger than 50 nm. The evaporation of pore water and loosely bound water under high temperature will cause the reorganization of aluminosilicate gels. The most likely consequence is the shrinkage of gels around pores (liquid phase) (Rovnaník, 2010; Lloyd, 2009), although the bulk volume may not change significantly (Zhang *et al.*, 2009a).

The effects of slag substitution on permeability of AAM binders were also studied by Zhang *et al.* (2010b), with the results shown in Figure 9.9. With 10–30% replacement of metakaolin by granulated blast furnace slag, the permeability was reduced by 10–20% at liquid/solid ratio of 0.60.

The reduced permeability was attributed to the decreased pore sizes and volume, as shown in Figure 9.10. The AAM binder without slag had a porosity of 24.1%, of which 61.5% were pores <10 nm, while the AAM binder with 10% slag substitution had a porosity of 22.3%, of which 65.8% of pores were <10 nm. When slag content was >10%, geopolymer had a relatively steady and low permeability, suggesting that

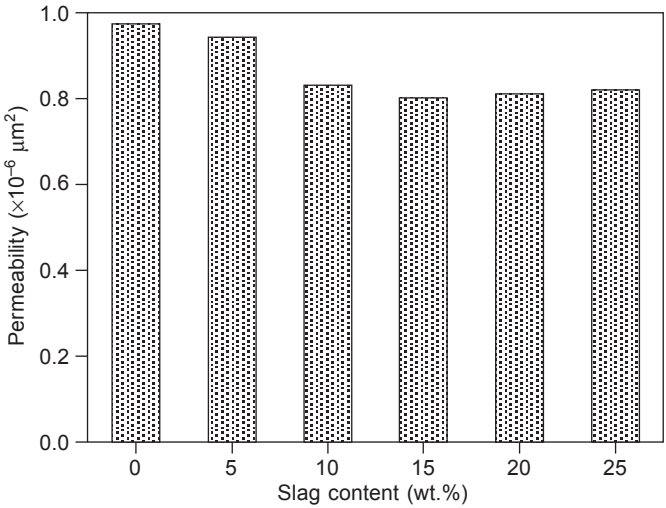

Figure 9.9 Effects of slag substitution on permeability of AAM binders that were synthesized by activation with $Na_2O{\cdot}1.2SiO_2$ solution at 20°C (reprinted from Zhang *et al.*, 2010b, Copyright © 2010, with permission from Elsevier).

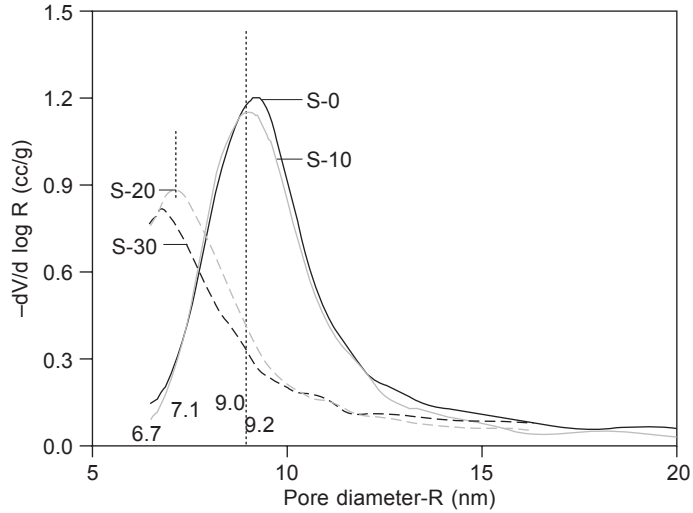

Figure 9.10 Effects of slag substitution on pore size distribution in AAM binders. Systems S-0, S-10, S-20, S-30 have 0, 10%, 20% and 30% slag substitutions, respectively (reprinted from Zhang *et al.*, 2010a, Copyright © 2010, with permission from Elsevier).

slag particles had some dense packing influence on geopolymer microstructure (Yip *et al.*, 2005). However, the substitution of slag should not be too high in the synthesis of low permeable AAMs, as it was observed that under laboratory conditions samples with more slag substitution possessed higher shrinkage. The shrinkage might cause micro-cracks, which become open channels for outside fluids.

9.3 Alkali-activated fly ash (AAFA) binders

9.3.1 Pore structure of AAFA binders

AAFA binders have been studied more extensively in recent years because they are more suitable than AAM binders for concrete manufacturing. It is well known that metakaolin needs a milling process and a high temperature heating process, usually at 500–900°C (Zhang *et al.*, 2009b), to obtain a reactive powder. In comparison, fly ashes do not require too much additional energy input. Fly ashes are spherical while metakaolin is layered in structure. This morphological difference leads to a much higher liquid requirement in metakaolin-based geopolymer paste than in fly ash-based geopolymer paste (Provis *et al.*, 2010). Metakaolin paste usually requires a liquid/metakaolin ratio of >0.6 by mass (Zhang *et al.*, 2009a, 2010a, 2010b), and mortars need ~1.0 (Rovnaník, 2010; Pacheco–Torgal *et al.*, 2011). If the liquid/solid ratio is low, a high pressure compaction process is required (Živica *et al.*, 2011), which is not desirable in most engineering production situations. In comparison, AAFA paste requires a liquid/ash ratio between 0.30 and 0.65 (Zhang *et al.*, 2012a), and 0.40–0.96 for concretes (Diaz–Loya *et al.*, 2011), which depends on the nature of fly ash and activator. It has been demonstrated that the activator solution is the major cost of the manufacture of alkali-activated binders (McLellan *et al.*, 2011). Therefore, the development of cost and performance comparable or superior AAFA binders to replace OPC is more interesting in actual applications.

Important factors that impact the pore structure of AAFA binders include fly ash properties, activator type and dosage, and curing conditions. The pore structure in AAFA binders is substantially different when fly ashes vary. Figure 9.11 presents the SEM images of five geopolymers. These geopolymers are synthesized using five different fly ashes at the same quantity of alkaline solutions (in terms of Na_2O and SiO_2 mass). The fly ashes require different additional water to obtain a similar workability. Specifically, fly ashes A and C are very fine and their mixtures at liquid/solid ratio of 0.39 exhibit high workability. Fly ashes B, D and E require some additional water, 0.2, 0.1 and 0.23, respectively (Zhang *et al.*, 2012a), to achieve a similar workability. The SEM images in Figure 9.11 show that AAFA binder E is the most porous one. The pore analysis by MIP method, as shown in Table 9.4, revealed that most pores in AAFA binders were between 20 and 500 nm. This pore size was much larger than in AAM binders. In comparison with normal cement pastes, such as the one in Table 9.3, only binders A and C had comparable or slightly larger pore size distribution. The other three all had much larger pores and higher porosities. Such porous AAFA binders are not expected to have low water permeability.

There is no doubt that the amount of additional water in the activator is one of the most important factors that affect the porosities of the AAFA binders. However, the particle size and packing density of fly ash are also important. As is well known, in AAFA systems only a fraction of fly ash particles (usually between 5 and 30% (Rattanasak *et al.*, 2011; Chindaprasirt *et al.*, 2011), at most 60% (Fernández–Jiménez *et al.*, 2006)) can be dissolved and react with alkali activator to form aluminosilicate gels. These gels are to fill the space between residual particles to reduce the porosity

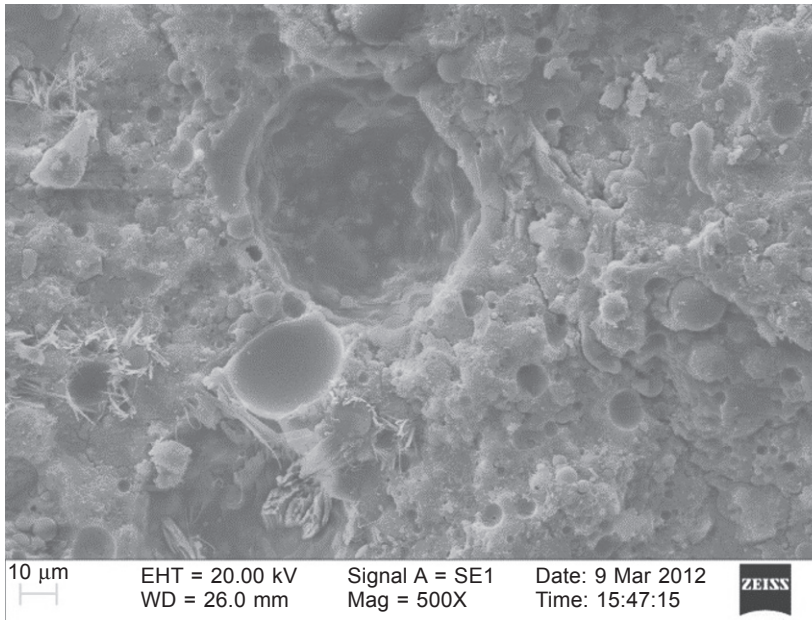

Figure 9.11 (a–e) SEM images of AAFA binders by alkali activation of fly ashes from different power stations. Fly ashes A, B, C, D and E have specific surface of 2.1, 2.3, 1.0, 0.9 and 0.6 m^2/g, respectively. The activator is a mixture of NaOH and $Na_2O{\cdot}2.0SiO_2$ and the curing is in sealed containers at 40°C for the first 24 h and followed by curing at 25°C for 27 days. More detailed information about physical and chemical features of the fly ashes and reaction conditions can be found in Zhang *et al.* (2012a).

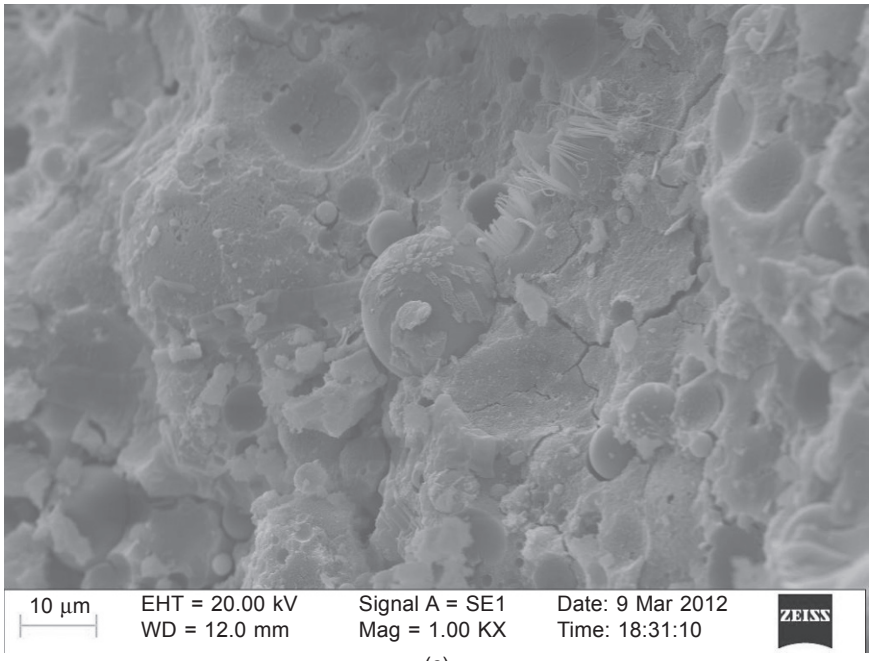

(c)

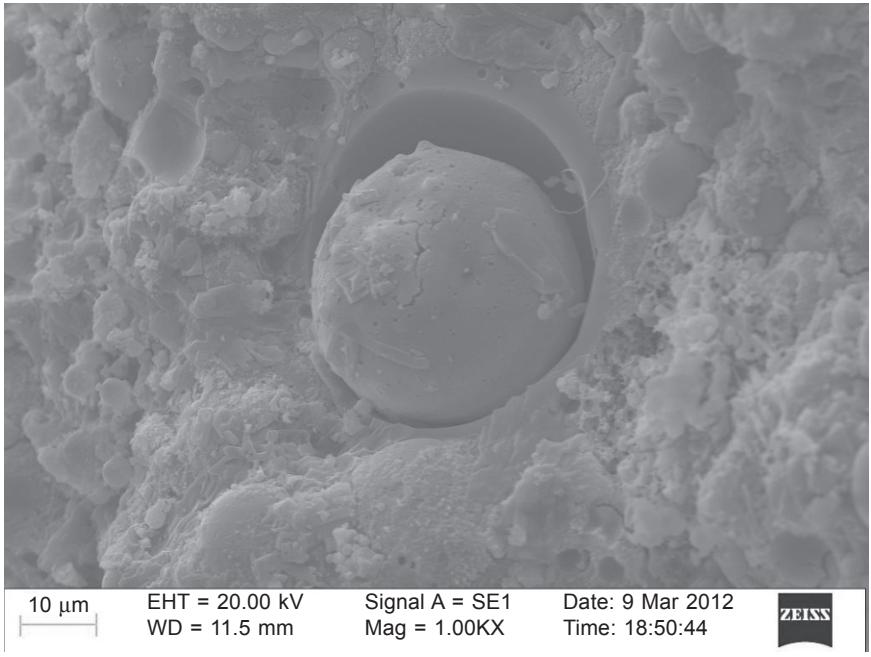

(d)

Figure 9.11 Continued

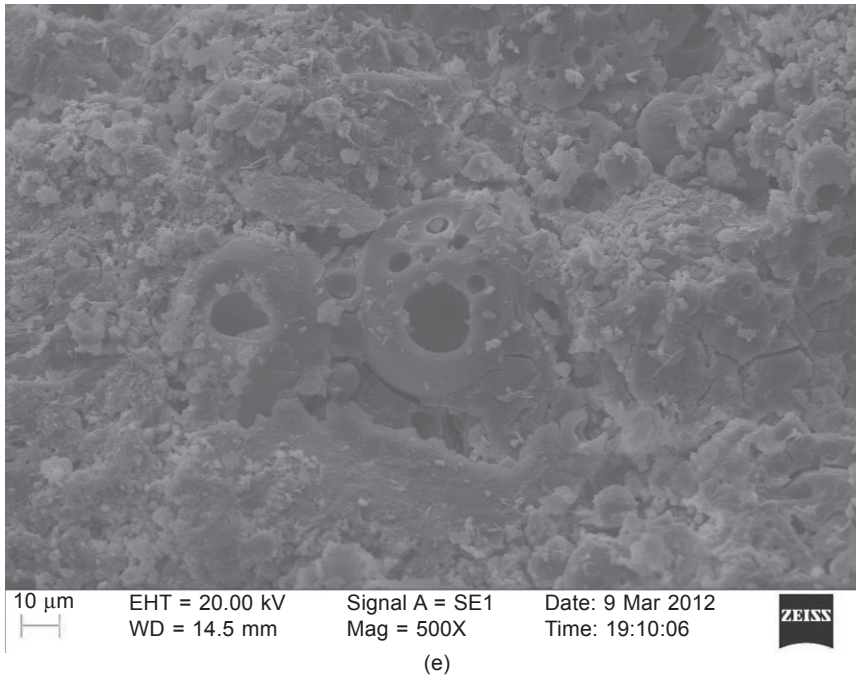

Figure 9.11 Continued

Table 9.4 Pore size distribution and porosity of AAFA binders synthesized with five different fly ashes

Binder	Pore size (nm)				Porosity (%)
	<20	<50	<100	>500	
A	16.0	55.3	65.5	4.1	21.7
B	0.7	34.1	32.2	14.7	35.9
C	0.5	51.1	63.8	5.8	27.4
D	0	4.2	50.2	13.5	29.2
E	0	1.5	4.5	34.2	41.6

in the final binder. Apparently, a high packing density, which usually comes with very fine ash particles, is critical in achieving a compact and strong binder.

The activator type also affects the pore size and porosity of AAFA binders to a large degree. In the early research by Palomo *et al*. (1999), it is noted that the binder activated by NaOH (12 M) solution was much more porous than the binder activated by the solution of KOH mixed with K_2SiO_3 with a modulus (SiO_2/K_2O ratio) of 0.63. The benefits and mechanisms of soluble silicate in activator to achieve compact binders are very similar to those in AAM systems. When $Ca(OH)_2$ is used as activation agent, the pores in binders are substantially different from those in

binders activated with alkali metal hydroxides and silicates (Komljenović *et al.*, 2010), as can be seen in Figure 9.12. The AAFA binder activated by $Ca(OH)_2$ produced typical C-A-S flocculation microstructure, and the pores are larger than in NaOH activated binder. As observed from the SEM images, the most compact binder is the one activated with $Na_2O{\cdot}1.5SiO_2$. The pore sizes are reduced from several micrometres in $Ca(OH)_2$, NaOH and $Na_2O{\cdot}0.5SiO_2$ activated binders to less than one nanometre in $Na_2O{\cdot}1.5\ SiO_2$ activated binders. This pore size feature was also

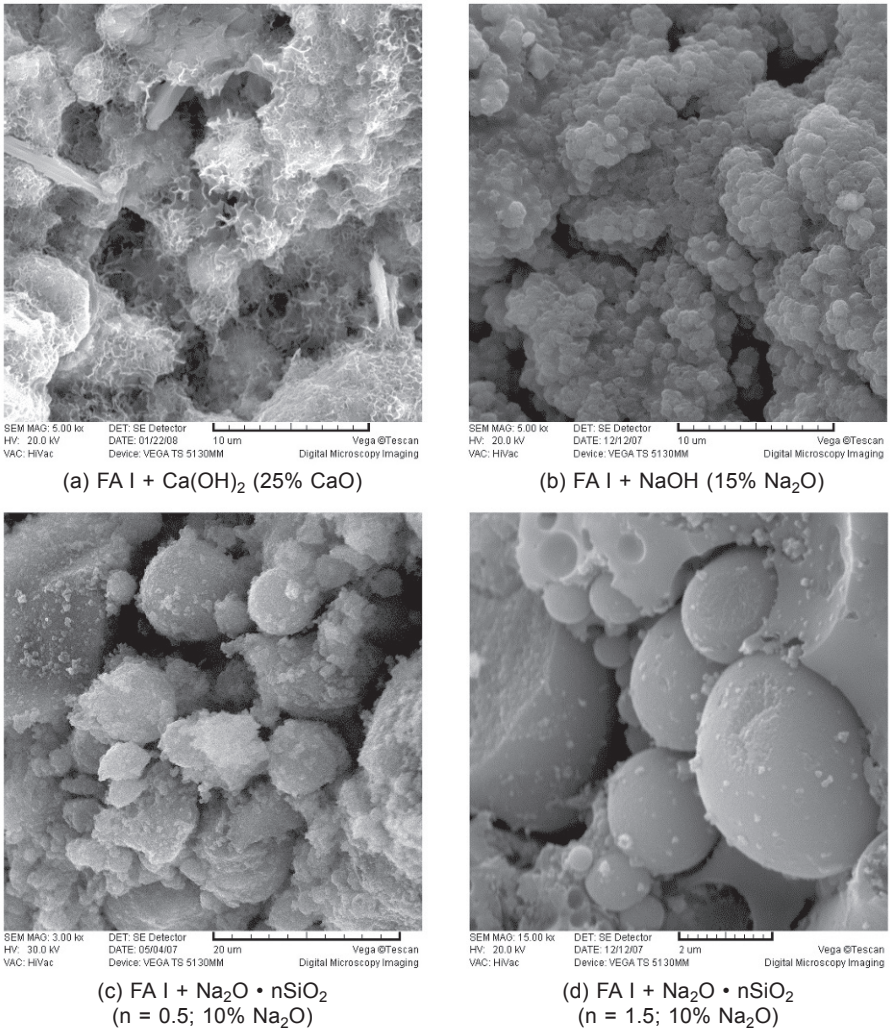

Figure 9.12 SEM images of AAFA binders by different activator solutions: (a) $Ca(OH)_2$ at CaO = 25%; (b) NaOH at Na_2O = 15%; (c) $Na_2O{\cdot}0.5SiO_2$ at Na_2O = 10%; and (d) $Na_2O{\cdot}1.5SiO_2$ at Na_2O = 10%. More detailed synthetic conditions can be found in Komljenović *et al.* (2010).

observed using SEM observation reported by many other researchers (Fernández-Jiménez and Palomo, 2005; Criado *et al*., 2012; Chi and Huang, 2013).

The curing conditions also have influences on the pore size in AAFA binders, very similar to AAM binders. Criado *et al*. (2012) investigated the curing humidity on the microstructure of AAFA binders. From their SEM observation it is noted that after 30 days of curing in air-tight containers with RH = 90% at 80°C the binder was much more compact than that cured at the same temperature but with RH = 40–50%.

9.3.2 Permeability, water absorption and chloride diffusion in AAFA binders

AAFA binders are expected to have lower permeability than normal cement binders because of much finer pore size, although their porosities may be similar. By using the Darcy method under a relatively low inlet pressure (0.7 MPa), the permeability of several AAFA binders prepared using different activators and curing conditions was tested in relation to their pore features (Ma *et al*., 2013), as shown in Figure 9.13. The Portland cement sample PC 0.4 (synthesized at w/c ratio of 0.4) had very similar total porosity as the sample 1.5–1.5 (denoting the modulus of activator is 1.5 and liquid/solid ratio is 1.5) at 7 days, but its water permeability was 10 times higher. As curing time increased, the total porosity did not change too much for AAFA binders but it decreased significantly for PC 0.4, so did their corresponding permeability. By using the Darcy method under relatively high inlet pressures, CO_2 permeability of AAFA binders was measured in comparison with hardened oil well cement paste by Nasvi *et al*. (2014). They found that at similar porosities, the CO_2 permeability of AAFA binders (0.0005–0.002 μD) is two to three orders lower than Class G cement (0.12–2.6 μD), depending on the mix compositions of AAFA. The reason for this much lower permeability is due to the finer pore size of AAFA than that of cement paste.

Beside of permeability, in concrete, the liquid transportation has another primary mechanism, namely capillary water absorption. Capillary absorption is the movement of water through the small pores in concrete in the absence of an externally applied hydraulic head, and is the result of surface interactions between the water and the pore wall. It is much faster than pressure permeability and is the primary transport mechanism for water in concrete structures under ambient conditions. In the following sections, water capillary absorption of AAFA binders is discussed in comparison with cement binders.

The author Zuhua Zhang and his colleague Zhu have designed the experimental works to examine the water absorption and chloride diffusion of AAFA binders in comparison with cement binders. The following are some of their unpublished data. They used a Class F Grade II fly ash (according to Chinese Standard GB/T 1596-2005) and $Na_2O{\cdot}1.0SiO_2$ (concentration = 35%) to prepare AAFA binders. The particle size distribution of the fly ash is shown in Figure 9.14. This fly ash had relatively coarse particles, and its specific surface area was estimated to be 0.82

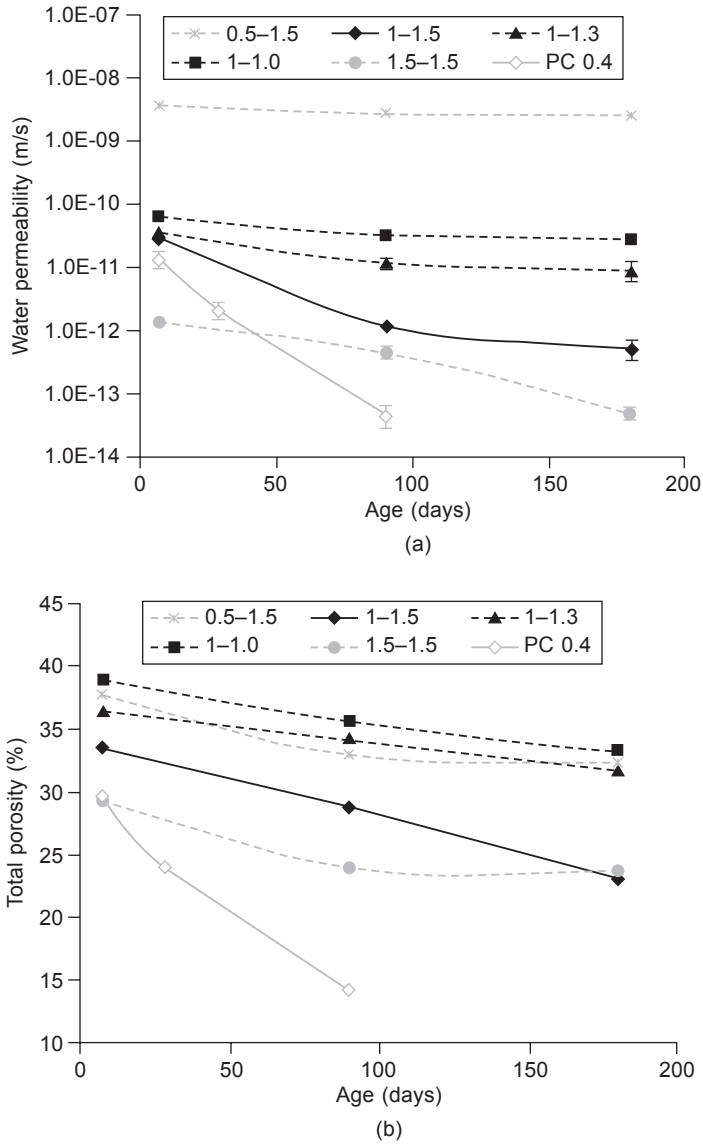

Figure 9.13 (a–d) Water permeability of AAFA binders and its relationship with porosity and pore size. The 'total porosity' refers to the total mercury intrusion volume at highest pressure, 'effective porosity' refers to the mercury volume by excluding ink-bottle porosity and 'threshold pore diameter' refers to the pore size corresponding to the highest mercury intrusion rate as size changes (reprinted from Ma *et al.*, 2013, Copyright © 2013, with permission from Elsevier).

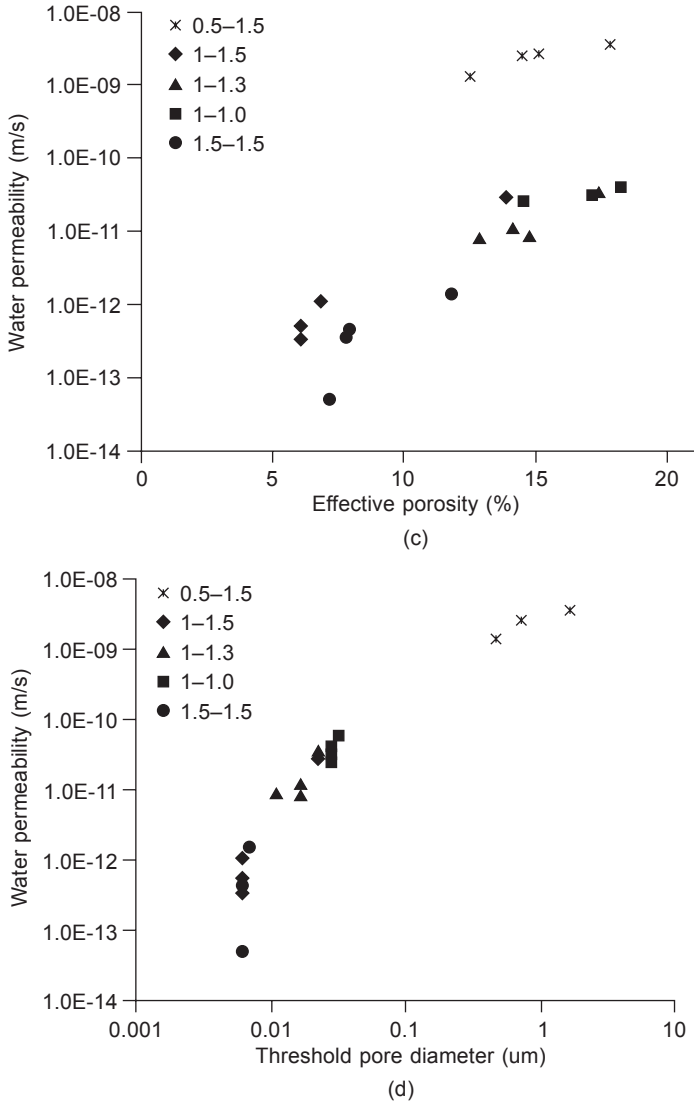

Figure 9.13 Continued

m^2/g as measured by a laser particle analyzer. This kind of Grade II fly ash required much high volume liquid, which was also found for those fly ashes with similar particle size and surface areas (Zhang *et al.*, 2012a). It was mixed with an activator solution at liquid/solid ratios of 0.6, 0.7 and 0.8. Trial mixtures at lower liquid/solid ratios than 0.6 were too stiff to fill the PVA moulds. A cement paste was prepared at a water/cement ratio of 0.35. AAFA pastes cast in moulds were cured in a well-designed procedure: sealed curing at 20°C for the first 24 h, followed by sealed

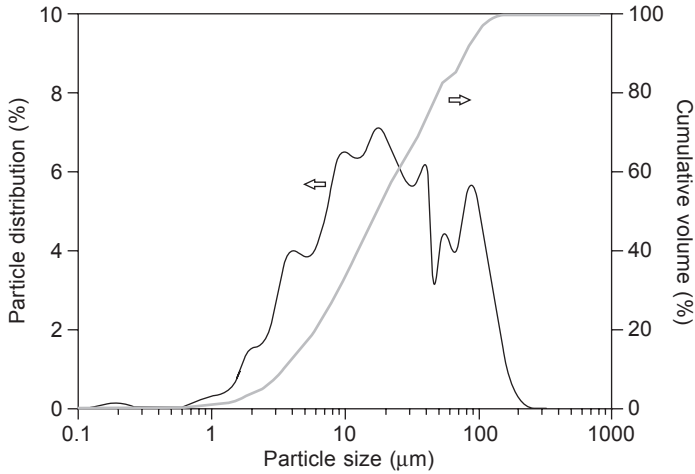

Figure 9.14 Particle size distribution of a Class F Grade II fly ash.

curing at 65°C for 48 h, de-moulded, then followed by sealed curing at 20°C for 7 days. The cement paste was sealed and cured at 20°C for the first 24 h, de-moulded and followed by water curing at 50°C for 15 days. These procedures were designed with the aim of achieving high maturity for the hardened samples.

The hardened AAFA binders and the cement binder were measured in two ways to obtain their water capillary absorption properties: one was measured on as-prepared samples after 24 h equilibration at RH = 90%, and the other was on samples after 24 h drying at 100°C. The water capillary absorption kinetics are shown in Figure 9.15.

It is clear that all of the three AAFA binders at different liquid/solid ratios have much higher capillary absorption rate and ratio than the cement binder. The as-prepared samples have very limited water loss under RH = 95%, 20°C conditions, and their water absorption is low. For those at 100°C and 24 h drying, a standard procedure recommend by ASTM C642-06, water absorption is very fast and reaches saturated absorption in 24 h. An increase of alkali activator dosage leads to an increased porosity, as reflected by the water absorption of the dried samples.

The pore structure of these binders is shown in Table 9.5, as determined by the MIP method. The pores in AAFA binder are mostly in a range of 10–50 nm. Portland cement binder has a larger pore size distribution, mainly from 20–200 nm. The porosities of AAFA binders are consistent with the water absorption ratio (Figure 9.15); however, the porosity of the cement binder is much lower than the water absorption ratio. This is due to its complex pore tortuosity, which makes it difficult for mercury fluid to intrude in. The capillary absorption has a close relationship with the porosity, less direct with pore size distribution.

The high porosity and high capillary absorption of AAFA binder are expected to lead to low resistance to chloride diffusion. To confirm this point, cylindrical samples of Ø20 mm × 80 mm were cast, cured at the conditions as described above, sealed

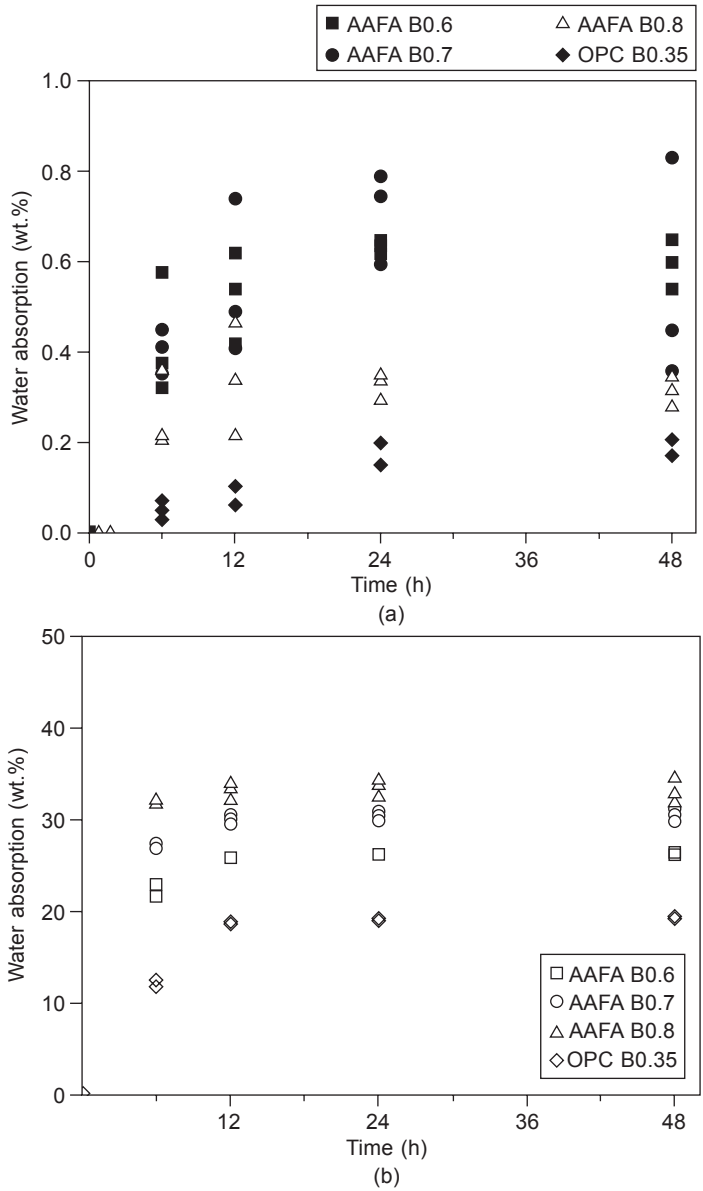

Figure 9.15 Water absorption of AAFA binders in comparison with OPC binders: (a) as-prepared samples; (b) 100°C × 24 h dried samples.

on surface with water-resistant resin and put in contact with saturated solution, as shown in Figure 9.16.

After 7 days of penetration, the samples were cut into four pieces with height of 20 mm, ground and dried. The chloride concentrations in each piece were determined by acid dissolution and $AgNO_3$ titration. Figure 9.17 shows the chloride concentration

Table 9.5 Pore size distribution and porosity of AAFA binders synthesized with different liquid/solid ratios, in comparison with a cement paste at w/c = 0.35

Binder	Liquid/solid ratio	Water/solid ratio	Pore size (nm)				Porosity (%)
			<10	<20	<50	>100	
B0.6	0.6	0.32	19.3	71.5	93.3	3.7	27.2
B0.7	0.7	0.36	24.6	76.4	93.2	4.4	31.2
B0.8	0.8	0.41	22.3	74.8	93.5	3.2	33.8
Cement	0.35	0.35	5.0	24.4	45.0	34.1	8.0

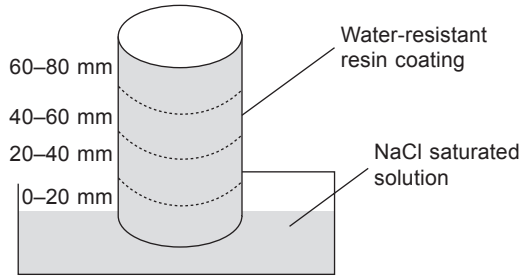

Figure 9.16 Chloride diffusion testing of AAFA binders under natural capillary absorption conditions at 20°C.

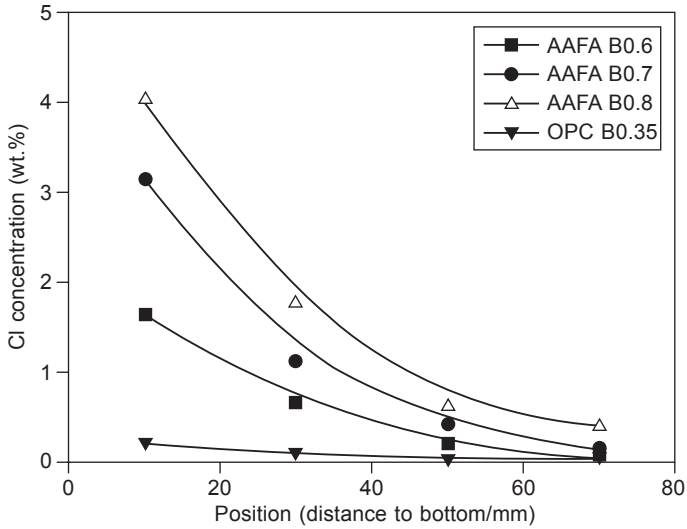

Figure 9.17 Distribution of chloride concentration in AAFA binders in contact with saturated NaCl solution, in comparison with OPC binder.

distribution of the three AAFA binders and the cement binder. It is very clear that AAFA binders have higher porosities, exhibiting much faster chloride diffusion compared with the cement binder.

The above data show that AAFA binders are not highly resistant to chloride diffusion/penetration. Regardless of external conditions, such as chloride concentration and liquid pressure, the permeability and water absorption properties of AAFA binders strongly depend on their formula. The liquid requirement is a critical factor in determining the final porosity. When a coarse fly ash (such as Class F Grade II or III fly ash according to GB/T 1596-2005) is used as single solid materials, the high liquid requirement usually leads to a high porosity. Moreover, as the pore sizes in AAFA binders are mostly between 20 and 100 nm, the capillary absorption force is very high. These properties may lead to fast penetration of chloride and other harmful ions in concretes (Wongpa *et al.*, 2010; Adam, 2009). Therefore, the utilization of fly ash in alkali-activated binder manufacturing needs to consider the pore sizes and porosity in the final products, and the possibility of high capillary absorption, permeability and ion diffusion rate.

9.4 Alkali-activated slag (AAS) binders

9.4.1 Pore structure of AAS binders

AAS binders have been extensively studied in the past decades, including chemical reaction mechanisms and engineering properties, and have been commercially produced and used in construction projects, most of which took place in the former Soviet Union and China (Shi *et al.*, 2006). Today there are AAS-based concretes on the market in Australia as well.

The microstructural features of AAS binders are different from AAM and AAFA binders, and also different from OPC binders. Figure 9.18 shows the comparison of typical microstructures of AAM, AASM (alkali-activated slag/metakaolin blend), AAS and OPC binders (Lecomte *et al.*, 2006). The AAM binder micrograph displays a relatively more homogeneous binding matrix than the other three. Compared to AAFA binders (Figures 9.11 and 9.12), AAS binders appear more compact. An important feature in AAS binders is that the micro-cracks appear throughout the matrix. This is a very common feature in AAS, as observed in SEM images in a lot of research (Adam, 2009; Brough and Atkinson, 2002; Gruskovnjak *et al.*, 2006; Palacios and Puertas 2007; Puertas *et al.*, 2004, 2006; Sakulich, 2009). This is probably due to the high shrinkage nature of AAS binders, if the drying procedure for sampling is not the main reason. However, crack-free microstructural images are observed in samples which are cut from bulk, immediately immersed in isopropanol and subsequently dried at 40°C for 24 h (Ben Haha *et al.*, 2011b). The penetration of a low viscosity epoxy resin into the binder may also help to reduce cracks during polishing (Ben Haha *et al.*, 2011b).

It is well established that AAS binders have finer pore size distribution than OPC binders (Shi *et al.*, 2006). However, the pore structure in AAS binders depends on many factors, such as alkali activator type and dosage, and curing/reaction conditions.

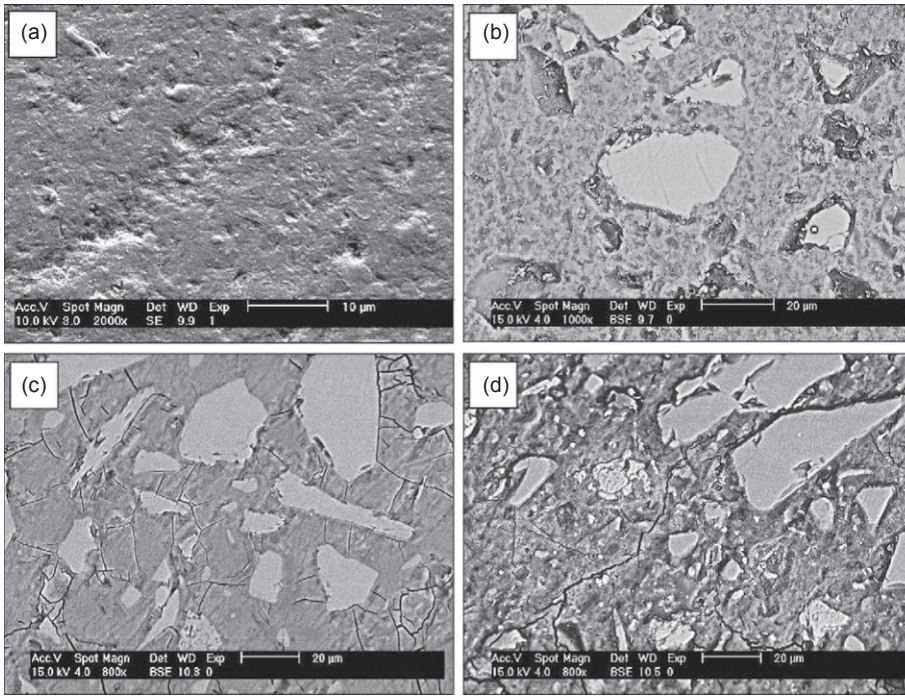

Figure 9.18 SEM images of alkali-activated metakaolin binder (a), alkali-activated metakaolin/slag (40/60) binder (b), alkali-activated slag binder (c), and hardened Portland cement binder (d). The alkali activator is a mixture of potassium metasilicate and potassium hydroxide solutions with K_2O/SiO_2 of 0.68. More detailed synthesis conditions can be found in Lecomte *et al.* (2006).

Alkali hydroxide-activated binders are more porous than alkali silicate-activated AAS binders because of the lack of soluble silicate (Shi, 1996; Ben Haha *et al.*, 2011a; Aydın and Baradan, 2014). Figure 9.19 shows the typical pore size distribution of three $Na_2O{\cdot}1.7SiO_2$ activated binders (Melo Neto *et al.*, 2008). At constant water/solid ratio of 0.48 (solids include the slag and Na_2O and SiO_2 in the activator), the maximum pore size changes from ~25 nm in the 2NS to smaller than 10 nm in the 4NS. The decreased pore size indicates the importance of soluble silicate in the densification of gel. Due to the high water/solid ratio used, the porosities in these binders, in a range of 20–40%, are much higher than the values reported in other research (Shi, 1996; Roy *et al.*, 2000). The utilization of $Na_2O{\cdot}nSiO_2$ and NaOH powder as dry activator generates a pore size distribution between 10 and 50 nm in the binders containing 15% Na_2O with Ms = 0.6 and 1.5 and the binder containing 5% Na_2O with Ms = 1.5 (Ravikumar and Neithalath, 2013). However, the binder containing 5% Na_2O with Ms = 1.5 shifts the main distribution to 20–100 nm (Ravikumar and Neithalath, 2013). From this point of view, the utilization of dry activator seems to have very limited influence on pore size distribution.

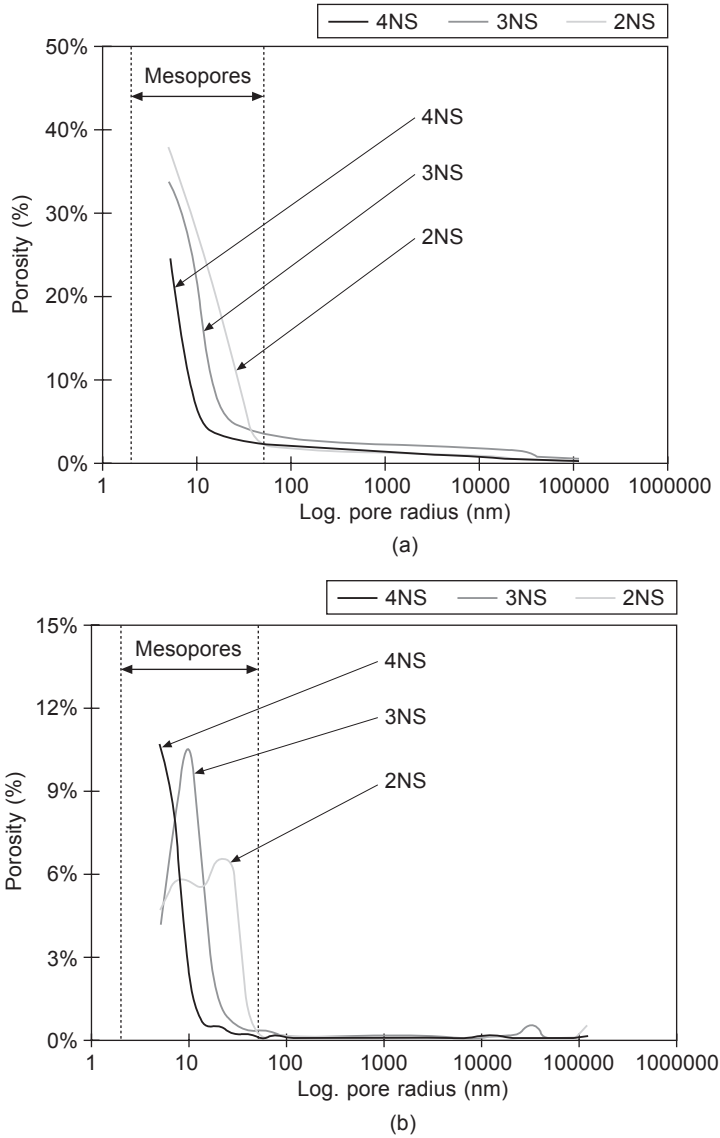

Figure 9.19 (a) Cumulative and (b) incremental pore size distribution of AAS binders. The activator is a sodium silicate solution with Ms = 1.7. '2NS', '3NS' and '4NS' refer to the concentrations of Na_2O in each binder 2.5%, 3.5% and 4.5%, respectively. More detailed synthetic conditions can be found in Melo Neto *et al*. (2008).

Curing conditions, such as time and humidity, have some influence on the pore structure in AAS binders. A very typical pore refinement trend in AAS binders is shown in Table 9.6. The paste is a mixture of slag with sodium silicate activator (dry) and lime slurry (1% lime in water) and cured under exposed conditions (Collins and

Table 9.6 Pore size distribution and porosity in sodium silicate-activated AAS binders

Age (d)	% mesopores (1.25–25 nm radius)	% macropores (25–5000 nm radius)	% voids/microcracks (5000–50,000 nm radius)	Porosity (%)
3	74.0	16.6	9.4	33
7	76.0	14.9	9.1	32
28	82.0	10.4	7.6	31
56	81.3	12.5	6.2	25

Source: Data are from Collins and Sanjayan (2001).

Sanjayan, 2001). Most of the pores in AAS binders are mesopores, from 1.25 to 25 nm. The pore sizes and volume continuously decrease with curing time, which is consistent with the pore refinement trend in other binders by liquid sodium silicate activation of different slags (Ben Haha *et al*., 2011a). The pore size distribution is affected by the curing humidity. A moist curing (water bath or sealed) leads to finer pore size, lower porosity and fewer micro-cracks than dry curing (exposed to air with RH = 50%) (Collins and Sanjayan, 2001).

9.4.2 Permeability of AAS binders

Direct measurements of the water permeability of AAS binders are less reported in the literature. Data of the permeable properties of AAS mortars and concretes are available (Shi, 1996; Ismail *et al*., 2013; Bernal *et al*., 2011). However, it is reasonable to expect that AAS binders have similar water permeability to AAM binders at an equivalent porosity level, considering their similar pore size distribution. Furthermore, given the fact that slag substitution of metakaolin provides benefits in reducing permeability, well-synthesized AAS binders are expected to have lower water permeability than AAM binders because of their lower porosities, compared to normal AAM binders.

The capillary water absorption property of AAS binders depends on the nature of raw materials and curing conditions. When mixed with aggregates, the capillary water absorption behaviour could be more complex (Aydın and Baradan, 2014; Ismail *et al*., 2013; Bernal *et al*., 2011). It is expected that AAS binders have much lower capillary water absorption than AAFA and AAM binders at the same activation conditions (Ismail *et al*., 2013; Bernal *et al*., 2011). Roy *et al*. (2000) measured the effective coefficients for steady state diffusion of chlorides through alkali-activated slag and slag/OPC binders, in comparison with OPC binders with and without activation (see Figure 9.20). The steady state diffusion of chlorides in AAS binder (slag replacement = 100%) is about 1.0×10^{-14} m^2/s, which is much lower than in OPC binders (1.4×10^{-13} m^2/s).

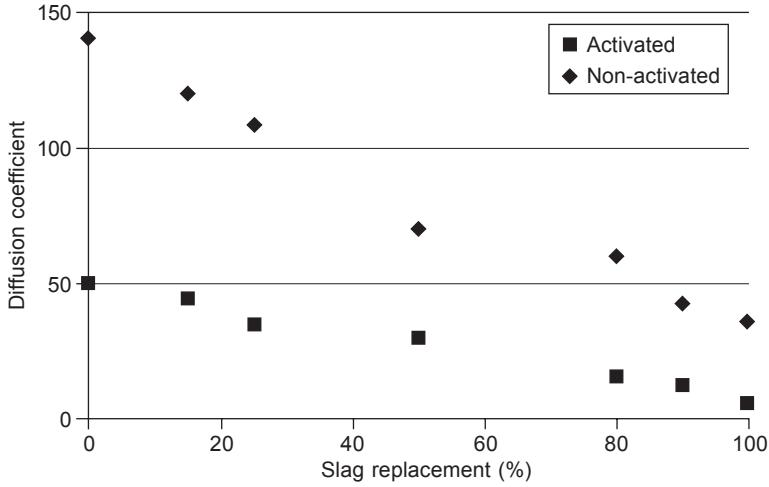

Figure 9.20 Effective diffusion coefficient (10^{-15} m^2/s) of pastes plotted as a function of the content of slag additive to OPC with and without alkali activation. The data are from Roy *et al*. (2000).

9.5 Conclusions and future trends

The compositions (solid materials and activator type) and curing conditions (temperature, humidity and duration) of alkali-activated binders have been shown to have significant impacts on their pore structure, and consequently their permeability. In general, for the same solid materials, binders formed by alkali silicate solution activation have much more compact microstructure than those by alkali hydroxide activation. This is because of the condensation effects of soluble silicate. When activated with sodium silicate solutions, AAM and AAS binders usually display smaller pore size distribution and lower porosities than AAFA binders and cement binders. These pore structure features endow AAM and AAS binders with lower permeability, lower capillary water absorption and lower chloride diffusion coefficient/rate than AAFA binders and Portland cement binders.

In future research into alkali-activated binders, the particle features of fly ashes should be considered as an important aspect. This is not only because of the chemical nature of fly ashes which vary from power station to power station, but also because their packing densities can be significantly different. This means that the activator requirement will be different if the ash source changes, and the pore structure and permeability of binders will be changed. Future research and development of alkali-activated binders should pay more attention to understanding the relationship between pore structure and durability of their concretes. The aggregates have significant impacts on the microstructure of concretes, particularly at the interface between aggregate particles and binder. Alkali-activated concretes may have substantially different permeability and liquid adsorption and diffusion behaviour than binders. This is a key issue for wide application of alkali-activated concretes.

References

Adam AA. Strength and durability properties of alkali activated slag and fly ash-based geopolymer concrete. PhD thesis. RMIT University, 2009.

Aydın S and Baradan B. Effect of activator type and content on properties of alkali-activated slag mortars. *Composites: B* 2014; 57: 166–172.

Backe KR, Lile OB, Lyomov SK, Elvebakk H and Skalle P. Characterising curing cement slurries by permeability, tensile strength and shrinkage, *SPE Drill Completion* 1999; 14: 162–167.

Ben Haha M, Le Saout G, Winnefeld F and Lothenbach B. Influence of activator type on hydration kinetics, hydrate assemblage and microstructural development of alkali activated blast-furnace slags. *Cem Concr Res* 2011a; 41: 301–310.

Ben Haha M, Lothenbach B, Le Saout G and Winnefeld F. Influence of slag chemistry on the hydration of alkali-activated blast-furnace slag – Part I: Effect of MgO. *Cem Concr Res* 2011b; 41: 955–963.

Bernal SA, Mejía de Gutiérrez R, Pedraza AL, Provis JL, Rodriguez ED and Delvasto S. Effect of binder content on the performance of alkali-activated slag concretes. *Cem Concr Res* 2011; 41: 1–8.

Bernal SA, Bílek V, Criado M, Fernández-Jiménez A, Kavalerova E, Krivenko PV, Palacios M, Palomo A, Provis JL, Puertas F, San Nicolas R, Shi C and Winnefeld F. Durability and testing - Degradation via mass transport, in *Alkali-Activated Materials: State-of-the-Art Report*, RILEM TC 224-AAM, Provis JL and van Deventer JSJ (eds), 2014, Springer/RILEM, Dordrecht, pp. 223–276.

Brough AR and Atkinson A. Sodium silicate-based, alkali-activated slag mortars Part I. Strength, hydration and microstructure. *Cem Concr Res* 2002; 32: 865–879.

Chandrasekhar S and Pramada PN. Microwave assisted synthesis of zeolite A from metakaolin. *Microporous Mesoporous Mater* 2008; 108; 152–161.

Chi M and Huang R. Binding mechanism and properties of alkali-activated fly ash/slag mortars. *Constr Build Mater* 2013; 40: 291–298.

Chindaprasirt P, Rattanasak U and Jaturapitakkul C. Utilization of fly ash blends from pulverized coal and fluidized bed combustions in geopolymeric materials. *Cem Concr Comp* 2011; 33: 55–60.

Collins F and Sanjayan JJ. Microcracking and strength development of alkali activated slag concrete. *Cem Concr Comp* 2001; 23: 345–352.

Criado M, Fernández Jiménez A, Sobrados I, Palomo A and Sanz J. Effect of relative humidity on the reaction products of alkali activated fly ash. *J Eur Ceram Soc* 2012; 32: 2799–2807.

Diaz-Loya EI, Allouche EN and Vaidya S. Mechanical properties of fly-ash-based geopolymer concrete. *ACI Mater J* 2011; 108: 300–306.

Duxson P, Provis JL, Lukey GC, Mallicoat S, Kriven WM and van Deventer JSJ. Understanding the relationship between geopolymer composition microstructure and mechanical properties. *Colloids Surf A* 2005; 269: 47–58.

Ershadi V, Ebadi T, Rabani AR, Ershadi L, Soltanian H. Reduction of set cement permeability in oil well to decrease the pollution of receptive environment using spherical nanosilica. In *2nd International Conference on Environmental Science and Technology, IPCBEE*, vol. 6. IACSIT Press, Singapore, 2011, pp. V1–101–104.

Fernández-Jiménez A and Palomo A. Composition and microstructure of alkali activated fly ash binder: effect of the activator. *Cem Concr Res* 2005; 35: 1984–1992.

Fernández-Jiménez A, de la Torre AG, Palomo A, López–Olmo G, Alonso MM and Arand MAG. Quantitative determination of phases in the alkaline activation of fly ash. Part II: Degree of reaction. *Fuel* 2006; 85: 1960–1969.

Goode JM. Gas and water permeability data for some common oilwell cements. *J Petrol Tech* 1962; 14: 851–854.

Gruskovnjak A, Lothenbach B, Holzer L, Figi R and Winnefeld F. Hydration of alkali-activated slag: comparison with ordinary Portland cement. *Adv Cem Res* 2006; 18: 119–128.

Ismail I, Bernal SA, Provis JL, San Nicolas R, Brice DG, Kilcullen AR, Hamdan S and Van Deventer JSJ. Influence of fly ash on the water and chloride permeability of alkali-activated slag mortars and concretes. *Constr Build Mater* 2013; 48: 1187–1201.

Kamseu E, Ceron B, Bignozzi MC, Tobias H, Muscio A, Leonelli E and Libbra A. Insulating behavior of metakaolin-based geopolymer materials assess with heat flux meter and laser flash techniques. *J Therm Anal Calorim* 2012; 108: 1189–1199.

Komljenović M, Baščarević Z and Bradić V. Mechanical and microstructural properties of alkali-activated fly ash geopolymers. *J Hazard Mater* 2010; 181: 35–42.

Lecomte I, Henrist C, Liégeois M, Maseri F, Rulmont A and Cloots R. (Micro)-structural comparison between geopolymers, alkali-activated slag cement and Portland cement. *J Eur Ceram Soc* 2006; 26: 3789–3797.

Lloyd RR. Accelerated ageing of geopolymers. In Provis JL and Van Deventer JSJ (eds), *Geopolymers: Structure, Processing, Properties and Industrial Applications*. Woodhead Publishing Limited, Cambridge, 2009, 139–166.

Ma Y, Hua J and Ye G. The pore structure and permeability of alkali activated fly ash. *Fuel* 2013; 104: 771–780.

McLellan BC, Williams RP, Lay J, Van Riessen A and Corder GD. Costs and carbon emissions for geopolymer pastes in comparison to ordinary Portland cement. *J Clean Prod* 2011; 19: 1080–1090.

Melo Neto AA, Cincotto MA and Repette W. Drying and autogenous shrinkage of pastes and mortars with activated slag cement. *Cem Concr Res* 2008; 38: 565–574.

Nasvi MCM, Ranjith PG and Sanjayan J. Effect of different mix compositions on apparent carbon dioxide (CO_2) permeability of geopolymer: suitability as well cement for CO_2 sequestration wells. *Appl Energy* 2014; 114: 939–948.

Okada K, Ooyama A, Isobe T, Kameshima Y, Nakajima A and MacKenzie KJD. Water retention properties of porous geopolymers for use in cooling applications. *J Eur Ceram Soc* 2009; 29: 1917–1923.

Pacheco-Torgal F, Moura D, Ding Y and Jalali S. Composition, strength and workability of alkali–activated metakaolin based mortars. *Constr Build Mater* 2011; 25: 3732–3745.

Palacios M and Puertas F. Effect of shrinkage-reducing admixtures on the properties of alkali-activated slag mortars and pastes. *Cem Concr Res* 2007; 37: 691–702.

Palomo A, Grutzeck MW and Blanco MT. Alkali-activated fly ashes: a cement for the future. *Cem Concr Res* 1999; 29: 1323–1629.

Provis JL, Duxson P and van Deventer JSJ. The role of particle technology in developing sustainable construction materials. *Adv Powder Technol* 2010; 21: 2–7.

Puertas F, Fernández-Jiménez A and Blanco-Varela MT. Pore solution in alkali-activated slag cement pastes: relation to the composition and structure of calcium silicate hydrate. *Cem Concr Res* 2004; 34: 139–148.

Puertas F, Palacios M and Vázquez T. Carbonation process of alkali-activated slag mortars. *J Mater Sci* 2006; 41: 3071–3082.

Rattanasak U, Pankhet K and Chindaprasirt P. Effect of chemical admixtures on properties of high-calcium fly ash geopolymer. *Intl J Miner Metal Mater* 2011; 18: 364–369.

Ravikumar D and Neithalath N. An electrical impedance investigation into the chloride ion transport resistance of alkali silicate powder activated slag concretes. *Cem Concr Comp* 2013; 44: 58–68.

Rovnaník P. Effect of curing temperature on the development of hard structure of metakaolin-based geopolymer. *Constr Build Mater* 2010; 24: 1176–1183.

Roy DM, Jiang W and Silsbee MR. Chloride diffusion in ordinary, blended, and alkali-activated cement pastes and its relation to other properties. *Cem Concr Res* 2000; 30: 1879–1884.

Sakulich AR. Characterization of environmentally-friendly alkali activated slag cements and ancient building materials. PhD thesis, Drexel University, 2009.

Shi C. Strength, pore structure and permeability of alkali-activated slag mortars. *Cem Concr Res* 1996, 26: 1789–1799.

Shi C, Krivenko PV and Roy D. *Alkali-Activated Cements and Concretes*. Taylor & Francis, New York, 2006.

Wongpa J, Kiattikomol K, Jaturapitakkul C and Chindaprasirt P, Compressive strength, modulus of elasticity, and water permeability of inorganic polymer concrete. *Mater Des* 2010; 31: 4748–4754.

Yip CK, Lukey GC and van Deventer JSJ. The coexistence of geopolymeric gel and calcium silicate hydrate at the early stage of alkaline activation. *Cem Concr Res* 2005; 35: 1688–1697.

Zhang L. The development of oil well cement slurries with high resistant properties of CO_2. Masters Thesis, Nanjing University of Technology, 2010 (in Chinese with English abstract).

Zhang Z, Yao X and Zhu H. Factors affecting strength of geopolymer predicted by back propagation neural network. *Bull Chinese Ceram Soc* 2008, 27: 640–645 (in Chinese with English abstract).

Zhang Z, Yao X and Zhu H. Activating process of geopolymer source material: kaolinite. *J Wuhan Uni Tech – Mater Sci* 2009a; 24: 132–136.

Zhang Z, Yao X, Zhu H and Chen Y. Role of water in the synthesis of calcined kaolin-based geopolymer. *Appl Clay Sci* 2009b; 43: 218–223.

Zhang Z, Yao X, Zhu H. Potential application of geopolymers as protection coatings for marine concrete II. Microstructure and anticorrosion mechanism. *Appl Clay Sci* 2010a; 49: 7–12.

Zhang Z, Yao X and Zhu H. Potential application of geopolymers as protection coatings for marine concrete I. Basic properties. *Appl Clay Sci* 2010b; 49: 1–6.

Zhang Z, Wang H and Provis JL. Quantitative study of the reactivity of fly ash in geopolymerization by FTIR. *J Sustain Cem-Based Mater* 2012a; 1: 154–166.

Zhang Z, Wang H, Provis JL, Bullen F, Reid A and Zhu Y. Quantitative kinetic and structural analysis of geopolymers. Part 1. The activation of metakaolin with sodium hydroxide. *Thermochim Acta* 2012b; 539: 23–33.

Zhang Z, Wang H, Provis JL, Bullen F and Reid A. Quantitative kinetic and structural analysis of geopolymers. Part 2. Thermodynamics of sodium silicate activation of metakaolin. *Thermochim Acta* 2013, 565: 163–171.

Živica V, Balkovic S and Drabik M. Properties of metakaolin geopolymer hardened paste prepared by high-pressure compaction. *Constr Build Mater* 2011; 25: 2206–2213.

Assessing the shrinkage and creep of alkali-activated concrete binders

10

S. E. Wallah[1], *D. Hardjito*[2]
[1]Sam Ratulangi University, Manado, Indonesia; [2]Petra Christian University, Surabaya, Indonesia

10.1 Introduction

Depending on the type of concrete structures, the effect of creep varies, but it is usually related to strain and deflection or stress redistribution. Creep can lead to excessive deflection of structural members and cause other serviceability problems, especially in high-rise buildings and long bridges. The other well-known effect of creep is that it causes loss of prestress. However, the presence of creep to some extent is also beneficial, because it could reduce the internal stress concentration induced by shrinkage, temperature changes or movement of supports (Gilbert, 1988; Neville, 2000).

Similarly, shrinkage is also a concern in concrete structures, since it is probably the most common cause of cracking. Shrinkage also causes axial deformation and warping which could lead to significant deflection; while the shrinkage induces tension, and resulting cracks, if not controlled, can lead to serviceability, durability and even shear strength failure (Gilbert, 1988; Rusch *et al*., 1983).

Although very important, topics of shrinkage and creep of concrete are considered unattractive to study, especially due to their dependence on time which requires long-term observational studies. This chapter elaborates the shrinkage and creep properties of Class F fly ash-based alkali-activated concrete, which are measured for a period of 1 year, the factors affecting them and methods to predict their values.

10.2 Shrinkage and creep in concrete

Creep is time-dependent increase in strain of hardened concrete under sustained stress. Under normal loading conditions, the instantaneous strain at the application of load includes not only the elastic strain but also some creep. However, normally creep is simply taken as the increase in strain above the initial elastic strain (Neville, 2000). In a loaded condition, a specimen also undergoes shrinkage as it dries, therefore this fact should be accounted for in calculating the actual creep. For practical simplification, creep might be calculated as the difference between

Handbook of Alkali-activated Cements, Mortars and Concretes. http://dx.doi.org/10.1533/9781782422884.2.265

total time deformation and shrinkage of a similar unloaded specimen stored under the same conditions through the same period. However, it should be noted that actually shrinkage and creep are not independent phenomena to which the principle of superposition can be applied.

Under constant temperature, the total strain at any time t may be expressed as the sum of the instantaneous, creep and shrinkage strain (Gilbert, 1988) as in Eq. (10.1).

$$\varepsilon\ (t) = \varepsilon_{e}\ (t) + \varepsilon_{c}\ (t) + \varepsilon_{sh}\ (t) \tag{10.1}$$

In a loaded specimen in equilibrium in which there is no moisture movement to or from the ambient medium, the time-dependent deformation is known as basic creep and the additional creep caused by drying is known as drying creep.

As illustrated in Figure 10.1, creep increases with time at a decreasing rate. The increase in creep is usually very rapid immediately after the load is applied. The rate of increase is decreasing significantly after several months and will be much smaller over longer periods. Creep continues for a very long time and the data of probably the longest period of measurement to date as reported by Troxell *et al.* (1958), show values for 10 years, 20 years and 30 years of respectively 1.26, 1.33 and 1.36 times the value of 1 year creep. Although concrete might continue to creep, it is usually assumed that creep is approaching a limiting value as the time after loading approaches infinity.

Many theories have been proposed to explain the origin and mechanism of creep in concrete as discussed extensively by Neville *et al.* (1983) and Bazant and Wittmann (1982). However, it seems that there is no single theory that could account for all the observed facts and phenomena of creep in concrete. It is generally agreed, however, that there are some main mechanisms which describe creep such as viscous flow of the cement paste, consolidation due to seepage or decomposition of interlayer hydrate water, delayed elasticity formed by the aggregates and gel crystals and local fracture (micro cracking and crystal failure) as well as recrystallisation and formation of new physical bonds (Gilbert, 1988; Neville *et al.*, 1983).

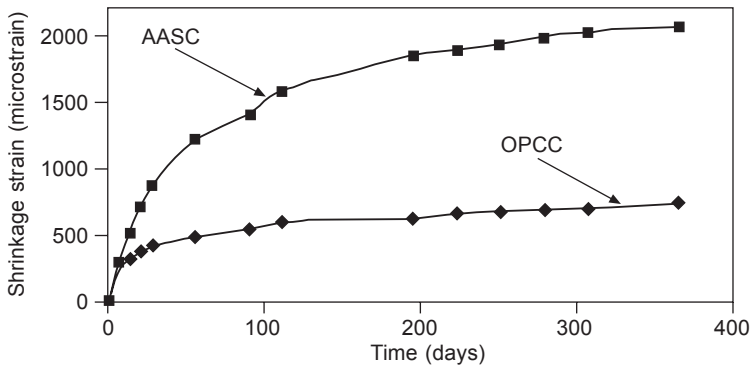

Figure 10.1 Drying shrinkage of OPC concrete (OPCC) as compared to AAS concrete (AASC) (reprinted from Collins and Sanjayan, 2000, Copyright © 2000, with permission from Elsevier).

There are many factors affecting the magnitude of creep and its rate of development. Bazant (1982) divided those factors into intrinsic factors and extensive factors. The intrinsic factors are related to material characteristics which are fixed after the concrete is cast, such as the design strength, the elastic modulus of aggregate, the fraction of aggregate in the concrete mix and the maximum aggregate size. The extensive factors which can vary after the casting include temperature, pore water content, age at loading, etc. Many studies are available such as those discussed by Neville *et al*. (1983) and Neville (2000). Gilbert (1988) summarised some important factors that influence the creep of concrete. High strength concrete creeps less than normal strength concrete. The same is true for concrete with higher aggregate content and larger maximum size of aggregate. Creep is also influenced by the factors that directly affect the concrete strength such as water–cement ratio and the cement type. The age of concrete at first loading affects the creep as the creep decreases for older concrete at first loading. Other factors are the humidity and temperature of the environment, in which the creep increases with the decrease in humidity or the increase in temperature. However, the effect of temperature is more significant at higher or elevated temperature. Another important factor affecting creep is the stress level. For the sustained stress of less than 50% of the compressive strength of concrete, the creep strain is approximately proportional to the stress level which is known as linear creep. The rate of increase in creep is faster at higher stress levels and becomes non-linear to stress.

The capacity of concrete to creep is usually expressed as the creep coefficient which is the ratio of creep strain at time t to instantaneous elastic strain in a specimen subjected to sustained stress as in Eq. (10.2):

$$\varphi(t) = \frac{\varepsilon_c(t)}{\varepsilon_e} \tag{10.2}$$

Another frequently used expression of creep is the proportionality factor relating stress to linear creep known as specific creep, $C(t)$, which is the creep strain at time t produced by a sustained unit stress, as shown in Eq. (10.3):

$$C(t) = \frac{\varepsilon_c(t)}{\sigma} \tag{10.3}$$

Shrinkage is the decrease in volume of concrete with time. Unlike creep, shrinkage is independent of the external actions to the concrete, as illustrated in Figure 10.1. There are various types of shrinkage in the concrete which should be distinguished. Gilbert (2002) divided the shrinkage into plastic shrinkage, chemical shrinkage, thermal shrinkage and drying shrinkage.

Plastic shrinkage occurs in wet concrete or when the concrete is still in plastic state due to loss of water by evaporation or suction by the underlying concrete or soil. This could lead to significant cracking during setting. The magnitude of plastic shrinkage is affected by temperature, ambient relative humidity and wind velocity (Neville, 2000). Plastic shrinkage also depends on the cement content of the mix and the water-to-cement ratio; it is greater for greater cement content and low water-to-cement ratio.

Chemical shrinkage is caused by various chemical reactions within the cement paste, including the hydration shrinkage. Thermal shrinkage is related to the liberation of the heat of hydration as Portland cement reacts with water.

Drying shrinkage is the reduction in volume which is primarily caused by the loss of water during the drying process. Drying shrinkage normally accounts for the biggest proportion of the total long-term shrinkage. Factors which affect the drying of concrete also affect the magnitude and rate of development of drying shrinkage. These factors include the type and content of cement or binder, water content and water-to-cement ratio, type of aggregates, maximum size and its proportion in the concrete, relative humidity and the size and shape of the member.

The aggregates play a significant role in affecting the shrinkage of concrete (de Larrard *et al.*, 1994; Neville, 2000). This is related to the restraining effect of the aggregate on shrinkage. The higher aggregate content results in smaller shrinkage and also concrete with aggregates of higher modulus or rougher surfaces is more resistance to the shrinkage process.

The higher water-to-cement ratio normally results in higher shrinkage due to interrelated effects. As the water/cement ratio increases, paste strength and stiffness decrease and as the water content increases, shrinkage potential increases because it also reduces the volume of restraining aggregates.

The relative humidity affects the magnitude of shrinkage as the rate of shrinkage is lower at higher values of relative humidity. The rate and magnitude of shrinkage decrease with an increase in the volume of concrete member, but the duration of shrinkage is longer for large members since more time is needed for shrinkage effects to reach the interior regions (de Larrard *et al.*, 1994).

The shrinkage strain of concrete, which is usually considered to be the sum of drying, chemical and thermal shrinkage components, continues to increase with time at a decreasing rate (Gilbert, 2002). And as for creep, shrinkage is also assumed to approach a final value as time approaches infinity.

10.3 Shrinkage in alkali-activated concrete

There are only few studies that have been reported related to shrinkage of alkali-activated concrete including geopolymer concrete. More studies have been conducted related to shrinkage of mortar and paste especially for alkali-activated slag. Therefore the following discussion will focus more on the studies of alkali-activated slag and fly ash-based geopolymer concrete.

Among the prime or source materials used for alkali-activated binders, slag is considered as a source material that has been used since the early development of this binder. Numerous studies have also been reported related to the development of alkali-activated slag binders. However, besides its certain properties which are superior to ordinary Portland concent (OPC), one of its drawbacks is that it has relatively much higher shrinkage compared to OPC. Several studies on alkali-activated slag (AAS) concrete such as reported by Collins and Sanjayan (1999a) confirm that fact.

Drying shrinkage of AAS concrete is about twice as much as that for OPC concrete and the difference tends to be higher as the age of concrete increases. This has also been observed previously by Douglas *et al*. (1992). Further studies by Collins and Sanjayan (2000) revealed that the high shrinkage of AAS concrete compared to OPC concrete (Figure 10.1) could be attributed to the pore size distribution rather than the amount of moisture loss, where it was observed in AAS paste that it has a much higher proportion of pore sizes (82%) within the mesopore region compared to OPC pastes (36.4%).

Another study by Collins and Sanjayan (1999b) found that the use of fully saturated blast furnace slag coarse aggregate to substitute the normal weight coarse aggregate could substantially improve the drying shrinkage of AAS concrete.

More studies on shrinkage of alkali-activated slag have been conducted, especially in paste or mortar states. Those studies tried to develop an understanding of the mechanism of shrinkage and to find or relate the effects of certain parameters that could influence the shrinkage as well as other properties of AAS. Those efforts also include finding the best way to reduce the shrinkage of AAS while retaining the other superior properties. The parameters studied include the types, dosage and combination of activators, the use of admixtures and additives, the types of aggregate and types of curing. The influence of some parameters on the shrinkage of AAS will be discussed in Section 10.5.

Extensive studies have been conducted by a research group at Curtin University of Technology, Australia, to develop fly ash-based geopolymer concrete and the results have been published and reported (Hardjito, *et al*., 2002, 2004a, 2004b, 2005; Hardjito and Rangan, 2005; Wallah *et al*., 2004, 2005; Wallah and Rangan, 2006; Sumajouw *et al*., 2005, 2007; Rangan *et al*., 2005, 2006). The results of those studies show that drying shrinkage of fly ash-based geopolymer concrete cured at elevated temperature is very low (Wallah and Rangan, 2006; Wallah, 2009). For up to one year measurement, the maximum shrinkage strain is only around 100 microstrain. However, the drying shrinkage for that cured at ambient condition is very much higher. This concrete was made using Class F fly ash as the source or prime material and alkaline solution consisting of the combination of sodium hydroxide and sodium silicate solution, while the aggregates used were the coarse and fine aggregates normally used for OPC concrete in the concrete industry.

The drying shrinkage was determined based on the standard test already developed for OPC concrete. In this case, Australian Standard, AS 1012.13 (1992), *Methods of testing concrete – Determination of the drying shrinkage of concrete for samples prepared in the field or in the laboratory* (Standards Australia 1992), was used.

Test specimens for the drying shrinkage test were 75 × 75 × 285 mm prisms with the gauge studs as shown in Figure 10.2. Three specimens were prepared for each type of test. In addition, for each type of test, four 100 × 200 mm cylindrical specimens were also prepared for compressive strength testing.

The shrinkage strain measurements started on the third day after casting the concrete. On the third day after casting, the specimens were demoulded and the first measurement was taken. Horizontal length comparator (Figure 10.3) was used for length measurements. The next measurement was taken on the fourth day of casting,

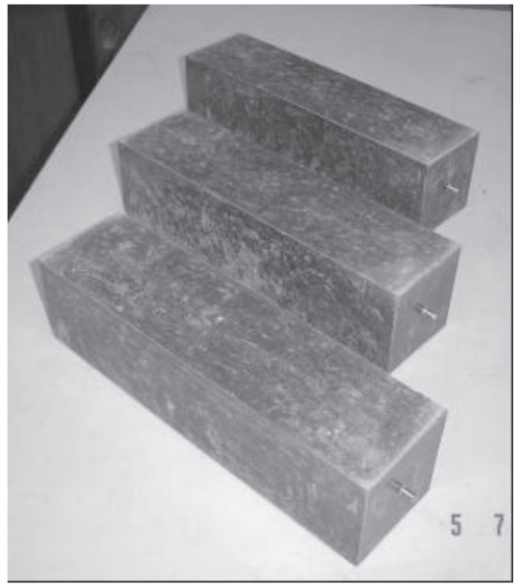

Figure 10.2 Specimens for drying shrinkage test.

Figure 10.3 Horizontal length comparator with a specimen.

considered as Day 1 for the drying shrinkage measurements. The measurements then continued every day in the first week, once a week until the fourth week, once in two weeks until the twelfth week, and then once in four weeks until one year.

During the drying shrinkage tests, the specimens were kept in a laboratory room where the temperature was maintained at approximately 23°C. The relative humidity of the room varied between 40% and 60%.

As stated previously, the drying shrinkage measurements commenced on the third day after casting. Therefore, the age 'zero' in the drying shrinkage strain versus age in days plots shown in the following figures represents three days after casting when the initial measurements were taken. The drying shrinkage shown in the following figures represents fly ash-based geopolymer concrete from two types of mixtures

(mixture-1 and mixture-2) in which mixture-1 resulted in higher strength compared to mixture-2. Two types of heat-curing, namely dry curing and steam curing, were applied at 60°C for 24 h. On the seventh day, compressive strengths of the mixtures ranged from 41 to 65 MPa.

Figures 10.4 and 10.5 show the plots of drying shrinkage strain versus age in days for the heat-cured test specimens. It can be seen from these figures that heat-cured fly ash-based geopolymer concrete undergoes very low drying shrinkage. For all test specimens, the final value of drying shrinkage strain after a period of one year was only around 100 microstrain.

The test data plotted in Figures 10.4 and 10.5 show that the drying shrinkage strains fluctuated slightly over the period of measurement. This could be attributed to the moisture movement from the environment to the concrete or vice versa, which causes reversible shrinkage or swelling of the concrete. Also, there were some minor differences in the measured values of drying shrinkage strains between

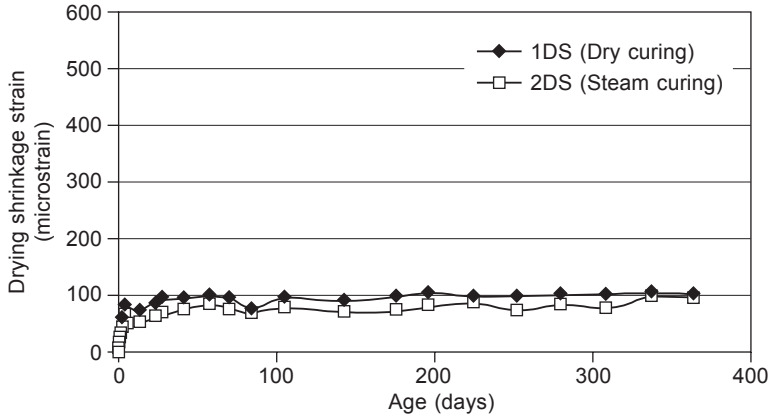

Figure 10.4 Drying shrinkage of heat-cured mixture-1 specimens.

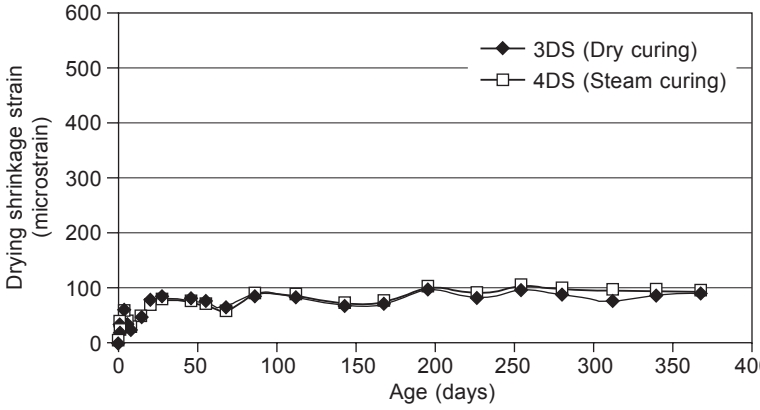

Figure 10.5 Drying shrinkage of heat-cured mixture-2 specimens.

dry- and steam-cured specimens. However, these variations are considered to be insignificant in the context of the very low drying shrinkage experienced by the heat-cured geopolymer concrete specimens.

Water is released during the chemical reaction process of geopolymers (Davidovits, 1999; Hardjito and Rangan, 2005) and in heat-cured fly ash-based geopolymer concrete, most of the water released during the chemical reaction may evaporate during the curing process. Because the remaining water contained in the micropores of the hardened concrete is small, the induced drying shrinkage is also very low. In addition, as for the creep (discussed in the next section), the presence of the 'micro-aggregates' in fly ash-based geopolymer concrete may also increase the restraining effect of the aggregates on drying shrinkage.

Conversely, fly ash-based geopolymer concrete cured at ambient condition experienced very much higher drying shrinkage compared to those cured at elevated temperature conditions. Figure 10.6 shows a comparison between drying shrinkage measurements up to 90 days of specimens made from the same mixture but experienced a different curing, ambient curing and heat curing at 60°C for 24 h. On the seventh day compressive strength of the specimens was 27 MPa for ambient-cured specimens and 61 MPa for heat cured specimens.

It can be seen that the drying shrinkage strains of the specimens cured in ambient conditions are manyfold larger than those experienced by the heat-cured specimens. As noted earlier, water is released during the chemical reaction process of geopolymers. In the specimens cured in ambient conditions, this water may evaporate over a period of time causing significantly large drying shrinkage strains, especially in the first two weeks as can be seen in Figure 10.6.

A study conducted by Lee (2007) reported the creep and shrinkage of inorganic polymer concrete (IPC). This concrete utilised materials similar to those for developing fly ash-based geopolymer concrete. Class C fly ash and Class F fly ash were used separately as precursor materials. Sodium silicate and sodium hydroxide and/or potassium hydroxide solution were used to activate this IPC. The aggregates used

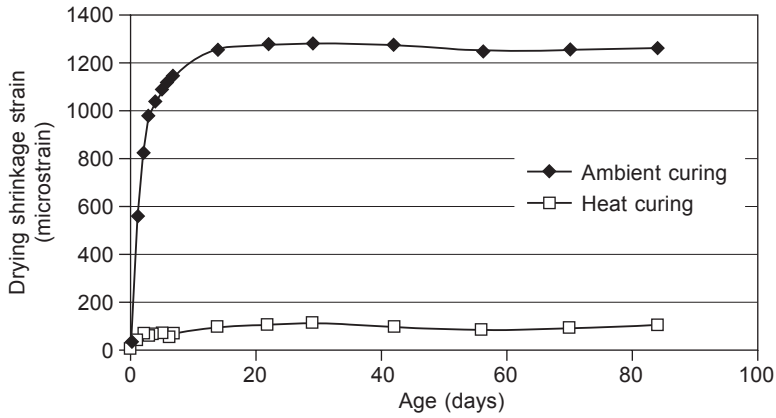

Figure 10.6 Drying shrinkage of heat-cured and ambient-cured specimens.

were aggregates commonly used in the concrete industry. The specimens were only cured at ambient conditions and sealed with plastic bag after demoulding and left in a plastic container at a temperature of around 21°C.

By following the procedures of determining drying shrinkage as in Australian Standard, AS 1012.13 (Standards Australia, 1992), and the seventh day after casing is considered as 'zero' reading, after 56 days it was obtained that the IPC utilising Class C fly ash has the lowest mean shrinkage strain (520 microstrain) which is lower than the control OPC specimens (820 microstrain), whereas the mean shrinkage strain for IPC utilising Class F fly ash varies from 550, 720 and 920 microstrain for concrete mixtures with nominal compressive strength of 20 MPa, 60 MPa and 45 MPa, respectively.

It is important to note that the study also reported that IPC may have a very high early age shrinkage potential and rate of shrinking in the first one or two days after casting. For that measurement, a newly developed method called image analysis was used. Although that method is not yet standard and the results still need to be confirmed or calibrated, the early age shrinkage should be a concern since it cannot be detected with the standard method such as AS 1012.13 (Standards Australia, 1992). That result is also in accordance with that reported by Neto *et al.* (2008) from the study of drying and autogenous shrinkage of pastes and mortars with activated slag cement (ASC). It was found that the bigger proportion of drying and autogenous shrinkage mostly occurs during the first three-day period after casting.

10.4 Creep in alkali-activated concrete

Among the properties of alkali-activated concrete including geopolymer concrete, creep is one property that is rarely studied or explored. Therefore very little information has been reported or published in that area. However, this does not imply that this property is not important, because creep is a very important property of concrete, especially as a structural material. Studies by the author (Wallah *et al.*, 2005; Wallah and Rangan, 2006; Wallah, 2010) give more information about creep behaviour of fly ash-based geopolymer concrete.

The creep behaviour of fly ash-based geopolymer concrete was studied for concrete incorporating Class F fly ash as source material. Like the study of drying shrinkage discussed in the previous section, the alkaline solution was a combination of sodium hydroxide and sodium silicate and the aggregates were those usually used in the concrete industry. Creep strains were measured for two geopolymer concrete mixtures, Mixture-1 and Mixture-2. Two types of curing, namely, dry curing and steam curing, were used.

Test specimens for the creep test were 150 × 300 mm cylinders as shown in Figure 10.7. Eight cylinder specimens were prepared for each test; three cylinders were for measuring the creep, two companion cylinders for measuring the drying shrinkage and the other three cylinders for the compressive strength test.

The creep tests were performed in accordance with the Australian Standard, AS

Figure 10.7 Creep test specimens.

1012.16-1996, *Methods of testing concrete – Determination of creep of concrete cylinders in compression* (Standards Australia, 1996). The sustained load was applied on the seventh day after casting of the specimens. The specimens were loaded at an early age of 7 days, and the sustained stress was taken as 40% of the mean compressive strength.

For strain measurement, demec gauge points were attached to the creep specimens and the companion shrinkage specimens as shown in Figure 10.8.

Before the creep specimens were loaded, the seventh day compressive strength of geopolymer concrete was determined by testing the three cylinders reserved for the compressive strength test. The creep specimens were applied with a load corresponding to 40% of the measured mean compressive strength of concrete. This load was maintained as the sustained load throughout the duration of the test. The strain values were measured and recorded immediately before and after the loading. Strains suffered by the control shrinkage specimens were measured at the same time

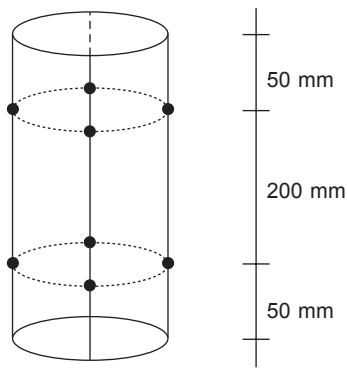

Figure 10.8 Location of demec gauge points on test cylinders.

as the strain measurements on creep specimens. The strain values were measured and recorded at 2 hours, 6 hours and then every day for the first week, after loading. The measurements then continued once a week until the fourth week. After that, the measurements were done once in two weeks until the twelfth week and then once every four weeks until one year.

The creep tests were conducted in a laboratory room where the temperature was maintained at about 23°C, and the relative humidity varied between 40% and 60% during the test. The compressive strength of the specimens ranged from 40–67 MPa while the sustained stresses were 16 to 27 MPa.

Table 10.1 gives the sustained stress and the instantaneous strain measured immediately after the application of the sustained load. Using these data, the instantaneous elastic modulus was calculated as sustained stress/instantaneous strain. The values of instantaneous elastic modulus, given in Table 10.1 are similar to those reported by Hardjito and Rangan (2005) and Hardjito *et al*. (2004b).

Figures 10.9–10.12 present the total strain and the drying shrinkage strain measured for a period of 52 weeks (one year). The total strain was measured on the specimens in the creep test rig, while the drying shrinkage strain was obtained from the companion unloaded specimens left in the vicinity of the creep specimens.

Table 10.1 Instantaneous strain and instantaneous elastic modulus

Test designation	Sustained stress (MPa)	Instantaneous strain (microstrain)	Instantaneous elastic modulus (MPa)
1CR	27	902	29,574
2CR	23	851	26,852
3CR	19	828	22,913
4CR	16	761	21,144

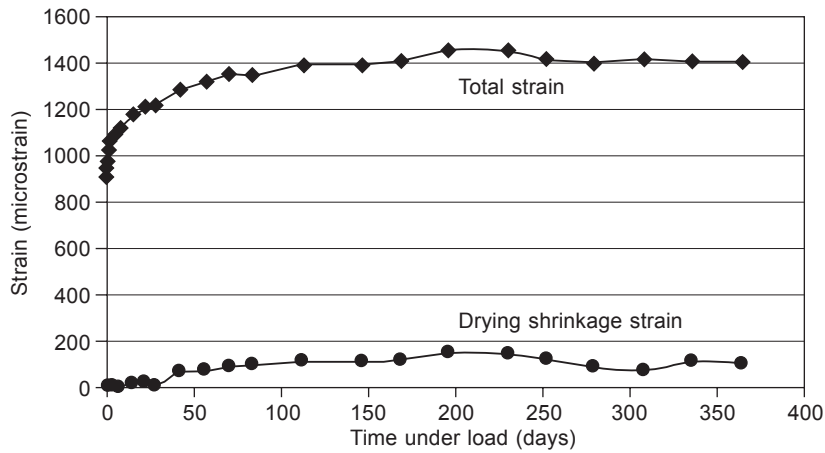

Figure 10.9 Total strain and drying shrinkage strain for 1CR.

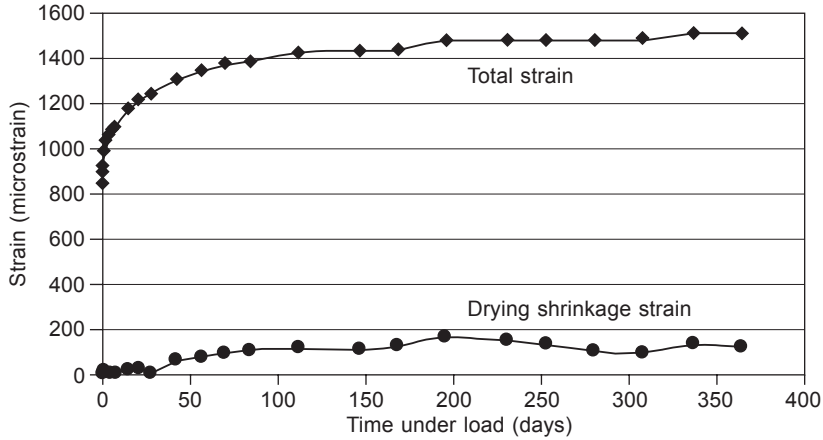

Figure 10.10 Total strain and drying shrinkage strain for 2CR.

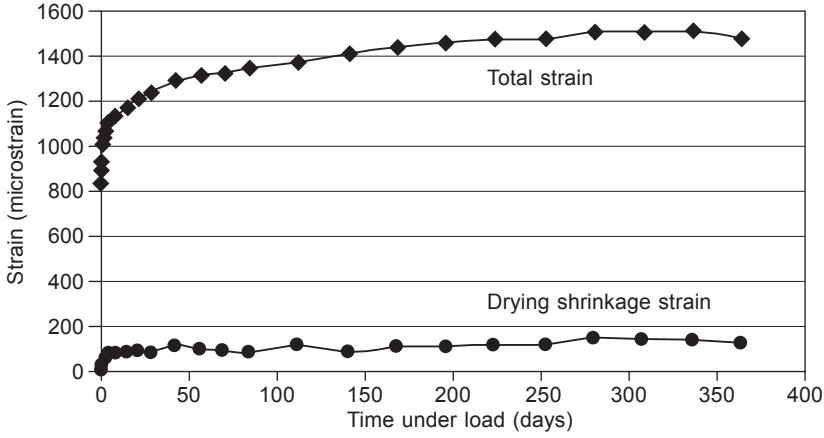

Figure 10.11 Total strain and drying shrinkage strain for 3CR.

Creep strain data were obtained by subtracting the drying shrinkage strain from the total strain. The creep strain including the instantaneous elastic strain data for specimens 1CR, 2CR, 3CR, and 4CR are presented in Figures 10.13–10.16, respectively.

The specific creep, defined as the creep strain per unit stress, data for the test specimens are presented in Figure 10.17.

The test results presented in those figures show that the creep data fluctuated slightly over the period of sustained loading. This might be due to variations in relative humidity of the laboratory room where the creep test rig was housed.

The test results generally indicate that fly ash-based geopolymer undergoes lesser creep than OPC concrete. Warner *et al*. (1998) illustrated that for OPC concrete the specific creep for 60 MPa concrete after one year was about 50–60 microstrain/

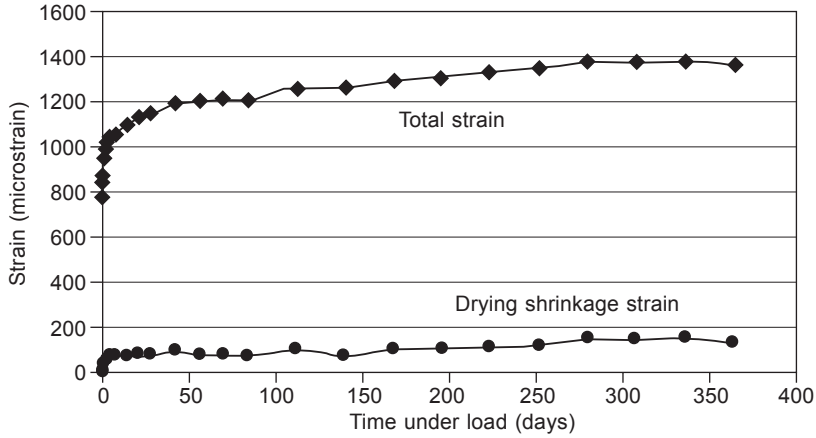

Figure 10.12 Total strain and drying shrinkage strain for 4CR.

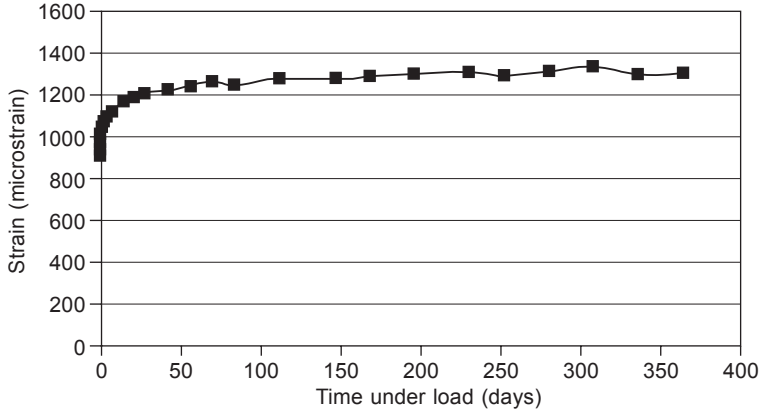

Figure 10.13 Creep strain data for 1CR.

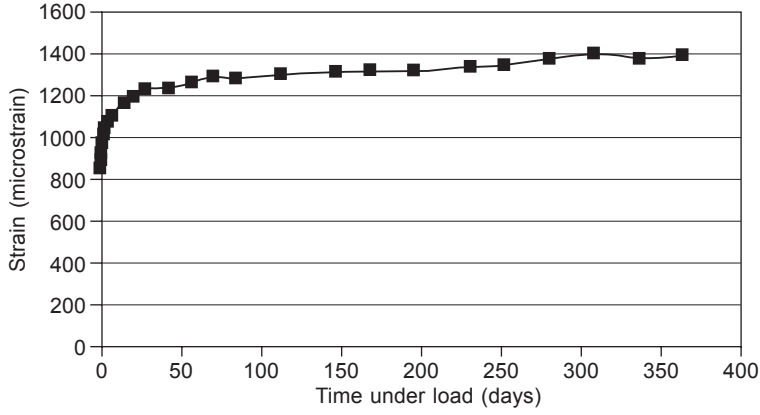

Figure 10.14 Creep strain data for 2CR.

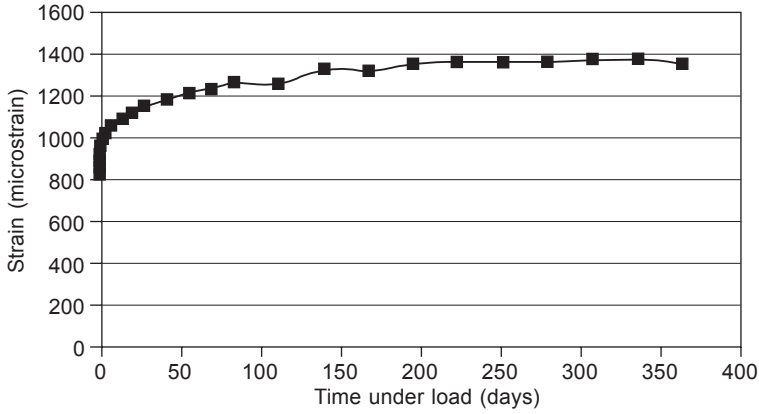

Figure 10.15 Creep strain data for 3CR.

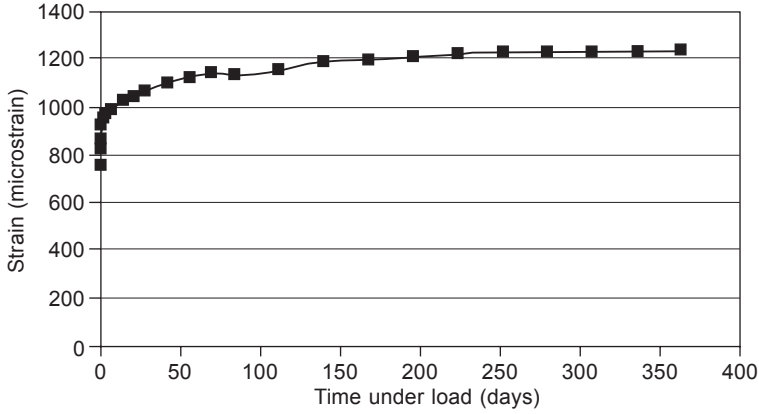

Figure 10.16 Creep strain data for 4CR.

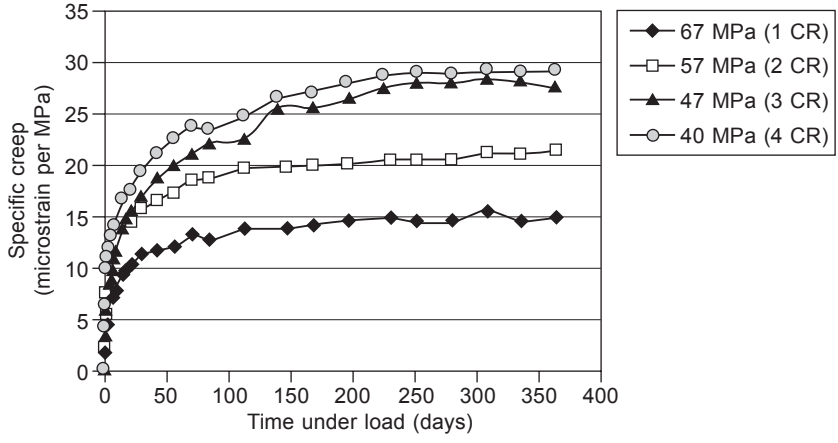

Figure 10.17 Specific creep.

MPa, while this value after six months was about 30–40 microstrain/MPa for 80 MPa concrete and about 20–30 microstrain/MPa for 90 MPa concrete. Similarly, Malhotra and Mehta (2002) reported that the specific creep of high-performance high volume fly ash (HVFA) concrete was about 24–32 microstrain/MPa after one year under loading. Those values are generally larger than the values given in Figure 10.17 for fly ash-based geopolymer concrete.

The effect of concrete compressive strength on the creep of fly ash-based geopolymer concrete is also illustrated in Figure 10.17. The test data show that the specific creep of geopolymer concrete decreased as the compressive strength increased. This test trend is similar to that observed in the case of OPC concrete as reported by Neville *et al*. (1983), Gilbert (1988), Warner *et al*. (1998) and Neville (2000).

The final values of specific creep of geopolymer concrete after one year of loading are summarised in Table 10.2. It can be seen that the final specific creep values differ significantly between geopolymer concretes with compressive strength of 47, 57 and 67 MPa, whereas this value for geopolymer concrete with compressive strength of 40 MPa is almost the same as that of 47 MPa concrete.

The creep strains of fly ash-based geopolymer concrete are generally smaller than that of OPC concrete. The exact reasons for this difference in behaviour are not known. However, it has been suggested by Davidovits (press. comm., 2005) that the smaller creep strains of fly ash-based geopolymer concrete may be due to a 'block-polymerisation' concept. According to this concept, the silicon and aluminium atoms in the fly ash are not entirely dissolved by the alkaline liquid. The 'polymerisation' that takes place only on the surface of the atoms is sufficient to form the 'blocks' necessary to produce the geopolymer binder. Therefore, the insides of the atoms are not destroyed and remain stable, so that they can act as 'micro-aggregates' in the system.

In OPC concrete, the creep is primarily caused by the cement paste. The aggregates are generally an inert component of the mixtures, and function to resist the creep of the cement paste. Therefore, the aggregate content in the concrete is a significant factor influencing the creep of the concrete as the creep will decrease with the increase in the quantity of the aggregates. The proportion of aggregates in the mixtures of fly ash-based geopolymer concrete used in this work is approximately similar to that used in OPC concrete. However, the presence of the 'micro-aggregates' due to the 'block-polymerisation' concept mentioned above gives the effect of increasing the aggregate content in the concrete. In other words, the presence of the 'micro-

Table 10.2 Final specific creep of geopolymer concrete after one-year loading

Designation	Compressive strength (MPa)	Final specific creep after one year loading ($\times 10^{-6}$/MPa)
1CR	67	15
2CR	57	22
3CR	47	28
4CR	40	29

aggregates' increases the creep resisting function of the fly ash-based geopolymer concrete which results in smaller creep compared to OPC concrete without 'micro-aggregates'.

As for shrinkage, Lee (2007) also reported the creep of inorganic polymer concrete (IPC) utilising Class C and Class F fly ash as precursor materials and the combination of sodium silicate and sodium hydroxide and/or potassium hydroxide as alkaline solutions. Each specimen category has two types of treatment, 'exposed' and 'sealed'. The measurements were taken up to 56 days of loading.

The types of treatment really affect the resulting behaviour of the specimens. The elastic response on initial loading shows a significant difference between the exposed and sealed specimens. The instantaneous elastic modulus of the 'exposed' IPC is much lower compared to that of 'sealed' IPC, while the specific creep (per MPa) at 28 days is much lower for 'sealed' specimens. A contrasting result was also shown by the different specimen treatment, in which none of the types of 'sealed' IPC having specific creep (per MPa) higher than that for control OPC concrete, but all types of 'exposed' IPC have higher specific creep compared to control OPC concrete.

Study of the creep behaviour of alkali-activated slag concrete utilising sodium hydroxide in combination with sodium carbonate and sodium silicate in combination with hydrated lime as activators by Collins and Sanjayan (1999a) revealed that OPC concrete has higher initial creep compared to AAS concrete, but after loading for 112 days, AAS concrete shows a slightly higher creep compared to OPC concrete.

10.5 Factors affecting shrinkage and creep

There are lots of parameters or factors affecting the shrinkage and creep of alkali-activated pastes, mortars and concretes and some of them will be discussed in this section.

As discussed in Section 10.3, the type of aggregates used could affect the shrinkage of resulting mortars or concretes. The replacement of normal weight coarse aggregate with fully saturated blast furnace slag coarse aggregate could reduce the drying shrinkage of alkali-activated concrete by about 40% (Collins and Sanjayan, 1999b).

One possible way to improve the properties of alkali-activated concrete is through the use of admixtures and additives. The use of air-entraining agent, water reducing and shrinkage reducing admixtures at proper dosage could significantly reduce the shrinkage of alkali-activated slag concrete (Bakharev *et al*., 2000). The addition of Portland cement or gypsum in certain proportions could also reduce the shrinkage of AAS concrete or mortar as reported by Rashad (2013) and Chang, *et al*. (2005). Use of reactive MgO as an additive to alkali-activated slag could reduce the drying shrinkage, as reported by Jin *et al*. (2014) from their study about the reactive MgO modified AAS (MAAS) pastes. From measurement up to 90 days, it was found that the use of highly reactive MgO considerably reduces the shrinkage, but more cracks

are generated when using highly reactive MgO content of more than 5%. On the other hand, use of medium reactive MgO does not increase the shrinkage at early age up to about one month, but the initial cracks are healed at later ages by hydration.

Curing types or conditions play an important role in the properties of alkali-activated binders including shrinkage (Bilim *et al.*, 2013; Jin *et al.*, 2014). Some other studies also confirm this fact. Heat curing was found to be effective in significantly reducing the drying shrinkage of alkali-activated mortars as shown by Aydin and Baradan (2012) who applied steam curing and autoclave curing to cure the AAS mortars. The effect of using heat curing to drying shrinkage was also observed for fly ash-based geopolymer concrete as has been discussed in Section 10.3. The use of heat curing, either dry curing or steam curing, significantly reduced the drying shrinkage of fly ash-based geopolymer concrete (Wallah and Rangan, 2006).

Higher content of slag in alkali-activated fly ash/slag pastes causes cracks due to autogenous shrinkage (Jang *et al.*, 2014), but internal curing by using pre-wetted lightweight aggregate can reduce or even eliminate autogenous shrinkage in alkali-activated slags through the same mechanism as in OPC, as shown by Sakulich and Bentz (2013). However, they also found that internal curing has nearly no effect on the total shrinkage as the total shrinkage is dominated by drying shrinkage.

Another factor affecting shrinkage of alkali-activated binders is activators. Type of activators, amount or dosage, and ratio are among parameters related to the use of activators. The activators usually used are sodium silicate, sodium or potassium hydroxide and sodium carbonate or a combination of those materials. Other types of activator are also used such as hydrated lime and gypsum (Collins and Sanjayan, 1999a; Neto *et al.*, 2010). Among the liquid sodium silicate, sodium hydroxide and sodium carbonate as activators for alkali-activated slag mortars, sodium carbonate AAS mortars resulted in lower or comparable drying shrinkage compared to that for OPC mortars, while liquid sodium silicate and sodium hydroxide AAS mortars have much higher drying shrinkage than OPC mortars (Atis *et al.*, 2009). Blast furnace slag activated with a combination of hydrated lime and gypsum has lower drying shrinkage than if it is activated with hydrated lime only (Neto *et al.*, 2010). Aydin and Baradan (2014) also observed the effects of activator type and content on properties of alkali-activated slag mortars including drying shrinkage. It was found from that study that the SiO_2/Na_2O (M_s) ratio plays an important role to the resulting drying shrinkage. The higher the M_s ratio, the higher the resulting drying shrinkage. However, for all ranges of M_s ratio, the drying shrinkage is still higher than that for PC mortar. Although AAS mortars activated by sodium silicate show higher compressive strength, lower water absorption characteristics, higher workability, lower porosity and a wide range of setting time than AAS activated by sodium hydroxide, they possess considerably higher drying shrinkage compared to AAS activated with sodium hydroxide.

Compressive strength seems not to be correlated with shrinkage, but it does for creep, as discussed in Section 10.4: higher compressive strength fly ash-based geopolymer concretes creep less than lower strength ones. As illustrated in Figure 10.17, the specific creep after one year loading is lower for higher compressive

strength, although the correlation of the rate of difference and the difference in compressive strength is still uncertain.

A different trend was observed for creep of inorganic polymer concrete (Lee, 2007). The difference seems to be dominated by the type of curing applied. Different curing type results in contrasting trend of creep in relation with compressive strength for the same type of IPC with Class F fly ash as source material but with different mixes for designed compressive strength purposes. For 'sealed' specimens, the specific creep at 28 days tends to be lower as the compressive strength increases, though the difference is not significant. However for 'exposed' specimens, the specific creep is higher for higher compressive strength and the difference is quite significant. These different types of curing between 'exposed' and 'sealed' not only result in different trends of creep as previously discussed, but also a difference in amount of creep strain. The 'sealed' specimens creep much less than the 'exposed' specimens.

10.6 Laboratory work and standard tests

There has been much laboratory work in the area of alkali-activated concretes, mortars and pastes. However, there is still no specific standard test and procedures for alkali-activated concretes, mortars and pastes. Most of the tests followed the standard procedures already developed for OPC-based binders. Possibly most of those standards are still suitable for alkali-activated binders, but probably some of them need to be evaluated. Some researchers have tried to develop their own test procedures to suit the needs of their research. For example, results of several studies indicated that alkali-activated binders seem to have quite high or significant early shrinkage, but many standard tests and procedures available for OPC binders could not accommodate the measurement of this early shrinkage. Moreover, most of the developed shrinkage test methods for concretes, mortars or pastes are for unrestrained or free shrinkage, while cracks are more likely to happen in restrained conditions due to the development of tensile stresses. Several test methods have been proposed to evaluate the crack of restrained specimens. One of them is the restrained ring-test, which is considered simple and economical. This test method is used to assess the shrinkage cracking potential of concrete mixtures and recommended by AASHTO (Hossain and Weiss, 2006).

Related to creep and shrinkage there are several standards developed for OPC binders that are usually used for studying alkali-activated binders. Those standards include ASTM C 512-02, *Standard test method for creep of concrete in compression*; ASTM C490/C490M-11 *Standard practice for use of apparatus for the determination of length change of hardened cement paste, mortar, and concrete*; ASTM C1608-12 *Standard test method for chemical shrinkage of hydraulic cement paste*; ASTM C157/C157M-08 *Standard test method for length change of hardened hydraulic-cement mortar and concrete*; AS 1012.16-1996, *Methods of testing concrete – Determination of creep of concrete cylinders in compression*; AS 1012.13-1992, *Methods of testing concrete – Determination of the drying shrinkage of concrete for samples prepared*

in the field or in the laboratory; and other equivalent standards applied to each country or region.

Figure 10.18 shows an example of equipment used for testing creep of concrete based on AS 1012.16-1996 (Standards Australia, 1996).

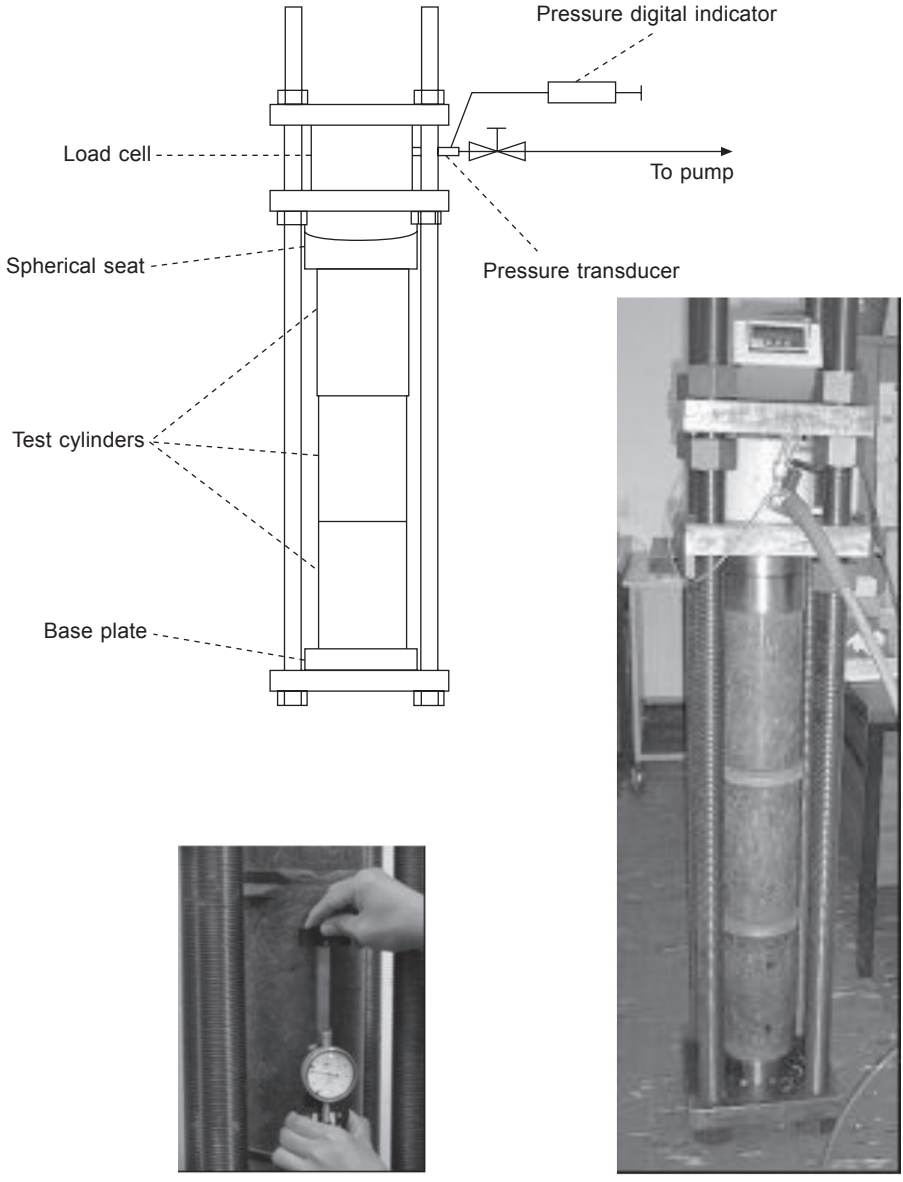

Figure 10.18 Creep test in laboratory.

10.7 Methods of predicting shrinkage and creep

Many methods have been developed to predict the creep and shrinkage of concrete, however, those methods were developed for OPC concrete. In this present situation, there is probably no prediction method for creep and shrinkage already developed specifically for alkali-activated concrete. Since the creep and shrinkage behaviour of alkali-activated concrete differ from those of OPC concrete, specific prediction methods need to be developed.

An example of using an available prediction method (developed for OPC concrete) to predict the creep and shrinkage of fly ash-based geopolymer concrete as reported by Wallah and Rangan (2006) will be presented here to give an overview of the suitability of the available method for newly developed fly ash-based geopolymer concrete.

Gilbert (2002) has proposed a simple method to calculate the creep coefficient of OPC concrete. This method is incorporated in Australian Standard for Concrete Structures AS3600 (2005). In this section, Gilbert's method is used to predict the creep coefficients of fly ash-based geopolymer concrete.

The Gilbert expression for calculating the creep coefficient is given by the following equation:

$$\varphi_{cc} = k_2 k_3 k_4 k_5 \varphi_{cc.b} \tag{10.4}$$

The factor k_2, given by Eq. (10.5), describes the development of creep with time and depends on the hypothetical thickness (t_h). In Eq. (10.5), t is the time (in days) since first loading and α_2 is given by Eq. (10.6).

$$k_2 = \frac{\alpha_2 t^{0.8}}{t^{0.8} + 0.15 t_h} \tag{10.5}$$

$$\alpha_2 = 1.0 + 1.12 e^{-0.008 t_h} \tag{10.6}$$

The factor k_3 is the maturity coefficient that depends on the strength ratio (f_{cm}/f'_c) as in Gilbert (2002). The f'_c is the characteristic compressive cylinder strength of concrete at 28 days and f_{cm} is the mean value of the compressive strength of concrete at the age of loading.

The factor k_4 accounts for the environment and is taken to be equal to 0.7 for an arid environment, 0.65 for an interior environment, 0.60 for a temperate environment and 0.5 for a tropical/coastal environment. The factor k_5 accounts for the relative humidity and the member size and is given by Eqs (10.7a) and (10.7b).
When

$$f'_c \leq 50 \text{ MPa: } k_5 = 1.0 \tag{10.7a}$$

When

$$50 \text{ MPa} < f'_c \leq 100 \text{ MPa: } k_5 = (2.0 - \alpha_3) - 0.02\,(1.0 - \alpha_3)\, f'_c \tag{10.7b}$$

where

$$\alpha_3 = \frac{0.7}{k_4 \alpha_2} \tag{10.8}$$

The hypothetical thickness (t_h) is given by Eq. (10.9), where A is the cross-sectional area of the member and u_e is that part of the perimeter of the member cross-section exposed to the atmosphere.

$$t_h = \frac{2A}{u_e} \tag{10.9}$$

The basic creep coefficient ($\varphi_{cc.b}$) depends on the characteristic compressive cylinder strength of concrete at 28 days (Gilbert, 2002).

An example of the comparison of the experimental results with the values calculated by Gilbert's method is given in Figure 10.19. Because the effect of age on the compressive strength of heat-cured fly ash-based geopolymer concrete is not significant, the strength ratio f_{cm}/f'_c is taken as equal to 1.0 and the maturity coefficient, $k_3 = 1.1$. The environmental factor, k_4 is taken as equal to 0.65 (interior environment) because the creep tests were conducted in an interior environment.

Figure 10.19 shows that the measured strains of fly ash-based geopolymer concrete are significantly smaller than the predicted values. As discussed in Section 10.4, the creep strains of fly ash-based geopolymer concrete are generally smaller than that of OPC concrete, and the method of prediction also confirms that fact. This also suggests the need for a new prediction method that is more suitable for fly ash-based geopolymer concrete.

For drying shrinkage strains, the measured shrinkage strains are also compared with the values predicted by a method proposed by Gilbert (2002). The method proposed by Gilbert divides the total shrinkage strain (ε_{cs}) into endogenous shrinkage (ε_{cse}) and drying shrinkage (ε_{csd}). Endogenous shrinkage is taken to be the sum of chemical and thermal shrinkage. The total shrinkage strain is given by Eq. (10.10) and the endogenous shrinkage at any time t (in days) after concrete placement is given by Eq. (10.11).

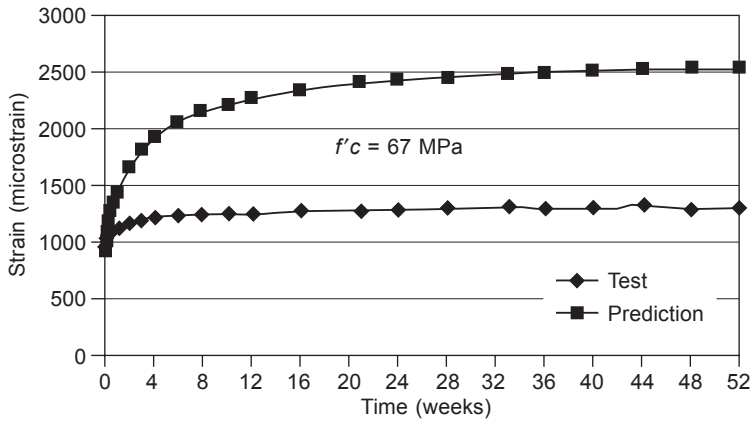

Figure 10.19 Correlation of test and predicted creep strain data.

$$\varepsilon_{cs} = \varepsilon_{cse} + \varepsilon_{csd} \tag{10.10}$$

$$\varepsilon_{cse} = \varepsilon^*_{cse}\,(1.0 - e^{-0.1t}) \tag{10.11}$$

Where ε^*_{cse} is the final endogenous shrinkage and may be taken as

$$\varepsilon^*_{cse} = (0.06\,f'_c - 1.0) \times 50 \times 10^{-6} \tag{10.12}$$

in which f'_c is in MPa.

The drying shrinkage at time t (in days) after the commencement of drying may be taken as

$$\varepsilon_{csd} = k_1 k_4 \varepsilon_{csd.b} \tag{10.13}$$

where $\varepsilon_{csd.b}$ is given by Eq. (10.14). In Eq. (10.14), $\varepsilon^*_{csd.b}$ depends on the quality of the local aggregates and may be taken as 800×10^{-6} for Sydney and Brisbane, 900×10^{-6} for Melbourne and 1000×10^{-6} elsewhere.

$$\varepsilon_{csd.b} = (1.0 - 0.008\,f'_c) \times \varepsilon^*_{csd.b} \tag{10.14}$$

The factor k_1 in Eq. (10.13) is given by Eq. (10.15), and the factor k_4, as for creep as discussed previously, is taken as equal to 0.7 for an arid environment, 0.65 for an interior environment, 0.6 for a temperate inland environment and 0.5 for a tropical or near-coastal environment.

$$k_1 = \frac{\alpha_1 t^{0.8}}{t^{0.8} + 0.15 t_h} \tag{10.15}$$

where

$$\alpha_1 = 0.8 + 1.2e^{-0.005 t_h} \tag{10.16}$$

and the hypothetical thickness, t_h is the same as given by Eq. (10.9).

An example of the measured shrinkage strains is compared with the predictions by Gilbert's method in Figure 10.20. In these calculations, the factor k_4 was taken as

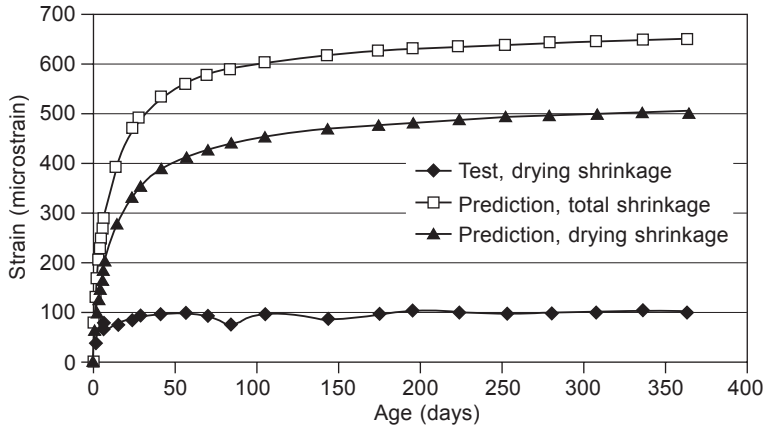

Figure 10.20 Comparison of test and predicted shrinkage strains.

equal to 0.65 as the test specimens were exposed to an interior environment and the value of f'_c was taken as the seventh-day compressive strength of the test specimens. It can be seen from Figure 10.20 that the measured drying shrinkage strains of heat-cured fly ash-based geopolymer concrete specimens are significantly smaller than the predicted values.

10.8 Future trends

Shrinkage remains a challenging and important topic for study because it is a property that seems to prevent a wider range of applications of alkali-activated concrete (AAC). Reducing the shrinkage, especially for AAC using slag as precursor material, is the biggest challenge. Although the shrinkage could be reduced significantly with suitable curing such as for fly ash-based geopolymer concrete with heat curing, the mechanisms of the causes still need to be explored and well understood. Suitable and accurate methods to observe the early age shrinkage also need to be developed. Likewise for creep of alkali-activated concrete, only very few studies have been reported or published. The effects of related parameters such as type of precursor materials, type of curing, type of activators, admixtures, and various age of loading still need to be investigated to confirm that creep of AAC is very small compared to ordinary Portland cement (OPC) concrete as shown by fly ash-based geopolymer concrete. The method used to predict the shrinkage and creep of OPC concrete is proved to be too inaccurate in its prediction of the properties of fly ash-based alkali-activated concrete. Thus, development of a more accurate method of prediction is imperative, taking into account the different mechanisms of hardening that take place, and factors affecting them. On the duration of observation, prolonged observation beyond one year is worth examining to be sure about the behaviour of shrinkage and creep development over a longer period.

References

Atis, C.D., Bilim, C., Celik, O. and Karahan, O. (2009), Influence of activator on the strength and drying shrinkage of alkali-activated slag mortar, *Construction and Building Materials*, 23(1), 548–555.

Aydin, S. and Baradan, B. (2012), Mechanical and microstructural properties of heat cured alkali-activated slag mortars, *Materials & Design*, 35, 374–383.

Aydin, S. and Baradan, B. (2014), Effect of activator type and content on properties of alkali-activated slag mortars, *Composites: Part B*, 57, 166–172.

Bakharev, T., Sanjayan, J.G., and Cheng, Y.B. (2000), Effect of admixtures on properties of alkali-activated slag concrete, *Cement and Concrete Research*, 30(9), 1367–1374.

Bazant, Z.P. (1982), Mathematical models for creep and shrinkage of concrete. In Z.P. Bazant and F.H. Wittmann (eds), *Creep and Shrinkage in Concrete Structures* (pp. 163–256). New York John Wiley & Sons.

Bazant, Z.P. and Wittmann, F.H. (eds) (1982), *Creep and Shrinkage in Concrete Structures*. New York, John Wiley and Sons.

Bilim, C., Karahan, O., Atis, C.D. and Ilkentapar, S. (2013), Influence of admixtures on the properties of alkali-activated slag mortars subjected to different curing conditions, *Materials & Design*, 44, 540–547.

Chang, J.J., Yeih, W. and Hung, C.C. (2005), Effects of gypsum and phosphoric acid on the properties of sodium silicate-based alkali-activated slag pastes, *Cement and Concrete Composites*, 27(1), 85–91.

Collins, F. and Sanjayan, J.G. (1999a), *W*orkability and mechanical properties of alkali-activated slag concrete, *Cement and Concrete Research*, 29, 455–458.

Collins, F. and Sanjayan, J.G. (1999b), Strength and shrinkage properties of alkali-activated slag concrete containing porous coarse aggregate, *Cement and Concrete Research*, 29(4), 607–610.

Collins, F. and Sanjayan, J.G. (2000), Effect of pore size distribution on drying shrinkage of alkali-activated slag concrete, *Cement and Concrete Research*, 30(9), 1401–1406.

Davidovits, J. (1999), Chemistry of Geopolymeric Systems, Terminology. Paper presented at the Géopolymère '99 International Conference, Saint-Quentin, France.

de Larrard, F., Acker, P. and Roy, R.L. (1994), Shrinkage creep and thermal properties. In S.P. Shah and S.H. Ahmad (eds), *High Performance Concretes and Applications* (pp. 65–114). London: Edward Arnold.

Douglas, E., Bilodeau, A. and Malhotra, V.M. (1992), *Properties and durability of alkali-activated slag concrete*, *ACI Materials Journal*, 89(5), 509–516.

Gilbert, R.I. (1988), *Time Effects in Concrete Structures*. Amsterdam: Elsevier.

Gilbert, R.I. (2002), Creep and shrinkage models for high strength concrete – proposal for inclusion in AS3600. *Australian Journal of Structural Engineering*, 4(2), 95–106.

Hardjito, D. and Rangan, B.V. (2005), Development and Properties of Low-Calcium Fly Ash-Based Geopolymer Concrete. Perth, Australia: Faculty of Engineering, Curtin University of Technology.

Hardjito, D., Wallah, S.E. and Rangan, B.V. (2002), Study on engineering properties of fly ash-based geopolymer concrete*, Journal of the Australasian Ceramic Society*, 38(1), 44–47.

Hardjito, D., Wallah, S.E., Sumajouw, D.M.J. and Rangan, B.V. (2004a), On the development of fly ash-based geopolymer concrete, *ACI Materials Journal*, 101(6), 467–472.

Hardjito, D., Wallah, S.E., Sumajouw, D.M.J. and Rangan, B.V. (2004b), The stress-strain behaviour of fly ash-based geopolymer concrete, In A.J. Decks and H. Hao (eds), *Development in Mechanics of Structures and Materials* (Vol. 2, pp. 831–834). Leiden: A.A. Balkema Publishers.

Hardjito, D., Wallah, S.E., Sumajouw, D.M.J. and Rangan, B.V. (2005), Fly ash-based geopolymer concrete, *Australian Journal of Structural Engineering*, 6(1), 77–86.

Hossain, A.B. and Weiss, J. (2006), The role of specimen geometry and boundary conditions on stress development and cracking in the restrained ring test, *Cement and Concrete Research*, 36, 189–199.

Jang, J.G., Lee, N.K. and Lee, H.K. (2014), Fresh and hardened properties of alkali-activated fly ash/slag pastes with superplasticizers, *Construction and Building Materials*, 50, 169–176.

Jin, F., Gu, K. and Al-Tabbaa, A. (2014), Strength and drying shrinkage of reactive MgO modified alkali-activated slag paste, *Construction and Building Materials*, 51, 395–404.

Lee, N.P. (2007), Creep and Shrinkage of Inorganic Polymer Concrete, Study Report, BRANZ.

Malhotra, V.M. and Mehta, P.K. (2002), *High-Performance, High-Volume Fly Ash Concrete: Materials, Mixture Proportioning, Properties, Construction Practice, and Case Histories*. Ottawa: Supplementary Cementing Materials for Sustainable Development Inc.

Neto, A.A.M., Cincotto, M.A. and Repette, W. (2008), Drying and autogenous shrinkage of pastes and mortars with activated slag cement, *Cement and Concrete Research,* 38(4), 565–574.

Neto, A.A.M., Cincotto, M.A. and Repette, W. (2010), Mechanical properties, drying and autogenous shrinkage of blast furnace slag activated with hydrated lime and gypsum, *Cement and Concrete Composites,* 32(4), 312–318.

Neville, A.M. (2000), *Properties of Concrete* (4th edn). Harlow: Pearson Education, Longman Group.

Neville, A.M., Dilger, W.H. and Brooks, J.J. (1983), *Creep of Plain and Structural Concrete*. London: Construction Press, Longman Group.

Rangan, B.V., Hardjito, D., Wallah, S.E. and Sumajouw, D.M.J. (2005), Fly ash-based geopolymer concrete: a construction material for sustainable development, *Concrete in Australia*, 31, 25–30.

Rangan, B.V., Wallah, S.E., Sumajouw, M.D.J. and Hardjito, D. (2006), Heat-cured, low-calcium, fly ash-based geopolymer concrete, *The Indian Concrete Journal*, 80(6), 47–52.

Rashad, A.M. (2013), Acomprehensive overview about the influence of different additives on the properties of alkali-activated slag – a guide for Civil Engineer, *Construction and Building Materials*, 47, 29–55.

Rusch, H., Jungwirth, D. and Hilsdorf, H.K. (1983), *Creep and Shrinkage, Their Effect on the Behaviour of Concrete Structures*. New York: Springer-Verlag.

Sakulich, A.R. and Bentz, D.P. (2013), *Mitigation of autogenous shrinkage in alkali activated slag mortars by internal curing*, *Materials and Structures*, 46, 1355–1367.

Standards Australia (1992), *Methods of testing concrete – Determination of the drying shrinkage of concrete for samples prepared in the field or in the laboratory*. AS 1012.13–1992.

Standards Australia (1996), *Methods of testing concrete – Determination of creep of concrete cylinders in compression*. AS 1012.16–1996.

Standards Australia (2005), *Australian Stardard for Concrete Structures*, AS 3600–2005.

Sumajouw, D.M.J., Hardjito, D., Wallah, S.E. and Rangan, B.V. (2005), Behaviour of geopolymer concrete columns under equal load eccentricities. Paper presented at the The Seventh ACI International Symposium on Utilization of High-Strength/High-Performance Concrete, Washington, DC.

Sumajouw, M.D.J., Hardjito, D., Wallah, S.E. and Rangan, B.V. (2007), Fly ash-based geopolymer concrete: study of slender reinforced columns, *Journal of Materials Science*, 42, 3124–3130.

Troxell, G.E., Raphael, J.M. and Davis, R.E. (1958), Long-time creep and shrinkage tests of plain and reinforced concrete, *Proc. ASTM*, 58, 1101–1102.

Wallah, S.E. (2009), Drying shrinkage of heat-cured fly ash-based geopolymer concrete, *Modern Applied Science*, 3(12), 14–21.

Wallah, S.E. (2010), Creep behaviour of fly ash-based geopolymer concrete, *Civil Engineering Dimension*, 12(2), 73–78.

Wallah, S.E. and Rangan, B.V. (2006), *Low-Calcium Fly Ash-Based Geopolymer Concrete: Long-Term Properties*, Research Report, Curtin University of Technology, Australia.

Wallah, S.E., Hardjito, D., Sumajouw, D.M.J. and Rangan, B.V. (2004), Geopolymer concrete: a key for better long-term performance and durability. Paper presented at the ICFRC

International Conference on Fibre Composites, High Performance Concretes and Smart Materials, Chennai, India.

Wallah, S.E., Hardjito, D., Sumajouw, D.M.J. and Rangan, B.V. (2005), Creep and shrinkage behaviours of fly ash-based geopolymer concrete. Paper presented at the Concrete 05, CIA 22nd Biennial Conference, Melbourne, Australia.

Warner, R.F., Rangan, B.V., Hall, A.S. and Faulkes, K.A. (1998), *Concrete Structures*. Melbourne: Longman.

Part Three

Durability of alkali-activated cement-based concrete binders

This page intentionally left blank

The frost resistance of alkali-activated cement-based binders

11

M. Cyr, R. Pouhet
Université de Toulouse, Toulouse, France

11.1 Introduction

In cold climates, frost action in the form of freezing and thawing cycles is one of the major problems that can lead to damage of concrete materials. It is generally recognized that durability problems related to cold weather conditions can take two principal forms:

- Internal cracking (Figure 11.1(a)) due to freezing and thawing cycles, which generally causes a loss of concrete strength and stiffness. It is often evaluated from the variation of strength or dynamic modulus of elasticity with freeze-thaw cycles.
- Surface scaling (Figure 11.1(b)) due to freezing in the presence of de-icing salts, which leads to a loss of concrete cover. The mass of scaling debris is usually the parameter measured to characterize this degradation.

Common points concerning both types of degradation are the need for high moisture content and a dependence on the porous network of the material. Usually, damage occurs when the material is saturated and its pore structure is not capable of resisting stresses due to the formation of ice. Since alkali-activated materials (AAM) are porous materials, they can be affected by frost.

This chapter describes the forms and mechanisms of frost in Portland cement concretes, and the parameters that could be significant in the evaluation of the susceptibility of AAM to freeze-thaw cycles. Existing data on the vulnerability of AAM to frost action are reported and discussed.

11.2 Frost in Portland cement concrete

11.2.1 Forms of frost damage

Frost damage in concrete, due to repeated freezing and thawing cycles, can take several forms. The most common types are treated here and concern internal cracking (Figure 11.1(a)) caused by progressive expansion of the cement paste with repeated freeze-thaw cycles, and surface scaling (Figure 11.1(b)) in the presence of moisture and de-icing salts. These types of deterioration do not necessarily happen at the same time.

Handbook of Alkali-activated Cements, Mortars and Concretes. http://dx.doi.org/10.1533/9781782422884.3.293

(a)

(b)

Figure 11.1 Deterioration of concrete due to frost attack: (a) internal cracking which led to significant loss of mass (photo courtesy of Richard Gagné); (b) surface scaling affecting the concrete cover (photo courtesy of Richard Gagné).

Other forms of damage, such as pop-outs and D-cracking, can also be seen. A pop-out is a small volume of concrete that has been separated from the overall concrete piece. It leaves a conical depression and the bottom of the hole is usually composed of a fragment of aggregate. The main cause is assumed to be the creation of stress resulting from freeze-thaw action within the coarse aggregate particle. The relief of this stress causes a crack in the aggregate and the surrounding paste and leads the concrete fragment near the concrete face to burst. D-cracking is characterized by

cracks that are usually parallel to joints and edges, with a pattern that can look like a large capital 'D'. The prime cause appears to be similar to that producing surface pop-out.

The best methods to limit the harmful effect of frost are to develop a proper network of bubbles in the matrix, or to design very high performance concrete that has compressive strength as high as 90 MPa. It should be noted that air entrainment has proved to be the easiest and most effective means of reducing the risk of damage to concrete by frost action.

11.2.2 Mechanisms and significant parameters of frost action

The mechanisms of frost damage have been attributed to several phenomena, which are partially due to the 9% expansion of water when it freezes: hydraulic pressure build-up as water is forced away from the freezing front (Powers, 1954, 1975), osmotic pressure gradients driving water towards the freezing centres (Powers and Helmuth, 1956: Helmuth, 1960), vapour pressure potentials (Litvan, 1972), and combinations of these processes. In the case of surface scaling, Rösli and Harnik (1980) also proposed a complementary hypothesis, stating that the phenomenon could be due to a mechanism of thermal shock, which implies a strong and brutal cooling of the concrete surface related to the endothermic reaction of the ice fusion when salts are used. The thermal gradient obtained would be sufficient to weaken the surface of the concrete. Most of these theories agree on the significant parameters responsible for frost damage in concrete.

11.2.2.1 Degree of saturation

As seen in Figure 11.2, concretes that have internal relative humidity below approximately 85% are normally not subject to internal damage from freezing,

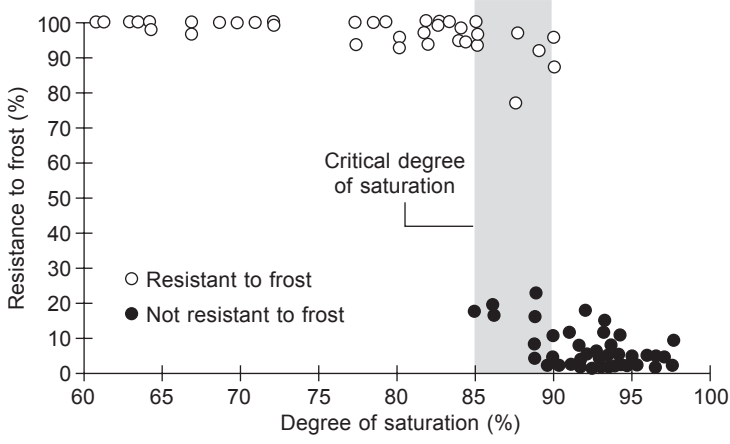

Figure 11.2 Effect of the degree of saturation on the frost resistance of concrete without air entrained. Data from Neville (1995).

whatever the concrete composition (ACI, 2008, Neville, 1995). A non-saturated paste contains pores that are filled with gas, and that provide a buffer volume in which the ice can be formed without exerting high stress on the pore walls.

11.2.2.2 Air-void

Frost damage is practically eliminated when a proper air-void system is achieved. Since air bubbles are practically never completely filled with water, ice can be formed without creating excessive internal pressure. For Portland cement concretes, it has been shown that the frost resistance is improved with increasing air content (Figure 11.3). In order to resist freeze-thaw cycles, it is generally recognized that concretes should contain more than 4% of air.

However, high air content is not enough to guarantee proper resistance to the effects of frost; air bubbles must be sufficiently close to one another to make sure that the internal stress generated by the ice is lower than the paste strength. Thus the essential parameter ensuring the efficiency of the protection provided by the air bubble network is the spacing factor. Figure 11.4 shows that, in the case of Portland cement concrete, this spacing factor should be lower than 500 μm to avoid internal cracking and lower than 200 μm to prevent surface scaling. The lower value for the second form of frost damage is due to the greater severity of the mechanisms involved in surface scaling. These values are usually achieved in Portland cement concrete by the use of an air-entraining admixture. However, the efficiency of air-entraining agents (AEA) in AAM is still a subject of discussion.

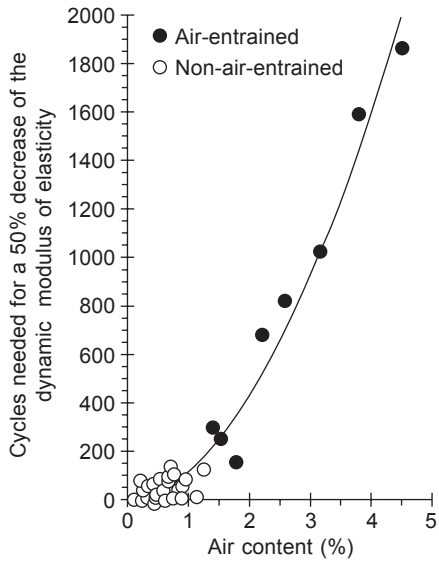

Figure 11.3 Effect of the air content on the frost resistance of Portland cement concrete. Data from Kosmatka *et al*. (2003).

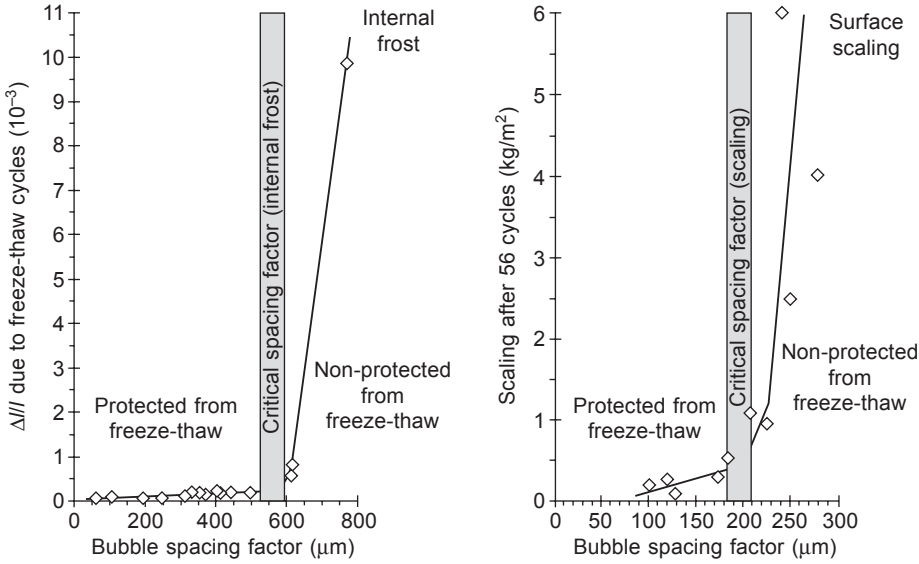

Figure 11.4 Spacing factors needed in the case of Portland cement concretes to protect the material against freeze-thaw cycles, for internal frost and surface scaling. Inspired from Gagné and Linger (2008), data from Pigeon and Langlois (1991) and Petersson (1993).

It has also been shown that the use of very active pozzolans such as silica fume in very high strength concretes (> 90 MPa) generally gives satisfactory behaviour in freeze-thaw cycles, without the need for a particular air void structure (Gagné *et al.*, 1990; Pigeon *et al.*, 1991). For other concretes of lower strength, a correct air void structure is almost always necessary (Gagné and Linger, 2008).

11.2.2.3 Water-binder ratio

Relatively high w/b (0.7–0.8) leads to mediocre freeze-thaw durability, even though the concrete contains entrained air (Gagné and Linger, 2008). Water-binder ratios of less than 0.5 or 0.3 for air-entrained or non-air-entrained concretes, respectively, are usually needed to reach an acceptable level of durability. At these levels, there is less freezable water and concrete has a higher resistance to internal stresses due to the formation of ice. Moreover, a decrease of w/b tends to decrease the size of pores, leading to less freeze-water at a given temperature, since the ice needs a lower temperature to form in smaller pores (Gagné and Linger, 2008).

11.2.2.4 Maturity of the concrete

As for air-void, many frost problems (especially for surface scaling) are eliminated when adequate maturity of the concrete is achieved, since it helps decrease porosity and permeability. Concretes with supplementary cementing materials (SCMs) are particularly vulnerable to short curing or to early freeze and thaw cycles. Numerous

examples of SCMs having low reaction kinetics (e.g., slag and fly ash) are reported in the literature concerning short curing times leading to insufficient frost resistance afterwards: see, for instance, Saric-Coric and Aitcin (2003).

11.3 Frost in alkali-activated binders – general trends and remarks

Alkali-activated materials possess a porous matrix and, although their microstructure can be different from that of Portland cement (Shi, 1996), some similarities can be expected regarding their behaviour against frost attack, which is primarily a physical phenomenon.

A few applications to real structures, for instance those reported in the book by Shi *et al*. (2005), were built in the 1980s and 1990s in countries where frost resistance is an issue. These structures were mainly composed of alkali-activated slag (AAS) concretes and seem to have resisted well even after many years of service.

- In Russia, several high residential buildings were built using AAS between 1986 and 1994 (e.g., in the city of Lipetsk). Visual observations carried out in 2000 indicated that the structures were in good condition with no cracking, deterioration or defects on the surface.
- AAS prestressed reinforced concrete railway sleepers, cast in 1988 near Tchudovo Railway Station between St Petersburg and Moscow (Russia), were still in good working condition after 13 years of service, as confirmed by a field inspection.
- An AAS concrete road 330 m long was cast between 1984 and 1990 in the city of Ternopol (Ukraine). The inspection made in 1999 showed that, compared to Portland cement concrete, the road made of AAS exhibited less surface deterioration.

To the best of the authors' knowledge, *in-situ* tests for frost attack of alkali-activated aluminosilicate binders are rare in the literature.

At laboratory scale, a few studies exist that assess the frost resistance of alkali-activated binders. The following detailed review separates AAMs into categories with respect to their vulnerability to freeze-thaw cycles: alkali-activated slag, alkali-alumino-silicate, and mixtures of the two, since the composition of the raw materials and the reaction products are very different for the two types of AAM.

As is often the case for literature on a subject that has not been extensively studied, it remains difficult to draw precise, accurate and incontestable conclusions on the frost resistance of AAM. However, some general tendencies, deduced from the following review, can still be highlighted.

11.3.1 Internal cracking of AAM

Most of the tests presented in the literature concern the study of internal cracking (e.g., ASTM C 666). A general trend for all kinds of AAM is that these materials can present good or fair frost resistance, for instance in the case of:

- alkali-activated slag (Byfors *et al.*, 1989; Douglas *et al.*, 1992; Gifford and Gillott, 1996; Puertas *et al.*, 2003; Fu *et al.*, 2011)
- alkali-activated fly ash (Sun, 2005; Sun and Wu, 2013; Škvára *et al.*, 2005, 2006; Slavik *et al.*, 2008)
- alkali-activated metakaolin (Bortnovsky *et al.*, 2007; Zhang *et al.*, 2008; Slavik *et al.*, 2008; Steinerova, 2011)

However, in a few cases, acceptable performance can be related to certain restrictions, for instance:

- The use of an efficient activator, such as sodium silicate, since others (e.g., sodium carbonate) can be less effective in protecting the concrete (Gifford and Gillott, 1996).
- The development of an appropriate air bubble network (Douglas *et al.*, 1992). Absence of entrained air could lead to marked weight loss, for instance in metakaolin-based AAM (Bucher *et al.*, 2011).
- The development of high strength, for instance greater than 86 MPa (Fu *et al.*, 2011).
- Avoidance of early freezing, since initial strength higher than 5 MPa is necessary for adequate protection (Byfors *et al.*, 1989).
- The use of reactive materials, since some raw materials having lower kinetics of reaction (e.g., some fly ashes) may lead to poor performance in comparison with other AAM (Puertas *et al.*, 2003, Slavik *et al.*, 2008).
- The need for aggregates in the mixtures, since the paste alone can be sensitive to frost attack (Steinerova, 2011).

11.3.2 Surface scaling of AAM

Literature specifically dedicated to this subject is scarce, so it might be difficult to detect a general trend. Sometimes, the tests presented measure the mass loss, but not on concrete plates and without the use of de-icing salts. A few authors give some results about surface scaling, the main conclusions being:

- mass loss of AAS can be equivalent to that in ordinary Portland cement (OPC) if the correct activator (e.g., sodium silicate) is used (Gifford and Gillott, 1996);
- AAFA without entrained air can have the same scaling behaviour as air-entrained OPC (Brooks *et al.*, 2010);
- as for OPC, the water/binder ratio has a very significant effect on scaling (Byfors *et al.*, 1989).

11.3.3 Importance and effect of air entrained in AAM

It seems that, as for OPC concrete, the air-void/bubble network plays a significant role regarding frost resistance. However, not all the literature agrees on the efficiency of air entraining agents, or the air content or critical spacing factor needed for fair protection of concrete against frost attack.

Some authors state that certain AEAs are efficient at producing a correct bubble network:

- Alkali-activated slag (Byfors *et al.*, 1989; Gifford and Gillott, 1996; Douglas *et al.*, 1992; Cai *et al.*, 2013).
- Alkali-activated fly ash (Škvára *et al.*, 2005, 2006; Sun, 2005; Sun and Wu, 2013; Shi, 2012, cited by Montes *et al.*, 2013).

However, not all available products are efficient (Gifford and Gillott, 1996) or allow a satisfactory size distribution of air bubbles to be obtained in the concrete (Byfors *et al.*, 1989). Higher doses of AEA may sometimes be required to reach the same air content as in OPC (Byfors *et al.*, 1989; Gifford and Gillott, 1996), but increasing AEA content does not necessarily lead to higher efficiency regarding frost resistance (Byfors *et al.*, 1989). In some cases, AEA can lead to instability of the entrained air (Douglas *et al.*, 1992), or may not permit a stable, uniform porous network to be obtained at all, for instance for some alkali-activated fly ash systems (Brooks *et al.*, 2010).

A few authors have shown that the air bubble spacing factor could present good correlation with frost resistance (Cai *et al.*, 2013), and AEA could produce an air bubble network that is efficient for the protection of concrete (Shi, 2012; Škvára *et al.*, 2005, 2006; Sun, 2005; Sun and Wu, 2013). However, the protection is not obtained systematically (Brooks *et al.*, 2010).

11.3.4 AAM vs. OPC

Comparisons of frost resistance between AAM and Portland cement are not often available in the literature but, when they are, it seems that the results converge towards similar conclusions, i.e. that AAMs show behaviour that is similar to or better than that of OPC (AAS: Gifford and Gillott, 1996; Krivenko, 1992; AAFA: Sun, 2005; Sun and Wu, 2013; Krivenko, 1992; Brooks *et al.*, 2010).

11.3.5 Freeze-thaw tests

On the one hand, as for other concrete pathologies, the conditions of accelerated frost tests can be relatively harsh, and one can wonder if this test is really representative of what happens in real structures. On the other hand, some authors have reported an improvement of concrete properties (e.g., strength, dynamic modulus) in the wet conditions of the freeze-thaw cycle tests (Puertas *et al.*, 2003; Zhang *et al.*, 2008; Bortnovsky *et al.*, 2007). This could be due to the activation of raw materials (slag, fly ash, metakaolin) during the test, leading to the formation of binding products and counteracting the effect of frost attack. This phenomenon might not be desirable in the evaluation of the frost resistance of a material. In order to avoid changes in the microstructure of AAM due to hydration or geopolymerization during freeze-thaw cycles, it could be judicious to postpone the beginning of the tests, especially for raw materials such as fly ash, which can have low kinetics of reaction.

11.4 Detailed review of frost resistance of alkali-activated slag (AAS) systems

Shi *et al.*'s (2005) book reports many studies on the frost resistance of alkali-activated slag systems carried out at the Kiev Civil Engineering Institute in the 1980s. Glukhovsky (1979) and Glukhovsky *et al.* (1988) studied the effect of the activator of the AAS on frost resistance and concluded that sodium silicate-activated slag concrete usually had the least porous structure, highest strength and best frost resistance. It was found that these concretes could resist between 300 and 1300 freeze-thaw cycles. Other concretes using soda-alkali melt as an activator only resisted 200–700 cycles (which was nevertheless better than Portland cement concrete for a given strength). It was also noted that the basicity of the slag had an effect on frost resistance, i.e. concrete made with acidic slag exhibited the worst performance. Timkovich (1986) completed these results by stating that sodium silicate-activated slag concrete, regardless of the basicity of the slag used, showed much better frost resistance in corrosive salt solutions than sodium carbonate-activated slag concrete and Portland cement concrete. Gerasimchuk (1982) also concluded on a better frost resistance of AAS compared to OPC in a study on lightweight alkali-activated slag concrete made with porous aggregates such as expanded perlite. These higher performances were attributed to the differences in structures and interfaces between cement paste and aggregate, and particularly the lower porosity of the AAS. Finally, Skurchinskaya and Belitsky (1989) found that no visible deterioration could be observed on sodium silicate-activated slag cement concrete after 45, 60 and 100 freeze–thaw cycles in 5% NaCl, $MgSO_4$ and $CaCl_2$, respectively.

Hakkinen (1986) (cited by Shi *et al.*, 2005) also concluded on better frost resistance of AAS in freeze-thaw testing, which indicated that alkali-activated slag cement concrete without air-entrainment could show better resistance than Portland cement concrete. However, air-entrained alkali-activated slag concrete suffered more damage than Portland cement concrete during the freeze-thaw tests.

Pu *et al.* (1988) (cited by Wang *et al.*, 1995) studied the frost resistance of AAS concretes having different strengths (low, medium and high) according to a Chinese standard in which the freezing took place in air. They found that no damage occurred after 200 freeze-thaw cycles for AAS concretes with strengths above 60 MPa and that weight loss was less than 0.118% for those with lower strength.

Byfors *et al.* (1989) studied the durability properties of a kind of alkali-activated slag called F-cement. These slags were activated using sodium hydroxide, sodium carbonate and an F-activator (NaOH 2.75%, Na_2CO_3 1%, lignosulfonate 1.5%, sodium gluconate 0.02%, and tributyl phosphate 0.02%). The specimens were used to study, among other things, early freezing, frost-salt scaling resistance, and the influence of air-entraining agents on the air bubble network. Different commercial AEAs (vinsol resin, alkylalcoholsulfonate tenside, polyglycolether-sulfonate tenside, and hollow plastic microspheres) were tested and it was concluded that it was possible to introduce air in the F-concrete on condition that the proportion of AEA was increased compared to those generally introduced in OPC. The size distribution

of air bubbles was considered satisfactory for two of the tested AEAs according to the criteria for OPC concrete (alkylalcoholsulfonate tenside and polyglycolether-sulfonate tenside).

Frost-salt scaling tests were also conducted on three F-concretes with water/binder ratios of 0.32, 0.40 and 0.50 (with and without AEA), according to a preliminary Swedish standard that recommends freezing in a 3% NaCl solution, and by measuring the accumulated mass of material scaled. It was observed that the water/binder ratio had a very significant effect on scaling (Figure 11.5), much more than the amount of AEA introduced into the mixtures. In fact, it was not possible to detect a trend regarding AEA content from these results. According to the authors, a study of the microstructure explained these findings as the structure was revealed to be very dense, with small capillary porosity and trapped permeability, a combination that makes it impossible for freezable water to be transported to the air pores.

Finally, the sensitivity of these concretes regarding early freezing was also tested by keeping specimens having different values of early strength at –20°C for 5 days. The compressive strength of the samples was measured after 91 days of post-curing. It was found that damage due to early freezing was seen only when the concrete had an initial strength lower than 5 MPa, i.e. the same value as for OPC.

Douglas *et al*. (1992) studied the properties and durability of alkali-activated slag concrete. They used granulated blast furnace slag and two different sodium silicates (M_s = 1.47 or 1.22), and all mixtures incorporated an air-entraining agent (sulfonated hydrocarbon type). For their freeze-thaw studies (based on ASTM C 666, Procedure A) they prepared prismatic specimens (76 mm × 102 mm × 390 mm) kept at 23°C in an atmosphere saturated with water for 14 days. Then the frost tests were carried out. They consisted of six 4 h freeze-thaw cycles, between 4.4°C and –17.8°C, per day. The lengths of the specimens were measured at 4.4°C, as were the loss of mass, the resonance frequency, and the pulse velocity, every 50 cycles up to 500 ± 10

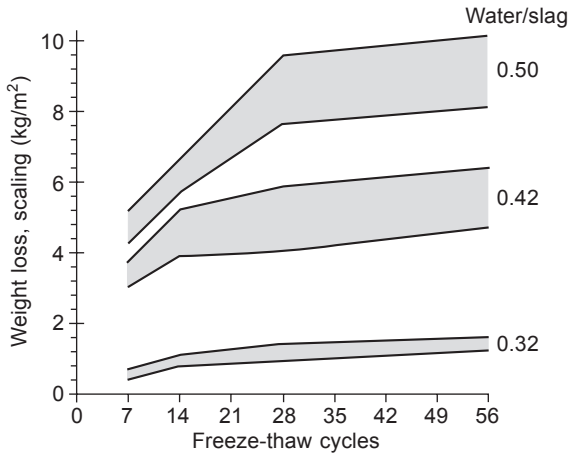

Figure 11.5 Weight loss due to scaling of alkali-activated slag concretes having different water/slag ratios. Data from Byfors *et al*. (1989).

cycles. The residual flexural strength was determined at the end of the 500 cycles. The specimens of reference concretes remained in a moist atmosphere.

Five mixtures having equivalent 28-day compressive strengths (around 30 MPa) were cast with a water/binder ratio of 0.48. The concrete formulations differed mainly in their sodium silicate/slag ratios (Table 11.1). The test results related to frost resistance are given in Table 11.1. The acceptable limits specified by ASTM C 666 correspond to a relative dynamic modulus of elasticity of 60% of the initial modulus, and 0.10% expansion. Among all the results, it was seen that the concrete prisms of Mixture 5 reached the specified limits before 300 cycles, whereas all the other concrete mixtures were below the specified values at 500 cycles, meaning that their frost resistance was good.

Measurements of the air-void spacing factors showed that, for all formulations, the values were between 270 and 380 μm (Table 11.1), which was higher, according to the authors, than the usual recommended limit of 220 μm for concrete resistant to freeze-thaw cycling. The air void spacing factor of Mixture 5 (377 μm) was probably responsible for the premature deterioration of this concrete. Moreover, it cannot be excluded that the mediocre behaviour of this mixture might have been due to its lower sodium silicate content (0.33 vs. 0.37–0.48, as seen in Table 11.1).

The authors pointed out that it was relatively easy to introduce air into fresh concrete but the small amount of air in the cured concrete indicated that entrained air was unstable. This instability could be due to incompatibility between the air-entraining agent and chemical admixtures used for activation of the slag, probably resulting in a coalescence of the air bubbles and leading to air loss during casting of the specimens.

Table 11.1 Properties of slag concretes and summary of test results in concrete prisms after 500 cycles of freezing and thawing

	Concrete mixtures				
	1	**2**	**3**	**4**	**5***
Sodium silicate/slag	0.48	0.48	0.39	0.37	0.33
Air content, fresh concrete (%)	6.2	5.2	7.3	7.2	5.7
Voids in hardened concrete (%)	3.9	4.2	4.5	6.2	4.7
Spacing factor of air bubbles (μm)	270	325	336	286	377
Initial compressive strength (MPa)	30.2	29.7	30.7	32.1	33.7
After 500 freeze-thaw cycles*					
Length variation (%)	+0.03	+0.04	+0.07	+0.09	+0.18
Weight variation (%)	–3.7	–1.0	–2.7	–2.9	–2.6
Variation of resonant frequency (%)	+1.8	+3.4	–1.4	–0.1	–29.9
Variation of pulse velocity (%)	–1.0	+0.8	–3.6	–8.1	–29.0
Relative dynamic modulus of elasticity (%)	104	107	97	100	50
Residual flexural strength (%)	62	63	58	67	32

* Mixture 5: test terminated at 300 cycles.
Source: Douglas *et al.*, 1992.

Gifford and Gillott (1996) presented a study of the durability of sodium carbonate or sodium silicate-activated blast furnace slag concrete against freeze-thaw (ASTM C 666). They also assessed the air-void parameter (ASTM C 457) by using an air-entraining agent that was a solution of various surface active agents (no further details available) especially designed for low-slump concrete or high-alkali cement. It should be noted that an attempt at using a commercially available AEA designed for Portland cement (aqueous solution of modified salts of a sulfonated hydrocarbon) was found to be ineffective for AAS.

Three types of concrete were studied (water-binder ratio of 0.44): one Portland cement concrete as the reference, and two AAS concretes activated by either sodium carbonate or sodium silicate (SiO_2/Na_2O = 1), at doses that provided 5.7 and 6.1% Na_2O relative to the slag mass, respectively. Lime slurry, used to delay the setting of the mixtures, was added to AAS concretes (8 kg/m^3). For each formulation, four prismatic specimens (75 mm × 75 mm × 350 mm) were cast for the freeze-thaw study, and two 100 mm × 200 mm cylinders for the study of air-void. Half the specimens were heated at 60°C for the first 6 h, while the other half was cured at room temperature. After 24 h, the samples were demoulded and stored in a moist-curing room until the time of testing. The results of freeze/thaw were noted every 35 cycles to measure the evolution of mass and dynamic modulus, up to 300 cycles (or until the modulus dropped below 60% of its initial value).

Several conclusions were drawn from the results:

- As for OPC, the workability of AAS concretes was improved when the amount of air in the mixture increased.
- In order to reach the same amount of entrained air in AAS concretes, it was necessary to double the AEA content in the sodium silicate AAS compared to OPC concrete. In the case of sodium carbonate, the AEA content reached four times that needed for OPC. The dosage of AEA thus depended on the nature and concentration of the activation solution. It was concluded that it was possible to create finely divided and closely spaced air bubbles in AAS concretes activated by sodium silicate using the same AEA as for OPC, but at higher doses.
- It was observed that the AAS specimens activated by sodium carbonate showed more weight loss and lower relative dynamic modulus than the other two mixtures. The sodium silicate AAS scaled the least, marginally less than the Portland cement specimens. The relative dynamic modulus of sodium silicate AAS was always higher than 80%, not far from that of the Portland cement mixture.
- The air-void parameters and durability against freeze-thaw for early-heated specimens were slightly lower than for those maintained in standard conditions.

Shi *et al*. (2005) studied the effect of freeze-thaw on AAS cement pastes compared with OPC, focusing on the electrolytes of the pore solution, which may have been the cause of the different deformations observed between these two matrices during freezing. It was found that, in the capillary pores of OPC, the solution froze spasmodically, while the freezing of the solution was more gradual in AAS cement pastes. Furthermore, the freezing point of the pore solution of AAS was considerably affected by the nature of the alkaline activator used. With potassium carbonate, the

freezing point of the eutectic mixture was –36°C whereas that of sodium carbonate was only –2.1°C. The lower freezing point of alkali-activated slag cement paste was also attributed to the differences in the pore structures between AAS and OPC, as AAS cement pastes contained more gel pores while Portland cement pastes had more capillary pores.

Fu *et al*. (2011) studied the effect of freeze-thaw cycles and mechanical damage on AAS concretes according to ASTM C 666 and GB/T50082-2009. They used blast furnace slag activated by a solution of sodium hydroxide and sodium silicate (modulus of 3.34). Five formulations of AAS concretes were assessed with six specimens per formulation (dimensions 100 mm × 100 mm × 400 mm). Mass and dynamic elastic modulus were then measured every 25 cycles up to 300 cycles.

The results showed a slight drop in the elastic dynamic modulus when the number of cycles increased (less than 12% at 300 cycles). Similarly, the percentage of weight lost was very low for all specimens as it remained below 1% at the end of the accelerated test. It should be noted that the strength of the concretes was higher than 86 MPa for all mixtures. According to the authors, these results were proof of the excellent freeze-thaw resistance of AAS concretes. The SEM analysis showed a symmetrical, compact structure, mainly composed of C-S-H with a low Ca/Si ratio and calcium-free aluminosilicates and zeolites, which made it difficult for water to penetrate into the concrete. In addition, the high compressive strength of AAS concretes further enhanced this ability to resist surface damage, which made it very durable regarding negative temperatures.

In another paper, the same team (Cai *et al*., 2013) used the same slag and activators to carry out a study focused on freeze-thaw resistance of alkali-slag concrete based on response surface methodology (RSM). RSM was applied to study the influence of the solution/slag ratio (A/S), slag content and sand ratio on the freeze-thaw resistance (ASTM C 666). Air-void structure was assessed using ASTM C 457-1998. A frost resistance coefficient D_F, defined as the ratio of dynamic elastic modulus after 300 freeze-thaw cycles to the initial dynamic elastic modulus, was used to evaluate the frost resistance. The empirical model used to plot the iso-response curves was calculated on the basis of 17 experiments chosen according to the Box–Behnken Design principle.

The analyses of response surfaces showed that the rank of the factors' significance for the AAS concrete frost resistance was solution/slag ratio > slag content > sand ratio. Lower solution/slag ratios and higher slag contents led to the best performances, while the sand content had very little influence on the results.

It was observed that the resistance to freeze-thaw ultimately depended on the porous network of the materials. The spacing coefficient and specific surface area of the air bubbles presented a fairly good correlation with the durability factor, with greater frost resistance for smaller air bubble spacing coefficient (Figure 11.6) and higher specific surface of air bubbles.

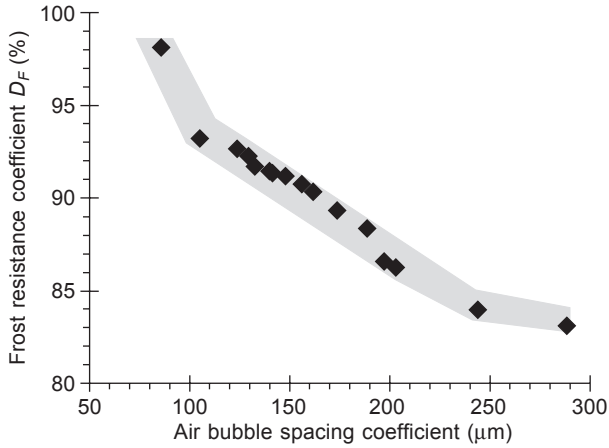

Figure 11.6 Relationship between air bubble spacing coefficient and the frost resistance coefficient D_F, defined as the ratio of dynamic elastic modulus after 300 freeze-thaw cycles to the initial dynamic elastic modulus. Data from Cai *et al.* (2013).

11.5 Detailed review of frost resistance of alkali-activated alumino-silicate systems

11.5.1 Alkali-activated fly ash systems

Davidovits and Comrie (1988) and then Davidovits *et al.* (1990), in two studies on the long-term durability of geopolymer based on observations of archaeological mortars, noted that the sodium-based geopolymers were not resistant to negative temperature and that only the mortar containing Na and K had resisted over time when they were in regions subject to the regular occurrence of freezing temperatures. Then Hermann *et al.* (1999) performed a freeze-thaw test on geopolymer cements according to the ASTM D 4842 standard (cycles between –20°C and +20°C), and observed no decrease in the compressive strength after 13 freeze-thaw cycles, no surface damage, and a total mass loss not exceeding 0.06%. A few years before, Kukko and Mannonen (1982) conducted freeze-thaw tests on F-concrete without air entrainment and found that the compressive strength increased after 100 freeze-thaw cycles (–20°C in air and 20°C in water).

Škvára *et al.*'s (2005, 2006) study of materials based on fly ash activated by an alkaline solution used freeze-thaw resistance tests carried out according to Czech standard CSN 72 2452 (no details given on the temperature and duration of the cycles). They prepared samples of dimensions 4 cm × 4 cm × 16 cm, which were stored at 40% RH and the ambient temperature of the laboratory for 28 days before starting the freeze-thaw tests. Mortars were made by mixing fly ash and sand with an alkaline solution containing NaOH and waterglass (M_s = 1.0–1.6, Na_2O 6–10%, w = 0.30–0.40) and were then heated between 60 and 80°C for 6 to 12 h in an open atmosphere. Seven formulations were made, incorporating some other materials (OPC, limestone in ground or aggregate form, and three different AEAs), but few

other details were given on the mixtures. In the freeze-thaw tests, samples were kept under water for 150 cycles and the results of compressive strengths were compared for each formulation, with controls maintained under laboratory conditions and broken at 28 days, 6 months and 1 year.

After 150 freeze-thaw cycles, no mass loss nor disintegration was observed on the specimens. The values of compressive strength obtained after these cycles were, on average, lower than those of the controls aged 28 days, except for the specimen with the AEA 2LN additive (Figure 11.7). Nevertheless, no damage or deformations were observed on the specimens at the end of the test. The authors therefore concluded that, in view of these results, it could be stated that the fly ash-based geopolymers were very resistant to freeze-thaw.

Brooks *et al*. (2010) studied high-performance concrete and lightweight concrete made with alkali-activated fly ash materials and, among other things, their behaviour towards freezing and thawing. They prepared 75 mm × 100 mm × 406 mm prisms by mixing fly ash and aggregates (fine and coarse) with a chemical activation solution of sodium hydroxide, concentrated sodium silicate and water (and also aluminium powder in the case of lightweight concrete), until a homogeneous mixture was obtained. The samples were then placed in a dry atmosphere (40–90°C) and demoulded after 12 h. The authors chose to study the effects of freeze-thaw on the AAM according to ASTM C 666, preferring the more severe test where freezing and thawing (temperature ranging from –18°C to 5°C) occurred under water immersion. The mixtures were prepared with and without an air-entraining agent (no further details). Visible changes and mass loss of AAM and OPC were followed for 300 freeze-thaw cycles. Note that the results can also be found in the work of Rostami and Brendley (2003).

As seen in Figure 11.8, AAFA concretes without air entrainment had a level of performance similar to that of air-entrained Portland cement concretes. The weight loss in the samples indicated that AAMs had a good resistance to freeze-thaw cycles,

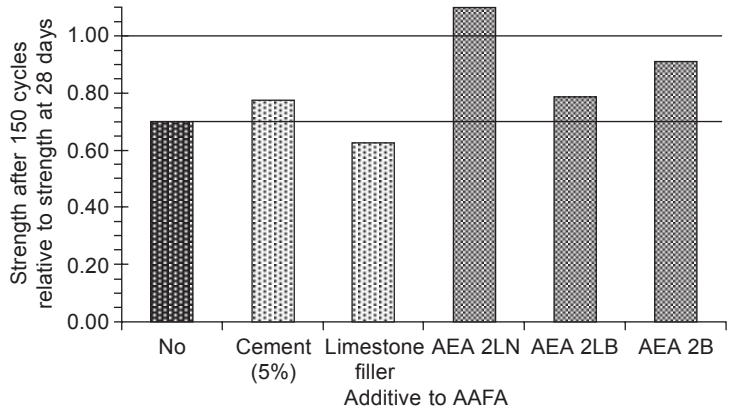

Figure 11.7 Compressive strength after 150 freeze-thaw cycles relative to 28 days of curing of mortars composed of activated fly ash, with and without additives. Data from Škvára *et al*. (2005, 2006).

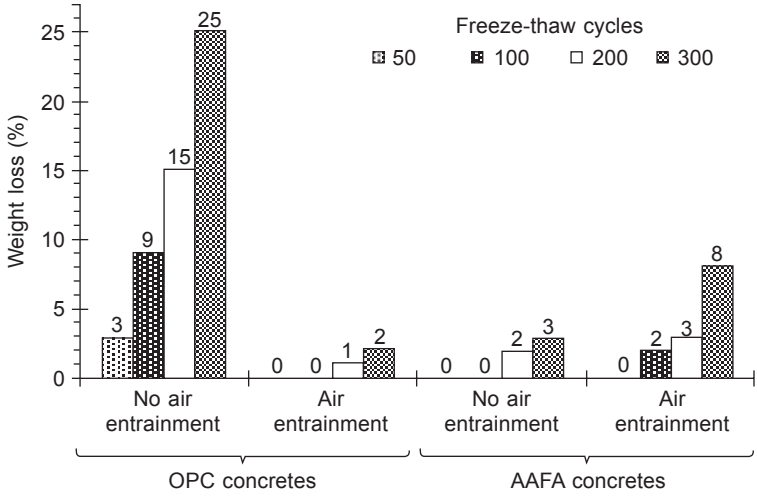

Figure 11.8 Weight loss after 50, 100, 200 and 300 freeze-thaw cycles of alkali-activated fly ash concretes compared to OPC concretes, with and without air entrainment. Data from Brooks *et al*. (2010) and Rostami and Brendley (2003).

but AEA did not increase their durability, since AAM with air entrainment presented more scaling than the formulation without AEA. According to Brooks *et al.*, this was due to the presence of entrained air, which significantly reduced the compressive strength of the mixtures (10–30% lower with AEA). It was concluded that the stable, uniform porous network obtained through the addition of AEA, which normally increases the resistance to freeze-thaw in OPC, was not formed in the AAM. The specimen without air entrainment performed better in freeze-thaw cycles and could thus be used outdoors without risk of damage. A study of the mass loss of AAM lightweight concrete with different formulations showed that concrete with lower density performed better regarding freeze-thaw cycles. AAM concrete with a density of 1200 kg/m^3, which had a compressive strength of 3 MPa and flexural strength of 0.8 MPa, could undergo 300 freeze-thaw cycles without any damage.

Sun (2005) and Sun and Wu (2013) studied the chemical and freeze-thaw resistance of alkali-activated fly ash (AAFA)-based inorganic mortars. The materials used in the study were Class F fly ash, silica fume, metakaolin, sodium hydroxide flakes, sodium sulfate and fine sand. A low cost sodium silicate solution was thus prepared by mixing the required amounts of NaOH flake with silica fume in distilled water, and the mixture was sealed and placed in a furnace at 75°C for 12 h, followed by slow cooling in air at room temperature before use.

For the freeze-thaw testing, air entraining agent (AEA: MB-VR, from Master Builders) was used (0.2% by weight relative to fly ash or Portland cement) in two of the four compositions: Portland cement mortar with and without air-entraining agent, and activated fly ash mortar with and without air-entraining agent. Mortar prisms of dimensions 23.5 mm × 23.5 mm × 50.8 mm were employed in the freeze-thaw tests, performed according to ASTM C666 (procedure A) for 300 cycles (alternately

lowering the temperature of the specimens from 4 to –18°C and raising it from –18 to 4°C in not less than 2 h and not more than 5 h).

As seen in Figure 11.9, the specimens of Portland cement mortar without AEA experienced the highest mass loss, which was 10 times higher than in specimens of Portland cement mortar with AEA. Both activated fly ash specimens (with or without entrained air) showed mass gains after 300 freeze-thaw cycles with no appreciable difference in mass change whether or not air entrainment was used (Figure 11.9). The strength study showed that the air-entraining agent used in this study had no negative effect on the compressive strength of activated FA mortars. Before the start of freeze-thaw testing the strength of AAFA mortars was around 41–42 MPa.

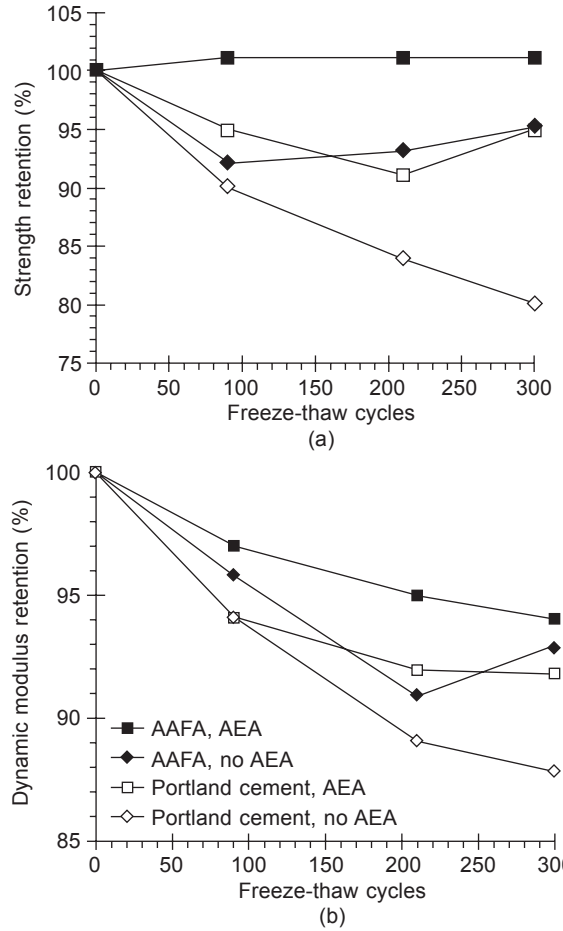

Figure 11.9 (a) Compressive strength retention (%) and (b) dynamic modulus retention (%) after 90, 210, and 300 freeze-thaw cycles of mixtures based on Portland cement with and without AEA, and of alkali-activated fly ash (AAFA) with and without AEA. (c) Mass change of the same mixtures after 300 freeze-thaw cycles. Data from Sun (2005) and Sun and Wu (2013).

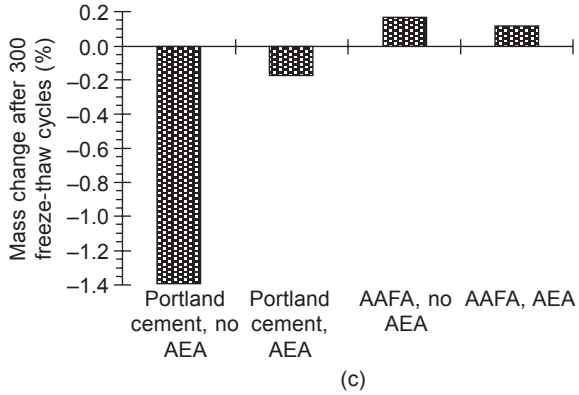

Figure 11.9 Continued

Figure 11.9 shows the compressive strength and dynamic modulus retained after 90, 210 and 300 freeze-thaw cycles for all four compositions. Specimens of Portland cement mortar without AEA deteriorated most seriously, showing about 20% strength loss after 300 cycles, while specimens of Portland cement mortar with AEA had lost only 5% after 300 cycles. Specimens of AAFA without AEA had lost 8% strength after 90 freeze-thaw cycles, and gradually regained some of their strength afterwards with a final loss of 5% at the end of the 300 cycles. AAFA with AEA specimens showed no change in compressive strength throughout the entire test. The study of dynamic modulus led to similar results, so the authors concluded that it was obvious that AAFA mortars had better freeze-thaw resistance than OPC mortars. Moreover, as for concrete, air entrainment could improve the freeze-thaw performance of fly ash mortars.

Shi (2012) (cited by Montes *et al.*, 2013) tested the resistance to freeze-thaw of specimens prepared from Class F fly ash according to standard ASTM C 666. He showed that, without AEA these geopolymers were unable to pass the test because they underwent complete degradation after only 100–120 cycles. In contrast, the addition of a small amount of AEA (0.25–1.5% per mass of ash) allowed those geopolymers to resist 300 cycles of freeze-thaw and retain over 90% of their elastic modulus.

11.5.2 Alkali-activated metakaolin systems

Bortnovsky *et al.* (2007) studied the development, the properties and the production of geopolymers based on the use of calcined shale or kaolin fly dusts, calcium-containing aluminosilicates, and an alkali activator composed of sodium waterglass with different silicate moduli (low and high). The paper focused on introducing two-component geopolymer binders produced under the commercial name Baucis. The tests performed included the freeze-thaw resistance according to EN 14617-5 (up to 100 cycles, freezing 2 h at –20°C and then thawing 2 h at +20°C in water).

All geopolymer mortar exhibited high freeze-thaw durability even after 100 cycles and the flexural strength values obtained at the end of the freeze-thaw test were higher than those obtained for the controls (180 days). Compressive strength values were below the controls, but reached 72% of the strength of the control in the worst case. Accelerated tests of durability (up to 15 cycles) were also carried out on the mortars. This test consisted of alternating scrubbing, drying and freezing of the sample during 1 week – 1 cycle, which, according to the authors, simulated 1 year of storage in outdoor weather conditions. The mortar sample strength values were sometimes higher, sometimes lower than those of control mixtures but without falling below 80% of the original values.

Steinerova (2011) published an article on the relationship between the properties of metakaolin-based geopolymer mortars and their porous structure. The geopolymer binder was prepared from a mixture of metakaolin (90% pure) with a solution of sodium hydroxide and sodium silicate (with ratios Si/Al = 1.4, Na/Al = 1 and H_2O/Na = 7.14), and a water/metakaolin ratio of 0.74. Quartz sand was used in a range of 0–93% by mass. After being demoulded at 24 h, mortar samples were placed in sealed plastic bags at ambient temperature for 28 days before being analysed. The study of freeze-thaw resistance consisted of comparing the average compressive strength of six specimens after 25 cycles of freeze-thaw (24 h cycles between –18°C and 20°C), and the average strength of six specimens kept at room temperature as controls. The results were expressed as the percentage of variation of resistance relative to the control, and the test was considered acceptable if the compressive strength remained higher than 75%. Young's modulus and flexural strength were also measured after 25 cycles.

The results showed that geopolymers could tolerate the 25 freeze-thaw cycles if they contained enough sand (more than 34%), otherwise the nanosized porous structure and the absence of mesopores in the 1–8 μm range did not allow the mortar to be frost resistant. The degradation of the geopolymer matrix containing only a small amount of sand might be due to a lack of accommodation of the freezing water in the porous network. According to the authors, the moisture expansion combined with the internal stress of the matrix were also suspected to be a cause of the destruction in the samples with low amounts of sand, a simple soak being enough to destroy pure geopolymer matrix (sudden occurrence of cracking upon contact with water). The increase in sand content (34% to 82%) allowed the mortars to withstand freeze-thaw cycles without showing cracking, as they remained above the limit of 75% of the controls' resistances. Above this limit, the frost resistance increased (up to 125%), mostly because both specimens (control and after freezing) already had very low strengths and because the excessive sand content led to the formation of coarse pores, which prevented full saturation.

Bucher *et al*. (2011) studied the frost resistance of a concrete made of metakaolin activated by a solution of sodium silicate and sodium hydroxide, without air-entrainment. The compressive strength of the concrete reached 55 MPa at 28 days. The freeze-thaw test was based on the French standard NF P18-424, on 7 cm × 7 cm × 28 cm specimens (tested at 28 days). It was seen that the absence of air-entrainment led to large weight losses after only 40 freeze-thaw cycles (Figure 11.10).

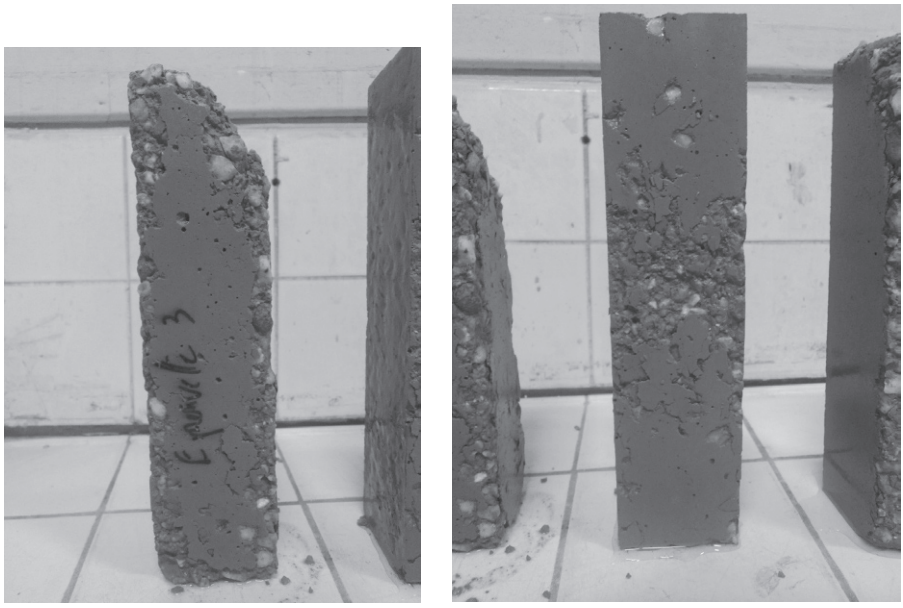

Figure 11.10 Metakaolin-based geopolymer concretes without AEA after 40 freeze-thaw cycles (Bucher *et al.*, 2011).

11.6 Detailed review of frost resistance of mixed systems

11.6.1 Alkali-activated slag/fly ash

Krivenko (1992) studied the properties of alkali-based cement concrete and noted that, depending on their composition, materials such as slag-alkaline binders, alkaline fly ash-binder, alkaline aluminate cements, or mixtures of these with OPC, could achieve better properties than the simple OPC binder, after more than 1000 freeze-thaw cycles. Ionescu and Ispas (1986) used a binder made with slag and fly ash, activated with liquid sodium silicate. The concretes had good resistance to 50–80 cycles of freeze-thaw exposure at 28 days of curing.

Puertas *et al.* (2003) studied the behaviour of three different alkali-activated cements reinforced with polypropylene fibres and, in particular, their resistance to freeze-thaw cycles. The three cements tested were: (a) GBFS activated by waterglass solution (Na_2SiO_3 + NaOH, Na_2O_{eq} = 4%) at room temperature, (b) aluminosilicate fly ash activated with 8 M NaOH and cured at 85°C for the first 24 h, and (c) 50% fly ash + 50% slag activated with 8 M NaOH solution at room temperature. In these tests, the dosage of fibre was 0.5% of the mortar volume. For the freeze-thaw testing, sets of three mortars of dimensions 4 cm × 4 cm × 16 cm were prepared for each formulation. After 28 days of cure, the mortars were subjected to 50 freeze-thaw cycles, with two cycles per day (3 h at –20°C, 0.5 h immersed in water, 3 h at –20°C,

and another 0.5 h immersed in water). For the rest of the time (17 h) the specimens were kept immersed in water.

The mechanical behaviour of mortars after 50 freeze-thaw cycles is presented in Figure 11.11. The most detrimental effect was observed on alkali-activated fly ash, where a significant drop in mechanical strength was found after the cycles. Compressive and flexural strength were observed to increase for mixtures containing alkali-activated slag. According to the authors, the activation of slag continued in the wet conditions of the test, resulting in the formation of a large amount of reaction product, which increased the mechanical strength. An increase was also seen, but to a lesser extent, for slag/fly ash mixtures and was due to the presence of slag in smaller quantities. It was concluded that slag-based materials have a strong resistance to negative temperatures because the freezing temperatures of alkaline metal solutions are below 0°C (about –15 to –20°C). It was also noted that the presence of fibre did not change the behaviour of the mortars regarding freeze-thaw cycles.

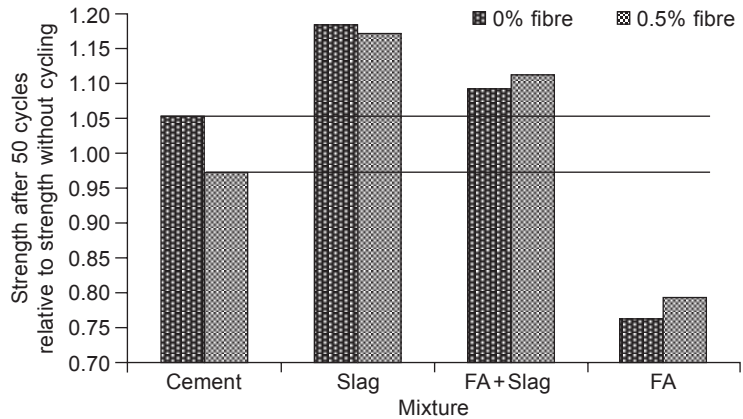

Figure 11.11 Compressive strength after 50 freeze-thaw cycles relative to strength without cycling of alkali-activated slag and fly ash systems, with and without polypropylene fibres. Data from Puertas *et al.* (2003).

11.6.2 Alkali-activated metakaolin/fly ash systems

Slavik *et al.* (2008) have studied the behaviour with respect to freeze-thaw cycles of geopolymer made of fluidized bed combustion bottom ash (FBC-BA) and thermally activated kaolinitic clay (i.e., metakaolin). The mixtures of the two products were activated with a solution of waterglass (composition 30.2% SiO_2 and 10.8% Na_2O) and 5 M NaOH (Figure 11.12). After 24 h, the specimens were demoulded and kept at 45% RH and 22°C for 28 days before starting the freeze-thaw tests. In accordance with European standard EN 14617-5:2005, the specimens were exposed to 50 freeze-thaw cycles (freezing for 2 h at –20°C and then thawing for 2 h at +20°C in water) and then tested for compressive strength. In parallel, compressive strength tests were also performed on specimens of the same age which had not been subjected to any negative temperatures.

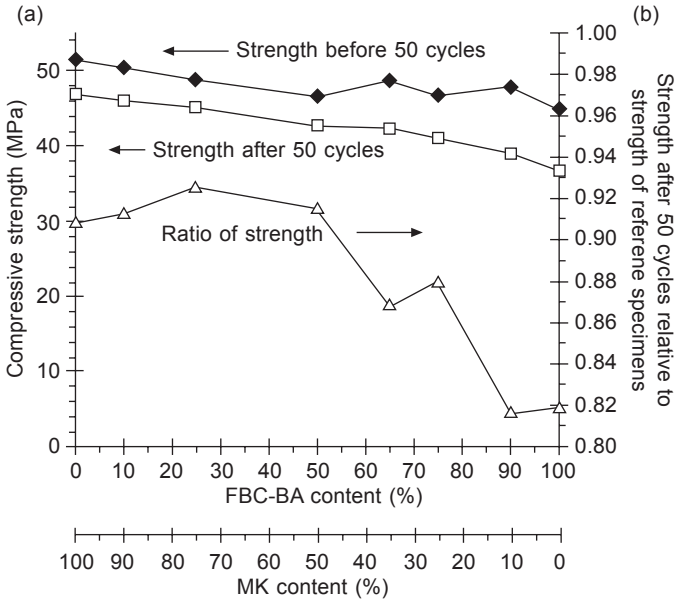

FBC-BA (g)	0	10	25	50	65	75	90	100
Metakaolin (g)	100	90	75	50	35	25	10	0
Waterglass (g)	100	90	85	80	70	65	60	55
5M NaOH (ml)	10	9	8	7.5	6.5	6	5.5	5

Figure 11.12 (a) Compressive strength and (b) relative strength of geopolymers made of fluidized bed combustion bottom ash and metakaolin after 50 cycles of freeze-thaw. Data from Slavik *et al*. (2008).

The study of compressive strength showed that the resistance declined a little when the amount of FBC-BA increased, and the same result was observed after 50 cycles of freeze-thaw. However, it should be noted that the amount of activating solution also decreased with the increase in fly ash content. After 50 freeze-thaw cycles, all samples underwent a moderate drop in resistance, which did not exceed 20% relative to the strength of control specimens. According to the authors, these results showed acceptable freeze-thaw resistance.

Zhang *et al*. (2008) studied, among other properties, the freeze-thaw resistance of metakaolin (MK)/fly ash-geopolymer composites manufactured by an extrusion technique and incorporating short PVA fibres. Four geopolymers made from kaolin calcined at 700°C for 12 h and Class F fly ash (in proportions ranging from 100% MK to 50% MK-50% FA) were activated by a solution of waterglass and NaOH. The samples were cured at 20°C and 100% R.H. for 28 days. The 9 h freeze-thaw cycles were carried out between 4.4 and –20°C on 90 mm × 75 mm × 6 mm thin plate specimens. The impact strength, stiffness and toughness of the four mixtures were measured before and after 20 freeze-thaw cycles. The results showed that the geopolymers tested possessed an excellent resistance to freeze-thaw cycles:

- For the 100% metakaolin mixture, no obvious change in the impact strength was seen relative to the same composite before the freeze-thaw cycles.
- The impact strength of mixtures with metakaolin and fly ash increased after the freeze-thaw cycles, especially for high fly ash content. As the impact behaviour of hardened cementitious paste was expected to be reduced after freeze-thaw cycles, the authors concluded that the increase was probably due to (a) the geopolymer structure, which was dense and compact so the water could not penetrate inside the plates and there was thus almost no freeze-thaw deterioration, or (b) the geopolymeric products still being formed over the long duration of freeze-thaw testing (about 10 days). Knowing that the kinetics of fly ash reaction is usually lower than that of metakaolin, the latter explanation seems plausible, and means that the freeze-thaw tests should be carried out after a longer cure, or for more cycles.

11.7 Future trends

There is an increasing interest in AAM applied to construction, including in countries experiencing negative temperatures. Current knowledge on the durability aspects of these materials does not allow their behaviour over time to be predicted, and thus requires further investigation, particularly in freeze-thaw conditions. *In-situ* and laboratory-scale tests are still needed to generalize the knowledge on frost resistance of all types of AAM. Several accelerated tests have been used in the literature to evaluate the frost resistance of AAM but it should be pointed out that accelerated tests are sometimes far from reality, so feedback is still needed to confirm the laboratory findings.

Durability related to freeze-thaw concerns two forms of damage but the literature tends to deal mainly with issues related to internal cracking. The surface scaling problem is an important issue requiring further study, especially testing that includes contact with salt solution.

The mechanisms responsible for damage due to freeze-thaw are mainly physical and are now well-known for Portland cement, as are the ways to reduce them. It is known that the use of AEA effectively reduces damage by creating a network of air bubbles. However, these chemical substances are usually combined with water and their stability and efficiency in the presence of strongly alkaline solution (such as waterglass) remain to be investigated.

Further work on mathematical models for freeze-thaw should complete the existing ones already developed for Portland cement-based materials. Such models could contribute to the understanding and prediction of the behaviour of AAM regarding the durability of concrete.

11.8 Sources of further information

Freeze-thaw is being treated by the 5-year RILEM Technical Committee 247-DTA (Durability testing of alkali-activated materials), set up in 2012 and chaired by

Professor John L. Provis. It is anticipated that the working groups will deliver a set of recommendations based on round-robin tests of standardized alkali-activated material mix designs according to specific freeze-thaw testing protocols. The recommendations will focus on answering the following questions:

- What is the best method for testing, in a laboratory environment, the likely frost resistance durability of an alkali-activated binder or concrete according to specific modes of degradation?
- Which parameters of mix design and/or sample conditioning show the greatest impact on the test outcomes, and how do these correspond to likely in-service performance?
- What recommendations can be made for the formulation of an alkali-activated material that is as resistant as possible to freeze-thaw?

References

ACI Committee 201 (2008), 'ACI 201.2 – Guide to Durable Concrete'.

Bortnovsky O, Dvořáková K, Roubíček P, Boušek J, Průdková Ž and Baxa P (2007), 'Development, properties, and production of geopolymers based on secondary raw materials', *3rd Int. Conf. on Alkali Activated Materials Research, Production and Utilization*, 83–96.

Brooks R, Bahadory M, Tovia F and Rostami H (2010), 'Properties of alkali-activated fly ash: high performance to lightweight', *International Journal of Sustainable Engineering*, 3 (3), 211–218.

Bucher R, Cyr M, Idir R and Habert G (2011), Etude de durabilité et analyse de cycle de vie des géopolymères à base de verre de recyclage et de métakaolin (in French), Université de Toulouse.

Byfors K, Klingstedt G, Lehtonen V, Pyy H and Romben L (1989), 'Durability of concrete made with alkali activated slag', Trondheim Conference, 1429–1466.

Cai L, Wang H and Fu Y (2013), 'Freeze–thaw resistance of alkali–slag concrete based on response surface methodology', *Construction and Building Materials*, 49, 70–76.

Davidovits J and Comrie D (1988), 'Archaeological long-term durability of hazardous waste disposal: preliminary results with geopolymer technologies', *Geopolymer '88*, 125–134.

Davidovits J, Douglas C C, Paterson J H and Ritcey D J (1990), 'Geopolymeric Concretes for Environnemental Protection', *Concrete International*, 12 (7), 30–40.

Douglas E, Bilodeau A and Malhotra V M (1992), 'Properties and Durability of Alkali-Activated Slag Concrete', *ACI Materials Journal*, 89, 509–516.

Fu Y, Cai L and Yonggen W (2011), 'Freeze–thaw cycle test and damage mechanics models of alkali-activated slag concrete', *Construction and Building Materials*, 25 (7), 3144–3148.

Gagné R and Linger L (2008), 'La durabilité des bétons en ambiance hivernale rigoureuse', in *La durabilité des bétons – Bases scientifiques pour la formulation de bétons durables dans leur environnement*, 2nd edn. Paris, Presses de l'école nationale des Ponts et Chaussées (ENPC).

Gagné R, Pigeon M and Aïtcin P-C (1990), 'Durabilité au gel des bétons de hautes performances mécaniques', *Materials and Structures*, 23, 103–109.

Gerasimchuk V L (1982), 'The influence of aggregates properties on the slag alkaline cement concrete structure and strength', PhD Thesis, Kiev Civil Engineering Institute, Kiev, USSR.

Gifford P M and Gillott J E (1996), 'Freeze-thaw durability of activated blast-furnace slag cement concrete', *ACI Materials Journal*, 93, 1994–1997.

Glukhovsky V D (1979), *Alkaline and Alkaline–Alkali-earth Hydraulic Binders and Concretes*, Kiev, USSR, Vysscha Shkola Publisher.

Glukhovsky V D, Krivenko PV, Rumyna GV and Gerasim chuk VL (1988), *The Manufacture of Concretes and Structures from Slag Alkaline Binders*, Kiev, USSR, Budivel'nik Publisher.

Hakkinen T (1986), 'Properties of alkali-activated slag concrete', VTT Research Notes No. 540, Technical Research Centre of Finland (VTT), Finland.

Helmuth R H (1960), 'Capillary size restrictions on ice formation in hardened Portland cement pastes', *4th International Symposium on the Chemistry of Cement*, 855–869.

Hermann E, Kunze C, Gatzweiler R, Kießig G and Davidovits J (1999), 'Solidification of various radioactive residues by géopolymère® with special emphasis on long-term stability', *Géopolymère '99 Proceedings*, 211–228.

Ionescu I and Ispas T (1986), *Properties and Durability of Some Concretes Containing Binders Based on Slag and Activated Ashes*, ACI Special Publication, vol 91, 1475–1493.

Kosmatka S H, Kerkhoff B and Panarese W C (2003), *Design and Control of Concrete Mixtures*, EB001, 14th edition, Portland Cement Association, Skokie, IL.

Krivenko P V (1992), 'Alkaline cements', *9th International Congress on the Chemistry of Cement*, 482–488.

Kukko H and Mannonen R (1982), 'Chemical and mechanical properties of alkali-activated blast furnace slag (F-concrete)', *Nord. Concr. Res*, No. I, 16.1–16.16.

Litvan G G (1972), 'Phase transitions of adsorbates: IV, Mechanism of frost action in hardened cement paste', *Journal of the American Ceramic Society*, 55, 38–42.

Montes C, Islam R, Shi J, Kupwade-Patil K and Allouche E N (2013), 'Towards a pre-cast geopolymer concrete pipe', *Pipelines 2013*, 534–542.

Neville A M (1995), *Properties of Concrete*, Harlow, Pearson Education.

Petersson P E (1993), 'Scaling resistance tests of concretes: Experience from practical use in Sweden', Atelier international sur la résistance des bétons aux cycles de gel-dégel en présence de sels fondants, Comité RILEM TC 117, Québec, 249–259.

Pigeon M and Langlois M (1991), 'Étude de la résistance au gel de bétons contenant un fluidifiant', *Revue canadienne de génie civil*, 18 (4), 581–589.

Pigeon M, Gagné R, Aitcin P-C and Banthia N (1991), 'Freezing and thawing tests of high-strength concretes', *Cement and Concrete Research*, 21, 844–852.

Powers T C (1954), 'Void spacing as a basis for producing air-entrained concrete', *Journal of the American Concrete Institute*, 50, 741–760.

Powers T C (1975), 'Freezing effects in concrete', in *Durability of Concrete*, ACI, SP-47, 1–11

Powers T C and Helmuth R A (1956), 'Theory of volume changes in hardened Portland cement paste during freezing', *Proceedings of the Highway Research Board*, 32, 285–297.

Pu X C, Gan CC, Wang SD and Yang CH (1988), *Summary Reports of Research on Alkali-Activated Slag Cement and Concrete*, 6 vols (in Chinese), Chongqing Institute of Architecture and Engineering.

Puertas F, Amat T, Fernández-Jiménez A and Vázquez T (2003), 'Mechanical and durable behaviour of alkaline cement mortars reinforced with polypropylene fibres', *Cement and Concrete Research*, 33 (12), 2031–2036.

Rösli A and Harnik A B (1980), 'Improving the durability of concrete to freezing, deicing salts', in *Durability of Building Materials and Components*, P J Sereda and G G Litvan (eds), ASTM, Philadelphia, STP 691, 464–473.

Rostami H and Brendley W (2003), 'Alkali ash material: a novel fly ash-based cement', *Environmental Science & Technology*, 37 (15), 3454–3457.

Saric-Coric M and Aitcin P-C (2003), 'Bétons à haute performance à base de ciments composés contenant du laitier et de la fumée de silice', *Canadian Journal of Civil Engineering*, 30, 414–428.

Shi C (1996), 'Strength, pore structure and permeability of alkali-activated slag mortars', *Cement and Concrete Research*, 26 (12), 1789–1799.

Shi C, Krivenko P V and Roy D (2005), *Alkali-Activated Cements and Concretes*, Abingdon, Taylor & Francis.

Shi J (2012), 'Response of geopolymer concrete to environmental loads', PhD Thesis, Louisiana Tech University Ruston, LA.

Skurchinskaya Zh. and Belitsky I V (1989), 'The regulation of setting processes in the slag-alkaline binders', in *III National Scientific and Practical Conference on Slag-Alkaline Cements, Concretes and Structures*, V D Glukhovsky (ed.), Kiev, USSR, I, 143–145.

Škvára F, Jilek T and Kopecky L (2005), 'Geopolymer materials based on fly ash', *Ceramics – Silikáty*, 49 (3), 195–204.

Škvára F, Doležal J, Svoboda P, Kopecký L, Pawlasová S, Lucuk M, Dvořáček K, Beksa M, Lenka M and Šulc R (2006), 'Concrete based on fly ash geopolymers', *IBAUSIL 2006 Conference Proceedings*.

Slavik R, Bednarik V, Vondruska M and Nemec A (2008), 'Preparation of geopolymer from fluidized bed combustion bottom ash', *Journal of Materials Processing Technology*, 200 (1–3), 265–270.

Steinerova M (2011), 'Mechanical properties of geopolymer mortars in relation to their porous structure', *Ceramics – Silikáty*, 55 (4), 362–372.

Sun P (2005), 'Fly ash based inorganic polymeric building materials', PhD Thesis, Wayne State University, Detroit, MI.

Sun P and Wu H-C (2013), 'Chemical and freeze-thaw resistance of fly ash-based inorganic mortars', *Fuel*, 111, 740–745.

Timkovich, V Yu (1986), 'Genesis of structure and strength of the slag alkaline cements and concretes', PhD Thesis, Kiev Civil Engineering Institute, Kiev, USSR.

Wang S-D, Pu X-C, Scrivener KL and Pratt PL (1995), 'Alkali-activated slag cement and concrete: a review of properties and problems', *Advances in Cement Research*, 7 (27), 93–102.

Zhang Y, Sun W, Li Z, Zhou X and Chau C (2008), 'Impact properties of geopolymer based extrudates incorporated with fly ash and PVA short fiber', *Construction and Building Materials*, 22 (3), 370–383.

The resistance of alkali-activated cement-based binders to carbonation

12

S. A. Bernal
University of Sheffield, Sheffield, UK

12.1 Introduction

The chemical reaction between a cement-based material and carbon dioxide (CO_2) is referred to as carbonation, and is one of the most harmful degradation processes that can drastically affect the long-term durability of civil infrastructure (Hobbs, 2001; Glasser *et al.*, 2008). A truly sustainable material must be durable, and therefore efforts have been focused in the past decade to understand the changes induced by carbonation in the microstructure of alkali-activated materials, and its consequent effects on permeability and mechanical strength, in order to predict service life performance (Bernal and Provis, 2014).

Carbonation of ordinary Portland cements (OPC) takes place when CO_2 from the atmosphere diffuses through the pore network of the material, and dissolves in the pore solution forming HCO_3^-. This anion is a weak acid, and reacts with the calcium-rich hydration products present in the matrix, mainly the portlandite ($Ca(OH)_2$), calcium silicate hydrate (C-S-H), calcium aluminate hydrates (C-A-H) and ettringite (Johannesson and Utgenannt, 2001; Fernández-Bertos *et al.*, 2004), promoting the formation of calcium carbonate polymorphs through a decalcification process. This leads to the decay of the strength-giving phases and a drop in the internal pH of the system, which facilitates the development of corrosion of steel components in reinforced concrete materials (Poonguzhali *et al.*, 2008).

In alkali-activated materials, the mechanism of carbonation is not yet fully understood, but it has been demonstrated that it is fundamentally a chemically controlled mechanism that occurs in two steps: (1) carbonation of the pore solution leading to a reduction in pH and the eventual precipitation of Na-rich carbonates, followed by (2) the decalcification of Ca-rich phases (mainly C-S-H, as portlandite usually does not form in these systems) and carbonation of secondary reaction products present in the system (Bernal *et al.*, 2012, 2013). These materials usually perform poorly when tested under accelerated carbonation conditions compared with Portland cement-based products; however, natural carbonation rates as low as 1 mm/year have been identified (Shi *et al.*, 2006) in aged structures based on alkali-activated binders. This indicates that the accelerated carbonation testing methods applied to alkali-activated materials are not accurately replicating what is experienced under

Handbook of Alkali-activated Cements, Mortars and Concretes. http://dx.doi.org/10.1533/9781782422884.3.319

natural carbonation conditions, and raises the need for further examination of the testing methods themselves.

12.2 Testing methods used for determining carbonation resistance

The relatively low concentration of CO_2 in the atmosphere (0.03–0.04%) makes carbonation a slow process in dense and chemically stable cementitious materials. This has led to the development of accelerated testing methods exposing the material to high CO_2 concentrations to induce carbonation. This is usually achieved through the use of climatic chambers where the exposure conditions such as temperature, relative humidity (RH) and concentration of CO_2 can be completely controlled. Table 12.1 shows a summary of the testing methods and protocols used for the assessment of the carbonation resistance of cementitious materials. It is important to note that carbonation resistance of alkali-activated materials has generally been tested using the same methods applied for Portland cement testing, but their applicability to these alternative binders still needs to be validated.

The reproducibility and repeatability of the results obtained by following different accelerated carbonation testing protocols has been strongly questioned (Sanjuán *et al*., 2003), and therefore comparison between carbonation results reported in different studies must be approached with care. It is evident that the accelerated carbonation conditions vary significantly depending on the protocol adopted, and in those cases where very high concentrations of CO_2 are used, it is important to consider the disruption suffered by the material, and to question the real meaning of the results in giving a good representation of a natural carbonation process. Accelerated carbonation results need then to be understood as an indicator of the potential durability of materials with comparable chemistry, when tested under similar exposure conditions.

The phenolphthalein method is widely used by the cement community to determine carbonation front; however, its applicability to the assessment of modern blended cements and alkali-activated materials is also questionable. This method is based on the changes in pH expected to occur in the specimens as a consequence of the CO_2 exposure. Considering the chemical differences between Portland cements and alkali-activated materials (i.e., the lack of portlandite ($Ca(OH)_2$) as a reaction product in most alkali-activated binders), changes in the pH of the pore solution can be easily registered using this method, instead of real decomposition via decalcification of the binding phases due to carbonation.

The effect of the different solvents (distilled water/ethanol) and concentrations used for the preparation of the phenolphthalein indicator in each of the carbonation testing methods described in Table 12.1 is largely unknown, with regard to the actual pH changes in the material. It is possible that this leads to different results in terms of measured carbonation depths, especially in alkali-activated

Table 12.1 Summary of accelerated test methods

Test	Sample preconditioning required	Indicator	Exposure conditions
BS EN 13295:2004	Specimens covered with a plastic film for 24 h, then demoulded and sealed again with a plastic film for 48 h, followed by curing of the specimens under water at 21 ± 2°C for 27 days. Afterwards the samples should be brought to an even moisture content, which is achieved by storing the samples at 21 ± 2°C and 60 ± 10 RH until constant weight, for a minimum of 14 days.	1 g of phenolphthalein dissolved in 70 mL of ethanol, diluted to 100 mL with distilled or deionised water	$[CO_2]$: 1%, *T*: 21 ± 2ºC RH: 60 ± 10%
RILEM CPC-18	Not specified	Solution of 1% phenolphthalein in 70% ethanol	$[CO_2]$: Not specified *T*: 20°C RH: 65%
Nordtest Method: NT Build 357	Specimens are stripped 1 day after casting, and cured in water at 20 ± 2ºC for 14 days, then cured in air at 50 ± 5% RH, 20 ± 2ºC until reaching a total of 28 days of curing	1 g phenolphthalein dissolved in 500 mL of distilled/ion exchanged water, and 500 mL ethanol	$[CO_2]$: 3%, *T*: Not specified RH: 55–65%
Portuguese Standard LNEC E391	Samples cured submerged in water for 14 days at 20 ± 2ºC, and stored in an enclosed environment at 50 ± 5% RH and 20 ± 2ºC until 28 days	0.1% of phenolphthalein in an alcoholic solution	$[CO_2]$: 5 ± 0.1% *T*: 23 ± 3ºC RH: 55–65%
French test method AFPC-AFREM (1997)	Specimens cured for 28 days are saturated with water prior to CO_2 exposure, and then oven dried at 40°C for 2 days.	0.1% of phenolphthalein in an alcoholic solution	$[CO_2]$: 50%, *T*: 20°C RH: 65%

materials, as a water-rich solution might promote the redissolution of dried pore solution remaining in the material after carbonation exposure, and reveal a fully alkaline surface, even though some chemical reaction with CO_2 has occurred. This is one limitation related to assessment of the susceptibility to carbonation of cementitious materials, especially alkali-activated binders, via accelerated carbonation testing. Consequently, the development and validation of testing protocols to estimate more accurately the long-term performance of these materials is required.

12.3 Factors controlling carbonation of cementitious materials

Carbonation of cements is controlled by the diffusivity and reactivity of the CO_2 within the bulk matrix (Fernández-Bertos *et al*., 2004), which is strongly dependent on the transport properties of the material, as well as the chemistry of the binding phases. Diffusivity of gaseous CO_2 is affected by the interconnectivity of the pore network and the carbonation exposure conditions, including CO_2 concentration, relative humidity and temperature (Houst and Wittmann, 1994; Fernández-Bertos *et al*., 2004). The reactivity of the CO_2 will depend on the CO_2 concentration, as well as the type of binder (Goñi *et al*., 2002), the gel maturity and pore solution chemistry (Fernández-Bertos *et al*., 2004), as this controls the nature and chemistry of the reaction products that will be present over the time of service, and consequently their susceptibility to react with CO_2.

In alkali-activated materials it could be expected that the diffusivity of CO_2 is controlled by the same variables as identified in conventional Portland cements, as this is a physically controlled mechanism that is mostly driven by the permeability of the material. However, the reactivity of CO_2 in these alternative binders strongly differs from what has been observed for Portland cements, as the chemistry and nature of reaction products forming is quite different, as will be discussed in the following sections.

12.4 Carbonation of alkali-activated materials

12.4.1 The role of exposure conditions

There are a limited number of published studies evaluating carbonation of alkali-activated materials, but there seems to be a general agreement that these materials are more susceptible to carbonation than conventional Portland cements, when tested under accelerated carbonation conditions, which is one of the major perceived limitations facing their adoption on an industrial scale.

Byfors *et al*. (1989) published one of the first studies of carbonation of alkali-activated materials, and identified that higher relative humidities (80%) promoted lower carbonation rates than identified in specimens carbonated at 50% relative humidity, and carbonation in F-concretes (plasticised alkali silicate-activated granulated blast furnace slag) is more intense when compared with OPC samples formulated to achieve comparable compressive strengths. Similar results were obtained by Bakharev *et al*. (2001), who observed a higher susceptibility to carbonation (associated with higher carbonation depths measured through phenolphthalein method) in concretes based on alkali-activated slag than in Portland cement concretes exposed to carbonated water (0.35 M solution of $NaHCO_3$).

In a later study, Deja (2002) identified comparable carbonation depths in alkali-activated slag mortars and concretes, and in reference samples based on Portland

cement, with increased compressive strengths at longer times of exposure to CO_2. These results were attributed to the refinement of the pore structure in both alkali-activated slag and Portland cement, associated with the precipitation of carbonates forming as the carbonation reaction progresses. It is important to note that the specimens were accelerated carbonated at a relative humidity of 90%, and in an atmosphere of 100% CO_2, and therefore the results of this particular study need to be interpreted with care when compared with natural exposure conditions. At very high relative humidity it is expected that the pores are fully saturated with moisture, and therefore, even using high CO_2 concentrations, the diffusivity of this gas through the pore network will be hindered, in both alkali-activated slag and Portland cement samples. This will reduce the likelihood of developing a carbonation process sufficiently representative to give a good indication of how these materials will perform under natural conditions during service.

Carbonation of cementitious materials is generally faster at intermediate relative humidity (50–70%), and decreases at higher and lower relative humidities (Papadakis *et al.*, 1991; Houst, 1996; Galan *et al.*, 2013). High humidity increases the fraction of pores filled with water, hindering the diffusion of gaseous CO_2, while at low humidity the pore network will not be sufficiently moist to promote the solvation and hydration of the carbon dioxide to form carbonic acid (Houst and Wittmann, 1994). Under intermediate moisture conditions, both reaction kinetics and diffusion of CO_2 are favoured, and therefore acceleration of the carbonation process is observed (Fernández-Bertos *et al.*, 2004; Galan *et al.*, 2013).

Bernal *et al.* (2014a) evaluated the effect of exposure conditions (relative humidity and CO_2 concentration) on the progress of accelerated carbonation of alkali-activated slag/metakaolin blended concretes, showing that the progress of carbonation is slightly higher when the test was conducted at 65% relative humidity, compared with specimens carbonated at relative humidities of 50% or 80%, consistent with that identified in conventional Portland cement; however, after longer periods of carbonation testing, the effect of the relative humidity became less pronounced. It is noted that in these alternative binders, the role of the relative humidity during accelerated carbonation testing goes far beyond the effect it can have in the saturation of the pore network and diffusivity of CO_2. This is related to a number of reasons, largely associated with the stability of the gel with respect to changes in humidity.

Alkali-activated slag binders can be more susceptible to shrinkage-related processes than Portland cement (Palacios and Puertas, 2007; Collins and Sanjayan, 2000, 2001), especially at early times of curing (Chi *et al.*, 2012), and the extent of shrinkage is strongly influenced by the nature and concentration of the alkaline activator (Melo Neto *et al.*, 2008). Dry conditions promote desiccation of the reaction products, especially in alkali-activated slag, leading to structural changes (Ismail *et al.*, 2013) and resulting in the superficial microcracking of the material, which facilitates the ingress of CO_2. Consequently, during the pre-conditioning of the specimens prior to accelerated carbonation testing, as required by the available standards and protocols shown in Table 12.1, it is likely that severe changes in the superficial permeability of the material take place as a result of drying shrinkage.

This can provide misleading indications regarding the mechanism of carbonation, compared to what can be experienced under natural carbonation conditions.

In both Portland cement (Castellote *et al*., 2009) and alkali-activated materials (Bernal *et al*., 2013), it has been identified that the concentration of CO_2 during accelerated carbonation testing plays a key role in inducing different structural changes in the binding products, and therefore, in the mechanism of accelerated carbonation. Changes in the pore solution of Portland cement carbonated specimens carbonated under different CO_2 concentrations and relative humidities have also been identified (Anstice *et al*., 2005). In alkali-activated cements, significant differences in the total porosity and capillary structure in these materials were observed as the CO_2 concentration of exposure increased from 1% to 3% (Bernal *et al*., 2014a). A recent study (Bernal *et al*., 2012) has demonstrated that the CO_2 concentration also affects the carbonation of the pore solution, as slight changes in temperature, relative humidity and CO_2 concentration lead to modification of phase equilibria in the system Na_2CO_3–$NaHCO_3$-CO_2-H_2O that can describe the carbonated pore solution of alkali-activated materials (Figure 12.1).

In alkali-activated binders it has been identified (Bernal *et al*., 2012, 2013) that under atmospheric CO_2 concentrations the formation of natron ($Na_2CO_3{\cdot}10H_2O$) is favoured; however, under accelerated carbonation testing conditions (CO_2 concentrations between 1% and 100%) the formation of nahcolite ($NaHCO_3$) prevails. Natron has a higher molar volume than nahcolite, meaning that under accelerated carbonation conditions nahcolite will fill much less space, and thus provide a greatly reduced degree of pore blockage in an alkali-activated binder than what could be expected under natural carbonation conditions. This, along with the differences in cracking due to sample conditioning as discussed above, indicates that the permeability developed by the material under natural carbonation conditions will differ from what is promoted under accelerated carbonation testing. Modifications of the carbonate/bicarbonate phase equilibrium favouring formation of bicarbonates (Figure 12.1) will lead to a more notable decrease in pH upon carbonation than would be observed in natural CO_2 environments, by as much as 2 pH units (Bernal *et al*., 2012). This will then render the pore solution environment in an accelerated test far more damaging to embedded steel reinforcing than is the case in actual service conditions.

12.4.2 The role of the binder composition

The mechanism of carbonation in alkali-activated materials is strongly dependent on the type of precursor used (slag or fly ash) (Bernal *et al*., 2013) and the nature and concentration of the activator used (Bernal *et al*., 2014c; Palacios and Puertas, 2006) as these parameters control the type of the reaction products formed.

Puertas *et al*. (2006) observed higher accelerated carbonation depths in slag-based mortars activated with sodium silicate than in sodium hydroxide activated specimens. This was mainly attributed to the differences in the composition and structure of the C-S-H product forming in each system. In the case of the silicate-activated slags the

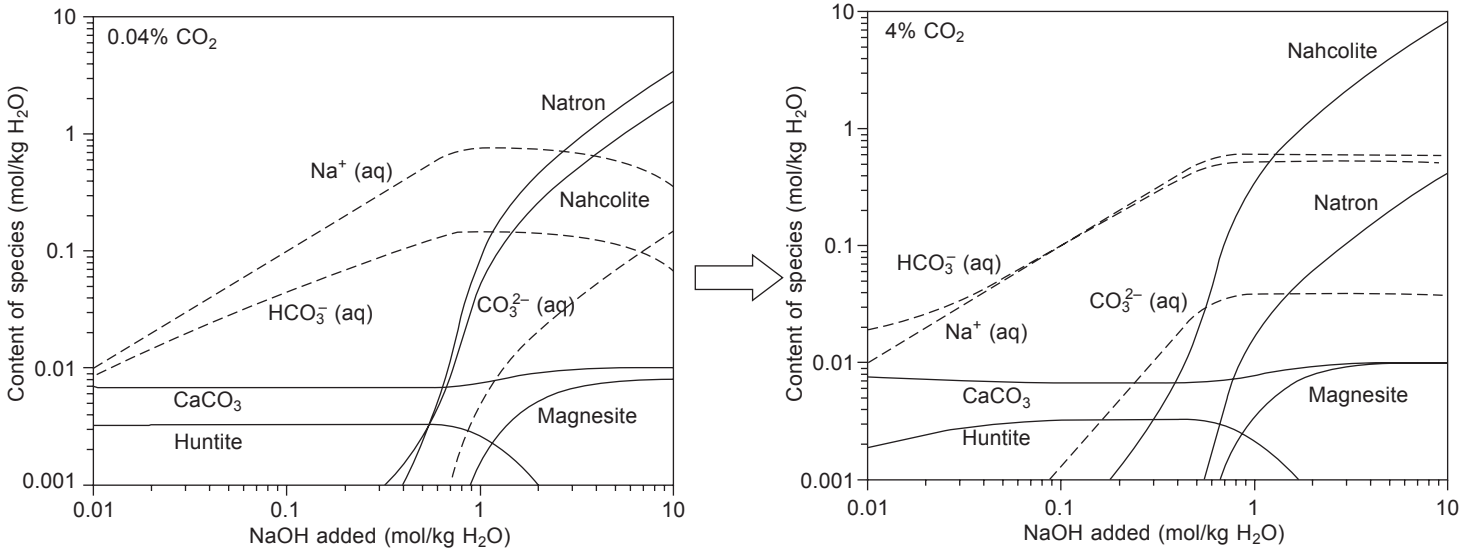

Figure 12.1 Differences in phase assemblages calculated from thermodynamic simulations of carbonation of NaOH solutions, as a function of NaOH concentration and CO_2 partial pressure. Data from Bernal *et al*. (2012).

C-S-H had a lower Ca/Si ratio (~0.8) than those formed when NaOH was used (Ca/Si ratio ~1.2). The higher Ca/Si ratio, along with the reduced silicate chain length observed in NaOH-activated slags, might favour the formation and precipitation of an increased amount of carbonate products to fill pore spaces when compared to silicate-activated slag products, and this could influence the diffusivity of CO_2 within the material. Natron and the calcium carbonate polymorphs calcite, vaterite and aragonite were identified as the main crystalline accelerated carbonation products of these silicate-activated slag binders (Palacios and Puertas, 2006).

Bernal *et al*. (2010) also determined the carbonation products forming in accelerated carbonated silicate-activated slags, but in that study calcite was the only calcium carbonate polymorph identified, along with trona ($Na_3(CO_3)(HCO_3)\cdot 2H_2O$). The differences in the carbonation products forming in these materials are mainly attributable to the exposure conditions used in each study. Specifically, the formation of trona will be favoured over natron with slight increments in the exposure temperature, independent of the CO_2 concentration of exposure (Bernal *et al*., 2012). The Mg-Ca carbonate huntite ($Mg_3Ca(CO_3)_4$) has also been observed as an accelerated carbonation product derived from the degradation of hydrotalcite (one of the secondary products in these binders) in the presence of high CO_2 concentrations (Bernal *et al*., 2013).

Most recently it was observed (Bernal *et al*., 2014b) that the MgO content of the slag influences the extension and the mechanism of carbonation of alkali-activated slags, so that an increased content of MgO in the slag promoted a significant reduction in the carbonation extent. This is associated with the formation of layered double hydroxides with a hydrotalcite-type structure as a secondary reaction product in systems with sufficient content of MgO (>5 wt.%) (Bernal *et al*., 2014b). Layered double hydroxides are materials that have the capacity to absorb CO_2 (León *et al*., 2010), and therefore it could be expected that a larger formation of this particular phase in these systems significantly contributes to enhancing the performance of alkali-activated slag binders when exposed to high CO_2 concentrations.

Prior to accelerated carbonation, silicate-activated slag pastes present a very cohesive and homogeneous structure as shown in Figure 12.2(a). In contrast, the carbonated paste (Figure 12.2(b)) exhibits a highly heterogeneous and porous structure. The surface of the carbonated pastes usually shows crystalline-like particles with dimensions of a few micrometres, accompanied by more irregular-shaped particles, identified as calcite. Chemical analysis of these pastes (Figure 12.2(c)) shows that the carbonation of the paste leads to the decalcification of the C-A-S-H type gel, along with the formation of a sodium-rich aluminosilicate-type product. These structural changes lead to the increased porosity and the reduced mechanical strength usually identified in accelerated carbonated silicate-activated slags.

Even though accelerated carbonation testing of alkali-activated slag materials is more damaging than is identified in Portland cement, it has been observed (Bernal *et al*., 2011) that an increased paste content in these concretes reduces the carbonation depth, so that the carbonation depths are comparable to those obtained in Portland cement concretes produced with similar mix designs. A similar trend has been identified in naturally carbonated silicate-activated slag concretes as shown

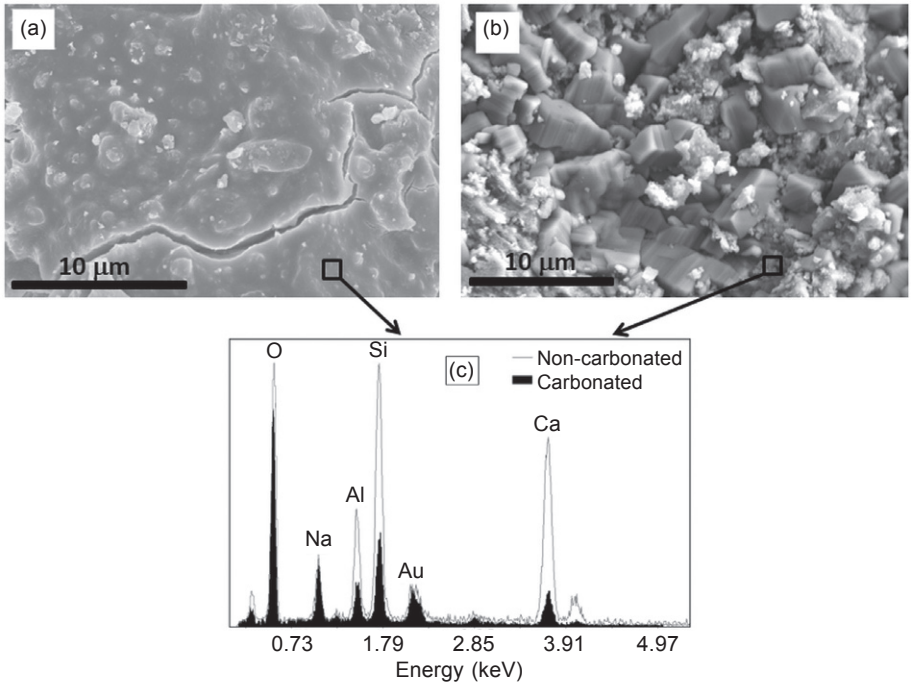

Figure 12.2 SEM images of silicate-activated slag binders before (a) and after (b) 1000 h exposure to 1% CO_2, and corresponding EDX data (c).

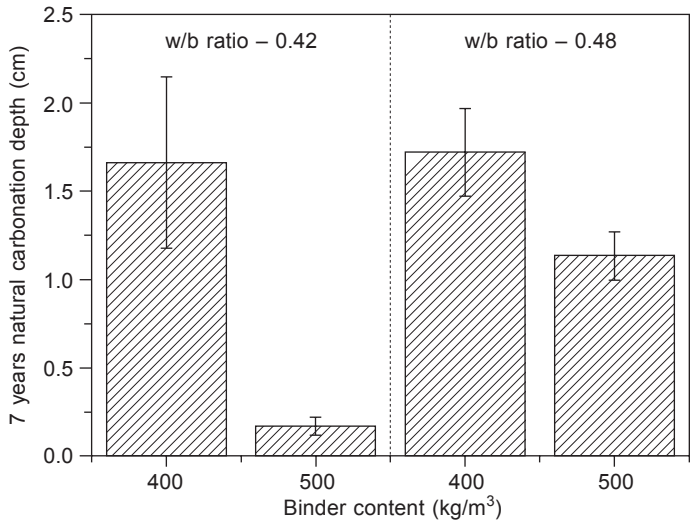

Figure 12.3 Natural carbonation depths of aged silicate-activated slag concretes, as a function of mix design. Error bars correspond to the value of one standard deviation among 16 measurements. Data from Bernal *et al*. (2014c).

in Figure 12.3, and this effect seems to be more significant when the concretes are formulated with lower water/binder ratios (Bernal *et al*., 2014c). The carbonation depth is also strongly dependent on the activation conditions, specifically the concentration of the activator, as higher concentration of alkalis in the pore solution is likely to attract a higher concentration of CO_2, favouring the formation of carbonic acid and carbonates, and therefore accelerating the carbonation reaction (Bernal *et al*., 2014c). This highlights that it is possible to tailor durability of alkali-activated materials to promote desired performance.

Accelerated carbonation testing methods are designed and intended to develop a better understanding about what is likely to occur when the material is in service. The study of de Castro *et al*. (2004) found a square-root dependence of carbonation rate on CO_2 concentration in Portland cement concretes when assuming diffusion control of carbonation, enabling comparison of the outcomes of the accelerated and natural carbonation testing for these concretes. Correlating accelerated and natural carbonation results of silicate-activated slag concretes using the de Castro equation, it has been demonstrated that the accelerated test is notably overpredicting the natural carbonation rate in these systems (Bernal *et al*., 2014c). The difference in the correlation between natural and accelerated carbonation between alkali-activated slag concretes and Portland cements has also been reported in Bernal *et al*. (2012), where a higher degree of aggressiveness of the accelerated test is observed in alkali-activated systems when the concentration of CO_2 increases above the natural concentration, compared with Portland cement concretes exposed under the same carbonation environment. This suggests that under accelerated carbonation testing conditions, if an alkali-activated concrete shows similar carbonation depths to a Portland cement concrete, it is likely that the durability of the alkali-activated material under natural carbonation conditions (and thus the service life) would be considerably greater.

Carbonation of alkali-activated fly ash, also referred to as fly ash geopolymers, has not been as broadly studied. Criado *et al*. (2005) identified the formation of nahcolite (sodium bicarbonate) in samples cured under atmospheric conditions, which was associated with the carbonation of the alkalis in the pore solution. This is consistent with a recent study (Bernal *et al*., 2013) assessing carbonation of fly ash geopolymers at different concentrations of CO_2 (1–5%). Formation of sodium carbonate heptahydrate ($Na_2CO_3{\cdot}7H_2O$) has been observed in young fly ash geopolymer specimens (1 day of curing) carbonated at 5% CO_2, which is an indication that carbonation in these systems promotes an internal CO_2 concentration gradient, associated with a more rapid drop in the internal relative humidity in the early stage of the CO_2 exposure, before a high CO_2 concentration is able to diffuse through the pore network to the binder. Structural changes in the geopolymer gel in carbonated specimens were not detected via ^{29}Si and ^{27}Al MAS NMR spectroscopy; however, carbonated samples presented a marked reduction in mechanical strength.

The partial substitution of slag for fly ash in alkali-activated binders promotes the formation of two distinctive binding products: a C-A-S-H gel formed through alkali silicate activation of slag, and an N-A-S-H gel (Puertas *et al*., 2000, Ismail *et al*., 2014). Under accelerated carbonation exposure, decalcification of the C-A-S-H

type gel is identified, the products of which coexist with an apparently unaltered N-A-S-H type gel resulting from the activation of fly ash, as well as various alkali and alkali-earth carbonate precipitates (Bernal *et al.*, 2013).

12.5 Remarks about accelerated carbonation testing of alkali-activated materials

The need to develop a standard methodology to assess carbonation performance of alkali-activated materials is evident. The availability of such a method is essential to develop a better understanding of the factors governing the mechanism of degradation of these materials. The information reported in the open literature must be interpreted considering that this is an indicator of the performance of materials produced with similar formulations and evaluated under comparable environmental conditions, as accelerated carbonation results of alkali-activated materials are strongly dependent on the carbonation testing environment parameters such as relative humidity, temperature and CO_2 concentration. It is not recommended to carry out accelerated carbonation testing of alkali-activated binders at CO_2 concentrations higher than 1% CO_2, and further work is required to determine accurate recommendations regarding other aspects of the testing procedure.

The relatively low natural carbonation rates identified in alkali-activated concretes suggest that these materials have a good resistance to carbonation during their service life, and accelerated carbonation tests are not replicating what is likely to take place in the long term. Changes in the carbonation reaction equilibria take place under accelerated carbonation conditions, especially in the interaction between CO_2 and pore solution, promoting poor performance results despite the low permeability and good mechanical strength identified in the specimens before accelerated carbonation testing. This highlights that further research in this area needs to be undertaken to determine how the testing conditions are affecting the outcomes of the tests conducted.

Little attention has been given to those factors that can be strongly affecting the performance of alkali-activated materials when assessed through accelerated carbonation tests, such as the effect of pre-conditioning of the specimens inducing desiccation of the hydrated products, carbonation shrinkage induced by decalcification of the binding products, and the chemistry of the pore solution. These factors can strongly influence how the phenolphthalein indicator might work, modifying the outcomes of tests. This suggests that further research in developing methods for measuring the progress of the carbonation front in alkali-activated materials needs to be conducted. Efforts in this area are being led and coordinated through the RILEM technical committee TC 247-DTA (Durability testing of alkali-activated materials).

References

Anstice, D. J., Page, C. L. and Page, M. M. 2005. The pore solution phase of carbonated cement pastes. *Cement and Concrete Research,* 35, 377–383.

Bakharev, T., Sanjayan, J. G. and Cheng, Y. B. 2001. Resistance of alkali-activated slag concrete to carbonation. *Cement and Concrete Research,* 31, 1277–1283.

Bernal, S. A. and Provis, J. L. 2014. Durability of alkali-activated materials: progress and perspectives. *Journal of American Ceramic Society,* 97, 997–1008.

Bernal, S. A., Mejía de Gutierrez, R., Rose, V. and Provis, J. L. 2010. Effect of silicate modulus and metakaolin incorporation on the carbonation of alkali silicate-activated slags. *Cement and Concrete Research,* 40, 898–907.

Bernal, S. A., Mejía de Gutierrez, R., Pedraza, A. L., Provis, J. L., Rodríguez, E. D. and Delvasto, S. 2011. Effect of binder content on the performance of alkali-activated slag concretes. *Cement and Concrete Research,* 41, 1–8.

Bernal, S. A., Provis, J. L., Brice, D. G., Kilcullen, A., Duxson, P. and Van Deventer, J. S. J. 2012. Accelerated carbonation testing of alkali-activated binders significantly underestimate the real service life: The role of the pore solution. *Cement and Concrete Research,* 42, 1317–1326.

Bernal, S. A., Provis, J. L., Walkley, B., San Nicolas, R., Gehman, J. D., Brice, D. G., Kilcullen, A., Duxson, P. and Van Deventer, J. S. J. 2013. Gel nanostructure in alkali-activated binders based on slag and fly ash, and effects of accelerated carbonation. *Cement and Concrete Research,* 53, 127–144.

Bernal, S. A., Provis, J. L., Mejía de Gutiérrez, R. and Van Deventer, J. S. J. 2014a. Accelerated carbonation testing of alkali-activated slag/metakaolin blended concretes: effect of exposure conditions. *Materials and Structures,* in press, DOI: 10.1617/s11527-014-0289-4.

Bernal, S. A., San Nicolas, R., Myers, R. J., Mejía de Gutiérrez, R., Puertas, F., Van Deventer, J. S. J. and Provis, J. L. 2014b. MgO content of slag controls phase evolution and structural changes induced by accelerated carbonation in alkali-activated binders. *Cement and Concrete Research,* 57, 33–43.

Bernal, S. A., San Nicolas, R., Provis, J. L., Mejía de Gutiérrez, R. and Van Deventer, J. S. J. 2014c. Natural carbonation of aged alkali-activated slag concretes. *Materials and Structures,* 47, 693–707.

Byfors, K., Klingstedt, G., Lehtonen, H. P. and Romben, L. 1989. Durability of concrete made with alkali-activated slag. In: Malhotra, V. M. (ed.), *3rd International Conference on Fly Ash, Silica Fume, Slag and Natural Pozzolans in Concrete*, ACI SP114. American Concrete Institute, 1429–1444.

Castellote, M., Fernandez, L., Andrade, C. and Alonso, C. 2009. Chemical changes and phase analysis of OPC pastes carbonated at different CO_2 concentrations. *Materials and Structures,* 42, 515–525.

Chi, M.-C., Chang, J.-J. and Huang, R. 2012. Strength and drying shrinkage of alkali-activated slag paste and mortar. *Advances in Civil Engineering,* 2012, 579732.

Collins, F. and Sanjayan, J. G. 2000. Cracking tendency of alkali-activated slag concrete subjected to restrained shrinkage. *Cement and Concrete Research,* 30, 791–798.

Collins, F. and Sanjayan, J. G. 2001. Microcracking and strength development of alkali activated slag concrete. *Cement and Concrete Composites,* 23, 345–352.

Criado, M., Palomo, A. and Fernández-Jiménez, A. 2005. Alkali activation of fly ashes. Part 1: Effect of curing conditions on the carbonation of the reaction products. *Fuel,* 84, 2048–2054.

De Castro, A., Ferreira, R., Lopes, A. M., Cacudo, O. and Carasek, H. 2004. Relationship between results of accelerated and natural carbonation in various concretes. In: Vázquez, E., Hendriks, C. and Janssen, G. (eds), *International RILEM Conference on the Use of Recycled Materials in Building and Structures*, Barcelona. RILEM Publications, 988–997.

Deja, J. 2002. Carbonation aspects of alkali activated slag mortars and concretes. *Silicates Industriels,* 67, 37–42.

Fernández-Bertos, M., Simons, S. J. R., Hills, C. D. and Carey, P. J. 2004. A review of accelerated carbonation technology in the treatment of cement-based materials and sequestration of CO_2. *Journal of Hazardous Materials,* B112, 193–205.

Galan, I., Andrade, C. and Castellote, M. 2013. Natural and accelerated CO_2 binding kinetics in cement paste at different relative humidities. *Cement and Concrete Research,* 49, 21–28.

Glasser, F. P., Marchand, J. and Samson, E. 2008. Durability of concrete – degradation phenomena involving detrimental chemical reactions. *Cement and Concrete Research,* 38, 226–246.

Goñi, S., Gaztañaga, M. T. and Guerrero, A. 2002. Role of cement type on carbonation attack. *Journal of Materials Research,* 17, 1834–1842.

Hobbs, D. W. 2001. Concrete deterioration: causes, diagnosis, and minimising risk. *International Materials Reviews,* 46, 117–144.

Houst, Y. F. 1996. The role of moisture in the carbonation of cementitious materials. *Internationale Zeitschrift für Bauinstandsetzen*, 2, 49–66.

Houst, Y. F. and Wittmann, F. H. 1994. Influence of porosity and water content on the diffusivity of CO_2 and O_2 through hydrated cement paste. *Cement and Concrete Research,* 24, 1165–1176.

Ismail, I., Bernal, S. A., Provis, J. L., Hamdan, S. and Van Deventer, J. S. J. 2013. Drying-induced changes in the structure of alkali-activated pastes. *Journal of Materials Science,* 48, 3566–3577.

Ismail, I., Bernal, S. A., Provis, J. L., San Nicolas, R., Hamdan, S. and Van Deventer, J. S. J. 2014. Modification of phase evolution in alkali-activated blast furnace slag by the incorporation of fly ash. *Cement and Concrete Composites,* 45, 125–135.

Johannesson, B. and Utgenannt, P. 2001. Microstructural changes caused by carbonation of cement mortar. *Cement and Concrete Research,* 31, 925–931.

León, M., Díaz, E., Bennici, S., Vega, A., Ordóñez, S. and Auroux, A. 2010. Adsorption of CO_2 on hydrotalcite-derived mixed oxides: sorption mechanisms and consequences for adsorption irreversibility. *Industrial and Engineering Chemistry Research,* 49, 3663–3671.

Melo Neto, A. A., Cincotto, M. A. and Repette, W. 2008. Drying and autogenous shrinkage of pastes and mortars with activated slag cement. *Cement and Concrete Research,* 38, 565–574.

Palacios, M. and Puertas, F. 2006. Effect of carbonation on alkali-activated slag paste. *Journal of the American Ceramic Society,* 89, 3211–3221.

Palacios, M. and Puertas, F. 2007. Effect of shrinkage-reducing admixtures on the properties of alkali-activated slag mortars and pastes. *Cement and Concrete Research,* 37, 691–702.

Papadakis, V. G., Vayenas, C. G. and Fardis, M. N. 1991. Experimental investigation and mathematical modeling of the concrete carbonation problem. *Chemical Engineering Science,* 46, 1333–1338.

Poonguzhali, A., Shaikh, H., Dayal, R. K. and Khatak, H. S. 2008. Degradation mechanism and life estimation of civil structures – A review. *Corrosion Reviews,* 26, 215–294.

Puertas, F., Martínez-Ramírez, S., Alonso, S. and Vázquez, E. 2000. Alkali-activated fly ash/slag cement: strength behaviour and hydration products. *Cement and Concrete Research,* 30, 1625–1632.

Puertas, F., Palacios, M. and Vázquez, T. 2006. Carbonation process of alkali-activated slag mortars. *Journal of Materials Science,* 41, 3071–3082.

Sanjuán, M. A., Andrade, C. and Cheyrezy, M. 2003. Concrete carbonation test in natural and accelerated conditions. *Advances in Cement Research,* 15, 171–180.

Shi, C., Krivenko, P. V. and Roy, D. M. 2006. *Alkali-Activated Cements and Concretes,* Abingdon, Taylor and Francis.

The corrosion behaviour of reinforced steel embedded in alkali-activated mortar

13

M. Criado
Instituto de Ciencia de Materiales de Madrid (CSIC), Madrid, Spain

13.1 Introduction

Reinforced concrete (RC) combines the good compression strength properties of concrete and the excellent mechanical strength properties of steel. Thus, RC materials can be used by designers, architects and civil engineers to meet high mechanical strength, fire resistance, durability, shape adaptability and low cost requirements (Grinda, 1995; Jiménez-Montoya *et al*., 1987). This explains why Portland cement has been the construction material *par excellence* for decades.

Corrosion of reinforcement steel is one of the main causes of the premature degradation of reinforced concrete structures. Steel rebars embedded in concrete are protected from corrosion by a thin oxide layer that is formed and maintained on their surfaces because of the highly alkaline environment of the surrounding concrete; with a pH usually in the range 12.5–13.5 (Bertolini *et al*., 2004; Page, 2007; Qiao and Qu, 2007).

However, with time, severe corrosion may occur in reinforced concrete structures (RCSs). Corrosion initiation in RCSs can be due to penetration of chloride ions or carbon dioxide (CO_2) to the steel surface. Chloride ions cause local destruction of the passive layer, leading to localized corrosion, while carbon dioxide reacts with the hydrated cement matrix to decrease the pH, leading to the loss of steel passivity and more generalized corrosion attack (Bertolini *et al*., 2004; Tommaselli *et al*., 2009). The steel corrosion occurs due to an electrochemical action, when metals of different nature are in electrical contact in the presence of water and oxygen. The process consists in the anodic dissolution of iron when the positively charged iron ions pass into the solution and the excess of negatively charged electrons goes to steel through the cathode, where they are absorbed by the electrolyte constituents to form hydroxyl ions. These in turn combine with the iron ions to form ferric hydroxide, which then converts to rust.

Apart from imposing the thermodynamic conditions required for self-renewal of the passivating layer, the concrete cover acts as a physical barrier to penetration of aggressive agents through its pores (Gónzalez *et al*., 1996; Gónzalez Fernández and Miranda Vidales, 2007). The less permeable and thicker the concrete cover, the longer will be the time needed for corrosion to appear and hence, the longer

Handbook of Alkali-activated Cements, Mortars and Concretes. http://dx.doi.org/10.1533/9781782422884.3.333

will be the service life of the RCS concerned (Tuutti, 1982). Figure 13.1 shows the Tuutti model that represents the different stages of the RCS corrosion initiation and propagation, thus governing the lifetime in service. The model represents the service life of a structure exposed to the action of carbonation and/or chloride ingress, in the absence of remedial interventions, as being the sum of two components:

- an initiation time, during which the cover zone of the concrete is penetrated by the aggressive agents until they reach sufficient concentration at the surface of the outermost steel bars to cause depassivation;
- a propagation time, during which the despassivated steel corrodes at a rate that eventually results in a limit stage being reached, usually identified by failure of serviceability associated with cracking or spalling of the concrete cover.

Corrosion of the steel bar damages the reinforced concrete structures in two ways. First, it reduces the cross-sectional area of steel bar. Second, it produces corrosion products with a larger volume than the steel itself. The volume increase induces the tensile stress in concrete, which results in cracking and eventual structural failure (Bertolini *et al.*, 2004; Poupard *et al.*, 2006; Bernal *et al.*, 2012).

An idea of the magnitude of the problem can be seen by the fact that losses attributed to RCS corrosion in Spain were of the order of 1.2×10^9 euros in 1995 (Grinda, 1995) and currently estimated direct and indirect costs of 3–4% of gross national product (GNP) in developed countries are connected to maintenance and repair operations (Bastidas *et al.*, 2012).

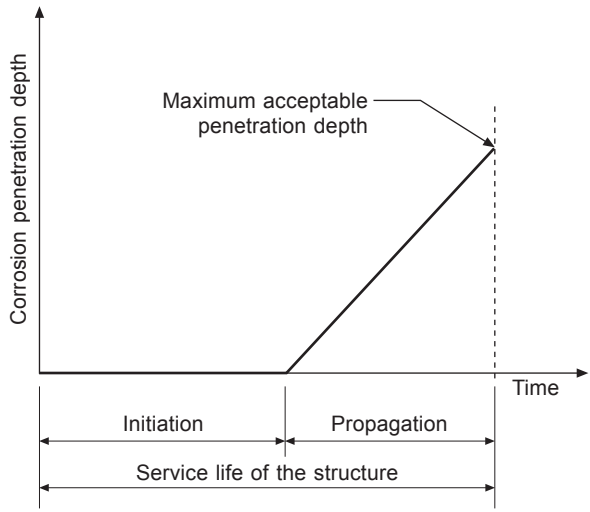

Figure 13.1 Service life model for reinforced concrete exposed in a corrosive environment.

13.2 Corrosion of reinforced alkali-activated concretes

13.2.1 Mechanisms for corrosion in reinforced concrete

For corrosion of steel in concrete to occur, the following conditions must all be satisfied: (a) the provision of an anode-cathode couple with at least part of the steel acting as an anode, (b) the maintenance of an electrical circuit (free-flowing ions), (c) the presence of moisture, and (d) the presence of oxygen (Gónzalez Fernández and Miranda Vidales, 2007).

There are two major processes that are coupled in corrosion attack on steels in concrete: carbonation reactions and pitting corrosion in the presence of chloride ions are shown in Figure 13.2. In carbonation, beginning at the surface of concrete and moving gradually towards the inner zones, the alkalinity of concrete may be neutralized by carbon dioxide from the atmosphere, so that the pH of the pore liquid of the concrete decreases to a value around 9 where the passive film is no longer stable. Chloride ions from the environment can penetrate into the concrete and reach the reinforcement; if their concentration at the surface of the reinforcement reaches a critical level, the protective layer may be locally destroyed (Bertolini *et al.*, 2004).

Carbonation of concrete leads to complete dissolution of the protective layer. Chlorides instead cause localized breakdown, unless they are present in very large amounts. Therefore:

- corrosion induced by carbonation can take place on the whole surface of steel in contact with carbonated concrete (general corrosion);

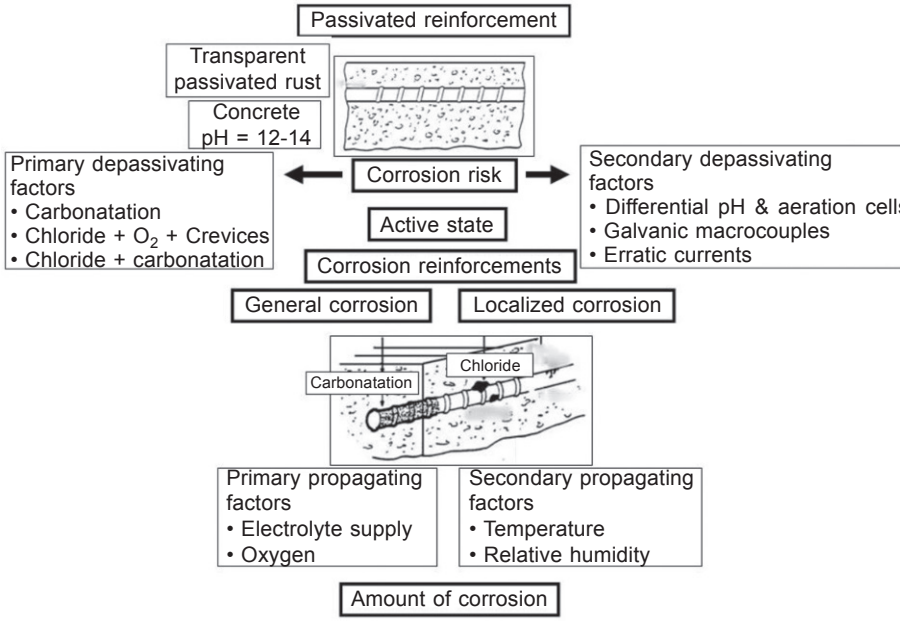

Figure 13.2 Schematic of reinforced concrete corrosion processes.

- corrosion by chlorides is localized (pitting corrosion), with penetrating attacks of limited area (pits) surrounded by non-corroded areas. Only when very high levels of chlorides are present (or the pH decreases) may the passive film be destroyed over wide areas of the reinforcement and the corrosion will be of a general nature.

13.2.2 Carbonation-induced corrosion

In moist environments, carbon dioxide present in the air forms an acid aqueous solution that can react with the hydrated cement paste and tends to neutralize the alkalinity of concrete (this process is known as carbonation).

The alkaline constituents of concrete are present in the pore liquid (mainly as sodium and potassium hydroxides) but also in the solid hydration products, e.g. $Ca(OH)_2$ or calcium silicate hydrate gel (C-S-H gel). Calcium hydroxide is the hydrate in the cement paste that reacts most readily with CO_2. The reaction that takes place in aqueous solution, can be written schematically as:

$$CO_2 + Ca(OH)_2 \xrightarrow{H_2O,\ NaOH} CaCO_3 + H_2O \quad (13.1)$$

Carbonation does not cause any damage to the concrete itself, although it may cause the concrete to shrink. Indeed, in the case of concrete obtained with Portland cement, it may even reduce the porosity and lead to an increase in strength (Chi *et al.*, 2002). However, carbonation has important effects on corrosion of embedded steel. The first consequence is that the pH of the pore solution drops from its normal values of pH 13–14, to values approaching neutrality. If chlorides are not present in concrete initially, the pore solution following carbonation is composed of almost pure water. This means that the steel in humid carbonated concrete corrodes as if it were in contact with water. A second consequence of carbonation is that chlorides bound in the form of calcium chloroaluminate hydrates and otherwise bound the hydrated phases may be liberated, making the pore solution more aggressive (Bertolini *et al.*, 2004).

The standard indicator used to determine carbonation depths in concretes is phenolphthalein (BS EN 14630:2006), which shows a colour change from pink/purple to colourless corresponding to the pH at which carbonate is converted to bicarbonate in solution. This pH also corresponds approximately to the pH at which steel is depassivated in pore solution environments, thus supporting its use as a measure of carbonation depth.

The rate of carbonation depends on both environmental factors (humidity, temperature, concentration of carbon dioxide) and factors related to the concrete (mainly its alkalinity and permeability).

- *Humidity*: The rate of diffusion of carbon dioxide within concrete is facilitated through the aerated pores. If the pore structures are dry, CO_2 diffuses inward readily but the carbonation reaction does not occur because of lack of water. If the pores are filled with water, the carbonation reaction rate is low because of slow CO_2 diffusion in water. Carbonation reaction only occurs when the pores are partially filled with water, which is normally the case at the surface of concrete (Bastidas *et al.*, 2012).

- *CO_2 concentration*: As the CO_2 content in the air increases, the carbonation rate increases.
- *Temperature*: An increase in temperature will raise the rate of carbonation.
- *Concrete composition*: The permeability of concrete has a remarkable influence on the diffusion of carbon dioxide and thus on the carbonation rate. A decrease in the water/cement ratio and an appropriate curing process, lead to a less porous cement matrix, which slows down the penetration of carbonation. Moreover, a higher alkalinity may decrease the carbonation rate.

13.2.3 Introduction of chloride ions

Chloride contamination of concrete is a frequent cause of corrosion of reinforcing steel. According to the European Standard EN 206-1 (2000), the maximum allowed chloride contents are 0.2–0.4% chloride ions by mass of binder for reinforced and 0.1–0.2% for prestressed concrete. Chloride ions can be introduced into concrete in two ways: contaminates in the mixing water, aggregates or admixtures, and exposure to deicing salts, seawater. Unlike the case of CO_2, the diffusion of Cl^- only takes place in the presence of water. If the concrete is dry, transport of Cl^- ions is impossible. If the concrete is semi-dry, there will be diffusion of chlorides from the surface to the inner concrete. With presence of cracks, the diffusion of Cl^- ion is enhanced. The diffusion resistance within the crack is compared to the diffusion resistance of the cover itself (Bastidas *et al.*, 2012).

Chlorides lead to a local breakdown of the protective oxide form on the reinforcement in alkaline concrete, so that a subsequent localized corrosion attack takes place (Zhang *et al.*, 2009). Areas no longer protected by the passive film act as anodes (active zones) with respect to the surrounding still passive areas where the cathodic reaction of oxygen reaction takes place. The morphology of the attack is that typical of pitting shown in Figure 13.3 (Bertolini *et al.*, 2004).

Once corrosion has initiated, a very aggressive environment will be produced

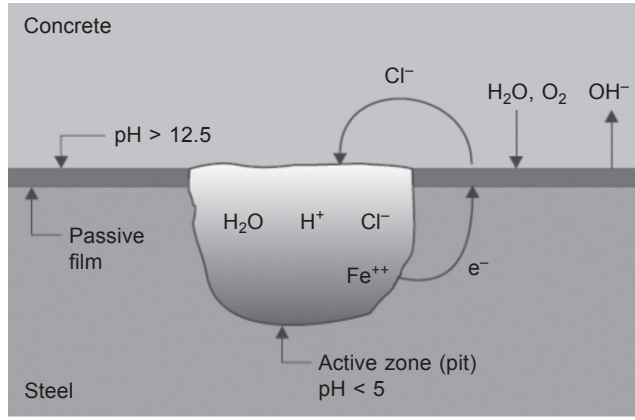

Figure 13.3 Schematic representation of pitting corrosion of steel in concrete

inside pits. In fact, current flowing from anodic areas to surrounding cathodic areas both increases the chloride content (chlorides, being negatively charged ions, migrate to the anodic region) and lowers the alkalinity (acidity is produced by hydrolysis of corrosion products inside pits). Conversely, the current strengthens the protective film on the passive surface since it tends to eliminate the chlorides while the cathodic reaction produces alkalinity. Consequently, both the anodic behaviour of active zones and the cathodic behaviour of passive zones are stabilized (Bertolini *et al*., 2004). In an attempt to overcome these problems, the construction sector is very interested in the development of new cement binder materials as an alternative to conventional Portland cement. In this respect, the most promising emerging approach is based on new raw materials suitable for alkaline activation, which originate from new binding materials generically known as alkaline cements.

13.3 Corrosion resistance in alkali-activated mortars

Considering that rebar corrosion is the main cause of reinforced concrete structure failure, the capacity of alkali-activated mortars to passivate steel rebars may be very important in guaranteeing the durability of RCS constructed using these new materials. Presumably, given its high alkalinity (even higher than OPC mortar) and concomitant position on the Pourbaix diagram, alkaline concrete should limit rebar corrosion to negligible levels. Several works (Miranda *et al*., 2005; Holloway and Sykes, 2005, Alcaide *et al*.. 2007; Bastidas *et al*., 2008; Aperador *et al*., 2009; Aperador Chaparro *et al*., 2012; Torres *et al*., 2010; Fernández-Jiménez *et al*., 2010; Criado *et al*., 2010, 2013) have demonstrated that alkali activated fly ash or slag mortars passivate steel reinforcement as rapidly and effectively as OPC mortars. They also show that the passivating capacity and permanence of the passive state, once reached, will depend on the nature and dosage of the binder, on the type of activator used, and on the environmental conditions.

13.3.1 Corrosion resistance in alkali-activated slag mortars

Regarding the corrosion of steel reinforcement embedded in slag mortar, Aperador *et al*. (2009) showed that the corrosion current density (i_{corr}) was higher in alkali-activated slag (AAS) than in the ordinary Portland cement (OPC) mortars exposed to accelerated carbonation environment. The slag was alkali-activated with a waterglass solution containing 5% Na_2O by weight of slag and a SiO_2/Na_2O ratio of 2.4. Cylindrical reinforced AAS and OPC specimens (76.2 mm diameter and 76.2 mm length) were prepared with a liquid/binder ratio of 0.4 to perform the experimental tests. Carbonation exposure was simulated by accelerated testing in a cabinet with 3% CO_2, 65% RH, and 25°C (AASA and OPCA specimens), and exposure in a laboratory environment with 0.03% CO_2, 65% RH, and 25°C (AASL and OPCL specimens).

Figure 13.4 shows E_{corr} values versus time for steel rebars embedded in AAS and OPC concrete in accelerated and laboratory exposure. In general, all the tested concretes showed similar behaviour with the exception of AASA. According to ASTM C 876-99 Standard (1999), the active potentials in the range from –0.2 V to –0.5 V vs. $Cu/CuSO_4$ up to 45 days observed for the AASA specimen indicate a 90% probability of corrosion. The AASL and OPCL concretes presented a 10% probability of corrosion after 45 days and 265 days of exposure in a laboratory environment, respectively.

Figure 13.5 shows R_p and i_{corr} values versus time for steel rebars embedded in carbonated and uncarbonated concretes. The AASA and AASL specimens showed the lowest R_p values: 4.65 kΩ cm^2 for AASA and 68.6 kΩ cm^2 for AASL after 45 days of experimentation. The OPCL and OPCA concretes showed the highest corrosion resistance after 80 days; with R_p values in the range from 640 to 1400 kΩ cm^2 (see Figure 13.5(a)). Nevertheless, the R_p value of the OPCA concrete dropped to 51 kΩ cm^2 after 265 days of experimentation, a behaviour that was attributed to the carbonation phenomenon. Figure 13.5(b) shows i_{corr} values, estimated from the R_p measurements using the Stern–Geary equation (Stern and Geary, 1957): $i_{corr} = B/R_p$, applying $\Delta E \pm 20$ mV at a scan rate of 0.16 mV s^{-1} and adopting a tentative value of 52 mV or 26 mV for the B constant for steel in the passive or active (corroding) state, respectively (Andrade and Alonso, 1996), versus time for steel rebars embedded in the two concretes. The AASA concrete showed the highest i_{corr}, with a value of 1.5 μA cm^{-2} after 45 days. The OPCL, OPCA and AASL specimens showed lower corrosion current densities of 0.02, 0.03 and 0.05 μA cm^{-2}, respectively. This behaviour is due to the fact that the carbonation rate is higher in AAS than in the respective OPC mortars, the calculated carbonation rate coefficients were 139 and 25 mm $(year)^{-1/2}$ for AAS and OPC, respectively, after 45 days of carbonation. It should be said that instead of the high aggressive environment tested (3% CO_2), the

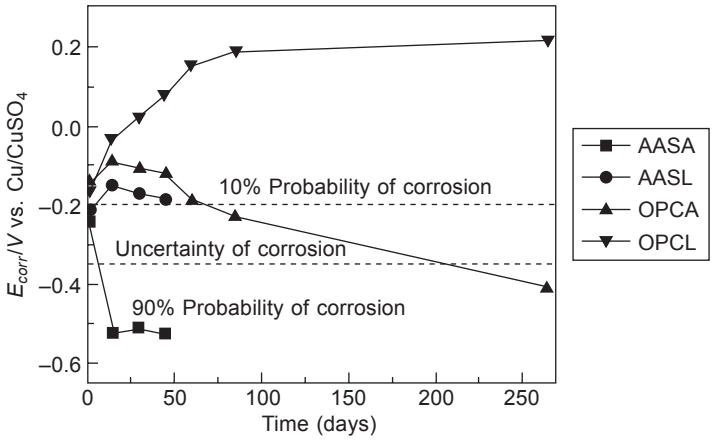

Figure 13.4 Corrosion potential (E_{corr}) versus time for steel rebars embedded in AAS and OPC concretes exposed to accelerated carbonation (AASA and OPSA) or a laboratory environment (AASL and OPCL).

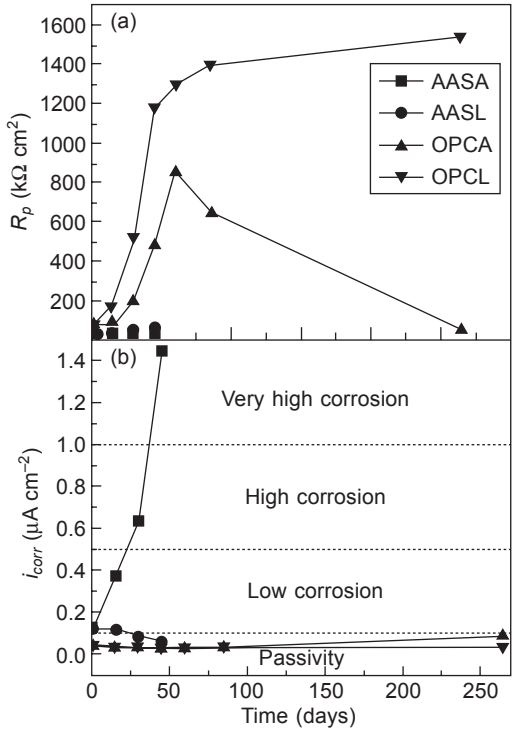

Figure 13.5 Polarization resistance (R_p) and corrosion current density (i_{corr}) versus time for steel embedded in AAS and OPC concretes with and without exposure to carbonation.

corrosion rate of steel embedded in both AAS and OPC concretes was very low. These findings are in good agreement and correlate with the reported E_{corr} results (Figure 13.4) and with those obtained from electrochemical impedance spectroscopy (EIS) data.

In other work (Aperador Chaparro *et al.*, 2012), the corrosion of reinforcing bars embedded in alkali-activated slag concrete subjected to chloride attack was studied. The slag was alkali-activated with a waterglass solution containing 5% Na_2O by weight of slag and a SiO_2/Na_2O ratio of 2.4. Cylindrical reinforced AAS and OPC specimens (76.2 mm diameter and 76.2 mm length) were prepared with a liquid/binder ratio of 0.4 to perform the experimental tests. Electrochemical measurements were carried out by immersing the specimens completely in 3.5% NaCl solution by weight of the slag.

Figure 13.6 shows the evolution of the rebar corrosion potential (E_{corr}) measured on AAS and OPC concrete exposed to 3.5% NaCl solution by weight of the slag, during 12 months immersion. For 0 months immersion (28 days of curing) the AAS and OPC concretes presented a 10% probability of corrosion, corresponding to a state of passivity based on the Pourbaix diagram. After 3 months of immersion the tested AAS and OPC concretes showed similar behaviour, the active potentials in the

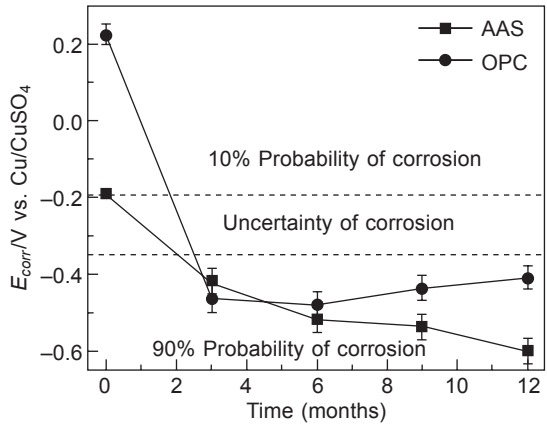

Figure 13.6 Corrosion potential (E_{corr}) vs. time for steel rebars embedded in AAS and OPC concretes immersed in a 3.5% NaCl solution by weight of the slag.

range from –0.2 to –0.6 V vs. Cu/CuSO$_4$, indicate a 90% probability of corrosion. E_{corr} evolutions of OPC concrete were constant after 6 months, and AAS specimens present the most negative corrosion potential values after 6 months.

Figures 13.7 and 13.8 show typical Nyquist plots for steel rebar embedded in AAS and OPC concrete exposed to a 3.5% NaCl solution, respectively. Measurements were performed at 0 (28 days of curing), 3, 6, 9 and 12 months. The electrical equivalent circuit (EEC) used to fit impedance data of steel embedded in both systems contains two distributed constant phase elements (CPE_1 and CPE_2) to consider the two relaxation time constants. The CPE_1–R_1 couple, which predominates at high frequencies, may be originated by the passive film and/or the dielectric properties of the concrete, while the CPE_2–R_2 couple, controlled at low frequencies, characterizes the corrosion process of the steel/concrete pore solution interface. R_Ω is the electrolyte resistance.

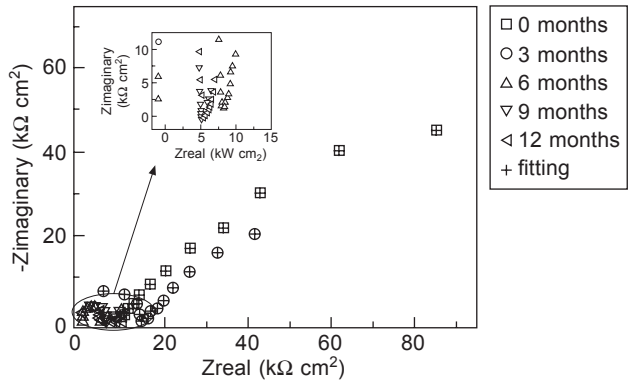

Figure 13.7 Nyquist plots for steel rebars embedded in AAS concrete exposed to 3.5% NaCl solution by weight of the slag.

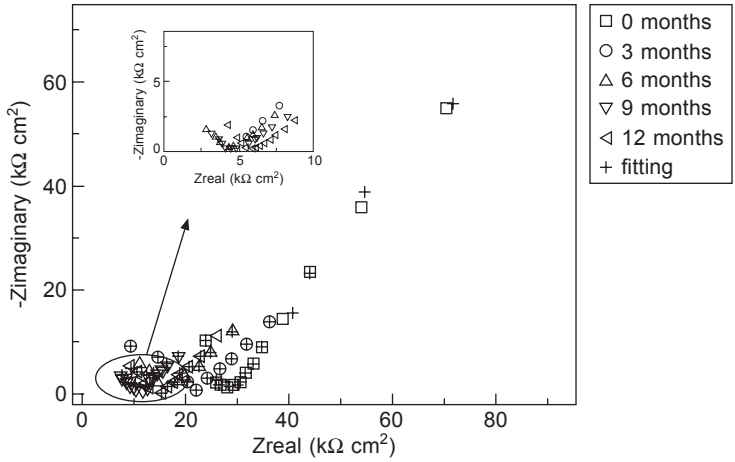

Figure 13.8 Nyquist plots after 108 days of experimentation for steel rebars embedded in OPC concrete exposed to 3.5 wt.% NaCl solution at 25ºC.

The high frequency process had a CPE_1 (Y_{P1}) for AAS in the range from 0.12×10^{-8} to 2.71×10^{-8} $Fcm^{-2}s^{-(1-\alpha 1)}$, for OPC in the range from 0.1×10^{-9} to 2.76×10^{-9} $Fcm^{-2}s^{-(1-\alpha 1)}$. At lower frequencies a capacitive behaviour was observed indicating a situation of passivity for AAS and OPC after 0 months, these value capacitive increments indicating the active condition of the rebar after 3 months of exposure for OPC concrete and 6 months for AAS specimens.

The impedance data could be interpreted in the following way. During the first 3 months of testing, the steel appears to show certain inertia to starting the corrosion process due to the passivation of the steel. The fitting process gives a R_2 value from 86 to 7 kΩ cm^2 for AAS concrete. The effect of chloride content in AAS concrete shows that R_2 decreases when the time of exposition increases. Accepting that the Stern–Geary equation can be applied, with an approximate B constant value of 26 mV, the resulting corrosion current density is low ($i_{corr} = 0.3$ μA cm^{-2}). For the OPC/steel system, the EIS results show a similar picture, with a depressed semicircle at high frequencies and a second semicircle also depressed at low frequencies, yielding an R_2 value from 58 to 7 kΩ cm^2. The estimated corrosion current density was low, of the order of 0.4 μA cm^{-2}. These results agree well with the DC data.

The passive state stability can also be affected by the inclusion of carbon fibres. A study was carried out to determine the effect of carbon fibre on the corrosion process of the embedded reinforcement in alkali-activated slag mortars (Alcaide *et al.*, 2007). The slag was alkali-activated with a waterglass solution containing 4% Na_2O by slag mass and a SiO_2/Na_2O ratio of 1.18. Alkali-activated slag (AAS) mortar prismatic specimens measuring $80 \times 55 \times 20$ mm were prepared with three different percentages of FC·(130 μm powder): 0, 1 and 3% and an activating solution/slag ratio of 0.56 (0.4% by binder weight of methylcellulose was added to facilitate fibre dispersion). After curing for seven days in water at 20°C, the specimens were

subjected to two types of attack: accelerated carbonation (with pure CO_2 and 70% RH) and partial immersion in a 0.5 M NaCl solution to simulate seawater.

Figure 13.9 shows the variation in corrosion rates over time in AAS mortars with alkaline cement and 0, 1 and 3% FC3 after exposure to accelerated carbonation. Note that during the process both the control and the sample with 1% FC3 were passivated while the 3% sample, surprisingly, was not. The maximum corrosion levels reached in the carbonation process came to 3.2 μA/cm^2, 4.8 μA/cm^2 and 5.7 μA/cm^2 for the control, 1% FC3 and 3% FC3, respectively. After around 50 days these values flattened at 0.7 μA/cm^2, 1.4 μA/cm^2, and 2.5 μA/cm^2, respectively. Consequently, as in Portland cement mortars, carbonation involves the development of the corrosion cell, whose kinetics are enhanced by the presence of carbonaceous materials (Garcés *et al.*, 2005).

Figure 13.10 shows the variation in corrosion rate in AAS mortars with 0, 1 and 3% FC3 partially submerged in seawater. Attention should first be drawn to

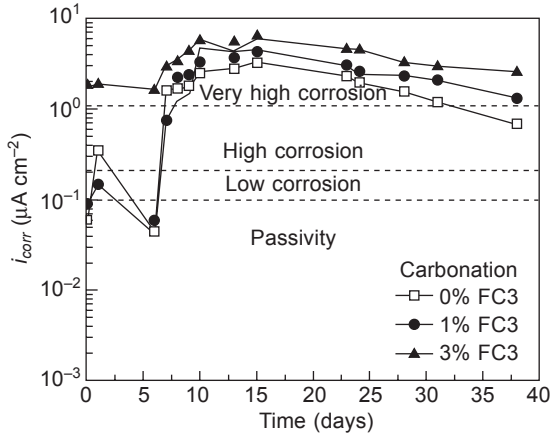

Figure 13.9 Evolution in corrosion rate in AAS mortars with different percentages of FC3, exposed to accelerated carbonation.

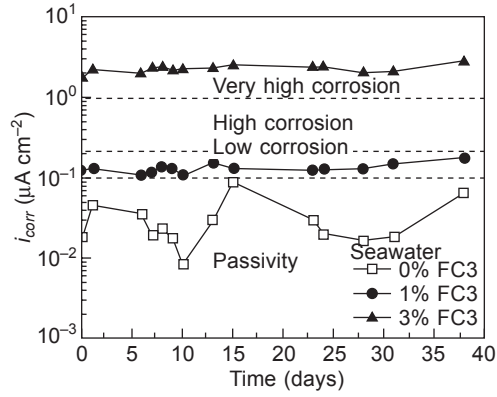

Figure 13.10 Evolution in corrosion rate in AAS mortars containing different percentages of FC3 and an activating solution/slag ratio of 0.56, partially submerged in seawater.

the behaviour of the control, with i_{corr} values of under 0.1 μA/cm^2 throughout: i.e., the steel maintains its passivity despite the aggressive environment. Moreover, the presence of 1% FC3 entailed no clear depassivation of the reinforcement, for the i_{corr} measurement stabilized at a mean value of around 0.1 μA/cm^2. The presence of 3% FC3, on the contrary, led to the development of the chloride-induced corrosion cell, with the mean i_{corr} value hovering around 2 μA/cm^2.

Taking into account that the addition of these conductive materials (FC3) in increasing proportions entails a progressive decline in concrete resistivity and that the carbonaceous materials are nobler than steel, they exert a galvanic couple effect on the metal, and the development of the corrosion cell is favoured. Therefore, the i_{corr} values recorded rise when the percentage of FC3 is increased.

13.3.2 Corrosion resistance in alkali-activated fly ash mortars

Regarding the corrosion of steel reinforcement embedded in fly ash mortar, Miranda *et al*. (2005) showed that the addition of 2% (by binder weight) of Cl^- in both fly ash and Portland cement mortars multiplies the corrosion rate by a factor of 100, approximately. The fly ash was activated with an 8 M NaOH solution and a 15% waterglass + 85% 12.5 M NaOH solution and Portland cement was hydrated with water. The sand/binder ratio employed was 2/1 and 3/1 for fly ash and cement mortars, respectively. Small prismatic specimens measuring 8 × 5.5 × 2 cm were prepared, which contained 0% and 2% (by binder weight) of Cl^- in the form of $CaCl_2$, added during the mixing operation.

Figures 13.11(a), 13.12(a) and 13.13(a) show the i_{corr} values, estimated from the R_p measurements taken, respectively, in the Portland cement mortar and the NaOH and 'water glass+ NaOH' activated fly ash mortars, at different specimen ages. The addition of chlorides multiplies the i_{corr} values by a factor of approximately 100 (from 0.01 to 1–10 μA/cm^2). Values of around 1 mA or higher are typical of active corrosion, whereas lower values correspond to passivated steel. Figures 13.11(b), 13.12(b) and 13.13(b) illustrate the changes recorded in the E_{corr} values. The findings are very similar for the three mortars in the passive state, ranging from –100 to –200 mV, and substantially more negative for fly ash than for cement mortars when passivation breaks down (around –600 mV compared with –300– –400 mV).

In the presence of the chloride anion, i_{corr} values appear to be higher in fly ash mortars than in Portland cement mortars. The explanation for this behaviour may very likely lie in the way the chloride dosage was defined with respect to cement weight. Contamination is higher in the former as a result of its proportionally higher cement content, with a sand/cement ratio of 2/1, compared with a ratio of 3/1 in the latter.

Bastidas *et al*. (2008) have studied the corrosion rates of steel rebars embedded in three types of fly ash mortars treated with three types of activators and with chloride additions using mainly electrochemical techniques. Mortar specimen composition is shown in Table 13.1. Experiments were performed on small prismatic specimens measuring 8 × 5.5 × 2 cm, which contained 0%, 0.2%, 0.4% and 2% chloride in

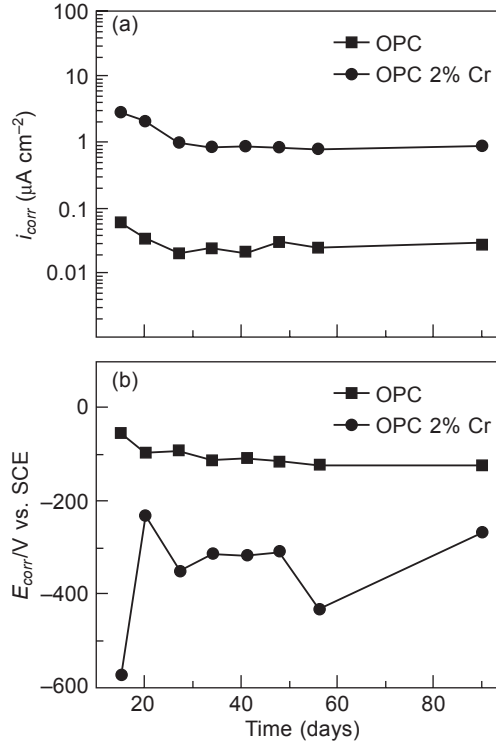

Figure 13.11 (a) i_{corr} and (b) E_{corr} values versus time, with steel electrodes symmetrically embedded in the Portland cement mortars without and with (2%) of Cl^- in relation to the cement weight.

relation to the binder material, in humidity cycles. Humidity cycles were performed to assess the chemical stability and thus the reliability of the fly ash matrix structure. The specimens were exposed to a cyclic environment: 94 days at 95% RH, point A, followed by 150 days in the laboratory atmosphere (dry environment, ≈30% RH), point B, and 220 days at 95% RH.

The corrosion current density (i_{corr}) value was estimated from the R_p measurements. Figure 13.14 shows the current density (i_{corr}) versus time for specimens in a cyclic RH experiment. It may be noted that: (i) the CR2 mortar remains in the passive state even with 2% Cl^- in the initial wet period and the intermediate dry period – an increase of two orders of magnitude in the i_{corr} may be observed with the rewetting of the CR2 mortar (see Figure 13.14(b)); and (ii) it is notable that with the CR3 mortar the humidity cycles also cause the loss of the passive state in the specimens with a low chloride content of 0.2 or 0.4% Cl^-.

The corrosion potential was monitored vs time as shown in Figure 13.15 for steel bars embedded in the CR1, CR2 and CR3 mortars with different chloride additions, using similar humidity cycles and the same specimens as in Figure 13.14: 100 days at 95% RH, point A, followed by 150 days in the laboratory atmosphere

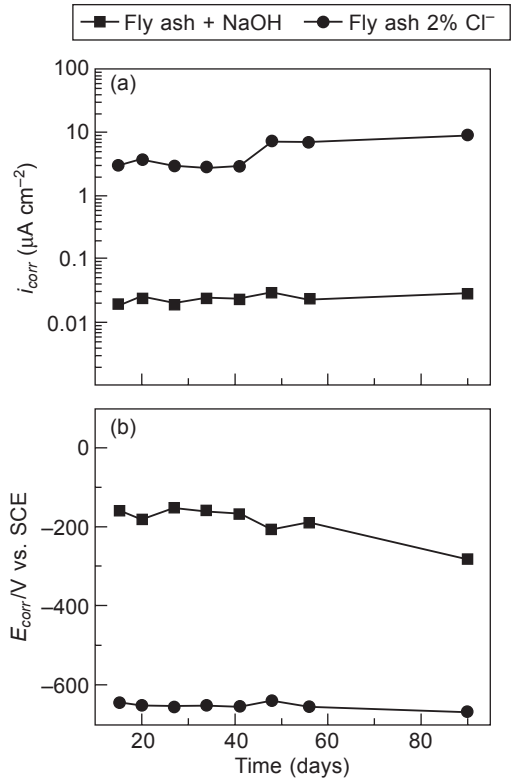

Figure 13.12 (a) i_{corr} and (b) E_{corr} values versus time, with steel electrodes symmetrically embedded in the fly ash + 8 M NaOH mortars without and with (2%) of Cl^- in relation to the cement weight.

(dry environment, ≈30% RH), point B, and 220 days at 95% RH. It may be noted that the CR2 mortar remains in the passive state even with 2% Cl^- in the initial wet period and the intermediate dry period. A decrease of 0.4 V (more active) may be observed in the E_{corr} when the specimens are moved from a dry environment to a wet environment (see Figures 13.15(b) and 13.15(c)). These changes in the E_{corr} may be attributed to the wetness of the pore network in the mortars. In contrast, the E_{corr} for passive electrodes is of the same order of magnitude in wet and dry conditions.

The carbon steel corrosion current density in the experimental conditions yielded similar values for the three tested materials: CR1, CR2 and CR3 mortars. Similar current density values were also obtained using polarization resistance and short duration galvanostatic pulses two orders of magnitude higher for activated electrodes than for passivated electrodes.

Absence of stability was observed in the passive state of specimens manufactured with CR3 mortar with 0.2 or 0.4% chloride additions and exposed to HR cycles (≈30%

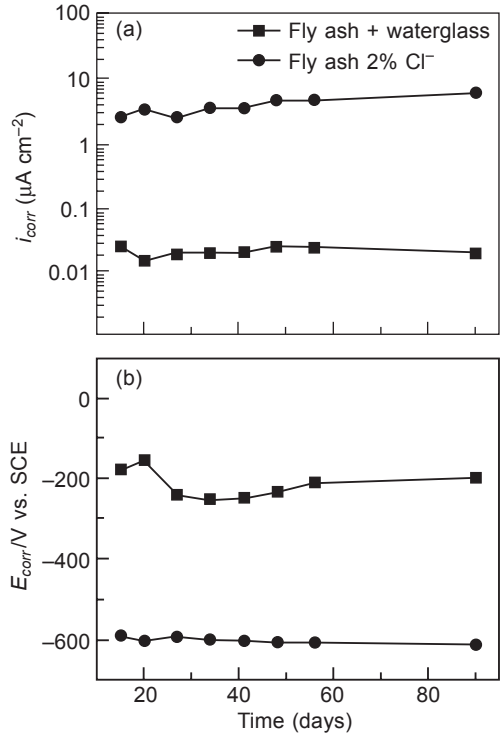

Figure 13.13 (a) i_{corr} and (b) E_{corr} values versus time, with steel electrodes symmetrically embedded in the fly ash + (15% waterglass + 85% 12.5 M NaOH) mortars without and with (2%) of Cl^- in relation to the cement weight.

Table 13.1 Mortar composition

Mortar matrix	Binder material	Sand/ binder ratio	Type of activator	Liquid/ binder ratio
CR1	Fly ash (FA)	2/1	15% waterglass, solution + 85% (12.5M NaOH) solution	0.5
CR2	70% FA + 30% OPC	2/1	15% waterglass, solution + 85% (12.5M NaOH) solution	0.5
CR3	58.8% FA + 25.2% OPC	2/1	8% pyramid, solid + 8% Na_2CO_3 solid water	0.4

RH and ≈95% RH). This behaviour was associated with a descending alkaline pH of the CR3 mortar compared to the pH of the CR1 and CR2 mortars and/or a high total porosity (Bastidas *et al.*, 2008).

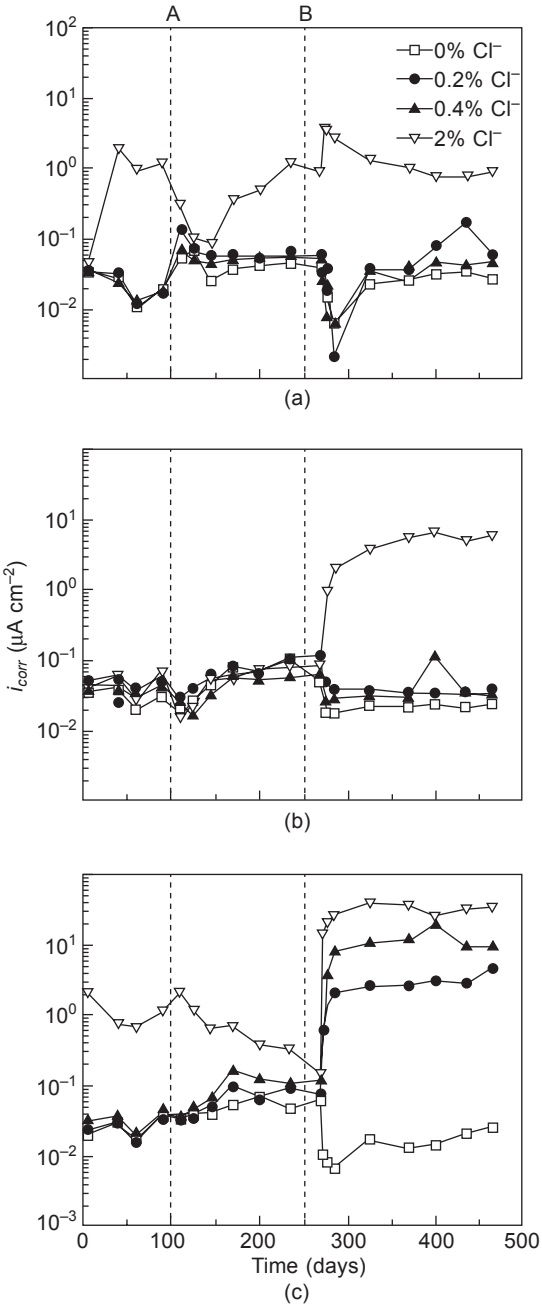

Figure 13.14 Corrosion current density (i_{corr}) versus time for carbon steel bars embedded in (a) CR1, (b) CR2 and (c) CR3 mortars for different chloride additions and in a cyclic environment: 100 days at a 95% RH, point A, followed by 150 days in the laboratory atmosphere (dry environment, ≈30% RH), point B, and 220 days at 95% RH.

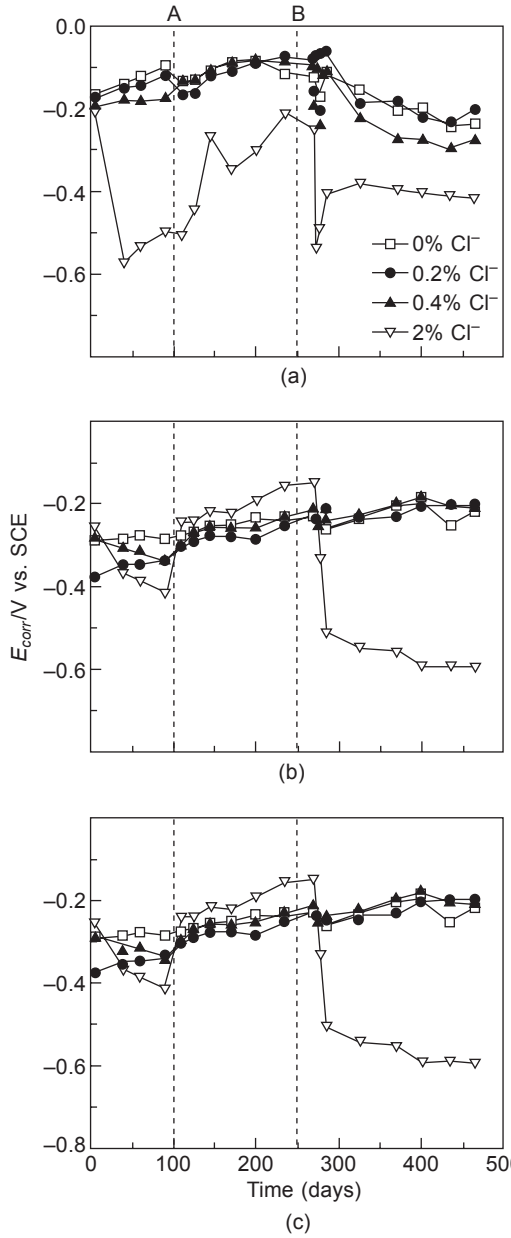

Figure 13.15 Corrosion potential (E_{corr}) versus time for carbon steel bars embedded in (a) CR1, (b) CR2 and (c) CR3 mortars for different chloride additions and in a cyclic environment: 100 days at 95% RH, point A, followed by 150 days in the laboratory atmosphere (dry environment, ≈30% RH), point B, and 220 days at 95% RH.

13.4 New palliative methods to prevent reinforced concrete corrosion: use of stainless steel reinforcements

Use of new corrosion prevention strategies is reported as a palliative method to increase the reinforced Portland or alkali-activated concrete service life, thus contributing to a reduction in the environmental impact and economic cost. Corrosion protection of steel rebar is often achieved by adding inhibitors in concrete, using high performance concrete mixtures, using protective coatings, using stainless steel and applying cathodic protection.

Currently, cathodic protection and replacement of C-steel rebars with stainless steel (SS) ones seem to be the most efficient solutions to guarantee the durability of reinforced concrete structures in highly aggressive environments (Pedeferri, 1996; Castro-Borges *et al.*, 2002). Stainless steels can be divided into four categories, based on their microstructure: ferritic, austenitic, martensitic and austenitic-ferritic (duplex). Only specific grades of austenic and duplex stainless steel are currently used in concrete, although also a ferritic type with 12% chromium has been proposed (Bertolini *et al.*, 2004). Austenitic SSs are characterized by much higher pitting potentials than C-steel, and much higher chloride content is required to depassivate them (Bertolini *et al.*, 1996; Gu *et al.*, 1996; Blanco *et al.*, 2006; Kouřil *et al.*, 2010). SSs have been used in a wide range of applications including highway bridges, car parks, coastal facilities and other structures where high chloride concentrations are expected (Baddoo, 2008). For an estimation of the service life of SS-reinforced structures, the critical chloride content is required, but this feature varies with service conditions including steel composition, surface finishing, metallurgical state (forming by hot or cold working, welding, etc.) and concrete chemistry (Angst *et al.*, 2009). For instance, the presence of scales on the steel surface can significantly impair the corrosion resistance, even for the most alloyed SSs (Kouřil *et al.*, 2010). Corrugated SS rebars exhibit poorer tensile properties and fatigue behaviour than those of plain rebars of the same compositions (Castro *et al.*, 2003). Corrugations formed by hot or cold working also have an important effect on the characteristics of the passive layer on SS rebars and, therefore, affect the corrosion behaviour of the SSs. On corrugated bars formed by cold working, the corrosion attack tends to be more localized and faster than on corrugated bars obtained by hot working (Paredes *et al.*, 2012).

SS composition has a paramount influence on the resistance to localized corrosion. Pitting resistance equivalent number (PREN) has been introduced in order to establish a ranking of resistance to pitting corrosion. This parameter is defined as %Cr + 3.3%Mo + 30%N and is used to assess the resistance to chloride-induced corrosion in acid and in neutral solutions (Herbsleb, 1982). However, its validity in alkaline environments such as concrete is still under discussion. Bertolini *et al.* (1996) observed that in alkaline solutions molybdenum has a lower influence on localized corrosion than in acid and neutral environments, while, in the same media, nickel is also maintained to contribute to SS corrosion resistance. Other studies (Bertolini

and Gastaldi, 2011) have demonstrated that both in alkaline solution and in concrete a high content of manganese or a high ferritic phase percentage in SSs have caused a significant decrease in the alloy corrosion resistance.

Although in the long term the choice of SS may be a more cost-effective alternative to cathodic protection, the high initial costs of SS have often limited its use. In order to decrease the initial cost of the structure, two possible ways have been studied, based on selective use of SS bars, i.e. limited to the more vulnerable parts of the structures, or on reduction in the cost of SS raw materials. As far as the latter choice is concerned, it must be stressed that nickel is subject to considerable price fluctuations due to stock market factors which have also induced the doubling of nickel price (Bertolini and Gastaldi, 2011). So, new austenitic SSs have been developed, where the nickel content has been partially substituted by other elements. In particular, N has been added because it is a strong austenite stabilizer and a solid solution strengthener (Milititsky *et al.*, 2008; Simmons, 2006). It also has a positive effect on pitting corrosion resistance (Baba *et al.*, 2002). Mn is also used because it is effective in increasing both the solubility of N in liquid steel and the fraction of austenite formed during solidification. The use of a new low nickel (Low-Ni) SS may even involve a saving of about 15–20% compared to conventional AISI 304 SS.

Low-Ni austenitic SSs exhibit attractive properties that are comparable to those of traditional austenitic SSs, such as good corrosion resistance, high strength and ductility levels and reduced tendency to SS sensitization (Di Schino *et al.*, 2002). Previous studies (García-Alonso *et al.*, 2007a,b) have shown that in sound OPC chloride-free mortar, the corrosion rate of C-steel is similar to that of traditional and Low-Ni austenitic SSs, while in the presence of chlorides it is at least 10 times higher than that of these SSs under similar conditions. Furthermore, Low-Ni SSs have a very similar corrosion behaviour to that of AISI 304 in solutions simulating both carbonated and uncarbonated chloride-contaminated concrete (Bautista *et al.*, 2006).

In light of these results, recent works have been carried out to study the corrosion behaviour of a new type of austenitic SS, with a low nickel content (Low-Ni) SS embedded in alkali-activated fly ash (AAFA) with different chloride additions (Criado *et al.*, 2011) and in carbonated AAFA and OPC mortars, partially immersed in distilled water containing increasing sodium chloride amounts, from 0.4 M saturation (Monticelli *et al.*, 2014).

The former work (Criado *et al.*, 2011) into the corrosion behaviour of a new type of austenitic SS embedded in AAFA mortar with different chloride additions and exposed to a ≈95% RH has demonstrated that Low-Ni SSs have a good corrosion behaviour, again quite comparable to that of AISI 304 SS. In these fly ash mortars, Low-Ni SSs exhibited i_{corr} values of the order of 0.001–0.01 μA cm^{-2} in the presence of chlorides, indicating the permanence of the passive state. Austenitic Low-Ni, AISI 304 SS and the reference C-steel were used as reinforcements. Their chemical composition is shown in Table 13.2. The content of nickel for Low-Ni SS is half the percentage for AISI 304 SS. The fly ash was activated with an 8 M NaOH solution (AAFA1 mortar) and a 15% waterglass + 85% 10 M NaOH solution (AAFA2 mortar). The sand/binder ratio employed was 2/1 and the liquid/solid ratio was 0.45. Small

Table 13.2 Chemical composition (% by weight[a]) of the tested austenitic Low-Ni SS, austenitic AISI 304 SS and carbon steel

Material	C	Si	Mn	P	S	Cr	Ni	Mo	Cu	N
Low-Ni	0.082	0.48	7.26	0.027	0.001	16.56	4.32	0.07	0.13	0.075
AISI 304	0.049	0.32	1.75	0.028	0.001	18.20	8.13	0.22	0.21	0.059
C-steel	0.45	0.22	0.72	<0.01	0.022	0.13	0.13	–	0.18	–

[a] The balance was Fe.

prismatic specimens measuring 8 × 5.5 × 2 cm were prepared, which contained 0%, 0.4% and 2% of Cl^- (with respect to binder weight) in the form of NaCl, and were added to fly ash.

Figures 13.16–13.19 show E_{corr} and i_{corr} values, estimated from the R_p measurements, versus time for (a) Low-Ni SS, (b) AISI 304 SS and (c) carbon steel rebar embedded in mortars AAFA1 and AAFA2, respectively, with different chloride additions (0, 0.4% and 2%). These figures showed a certain similarity between the corrosion behaviour of Low-Ni SS, AISI 304 SS and the carbon steel rebar in the absence of chlorides. These steels exhibited E_{corr} values around –100 to –200 mV vs SCE and i_{corr} values of the order of 0.01 μA cm^{-2}.

According to the results, the Low-Ni SS and AISI 304 SS embedded in mortar AAFA1 with 0.4% and 2% chlorides (Figure 13.16) showed E_{corr} values hundreds of millivolts higher (more noble) than the carbon steel rebar (≈ –500 mV vs. SCE). In contrast, the addition of 0.4% chloride did not cause a breakdown of passivity for the carbon steel rebar embedded in mortar AAFA2 (see Figure 13.17). The breakdown of passivity depends on the material characteristics to allow the diffusion of chlorides through its porous canal network (Batis *et al.*, 2005). A possible explanation for this behaviour was that the addition of a small amount of waterglass (15%) to the activating solution prompts the precipitation of a dense and compact reaction product (Fernández-Jiménez *et al.*, 2006), leading to a system with a slightly lower porosity (see Figure 13.20), through a blocking and pore refinement process. Therefore, a lower porosity implies a greater difficulty in the mobility of chloride ions to the steel surface.

The evolution of i_{corr} over time (Figures 13.18 and 13.19) showed differences in the i_{corr} value of around two or three orders of magnitude in the specimens with 0.4% and 2% chlorides (with these chloride additions, carbon steel had lost its passivity and it corroded at high corrosion rates, i_{corr} = 1–10 μA cm^{-2}, except in mortar AAFA2 with chlorides additions of 0.4%, see Figure 13.19), while the SSs, including the new Low-Ni SS, still exhibited i_{corr} values of the order of 0.001–0.01 μA cm^{-2}.

Therefore, the new Low-Ni SS does not present significant changes in E_{corr} and i_{corr} values, thus indicating the permanence of the passive state. The effect caused by the reduced Ni-content is almost balanced by the beneficial effect of other additives such as manganese or nitrogen, present in higher concentration than in AISI 304 SS. In this study and in the literature (García-Alonso *et al.*, 2007a,b), the influence

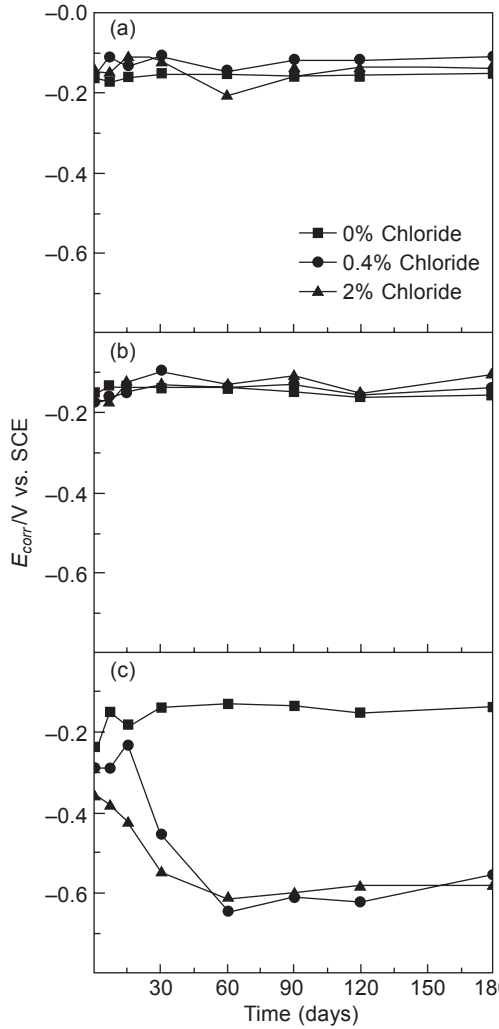

Figure 13.16 Corrosion potential (E_{corr}) versus time for (a) Low-Ni SS, (b) AISI 304 SS and (c) carbon steel rebar embedded in mortar AAFA1 for different chloride additions and exposed to a ≈95% RH.

of the metal base composition on the corrosion process has proved not to be a very important factor, and the Low-Ni SS embedded in the AAFA1 and AAFA2 chloride-polluted mortars has a good durability.

Corrosion behaviour of a low nickel austenitic SS in carbonated chloride-polluted alkali-activated fly ash mortar also demonstrated the very good performance of this new SS, which has a slightly lower pitting resistance than the more expensive AISI 304 SS (Monticelli *et al.*, 2014). The reinforcements used in this study were also austenitic Low-Ni, AISI 304 SS and the reference C-steel (their chemical composition

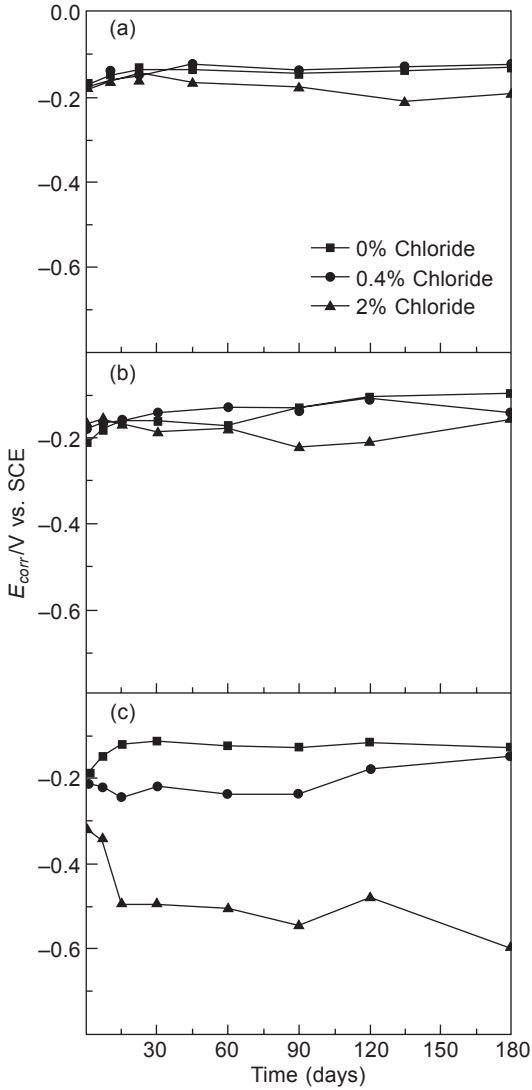

Figure 13.17 Corrosion potential (E_{corr}) versus time for (a) Low-Ni SS, (b) AISI 304 SS and (c) carbon steel rebar embedded in mortar AAFA2 for different chloride additions and exposed to a ≈95% RH.

was shown in Table 13.2). The fly ash was activated with an 8 M NaOH solution (AAFA1 mortar) and a 15% waterglass + 85% 10 M NaOH solution (AAFA2 mortar) and Portland cement was hydrated with water. The sand/fly ash and sand/cement ratio employed was 2 and 3, respectively. In all mortar types the liquid/binder ratio was 0.6 favouring carbonation. Prismatic mortar specimens, with dimensions of 8 × 5.5 × 2 cm were prepared. The AAFA and OPC mortars underwent hardening,

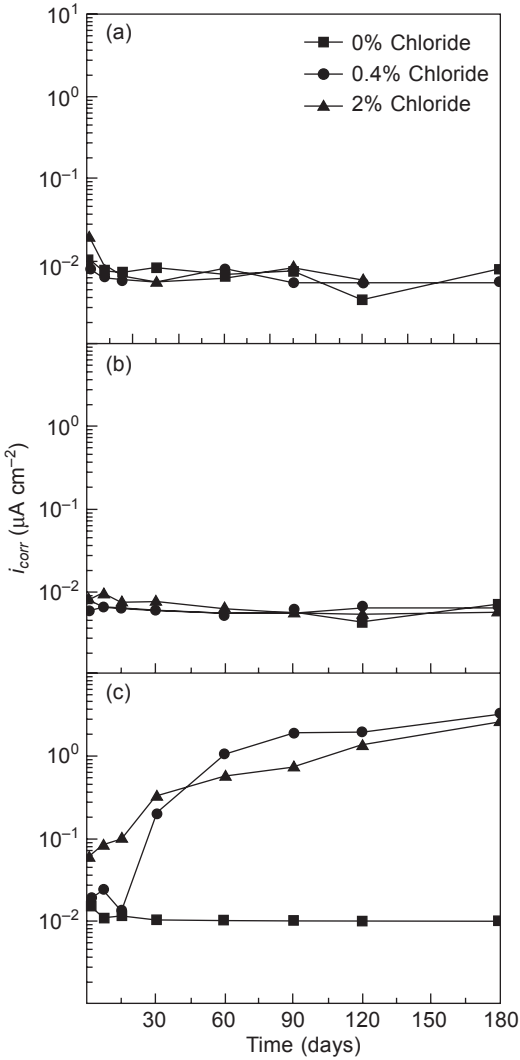

Figure 13.18 Corrosion current density (i_{corr}) versus time estimated from the R_p measurements for (a) Low-Ni SS, (b) AISI 304 SS and (c) carbon steel rebar embedded in mortar AAFA1 for different chloride additions and exposed to a ≈95% RH.

carbonation steps and partial immersion in water containing increasing chloride additions, according to the scheme reported in Table 13.3.

Figures 13.21 and 13.22 and Table 13.4 report anodic polarization curves recorded on Low-Ni SS and AISI 304 SS rebars embedded in carbonated mortars exposed to chloride solutions for 650 days exhibiting the highest and the lowest R_p value in each SS/mortar system. Low-Ni SS bars with high R_p values (mainly higher than 10^8 Ω cm^2, Figure 13.21(a)) exhibited passive corrosion conditions with i_{corr} values around

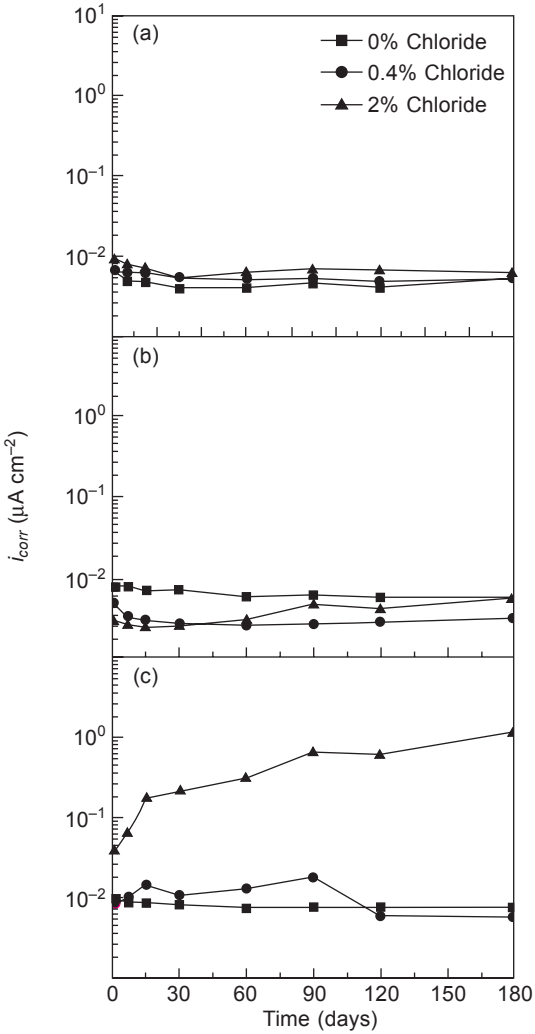

Figure 13.19 Corrosion current density (i_{corr}) versus time estimated from the R_p measurements for (a) Low-Ni SS, (b) AISI 304 SS and (c) carbon steel rebar embedded in mortar AAFA2 for different chloride additions and exposed to a ≈95% RH.

3–5 × 10^{-9} A cm^{-2} (as evaluated by the Tafel method) and E_{corr} values nobler or equal to –0.20 V (Table 13.4). Among these rebars, those exposed to AAFA mortars exhibited E_{pit} values clearly detectable by a sharp anodic current increase, occurring at +0.10 V in AAFA1 and +0.14 V in AAFA2 (Table 13.4). In OPC anodic currents increased rather continuously over three orders of magnitude. So, in this mortar E_{pit} was assigned to the potential at which an anodic current density of 1 × 10^{-7} A cm^{-2} was exceeded (+0.09 V_{SCE}). Table 13.4 shows that E_{pit} values increased in the order: OPC ≤ AAFA1 < AAFA2.

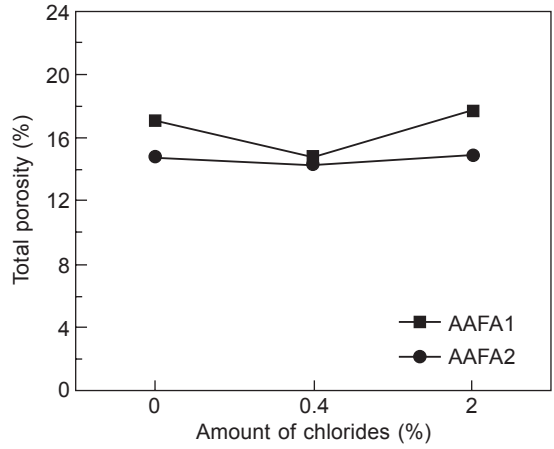

Figure 13.20 Total porosity results for mortars AAFA1 and AAFA2 after 90 days of ageing.

Table 13.3 Hardening (steps I and II), carbonation (III) and exposure steps for reinforced mortar specimens. During step IV C-steel reinforced slabs were immersed in 0.2 M chloride solutions

Steps	AAFA mortars	OPC mortars
I	20 h at 85°C, 100% RH	20 h at room temperature, 100% RH
II	28 days at the laboratory atmosphere	
III	60 days at room temperature, 65% RH, P_{CO_2} = 1 atm	
IV	650 days of partial immersion in NaCl solutions of increasing concentrations, starting from 0.4 M up to saturation (150 days in 0.2 M NaCl solution, for C-steel).	

Source: Criado *et al.*, 2012.

The Low-Ni SS bars with the lowest R_p values (from about 10^5 to 10^6 Ω cm^2, Figure 13.21(b)) showed polarization curves had shifted to higher currents with i_{corr} between 4×10^{-8} and 2×10^{-7} A cm^{-2}. Even if these i_{corr} values are rather low, they are around 1–2 orders of magnitude higher than those measured from the curves in Figure 13.21(a). Moreover, they are the result of a localized corrosion attack in progress, thus they may correspond to significant local penetration rates. Under these conditions, E_{corr} values of –0.4 V or more negative were measured. Table 13.4 shows that on low R_p rebars the potentials at which new pits form (E_{pit}) are only 40–80 mV lower than those obtained on the high R_p rebars (Figure 13.21(a)) and again increase according to the sequence: OPC < AAFA1 < AAFA2. These findings suggest that the potential of new pit formation is scarcely dependent on the pre-existence of a localized corrosion attack on the metal. It also only slightly depends on the mortar

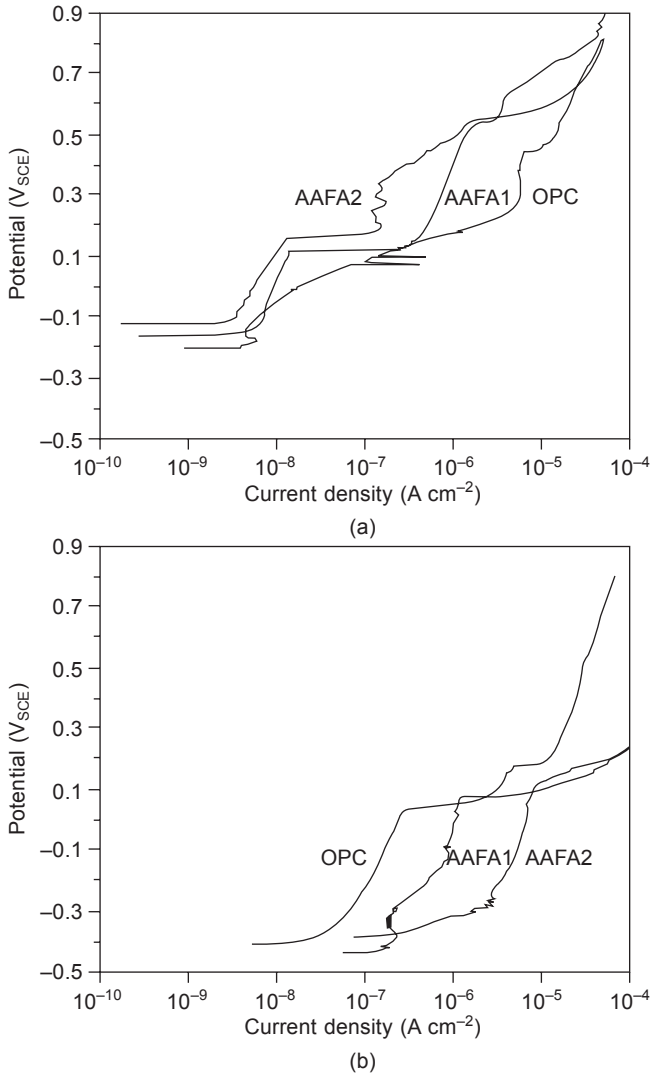

Figure 13.21 Anodic polarization curves recorded on Low-Ni SS rebars embedded in carbonated mortars and exposed to chloride solutions for 650 days: (a) high R_p values; (b) low R_p values.

type, with AAFA mortars exhibiting a somewhat higher protection against new pit formation.

Figures 13.22(a) and 13.22(b) show the polarization curves obtained on AISI 304 bars with the highest ($> 1 \times 10^8$ Ω cm^2) and the lowest (OPC: 1.2×10^6 Ω cm^2; AAFA1: 5.9×10^6 Ω cm^2; AAFA2: 3.8×10^7 Ω cm^2) R_p values, respectively. From Figure 13.22(a), i_{corr} values around 4–5 $\times 10^{-9}$ A cm^{-2} are evaluated, with E_{corr} of –0.12 V or nobler. In Figure 13.22(b), unaltered i_{corr} values are found for rebars

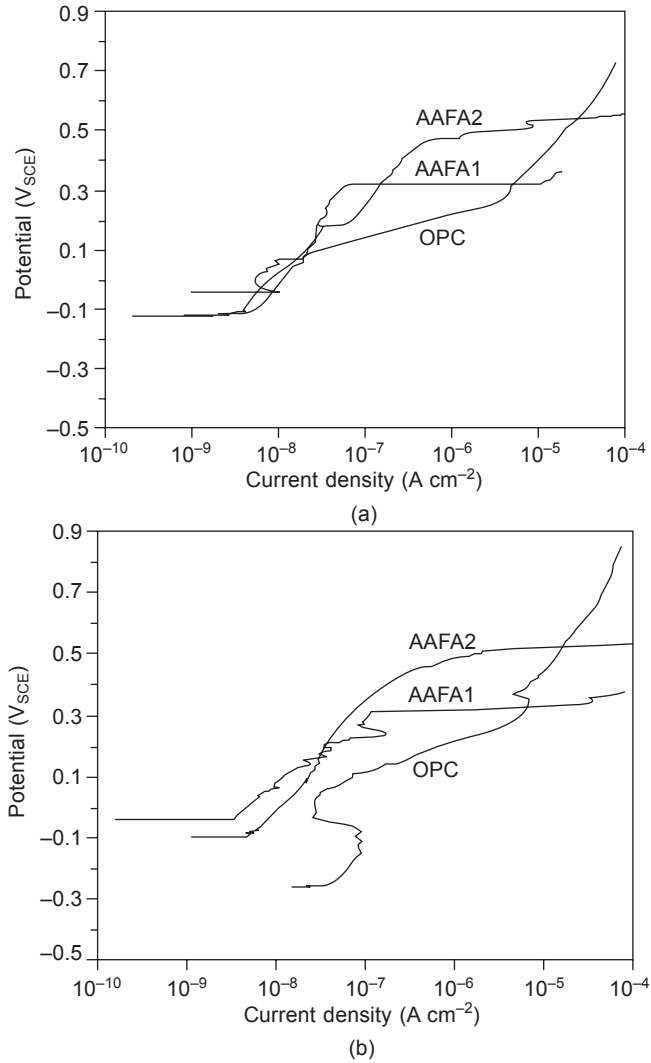

Figure 13.22 Anodic polarization curves recorded on AISI 304 SS rebars embedded in carbonated mortars and exposed to chloride solutions for 650 days: (a) high R_p values; (b) low R_p values.

in AAFA mortars, characterized by the lowest, but still rather high, R_p values (5.9×10^6 and 3.8×10^7 Ω cm^2). These R_p values indicate the persistence of passive corrosion conditions, as also suggested by the nobler corresponding E_{corr} (–0.04 and –0.10 V). Instead, the AISI 304 SS rebar exposed to OPC (with R_p of 1.2×10^6 Ω cm^2) shows an i_{corr} value of one order of magnitude higher (3.6×10^{-8} A cm^{-2}) and slightly more active E_{corr} values (–0.26 V, Table 13.4). The comparison of Figures 13.22(a) and 13.22(b) evidences that E_{pit} values of AISI 304 are almost independent

Table 13.4 E_{corr}, i_{corr} and E_{pit} values obtained from anodic polarization curves recorded on Low-Ni and AISI 304 SSs in mortars after 650 days of exposure to chloride solutions

SS	AAFA1				AAFA2				OPC			
	R_p (Ω cm^2)	E_{corr} (V_{SCE})	i_{corr} (A cm^{-2})	E_{pit} (V_{SCE})	R_p (Ω cm^2)	E_{corr} (V_{SCE})	i_{corr} (A cm^{-2})	E_{pit} (V_{SCE})	R_p (Ω cm^2)	E_{corr} (V_{SCE})	i_{corr} (A cm^{-2})	E_{pit} (V_{SCE})
Low-nickel	7.0×10^7	–0.16	5×10^{-9}	+0.10	2.4×10^8	–0.12	3×10^{-9}	+0.14	1.1×10^8	–0.20	5×10^{-9}	+0.09
	1.7×10^5	–0.44	1.3×10^{-7}	+0.05	9.3×10^4	–0.39	2.2×10^{-7}	+0.10	1.0×10^6	–0.41	3.6×10^{-8}	+0.01
AISI 304	3.2×10^8	–0.12	4×10^{-9}	+0.31	3.9×10^8	–0.12	5×10^{-9}	+0.47	1.6×10^8	–0.05	5×10^{-9}	+0.14
	5.9×10^6	–0.04	4×10^{-9}	+0.29	3.8×10^7	–0.10	5×10^{-9}	+0.50	1.2×10^6	–0.26	3.6×10^{-8}	+0.11

Note: The parameters reported refer to the bars exhibiting the highest and the lowest R_p values, in each SS/mortar system. The corresponding R_p values are also reported.

of i_{corr}, as also found for Low-Ni SS, and vary significantly with the mortar type. In both figures they increase according to the following order: OPC (+0.11/+0.14 V) < AAFA1 (+0.29/+0.31 V) < AAFA2 (+0.47/+0.50 V). These tests suggest that SSs, and particularly AISI 304, have a higher pitting resistance in AAFA than OPC mortars. In the latter mortar, both the slightly higher chloride content and the presence of more significant inhibiting bicarbonate/carbonate concentrations may contribute to this effect.

With the aim to actually assess the risk of pitting attack on SSs in the studied systems under the severe corrosion conditions investigated, at the end of the exposure to chloride solutions all the slabs were broken and the fraction of rebars showing localized corrosion (among those not affected by electrochemical polarization) was evaluated. The fraction of rebars which showed localized attack in each SS/mortar system is reported in Table 13.5. The last column shows the percentage of rebars of each SS suffering localized attack in all mortars, while the last row reports the percentage of all SS rebars exhibiting localized attack in each mortar type. Table 13.5 evidences that AISI 304 is more resistant to pitting (only 11% of rebars suffering localized attack), but the cheaper Low-Ni exhibits an acceptable performance (pits or stains on 28% of rebars). Moreover, even if some caution is necessary, given the limited number of rebars tested, Table 13.5 indicates that the protectiveness against pitting corrosion offered by OPC mortar to both SSs is lower than that offered by AAFA mortars, where only 17% of all the rebars underwent localized attack.

Table 13.5 Fraction of rebars with pits and stains in each SS/mortar system. Aggregated results are also presented

SS type	Mortars			
	AAFA1	AAFA2	OPC	All mortars
	Fraction of rebars with localized attack			
Low-Ni	1/6	2/6	2/6	0.28
AISI 304	1/6	0/6	1/6	0.11
Both SSs	0.17	0.17	0.25	

13.5 New palliative methods to prevent reinforced concrete corrosion: use of corrosion inhibitors

Corrosion inhibitors may be a good alternative to other protection methods or classical repair methods due to their lower cost and easy application. Corrosion inhibitors can prolong either the initiation period (raising the chloride threshold value or reducing chloride penetration) or the propagation period (reducing the overall corrosion rate) (Broomfield, 1999; Bertolini *et al.*, 2004; Raupach *et al.*, 2007; Söylev and Richardson, 2008). Corrosion inhibitors can be classified in different ways: according to their application methods, according to their mechanism of protection, or their content.

The main application methods for corrosion inhibitors are:

- added to fresh concrete as an admixture
- applied on the hardened concrete surface, so-called penetrating corrosion inhibitor (also migrating corrosion inhibitor and surface-applied corrosion inhibitor).

The inhibitors can also:

- be added to repair mortars, or
- be used as a surface treatment on the reinforcement bars before concreting.

According to the different mechanisms of protection, corrosion inhibitors may be anodic, cathodic or mixed.

- Anodic inhibitors act on the dissolution of the steel and they reduce the corrosion rate by an increase in the corrosion potential of the steel. The most commonly used anodic inhibitor is calcium nitrite ($Ca(NO_2)_2$). Sodium nitrite, sodium benzoate and sodium chromate have also been used.
- Cathodic inhibitors act on the oxygen reaction on the steel surface and they reduce the corrosion rate by a decrease in corrosion potential. The most commonly used cathodic inhibitors are sodium hydroxide and sodium carbonate, which are supposed to increase the pH near the steel, and reduce the oxygen transport by covering the steel surface. Phosphates, silicates and polyphosphates are also used.
- Mixed inhibitors act on both anodic and cathodic sites and they reduce the corrosion rate without a significant change in the corrosion potential, generally by surface adsorption over the surface of the steel in contact with the inhibitor and consequently forming a thin protective layer. In mixed type inhibitors, material with the hydrophobic group that has polar groups such as N, S, OH is effective. Organic polymer compounds such as amine and aminoalcohol (AMA) are also used.

Corrosion inhibitors have been used successfully in steel pipelines, tanks, etc., for many decades. Their use in concrete, however, is more recent and more limited. Early studies are focused on the use of corrosion inhibitors as additives for the concrete mix, showing the most effective to be calcium nitrite ($Ca(NO_2)_2$) (Berke and Rosenberg, 1989; Söylev and Richarson, 2008) due to its oxidant properties and its ability to heal defects in the passive layer on steel. However, nitrites are considered to be toxic substances (Hellawell, 1988), and there is growing interest to develop environmentally friendly substances that can act as corrosion inhibitors. Several studies have been conducted to evaluate the effectiveness of chemical admixtures in inhibiting reinforcement corrosion (Elsener, 2001; Troconis de Rincón *et al*., 2002; Ngala *et al*., 2002, 2003; Dhouibi *et al*., 2003; Muralidharan *et al*., 2004; Al-Mehthel *et al*., 2009). These studies have concentrated on calcium nitrite, sodium monofluorophosphate, zincates, citrates, etc. In recent years, corrosion inhibitors have included blends based on organic compounds which penetrate the concrete cover to reach the rebars in structures in service (Jamil *et al*., 2004, 2005).

Previous papers have reported studies to evaluate the inhibitive action of several organic compounds on the corrosion of carbon steel in a synthetic solution simulating the pore chemistry of a carbonated concrete and in a carbonated OPC concrete

(Trabanelli *et al*., 2002, 2005). In synthetic solution, benzoate (BEN), its amino-derivates (2-aminobenzoate (2AMB) or *N*-phenyl-2-aminobenzoate (PhAMB)), and dicarboxylates are able to form a long-lasting film on the steel surface. Their efficiency improves with time. Among the additives tested as inhibitors in carbonated concrete, only BEN and 2AMB exhibit inhibition efficiency (IE) on rebar corrosion. In the presence of 2AMB an IE of around 60% is measured after 400 days of exposure. Sodium salts of the aminobenzoic acids (2AMB and 3AMB) have proved to act as anodic inhibitors to reduce both critical passivation and passive currents on the steel and to maintain the free corrosion potential of steel in the passive region. On the other hand, in alkaline synthetic solutions containing chlorides, disodium β-glycerol phosphate (GPH) forms an impervious surface film on the steel which hinders the onset of localized attack. Results obtained after six months of exposure to chloride-polluted mortars reveal a 90% IE with GPH (Monticelli *et al*., 2000). Finally, tests have been performed in a synthetic solution to verify whether the simultaneous use of GPH and 2AMB is compatible and whether their addition can efficiently hinder the corrosion attack in the presence of both chlorides and carbonation (Monticelli *et al*., 2011). The concentration of these two substances has been varied to determine the lowest concentration necessary to reduce corrosion to an acceptable level. The results suggest that a mixture of 0.05 M GPH and 0.05 M 2AMB ensures a high IE (above 93%) in 100 h of testing.

Therefore, as 3AMB acts as anodic inhibitor able to reduce both critical passivating and passive currents on steel under carbonation conditions, while GPH and PhAMB form a film on steel which inhibits pitting corrosion in chloride polluted concrete, mixtures of GPH with 3AMB, and GPH with PhAMB have been tested as corrosion inhibitors (Criado *et al*., 2012), in both a synthetic solution (simulating the mortar pore chemistry in the presence of chlorides and carbonation) and in carbonated OPC and FA mortars partially immersed in an aqueous solution containing 1% (by binder weight) chlorides.

The fly ash was activated with an 8 M NaOH solution (FAA mortar) and a 15% waterglass + 85% 10 M NaOH solution (FAB mortar) and Portland cement was hydrated with water. The sand/FAA or FAB and sand/OPC ratios used in the mortars were 2 and 3, respectively. In all mortars types the liquid/binder ratio was 0.6 favouring carbonation. Prismatic mortar specimens, with dimensions of $8 \times 5.5 \times 2$ cm were prepared. The mortar slabs were subjected to the following procedure: (i) a hardening step involving 28 days ageing in laboratory atmosphere conditions at room temperature; (ii) a carbonation step involving 60 days exposure in a carbonation chamber at 65% RH, $\approx$1 atm pressure of CO_2 and room temperature; and (iii) a step of 150 days partial immersion (2 cm depth) in 1% (by binder weight) chloride solution, both in the absence and the presence of the tested inhibitors. The chloride/binder ratio was 0.01 and in the presence of the inhibiting mixtures the following ratios were ensured: [GPH]:[3AMB]:[Cl^-] was 1:1:4 (0.05 M GPH with 0.05 M 3AMB, Mix A), and [GPH]:[PhAMB]:[Cl^-] was 1:saturated:4 (0.05 M GPH with saturated PhAMB, Mix B).

Figure 13.23 shows the Nyquist plots recorded for carbonated OPC, FAA and FAB mortars after 150 days of partial immersion in a chloride solution (1% chlorides in

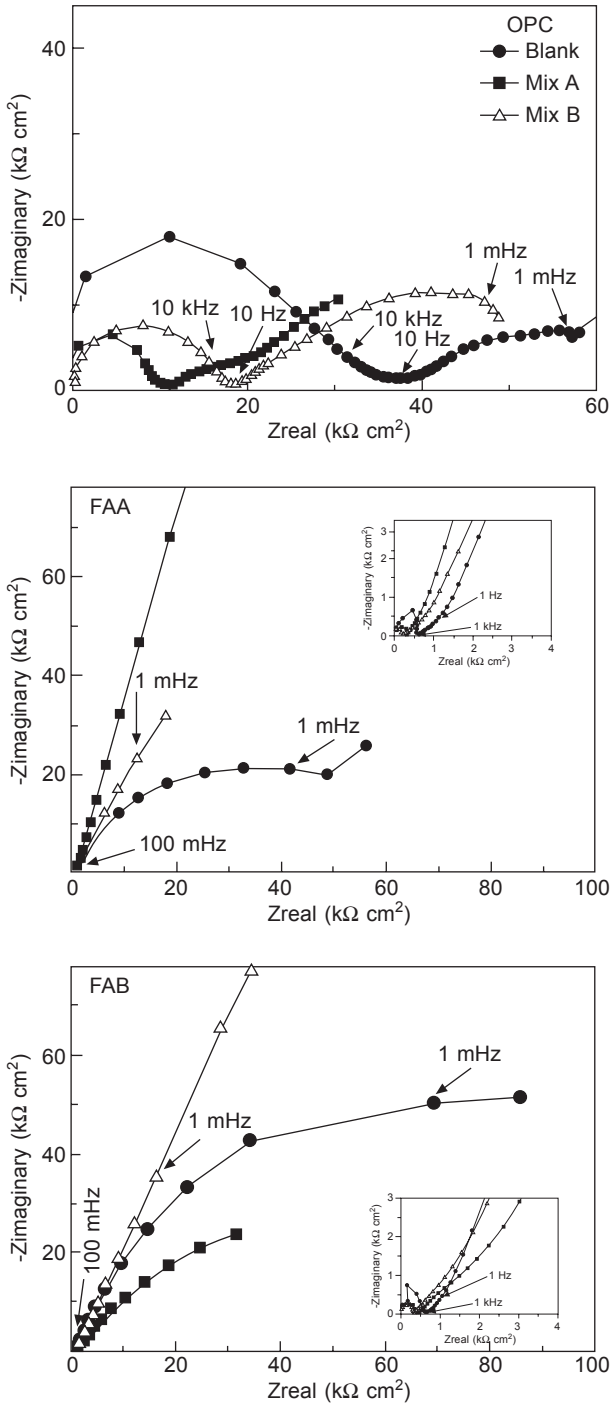

Figure 13.23 Nyquist plots for carbon steel embedded in carbonated OPC, FAA and FAB mortars at 150 days of partial immersion in distilled water polluted with 1% NaCl in the absence (blank solution) and the presence of inhibitor, Mix A or Mix B.

relation to the binder) in the absence and presence of the inhibiting mixtures. The behaviour after 20 or 70 days exposure was similar to that after 150 days, and for this reason these plots were omitted. In general, capacitive behaviour was obtained, characterized by the presence of a capacitive arc at high frequency (usually in the 10^6–10^4 Hz range for OPC mortars and the 10^6–10^3 Hz range for FA mortars), most likely connected with the dielectric properties of the mortar, followed by a poorly defined second semicircle in the 10^4–10 Hz frequency range for OPC mortars and in the 10^3–1 Hz range for FA mortars, which was attributed to the characteristics of a corrosion product layer, adherent to the reinforcing bars. The impedance response collected at lower frequencies may be associated with the carbon steel corrosion process.

The electrical equivalent circuit (EEC) used to fit the impedance data of reinforced carbonated mortar specimens and subsequent partial immersion conditions in a distilled water solution polluted with 1% chlorides contains: Re is the electrolyte resistance, the R_{HF}–CPE_{HF} couple predominating at high frequencies may be associated to the dielectric properties of the mortar cover, the R_{prod}–CPE_{prod} couple characterizes the layer of corrosion products on the steel surface, and the R_{CT}–CPE_{LF} combination controlling the low frequency portion of the diagrams (and also containing a Warburg impedance element (W), in the case of OPC mortar immersed in Mix A or Mix B) is related to the electrochemical properties of the corroding carbon steel rebar. In particular, R_{CT} corresponds to the charge transfer resistance and CPE_{LF} to the double-layer capacitance of the carbon steel/mortar interface.

From the Nyquist plots of the EIS diagrams, polarization resistance *(R_p)* values were estimated by subtracting the contribution of the mortar pore solution and, wherever present, of the inorganic film from the low frequency intercept of the arc collected in the lowest frequency region. These values, evaluated in both uninhibited (blank solution) and inhibited (Mix A or Mix B) carbonated chloride-polluted OPC, FAA and FAB mortars during 150 days of partial immersion in distilled water containing 1% chlorides (vs. binder), are reported in Figure 13.24. In OPC mortar, the R_p values were about 3×10^4 Ω cm^2 after 20 days of immersion and remained more or less unchanged during the whole exposure period. Uninhibited carbonated chloride-polluted FAA and FAB mortars exhibited higher R_p values ($1–3 \times 10^5$ Ω cm^2), indicating lower corrosion rates.

The penetration of the inhibitor mixtures in the OPC mortars only slightly reduced the reinforcement corrosion rates. In fact, the R_p values obtained by impedance fitting were $4–9 \times 10^4$ Ω cm^2 (Figure 13.24).

Table 13.6 collects the inhibition efficiency (*IE*), in %, of the mixtures calculated using the formula:

$$IE = \left(\frac{R_{pinh} - R_{pblank}}{R_{pinh}} \right) \times 100 \tag{13.2}$$

where R_{pinh} and R_{pblank} are the polarization resistance values estimated from the Nyquist plots in the presence and absence of the inhibitors, respectively. It can be noticed that the penetration of Mix A and Mix B into the OPC mortar led to

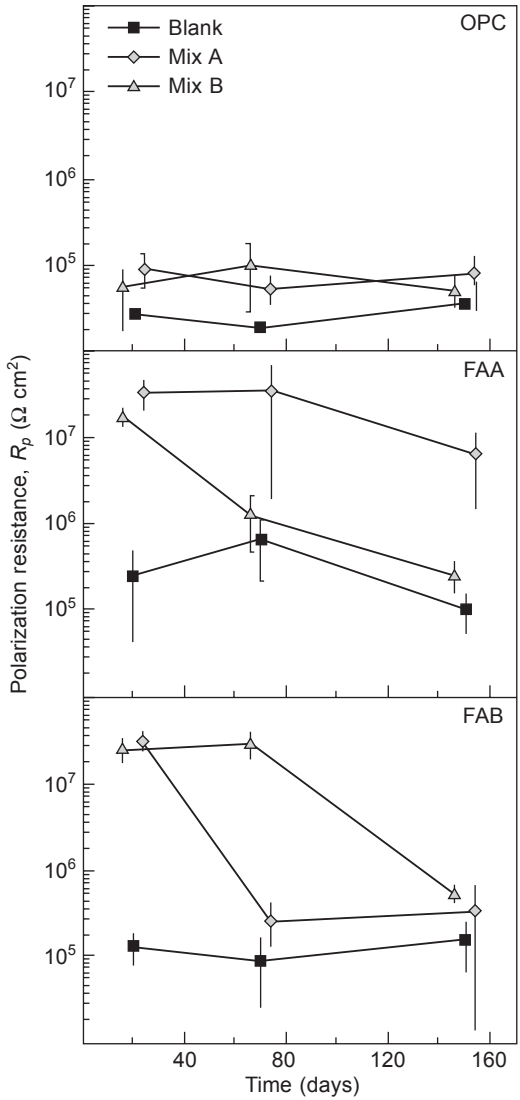

Figure 13.24 Variation in R_p with time for steel rebars embedded in uninhibited (blank) and inhibited (Mix A or Mix B) carbonated OPC, FAA and FAB mortars immersed in 1% chloride solution.

IE values of 70% and 50%, respectively, after 20 days of exposure, but that these values decreased to about 60% with Mix A and 30% with Mix B at the end of the exposure time of 150 days.

EIS data recorded in carbonated chloride-polluted FAA and FAB mortars containing the inhibitor mixtures showed one capacitive loop at frequencies lower than 1 Hz (1–10^{-4} Hz), connected to the corrosion process (Figure 13.23). The initial R_p values were around 2.5×10^7 Ω cm^2, i.e. about two orders of magnitude higher than those

obtained in the corresponding blank mortars. The *IE* of the mixtures was close to 99%. After 150 days in FAA mortar with Mix A, very high R_p values of about 6×10^6 Ω cm^2 were still shown, with an *IE* of about 99%. Even in FAA mortar with Mix B, and in FAB mortar with both mixtures (Mix A and Mix B), the inhibiting effects were maintained during the long exposure periods, but decreasing R_p values were measured (Figure 13.24). The corresponding *IE* values always remain higher than or equal to 50%, throughout the exposure time (Table 13.6). In general, the inhibiting efficiencies appeared higher in the FAA and FAB than in the OPC system, where steel is exposed to a higher chloride concentration.

Table 13.6 Inhibition efficiency (*IE*) (%) values for carbonated OPC, FAA and FAB mortars in partial immersion in 1% chloride solution, inhibited with Mix A or Mix B

Time (days)	Inhibitor efficiency (IE) (%)					
	OPC+Mix A	OPC+Mix B	FAA+Mix A	FAA+Mix B	FAB+Mix A	FAB+Mix B
20	69	51	99	98	99	99
70	63	81	98	49	65	99
150	56	33	98	60	51	69

13.6 Future trends

Although the results demonstrate that alkaline cements can provide passivation to reinforcements as efficiently and permanently as conventional Portland cement, they also show that this passivity depends on the type and dosage of binder, on the type of activators used and on the environmental conditions, so from a scientific, technical and economic viewpoint there is a need for more results on the subject in order to build up a database and avoid unnecessary risks regarding the durability of reinforced structures manufactured with these new materials. Moreover, future work should focus on the study of the nature and the integrity of the hydration products forming at the mortar–steel interface, which play a substantial role in governing metal passivation and de-passivation. Focus should also be on the study of morphological aspects and chemical compositions of the corrosion products deposited on the steel surface, so exerting influence on steel–mortar interface microstructure and on material behaviour.

The use of new corrosion prevention strategies could increase the reinforced alkali-activated concrete service life. These strategies can be encompassed in the following:

- the reduction of permeability of concrete: the use of high-quality, impermeable concrete with a low water/cement (w/c) ratio and adequate mixing and pouring of concrete cover can do much to alleviate the corrosion problem;
- protective coatings on the concrete: treatments with water-repellant materials, such as use

of overlays of asphalt or polymer concrete, can be very effective, as overlays of this type offer low permeability, good crack resistance and good bonding properties;
- protective coatings on the steel: submicron films inhibit corrosion by providing a chemically inert barrier to the diffusion of corrosion initiating species; and
- suppression of the electrochemical process: suppression of the electrochemical corrosion of iron is the basis of cathodic protection. If the current supplied to the rebar is sufficiently large, the iron is made cathodic and corrosion is prevented. A sacrificial anode, such as zinc or magnesium bars, can be buried close to the structure to reduce the corrosion of steel rebars.

13.7 Sources of further information and advice

More information can be found in the following sources:

- Shi, C., Krivenko, P.V. and Roy, D. (2006) *Alkali-Activated Cement and Concretes*. London: Taylor and Francis.
- Pacheco-Torgal, F., Abdollahnejad, Z., Camoes, A.F., Jamshidi, M. and Ding, Y. (2012) 'Durability of alkali-activated binders: a clear advantage over Portland cement or an unproven issue?', *Construcc Build Mater*, 30, 400–405.
- van Deventer, J.S.J., Provis, J.L., Duxson, P. and Brice, D.G. (2010) 'Chemical research and climate change as drivers in the commercial adoption of alkali activated materials', *Waste Biomass Valor*, 1, 145–155.
- www.rilem.org. Durability testing of alkali-activated materials.

Advice can be obtained from the following research groups:

- Instituto de Metarlurgia, Universidad Autónoma de San Luis de Potosí, San Luis de Potosí, México.
- National Centre for Metallurgical Research (CENIM), CSIC, Madrid, Spain.
- Eduardo Torroja Institute of Construction Sciences (IETCC), CSIC, Madrid, Spain.
- Departament of Materials, University of Oxford, Oxford, United Kingdom.
- Universidad de Alicante, Alicante, Madrid, Spain.
- Composite Materials Group, Universidad del Valle, Cali, Colombia.
- Department of Metallurgical Engineering, Universidad Pedagógica y Tecnológica de Colombia, Tunja, Colombia.
- Department of Mechatronics Engineering, Universidad Militar Nueva Granada, Bogotá, Colombia.
- Corrosion and Metallurgical Study Centre 'A. Daccò', University of Ferrara, Ferrara, Italy.

Acknowledgements

The author would like to acknowledge the Juan de la Cierva contract (ref. JDC-2010) financed by the Spanish Ministry of Science and Innovation.

References

Alcaide, J.S., Alcocel E.G., Puertas, F., Lapuente, R. and Garcés, P. (2007) 'Carbon fibre-reinforced, alkali-activated slag mortars', *Mater Construcc*, 57 (288), 33–48.

Al-Mehthel, M., Al-Dulaijan, S., Al-Idi, S.H., Shameem, M., Ali, M.R. and Maslehuddin, M. (2009) 'Performance of generic and proprietary corrosion inhibitors in chloride contaminated silica fume cement concrete', *Construcc Build Mater*, 23, 1768–1774.

Andrade, C. and Alonso, C. (1996) 'Corrosion rate monitoring in the laboratory and on-site', *Construcc Build Mater*, 10, 315–328.

Angst, U., Elsener, B., Larsen, C.K. and Vennesland, Ø. (2009) 'Critical chloride content in reinforced concrete – a review', *Cement Concrete Res*, 39, 1122–1138.

Aperador, W., Mejía de Gutiérrez, R. and Bastidas, D.M. (2009) 'Steel corrosion behaviour in carbonated alkali-activated slag concrete', *Corros Sci*, 51, 2027–2033.

Aperador Chaparro, W., Bautista Ruiz, J.H. and Torres Gómez, R.J. (2012) 'Corrosion of reinforcing bars embedded in alkali-activated slag concrete subjected to chloride attack', *Mater Res*, 15, 57–62.

ASTM C 876–99 Standard (1999) *Standard test for half-cell potentials of uncoated reinforcing steel in concrete*, West Conshohocken, PA, American Society for Testing and Materials.

Baba, H., Kodara, T. and Katada, Y. (2002) 'Role of nitrogen on the corrosion behaviour of austenitic stainless steels', *Corros Sci*, 44, 2393–2407.

Baddoo, N.R. (2008) 'Stainless steel in construction: a review of research, applications, challenges and opportunities', *J Construcc Steel Res*, 64, 1199–1206.

Bastidas, D.M., Fernández-Jiménez, A., Palomo, A. and Gónzalez, J.A. (2008) 'A study on the passive state stability of steel embedded in activated fly ash mortars', *Corros Sci*, 50, 1058–1065.

Bastidas, D.M., Llorente, I. and Criado, M. (2012) 'Corrosion and environmental aspects of cements and reinforced concrete', in Rivera S.M. and Pena Diaz A.L. (eds), *Brick and Mortar Research*, New York, Nova Science Publishers.

Batis, G., Pantazopoulou, P., Tsivilis, S. and Badogiannis, E. (2005) 'The effect of metakaolin on the corrosion behaviour of cement mortars', *Cement Concrete Comp*, 27, 125–130.

Bautista, A., Blanco, G. and Velasco, F. (2006) 'Corrosion behaviour of low-nickel austenitic stainless steel reinforcements: a comparative study in simulated pore solutions', *Cement Concrete Res*, 36, 1922–1930.

Berke, N.S. and Rosenberg, A. (1989) 'Technical review of calcium nitrite inhibitor in concrete', *Transport Res Rec*, 1211, 18–21.

Bernal, S.A., Provis, J.L., Kilcullen, A., Duxson, P and van Deventer, J.S.J. (2012) 'Acelerated carbonation testing of alkali-activated binders significantly underestimates service life: the role of pore solution chemistry', *Cement Concrete Res*, 42, 1317–1326.

Bertolini, L. and Gastaldi, M. (2011) 'Corrosion resistance of low-nickel duplex stainless steel rebars', *Mater Corros*, 62, 120–129.

Bertolini, L., Bolzoni, F., Pastore, T. and Pedeferri, P. (1996) 'Behaviour of stainless steel in simulated concrete pore solution', *Br Corros J*, 31, 218–222.

Bertolini, L., Elsener, B., Pedeferri, P. and Polder, R. (2004) *Corrosion of Steel in Concrete – Prevention, Diagnosis, Repair*. Weinheim, Wiley-VCH.

Blanco, G., Bautista, A. and Takenouti, H. (2006) 'EIS study of passivation of austenitic and duplex stainless steels reinforcements in simulated pore solutions', *Cement Concrete Compos*, 28, 212–219.

Broomfield, J.P. (1999) 'Corrosion inhibitors for steel in concrete', *Concrete Int*, 33, 44–47.

BS EN 14630:2006 (2006) Products and systems for the protection and repair of concrete structures. Test methods. Determination of the carbonation depth in a hardened concrete through the phenolphthalein method.

Castro, H., Rodriguez, C., Belzunce, F.J. and Cantelli, A.F. (2003) 'Mechanical properties and corrosion behaviour of stainless steel reinforcing bars', *J Mater Process Technol*, 143–144, 134–137.

Castro-Borges, P., de Rincón, O.T., Moreno, E.I., Torres-Acosta, A.A., Martínez-Madrid, M. and Knudsen, A. (2002) 'Performance of a 60-year-old concrete pier with stainless steel reinforcement', *Mater Perform*, 41, 50–55.

Chi, J. M., Huang, R. and Yang, C.C. (2002) 'Effects of carbonation on mechanical properties and durability of concrete using accelerated testing method'. *J Mar Sci Tech*, 10, 14–20.

Criado, M., Fernández Jiménez, A. and Palomo A. (2010) 'Corrosion behaviour of steel embedded in activated fly ash mortars', *1st Int. Conf. on Advances in Chemically-Activated Materials (CAM'2010-China), in conjunction 7th Int. Symp. on Cement and Concrete (ISCC 2010)*, Jinan, China.

Criado, M., Bastidas, D.M., Fajardo, S., Fernández-Jiménez, A. and Bastidas, J.M. (2011) 'Corrosion behaviour of a new low-nickel stainless steel embedded in activated fly ash mortars', *Cement Concrete Comp*, 33, 644–652.

Criado, M., Monticelli, C., Fajardo, S., Gelli, D., Grassi, V. and Bastidas, J.M. (2012) 'Organic corrosion inhibitor mixtures for reinforcing steel embedded in carbonated alkali-activated fly ash mortar', *Construcc Build Mater*, 35, 30–37.

Criado, M., Martínez-Ramírez, S., Fajardo, S., Gómez, P.P. and Bastidas, J.M. (2013) 'Corrosion rate and corrosion product characterization using Raman spectroscopy for steel embedded in chloride polluted fly ash mortar', *Mater Corros*, 64, 372–380.

Dhouibi, L., Triki, E., Salta, M., Rodrigues, P. and Raharinaivo, A. (2003) 'Studies on corrosion inhibition of steel reinforcement by phosphate and nitrite', *Mater Struct*, 36, 530–540.

Di Schino, A., Barteri, M. and Kenny, J.M. (2002) 'Fatigue behaviour of a high nitrogen austenitic stainless steel as a function of its grain size', *J Mater Sci Lett*, 21, 1969–1971.

Elsener, B. (2001) *Corrosion Inhibitors for Steel in Concrete. State of the Art Report*, EFC Publication No. 35, London, Maney Publising.

EN 206-1 (2000) *Concrete: Specification, Performance, Production and Conformity.*

Fernández-Jiménez, A., Palomo, A. and Criado, M. (2006) 'Alkali activated fly ash binders: a comparative study between sodium and potassium activators', *Mater Construcc*, 56, 51–65.

Fernández-Jiménez, A., Miranda, J.M., Gónzalez, J.A. and Palomo A. (2010) 'Steel passive state stability in activated fly ash mortars', *Mater Construcc*, 60 (300), 51–65.

Garcés, P., Fraile, J., Vilaplana-Ortego, E., Cazorla-Amorós, D., Alcocel, E.G. and Andión, L.G. (2005) 'Effect of carbon fibers on the mechanical properties and corrosion levels of Portland cement mortars', *Cement Concrete Res*, 35, 324–331.

García-Alonso, M.C., Escudero, M.L., Miranda, J.M., Vega, M.I., Capilla, F., Correia, M.J., Salta, M., Bennani, A. and González, J.A. (2007a) 'Corrosion behaviour of new stainless steels reinforcing bars embedded in concrete', *Cement Concrete Res*, 37, 1463–1471.

García-Alonso, M.C., González, J.A., Miranda, J., Escudero, M.L., Correia, M.J., Salta, M. and Bennani, A. (2007b) 'Corrosion behaviour of innovative stainless steels in mortar', *Cement Concrete Res*, 37, 1562–1569.

Gónzalez, J.A., Feliu, S., Rodríguez, P., Ramirez, E., Alonso, C. and Andrade, C. (1996) 'Some questions on the corrosion of steel in concrete. Part I: When, how and how much steel corrodes', *Mater Struct*, 29, 40–46.

Gónzalez Fernández, J.A. and Miranda Vidales J. (2007) *Corrosión en las estructuras de hormigón armado: Fundamentos, medida, diagnosis y prevención*. Madrid, Biblioteca de Ciencias.

Grinda, E.G. (1995) *El Hormigón Armado,* Madrid, Tectónica, ATC Ediciones.

Gu, P., Elliot, S., Beaudoin, J.J. and Arsenault, B. (1996) 'Corrosion resistance of stainless steel in chloride contaminated concrete', *Cement Concrete Res*, 26, 1151–1156.

Hellawell, J.M. (1988) 'Toxic substances in rivers and streams', *Environ Pollu*, 50, 61–85.

Herbsleb, G. (1982) 'The influence of SO_2, H_2S and CO on pitting corrosion of austenitic chromium–nickel stainless steels with up to 4 wt.% molybdenum in 1 M NaCl', *Mater Corros*, 33, 334–340.

Holloway, M. and Sykes, J.M. (2005) 'Studies of the corrosion of mild steel in alkali-activated slag cement mortars with sodium chloride admixtures by a galvanostatic pulse method', *Corros Sci*, 47, 3097–3110.

Jamil, H.E., Shiri, A., Boulif, R., Bastos, C., Montemor, M.F. and Ferreira, M.G.S. (2004) 'Electrochemical behaviour of amino-alcohol based inhibitor used to control corrosion of reinforcing steel', *Electrochim Acta*, 49, 2753–2760.

Jamil, H.E., Shiri, A., Boulif, R., Montemor, M.F. and Ferreira, M.G.S. (2005) 'Corrosion behaviour of reinforcing steel exposed to an amino alcohol based corrosion inhibitor', *Cement Concrete Compos*, 27, 671–678.

Jiménez-Montoya, P., García-Meseguer, A. and Morán-Cabre, F. (1987) *Hormigón Armado*, Barcelona, Gustavo Gili.

Kouřil, M., Novák, P. and Bojko, M. (2010) 'Threshold chloride concentration for stainless steels activation in concrete pore solutions', *Cement Concrete Res*, 40, 431–436.

Milititsky, M., DeWispelaere, N., Petrov, R., Ramos, J.E., Reguly, A. and Hänninen, H. (2008) 'Characterization of the mechanical properties of low-nickel austenitic stainless steels', *Mater Sci Eng A*, 498, 289–295.

Miranda, J.M., Fernández-Jiménez, A., Gónzalez, J.A. and Palomo, A. (2005) 'Corrosion resistance in activated fly ash mortars', *Cement Concrete Res*, 35, 1210–1217.

Monticelli, C., Frignani, A. and Trabanelli, G. (2000) 'A study on corrosion inhibitors for concrete application', *Cement Concrete Res*, 30, 635–642.

Monticelli, C., Frignani, A., Balbo, A. and Zucchi. F. (2011) 'Influence of two specific inhibitors on steel corrosion in a synthetic solution simulating a carbonated concrete with chlorides', *Mater Corros*, 62, 178–186.

Monticelli, C., Criado, M., Fajardo, S., Bastidas, J.M., Abbottoni, M. and Balbo, A. (2014) 'Corrosion behaviour of a low Ni austenitic stainless steel in carbonated chloride-polluted alkali-activated fly ash mortar', *Cement Concrete Res*, 55, 49–58.

Muralidharan, S., Saraswathy, V., Merlin Nima, S.P. and Palaniswamy, N. (2004) 'Evaluation of a composite corrosion inhibiting admixtures and its performance in Portland pozzolana cement', *Mater Chem Phys*, 86, 298–306.

Ngala V.T., Page C.L. and Page M.M. (2002) 'Corrosion inhibitor systems for remedial treatment of reinforced concrete. Part 1: Calcium nitrite', *Corros Sci*, 44, 2073–2087.

Ngala V.T., Page C.L. and Page M.M. (2003) 'Corrosion inhibitor systems for remedial treatment of reinforced concrete. Part 2: Sodium monofluorophosphate', *Corros Sci*, 45, 1523–1537.

Page, C.L. (2007) 'Corrosion and protection of reinforcing steel in concrete', in Page C.L. and Page M.M. (eds), *Durability of Concrete and Cement Composites*, Cambridge, Woodhead Publishing Limited.

Paredes, E.C., Bautista, A., Alvarez, S.M. and Velasco, F. (2012) 'Influence of the forming process of corrugated stainless steel on their corrosion behaviour in simulated pore solutions', *Corros Sci*, 58, 52–61.

Pedeferri, P. (1996) 'Cathodic protection and cathodic prevention', *Construcc Build Mater*, 10, 391–402.

Poupard, O., L'Hostis, V., Catinaud, S. and Petre-Lazar, I. (2006) 'Corrosion damage diagnosis of a reinforced concrete beam after 40 years natural exposure in marine environment'. *Cement Concrete Res*, 36, 504–520.

Qiao, G. and Qu, J. (2007) 'Corrosion monitoring of reinforcing steel in cement mortar by EIS and ENA', *Electrochim Acta*, 52, 8008–8019.

Raupach M., Elsener, B., Polder, R. and Mietz, J. (2007) *Corrosion of Reinforcement in Concrete: Mechanisms, Monitoring, Inhibitors and Rehabilitation Techniques*, Cambridge, Woodhead Publishing Limited.

Simmons, J.W. (1996) 'Overview: high-nitrogen alloying of stainless steels', *Mater Sci Eng A*, 207, 159–169.

Söylev, T.A. and Richardson, M.G. (2008) 'Corrosion inhibitors for steel in concrete: state-of-the-art report', *Construcc Build Mater*, 22, 609–622.

Stern, M. and Geary, A.L. (1957) 'Electrochemical potential I. A theoretical analysis of the shape of polarization curves', *J Electrochem Soc*, 104, 56–63.

Tommaselli, M.A.G., Mariano, N.A. and Kuri, S.E. (2009) 'Effectiveness of corrosion inhibitors in saturated calcium hydroxide solutions acidified by acid rain components', *Construcc Build Mater*, 23, 328–333.

Torres, R., Aperador, W., Vera, E., Ortiz, C. and Mejía de Gutiérrez, R. (2010) 'Estudio de la corrosión del acero embebido en concreto aas sometido a cloruros', *Dyna*, 77, 52–59.

Trabanelli, G., Monticelli, C., Grassi, V., Frignani, A. and Zucchi, F. (2002) *Giornate Nazionali sulla Corrosione e Protezione*, 5th edn. Bergamo, Italy, AIM.

Trabanelli, G., Monticelli, C., Grassi, V. and Frignani, A. (2005) 'Electrochemical study on inhibitors of rebar corrosion in carbonated concrete', *Cement Concrete Res*, 35, 1804–1813.

Troconis de Rincón, O., Pérez, O., Paredes, E., Caldera, Y., Urdaneta, C. and Sandoval, I. (2002) 'Long-term performance of ZnO as a rebar corrosion inhibitor', *Cement Concrete Compos*, 24, 79–87.

Tuutti, K. (1982) *Corrosion of Steel in Concrete*. Report Fo 4.82, Swedish Cement and Concrete Institute, Stockholm.

Zhang, F., Pan, J. and Lin, C. (2009) 'Localized corrosion behaviour of reinforcement steel in simulated concrete pore solution', *Corros Sci*, 51, 2130–2138.

The resistance of alkali-activated cement-based binders to chemical attack

14

Z. Baščarević
University of Belgrade, Belgrade, Serbia

14.1 Introduction

A binder material in practice can come in contact with a wide range of aggressive aqueous solutions. Sulphate ions present in groundwater or soils surrounding a concrete structure can represent a threat to its long-term durability. Sulphate attack on hydrated Portland cement concrete comprises a series of chemical reactions between sulphate ions and the components of the hardened cement (Alexander *et al.*, 2013). These reactions may lead to the deterioration of concrete structure.

The attack by acidic solutions also represents a topic of growing significance due to increasing damage to concrete structures globally (Alexander *et al.*, 2013). Acidic media originate usually from industrial processes but can be due to urban activity and natural occurrences. Concrete exposed to acid rain (Xie *et al.*, 2004) or used in agricultural construction (De Belie *et al.*, 1997) and wastewater treatment plants (Beddoe and Dorner, 2005) can suffer significant deterioration. Probably the most important cause of acid-induced damage to concrete is biogenic sulphuric acid corrosion which often takes place in sewer pipes (Monteny *et al.*, 2000; Gutiérrez-Padilla *et al.*, 2010).

Water is always present in chemical deterioration processes, since it acts as a solvent for aggressive agents, and it helps to transport these aggressive agents and their reaction products (Alexander *et al.*, 2013). Leaching of concrete by flowing water has caused severe damage in dams, pipes and tunnels, and is potentially important for the long-term storage of nuclear wastes (Shi and Stegemann, 2000; Glasser *et al.*, 2008). There are also some applications where a binder material can be exposed to alkaline solutions, such as soils with high Na_2CO_3 content or humid environments.

Most degradation processes of hydrated Portland cement are associated with leaching of portlandite, $Ca(OH)_2$, from the pore solution and decalcification of calcium silicate hydrate, C–S–H (Alexander *et al.*, 2013). In the case of sulphate attack on hydrated Portland cement, deterioration of Portland cement concrete is usually caused by the formation of expansive secondary ettringite and gypsum in the hardened cement paste, resulting from reactions of sulphate ions with aluminate phases and portlandite. Due to different chemistry of the pore solution (Lloyd *et al.*, 2010) and different binder gel composition (Shi *et al.*, 2006; Fernández-Jiménez and

Handbook of Alkali-activated Cements, Mortars and Concretes. http://dx.doi.org/10.1533/9781782422884.3.373

Palomo, 2009) of alkali-activated materials, these binders usually perform better in aggressive aqueous solutions than Portland cement.

14.2 Resistance to sodium and magnesium sulphate attack

14.2.1 Background

External sulphate attack refers to the deterioration of a binder material resulting from chemical reactions occurring when a binder is exposed to a solution containing a high concentration of dissolved sulphates. Foundations and/or parts of structures in contact with groundwater and soils in arid regions or concrete in contact with wastewaters may be subject to sulphate attack (Alexander *et al.*, 2013).

Upon contact of hydrated Portland cement with sulphate solution, diffusion of sulphate ions into the structure of the hardened cement occurs. Diffusion is followed by reactions of sulphate ions with some of the phases present in the structure. The main reaction products of sulphate attack on hydrated Portland cement are gypsum, ettringite, thaumasite or mixtures of these phases (Glasser *et al.*, 2008). The formation of these phases can cause expansion, stress, strength loss, and finally deterioration of the material. Occurrence and the extent of deterioration of hardened Portland cement structure in contact with a sulphate solution depend on the type of Portland cement, water/binder ratio, pH of the sulphate solution, concentration of sulphate ions, type of cation accompanying the sulphate ions, temperature, etc. (Neville, 2004; Santhanam *et al.*, 2001; Messad *et al.*, 2009).

Although there are numerous investigations on the effects of sulphate solutions on hydrated Portland cement structures (Neville, 2004), at the moment, there is no standard method in Europe for testing the resistance of cementitious materials to sulphate attack (CEN/TR 15697:2009). Probably the most widely used test procedure for assessment of sulphate resistance of ordinary and blended Portland cement is ASTM C1012. This standard uses expansion of $25 \times 25 \times 285$ mm mortar bars, after the immersion in 50 g/L solution of sodium sulphate, as a measure for evaluation of sulphate resistance of Portland cement. Several other sulphate resistance testing procedures are often used, such as Koch-Steinegger, SVA, Wittekind, etc. (see CEN/TR 15697:2009 and Alexander *et al.*, 2013, for detailed discussion on sulphate resistance test methods).

Due to generally lower content of calcium in alkali-activated binders than in hydrated Portland cement, it should be expected that the mechanism of sulphate attack on alkali-activated binders is different. Therefore, some test parameters used to assess sulphate resistance of Portland cement should probably be modified in order to provide a proper evaluation of resistance of alkali-activated binders to sulphate attack (Bernal and Provis, 2014). Currently, there is an ongoing work of RILEM Technical Committee DTA: Durability testing of alkali-activated materials on providing recommendations regarding appropriate test methodologies for testing

durability of alkali-activated binders. One of the areas which will be given special attention is sulphate attack on alkali-activated binders.

The following subsections will provide an overview on previous work done on investigating sulphate attack on alkali-activated binders. The review is roughly divided into three subsections, according to the chemistry of the alkali-activated binders. High-calcium alkali-activated binders are usually obtained from calcium-rich starting materials, such as granulated blast furnace slag. Although alkali-activated binders based on blends of blast furnace slag and an aluminosilicate material, such as fly ash, have intermediate calcium content, sulphate resistance of these materials has also been analysed in the subsection dealing with high-Ca alkali-activated binders. The second subsection will be focused on sulphate resistance of low-calcium alkali-activated binders, based on aluminosilicate source materials, such as fly ash and metakaolin. Some results on sulphate resistance of hybrid Portland cement–alkali-activated aluminosilicate systems will be given in the third subsection.

14.2.2 Sulphate attack resistance of high-calcium alkali-activated binders

Bakharev *et al*. (2002) investigated resistance to sulphate attack of alkali-activated granulated blast furnace slag using the ASTM C1012 test procedure. Alkali-activated slag concrete specimens were immersed in 5% Na_2SO_4 and 5% $MgSO_4$ solutions for a period of up to 12 months. Ordinary Portland cement (OPC) concrete samples were subjected to the same treatment for comparison. Up to 60 days, strength development was the same for both alkali-activated slag and Portland cement concretes in both environments. After that time, strength reduction in Portland cement concrete was higher than in alkali-activated slag samples in both of the sulphate solutions (see Figures 14.1 and 14.2). After 12 months of exposure to the Na_2SO_4 solution, the

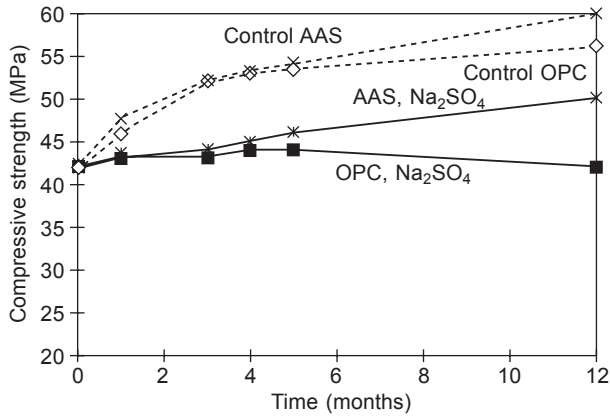

Figure 14.1 Compressive strength of ordinary Portland cement (OPC) and alkali-activated slag (AAS) concrete samples subjected to 5% Na_2SO_4 solution. Data obtained from Bakharev *et al*. (2002).

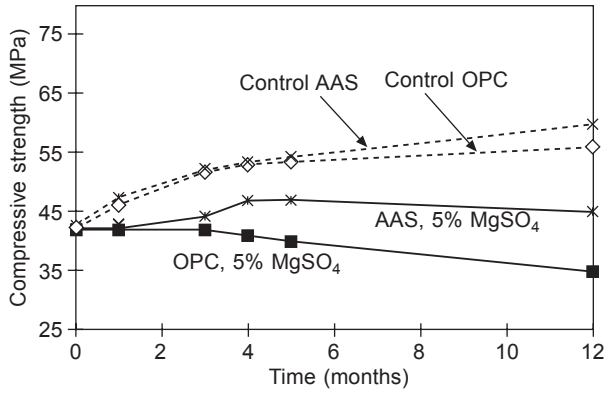

Figure 14.2 Compressive strength of ordinary Portland cement (OPC) and alkali-activated slag (AAS) concrete samples subjected to 5% $MgSO_4$ solution. Data obtained from Bakharev *et al.* (2002)

strength decrease was up to 17% for alkali-activated slag concrete and up to 25% for Portland cement concrete. The reduction of concrete compressive strength was more substantial in the $MgSO_4$ solution for both types of binders: after 12 months in the $MgSO_4$ solution, the strength decrease was up to 37% for Portland cement concrete and 23% for alkali-activated slag samples. Structural characterization of mortars from the surface of alkali-activated slag and Portland cement samples by X-ray diffraction analysis indicated different degradation products. In Portland cement samples, ettringite was present in the sample exposed to Na_2SO_4 solution, and considerable amounts of ettringite and gypsum were found in the sample exposed to $MgSO_4$. Meanwhile, no gypsum or ettringite were present in the alkali-activated slag sample exposed to Na_2SO_4 solution, while a considerable amount of gypsum was present in samples exposed to $MgSO_4$ solution. As a result of gypsum formation, cracks at the corners of alkali-activated slag specimens and some softening of the concrete occurred after the exposure to the $MgSO_4$ solution.

Puertas *et al.* (2002) investigated sulphate resistance of alkali-activated granulated blast furnace slag using variants of two different testing methods: ASTM C1012 and Koch-Steinegger. Blast furnace slag mortar samples were prepared using both sodium silicate and sodium hydroxide solutions as activator. Additionally, sulphate resistance of 50% slag + 50% fly ash mixture activated with 10 M NaOH solution was evaluated. Sodium silicate activated slag samples, and slag/fly ash mixture showed good sulphate resistance. However, mortars prepared from slag activated with NaOH showed 15–25% lower strength after exposure to the sodium sulphate solution, compared to the reference samples cured in water. Traces of ettringite were detected in these samples.

More recently, resistance to sulphate attack of alkali-activated granulated blast furnace slag concrete was evaluated after five cycles of immersion in saturated sodium sulphate solution for 24 h followed by drying of the samples at 105 ± 5°C for 24 h (Chi, 2012). The testing method was adopted from ASTM C88. Alkali-

activated slag concrete had lower weight loss compared to OPC concrete. However, no regular trends were observed in the reduction of compressive strength of the concrete samples. Some of the alkali-activated slag samples showed some strength increase after the treatment with the sulphate solution, for example, alkali-activated slag samples cured at relative humidity of 80% and at temperature of 60°C prior to testing.

The effects of external sulphate attack on mechanical properties and microstructure of alkali-activated granulated blast furnace slag were recently investigated by Komljenović *et al*. (2013). Alkali-activated slag mortar samples were immersed in 5% Na_2SO_4 solution for up to 90 days. At the same time, control samples of alkali-activated slag were cured in humid chamber, and Portland-slag cement (CEM II) was used as a benchmark material. Exposure to the sulphate solution caused a decrease in strength of Portland cement mortars, but not of alkali-activated slag samples. Strength loss of Portland cement mortars in sulphate solution was attributed to the formation of ettringite and gypsum. On the other hand, alkali-activated slag did not show significant structural alteration. Good resistance of alkali-activated slag to sulphate attack was attributed to the absence of portlandite and the unavailability of aluminium, substituted in C–S–H(I) or present in hydrotalcite gel, for reaction with sulphates.

Sulphate resistance of alkali-activated fly ash/slag (1:1 mass ratio) binder has been studied recently by Ismail *et al*. (2013). Alkali-activated fly ash/slag binder pastes, prepared with different water/binder ratios, were immersed in 50 g/L $NaSO_4$ and 50 g/L $MgSO_4$ solutions for 3 months. It was found that decreasing the water/binder ratio increases the resistance to sulphate attack. Nevertheless, the cation accompanying the sulphate ion had more pronounced effect on sulphate resistance of the alkali-activated binders. No evident physical changes were observed in the alkali-activated binder samples after the exposure to the $NaSO_4$ solution. Ismail *et al*. (2013) suggested that alkali-activated binder continued to stabilize and develop in the presence of the $NaSO_4$ solution and noted that $NaSO_4$ is often used as an activator in alkali-activated slag systems. On the other hand, $MgSO_4$ was more aggressive to the alkali-activated binder pastes than $NaSO_4$ solution. The presence of magnesium led to decalcification of the Ca-rich gel phases present in the alkali activated fly ash/slag system, causing degradation of the binder and precipitation of gypsum.

14.2.3 Sulphate attack resistance of low-calcium alkali-activated binders

Most of the previous studies concluded that alkali-activated binders obtained by activation of aluminosilicate materials show good resistance to sulphate attack, especially to the attack of Na_2SO_4 solution. Palomo *et al*. (1999) subjected $1 \times 1 \times 6$ cm alkali-activated metakaolin paste samples to the effects of 4.4% Na_2SO_4 solution for a period of up to 270 days. A fluctuation in strength was observed during the first three months of testing both in the control (immersed in water) and in the samples exposed to the sulphate solution. After that period, there was an increase in strength

in both groups of samples. Some traces of faujasite-type zeolitic phase were detected after 56 days of investigation, both in the control and in the samples exposed to the Na_2SO_4 solution. No significant changes in the structure were detected by the infrared spectroscopy of the alkali-activated binder after the sulphate resistance testing.

Fernández-Jiménez *et al*. (2007) observed similar behaviour when alkali-activated fly ash mortar samples were tested for sulphate resistance. After fluctuations in strength at the early stages of the investigation, an increase in strength was observed both in the samples immersed in 4.4% Na_2SO_4 solution and in control samples cured in air. No significant differences were observed in sulphate resistance of the alkali-activated fly ash samples prepared with sodium hydroxide and sodium silicate solutions as activators. Electron microscopy of the alkali-activated binder revealed crystals of Na_2SO_4 salts in the pores of the material after 365 days in the Na_2SO_4 solution.

Compressive strength of alkali-activated fly ash paste samples subjected to 5% Na_2SO_4, 5% $MgSO_4$ and 5% Na_2SO_4 + 5% $MgSO_4$ solutions fluctuated throughout the entire testing period in a study conducted by Bakharev (2005a). However, the least changes in alkali-activated binders' properties were found in more concentrated sulphate solution, i.e. in the 5% Na_2SO_4 + 5% $MgSO_4$ solution. The strength losses observed in the Na_2SO_4 and $MgSO_4$ solutions were attributed to migration of alkalis from the specimens into the solution. Based on infrared analysis of alkali-activated fly ash specimens after the immersion in sulphate solutions, it was suggested that sulphate attack had caused an increase in a chain length of aluminosilicate gel. Also, when sodium silicate was used as an alkaline activator, the infrared analysis of the alkali-activated fly ash binder indicated that exposure of the samples to the Na_2SO_4 solution resulted in an increase in the Si/Al atomic ratio in the aluminosilicate gel. The alkali-activated binder prepared using sodium hydroxide as alkaline activator had the best performance in the sulphate solutions, which was attributed to a stable cross-linked aluminosilicate polymer structure.

Škvara *et al*. (2005) investigated resistance to sulphate attack of paste and mortar samples prepared from alkali-activated fly ash. The alkali-activated binder samples were immersed in 44 g/L Na_2SO_4 and 5 g/L $MgSO_4$ solutions for a period of up to 720 days. Compressive strength of the alkali-activated fly ash mortars exposed to the effects of the sulphate solutions increased over the whole period of testing. No significant changes in mass and dimensions of the samples were observed during the investigation and no new crystalline phases were detected in the structure of alkali-activated fly ash after the treatment with the sulphate solutions.

Recently, sulphate resistance of alkali-activated lignite bottom ash samples was tested in accordance with ASTM C1012 (Sata *et al*., 2012). Ordinary Portland cement was subjected to the same treatment for comparison. It was concluded that alkali-activated ash mortars were less susceptible to attack by 5% Na_2SO_4 solution than OPC. Alkali-activated bottom ash mortars showed significantly lower expansion after 360 days in the sulphate solution compared to the OPC specimens.

Alkali-activated binder prepared from high calcium (~17% CaO) fly ash showed presence of calcium silicate phases in the structure. Mortars samples prepared from this alkali-activated binder showed some strength loss after 6 months of immersion in 5% $MgSO_4$ solution (Chindaprasirt *et al*., 2013). X-ray diffraction analysis of the

white deposit from the surface of the samples indicated the presence of gypsum and magnesium hydroxide, among other phases.

14.2.4 Sulphate attack resistance of hybrid binders

In recent years, much attention has been paid to hybrid Portland cement–alkali-activated aluminosilicate systems (Shi *et al.*, 2011; García-Lodeiro *et al.*, 2013). This new type of alkali-activated binder, so-called hybrid cement, consists of high volume (usually more than 60%) of a supplementary cementitious material (e.g. fly ash, slag), Portland cement clinker and small quantity of an alkaline activator.

Fernández-Jiménez *et al.* (2013) investigated resistance to sulphate attack of the hybrid binder produced by blending two types of slag (blast furnace slag and zinc slag) with an activator and 12% of Portland cement clinker. Mortar specimens prepared from hybrid binder were cured in a humid chamber for 28 days and then submerged in 4.4% Na_2SO_4 solution for a period of up to 90 days. High durability Portland cement samples were subjected to the same treatment for comparison. Compressive strength of both groups of samples was observed to increase with time in the Na_2SO_4 solution. While X-ray diffraction analysis of the Portland cement specimens treated with the sulphate solution indicated formation of ettringite, only some small ettringite crystals in the pores of the hybrid binder were detected by electron microscopy. The quantity of the ettringite formed in the structure of the hybrid binder was insufficient to be detected by X-ray diffraction analysis.

14.2.5 Concluding remarks regarding sulphate attack

Alkali-activated binders generally perform well when exposed to sulphate solution. However, lack of the most suitable method for testing sulphate attack on Portland cement has affected the work on sulphate resistance of alkali-activated binders. Testing conditions varied in terms of the time of exposure, the type of samples used (paste, mortar and concrete) and, in terms of test parameters used to assess sulphate resistance of alkali-activated binders (expansion, weight loss, compressive strength, etc.). It seems that mechanism of sulphate attack on alkali-activated binders is not yet fully understood, primarily due to a wide range of the compositions of alkali-activated binders.

Nevertheless, based on the results of the previous work done on investigating sulphate attack on alkali-activated binders, and the available standards and test protocols for Portland cement, some recommendations regarding future work on evaluating the sulphate resistance of alkali-activated binders can be made. Several important testing parameters should be kept in mind when selecting the most suitable test method for sulphate attack on alkali-activated binders.

- *Type of samples (paste, mortar or concrete).* Durability of the final product can only be assessed by testing concrete samples. However, testing of concrete requires large samples, duration of the testing will be long as a result of a large cross section of the sample and

use of non-standardized aggregate will reduce reproducibility of the test. Standardized laboratory testing of pastes and mortars could bring important outcomes and promote interlaboratory dissemination of results.

- *Mix design of the samples*. Durability of binder materials is strongly affected by their permeability, i.e. porosity. Higher water/binder ratio will accelerate deterioration and help to achieve discrimination in a reasonable timescale. However, high water/binder ratios would differ from the ratios used for concretes to be applied in construction.
- *Curing of the samples before the testing*. Depending on their composition, some alkali-activated binders need heat curing. Curing of the alkali-activated binders under water or in limewater prior to sulphate resistance testing, or as control samples, is not always suitable, as leaching of the alkali can occur. In that case, curing of alkali-activated binder in a humid chamber would be a better option. The age of the alkali-activated binder samples before the testing could be fixed (for example, 28 days).
- *Aggressive solution*. In order to accelerate the deterioration of binder material, usually high concentrations of sulphate ions are used. The results obtained in highly concentrated sulphate solution can be different from the performance of the binder in the field, where lower concentrations of sulphate ions are present. Studies of sulphate attack on alkali-activated binders indicated that cation accompanying the sulphate ions had a pronounced effect on sulphate resistance, as $MgSO_4$ solution was more aggressive to alkali-activated binders than Na_2SO_4 solution. Control of the sulphate solution pH is also very important. Leaching of the alkali from the binder structure can lead to a significant increase in pH of the solution (Baščarević *et al.*, 2014).
- *Pass/fail criteria*. Testing of alkali-activated binders in sodium sulphate solutions according to test procedures used to investigate Portland cement in most cases did not promote expansion or cracking of the material. It seems that compressive strength of the samples, or relative strength of specimens stored in the sulphate solution and in humid chamber, would be a more suitable option. Pass/fail criteria should be based on the residual strength of the specimens after reasonably long testing in the sulphate solution.

14.3 Resistance to acid attack

14.3.1 Background

Since their development, alkali-activated binders have been advertised as being highly resistant to the effects of acidic solutions (Shi *et al.*, 2006; Fernández-Jiménez and Palomo, 2009). Acid attack on a binder material, whether Portland cement of alkali-activated binder, occurs via degradation of a binder by ion exchange reactions. It is well known that all hydrated Portland cement compounds are stable only in solutions with well-defined ranges of concentrations for Ca^{2+} and OH^- ions (Pavlik, 1994a; Alexander *et al.*, 2013). Due to a lower calcium content in alkali-activated binders, the acid-induced corrosion processes in alkali-activated binder materials and Portland cement are expected to be different (Fernández-Jiménez and Palomo, 2009).

Hydrated paste of Portland cement is highly alkaline and can be easily attacked by acidic solutions (Pavlik 1994a; Pavlik and Uncik, 1997; Beddoe and Dorner, 2005). Acidic solutions react with hydrated and unhydrated compounds of hardened Portland cement and decompose them. As the pH value of the hydrated Portland

cement pore solution decreases, calcium hydroxide (12.6), ettringite (10.7), calcium silicate hydrate (~10.5) and finally calcium aluminate and ferrite hydrates decompose successively until a silica gel residue is obtained at pH values below roughly 2 (the values in parentheses referring to pH stability; Beddoe and Dorner, 2005). The end products of the acid attack on hydrated Portland cement are generally the calcium salts of the acid and a decalcified residue of the cement hydration products (Pavlik and Uncik, 1997).

High-calcium alkali-activated binders, such as alkali-activated granulated blast furnace slag, are expected to show superior acid corrosion resistance compared to Portland cement, due to the absence of portlandite and low Ca/Si ratio in the binder. On the other hand, highly cross-linked three-dimensional aluminosilicate structure of low-calcium alkali-activated binders, e.g. alkali-activated fly ash or metakaolin binders, should provide good performance of these binders in acidic solutions.

14.3.2 Acid corrosion resistance of high-calcium alkali-activated binders

Shi and Stegemann (2000) investigated acid corrosion resistance of several cementing materials, including alkali-activated blast furnace slag and ASTM Type I Portland cement. Hardened cement pastes were exposed to pH 3 nitric acid, pH 3 acetic acid, and pH 5 acetic acid solutions for 580 days period. Corroded depth was used as a measure of acid-induced degradation of the cementing materials. It was found that all the cement pastes corroded faster in acetic acid than in nitric acid, and when the pH of the acetic acid was decreased to 3, the differences in acid corrosion resistance of the cementing materials became more obvious. The alkali-activated blast furnace slag pastes were less corroded than Portland cement pastes in all the acidic media. Although no pore structure test of the investigated cementing materials was done, it was suggested that the differences in acid corrosion resistance of the cement pastes were caused by the nature of their hydration products, rather than their porosity. These findings were later confirmed by Shi (2003).

Bakharev *et al*. (2003) studied acid corrosion resistance of alkali-activated blast furnace slag and Portland cement concrete specimens immersed in pH 4 acetic acid. After 12 months in the acidic solution, Portland cement specimens had about 47% and alkali-activated slag samples had about 33% strength reduction, compared to the samples cured in water. Also, at the end of the investigation, a depth of the pH reduction of the concrete samples, determined by phenolphthalein method, was much higher for Portland cement samples (22 mm) than for alkali-activated slag concrete (16 mm). Thus, alkali-activated slag concrete showed higher acetic acid resistance compared to Portland cement concrete, attributed to low content of Ca and low average Ca/Si ratio of C-S-H in slag paste.

More recently, Bernal *et al*. (2012) investigated acid resistance of alkali-activated granulated blast furnace slag mortar samples in comparison to Portland cement. The mortar samples were exposed to pH 3 hydrochloric, nitric and sulphuric acid solutions, as well as to pH 4.5 acetic acid solution. Negligible changes in compressive strength

were identified both in Portland cement and alkali-activated slag mortars during exposure to mineral acids. After an initial drop in strength in all the alkali-activated slag samples, there was a substantial increment in the mechanical strength with the time of exposure in specimens exposed to nitric and sulphuric acid (attributed to maturity effects in the undamaged core), and a slight reduction in the mechanical strength of specimens exposed to hydrochloric acid. On the other hand, exposure to acetic acid caused significant reduction in strength in both Portland cement and alkali-activated slag mortars, indicating that acetic acid was more aggressive than the mineral acids used in this study. These findings were in line with the previous results (Shi and Stegemann, 2000; Shi, 2003). It is well known that aggressiveness of an acid towards a calcium silicate-based binder such as Portland cement or alkali-activated slag depends on the strength of the acid (i.e., its ability to dissociate) and the solubility of its calcium salts (Alexander *et al.*, 2013). Although acetic acid is a weak acid, its high aggressiveness towards binder materials is attributed to the high solubility of calcium acetate. In order to provide an additional explanation, Pavlik (1994b) suggested that the differences between nitric and acetic acid attack on Portland cement were caused by a buffering effect of the acetic acid solution in the corroded layer. Bernal *et al*. (2012) also pointed out that the solutions of acetic acid in water have a lower surface tension than either pure water or aqueous mineral acids, which may lead to a higher degree of wetting and penetration of the acidic solution into the pore network of the solid binder.

Although exposure to acetic acid caused strength loss and a substantial increment in porosity in both Portland cement and alkali-activated slag mortars, Bernal *et al*. (2012) emphasized that alkali-activated slag performed better than Portland cement, retaining 75% of their original strength after 150 days of exposure to acetic acid (see Figure 14.3). Higher stability of alkali-activated slag binder under acetic

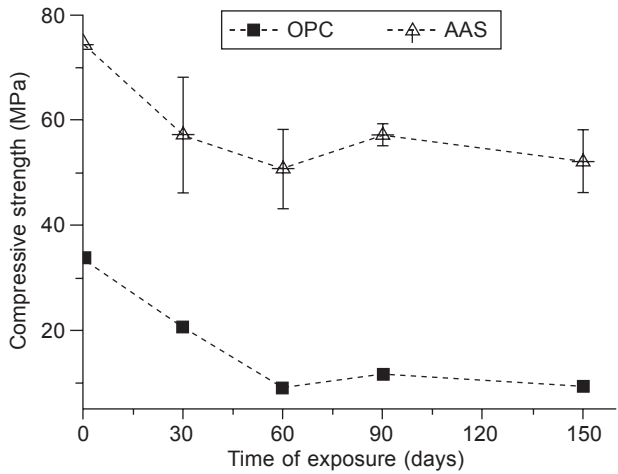

Figure 14.3 Compressive strengths of Portland cement (OPC) and alkali-activated slag (AAS) mortars as a function of the time of exposure to pH 4.5 acetic acid. Data obtained from Bernal *et al*. (2012).

acid attack is attributed to lower initial permeability, higher alkalinity of the pore solution and low CaO/SiO_2 ratio in the alkali-activated slag system. Decalcification of the alkali-activated slag binder through formation of calcium acetate leaves a residual aluminosilicate type gel in the corroded area, which is less soluble and more mechanically sound than the silicate gel formed in Portland cement binders, thus contributing to the higher acid resistance of alkali-activated slag binder.

Acid corrosion resistance of alkali-activated fly ash and granulated blast furnace slag mixture was studied by Allahverdi and Škvára (2001a, 2001b, 2005, 2006). Fly ash and slag were mixed in equal proportions and alkali activated. After 28 days of curing, paste samples were exposed to pH 1, 2 and 3 nitric acid solutions (Allahverdi and Škvára, 2001a, 2001b) and pH 1, 2 and 3 sulphuric acid solutions (Allahverdi and Škvára, 2005, 2006). Upon the exposure of the alkali-activated fly ash/slag binder to pH 1 and pH 2 nitric acid, fine shrinkage cracks and relatively hard and brittle corroded layers were observed. Exposure of the material to pH 3 nitric acid led to almost no changes in appearance of the samples, with a formation of relatively soft and easily removable surface layer. Based on the structural characterization of the binder material, Allahverdi and Škvára (2001b) suggested a reaction mechanism of the acid corrosion of the alkali-activated binder. According to these authors, the acid corrosion reaction of the alkali-activated binder occurs via the following steps:

1. Leaching of calcium and sodium (charge compensating cations in the binder gel network); these ions are exchanged by H^+ or H_3O^+ ions from the acidic solution along with an electrophilic attack by acid protons on Si–O–Al bonds in the aluminosilicate gel network, resulting in the ejection of tetrahedral aluminium from the structure.
2. Framework vacancies are mostly re-occupied by silicon atoms resulting in a formation of an imperfect highly siliceous network; the ejected aluminium atoms are octahedrally coordinated and accumulate in the intraframework space.

Exposure of the alkali-activated fly ash/slag binder to pH 1 sulphuric acid resulted in significant expansion and formation of a hard corroded layer (Allahverdi and Škvára, 2005). After the exposure to pH 2 sulphuric acid a slight expansion, very fine cracks and hard corroded layer were observed, while the exposure to pH 3 sulphuric acid led to a formation of soft and easily removed surface layer (Allahverdi and Škvára, 2006). Examination of the alkali-activated fly ash/slag binder after the exposure to pH 1 sulphuric acid by scanning electron microscopy revealed the presence of gypsum crystals in the corroded layer. The authors concluded that the deposition of gypsum inside corroded matrix provided a protective effect, inhibiting the total process of deterioration in acidic solution. On the other hand, Allahverdi and Škvára (2006) suggested that the mechanism of the sulphuric acid attack at pH 2 and 3 resembled the one suggested for nitric acid attack (Allahverdi and Škvára, 2001b).

14.3.3 Acid corrosion resistance of low-calcium alkali-activated binders

Rostami and Brendley (2003) studied acid corrosion resistance of alkali-activated fly ash immersed in 100% solution of acetic and 20% solutions of nitric, hydrochloric

and sulphuric acid. Based on weight loss of the concrete samples after 1 year of testing in the acetic solution, the authors concluded that alkali-activated material was more resistant than Portland cement. Visual examination of the samples exposed to 70% nitric acid confirmed superior resistance of the alkali-activated binder, as the Portland cement concrete showed severe damage after 2 h in the acidic solution, while alkali-activated fly ash concrete showed no signs of degradation after more than one week in 70% nitric acid.

Alkali-activated fly ash pastes showed mass loss and decrease in compressive strength after 6 months of immersion in 5% sulphuric and acetic acids (Bakharev, 2005b). The sulphuric acid was more aggressive to the alkali-activated material than the acetic acid, but the strength of these acidic solutions was also different, as sulphuric acid solution had pH 0.8 and acetic acid solution had a pH value of 2.4. Bakharev (2005b) concluded that the exposure to the acidic solutions caused depolymerization and dealumination of aluminosilicate binder gel structure. It was suggested that durability properties of the alkali-activated fly ash pastes depended on the type of the alkali activator solution used (alkali hydroxide or alkali silicate solution). Nevertheless, all alkali-activated fly ash samples investigated in this study showed higher acid resistance than Portland cement pastes and Portland cement paste with 20% fly ash replacement.

Fernández-Jiménez *et al.* (2007) studied acid corrosion resistance of alkali-activated fly ash and Portland cement mortars in pH 1 hydrochloric acid. Structural characterization of the alkali-activated fly ash binder upon the exposure to hydrochloric acid revealed an increase in the content of amorphous phases in the structure. At the same time, aluminium and zeolites content in the aluminosilicate structure decreased. The authors concluded that treating of alkali-activated fly ash binder with highly acidic solution triggered dealumination of the aluminosilicate structure. Aluminosilicate depolymerization was followed by condensation of silicon-rich polymeric ions. However, alkali-activated fly ash mortars performed better than Portland cement mortars: compressive strength of alkali-activated fly ash mortars declined by approximately 23–25% after 90 days in the acidic solution, whereas in the Portland cement mortars strength decreased at nearly twice that rate (47%). Weight loss of alkali-activated fly ash mortars was lower than in Portland cement mortars.

Later study on the hydrochloric acid resistance of alkali-activated fly ash concrete, which combined the effects of acidic conditions and high temperature, also indicated that alkali-activated binder performed better than Portland cement concrete (Chaudhary and Liu, 2009). A more recent investigation by Temuujin *et al.* (2011) showed that treating the alkali-activated fly ash pastes with 18% hydrochloric acid caused leaching of Fe, Al and Na. Consequently, a weight loss and a strength reduction of the samples were observed after only 5 days of the investigation. Sodium chloride was identified as a corrosion product of the acid attack, originating from neutralization reaction of sodium hydroxide with the hydrochloric acid.

Recently, Lloyd *et al.* (2012) reported a comprehensive study of factors influencing the resistance of alkali-activated fly ash binder to pH 1 sulphuric acid. Of the factors examined, replacement of fly ash by granulated blast furnace slag and

increased alkali content were found to have the strongest positive influence on the resistance to corrosion (see Figure 14.4), while the effects of water-to-binder ratio and the content of dissolved silica in the activating solution were less pronounced. Alkali type and the presence of aggregate were found to have no significant effect on resistance to the acid under the examined conditions. The authors emphasized that the measurement of corroded depth is much more sensitive to the acid-induced degradation mechanism of alkali-activated binder than mass loss, and recommended it for future studies in this field (Lloyd *et al.*, 2012; Provis *et al.*, 2009). Comparison between the corroded depths of several different types of binders in pH 1 sulphuric acid showed that Portland cement paste performed best, followed by alkali-activated

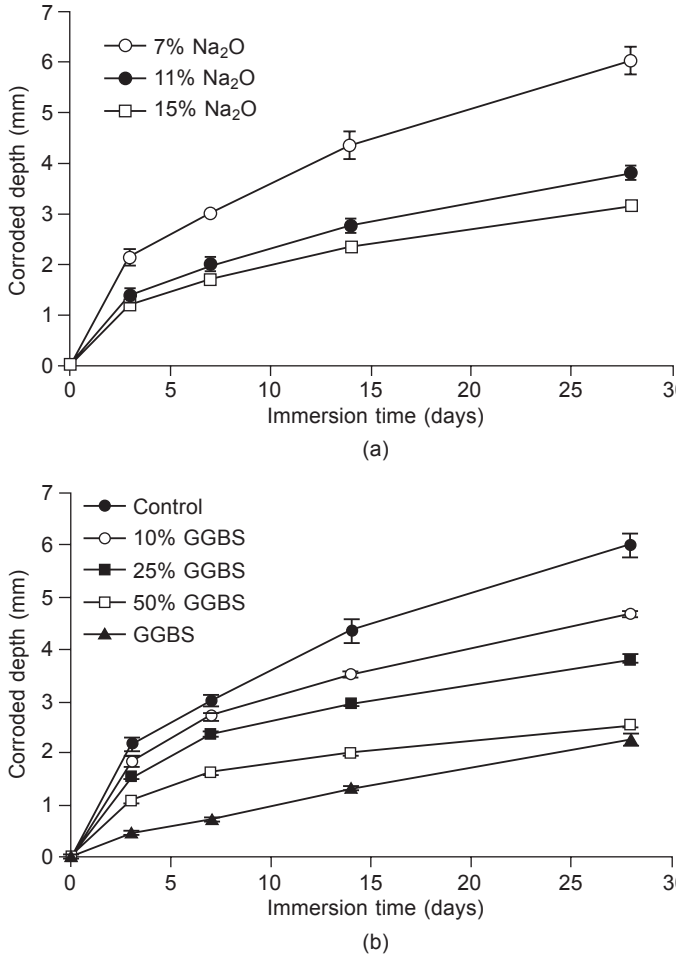

Figure 14.4 Factors influencing the resistance of alkali-activated fly ash binder to pH 1 sulphuric acid: (a) the effect of alkali (sodium) content, (b) the effect of granulated blast furnace slag content. Data obtained from Lloyd *et al.* (2012).

slag and alkali-activated fly ash. These results were opposite to those of Shi and Stegemann (2000), who reported that Portland cement corroded more rapidly than alkali-activated slag paste in pH 3 acidic solutions. Lloyd *et al*. (2012) suggested that direct comparison between alkali-activated binders and Portland cement, with regard to field performance, is hindered somewhat by the fact that paste rather than concrete samples were examined for acid corrosion resistance, and the absence of an interfacial transition zone region in alkali-activated binder concrete is expected to provide a significant performance advantage over Portland cement concrete. There were also notable differences in curing of the alkali-activated binder samples prior to the acid attack in these two investigations: Shi and Stegemann (2000) tested acid resistance of the samples cured for one year, while Lloyd *et al*. (2012) examined the samples after 28 days of curing.

Sun and Wu (2013) reported that both alkali-activated fly ash and Portland cement mortars deteriorated in 3% sulphuric acid. On the other hand, Ariffin *et al*. (2013) found that concrete specimens prepared with alkali-activated pulverized fuel ash and palm oil fuel ash showed higher resistance to 2% sulphuric acid attack compared to Portland cement concrete. Blended alkali-activated binder had lower mass loss and higher residual compressive strength than Portland cement concrete. After 18 months of exposure to 2% sulphuric acid, strength loss of alkali-activated concrete was 35%, while Portland cement concrete lost 68% of its initial strength. Sata *et al*. (2012) compared sulphuric acid resistance of mortars prepared by alkali activation of lignite bottom ash to the resistance of Portland cement and high volume fly ash mortars. After 120 days in 3% sulphuric acid solution, alkali-activated binder mortars showed significantly lower weight loss than Portland cement-based mortars.

Acid corrosion resistance of alkali-activated binder synthesized from low calcium ferronickel slag was assessed by exposing the samples to 1 N hydrochloric acid and simulated acid rain (sulphuric and hydrochloric acids, 60 : 40 wt.%, pH 3) solutions (Komnitsas *et al*., 2007). Strength loss of approximately 20% was observed in both of the acidic solutions. Halite, NaCl, was detected in the surface layer of the specimens immersed in hydrochloric acid.

Pacheco-Torgal *et al*. (2010, 2011) investigated durability performance of alkali-activated binder based on calcined tungsten mine waste mud. The acid resistance of waste mud mortars was assessed by immersion of the samples in 5% sulphuric, hydrochloric and nitric acid solutions. When a limestone aggregate was used, both alkali-activated and Portland cement mortars showed high weight losses after immersion in acidic solutions. On the other hand, waste mud mortars without limestone aggregate showed good acid resistance, superior to the acid resistance of Portland cement mortars. This was attributed to the fact that alkali-activated binders had low water absorption and low content of calcium.

Alkali-activated metakaolin paste samples showed no significant signs of acid corrosion after immersion in 0.001 N (pH 3) sulphuric acid solution for 270 days (Palomo *et al*., 1999). After a fluctuation in flexural strength during the first three months of immersion, there was a strength recovery with the time of exposure of the samples. It was observed that small amounts of a crystalline zeolite belonging to the faujasite family began to form after 180 days in the acidic solution.

Recently, Burciaga-Díaz and Escalante-García (2012) assessed the acid corrosion resistance of two different alkali-activated metakaolin paste samples. The samples were exposed to 0.5 N hydrochloric acid solution isothermally at 60°C, for up to 10 days. The starting pH of the solution was 0.8, and reached values of up to 3.7 by the end of the investigation. The alkali-activated metakaolin paste sample with SiO_2/Al_2O_3 molar ratio of 2.6 and starting compressive strength of 55.4 MPa showed strength loss of only 4% after 10 days of testing. On the other hand, alkali-activated binder with SiO_2/Al_2O_3 molar ratio of 3.0 and starting compressive strength of 81 MPa lost 14.6% of its strength after 2 days in the acidic solution and showed total strength reduction of 31.3% at the end of the investigation. Infrared spectroscopy and electron microscopy of the binders after the exposure to the acidic solution suggested that the deterioration was due to the destruction of the polymeric network and migration of Na and Al towards the solution. X-ray diffraction showed that NaCl precipitated in the aqueous medium. However, the authors concluded the chemical resistance of the alkali-activated metakaolin binder was good considering the aggressiveness of the acidic solution.

Gao *et al.* (2013) also investigated acid resistance of binder prepared from metakaolin as a starting material. A mixture of potassium hydroxide and silica fume was used as an alkaline activator. The alkali-activated binder paste samples were immersed in 0.01 N hydrochloric acid solution (pH 2) for 28 days. Analyses of the acidic solutions after the immersion of the binder material indicated high concentrations of potassium ions in the solution. The compressive strength of the samples slightly decreased after the exposure to the hydrochloric acid. Based on X-ray diffraction and electron microscopy analyses of the binder material after the acid attack, the authors concluded that the binder network structure remained intact after the immersion in the acidic solution.

14.3.4 Acid corrosion resistance of hybrid binders

Recently, Donatello *et al.* (2013) examined acid resistance of a hybrid cement binder which contained 78% fly ash, 18% Portland cement clinker and 4% Na_2SO_4. The hybrid binder and Type II Portland cement mortars were exposed to 0.1 N hydrochloric acid solution for 90 days. Prior to acid resistance examination, strengths of hybrid cement and Portland cement mortars were 37.2 and 54.1 MPa, respectively. After 90 days in hydrochloric acid (0.1 N), compressive strengths were reduced by 85–90% in both sets of mortars. The Portland cement mortar showed higher initial acid resistance than the hybrid cement. This was explained by the presence of high quantities of portlandite and calcite, which acted as acid buffers. Structural characterization of the binder materials after the exposure to the acidic solution indicated that both pastes showed characteristic signs of acid attack on cementitious gel structures, with a formation of colloidal silica gel.

Fernández-Jiménez *et al.* (2013) investigated durability of the hybrid binder obtained by blending 12% Portland cement clinker with two types of slag (blast furnace slag and zinc slag) and alkaline activator. High durability Portland cement was used as a control material in this study. After 90 days in 0.1 N hydrochloric acid

(pH 1.5) compressive strength declined substantially in both cements (~90%). Thus, the acid resistance of the hybrid binder was wholly comparable to the performance of conventional Portland cement.

14.3.5 Concluding remarks regarding acid attack

The available literature on acid corrosion resistance of alkali-activated materials indicates that alkali-activated binders generally perform well in acidic solutions. Due to a wide range of acid exposure conditions which are of interest in practice, various non-standardized test protocols were used in order to assess acid corrosion resistance of alkali-activated binders. Testing conditions varied in terms of the strength of the acid used, the concentration of the acidic solution, the time of the exposure and the type of the samples used (paste, mortar or concrete). Also, different measures of acid induced degradation of the binder materials (weight loss, compressive strength, corroded depth, etc.) were used. In most of the studies, an alkali-activated binder performed better than Portland cement specimens subjected to the same acid solution treatment.

Some of the recommendations given in the previous section regarding future work on sulphate attack on alkali-activated binders can also be applied in future investigations of acid attack on alkali-activated binders, especially those regarding type of samples or curing of the samples before testing. However, more attention should be devoted to selecting appropriate acidic solutions. Some of the previous works on acid attack on alkali-activated binders applied rather drastic testing conditions, in terms of type and concentration of the acidic solutions used. Whenever the results can be obtained after a reasonable time of testing, use of acidic solutions that are expected to be met in practice should be favoured. Also, it seems that no work has been done on investigating biogenic sulphuric acid corrosion of alkali-activated binders.

Selecting a proper measure of acid-induced degradation of alkali-activated binders is also very important. Monitoring the mass loss of the binder may not always be the best way to investigate acid attack, since degradation of alkali-activated material in an acidic solution can be both due to leaching and dissolution of the binder and due to deposition of degradation products inside the structure. Recently, corroded depth has been recommended as a much more sensitive measure of the acid-induced degradation mechanism of alkali-activated binders than mass loss. On the other hand, some authors consider that measuring compressive strength loss can be complicated by the increase in strength of the undamaged core of the alkali–binder sample. It seems that, in order to provide a proper evaluation of alkali-activated binders' resistance to acid attack, multiple indicators of acid-induced degradation should be used.

14.4 Decalcification resistance

Decalcification is usually described as the process of degradation of hydrated Portland cement in pure water involving dissolution and leaching of calcium ions from

portlandite, $Ca(OH)_2$, and calcium silicate hydrate, C-S-H (Glasser *et al*., 2008). This phenomenon usually affects structures that have been in contact with water for long periods: dams, tunnels, water pipes, etc. Decalcification of cement-based materials has been identified as an important issue for nuclear waste storage (Shi and Stegemann, 2000; Glasser *et al*., 2008; Komljenović *et al*., 2012; Wan *et al*., 2013).

Different testing procedures were developed to assess the resistance of binder materials to decalcification. Since calcium leaching is a relatively slow process, a wide range of accelerated tests have been developed. The majority of these procedures are carried out with strongly acidified solutions like ammonium nitrate, NH_4NO_3, instead of water (Glasser *et al*., 2008). Decalcification by highly concentrated (6 M) NH_4NO_3 solution offers some key advantages compared to leaching by water. The rate of leaching is increased by two orders of magnitude (Carde and François, 1997; Heukamp *et al*., 2001; Puertas *et al*., 2012) and additionally, the leaching reaction in 6 M NH_4NO_3 solution is almost a pure decalcification, i.e. there is no altering in content of silicon, even at very low ratios of Ca/Si = 0.3 (Chen *et al*., 2006).

Decalcification resistance of alkali-activated granulated blast furnace slag has been investigated recently by Komljenović *et al*. (2012). Alkali-activated binder was exposed to the effects of the concentrated (6 M) NH_4NO_3 solution for 90 days. Simultaneously, a set of control (reference) alkali-activated slag samples was cured in a humid chamber. Portland-slag cement (CEM II) was used as a benchmark material and the decalcification process was investigated under equal conditions for both materials.

Exposure of mortar samples to 6 M NH_4NO_3 solution led to a decrease in strength, both in alkali-activated binder and Portland cement. However, decrease in strength was significantly lower in alkali-activated slag mortars. After 60 days of investigation, the relative strength of Portland cement (degraded/reference) was 0.19 and remained unchanged after additional 30 days of testing. Over the same period, changes in alkali-activated slag mortar strength were considerably lower: relative strength of the alkali-activated slag mortars was 0.91 after 60 days and 0.85 after 90 days of testing.

X-ray microanalysis of the alkali-activated slag binder after the immersion in NH_4NO_3 solution showed that sodium from the pore solution was leached almost completely after the first 30 days of testing. Decrease in Ca/Si atomic ratio from an initial value of 0.84 to 0.33 after 90 days in solution, indicated leaching of calcium from the structure. A very low ratio of Ca/Si (~0.3) was explained by the coexistence of calcium silicate hydrate, C–S–H(I), with low Ca/Si ratio and polymerized silica gel. Al/Si atomic ratio in alkali-activated slag samples after exposure to NH_4NO_3 solution ranged in a very narrow interval from 0.14 (initial) to 0.15 (after 90 days in the solution). In the same period, the Al/Si ratio in the reference samples showed an increase. It was suggested that a small change in this ratio in alkali-activated binder after the immersion in NH_4NO_3 solution could be related to aluminium leaching, i.e. to a lower degree of its substitution in the C–S–H(I) structure. Analysis of Mg/Si versus Al/Si ratio indicated the presence of a phase similar to hydrotalcite, probably finely dispersed Mg-Al hydroxide gel within C–S–H(I). After the immersion of the alkali-activated binder in NH_4NO_3 solution, the Mg/Al atomic ratio decreased and

there was an indication that no aluminium was incorporated into C-S-H. The detected decrease in the Mg/Al atomic ratio was attributed to magnesium leaching from hydrotalcite gel and/or aluminium leaching from C–S–H gel; the released aluminium could then be incorporated into polymerized silica gel, resulting in formation of aluminosilicate gel.

Correlation of compressive strength of mortars with the results of structural characterization showed that decrease in strength was related to the decrease in Ca/Si ratio. Dissolution of portlandite due to the effects of NH_4NO_3 solution had a destructive effect on mechanical properties of Portland cement mortars. After almost complete leaching of portlandite (after 30 days in the solution, Ca/Si ~ 2.0), a further decrease in strength of CEM II mortars occurred due to the dissolution of C–S–H, until it reached minimal, or the so-called residual strength, with ratio Ca/Si ~1.4 (after 60 days in NH_4NO_3 solution). In alkali-activated slag samples portlandite was not detected and decalcification of C–S–H with low Ca/Si ratio resulted in a thick protective layer of silica gel. Hence, alkali-activated slag samples showed substantially lower decrease in strength after the immersion in NH_4NO_3 solution.

Komljenović *et al*. (2012) concluded that very pronounced decalcification resistance of alkali-activated slag was due to the absence of portlandite, high level of polymerization of silicate network (low Ca/Si atomic ratio ~ 0.8), a relatively low level of aluminium substitution for silicon in C–S–H(I) gel structure (up to 20% of bridging tetrahedra), as well as due to the formation of a protective layer of polymerized silica gel.

The effects of 6 M NH_4NO_3 solution on properties of alkali-activated fly ash binder were investigated recently by Baščarević *et al*. (2013). It was found that immersion in the concentrated NH_4NO_3 solution (starting pH ~ 4) had almost similar effects on the structure of the alkali-activated binder as the acid attack. Exposure of the alkali-activated fly ash samples to NH_4NO_3 solution caused leaching of alkali cations and breaking of Si–O–Al bonds in aluminosilicate gel structure. Consequently, compressive strength of the alkali-activated fly ash mortars decreased approximately 20% after 28 days in the solution. Further examination (up to 540 days) indicated that reparation of structural defects, formed by breaking of Si–O–Al bonds, occurred. Defects in the structure were re-occupied by silicon forming more siliceous structure, which resulted in a subsequent fluctuation in compressive strength.

As noted previously, decalcification resistance of a binder material is of great importance in the structures used for radioactive waste disposal containers. Previous studies showed that alkali-activated cements have a high potential for use in stabilization/solidification of hazardous and radioactive wastes (Shi and Fernández-Jiménez, 2006; Vance and Perera, 2009; Provis, 2009; Nikolić *et al*., 2014). The results of Komljenović *et al*. (2012) confirmed that in stabilization/solidification processes, alkali-activated slag represents a more promising option than Portland cement due to the significantly higher resistance to decalcification.

14.5 Resistance to alkali attack

There are certain applications where binder materials can be exposed to highly alkaline solutions. For example, concretes that are resistant to alkaline soil conditions are necessary in construction applications in many parts of the world, where high levels of sodium carbonate in soils can increase the soil pH to around 9 or higher (Sindhunata *et al.*, 2008). Alkali resistance would also be important in conditions where a binder material is exposed to moisture, as the pore solution within alkali-activated binders is highly alkaline (Sindhunata *et al.*, 2008). Exposure of Portland cement pastes to the conditions that simulated exposure to moisture (pH 11.5 calcium hydroxide solution) caused leaching of portlandite from the pore solution as well as leaching of calcium from C–S–H, which resulted in increased porosity of the samples (Revertegat *et al.*, 1992).

Alkali resistance of alkali-activated fly ash binder was assessed by immersion of the material in various alkaline and carbonate solutions: 1, 5 and 8 M sodium and 5 M potassium hydroxide solutions, 2.2 M (saturated) sodium carbonate and 2.5 M potassium carbonate solution, as well as in distilled water for 90 days (Sindhunata *et al.*, 2008). It was found that 1 M NaOH (pH ~14), carbonate solutions (~11) and water showed similar trends in terms of leaching of binder gel elements (Si and/or Al). The pH of water was not monitored, but it was certain that it had become significantly alkaline due to the release of free alkali from the binder. These solutions had remarkably little effect on alkali-activated fly ash structure. On the other hand, more concentrated hydroxide solutions (pH >14) led to a more significant extent of Si and Al leaching, as well as to the collapse of the pore network. Small quantities of zeolites from the initially X-ray amorphous gel were observed in the alkali-activated binder after the immersion in 5 and 8 M hydroxide solutions.

More aggressive testing conditions were applied in a recent alkali corrosion resistance study conducted by Temuujin *et al.* (2011). Alkali-activated fly ash samples were exposed to 14 M NaOH solution with liquid-to-solid ratio of approximately 5. After only 5 days in the solution, Si was leached at high levels, while Al leach rates were lower. Leaching caused weight reduction of the alkali-activated fly ash samples (~20% after 5 days of testing). No new crystalline phases were detected in the alkali-activated binder structure upon the exposure to the highly concentrated hydroxide solution. Compressive strength of the alkali-activated fly ash pastes after the immersion in the 14 M NaOH had high standard deviations and no reliable conclusions about the strength changes could be made.

Recently, Gordon *et al.* (2011) investigated durability of alkali-activated fly ash/granulated blast furnace slag mixtures (2:1) when exposed to concentrated (2.5 M) potassium carbonate solution and distilled water. Different binder formulations in terms of SiO_2/Al_2O_3, Na_2O/SiO_2 and H_2O/Na_2O were investigated. Most of the alkali-activated binders examined in this study showed substantial strength loss after the immersion in the carbonate solution. Performance of the alkali-activated binders in alkaline solutions was found to depend greatly on porosity of the binder.

As seen from the works of Sindhunata *et al*. (2008) and Temuujin *et al*. (2011), alkali-activated fly ash binders would be a suitable option for applications in moderately alkaline conditions, such as soils with high Na_2CO_3 content or humid environments. Applications in highly alkaline environments (pH >14) are somewhat limited due to the leaching of silicon from the binder structure in these conditions. On the other hand, alkali-activated fly ash/granulated blast furnace slag mixtures showed poor resistance to the potassium carbonate solution (Gordon *et al*., 2011). Clearly, more work needs to be done in order to make a positive or negative report on the effects of highly alkaline conditions on engineering properties of alkali-activated binders, such as compressive strength of mortar or concrete samples.

14.6 Conclusions

A binder material in service can come in contact with a wide range of aggressive aqueous solutions, such as solutions with high concentrations of sulphate ions, various acidic solutions, or solutions with high concentrations of alkali. Alkali-activated binders usually show superior resistance to chemical attack by aggressive aqueous solutions, compared to Portland-cement.

Generally good resistance of high-calcium alkali-activated binders to sulphate attack can be attributed to the absence of portlandite and the unavailability of aluminium for reaction with sulphates. Low-calcium alkali-activated binders also show good resistance to sodium sulphate solutions. However, several studies have shown that $MgSO_4$ solution is more aggressive to alkali-activated binder than Na_2SO_4 solution. Generally, more work is required to validate sulphate resistance of alkali-activated binders under the conditions met in service.

In most of the previous acid attack studies, an alkali-activated binder performed better than Portland cement specimens subjected to the same acid solution treatment. Higher acid resistance of high-calcium alkali-activated binders can be attributed to lower content of Ca and lower average Ca/Si ratio of C-S-H in the structure, compared to Portland cement. Although acid attack on low-calcium alkali-activated binders usually leads to depolymerization and dealumination of aluminosilicate structure, these binders also show acid corrosion resistance superior to that of Portland cement. Future work on acid attack resistance of alkali-activated binders should focus on testing the alkali-activated binders in acidic conditions expected in practice, especially in microbiologically induced aggressive environments. Special attention should be paid to selecting a proper measure of acid-induced degradation of alkali-activated binders.

A study on decalcification resistance of alkali-activated slag showed that this binder represents a promising option for applications where long-term contact with water is expected, particularly for stabilization/solidification of hazardous and radioactive wastes. Further work is required to validate resistance of alkali-activated binders to alkali attack.

14.7 Sources of further information and advice

Shi C., Krivenko P.V. and Roy D.M. (2006) *Alkali-Activated Cements and Concretes*, Taylor & Francis, Abingdon.

Provis J.L. and van Deventer J.S.J. (eds) (2009) *Geopolymers: Structures, Processing, Properties and Industrial Applications*, Woodhead Publishing, Cambridge.

Alexander M., Bertron A. and De Belie N. (eds) (2013) *Performance of Cement-Based Materials in Aggressive Aqueous Environments*, State-of-the-Art Report, RILEM TC 211 – PAE, Series: RILEM State-of-the-Art Reports, Vol. 10, Springer, New York.

References

Alexander M., Bertron A. and De Belie N. (eds) (2013) *Performance of Cement-Based Materials in Aggressive Aqueous Environments*, State-of-the-Art Report, RILEM TC 211 – PAE, Series: RILEM State-of-the-Art Reports, Vol. 10, Springer, New York.

Allahverdi A. and Škvára F. (2001a) 'Nitric acid attack on hardened paste of geopolymeric cements, Part 1', *Ceram – Silik*, 45 (3), 81–88.

Allahverdi A. and Škvára F. (2001b) 'Nitric acid attack on hardened paste of geopolymeric cements, Part 2', *Ceram – Silik*, 45 (4), 143–149.

Allahverdi A. and Škvára F. (2005) 'Sulfuric acid attack on hardened paste of geopolymer cements, Part 1. Mechanism of corrosion at relatively high concentrations', *Ceram – Silik*, 49 (4), 225–229.

Allahverdi A. and Škvára F. (2006) 'Sulfuric acid attack on hardened paste of geopolymer cements Part 2. Corrosion mechanism at mild and relatively low concentrations', *Ceram-Silik,* 50 (1), 1–4.

Ariffin M.A.M., Bhutta M.A.R., Hussin M.W., Mohd Tahir M. and Aziah N. (2013) 'Sulfuric acid resistance of blended ash geopolymer concrete', *Constr Build Mater* 43, 80–86.

ASTM C1012/C1012M-13 *Standard Test Method for Length Change of Hydraulic–Cement Mortars Exposed to a Sulfate Solution*.

Bakharev T. (2005a) 'Durability of geopolymer materials in sodium and magnesium sulfate solutions', *Cem Concr Res*, 35, 1233–1246.

Bakharev T. (2005b) 'Resistance of geopolymer materials to acid attack', *Cem Concr Res*, 35, 658–670.

Bakharev T., Sanjayan J.G. and Cheng Y.-B. (2002) 'Sulfate attack on alkali-activated slag concrete', *Cem Concr Res*, 32, 211–216.

Bakharev T., Sanjayan J.G., Cheng Y.-B. (2003) 'Resistance of alkali-activated slag concrete to acid attack', *Cem Concr Res*, 33, 1607–1611.

Baščarević Z., Komljenović M., Miladinović Z., Nikolić V., Marjanović N., Žujović Z. and Petrović R. (2013) 'Effects of the concentrated NH_4NO_3 solution on mechanical properties and structure of the fly ash based geopolymers', *Constr Build Mater*, 41, 570–579.

Baščarević Z., Komljenović M., Miladinović Z., Nikolić V., Marjanović N. and Petrović R. (2014) 'Impact of sodium sulfate solution on mechanical properties and structure of fly ash based geopolymers', *Mater Struct*, DOI: 10.1617/s11527-014-0325-4.

Beddoe R.E. and Dorner H.W. (2005) 'Modelling acid attack on concrete: Part I. The essential mechanisms', *Cem Concr Res*, 35, 2333–2339.

Bernal S.A. and Provis J.L. (2014) 'Durability of alkali-activated materials: progress and perspectives', *J Am Ceram Soc*, 97, 997–1008.

Bernal S.A., Rodríguez E.D., Mejía de Gutiérrez R. and Provis J.L. (2012) 'Performance of alkali-activated slag mortars exposed to acids', *J Sustain Cement-Based Mater*, 1 (3), 138–151.

Burciaga-Díaz O. and Escalante-García J.I. (2012) 'Strength and durability in acid media of alkali silicate-activated metakaolin geopolymers', *J Am Ceram Soc*, 95, 2307–2313.

Carde C. and François R. (1997) 'Effect of the leaching of calcium hydroxide from cement paste on mechanical and physical properties', *Cem Concr Res*, 27, 539–550.

CEN/TR 15697:2009 *Cement – Performance Testing for Sulfate Resistance – State of the Art Report*.

Chaudhary D. and Liu H. (2009) 'Influence of high temperature and high acidic conditions on geopolymeric composite material for steel pickling tanks', *J Mater Sci*, 44, 4472–4481.

Chen J.J., Thomas J.J. and Jennings H.M. (2006) 'Decalcification shrinkage of cement paste', *Cem Concr Res*, 36, 801–809.

Chi M. (2012) 'Effects of dosage of alkali-activated solution and curing conditions on the properties and durability of alkali-activated slag concrete', *Constr Build Mater*, 35, 240–245.

Chindaprasirt P., Rattanasak U. and Taebuanhuad S. (2013) 'Resistance to acid and sulfate solutions of microwave-assisted high calcium fly ash geopolymer', *Mater Struct*, 46, 375–381.

De Belie N., Debruyckere M., Van Nieuwenburg D. and De Blaere B. (1997) 'Attack of concrete floors in pig houses by feed acids: influence of fly ash addition and cement-bound surface layers', *J Agric Engng Res*, 68, 101–108.

Donatello S., Palomo A. and Fernández-Jiménez A. (2013) 'Durability of very high volume fly ash cement pastes and mortars in aggressive solutions', *Cem Concr Comp*, 38, 12–20.

Fernández-Jiménez A. and Palomo A. (2009) 'Chemical durability of geopolymers', in Provis, J.L. and van Deventer, J.S.J. (eds) *Geopolymers: Structure, Processing, Properties and Industrial Applications*, Woodhead Publishing, Cambridge, 167–193.

Fernández-Jiménez A., Garcıa-Lodeiro I. and Palomo A. (2007) 'Durability of alkali-activated fly ash cementitious materials', *J Mater Sci*, 42, 3055–3065.

Fernández-Jiménez A., Flores E., Maltseva O., García-Lodeiro I. and Palomo A. (2013) 'Hybrid alkaline cements. Part III. Durability and industrial applications', *Rev Rom Mater*, 43, 195–200.

Gao X.X., Michaud P., Joussein E. and Rossignol S. (2013) 'Behavior of metakaolin-based potassium geopolymers in acidic solutions', *J Non-Cryst Solids*, 380, 95–102.

García-Lodeiro I., Fernández-Jiménez A. and Palomo A. (2013) 'Variation in hybrid cements over time: alkaline activation of fly ash–Portland cement blends', *Cem Concr Res*, 52, 112–122.

Glasser F.P., Marchand J. and Samson E. (2008) 'Durability of concrete – degradation phenomena involving detrimental chemical reactions', *Cem Concr Res*, 38, 226–246.

Gordon L.E, Provis J.L. van Deventer J.S.S (2011) 'Durability of fly ash/GGBFS based geopolymers exposed to carbon capture solvents', *Adv Appl Ceram*, 10 (8), 446–452.

Gutiérrez-Padilla M.G.D., Bielefeldt A., Ovtchinnikov S., Hernandez M. and Silverstein J. (2010) 'Biogenic sulfuric acid attack on different types of commercially produced concrete sewer pipes', *Cem Concr Res*, 40, 293–301.

Heukamp F.H., Ulm F-J. and Germaine J.T. (2001) 'Mechanical properties of calcium-leached cement pastes: triaxial stress states and the influence of the pore pressures', *Cem Concr Res*, 31, 767–774.

Ismail I., Bernal S.A., Provis J.L., Hamdan S. and van Deventer J.S.J. (2013) 'Microstructural changes in alkali activated fly ash/slag geopolymers with sulfate exposure', *Mater Struct*, 46, 361–373.

Komljenović M., Baščarević Z., Marjanović N. and Nikolić V. (2012) 'Decalcification resistance of alkali-activated slag', *J Hazard Mater*, 233–234, 112–121.

Komljenović M., Baščarević Z., Marjanović N. and Nikolić V. (2013) 'External sulfate attack on alkali-activated slag', *Constr Build Mater*, 49, 31–39.

Komnitsas K., Zaharaki D. and Perdikatsis V. (2007) 'Geopolymerisation of low calcium ferronickel slags', *J Mater Sci*, 42, 3073–3082.

Lloyd R.R., Provis J.L. and van Deventer J.S.J. (2010) 'Pore solution composition and alkali diffusion in inorganic polymer cement', *Cem Concr Res*, 40, 1386–1392.

Lloyd R.R., Provis J.L. and van Deventer J.S.J. (2012) 'Acid resistance of inorganic polymer binders. 1. Corrosion rate', *Mater Struct*, 45, 1–14.

Messad S., Carcasses M. and Linger L. (2009) 'Design of an accelerated test method for external sulfate attack', in: Alexander M.G. and Bertron A. (eds) *Concrete in Aggressive Aqueous Environments – Performance, Testing and Modeling*, RILEM TC 211-PAE Final Conference 3–5 June 2009, Toulouse, France, RILEM Publications SARL.

Monteny J., Vincke E., Beeldens A., De Belie A., De Belie N., Taerwe L., Van Gemert D. and Verstraete W. (2000) 'Chemical, microbiological, and *in situ* test methods for biogenic sulfuric acid corrosion of concrete', *Cem Concr Res*, 30, 623–634.

Neville A. (2004) 'The confused world of sulfate attack on concrete' *Cem Concr Res*, 34, 1275–1296.

Nikolić V., Komljenović M., Marjanović N., Baščarević Z. and Petrović R. (2014) 'Lead immobilization by geopolymers based on mechanically activated fly ash' *Ceram Int*, 40, 8479–8488.

Pacheco-Torgal F. and Jalali S. (2011) 'Resistance to acid attack, abrasion and leaching behavior of alkali-activated mine waste binders', *Mater Struct*, 44, 487–498.

Pacheco-Torgal F., Castro-Gomes J. and Jalali S. (2010) 'Durability and environmental performance of alkali-activated tungsten mine waste mud mortars', *J Mater Civ Eng*, 22, 897–904.

Palomo A., Blanco-Varela M.T., Granizo M.L., Puertas F., Vazquez T. and Grutzeck M.W. (1999) 'Chemical stability of cementitious materials based on metakaolin', *Cem Concr Res*, 29, 997–1004.

Pavlik V. (1994a) 'Corrosion of hardened cement paste by acetic and nitric acids. Part I: Calculation of corrosion depth', *Cem Concr Res*, 24, 551–562.

Pavlik V. (1994b) 'Corrosion of hardened cement paste by acetic and nitric acids, Part II: Formation and chemical composition of the corrosion products', *Cem Concr Res*, 24, 1495–1508.

Pavlik V. and Uncik S. (1997) 'The rate of corrosion of hardened cement pastes and mortars with additive of silica fume in acids', *Cem Concr Res*, 27, 1731–1745.

Provis, J.L. (2009) 'Immobilization of toxic waste in geopolymers', in: Provis J.L. and van Deventer J.S.J. (eds) *Geopolymers: Structure, Processing, Properties and Industrial Applications*, Woodhead Publishing, Cambridge, 421–440.

Provis J.L., Lloyd R.R. and van Deventer J.S.J. (2009) 'Mechanism and implications of acid attack on fly ash and fly ash-slag inorganic polymers' in: Alexander M.G. and Bertron A. (eds) *Concrete in Aggressive Aqueous Environments – Performance, Testing and Modeling*, RILEM TC 211–PAE Final Conference 3–5 June 2009, Toulouse, France, RILEM Publications SARL.

Puertas F., de Gutierrez R., Fernandez-Jimenez A., Delvasto S. and Maldonado J. (2002)

'Alkaline cement mortars: chemical resistance to sulfate and seawater attack', *Mater Constr*, 52 (267), 55–71.

Puertas F., Goñi S., Hernández M.S., Varga C. and Guerrero A. (2012) 'Comparative study of accelerated decalcification process among C_3S, grey and white cement pastes', *Cem Concr Comp*, 34, 384–391.

Revertegat E., Richet C. and Gégout P. (1992) 'Effect of pH on the durability of cement pastes', *Cem Concr Res*, 22, 259–272.

RILEM Technical Committee DTA: Durability testing of alkali-activated materials, http://www.rilem.org/gene/main.php?base=8750&gp_id=290 (accessed 24 February 2014).

Rostami H. and Brendley W. (2003) 'Alkali ash material: a novel fly ash-based cement', *Environ Sci Technol*, 37, 3454–3457.

Santhanam M., Cohen M.D. and Olek J. (2001) 'Sulfate attack research – whither now?' *Cem Concr Res*, 31, 845–851.

Sata V., Sathonsaowaphak A. and Chindaprasirt P. (2012) 'Resistance of lignite bottom ash geopolymer mortar to sulfate and sulfuric acid attack', *Cem Concr Comp*, 34, 700–708.

Shi C. (2003) 'Corrosion resistance of alkali-activated slag cement', *Adv Cem Res*, 15 (2), 77–81.

Shi C. and Fernández-Jiménez A. (2006) 'Stabilization/solidification of hazardous and radioactive wastes with alkali-activated cements', *J Hazard Mater*, B137, 1656–1663.

Shi C. and Stegemann J.A. (2000) 'Acid corrosion resistance of different cementing materials', *Cem Concr Res*, 30, 803–808.

Shi C., Krivenko P.V. and Roy D. (2006) *Alkali-Activated Cements and Concretes*, Taylor & Francis, Abingdon.

Shi C., Fernández Jiménez A. and Palomo A. (2011) 'New cements for the 21st century: the pursuit of an alternative to Portland cement', *Cem Concr Res*, 41, 750–763.

Sindhunata, Provis J.L., Lukey G.C., Xu H. and van Deventer J.S.J. (2008) 'Structural evolution of fly ash based geopolymers in alkaline environments', *Ind Eng Chem Res*, 47, 2991–2999.

Škvara F., Jilek T. and Kopecky L. (2005) 'Geopolymer materials based on fly ash', *Ceram – Silik*, 49 (3), 195–204.

Sun P. and Wu H-C. (2013) 'Chemical and freeze–thaw resistance of fly ash-based inorganic mortars', *Fuel*, 111, 740–745.

Temuujin J., Minjigmaa A., Lee M., Chen-Tan N. and van Riessen A. (2011) 'Characterisation of class F fly ash geopolymer pastes immersed in acid and alkaline solutions', *Cem Concr Comp*, 33, 1086–1091.

Vance E.R. and Perera D.S. (2009) 'Geopolymers for nuclear waste immobilization' in: Provis, J.L. and van Deventer, J.S.J. (eds) *Geopolymers: Structure, Processing, Properties and Industrial Applications*, Woodhead Publishing, Cambridge, 401–420.

Wan K., Li L. and Sun W. (2013) 'Solid–liquid equilibrium curve of calcium in 6 mol/L ammonium nitrate solution', *Cem Concr Res*, 53, 44–50.

Xie S., Li Q. and Zhou D. (2004) 'Investigation of the effects of acid rain on the deterioration of cement concrete using accelerated tests established in laboratory', *Atmos Environ*, 38, 4457–4466.

Resistance to alkali-aggregate reaction (AAR) of alkali-activated cement-based binders

15

M. Cyr, R. Pouhet
Université de Toulouse, Toulouse, France

15.1 Introduction

The alkali-aggregate reaction (AAR) is an endogenous reaction that usually occurs in Portland cement concretes. It is generated from the internal components of the initial concrete mixture, without the need for exterior aggressive agents. The reaction products are expansive compounds, which induce stresses and hence cracking in concrete. Many international congresses have been dedicated to this concrete pathology (1st to 14th ICAAR, 1974–2012). The two principal types of AAR are the alkali-silica reaction (ASR) and the alkali-carbonate reaction (ACR), the former being much more frequent than the latter.

The alkali-silica reaction (ASR) was first identified in the 1940s (Stanton, 1940) and occurs when the amorphous or poorly crystallized silica phase in an aggregate (e.g., chert, flint, chalcedony or opaline sandstone) is attacked and dissolved by the alkali hydroxides in the concrete pore solution. The formation of an alkali-silica gel leads to concrete swelling and cracking. ASR will develop only if there is a sufficient amount of alkalis in the concrete pore solution and a sufficient moisture level in the concrete and reactive aggregate.

The alkali-carbonate reaction (ACR) involves the de-dolomitization (decomposition of dolomite into brucite and calcite) of carbonate rocks by strongly alkaline solutions, which gives expansive products (Swenson, 1957; Swenson and Gillott, 1964; Deng and Mingshu, 1993). The expansion often occurs within the aggregate particle, causing cracks and thus deleterious expansion of the mass. Some authors report that the dissolution of dolomite could expose silicate minerals initially enclosed in the limestone and so produce alkali-silica or -silicate gels (Gillott, 1964; Hudec, 1990).

One of the common points concerning both ASR and ACR is that the alkali content in the mixture has to be high if abnormal expansion of the concrete is to occur. Knowing that alkali-activated materials (AAM) involve large amounts of alkalis to activate the binder (slag, fly ash, metakaolin, etc.), and that the activators used (mainly alkali silicate, alkali carbonate or alkali sulfate) lead to highly alkaline pore solutions in the hardened mixtures, many concerns can be expressed in regard to AAR.

This chapter reports the mechanisms of AAR and existing data about the vulnerability

Handbook of Alkali-activated Cements, Mortars and Concretes. http://dx.doi.org/10.1533/9781782422884.3.397

of AAM to AAR. The alkali-silica reaction is the principal form of AAR treated here since very few results are available for ACR in alkali-activated systems.

15.2 Alkali-silica reaction (ASR) in Portland cement concrete

15.2.1 Visual and microscopic manifestations of ASR

The alkali-silica reaction in Portland cement concretes can be found in various kinds of structures. Figure 15.1 shows a hydraulic dam in which ASR was detected (Sellier *et al*., 2009). The cracking map pattern is a typical indicator of ASR, and the network of cracks appears when the pressure exerted by the gel exceeds the tensile strength of the concrete, which is generally about 10% of its compressive strength. The expansion can also lead to relative displacements of different portions of the structure, which could cause serviceability problems. However, because of the slow kinetics of ASR deterioration, the risk of catastrophic failure is low since the reaction could take many years to develop. Note that surface deposits (efflorescence) of ASR gel or calcium carbonate can be found along cracks in concrete (Figure 15.1). Popouts caused by a fragment breaking out of the surface of the concrete can also be seen. They leave a hole that is usually 25–50 mm in diameter.

At macroscopic scale, the observation of ASR-affected concretes reveals traces of gel in pores and at the interface between paste and aggregates (circles on Figure

Figure 15.1 View of an ASR cracking pattern in a dam.

15.2). Reaction rims are also seen around reactive aggregates (arrows on Figure 15.2). At microscopic scale (Figure 15.3(a), (b)), the reaction products of ASR have a typical morphology and composition that can easily be identified using scanning electron microscopy (SEM) and energy dispersive X-ray spectrometry (EDX). Smooth textures are usually characteristic of young gels (Figure 15.3(c)), while older gels often crystallize as rosette shapes (Figure 15.3(d)).

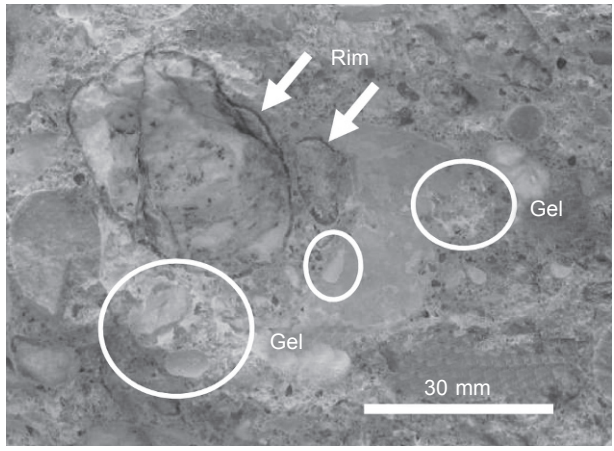

Figure 15.2 Visual observation of dam concrete affected by ASR (same concrete as Sellier *et al.*, 2009). Circles show traces of gel in pores and aggregate prints.

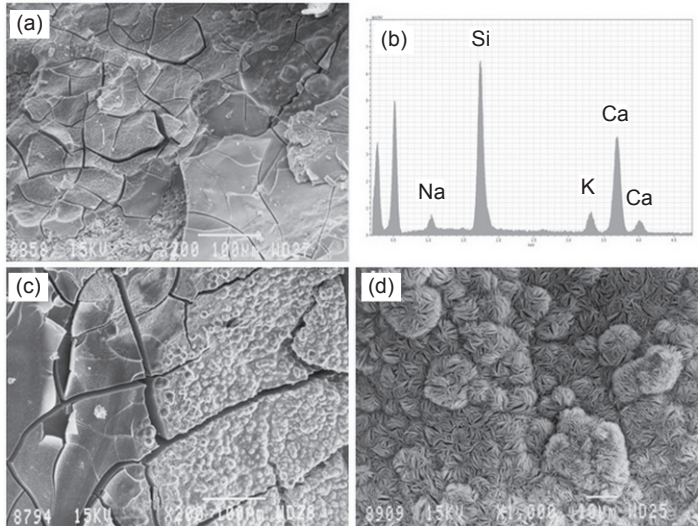

Figure 15.3 Typical morphologies and composition of ASR reaction products obtained with scanning electron microscopy (SEM) and energy dispersive X-ray spectrometry (EDX). (a, b, c) SEM micrographs and EDX spectrum of ASR gel (cracks were provoked by drying in the microscope chamber), (d) Rosette-type morphology of crystallized gel.

In the laboratory, the main tests to identify reactive aggregates or reactive concrete formulations are based on expansion measurements, although other kinds of tests can be performed, such as petrographic examination, chemical tests, etc. Due to the long time needed for ASR to develop, these tests usually need to be accelerated for laboratory use. The main problem is thus to make sure that the accelerated tests do not lead to a denaturation of the phenomenon that could result in misleading information. This key point was studied and discussed for several years in the case of Portland cement concretes, and it must be expected that the same will happen for AAM.

15.2.2 Mechanisms of ASR

The presence of alkalis and reactive silica is necessary conditions for ASR to occur. In Portland cement concretes, alkalis come mainly from the cement, but aggregates, mineral additives and organic admixtures can also contribute some alkali and are usually taken into account. Concrete is usually recognized as being free of abnormal expansion due to ASR if the alkali content in the mixture does not exceed 3–5 kg of Na_2O_{eq} per m^3 of concrete (Rogers and Hooton, 1991; Hobbs, 1993; Thomas *et al*., 1996; Shehata and Thomas, 2000). It should be noted that, in the case of AAM, the alkali content could reach values of more than 40 kg per m^3.

The different forms of SiO_2 that have been reported to be alkali-reactive include opal or opaline silica, chalcedony, cristobalite, tridymite, microcrystalline, cryptocrystalline and highly-strained quartz, and amorphous silica found in volcanic or artificial glasses (Sims and Nixon, 2003). Many aggregates in the world can be completely or partly composed of one or more of these forms of reactive silica. Most of them are listed by RILEM TC 191-ARP (Sims and Nixon, 2003), the main ones being: andesite, chert, granite, gneiss, greywacke, siliceous limestone, quartzite, rhyolite, sandstone and tuff. The silica in aggregates is composed of siloxane bridges (Si-O-Si), and surfaces, both external and internal, are covered with silanol groups (Si-OH).

ASR in concrete is initiated by the dissolution of the different forms of active silicates present in the aggregate. Dent Glasser and Kataoka (1981a, 1981b) identified two mechanisms leading to the dissolution of silica in the concrete environment: hydroxyl ion attack of siloxane bridges (Eq. 15.1) and reaction of hydroxide ions with silanol groups (Eq. 15.2)

$$\equiv Si - O - Si \equiv +20H^- \rightarrow \equiv Si - O^- + {}^-O - Si \equiv + H_2O \quad (15.1)$$

$$\equiv Si - OH + OH^- \rightarrow \equiv Si - O^- + H_2O \quad (15.2)$$

The negatively charged $Si–O^-$ species attracts positive charges such as Na^+, K^+ and Ca^{2+}, which diffuse into the reaction product in sufficient numbers to balance the charge on the negatively charged groups. The approximate stoichiometry of the reaction product, when considering sodium, would be $Na_{0.38}SiO_{2.19}$ (Dent Glasser and Kataoka, 1981a).

The reaction product is usually identified as a gel-like structure that has a higher specific volume than that of the replaced SiO_2. According to Glasser (1992), this

creates swelling pressure, expansion and cracking that are characteristic of the alkali-silica reaction. The gel could also permeate through part of the connected porous volume between aggregate and cement paste and fill a part of the connected porosity (Jones, 1988). Since this gel is confined by the cement paste this leads to a high internal pressure. Several experiments showed the occurrence of 4 MPa osmotic pressures (Pacheco-Torgal and Jalali, 2011). Such tensions are higher than the tensile strength of concrete thus leading to concrete cracking.

Other hypotheses have been put forward to explain the expansion behaviour related to the production of the gel: osmotic pressure (Dent-Glasser, 1979; Diamond, 1989), double layer theory (Prezzi *et al.*, 1998), crystallization pressure theory (Dron *et al.*, 1997), and aggregate swelling theory (Garcia-Diaz *et al.*, 2006). The reader is invited to see the specific papers for more information on each topic.

15.3 Alkali-aggregate reaction (AAR) in alkali-activated binders – general remarks

A few studies exist on the assessment of alkali-aggregate reaction of alkali-activated binders. Most of them use tests such as ASTM C1260, in which the reaction is accelerated by keeping mortar samples in 1 M NaOH solution at 80°C for 14 days. This test is quite rapid, since the results are available in two weeks, but the conditions of the tests are relatively harsh and one can wonder if this test is really representative of what can be found in real structures.

To the best of our knowledge, no *in situ* tests are reported in the literature for AAR of alkali-activated binders, except maybe the tests on some long-term constructions in Russia and China reported by Shi *et al.* (2005), where it was not known whether the aggregates were potentially reactive or not.

The following review separates AAM into two categories with respect to their vulnerability to AAR: alkali-activated slag and alkali-alumino-silicate. The compositions of the raw materials are very different for the two types of AAM; the former contain large amounts of calcium while the latter usually have much less of this element. The presence of calcium could have a significant influence on the swelling of cement-based materials containing alkali-reactive aggregates (Diamond, 1989).

15.4 AAR in alkali-activated slag (AAS)

15.4.1 General trends

The existence of alkali-aggregate reaction in alkali-activated slag is quite controversial and the literature remains divergent. Ground granulated blast-furnace slags are recognized to be efficient in counteracting the effect of ASR in Portland cement-based systems (see, for instance, Hogan, 1983; Thomas and Innis, 1998), and it might

be expected that their use as the only binder should lead to limited ASR effects. However, the reality is more complicated than that, partly due to the presence of a large amount of alkalis in AAS.

In terms of expansion due to ASR, the literature about AAS can be divided into three categories: slight expansion lower than or similar to that of ordinard portland cement (OPC), expansion that cannot be neglected but remains lower than in OPC, and significant expansion that is higher than in OPC. Figure 15.4 summarizes these different states of expansion, for data available in eight papers taken from the literature (Bakharev *et al*., 2001; Gifford and Gillott, 1996; Chen *et al*., 2002; Metso, 1982; Al-Otaibi, 2007; Fernández-Jiménez and Puertas, 2002; Puertas *et al*., 2009; Wang *et al*., 2010). This figure presents the ratios of the expansion of a given mixture (mortar or concrete) relative to the limit proposed in the standard used for the test. A value higher than 1 means that the expansion was higher than the limit suggested in the standard for the mixture to be considered as non-reactive regarding ASR. The data below the figure give the main details of the tests and mixtures. The black bars represent the mixtures made of OPC, while the grey bars are for alkali-activated slag (AAS) systems.

Although it is almost impossible to generalize about the effect of slag in AAS regarding ASR from these data, it is nevertheless possible to point out a few general trends.

- It can be seen from Figure 15.4 that AAS expanded less than OPC, most of the time. Only four AAS mixtures showed expansion higher than OPC (in A1, A2 and D3 of Figure 15.4).
- On the other hand, this does not mean that AAS led to negligible expansion. In fact, of the 40 AAS considered (from eight different papers), 11 were above or at the permitted expansion limit, i.e. around a quarter of the mixtures.
- From the different papers (detailed in the next section), it can be affirmed that waterglass is usually connected with more expansion than other activators, that the increase of the alkali content usually leads to higher expansion, and that the expansion remains under the acceptable limit when non-reactive aggregates are used.

However, it remains difficult to highlight the causes of such results, because of the large differences in the experimental parameters (e.g. differences in type of mixtures used, tests carried out, etc.). Moreover, several characteristics that would have been necessary for the data to be analysed correctly and completely were missing.

15.4.2 Slight expansion, lower than or similar to that of OPC

Al-Otaibi (2007) conducted a study on the durability of alkali-activated slag with ground granulated blast-furnace slag. In this study, the author presented several aspects of durability including a study of the alkali-silica reaction (ASR). The study lasted for up to one year and reported the dimensional changes of eight different concretes (specimen size: $7.5 \times 7.5 \times 28$ cm) exposed to a relative humidity of 100% and a temperature of 60°C (test in compliance with BSI DD218 Draft:1995, now replaced by BS 812-123:1999). The aggregate was from the Thames Valley and was identified

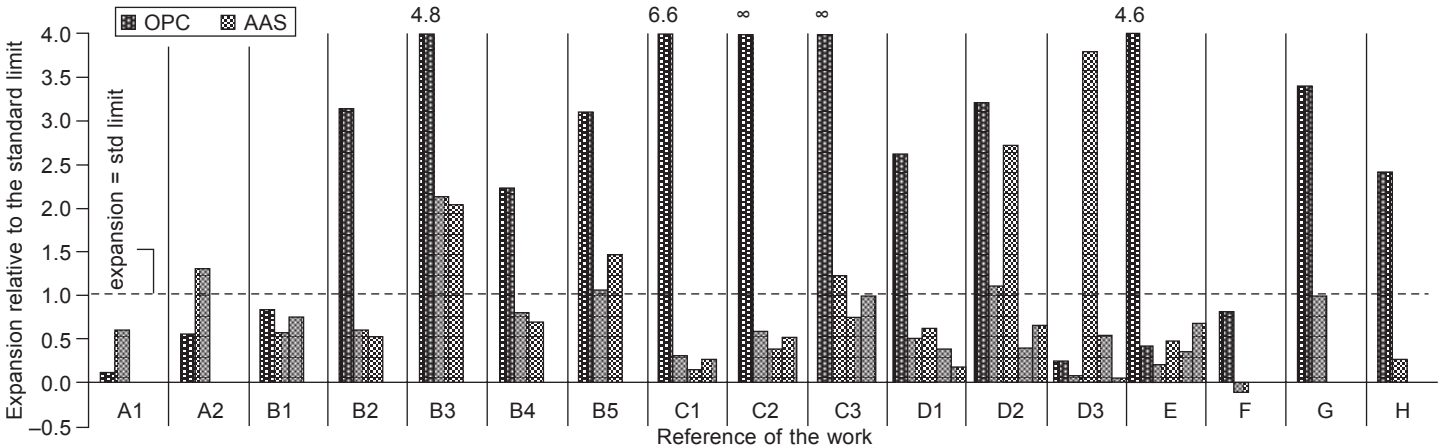

	Reference	Test	Temperature	Age of test	Std Limit	Explanation of the different AAS mixtures
A1, A2	Bakharev *et al.* (2001)	ASTM C 1293	38°C	1 year	0.04%	A1: non-reactive aggregate A2: reactive aggregate
B1 to B5	Gifford and Gillott (1996)	CSA A23.2-14A-94	38°C	1 year	0.04%	B1: non-reactive aggregate B2: reactive (ASR) aggregate S1 B3: reactive (ASR) aggregate S2 B4: reactive (ASR) aggregate V B5: reactive (ASR) aggregate B AAS activated with Na_2CO_3 or Na_2SiO_3
C1 to C3	Chen *et al.* (2002)	based on ASTM C227	38°C	180 days	0.1%	C1, C2 and C3: 2, 3.5 and 5% alkalis, respectively AAS activated with waterglass, NaOH, Na_2CO_3 or Na_2SO_4
D1 to D3	Metso (1982)	based on ASTM C227	40°C	70 days	0.1%	D1, D2 and D3: 3, 8 and 15% of opal, respectively Two types of slag, activated with 1.5 or 2.4% Na
E	Al-Otaibi (2007)	BSI Draft DD218 (1995)	60°C	1 year	0.04%	AAS activated with sodium silicate or sodium metasilicate, with Na_2O content of 4 or 6% Two OPC references: doped and non-doped with alkalis
F	Fernández-Jiménez and Puertas (2002)	ASTM C1260-94	80°C	16 days	0.1%	
G	Puertas *et al.* (2009)	ASTM C1260-94	80°C	14 days	0.1%	
H	Wang *et al.* (2010)	ASTM C1260-94	80°C	14 days	0.1%	

Figure 15.4 Ratios of the expansion relative to the limit proposed in the standard used for the ASR test, for Portland cement and alkali-activated slag systems.

as greywacke, which was recognized to present deleterious expansion attributed to ASR. Of these eight mixtures, four were used as references with Portland cement (OPC class 42.5 N, w/c = 0.48): 100% OPC, and 60% slag–40% OPC, each being cast with and without addition of extra alkalis. AAS concretes were composed of slag activated by either sodium silicate (SS) or sodium metasilicate (MET), having silicate moduli (M_s) of 1.65 and 1, respectively. Both activators were used to reach Na_2O contents of 4% (SS4 and MET4) and 6% (SS6 and MET6).

After a year of measurement, the author concluded (Figure 15.5(a)) that swelling was less for AAS and plain references (i.e., without added alkalis) than for the alkali-doped concretes (100% OPC and 40% OPC–60% slag). The expansion of AAS concretes reached the same order of magnitude as OPC concretes, without added alkalis (Figure 15.5(b)). These concretes presented lower expansion than the limit fixed by the test at 1 year (0.04%), although AAS contained large amounts of alkalis. The general trend was that an increase in alkali content, for a given activator, led to higher expansions: 0.008% for SS4 as against 0.020% for SS6, and 0.014% for MET4 as against 0.027% for MET6. In these tests, metasilicate gave higher expansions than sodium silicate. The author explained these results on the basis of the literature (Talling and Brandstetr, 1989) saying that, in AAS, 80% of the alkalis could be combined in the different hydration products and were therefore less likely to be involved in an alkali-silica reaction. However, it should be noted that the kinetics of expansion was still high after 1 year, especially for higher Na contents. This means that the expansion was probably not over and that ASR could continue at later ages.

Wang *et al*. (2010) carried out a parametric study on the ASR of AAS. They activated slag/metakaolin mixtures (mass ratio of 7/3) with solutions of waterglass mixed with NaOH. The sand used was a mixture of quartz glass (as active aggregate) and standard sand (as non-active aggregate). An accelerated test based on the ASTM C1260-94 standard was used for 28 days on the specimen kept in 1 M NaOH at 80°C.

The study on aggregates showed a significant expansion of OPC for the quartz glass and negligible expansion for standard sand after 14 days in 1 M NaOH. The expansion results on slag-based geopolymer allowed various observations to be made:

- All AAS mixtures presented expansion lower than the standard limit of 0.1%.
- A pessimum effect was highlighted for quartz glass when used at 15% in AAS activated with 4% Na_2O.
- The increase in waterglass content (by Na_2O%) from 3 to 5% involved a decrease in the expansion, probably due to a significant gain in the compressive strength of the mortars when the Na_2O concentration was raised.
- At a given Na_2O content (5%), the lowest modulus of waterglass (SiO_2/Na_2O = 1.2) led to the lowest expansion.
- The comparison of OPC and AAS (5% Na_2O) showed that the former expanded nine times more than the latter. According to the authors, the silica of both slag and reactive aggregates was dissolved by the activator and reacted rapidly with the alkalis participating in the chemical reaction, meaning that alkalis were no longer available for ASR.

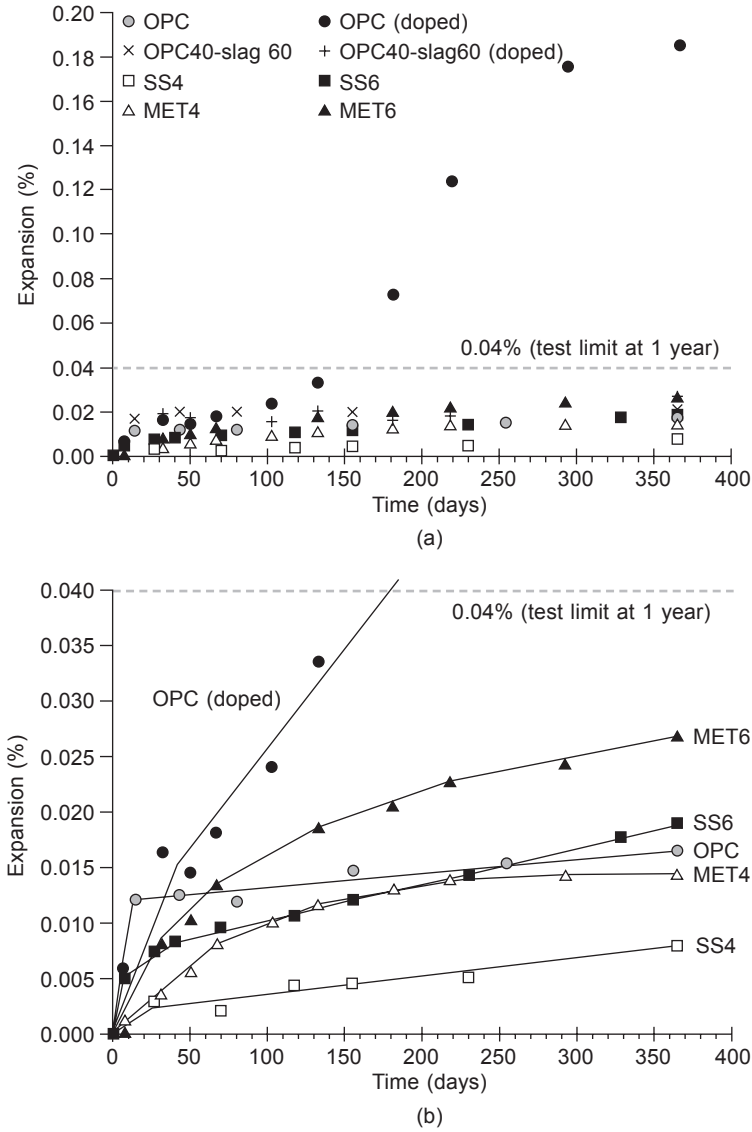

Figure 15.5 (a, b) ASR expansion of concrete mixtures cured at 60°C for 1 year. Mixtures were composed of Portland cement (OPC) and 40% cement + 60% slag (OPC40-slag60), both with and without added alkalis, and slag activated by sodium silicate (SS) and sodium metasilicate (MET) at Na_2O contents of 4% (SS4 and MET4) and 6% (SS6 and MET6). Data from Al-Otaibi (2007).

15.4.3 Non-negligible expansion but lower than that of OPC

Metso (1982) was one of the first to study alkali-aggregate reaction in alkali-activated slag mixtures. Two kinds of granulated blast furnace slag were used (RRGR and

OVGR), differing mainly by their composition: 35.1% SiO_2 and 1.89% Na_2O_{eq} for RRGR, vs. 40.4% SiO_2 and 1.12% Na_2O_{eq} for OVGR. The slags were activated using F-admixture at three concentrations of sodium: 1.6%, 2.4% and 3.9% of pure Na calculated from the weight of slag. The expansion was compared for mixtures composed of a low-alkali Portland cement and an ordinary Portland cement (water/cement ratio of 0.485). Opal was used in the aggregate, at different rates: 3%, 8% and 15% per mass of aggregates. Tests were carried out according to ASTM C277-71, i.e. curing at 40°C, but also at 20°C and 80°C.

The main result is summarized in Figure 15.6. A pessimum effect of opal was highlighted for OPC and some AAS mixtures. The general trend was that AAS expanded less than OPC, especially for low opal content (3%). At 8% opal, only slag RRGR at 2.4% Na came close to the reference, otherwise the expansions were much lower (although RRGR 1.5% Na was higher than the limit of 0.1%). At 15% opal, RRGR at 2.4% Na presented a very high expansion compared to the other mixtures, showing that AAS can be highly alkali-reactive. The author concluded that different slags may have different behaviour regarding ASR, even if they are activated with the same concentration of sodium. He also stated that the increase in the amount of Na strengthened the ASR susceptibility.

Shi (1988) made a study of alkali-activated Portland phosphorus slag cement using a rapid autoclave method (from Tang *et al.*, 1989) and found that the expansion of a low-alkali-activated slag tested with opal did not exceed the limit value of 0.1%. In a later work (Shi, 2003), he stated that alkalis in AAS paste could exist in three forms, as for OPC: (1) incorporated into C-S-H, (2) physically adsorbed on the surface of hydration products, and (3) free in pore solution. However, unlike OPC, the C-S-H from AAS had a very low Ca/Si ratio, and thus a much higher capacity to fix alkalis. As alkalis were more concentrated in C-S-H, it was expected that less free alkali would be available for ASR than originally assumed. A series of studies

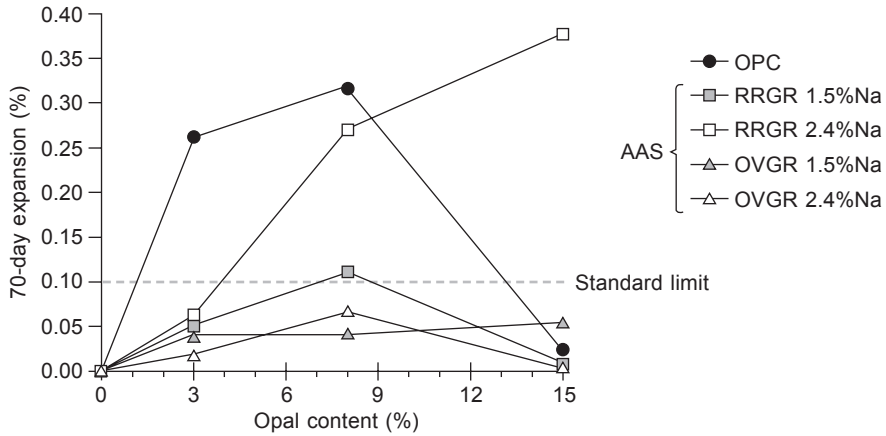

Figure 15.6 Expansion at 70 days of mortars made with 3, 8 and 15% opal. Comparison of OPC with AAS from two different slags activated at 1.5 and 2.4% Na. Data from Metso (1982).

involving Pu and Yang (Pu and Chen, 1991; Pu and Yang, 1994; Yang, 1997; Yang *et al*., 1999) were carried out in the 1990s on the alkali-aggregate reaction in alkali-activated slag cements. Pu and Chen (1991) and Yang (1997) noted that the addition of silica fume could eliminate expansion caused by AAR in AAS. Moreover, the use of 30–50% of low-calcium fly ash was found to reduce the expansion of AAS cement below the accepted limit (Yang, 1997). Pu and Yang (1994) made a study using a rapid autoclave method (from Tang *et al*., 1989) and arrived at the conclusion that AAR took place in AAS matrices, the expansion due to this reaction depending on the activator used and the reactive aggregate content. Thus in NaOH-based slags, non-destructive expansion was found with up to 15% of reactive aggregate, whereas in carbonate or sodium silicate-based systems, the reactive aggregate content could be much higher, i.e. up to 50%. Yang (1997) and Yang *et al*. (1999) investigated several factors affecting the alkali-aggregate reaction, such as the basicity of slags or the concentration of activator. The main conclusions were as follows:

- The expansion developed mainly during the first 30–60 days and reached a plateau thereafter, whatever activator used. Furthermore, this expansion increased with the alkali concentration or the basicity of slags, or the reactive aggregate content (up to 30%).
- For an equal NaOH content, it was found that the sodium silicate-activated slag cement showed the highest expansion (up to 0.25% with 30% of silica glass) and the NaOH-activated slag cement the lowest expansion (up to 0.05% with 30% of silica glass).
- When reactive aggregate content was less than 5%, the expansion of alkali-activated cement systems was within the expansion limit, regardless of the alkali dosage and the nature of activators.

In 1996, a study conducted by Gifford and Gillott (1996) addressed the alkali-silica reaction (ASR) and alkali-carbonate reaction (ACR) in alkali-activated slag (AAS) concretes. AAS was made of a slag (containing SiO_2 = 33.5%, Al_2O_3 = 12.5%, CaO = 39.3%, MgO = 11.7%, Na_2O_{eq} = 0.8% by mass, Blaine fineness = 340 m²/kg) and an activator composed of either sodium silicate or sodium carbonate dissolved in mixing water to reach 6% of Na_2O_{eq} per mass of slag. The comparison was made with concretes formulated with Portland cement (CSA Type 10), w/c ratio of 0.43, and an alkali content boosted with a NaOH solution to obtain an Na_2O_{eq} of 1.25% (by mass of cement). Six sources of Canadian aggregate were used: one non-reactive aggregate, four siliceous aggregates (potentially reactive to ASR) and one dolomitic limestone (potentially reactive to ACR). The study was conducted according to CSA A23.2-14A-94, on 7.5 × 7.5 × 30.5 cm prisms cured at 38°C and 100% RH over a period of one year. The expansion limit for the concrete to be considered as non-reactive was 0.04%.

The expansion measurements on specimens at 1 year (Figure 15.7) showed that all OPC concretes with reactive aggregates led to abnormal expansions, exceeding the 0.04% limit of the standard. Concerning AAS, concretes exhibited expansions significantly lower than those displayed by the OPC concretes. However, as seen in Figure 15.7, two of the reactive aggregates (S2 and B) led to expansions higher than the standard limit, for both types of activator (without being able to conclude which was the worse activator regarding ASR).

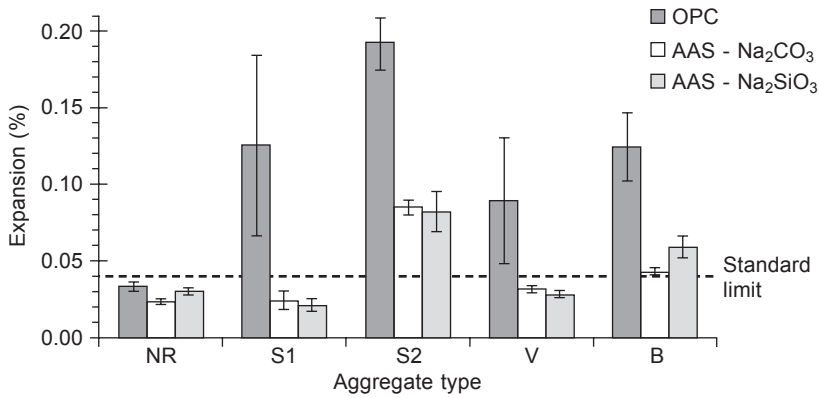

NR: Control–crushed dolostone (innocuous)
S1: Partly crushed gravel (–75% reactive quartz-bearing particles)
S2: Crushed siliceous limestone (small amount of microscopic chalcedony, black chert)
V: Crushed gravel (small amount of chert particles)
B: Crushed gravel (small amount of chert particles)

Figure 15.7 Expansion at 1 year of OPC and AAS concretes cured at 38°C and containing one non-reactive and four ASR-reactive aggregates. Data from Gifford and Gillott (1996).

The available data did not allow the reasons for such results to be fully understood. However, the high alkalinity of AAS was thought to lead to a rapid dissolution of reactive silica in the aggregates during the early period of hardening. Moreover, it was supposed that the viscous alkali-silica gel could be more easily accommodated in the porosity of AAS systems than in OPC concrete.

It should be noted that this study also evaluated one aggregate (dolomitic limestone) regarding alkali-carbonate reaction. The results showed very significant damage on the OPC and even more visible damage was observed on AAS with the same aggregates, with an expansion twice that of the cement (OPC = 0.305%, Na_2CO_3-activated AAS = 0.720% and $Na_2O.SiO_2$-activated AAS = 0.617%). The authors concluded that ACR was due to the increased alkalinity of AAS systems, which could involve dedolomitization and subsequent swelling of dry clay minerals when they were exposed to water.

Fernández-Jiménez and Puertas (2002) made AAS using Spanish granulated blast furnace slag, with a specific surface area of 460 m^2/kg, mixed with a solution of NaOH (4% Na_2O per mass of slag). The solution/slag ratio was 0.57. The aggregate used was opal with a reactive silica content of 21%. The comparison was made with CEM I 42.5. The authors used standardized test ASTM C1260-94, with specimens ($2.5 \times 2.5 \times 23$ cm) stored at 80°C in containers with deionized water or 1 M NaOH solution.

They found that, for the same storage conditions, cement showed higher expansion than AAS, while for the same matrix, conservation in 1 M of NaOH solution was more likely to trigger swelling. At 16 days, OPC in the NaOH solution had almost reached the expansion limit of 0.1%, while AAS in similar conditions was still in a shrinkage phase (Figure 15.8). It took close to 80 days for AAS to achieve 0.1% of expansion, but the mortar continued to swell until the end of the test, at 140 days.

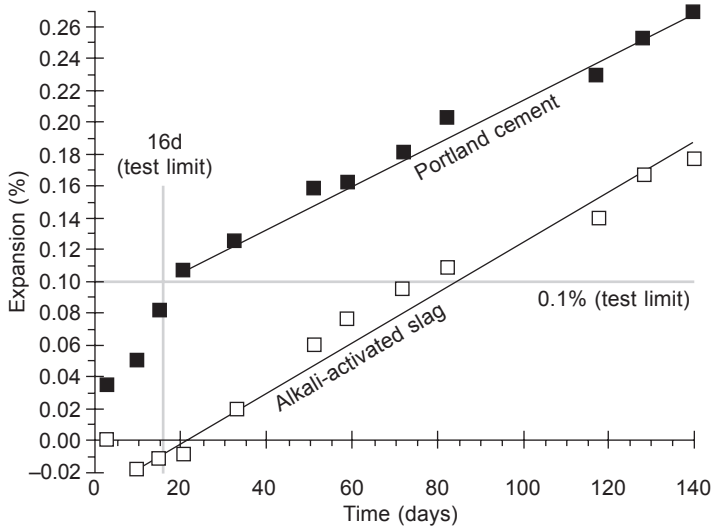

Figure 15.8 Expansion of OPC and AAS mortars kept in 1 M NaOH at 80°C. Data from Fernández-Jiménez and Puertas (2002).

The expansion of OPC and AAS in water (80°C) was not critical up to 140 days. The SEM analysis of AAS showed a good paste-aggregate interface with some microcracks, most numerous in the case of NaOH immersion. The main reaction product of AAS in the two curing conditions was calcium silicate hydrate but, in the case of AAS-NaOH, some rosette crystals typical of ASR were found.

It was deduced from these tests that, without external alkali supply, AAS does not swell. In contrast, an external alkali supply (e.g. 1 M NaOH solution) leads to the formation of a reaction product typical of ASR and probably contributing to the expansion of the specimen. The fact that the swelling produced in AAS was slower than for OPC was attributed to the competition for alkalis between the slag and the reactive aggregate. The authors concluded that the accelerated test used (80°C in 1 M NaOH) was probably unsuitable for the study of ASR in AASs, due to their slower rate of expansion in the first days of the test.

Chen *et al*. (2002) studied the behaviour of different alkali-activated slag cements (AAS) in the presence of ASR-reactive aggregates. They used three different blast furnace slags, named S1 (basic slag), S2 (neutral slag) and S3 (acid slag), and comparison was made with an ordinary Portland cement. Alkaline activation of the slag was achieved using four different solutions: Na_2CO_3, NaOH, Na_2SO_4 and an industrial waterglass solution (modulus 3.29). The reactive aggregates used in this study were quartz glass, previously crushed and sieved, and non-reactive aggregates were standard Chinese sand. Six samples of each mixture were prepared (dimensions $10 \times 10 \times 60$ mm), with a cement/aggregate ratio of 1:2.25 and w/c of 0.4. They were kept at 20°C and RH of 95% for the first 24 h. After the initial measurements, the samples were placed in a sealed container at 38°C and 95% RH.

The main results and conclusions were as follows:

- Whatever the amount of alkali, the type of reactive aggregates, or the aggregate size, the maximum expansion was always reached for the system with waterglass, while the lowest expansion was always measured for the NaOH system.
- The expansion increased with the quantity of alkalis used in the mixtures. For instance, the expansion of the AAS–waterglass mortar increased from 0.04% to 0.16% when the amount of alkali changed from 2% to 6.5%. However, it was pointed out that no expansion measured for an alkali content equal to or less than 5% exceeded 0.1%, and such expansions were therefore probably not destructive.
- The basic slag (S1) resulted in the greatest expansion (0.08% at 180 days), while the use of acid slag (S3) significantly reduced the expansion (0.03% at 180 days), neutral slag giving an intermediate value of 0.5% after the same time. The authors therefore concluded that the use of acid slag should be recommended to reduce the impact of the AAR, knowing that it might decrease the activity of the AAS.
- The expansion of AAS mixtures was systematically lower than that of OPC. The authors explained this difference in behaviour by means of three reasons/mechanisms: firstly, since slags are inhibitors of AAR, and as they are the main component of AAS, it would make sense that the expansion should be smaller than in OPC; second, the alkali of AAS participated in an independent reaction leading to the formation of alkaline hydrate and thereby reduced the amount of free alkali; and third, the gel formed in the AAS absorbed alkalis very strongly, which significantly reduced the free alkali activity.

Puertas *et al*. (2009) studied the effect of aggregate type on the AAR behaviour of alkali-activated slag (AAS) compared to OPC mortars. The slag (vitreous content of 99%) was activated by a waterglass solution containing 4% Na_2O by slag mass and a SiO_2/Na_2O ratio of 1.08. Three types of aggregates were used: two calcareous sands (reactive and non-reactive) and one siliceous sand. AAR tests were run according to the ASTM C1260-94 standard ($2.5 \times 2.5 \times 28.7$ cm specimens) at 80°C in 1 M solution of NaOH. Volume stability, compressive strength, microstructural and mineralogical characterization were monitored for up to 4 months on OPC and AAS samples.

The results showed the following:

- At 14 days, the expansion of OPC mortar with siliceous aggregate was 3.6 times the accepted limit fixed by the standard (0.36% vs. 0.10%). For the same age and aggregate, the AAS mortar was at the limit of 0.10%. So even though the expansion of AAS was much lower than that of OPC, it cannot be considered negligible. The expansion of these two mortars continued up to 4 months and was still in progress at the end of the test. The compressive strength of OPC and AAS siliceous mortars decreased between 14 days and 4 months. SEM observations confirmed that the aggregate was attacked for OPC and AAS in accelerated conditions. The ASR gels in AAS mortars looked like rosettes, with a lower concentration of calcium than OPC ASR gels.
- The expansions at 14 days and 4 months for calcareous aggregate mortars were very low, for both OPC and AAS mixtures. SEM study showed that the surface of the non-reactive calcareous aggregate was attacked, which resulted in the formation, at the paste/aggregate interface, of a whiteish gel having a high calcium content. This gel improved cohesion between paste and aggregate and explained, according to the authors, the low porosity and high strength of AAS mortar. Finally, although no adverse effects were observed on the strength with the reactive calcareous sand, the SEM observations showed that alkali-calcareous aggregate reactions did take place after 14 days.

Krivenko *et al*. (2013) studied the mechanisms of AAR prevention in slag-based systems. Five different aggregates (olivine, basalt, andesite, perlite and quartz) were used for the tests. The alkaline activation of the mixtures was achieved by using sodium carbonate and sodium metasilicate pentahydrate. The expansion tests, carried out on mortar specimens (2.5 × 2.5 × 28.5 cm) at 100% RH and two temperatures (38°C and 70°C), showed that the alkali-activated slag cement (2.5% Na_2O_{eq}) presented:

- expansions much lower than the critical expansion limit for both tests, the maximum expansion obtained (for andesite aggregate) being less than 25% of the acceptable limit; the use of 15% of metakaolin in the mixtures led to zero-expansion or even to a slight shrinkage for all aggregates;
- higher expansion than low-alkali Portland cement (0.22% Na_2O_{eq}), but this expansion was still considered as admissible since it was well below the critical expansion limit;
- much lower expansion than high-alkali Portland cement (1.3% Na_2O_{eq}) and alkali-activated slag Portland cement (60% of slag by mass and 2.5% of Na_2O_{eq}), especially for highly reactive aggregates (andesite).

Low expansion in alkali-activated slag mortars was attributed to the active Al_2O_3 contained in the slag glass (and probably in metakaolin when this additive was used). SEM observations of the ITZ showed the formation of alkaline aluminosilicate zeolite-like hydrates ($Na_2O \bullet Al_2O_3 \bullet mSiO_2 \bullet nH_2O$), favoured by the high alkali content and the presence of aluminium oxide. This dense, sound, impermeable hydrate formed a shell around the aggregate grains, which could stop further development of the destructive reaction. Therefore the free aluminium was believed to play a very important role in these systems because it would significantly control the structure of the gels formed, and thus determine whether the gels were destructive or beneficial.

15.4.4 Significant expansion higher than OPC

Hakkinen (1986) studied the properties of alkali-activated slag concrete and found that the expansion of AAS increased as the alkali content increased from 2.2% to 5.3% for an opal content of 8%. But when the amount of alkali was about 2% by mass of slag (typical alkali content for this kind of concrete), the measured expansion was not higher than in OPC. This study also showed that the expansion increased when the opal content increased (from 3 to 15%) for a given alkali content of 2.4%. So the conclusion was that the expansion was associated with the pessimum SiO_2/Na_2O ratio of alkali-silica reaction gel. This was in agreement with the result obtained by Hobbs (1988) who noted that the pessimum ratio varied with the aggregate-to-cement ratio, and Zhang and Groves (1990) who found that the pessimum SiO_2/Na_2O ratio was around 12–13.

Bakharev *et al*. (2000) used the ASTM C 1293 standard for a 22-month study of concrete prisms (7.5 × 7.5 × 28.5 cm) cured in moist conditions at 38°C. All concretes were designed to reach 40 MPa at 28 days. They were made of either

reactive coarse aggregates from Queensland (Australia) or non-reactive aggregates. The blast furnace slag, supplied with 2% blended gypsum, had a basicity coefficient ($CaO + MgO/SiO_2 + Al_2O_3$) of 0.93 and was ground to a fineness of 460 m^2/kg. It was activated by a solution of sodium silicate and sodium hydroxide having a modulus (mass ratio of SiO_2 to Na_2O) of 0.75. The prepared AAS concrete contained 4% Na by mass in proportion to slag. The reference concrete (w/c = 0.5) was made with Portland cement.

The main conclusion of these tests was that AAS concrete was more likely to be deteriorated by ASR than OPC. The results of the dimensional change over time showed a significant, fast expansion of AAS made with reactive aggregates, the limit of 0.04% indicated by the standard being reached in less than 2 months. In contrast, expansion of OPC did not exceed 0.025% at 12 months and specimens did not present any visual damage at 22 months, whereas surface cracks were visible for AAS. Although the 0.04% limit was not reached for AAS in the case of non-reactive aggregates, the expansion could not be neglected (0.025% at 22 months), as it was higher than that of the OPC reference. Evidence of ASR reaction products in the matrix was confirmed by SEM-EDX, showing the presence of an alkali silica gel (containing Si, O, Ca, Na, K) which was found at the interface with the aggregates. According to the authors, the greater expansion of AAS compared to OPC was explained by the very high concentration of alkalis in the pore solution. However, they claimed that expansion in slag concretes could be mitigated by their rapid strength development.

15.5 AAR in alkali-activated fly ash and metakaolin

In contrast to the findings for alkali-activated slag, almost all the papers in the literature agree that the use of alumino-silicate as a raw material usually involves less abnormal swelling due to AAR, even with very reactive aggregates.

Between 1994 and 2005, Davidovits reported a series of experiments comparing the AAR behaviours of OPC and geopolymer. In 1994, he pointed out that, according to the ASTM C227 standard, no deterioration due to expansion should appear in geopolymers, although they contain more than 9.2% alkali (Davidovits, 1994). In the author's opinion, the explanation was provided by ^{29}Si and ^{27}Al NMR tests, which showed that the geopolymers were the synthetic analogues of natural pozzolan, well known for effectively suppressing the effects of alkali-aggregate reaction. A few years later, Davidovits *et al*. (1999) used an accelerated expansion test in a saturated NaCl bath to show that a geopolymer with 10% alkali content reached only a fifth of the expansion experienced by mortar made with a CEM I 42.5R cement (0.05% vs. 0.25% at 14 days). Davidovits (1999, 2005) again confirmed the conclusion of his previous work, by presenting a curve where zero expansion was found for a potassium based geopolymer (9.2% alkali content) subjected to the ASTM C227 accelerated test.

15.5.1 Alkali-activated fly ash systems

Two studies partly or totally dedicated to ASR of activated fly ash (AAFA) systems were carried out by Fernández-Jiménez *et al*. (2007) and García-Lodeiro *et al*. (2007). The authors used a standardized test (ASTM C1260) to evaluate the ASR of AAFA systems compared to one containing Portland cement, by measuring the dimensional variation of 2.5 × 2.5 × 28.5 cm samples immersed in a 1 M solution of sodium hydroxide at 85°C (instead of 80°C as specified in the standard). In OPC systems, the expansion must be below 0.1% after 16 days of immersion to indicate innocuous behaviour in most cases.

In the work of Fernández-Jiménez *et al*. (2007), the expansion tests were carried out with a siliceous sand composed of quartz and calcite, commonly used to make concrete in Spain and regarded as non-reactive. García-Lodeiro *et al*. (2007) studied the behaviour of three different types of mortar for OPC and AAFA systems: one containing the non-reactive siliceous sand, one made of opal sand, and finally one that was a mixture of 90% non-reactive sand and 10% opal sand.

The binder in the Portland cement references was a CEM I with low alkali content (Na_2O_{eq} of 0.46%). AAFA mortars were made with two similar Spanish Type F fly ashes, with low calcium content (CaO = 3.21% and 2.44%) and a SiO_2/Al_2O_3 ratio around 2.1. The activating solution was composed of an 8 M NaOH solution or a mixture of 85% 12.5 M NaOH + 15% sodium silicate ($SiO_2/Na_2O = 0.16$). The sand/binder mass ratio of the mortars was 2.25 and the liquid/solid ratio was 0.47. The mortars were initially cured for 20 h at 85°C and a RH of 99%. The details of the mortar mixtures are given in Table 15.1.

Table 15.1 Mixture details for ASR expansion tests (ASTM C1260: 85°C in 1 M NaOH) carried out by Fernández-Jiménez *et al.* (2007) and García-Lodeiro *et al.* (2007) on Portland cement and alkali-activated fly ash systems

Ref	Mixture	Sand	Binder	Activator	Sand/binder	Liquid/solid
A Fernández-Jiménez *et al.* (2007)	OPC	NR[a]	CEM I	–	2.25	0.47
	AAFAN		Fly ash A	8M NaOH		
	AAFAW			85% 12.5M NaOH 15% sodium silicate[b]		
B García-Lodeiro *et al.* (2007)	OPC1	NR	CEM I	–		
	AAFA1		Fly ash B	8M NaOH		
	OPC3	90% NR 10% opal	CEM I	–		
	AAFA3		Fly ash B	8M NaOH		

[a] NR: non-reactive siliceous sand.
[b] $SiO_2/Na_2O = 0.16$.

The expansion results for immersion of up to 16 days are given in Figure 15.9(a). The tests were prolonged to 90 days (García-Lodeiro *et al*., 2007 – B in the figures) and 180 days (Fernández-Jiménez *et al*., 2007 – A in the figures), as shown in Figure 15.9(b).

It was seen that all reference mortars with Portland cement showed very high expansions, the value of 0.1% being exceeded before the ninth day. The expansions of more than 0.20% at 16 days after casting were indicative of potentially deleterious expansion, according to ASTM C1260. The maximum expansion was obtained for OPC3, which contained 10% of opal (pessimum effect of this aggregate; Hobbs, 1988). It is noteworthy that the siliceous sand, considered by the authors as non-reactive, presented much higher expansion values than the limit imposed by the test. This could be due to the presence of cryptocrystalline quartz in its structure.

Generally speaking, the alkali-activated fly ash mortars presented much lower expansions than their OPC replicate. However, it cannot be stated that AAFA systems are completely safe regarding ASR swelling. On the one hand, some results were indicative of innocuous behaviour (expansion < 0.1% at 16 days), for instance AAFA mixtures with siliceous sand as the sole aggregate and NaOH as the sole activator. On the other hand, a few AAFA mortars showed disturbing behaviour:

- AAFAW, containing a siliceous sand and an activator made of 15% of sodium silicate and 85% of 12.5 M NaOH, showed significant expansion in the first days of the test, and

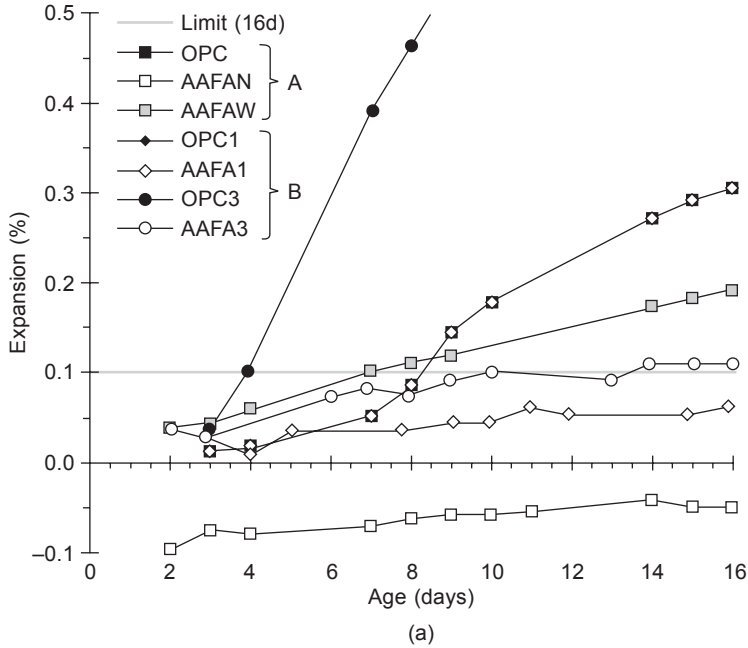

Figure 15.9 Expansion of mortars made of Portland cement (OPC) or activated fly ash (AAFA) up to 16 days (a) and 180 days (b), according to ASTM C1260 (85°C in 1 M NaOH). Data from Fernández-Jiménez *et al*. (2007) (A) and García-Lodeiro *et al*. (2007) (B).

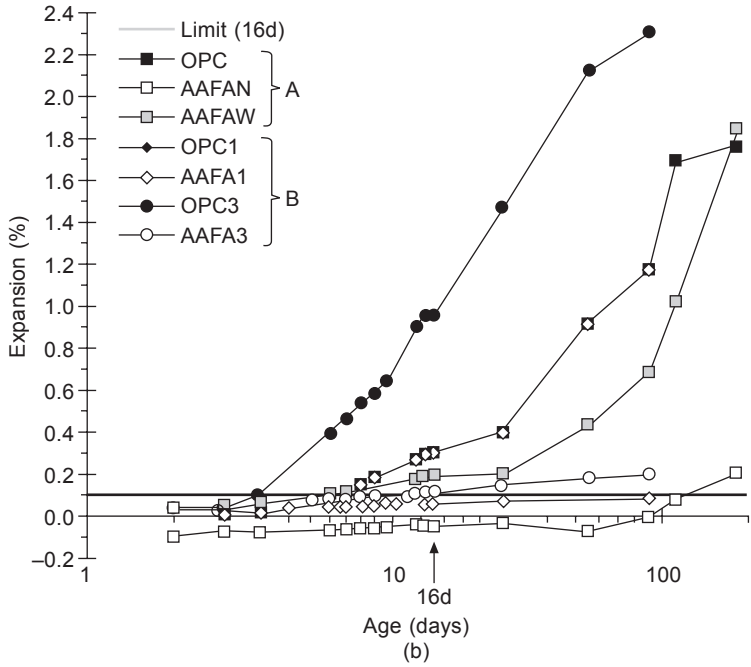

Figure 15.9 Continued

followed a trend similar to that of OPC. However, no surface cracking was seen after 16 days. According to the authors, the conditions of the accelerated test may have caused the formation of ASR-expansive products and/or zeolites that were believed to be the cause of a certain amount of stress, which would contribute to the expansion detected.

- AFAN, composed of a siliceous sand and activated by a 8 M NaOH solution, presented an increase in its kinetics of expansion after 100 days, raising the question of whether the ASR was only delayed. However, it should be said that 100 days at 85°C in 1 M NaOH solution could represent a very long period of *in situ* conservation.
- AAFA3, made of 10% opal sand, had an expansion slightly higher than the limit of 0.1% at 16 days.
- The expansion results of AAFA2, containing 100% opal sand and activated by an 8 M NaOH solution, were not presented in the paper due to the early deterioration of the specimens. This was probably caused by an almost immediate dissolution of highly reactive silica from the opal, as proved by the disappearance of the characteristic XRD peak of this mineral (see Figure 15.9 – B, from García-Lodeiro *et al.*, 2007).

In both papers, studies were also made with SEM/EDX and XRD to better understand the mechanisms of ASR in OPC and AAFA matrices. OPC systems (García-Lodeiro *et al.*, 2007) showed the presence of gel with high sodium concentration at 16 days and gel morphology such as ‘rosette’, ‘pseudo-rosette’ or ‘rod’ at 90 days. A decrease in the portlandite content, characterized by a decrease of XRD-peak intensities, was found between 16 and 90 days. This was interpreted as an incorporation of calcium in the ASR gels.

In AAFAN, SEM observations at 16 days did not reveal the formation of the gel structure typical of ASR, but crystalline phases of zeolites were found: hydroxysodalite, herschelite and zeolite P (Fernández-Jiménez *et al.*, 2007). The presence of zeolite P was explained by the very aggressive conditions to which the specimens were subjected. At 180 days, SEM observation showed small amounts of alkali-silicate gel containing calcium (Ca/Si = 0.15 and Na/Si = 0.72) with pseudo-rosette morphology, and a supplementary zeolite phase: analcime (Si/Al = 2.40 and Na/Al = 1.26) (Fernández-Jiménez *et al.*, 2007). This might explain the increase in the kinetics of expansion of this mortar after 100 days.

For AAFA1, García-Lodeiro *et al.* (2007) mainly found an amorphous phase without calcium at 90 days and the presence of zeolites P, but also very few alkali-aggregate reaction products with pseudo-rosette morphology. The same observations were made for AAFA3, with a greater amount of zeolite, probably due to the 10% of highly reactive silica introduced by the opal.

Although some evidence of an attack of the aggregates was found in the case of AAFA, expansions were lower than in OPC systems. According to the authors of these papers, this could be for a variety of factors:

- A deficiency in calcium, which plays an essential role in ASR, as already stated in various studies (Dent Glasser and Kataoka, 1982; Chatterji, 1979; Thomas, 1998). Several authors (Bleszynski and Thomas, 1998; Shehata and Thomas, 2000) proved that the addition of $Ca(OH)_2$ promoted ASR-induced expansion and others (Hou *et al.*, 2004) revealed a direct relationship between portlandite uptake and the formation of ASR gels.
- Alkali-silicate gel with pseudo-rosette morphology would be sufficiently fluid to seep through cracks and partially or completely fill the gaps in the matrix, thereby attenuating expansion.
- The increased zeolite concentration due to the ASR would not be harmful because zeolites normally form as a precipitate in the pre-existing pores in the matrix, so their growth would not cause stress that could lead to the formation of cracks.

However, it must be kept in mind that more realistic conditions of conservation (than 85°C in 1 M NaOH solution) still need to be tested to confirm the possibly innocuous behaviour of alkali-activated fly ash systems.

15.5.2 Alkali-activated metakaolin systems

Results for metakaolin-based geopolymers are scarce. Li *et al.* (2005, 2006) compared the ASR behaviour of cement-based binders (Portland cement and slag, fly ash and silica fume) to that of one geopolymer composed of metakaolin, fly ash, silica fume and alkali-activator. The alkali content in the geopolymer reached 12.1%. The reactive aggregate was a crushed quartz glass with an amorphous silica content of more than 90%. The ASR test was based on ASTM C441, itself based on ASTM C227 (38°C). The results showed that the higher expansions were obtained for mortars containing Portland cement only, followed by mixtures with pozzolans (65–82% reduction of expansion). The geopolymer mortar, which contained a much higher alkali content than OPC-based mortars (12.1% vs. less than 1%), led to negligible length variations

(0.01% at 14 days and –0.03% at 90 days). According to the authors, 'geopolymer does not generate any dangerous alkali-silica reaction' since there would not be enough free alkalis to react with the reactive aggregate and thus produce alkali-silica gel, because Na^+ and K^+ are fixed in the framework cavities of SiO_4 and AlO_4 to balance the negative charge of Al^{3+}.

Experiments have recently been performed in our laboratory on the ASR reactivity of geopolymer made of flash-calcined metakaolin in the presence of aggregates with different reactive silica contents in comparison with OPC. The raw material used in this study was a metakaolin made with a 'flash' calcination (temperature around 700°C for a few tenths of a second) and the activation was achieved with a commercial waterglass solution ($Na_2O \bullet nSiO_2 \bullet mH_2O$) having a SiO_2/Na_2O ratio of 1.68. The OPC mortar was composed of CEM I 52.5 N having a w/c ratio of 0.5. The alkali concentration was boosted to 8 kg/m^3 by adding pure KOH during the preparation to ensure the reactivity of the aggregates. To make the study exhaustive, five aggregates of different natures and compositions were chosen: one was selected for its low reactivity regarding ASR (quartz), while the other four were aggregates recognized to be alkali-reactive (quartzite, siliceous limestone, crushed glass and alluvial sand with opal). An accelerated test was carried out on each specimen, in which the size, mass and dynamic Young's modulus were monitored over time for up to 250 days, with a cure at 60°C in a humid environment. Figure 15.10 presents the evolution of the expansions measured over time for each sand and binder used. The results clearly show a large difference in behaviour between the two binders from the beginning of the test. The expansions measured for the geopolymers varied between –0.02% and 0.03%, while the variations found for OPC were between 0.04% for the least reactive aggregate and almost 0.3% for sand containing opal.

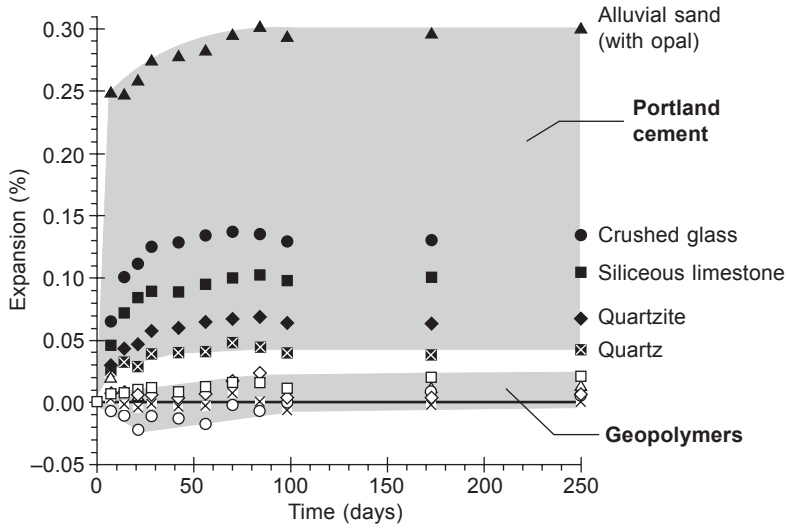

Figure 15.10 Expansion at 60°C of mortars composed of Portland cement or alkali-activated metakaolin (geopolymer), and containing different kinds of alkali-reactive aggregates.

Further analysis by SEM showed the presence of amorphous alkali-silicate gel at the interface between the geopolymer and the crushed glass aggregates (Figure 15.11). These results indicate that flash-metakaolin-based geopolymer seemed to resist ASR better than Portland cement mortars did. A gel formation at the interface between the geopolymer paste and the alkali-reactive aggregates seems probable but, unlike in OPC, would not be expansive.

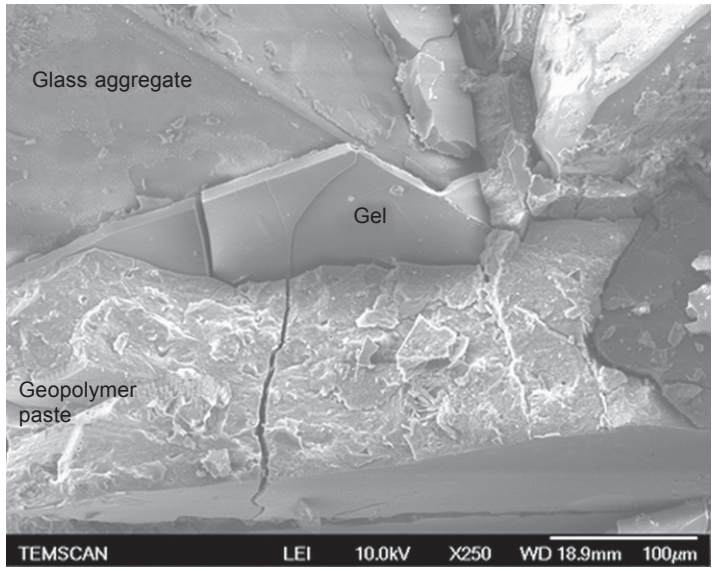

Figure 15.11 SEM micrograph of an amorphous alkali-silicate gel at the interface between MK-geopolymer and crushed glass aggregates. Mortar kept at 60°C for 250 days.

15.6 Future trends

Many important topics require further research:

- Since the interest in AAM is continuing to increase, these materials need to be further characterized regarding durability aspects such as AAR, in order to arrive at standards that will help their use in concrete. There are currently not enough experimental results (*in situ* and at a laboratory scale) for general conclusions to be drawn on the behaviour of AAM with respect to alkali-aggregate reaction.
- The results of accelerated tests need to be compared with the *in-situ* behaviour of concrete in real structures. It has been pointed out that accelerated tests are sometimes far from reality, so feedback from experience is still necessary to confirm the laboratory conclusions.
- Mechanisms explaining why AAM are sometimes affected (or not) by AAR need to be assessed. Some hypotheses have been put forward but most of them lack sufficient, convincing proof.
- Since calcium is crucial in ASR, calcium-based alkali-activated materials deserve a special attention concerning ASR mitigation measures.

- Mathematical models for AAR should complement the models already developed for Portland cement-based materials. These models could help in understanding and predicting the behaviour of AAM regarding the durability of concrete.

15.7 Sources of further information

This chapter has presented an overview of the susceptibility of alkali-activated binders to AAR, based on the knowledge currently available in the literature. Further information on this subject may be found in books devoted to AAM, such as those by Shi *et al*. (2005) and Provis and van Deventer (2009).

AAR is also being considered by the 5-year RILEM Technical Committee 247-DTA (Durability testing of alkali-activated materials), chaired by Professor John L. Provis and initiated in 2012. It is anticipated that the working groups will deliver a set of recommendations based on round-robin tests of standardized alkali-activated material mix designs according to specific AAR testing protocols. The recommendations will focus on answering the following questions:

- What is the best method for testing, in a laboratory environment, the likely AAR durability of an alkali-activated binder or concrete according to specific modes of degradation?
- Which parameters of mix design and/or sample conditioning show the greatest impact on the test outcomes, and how do these correspond to likely in-service performance?
- What recommendations can be made for the formulation of an alkali-activated material that is as resistant as possible to AAR?

References

1st ICAAR, Aalborg Portland R and D seminar on alkali-silica reaction, Karlstrup, Denmark, 1974.
2nd ICAAR, Symposium on AAR, preventative measures, Reykjavik, Iceland, 1975.
3rd ICAAR, The effects of alkalis on the properties of concrete, Wexham Springs, London 1976.
4th ICAAR, The effects of alkalis in cement and concrete, Purdue University, Indiana, USA, 1978.
5th ICAAR, The effects of alkalis in cement and concrete, Cape Town, South Africa, 1981.
6th ICAAR, Alkalis in concrete, research and practice, Copenhagen, Denmark, 1983.
7th ICAAR, Concrete alkali-aggregate reactions, Ottawa, Canada 1987.
8th ICAAR, Alkali-aggregate reaction, Kyoto, Japan, 1989.
9th ICAAR, Alkali-aggregate reaction in concrete, London, UK 1992.
10th ICAAR, Alkali-aggregate reaction in concrete, Melbourne, Australia, 1996.
11th ICAAR, Alkali-aggregate reaction in concrete, Quebec City, Canada, 2000.
12th ICAAR, Alkali-aggregate reaction in concrete, Beijing, China, 2004.
13th ICAAR, Alkali-aggregate reaction in concrete, Trondheim, Norway, 2008.
14th ICAAR, Alkali-aggregate reaction in concrete, Austin, Texas, USA, 2012.
Al-Otaibi S (2007), 'Durability of concrete incorporating GGBS activated by water-glass', *Construction and Building Materials*, 22(10), 2059–2067.

ASTM C 227 – 03(2003), Standard test method for potential alkali reactivity of cement-aggregate combinations (mortar-bar method).

ASTM C 441 – 02a(2002), Standard test method for effectiveness of pozzolans or ground blast-furnace slag in preventing excessive expansion of concrete due to the alkali-silica reaction.

Bakharev T, Sanjayan J G and Cheng Y B (2001), 'Resistance of alkali-activated slag concrete to alkali–aggregate reaction', *Cement and Concrete Research*, 31(2), 331–334.

Bleszynski R F and Thomas M D A (1998), 'Microstructural studies of alkali-silica reaction in fly ash concrete immersed in alkaline solutions', *Advanced Cement Based Materials*, 7, 66–78.

Chatterji S (1979), 'The role of $Ca(OH)_2$ in the breakdown of Portland cement concrete due to alkali-silica reaction', *Cement and Concrete Research*, 9, 185–188.

Chen Y, Pu X, Yang C and Ding Q (2002), 'Alkali aggregate reaction in alkali slag cement mortars', *Journal of Wuhan University of Technology-Mater, Sci. Ed*, 17(3), 60–62.

Davidovits J (1994), 'High-Alkali Cements for 21st Century Concretes', *Concrete Technology: Past, Present and Future*, Vol. 35, pp. 383–397.

Davidovits J (1999), 'Chemistry of geopolymeric systems, Terminology', *Géopolymère '99 Proceedings*, 9–40.

Davidovits J (2005), 'Geopolymer chemistry and sustainable development. The poly(sialate) terminology: a very useful and simple model for the promotion and understanding of green-chemistry', in Davidovits J (ed.) *Geopolymer: Green Chemistry and Sustainable Development Solutions*, Institut Géopolymère, Saint-Quentin, 9–16.

Davidovits J, Buzzi L, Rocher P, Gimeno D, Marini C and Tocco S (1999), 'Geopolymeric cement based on low cost geologic materials: results from the European research project Geocistem', *Géopolymère '99 Proceedings*, Vol. 2, pp. 83–96.

Deng M and Mingshu T (1993), 'Mechanism of dedolomotization and expansion of dolomitic rocks', *Cement and Concrete Research,* 23(6), 1397–1408.

Dent Glasser L S (1979), 'Osmotic pressure and the swelling of gels', *Cement and Concrete Research*, 9, 515–517.

Dent Glasser L S and Kataoka N (1981a), 'The chemistry of alkali-aggregate reactions', in *Proceedings of the Fifth International Conference on Alkali-Aggregate Reactions*, Cape Town, South Africa, paper S252/23, 66.

Dent Glasser L S and Kataoka N (1981b), 'The chemistry of alkali-aggregate reactions', *Cement and Concrete Research*, 11(1), 1–9.

Dent Glasser L S and Kataoka N (1982), 'The role of calcium in the alkali–aggregate reaction', *Cement and Concrete Research*, 12, 321–331.

Diamond S (1989), 'ASR – another look at mechanisms', in *8th International Conference on Alkali-Aggregate Reaction in Concrete*, 83–94.

Dron R, Brivot F and Chaussadent T (1997), 'Mechanism of the alkali-silica reaction', in *Proceedings of the 10th International Congress on the Chemistry of Cement*, Gothenburg, Vol. 4: Performance and Durability of Cementitious Materials, 8.

Fernández-Jiménez A and Puertas F (2002), 'The alkali–silica reaction in alkali-activated granulated slag mortars with reactive aggregate', *Cement and Concrete Research*, 32, 1019–1024.

Fernández-Jiménez A, García-Lodeiro I and Palomo A (2007), 'Durability of alkali-activated fly ash cementitious materials', *Journal of Materials Science*, 42, 3055–3065.

Garcia-Diaz E, Riche J, Bulteel D and Vernet C (2006), 'Mechanism of damage for the alkali–silica reaction', *Cement and Concrete Research*, 36(2), 395–400.

García-Lodeiro I, Palomo A and Fernández-Jiménez A (2007), 'Alkali–aggregate reaction in activated fly ash systems', *Cement and Concrete Research*, 37(2), 175–183.

Gifford P M and Gillott J E (1996), 'Alkali-silica reaction (ASR) and alkali-carbonate reaction (ACR) in activated blast furnace slag cement (ABFSC) concrete', *Cement and Concrete Research*, 26(1), 21–26.

Gillott J E (1964), 'Mechanisms and kinetics of expansion in the alkali-carbonate rock reaction', *Canadian Journal of Earth Science,* 1, 121–145.

Glasser F P (1992), 'Chemistry of alkali-aggregate reaction, in Swamy, R. N. (ed.) *The Alkali-Silica Reaction in Concrete*. Blackie and Son, London.

Hakkinen T (1986), 'Properties of alkali-activated slag concrete', *VTT Research*, 540, Technical Research Centre of Finland (VTT), Finland.

Hobbs D (1988), *Alkali-silica reaction in concrete*, Thomas Telford, London.

Hobbs D W (1993), 'Deleterious alkali–silica reactivity in the laboratory and under field conditions', *Magazine of Concrete Research*, 45(163), 103–112.

Hogan F J (1983), 'The effect of blastfurnace slag cement on alkali aggregate reactivity: a literature review', *Cement, Concrete and Aggregates*, 7, 100–107.

Hou X, Stuble L J and Kirkpatrick R J (2004), 'Formation of ASR gel and the role of CSH and portlandite', *Cement and Concrete Research,* 34, 1683–1696.

Hudec P P (1990), 'Common factors affecting alkali reactivity and frost durability of aggregates', in Baker J M, Davies H, Majumdar A J and Nixon P J (eds) *Durability of Building Materials and Components, Proceedings of the Fifth International Conference*, E & FN Spon, London.

Jones T N (1988), 'A new interpretation of alkali-silica reaction and expansion mechanisms in concrete', *Chemistry and Industry*, 40–44.

Krivenko P, Drochytka R, Gelevera A and Kavalerova E (2013), 'Mechanism of preventing the alkali–aggregate reaction in alkali activated cement concretes', *Cement and Concrete Composites*, 45, 157–165.

Li K-L, Huang G-H, Chen J, Wang D, Nanjing X T and Co H T (2005), 'Early mechanical property and durability of geopolymer', in Davidovits J (ed.) *Geopolymer: Green Chemistry and Sustainable Development Solutions*, Institut Géopolymère, Saint-Quentin, 117–120.

Li K, Huang G, Jiang L-H, Cai Y-B, Chen J and Ding J-T (2006), 'Study on abilities of mineral admixtures and geopolymer to restrain ASR', *Key Engineering Materials*, 302–303, 248–254.

Metso J (1982), 'The alkali reaction of alkali-activated Finnish blast furnace slag', *Silicates industriels*, 4–5, 123–127.

Pacheco-Torgal F and Jalali S (2011), *Eco-efficient Construction and Building Materials*, Springer Verlag, London.

Prezzi M, Monteiro J M and Sposito G (1998), 'The alkali-silica reaction. Part I: Use of the double layer theory to explain the behaviour of reaction-products gels', *ACI Materials Journal*, 94, 3–10.

Provis J L and van Deventer J S J (2009), *Geopolymers: Structures, Processing, Properties and Industrial Applications*, Woodhead Publishing Limited, Cambridge.

Pu X and Chen M (1991), 'The preventive effect of silica fume on alkali-silica reactive expansion in alkali-slag concrete (JK) concrete', *International Symposium on Concrete Engineering*, Nanjing, P.R. China, 1197–1202.

Pu X and Yang C (1994), 'Study on alkali-silica reaction of alkali-slag concrete', in Krivenko P V (ed.) *1st International Conference on Alkaline Cements and Concretes*, Kiev, Ukraine, 2, 897–906.

Puertas F, Palacios M, Gil-Maroto A and Vázquez T (2009), 'Alkali-aggregate behaviour of alkali-activated slag mortars: effect of aggregate type', *Cement and Concrete Composites*, 31(5), 277–284.

Rogers C A and Hooton R D (1991), 'Reduction in mortar and concrete expansion with reactive aggregates due to alkali leaching', *Cement, Concrete and Aggregates*, 13(1), 42–49.

Sellier A, Bourdarot E, Multon S, Cyr M and Grimal E (2009), 'Combination of structural monitoring and laboratory tests for the assessment of AAR-swelling – application to a gate structure dam', *ACI Materials Journal*, 106(3), 281–290.

Shehata M H and Thomas M D A (2000), 'The effect of fly ash composition on the expansion of concrete due to alkali–silica reaction', *Cement and Concrete Research*, 30(7), 1063–1072.

Shi C (1988) 'Alkali-aggregate reaction of alkali-slag cements (in Chinese)', *Concrete and Cement Products*, 4, 28–32.

Shi C (2003), 'On the role and state of alkali ions during the hydration of alkali activated slag cement', in *Proceedings of the 11th International Congress on the Chemistry of Cement*, Durban, South Africa, 2097–2105.

Shi C, Pavel V K and Della R (2005), *Alkali-Activated Cements and Concretes*, Taylor & Francis, New York.

Sims I and Nixon P (2003), 'RILEM TC 191-ARP: Alkali-reactivity and prevention – Assessment, specification and diagnosis of alkali-reactivity, RILEM Recommended Test Method AAR-I: Detection of potential alkali-reactivity of aggregates – Petrographic method', *Materials and Structures*, 36, 480–496.

Stanton T E (1940), 'Expansion of concrete through reaction between cement and aggregate', *Proceedings of the American Society of Civil Engineers*, 66, 1781–1811. (Also published with discussions in 1942 *ASCE Transactions*, 107, 54–126.)

Swenson E G (1957), 'A Canadian reactive aggregate undetected by ASTM tests', *ASTM Bulletin*, 226, 48–51.

Swenson E G and Gillot J E (1964), 'Alkali-carbonate rock reaction', *Highway Research Board Bulletin*, 275, 18–31.

Tailing B and Brandstetr J (1989), 'Present state and future of alkali-activated stag concretes', *ACI Special Publication*, 114, 1519–1546.

Tang M, Han S and Zhen S (1989), 'A rapid method for identification of alkali reactivity of aggregates', *Cement and Concrete Research*, 13(2), 417–422.

Thomas M D A (1998), 'The role of calcium in alkali–silica reaction', in Cohen M, Mindess S and Skalny J P (eds) *Materials Science of Concrete – The Sidney Diamond Symposium*, American Ceramics Society, Westerville, OH, 325–337.

Thomas M D A and Innis F A (1998), 'Effect of slag on expansion due to alkali-aggregate reaction in concrete', *ACI Materials Journal*, 95(6), 716–724.

Thomas M D A, Blackwell B Q and Nixon P J (1996), 'Estimating the alkali contribution from fly ash to expansion due to alkali-aggregate reaction in concrete', *Magazine of Concrete Research*, 48(177), 251–264.

Wang Q, Ding Z Y, Li L, Zhang C Y and Sui Z T (2010), 'Effect of alkali-activator on alkali-aggregate reaction of slag-based geopolymer', in *First International Conference on Advances in Chemically-activated Materials*, 131–138.

Yang C (1997), 'Alkali-Aggregate Reaction of Alkaline Cement Systems', PhD Thesis, Chongqing Jiangzhu University, Chongqing, P.R. China.

Yang C, Pu X and Wu F (1999), 'Studies on alkali-silica reaction (ASR) expansions of alkali activated slag cement mortars', in Krivenko P V (ed.) *2nd International Conference on Alkaline Cements and Concretes*, Kiev, Ukraine, 101–108.

Zhang X and Groves G W (1990), 'The alkali-silica reaction in OPC/silica glass mortar with particular reference to pessimum effects', *Advances in Cement Research*, 3(9), 9–13.

The fire resistance of alkali-activated cement-based concrete binders

16

D. Panias, E. Balomenos, K. Sakkas
National Technical University of Athens, Athens, Greece

16.1 Introduction

Fire played and still plays an important role for all cultures and religions. It has several symbolic meanings, from inspiration to hell, and has been regarded as the means that can warm and illuminate but at the same time can cause pain and death to human beings. Therefore, the fear of uncontrolled fires and the attempt to avoid their consequences were and still remain an important objective for human civilization.

16.1.1 Fire and consequences

The consequences from uncontrolled fire incidents are enormous for human life as well as human assets. The US National Fire Protection Association reported (Domich, 2004) that in 2002 almost 1.7 million fires took place in the United States, causing 3380 deaths, over 18,000 injuries and US$10.3 billion economic losses. In addition, fires in underground constructions cause tremendous disaster putting at risk the lives of many people and having enormous economic consequences (Beard and Carvel, 2005; Sakkas *et al*., 2013a) as can be seen in Table 16.1, where a number of serious accidents recorded internationally since 1996 is reported.

Besides the impacts on human lives and assets, fires can cause significant damage to physical structures (Khoury, 2000; Phan, 2008; Peng *et al*., 2006; Sakkas *et al*., 2013b). The two most sensitive components of every construction are the structural concrete and steel. Although concrete is an incombustible material, it suffers serious damage during a fire incident (concrete spalling and mechanical properties degradation) that is caused by the spontaneous release of great amounts of heat and aggressive fire gasses. Concrete spalling phenomena and substantial reduction of concrete mechanical strengths can normally be observed at temperatures higher than 300°C (Sakkas *et al*., 2013b). Structural steel (A36 and A992) and high strength alloy steels lose approximately 10% of their strength upon heating to 315°C, undergo significant deformations upon heating at temperatures higher than 430°C and generally are considered to have undergone structural disintegration at temperatures between 550 and 600°C (Sakkas *et al*., 2013b; Edwards and Gamble, 1986; FPPR, 1994).

The avoidance of the harmful and destructive effects of fire within a construction

Handbook of Alkali-activated Cements, Mortars and Concretes. http://dx.doi.org/10.1533/9781782422884.3.423

Table 16.1 Significant tunnel fire events recorded since 1996

Year	Tunnel	Human casualties	Repair cost [M€]	Loss of revenue [M€]
1996	Eurotunnel	2 injured	49	203
1999	Mont Blanc	41 deaths	189	203
1999	Tauern	12 deaths	8.5	20
2001	St. Gothard	11 deaths	Not available	Not available
2005	Frejus	2 deaths	2	3
2006	Viamala	9 deaths	Not available	Not available
2007	Burnley	3 deaths	Not available	Not available
2007	Santa Clarita	3 deaths	Not available	Not available
2009	Eiksund	5 deaths	Not available	Not available
2010	Wuxi Lihu	24 deaths	Not available	Not available
2011	Fjord	–	Not available	Not available
2012	Wallasey	–	Not available	Not available
2013	Brattli	–	Not available	Not available

is the subject of fire engineering that applies science and engineering principles to improve the fire resistance of constructions and to eliminate simultaneously the severity of fire incidents. One of the disciplines of fire engineering is the passive and active fire protection of constructions.

16.1.2 Passive and active fire protection

The protection of constructions against fires necessitates a holistic approach combining the application of active and passive fire protection methods as well as management systems (such as evacuation procedures, communication procedures, compartmentalization, smoke extraction, etc.). The active fire protection measures operate only in the event of a fire. By definition, active systems require to be switched on, either by manual or automatic means, to be effective. The most common forms of active fire protection used in constructions are fire suppression systems (fire extinguishers and water sprinklers), fire detection systems and hypoxic air as well as ventilation systems (Beard and Carvel, 2005; Brinson, 2010; Mawhinney and Trelles, 2010; Chiti, 2011). On the other hand, passive fire protection measures are those related to the features of the construction itself. They are an integral part of the construction, present throughout its lifetime and serving as a fire spreading barrier as well as a thermal energy barrier preventing the failure of construction elements. The passive fire protection systems (Davidson *et al.*, 2013; Zellei, 2013; ASFP, 2013) involve application of special mortars and boards as well as radiation shielding (Domich, 2004). The cementitious mortars used for the protection are sprayed on the construction element surface. They not only prevent the mechanical deterioration of concrete structures exposed to fires above 300°C, but also deter explosive spalling of concrete. The boards used for the passive fire protection are incombustible, made of endothermic materials such as gypsum or calcium silicate

reinforced by inert fibers to avoid their disintegration. They are not effective for high temperature and long-duration fires. Finally, radiation shielding has, as a target, to limit the amount of radiation produced by a fire that reaches a structural element (e.g., polished sheet metal reflector). It cannot be applied for the protection of an entire structural system but for the protection of a specific structural element from local thermal radiation exposure. The materials used for passive fire protection are tested through standard tests issued by several authorities worldwide to determine their fire resistance performance.

16.1.3 Fire resistance

Fire resistance is the property of materials or their assemblies that prevents or retards the passage of excessive heat, hot gasses or flames under conditions of use (NYCBC, 2008). Fire resistance of materials is quantified by means of fire resistance rating. Fire resistance rating is typically determined by measuring the ability of a passive fire protection material or assembly to withstand a standard fire resistance test. This is quantified either as a measure of period of time for which a material or assembly withstands a specific fire resistance test, or by evaluating through quantifiable criteria set by a specific fire resistance test, the ability of a material or assembly to perform a specific structural functionality.

The development of standard fire resistance tests for rating the resistance of passive fire protection materials or assemblies for specific applications made necessary the development of standard international time–temperature curves that simulate specific types of fires.

16.1.4 Standard fire scenarios

Several types of fire incidents have been observed in constructions and therefore, several fire scenarios have been developed in order to simulate those that occur most frequently. The developed standard fire scenarios used in testing, analysis and design of fire resistance rating of fire protection systems and materials are given in Figure 16.1. There are basically three families of developed standard fire scenarios (Khoury, 2000): (a) for buildings, (b) for offshore and petrochemical industries, and (c) for tunnels.

16.1.4.1 (a) Fire scenarios for buildings (Collette, 2007; EFNARC, 2006)

The international standard ISO 834 time–temperature curve simulates cellulosic fires. This curve is the best one to test the fire resistance of materials subjected to a fire hazard based on the burning rate of general combustible building materials and building contents such as timber, paper, fabric, etc. Therefore, it is appropriate for the fire resistance assessment of fire protection systems in ordinary buildings but may also be used for fire testing of tunnel linings. The standard ISO 834 time–temperature curve represents the least severe fire scenario.

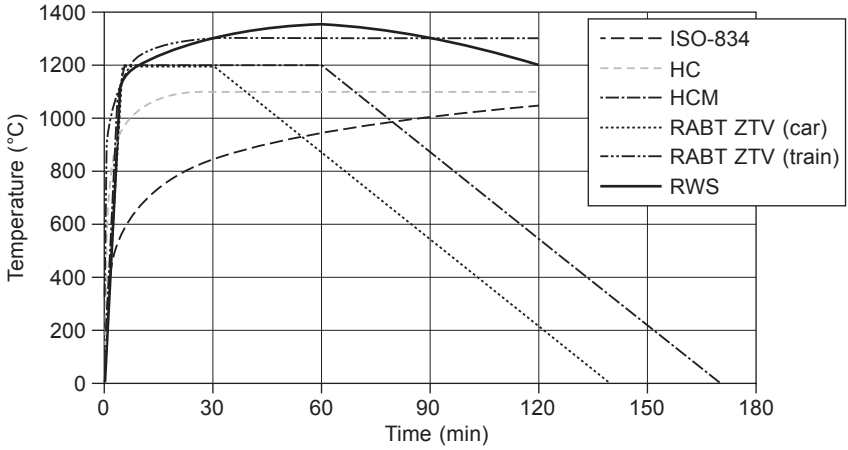

Figure 16.1 Standard fire scenarios (ISO: International standard organization; HC: Hydrocarbon curve; HCM: Hydrocarbon modified curve; RWS: Rijkswaterstaat).

16.1.4.2 (b) Fire scenarios for offshore and petrochemical industries (Collette, 2007; EFNARC, 2006)

The hydrocarbon curve (HC) simulates the burning rates for certain materials such as petrol gas, chemicals, etc., which are in excess of the burning rate of cellulosic materials. Therefore, the HC time–temperature curve is used within offshore and petrochemical industries where the fires are often less contained and generally where small hydrocarbon fires might occur.

This fire scenario is more severe than the ISO 834 one, especially during the initial fire growth stage where the temperature exceeds 1000°C within the first 10 min. The HC curve has also been used for the fire resistance rating of tunnel linings.

16.1.4.3 (c) Fire scenarios for tunnels (Maevski, 2011; EFNARC, 2006)

Fires in tunnels are more severe than the ones in offshore and petrochemical industries as well as in buildings. Therefore, more severe fire scenarios have been developed simulating higher burning rates and higher maximum temperatures.

The RATB-ZTV time–temperature curves were developed in Germany to set requirements for tunnel fires. The RATB-ZTV curves are based on hydrocarbon fires and are characterized by a high temperature rise in the initial fire growth stage where the temperature reaches 1200°C within 5 min. The duration of the fully developed fire stage is shorter than the other fire scenarios describing better simple truck fire incidents in tunnels.

The hydrocarbon modified (HCM) time–temperature curve was developed to simulate a hydrocarbon-based fire with very high temperature gradient during the initial fire growth stage, very high maximum temperature (1300°C) during the fully developed fire stage and longer duration at high temperatures of the fully developed fire stage.

Finally, the RWS (Rijkswaterstaat) time–temperature curve is the most severe fire scenario, simulating a 50m^3 fuel (oil or petrol) tanker fire with a fire load of 300 MW lasting up to 120 minutes. RWS fire scenario is characterized by a very high temperature rise during the initial fire growth stage, reaching a maximum temperature of 1350°C within 1 h. RWS is the adopted standard curve in many countries all over the world for the fire resistance rating assessment of fire protection materials for concrete tunnel linings.

16.1.5 Fire resistance and alkali-activated binders

Alkali-activated binders share the following physicochemical characteristics (Davidovits, 2011):

- They are totally inorganic polymeric materials and therefore are incombustible.
- They have ceramic-like properties that render them resistant upon heating at high temperatures due to formation of several crystalline aluminosilicate phases with potentially high melting points (>1100°C). Therefore, they retain their structural integrity at elevated temperatures.
- They are endothermic materials due to the contained geopolymeric water (physically and chemically bound water) and therefore have high potential to absorb heat due to high heat capacity of water. The endothermicity of materials is a well-established and proven property in fire engineering applications.
- They have thermal conductivity values in the region of 0.1–0.3 W/m.K, which is relatively low in comparison to the other commonly used structural building materials and almost identical or comparable to the marketable fire resistant materials (Sakkas *et al.*, 2013c). Therefore, alkali-activated binders have the ability to operate as an efficient heat flux barrier (Giannopoulou and Panias, 2008).

The above features render alkali-activated binders suitable candidates for passive fire protection applications under intermediate exposure temperatures (< 900°C). By controlling the chemical composition of alkali-activated binders, materials with very high fire resistance ratings can be produced that are capable of withstanding exposure temperatures as high as 1350°C (Sakkas *et al.*, 2013c).

16.2 Theoretical analysis of the fire performance of pure alkali-activated systems (Na_2O/K_2O)-SiO_2-Al_2O_3

The basic function of a fire resistant material is to set a barrier that prevents or retards the transfer of excessive heat and the spreading of hot gasses and flames for a time period during a fire incident. The transfer of excessive heat is related to the thermal conductivity and endothermicity of materials. The spreading of fire, hot gasses and flames is related to the incombustibility and structural integrity of materials that permit them to act as an effective barrier. The structural integrity can be theoretically predicted through the calculation of ternary phase diagrams

and equilibrium compositions in pure alkali-activated binding systems under the high temperatures occurring in fire incidents. The FactSage 6.4 software with its thermodynamic models and databases was used for the calculation of ternary phase diagrams that describe the most important alkali-activated binding systems. The calculated liquidus temperature surfaces in ternary Na_2O-SiO_2-Al_2O_3 phase diagram are shown in Figure 16.2.

In the binary Na_2O-SiO_2 system three phases are formed upon heating as is shown in Figure 16.2: sodium orthosilicate ($2Na_2O.SiO_2$), sodium silicate ($Na_2O.SiO_2$) and sodium disilicate ($Na_2O.2SiO_2$). The melting temperatures of these phases are 1078°C for sodium orthosilicate, 1089°C for sodium silicate and 874°C for sodium disilicate (Verein Deutscher Eisenhüttenleute, 2008), which are lower than the temperatures developed (1100°C) during the cellulosic (ISO 834) and the small hydrocarbon (HC) fires. Therefore the pure sodium silicate systems cannot be used for production of fire resistant binders. The doping of pure sodium silicate systems with aluminum has a beneficial effect on the fire resistant performance of sodium aluminosilicate binders as is seen in Figure 16.2. The presence of aluminum results in the formation of three new sodium aluminosilicate phases: albite ($Na_2O.Al_2O_3.6\ SiO_2$), a low alumina phase with melting point 1118°C (Verein Deutscher Eisenhüttenleute, 2008; Greig and Barth, 1938), and the two high alumina allotropic phases nepheline and carnegieite ($Na_2O.Al_2O_3.2SiO_2$). Nepheline is stable at temperatures lower than

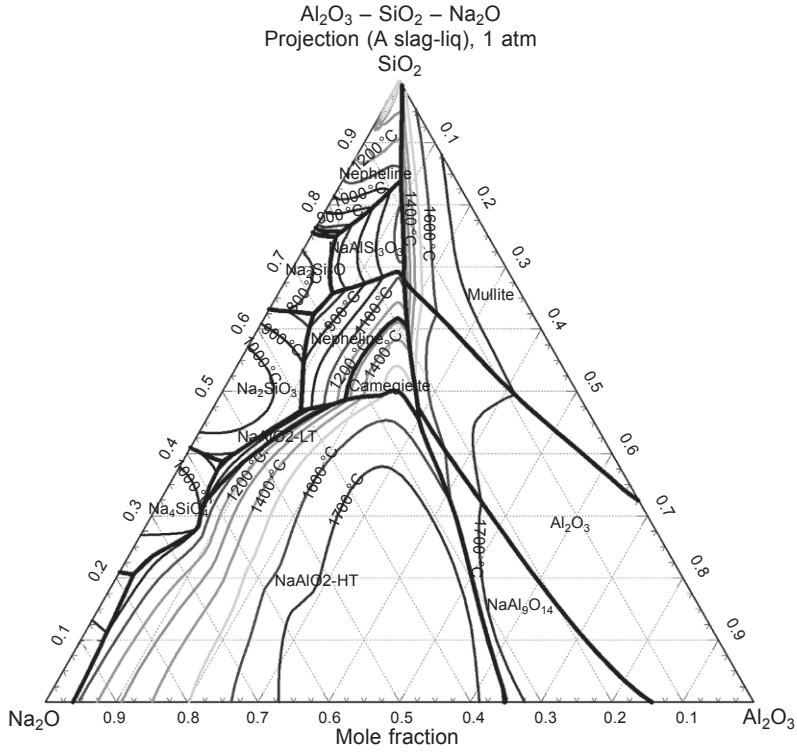

Figure 16.2 Calculated liquidus temperature surfaces in Na_2O-SiO_2-Al_2O_3 system.

1256°C while carnegieite melts at 1526°C. Geopolymeric compositions located in the stability area of albite have liquidus temperatures between 730 and 1100°C and therefore cannot resist the less intense cellulosic (ISO 834) and small hydrocarbon (HC) fire scenarios. Shifting the geopolymeric compositions towards the stability area of nepheline, a region can be defined where the liquidus temperatures are between 1100 and 1256°C. Sodium-activated binders located in this area have the potential to withstand the temperatures observed during the less intense cellulosic (ISO 834) and small hydrocarbon (HC) fire scenarios. Furthermore, in a smaller portion of this region the liquidus temperatures are between 1200 and 1256°C showing geopolymeric compositions with potential to resist more intense fire scenarios like the ones described by the RATB-ZTV time–temperature curves.

In order to prove theoretically the good prospects for fire resistant materials in the nepheline region, the solidus temperatures of some geopolymeric compositions as well as the percentage of material melted between the solidus and liquidus temperatures were calculated utilizing the FactSage 6.4 thermochemical software. The results are shown in Figure 16.3 and the positions of all studied compositions in the nepheline region (1–7) are also given in Figure 16.4. Although the materials have liquidus temperatures in the range 1100–1250°C, they also have substantially lower solidus temperatures in the range 700–1000°C and the partially melted material at 1100°C is higher than 60% of the mass of totally dehydrated geopolymeric compositions. Therefore, the sodium-activated binders at high temperatures (≥1100°C) are transformed into very viscous materials that can creep under the influence of gravity thus losing their structural integrity and consequently their fire resistance performance. Therefore, the geopolymeric compositions in the nepheline region are not capable of withstanding the temperatures observed even during the less intense

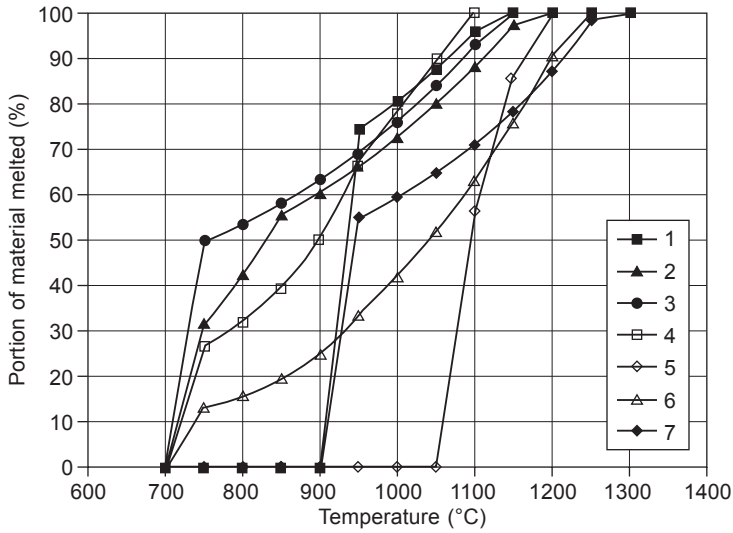

Figure 16.3 Percentage portion of totally dehydrated geopolymeric compositions melted between solidus and liquidus temperatures (nepheline region in Na_2O-SiO_2-Al_2O_3).

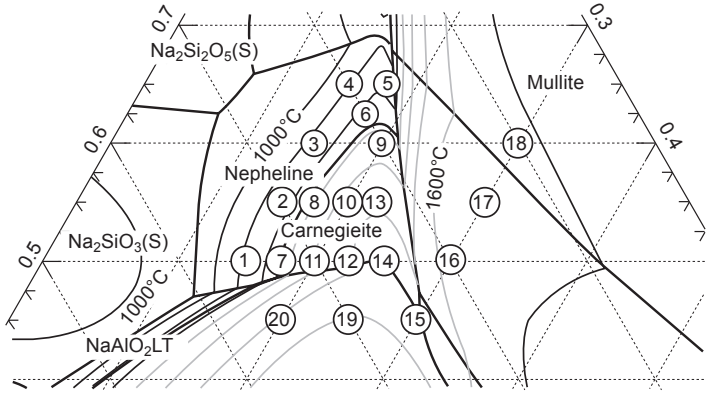

Figure 16.4 Positioning of all studied totally dehydrated geopolymeric compositions in Na_2O-SiO_2-Al_2O_3 system.

standard cellulosic (ISO 834) and small hydrocarbon (HC) fire scenarios and for this reason their fire resistance performance is unsuitable. All the compositions are suitable for fires with a highest temperature not exceeding 700°C. Compositions 1 and 7 are fire resistant for temperatures lower than 900°C while composition 5 is suitable for temperatures lower than 1050°C.

In the stability area of carnegieite the liquidus temperatures vary from 1256°C to almost 1550°C, designating a region of geopolymeric compositions with very promising fire resistant properties. Na-activated binders within this area have the potential to withstand the most severe standard fire scenarios like the RWS and HCM ones. The calculated solidus temperatures of some geopolymeric compositions in the carnegieite region (8–15 as shown in Figure 16.4) as well as the percentage of material melted between the solidus and liquidus temperatures are shown in Figure 16.5. All

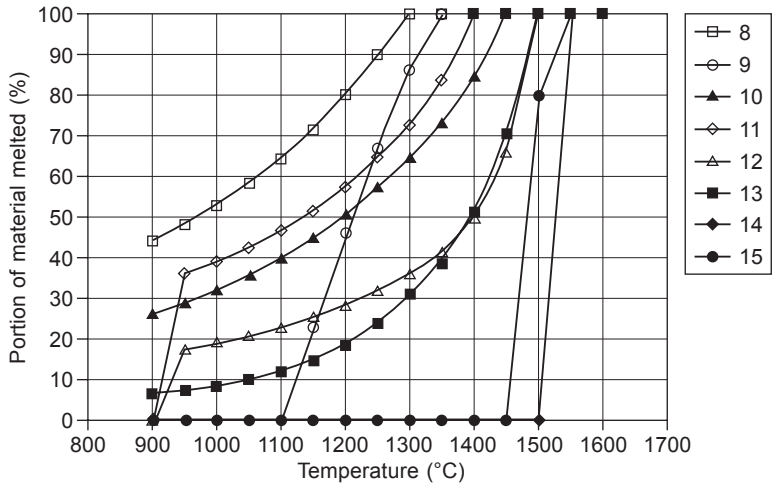

Figure 16.5 Percentage portion of totally dehydrated geopolymeric compositions melted between solidus and liquidus temperatures (carnegieite region in Na_2O-SiO_2-Al_2O_3).

compositions have very high liquidus temperatures (1300–1525°C) but a big gap exists between their solidus and liquidus temperatures. The only exception is related to composition 14 which has the stoichiometry of carnegieite ($Na_2O.Al_2O_3.2SiO_2$) and therefore there is no difference between the solidus and liquidus temperatures. This sodium-activated binder exhibits excellent fire resistance performance, having the ability to withstand the most severe standard fire scenarios like the RWS and HCM ones without losing its structural integrity, and therefore can be applied to the most demanding passive fire protection applications. The geopolymeric compositions (12, 13 and 15) in the direct vicinity of composition 14 have inferior fire resistance performance. Composition 15 has a small gap between the solidus and liquidus temperatures (Figure 16.5) and therefore can resist the most severe standard fire scenarios like the RWS and HCM. Compositions 9, 12 and 13 have potential to withstand the less intense standard cellulosic (ISO 834) and small hydrocarbon (HC) fire scenarios, although an amount of 0–22% of materials is melted at 1100°C. The other compositions (8, 10 and 11) do not have acceptable fire resistant properties in relation to the standard fire scenarios used for their evaluation.

Finally, in the Na_2O-SiO_2-Al_2O_3 system there are the stability areas of mullite, alumina and sodium aluminate where the highest liquidus temperatures of this system are located (Figure 16.2). The calculated solidus temperatures and the percentage of melted material of some geopolymeric compositions (15–20 as shown in Figure 16.4) are shown in Figure 16.6. All compositions have very high liquidus temperatures (>1500°C) but there is a big gap between solidus and liquidus temperatures making them inappropriate to resist the most severe fire scenarios (RWS and HCM). Composition 16 has a solidus temperature at 1200°C and therefore can resist the RATB-ZTV fire scenario. Composition 19 has a low solidus temperature (900°C)

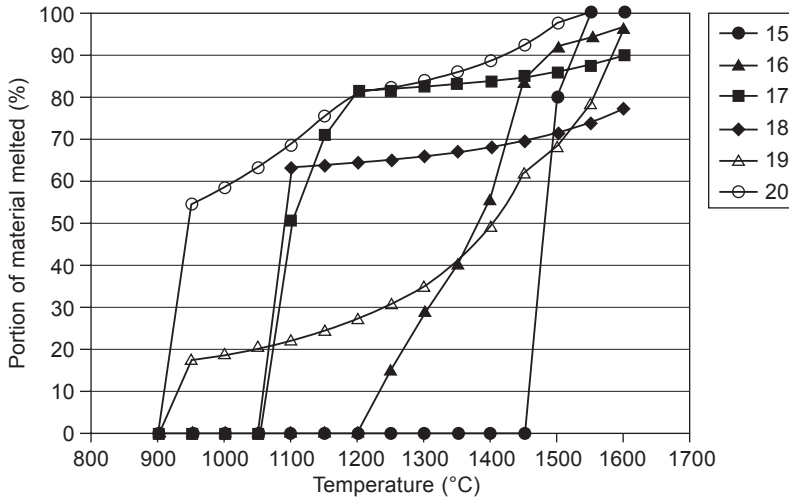

Figure 16.6 Percentage portion of totally dehydrated geopolymeric compositions melted between solidus and liquidus temperatures (mullite, alumina and sodium aluminate regions in Na_2O-SiO_2-Al_2O_3).

but an only 22% of material is melted at 1100°C making it a good fire resistant material for cellulosic fires. All the remaining compositions (16, 18 and 20) are inappropriate for fire resistance applications even for the less intense cellulosic fire scenarios because more than 50% of materials is melted at 1100°C.

The main conclusion for the pure Na_2O-SiO_2-Al_2O_3 system is that there is a very small region around the mineral composition of carnegieite (14) where a very restricted number of geopolymeric formulations (9, 12, 13, 15, 16 and 19) with very good to excellent fire resistance properties are located.

The ternary K_2O-SiO_2-Al_2O_3 system (Verein Deutscher Eisenhüttenleute, 2008; Mrazova and Klouzkova, 2009; Hong, 2005; Morey, 1964) is shown in Figure 16.7. Three compounds are present in the binary K_2O-SiO_2 system: potassium silicate ($K_2O.SiO_2$, with melting point at 976°C), potassium disilicate ($K_2O.2SiO_2$, with melting point at 1045°C) and potassium tetrasilicate ($K_2O.4SiO_2$, with melting point at 770°C). The melting temperatures are substantially lower than the temperatures developed during the less intense fire scenarios, and therefore the pure potassium silicate system, like the sodium silicate one, cannot be used for production of fire resistant binders.

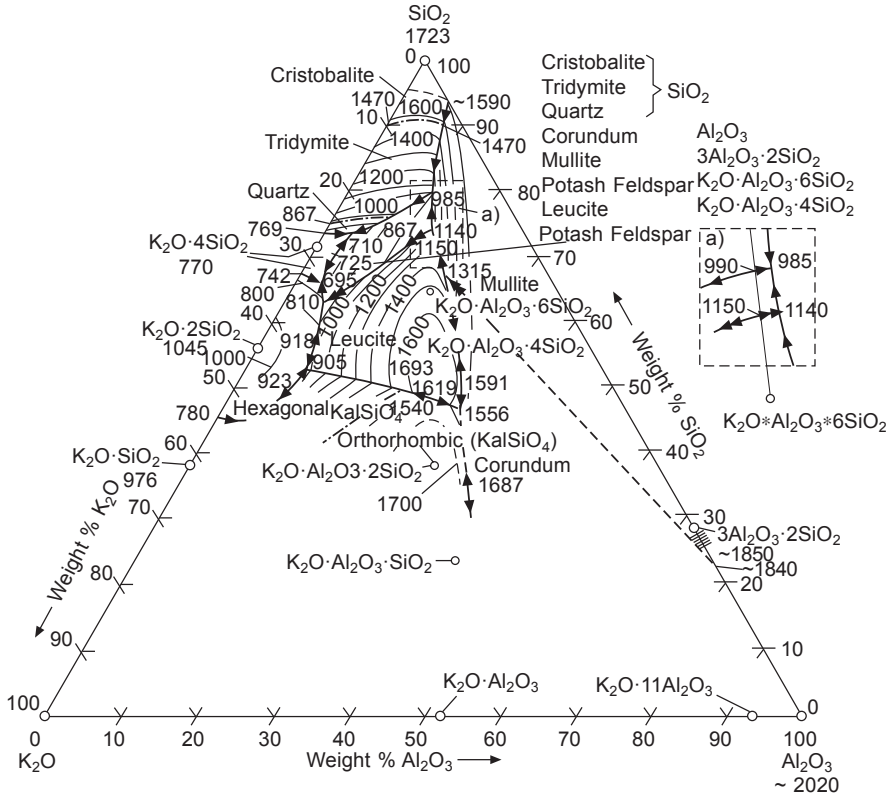

Figure 16.7 Liquidus temperature surfaces in K_2O-SiO_2-Al_2O_3 system (Verein Deutscher Eisenhüttenleute, Slag Atlas, Copyright 1995 Verlag Stahleisen GmbH, Düsseldorf, Germany).

The fire resistance behavior of the potassium silicate system changes dramatically with the addition of alumina. Four potassium aluminosilicate compounds are formed. The potash feldspar ($K_2O.Al_2O_3.6SiO_2$) that melts incongruently at 1150°C is the less refractory phase. Potash feldspar melts at about the same temperature as its analogue soda feldspar (albite) but its melting leads to the formation of solid leucite ($K_2O.Al_2O_3.4SiO_2$) and a more siliceous melt which is so viscous that flows very slowly causing a more refractory effect in relation to its analogue soda feldspar (Morey, 1964). Leucite is a refractory compound with melting temperature at 1693°C. Its field occupies a large area at the center of the K_2O-SiO_2-Al_2O_3 system in which the liquidus temperatures vary between 810°C, at the edge very close to the binary of the K_2O-SiO_2 system, and 1693°C, the congruent melting point of leucite. Therefore, there is a broad region of geopolymeric compositions in the leucite field with liquidus temperatures higher than 1350°C that renders the K-activated binders located in this region very promising fire resistant candidates. In addition to leucite, the compound $K_2O.Al_2O_3.2SiO_2$, which is an analogue of nepheline/carnegieite, is formed in the ternary K_2O-SiO_2-Al_2O_3 system as shown in Figure 16.7. Several polymorphs of this compound exist: the hexagonal one with the two isomorphs, kalsilite and kaliophilite, and the orthorhombic one (Morey, 1964; Cook *et al.*, 1977). The transition from the hexagonal to the orthorhombic form takes place at about 1540°C. The compound $K_2O.Al_2O_3.2SiO_2$ melts congruently near or above 1750°C. Finally, the compound $K_2O.Al_2O_3.SiO_2$ with a melting point well above 1700°C exists in the ternary K_2O-SiO_2-Al_2O_3 system designating together with the orthorhombic compound $K_2O.Al_2O_3.2SiO_2$ a field below the leucite one with extremely high liquidus temperatures (> 1540°C) and therefore very promising fire resistant properties.

The K_2O-SiO_2-Al_2O_3 system has higher refractoriness in relation to the Na_2O-SiO_2-Al_2O_3 one. This is attributed to the existence of three potassium aluminosilicate compounds ($K_2O.Al_2O_3.4SiO_2$, $K_2O.Al_2O_3.2SiO_2$ and $K_2O.Al_2O_3.SiO_2$) with congruent melting points higher than 1693°C in relation to the existence of only one compound (carnegieite, $Na_2O.Al_2O_3.2SiO_2$) in the Na_2O-SiO_2-Al_2O_3 system with substantially lower congruent melting point at 1526°C. In addition, although albite ($Na_2O.Al_2O_3.6SiO_2$) and potash feldspar ($K_2O.Al_2O_3.6SiO_2$) melt at almost identical temperatures, the potash feldspar melt has substantially higher viscosity, rendering its flowing an insignificant phenomenon and giving it a more refractory effect. Therefore the K_2O-SiO_2-Al_2O_3 system is without any doubt more advantageous than the Na_2O-SiO_2-Al_2O_3 one for fire resistance applications.

16.3 Theoretical analysis of the fire performance of calcium containing alkali-activated systems CaO-(Na_2O/K_2O)-SiO_2-Al_2O_3

The quaternary CaO-Na_2O-SiO_2-Al_2O_3 system is divided in the ternary systems Na_2O-SiO_2-Al_2O_3, CaO-Na_2O-SiO_2, CaO-SiO_2-Al_2O_3 and CaO-Na_2O-Al_2O_3. The system

Na_2O-SiO_2-Al_2O_3 has been analyzed and presented in Figure 16.2. The addition of CaO in the binary Na_2O-SiO_2 system results in the formation of new binary as well as ternary compounds. The new binary compounds belong to the system CaO-SiO_2 (Morey, 1964). Tricalcium silicate ($3CaO.SiO_2$) is melted incongruently, forming CaO and a silicate melt at 2070°C. Dicalcium silicate ($2CaO.SiO_2$) and calcium silicate ($CaO.SiO_2$) melt congruently at 2130°C and 1544°C, respectively. Finally, tricalcium disilicate ($3CaO.2SiO_2$) melts incongruently at 1464°C, forming 2CaO. SiO_2 and a silicate melt. Five new ternary compounds form in the system, CaO-Na_2O-SiO_2 (Morey, 1964). Two compounds ($Na_2O.2CaO.3SiO_2$, $Na_2O.2CaO.2SiO_2$) have congruent melting at 1284°C and 1450°C, respectively, while three compounds ($Na_2O.3CaO.6SiO_2$, $2Na_2O.CaO.3SiO_2$, $4Na_2O.3CaO.5SiO_2$) melt incongruently at 1060°C, 1141°C and 1130°C, respectively. As a general conclusion, the addition of CaO in the Na_2O-SiO_2 system increases its refractoriness due to formation of several compounds that melt at substantially higher temperatures in relation to the sodium silicate ones. This is clearly seen by comparing the changes in the neighborhood of the side Na_2O-SiO_2 of the triangular diagrams shown in Figures 16.8–16.10 where the effect of CaO addition on the liquidus curves of the Na_2O-SiO_2-Al_2O_3 system has been theoretically calculated.

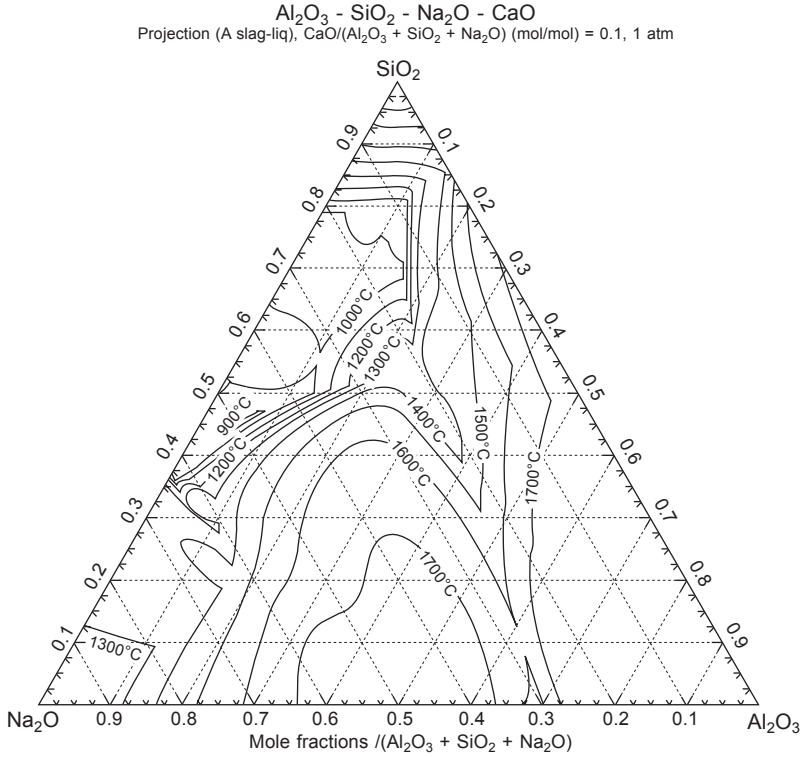

Figure 16.8 Effect of CaO addition (7.31% w/w) on the liquidus curves of the Na_2O-SiO_2-Al_2O_3 system.

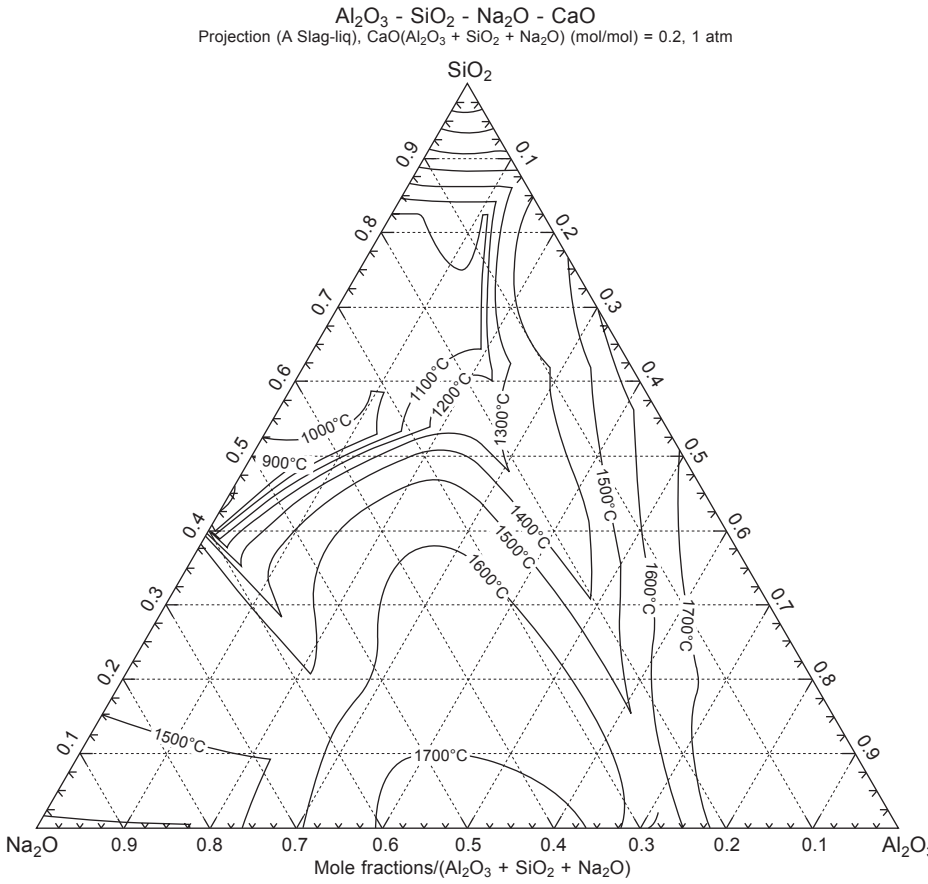

Figure 16.9 Effect of CaO addition (13.63% w/w) on the liquidus curves of the Na_2O-SiO_2-Al_2O_3 system.

The CaO addition to the binary highly refractory SiO_2-Al_2O_3 system forms new binary calcium aluminate as well as ternary calcium aluminosilicate compounds (Morey, 1964). The $12CaO.7Al_2O_3$, $CaO.Al_2O_3$ and $CaO.2Al_2O_3$ melt congruently at 1458°C, 1600°C and 1750°C, respectively, while $3CaO.Al_2O_3$ and $CaO.6Al_2O_3$ have incongruent melting at 1535°C and 1850°C, respectively. Two ternary calcium aluminosilicate compounds are formed: the anorthite ($CaO.Al_2O_3.2SiO_2$) and the gehlenite ($2CaO.Al_2O_3.SiO_2$), which melt congruently at 1555°C and 1590°C, respectively. All the new compounds mentioned above are melted at temperatures lower than the melting point of mullite ($3Al_2O_3.2SiO_2$, 1850°C) and therefore the CaO addition decreases the refractoriness of the binary Al_2O_3–SiO_2 system. This is seen in Figures 16.8–16.10 by comparing the changes in the liquidus curves in the area beside the axis Al_2O_3–SiO_2 of the triangular Na_2O-SiO_2-Al_2O_3 diagram.

No reliable data exist for the system Na_2O-Al_2O_3 which is dominated by the compound $Na_2O.Al_2O_3$ which melts at a temperature higher than 1850°C (Figure 16.2).

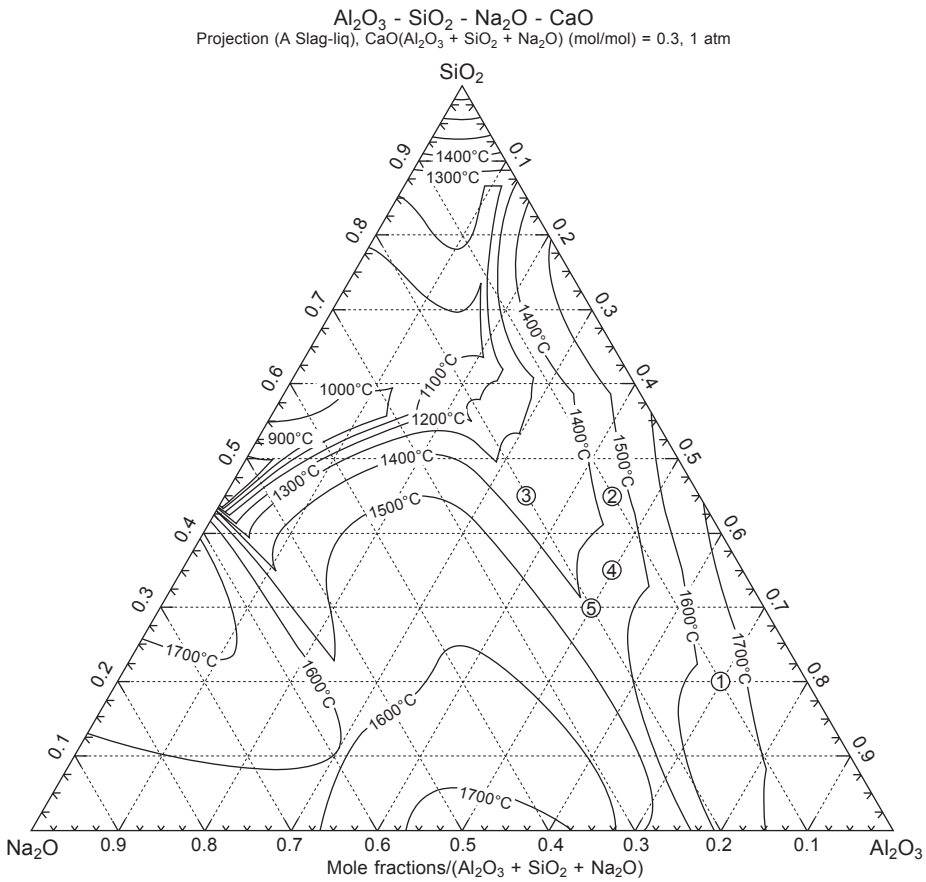

Figure 16.10 Effect of CaO addition (19.13% w/w) on the liquidus curves of the Na_2O-SiO_2-Al_2O_3 system.

The CaO addition induces the formation of the above-mentioned calcium aluminate compounds as well as of two ternary sodium calcium aluminate compounds: the $Na_2O.8CaO.3Al_2O_3$ which melts incongruently at 1508°C and the $2Na_2O.3CaO.5Al_2O_3$ which does not dissociate or melt up to 1630°C (Morey, 1964). The CaO addition improves the refractoriness of the Na_2O-Al_2O_3 system in the area of very rich Na_2O compositions as is shown in Figures 16.8–16.10, while diminishing the refractoriness in the area of medium and rich Al_2O_3 compositions.

The total effect of CaO addition on the Na_2O-SiO_2-Al_2O_3 system is summarized by the shift of the liquidus curves towards the Al_2O_3 sector and Na_2O-Al_2O_3 axis. This has a detrimental effect on the fire resistance performance of compositions that had excellent thermal behavior in the absence of CaO (stoichiometric carnegieite composition) as shown in Figure 16.11. The addition of CaO changes the system's stoichiometry forming less refractory compounds that decrease the liquidus temperature and causing a big gap between the liquidus and the solidus temperatures destroying the fire performance of materials.

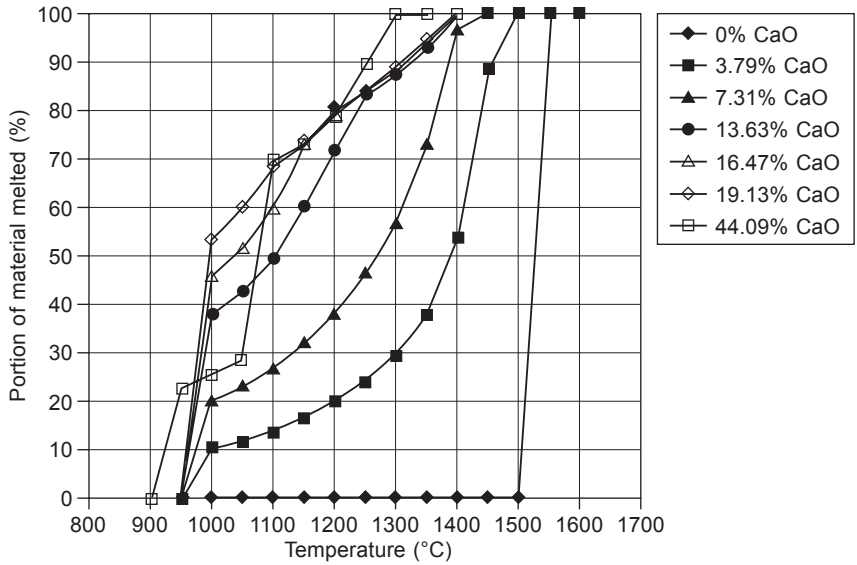

Figure 16.11 Percentage portion of totally dehydrated geopolymeric compositions melted between solidus and liquidus temperatures as a function of CaO addition (stoichiometric carnegieite composition in the Na_2O-SiO_2-Al_2O_3 system).

The heat behavior of five compositions in the high alumina area of the CaO-doped (19.13% w/w) Na_2O-SiO_2-Al_2O_3 system (depicted in Figure 16.10) is shown in Figure 16.12. All compositions can resist the cellulosic and the hydrocarbon standard

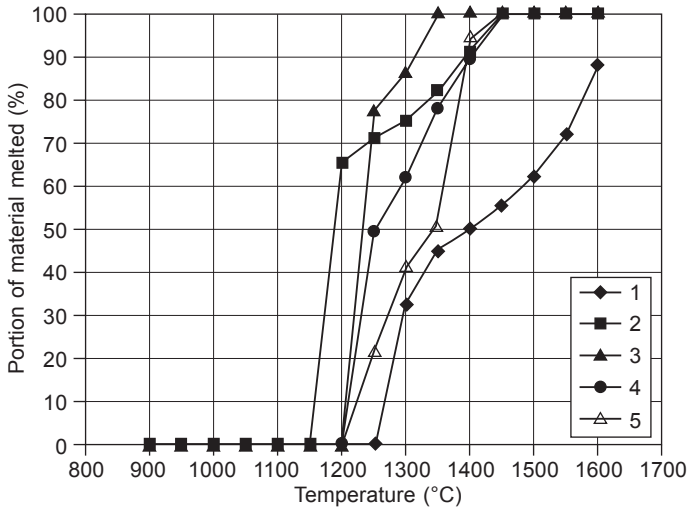

Figure 16.12 Percentage portion of totally dehydrated geopolymeric compositions melted between solidus and liquidus temperatures in the Al_2O_3 domain of the CaO-doped (19.13% w/w) Na_2O-SiO_2-Al_2O_3 system (Figure 16.10).

fire curves. Compositions 1, 3, 4 and 5 can resist additionally the RABT-ZTV fire curves. Finally, no composition can resist the most severe fire scenarios RWS and HCM.

In general, the effect of CaO addition in the K_2O-SiO_2-Al_2O_3 system is almost identical to the one in the Na_2O-SiO_2-Al_2O_3 system. In the system K_2O-SiO_2-CaO several ternary potassium calcium silicate compounds are formed that together with the binary calcium silicate ones improve the heat behavior of the pure K_2O-SiO_2 system. The CaO addition decreases the refractoriness of the binary Al_2O_3-SiO_2 system as well as the refractoriness in the poor K_2O domain of the binary K_2O-Al_2O_3 system due to formation of eutectic mixtures (Morey, 1964; Verein Deutscher Eisenhüttenleute, 2008). Therefore, there is a shift of the liquidus curves toward the Al_2O_3 domain of the K_2O-SiO_2-Al_2O_3 system which has a detrimental effect on the fire resistance performance of this system. This can be seen in Figure 16.13, where the plane $K_2O.Al_2O_3.4SiO_2$–$CaO.Al_2O_3.2SiO_2$–SiO_2 of the quaternary CaO-K_2O-Al_2O_3-SiO_2 system is depicted (Morey, 1964). The addition of CaO on leucite

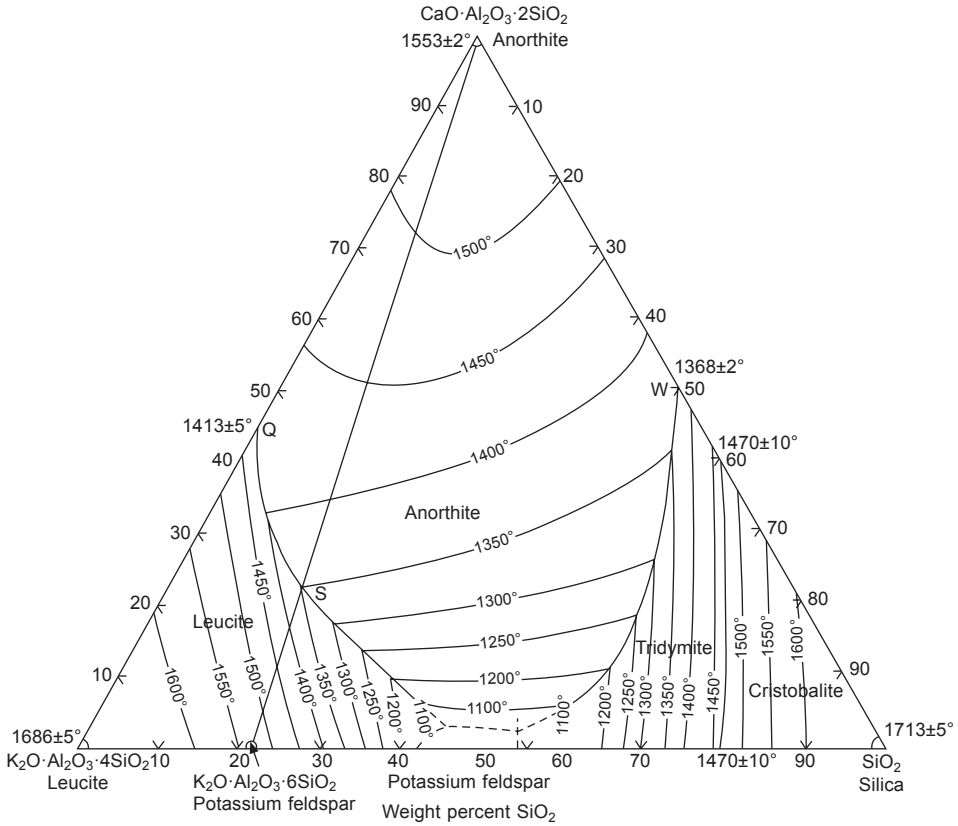

Figure 16.13 The plane $K_2O.Al_2O_3.4SiO_2$-$CaO.Al_2O_3.2SiO_2$-SiO_2 of the quaternary CaO-K_2O-Al_2O_3-SiO_2 system (Copyright 1964 6th Edition, *Data of Geochemistry*, United States Government Printing Office, Washington, with kind permission from US Geological Survey).

composition (axis $K_2O.Al_2O_3.4SiO_2$–$CaO.Al_2O_3.2SiO_2$) diminishes the liquidus temperatures of the system and therefore affects negatively the fire performance of the potassium-activated binders. Finally, it has to be noticed once more that the K_2O siliceous melts are significantly more viscous than the Na_2O siliceous ones (Morey, 1964), giving the potassium-activated binders more refractoriness than their sodium analogues.

16.4 Theoretical analysis of the fire performance of iron containing alkali-activated systems FeO-(Na_2O/K_2O)-SiO_2-Al_2O_3

The FeO addition in the binary Na_2O-SiO_2 system creates two main phases in addition to the sodium silicate ones (Figure 16.14): the compound fayalite ($2FeO.SiO_2$) with melting point at 1205°C and the compound $Na_2O.FeO.SiO_2$ which melts incongruently at 976°C. The FeO addition shifts the compositions toward the fayalite field, which is characterized by low liquidus temperature curves, and therefore does not improve the fire performance of the Na_2O-SiO_2 system.

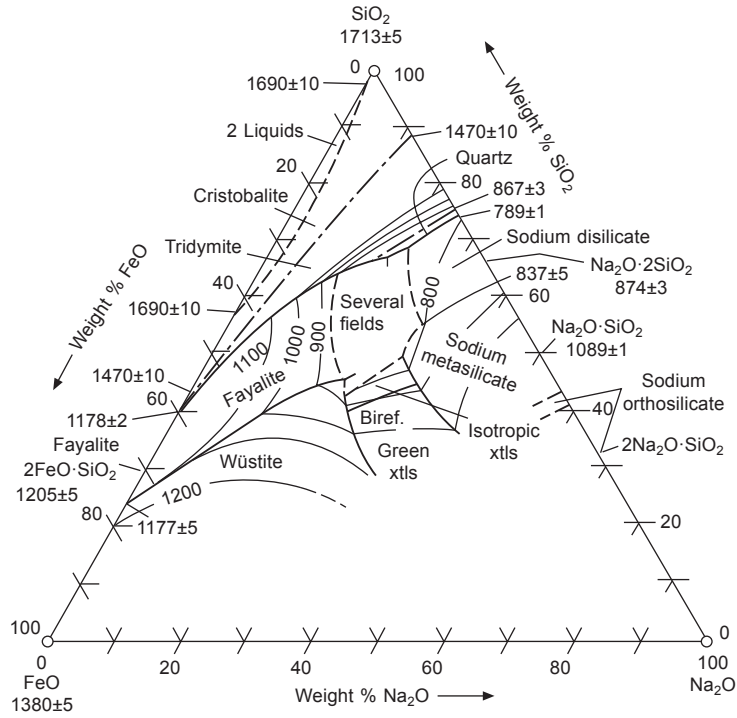

Figure 16.14 FeO-Na_2O-SiO_2 system (Verein Deutscher Eisenhüttenleute, Slag Atlas, Copyright 1995 Verlag Stahleisen GmbH, Düsseldorf, Germany).

The FeO addition in the Al_2O_3-SiO_2 system (Figure 16.15) creates two new compounds: the iron cordierite ($2FeO.2Al_2O_3.5SiO_2$), which has a very small narrow field almost in the middle of the triangular phase diagram FeO-Al_2O_3-SiO_2 and melts incongruently at 1210°C, and the refractory binary compound $FeO.Al_2O_3$ (hercynite) with melting point at 1780°C. In the FeO-Al_2O_3-SiO_2 system the fields of mullite, corundum and hercynite designate a region rich in alumina and poor in silica with very high refractoriness.

The effect of FeO addition on the liquidus curves of the ternary Na_2O-SiO_2-Al_2O_3 system is shown in Figures 16.16–16.18. The addition of FeO moves the liquidus curves toward the Al_2O_3 vertex of the triangular diagrams, destroying thus the fire resistance of the best composition (carnegieite stoichiometry) in the pure Na_2O-SiO_2-Al_2O_3 system as shown in Figure 16.19.

Indeed, the addition of FeO (0–23.29 %w/w) on the one hand decreases the liquidus temperature from 1550°C to 1330°C, and on the other hand increases the gap between liquidus and solidus temperatures. Although the pure stoichiometric carnegieite composition is thermally stable at temperatures as high as 1500°C (resisting the most

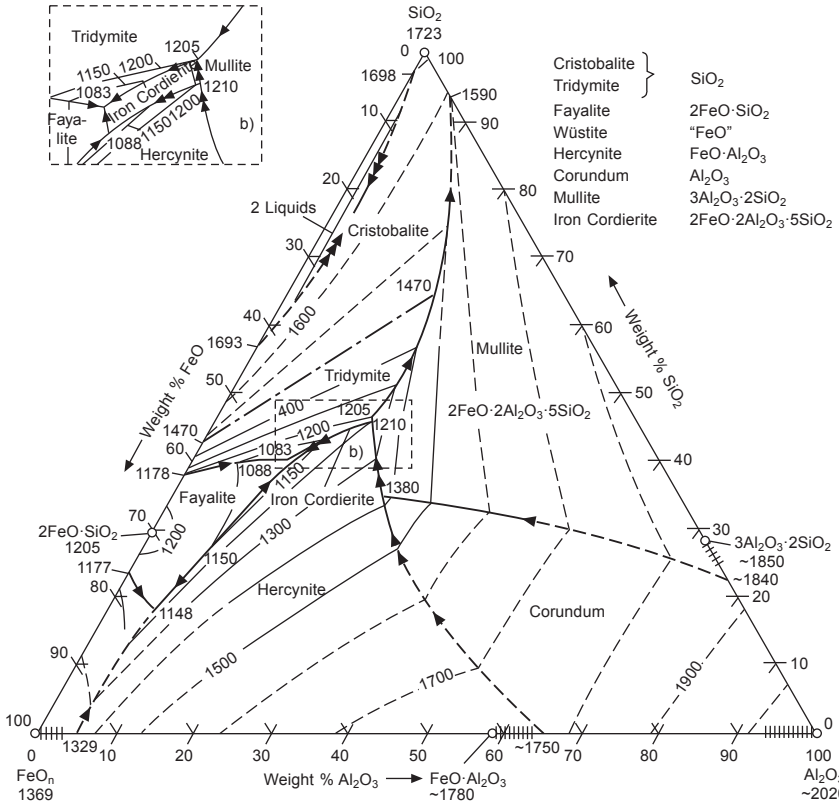

Figure 16.15 FeO-Al_2O_3-SiO_2 system (Verein Deutscher Eisenhüttenleute, Slag Atlas, Copyright 1995 Verlag Stahleisen GmbH, Düsseldorf, Germany).

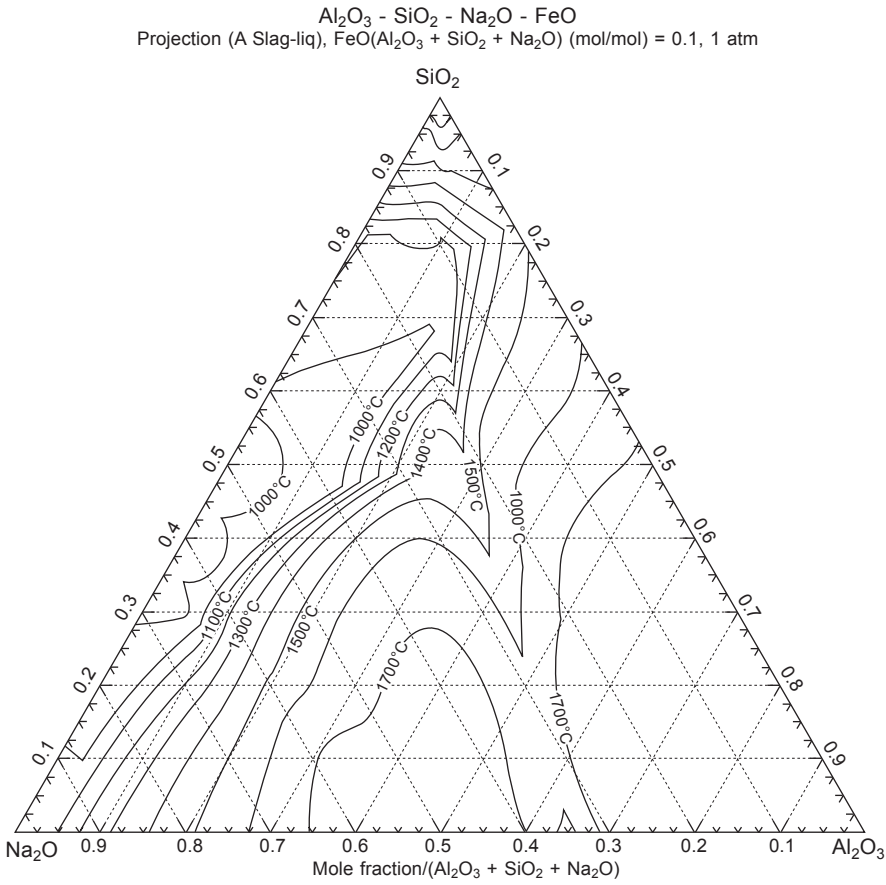

Figure 16.16 Effect of FeO addition (9.19% w/w) on the liquidus curves of the Na_2O-SiO_2-Al_2O_3 system.

severe RWS fire curve), all the FeO-doped carnegieite compositions are thermally stable up to 1150°C (resisting only the less severe cellulosic and HC fire curves) having undergone significant degradation of their fire resistance performance. As in the case of CaO doping, the shift of the liquidus curves toward the Al_2O_3 corner of the Na_2O-SiO_2-Al_2O_3 system due to FeO doping renders this rich alumina domain a promising area for fire resistant alkali-activated binders.

The effect of FeO addition in the pure K_2O-SiO_2-Al_2O_3 system is expected to be identical to the one in the Na_2O-SiO_2-Al_2O_3 system. The new compounds added in the system are the $K_2O.FeO.3SiO_2$ (congruent melting point at 900°C), $K_2O.FeO.5SiO_2$ (congruent melting point around 900°C), fayalite, iron cordierite and the refractory hercynite. As can be seen in Figure 16.20, the FeO addition to the K_2O-SiO_2 system moves the compositions toward the $K_2O.FeO.3SiO_2$, $K_2O.FeO.5SiO_2$ and mainly $2FeO.SiO_2$ domains which are characterized by low liquidus temperature

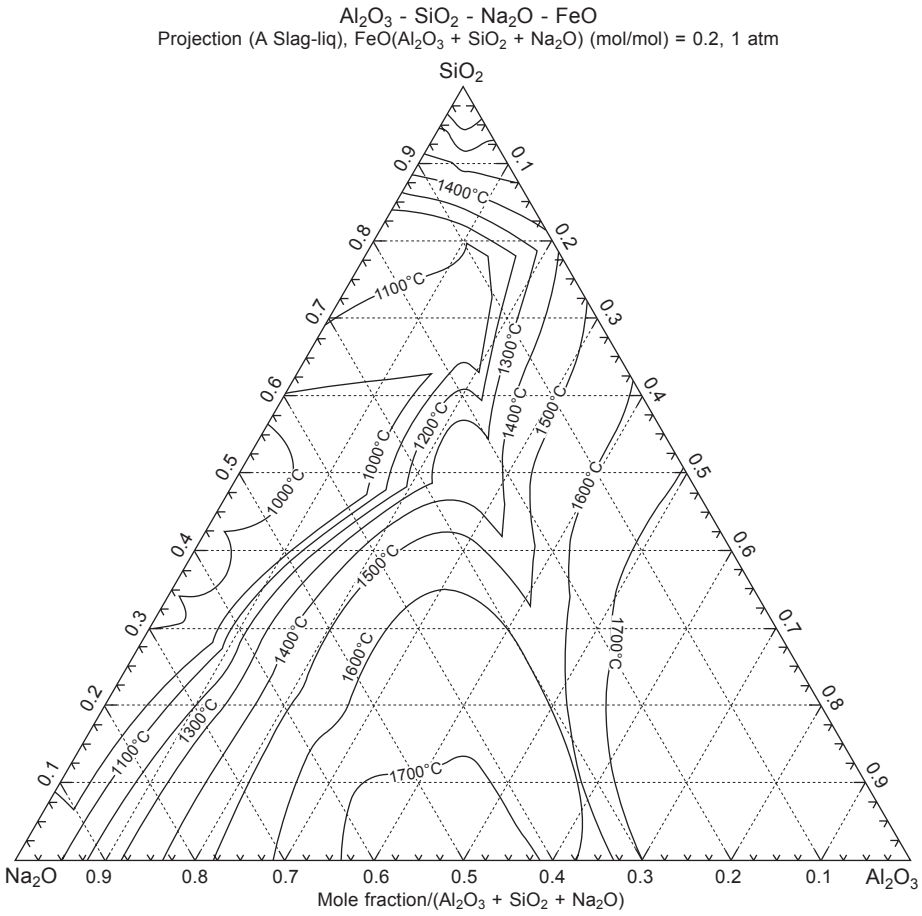

Figure 16.17 Effect of FeO addition (16.83% w/w) on the liquidus curves of the Na_2O-SiO_2-Al_2O_3 system.

curves and therefore are not interesting compositions from a fire resistance point of view.

The fire resistance performance of the FeO-doped K_2O-SiO_2-Al_2O_3 system is determined by the presence of alumina which adds to the system the refractory compounds of mullite and hercynite (Figure 16.15) as well as leucite and kaliophilite (Figure 16.7). Therefore, the rich-in-alumina domain of the FeO-doped K_2O-SiO_2-Al_2O_3 system far from the fayalite and silica fields and close to the leucite as well as hercynite fields has the highest potential for geopolymeric compositions with very good fire resistance performance as shown in Figure 16.21.

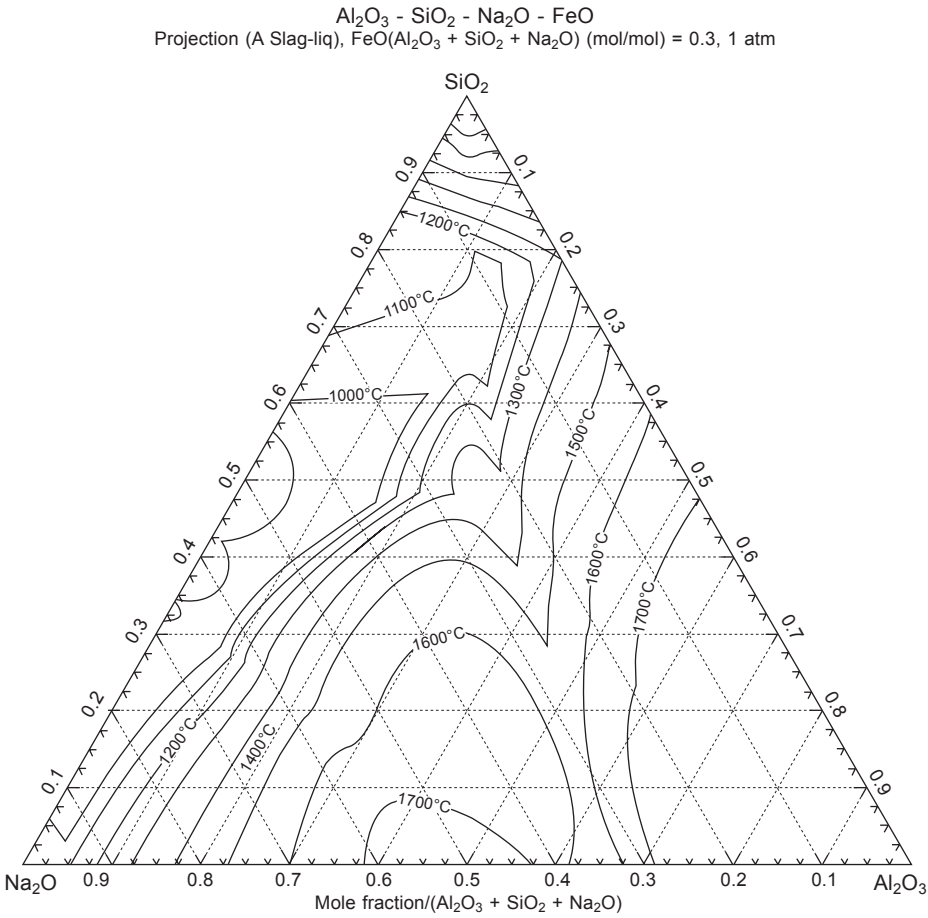

Figure 16.18 Effect of FeO addition (23.29% w/w) on the liquidus curves of the Na_2O-SiO_2-Al_2O_3 system.

16.5 Fire resistant alkali-activated composites

Fire resistant alkali-activated binders have been developed since 1970, when J. Davidovits carried out research into new heat resistant materials as an aftermath of various catastrophic fires in France. Since then, a lot of research has taken place in order to develop fire resistant geopolymers as well as geopolymer concretes and composites (www.geopolymer.org).

A high temperature composite called GPMC was developed by Géopolymère SA and used as a filter frame for air filtration in sterilization tunnels (Buchler, 1999). The composite included a silica fibre fabric that was impregnated with a fluoro-poly (sialate-disiloxo) geopolymeric resin. The composite had a flexural strength of 25MPa, was incombustible, did not release smoke upon high temperature

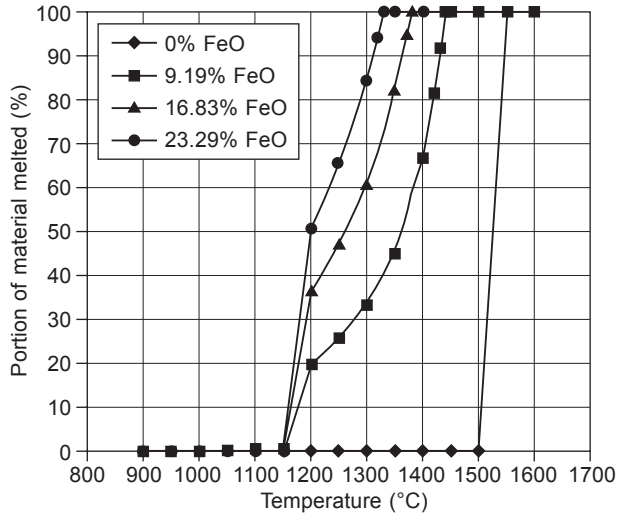

Figure 16.19 Percentage portion of totally dehydrated geopolymeric compositions melted between solidus and liquidus temperatures as a function of FeO addition (stoichiometric carnegieite composition in the Na_2O-SiO_2-Al_2O_3 system).

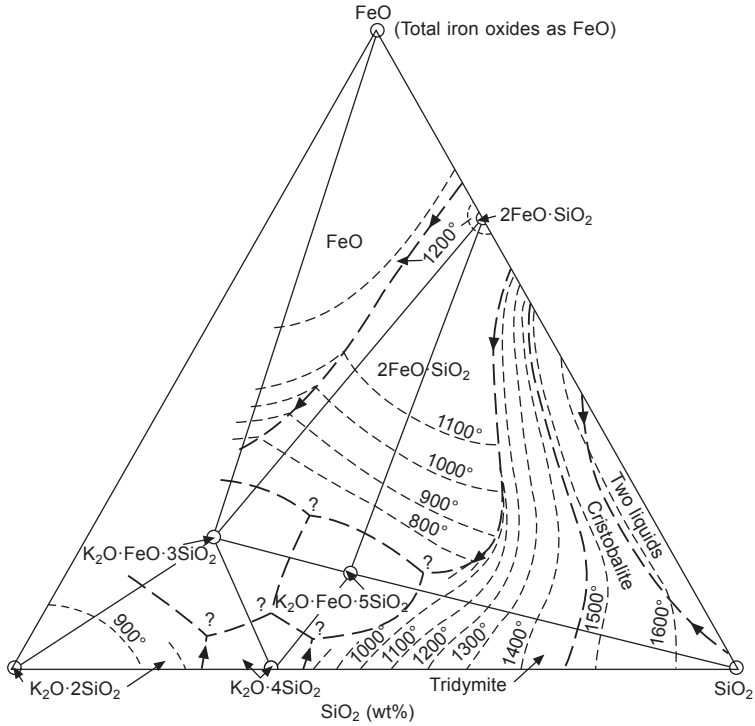

Figure 16.20 FeO-K_2O-SiO_2 system (Copyright 1964 6th Edition, *Data of Geochemistry*, United States Government Printing Office, Washington, With kind permission from U.S. Geological Survey).

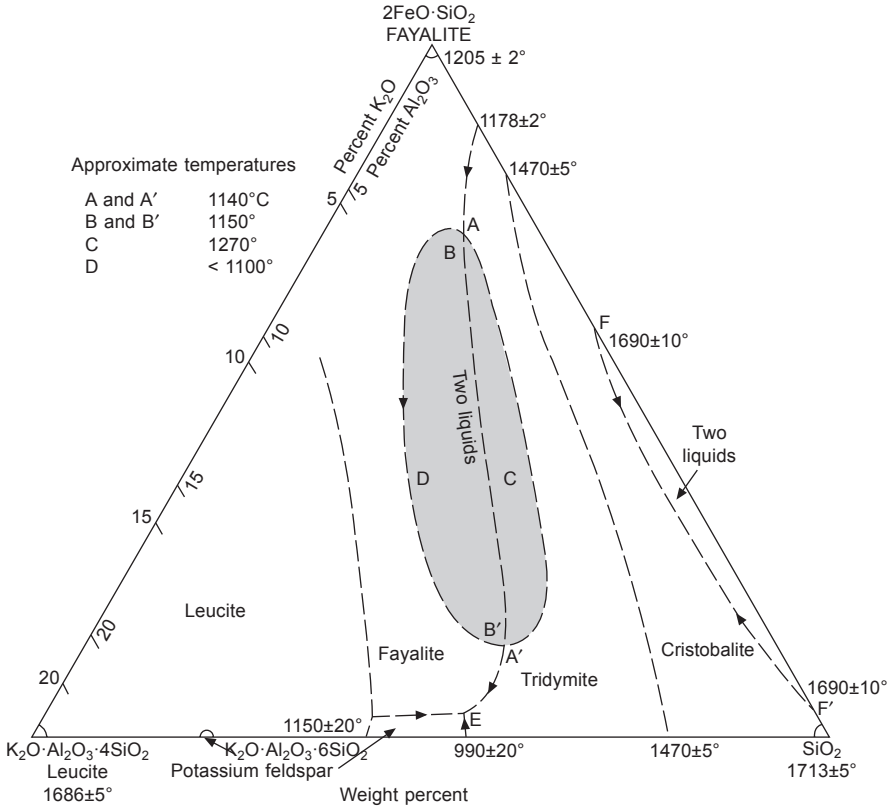

Figure 16.21 Preliminary study of the section leucite-fayalite-SiO_2 of the quaternary FeO-K_2O-SiO_2-Al_2O_3 system (Copyright 1964 6th Edition, *Data of Geochemistry*, United States Government Printing Office, Washington, with kind permission from US Geological Survey).

exposure, and was fire resistant at temperatures up to 600°C. A geopolymer carbon composite heat shield for racing car manufacture was developed by Géopolymère SA in 1994. This composite was able to withstand the heat stress of 600°C for 2–3 h (Davidovits, 2011). Later, in 1999, a more sophisticated fire and heat resistant geopolymer-carbon laminate was introduced on an American All Racers CART that could be used during the entire season (10 races) without being damaged (Davidovits, 2011).

In 1996 the Federal Aviation Administration (FAA) initiated a research program to develop low cost, environmentally friendly, fire resistant materials for use in aircraft composites and cabin interior applications. The goal of the program was to eliminate cabin fire as cause of death in aircraft accidents. It was proved that the carbon fabric-reinforced potassium aluminosilicate resin (with an empirical formula $Si_{32}O_{99}H_{24}K_7Al$) did not ignite, burn, or release any heat or smoke even after extended exposure to high heat flux (50 kW/m^2) while at the same time geopolymer composites had substantial

residual strength after the simulated fire test (Lyon, *et al*., 1997). The geopolymer-carbon fabric laminate was proved to have maximum temperature capability higher than 800°C. The manufacturing of fire resistant biocomposite sandwich plates using waste sawdust as filler and an inorganic potassium aluminosilicate binder was studied by Giancaspro *et al*. (2008). The biocomposite plates contained 29% and 34% w/w inorganic binder and some of them were strengthened with carbon and glass fiber reinforcements to create a more durable sandwich structure. All specimens passed the FAA requirements for heat release and smoke emission and showed superior heat release rates during 5 min of fire exposure. A thin layer of a fire-resistant paste composed of geopolymer and hollow glass microspheres was applied to high-strength fiber facings to create a composite material that serves as a protective fire barrier improving the fire resistance of balsa sandwich panels (Giancaspro *et al*., 2006). The fire performance of this material was evaluated and the results showed that a 1.8 mm thick layer of fireproofing satisfies the FAA requirements for both heat release and smoke emission.

Two different types of syntactic foams made by embedding randomly dispersed spheres (ceramic as well as expanded polystyrene beads) in fire resistant, polysialate matrix were developed by Papakonstantinou *et al*. (2008). The foams with the ceramic spheres were not affected by fire exposure during the tests, exhibited remarkable stability, and passed the FAA requirements for both heat release and smoke emission. The foams with the expanded polystyrene spheres exhibited flaming combustion during the fire tests, but the heat release remained below the acceptable FAA levels. It was concluded that the polysialate matrix serves as an insulator, limiting the heat release and smoke emission to acceptable FAA levels.

Thermal silica-based K-geopolymers reinforced by 45, 53 or 60 vol.% of unidirectional carbon fibers, basalt rovings, or E-glass were fabricated by Hung *et al*. (2011). The K-geopolymer reinforced composites exhibited very good thermal-mechanical properties, retaining nearly 50% of flexural strength even after severe thermal exposure for 1 h in oxidation environment up to 600°C for basalt and E-glass and 1000°C for carbon fiber reinforced composites. The geopolymer resins could protect in general the carbon fibers from oxidation, although approximately 14% w/w of carbon fibers was oxidized at temperatures higher than 800°C. In addition, the composites had very good thermal dimensional stability and non-toxic fumes and smokes were generated during thermal exposure.

Foamed and unfoamed metakaolin-based geopolymers reinforced with polyprolylene fibres were developed and their thermal performance was investigated under the standard ISO 834 fire curve (Rickard *et al*., 2013) in order to assess their suitability for high temperature applications such as thermal barriers and fire resistant panels. The fire testing was conducted on 50 mm thick panels with an exposure size of 200 × 200 mm. The results showed that the fire rating of the samples was at least 60 min (the time needed for the average temperature of the cold side of samples to exceed 165°C). The best performing sample was the unfoamed geopolymer which had a fire rating of 97 min. Although the foamed samples had reduced thermal conductivities, their ability to insulate during a fire was not improved due to their lower water content. The best performing foamed sample achieved a fire rating of

82 min which is only 15 min less than the unfoamed sample while exhibiting the desirable properties of a low density material.

16.6 Fire resistant alkali-activated cements, concretes and binders

Since 1985, French and English nuclear power stations have equipped their plants with air filters in which joints and dust-free sealants are made of geopolymer. A fire or heat resistant air filter for nuclear power plants is expected to resist hot air (temperature resistance up to 500°C for 15 min is required) and must be incombustible and water resistant. The company Géopolymère SA developed Geopolymite SP7 and SP20 sealing cements for fire resistant air filters in nuclear power plants, which were castable compounds based on fluoro-poly (sialate-disiloxo) matrix (Buchler, 1999). In addition, and in order to comply with the increased safety standards for nuclear power plants in case of fire, Géopolymère SA developed a new Geopolymite sealing resin GPS45 which was based on a polysialate penta-disiloxo matrix (Buchler, 1999).

Cordi-Géopolymère SA developed (Na,Ca)-Poly(sialate) and (K,Ca) Poly(sialate-siloxo) cements and binders with excellent fire resistant properties up to 1200°C (Davidovits, 1999). This excellent behavior was attributed to: (a) the unique structure of the tecto-alumino-silicate type 3D networks that possesses nano-porosity allowing physically and chemically bonded water to evaporate without causing damage to geopolymers during their exposure to fire, and (b) the high endothermicity of materials due to physically and chemically bonded water.

HT Troplast AG had developed a poly-silico-oxo-aluminate material with the brand name 'Trolit' (Liefke, 1999) that is incombustible with low thermal conductivity (≥0.037 W/mK) and bulk density 100–800 kg/m^3 for 'Trolit' foam and 1500–3000 kg/m^3 for 'Trolit' compact material. Depending on the formulation, its temperature resistance was between 1000 and 1200°C. The material was most suited for fire-proof heat insulation or heat-resistant soundproofing.

The Australian Research Organization CSIRO developed a new fire resistant coating material called hybrid inorganic polymer system – HIPS (Figure 16.22), which is composed mainly of an inorganic geopolymer resin and a small amount of polymer additives (CSIRO, n.d.). HIPS can withstand temperatures of over 1000°C and has the potential to form thin fireproof coatings on timbers and on metals as well as protecting brickwork, either as a thin coating or as a render. In addition, HIPS coatings are free of volatile organic compounds, do not burn or produce heat, and do not release smoke or toxic chemicals at temperatures up to 1200°C.

Barbosa and McKenzie (2003) investigated the thermal behavior of inorganic polymers derived from metakaolinite with compositional ratios SiO_2/Al_2O_3 = 3.3 and Na_2O/SiO_2 = 0.25. The inorganic polymers were endothermic and exhibited remarkable thermal stability until the onset of melting at around 1300°C. In addition, their composites with granular inorganic fillers exhibited again good thermal behavior with little detectable reaction between the filler and the matrix up to 1000°C.

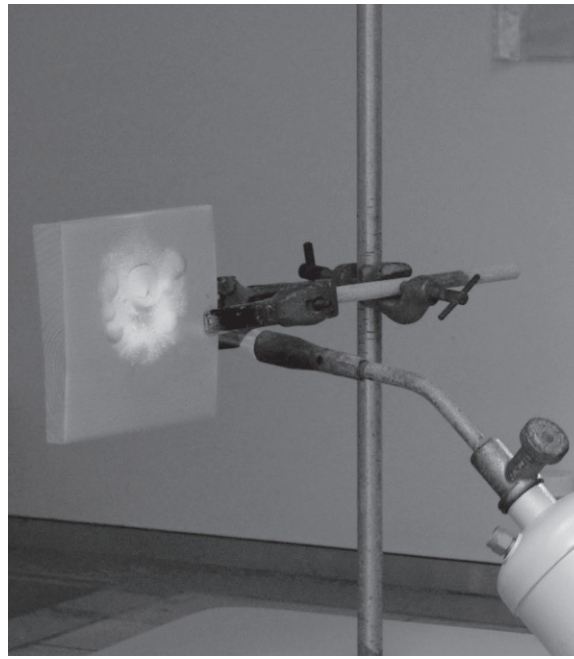

Figure 16.22 HIPS fireproof coatings (with kind permission from CSIRO).

Geopolymers based on metakaolinite were developed in order to protect concrete substrates from fires (Varela and Privorotskaya, 2005). Two geopolymeric coatings with Si/Al molar ratios of 2 and 6 were developed and proved effective thermal barriers for concrete protection up to 800°C. The geopolymer with the higher Si/Al ratio presented minimal deterioration and absence of cracks besides providing a stronger bond to the concrete substrate. Hu *et al*. (2009) investigated the mechanical and heat resistance properties of geopolymer-lightweight aggregate refractory concrete (GLARC) at 950°C. GLARC was prepared by mixing a sodium-activated binder based on metakaolin and lightweight aggregates (haydite). The results showed that the GLARC possesses excellent heat resistance at 950°C, retaining 40–55% of its original mechanical strength that is affected by the thickness of geopolymer gel that covers the surface of aggregate. For optimal performance, the quantity of geopolymer gel per surface area of haydite aggregates with size of 1.18–4.75 mm should be in the range of 0.3–0.5 mg/mm^2.

The thermal behavior of Na- and K-based geopolymers made using Class F fly ash was studied in the temperature range 800–1200°C. The thermal stability of Na-activated binders was rather low and rapid deterioration of their strength at 800°C was observed, which was attributed to a dramatic increase in the average pore size. The K-activated binders had better thermal stability than the Na-activated ones and the deterioration of strength started at 1000°C (Bakharev, 2006; Hardjito and Tsen, 2008). Geopolymers prepared by alkali activation (a mixture of sodium silicate and potassium hydroxide) of Class F fly ash exhibited increased mechanical strength

of about 53% after exposure to 800°C (Kong *et al.*, 2007; Kong and Sanjayan, 2008). This was attributed on the one hand to the large number of small pores which facilitate the escape of moisture during heating and thus causing minimal damage to the geopolymer matrix, and on the other hand to the sintering reactions of unreacted fly ash particles. However, geopolymer/aggregate composites with identical geopolymer binder formulations exhibited decreased strength by up to 65% after the exposure to 800°C (Kong and Sanjayan, 2008). This was attributed to the expansion of coarse aggregates (basalt or slag) that caused contraction to the geopolymeric matrix deteriorating the mechanical strength of the composite (Kong and Sanjayan, 2010).

In order to understand better this oppositional behavior of fly ash-based geopolymers at high temperatures, Pan *et al.* (2009) investigated the mechanisms for strength gain or loss of geopolymer mortar after exposure at 800°C for 2 h. The results indicated that ductility of geopolymeric mortars plays an important role in the strength losses or gains at high temperatures. There are two opposing processes responsible for the strength losses or gains in geopolymeric mortars: (1) the strength gain is attributed to further geopolymerization and/or sintering at elevated temperatures; (2) the strength loss is attributed to the damage of the mortar because of thermal incompatibility arising from non-uniform temperature distribution. Geopolymeric mortars with high ductility have high capacity to accommodate thermal incompatibilities and thus suppress mechanism (2) giving rise to mechanism (1) and to strength gain or reduced strength loss at high temperatures (Pan *et al.*, 2009; Guerrieri and Sanjayan, 2010).

The thermal resistance of potassium activated mortars from Class F fly ash with a mixture of sand/bottom ash aggregates was studied by Hardjito and Fung (2010). In order to test the thermal resistance the samples were subjected to thermal exposure of 400°C, 700°C and 1000°C at an incremental rate of 10°C/min from room temperature, remained at the desired temperature for 3 h and then were allowed to cool naturally to room temperature and the compressive strength was measured the next day. The results showed that after exposure to elevated temperature the compressive strength of the geopolymer mortars with lower bottom ash as aggregates (0–25%) was decreased while the one of mortars with higher bottom ash content (50–100%) was increased.

Van Riessen *et al.* (2009) compared the behavior of a fly ash-based geopolymer concrete and a Portland cement concrete, both with a compressive strength of approximately 75 MPa, at elevated temperature. The specimens were rectangular slabs, 780 mm long and 360 mm wide with a thickness of 200 mm, reinforced with 100×100 mm steel mesh with a bar diameter of 6 mm. The specimens were exposed to the Eurocode EN1991-1-2 standard hydrocarbon fire on one side. After the end of the fire test severe spalling was observed on the Portland cement concrete, while no spalling phenomena appeared on the geopolymer concrete, which thus exhibited very good fire resistance performance. The same behavior was also observed by Zhao and Sanjayan (2011) as well as Dao and Forth (2013), who had developed Class F fly ash-based geopolymer and Portland cement concretes and then exposed them to temperatures as high as 1000°C. After the tests it was observed that no spalling

appeared in geopolymer concretes that were converted into ceramic materials, whereas Portland cement concretes exhibited severe spalling and were more or less disintegrated.

Finally, Temuujin *et al*. (2010) developed and tested Class F fly ash-based Na-geopolymers as fire resistant coatings on steel. The heat insulating characteristics of the coatings were measured following the Australian standard 1530.4 and the standard time–temperature curve ISO-834. The insulating capacity of the samples was calculated by measuring the time necessary for the unexposed side to reach a temperature of 180°C above the ambient temperature. The compositions of Na-geopolymers had a fixed Na/Al molar ratio of 1 while the Si/Al molar ratio varied between 1 and 3.5. The fire resistance measurements were performed on coated mild steel with dimensions of 15 × 15 cm and the coating thickness was fixed at 0.6 mm and 1.5 mm. The best adhesive strength of the coating to steel was observed for the alkali-activated binder with Si/Al molar ratio of 3.5 and was measured higher than 3.5 MPa. The best geopolymer coating had a Si/Al molar ratio of 3.5, a water/cement mass ratio at 0.25 and a measured insulating capacity of 9 min.

Several geopolymers were synthesized from industrial wastes such as fly ash, alumina red mud, ferronickel slag, perlite superfines and bentonite tailings, and their behavior upon exposure at high temperatures was studied (Giannopoulou and Panias, 2008). Round geopolymeric discs 210 mm in diameter and 10 mm thick were prepared and then their front-side was exposed to a propane flame with temperature higher than 1100°C for 100 min. The reverse-side temperature was measured during the whole test and the results are shown in Figure 16.23. The reverse-side temperature at thermal equilibrium reaches around 400°C in all samples with the only exception of bentonite geopolymer which reaches 200°C, exhibiting superior fire resistance performance.

Geopolymers are highly endothermic materials, principally due to large amount of water entrapped inside their structure. This is obvious during the unsteady thermal state (first minutes after their exposure to a fire) of the test and becomes impressive in the case of bentonite geopolymer where the temperature is kept constant at almost 100°C for the first 20 min of the test. In general, the materials behave as high temperature insulators such as calcium silicate, rockwool and some proprietary insulation solids (perlite mixtures and vermiculite bonded with sodium silicate) with very good thermal stability indicating, thus, their application potential as fireproofing materials in construction sector.

Cheng and Chiu (2003) developed fire resistant K-based geopolymers using granulated blast furnace slag as raw material. In order to investigate the fire resistance, a 10 mm thick panel of K-geopolymer was exposed to an 1100°C flame and the reverse-side temperature was measured as a function of time. The materials behaved well and the measured reverse-side temperature reached 240–283°C after 35 min. It was also found that the fire resistant characteristics can be improved by increasing the KOH concentration or the amount of added metakaolinite. In addition, Cheng (2003) developed fire resistant geopolymers using waste serpentine cuttings. Their fire resistance was tested in the same way as in the previous research and the results showed that the measured back-side temperatures reached less than 450°C after 30

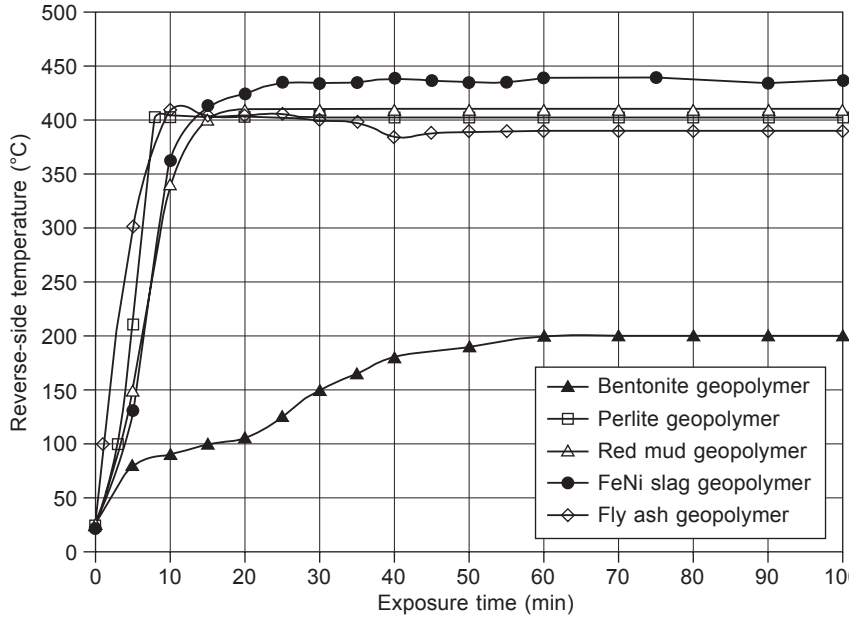

Figure 16.23 Reverse-side temperature as a function of exposure time to a propane flame (≈1100°C) of several geopolymeric materials prepared from industrial wastes (Giannopoulou and Panias, 2008).

minutes indicating inferior fire resistance performance in relation to the blast furnace slag-based geopolymers.

The behavior of Zeobond E-Crete™ 40 geopolymer concrete (www.zeobond.com/products-e-crete.html) derived with sodium activation of coal fly ash and metallurgical slag blended with fine and coarse aggregates (quartz sand and crushed granite) was studied at high temperatures (Provis, 2010). The thermal behavior of the geopolymer concrete was tested in pilot-scale tests, using a furnace and following the standard time–temperature ISO-834 profile reaching the maximum temperature of 1100°C and lasting 4 h. The one face of specimen of size 122 × 122 × 15 cm was exposed to the elevated temperature and the temperature along the specimen was measured with thermocouples that were located in different places. The temperature after the 4 h test, at 25 mm and 50 mm from the exposed face, was about 850°C and 600°C, respectively, while the observed maximum unexposed face temperature was 105.3°C which is lower from the maximum allowable temperature of 139°C imposed by the ASTM E 119 standard. The results showed an apparent flattening of the rate of temperature increase at a temperature between 100 and 160°C, which was attributed to the high specific heat capacity and latent heat of vaporization of water. Spalling phenomena were not observed in any of the tested samples (Figure 16.24), which retained their structural integrity and at the end of the test were able to be lifted and stacked using a forklift without any difficulty or fragility. The exposed surfaces of the samples where whitened, slightly dusty and soft but the

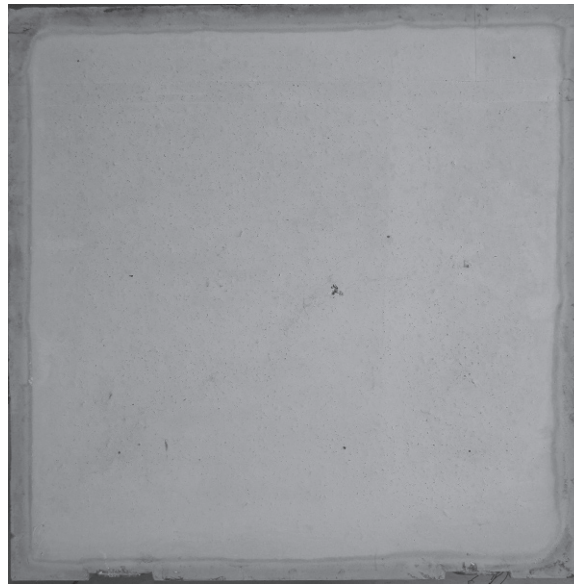

Figure 16.24 Photograph of the exposed face of an E-Crete 40 geopolymer concrete sample after a fire test following the Standard ISO-834 time-temperature curve (with kind permission from Jannie S.J. van Deventer).

bulk of the sample (which had sustained exposure to temperatures of up to 800°C) did not show structural failure. The performance of E-Crete 40 geopolymer concrete under fire testing conditions was very satisfactory, as the rate of thermal transport was low and the degree of structural damage to the materials during a 4-h fire test was minor.

16.7 Passive fire protection for underground constructions

Sakkas *et al.* (2013b) developed inorganic polymeric materials from FeNi slag, that is an iron-rich slag (>35% FeO) produced in ferronickel production, for passive fire protection of underground constructions. The FeNi slag was activated with 7 M NaOH solution and the geopolymeric paste was formed by mixing the FeNi slag and the activating solution at a ratio 4 g/mL. The paste was cured at ambient temperature for 96 h. Small lab-scale geopolymeric plates with dimensions 300 × 150 × 10 mm were prepared and tested for the determination of their fire performance. The plates were placed horizontally on a metallic tripod and its front-side surface was exposed to a propane flame with temperature higher than 1100°C for 120 min (Figure 16.25(a)), while the reverse-side and front-side temperatures were measured every 5 min through a laser, high performance infrared thermometer (Figure 16.25(c)).

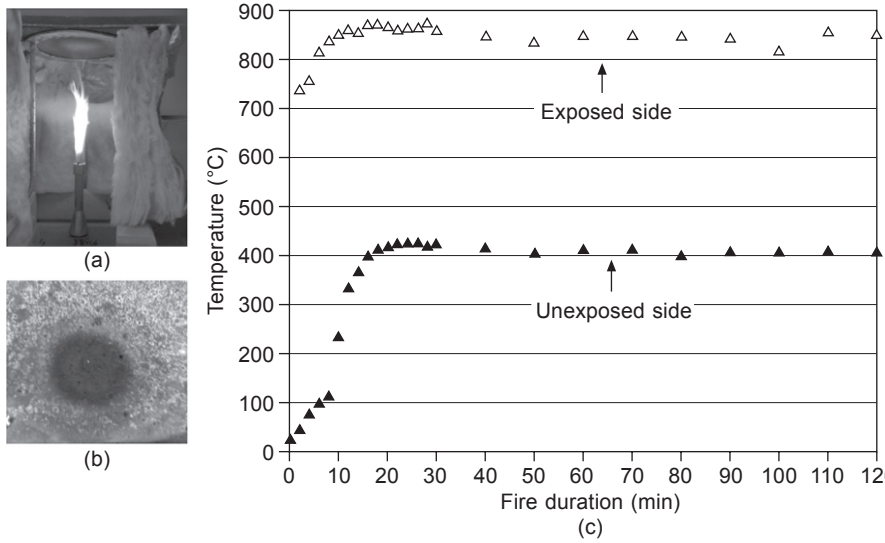

Figure 16.25 (a) Set up of lab-scale fire test; (b) fire exposed surface of FeNi Geopolymer slab after the fire test; (c) temperature–time curves of exposed and unexposed surfaces of FeNi geopolymer during the fire test.

The lab-scale experiments showed that the FeNi slag-based inorganic polymers can effectively set a flame and a temperature barrier achieving at thermal equilibrium a high temperature gradient of 41°C/mm that was attributed to its low thermal conductivity (0.135 W/m.K). Moreover, the material during the fire test was not thermally degraded, avoiding the formation of cracks and spalling phenomena as shown in Figure 16.25(b). Alterations in the microstructure of material were observed during the fire test that appeared as color changes on the exposed side (Figure 16.25(b)) and were attributed to phase transformations taking place during heating.

The lab-scale tests proved that the FeNi slag-based inorganic polymer has a good thermal insulating capacity which may render it a promising material for passive fire protection of underground constructions. The ability of this material to offer passive fire protection of concrete was evaluated following the EFNARC (European Federation of National Associations Representing producers and applicators of specialist building products for Concrete) guidelines (Sakkas *et al.*, 2013c). Composite specimens with dimensions 15 × 15 × 15 cm consisting of 5 cm thick Na-geopolymer material and 10 cm thick concrete slab were prepared (Figure 16.26(a)). The adhesion between the two materials was enhanced by steel anchors, placed during material preparation. The specimens were subjected to thermal loading in a specially designed furnace (Figure 16.26(b)) by exposing the geopolymer surface to prescribed temperatures according to the ISO-834 time–temperature curve. The temperature at the geopolymer/concrete interface was measured by using a 'K'-type thermocouple, while the temperature at the back surface of the concrete slab, with a high performance infrared thermometer (Figure 16.27).

(a)

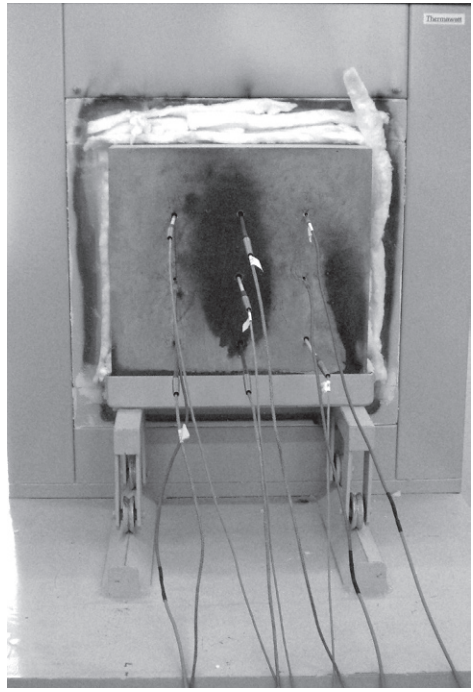

(b)

Figure 16.26 (a) Composite Na-geopolymer/cement concrete specimens; (b) fire test in a specially designed furnace.

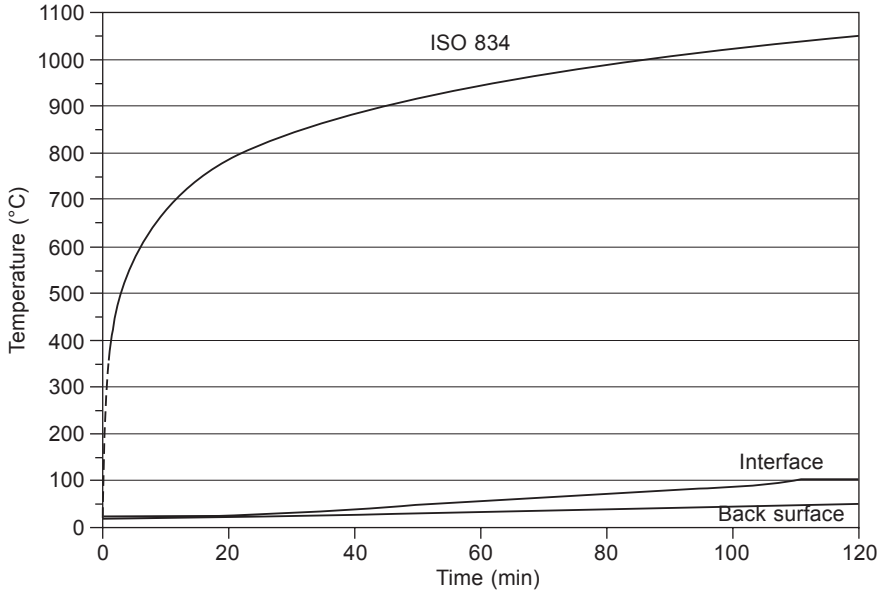

Figure 16.27 Temperature–time curves of ISO 834 standard fire scenario as well as Na-geopolymer/cement concrete and back cement concrete surfaces during the fire test (from Sakkas *et al.*, 2013c, with kind permission from Springer Science and Business Media).

The sodium-based geopolymer was proved to be an effective heat flux barrier keeping the temperature at the geopolymer–conrete interface at around 100°C and thus offering very successful passive fire protection to structural concrete and steel from cellulosic fires. Furthermore, some cracks were observed on the exposed face of the Na-geopolymer after the test, formed due to the sudden loss of geopolymeric water, which, however, were less than 6 mm wide and 25 mm deep, which are the specific performance criteria set by the standard ISO 834-1:1999(E) for the evaluation of integrity of fire resistant materials.

The Na-geopolymer was also tested against the most severe RWS fire load curve but it failed to pass the performance criteria as a passive fire protection material. Although the Na-geopolymer set an efficient thermal barrier, it was disintegrated during the test due to intense creeping phenomena attributed to its partial melting between 1200 and 1350°C.

In order to develop a FeNi slag-based geopolymer material for passive fire protection of concrete tunnels linings, Sakkas *et al.* (2013c) switched to a material design utilizing a potassium-based activator of the slag instead of a sodium one. The basic idea was to create a chemical composition in the material such that upon heating at high temperatures, FeO (which is a substantial FeNi slag component with concentration almost 35% w/w) would be bound in the refractory aluminate phase of hercynite, $FeO.Al_2O_3$ (melting point 1780°C), and SiO_2 (which is the other major component of FeNi slag with concentration 41% w/w) would be bound in the refractory phase of leucite $K_2O.Al_2O_3.4SiO_2$ (melting point at 1693°C). To achieve the above

design targets, the potassium activation and the doping with alumina of the FeNi slag were necessary. The procedure for testing the fire performance of K-geopolymer was exactly the same as the one followed for Na-geopolymer. The potassium-based geopolymer was proved to be an effective heat flux barrier and succeeded in the passive fire protection test simulating the most severe RWS fire load curve (Figure 16.28). The maximum temperature achieved at the geopolymer–concrete interface was 280°C at the end of the fire test, which is 100°C lower than the performance requirements for an efficient fire resistant material set by the EFNARC for a passive fire protection test with the RWS fire loading curve. The temperature on the back surface of the concrete slab did not exceed 70°C during the whole duration of the fire test, which means that across the concrete slab the temperature varied between 70°C and 280°C.

The K-geopolymer remained on top of the concrete slab without any change in its geometry as well as any mechanical damage or cracks after the end of the fire test (Figure 16.29). The surface of the K-geopolymer exposed directly at 1350°C (Figure 16.29(b)) remained almost unchanged without cracks except some local, small in extent and not deep, superficial scaling. The K-geopolymer after the fire test became tougher and stronger and the fire helped in improving the mechanical properties of the material. The adhesion of the K-geopolymer/concrete through the steel anchors proved to be excellent and the steel anchors used did not undergo visible deformations or structural disintegration.

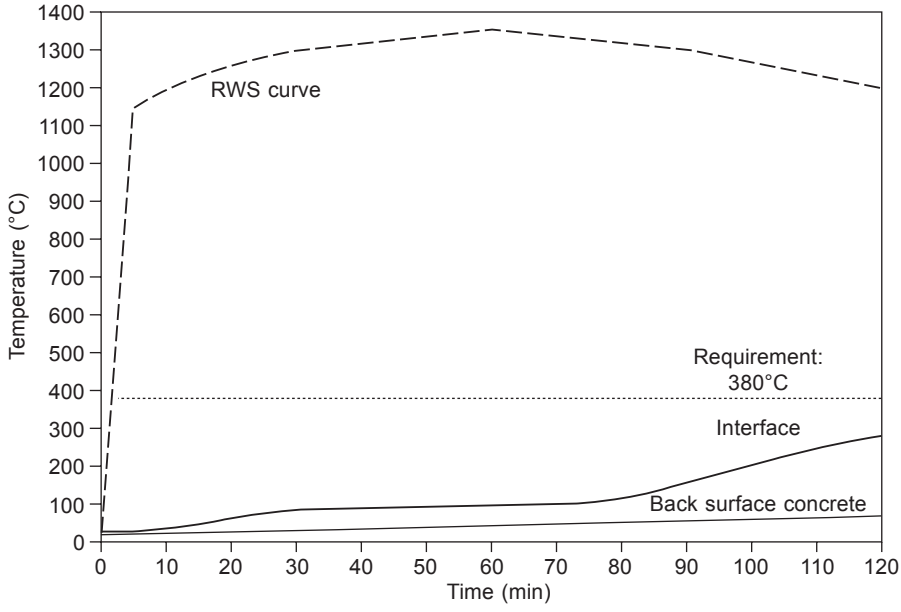

Figure 16.28 Temperature–time curves of RWS standard fire scenario as well as K-geopolymer/cement concrete and back cement concrete surfaces during the fire test (from Sakkas *et al.*, 2013c, with kind permission from Springer Science and Business Media).

(a)

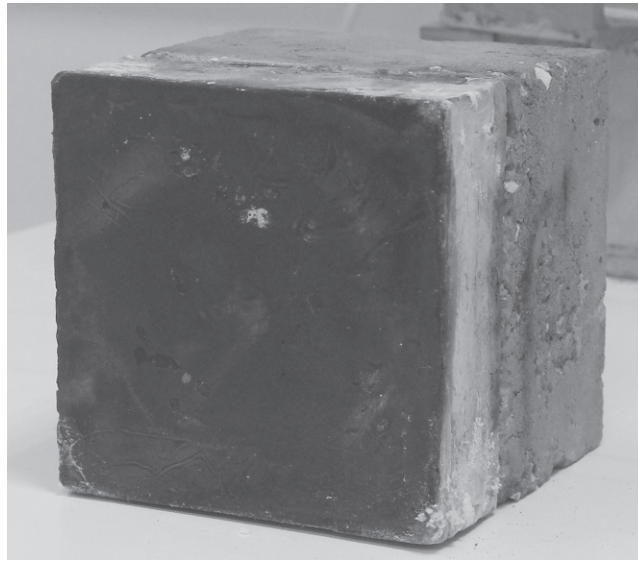

(b)

Figure 16.29 K-Geopolymer/cement concrete composite specimen before (a) and after (b) the test with the RWS standard fire scenario (from Sakkas *et al.*, 2013c, with kind permission from Springer Science and Business Media).

16.8 Future trends

Alkali-activated binders will continue to be very attractive candidates as the polymeric matrix of fire resistant composite materials such as fiber reinforced composites.

The advantages of alkali-activated binders (such as high operating temperature, low processing temperature, incombustibility) in relation to the organic polymer counterparts, their compatibility with all the marketable types of fibers and the pressure of the industry (especially the aviation one) for new materials with improved fire resistance performance render their application very attractive. The replacement of cement concrete from geopolymer concrete has been proved very advantageous. Geopolymer concrete can achieve high compressive strengths comparable with the ones of cement concrete, while at the same time having substantially better fire resistance performance, avoiding the spalling phenomena even at very high exposure temperatures and in some cases has improved mechanical strength after exposure in fire. The massive replacement of cement concrete does not seem to be feasible for several reasons. The most important one is the market availability of sodium hydroxide. If the world production of NaOH, that is almost 50 million tons, was utilized in geopolymerization technology, the amount of geopolymeric cement produced would be around 850 million tones which is only a quarter of the global production of cement (3.4 billion tons). Therefore, the partial substitution of cement concrete in specific applications necessitating greater protection from fire or, even better, the protection of cement concrete with fire resistant superficial layers from geopolymeric cement or concrete seems to be more reasonable and attractive. The excellent performance of alkali-activated binders in fires (effective fire and smoke spread as well as thermal barriers, incombustibility, proved structural integrity) renders them very good candidates for passive fire protection of cement concrete. Applications for passive fire protection of concrete linings in tunnels or generally in underground constructions seem to be reasonable and very attractive.

The passive fire protection of steel structures in buildings (encasement in insulating materials) is another attractive area for alkali-activated binders. The state of the art materials are traditional concrete and autoclaved aerated concrete as well as boards from calcium silicate, gypsum and mineral wool. Taking into account that alkali-activated binders have superior or identical fire performance with the above materials and superior or slightly better thermal conductivity values (0.1–0.3 W/m.K instead of 1–3 W/m.K for concrete and 0.2–0.8 W/m.K for cement, calcium silicate and gypsum plasters), geopolymeric plasters seem to be attractive substitutes for steel encasing insulating materials.

16.9 Sources of further information

- UK Passive Fire Protection Federation, http://pfpf.org/
- Promat, http://www.promat-spray.com/
- BASF, http://www.basf-admixtures.ch/de/publikationen/Documents/Fireshield_070508.pdf
- SIKA AG, http://www.sika.com/en/system/search.html?q=Fire+Protection
- NU-CORE, http://www.nu-core.com.au/fr-geocomposite.html
- Alexander Khoury and Yngve Anderberg, ‘Concrete spalling review’, 2000 (http://www.cob.nl/kennisbank/webshop/artikel/fire-safety-design-concrete-spalling-review.html).

- D.J. Naus, 'The effect of elevated temperature on concrete materials and structures – a literature review', 2005 (http://info.ornl.gov/sites/publications/files/Pub1043.pdf)

References

ASFP (2013) *Ensuring Best Practice for passive fire protection in buildings*, Association for Specialist Fire Protection, Available from: http://www.pfpf.org/pdf/publications/best_practice_guide.pdf (accessed 13 October 2013).

Bakharev T. (2006) 'Thermal behaviour of geopolymers prepared using class F fly ash and elevated temperature curing', *Cem Concr Res*, 36, 1134–1147.

Barbosa V. and McKenzie K. (2003) 'Thermal behavior of inorganic polymers and composites derives from sodium polysialate', *Mater Res Bull*, 38, 319–331.

Beard A. and Carvel R. (2005) *The Handbook of Tunnel Fire Safety*, London: Thomas Telford.

Brinson A. (2010) 'Active fire protection in tunnels', *4th International Symposium on Tunnel Safety and Security*, Frankfurt, 47–58.

Buchler C. (1999) 'Uses of Geopolymite resins and GPMC composites in the field of air filtration at high temperatures', *Proceedings of the 2nd International Conference Geopolymere '99*, Saint-Quentin, France, 181–187.

Cheng T.W. (2003) 'Fire-resistant geopolymer produced by waste serpentine cutting', *Proceedings of the 7th International Symposium on East Asian Resources Recycling Technology*, Taiwan, 431–434.

Cheng T.W. and Chiu J.P. (2003) 'Fire-resistant geopolymer produced by granulated blast furnace slag', *Miner Eng*, 16, 205–210.

Chiti S. (2011) 'A pilot study on hypoxic air performance at the interface of fire prevention and fire suppression', *Proceedings of the 5th FIRESHEAT symposium*, Edinburgh, 79–90.

Collette K.A. (2007) *Comparisons of Structural Designs in Fires*, Masters Thesis, Worcester Polytechnic Institute.

Cook L.P., Roth R.S., Parker H.S. and Negas T. (1977) 'The system K_2O-Al_2O_3-SiO_2. Part 1. Phases on the $KAlSiO_4$-$KAIO_2$ join', *Am Mineral*, 62, I180–l190.

CSIRO (n.d.) *HIPS fireproof coatings can really take the heat*, Available from: http://www.csiro.au/Portals/Media/2009/HIPS-fireproof-coatings.aspx (accessed 29 November 2013).

Dao D.V. and Forth J.P. (2013) 'Investigation of the behaviour of geopolymer mortar after heating to elevated temperatures', *Proceedings of the 3rd International conference on sustainable construction materials and technologies*, Kyoto, Japan. Available from: http://www.claisse.info/Proceedings.htm (accessed 3 December 2013).

Davidovits J. (1999) 'Fire proof geopolymeric cements', *Proceedings of the 2nd International Conference Geoplymere '99*, Saint-Quentin, France, 165–169.

Davidovits J. (2011) Geopolymer Chemistry and Applications, 3rd edn, Saint-Quentin: Institut Géopolymère.

Davidson M.T., Harik I.E. and Davis D.B. (2013) 'Fire impact and passive fire protection of infrastructure: state of the art', *J Perform Constr Facil*, 27, 135–143.

Domich P.D. (2004) *Fire Protection of Structural Steel in High-Rise Buildings*, National Institute of Standards and Technology GCR 04-872.

Edwards W.T. and Gamble W.L. (1986) 'Strength of grade 60 reinforcing bars after exposure to fire temperatures', *Concr Int*, 8, 17–19.

EFNARC (2006) *Specifications and Guidelines for Testing of Passive Fire Protection for Concrete Tunnels Linings* (www.efnarc.org).

FPPR (1994), *Assessing the Condition and Repair Alternatives of Fire Exposed Concrete and Masonry Members: Fire Protection Planning Report of the National Codes and Standards Council of the Concrete and Masonry Industries*, Illinois, USA.

Giancaspro J., Balaguru P. and Lyon R. (2006) 'Use of inorganic polymer to improve the fire response of balsa sandwich structures', *J Mater Civ Eng*, 18(3), 390–397.

Giancaspro J., Papakonstantinou C. and Balaguru P. (2008) 'Fire resistance of inorganic sawdust biocomposite', *Compos Sci Technol*, 68, 1895–1902.

Giannopoulou I. and Panias D. (2008) 'Fire resistant geopolymers synthesized from industrial wastes', *World J Eng*, 5(3), 130–131.

Greig J.W. and Barth T.F.W. (1938) 'The system, $Na_2O.Al_2O_3.2SiO_2$ (Nephelite, Carnegieite) – $Na_2O.Al_2O_3.6SiO_2$ (Albite)', *Am J Sci*, 35-A, 93–112.

Guerrieri M. and Sanjayan J. (2010) 'Behavior of combined fly ash/slag-based geopolymers when exposed to high temperatures', *J Fire Mater*, 34, 163–175.

Hardjito D. and Fung S.S. (2010) 'Parametric study on the properties of geopolymer mortar incorporating bottom ash', *Concrete Res Lett*, 1, 115–124.

Hardjito D. and Tsen M.Z. (2008) 'Strength and thermal stability of fly ash-based geopolymer mortar', *Proceedings of the 3rd International Conference ACF/VCA2008 on Sustainable Concrete Technology and Structures in Local Climate and Environment conditions*, Ho Chi Minh City, Vietnam, 144–150.

Hong L. (2005) *Formation of β-Eucryptite and β-Sposumene from Topaz mixtures*, PhD Thesis in Ceramic and Materials Engineering, School in Materials Science and Engineering, Faculty of Science, University of New South Wales, Sydney, Australia.

Hu S., Wu J., Yang W., He Y., Wang F. and Ding Q. (2009) 'Preparation and properties of geopolymer-lightweight aggregate refractory concrete', *J Cent S U Technol*, 16, 914–918.

Hung T.D., Louda P., Kroisova D., Bortnovsky O. and Xiem N.T. (2011) 'New generation of geopolymer composite for fire-resistance', in Tesinova P (ed.) *Advances in Composite Materials – Analysis of Natural and Man-Made Materials*, Rijeka: InTech, 73–94.

Khoury G.A. (2000) 'Effect of fire on concrete and concrete structures', *Prog Struct Eng Mater*, 2, 429–447.

Kong D. and Sanjayan J. (2008) 'Damage behavior of geopolymer composites exposed to elevated temperatures', *Cem Concr Compos*, 30, 986–991.

Kong D. and Sanjayan J. (2010) 'Effect of elevated temperatures on geopolymer paste, mortar and concrete', *Cem Concr Res*, 40, 334–339.

Kong D., Sanjayan J. and Sagoe-Crentsil K. (2007) 'Comparative performance of geopolymers made with metakaolin and fly ash after exposure to elevated temperatures', *Cem Concr Res*, 37, 1583–1589.

Liefke E. (1999) 'Industrial applications of foamed inorganic polymers', *Proceedings of the 2nd International Conference Geopolymere '99*, Saint-Quentin, France, 189–199.

Lyon R.E., Balaguru P.N., Foden A., Sorathia U., Davidovits J. and Davidovics M. (1997) 'Fire resistant aluminosilicate composites', *J Fire Mater*, 21, 67–73.

Maevski I.Y. (2011) *Design Fires in Road Tunnels, National Cooperative Highway Research Program*, Washington, DC, Transportation Research Board (www.TRB.org).

Mawhinney J.R. and Trelles J. (2010) 'Performance testing of fire protection systems in tunnels – integrating test data with CFD simulations', *Proceedings of the 4th International Symposium on Tunnel Safety and Security*, Frankfurt, 297–309.

Morey G.W. (1964) Chapter L. '*Phase-equilibrium relations of the common rock-forming oxides except water, Data of Geochemistry*, 6th edn, Washington, DC: US Government Printing Office.

Mrazova M. and Klouzkova A. (2009) 'Leucite porcelain fused to metals for dental restoration', *Ceram Silikaty*, 53(3), 225–230.

NYCBC (2008) 'Fire resistance rated construction', New York City Building Code, New York, 95–166. Available from: http://archive.org/details/gov.law.nyc.building.2008 (accessed 13 October 2013).

Pan Z., Sanjayan J.G. and Rangan B.V. (2009) 'An investigation of the mechanisms for strength gain or loss of geopolymer mortar after exposure to elevated temperature', *J Mater Sci*, 44, 1873–1880.

Papakonstantinou C., Giancaspro J. and Balaguru P. (2008) 'Fire response and mechanical behavior of polysialate syntactic foams', *Composites: Part A*, 39, 75–84.

Peng G.F., Yang W.W., Zhao J., Liu Y.F., Bian S.H. and Zhao L.H. (2006) 'Explosive spalling and residual mechanical properties of fiber toughened high-performance concrete subjected to high temperatures', *Cem Concr Res*, 36, 723–727.

Phan L.T. (2008) 'Pore pressure and explosive spalling in concrete', *Mater Struct*, 41, 1623–1632.

Provis J. (2010) 'Fire resistance of geopolymer concretes', Final Project report – Grant FA23860814096, Available from: http://www.defensetechbriefs.com/component/content/article/8261 (accessed 1 December 2013).

Rickard W., Vickers L. and van Riessen A. (2013) 'Performance of fibre reinforced, low density metakaolin geopolymers under simulated fire conditions', *Appl Clay Sci*, 73, 71–77.

Sakkas K., Nomikos P., Sofianos A. and Panias D. (2013a) 'Slag based geopolymer for passive fire protection of tunnels', *Proceedings of the World Tunnel Congress 2013*, Geneva, 343–349.

Sakkas K., Nomikos P., Sofianos A. and Panias D. (2013b) 'Inorganic polymeric materials for passive fire protection of underground constructions', *J Fire Mater*, 37–140–150.

Sakkas K., Nomikos P., Sofianos A. and Panias D. (2013c) 'Utilisation of FeNi-slag for the production of inorganic polymeric materials for construction or for passive fire protection', *Waste Biomass Valor*, Published online: 17/11/2013 (doi: 10.1007/s12649-013-9278-z).

Temuujin J., Minjigmaa A., Rickard W., Lee M., Willimas I. and van Riessen A. (2010) 'Fly ash based geopolymer thin coatings on metal substrates and its thermal evaluation', *J Hazard Mater*, 180, 748–752.

Van Riessen A., Rickard W. and Sanjayan J. (2009) 'Thermal properties of geopolymers', in Provis J.L. and van Deventer J.S.J. (eds) *Geopolymers: Structure, Processing, Properties and Industrial Applications*, Cambridge: Woodhead Publishing, 315–342.

Varela B. and Privorotskaya N. (2005) 'The use of geopolymers as concrete coatings for fire protection', *Proceedings of the World Congress Geopolymer 2005*, 209–211.

Verein Deutscher Eisenhüttenleute (2008), *Slag Atlas*, 2nd edn, Dusseldorf: Verlag Stahleisen GmbH.

Zellei J. (2013) 'Recent European tendencies in the passive fire protection of steel constructions', in Jármai K. and Farkas J. (eds) *Design, Fabrication and Economy of Metal Structures*, New York: Springer, 421–427.

Zhao R. and Sanjayan J.G. (2011) 'Geopolymer and Portland cement concretes in simulated fire', *Mag Concrete Res*, 63, 163–173.

This page intentionally left blank

Methods to control efflorescence in alkali-activated cement-based materials

17

A. Allahverdi[1,2], *E. Najafi Kani*[3], *K. M. A. Hossain*[2], *M. Lachemi*[2]
[1]Iran University of Science and Technology, Tehran, Iran; [2]Ryerson University, Toronto, ON, Canada; [3]Semnan University, Semnan, Iran

17.1 An introduction to efflorescence

Efflorescence refers to the formation of a surface deposit which occurs in both natural and built environments. It is formed when soluble constituents are dissolved by water migrating through a porous material and then precipitating onto its surface by chemical reaction and/or evaporation of the salt solution. Efflorescence usually consists of salts that originate from the material itself or the surrounding environment. In cement-based materials, it therefore may be a symptom of attack by aggressive chemicals (such as sulphate) that affect the material performance.

This chapter, however, does not consider efflorescence caused by chemical attack. It must also be noted that efflorescence is distinct from the process of atmospheric carbonation. Carbonation usually results in pH reduction of the material followed by binder degradation. It may also include the deposition of carbonation reaction products in the bulk of the material, which may or may not be visible to the naked eye. Efflorescence, however, causes the formation of visible surface deposits, and may or may not be accompanied by further degradation of the binder.

17.1.1 Definition and effects

In chemistry, efflorescence means the growth of salt crystals on a surface caused by evaporation of salt-laden water. ACI 116R-90 defines efflorescence as 'a deposit of salts, usually white, formed on a surface, the substance having emerged in solution from within either concrete or masonry and subsequently been precipitated by evaporation'. The British Standard Glossary, BS6110: Subsection 1.3.7:1991 defines efflorescence as a 'crystalline deposit of soluble salts on a surface that results from the migration and evaporation of water' (Neville, 2002).

In porous construction and building materials, therefore, efflorescence is referred to as a deposit, usually white in color, that occasionally develops on the surface of the material. It is usually harmless and may only present a cosmetic problem, but in some cases excessive efflorescence can cause expansion in regions close to surfaces that may finally disrupt the material surface.

Handbook of Alkali-activated Cements, Mortars and Concretes. http://dx.doi.org/10.1533/9781782422884.3.463

In cement-based materials, efflorescence is a surface defect usually with no important structural consequences. It is a deposit of crystalline slats, usually loose, white and fluffy, that forms on or near the surface of the material. There exist different types of efflorescence forming by the same general mechanisms. The most relevant types of concern are efflorescence of calcium carbonate in Portland cement and efflorescence of sodium carbonate in alkali-activated or geopolymer binders.

The initial occurrence of the efflorescence is primarily considered as an aesthetic defect. However, if not controlled, continued efflorescence can become a functional defect affecting the integrity of the material. The defects begin from the surface regions and continue inward to the internal regions. The weakened surface regions of the material can be spalled over time due to increasing internal stresses caused by efflorescence crystallization pressure and/or through freeze/thaw cycling. In the case of coated concrete, the primary danger is potential bond failure between the coat and the underlying cementitious components. The crystallization of soluble salts, especially those that form in the adhesive–cladding interface, can exert disintegrating stresses that simply result in spalling or bond failure.

17.1.2 Types of efflorescence

There are two main types of efflorescence (Kresse, 1989; Bensted, 2000):

- primary efflorescence
- secondary efflorescence

Primary efflorescence typically occurs during the initial cure of the cement-based material. It is due to the hydration process during the setting of cement and involves the water used in the preparation of the material. When mixing water is being driven out as a result of hydration heat of cement, it brings the soluble constituents of the cement paste to the surface where mainly water evaporation results in the efflorescence formation. This type of efflorescence, which develops as a whitish bloom or color fade, is not deleterious to the performance of the material and is not usually considered significant. Primary efflorescence cannot be completely eradicated, but it is quite soft and the surface of the material can be simply cleaned by brushing off.

Secondary efflorescence is related largely to free water of the cementitous material and/or outside water like rain or groundwater and develops later, sometimes after months or even years from the start of the hydration reactions. All cement-based materials are susceptible to secondary efflorescence that appears as a uniform discoloration and/or as localized surface encrustations where water exits the material. The amount and the character of the deposits vary according to the type of cement and chemical admixtures used and also the atmospheric conditions.

The effects of secondary efflorescence are usually seen as color modifications, varying over the surface and changing with time. Iron oxide, dust, or dirt present in the surrounding environment can also take part in this color modification resulting in the formation of stained efflorescence. In rare cases, severe secondary efflorescence over long periods of time can put the structural integrity of the material at risk.

17.1.3 Formation mechanism and influencing factors

The mechanism for efflorescence formation can be described by discussing the chemical reactions and the physical processes involved under favorable conditions. Efflorescence is caused by a combination of circumstances including: presence of soluble constituents, presence of water to dissolve the soluble constituents, and a transporting force that moves the solution toward the surface such as gravity, capillary action, hydrostatic pressure, or evaporation.

In both Portland and alkali-activated cements, efflorescence is mainly caused by carbonates. In Portland cement-based materials, it mainly consists of calcium carbonate resulting from the reaction between calcium hydroxide of the hydrated cement paste and carbon dioxide from the atmosphere. As the Portland cement sets or hardens, free calcium hydroxide is formed which is soluble in water even if only to a slight extent. Consequently, it migrates to the concrete surface either after already being dissolved in the mixing water of the fresh concrete, or through the hardened concrete when exposed to the effects of rain or dew. Having reached the surface of the concrete, the calcium hydroxide reacts with carbon dioxide in the air to form water-insoluble calcium carbonate (Kresse, 1989; Bensted, 2000; Mohamed Sutan and Hamdan, 2013):

$$Ca(OH)_{2\ (dissolved)} + CO_{2\ (dissolved)} \rightarrow CaCO_{3\ (solid)} + H_2O_{\ (liquid)}$$

The reaction may happen in the pore solution of the concrete, but if evaporation rates are fast enough, calcium hydroxide precipitates on the concrete surface and subsequently reacts with atmospheric carbon dioxide when sufficient moisture becomes available on the surface (carbon dioxide reacts only if dissolved in water). If the surface of the concrete is not very moist and enough air has access to the surface, atmospheric carbon dioxide diffuses into the surface regions, dissolves in the pore solution and reacts with calcium hydroxide.

Formation of calcium carbonate in the pore solution can gradually block the capillary pores. In this case, the process of efflorescence formation can come to a halt. If the surface of the concrete is very moist or covered with a film of condensation, the calcium hydroxide spreads over the concrete surface and reacts with carbon dioxide to form a layer of calcium carbonate that is insoluble in water and makes stain removal difficult. Although the formation of calcium carbonate inside the capillary pores can effectively seal them and halt the formation of primary efflorescence, later when concrete is exposed to drying out, secondary efflorescence can start and continue. The formation and deposition of calcium carbonate on the concrete surface creates a concentration gradient in relation to the interior of the capillary system. This results in continuous diffusion of calcium hydroxide from deeper concrete layers to the surface pores as long as there exists a concentration gradient (Mohamed Sutan and Hamdan, 2013; Kresse, 1987, 1991).

The drying out of the concrete at the surface is therefore one of the main factors influencing efflorescence formation. Efflorescence usually results from a combination of factors rather than having a single cause. Of these factors, the most important ones are generally considered to be type of cement and admixtures, mix proportion and

water content, poor compaction of the concrete, insufficient curing, and atmospheric conditions that cause a rapid drying out of the concrete (Kresse, 1987, 1991; Deichnel, 1982; Neville, 2011).

In concrete materials usually cement is the principal source of the soluble salts. The amount of soluble salts therefore increases with increasing cement content of the concrete, the alkali content of cement and the cement fineness. In the case of Portland cement, incorporation of materials exhibiting pozzolanic properties reduces efflorescence formation by consuming part of the calcium hydroxide in pozzolanic hydration reactions. In addition, these materials produce a finer pore structure, which will reduce water permeability. Chemical admixtures may also influence efflorescence formation depending on their composition, their chemical interaction with soluble salts present in cement and how they are used.

Aggregates usually do not take part in efflorescence formation unless being contaminated with soluble salts (e.g., sea water slats and/or soluble sulphates). Water content of the fresh concrete influences the volume and the continuity of the pore structure and therefore determines the amount and the rate of both water and salt transfer. Improper concreting practices including insufficient mixing, inconsistent compaction and even inadequate mixing sequence result in a non-uniform pore structure, which may increase the risk of efflorescence formation or cause localized areas of efflorescence.

Curing humidity is another important factor. At low humidity, fresh concrete starts drying especially if exposed to sun and wind. When water evaporates from the concrete surfaces, it is easily replaced by transfer of mixing water from concrete internal regions. This in turn produces a layer of calcium carbonate efflorescence that temporarily blocks the surface pores of the concrete and prevents the subsequent ingress of water for continued curing. Such a concrete not only will not gain enough strength, but also will remain relatively permeable and prone to continued efflorescence formation.

In summary, a porous and permeable concrete is more prone to efflorescence formation, especially when subjected to repeated cycles of wetting and drying. In this case, there might be no distinction between primary and secondary efflorescence since the mechanism of their formation is virtually identical (Kresse, 1987).

It is not possible to completely eliminate efflorescence formation in cement-based materials. Long-term experiences on calcium-based hydrating products, however, resulted in the development of some rules of thumb to avoid or greatly reduce the potential for efflorescence formation. These include:

- minimizing free soluble salts from raw materials
- minimizing concrete permeability
- avoiding the exposure of concrete to uneven moisture conditions.

Use of quality materials in an optimized mix design is very important. Composite cements containing pozzolanic materials are usually better than plain cements. Soluble constituents in the cement including alkali, alkali sulphate and free lime must be kept at minimum possible levels. In addition, aggregates and mixing water contaminated with significant quantities of soluble salts should be avoided.

Permeability of the concrete must be minimized by using graded aggregates and sufficient amount of cement, keeping the water-to-cement ratio as low as possible and applying an effective compaction. Using too little cement leads to a low density and a high permeability. On the other hand, a high amount of cement requires higher water content that may again lead to higher permeability as a result of increased shrinkage cracks. In some cases, it may also be necessary to seal the external surface of the concrete by producing a dense impermeable surface finish. In any case, however, the concrete must be well cured at suitable and consistent conditions to ensure adequate hydration of cement.

Concrete's exposure to uneven moisture conditions, condensation and cycles of wetting-drying should be avoided both before and after curing. It is also necessary to maintain a uniform temperature inside the concrete.

After efflorescence formation, it is necessary firstly to identify its cause. When the cause is known, appropriate removal and prevention methods can be sought. If concrete is in contact with an external source of soluble salts, then it is necessary to identify the composition of the efflorescence, because it may indicate ingress of aggressive salts affecting concrete's durability.

Efflorescence may gradually be removed from exposed surfaces by acid rain or by normal abrasion, but if necessary chemical and/or mechanical methods are also available. Chemical removal is usually based on washing the concrete surface with dilute acid, but it may alter the color and the texture of the concrete surface. Mechanical methods include brushing the concrete surface with a stiff bristle brush or cleaning it with high pressure water jetting. Sand blasting may also be effective but it may alter the texture of the concrete surface.

In alkali-activated or geopolymer binders, efflorescence usually consists of sodium carbonate resulting from the reaction between excess sodium oxide remaining unreacted in the material and the carbon dioxide of the atmosphere:

$$2Na(OH)_{\text{(dissolved)}} + CO_{2\ \text{(dissolved)}} \rightarrow Na_2CO_{3\ \text{(solid)}} + H_2O_{\text{(liquid)}}$$

The mechanism and the influencing factors for alkali-activated or geopolymer binder are all the same. The type, nature and the characteristics of the efflorescence, however, are different.

17.2 Efflorescence formation in alkali-activated binders

In recent decades, researchers have investigated the possibility of utilizing a broad range of precursors as raw materials in the production of alkali-activated or geopolymer binders. Experiences in this field, however, confirmed that these binders are more prone to efflorescence formation and severe efflorescence may even put their structural integrity at risk. In spite of the importance of the problem, relatively less attention has been paid to the efflorescence phenomenon.

17.2.1 Alkali-activated binders and their susceptibility to efflorescence formation

These binders are produced by reactions between alkaline solutions usually alkali metal silicates or hydroxides and solid aluminosilicate precursors (Davidovits, 1991, 2008). Provis *et al*. (2005) presented a simplified model for the mechanism of alkali activation of a solid aluminosilicate precursor into a synthetic amorphous or nano-crystalline binder. Their model starts with dissolution of solid aluminosilicate source in alkali-activator and oligomerization of silicate and aluminate monomers. Depending on the processing conditions, the aluminosilicate oligomers produced could form either amorphous aluminosilicate gel upon polymerization and gelation or nano-crystalline zeolite phase upon nucleation and crystallization.

The main role of alkalis in the reaction processes involved is initially to generate a sufficiently high pH medium to start the breakdown of the covalent bonds (Si-O-Si and Al-O-Si) of the precursor, and then to charge-balance the growing aluminosilicate gel framework (Duxson *et al*., 2005a). Alkali concentration of the activator is one of the most important parameters strongly influencing the formation mechanisms and the properties of the binder, because it determines the extent of chemical reactions and the microstructure densification (Lloyd *et al*., 2009; Najafi Kani and Allahverdi, 2009a).

Alkali-activated binders formulated with sodium-based activators are more prone to efflorescence formation. It is also reported that formulations with higher Na_2O/Al_2O_3 ratios containing higher excess sodium oxide remaining unreacted in the material suffer from more severe efflorescence (Najafi Kani and Allahverdi, 2009a; Allahverdi *et al*., 2008; Škvára *et al*., 2009a; Temuujin and van Riessen, 2009; Pacheco-Torgal and Jalali, 2010). This is due to the relative mobility of the sodium cations within the aluminosilicate framework, particularly when the material is exposed to cycles of wetting/drying or moisture transfer. It is generally believed that in comparison to Portland cement, alkali-activated binders are more prone to efflorescence formation. This higher tendency toward efflorescence formation is due to the following characteristics, particularly if the binder is produced from relatively low reactive precursors and highly concentrated activators:

- open microstructure resulting in higher permeability (Škvára *et al*., 2009b)
- high alkali concentration in the pore solution (Lloyd *et al*., 2010)
- weak binding property of sodium cations in the aluminosilicate framework (Szklorzova and Bilek, 2008; Škvára *et al*., 2008; Bortnovsky *et al*., 2008).

17.2.2 A brief literature survey

In research work on the possibility of utilizing a pumice-type natural pozzolan as the aluminosilicate source material in the production of alkali-activated or geopolymer cement, Allahverdi *et al*. (2008) considered the extent of efflorescence formation as a soundness determining parameter. To evaluate the extent of efflorescence formation, they placed 28-day cured cubic paste specimens 2 cm^3 in size in 50 ml

water individually and kept them in open-air atmosphere at 25°C until the water was evaporated completely. Based on a qualitative comparison, they showed that the extent of efflorescence formation is a function of not only the Na_2O concentration of alkali activator, but also the silica modulus of alkali activator and the water-to-binder ratio. The effect of Na_2O concentration, however, was claimed to be more pronounced than the other two factors. Comparing the results of 28-day compressive strength measurements to those of efflorescence tests, they also concluded that a relatively high compressive strength attainable at relatively higher Na_2O concentration does not necessarily indicate soundness and durability.

In their works on material and structural characterization of alkali-activated low-calcium brown coal fly ash and the influence of the temperatures ranging from 20 to 1000°C on properties of aluminosilicate polymer or alkali-activated binder based on brown coal fly ash, Škvára *et al*. (2008, 2009b) elaborated the susceptibility of alkali-activated binders to exhibit efflorescence formation. Based on results obtained from ^{23}Na NMR MAS spectra, they claimed that alkali metals are rather bonded to Al in Si-O-Al chain structure in the form of $Na,K(H_2O)_n^+$ than as Na^+,K^+. The bond of alkali metals in the form of $Na,K(H_2O)_n^+$ complex is weaker than the direct bond of Na^+. This model of bonding of the Na atom helps to explain the ease in leaching of alkali metals out of the alkali-activated binders (regardless of whether prepared from fly ash or metakaolin) and efflorescence formation. They showed that the tendency for efflorescence formation declines substantially by firing the material at temperatures higher than 600°C. Such a high temperature treatment eliminates the H_2O content of the structure and results in the transformation of alkali metal bonds. They reported the presence of hydrates of the type $Na_2CO_3{\cdot}nH_2O$ and $Na_6(SO_4)(CO_3,SO_4){\cdot}nH_2O$ in typical efflorescence observed in their studies.

Temuujin *et al*. (2009) investigated the influence of CaO and $Ca(OH)_2$ on mechanical properties of geopolymer pastes developed from fly ash. Considering two different curing temperatures including 20°C (ambient temperature) and 70°C, they reported that all the samples cured at ambient temperatures exhibited efflorescence formation. They explained that at ambient temperatures the dissolution rates are low and result in the presence of residual excess alkaline solution in the material. Analytical studies performed on some fragments of efflorescence by SEM-EDS and XRD clarified the nature of the efflorescence as sodium phosphate hydrate ($Na_3PO_4{\cdot}12H_2O$) instead of sodium carbonate hydrate ($Na_3H(CO_3){\cdot}2H_2O$). They attributed the formation of sodium phosphate hydrate to the presence of 1.3 wt.% P_2O_5 in the fly ash and explained that a strong alkaline medium could readily dissolve the phosphate content of the material and enable it to recrystallize as sodium phosphate efflorescence. This observation, however, is contrary to Davidovits, suggestion (Davidovits, 2008) that phosphates are able to form geopolymer structures such as poly(sialate-siloxo)/phosphate or phospho-silioxonate geopolymer.

Allahverdi *et al*. (2010) investigated the influence of sodium oxide concentration on different physico-mechanical properties and efflorescence formation of alkali-activated blast furnace slag. They considered mix designs of the same silica modulus (M_s = 0.6) and different sodium oxide concentrations ranging from 1 to 6% by weight of slag. The tendency of the mix designs for efflorescence formation was

evaluated qualitatively in a similar way as explained in their earlier work (Škvára *et al*., 2009a). They reported that, based on observations, mixes with 1 and 2 wt.% sodium oxide concentration showed a relatively slight tendency for efflorescence formation, mixes containing 3 wt.% sodium oxide exhibited a relatively moderate tendency for efflorescence formation, and mixes containing higher concentrations of sodium oxide (4, 5 and 6 wt.%) displayed a relatively severe tendency for efflorescence formation.

Pacheco-Torgal and Jalali (2010) considered the tendency for efflorescence formation as a criterion of structural stability for alkali-activated binder based on calcined tungsten mine waste mud. While alkali-activated binder produced from plain mine waste mud calcined at different temperatures did not suffer from efflorescence formation, alkali-activated mortars based on mine waste mud calcined with sodium carbonate exhibiting relatively high early compressive strengths presented a high amount of efflorescence formation after water immersion. This indicates that even a relatively high early compressive strength does not always mean a stable structure formation.

Allahverdi *et al*. (2011) investigated the influence of blast furnace slag on basic engineering properties and efflorescence formation of natural pozzolan-based geopolymer cement. They studied different mix designs of the same silica modulus ($M_s = 0.6$) and different sodium oxide concentrations ranging from 4 to 6% by weight of binder. The water-to-dry binder ratio (w/c ratio) was adjusted at four different values of 0.26, 0.28, 0.30 and 0.32 and blast furnace slag was used at four different replacement levels of 0, 5, 15 and 25% by weight of binder. The obtained results showed that incorporation of the blast furnace slag did not provide any improvement in strength behavior of the studied natural pozzolan-based geopolymer cement, but an optimum amount of which was beneficial in reducing the efflorescence formation. They claimed that the geopolymer cement mix comprising 5 wt.% blast furnace slag and 8 wt.% Na_2O with a w/c ratio of 0.30 exhibited the highest 28-day compressive strength of 36 MPa with the least tendency for efflorescence formation. They measured the tendency of the mixes for efflorescence formation qualitatively as explained in their earlier work (Škvára *et al*., 2009a).

Najafi Kani *et al*. (2012) focused their work on controlling efflorescence formation in a geopolymer binder based on a pumice-type natural pozzolan. They showed that efflorescence formation can be reduced and controlled either by the addition of alumina-rich admixtures or by hydrothermal curing. Each of these techniques provides benefits to the binder structure by enhancing the binder structure formation process.

Škvára *et al*. (2012) reviewed the existing models for Na(K) bonds in (Na,K)-A-S-H gels and claimed that this bond still is an insufficiently resolved issue with significant consequences for efflorescence in alkali-activated or geopolymer cements. They also obtained interesting results in their studies supported by a series of long-term leaching experiments on alkali-activated fly ash and metakaolin in deionized water. Based on compressive strength measurements, studies by NMR MAS (^{29}Si, ^{27}Al, ^{23}Na) and SEM, and also modeling the leaching phenomenon, they compared the leached and unleached gels and showed that almost all the alkalies can be simply

leached out without affecting the gel skeletal structure and without any significant loss in strength.

They therefore concluded that the main role of alkalis in the process of alkali activation is to create a strong base environment for dissolution of glass phases from precursor materials and after gel formation, alkalis remain in the nanostructure of (N, K)-A-S-H gel weakly as unnecessary load-bearing remnants from activating solution. They used the Barbosa model (Barbosa *et al.*, 2000) to interpret the weak Na(K) bond in (N, K)-A-S-H gels. According to this model, the gel can be considered as randomly oriented Al, Si polymeric chains providing cavities of sufficient size to accommodate the charge-balancing hydrated Na(K) ions in the form of $Na(H_2O)_n^+$, $K(H_2O)_n^+$. The positively-charged alkali cations can be replaced with other cations present in the system. The most probable is H_3O^+, but $Al(OH)_2^+$ or $Al_n(OH)_m^{(3n-m)+}$ could also compensate the negative charge (Cloos *et al.*, 1969). The presence of other cations (Fe, Mn and Ca) in the precursors can also easily balance the negative charge on Al^{IV}.

17.3 Efflorescence formation control in alkali-activated binders

After reviewing an outline of the general features of efflorescence, its effects and consequences, types of efflorescence, formation mechanism and also a brief literature survey on efflorescence formation in alkali-activated binders, the remaining part of the chapter is devoted to efflorescence controlling methods in alkali-activated binders, which is a new field of research in developing alkali-activated or geopolymer binders.

17.3.1 Efflorescence control methods

Three different methods can be used to reduce efflorescence formation in an alkali-activated or geopolymer binder. Firstly adjustment of chemical formulation of the alkali activator used, secondly applying different curing conditions to increase the extent of reaction of the materials, and thirdly utilizing different admixtures to enhance microstructure densification. For achieving a sound and durable alkali-activated or geopolymer binder product, the geopolymer aluminosilicate source material should be considered at first and due to its composition, molecular structure, crystalline structure and phases, and its reactivity and solubility in alkaline activator, one or a combination of more efflorescence control methods should be applied.

Here, it is worth reviewing the effectiveness of the three efflorescence control methods applied on a geopolymer binder based on a pumice-type natural pozzolan (Najafi Kani *et al.*, 2012).

17.3.2 Adjustment of chemical formulation

To investigate the effect of alkali activator chemical composition adjustment on efflorescence control, geopolymer binder based on a pumice-type natural pozzolan has been selected. The natural pozzolan used in this work was of the pumice type obtained from mountains located in the south east of Iran. The pozzolan was ground in a closed circuit industrial mill to a Blaine specific surface area of 305 m^2/kg with mean particle size of 32 micron. The chemical composition determined in accordance with the standard procedures of ASTM C311 was SiO_2 = 61.57, Al_2O_3 = 18.00, CaO = 6.69, Fe_2O_3 = 4.93, MgO = 2.63, K_2O = 1.95, Na_2O = 1.65 with LOI = 2.15 and basicity factor [(CaO + MgO)/(SiO_2 + Al_2O_3)] of 0.84.

The natural pozzolan was also characterized for its crystalline phases. The crystalline mineral phases determined by X-ray diffractometry (Philips X'pert diffractometer, CuKα radiation, 2°/min, divergence and anti-scatter slits 1° each, receiving slit 0.01 mm) revealed the presence of the minerals anorthite (a feldspar mineral), cordierite and tremolite (amphiboles), and biotite (mica), as well as a small amount of quartz. Commercial sodium silicate solution (mass ratio SiO_2/Na_2O = 0.92 and SiO_2 content of 31.36 wt.%) and industrial-grade NaOH (99% purity) were used throughout all experiments (Najafi Kani *et al.*, 2012).

The chemical composition of the alkali activator studied is shown in Table 17.1. For qualitative evaluation based on visual observation, 28-day cured 2 cm cube paste specimens were individually immersed in 40 ml of distilled water and kept in open-air atmosphere at 25°C for complete evaporation of water. Quantitative evaluation was based on determining alkali salt leachability by adding 1.0000 ± 0.0001 g of ground hardened paste into 20 ml of distilled water in a covered container. After 24 h, the solution was centrifuged to remove solids and placed in an oven to evaporate the water, leaving only the leached soluble salts, which were then weighed. Studied mix compositions exhibiting relatively higher 28-day compressive strengths (shown in Table 17.1) were selected to determine the leachability of alkali, as a quantitative measure of the tendency toward efflorescence (Najafi Kani *et al.*, 2012).

The extent of efflorescence at the end of the qualitative (water evaporation) test shows that mixes G2 and G9 show a clearly lower efflorescence compared to the other mixes. Figure 17.1 shows the extent of efflorescence at the end of the qualitative (water evaporation) test in a selection of mixes (G2, G14, and G23). Sample G2 (Figure 17.1(a)) was selected because it showed the lowest extent of efflorescence. Sample G14 (Figure 17.1(b)) displayed the highest 28-day compressive strength and sample G23 (Figure 17.1(c)) showed the highest extent of efflorescence.

Figure 17.2 shows the extent of sodium leaching (as an indirect but quantitative measure of efflorescence) of the same samples, with comparison to their compressive strengths, and the data are fundamentally consistent with the qualitative extents of efflorescence. Geopolymer mixes with higher Na/Al molar ratios show a higher extent of alkali leaching, indicating a stronger tendency toward efflorescence (Najafi Kani *et al.*, 2012). The alkali leaching here appears to follow the known trend in pore solution chemistry as a function of alkali content, where higher Na/Al ratios give more alkaline pore solutions (Lloyd *et al.*, 2010); the effect of permeability (which

Table 17.1 Chemical composition and compressive strength of geopolymer mixes

Mix name	Chemical composition		28-day compressive strength (MPa)
	Activator SiO_2/Na_2O molar ratio	Total Na/Al molar ratio	
G1	0.30	0.61	20.0 ± 2.0
G2	0.45	0.61	27.5 ± 2.0
G3	0.60	0.61	25.0 ± 2.0
G4	0.75	0.61	17.5 ± 2.0
G5	0.90	0.61	13.7 ± 2.0
G6	0.30	0.77	15.0 ± 1.0
G7	0.45	0.77	22.5 ± 1.0
G8	0.60	0.77	26.2 ± 1.0
G9	0.75	0.77	32.5 ± 1.0
G10	0.90	0.77	20.0 ± 1.0
G11	0.30	0.92	12.5 ± 1.0
G12	0.45	0.92	17.5 ± 1.0
G13	0.60	0.92	35.0 ± 1.0
G14	0.75	0.92	45.0 ± 1.0
G15	0.90	0.92	32.5 ± 1.0
G16	0.30	1.08	17.5 ± 1.0
G17	0.45	1.08	25.0 ± 1.0
G18	0.60	1.08	37.5 ± 1.0
G19	0.75	1.08	27.5 ± 1.0
G20	0.90	1.08	22.5 ± 1.0
G21	0.30	1.23	15.0 ± 1.0
G22	0.45	1.23	22.5 ± 1.0
G23	0.60	1.23	33.7 ± 1.0
G24	0.75	1.23	28.7 ± 1.0
G25	0.90	1.23	25.0 ± 1.0

Source: Reprinted from Najafi Kani *et al.*, 2012, Copyright © 2012, with permission from Elsevier.

generally decreases with increasing extent of reaction, and thus would be expected to decrease at higher Na/Al contents) appears secondary when comparing different mix designs.

Comparing 28-day compressive strengths and alkali leachability reveals that the highest achievable compressive strength (attainable at an optimum Na/Al molar ratio of 0.92 for mix G14) does not necessarily result in soundness and durability. In fact, mixes with lower Na/Al molar ratios, i.e. G2 and G9, show a lower extent of alkali leaching and consequent efflorescence, showing that, in the absence of additives or heat curing, there appears to be a need to compromise between achieving the highest strength which is achieved with a denser microstructure, corresponding to a

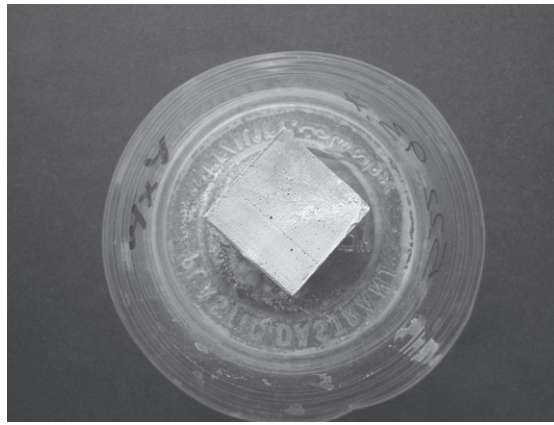

(a)

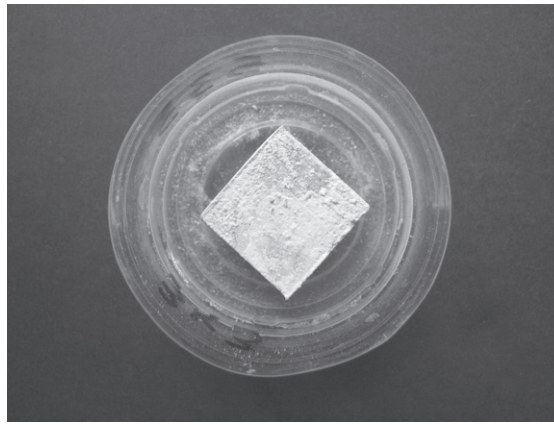

(b)

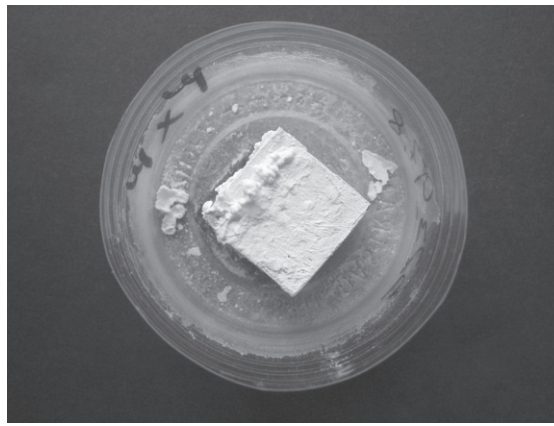

(c)

Figure 17.1 Photographs of specimens tested qualitatively for their efflorescence extent, at the end of the test period: (a) G2, (b) G14, and (c) G23.

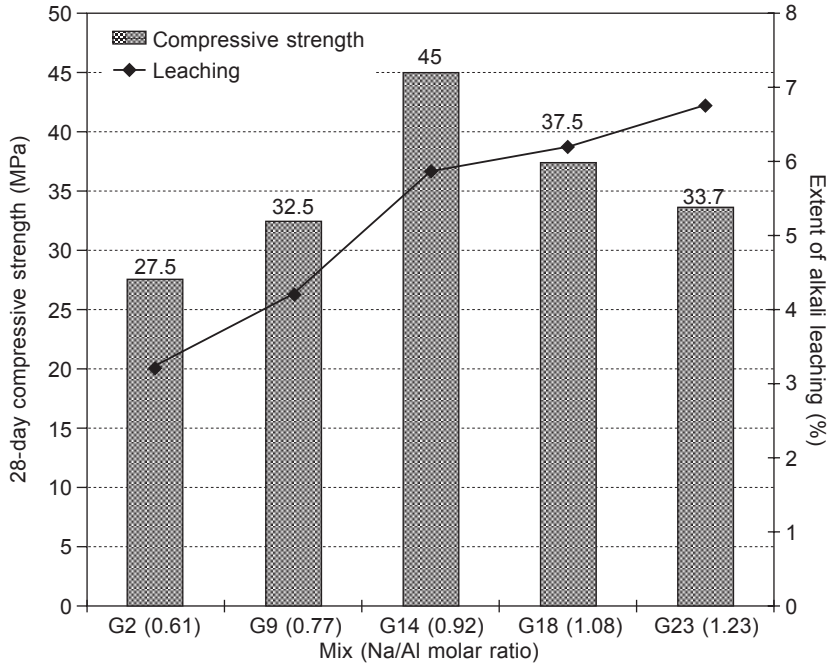

Figure 17.2 Comparison of the extent of alkali leaching and 28-day compressive strength for mixes G2, G9, G14, G18 and G23 (reprinted from Najafi Kani *et al.*, 2012, Copyright © 2012, with permission from Elsevier).

higher extent of reaction (Duxson *et al.*, 2005b), and controlling the concentration of mobile alkali in the pore solutions to prevent efflorescence.

17.3.3 Application of curing conditions

To investigate the effect of hydrothermal curing on efflorescence formation, specimens of mixes G2 and G9 were cured hydrothermally in a steam saturated atmosphere at temperatures of 45, 65, 85, 105, and 125°C for 20 h, after 7 days of precuring at ~95% relative humidity (RH) at 25°C (Najafi Kani *et al.*, 2012).

Figures 17.3 and 17.4 show the variations in the extent of alkali leachability and compressive strength as a function of hydrothermal curing temperature for mixes G2 and G9, respectively (Najafi Kani *et al.*, 2012). The baseline curing regime was a simple 28-day curing period in 95% RH at room temperature (RT); hydrothermal (HT) curing was applied at temperatures of 45, 65, 85, 105, and 125°C for 20 h, following 7 days of precuring at 25°C and 95% RH. As seen for both mixes, hydrothermal curing at temperatures higher than 65°C results in reduced efflorescence extent and increased compressive strength. Hydrothermal treatment at the lowest applied temperature of 45°C also increases the extent of efflorescence, but results in reduced compressive strength. The improvements brought about at temperatures higher than

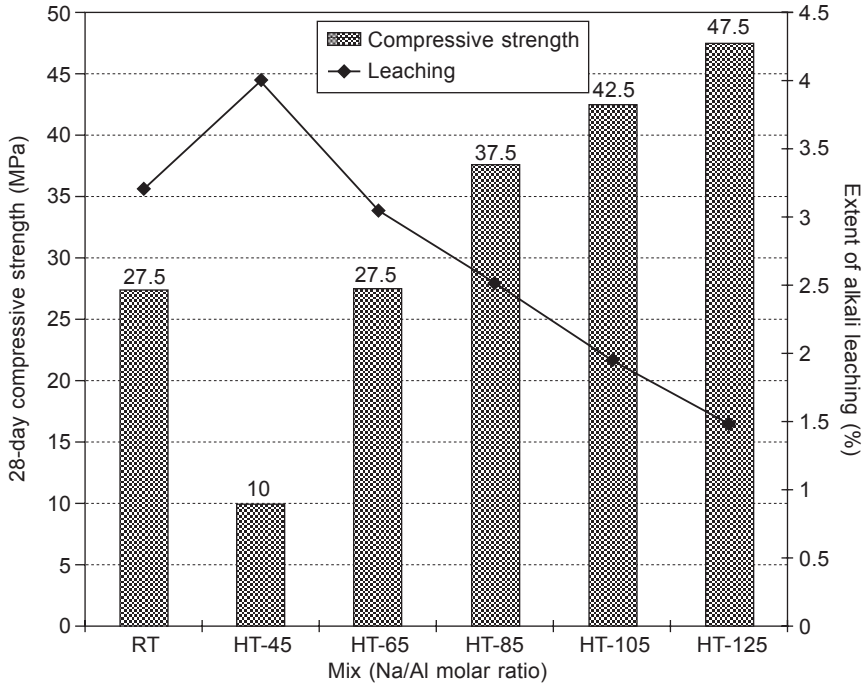

Figure 17.3 Effect of hydrothermal curing on efflorescence extent and compressive strength of mix G2 (reprinted from Najafi Kani *et al.*, 2012, Copyright © 2012, with permission from Elsevier).

65°C may be attributed to the higher extent of geopolymerization reactions which can be achieved at these temperatures in these systems (Najafi Kani and Allahverdi, 2009b).

17.3.4 Utilization of special additives

To investigate the application of special additives on controlling the efflorescence formation, 5 Al-rich mineral admixtures including metakaolin (Zigma International, India), ground granulated blast furnace slag (Isfahan Steel Complex, Iran), and the three different calcium aluminate cements of Secar 71 (Kerneos, France), Secar 80 (Kerneos, France) and Koracast (Iran Refractory Products, Iran) were incorporated into the dry binder mixes at replacement levels of 2, 4, 6, and 8 wt.%. The chemical compositions of the admixtures are given in Table 17.2 (Najafi Kani *et al.*, 2012).

Tables 17.3 and 17.4 show the variations in the extent of alkali leaching as a function of replacement percentage of natural pozzolan by different admixtures, for mixes G2 and G9, respectively. In the case of slag or metakaolin, a very minor decrease in the tendency towards efflorescence is observed, and only at the lowest replacement level of 2 wt.%. All three types of calcium aluminate cements, however,

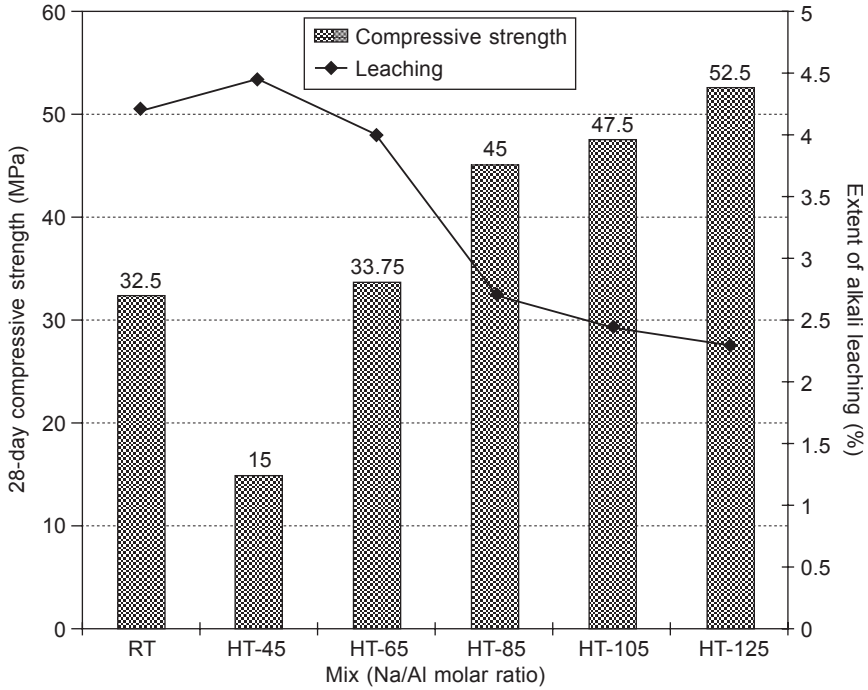

Figure 17.4 Effect of hydrothermal curing on efflorescence extent and compressive strength of mix G9 (reprinted from Najafi Kani *et al.*, 2012, Copyright © 2012, with permission from Elsevier).

Table 17.2 Chemical composition of the additives used (wt.% as oxides, as determined by X-ray fluorescence)

Component	SiO_2	Al_2O_3	Fe_2O_3	CaO	MgO	SO_3	K_2O	Na_2O
Secar 71	0.55	70.20	0.20	28.30	0.20	0.10	0.10	0.25
Secar 80	0.30	79.00	0.20	20.00	0.10	0.10	–	0.15
Koracast	–	94.00	0.10	5.40	–	–	–	–
Blast furnace slag	36.06	9.16	0.70	36.91	10.21	1.15	0.70	0.48
Metakaolin	56.50	38.30	0.50	0.15	0.18	–	0.23	0.35

Source: Reprinted from Najafi Kani *et al.*, 2012, Copyright © 2012, with permission from Elsevier.

provide a considerable positive effect in efflorescence reduction for both mixes G2 and G9. The optimum replacement levels for calcium aluminate cements (Secar 71, Secar 80, and Koracast) are 6, 8, and 6 wt.%, respectively (Najafi Kani *et al.*, 2012).

The reasons for the limited effects of addition of slag and metakaolin could be attributed to the differences between the form and the concentration of alumina in slag and metakaolin compared to high-alumina cements. In high-alumina cements,

Table 17.3 Effect of admixtures on alkali leaching (as a proxy for efflorescence extent) in mix G2

Weight % of admixture	Extent of efflorescence (%)				
	Secar 71	Secar 80	Koracast	Slag	Metakaolin
0	3.20	3.20	3.20	3.20	3.20
2	2.79	2.81	3.01	2.84	3.09
4	2.28	2.45	2.82	3.22	3.25
6	**1.25**	2.31	2.12	3.45	3.64
8	**1.26**	1.48	2.12	3.52	3.79

Source: Reprinted from Najafi Kani *et al.*, 2012, Copyright © 2012, with permission from Elsevier.

Table 17.4 Effect of admixtures on alkali leaching (as a proxy for efflorescence extent) in mix G9

Weight % of admixture	Extent of efflorescence (%)				
	Secar 71	Secar 80	Koracast	Slag	Metakaolin
0	4.20	4.20	4.20	4.20	4.20
2	3.52	3.66	3.72	3.30	3.41
4	3.02	3.02	3.56	4.08	4.14
6	**2.08**	2.95	3.25	4.53	4.65
8	**2.08**	2.18	3.25	5.89	5.99

Source: Reprinted from Najafi Kani *et al.*, 2012, Copyright © 2012, with permission from Elsevier.

alumina is present in the form of calcium aluminates, whereas in the case of slag and metakaolin it is in the form of aluminosilicates. This important difference not only results in different behavior in geopolymerization reactions, but will also lead to the formation of different reaction products. Also, the alumina supplied in highly reactive form by the high-alumina cements – which is more readily available compared to that supplied by slag or metakaolin due to the fact that it is not associated with Si – means that more alumina enters into the geopolymerization reactions. This strengthens the tetrahedral geopolymer gel network which is generated by alkali activation of the pozzolan (which has reasonably low Al availability), and also leads to binding of the alkalis into a charge-balancing role in the gel, hence resulting in a lower extent of alkali leaching and efflorescence (Najafi Kani *et al.*, 2012).

It is interesting to note that the greatest influence on alkali leaching was shown by Secar 71, with the lowest Al and highest Ca content of the three high-alumina cements tested; this again highlights that it is the availability of calcium, not simply its presence, which is the most important point here, as the Al is more readily available from the $CaAl_2O_4$ phase which dominates Secar 71 than from the $CaAl_4O_7$ and Al_2O_3 phases which are present in higher concentrations along with the $CaAl_2O_4$ in Secar 80 (Najafi Kani *et al.*, 2012).

Figure 17.5 shows the specimens of mix G2 tested qualitatively for their efflorescence

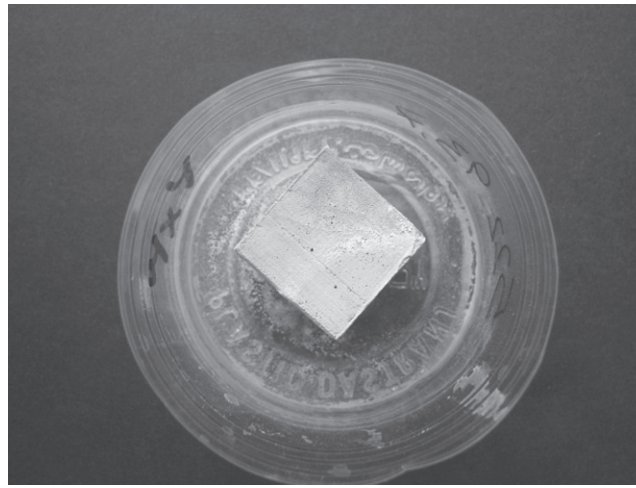

(a)

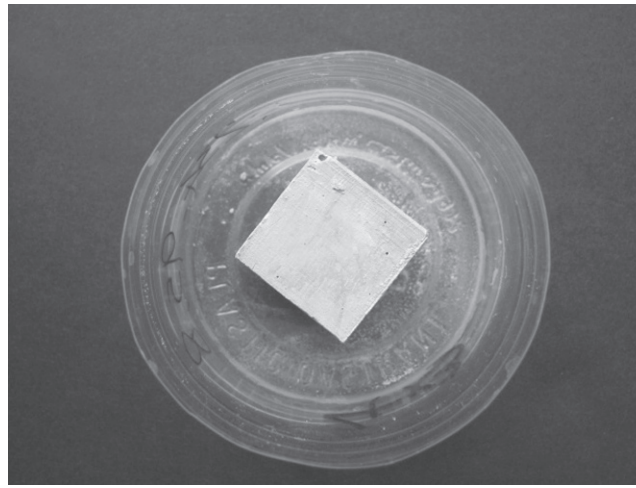

(b)

Figure 17.5 Specimens of mix G2 tested qualitatively for their efflorescence extent, without (a) and with (b) 6 wt.% Secar 71.

extent, without admixtures (Figure 17.5(a)) and with optimum percentages of the Secar 71 calcium aluminate cement (Figure 17.5(b)). The effectiveness of the admixture in reducing efflorescence is particularly visible for mix G2. Tests with the other calcium aluminate cements (Secar 80 and Koracast) also showed similar reductions in the formation of visible efflorescence deposits on the samples.

FTIR spectroscopy analysis of samples G2 and G9 with and without 6 wt.% Secar 71 (Table 17.5) shows that the addition of the high-alumina cement leads to an increase in the wavenumber of the Si-O-(Si,Al) asymmetric stretch peak, which is the

Table 17.5 Si-O-(Si,Al) asymmetric stretch peak positions in FTIR spectra of samples G2 and G9, with and without Secar 71

Peak positions (cm^{-1})	Secar 71 content	
	0%	6%
Mix G2	998	1007
Mix G9	996	1004

Source: Reprinted from Najafi Kani *et al*., 2012, Copyright © 2012, with permission from Elsevier.

strongest peak in the infrared spectrum of almost all geopolymeric materials, and is a key diagnostic region describing geopolymer gel network structures (Hajimohammadi *et al*., 2010; Rees *et al*., 2007).

An increase in the wavenumber of this peak could be due to one of two factors, either an increase in network connectivity or a decrease in the level of Al substitution (Hajimohammadi *et al*., 2010). Given that the addition of Secar 71 is supplying additional Al into the mixes, decreased Al substitution into the gels of the blended binders is unlikely, and thus the increase in FTIR peak positions is attributed to an increase in gel connectivity with the addition of the high-alumina cements. The higher compressive strengths observed after adding Secar 71 may also be attributed to the stronger bonding of the three-dimensional gel matrix with increased connectivity. Geopolymerization reactions in the presence of the high-alumina cement admixtures will result in the formation of a more crosslinked aluminosilicate gel, which in turn produces a dense, higher-strength molecular structure upon polycondensation. This is in accordance with previous work on systems based on natural pozzolan (Najafi Kani and Allahverdi, 2009b); similar trends were also observed for the samples cured hydrothermally (Najafi Kani and Allahverdi, 2009b).

The most important reason for the positive effects of the high-alumina cement Secar 71 in efflorescence reduction and increasing mechanical strength is the production of higher amounts of aluminosilicate gel, due to the higher amounts of alumina available to participate in the geopolymerization reactions. This is the most likely reason for higher compressive strength in cementing mixes containing alumina cements compared to mixes containing slag and metakaolin; the presence of additional Al leads to a higher degree of crosslinking in the binder gel (as seen in the FTIR data), and the binder structure develops higher strength in addition to the stronger binding of alkalis which reduces efflorescence. If the key effect was due to the calcium contained in the admixture, the slag would be expected to have a stronger effect than Secar 71 due to its higher Ca content (Najafi Kani *et al*., 2012).

As a conclusion, efflorescence is sometimes an issue in geopolymeric binders, but can be reduced either by precise selection of chemical composition, the addition of alumina-rich admixtures and or by hydrothermal curing. Each of these techniques provides benefits to the binder structure by enhancing the binder structure formation

process. Hydrothermal curing at temperatures of 65°C or higher also provides a significant effect in efflorescence reduction, as well as slight strength improvements. The addition of high-alumina cements is particularly beneficial; an optimum dosage of calcium aluminate cement, especially Secar 71, as an admixture is more effective than hydrothermal curing in reducing the extent of efflorescence in the natural pozzolan-based geopolymer binders studied. The additional alumina supplied by the high-alumina cement admixtures leads to an increased extent of crosslinking in the geopolymer binder, reduces the mobility of alkalis (which is the key cause of efflorescence in these materials), and also generates a hardened geopolymer binder product with markedly improved mechanical properties compared to the systems with no admixtures (Najafi Kani *et al.*, 2012).

17.4 Conclusions

Alkali-activated or geopolymer binders are prone to efflorescence formation that may even put their soundness at risk. Attention therefore must be paid to efflorescence formation potential when developing alkali-activated or geopolymer binders. Published data confirm that the highest achievable compressive strength does not necessarily result in soundness and it is necessary to compromise between achieving the highest strength and controlling the concentration of mobile alkali in the pore solutions to prevent efflorescence. In addition to the careful adjustment of the chemical composition, hydrothermal curing and utilization of Al-rich mineral admixtures such as calcium aluminate cements provide positive effects in reduction of efflorescence. Suitable Al-rich mineral admixtures represent the greatest effect in controlling efflorescence. This effect can be attributed to their dissolution extent in alkaline media that releases relatively high amounts of alumina for the aluminosilicate geopolymer gel formation. This in turn leads to an increased extent of crosslinking in the geopolymer binder, reduces the mobility of alkalis, which is the key cause of efflorescence in these materials, and also improves the mechanical properties of the material (Najafi Kani *et al.*, 2012).

References

Allahverdi, A., Mehrpor, K. and Najafi Kani, E. (2008) 'Investigating the possibility of utilizing pumice-type natural pozzolan in production of geopolymer cement', *Ceram Silik*, 52(1), 16–23.

Allahverdi, A., Shaverdi, B. and Najafi Kani, E. (2010) 'Influence of sodium oxide on properties of fresh and hardened paste of alkali-activated blast-furnace slag', *Int J Civ Eng*, 8(4), 304–314.

Allahverdi, A., Najafi Kani, E. and Yazdanipour, M. (2011) 'Effects of blast furnace slag on natural pozzolan-based geopolymer cement', *Ceram Silik*, 55 (1), 68–78.

Barbosa, V. F. F., MacKenzie, K. J. D. and Thaumaturgo, C. (2000) 'Synthesis and

characterisation of materials based on inorganic polymers of alumina and silica: sodium polysialate polymers', *Int J Inorg Mater*, 2, 309–317.

Bensted, J. (2000) 'Efflorescence – prevention is better than cure', *Concr*, 34, 40–41.

Bortnovsky, O., Dědeček, J., Tvarůžkova, Z., Sobalik, Z. and Šubrt, J. (2008) 'Metal ions as probes for characterization of geopolymer materials', *J Am Ceram Soc*, 1, 3052–3057.

Cloos, P., Léonard, A.J., Moreau, J.P., Herbillon, A. and Fripiat, J.J. (1969) 'Structural organization in amorphous silico-aluminas', *Clays Clay Miner*, 17, 279–287.

Davidovits, J. (1991) 'Geopolymers – inorganic polymeric new materials', *J Therm Anal*, 37(8), 1633–1656.

Davidovits, J. (2008) *Geopolymer Chemistry and Applications*, Institute Geopolymere, Saint-Quentin, France.

Deichnel, T. (1982) 'Efflorescence-origins, causes, counter-measures', *Betonwerk+Fertigteil-Technik*, 48, 590–597.

Duxson, P., Lukey, G. C., Separovic, F. and van Deventer, J. S. J. (2005a) 'Effects of alkali cations on aluminum incorporation in geopolymeric gels', *Ind Eng Chem Res*, 44(40), 832–839.

Duxson, P., Provis, J. L., Lukey, G. C., Mallicoat, S. W., Kriven, W. M. and van Deventer, J. S. J. (2005b) 'Understanding the relationship between geopolymer composition, microstructure and mechanical properties', *Colloid Surf A: Physicochem Eng Aspects*, 269(1–3), 47–58.

Hajimohammadi, A., Provis, J. L. and van Deventer, J. S. J. (2010) 'The effect of alumina release rate on the mechanism of geopolymer gel formation', *Chem Mater*, 22, 5199–5208.

Kresse, P. (1987) 'Efflorescence-mechanism of occurrence and possibilities of prevention', *Betonwerk+Fertigteil-Technik*, 53, 160–168.

Kresse, P. (1989) 'Coloured concrete and its enemy: efflorescence', *Chem Ind*, 4, 93–95.

Kresse, P. (1991) 'Efflorescence and its prevention', *Betonwerk+Fertigteil-Technik*, 57, 84–88.

Lloyd, R.R., Provis, J. L., Smeaton, K. J. and van Deventer, J. S. J. (2009) 'Spatial distribution of pores in fly ash-based inorganic polymer gels visualised by Wood's metal intrusion', *Micropor Mesopor Mater*, 126(1–2), 32–39.

Lloyd, R. R., Provis, J. L. and van Deventer, J. S. J. (2010) 'Pore solution composition and alkali diffusion in inorganic polymer cement', *Cem Concr Res*, 40(9), 1386–1392.

Mohamed Sutan, N. and Hamdan, S. (2013) 'Efflorescence phenomenon on concrete structures', *Adv Mater Res*, 626, 747–750.

Najafi Kani, E. and Allahverdi, A. (2009a) 'Effects of chemical composition on basic engineering properties of inorganic polymeric binders based on natural pozzolan', *Ceram Silik*, 53(3), 195–204.

Najafi Kani, E. and Allahverdi, A. (2009b) 'Effects of curing time and temperature on strength development of inorganic polymeric binders based on natural pozzolan', *J Mater Sci*, 44(12), 3088–3097.

Najafi Kani, E., Allahverdi, A. and Provis, J. L. (2012) 'Efflorescence control in geopolymer binders based on natural pozzolan', *Cem Concr Comp*, 34(1), 25–33.

Neville, A. (2002) 'Efflorescence – surface blemish or internal problem? Part 1: The knowledge', *Concr Int*, 24(8), 86–90.

Neville, A. M. (2011) *Properties of Concrete*, 5th edn, Harlow, Prentice-Hall.

Pacheco-Torgal, F. and Jalali, S. (2010) 'Influence of sodium carbonate addition on the thermal reactivity of tungsten mine waste mud based binders', *Construct Build Mater*, 24(1), 56–60.

Provis, J. L., Duxson, P., van Deventer, J. S. J. and Lukey, G. C. (2005) 'The role of

mathematical modeling and gel chemistry in advancing geopolymer technology', *Chem Eng Res Des*, 83, 853–860.

Rees, C. A., Provis, J. L. and van Deventer, J. S. J. (2007) 'Attenuated total reflectance Fourier transform infrared analysis of fly ash geopolymer gel aging', *Langmuir*, 23, 8170–8179.

Škvára, F., Pavlasova, S., Kopecký, L., Myškova, L. and Alberovska, L. (2008) 'High temperature properties of fly ash-based geopolymers', *3rd International Symposium on Non-Traditional Cement and Concrete*, Czech Republic, Brno, 741–750.

Škvára, F., Kopecký, L., Myškova, L., Šmilauer, V., Alberovska, L. and Vinšova, L. (2009a) 'Aluminosilicate polymers – influence of elevated temperatures, efflorescence', *Ceram Silik*, 53(4), 276–82.

Škvára, F., Kopecký, L., Šmilauer, V. and Bittnar, Z. (2009b) 'Material and structural characterization of alkali activated low-calcium brown coal fly ash', *J Hazard Mater*, 168, 711–720.

Škvára, F., Šmilauer, V., Hlaváček, P., Kopecký, L. and Ćilová Z. (2012) 'A weak alkali bond in (N,K)-A-S-H gels: evidence from leaching and modeling', *Ceram Silik*, 56(4), 374–382.

Szklorzova, H. and Bilek, V. (2008) 'Influence of alkali ions in the activator on the performance of alkali-activated mortars', *3rd International Symposium on Non-Traditional Cement and Concrete*, Czech Republic, Brno, 777–784.

Temuujin, J. and van Riessen, A. (2009) 'Effect of fly ash preliminary calcination on the properties of geopolymer', *J Hazard Mater*, 164(2–3), 634–639.

Temuujin, J., van Riessen, A. and Williams, R. (2009) 'Influence of calcium compounds on the mechanical properties of fly ash geopolymer pastes', *J Hazard Mater*, 167, 82–88.

This page intentionally left blank

Part Four

Applications of alkali-activated cement-based concrete binders

This page intentionally left blank

Reuse of aluminosilicate industrial waste materials in the production of alkali-activated concrete binders

18

J. Payá[1], *J. Monzó*[1], *M. V. Borrachero*[1], *M. M. Tashima*[2]
[1]Universitat Politècnica de València, València, Spain; [2]UNESP – Univ. Estadual Paulista, Ilha Solteira, Brazil

18.1 Introduction

In today's world, one of the major issues facing communities is the management of resources (water, soil, air, energy) and the environmental consequences associated with the increase of the waste generated (solid, liquid and gaseous residues).

It is generally accepted that the following solutions must be enhanced: a reduction in the consumption of non-renewable raw materials (to Reduce), a recycling of wastes in similar applications from which they are generated (to Recycle), a recovery of wastes through their reuse in other applications (to Reuse), or a recovery of various/selected components, energy or elements that are part of the waste (to Recover). These four actions (the four Rs, R^4) could deliver important enhancements to the environment and, consequently, to society. However, we should not forget the fifth R, which is an activity that will enhance the environmental sustainability of society: research (to Research). Using the R^5 function (the five Rs), all processes and activities from environmental, economic, technological and social points of view can be optimized (see Figure 18.1).

Many interesting studies on reusing wastes produced by different human activities (urban, agricultural and industrial) have been carried out, as one of the major challenges is related to the development of alternative cements for replacing, totally or partially, the synthetic material most widely produced at present: ordinary Portland cement, OPC (Flatt *et al*., 2012). In this respect, alkali-activated materials (AAMs) have recently become one of the most promising binders for the future (Shi *et al*., 2011; Pacheco-Torgal *et al*., 2008a, 2008b; Majidi, 2009; Komnitsas and Zaharaki, 2007; Van Deventer *et al*., 2010).

Industrial by-products such as fly ash (FA, derived from coal combustion power plants) and ground granulated blast furnace slag (BFS, derived from the iron-making industry) have been used as precursors in many cases for preparing AAMs. Synthetic precursors produced from clays (metakaolin, MK) are also used, although this

Handbook of Alkali-activated Cements, Mortars and Concretes. http://dx.doi.org/10.1533/9781782422884.4.487

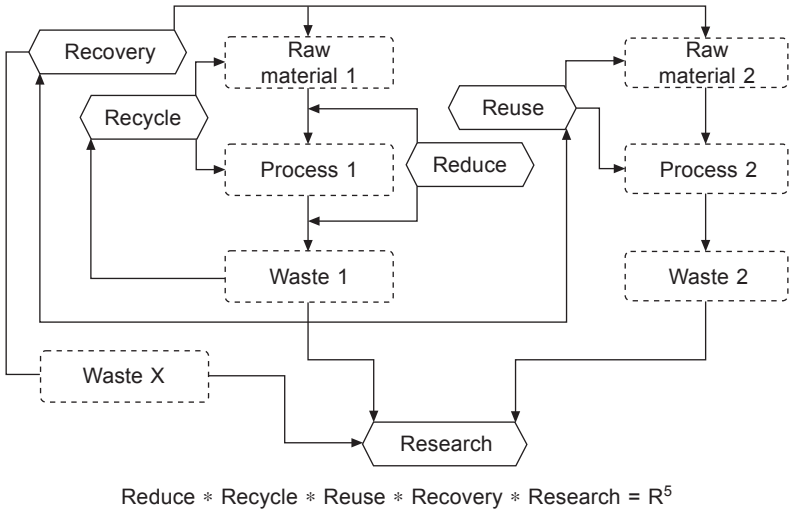

Figure 18.1 The five attitudes (R^5) for sustainability in the modern society.

type of precursor is not a waste. A wide range of studies on the above-mentioned precursors have been reported (Shi *et al*., 2006; Provis and van Deventer, 2009) and many aspects of the geopolymeric reaction (proportioning, mixing, curing) and the performance of pastes, mortars and concrete (mechanical properties, microstructure, durability) have been described and analyzed.

On the one hand, many diverse wastes are currently produced, sometimes having similar characteristics to precursors (BFS, FA, MK) and sometimes not. Therefore, it is important to take into account the fact that these 'new' precursors are generated in huge amounts. On the other hand, the production of FA could decay in the future due to the use of alternative energy sources with lower CO_2 emissions, and BFS availability being highly dependent on the exploitation of iron ores (steel production is closely related to the recycling of scrap). These facts could limit the use of these traditional precursors, and thus, the study and development of new precursors for AAMs is necessary in order to propose this type of binders as cements for the future.

Wastes can be grouped according to type of source:

- energy production
- metallurgy
- mining
- ceramics/glass industries
- construction and demolition of buildings and infrastructures
- chemical and petrochemical industries
- agro-industries.

In this chapter, recent developments in the use of these wastes or combination of them with traditional precursors are summarized.

18.2 Bottom ashes

Bottom ashes are granular waste materials usually generated from combustion of coal or other fuels, which are collected in the bottom hopper of the burning furnace. Power generation from coal combustion is the main energy source world wide. During this process, fly ash and coal bottom ash (CBA) are generated as residue. These wastes present similar chemical composition; however, the main differences are the shape and the size of the particles. Several studies have been performed regarding the use of CBA as a supplementary cementitious material (Cheriaf *et al.*, 1999). The use of CBA as an aluminosilicate source material in the production of alkali-activated binders has also been reported (Topçu and Toprak, 2011; Chindaprasirt *et al.*, 2009, 2013; Chen *et al.*, 2012). Nevertheless, other waste materials and fuels can also generate bottom ashes (Chen *et al.*, 2009; Yamaguchi and Ikeda, 2010; Yang *et al.*, 2013; Yamaguchi *et al.*, 2013; Lancellotti *et al.*, 2013). In order to facilitate the discussion, this topic is presented in three sections according to the combustion process.

18.2.1 Coal thermal power plant

The use of coal bottom ash from thermal power plant as alkali-activated binders is reported in some studies (Sathonsaowaphak *et al.*, 2009; Boonserm *et al.*, 2012; Sata *et al.*, 2012; Chindaprasirt *et al.*, 2009). In general terms, the flowability and the compressive strength of the geopolymer can be improved with an increase of the CBA fineness (Sathonsaowaphak *et al.*, 2009).

Chindaprasirt *et al.* (2009) performed a comparative study on the characteristics of coal fly ash and CBA geopolymers. The results showed that fly ash is more reactive than bottom ash and promotes a higher degree of geopolymerization.

Chotetanorm *et al.* (2013) compared three degrees of fineness for CBA with high-calcium content. The finely ground CBA mortar yielded 40–54.5 MPa of compressive strength at 28 days of curing (room temperature) and with an initial 48-hour thermal curing at 75ºC. In the same study, authors concluded that the threshold values of intruded volume, pore sizes and rate of sorptivity of geopolymeric mortars were directly related to CBA fineness and water/CBA ratio.

In another study, Sata *et al.* (2012) showed that CBA geopolymeric mortars were less susceptible to the attack of 5% sodium sulfate solutions and sulfuric acid solution when compared to the Portland cement mortar, due to the more stable crosslinked aluminosilicate polymer structure as compared to the calcium silicate hydrate structure formed in Portland cement hydration.

18.2.2 Circulating fluidized bed combustion coal ashes

The first study that described the use of fluidized bed combustion bottom ash was performed by Slavik *et al.* (2008). According to the authors, the compressive strength after 90 days was about 50 MPa and specimens showed an increase in the compressive

strength after wet-dry tests, probably due to the increment on the temperature that accelerates the geopolymerization reaction.

According to Chindaprasirt and Rattanasak (2010), blended fluidized bed combustion fly ash and bottom ash have the potential to be used as a source material for making geopolymer. For these systems, geopolymeric mortars with 34–44 MPa in compression can be obtained (see Figure 18.2), depending on the fineness of FBC ash; C class (coarse size), M class (medium size) and F class (Fine size).

Xu *et al.* (2010) demonstrated that mechanical properties of CBA geopolymers strongly depend upon the chemical compositions of the initial reacting systems, yielding 52.9 MPa, in compressive strength, for the optimal mix. In the same study, the authors observed by SEM images that geopolymers exposed to 1050ºC presented traces of formation of albite, which was confirmed by the XRD patterns. It is important to highlight that specimens exposed up to 800ºC did not present any microstructural change.

Topçu and Toprak (2011) also demonstrated that geopolymers with CBA can be manufactured even at room temperature and concluded that curing conditions produced a strong effect on the compressive strength development of geopolymeric binders based on CBA.

18.2.3 Incineration of municipal solid waste

Incineration is a burning process to reduce the volume and weight of wastes and to recover energy. From this process, a granular ash, also named bottom ash,

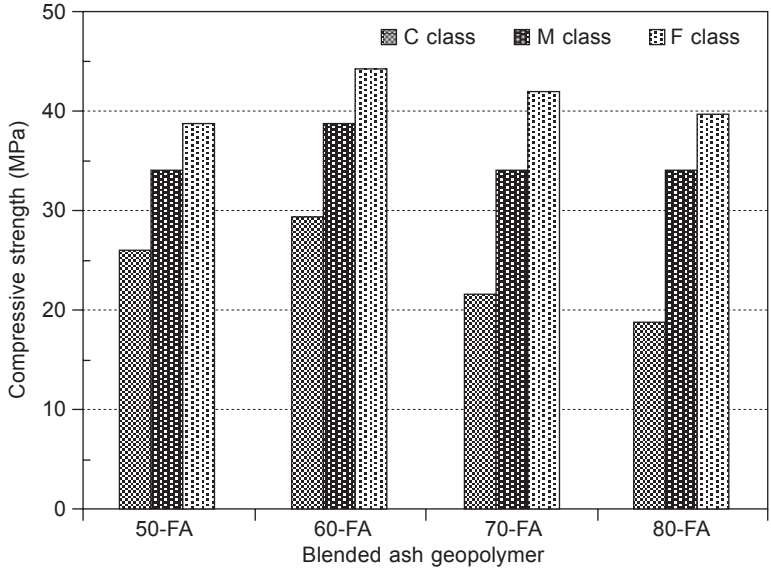

Figure 18.2 Compressive strength of different FCB–fly ash blended geopolymer mortars at age of 7 days (reprinted from Chindaprasirt and Rattanasak, 2010, Copyright © 2010, with permission from Elsevier).

is generated with variable chemical composition, depending on the incinerated residue.

Lancellotti *et al*. (2013) studied the ashes generated from incineration of municipal solid waste (MSW). These bottom ashes (MSWBA) were mixed with metakaolin (MK) in the production of geopolymers with up to 80 wt.% of bottom ash. After 15 days of curing, geopolymeric samples were immersed in water for 48 h to assess the chemical stability of samples; none of the compositions changed their aspect except geopolymer containing 80 wt.% of MSWBA. Similarly, FTIR analysis, XRD studies and SEM/EDS images demonstrated that MSWBA is a suitable source material for producing metakaolin blended geopolymers with high percentages of MSWBA (50–70 wt.%).

Similarly, Yamaguchi *et al*. (2013) used ashes from incinerated urban wastes for geopolymer production. The starting ash presented high CaO, Al_2O_3 and SiO_2 contents and amorphous structure. Geopolymeric pastes yielded up to 16 MPa in flexural strength when cured at 80ºC with 100% RH.

Another incinerated waste is reservoir sludge that was calcined at different temperatures 500–900ºC for application in geopolymers (Chen *et al*., 2009). The authors obtained a maximum compressive strength of 56.2 MPa at 28 days of curing for reservoir sludge calcined at 850ºC. Yang *et al*. (2013) produced foamed reservoir sludge geopolymers with water absorption up to 90% and more than 80% of the pores were less than 0.3 mm in diameter. The use of sewage sludge ash in alkali-activated binders was also reported by Yamaguchi and Ikeda (2010). Geopolymers based on sewage sludge/fly ash yielded flexural strength in the range of 4–5.5 MPa and presented an amorphous structure characteristic of geopolymeric gels.

18.3 Slags (other than blast furnace slags (BFS)) and other wastes from metallurgy

The metallurgic industry generates different types of wastes, the main ones being those corresponding to slags produced in the metal extraction processes or in the refinement of metals. Selected types of slags from different thermo-chemical processes are presented, and their applications in the formulation of alkali-activated binders are discussed.

Pontikes *et al*. (2013) studied slags from non-ferrous metallurgy. These slags are Fe rich, with Si as a minor constituent, and with low levels of Al. Slag is produced in a pilot-plant facility through a plasma reactor. The slag was cooled in four different ways, namely ‘slag pot’ (SP), ‘layer’ (L), ‘layer + water’ (LW) and ‘water quenching’ (WQ). The effect of cooling rates on slag microstructure for a specific Al/Fe ratio has been studied. Results showed that high cooling rates led to a predominantly amorphous material. For lower cooling rates the content of amorphous phase varied from 52 wt.% to 12 wt.%. Spinel was the primary phase precipitating, whereas, for the lowest cooling rate investigated, pyroxenes formed as well. The activating solution was composed of 50 wt.% 10 M NaOH and 50 wt.% Na–silicate

solution. Regarding compressive strength, samples prepared from SP slag achieved < 5 MPa at 28 days, which is not sufficient to produce a material with interesting engineering properties. Samples from L slag had compressive strength in the range of 10–15 MPa at 28 days but after 90 days higher values were recorded. Finally, samples from WQ slags produced materials with compressive strength exceeding 60 MPa after 28 days.

Zinc slag generated during the imperial smelting process (ISP) all over the world is simply dumped. Some occasional research attempts, seen in the literature, are limited to its use as a replacement for aggregates in construction applications. Alex *et al*. (2013) studied the effect of milling environment (air and CO_2, see Figure 18.3) on the reactivity of milled zinc slag and on properties of geopolymers synthesized using the slag milled in different atmospheres. Both air and CO_2-milled slag showed good geopolymerization behavior leading to high compressive strength of the geopolymeric products. The initial strength (1 day) values were significant: around 20 and 10 MPa for CO_2-milled and air-milled slag, respectively. The maximum compressive strength after 28 days in the case of air-milled slag was 73 MPa while that of CO_2-milled slag was 88 MPa.

A similar study on the influence of the milling environment on the activation of Cu–Ni slag and the structure and properties of geopolymers synthesized using the activated slag was carried out by Kalinkin *et al*. (2012). Compressive strengths for the geopolymeric samples prepared using slag mechanically activated in air were 50.5, 74.6, 81.1, 82.8, and 89.5 MPa, after curing for 1, 7, 28, 150, and 360 days, respectively. The corresponding values for those geopolymeric samples prepared using slag mechanically activated in CO_2 were 53.8, 77.4, 94.4, 106.0, and 119.0

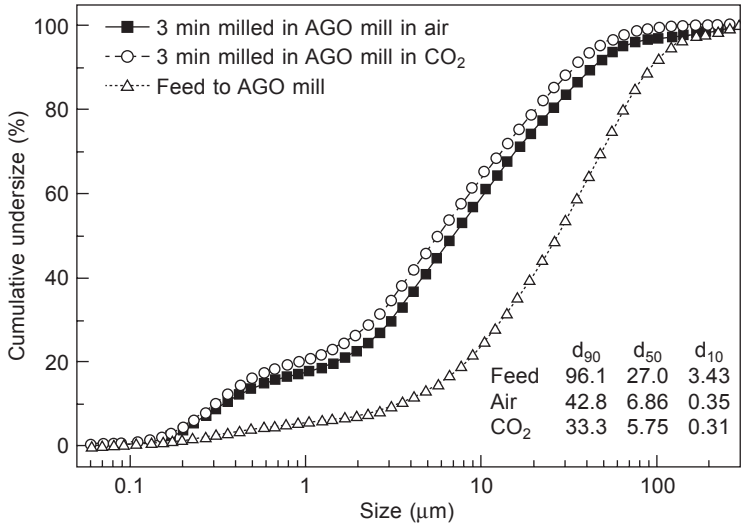

Figure 18.3 Particle size distributions of unground zinc slag and samples milled in an AGO mill for 3 min in air and CO_2 medium (reprinted from Alex *et al*., 2013, Copyright © 2013, with permission from Elsevier).

MPa, respectively. Results showed that mechanical activation of the slag in carbon dioxide gas (P = 105 Pa) in a planetary mill led to an increase of the compressive strength of the geopolymer when compared with the mechanical activation in air.

The feasibility of geopolymer synthesis formed from low calcium electric arc ferronickel slags has been investigated by Komnitsas *et al*. (2007), in order to elucidate the main mechanism involved. The durability of specimens is almost unaffected when immersed in distilled and seawater or subjected to freeze-thawing cycles over a period of 4 months. On the contrary, noticeable loss of strength is observed when geopolymers are immersed in 1 N HCl or simulated acid rain solutions. In a different paper, Komnitsas *et al*. (2009) studied the effect of synthesis parameters on the compressive strength of low-calcium ferronickel slag inorganic geopolymers and concluded that the main factors were the mineralogy of raw materials, types of additives used, the initial water content, the alkali concentration and type of activator, pre-curing period as well as heating temperature and heating and aging period. Geopolymers based on ferronickel slag have also been studied by Maragkos *et al*. (2009). The results showed that the ferronickel slag is an excellent raw material for the production of inorganic geopolymers. Those produced under optimum synthesis conditions presented high compressive strength (118 MPa), as well as extremely low water absorption (0.7–0.8%).

Geopolymerization of the red mud generated in primary aluminum production and the slag generated in ferronickel production was studied by Giannopoulou *et al*. (2009). The inorganic polymeric materials produced by geopolymerization of the red mud developed compressive strength values up to 21 MPa and presented water absorption lower than 3%, while the geopolymerization of the ferronickel slag resulted in materials with compressive strength higher than 110 MPa and extremely low water absorption (< 1%).

Geopolymer made of lead slag produced under laboratory conditions was synthesized by Onisei *et al*. (2012). For the inorganic polymer with lead slag, the binding phase contains, on average, more than 50 wt.% PbO, with also relatively high levels of Fe, Si and Zn compounds; the average Si/Al ratio was approximately 33. Despite crack formation, the mechanical properties were acceptable. To overcome the Al deficiency, inorganic polymers of fly ash/lead slag mixtures were developed. Regarding the properties of fly ash and lead slag inorganic polymers, compressive strength is higher than 35 MPa in all cases and water absorption diminishes as the lead slag content increases.

18.4 Mining wastes

Mining is probably one of the most important global activities in the generation of high volume wastes. This type of wastes, called mine tailings, is usually inert from chemical and environmental points of view. In some specific cases, such as copper and tungsten mine tailings, due to their chemical and mineralogical composition, they are appropriate for using in alkali-activated binders.

Ahmari and Zhang have focused their research on copper mine tailing (MT) geopolymeric bricks. The procedure for producing the bricks simply includes mixing the tailings with an alkaline solution, forming the brick by compressing the mixture and curing at a slightly elevated temperature. Bricks met the ASTM requirements (Ahmari and Zhang, 2012). Durability and leaching behavior of geopolymeric bricks were studied. The results indicated that although there was a substantial strength loss after immersion in pH = 4 and 7 solutions, the water absorption and weight loss were not significant. The leaching analyses showed that the heavy metals are effectively immobilized in the MT-based geopolymeric bricks, which was attributed to the incorporation of heavy metals in the geopolymeric network (Ahmari and Zhang, 2013a). The enhancement of copper mine tailings-based geopolymeric bricks with cement kiln dust (CKD) was studied (Ahmari and Zhang, 2013b). When CKD was used, an increase of unconfined compressive strength (UCS) and improvements in durability were produced. The effects of activator type/concentration and curing temperature on alkali-activated binder based on copper mine tailings were studied (Ahmari *et al*., 2012a). Some alkaline activators at different compositions, concentrations and curing temperatures were considered (see Table 18.1). The results indicated that sodium hydroxide concentration and curing temperature are two important factors that affect the UCS and microstructural properties of the alkali-activated MT binder.

Zhang *et al*. (2011) studied the viability of geopolymerization of copper mine tailings adding different amounts of fly ash in order to decrease the high Si/Al ratio of the mine tailings. The results showed that the Si/Al ratio and the alkalinity have very important effects on the mechanical and microstructural properties of the mine tailings-based geopolymers.

Pacheco-Torgal *et al*. (2008c, 2008d, 2008e, 2008f, 2009, 2010) have carried out exhaustive studies on tungsten mine waste. Tungsten mine waste mud (TMWM) geopolymeric binder is a new cementitious material with a very high early age strength, low water absorption and very good adhesion to ordinary Portland cement (OPC) concrete (Pacheco-Torgal *et al*., 2008c, 2008f). It is obtained from dehydroxylated mine waste powder mixed with calcium hydroxide and activated with NaOH and waterglass solutions. The results showed that techniques and procedures for assessing OPC fresh mixtures are not recommended to evaluate TMWM binders. Unrestrained shrinkage of TMWM binders is lower than observed for OPC binders, being even lower than some traditional alkali-activated binders (Pacheco-Torgal *et al*., 2008d).

Table 18.1 Activator type/concentration and curing temperature conditions for alkali-activated binder based on copper mine tailings

Type of activator	[NaOH] (M)	Curing temperature (°C)
NaOH	5, 10 and 15	60, 75, 90 and 120
NaOH + sodium silicate (SS)[a]		60
NaOH + sodium aluminate (SA)[b]		90

[a]SS/NaOH solution = 0.5–2.5; [b]SA/NaOH mass = 0.4–3.1.
Source: Adapted from Ahmari *et al*., 2012a.

The effect of the aggregate/binder ratio, the aggregate dimension and aggregate type (schist, granite and limestone) in the microstructure and mechanical behavior of tungsten mine waste geopolymeric pastes and mortars were investigated (see Figure 18.4). In contrast with the porous typical interfacial transition zone of Portland cement mixtures, a dense and a uniform interfacial transition zone was detected in tungsten mine waste geopolymeric-based binders (Pacheco-Torgal *et al*., 2008e).

Research on geopolymeric mine waste mud (GMWM) binder's hydration products has been carried out. Results showed that a new crystalline phase, phlogopite with a trioctahedral layered structure, was formed as a result of the geopolymerization process (Pacheco-Torgal *et al*., 2009).

Durability and environmental performance of TMWM mortars were carried out. This study showed that TMWM binders have higher acid and abrasion resistance than OPC-based concrete mixtures. The environmental assessment of the TMWM binders showed that it can be considered inert from an environmental point of view and it could be used as a construction material (Pacheco-Torgal *et al*., 2010).

Silva *et al*. (2012) studied the behavior of alkali-activated TMWM after immersion in water. A mixture of waterglass and sodium hydroxide as an activating solution

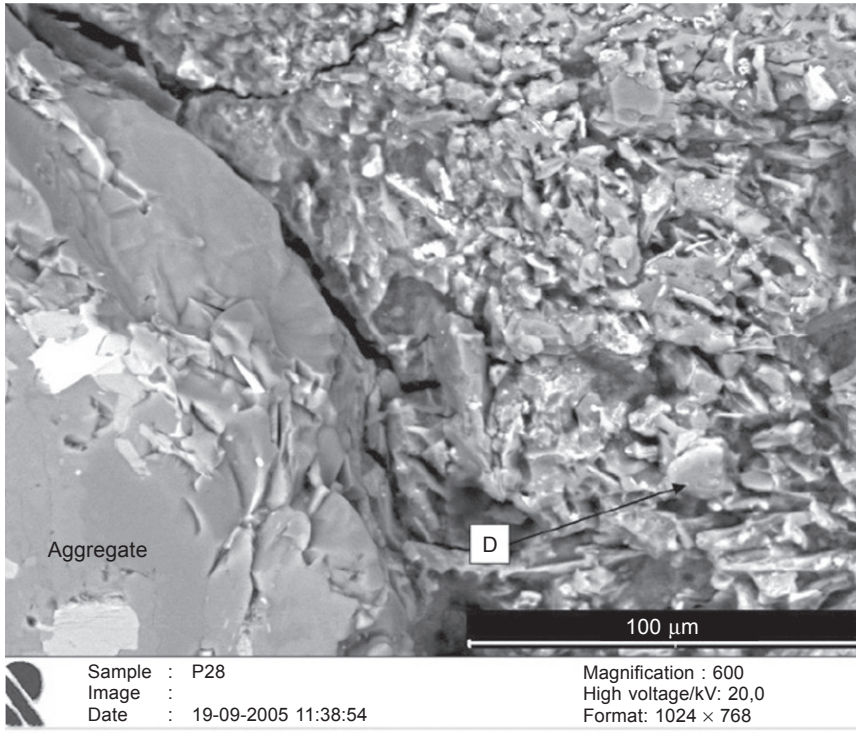

Figure 18.4 SEM micrograph of interfacial transition zone in tungsten mine waste geopolymeric mortars made with granitic coarse aggregates. Area D presents a sodium content of 3.4% (%Na_2O) obtained by EDS (reprinted from Pacheco-Torgal *et al*., 2008e, Copyright © 2008, with permission from Elsevier).

was used. Additional specimens with high water content (10% in relation to mass precursor) were cured for several weeks at 20ºC and 40% RH, 80ºC and 130ºC dry conditions. Afterwards, specimens were immersed in water for different periods. Alkali-activated specimens cured at room conditions (20ºC 40% RH) partially disintegrated when immersed in water. Disintegration of specimens was due to deficient geopolymeric reaction (partial alkali-activation reaction), which could have been caused by an insufficient concentration of NaOH solution.

Castro-Gomes *et al*. (2012) have developed new geopolymer-based composite materials, obtained from non-contaminated waste-rock tailings. These materials could have interesting properties for technical-artistic value added applications, such as conservation, restoration and/or rehabilitation of historic monuments, sculptures, decorative and architectural interventions, or simply as materials for building coatings.

Komnitsas and Zaharaki (2007) have published an interesting paper about minerals and geopolymerization. The paper presented a brief history and review of geopolymer technology, summarized and critically analyzed the most important research findings over the last 25 years. Finally, the paper proposed further research and development topics and suggested steps forward (see Figure 18.5) to improve the potential of geopolymerization focusing on the utilization of mining and metallurgical wastes and by-products, the synthesis properties and the stabilization of hazardous wastes.

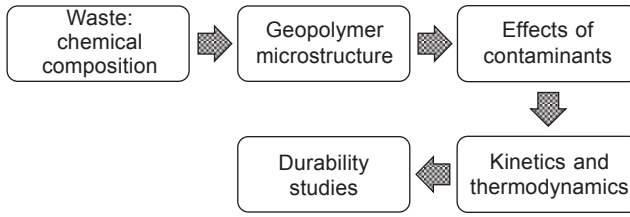

Figure 18.5 Proposed steps to improve the potential development of geopolymerization technology (adapted from the text in Komnitsas and Zaharaki, 2007).

18.5 Glass and ceramic wastes

In this section, waste materials whose synthetic routes are based on high temperature processes are analyzed. The application of different types of glasses in geopolymer production is described: glass waste from industrial manufacture, glass cullet, glass from plasma treatment, solar panel waste glass. Applications using scraps from traditional ceramic materials are also described: bricks, tiles, porcelain and stoneware.

18.5.1 Glasses

Municipal waste streams across the world generate millions of tons of glass every year. In the United States, about 12 million of tons of waste glass are generated

annually, only 25% of which is recycled. Glass powder is rich in silica, and when activated with alkalis can result in the formation of sodium silicate gel. Preliminary studies have been reported on the alkali activation of glass powder/blast furnace slag, using NaOH and NaOH/Na_2CO_3 solutions as activating reagents (Torres *et al*., 2009). According to the test results, the best compressive strength value was 27.7 MPa for pastes prepared with 30/70 waste glass/slag and activated with NaOH/Na_2CO_3. The authors also observed that the increase of the glass waste content promoted a decrease in the mechanical properties of alkali-activated pastes.

Other attempts have been made using glass cullet/clay mixtures (Carvalho *et al*., 2008). Optimized formulations showed an interesting mechanical strength of 20 MPa, after 48 h of curing at room temperature. The addition of foundry sand as an aggregate minimized shrinkage upon curing and increased the density of the specimens. In addition, the curing conditions are also decisive in determining the final characteristics of the materials. Curing in room conditions had a beneficial effect on the mechanical strength, contradicting some reported results in the literature. This was probably related to a slower and well-controlled curing process conducted at room temperature.

Idir *et al*. (2011) and Cyr *et al*. (2012) have reported the production of geopolymer from cullet glass without any additional mineral admixture. Idir *et al*. (2011) used glass obtained from glass bottles. The assessed parameters were the fineness of the glass, the geopolymerization temperature (20, 40 and 60ºC) and the nature and concentration of the activator solution (KOH, NaOH). The results showed that the cullet of soda-glass activated with KOH or NaOH had good mechanical strengths (60 MPa for optimal conditions) but high fineness of glass yielded better mechanical performance. In addition, it was not necessary to use high curing temperature (60ºC) to obtain high performance, although the optimal curing temperature was 40ºC. KOH was the activating reagent which yielded the highest performance.

Cyr *et al*. (2012) extended the previous research, and concluded that waterglass was not necessary for the setting of geopolymers, contrarily to metakaolin-based geopolymers. The authors also demonstrated that the durability of glass cullet geopolymers is affected by water conservation, probably due to a lack of aluminum. Optimization was still needed and long-term durability tests should be carried out.

Other glass wastes have been used in geopolymer production. Tashima *et al*. (2013a) used a waste from glass fiber manufacturing: the vitreous calcium aluminosilicate (VCAS). The authors analyzed the influence of curing time on the microstructure and mechanical strength development of alkali-activated binders based on VCAS (see Figure 18.6). Compressive strength values around 77 MPa after three days of curing at 65ºC were obtained. A mathematical model of compressive strength development of mortars was proposed in the range 4–72 h curing time. This mathematical model was:

$$R_c = a \times (1 - b^t) \tag{18.1}$$

where R_c is the compressive strength (MPa), t is the curing time (h) and a and b are 120.45 and 0.9863 MPa, respectively.

In another paper, Tashima *et al*. (2012a) activated VCAS using NaOH and KOH

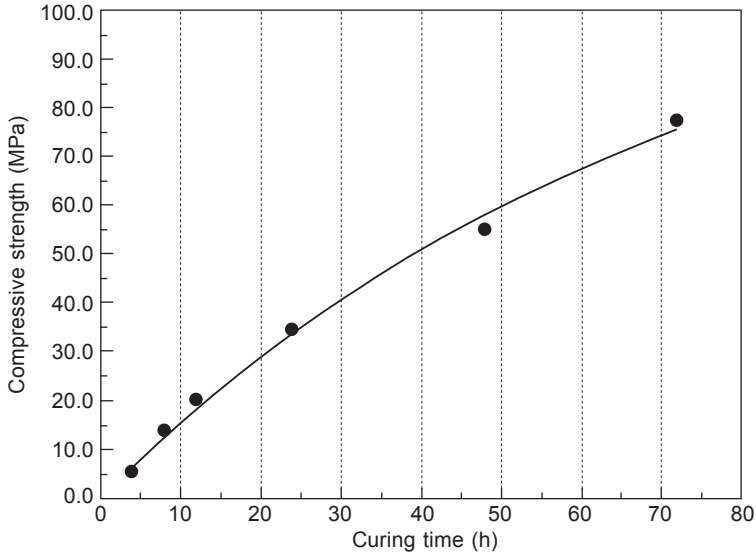

Figure 18.6 Compressive strength development of alkali-activated VCAS mortars. Solid circles are experimental data and solid line is fitting curve according to Eq. (18.1) (from Tashima *et al.*, 2013a, with kind permission from Springer Science and Business Media).

solutions. The results showed that the type of cation and the concentration of the activating solution play a key role in determining changes in the microstructure of pastes. VCAS mortars had compressive strength in the range of 20–77 MPa when cured at 65ºC for three days, with higher compressive strengths obtained for NaOH compared to KOH-based systems. In addition, alkali-activated mortars based on VCAS cured at room temperature were also evaluated in a third paper (Tashima *et al.*, 2013b). Mortars yielded 78.5 and 89.5 MPa compressive strength values after 91 and 360 days of curing, respectively. The microstructure of these mortars was amorphous and no crystalline phases were detected by X-ray analysis.

In a recent paper, Redden and Neithalath (2014) used a glass powder that is a by-product of industrial and highway safety glass bead manufacturing with pozzolanic properties (Schwarz and Neithalath, 2008; Schwarz *et al.*, 2008). This is a silica-rich glass powder that can be activated using high concentrations of NaOH and high curing temperatures (50 and 75ºC) at 48 and 72 h. However, high curing temperatures and long-term curing times adversely influenced the strength of glass powder-based binders when higher alkalinity was used in the activation process. In this case, a porous and disconnected microstructure was observed. The lack of hydrolytic stability of sodium silicate gels formed was evident because of the drastic strength loss under moisture curing conditions. Silica depolymerization in sodium silicate gels could explain this strength loss. The doping of this system with Ca and Al, by means of addition of ground granulated blast furnace slag and metakaolin, respectively, allowed a better control of the strength loss under moisture exposure.

Hao *et al*. (2013) analyzed the effect of solid/liquid ratio (0.4–1.0) on the properties of geopolymer where part of metakaolin was replaced by solar panel waste glass (0–40% range) using as activating solutions NaOH/waterglass mixtures. The experimental results indicated that geopolymer containing 10% solar panel waste glass at solid/liquid ratio of 1.0 had higher compressive strength at 1 day (57.6 MPa) and 7 days (64 MPa) curing time than geopolymer without solar panel waste glass. The experimental results showed that the degree of the geopolymerization is higher if the solid/liquid ratio is increased. Additionally, as the amount of solar panel waste glass increased, the reaction degree of the geopolymer decreases, resulting in a microstructure with lower density and higher porosity.

Kourti *et al*. (2010a, 2010b, 2011a, 2011b) have published various papers, where glass produced from DC plasma treatment of air pollution control (APC) residues was used for geopolymer production. APC residues are hazardous wastes produced from cleaning gaseous emissions at energy-from-waste (EfW) facilities processing municipal solid waste (MSW). APC residues have been blended with glass-forming additives and treated using DC plasma technology to produce a high calcium aluminosilicate glass.

Kourti *et al*. (2010a, 2010b) prepared geopolymers from the glass produced by the DC plasma treatment of APC residues. The effect of activating solutions with NaOH (2–12 M)/sodium silicate (Si/Al 2.6), and with a constant solid/liquid ratio of 3.4 was assessed. The pastes were cured at room temperature. These residues of APC, due to high calcium content, could cause the formation of some amorphous calcium silicate hydrate (C-S-H) gels. Samples prepared with 6 M NaOH or above yielded high compressive strengths, ranking between 80 and 110 MPa after 28 days and 100 and 140 MPa after 92 days' room curing time. Density and water absorption also depended on the sodium hydroxide concentration; high NaOH concentrations increased density and result in a decrease of absorption, which was relatively low (8–10%).

Kourti *et al*. (2011a) investigated in depth the properties of geopolymers prepared with this residue, with the same previous optimal conditions (NaOH 6 M). They concluded that APC glass geopolymer is a composite consisting of a binder phase and unreacted APC glass particles which act as reinforcement rather than a pure geopolymer. The binder phase was a three-dimensional geopolymeric network that contains C-S-H gel and probably Al modified C-S-H gel. The excellent mechanical properties of APC glass geopolymers (110 MPa at 28-day room curing time) can be attributed to these microstructural characteristics. These geopolymers also exhibited high density (2.3 g/cm^3), low porosity (5.5%) and low water absorption (11%), good resistance to freeze/thaw test (2% of weight loss after 92 cycles), low leaching and high acid resistance.

In a subsequent paper, Kourti *et al*. (2011b) compared the properties of geopolymers from glass derived from DC plasma treatment of APC residues with a geopolymer prepared, in a similar way, from metakaolin or blast furnace slag (BFS). The results showed that APC glass geopolymer exhibited significantly higher compressive strength values than metakaolin or BFS geopolymers.

18.5.2 Bricks, tiles and porcelain

Ceramic wastes are generated not only by industry but also by the construction sector. Approximately 45% of construction and demolition wastes are ceramic in nature. Accordingly with the source of raw materials, different ceramic materials can be distinguished: structural ceramic products (i.e., bricks, roofing tiles, vaults, etc.), ceramic tiles and stoneware.

A review survey by Stock (2011) reported a world tile production of 9 million m^2 in 2010 of which 96% was accounted for by the 30 major manufacturing countries. According to Pacheco-Torgal and Jalali (2010), the amount of waste generated by the European ceramic industry is typically 3–7% by weight of total production.

Puertas *et al*. (2006) assessed six different ceramic wastes activated with NaOH and sodium silicate solution. After 8 curing days at 40ºC, alkali-activated pastes yielded maximum compressive strength of 13 MPa. Apparently, the amount of vitreous phase in ceramic waste and the nature of the activator did not have a strong influence on the development of strength in these alkali-activated systems. Alkali-activated pastes showed that feldspar phases are susceptible to dissolution and reaction with the alkaline solution.

Reig *et al*. (2013a) presented a work about alkali-activated pastes and mortars based on clay brick wastes activated with NaOH and sodium silicate solution. The type and concentration of activating solution were optimized to produce mortars that yielded up to 50 MPa after 7 curing days at 65ºC. Thermogravimetric analysis (TGA) identified the formation of zeolitic structures just for low alkaline solution concentration.

In another paper (Reig *et al*., 2013b), two different geopolymeric binders that consist of two ceramic waste materials, porous red clay brick and porcelain stoneware, with very different sintering temperatures and chemical composition, have been developed. The effect of the activating solution concentration on mechanical strength and microstructure of the prepared binders have been studied. For mortars with red clay brick powder, compressive strengths in the range 29–41 MPa depending on the water/binder ratio and activator/binder ratio were obtained. For alkali activation process of porcelain stoneware, the addition of $Ca(OH)_2$ was necessary to produce alkali-activated mortars with compressive strength about 30 MPa after 7 curing days at 65ºC.

Sun *et al*. (2013) activated a ceramic waste composed by a mixture of tiles, pan forms and blocks with a mixture of alkali hydroxides and/or sodium/potassium silicate solutions (see Table 18.2). The geopolymer with optimal mix gave a compressive strength of 71.1 MPa (see Figure 18.7). In addition, the waste ceramic-based geopolymer exhibited favorable thermal exposures. A higher compressive strength was even acquired after 2 hours of calcination at 1000ºC, which may be due to the viscous sintering and the completion of further geopolymerization reaction at high temperature.

Table 18.2 Composition of activating solutions for geopolymers containing ceramic waste

Activating solution	Geopolymer ID	Content (wt.%)			
		KOH	NaOH	SiO_2	H_2O
A1	GA1	–	24.84	22.34	52.82
A2	GA2	–	22.0	23.18	54.81
A3	GA3	–	19.87	23.82	56.31
B1	GB1	16.55	11.85	21.28	50.32
B2	GB2	14.73	10.55	22.21	52.51
B3	GB3	13.15	9.70	22.92	54.19
C1	GC1	–	30.10	–	69.90
C2	GC2	40.38	–	–	59.62
C3	GC3	12.15	16.88	–	59.97

Source: Reprinted from Sun *et al.*, 2013, Copyright © 2013, with permission from Elsevier.

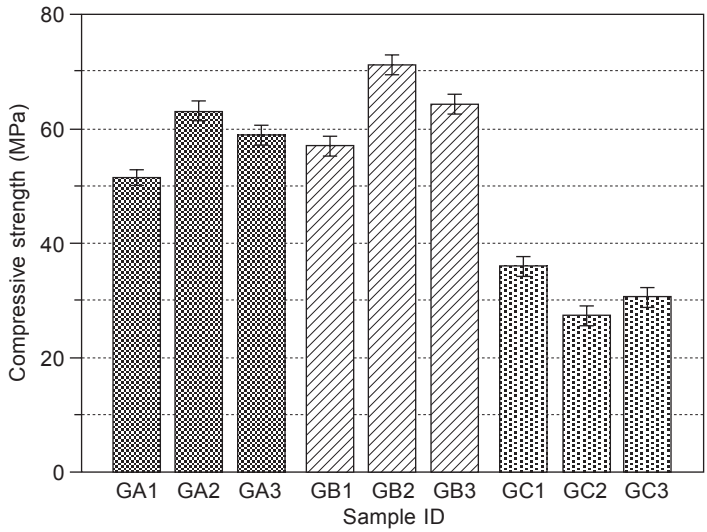

Figure 18.7 Compressive strength values for geopolymers cured at 28 days, prepared with activating solutions summarized in Table 18.2 (reprinted from Sun *et al.*, 2013, Copyright © 2013, with permission from Elsevier).

18.6 Construction and demolition wastes (CDW)

Construction and demolition wastes (CDW) are a growing problem in many countries. In the US, CDW represents about one-third of the volume of materials in landfill areas (Kibert, 2000). In the European Union it was estimated that 0.5–1 ton per capita of CDW is generated annually. The valorization of CDW is usually faced with the

problem of how to recycle/valorize coarse aggregates in Portland cement concrete (Pacheco-Torgal *et al.*, 2013).

Very limited research has been conducted on recycling waste concrete via geopolymerization. Yang *et al.* (2009a) prepared a geopolymer concrete using a mixture of recycled construction aggregate (40%) and natural aggregates. The geopolymeric matrix was prepared with a mixture of waste concrete powder and metakaolin (5–25%). The activating solution was prepared using NaOH/waterglass (0.5–1.3 mass ratio) and the compressive strength of geopolymeric concrete formed yielded about 40 MPa after 28 curing days at room temperature.

Yang *et al.* (2009b, 2009c) have also studied the properties of concrete sludge-based geopolymers. In this case, the concrete sludge powder and silica sand were mixed with different quantities of metakaolin (10–40%) and NaOH/waterglass solution was used as an alkaline activator solution. To improve the mechanical properties, silica fume was added to the binding matrix (0–10%) to replace part of the concrete sludge. In these specimens, the silica fume offered active SiO_2, which was advantageous for geopolymer production, improving the mechanical properties of mortars and made the structure much denser.

Ahmari *et al.* (2012b) studied the production of geopolymeric binder pastes from ground waste concrete (GWC) powder mixed with Class F fly ash (FA). The results indicated that the inclusion of GWC improved the compressive strength of geopolymeric binder up to a certain GWC content. In the current experiment, 50% was found as the optimum GWC content for 5 and 10 M NaOH and waterglass/NaOH ratio of 1 and 2. In this case, the highest compressive strength was obtained using a low Ca/Si ratio (0.25), which suggests formation of low calcium C-S-H gel in the geopolymeric system. Increasing NaOH concentration resulted in higher compressive strength, especially for GWC content less than 50%. Addition of waterglass also improved strength values. In addition, SEM/EDX, XRD and FTIR analysis confirmed that Ca in GWC enhances the strength, mainly due to the formation of low calcium semi-crystalline CSH gel, which coexists with the geopolymeric gel and the incorporation of Ca^{2+} into the geopolymer network as charge balancing cation.

Khater (2012) studied the effect of calcium in the form of hydrated lime on the geopolymeric binders cured at room temperature and at 40ºC. A mixture of demolished walls, demolished concrete and metakaolin (added in order to increase alumina content) was prepared. The results showed that the addition of calcium improved the compressive strength after 90 days of curing at room temperature in water saturation conditions. After drying the pastes at 80ºC for 24 h, an enhancement in mechanical properties occurred. This was probably related to the calcium silicate hydrate transformation into a crystallized form that increases the rate of hydration as well as the compressive strength. In addition, curing at room temperature in tap water gave better microstructural and mechanical properties compared to those observed for same systems cured at 40ºC (100% RH).

Lampris *et al.* (2009) have investigated the geopolymerization of silt generated from aggregate and waste washing plants, in the preparation of aggregate. Silt from aggregate washing plants was characterized and blended with either metakaolin or fly ash (FA) and activated under a range of conditions. On one hand, silt geopolymers

cured at room temperature had average 7-day compressive strengths of 18.7 MPa (see Figure 18.8). Curing for 3 days at 60ºC and then at room temperature yielded slight higher values. And curing specimens for 24 h at 105ºC gave a value of 39.7 MPa for compressive strength and microstructure analysis confirmed an increase of density. On the other hand, partial substitution of silt by metakaolin or FA increased average compressive strengths to 30.5 MPa and 21.9 MPa, respectively.

Payá *et al*. (2012) evaluated the use of hydrated-carbonated Portland cement as a raw material in the production of geopolymers. The hydrated Portland cement was intensively carbonated by using carbon dioxide, in order to decompose C-S-H and C-A-H compounds and produced reactive silica and alumina. The results showed that produced geopolymers were mechanically stable and yielded compressive strengths higher than 10 MPa for mortars cured at 65ºC for 3 days. The authors concluded that alkaline activation of hydrated-carbonated Portland cement could be considered a low CO_2-emission binder.

Finally, alkali-activated mixtures of waste brick powder and concrete powder were reported (Allahverdi and Kani, 2009). In this study, final setting times of systems prepared with different proportions of these powders ranged from 100 to 250 minutes. In addition, the results obtained for 28-day compressive strength confirmed that waste brick was more suitable than waste concrete for geopolymerization reactions.

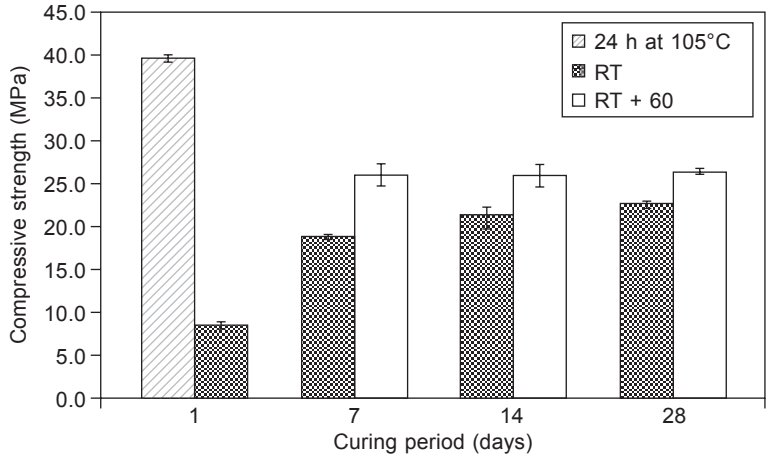

Figure 18.8 Effect of curing conditions on compressive strength of silt geopolymers. RT: room temperature curing; TR+60: 3 days curing at 60ºC and then room temperature curing (reprinted from Lampris *et al*., 2009, Copyright © 2009, with permission from Elsevier).

18.7 Wastes from agro-industry

Agro-industrial activities have been introduced worldwide and huge amounts of different types of residues are being produced, either on the same farm field or in related industries. This type of residues could be valorized through energy recovery. The use of biomass in energy production is at present and in the near future the

most important route of recovery. The energy recovery process from this type of waste generates another type of waste (ashes), so one can extract an additional or a second valorization. This second stage can lead to materials being obtained with high added value: pozzolanic materials for the manufacture of cement and Portland cement-based concrete. Additionally, these ashes could be used as a mineral precursor for production of alkali-activated cements (geopolymers) or, moreover, as a raw material in the manufacture of activating solutions.

Many types of ashes produced from agro-wastes have been characterized and their behavior in Portland cement mixtures has been reported (Payá *et al*., 2010): ashes from rice husk, sugarcane bagasse, sugarcane straw, palm oil fuel, wheat straw, corn cob, eucalyptus wood (bark) and bamboo leaf. Most of these ashes, in their chemical composition, present silicon dioxide (SiO_2) as their main component. An increase in their reuse could provide a substantial benefit in waste management and the development of commercial applications.

These silica-rich ashes are also good candidates to prepare alkali-activated cements. The low Al_2O_3 content in the agro-wastes makes necessary the combination with other types of wastes, such as coal fly ashes (FA) or blast furnace slag (BFS).

Rice husk ash (RHA) is the most studied agro-waste in geopolymers. Usually, RHA contains higher than 90% SiO_2. A preliminary study (Rattanasak *et al*., 2010) of the reactivity of RHA/aluminum hydroxide mixtures demonstrated that an external source of aluminum (2.5–10% by weight) was necessary for preparing geopolymers. However, these mixtures activated with NaOH/sodium silicate were not stable under water, and disintegrated.

The good behavior of the alkaline activation of RHA/FA mixtures has been reported in several papers (Detphan and Chindaprasirt, 2009; Rüscher *et al*., 2011; Riahi *et al*., 2012). Detphan and Chindaprasirt (2009) reported the behavior of RHA/FA geopolymers activated with NaOH, sodium silicate and heat in the following proportions: 0/100, 20/80, 40/60 and 60/40. Compressive strengths in the 12.5–56.0 MPa range were reported. The authors also reported that the compressive strength was increased with the fineness of the RHA, which was attributed to the increase in the surface area and reactivity. Riahi *et al*. (2012) also studied this RHA/FA system, and they found that 90ºC was the optimum curing temperature for activating the geopolymerization, and good behavior was found for 5 M or 8 M NaOH activator by mixing with sodium silicate solution.

RHA was also reacted with another type of mineral addition: red mud (RM) or diatomaceous earth (DE). In the case of RHA/RM mixtures (He *et al*., 2013), it must be taken into account that RM waste contained high proportions of alumina (14.0%) and sodium aluminate (23.0%), which favored the geopolymerization process. In this case, 4 M NaOH solution was necessary for activating the mineral mixture. The best behavior was found for a RHA/RM = 0.5 ratio, yielding 20.46 MPa in compression test after 49 days of curing at room temperature. RHA/DE mixtures (Pimraksa *et al*., 2011) were designed for preparing low bulk density geopolymers (1 g/cm^3). The alumina source was diatomaceous earth (10–14%), and its replacement by using RHA; SiO_2/Al_2O_3 ratios were in the range 16.6–33.5. RHA provided large amounts

of dissolved silicate ions and led to an increase in the compressive strength of these low density geopolymers.

Many types of agro-wastes can be used as fuel (biomass) in power plants. In Asia, it is very common to use a mixture of rice husk and eucalyptus bark. In this way, rice husk-bark ash (RHBA) is produced in large amounts. This ash is also characterized by high SiO_2 content (higher than 80%), low loss on ignition (3–5%) and low Al_2O_3 (<1%) and CaO (<5%) contents. RHBA-FA mixtures have been intensively studied (Nazari *et al*., 2011, 2012; Songpiriyakij *et al*., 2010). RHBA/FA mixtures (Nazari *et al*., 2011) were in the 20/80 and 40/60 range, using a sodium silicate/sodium hydroxide solution ratio of 2.5. The best NaOH solution concentration was 12 M, yielding compressive strength higher than 25 MPa after curing for 36 hours at 80ºC. Selected samples of FA and RHBA with different fineness were tested, finding that the combination of the finest mineral additions resulted in the best mechanical behavior (more than 35 MPa after 7 days of curing, and more than 45 MPa after 28 days). In a similar study, Songpiriyakij *et al*. (2010) studied RHBA/FA mixtures in the 0/100 to 100/0 range. The best mechanical results were observed for the 60/40 ratio, in which the SiO_2/Al_2O_3 ratio was 15.91 (see Figure 18.9). The degree of reaction was determined in these mixtures, and no match with the strength development was found, meaning that not only the degree of reaction but also the nature of the developed matrix in the geopolymerization process was responsible for the compressive strength.

Bark fly ash (BFA) was also studied as a source of mineral materials (Rajamma *et al*., 2012). In this case, the proportion of CaO was significantly high (24.0%), and also the Al_2O_3 content (8.5%). Geopolymers using BFA or BFA/metakaolin (MK)

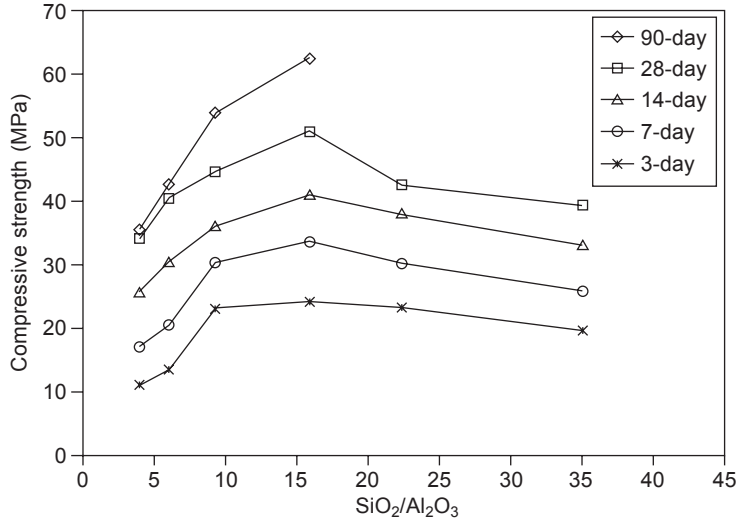

Figure 18.9 Compressive strength of alkali-activated FA/RHA mixtures vs. SiO_2/Al_2O_3 ratio (reprinted from Songpiriyakij *et al*., 2010, Copyright © 2010, with permission from Elsevier).

were developed. Compressive strength of BFA geopolymeric pastes increased with the increase of NaOH content (from 8 M to 18 M) and strengths in the 8–12 MPa were achieved. Better results using BFA/MK mixtures were obtained: replacement of 20–40% of BFA by MK produced a strength gain, yielding compressive values in the 12–16 MPa range. Mortars were also prepared, and better mechanical behavior was observed: 100/0 BFA/MK mortar had 14–18 MPa in compression, 22–29 MPa for 80/20 samples, and 36–39 MPa for 60/40 mortars.

Palm oil fuel ashes (POFA) were also tested in alkali-activated systems. Palm oil shell and husk are used as a fuel in boilers in palm oil mills to produce steam for electricity. The resulting ash usually contains a high proportion of SiO_2 (>50%) and significant amounts of CaO (>5%). In some cases, the loss on ignition (LOI) value is high (>5%). POFA has been used in mixtures with BFS (Karim *et al*., 2013; Yusuf *et al*., 2014), FA (Ariffin *et al*., 2011, 2013) and MK (Ismail *et al*., 2013). Ultrafine POFA is a very interesting material for preparing POFA/BFS systems (Yusuf *et al*., 2014): in the case of 80/20 ratio, 71.2 MPa of strength was reached after 28 days of of curing after 60ºC-24 h of precuring. For the POFA/FA system (Ariffin *et al*., 2011), interesting results were found for the 70/30 mixture, being the compressive strength of 25 MPa after 28 days of curing at room temperature (28ºC).

Sugarcane bagasse ash (SCBA) has also been studied for mineral addition in alkali-activated systems. Its activation was not successfully achieved without the participation of an additional mineral admixture: studies on SCBA/BFS (Castaldelli *et al*., 2013, 2014), SCBA/FA (Castaldelli *et al*., 2014) and SCBA/MK mixtures (Tippayasam *et al*., 2010) have been carried out. Castaldelli *et al*. (2013, 2014) showed good performance of 40/60 SCBA/BFS systems activated through a mixture of NaOH solution and waterglass. Thus, compressive strength of 42 MPA was reached after curing for 3 days at 65ºC. The strength development at room temperature was slower, yielding 30 MPa after 7 days and 50 MPa after 28 days. The geopolymeric matrix developed with time, reaching 70 MPa after 270 days. For the SCBA/FA system, the presence of unburned matter in the SCBA is critical, and the setting and hardening in a geopolymeric mixture did not occur (Castaldelli *et al*., 2014). For preparing good performance mortars, SCBA may be previously calcined at 600ºC for removing organics. SCBA/FA mixture (25/75) was activated using a mixture of potassium hydroxide and potassium silicate (8 M in K^+, and 0.65 SiO_2/K_2O molar ratio). Compressive strength of mortars cured for 3 and 7 days at 65ºC yielded 33.5 and 36.4 MPa, respectively.

Recently, a new approach to using agro-wastes in the preparation of geopolymers has been presented: the synthesis of alkali activator by reaction of NaOH and rice husk ash. Bouzón *et al*. (2014) have developed a method in which an aqueous mixture of NaOH and RHA is refluxed for 5–240 minutes. The highest silica dissolution was achieved for 60 minutes of refluxing (see Figure 18.10). The method was applied to as-received and to a ground RHA, and no significant differences were found for the first 120 minutes of refluxing. Geopolymeric mortars were prepared using spent FCC catalyst, and a comparison was established using a control activator prepared by mixing appropriate quantities of NaOH, waterglass and water. This control

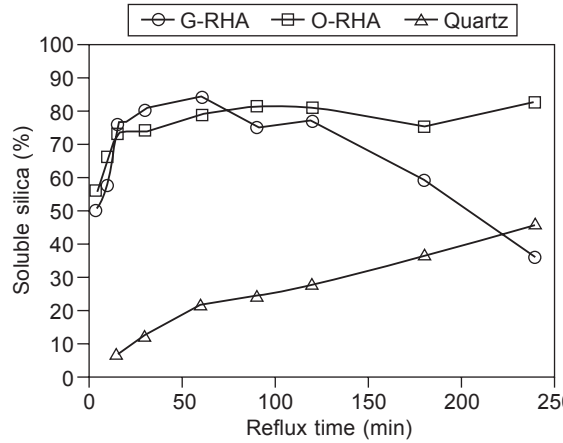

Figure 18.10 Soluble silica content (%) versus reflux time in NaOH solution for original rice husk ash (O-RHA), ground rice husk ash (G-RHA) and quartz (reprinted from Bouzón *et al.*, 2014, Copyright © 2014, with permission from Elsevier).

mortar yielded 40.9 MPa (1 day curing at 65ºC), whereas equivalent mortars using 60 minutes refluxed NaOH/RHA mixture yielded 35 MPa for as-received RHA and 42 MPa for ground RHA.

Mejía *et al*. (2013) tested RHA as a source of silica in FA/BFS systems. Two RHA samples were compared, which differed in the content of amorphous silica (amorphous RHA = 94.7% and crystallized RHA = 27.7%) In this case, the NaOH/RHA suspension was stored for 1 day at room temperature. Mechanical performance of BFS, FA and FA/BFS pastes prepared with NaOH and waterglass was significantly better than those obtained for NaOH/RHA activated pastes. Despite amorphous RHA yielding better behavior, apparently part of the crystallized silica was dissolved in the preparation of the alkaline activator.

18.8 Wastes from chemical and petrochemical industries

The use of wastes from the chemical and petrochemical industries as an aluminosilicate precursor in alkali-activated binders is described in this section. Essentially, this topic is divided into three main sections. The first section makes a brief discussion about cement kiln dust (CKD), probably the most important chemical and petrochemical waste in volume. The second section is related to the use of fluid catalytic cracking catalyst residue (spent FCC), an aluminosilicate source with similar chemical composition to metakaolin. In the last section, other minor wastes such as wastepaper sludge, flue gas desulphurization (FGD) waste and waste from treatment of chlorosilane production are reported.

18.8.1 Cement kiln dust

Cement kiln dust (CKD) is an industrial waste material collected from cement kiln exhaust gases during Portland cement production. In the production of Portland cement, clay and calcium carbonate are finely ground, mixed and calcined at 1450ºC. During this process, calcium silicate is the main product formed and a dust named CKD is generated. The air pollution control devices in Kilns (cyclones, electrostatic precipitators or bag house) are responsible for capturing fine-grained particles of raw materials, partially processed feed and components of final product carried out from the kiln by exhaust gases (Ahmari and Zhang, 2013b). Approximately 5% of clinker production is generated from CKD.

Depending on the chemical composition of CKD (alkali and chloride content), this material can be recycled in cement production. In most cases, it has been used for different purposes such as agriculture (Adaska and Taubert, 2008), water treatment, soil stabilization (Peethamparan *et al*., 2008) and filler for concrete and mortars (Maslehuddin *et al*., 2008; Kunal *et al*., 2012; Siddique, 2006).

The reuse of CKD in alkali-activated systems is related to the improvement of physical and mechanical properties and durability aspects of alkali-activated binders, mainly due to its latent hydraulic substances. Hence, CKD is always used in binary systems such as fly ash/CKD, slag/CKD, metakaolin/CKD and mining waste/CKD (Buchwald and Schulz, 2005; Ahmari and Zhang, 2013b). Wang *et al*. (2004) studied the effect of curing temperature and sodium hydroxide concentration on hydration and strength development of binary systems 50% CKD–50% fly ash. In this type of system, the major crystalline phase found by the authors was ettringite, which contributes to stiffening, setting and early strength development. The presence of calcium hydroxide was also observed (resulting from the CKD hydration), promoting the pozzolanic reaction for the CKD–fly ash system.

In the same way, Cabrera-Fuentes *et al*. (2011) investigated alkali-activated fly ash blends containing 0, 5 and 20 wt.% CKD activated with alkaline solution with solid/liquid ratio of 0.4 and SiO_2/Na_2O ratio of 0.19 and 1.17. Pastes were cured for 28 days at 85ºC and a relative humidity of 95%. According to the authors, an increment of the amount of CKD decreases the mechanical strength up to 45%, depending on the activating solution. XRD patterns showed a deviation on the baseline in the range $2\theta = 20–35^{o}$, associated to the presence of N-A-S-H gel that is responsible for the mechanical properties of these materials.

Buchwald and Schulz (2005) used two different CKD in the production of alkali-activated binders based on slag/CKD, fly ash/CKD and metakaolin/CKD. The results verified the suitability of these CKD-based materials. Slag/CKD pastes yielded higher compressive strength than the other system, reaching 12–22 MPa after 28 days of curing.

Ahmari and Zhang (2013b) assessed binary systems of mining tailings/CKD for alkali-activated binders. The results obtained demonstrated that CKD is responsible for enhancing the physical and mechanical properties and the durability of mining tailing-based geopolymeric bricks.

18.8.2 Fluid catalytic cracking catalyst residue (spent FCC)

Fluid catalytic cracking catalyst residue is a waste material generated during the catalytic process for petrol production in the petrochemical industry. About 160,000 tons of spent FCC is produced annually by this industry (Rodríguez *et al.*, 2013). Several studies reported the use of spent FCC as a pozzolanic material both in OPC and hydrated lime systems (Payá *et al.*, 2003a, 2003b).

Tashima *et al.* (2012b) reported the first study related to the use of spent FCC in the production of alkali-activated systems. The authors observed that an increment on the [Na^+] promotes an increase in the compressive strength of mortars cured for 3 and 7 days at 65ºC. Nevertheless, no differences were observed on curing for 3 or 7 days at 65ºC. The influence of SiO_2/Na_2O molar ratio for a fixed Na^+ concentration and H_2O/spent FCC of 0.6 was also assessed. For SiO_2/Na_2O of 0.29 and 1.19, mortars yielded about 10 MPa and 68 MPa, respectively, when cured for 3 days at 65ºC.

Tashima *et al.* (2013c) reported a study of alkali-activated materials based on spent FCC analyzing the influence of SiO_2/Na_2O and H_2O/spent FCC ratio on mechanical strength and microstructure. The XRD patterns of alkali-activated pastes demonstrated that faujasite was dissolved in an alkaline medium, forming amorphous products. The compressive strength of mortars cured for 3 days at 65ºC was in the range 26.4 to 83.6 MPa, depending on the SiO_2/Na_2O molar ratio and H_2O/spent FCC mass ratio (see Figure 18.11). A reduction of the H_2O/spent FCC ratio from 0.6 to 0.45 promotes a significant reduction in the total porosity of mortar (about 25%).

Recently, Tashima *et al.* (2014) reported an experimental study related to the use of sodium and potassium silicate in the production of alkali-activated binders

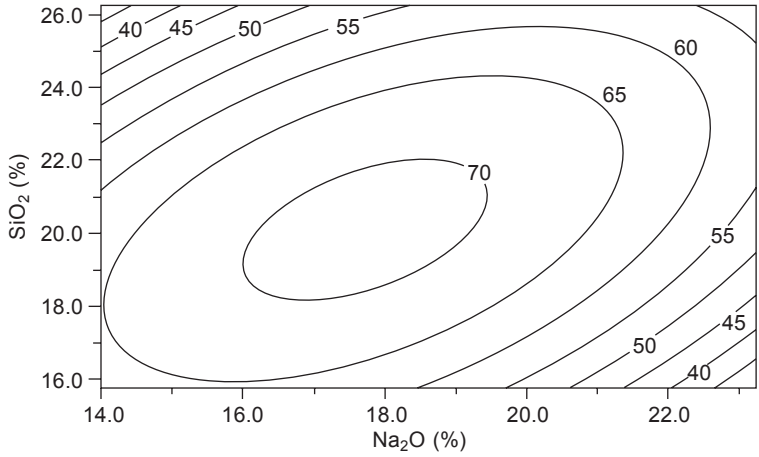

Figure 18.11 Non-linear fitting surface of compressive strength for alkali-activated mortars based on spent FCC with different proportions of Na_2O and SiO_2 in the alkali activator (reprinted from Tashima *et al.*, 2013c, Copyright © 2013, with permission from Elsevier).

based on spent FCC. Results indicated that even possessing less water in the potassium activating solution, mortars activated with sodium silicate solution yielded similar compressive strength when cured at room temperature and at 65ºC for 3 days.

Rodríguez *et al*. (2013) presented a microstructural analysis of alkali-activated binders based on spent FCC by means of X-ray diffraction (XRD), Fourier transform infrared spectroscopy (FTIR), scanning electron microscopy (SEM) and nuclear magnetic resonance (NMR). According to the authors, the remnant dealuminized zeolites in the unreacted spent FCC are readily dissolved, even when activation is carried out under relatively low alkalinity conditions, indicating the high reactivity of this precursor. Similarly, the alkali activation of spent FCC led to the dissolution of faujasite, as observed by Tashima *et al*. (2013c). In conclusion, the authors considered spent FCC as a useful material for production of geopolymeric binders.

Bouzón *et al*. (2014) proposed the use of refluxed rice husk ash/NaOH suspension in the production of alkali-activated binders based on spent FCC. The results obtained showed that spent FCC mortars activated with rice husk ash/NaOH yielded compressive strengths ranging from 31 to 41 MPa, similar to mortars prepared with waterglass/NaOH.

18.8.3 Other waste

Geopolymeric mortars based on wastepaper sludge/fly ash were investigated by Yan and Sagoe-Crentsil (2012). According to the authors, the addition of wastepaper sludge promotes a reduction in the flow of mortars, diminishing the compressive strength in the range 8–48%, depending on the wt.% incorporation of paper sludge. The positive effect is the significant reduction in the drying shrinkage (34–64%) when compared to reference geopolymeric mortar (only fly ash).

Santa *et al*. (2013) assessed geopolymeric binders which were synthesized from bottom coal ash and calcined paper sludge. In this study, wastepaper sludge was previously treated with 1.5 M HCl, washed with deionized water and filtered to remove the residue of calcium chloride. After that, the material was dried in an oven at 100ºC for 24 h and calcined at 850ºC for 2 h, obtaining an amorphous aluminosilicate material. The compressive strength for bottom ash/wastepaper ratio 2/1 was about 10–25 MPa at 90 days room curing time.

Guo *et al*. (2013) studied the use of flue gas desulphurization (FGD) gypsum in fly ash geopolymers. The FGD, after calcination at 800ºC, when mixed with fly ash, formed an amorphous geopolymeric gel with the presence of some crystalline phases such as calcite and bassanite.

The silica residue from waste treatment of chlorosilane production has also been used in the production of alkali-activated binders (Gluth *et al*., 2013). In this case, sodium aluminate was used as alkaline solution and according to the XRD pattern, the main reaction product was an amorphous gel and zeolite A. According to the authors, silica residue can be used in the production of geopolymers or even together with sodium aluminate as a starting material for one-part geopolymer.

18.9 Future trends

Different types of wastes, produced from diverse activities, are suitable for preparing alkali-activated materials. These wastes differ from 'conventional' or 'traditional' precursors such as blast furnace slag, fly ash and metakaolin. However, in the future, relationships must be established among them, in order to assess the potential usefulness of these 'new/alternative' precursors. Obviously, standards are necessary for alkali-activated cements; and once corresponding regulations are approved, there will be a time to evaluate the usefulness of all these types of wastes according to the standards.

On one hand, in the coming years, most precursors will probably not belong to the 'conventional' category, due to the high availability and appropriate characteristics of 'new' precursors. Alternative routes must be assessed for optimizing their properties and reactivity, and different options for preparing 'blended' precursors may be explored.

On the other hand, in terms of alkaline activator synthesis, there will be a challenge to overcome: the activator is the component that has the largest carbon and ecological footprints (Turner and Collins, 2013; Weil *et al*., 2009). Specifically, waterglass solution has the most important carbon footprint, and the minimization in its dosage and the sustainability in its manufacture may be enhanced. Further research in the use of diverse alkali-rich wastes may be carried out.

Another topic to be developed is related to the durability: in the case of this type of wastes, this point has been shown to be critical due to the variability in the source and in the chemical/physical/mineralogical properties of the precursors.

Finally, user-friendly products may be commercialized and, specifically, alternative, low cost and environmentally friendly construction materials may be designed and tested.

The alkali activation technology based on this type of wastes has a special focus on developing countries, due to the availability of new and cheaper products with good properties, based on self-generated wastes. This practice would allow diminished dependence on Portland cement, considered a critical topic in developing countries.

18.10 Sources of further information and advice

- *Alkali-Activated Cements and Concretes*. Caijun Shi, Pavel V. Krivenko and Della Roy. Taylor & Francis. ISBN10: 0–415–70004–3
- *Geopolymer Chemistry and Applications*. Joseph Davidovits. Institut Géopolymère. ISBN-10: 2951482019
- *Geopolymers: Structure, Processing, Properties and Industrial Applications*. John L. Provis and Jannie S. J. van Deventer. Woodhead Publishing. ISBN 978-1-84569-449-4
- 'Geopolymer technology: the current state of the art'. P. Duxson, A. Fernández-Jiménez, J. L. Provis, G. C. Lukey, A. Palomo, J. S. J. van Deventer. *J Mater Sci* (2007) 42: 2917–2933.

- Commonwealth Scientific and Industrial Research Organisation (CSIRO): http://www.csiro.au/en
- Geopolymer Alliance: http://www.geopolymers.com.au/
- Geopolymer Institute: http://www.geopolymer.org/
- The World Bank, Urban Development: http://www.worldbank.org/en/topic/urbandevelopment
- United Nations, Economic Comission for Africa: http://www.uneca.org/publications/africa-review-report-waste-management-main-report

Acknowledgement

This work has been developed under the GEOCEDEM Project BIA 2011-26947 (Spanish Ministry of Science and Innovation, co-funded by FEDER).

References

Adaska, W.S. and Taubert, D.H. (2008) 'Beneficial uses of cement kiln dust', *50th Cement Industry Technical Conf*, 1–19.

Ahmari, S. and Zhang, L. (2012) 'Production of eco-friendly bricks from copper mine tailings through geopolymerization', *Const Build Mater* 29, 323–331.

Ahmari, S. and Zhang, L. (2013a) 'Durability and leaching behavior of mine tailings-based geopolymer bricks', *Construct Build Mater* 44, 743–750.

Ahmari, S. and Zhang, L. (2013b) 'Utilization of cement kiln dust (CKD) to enhance mine tailings-based geopolymer bricks', *Construct Build Mater* 40, 1002–1011.

Ahmari, S., Zhang, L. and Zhang, J. (2012a) 'Effects of activator type/concentration and curing temperature on alkali-activated binder based on copper mine tailings', *J Mater Sci* 47, 5933–5945.

Ahmari, S., Ren, X., Toufigh, V. and Zhang, L. (2012b) 'Production of geopolymeric binder from blended waste concrete powder and fly ash', *Const Build Mater* 35, 718–729.

Alex, T.C., Kalinkin, A.M., Nath, S.K., Gurevich, B.I., Kalinkina, E.V., Tyukavkina, V.V., and Kumar, S. (2013) 'Utilization of zinc slag through geopolymerization: influence of milling atmosphere', *Int J Miner Process* 123, 102–107.

Allahverdi, A. and Kani, E.N. (2009) 'Construction wastes as raw materials for geopolymer binders', *Int J Civ Eng* 7, 154–160.

Ariffin, M.A.M., Hussin, M.W. and Bhutta, M.A.R. (2011) 'Mix design and compressive strength of geopolymer concrete containing blended ash from agro-industrial wastes', *Adv Mater Res* 339, 452–457.

Ariffin, M.A.M., Bhutta, M.A.R., Hussin, M.W., Tahir, M.M. and Aziah, N. (2013) 'Sulfuric acid resistance of blended ash geopolymer concrete', *Construct Build Mater* 43, 80–86.

Boonserm, K., Sata, V., Pimraksa, K. and Chindaprasirt, P. (2012) 'Improved geopolymerization of bottom ash by incorporating fly ash and using waste gypsum as additive', *Cem Concr Compos* 34, 819–824.

Bouzón, N., Payá, J., Borrachero, M.V., Soriano, L., Tashima, M.M. and Monzó, J. (2014) 'Refluxed rice husk ash/NaOH suspension for preparing alkali activated binders', *Mater Lett* 115, 72–74.

Buchwald, A. and Schulz, M. (2005) 'Alkali-activated binders by use of industrial by-products', *Cem Concr Res* 35, 968–973.

Cabrera-Fuentes, A.B., Fernández-Jiménez, A. and Palomo, A. (2011) 'Alkaline activation of blended fly ash and cement kiln dust', *Proceedings of the 13th International Congress on the Chemistry of Cement,* 212–218.

Carvalho, J., Carvalho, P., Pinto, A.T. and Labrincha, J.A. (2008) 'Activation of mixtures of natural clay and glass cullet rejects', *Clay Miner* 43, 657–667.

Castaldelli, V.N., Akasaki, J.L., Melges, J.L.P., Tashima, M.M., Soriano, L., Borrachero, M.V., Monzó, J. and Payá, J. (2013) 'Use of slag/sugar cane bagasse ash (SCBA) blends in the production of alkali-activated materials', *Materials* 6, 3108–3127.

Castaldelli, V.N., Tashima, M.M., Melges, J.L., Akasaki, J.L., Monzó, J., Borrachero, M.V., Soriano, L. and Payá, J. (2014) 'Preliminary studies on the use of sugar cane bagasse ash (SCBA) in the manufacture of alkali activated binders', *Key Eng Mater* 600, 689–698.

Castro-Gomes, J.P., Silva, A.P., Cano, R.P., Durán Suarez, J. and Albuquerque, A. (2012) 'Potential for reuse of tungsten mining waste-rock in technical-artistic value added products', *J Clean Product* 25, 34–41.

Chen, C., Li, Q., Shen, L. and Zhai, J. (2012) 'Feasibility of manufacturing geopolymer bricks using circulating fluidized bed combustion bottom ash', *Environ Technol* 33, 1313–1321.

Chen, J., Huang, J. and Chang Y. (2009) 'A preliminary study of reservoir sludge as a raw material of inorganic polymers', *Cons Build Mater* 23, 3264–3269.

Cheriaf, M., Rocha, J.C. and Péra, J. (1999) 'Pozzolanic properties of pulverized coal combustion bottom ash', *Cem Concr Res* 29, 1387–1391.

Chindaprasirt, P. and Rattanasak, U. (2010) 'Utilization of blended fluidized bed combustion (FBC) ash and pulverized coal combustion (PCC) fly ash in geopolymer', *Waste Manage* 30, 667–672.

Chindaprasirt, P., Jaturapitakkul, C., Chalee, W. and Rattanasak, U. (2009) 'Comparative study on the characteristics of fly ash and bottom ash geopolymers', *Waste Manage* 29, 539–543.

Chindaprasirt, P., Thaiwitcharoen, S., Kaewpirom, S. and Rattanasak, U. (2013) 'Controlling ettringite formation in FBC fly ash geopolymer concrete', *Cem Concr Compos* 41, 24–28.

Chotetanorm, C., Chindaprasirt, P., Sata, V., Rukzon, S. and Sathonsaowaphak, A. (2013) 'High-calcium bottom ash geopolymer: sorptivity, pore size, and resistance to sodium sulfate attack', *J Mater Civ Eng* 25, 105–111.

Cyr, M., Idir, R. and Poinot, T. (2012) 'Properties of geopolymer mortars made of glass cullet', *J Mater Sci* 47, 2782–2797.

Detphan, S. and Chindaprasirt, P. (2009) 'Preparation of fly ash and rice husk ash geopolymer', *Int J Miner Metall Mater* 16, 720–726.

Flatt, R.J., Roussel, N. and Cheeseman, C.R. (2012) 'Concrete: an eco-material that needs to be improved', *J Eur Ceram Soc* 32, 2787–2798.

Giannopoulou, I., Dimas, D., Maragkos, I. and Panias, D. (2009) 'Utilization of metallurgical solid by-products for the development of inorganic polymeric construction materials', *Global Nest J* 11, 127–136.

Gluth, G.J.G., Lehmann, C., Rübner, K. and Kühne, H.C. (2013) 'Geopolymerization of silica residue from waste treatment of chlorosilane production', *Mater Struct* 46, 1291–1298.

Guo, X., Shi, H. and Dick, W.A. (2013) 'Utilization of thermally treated flue gas desulfurization (FGD) gypsum and class-C fly ash (CFA) to prepare CFA-based geopolymer', *J Wuhan Univ Technol*, 132–138.

Hao, H., Lin, K., Wang, D., Chao, S., Shiu, H., Cheng, T. and Hwang, C. (2013) 'Utilization of solar panel waste glass for metakaolinite-based geopolymer synthesis', *Environ Prog Sust Ener* 32, 797–803.

He, J., Jie, Y., Zhang, J., Yu, Y. and Zhang, G. (2013) 'Synthesis and characterization of red mud and rice husk ash-based geopolymer composites', *Cem Concr Compos* 37, 108–118.

Idir, R., Cyr, M., Poinot, T. and Khelil, N. (2011) 'Properties of geopolymer mortars made of glass cullet', *Proceedings of the 13th International Congress on the Chemistry of Cement*, 451–457.

Ismail, M., Yusuf, T.O., Noruzman, A.H. and Hassan, I.O. (2013) 'Early strength characteristics of palm oil fuel ash and metakaolin blended geopolymer mortar', *Adv Sci Tech* 690–693, 1045–1048.

Kalinkin, A.M., Kumar, S., Gurevich, B.I., Alex, T.C., Kalinkina, E.V., Tyukavkina, V.V., Kalinnikov, V.T. and Kumar, R. (2012) 'Geopolymerization behavior of Cu–Ni slag mechanically activated in air and in CO_2 atmosphere', *Int J Miner Process* 112–113, 101–106.

Karim, M.R., Zain, M.F.M., Jamil, M. and Lai, F.C. (2013) 'Fabrication of a non-cement binder using slag, palm oil fuel ash and rice husk ash with sodium hydroxide', *Constr Build Mater* 49, 894–902.

Khater, H.M. (2012) 'Effect of calcium on geopolymerization of aluminosilicate wastes', *J Mater Civ Eng* 24, 92–101.

Kibert, C.J. (2000) 'Deconstruction as an essential component of sustainable construction', *Proceedings of the Second Southern African Conference on Sustainable Development in the Built Environment*, 1–5.

Komnitsas, K. and Zaharaki, D. (2007) 'Geopolymerisation: a review and prospects for the minerals industry', *Miner Eng* 20, 1261–1277.

Komnitsas, K., Zaharaki, D. and Perdikatsis, V. (2007) 'Geopolymerisation of low calcium ferronickel slags', *J Mater Sci* 42, 3073–3082.

Komnitsas, K., Zaharaki, D., and Perdikatsis, V. (2009) 'Effect of synthesis parameters on the compressive strength of low-calcium ferronickel slag inorganic polymers', *J Hazard Mater* 161, 760–768.

Kourti, I., Rani, D.A., Deegan, D., Cheeseman, C.R. and Boccaccini, A.R. (2010a) 'Development of geopolymers from plasma vitrified air pollution control *residues* from energy from waste plants', in Singh, D., Zhu, D. and Zhou, Y. (eds) *Design, Development, and Applications of engineering ceramics and composites*, New York: John Wilky & Sons, 297–304.

Kourti, I., Rani, D.A., Deegan, D., Boccaccini, A.R. and Cheeseman, C.R. (2010b) 'Production of geopolymers using glass produced from DC plasma treatment of air pollution control (APC) residues', *J Hazar Mater* 176, 704–709.

Kourti, I., Rani, A.D., Guerrero, A., Deegan, D., Boccaccini, A.R. and Cheeseman, C.R. (2011a) 'Geopolymers prepared from DC plasma treated air pollution control (APC) residues glass: properties and characterization of the binder phase', *J Hazar Mater* 196, 86–92.

Kourti, I., Rani, A.D., Boccaccini, A.R. and Cheeseman, C.R. (2011b) 'Geopolymers from DC plasma-treated air pollution control residues, metakaolin and granulated blast furnace slag', *J Mater Civ Eng* 23, 735–740.

Kunal, Siddique, R. and Rajor, A. (2012) 'Use of cement kiln dust in cement concrete and its leachate characteristics', *Resour Conserv Recyl* 61, 59–68.

Lampris, C., Lupo, R. and Cheeseman, C.R. (2009) 'Geopolymerisation of silt generated from construction and demolition waste washing plants', *Waste Manage* 29, 368–373.

Lancellotti, I., Ponzoni, C., Barbieri, L. and Leonelli, C. (2013) 'Alkali activation processes for incinerator residues management', *Waste Manage* 33, 1740–1749.

Majidi, B. (2009) 'Geopolymer technology, from fundamentals to advanced applications: a review', *Mater Tech* 24, 79–87.

Maragkos, I., Giannopoulou, I. and Panias, D. (2009) 'Synthesis of ferronickel slag-based geopolymers', *Miner Eng* 22, 196–203.

Maslehuddin, M., Al-Moudi, O.S.B., Shameem, M., Rehman, M.K. and Ibrahim, M. (2008) 'Usage of cement kiln dust in cement products – research review and preliminary investigations', *Construct Build Mater* 22, 2369–2375.

Mejía, J.M., Mejía de Gutiérrez, R. and Puertas, F. (2013) 'Rice husk ash as a source of silica in alkali-activated fly ash and granulated blast furnace slag systems', *Mater Constr* 63, 361–375.

Nazari, A., Bagheri, A. and Riahi, S. (2011) 'Properties of geopolymer with seeded fly ash and rice husk bark ash', *Mater Sci Eng A* 528, 7395–7401.

Nazari, A., Riahi, S. and Bagheri, A. (2012) 'Designing water resistant lightweight geopolymers produced from waste materials', *Mater Des* 35, 296–302.

Onisei, S., Pontikes, Y., van Gerven, T., Angelopoulos, G.N., Veleae, T., Predicae, V. and Moldovana, P. (2012) 'Synthesis of inorganic polymers using fly ash and primary lead slag', *J Hazard Mater* 205–206, 101–110.

Pacheco-Torgal, F. and Jalali, S. (2010) 'Reusing ceramic wastes in concrete', *Construct Build Mater* 24, 832–838.

Pacheco-Torgal, F., Castro-Gomes, J. and Jalali, S. (2008a) 'Alkali-activated binders: a review. Part 1: Historical background, terminology, reaction mechanisms and hydration products', *Construct Build Mater* 22, 1305–1314.

Pacheco-Torgal, F., Castro-Gomes, J. and Jalali, S. (2008b) 'Alkali-activated binders: a review. Part 2: About materials and binders manufacture', *Construct Build Mater* 22, 1315–1322.

Pacheco-Torgal, F., Castro-Gomes, J.P. and Jalali, S. (2008c) 'Investigations on mix design of tungsten mine waste geopolymeric binder', *Construct Build Mater* 22, 1939–1949.

Pacheco-Torgal, F., Castro-Gomes, J.P. and Jalali, S. (2008d) 'Properties of tungsten mine waste geopolymeric binder', *Construct Build Mater* 22, 1201–1211.

Pacheco-Torgal, F., Castro-Gomes, J.P. and Jalali, S. (2008e) 'Investigations of tungsten mine waste geopolymeric binder: strength and microstructure', *Construct Build Mater* 22, 2212–2219.

Pacheco-Torgal, F., Castro-Gomes, J.P. and Jalali, S. (2008f) 'Adhesion characterization of tungsten mine waste geopolymeric binder: influence of OPC concrete substrate surface treatment', *Construct Build Mater* 22, 154–161.

Pacheco-Torgal, F., Castro-Gomes, J.P. and Jalali, S. (2009) 'Tungsten mine waste geopolymeric binder: preliminary hydration products investigations', *Construct Build Mater* 23, 200–209.

Pacheco-Torgal, F., Castro-Gomes, J.P. and Jalali, S. (2010) 'Durability and environmental performance of alkali-activated tungsten mine waste mud mortars', *J Mater Civ Eng* 22, 897–904.

Pacheco-Torgal, F., Tam, V., Labrincha, J., Ding, Y. and de Brito, J. (2013) *Handbook of Recycled Concrete and Demolition Waste*, Cambridge: Woodhead Publishing.

Payá, J., Monzó, J., Borrachero, M.V. and Velázquez, S. (2003a) 'Evaluation of the pozzolanic activity of fluid catalytic cracking catalyst residue (FC3R). Thermogravimetric analysis studies on FC3R-Portland cement pastes', *Cem Concr Res* 33, 603–609.

Payá, J., Monzó, J., Borrachero, M.V., Velázquez, S. and Bonilla, M. (2003b) 'Determination

of the pozzolanic activity of fluid catalytic cracking residue: thermogravimetric analysis studies on FC3R-lime pastes', *Cem Concr Res* 33, 1085–1091.

Payá, J., Monzó, J. and Borrachero, M.V. (2010) 'Outstanding aspects on the use of rice husk ash and similar agrowastes in the preparation of binders', *Proceedings of the 1st Pro-Africa Conference: Non-conventional Building Materials Based on Agroindustrial Wastes, Pirassununga, Brazil*.

Payá, J., Borrachero, M.V., Monzó, J., Soriano, L. and Tashima, M.M. (2012) 'A new geopolymeric binder from hydrated-carbonated cement', *Mater Lett* 74, 223–225.

Peethamparan, S., Olek, J. and Lovell, J. (2008) 'Influence of chemical and physical characteristics of cement kiln dusts (CKDs) on their hydration behavior and potential suitability for soil stabilization', *Cem Concr Res* 38, 803–815.

Pimraksa, K., Chindaprasirt, P., Rungchet, A., Sagoe-Crentsil, K. and Sato, T. (2011) 'Lightweight geopolymer made of highly porous siliceous materials with various Na_2O/Al_2O_3 and SiO_2/Al_2O_3 ratios', *Mater Sci Eng A* 528, 6616–6623.

Pontikes, Y., Machiels, L., Onisei, S., Pandelaers, L., Geysen, D., Jones, P.T. and Blanpain, B. (2013) 'Slags with a high Al and Fe content as precursors for inorganic polymers', *Appl Clay Sci* 73, 93–102.

Provis, J.L. and van Deventer, J.S.J. (2009) *Geopolymers: Structure, Processing, Properties and Industrial Applications*, Cambridge: Woodhead Publishing.

Puertas, F., Barba, A., Gazulla, M.F., Gómez, M.P., Palacios, M. and Martínez-Ramírez, S. (2006) 'Ceramic wastes as raw materials in Portland cement clinker fabrication: characterization and alkaline activation', *Mater Const* 56, 73–84.

Rajamma, R., Labrincha, J.A. and Ferreira, V.M. (2012) 'Alkali activation of biomass fly ash-metakaolin blends', *Fuel* 98, 265–271.

Rattanasak, U., Chindaprasirt, P. and Suwanvitaya, P. (2010) 'Development of high volume rice husk ash alumino silicate composites', *Int J Miner Metall Mater* 17, 654–659.

Redden, R. and Neithalath, N. (2014) 'Microstructure, strength, and moisture stability of alkali activated glass powder-based binders', *Cem Concr Compos* 45, 46–56.

Reig, L., Tashima, M.M., Borrachero, M.V., Monzó, J., Cheeseman, C.R. and Payá, J. (2013a) 'Properties and microstructure of alkali-activated red clay brick waste', *Const Build Mater* 43, 98–106.

Reig, L., Tashima, M.M., Borrachero, M.V., Monzó, J. and Payá, J. (2013b) 'Alkaline activation of ceramic waste materials', *Waste Biomass Valor* 4, 729–736.

Riahi, S., Nazari, A., Zaare, D., Khalaj, G., Bohlooli, H. and Kaykha, M.M. (2012) 'Compressive strength of ash-based geopolymers at early ages designed by Taguchi method', *Mater Des* 37, 443–449.

Rodríguez, E.D., Bernal, S.A., Provis, J.L., Gehman, J.D., Monzó, J., Payá, J. and Borrachero, M.V. (2013) 'Geopolymers based on spent catalyst residue from a fluid catalytic cracking (FCC) process', *Fuel* 109, 493–502.

Rüscher, C.H., Mielcarek, E.M., Wongpa, J. and Jaturapitakkul, C. (2011) 'Silicate-, aluminosilicate and calciumsilicate gels for building materials: chemical and mechanical properties during ageing', *Eur J Mineral* 23, 111–124.

Santa, R.A.A.B., Bernardin, A.M., Riella, H.G. and Kuhnen, N.C. (2013) 'Geopolymer synthesized from bottom coal ash and calcined paper sludge', *J Clean Prod* 57, 302–307.

Sata, V., Sathonsaowaphak, A. and Chindaprasirt, P. (2012) 'Resistance of lignite bottom ash geopolymer mortar to sulfate and sulfuric acid attack', *Cem Concr Compos* 34, 700–718.

Sathonsaowaphak, A., Chindaprasirt, P. and Pimraksa, K. (2009) 'Workability and strength of lignite bottom ash geopolymer mortar', *J Hazard Mater* 168, 44–50.

Schwartz, N. and Neithalath, N. (2008) 'Influence of a fine glass powder on cement hydration: comparison to fly ash and modeling the degree of hydration', *Cem Concr Res* 38, 429–436.

Schwartz, N., Cam, H. and Neithalath, N. (2008) 'Influence of a fine glass powder on the durability characteristics of concrete and its comparison to fly ash', *Cem Concr Compos* 30, 486–496.

Shi, C., Krivenko, P.V. and Roy, D. (2006) *Alkali-Activated Cements and Concretes*, London: Taylor & Francis.

Shi, C., Fernández-Jiménez, A. and Palomo, A. (2011) 'New cements for the 21st century: the pursuit of an alternative to Portland cement', *Cem Concr Res* 41, 750–763.

Siddique, R. (2006) 'Utilization of cement kiln dust (CKD) in cement mortar and concrete – an overview', *Resour Conserv Recyl* 48, 315–338.

Silva, I., Castro-Gomes, J.P. and Albuquerque, A. (2012) 'Effect of immersion in water partially alkali-activated materials obtained of tungsten mine waste mud', *Construct Build Mater* 35, 117–124.

Slavik, R., Bednarik, V., Vondruska, M. and Menec, A. (2008) 'Preparation of geopolymer from fluidized bed combustion bottom ash', *J Mater Process Tech* 200, 265–270.

Songpiriyakij, S., Kubprasit, T., Jaturapitakkul, C. and Chindaprasirt, P. (2010) 'Compressive strength and degree of reaction of biomass- and fly ash-based geopolymer', *Constr Build Mater* 24, 236–240.

Stock, D. (2011) 'World production and consumption of ceramic tiles', *Tiles Today* 73, 50–58.

Sun, Z., Cui, H., An, H., Tao, D., Xu, Y., Zhai, J. and Li, Q. (2013) 'Synthesis and thermal behavior of geopolymer-type material from waste ceramic', *Const Build Mater* 49, 281–287.

Tashima, M.M., Soriano, L., Borrachero, M.V., Monzó, J., Cheeseman, C.R. and Payá, J. (2012a) 'Alkali activation of vitreous calcium aluminosilicate derived from glass fiber waste', *J Sust Bas Cem Mat* 1, 83–93.

Tashima, M.M., Akasaki, J.L., Castaldelli, V.N., Soriano, L., Monzó, J., Payá, J. and Borrachero, M.V. (2012b) 'New geopolymeric binder based on fluid catalytic cracking catalyst residue (FCC)', *Mater Lett* 80, 50–52.

Tashima, M.M., Soriano, L., Borrachero, M.V., Monzó, J. and Payá, J. (2013a) 'Effect of curing time on microstructure and mechanical strength development of alkali activated binders based on vitreous calcium aluminosilicate (VCAS)', *Bull Mater Sci* 36, 245–249.

Tashima, M.M., Soriano, L., Monzó, J., Borrachero, M.V. and Payá, J. (2013b) 'Novel geopolymeric material cured at room temperature', *Adv Appl Cer* 112, 179–183.

Tashima, M.M., Akasaki, J.L., Melges, J.L.P., Soriano, L., Monzó, J., Payá, J. and Borrachero, M.V. (2013c) 'Alkali activated materials based on fluid catalytic cracking catalyst residue (FCC): influence of SiO_2/Na_2O and H_2O/FCC ratio on mechanical strength and microstructure', *Fuel* 108, 833–839.

Tashima, M.M., Soriano, L., Akasaki, J.L., Monzó, J., Payá, J. and Borrachero, M.V. (2014) 'Spent FCC catalyst for preparing alkali-activated binders: an opportunity for a high-degree valorization', *Key Eng Mater* 600, 709–716.

Tippayasam, C., Boonsalee, S., Sajjavanich, S., Ponzoni, C., Kamseu, E. and Chaysuwan, D. (2010) 'Geopolymer development by powders of metakaolin and wastes in Thailand', *Adv Sci Tech* 69, 63–68.

Topçu, I.B. and Toprak, M.U. (2011) 'Properties of geopolymer from circulating fluidized bed combustion coal bottom ash', *Mat Sci Eng A – Struct* 528, 1472–1477.

Torres, J.J., Palacios, M., Hellouin, M. and Puertas, F. (2009) 'Alkaline chemical activation of

urban glass wastes to produce cementitious materials', *1st Spanish National Conference on Advances in Materials Recycling and Eco-Energy*, 111–114.

Turner, L.K. and Collins, F.G. (2013) 'Carbon dioxide equivalent (CO_2-e) emissions: a comparison between geopolymer and OPC cement concrete', *Constr Build Mater* 43, 125–130.

Van Deventer, J.S.J., Provis, J.L., Duxson, P. and Brice D.G. (2010) 'Chemical research and climate change as drivers in the commercial adoption of alkali activated materials', *Waste Biomass Valor* 1, 145–155.

Wang, K., Shah, S. and Mishulovich, A. (2004) 'Effects of curing temperature and NaOH addition on hydration and strength development of clinker-free CKD-fly ash binders', *Cem Concr Res* 34, 299–309.

Weil, M., Dombroswski, K. and Buchwald, A. (2009) 'Life-cycle analysis of geopolymers', in Provis, J.L. and van Deventer, J.S.J. (eds), *Geopolymers: Structure, Processing, Properties and Industrial Applications*, Cambridge: Woodhead Publishing, 194–210.

Xu, H., Li, Q., Shen, L., Wang, W. and Zhai, J. (2010) 'Synthesis of thermostable geopolymer from circulating fluidized bed combustion (CFBC) bottom ashes', *J Hazard Mater* 175, 198–204.

Yamaguchi, N. and Ikeda, K. (2010) 'Preparation of geopolymeric materials from sewage sludge slag with special emphasis to the matrix compositions', *J Ceram Soc Japan* 118, 107–112.

Yamaguchi, N., Nagaishi, M., Kisu, K., Nakamura, Y. and Ikeda, K. (2013) 'Preparation of monolithic geopolymer materials from urban waste incineration slags', *J Ceram Soc Japan* 121, 847–854.

Yan, S. and Sagoe-Crentsil, K. (2012) 'Properties of wastepaper sludge in geopolymer mortars for masonry applications', *J Environ Manage* 112, 27–32.

Yang, K., Lo, C. and Huang J. (2013) 'Production and properties of foamed reservoir sludge inorganic polymer', *Cem Concr Compos* 38, 50–56.

Yang, Z.X., Ha, N.R., Jang, M.S. and Hwang, K.H. (2009a) 'Geopolymer concrete fabricated by waste concrete sludge with silica fume', *Mater Sci Forum* 620–622, 791–794.

Yang, Z.X., Ha, N.R., Hwang, K.H. and Lee, J.K. (2009b) 'A study of the performance of a concrete sludge-based geopolymer', *J Ceram Process Res* 10, s72–s74.

Yang, Z.X., Ha, N.R., Jang, M.S., Hwang, K.H. and Lee, J.K. (2009c) 'The effect of SiO_2 on the performance of inorganic sludge-based structural concretes', *J Ceram Process Res* 10, 266–268.

Yusuf, M.O., Johari, M.A.M., Ahmad, Z.A. and Maslehuddin, M. (2014) 'Evolution of alkaline activated ground blast furnace-ultrafine palm oil fuel ash based concrete', *Mater Des* 55, 387–393.

Zhang, L., Ahmari, S. and Zhang, J. (2011) 'Synthesis and characterization of fly ash modified mine tailings-based geopolymers', *Construct Build Mater* 25, 3773–3781.

Reuse of recycled aggregate in the production of alkali-activated concrete

19

P. Chindaprasirt[1], *T. Cao*[2]
[1]Khon Kaen University, Khon Kaen, Thailand; [2]Surface Design Consulting Pty Ltd, Sydney, NSW, Australia

19.1 Introduction

Waste arising from construction and demolition constitutes one of the largest waste streams in many countries (Limbachiya *et al*., 2004). It has been estimated that the global concrete industry consumes approximately 10 billion tons of sand and rocks (2002 data) and produces over 1 billion tons of construction and demolition waste annually (Mehta, 2002). About 300 million tons of construction and demolition wastes are generated in the US (Nassar and Soroushian, 2012; CSI, 2012) whereas 200 million tons are generated in China (Xiao *et al*., 2012), 77 million tons in Japan (CSI, 2012) and 450–510 million tons in Europe (Matias *et al*., 2013; CSI, 2012) annually. Disposal of construction and demolition waste is therefore a major issue in terms of social, economic and environmental concerns. The recycling of construction and demolition waste into new engineering construction, including its use as aggregate in new concrete, is now considered an integral part of building green with concrete. The LEED (2000) rating system devised by the US Green Building Council, for example, awards points for certification for using post-consumer recycled materials such as construction and demolition waste in new construction.

It must be noted that aggregates are the major component of concrete by volume; however, they are inherently low carbon products. UK data suggest that the use of recycled aggregate in structural concrete can lead to reduction in ECO_2 (equivalent carbon dioxide) only when the source is local to minimize the impact of transportation (MPA, 2011; Thomas *et al*., 2009). Besides ECO_2, the factors to balance are resource depletion and implications on mix design. The impact on reducing depletion of natural resources would be more significant when construction and demolition waste can be used in large quantities/percentages to replace natural aggregates in concrete. The fact that the EU has set an ambitious target of 70% recycling target for 2020 (Saez *et al*., 2011; del Rio Merino *et al*., 2011, Pacheco-Torgal, 2013) is an indication of the importance of this issue.

When used in normal concrete, the performance of recycled concrete aggregate and hence its content in new concrete is limited by the quantity and properties of the cement paste adhered to the recycled aggregate particles (Hansen and Narud, 1989; Tavakoli and Soroushian, 1996b). Stringent selection of recycled concrete aggregate,

Handbook of Alkali-activated Cements, Mortars and Concretes. http://dx.doi.org/10.1533/9781782422884.4.519

particularly in regard to the qualities of original concrete, would be necessary for their use at high percentage. This is not practical in all cases and is impossible for recycled aggregate containing a significant amount of material other than crushed concrete.

Alkali-activated cements–slag, metakaolin and fly ash-based alkali-activated cements are the types of binders attracting a high level of interest worldwide in recent years based on the number of published technical and scientific papers and patents. Alkali-activated cement can be used to replace Portland cement in making concrete and other cementitious products due to their advantages of low energy cost, high strength and excellent durability. The combined use of alkali-activated cement and recycled concrete aggregate in making concrete is of great interest since the combination could potentially lead to the maximum utilization of recycled concrete aggregate without loss of engineering properties. Work in this area is somewhat limited. This section provides some descriptions of recycled aggregate, recycled aggregate concrete and the alkali-activated recycled aggregate concrete.

19.2 A brief discussion on recycled aggregates

Recycled aggregate is defined as aggregate resulting from the processing of inorganic or mineral material previously used in construction (BS EN 12620, 2013; MPA, 2013). When consisting mainly of crushed concrete, it may be classified as recycled concrete aggregate (RCA). Information on processing old concrete into RCA can readily be found in the literature (ACI 555R-01, 2001). When it contains substantial quantities of materials other than concrete, it is classified as general recycled aggregate (RA).

Recycled aggregate and recycled concrete aggregate are covered in some national standards for concrete such as BS EN 12620 (2013). In this standard, coarse recycled aggregates are classified according to the proportions of constituent materials including amounts of concrete/concrete products/mortar/concrete masonry units; unbound aggregate/natural stone/hydraulically bound aggregate; clay masonry units/calcium silicate masonry units/aerated non-floating concrete); bituminous materials; glass; floating material in volume; and other materials including gypsum plaster; clay and soil, metals; and non-floating wood, plastic and rubber.

In Australia, recycled aggregates are classified into the following groups (CCAA, 2008):

1. Recycled concrete aggregate (RCA) which is produced by crushing sound, clean demolition waste of at least 95% by weight of concrete and having a total contaminant level typically lower than 1% of bulk mass.
2. Recycled concrete and masonry (RCM) which is graded aggregate produced from sorted and clean waste concrete and masonry typically for road sub-base applications.
3. Reclaimed aggregate which is aggregate reclaimed from concrete returned to a batching plant by separating the aggregates from the water–cement slurry.
4. Reclaimed asphalt pavement (RAP) which is a reuse of old asphalt concretes as the aggregate base for new asphaltic concrete.

5. Reclaimed asphalt aggregate (RAA) which is a product of a specialized method to produce reclaimed coarse aggregate and recycled asphalt granules from waste asphalt concrete and concrete dust.
6. Glass cullet sand.
7. Scrap tyre chips and crumb rubber aggregate.
8. Used foundry sand or spent foundry sand.

19.2.1 Recycled concrete aggregate (RCA)

Coarse RCA complies to the requirements of maximum 5% masonry content, 5% fine materials, 0.5% lightweight material, 5% asphalt, 1% foreign material and 1% acid soluble sulfate, and is suitable for use in concrete as per BS 8500-2 (2006). In designated concrete RC20/25 to RC40/50, RCA can automatically be used at 20% of coarse aggregate (MPA, 2011). For designated concrete GEN0(C6/8) to GEN3(C16/20), there are no general restrictions on the proportion of RCA or RA as long as aggregate durability criteria are met (MPA, 2011). While it is indicated in BS 8500-2 (2006) that fine RCA and fine RA may be suitable for use in concrete, their use is left to the project specification which can take account of the particular source of RCA or RA.

The Australian Standard HB 155 (2002) suggests two classes of aggregate with Class 1A-RCA containing less than 0.5% brick content. The CCAA (2008) indicates that this class of RCA can be used to replace natural aggregate to 30% in concrete for sidewalks, kerbs and gutters and in structural concrete (with mix adjustment) resulting in inferior permeability and shrinkage properties. Published literature indicates that RCA has higher water absorption rates than virgin aggregates due to the high volume fraction of cement mortar adhering to the aggregate particles (Hansen, 1986; Kasami *et al*., 1998; Shayan and Xu, 2003). The presence of the adherent mortar and brick content in the RCA usually results in a lower relative density of RCA (5–10% lower). Abrasion loss of RCA tends to be higher than virgin aggregates. However, it is noted in ACI 555R-01 (2001) that most RCA will meet the abrasion loss requirements specified in ASTM C33-13 (2013).

In regard to the influence of RCA on fresh concrete properties (Yang *et al*., 2008; Rashwan and Abourizk, 1997), it has been noted that workability decreases and water demand increases as the RCA content increases. This has been attributed to the inclusion of fine materials in RCA. There appears to be an increase in entrapped air in concrete containing RCA. Furthermore, finishability of concrete tends to be poorer with RCA.

In regard to the hardened concrete properties (De Brito and Saikia, 2013; Hansen, 2004; Khatib, 2005), it is known that concrete compressive strength decreases between 5 and 25% when coarse RCA is used and between 15 and 40% when both coarse and fine RCA are used. Flexural strength is also adversely affected, especially when fine RCA is incorporated in the concrete (Sheen *et al*., 2013). Properties affecting durability of concrete (Gomes and Brito, 2009; Thomas *et al*., 2013; Kou and Poon, 2013; Salem *et al*., 2003) such as chloride resistance, gas permeability, water sorptivity and freeze-thaw resistance are generally adversely affected with increases in the

quantities of RCA in the concrete mix. Creep and shrinkage of concrete containing RCA (Tavakoli and Soroushian, 1996a; Domingo-Cabo *et al*., 2009; Rao *et al*., 2007) are also higher and are related to the content of paste or mortar in RCA.

19.2.2 Recycled concrete and masonry (RCM)

Recycled concrete and masonry (RCM) aggregate can be described as graded aggregate produced from sorted and clean waste concrete and masonry. The RCM material may contain brick, gravel crush rock or other forms of stony materials as blended materials. Class 1B-RCA as per HB 155 (2002) is an RCM aggregate. Class 1B-RCA is essentially Class 1A-RCA blended with no more than 30% crushed brick. This type of material is considered suitable for granular base course and sub-base material (CCAA, 2008; Cameron *et al*., 2012; Azam and Cameron, 2013). While it has been established that concrete can be produced successfully with RCM, practical use of RCM as coarse aggregate in concrete is somewhat limited due to high and unpredictable water demand, poorer workability, lower mechanical properties and higher shrinkage associated with high brick content (Azam and Cameron, 2013; Debieb and Kenai, 2008; Khalaf and De Venny, 2004; Correia *et al*., 2006). However, in recent years, it has been established that RCM consists of two main types of materials, namely concrete block and clay brick type masonry. It is therefore expected that information regarding the use of RCM should be better organized and compiled which in turn will foster the better use of recycled aggregate.

19.2.3 Recycled aggregate from other materials

Glass cullet has been used in different construction applications including cement replacement, aggregate replacement in concrete, road beds, pavement, trench fill, drainage medium, etc.; and in general use applications including abrasives, fluxes/additives, manufacturing of fiberglass insulation and foam insulation. When used as sand replacement, there is some indication that there can be a noticeable reduction in compressive strength (CCAA, 2008). This is, however, not consistently observed (Oliveira *et al*., 2008; Sangha *et al*., 2004; Limbachiya, 2009; Taha and Nounu, 2009). The main issue with waste glass sand in concrete is the risk of potential alkali-silica reaction. This risk can be effectively managed using blended cement (Du and Tan, 2013; Topçu *et al*., 2008) containing fly ash and/or ground granulated blast furnace slag.

Scrap tire chips and crumb rubber aggregate have also been used in mortars and concretes. Rubber concrete has been recommended for applications where vibration damping or where resistance to impact or blast or where high plastic energy absorption is required. Concrete with rubber aggregate has also been recommended for applications such as trench filling and pipe bedding, low strength flowable concrete, nailing concrete and stone backing. A summary of properties of concrete containing rubber aggregate can be found in the literature (Siddique, 2008).

19.3 Properties of alkali-activated recycled aggregate concrete

It has been noted in the literature that in conventional concrete, aggregate forms a rigid skeleton of granular elements which are responsible for compressive strength whereas in geopolymers most of the compressive strength is related to the matrix characteristics (Pacheco-Torgal *et al*., 2012c). Alkali-activated cement/geopolymer is also known to be a good material for immobilizing a wide range of harmful elements (Hermann *et al*., 1999) and is less susceptible to alkali-silica reaction induced expansion (García-Lodeiro *et al*., 2007). These characteristics suggest that alkali-activated cement concrete is more suitable for use with recycled aggregates. Alkali-activated cement would lessen the impact of recycled aggregate and the problem of impurities in recycled aggregates on the hardened properties and durability of concrete. It has been indicated that concrete with 28-day compressive strength of 20–99 MPa can be produced with low grade aggregates including recycled aggregates (Chen *et al*., 2004).

19.3.1 Alkali-activated cement concrete containing RCA

Published results (Shi *et al*., 2012a) on compressive strength development of alkali-activated cement concrete containing recycled aggregate indicate that, similar to the case of normal concrete, the strength of alkali-activated cement concrete reduces with increased recycled aggregate percentage in concrete as shown in Table 19.1. However, high 28-day compressive strengths of 71.5 and 54.5 MPa can still be obtained for mixes with high percentages of recycled aggregate of 50 and 100% with alkali-activated fly ash concrete in comparison to that with normal aggregate. Compressive strength development of alkali-activated fly ash concrete containing RCA as reported by Galvin and Lloyd (2011) also suggests that the incorporation of RCA reduces the strength of concrete but the reduction is at an acceptable level.

Table 19.1 Compressive strength of normal concrete and alkali-activated cement concrete containing recycled aggregate

Concrete	Compressive strength (MPa)									
	3-Day	SD	7-Day	SD	28-Day	SD	60-Day	SD	90-Day	SD
RAC0	22.51	0.13	36.94	0.94	49.98	0.41	51.72	0.67	62.42	0.44
RAC50	22.41	0.19	36.08	0.2	44.9	0.76	46.51	0.64	53.63	0.62
RAC100	22.04	0.38	36.37	0.35	44.58	0.18	45.6	0.7	50.79	0.7
GRC0	74.37	2.31	80.58	1.87	85.66	1.58	86.15	0.9	88.22	1.07
GRC50	61.11	1.81	67.72	0.29	71.59	1.66	71.72	1.57	71.97	1.91
GRC100	47.77	1.27	50.83	0.37	54.66	1.73	54.95	0.97	55.09	1.27

Note: RAC is normal Portland cement concrete with recycled aggregate, GRC is fly ash geopolymer concrete with recycled aggregate. SD is standard deviation.
Source: Reprinted from Shi *et al*., 2012a, Copyright © 2012, with permission from Elsevier.

The 28-day compressive strength of 40% RCA concrete was reduced to 25.5 MPa compared with 33.0 MPa of the control concrete and the 90-day strength of 40% RCA concrete was reduced to 30.0 MPa compared with 35.5 MPa of the control. In other investigations, instead of strength reduction, increase in compressive strength was even observed with increased amount of RCA (Sanusi *et al.*, 2011). This has been attributed to the additional formation of C-S-H from calcium present in the RCA. The acceptable strength values of alkali-activated concrete with RCA allow its use in various construction works and in some structural applications, especially when strength is not the prime concern.

19.3.2 Lightweight alkali-activated concrete containing recycled aggregate

Crushed lightweight aggregate concrete (LWAC) can also be used as an aggregate in concrete (recycled LWAC-aggregate) (European Union – Brite EuRam III, 2000). Crushed waste lightweight concrete block has been used successfully as recycled aggregates for making lightweight alkali-activated concrete using NaOH, sodium silicate and fly ash (Posi *et al.*, 2013) with acceptable 28-day compressive strength of 1.0–16.0 MPa, density of 860–1400 kg/m^3, water absorption of 10–31%, porosity of 12–34%, and modulus of elasticity of 2.9–9.9 GPa. The strength slightly increases with the increase in the amount of fine recycled lightweight aggregate content (reduced recycled coarse aggregate) as shown in Figure 19.1. The fine aggregate

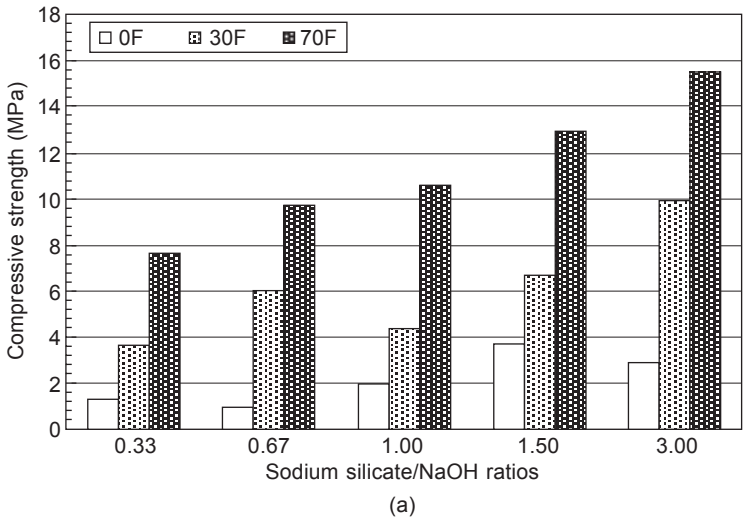

Figure 19.1 Compressive strength of lightweight alkali-activated concrete made with recycled lightweight aggregate from lightweight concrete block (a) with various sodium silicate to NaOH ratios and (b) with various NaOH concentrations (M) (reprinted from Posi *et al.*, 2013, Copyright © 2013, with permission from Elsevier). Note: 0F = 0% fine aggregate, 30F = 30% fine aggregate, 70F = 70% fine aggregate.

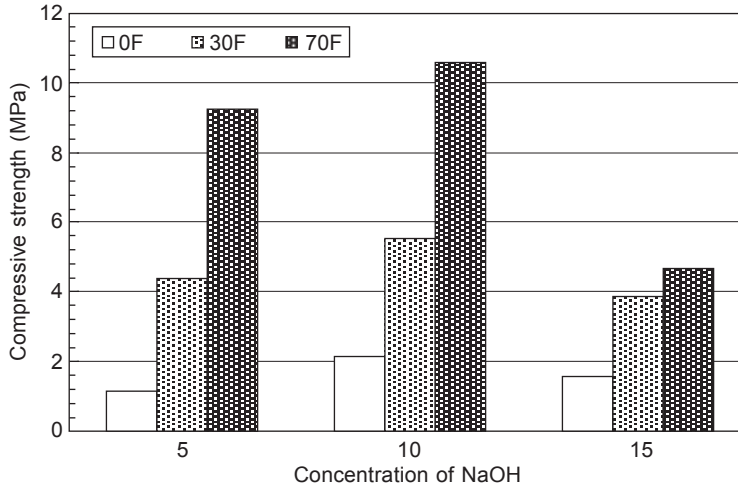

Figure 19.1 Continued

with high surface area offers better bonding between alkali-activated matrix and fine aggregate than that of coarser aggregate, and thus the increase in fine aggregate from 0% to 70% results in concrete with increased strength. Also, the increase in the amount of fine aggregate results in an increase in concrete density due to the higher density of fine recycled lightweight aggregate. Strength development is improved with the increases in sodium silicate content (sodium silicate/NaOH of 0.33–3.0) and curing temperature of 25–60°C with the optimum NaOH concentration of 10 M. These findings are in line with the results reported on the normal Class C fly ash alkali-activated system (Sathonsaowaphak *et al.*, 2009; Chindaprasirt *et al.*, 2007; Somna *et al.*, 2011; Lee and van Deventer, 2002).

19.3.3 Pervious alkali-activated concrete containing recycled aggregates

Alkali-activated fly ash binder has been used for making pervious concrete containing normal aggregate with satisfactory strength (Tho-in *et al.*, 2012). Furthermore, pervious alkali-activated concrete can also be made with RCA and recycled clay brick as coarse aggregates with acceptable properties in comparison to natural coarse aggregates. Sata *et al.* (2013) used 4.5–9.5 mm single-size RCA and recycled clay brick aggregate for making pervious concrete using high-calcium fly ash, sodium silicate and NaOH. Results indicated the normal trend of strength development for normal recycled aggregate, i.e. the strength of concrete reduced with the use of recycled aggregate, which is in line with the published results on normal recycled aggregate concrete (Hansen, 1986) and on pervious recycled aggregate concrete (Tho-in *et al.*, 2012). For mixes with 15 M NaOH, the compressive strengths of

normal aggregate (NA), recycled concrete (RC) aggregate and recycled clay brick (RB) aggregate concretes were 13.6, 10.0 and 4.0 MPa, respectively (Sata *et al*., 2013). This is due to the difference in the strengths of recycled aggregates as can be observed from the fractured surfaces of the concretes shown in Figure 19.2. The

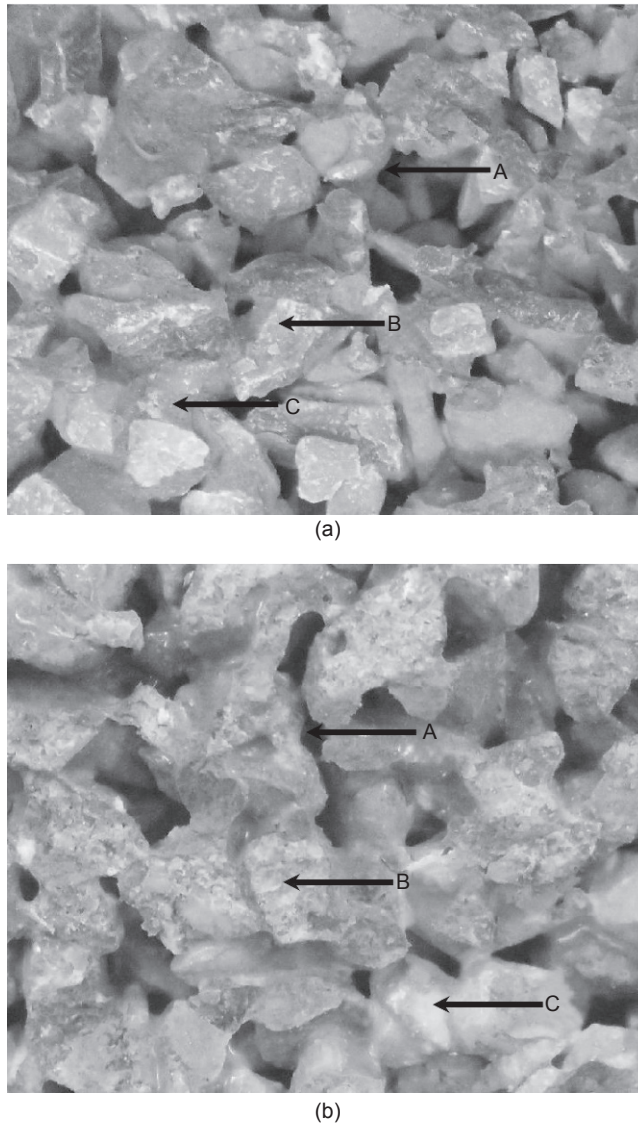

Figure 19.2 Fracture surfaces of alkali-activated pervious concretes: (a) normal aggregate; (b) recycled concrete aggregate; and (c) recycled clay brick aggregate (reprinted from Sata *et al*., 2013, Copyright © 2013, with permission from Elsevier). Note: A = void, B = fractured aggregate, C = alkali activated paste.

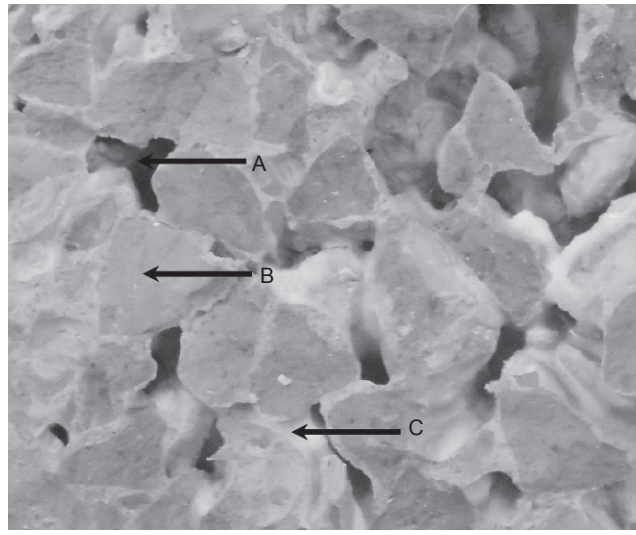

(c)

Figure 19.2 Continued

recycled clay brick aggregate is the weakest and shows the largest fractured surface and is followed in turn by recycled concrete aggregate and normal aggregate. The same authors reported further that the average ratio of splitting tensile to compressive strengths of pervious geopolymer concrete was 14.4%, which was slightly higher than 8–14% for conventional concrete. The high tensile strength ratio is the common feature found and this suggests the better bonding of alkali-activated binders than that of the conventional Portland cement binder system (Shi *et al.*, 2012a).

19.3.4 Controlled low-strength and other recycled alkali-activated concretes

In a study on the utilization of recycled concrete aggregate, Achtemichuk *et al.* (2009) used slag and high calcium fly ash at dosages of 5–30% by weight in combination with recycled concrete aggregate to produce controlled low-strength materials without using Portland cement. The same authors suggested that in addition to hydraulic activity, the pozzolanic reaction of slag and high calcium fly ash was activated by the alkalis and calcium hydroxide presented in the residual paste of the RCA and this resulted in adequate strength development of controlled low-strength materials, especially when slag was used.

The silica and alumina in Portland cement paste can be reused as starting materials for geopolymers (Payá *et al.*, 2012). The authors induced carbonation of hydrated Portland cement to transform C-S-H and C-A-H to silica and alumina gels and then alkali activated with a NaOH/waterglass solution. The geopolymer mortars are mechanically stable with compressive strength over 10 MPa after 65°C curing for 3

days. The result confirms the possibilities for reuse of the cement-rich components of construction and demolition waste.

Recycled materials can also be used as sand replacement in the alkali-activated system. Vavro *et al*. (2011) studied the use of recycled clay brick and recycled concrete block for sand replacement in slag/NaOH/sodium silicate system. The recycled clay brick and concrete block were ground to maximum particle size of 2 mm and used to replace natural sand at 50% and 100% levels. The concrete strength was reduced with the increase in replacement level due to the relatively low strength of fine aggregate from brick and block compared with that of natural sand. The 28-day strength of AAS concretes with 50% clay brick and concrete block were 52.0 and 72.7 MPa and those with 100% clay brick and concrete block were 41.7 and 40.7 MPa compared with 87.8 MPa of AAS concrete with 100% natural sand. The strength of recycled concrete aggregate concrete is greater than that of recycled brick aggregate concrete due to the higher strength of recycled concrete aggregate compared to that of recycled brick aggregate. Although the strength of recycled aggregate concrete is lower, its durability performance in terms of resistance to hydrochloric acid attack, freeze-thaw environment and to water and chemical de-icing agents is acceptable. The same authors suggested that alkali-activated materials containing recycled concrete and recycled brick as fine aggregate have good prospects.

19.4 Other alkali-activated recycled aggregate concrete

19.4.1 Waste glass

Soda-glass cullet powder (Blaine fineness of 1000–4000 cm^2/g) has been used to produce geopolymers (Cyr *et al*., 2012). In contrast to fly ash or metakaolin-based geopolymers, waterglass is not needed for the setting of glass cullet geopolymers. To obtain acceptable mechanical performance, high fineness of glass and temperature in the range of 40–60°C are required for activation using KOH and NaOH. Alkali-activated Class F fly ash cement with glass aggregates has also been studied. The issue of alkali-silica reaction (ASR) induced expansion is not a significant problem with alkali-activated fly ash cement mortar in comparison to the use of glass aggregate in normal mortar and concrete. Concretes made from alkali-activated fly ash with pulverized glass have also been investigated (Berry *et al*., 2011). Outstanding early strength and continued strength gain over a long period as well as good durability characteristics have been observed. An alkali-activated fly ash with glass aggregate called ‘ashcrete’ was also developed by Xi *et al*. (2004). This ashcrete has high strength and develops high early strength which makes it very suitable for the precast concrete industry.

When used in alkali-activated slag using NaOH and NaOH/Na_2CO_3 solutions, glass powder was found to be less effective than ground granulated blast furnace slag with other alkali-activated systems in regard to the strength development of the resultant alkali activated cement (Torres *et al*., 2009). In general, temperature or

mechano-chemical activation, or both, would be needed for the effective re-use of waste glass in alkali-activated cement concrete. The same author, however, reported that it is possible to use up to 50% ground waste glass blended with slag activated with NaOH/Na_2CO_3 solutions cured at a low temperature of 25°C to produce mixes with reasonable compressive strengths.

The use of recycled waste material such as waste glass as sand replacement has also been tried in alkali-activated concrete. Xie *et al*. (2003) studied the use of waste glass/fly ash/sodium silicate concrete. The glass aggregate showed much reduced ASR expansion in the alkali-activated system compared with that of Portland cement mortar where even a small substitution of natural aggregate by waste glass caused severe expansion. The same author reported that even when all natural aggregate is replaced by glass aggregates, the alkali-silica reaction expansion of the waste glass alkali-activated mortar is still within the limits as per ASTM C1260-07 (2007). This indicates that in alkali-activated mortar, waste glass is a safe aggregate in terms of alkali-silica reaction potential for reactive aggregates.

19.4.2 Circulation fluidized bed combustion bottom ash

CFBC (circulation fluidized bed combustion) bottom ash has also been used as a source material for making geopolymer (Chindaprasirt and Rattanasak, 2010; Boonserm *et al*., 2012; Topçu and Toprak, 2011) and also as aggregates (Li *et al*., 2013). When used as aggregate to replace sand (Li *et al*., 2013), the best results of the geopolymer mortar are obtained when the ratio of CFBC bottom ash to fly ash is in the range of 0.75–1.25 with sodium hydroxide and sodium silicate solution at modulus of 1.2. Strengths of 60 MPa and 10 MPa for compressive and flexural strengths, respectively, were achieved and were much higher than geopolymeric mortar made with natural sand aggregates. The mortars showed higher compressive and flexural strengths than those with standard sand due to better bonding and denser microstructures. Microstructure observation by the same authors suggested the improvement in bonding of bottom ash aggregate by reporting that no distinct gap could be identified between bottom ash particle and alkali-activated binder as compared to the observable void at boundaries between sand and alkali-activated binders.

19.4.3 Artificial lightweight aggregate from by-product materials

Procedures and technologies used in the manufacture of alkali-activated cement concrete have also been applied to the production of lightweight aggregate for concrete (Jo *et al*., 2007; Bui *et al*., 2012, 2013) from waste and by-product materials such as fly ash, sewage sludge and waste glass. This is a related recycle aggregate which shared a similar name but is slightly different type of recycled aggregate. This artificial recycled aggregate is normally made from industrial by-products. Jo *et al*. (2007) made artificial recycled lightweight aggregate from alkali-activated fly ash. Fly ash/NaOH/

sodium silicate/MnO_2 paste cured at 50°C produces a high compressive strength of 33.9 MPa. This paste was crushed and used as alkali-activated recycled lightweight aggregate with specific gravity (SSD), water absorption, unit weight, and solid volume percentages of 1.85, 11.8%, 972 kg/m^3 and 58.6%, respectively. Bui *et al*. (2012) also tested artificial recycled aggregate made from industrial by-products, namely, Class F fly ash, ground granulated blast furnace slag and rice husk ash using NaOH and sodium silicate at modulus of 1.5 as activators. The manufactured lightweight aggregate unit weights were 770–1060 kg/m^3. High performance concretes were made with these aggregates with unit weights of 1840–2060 kg/m^3 and 28-day compressive strengths of 14.8–38.1 MPa. Chindaprasirt *et al*. (2009) prepared lightweight aggregate from rice husk ash activated with sodium hydroxide solution and temperature cured to obtain hardened alkali-activated paste which was then crushed and heated to form alkali-activated lightweight aggregate with density of 0.20–0.40 g/cm^3. Two to four present boric acid by weight of RHA was incorporated to this mixture to make the paste stable and not disintegrate in boiling water. As shown in Figure 19.3(a), rice husk ash/10 M NaOH/2% boric acid paste after curing at 115°C contains RHA particles, sodium silicate matrix and some needle-like hydration products. After heating at 500°C, the lightweight alkali-activated rice husk ash aggregate is formed and the texture is quite homogeneous with some pores as shown in Figure 19.3(b). With literature support, it is shown here that the activated recycled aggregates offer a good alternative for the utilization of industrial by-products.

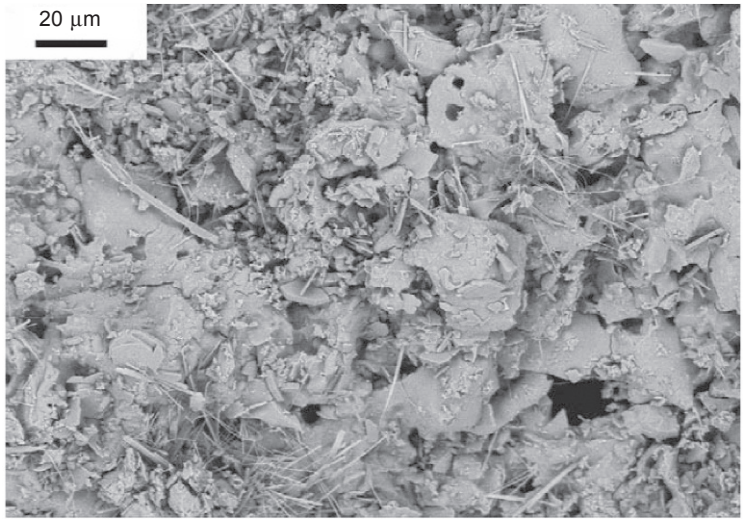

Figure 19.3 Morphology of lightweight aggregate made from rice husk ash/10 M NaOH/2% boric acid: (a) paste cured at 115°C and (b) lightweight aggregate after heating at 500°C (reprinted from Chindaprasirt *et al*., 2009, Copyright © 2009, with permission from Elsevier).

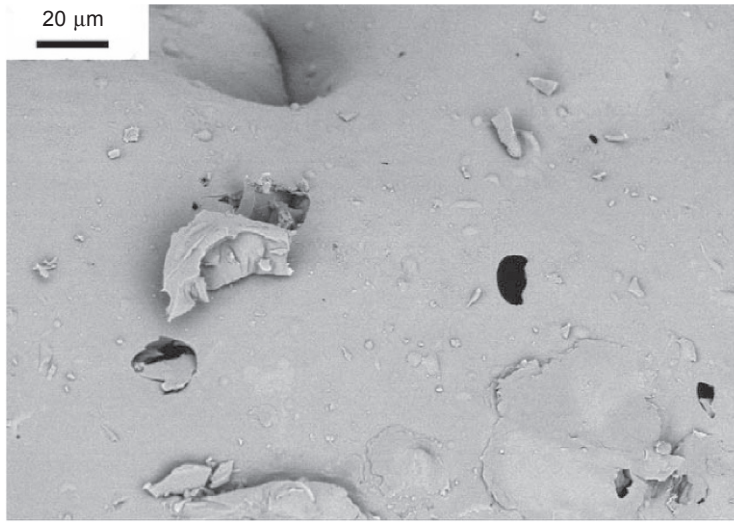

(b)

Figure 19.3 Continued

19.4.4 Waste rubber, plastic, ceramic and other materials

Other recycled materials can also be used as aggregate in alkali-activated cement concrete. Initial research work has indicated that waste rubber shreds from used tires (<0.9 mm) can be solidified into geopolymeric matrix (Skoba *et al*., 2005). As expected, the waste rubber–geopolymer composite is more elastic than the geopolymer materials and the compressive strength reduces as the rubber content increases. It should be noted that geopolymer composites with plastic fillers, ceramic fillers, fibre reinforcement (organic and inorganic fibres) and/or fabric reinforcement have been successfully produced (Natali *et al*., 2011; Shaikh, 2013; Sakulich, 2011; Wang *et al*., 2005; Alomayri and Low, 2013; Chindaprasirt *et al*., 2013; Medri and Landi, 2014) with good properties such as flexural strength and fracture toughness. These findings indicate that a wide range of waste materials can be used with geopolymeric materials and alkali-activated binders to manufacture engineering components.

Other wastes such as bottom ash (BA) and spent foundry sand (FS) are also used in combination with RCA as 100% recycled aggregate in making alkali-activated fly ash concrete (Slabbert, 2008). The mixes were made with water-to-geopolymer solid ratio of 2.0 with 4% superplasticizer using 8 M NaOH and sodium silicate as alkali activators and cured at 60°C for 24 h. The geopolymer concrete with aggregates RCA:BA:FS of 70:10:20 showed 28-day strength of 4.4 MPa and can be used in a low specification geopolymer concrete such as alkali-activated masonry concrete block.

19.5 Future trends

The need to reuse recycled materials for making concrete is and will continue to be very important in the future for the sustainability of the construction industry. Knowledge in this field is therefore needed to specifically manage the waste from recycled concrete, demolition and other wastes. Concrete is a material used worldwide and the volume used is very large. Effort is therefore needed for the accumulation of basic information for reusing recycled materials as inert aggregate or as a constituent for active binders. For example, the work of Ahmari *et al*. (2012) on production of geopolymeric binders from blended waste concrete powder and fly ash is very important and should set the tone for future work to completely recycle and utilize waste concrete in a sustainable and environmentally friendly way.

The research in this area is at an early stage and a lot more is needed for the sustainable use of recycled aggregate. Shi *et al*. (2012b) are pioneering the application of this recycled aggregate concrete to a more complex structural use by studying the strength and ductility of steel tubular stub columns filled with geopolymeric recycled aggregate. This opens the scope for the wider application of recycled concrete, demolition and other waste as aggregates in structural concrete composites.

19.6 Sources of further information and advice

The information on alkali-activated recycled aggregate concrete is limited. However, much of the information on alkali-activated cement and concrete and on the recycled aggregate does exist. In order to build up the base of knowledge on this subject, it is advantageous to go through some of the references as follows.

1. Books on alkali-activated cement and geopolymers by Shi *et al*. (2006), Provis and van Deventer (2009) and Davidovits (2011).
2. Papers on the review of alkali-activated concrete by Duxson *et al*. (2007), Pacheco-Torgal *et al*. (2012a, 2012b); Komnitsas and Zaharaki (2007) and Rashad (2013).
3. Books on recycled aggregate and concrete by Hansen (1986), Siddique (2008), Pacheco-Torgal *et al*. (2013) and De Brito and Saikia (2013).
4. Papers on the review and new knowledge of recycled aggregate concrete by Khalaf and De Venny (2004), Ismail and Ramli (2013) and Cree *et al*. (2013).

It is likely that the subject of alkali-activated recycled aggregate concrete will be researched and extensive results will be published.

References

Achtemichuk, S., Hubbard, J., Sluce, R. and Shehata, M. H. (2009), 'The utilization of recycled concrete aggregate to produce controlled low-strength materials without using Portland cement', *Cem Concr Compos*, 31, 564–569.

ACI 555R-01 (2001), *Removal and Reuse of Hardened Concrete*, ACI Committee 555, American Concrete Institute, Farmington Hills, MI.

Ahmari, S., Ren, X., Toufigh, V. and Zhang, L. (2012), 'Production of geopolymeric binder from blended waste concrete powder and fly ash', *Constr Build Mater*, 35, 718–729.

Alomayri, T. and Low, I. M. (2013), 'Synthesis and characterization of mechanical properties in cotton fiber-reinforced geopolymer composites', *J Am Ceram Soc*, 1, 30–34.

ASTM C33-13 (2013), *Standard specification for concrete aggregates, American Society for Testing and Materials, Book of Standards Vol. 04.02*, West Conshohocken, PA.

ASTM C1260-07 (2007), *Standard test method for potential alkali reactivity of aggregates (mortar-bar method), American Society for Testing and Materials, Book of Standards Vol. 04.02*, West Conshohocken, PA.

Azam, A. and Cameron, D. (2013), 'Geotechnical properties of blends of recycled clay masonry and recycled concrete aggregates in unbound pavement construction', *J Mater Civ Eng*, 25, 788–798.

Berry, M., Stephens, J. and Cross, D. (2011), 'Performance of 100% fly ash concrete with recycled glass aggregate', *ACI Mater J*, 108, 378–384.

Boonserm, K., Sata, V., Pimraksa, K. and Chindaprasirt, P. (2012), 'Improved geopolymerization of bottom ash by incorporating fly ash and using waste gypsum as additive', *Cem Concr Compos*, 34, 819–824.

BS 8500-2 (2006), *Concrete-complementary British standard to BS EN 206-1- Part 2: specification constituent materials and concrete*, British Standards Institution, London.

BS EN 12620 (2013), *Aggregates for concrete*, British Standards Institution, London.

Bui, L. A-T., Hwang, C-L., Chen, C-T., Lin, K-L. and Hsieh, M-Y. (2012), 'Manufacture and performance of cold bonded lightweight aggregate using alkaline activators for high performance concrete', *Constr Build Mater*, 35, 1056–1062.

Bui, L. A-T., Hwang, C-L., Lin, K-L., Chen, Y-Y. and Young, M-P. (2013), 'Development of lightweight aggregate from sewage sludge and waste glass powder for concrete', *Constr Build Mater*, 47, 334–339.

Cameron, D. A., Rahman, M. M. and Azam, A. H. (2012), 'Recycled clay masonry and recycled concrete aggregate blends in pavement', *Geo-Congress 2012*, Oakland, CA, 1532–1541.

CCAA (2008), *Use of recycled aggregates in construction*, Report, Cement Concrete and Aggregates Australia, Mascot, NSW, Australia.

Chen, J.-X., Chen, H.-B., Xiao, P. and Zhang, L.-F. (2004), 'A study on complex alkali-slag environmental concrete', *Proceedings of the International Workshop on Sustainable Development and Concrete Technology (Workshop Proceedings, 2004 Iowa State University)*, Beijing, China.

Chindaprasirt, P. and Rattanasak, U. (2010), 'Utilization of blended fluidized bed combustion (FBC) ash and pulverized coal combustion (PCC) fly ash in geopolymer', *Waste Manage*, 30, 667–672.

Chindaprasirt, P., Chareerat, T. and Sirivivatnanon, V. (2007), 'Workability and strength of coarse high calcium fly ash geopolymer', *Cem Concr Compos*, 29, 224–229.

Chindaprasirt, P., Jaturapitakkul, C. and Rattanasak, U. (2009), 'Influence of fineness of rice husk ash and additives on the properties of lightweight aggregate', *Fuel*, 88, 158–162.

Chindaprasirt, P., Thaiwitcharoen, S., Kaewpirom, S. and Rattanasak, U. (2013), 'Controlling ettringite formation in FBC fly ash geopolymer concrete', *Cem Concr Compos*, 41, 24–28.

Correia, J. R., Brito, J. and Pereira, A. S. (2006), 'Effects on concrete durability of using recycled ceramic aggregates', *Mater Struct*, 39, 169–177.

Cree, D., Green, M. and Noumowé, A. (2013), 'Residual strength of concrete containing recycled materials after exposure to fire: a review', *Constr Build Mater*, 45, 208–223.

CSI (2012), *Recycling concrete, Report, the cement sustainability initiative (CSI), World Business Council for Sustainable Development*, Switzerland, Available from: http://www.wbcsdcement.org/pdf/CSI-RecyclingConcrete-FullReport.pdf

Cyr, M., Idir, R. and Poinot, T. (2012), 'Properties of inorganic polymer (geopolymer) mortars made of glass cullet', *J Mater Sci*, 47, 2782–2797.

Davidovits J. (2011), *Geopolymer Chemistry and Applications*, 3rd edn, Institut Géopolymère, Saint-Quentin, France.

De Brito, J. and Saikia, N. (2013), *Recycled Aggregate in Concrete – Use of Industrial, Construction and Demolition Waste*, Springer, New York.

Debieb, F. and Kenai, S. (2008), 'The use of coarse and fine crushed bricks as aggregate in concrete', *Constr Build Mater*, 22, 886–893.

del Rio Merino, M., Navarro, J. and Saez, P. (2011), 'Legal aspects which implement good practice measures in the management of construction and demolition waste', *Open Constr Build Tech J*, 5 (Suppl 2-M2), 124–130.

Domingo-Cabo, A., Lázaro, C., López-Gayarre, F., Serrano-López, M. A., Serna, P. and Castaño-Tabares, J. O. (2009), 'Creep and shrinkage of recycled aggregate concrete', *Constr Build Mater*, 23, 2545–2553.

Du, H. and Tan, K. H. (2013), 'Use of waste glass as sand in mortar: Part II – Alkali–silica reaction and mitigation methods', *Cem Concr Compos*, 35, 118–126.

Duxson, P., Fernández-Jiménez, A., Provis, J. L., Lukey, G. C., Palomo, A. and van Deventer, J. S. J. (2007), 'Geopolymer technology: the current state of the art', *J Mater Sci*, 42, 2917–2933.

European Union – Brite EuRam III (2000), *Recycling lightweight aggregate concrete, EuroLightCon: Economic design and construction with light weight aggregate concrete*, Document BE96-3942/R26, European Union, Brussels.

Galvin, B. and Lloyd, N. (2011), 'Fly ash based geopolymer concrete with recycled concrete aggregate', *Proceedings of the Concrete 2011 Conference*, The Concrete Institute of Australia, Perth, Australia.

García-Lodeiro, I., Palomo, A. and Fernández-Jiménez, A. (2007), 'Alkali–aggregate reaction in activated fly ash systems', *Cem Concr Compos*, 37, 175–183.

Gomes, M. and Brito, J. (2009), 'Structural concrete with incorporation of coarse recycled concrete and ceramic aggregates: durability performance', *Mater Struct*, 42, 663–675.

Hansen, T. (1986), 'Recycled aggregates and recycled aggregate concrete: second state-of-the-art report developments 1945–1985', *Mater Struct*, 19, 201–246.

Hansen, T. C. (2004), *Recycling of demolished concrete and masonry* (RILEM Report, No. 6), Taylor & Francis CRC, New York.

Hansen, T. C. and Narud, H. (1989), 'Strength of recycled concrete made from crushed concrete coarse aggregate', *Concr Int*, 5, 78–83.

HB 155 (2002), *Guide to the use of recycled concrete and masonry materials,* Standards Australia, Sydney.

Hermann, E., Kunze, C., Gatzweiler, R., Kiebig, G. and Davidovits, J. (1999), 'Solidification of various radioactive residues by geopolymer with special emphasis on long term stability', *Proceedings of the Géopolymère '99 international conference*, Geopolymer Institute, Saint-Quentin, France.

Ismail, S. and Ramli, M. (2013), 'Engineering properties of treated recycled concrete aggregate (RCA) for structural applications', *Constr Build Mater*, 44, 464–476.

Jo, B-W., Park, S-K. and Park, J-B. (2007), 'Properties of concrete made with alkali-activated fly ash lightweight aggregate (AFLA)', *Cem Concr Compos*, 29, 128–135.

Kasami, H., Shimizu, K. and Kudoh, Y. (1998), 'Experimental study on the effect of adhered cement mortar on the properties of recycled aggregate: Part 3 – Effect of adhered cement mortar on the density and absorption of recycled aggregate', in *Summaries of Technical Papers of Annual Meeting*, Architectural Institute of Japan, Tokyo, 689–690.

Khalaf, F. and De Venny, A. (2004), 'Recycling of demolished masonry rubble as coarse aggregate in concrete: review', *J Mater Civ Eng*, 16, 331–340.

Khatib, J. M. (2005), 'Properties of concrete incorporating fine recycled aggregate', *Cem Concr Res*, 35, 763–769.

Komnitsas, K. and Zaharaki, D. (2007), 'Geopolymerisation: a review and prospects for the minerals industry', *Miner Eng*, 20, 1261–1277.

Kou, S-C. and Poon, C-S. (2013), 'Long-term mechanical and durability properties of recycled aggregate concrete prepared with the incorporation of fly ash', *Cem Concr Compos*, 37, 12–19.

Lee, W. K. W. and van Deventer, J. S. J. (2002), 'The effect of ionic contaminants on the early-age properties of alkali-activated fly ash-based cements', *Cem Concr Res*, 32, 577–584.

LEED (2000), *Green building rating system™ version 2.0*, LEED (Leadership in Energy and Environmental Design), US Green Building Council, Washington, DC.

Li, Q., Chen, C., Shen, L. and Zhai, J. (2013), 'Manufacturing F-fly ash based geopolymer mortars using CFBC bottom ash as fine aggregates', *J Chem Soc Pak*, 35, 314–319.

Limbachiya, M. C. (2009), 'Bulk engineering and durability properties of washed glass sand concrete', *Constr Build Mater*, 23, 1078–1083.

Limbachiya, M. C., Koulouris, A., Roberts, J. and Fried, A. (2004), 'Performance of recycled aggregate concrete', in N. Kashino, Y. Ohama, *RILEM International Symp. on Environment-Conscious Materials and Systems for Sustainable Development*, RILEM Publications SARL, 127–136.

Matias, D., de Brito, J., Rosa, A. and Pedro, D. (2013), 'Mechanical properties of concrete produced with recycled coarse aggregates – influence of the use of superplasticizers', *Constr Build Mater*, 44, 101–109.

Medri, V. and Landi, E. (2014), 'Recycling of porcelain stoneware scraps in alkali bonded ceramic composites', *Ceram Int*, 40, 307–315.

Mehta, P. K. (2002), 'Greening of the concrete industry for sustainable development', *Concr Int*, 24, 23–28.

MPA (2011), *Specifying sustainable concrete: Understanding the role of constituent materials*, Mineral Products Association (MPA), London.

MPA (2013), *Cement fact sheet 6: Use of recycled aggregates in concrete*, Mineral Products Association (MPA), London.

Nassar, R.-U.-D. and Soroushian, P. (2012), 'Strength and durability of recycled aggregate concrete containing milled glass as partial replacement for cement', *Constr Build Mater*, 29, 368–377.

Natali, A., Manzi, S. and Bignozzi, M. C. (2011), 'Novel fiber-reinforced composite materials based on sustainable geopolymer matrix', *Procedia Engineering*, 21, 1124–1131.

Oliveira, L. A., Castro Gomes, J. P. and Santos, P. (2008), 'Mechanical and durability properties of concrete with ground waste glass sand', *11th International Conference on Durability of Building Materials and Components*, Istanbul, Turkey.

Pacheco-Torgal, F. (2013), Introduction to the recycling of construction and demolition waste (CDW), in Pacheco-Torgal, F., Tam, V.W.Y., Labrincha, J.A., Ding, Y. and de Brito, J. (eds) *Handbook of Recycled Concrete and Demolition Waste*, Woodhead Publishing Limited, Cambridge, 1–6.

Pacheco-Torgal, F., Abdollahnejad, Z., Camões, A. F., Jamshidi, M. and Ding, Y. (2012a), 'Durability of alkali-activated binders: a clear advantage over Portland cement or an unproven issue?', *Constr Build Mater*, 30, 400–405.

Pacheco-Torgal, F., Abdollahnejad, Z., Miraldo, S., Baklouti, S. and Ding, Y. (2012b), 'An overview on the potential of geopolymers for concrete infrastructure rehabilitation (Review)', *Constr Build Mater*, 36, 1053–1058.

Pacheco-Torgal, F., Ding, Y., Miraldo, S., Abdollahnejad, Z. and Labrincha, J. A. (2012c), 'Are geopolymers more suitable than Portland cement to produce high volume recycled aggregates HPC?', *Constr Build Mater*, 36, 1048–1052.

Pacheco-Torgal, F., Tam V., Labrincha J., Ding Y. and de Brito J. (eds) (2013), *Handbook of Recycled Concrete and Demolition Waste*, Woodhead Publishing Limited, Cambridge.

Payá, J., Borrachero, M. V., Monzó, J., Soriano, L. and Tashima, M. M. (2012), 'A new geopolymeric binder from hydrated-carbonated cement', *Mater Lett*, 74, 223–225.

Posi, P., Teerachanwit, C., Tanutong, C., Limkamoltip, S., Lertnimoolchai, S., Sata, V. and Chindaprasirt, P. (2013), 'Lightweight geopolymer concrete containing aggregate from recycle lightweight block', *Mater Des*, 52, 580–586.

Provis, J.L., and van Deventer J.S.J. (2009), *Geopolymers: Structures, Processing, Properties and Industrial Applications,* Woodhead Publishing Limited, Cambridge.

Rao, A., Jha, K. N. and Misra, S. (2007), 'Use of aggregates from recycled construction and demolition waste in concrete', *Resour Conserv Recy*, 50, 71–81.

Rashad, A. M. (2013), 'A comprehensive overview about the influence of different additives on the properties of alkali-activated slag – a guide for civil engineer', *Constr Build Mater*, 47, 29–55.

Rashwan, M. S. and Abourizk, S. (1997), 'The properties of recycled concrete. factors affecting strength and workability', *Concr Int*, 19, 56–60.

Saez, P., del Rio Merino, M., Amores, C. and Gonzalez, A. (2011), 'European legislation and implementation measures in the management of construction and demolition waste', *Open Constr Build Tech J*, 5 (Suppl 2-M6), 156–161.

Sakulich, A. R. (2011), 'Reinforced geopolymer composites for enhanced material greenness and durability', *Sustain Cities Soc*, 1, 195–210.

Salem, R. M., Burdette, E. G. and Jackson, N. M. (2003), 'Resistance to freezing and thawing of recycled aggregate concrete', *ACI Mater J*, 100, 216–221.

Sangha, C. M., Alani, A. M. and Walden, P. J. (2004), 'Relative strength of green glass cullet concrete', *Mag Concr Res*, 56, 293–297.

Sanusi, O., Tempest, B. and Ogunro, V. O. (2011), 'Mitigating leachability from fly ash based geopolymer concrete using recycled concrete aggregate (RCA)', *Geo-Frontiers*, 1315–1324.

Sata, V., Wongsa, A. and Chindaprasirt, P. (2013), 'Properties of pervious geopolymer concrete using recycled aggregates', *Constr Build Mater*, 42, 33–39.

Sathonsaowaphak, A., Chindaprasirt, P. and Pimraksa, K. (2009), 'Workability and strength of lignite bottom ash geopolymer mortar', *J Hazard Mater*, 168, 44–50.

Shaikh, F. U. A. (2013), 'Review of mechanical properties of short fibre reinforced geopolymer composites', *Constr Build Mater*, 43, 37–49.

Shayan, A. and Xu, A. (2003), 'Performance and properties of structural concrete made with recycled concrete aggregate', *ACI Mater J*, 100, 371–380.

Sheen, Y-N., Wang, H-Y., Juang, Y-P. and Le, D-H. (2013), 'Assessment on the engineering properties of ready-mixed concrete using recycled aggregates', *Constr Build Mater*, 45, 298–305.

Shi, C., Krivenko, P.V. and Roy, D. (2006), *Alkali-Activated Cements and Concretes*. Taylor & Francis, Abingdon.

Shi, X. S., Collins, F. G., Zhao, X. L. and Wang, Q. Y. (2012a), 'Mechanical properties and microstructure analysis of fly ash geopolymeric recycled concrete', *J Hazard Mater*, 237–238, 20–29.

Shi, X. S., Wang, Q. Y., Zhao, X. L. and Collins, F. (2012b), 'Experimental study on strength and ductility of steel tubular stub columns filled with geopolymeric recycled concrete', in Gardner, L. (ed.) *Tubular Structures XIV,* CRC Press, Boca Raton, FL, 757–764.

Siddique, R. (2008), *Waste Materials Aand By-Products in Concrete*, Springer-Verlag, Berlin, Heidelberg.

Skoba, O., Bednarik, V., Vondruska, M., Slavik, R. and Hanzlieek, T. (2005), 'Solidification of waste tire-shreds by geopolymerization', *Green Chemistry and Sustainable Development Solutions, Proceedings of the World Congress, Geopolymer 2005*, Institut Geopolymere, Saint-Quentin, France.

Slabbert, M. C. (2008), 'Utilising waste products from Kwinana industries to manufacture low specification geopolymer concrete', Masters Thesis, Curtin University of Technology, Perth, Australia.

Somna, K., Jaturapitakkul, C., Kajitvichyanukul, P. and Chindaprasirt, P. (2011), 'NaOH-activated ground fly ash geopolymer cured at ambient temperature', *Fuel*, 90, 2118–2124.

Taha, B. and Nounu, G. (2009), 'Utilizing waste recycled glass as sand/cement replacement in concrete', *J Mater Civ Eng*, 21, 709–721.

Tavakoli, M. and Soroushian, P. (1996a), 'Drying shrinkage behaviors of recycled aggregate concrete', *Concr Int*, 18, 58–61.

Tavakoli, M. and Soroushian, P. (1996b), 'Strengths of recycled aggregate concrete made using field-demolished concrete as aggregate', *ACI Mater J*, 93, 182–190.

Tho-in, T., Sata, V., Chindaprasirt, P. and Jaturapitakkul, C. (2012), 'Pervious high-calcium fly ash geopolymer concrete', *Constr Build Mater*, 30, 366–371.

Thomas, A., Lombardi, D. R., Hunt, D. and Gaterell, M. (2009), 'Estimating carbon dioxide emissions for aggregate use', *Proceedings of the ICE – Engineering Sustainability*, 162, 135–144.

Thomas, C., Setién, J., Polanco, J. A., Alaejos, P. and Sánchez de Juan, M. (2013), 'Durability of recycled aggregate concrete', *Constr Build Mater*, 40, 1054–1065.

Topçu, İ. B. and Toprak, M. U. (2011), 'Properties of geopolymer from circulating fluidized bed combustion coal bottom ash', *Mater Sci Eng A*, 528, 1472–1477.

Topçu, İ. B., Boğa, A. R. and Bilir, T. (2008), 'Alkali–silica reactions of mortars produced by using waste glass as fine aggregate and admixtures such as fly ash and Li_2CO_3', *Waste Manage*, 28, 878–884.

Torres, J., Palacios, M., Hellouin, M. and Puertas, F. (2009), 'Alkaline chemical activation of urban glass wastes to produce cementitious materials', *The 1st Spanish National Conference on Advances in Materials Recycling and Eco-Energy*, Madrid.

Vavro, M., Boháčová, J., Mec, P., Tomková, V., Vlček, J. and Staněk, S. (2011), 'Alkali-activated building materials based on blast furnace slag and non-standard aggregates', *Transactions of the VŠB – Technical University of Ostrava. Construction Series, XI,* 2, 1–8.

Wang, H., Li, H. and Yan, F. (2005), 'Reduction in wear of metakaolinite-based geopolymer composite through filling of PTFE', *Wear*, 258, 1562–1566.

Xi, Y., Li, Y., Xie, Z. and Lee, J. S. (2004), 'Utilization of solid wastes (waste glass and rubber particles) as aggregates in concrete', *Proceeding of the International Workshop on Sustainable Development and Concrete Technology*, Beijing, China.

Xiao, J., Li, W., Fan, Y. and Huang, X. (2012), 'An overview of study on recycled aggregate concrete in China (1996–2011)', *Constr Build Mater*, 31, 364–383.

Xie, Z., Xiang, W. and Xi, Y. (2003), 'ASR potentials of glass aggregates in water-glass activated fly ash and Portland cement mortars', *J Mater Civ Eng*, 15, 67–74.

Yang, K. H., Chung, H. S. and Ashour, A. F. (2008), 'Influence of type and replacement level of recycled aggregates on concrete properties', *ACI Mater J*, 105, 289–296.

Use of alkali-activated concrete binders for toxic waste immobilization

20

I. Lancellotti, L. Barbieri, C. Leonelli
Università degli Studi di Modena e Reggio Emilia, Modena, Italy

20.1 Introduction and EU environmental regulations

Directive 2008/98/EC, implemented in Italy by Legislative Decree 205 of 2010, aims to help the European Union (EU), to move closer to a 'recycling society', seeking to avoid waste and to use them as resources. The main objectives are to strengthen the principles of producer responsibility and the actual implementation of the hierarchy shown in Figure 20.1, according to which safe management is encouraged by various means (including economic). This second model requires a more advanced technological system of management based on 'using the best technologies'.

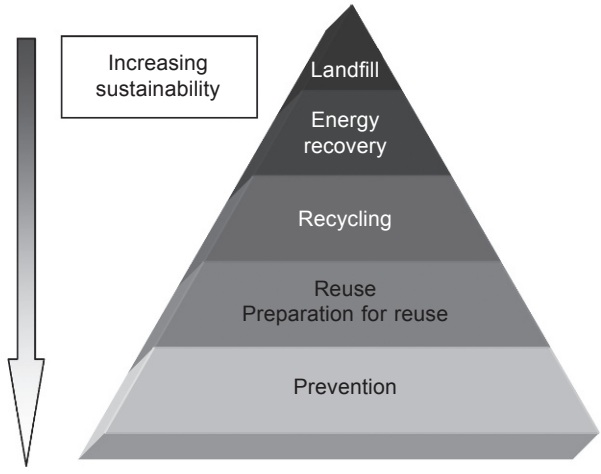

Figure 20.1 Waste management hierarchy.

Handbook of Alkali-activated Cements, Mortars and Concretes. http://dx.doi.org/10.1533/9781782422884.4.539

20.2 Definition of waste

Waste is classified either according to origin (urban and special waste) or to the hazardous characteristics (hazardous and non-hazardous). All wastes are identified by a six-digit code, the list of which is divided into 20 classes, each of which groups wastes arising from the same production cycle (EWC 2002). Within the list, hazardous waste is marked with an asterisk.

'Dangerous substance' means any substance classified as dangerous according to Directive 67/548/EEC (Council Directive 67/548/EEC of 27 June 1967 on the approximation of laws, regulations and administrative provisions relating to the classification, packaging and labelling of dangerous substances) and following amendments: this classification is subject to updating, as the research and knowledge in this field are constantly changing.

The so-called 'heavy metals' are antimony, arsenic, cadmium, chromium (VI), copper, lead, mercury, nickel, selenium, tellurium, thallium and tin. They may be present either in pure form or combined with other elements in chemical compounds.

20.3 Overview of inertization techniques

The inertization process of a waste consists in binding it to an inert matrix (inorganic or organic), through a chemical and/or physical process. The goal is to decrease the pollution potential and the dangerousness of waste, preventing or minimizing the transfer of pollutants into the environment and reducing the area available for leaching, in such a way as to render the waste suitable for subsequent phases of landfilling for non-hazardous waste, or for recovery. The processes of inertization, summarized in Table 20.1, can be applied to the treatment of contaminated soil, solid or liquid waste arising from washing or incineration, radioactive waste, removal and safety of toxic and hazardous waste.

They can be roughly divided into two categories:

1. *Heat treatments techniques*, which are those techniques that adopt high temperatures for the thermal destruction of the waste. They are: vitrification, glass-ceramization (1300–1500°C), and treatment with plasma torch (7000–13,000°C depending on the type of torch used).
2. *Cold processes*, characterized by temperatures between 25 and 150°C and different mechanisms: stabilization/solidification (S/S) obtained with hydraulic binders based on inorganic (e.g., cement, lime, clay) or organic (e.g., thermoplastics, macroencapsulating compounds, polymers) reagents.

Table 20.1 Hot and cold inertization techniques

Heat treatments	Cold techniques (stabilization/solidification)
Vitrification Glass-ceramization Plasma torch	Inorganic: cement/silicates, lime, clay Organic reagents: thermoplastics, resins, polymers

20.4 Cold inertization techniques: geopolymers for inertization of heavy metals

The increasingly urgent need for the use of industrial inorganic waste as raw material for new materials raises the possibility of geopolymers as an alternative to the traditional Portland cement/concrete. These alkali-activated materials can, in fact, be considered a resource in sustainable waste management as it is possible to formulate them starting from waste, mostly aluminosilicates, which are not dangerous, but it is also possible to design and use them as matrices for inertization of hazardous waste containing heavy metals. In this sense we can define geopolymerization of waste materials as a technique that combines the alkaline activation of the aluminosilicate and/or phosphate component to act as matrix and the dissolution/activation/hydrolyzation of the surface of the particles of waste. The surface reactivity is in fact responsible for the bond that is formed between the waste particles and the aluminosilicate matrix immobilizing the heavy metal ions. The nature of the waste, in terms of mineralogy, alumina and silica contents, particle size, surface area and morphology, significantly affect the reactivity of the waste itself.

To assess the real effectiveness of the immobilization of heavy metals, several authors have introduced salts of heavy metals, such as Pb, Cu, Cr, Cd, etc., and have evaluated the immobilization through leaching tests in different solvents. The matrices used for these studies (Phair and van Deventer, 2001; Phair *et al.*, 2004; van Jaarsveld *et al.*, 1999; Hanzlìcekw and Steinerovà-Vondràkova, 2006; Palomo and Palacios, 2003; Zhang *et al.*, 2008a, 2008b; Xu *et al.*, 2006) include kaolin, metakaolin and cement added with coal fly ash and/or blast furnace slag.

The leaching tests have been recognized by the scientific and regulatory community to be the most effective way to evaluate the efficiency of chemical immobilization of heavy metals. The leaching process is a very complex phenomenon which requires the strict control of several parameters including particle size distribution, pH of eluating solution, temperature, contact time, stirring, liquid/solid ratio, etc.

The leaching of the immobilized species can be due to degradation and disruption of the matrix or their release from an intact matrix, similar to the phenomenon of ion exchange. The results presented below belong to the second type as the conditions of the leaching tests are not sufficiently severe to degrade the aluminosilicate matrix of geopolymer.

20.4.1 Lead, copper, chromium and cadmium

In studies related to the efficiency of the immobilization of lead and copper cations, often the two are added together so as to compare an ion small transition, Cu^{+2}, and a larger one belonging to one of the main groups of the periodic table, Pb^{+2}. The studies were conducted through the dynamic toxicity characteristic leaching procedure (TCLP) leaching test in acetic acid (US EPA, 1986). In particular for lead it was observed that the immobilization is strongly controlled by different factors one of which is the influence exerted by the type of cation present in alkaline solution used

to activate the matrix and the waste; it is possible to hypothesize a relevant role of sodium in the leaching process of Pb-containing geopolymer.

Keeping constant the alkaline metal of the activator solution, such as sodium, the effectiveness of the immobilization of lead varies significantly: the most effective immobilization is recorded for the solution of NaOH, which also corresponds to the higher pH, rather than the sodium silicate having the mixture of the two solutions, which has an intermediate behaviour (Phair and van Deventer, 2001; Phair *et al*., 2004).

Compared to lead, copper is immobilized with less efficiency because of its smaller ionic radius that makes it more mobile, facilitating the diffusion and leaching processes, for example with respect to Co and Ni (Phair and van Deventer, 2001; Phair *et al*., 2004; van Jaarsveld *et al*., 1999; Hanzlìcekw and Steinerovà-Vondràkova, 2006). A similar behaviour to lead has been observed, however, also for copper: again the activating solutions containing sodium show a higher efficiency than those with potassium. This behaviour suggests a greater influence of the basicity of the alkaline solutions, rather than the size of the hydration sphere of the different cations which leads to the formation of precipitates strongly retained by the matrix.

Chromium, a metal widespread in the environment and present in many types of industrial wastes, is particularly toxic and mobile in its form of Cr(VI) and its introduction into a Portland cement has a deleterious effect on the mechanical properties. In fact, when it is inserted as CrO_3 in Portland cement admixed with coal ash, the setting and the mechanical performance of the material are inhibited significantly (Palomo and Palacios, 2003). Instead, when the insertion occurs in a matrix of blast furnace slag through alkaline activation, immobilization is not only effective, but an improvement is also observed in the mechanical properties of the material. The immobilization can also be favoured by reducing conditions due to the presence of sulphide ions that lead to a partial reduction of Cr(VI) to Cr(III) (Zhang *et al*., 2008a).

Xu *et al*. (2006) studied the influence of the concentration of the alkaline solution and the curing time of geopolymeric materials (based on metakaolin and coal ash) on the immobilization of Cu, Cd, Pb and Cr. A stronger influence of the studied parameters was observed on Cu and Cd inertization rather than on Pb and Cr. In particular, the conditions favourable for inertizing Cu and Cd correspond to high pH and short curing time. Under any condition, however, the efficiency of immobilization of Pb and Cr is greater than that of Cu and Cd.

Another parameter that might influence the effectiveness of immobilization of heavy metals is the type of salt with which they occur in the inertizing matrix (Zhang *et al*., 2008b). In particular the effectiveness of inertizing of Pb, Cr and Cd was evaluated with static tests in acid (sulfuric acid to pH 1), saline (Na_2CO_3 and $MgSO_4$) and in distilled water because the resistance of heavy metal-containing geopolymers to leaching in different environments depends very strongly on both the nature of the heavy metal and the aggressive components of the leaching solution.

H_2SO_4 leaching in general shows the highest rate of metals release than the other leach solutions tested. Pb is immobilized very effectively by a chemical binding mechanism in geopolymers, meaning that its addition in a soluble chemical form is

actually preferable (Figure 20.2). Cd immobilization depends on the solubility of a hydroxide phase, and so is very effective at high pH but poor at low pH (Onisei *et al*., 2012). The studies reported allow us to hypothesize that the immobilization of lead is to be charged to a chemical bond between Pb^{2+} and the matrix with the formation of silicate phases rather than to an adsorption or physical entrapment.

When chromium and lead are placed in the geopolymeric matrix in the form of combined salt, $PbCrO_4$ the release of chromium is greater than that of lead. If the chromium is introduced as a soluble salt, Na_2CrO_4, in the absence of reducing agents is easily leached, while in the presence of sulphide ions is easily reduced and forms $Cr(OH)_3$ and therefore its immobilization is more effective compared to the less soluble $PbCrO_4$, that, remaining unchanged, is subject to leaching.

Cadmium shows a strong dependence on the medium used for the release test, in fact, showing good chemical resistance in water and salt solutions, while the same decreases drastically in sulphuric acid, probably due to the fact that cadmium is immobilized as the hydroxide, $Cd(OH)_2$, which is particularly soluble in acidic environment (Zhang *et al*., 2008b). Conversely cadmium, being a divalent ion like calcium, is immobilized effectively in calcic matrices such as those based on Portland cement and blast furnace slag activated with alkali.

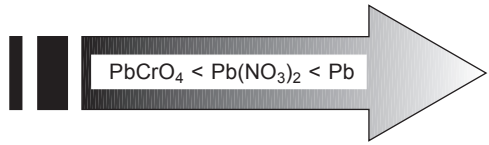

Figure 20.2 Efficiency of Pb immobilization in Na_2CO_3 solution in function of the form in which Pb is introduced into the matrix.

20.4.2 Arsenic

Arsenic is particularly important due to its high toxicity and solubility and the ease with which it is found in various waste streams. Arsenic is quite effectively immobilized in matrices based on Portland cement. Its immobilization in geopolymers was studied when it is introduced in the form of complex waste containing many metals and has proven only partially effective. Some authors have shown that arsenic contained in coal fly ashes is leached more when the ashes are in geopolymer with respect to the ashes on their own (Álvarez-Ayuso *et al*., 2008).

Fernández-Jiménez *et al*. (2005) studied matrices of coal fly ash and metakaolin containing arsenic introduced as $NaAsO_2$. The leaching has been studied through the TCLP test and ANS 16.1 (American Nuclear Society 16.1). The data showed that arsenic is incorporated more effectively from the matrix containing the fly ash compared to that of only metakaolin. However, the leaching exceeds the legal limits and therefore arsenic cannot be considered inert. The use of mixed systems based on blast furnace slag, rich in calcium, and coal fly ash could represent a better solution given that calcium promotes inertization of arsenic.

To summarize, there are many parameters that can influence the immobilization of

heavy metals, of which the pH plays an important role. In Figure 20.3 the influence of pH on heavy metals is shown. For example, arsenic is not effectively incorporated in the geopolymer in the whole pH range, whereas cadmium is incorporated at alkaline pH, while it is leached at acid pH. Cr, Ni, Sn are inert throughout the pH range (Waijarean *et al.*, 2014). A summary of the efficacy of the incorporation of the geopolymeric matrix in respect of the different elements of the periodic table is shown in Figure 20.4.

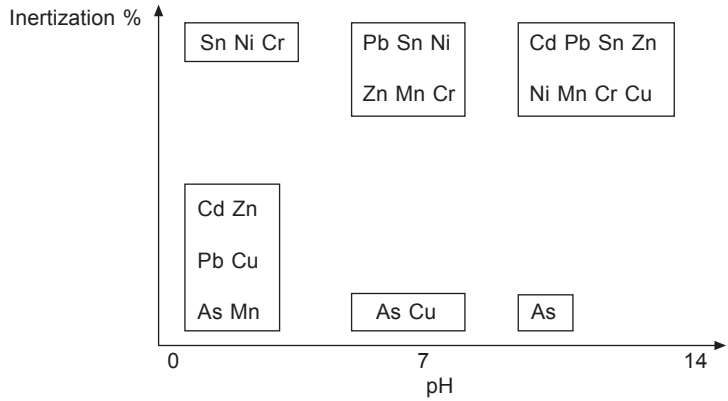

Figure 20.3 pH influence on heavy metal inertization.

20.5 Cold inertization techniques: geopolymers for inertization of anions

20.5.1 Sulphates and nitrates

While many studies are present in the literature on heavy metal immobilization in geopolymers, so far a limited number of studies have attempted to elucidate the effect of anions on geopolymer properties (Criado *et al.*, 2010; Desbats-Le Chequer and Frizon, 2011; Lee and van Deventer, 2002; Komnitsas *et al.*, 2013). These studies have focused on the effect of anions on fly ash, metakaolin and ferronickel slag-based geopolymers.

For sulphates, TCLP results, investigating the effect of sulphate and nitrate ions on heavy metal immobilization during the production of geopolymers from low calcium ferronickel slag, show that with the exception of Cr, which has quite low concentration in the extract, high concentrations of Pb, Cu and Ni are detected in the extract when these metals are added as sulphate ions in the starting mixture. Geopolymers exhibit increased toxicity in terms of Pb release whereas no TCLP limits are available for Ni and Cu. The concentration of these two elements, Ni and Cu, in the extract is considered high (25–50 mg/L). Thus increased risk for contamination of soils and groundwater could be envisaged if wastes containing Ni and Cu in the form of sulphate or nitrate salts are geopolymerized and disposed of without proper

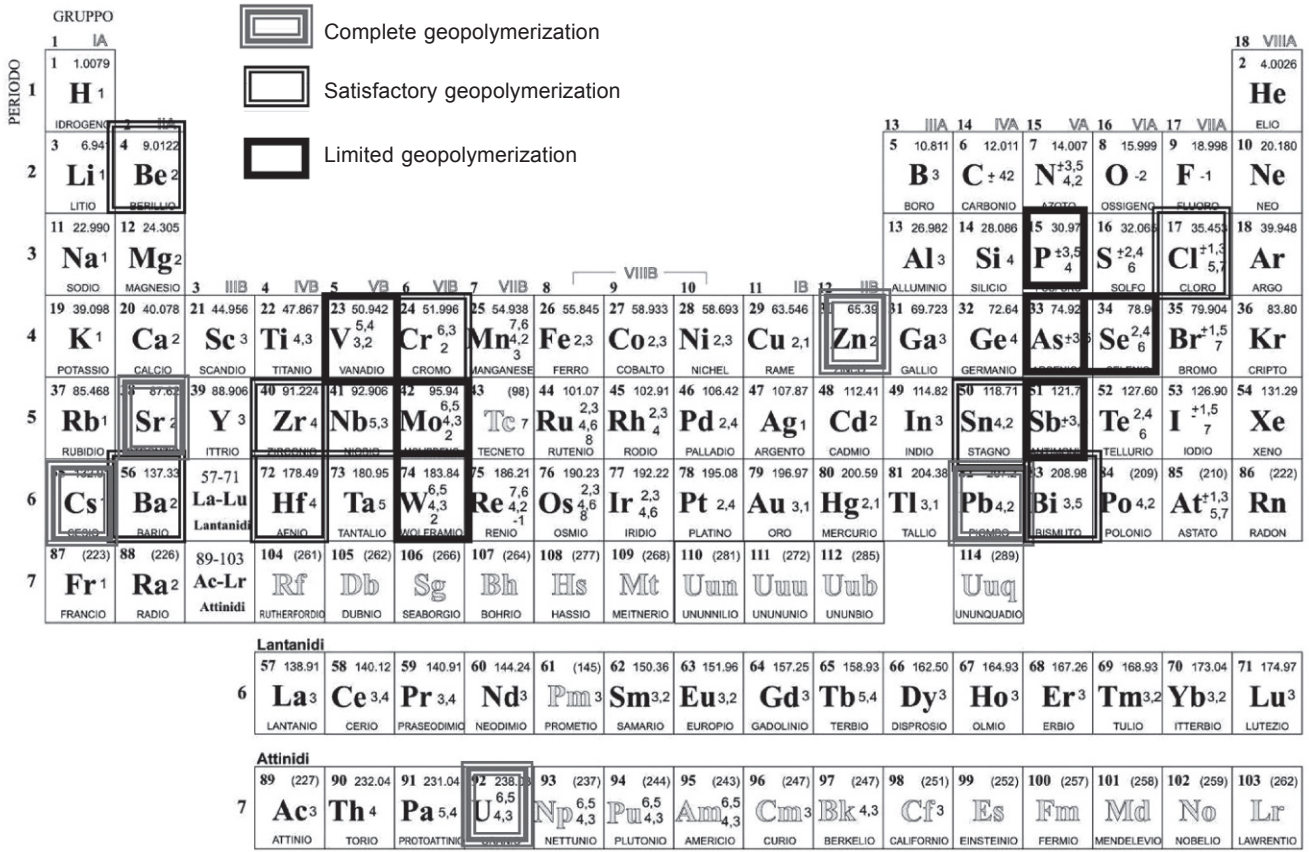

Figure 20.4 Summary of the efficiency of single element immobilization introduced in geopolymers (based on the available literature data).

care in the environment. Also the compressive strength of geopolymers is negatively affected by the presence of NO_3^- or SO_4^{-2} ions in the starting mixture. Both anions consume most of the available alkali activator moles, hinder geopolymerization reactions and thus the quantity of the gel produced is limited and scarcely connected (Komnitsas *et al.*, 2013).

20.5.2 Chlorides

Lee and van Deventer (2002) found that chloride salts such as KCl, $CaCl_2$ and $MgCl_2$ were detrimental to geopolymer obtained by the activation of fly ash and kaolin. They decreased the product durability by gradually causing precipitation and crystallization in the aluminosilicate gel which is the binding phase of geopolymer. On the other hand, carbonate salts, K_2CO_3 and $CaCO_3$, were beneficial by lowering the dissolved water contents and preventing hydrolytic attacks on the gels. A new crystalline phase, probably calcium silicate chloride ($Ca_2SiO_3Cl_2$), was found in the geopolymer systems investigated and was exclusive to the chloride-affected geopolymers. Experimental data gathered in Lee and van Deventer (2002) suggest that, regardless of chloride salt contamination or excessive alkalinity, the most likely mechanism associated with product deterioration in geopolymers is hydrolytic attack on the primary aluminosilicate gel, which is produced directly from alkali activation on the solid raw material.

20.5.3 Sulphides

Sulphides, S^{2-} ions, studied by Zhang *et al.* (2008a), play a critical role in the immobilization of Cr(VI) in alkali-activated fly ash matrices, by reducing Cr(VI) to Cr(III) and enabling precipitation in highly insoluble forms. A little addition (0.5%) of S^{2-} as $Na_2S{\cdot}9H_2O$ has been shown here to be highly effective in immobilizing Cr against attack by deionized water or mineral salt solutions for at least 90 days. Leaching in H_2SO_4 solution remains more problematic, most likely due to the re-oxidation of the Cr to highly mobile Cr(VI) species, but the addition of sulphide still provides a major increase in leaching resistance compared to a simple geopolymer binder (Figure 20.5). Addition of the Cr as a sparingly soluble salt actually provides less effective immobilization than does addition as a highly soluble salt in the presence of sulphides.

20.6 Immobilization of complex solid waste

Fly ash from electric arc furnaces for steel production, containing Zn, Pb, Cr, Cd, and electrostatic precipitator and fabric filter fly ash from incineration of municipal waste containing Cd, Cr, Cu, Ni, Pb, CO_3^{2-}, Cl^- and SO_4^{2-} are classified as hazardous waste. They were mixed with blast furnace slag, coal ash and kaolin/metakaolin and

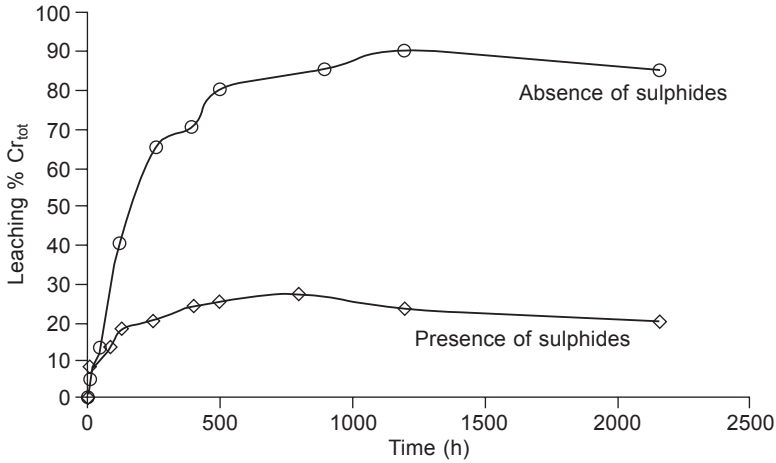

Figure 20.5 Percentage of Cr extraction in H_2SO_4 leaching solution (pH = 1) from geopolymer containing 0.5% Cr, added as Na_2CrO_4, as a function of sulphide presence (data elaborated from Zhang *et al*., 2008b).

activated with potassium or sodium silicate (Fernández Pereira *et al*., 2009; Galiano *et al*., 2011; Lancellotti *et al*., 2010).

The inertization efficiency was assessed by release test in distilled water for 24 hours (EN 12457-4, 2002). The inertization efficiency was also assessed by release test in acetic acid (US EPA, 1986) and in distilled water acidified to pH = 4 with nitric acid (NEN 7345, 1993) (which indicates the maximum amount of contaminant that can be leached in extreme conditions) and compared with the behaviour of a matrix based on Portland cement. Fernández Pereira *et al*. (2009) have also analyzed the behaviour of Zn, which has been little studied, but which is important since it has a deleterious effect on the hardening/curing of Portland cement because of Ca–Zn interactions that lead to the precipitation of calcium zincate on the surface of the cement grains and therefore its inclusion in this matrix is not very suitable. In this context, it is expected that geopolymers with low calcium content can be a good matrix for the immobilization of this metal. Mináriková and Skvara (2006) have observed that the introduction of zinc in geopolymers leads to a reduction of the compressive strength, but the setting time is not delayed as in Portland cement.

20.6.1 Ashes from electric arc furnaces

The response of the material to leaching is a function of the leaching medium:

- Test in distilled water (EN 12457-4, 2002): the concentration of the metals is less in the geopolymeric matrix with respect to Portland cement using either potassium or sodium silicate. The lower values of heavy metals, however, are those with potassium activation. The resulting materials show leaching values which are acceptable for being disposed of in landfills for non-hazardous waste.

- Test in acetic acid (EPA TCLP (US EPA, 1986)) with a solution at pH 4.93: leaching of different metals varies significantly. The geopolymer only immobilizes Cr, while Pb, Zn and Cd exceed the limits. This behaviour is strongly linked to the alkalinity of the matrix and to the ability of the solid to neutralize the acidic solution, greater in the Portland cement compared to the geopolymer. The strong leaching of Pb, Zn and Cd in the ash from the electric arc is due to the fact that these metals are in the form of oxides and chlorides which are soluble in a medium with a pH close to neutrality.
- Test in nitric acid (NEN 7345, 1993): Zn and Cr exhibit low leaching and good immobilization (90–100%) either in cement or in geopolymeric matrices, whereas, Pb and Cd show a very variable immobilized fraction (Pb = 30–95% and Cd = 47–91%) with lower values for the geopolymeric matrix.

20.6.2 Fly ash from urban incinerator

For the fly ash from an incinerator it was observed that, depending on the test used, the behaviour of the different matrices, based on metakaolin or Portland cement, is different.

The matrix effects and leaching agent can be summarized as follows.

- Test in distilled water (EN 12457-4, 2002): Zn (particularly because of its high concentration in the initial waste), Co, Ni, Cu and Sn are less leachable metals. In contrast, Mo, V and Cr, elements that typically form oxyanions, showed the worst results regardless of the matrix in which they are located. Materials prepared by activation with potassium and high calcium content (blast furnace slag and Portland cement) have obtained the best results. Ba and Pb are less effectively incorporated into the calcium matrix (Portland), and Sb in the geopolymers. This last element is the most problematic for inertizing in geopolymers. The above highlights once again the influence of the calcium present in the matrix on the immobilization of different metals.
- Test in acetic acid (EPA TCLP (US EPA, 1986)): the results were compared with the limits set by the US Environmental Protection Agency (US EPA; www.epa.gov) for As, Cr, Cu, Zn, Pb, Ba, Cd, Hg, and Se. Concentrations of the metals were below the limits, but the best performances were obtained for metakaolin-based geopolymers activated with potassium.
- Test in nitric acid (NEN 7345, 1993): Ba, Zn, Pb, Cr and Cd show concentrations below detectable limits. Comparing the different matrices, there is a lower release of Zn and Cr matrices with Portland cement and with blast furnace slag gepolymers, a fact probably related to the high alkalinity of the calcium-containing matrices. Conversely Ba shows worse behaviour in the calcic environment, according to the test in UNI 10802:2013, probably because of chemical interactions with the aluminosilicate lattice characteristic of geopolymers, which are able to immobilize them effectively.
- GANC test (generalized acid neutralization capacity test) (Isenburg and Moore, 1992): this test is used to quantify the equivalents of acetic acid necessary to reduce the pH of an aqueous solution in contact with a solid. Thus it provides information on chemical neutralization, speciation and mobility during leaching of toxic metals from waste stabilized. The metals Zn, Pb and Cd showed amphoteric behaviour irrespective of the matrix. In particular, in geopolymers they show less leaching at neutral pH and acid.

In addition to the studies of the immobilization of heavy metals through the release

test (UNI 10802:2013), the problem related to the presence of anions and their relative stability in the geopolymeric matrix is another important issue. Lancellotti *et al*. (2010) have conducted an investigation into the immobilization of soluble anions such as chlorides in metakaolin-based geopolymers containing a mixture of ashes from electrostatic and fabric filters following incineration of municipal waste. The activation was performed with sodium hydroxide and silicate and the leaching results show a significant decrease in the release of all metals with respect to as-received ashes. The leaching values were lower than the limits imposed by Italian law for the landfill for non-hazardous waste (DM 30/08/2005). An important effect was evidenced for Cd, Pb and Cu, which were strongly released from both ashes in the as-received state, while they are completely immobilized in the geopolymeric matrix. Cr behaved differently since it was partially released from the geopolymer containing ash from the fabric filter. Even though Cr values were maintained below the limits for a landfill for non-hazardous waste, its release was strongly influenced by the presence of chloride ions that facilitate its leakage despite being contained in these ashes in an amount lower than in the ash from the electrostatic precipitator. Assuming the chromium is in the form of insoluble hydroxide, it may be more leachable in solutions containing chlorides which are able to reduce the range of stability of the hydroxide of chromium in both acidic and alkaline conditions, promoting the dissolution in the form of Cr^{3+} and CrO_3^{3-}, respectively (Lancellotti *et al*., 2010).

The release of chlorides in geopolymers shows that the sample containing the ashes from the fabric filter presents higher values of leakage due both to the higher content of this anion in the ash itself and the co-presence of soluble cations. In the reference, which contains the ashes from the incinerator, the release of Na is very low and this indicates that both Na^+ and Cl^- come from the soluble salts in the ash and not just from the alkaline solution used as an activator. From these data the greater ability is apparent of the geopolymer containing ash from the electrostatic precipitator to retain only 30% the chlorides that are released, while this percentage increases to 81% for the material containing ash from the fabric filter.

The parameters of the production process of geopolymers can have a significant influence on the leaching of heavy metals. Izquierdo *et al*. (2010) studied the influence of open and closed conditions adopted for the aging stage in geopolymers obtained from blast furnace slag and coal fly ash enriched in Cu, Ni, P, Sn and Zn deriving from the co-combustion of sewage sludge. The activation was done with potassium silicate and the leaching test performed in open and closed solution vessels. In water (EN 12457-4, 2002) Mo, probably present in the form of soluble salts, is leached up to 75%. As, B, Se and V show a significant mobility (up to 10% of their initial content) linked to their presence in the form of soluble salts, which precipitate during the aging process rather than during the early stages of reticulation of the matrix. The mobility of all other metals such as Ba, Be, Bi, Cd, Co, Cu, Ni, Hf, Nb, and Pb, and also traces of rare earths, is very low and independent of the curing conditions. These results are reproducible for use in both the test EN 12457-4 and the test EA NEN 7375 (2004).

The ashes of urban incinerators could be subjected to pre-treatment before their geopolymerization. Given the high concentration of soluble ions, Zheng *et al*. (2011)

conducted a study on the influence of a washing pre-treatment on ash from fabric filter. The results showed that the washing leads to higher values of mechanical resistance and to a reduction in the leaching fraction of Cr, Cu and Zn. This behaviour confirms the feasibility of a combined process of washing/immobilization, although an assessment is necessary of the appropriate management of the washing waters rich in K^+, Na^+, and Cl^- (Zheng *et al*., 2011).

20.6.3 Electroplating sludge

The introduction of electroplating sludge containing heavy metals, significantly reduced the rate of strength development in geopolymers obtained using water treatment residue (WTR) as an aluminosilicate material. Decrease in strength resulted from the deposition of insoluble metal compounds, such as zinc oxide, zinc chromium oxide and sodium iron oxide, on the surface of the raw material, interfering with the geopolymerization reactions. The formation of insoluble sodium aluminum iron hydrate silicate indicated that the dissolved Si and Al from the aluminosilicate structure present in WTR under the highly alkaline conditions reacted with the heavy metals present in the sludge instead of forming an aluminosilicate network (Waijarean *et al*., 2014). Leaching tests are still under investigation.

20.7 Immobilization of complex liquid waste

20.7.1 Ceramic industry liquors

In the traditional ceramic industry the use of heavy metals as colorants (in liquid form) and pigments (in powdery form) is very diffused as they are good chromospheres at high temperatures (above 950°C). The glazing process is the manufacturing stage during which they are mainly used, hence waste deriving from this section of the plant is richer in hazardous compounds. One of these, in liquid form, was immobilized in geopolymeric matrix (Lancellotti *et al*., 2013). This waste is collected at the plant in liquid homogeneous form composed prevalently of aqueous solutions of metal compounds which develop colours during the firing cycle. The colorant solution contains Fe, Mo, Mn, Co, Cr, depending on the final colour, together with mineralizers and complexes. One of the innovative aspects of this research is the exploitation of water content of the as-collected waste and the absence of a drying step, the latter being a common step in the management of the majority of liquid hazardous wastes.

The results obtained by the introduction of a complex liquid wastes into a geopolymer matrix highlight that, from an environmental point of view, the waste is successfully incorporated into the inorganic polymeric matrix. Geopolymers, based on metakaolin and sodium silicate compositions, stabilize the Cr-bearing liquor as it emerges from the industrial productive cycle with no need for any pre-treatment. Leaching studies of the consolidated material show a release of Cr which allows

disposal in a landfill site suitable for wastes that are not dangerous. The absence of a drying pre-treatment reduces both the use of energy and handling necessary for the management of this kind of hazardous liquid waste. The abundance of literature on heavy metal immobilization by means of geopolymerization makes this encouraging also for liquid wastes containing metals different from chromium.

20.7.2 Red mud/Bayer process hazardous waste

The geopolymerization of red mud, a major industrial waste from alumina refining with the Bayer process, has been investigated since 2005 (Sagoe-Crentsil and Brown, 2005; Cundi *et al.*, 2005) (Table 20.2). Due to its highly caustic nature, with a pH in the range of 10.5–12.5, free alkali content from 3 to 5%, coupled with fine particles (particle size from +90 to –200 mesh), this abundant industrial waste (world annual production of 21 million tons of aluminum generates 82 million tons of sludge; Hajjaji *et al.*, 2013) could cause serious environmental problems. Due to its risky nature, red mud waste is usually managed by discharge into engineered or natural impoundment reservoirs, with subsequent dewatering by gravity-driven consolidation and sometimes followed by capping for closure. Every country has to face the problem of finding suitable disposal sites or propose a sensitive re-use of tons of waste produced yearly, posing a very serious and alarming environmental problem. The route of neutralization requires lowering the pH below 9 with an optimum value of 8.5–8.9 before it becomes environmentally benign (Hanahan *et al.*, 2004). Neutralization is carried out via different techniques, such as acid neutralization, CO_2 treatment, seawater neutralization, bioleaching and sintering (Rai *et al.*, 2012), but research nowadays is directed towards its utilization. It can be used as a building material in bricks, blocks, lightweight aggregates, in the cement industry as cements, and special cements, in the concrete industry in paints and pigments, and in the environmental field for pollution control by acting as an adsorbent for cleaning of industrial gases.

A number of publications (Dimas *et al.*, 2009; Zhang *et al.*, 2010; Giannopoulou *et al.*, 2009; Kumar and Kumar, 2013; Hajjaji *et al.*, 2013) suggested the potential

Table 20.2 Typical composition of red mud

Oxide	wt.%
Fe_2O_3	30–60
Al_2O_3	10–20
SiO_2	3–50
Na_2O	2–10
CaO	2–8
TiO_2	trace–25
Minor elements (K, Cr, V, Ba, Cu, Mn, Pb, Zn, P, F, S, As, etc.)	traces

Source: Red mud Project. http://www.redmud.org/

use of red mud mixed with other aluminosilicates (such as fly ash if not metakaolin) for the production of inorganic polymeric materials that could be used as massive bricks. The high compressive strength (up to 20 MPa), very low water absorption (about 3%), satisfactory apparent density, and excellent fire resistance proved that the red mud-based geopolymeric materials have promising properties and have the potential to be used as artificial structural elements in the construction sector.

A pilot study was presented in 2010 (Zhang *et al.*, 2010) investigating the potential of reusing red mud mixed with fly ash and sodium silicate to obtain a cementitious material that can be used in roadway construction.

Recently, attentions has also focused on another hazardous waste coming from bauxite processing, i.e. the Bayer liquor (van Riessen *et al.*, 2013) composed of 15:Al_2O_3, 24:Na_2O, 61:H_2O (wt.%). In addition, the amount of Bayer liquor used to replace NaOH did not have any impact on the compressive strength (45 MPa). This outcome clearly indicates that the contaminants in the plant liquor have no detrimental impact on geopolymerization or strength development.

20.8 Conclusions

Room temperature alkali activation has been developed in the past few years for inertization of toxic and hazardous wastes and very interesting results have been presented. The role of heavy metals as well as that of the anions has still to be further investigated in order to predict the chemical and structural stability of the final materials. Very few liquid wastes have been investigated at present, but it will be of great interest to use the water contained in the waste to create the necessary alkaline environment requested for a proper geopolymerization.

References

Álvarez-Ayuso E, Querol X, Plana F, Alastuey A, Moreno N, Izquierdo M, Font O, Moreno T, Diez S, Vázquez E and Barra M (2008), 'Environmental, physical and structural characterisation of geopolymer matrixes synthesised from coal (co-)combustion fly ashes', *J. Hazard Mater*, 154(1–3), 175–183.

American Nuclear Society 16.1, *Measurement of the leachability of solidified low-level radioactive wastes by a short-term test procedure*. American Nuclear Society, La Grange Park, IL.

Criado M., Jiménez A F and Palomo A (2010), 'Effect of sodium sulfate on the alkali activation of fly ash', *Cement and Concrete Compos*, 32, 589–594.

Cundi W, Hirano Y, Terai T, Vallepu R, Mikuni A and Ikeda K (2005), 'Preparation of geopolymeric monoliths from red mud–PFBC ash fillers at ambient temperature', *Proceedings of 4th World Congress on Geopolymer*, France, 85–87.

Desbats-Le Chequer C and Frizon F (2011), 'Impact of sulfate and nitrate incorporation on potassium- and sodium-based geopolymers: geopolymerization and materials properties', *J Mater Sci*, 46, 5657–5664.

Dimas D D, Ioanna P and Panias D (2009), 'Utilization of alumina red mud for synthesis of inorganic polymeric materials', *Mineral Processing and Extractive Metallurgy Review*, 30(3), 211–239.

EA NEN7375 (2004), *Leaching characteristics of granular building and waste materials. Determination of the availability of inorganic components for leaching: the tank test*. Environment Agency, London.

EN 12457-4:2002, *Characterisation of waste – Leaching – Compliance test for leaching of granular waste materials and sludges*.

EWC (2002) *European Waste Catalogue and Hazardous Waste List*, Environmental Protection Agency, Ireland.

Fernández-Jiménez A, Macphee D E, Lachowski E E and Palomo A (2005), 'Fixing arsenic in alkali activated cementitious matrices', *J Am Ceram Soc*, 88(5), 1122–1126.

Fernández Pereira C, Galiano Y L, Querol X, Antenucci D and Vale J (2009), 'Waste stabilization/solidification of an electric arc furnace dust using fly ash-based geopolymers', *Fuel*, 88(7), 1185–1193.

Galiano Y L, Fernández Pereira C and Vale J (2011), 'Stabilization/solidification of a municipal solid waste incineration residue using fly ash-based geopolymers', *J Haz Mat*, 185(1), 373–381.

Giannopoulou I, Dimas D, Maragkos I and Panias D (2009), 'Utilization of metallurgical solid by-products for the development of inorganic polymeric construction materials', *Global NEST J*, 11 (2), 127–136.

Hajjaji W, Andrejkovičová S, Zanelli C, Alshaaer M, Dondi M, Labrincha J A and Rocha F (2013), 'Composition and technological properties of geopolymers based on metakaolin and red mud', *Materials & Design*, 52, 648–654.

Hanahan C, McConchie D, Pohl J, Creelman R, Clark M and Stocksiek C (2004), 'Chemistry of seawater neutralization of bauxite refining residues (red mud)', *Env Eng Sci*, 21, 125–138.

Hanzlìcekw T and Steinerovà-Vondràkova M (2006), 'Immobilization of toxic metals in solidified systems of siloxo-sial networks', *J Am Ceram Soc*, 89(3), 968–970.

Isenburg J and Moore M (1992), 'Generalized acid neutralization capacity test', in Gilliam T M and wiles C C (eds) *Stabilization and Solidification of Hazardous, Radioactive and Mixed Wastes*. ASTM STP 1123.

Izquierdo M, Querol X, Phillipart C, Antenucci D and Towler M (2010), 'The role of open and closed curing conditions on the leaching properties of fly ash-slag-based geopolymers', *J Haz Mat*, 176(1–3), 623–628.

Komnitsas K, Zaharaki D and Bartzas G (2013), 'Effect of sulphate and nitrate anions on heavy metal immobilisation in ferronickel slag geopolymers', *Appl Clay Sci*, 73, 103–109.

Kumar A and Kumar S (2013), 'Development of paving blocks from synergistic use of red mud and fly ash using geopolymerization', *Constr and Build Mater*, 38, 865–871.

Lancellotti I, Kamseu E, Michelazzi M, Barbieri L, Corradi A and Leonelli C (2010), 'Chemical stability of geopolymers containing municipal solid waste incinerator fly ash', *Waste Manag*, 30, 673–679.

Lancellotti I, Ponzoni C, Barbieri L and Leonelli C (2013), 'Inertization of chromium liquid waste in inorganic polymers via alkali activation of metakaolin', *Envir Eng and Manag J*, 12(S11), 39–42.

Lee W K W and van Deventer J S J (2002), 'The effects of inorganic salt contamination on the strength and durability of geopolymers', *Colloids and Surfaces A*, 211, 115–126.

Mináriková M and Skvara F (2006), 'Fixation of heavy metals in geopolymeric materials based on brown coal fly ash', *Ceramics Silikaty*, 50, 200–207.

NEN 7345 (1993), *Leaching characteristics of soil, construction materials and wastes leaching tests – determination of the release of inorganic constituents for leaching from construction materials and waste materials*, NNI (Dutch Standards Institute), Delft, The Netherlands.

Onisei S, Pontikes Y, van Gerven T, Angelopoulos G N, Velea T, Predica V and Moldovan P (2012), 'Synthesis of inorganic polymers using fly ash and primary lead slag', *J Haz Mat*, 205–206, 101–110.

Palomo A and Palacios M (2003), 'Alkali-activated cementitious materials: alternative matrices for the immobilisation of hazardous wastes: Part II. Stabilisation of chromium and lead', *Cem Concr Res*, 33(2), 289–295.

Phair J W and van Deventer J S J (2001), 'Effect of silicate activator pH on the leaching and material characteristics of waste-based inorganic polymers', *Minerals Eng*, 14(3), 289–304.

Phair J W, van Deventer J S J and Smith J D (2004), 'Effect of Al source and alkali activation on Pb and Cu immobilisation in fly-ash based "geopolymers"', *Appl Geochem*, 19(3), 423–434.

Rai S, Wasewar K L, Mukhopadhyay J, Kyoo Yoo C and Uslu H (2012), 'Neutralization and utilization of red mud for its better waste management', *Arch Environ Sci*, 6, 13–33.

Sagoe-Crentsil K and Brown T (2005), 'Bayer process waste stream as potential feedstock material for geopolymer binder systems', *Proceedings of the 7th International Alumina Quality Workshop*, Perth, 214–217.

UNI 10802: 2013 *Wastes: Manual sampling and preparation of sample and analysis of eluates*. Italian Organization for Standardization (UNI).

US EPA (1986), *Test methods for evaluating solid wastes, toxicity characteristic leaching procedure (TCLP), Method 1311 SW-846*, 3rd edn, Environmental Protection Agency, Washington, DC.

van Jaarsveld J G S, van Deventer J S J and Schwartzman A (1999), 'The potential use of geopolymeric materials to immobilise toxic metals: Part II. Material and leaching characteristics', *Minerals Eng*, 12(1), 75–91.

van Riessen A, Jamieson E, Kealley C S, Hart R D and Williams R P (2013), 'Bayer-geopolymers: an exploration of synergy between the alumina and geopolymer industries', *Cement and Concrete Compos*, 41, 29–33.

Waijarean N, Asavapisit S and Sombatsompop K (2014), 'Strength and microstructure of water treatment residue-based geopolymers containing heavy metals', *Constr and Build Mater*, 50, 486–491.

Xu J Z, Zhou Y L, Chang Q and Qu H Q (2006), 'Study on the factors affecting the immobilization of heavy metals in fly ash-based geopolymers', *Mater Lett*, 60(6), 820–822.

Zhang G, He J and Gambrell R P (2010), 'Synthesis, characterization, and mechanical properties of red mud-based geopolymers', *J Transp Res Board*, 2167, 1–9.

Zhang J, Provis J L, Feng D and van Deventer J S J (2008a), 'The role of sulfide in the immobilization of Cr(VI) in fly ash geopolymers', *Cem Concr Res*, 38(5), 681–688.

Zhang J, Provis J L, Feng D and van Deventer J S J (2008b), 'Geopolymers for immobilization of Cr^{6+}, Cd^{2+}, and Pb^{2+}', *J Haz Mat*, 157(2–3), 587–598.

Zheng L, Wang C, Wang W, Shi Y and Gao X (2011), 'Immobilization of MSWI fly ash through geopolymerization: effects of water-wash', *Waste Manag*, 31(2), 311–317.

The development of alkali-activated mixtures for soil stabilisation

21

P. Sargent
AECOM, Newcastle upon Tyne, UK

21.1 Introduction

Chemical (admixture) stabilisation introduces cementitious materials to soft problematic soils, with a view to improving their engineering properties including strength and durability. Portland cement (CEM-I; BS EN: 197-1) and lime have long been utilised as binders; the former is considered more favourable in providing rapid strength enhancements (Rogers *et al.*, 2000; Hossain, 2010; Jegandan *et al.*, 2010). The presence of soil water and calcium silicates/aluminates within the binders react to form hydration products including calcium silica hydroxide (C-S-H) and calcium aluminate hydroxide (C-A-H) gels.

Negative environmental and financial issues are associated with utilising CEM-I and lime as binders; specifically high energy consumption, financial cost, greenhouse gas and carbon emissions. The continued use of these binders is not sustainable. Hence, there is a need to identify more environmentally and financially sustainable replacement binders. These binders should provide engineering performances that are either comparable or surpass those of CEM-I and lime within similar curing times.

A popular route for selecting new binders has been to recycle industrial by-products (IBPs), preferably those which are alumino-silicate based (i.e., pozzolanic). The introduction of alternative alkali activators such as sodium hydroxide to these IBPs, can increase the rate at which the mechanical properties of stabilised soils are improved by increasing soil pH, thereby allowing pozzolanic reactions and cementitious bonding to occur (Palomo *et al.*, 1999).

The primary aim of this chapter is to present the most up-to-date literature on the development and use of alkali-activated cements as binders for chemical soil stabilisation. The first few sections address the basic mechanisms of chemical soil stabilisation, traditionally used binders and this technique's applicability in geotechnics. Findings from recent research on sustainability in terms of environmental and financial costs will then be presented, outlining the need for new sustainable binders. The final sections will then present findings from recent laboratory-based research on the development of new alkali-activated cement mixtures, in addition to possible future trends in this research area.

Handbook of Alkali-activated Cements, Mortars and Concretes. http://dx.doi.org/10.1533/9781782422884.4.555

21.2 Basic mechanisms of chemical soil stabilisation

There are five main reactions which occur between the binder and the soil to be stabilised: cation exchange, flocculation/agglomeration, hydration, pozzolanic reactions and potentially carbonation. Cation exchange and flocculation/agglomeration occur immediately upon mixing and can last for up to a few hours afterwards. Hydration takes place up to one month post-mixing, whereas pozzolanic reactions occur over a longer time-scale, i.e. months or years.

21.2.1 Cation exchange

Immediately upon mixing, the introduction of a binder to the soil releases calcium ions, which can exchange with metal ions (e.g., Na^+ and Al^{3+}) incorporated within the soil's clay lattice (Rogers and Glendinning, 1996). This process is referred to as cation exchange, which results in numerous physical changes to the soil. One of the first changes to occur is a reduction in the electric double (adsorbed water) layer surrounding clay particles (Rogers and Glendinning, 1996). The physical arrangement of clay particles dictates the size of the electric double layer; parallel arrangements allow larger envelopes to form compared with 'edge-to-face' arrangements. A reduction in the electric double layer thickness means that clay particles are less prone to the addition of water. The second change experienced is flocculation, whereby van der Waals forces overcome the repulsion of the negatively charged clay particles, bringing them into close proximity with each other and further reducing the thickness of the adsorbed water layer (Figure 21.1).

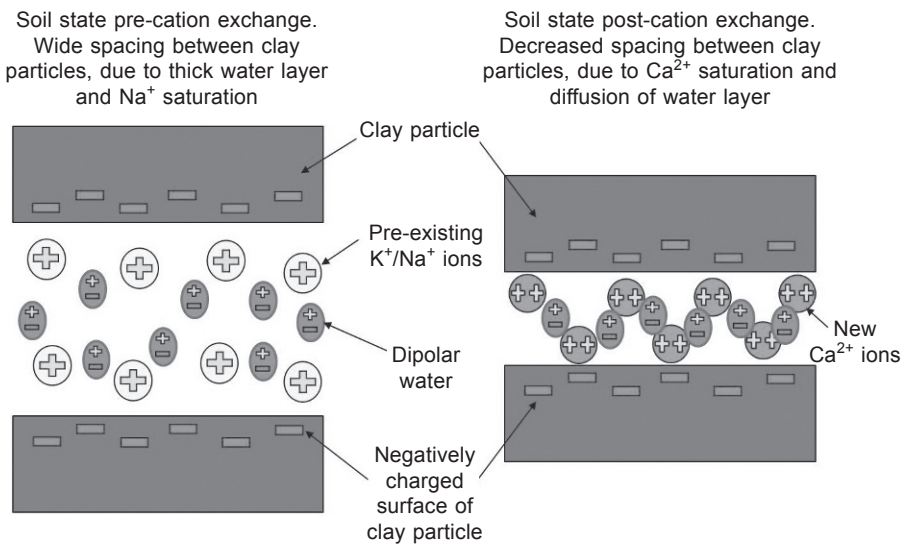

Figure 21.1 Diagram demonstrating cation exchange within soils, which occurs immediately upon introducing a binder such as lime or cement.

The aforementioned changes result in numerous textural and strength changes within the soil; namely a transition from a medium–high plastic clay to a more granular and friable soil characterised by a lower plasticity index. This results in an increase in the friction angle between agglomerate matter and consequently an increase in shear strength (Rogers and Glendinning, 1996).

Some of the most common cations involved in cation exchange include aluminium (Al^{3+}), calcium (Ca^{2+}), magnesium (Mg^{2+}), potassium (K^{+}), ammonium (NH_4^{+}), sodium (Na^{+}) and hydrogen (H^{+}). A cation's adsorption potential is influenced by valence and atomic weight, whereby the higher these values, the higher the cation's adsorption level.

21.2.2 Flocculation

Flocculation/agglomeration occurs immediately post-mixing, involving the restructuring of negatively charged clay particles which are surrounded by a positively charged cation shell. The cation shell's thickness depends on the level of charge; the higher the charge the thicker the shell. Initially, the clay particles are dispersed and occur in a parallel arrangement, due to their negative surface charge and positively charged cation shells repelling each other. This repulsion may be overcome by van der Waals forces, causing particles to flocculate and give a new edge-to-face orientation (Figure 21.2).

There are two divisions of flocculators: good flocculators are ions with larger hydrated radii and higher valences (≥2+) (Sumner and Naidu, 1998), including Ca^{2+} and Mg^{2+}; poor flocculators include ions with smaller hydrated radii and lower valences, including Na^{+} and K^{+}. As a result of flocculation, soils gain improved

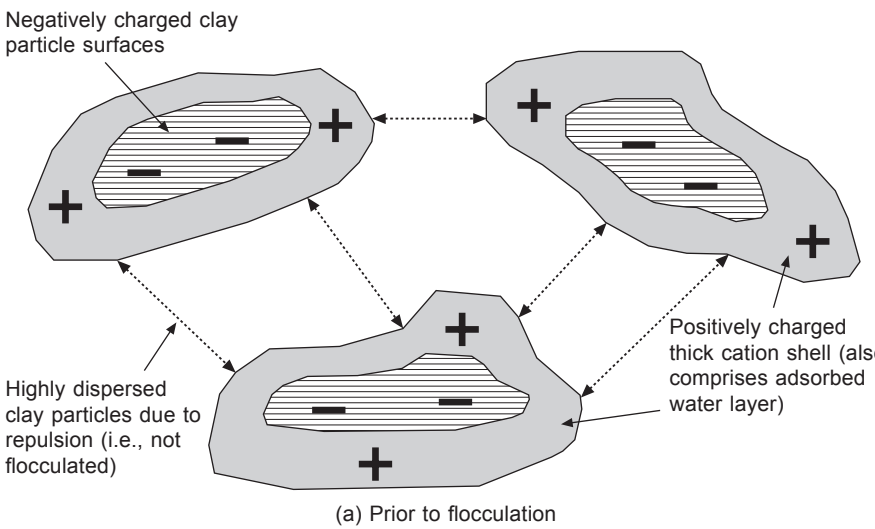

Figure 21.2 Illustration of the state of a soil (a) prior to and (b) post flocculation.

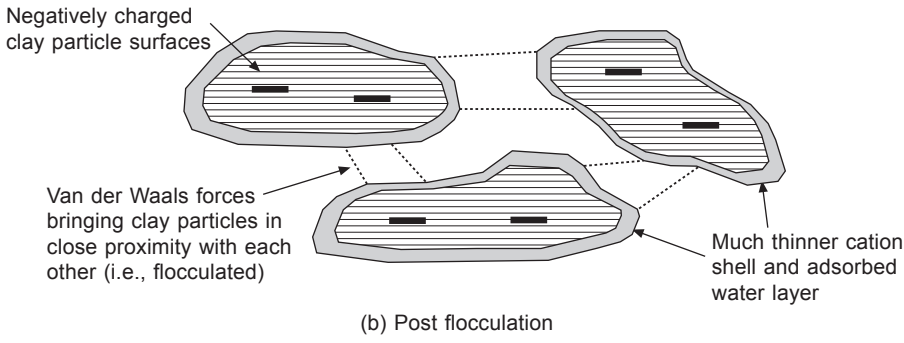

Figure 21.2 Continued

engineering performances, specifically by increasing the plastic limit, increasing shear strength and the development of a granular texture.

21.2.3 Hydration

Hydration occurs when combining water with lime or cement (Eq. 21.1). The hydration of quicklime is exothermic (Figure 21.3); whereby occasionally the amount of heat produced can cause a soil's pore water to boil (Bergado *et al*., 1996). Upon mixing, the soil's water content instantly decreases as the water is consumed during hydration. This drying process is key in improving soft soils with high moisture contents. According to Bergado *et al*. (1996), the moisture content of the soil must be sufficiently high in order for the quicklime to be completely slaked. There must also be sufficient amounts of water post-evaporation due to the heat produced during slaking, to ensure that ion exchange occurs between calcium ions of hydrated lime and alkali ions of clay minerals (Bergado *et al*., 1996).

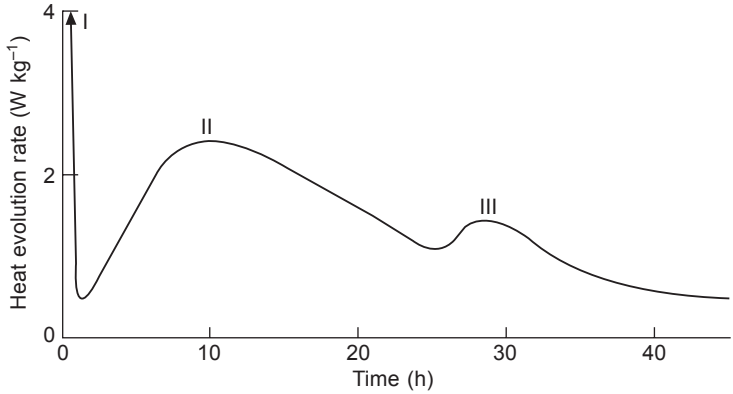

Figure 21.3 Heat evolution during hydration of ordinary Portland cement at 20°C and a water–cement ratio of 0.4. Note the three maxima (I, II and III) in hydration reaction rates. Courtesy of Bye (2011). Reproduced with permission from the Institution of Civil Engineers.

$$CaO + H_2O \rightarrow Ca(OH)_2 + Heat \quad (21.1)$$

The calcium oxide reaction product from Eq. (21.1) dissociates in the pore water, which increases its electrolytic concentration and pH (Eq. 21.2), thereby dissolving SiO_2 and Al_2O_3 from the soil's clay particles (Bergado *et al.*, 1996). These will collectively allow ion exchange, flocculation and pozzolanic reactions to occur (Bergado *et al.*, 1996).

$$Ca(OH)_2 \rightarrow Ca^{++} + 2(OH)^- \quad (21.2)$$

There are two mechanisms involved during hydration: 'through solution' and 'topochemical' (Kurtis, 2007). Through solution involves the dissolution of anhydrous compounds towards their ionic constituents, hydrate formation within the solution and ultimately their precipitation, given their low solubility (Kurtis, 2007). The topochemical mechanism (solid state hydration) involves reactions that occur on anhydrous cement compound surfaces whilst not going into solution (Kurtis, 2007). Five key phases occur upon mixing cement with soil water; firstly the cement particles undergo dissolution followed by increases in ionic concentration levels within the water. Once ionic concentrations have become sufficiently high, compounds develop within solution, whereby once ionic concentration has become saturated these compounds precipitate as solid hydration products. These products form close to or on the surfaces of anhydrous cement particles (Kurtis, 2007).

Four main strength-producing compounds exist within CEM-I, two are silicate-based, two are aluminate-based. Tricalcium silicate (C_3S) hydrates and hardens quickly and accounts for any early setting and strength gains (3 hours–14 days post-mixing).

The second main hydrated cement compound is dicalcium silicate (C_2S) which hydrates and hardens relatively slowly. Rather than contributing towards initial strength gains, the strengthening effects of C_2S are observed at a later stage; normally between 7 and 14 days (Kurtis, 2007). Higher levels of heat are associated with C_3S hydration than with C_2S. The two aluminate-based hydrated cement compounds are tricalcium aluminate (C_3A) and tetracalcium aluminoferrite (C_4AF), whereby the former releases considerable amounts of heat during the first couple of days of curing and is most useful in terms of initial strength development; whereas, the C_4AF hydrates quickly and decreases the clinkering temperature, contributing very little towards strength development (Kurtis, 2007).

All four of the aforementioned compounds are important for providing strength gains. Immediately upon mixing, the cement hydrates very rapidly and produces primary cementitious products (a.k.a. major hydration products), these being hydrated calcium silicates (C_2SH_x and $C_3S_2H_x$) and aluminates (C_3AH_x and C_4AH_x) and hydrated lime (Bergado *et al.*, 1996). The cement particles then create bonds between adjacent cement grains and undisturbed soil particles during the hardening phase, ultimately creating a stronger soil–cement skeleton.

By hydrating both C_3S and C_2S, C-S-H and calcium hydrates (CH) are produced (Figure 21.4); however, C_2S produces significantly lower amounts of CH, which is vital for durability purposes within sulphate-bearing soils (Kurtis, 2007). As is

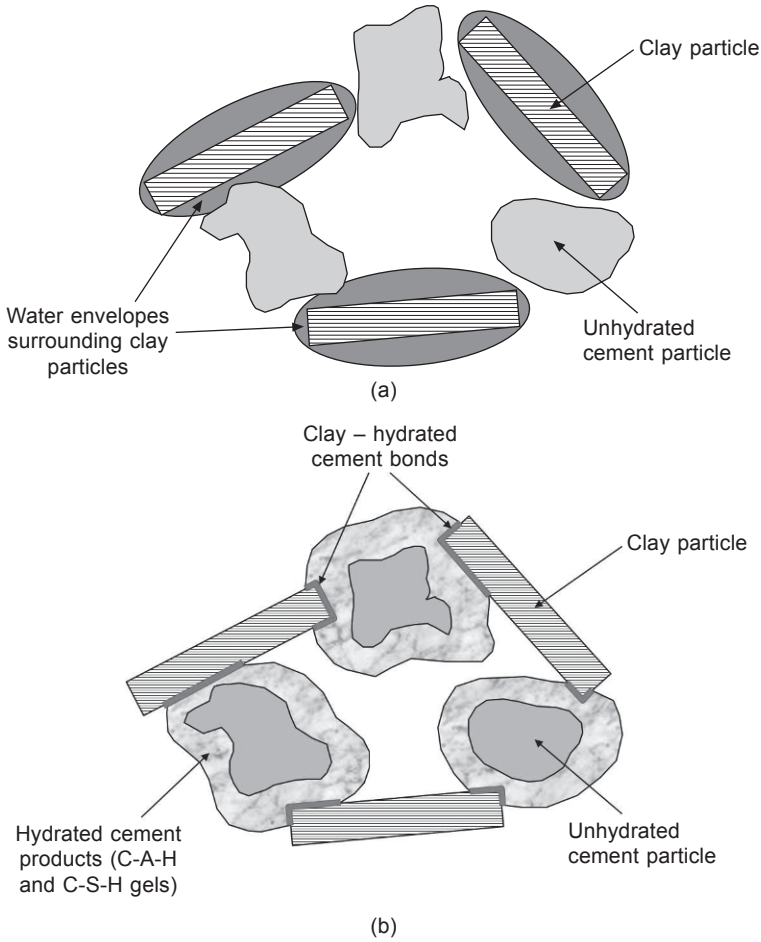

Figure 21.4 The typical state of a soil mixed with cement (a) prior to hydration and (b) after a few weeks curing, whereby the cement has reacted with the soil water and produced hydrated cementitious gels.

commonly known for most chemical reactions, temperature influences the rate of hydration.

C-S-H gels are generally poorly understood regarding their mineralogical structure, due to their wide variation from amorphous to poorly crystalline (Kurtis, 2007). C-S-H is the primary strengthening mineral within CEM-I via ionic and van der Waals bonds, whereby it takes up to 60% of the hydrated cement paste and takes up large surface areas of up to 700 m^2/g (Kurtis, 2007).

According to Kurtis (2007), as the hydration rates of the aforementioned five phases can significantly differ, factors such as the rate of cement hardening, the amount of time required for cement to stiffen and the setting time will ultimately depend on the cement composition. Cement hydration also leads to an increase in

the soil pore water's pH as a direct consequence of the dissociation of the hydrated lime (Bergado *et al.*, 1996).

21.2.4 Pozzolanic reactions

Pozzolanic reactions occur over long time scales (months to years). The main mechanism involves the transportation of calcium hydroxide via water within the soil to combine with the aluminate and/or silicate clay minerals (Duxson *et al.*, 2007). The high surface area aluminate and silicate minerals are pozzolan phases, which in the presence of water and an alkali (e.g., calcium) produce cementitious materials, comprising calcium silicates and aluminate hydrates (Bergado *et al.*, 1996). Any dissolved Ca^{2+} ions within the soil then react with any dissolved SiO_2 and Al_2O_3 located on clay particles to produce hydrated gels of C-S-H and C-A-H, which cement soil particles together as can be seen in Figure 21.5.

$$Ca^{2+} + 2(OH)^{-} + SiO_2 \rightarrow C–S–H \tag{21.3}$$

$$Ca^{2+} + 2(OH)^{-} + Al_2O_3 \rightarrow C–A–H \tag{21.4}$$

Pozzolanic reactions consume part of the soil's water content. This is preferable in terms of engineering performance of the stabilised soil, as the material becomes stiffer and less susceptible to volume shrinkage/swelling. The soil–binder mixtures cure and produce stronger, cementitious soil matrices known as 'geopolymers' (Sherwood, 1993), which will be able to resist dissolution and soil erosion.

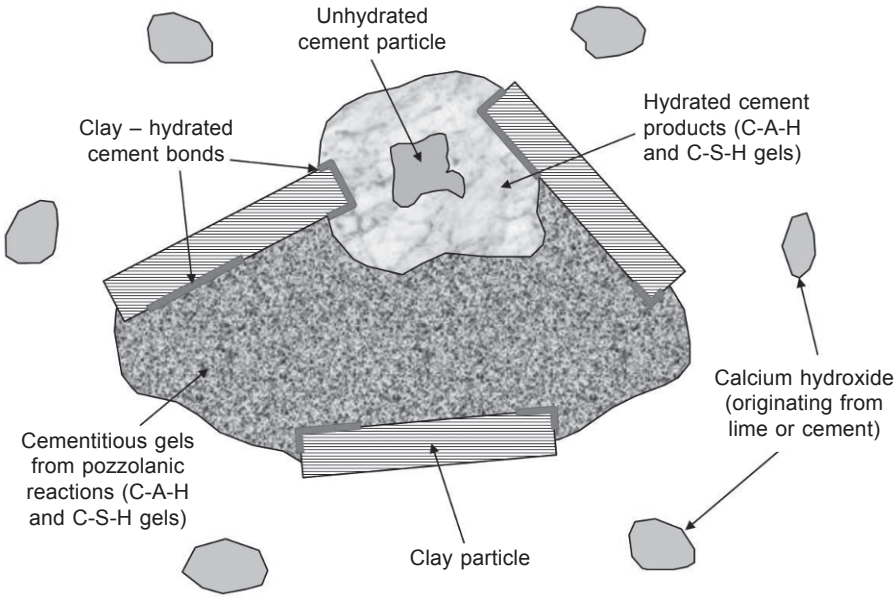

Figure 21.5 Cementitious bonding products formed during hydration and long-term pozzolanic reactions.

According to Bergado *et al*. (1996) and Diamond and Kinter (1965), pozzolanic reactions are not complete until five years post-mixing. The solubility potential of silicates and aluminates within the soil, their likelihood of reacting with lime/cement and cementitious bond formation rely heavily on soil pH. According to Davidson *et al*. (1965), pozzolanic reactions only occur when soil pH is ≥10.5, as this is when SiO_2 and Al_2O_3 become soluble. Broms (1984) and Palomo *et al*. (1999) suggest that if samples cure at higher temperatures during the first 5 hours post-mixing, reaction rates are increased, resulting in further improved strengths.

21.3 Chemical stabilisation techniques

Chemical treatment is a versatile ground improvement technique, which is suitable for stabilising various soils up to 25 m depth. A key advantage of this technique is that a large range of binders are available for selection, each having their own unique set of physicochemical properties that are advantageous in stabilising a soil. Both the soil's and binder's material properties must be carefully studied prior to stabilisation, as a binder may show impressive strength gains within one soil and damaging effects in another.

21.3.1 Surface and shallow soil mixing

Surface and shallow mixing are low cost techniques for enhancing the mechanical properties of soft soils, which cover large areas (Topolnicki, 2004). Surface mixing involves the incorporation of a lime or cement-based binder (dry or wet) within the top 250 mm of soil at air temperatures > 7°C (Figure 21.6). This technique has long been used in the United States and Australia for treating soft subgrades.

Prior to mixing, the binder may be applied by spreading either a dry powder or slurry. Soils which are most suitable for surface mixing are characterised by clay contents > 10%, plasticity index (PI) > 20, an activity PI–clay content ratio > 0.75 and a sulphate content < 1%.

For stabilising the subgrade, the typical binder dosage should be > 2.5%. Once the binder has been mixed into the soil, an uneven surface is produced. Thus, a roller follows behind the mixer to compact the stabilised soil. The main advantage of using surface mixing is negating the need to remove poor soil away from site. Onsite stabilisation reduces the amount of binder/aggregate that would be required if significant quantities of poor soil were to be replaced. Depending on the soil and binder type, additional binder may be introduced to increase strength gain rates. Numerous disadvantages are associated with surface mixing, the most serious of which is dust and atmospheric pollution caused by plant equipment.

Shallow mixing involves treatment up to 3 m depth, whereby large diameter augers and mass mixers stabilise a specific volume of soil (Topolnicki, 2004), commonly called 'mass stabilisation'. The uppermost soil layers may be insufficiently strong to support heavy mixing equipment. Therefore mass mixers/augers should either be

Figure 21.6 Photograph of surface mixing taking place at a site in India (courtesy of Wirtgen Group, 2014).

suspended from a crane or mounted to a cantilever. It is normal practice to initially stabilise a 2 m wide × 5 m long × 3 m deep block of soil that is positioned onsite so it is within the crane's operational range (Topolnicki, 2004). One major disadvantage with shallow mixing is high emissions. To reduce such emissions, mixing tools may be fitted with a hood/bottom-opened cylinder, temporary low-pressure blowers, vacuum pumps, dust collectors, fume incinerators and activated carbon scrubbers (Topolnicki, 2004).

21.3.2 Deep soil mixing

Deep soil mixing (DSM) is used for various geotechnical applications on- and offshore, ranging from environmental remediation to ground improvement for construction purposes including foundations, excavation wall support, liquefaction mitigation, slope stabilisation and embankment hydraulic cut-off walls. DSM involves the mechanical disturbance of a soil via auger mixing up to depths of 25 m (Quasthoff, 2012). Once the auger has been drilled to the required depth, its rotation direction is then reversed and retrieved whilst a binder is pumped through the auger drill bit. The auger's rate of rotation and binder flow must remain constant during mixing, to ensure homogeneous stabilised soil columns are produced. Various auger drill bits are available for use in DSM; whereby the drill bit used depends upon the DSM column diameter required and the soil being stabilised. The fins of the all drill bits are orientated to ensure compaction occurs along the column's length upon auger retraction.

DSM has numerous advantages over other deep ground improvement techniques, including its applicability within a wide variety of soils and its minimal environmental impact due to low levels of vibration, noise and spoil. DSM has high levels of productivity, making it economical for larger projects (Topolnicki, 2004). The desired engineering properties of DSM soils are easily adjustable, as are the column spacing and their installation pattern (Figure 21.7).

For chemical treatment, there are dry and wet mixing methods. Dry mixing involves a dry binder being injected under compressed air into the surrounding soil via nozzles at the tips of the auger mixing tool's blades (Figure 21.8). A similar

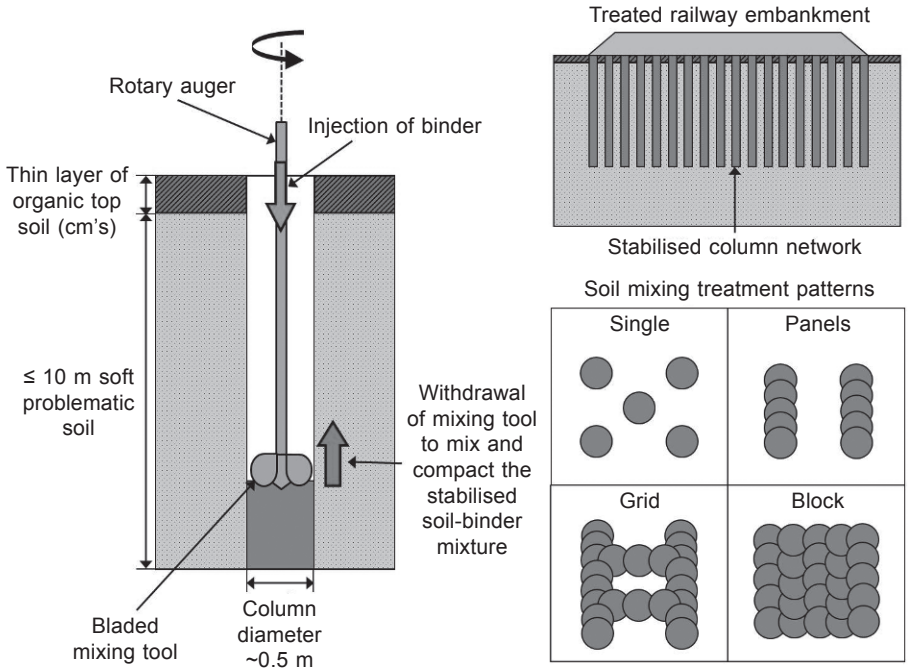

Figure 21.7 Illustration of the DSM technique and its application in ground improvement.

Figure 21.8 Dense network of solidified DSM columns (courtesy of Treviicos, 2013).

process is involved for wet mixing, whereby the binder slurry is supplied from a delivery pump. However, more expensive plant equipment is required, namely a water tank, a temporary storage tank and large silos (Topolnicki, 2004). When determining whether to use wet or dry mixing, the soil's moisture content must be considered. Cohesive soils with moisture contents of 60–200% are most suited for dry mixing (Topolnicki, 2004).

For soils with moisture contents < 20% and/or lower than the soil's plastic limit, the volume of water within the soil would be insufficient for hydration. For DSM projects where high strength columns are essential, wet mixing should be used as it provides higher levels of homogeneity due to longer mixing times. Dry mixing tends to be used when using either a combination of cement and lime or IBPs as binders.

Dry mixing is preferred over wet mixing in regions where long periods of cold temperatures, freeze and thaw cycles are experienced (e.g., Scandinavia) as water-based delivery systems are prone to freezing (Topolnicki, 2004; Quasthoff, 2012). When installing DSM columns through harder stratified soils, wet mixing should be used as the slurry acts as a lubricant, aids and ensures higher torque capacity and consistent strengths along the length of the columns (Topolnicki, 2004).

Since DSM was pioneered in Scandinavia and Japan during the 1960s, the technique has become increasingly popular. Countries including Belgium, Germany, China and US commonly use the technique (Topolnicki, 2004); whereas the UK has only used it since the 1990s (Al-Tabbaa, 2003). For dry and wet DSM, lime and cement have predominantly been used as binders since the 1970s, based on their high strength performance. Where DSM is used for environmental remediation, cementitious binders are substituted with chemical oxidation agents and reactive materials (Topolnicki, 2004).

The strength of DSM soils depends on numerous factors, including the blade rotation number, the mixing energy used, the binder dosage and soil type (Topolnicki and Pandrea, 2012). Table 21.1 summarises the expected engineering properties of DSM soils after 28 days.

Table 21.1 Summary of typical unconfined compressive strength (UCS) and permeability values expected after 28 days curing for various soil types and binder dosages

Soil type	Binder dosage (kg/m^3)	Expected permeability, k (ms^{-1})	Expected UCS (MPa)
Sludge	250–400	1×10^{-8}	0.1–0.4
Peat/Organic silts and clays	150–350	5×10^{-9}	0.2–1.2
Soft clays	150–300	5×10^{-9}	0.5–1.7
Medium–hard clays	120–300	5×10^{-9}	0.7–2.5
Silts and silty sands	120–300	1×10^{-8}	1.0–3.0
Fine–medium sands	120–300	5×10^{-8}	1.5–5.0
Coarse sands and gravels	120–250	1×10^{-7}	3.0–7.0

Source: Data courtesy of Geo-Con, Inc. (1998) and FHWA (2001).

21.4 Soil suitability for chemical treatment

The characteristics of both the stabilisation reactions and the end-products are controlled by numerous key factors associated with the nature of the soil; namely mineralogy, soil grading, cation exchange capacity (CEC) surface area and moisture content. Given that such properties vary greatly between soils, chemical stabilisation may not be suitable for treating all soils.

From Figure 21.9, chemical treatment may be used for soils comprising fine clays to medium/coarse sands. Soils which are deemed suitable for soil mixing include most silts, clays, peats and some non-cohesive granular soils. Soils are required to have a moisture content of ≥20% for DSM to be effective (Quasthoff, 2012). Generally, cohesive fine grained soils achieve better engineering performances after chemical treatment compared with non-cohesive coarse grained soils.

To understand a soil's capacity to react with binders and ultimately produce cementitious gels, workers including Sargent *et al*. (2013) have determined that it is necessary to conduct specific surface area and CEC analyses. Other factors including the organic and sulphate contents of soils also have a role in assessing whether a soil is suitable for chemical treatment.

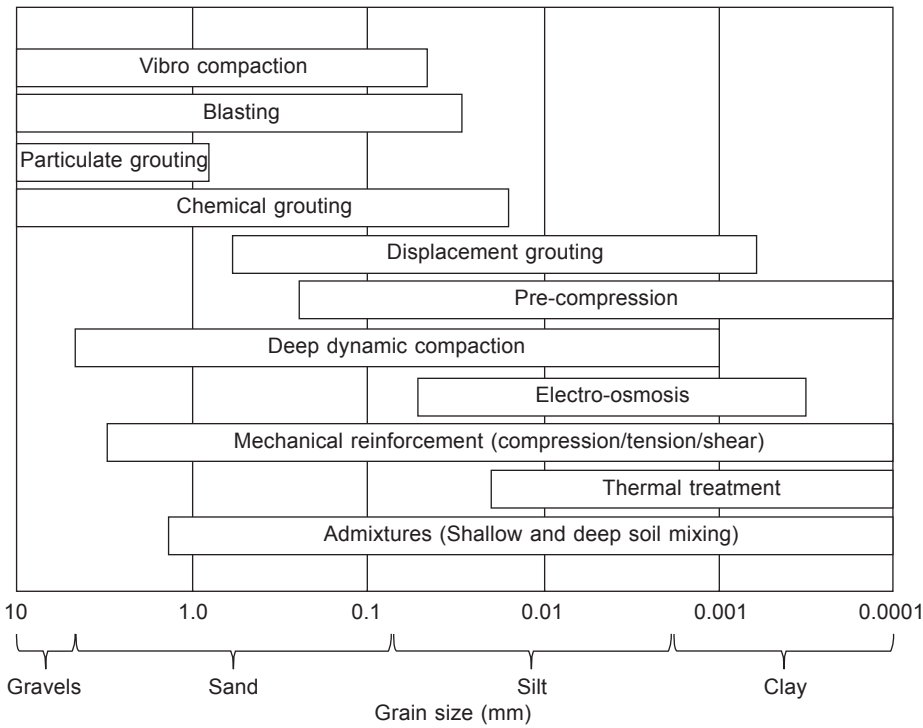

Figure 21.9 Graph showing the influence of a soil's PSD on the applicability of ground improvement techniques which can be used.

21.4.1 Surface area and cation exchange capacity

Quantifying the specific surface area of a soil provides insights into its CEC and particle size distribution. Clay particles have high surface areas, therefore soils with high surface area values indicate high clay contents. This implies that the soil's CEC is likely to be high, suggesting that the soil would be well suited to chemical stabilisation. One of the most widely used techniques for determining the specific surface area of soils is the Brunauer Emmett Teller (BET) method, which involves nitrogen gas adsorption on particle surfaces (Brunauer *et al.*, 1938).

CEC provides an estimate of the net negative charge on soil particulate matter as a result of isomorphous substitution and broken bonds at boundaries (Terzaghi *et al.*, 1996), i.e. the number of sites within a soil which are able to attract, retain and exchange cations. Large proportions of most soils comprise clay minerals and organic matter, both of which are characterised by negative surface charges, implying that they must attract cation elements of the opposite charge. Cations which neutralise negative surface charges within water are able to be exchanged with other cations, which depends upon the cation concentrations within the soil water and their electrovalences (Terzaghi *et al.*, 1996).

Out of kaolinite, illite and montmorillonite, montmorillonite has the highest CEC (Table 21.2), due to its structure comprising multiple single unit sheets (Terzaghi *et al.*, 1996).

Soils containing clay minerals with high CEC values will experience more significant mechanical changes upon mixing compared with those containing clay minerals with low CEC values (Rogers and Glendinning, 1996). Low CEC values are representative of soils characterised by low organic matter contents and low clay/high sand contents (Figure 21.10), which can be expected from river alluvium deposits (Cooper, 2009). A soil's surface area can influence its physical and chemical characteristics, whereby a larger surface area provides more cation exchange surfaces.

Knowledge about the CEC and surface area properties of a soil provides an insight into its potential cementitious gel formation. By using CEC values obtained from laboratory testing and Eq. (21.5) (Meunier, 2005), the CEC-related charge density (σ_{CEC}) may be calculated:

$$\sigma_{\mathrm{CEC}} = \frac{e(\mathrm{CEC} \times 10^{-2})}{2\,ab} \tag{21.5}$$

where e = the elementary charge, which has a constant value of 1.6022×10^{-2} C,

Table 21.2 Summary of cation exchange capacity values of the three principal clay minerals

Clay mineral	Cation exchange capacity (meq/g)
Kaolinite	0.03–0.1
Illite	0.2–0.3
Montmorillonite	0.8–1.2

Source: Values courtesy of Terzaghi *et al.*, 1996. Reproduced with permission from John Wiley & Sons, Inc.

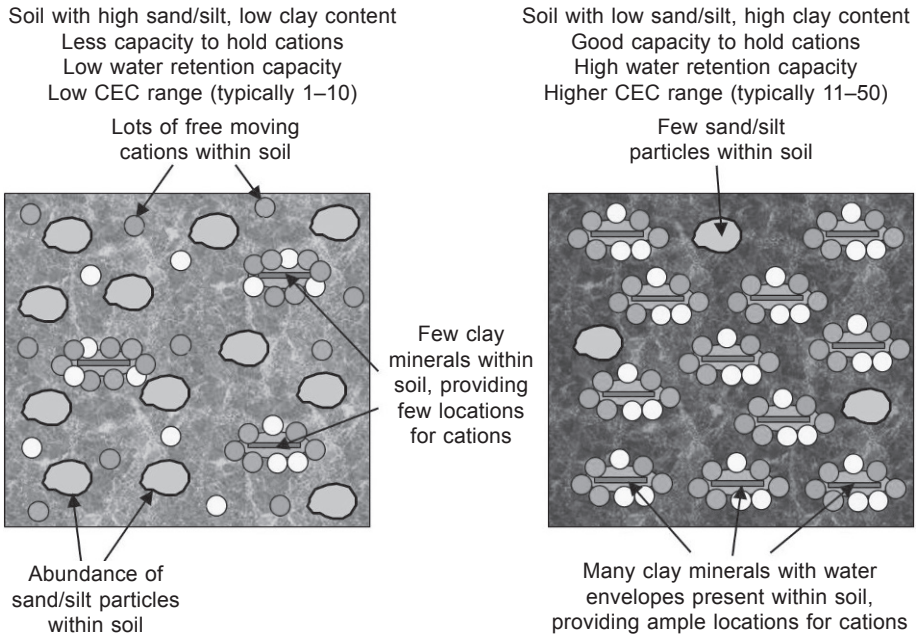

Figure 21.10 Schematic showing how cation exchange capacity varies between soils that are predominantly composed of sand/silt and those of mainly clay particles.

and a and b are unit cell parameters for the clay mineral in the x-y plane, where for kaolinite $a = 0.531$ nm and $b = 0.92$ nm; values taken from Meunier, 2005.

Following Table 21.3, low surface area, organic matter and CEC values can be expected of sandy and silty soils such as loam and alluvium (Ersahin *et al.*, 2006).

Table 21.3 Summary of surface area, organic matter and CEC characteristics typically expected for various soils

Soil No.	Particle size distribution (%)			Texture class	Specific surface area (m^2/g)	Organic matter (%)	Cation exchange capacity (cmol/kg)
	Clay	Silt	Sand				
1	61.2	11.4	27.3	C	234.1	2.0	37.4
2	35.7	11.3	53.0	SiCL	122.6	1.8	22.8
3	14.0	27.5	58.5	SiL	68.4	1.3	14.6
4	35.0	26.0	39.0	CL	133.7	2.4	26.1
5	7.7	58.3	34.0	SL	43.0	0.65	11.0
6	49.0	25.0	26.0	SCL	146.0	2.4	19.3
7	18.0	33.0	49.0	L	53.4	1.2	14.8

Note: C = Clay, SiCL = Silty clay loam, SiL = Silty loam, CL = Clay loam, SL = Sandy loam, SCL = Sandy clay loam and L = Loam. The texture classification scheme used by Ersahin *et al.* (2006) was that of the USDA.
Source: Adapted from Ersahin *et al.*, 2006. Reproduced with permission from Elsevier.

21.4.2 Other factors

Although CEC and surface area have a considerable role in dictating a soil's suitability for chemical treatment, other parameters to consider include particle size distribution, organic and sulphate contents.

Soils containing high fines contents which are chemically treated produce the most impressive strengths (Puppala *et al*., 2008). This is related to surface area characteristics; whereby soils with higher surface areas are characterised by relatively high CEC values, which are ideal for cementitious bonding and strength development.

Chemical treatment has long been applicable for soft clayey soils with high degrees of total organic matter (TOM). However, the level of improvement gained for soils with high TOM values will be of lower magnitude compared with that achieved by soils with low TOM values. Delle Site (2000) provides a conversion factor of 1.724 to convert total organic carbon (TOC) values to TOM.

TOM interferes with the chemical reactions occurring between the soil and binder. The higher the degree of a soil's organic matter decomposition (OMD), the stronger the soil will be upon stabilisation. Prior to stabilisation, a soil's TOM value affects its Atterberg limits and pH (Puppala *et al*., 2008). Oven and air drying such soils increases acidity and reduces plasticity. Once treated with lime-cement, Puppala *et al*. (2008) documented poor strength developments, which were attributed to the soil becoming more plastic rather than more acidic. A large fraction of a soil's organic content comprises humified material, which has adverse effects on strength development (Puppala *et al*., 2008). The presence of lime in organic soils inhibits strength development, as it increases organic solubility, resulting in higher degrees of homogenisation in terms of organic distribution within the soil (Puppala *et al*., 2008). Hence for organic soils, the use of CEM-I is preferred over lime or lime-cement.

The final aspect of a soil's chemistry to consider is sulphate content. Soils with sulphate contents > 3000 ppm are problematic, whereby ettringite formation is inevitable. For such soils, Little and Nair (2009) recommend that whilst it is impossible to fully solubilise all sulphates, water should be used to thoroughly mix the soil to ensure that sulphates and all possible ettringite formation sites are homogeneously distributed.

Sulphates occur as gypsum but are not uniformly distributed through the soil column; they most commonly occur in seams or as lenses. Climate has an impact on ion movement within soils; whereby in dry arid climates where evaporation is common, sulphates are located within the shallow surface. For wet humid climates, sulphates may be found at greater depths due to water infiltration. However, capillary action can cause water and sulphate sources to rise towards the surface (Little and Nair, 2009). Local terrain, geological and hydrological conditions also influence sulphate distribution. In regions characterised by hilly topography, (gravitational) surface and sub-surface water flow are common, which results in soils with high moisture and sulphate contents, along with high potentials of ettringite formation and surface heave on valley floors.

Clay-rich soils have higher moisture-retention capabilities, and higher sulphate

and salinity contents compared with most other soils (Little and Nair, 2009). These characteristics are key for ettringite and thaumasite production, which are hydrous calcium aluminate sulphate (Aft) minerals as can be observed in Figure 21.11 (Wilkinson *et al*., 2010a). These cause volumetric expansion within soils that have been stabilised with calcium-based binders (Little and Nair, 2009). In contrast to soils containing high organic contents, the presence of lime does not inhibit strength development as it decreases organic solubility and does not interfere with chemical reactions between the soil and lime (Puppala *et al*., 2008).

The high surface areas of ettringite and thaumasite provide high reactivity rates, which allow reactants to become available as soluble ions (Little and Nair, 2009). Hence, ettringite formation in CEM-I concrete is rapid and relies on the matrix sulphate content, whereas for stabilised soils, ion availability in solution depends on the soil's mineralogy, degree of initial flocculation and dissolution properties (Little and Nair, 2009).

In chemical stabilisation, there are two phases of ettringite formation (Little and Nair, 2009); the first occurs during initial hydration and does not present any damaging effects. The second stage occurs later in the curing process when the soil's cemented matrix has been established, which may lead to deterioration. The environmental and weathering conditions which soil particles are subjected to create higher levels of heterogeneity compared with CEM-I, meaning that fewer ions are available in solution to produce ettringite in stabilised soils compared with cement pastes (Little and Nair, 2009). Thus, ettringite does not form as rapidly in stabilised soils as it does in cement.

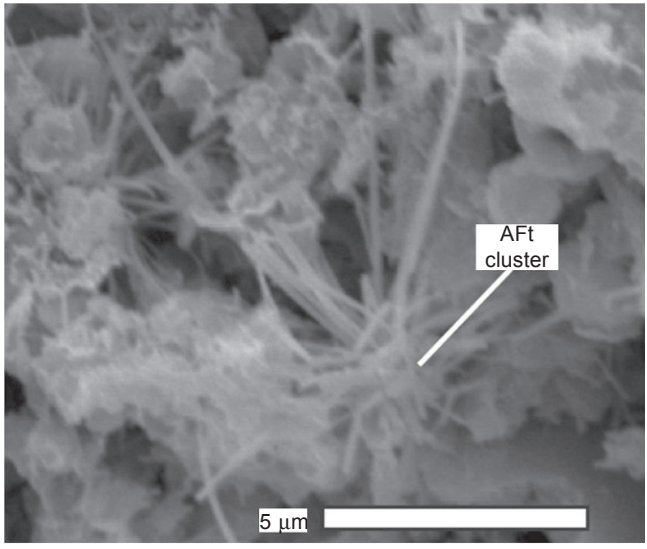

Figure 21.11 Ettringite (AFt) formation within PFA-stabilised Ginifer soil after 28 days. Courtesy of Wilkinson *et al*. (2010a). Reproduced with permission from the Institution of Civil Engineers.

No single binder will necessarily be suited for stabilising all problematic soil types, due to the natural complexity of soils. It is common for binders to comprise two or three materials, as the chemistry of a single material may not be as efficient in creating the ideal conditions for cementitious bond formation compared with the use of two or three materials. A soil's chemistry and basic geotechnical classification dictate the binder design to be used for its stabilisation. It is strongly advised that EuroSoilStab (2002) be studied prior to treatment, in order to select the most appropriate binder mix for stabilising the problematic soil at hand.

21.5 Traditional binder materials

Since the 1960s, there have been various binders that have been widely used, depending on the soil type to be stabilised. The ideal binder should bond soil particles together and waterproof the material. However, not all binders are able to do both within all soils. The performance of binders whose primary aim is to bond soil particles depends upon the strength of the stabilised soil's matrix, whether bonds form between soil particles and the matrix and whether individual or agglomerations of soil particles are bonded with each other (Sherwood, 1993). Binders will not completely waterproof a soil; however, they will ensure less water absorption, whereby their purpose is to ensure that the soil's moisture content is kept to a minimum. The performance of such binders is measured by how much the soil's permeability has been reduced (Sherwood, 1993).

The presence of soil water and calcium silicates/aluminates within binders reacts to form C-S-H and C-A-H gels via long-term pozzolanic reactions when soil pH levels are ≥ 10.5 (Davidson *et al.*, 1965). The mixtures then cure and produce stronger, cementitious soil matrices known as 'geopolymers' (Sherwood, 1993). Cement and lime have long been utilised as binders, where the former is more favourable in providing rapid strength enhancements (Rogers *et al.*, 2000; Hossain, 2010; Jegandan *et al.*, 2010). The primary components of Portland cement are tri- and di-calcium silicates. Other constituents may be added to produce advanced cement blends that are more suitable than type-I cement (CEM-I) for specific engineering purposes. CEM-I is most commonly used in soil stabilisation, due to its availability and low cost over other cements (Bergado *et al.*, 1996).

Lime originates from the calcination of chalk or limestone, where calcitic lime may be utilised as either quicklime or slaked lime. Lime treatment is generally used to modify expansive soils by drying the soil and allowing for compaction (Christopher *et al.*, 2006). Additionally, lime may be used to prepare soils for subsequent cement stabilisation (Christopher *et al.*, 2006).

Both lime and cement are available as fine grained powders, making them ideal for dry soil mixing. However, they may also be combined with water to produce slurries (Sherwood, 1993). This eliminates dust emissions and produces more homogeneous soil–binder mixtures, although using slurries is less applicable in highly saturated soils compared with dry powders.

21.6 Alkali-activated waste products as environmentally sustainable alternatives

Negative environmental issues are associated with utilising CEM-I and lime in soil stabilisation, as their production requires large amounts of energy. Dust and sulphur dioxide (SO_2) aerosol emissions from manufacturing plants can pose serious health risks including long-term respiratory diseases. SO_2 is also a primary contributor to trans-boundary pollution via acid rain. CEM-I/lime manufacture also produces high CO_2 emissions, accounting for 5–7% of global CO_2 emissions (Bye, 2011; McLellan *et al.*, 2011). Heavy elements including lead are present within the raw materials and fuels involved in cement manufacture (Bye, 2011), which can be toxic at high concentrations. Environmental pollution has been regulated in the UK since 1805 by the UK Alkali Act and by the Integrated Pollution Prevention and Control Directive (IPCC) in the EU (Bye, 2011).

It has become a priority for the cement/lime manufacture and construction industries to develop new cementitious binders and become more environmentally sustainable (energy consumption and greenhouse gas emissions). New binders should provide engineering performances that are either comparable or surpass those of CEM-I and lime within similar curing times. A popular route for selecting new materials has been the development of geopolymers, which are synthetic alkali alumino-silicates produced when combining a solid alumina-silicate with a highly concentrated aqueous alkali hydroxide or silicate solution (Duxson *et al.*, 2007). Geopolymers commonly use alumino-silicate based (i.e., pozzolanic) industrial by-products (IBPs) (Bye, 2011), which are able to produce high compressive strengths, low shrinkage levels, acid and fire resistance and low thermal conductivity (Duxson *et al.*, 2007; Weil *et al.*, 2009). Also, IBP geopolymers production costs are up to 30% lower than that for CEM-I (Duxson *et al.*, 2007). McLellan *et al.* (2011) conducted a sustainability comparison study between CEM-I and Australian geopolymers, which revealed that geopolymers reduced greenhouse gas emissions by 44–64%.

Popularly used IBPs include ground granulated blast furnace slag (GGBS) from pig iron manufacture, steel slag (SS) and pulverised fly ash (PFA) from coal combustion in power plants, where type C PFA is preferred over type F PFA due to its higher reactivity and better cementitious properties (McCarthy *et al.*, 1984). Red gypsum (RG) as a waste from titanium dioxide (TiO_2) manufacture has recently been developed as a binder (Hughes *et al.*, 2011; Gazquez *et al.*, 2013). From the aforementioned materials, GGBS and type C PFA tend to be the most preferred binders due to the high strengths which they typically achieve. With regard to SS, type F PFA and RG, these tend to be used in combination with other cementitious wastes (GGBS) to produce higher strengths, due to factors including low tricalcium silicate content (Shi *et al.*, 2006). Ashes produced from burning certain organic materials including rice husk and wood may also be used as binders, due to their high levels of pozzolanicity and reactivity, in addition to their high CaO and silica contents (Abu Bakar *et al.*, 2011; Zain *et al.*, 2011; Supancic and Obernberger, 2012).

Certain IBPs require alkali activation in order to initiate pozzolanic reactions, cementitious bond formation and to increase the rate at which mechanical properties

are improved by increasing soil pH (Palomo *et al.*, 1999). Such materials may be sourced naturally or synthetically, although the latter incurs high costs and negative environmental impacts. Alkali silicates (sodium silicate) are the most useful activators. Lime and metakaolin are less popular due to environmental impacts, poor early strength development, long setting times (Moranville-Regourd, 1998; Shi *et al.*, 2006) and the fact that metakaolin requires large volumes of water, which increases a soil's porosity and decreases its stiffness (Duxson *et al.*, 2007).

21.7 Financial costs of traditional versus alkali-activated waste binders

Financial cost in terms of energy consumption, transportation and market price is a significant factor to consider in determining whether alkali-activated geopolymers can become sustainable replacements for CEM-I/lime. If geopolymers are to become serious competitors, their financial cost must be similar to or lower than that for CEM-I and lime. The inclusion of alkali activators within geopolymers significantly increases their overall cost due to the amount of fuel and electricity required in their production (Figure 21.12) (McLellan *et al.*, 2011).

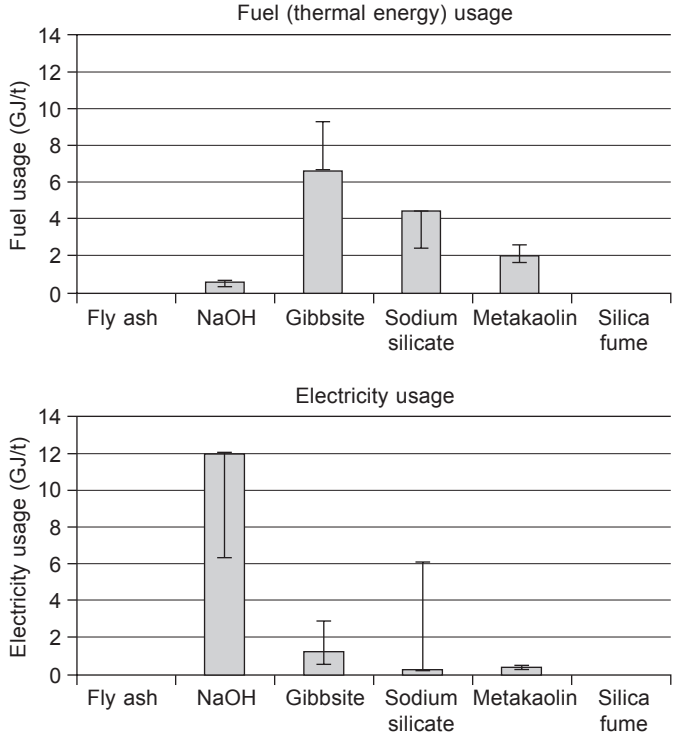

Figure 21.12 Energy usage for geopolymers feedstock production in Australia. Reprinted from McLellan *et al.* (2011), Copyright © 2011, with permission from Elsevier.

However, given that IBPs have no production costs and make up > 80% by dry weight of geopolymers, their inclusion compensates for the high cost of alkali materials. For the Australian geopolymers studied by McLellan *et al.* (2011), the overall cost of most mixtures was not much greater than that of CEM-I, although their transportation costs were considerably higher (Figure 21.13). This therefore raises doubts about the merits of using geopolymers. However, McLellan *et al.*'s (2011) findings were restricted to production and transportation within Australia, where transportation distances can vary greatly. Hence, McLellan *et al.*'s (2011) findings may not be truly representative of transportation costs incurred in other parts of the world where geopolymers are manufactured.

Wherever geopolymers are intended for use, careful assessments should be conducted to ensure that the distances between the binder source and treatment site are minimised, as this influences their overall sustainability, market price

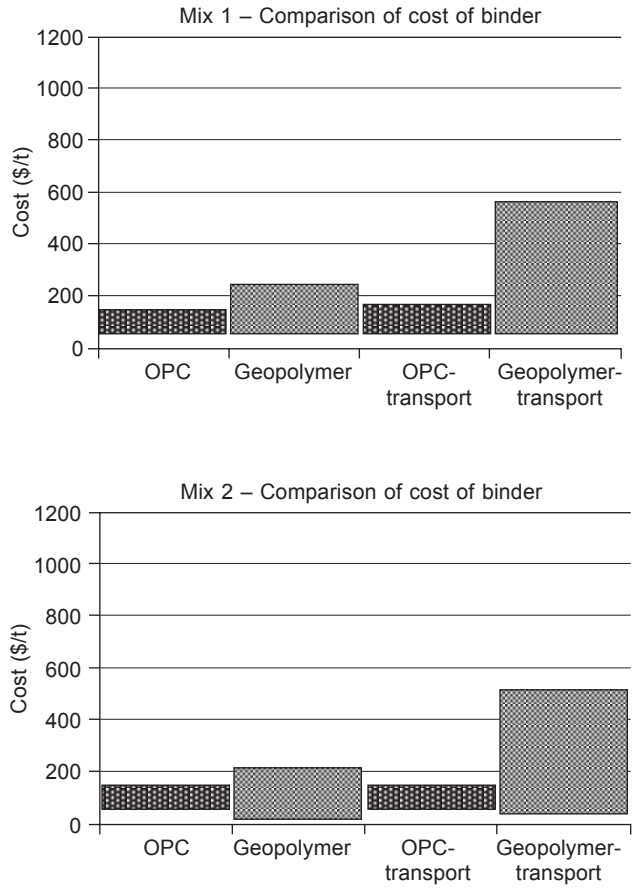

Figure 21.13 Summary of the overall costings for the four Australian geopolymers compared with CEM-I. Reprinted from McLellan *et al.* (2011), Copyright © 2011, with permission from Elsevier.

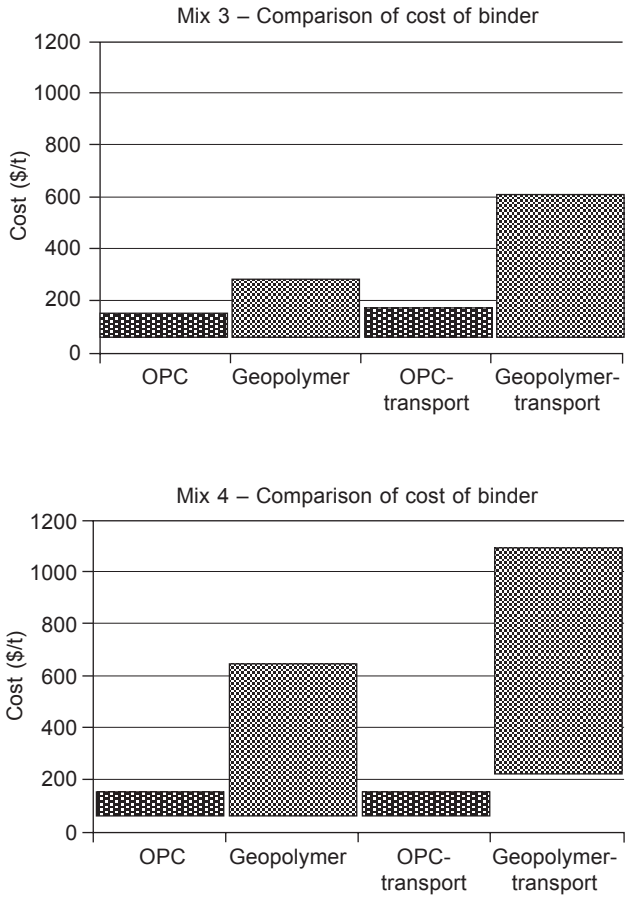

Figure 21.13 Continued

and competitiveness against CEM-I/lime. The market price of NaOH and sodium silicate are considerably higher than other alkalis and IBPs. However, alkalis are only required in small quantities to activate pozzolanic reactions. To summarise, although the inclusion of alkalis within geopolymers can incur high costs due to their production and transport and appear to make geopolymers less able to compete against CEM-I/lime, geopolymers are capable of achieving strengths which surpass those of CEM-I/lime.

21.8 Recent research into the engineering performance of alkali-activated binders for soil stabilisation

There is extensive literature on the laboratory investigation of chemically stabilised soils. There are two main types of laboratory investigations which are conducted

on chemically treated soils: those which examine the mechanical (engineering) performance and those which examine how the mineralogy of stabilised soils change with curing, in order to account for engineering performance enhancements. A number of studies from both types of investigation are presented here.

21.8.1 Al-Tabbaa et al. – Cambridge University, UK

Some of the first studies on the laboratory characterisation of stabilised soils in the UK using IBP-based binders were those by Al-Tabbaa and Evans (1998, 1999). Their studies aimed to develop soil–grout mixtures that were suitable for stabilising soils (made ground, sands and gravels) in terms of strength and environmental remediation, which had been contaminated with organic compounds and heavy metals on a former chemical works site in West Drayton, Middlesex. There was also an emphasis on using as little cement/grout as possible to meet economic and environmental criteria. The binders used included CEM-I, PFA, bentonite and lime to increase soil pH. A soil–grout ratio of 5:1, a water–dry grout ratio of 0.42:1 and a soil–dry grout ratio of 5:1/7:1 were always maintained. After 28 days curing, the mixtures tested reached unconfined compressive strength (UCS) values of 350–1100 kPa, leachate pH values of 6.5–10.5, reasonable wet-dry but poor freeze-thaw durability performances, low permeabilities of 0.2–2.0 $\times$ 10^{-9} ms^{-1} and low M_v values of 2 $\times$ 10^{-6} m^2/kN. These results suggested that the treatment methodology employed by Al-Tabbaa and Evans (1998) was appropriate for treating the West Drayton site. This led to their 1999 paper, which simplified (in terms of the contaminants present) and homogenised the West Drayton site's conditions, thereby allowing correlations to be made between the 1998 treatability study and the properties of the lab-scale *in-situ* treated soil, and secondly between the lab and field-scale modelling of the soil stabilisation conducted.

21.8.2 Hughes et al. – Newcastle University, UK

Hughes and Glendinning (2004) stabilised a site near Sandling in Kent (UK) characterised by 5 m of problematic peaty soils, which underlie a section of the Channel Tunnel Rail Link (CTRL). Given the poor ground conditions and the CTRL's importance, stabilised soils were required to achieve minimum undrained shear strengths of 100 kPa and a Young's modulus of 10 MPa after 28 days (Hughes and Glendinning, 2004). The study's main aim was to assess RG's suitability when combined with GGBS as an alternative to lime/CEM-I, in terms of cost and engineering performance. Hughes and Glendinning (2004) conducted both field and laboratory testing using a range of GGBS/RG ratios at a dosage of 200 kg m^{-3}. Once 27 DSM columns had been installed, Hughes and Glendinning (2004) conducted *in-situ* standard column penetration (SCPT) and cone penetration tests after 7 and 56 days curing. Cores were recovered from the columns for laboratory testing; namely quick undrained unconsolidated triaxial, durability (wet-dry and freeze-thaw) pH and mineralogical analyses (XRD, SEM).

Hughes and Glendinning (2004) documented a good correlation between the *in-situ* SCPT and laboratory undrained shear strengths. However, there were a few exceptions where there was a poor correlation (Figure 21.14), whereby laboratory strengths were higher than the *in-situ* strengths. This may be attributed to continued strength development of laboratory samples between sample recovery and their testing (Hughes and Glendinning, 2004). Additionally, the unusually low laboratory strengths may be due to sample disturbance and weakening during transport.

Using a GGBS–RG ratio of 75:25 produced the most impressive strengths, which met the required design criteria and exceeded those achieved by using CEM-I (Hughes and Glendinning, 2004). Durability results were also encouraging, as little damage was incurred to the columns and the GGBS–RG's overall performance was comparable to CEM-I.

Although pH may have an impact on DSM column strength development, pH values > 10.5 did not guarantee higher shear strengths (Hughes and Glendinning, 2004). Humic acids within the peaty soils interfered with the soil–cement reactions (Hughes and Glendinning, 2004), which may explain the low pH and strength values of certain mixtures. Using an alkali activator is recommended to raise the pH of such samples and thus promote pozzolanic reactions.

Further to their 2004 study, Hughes *et al*. (2011) investigated RG's effectiveness in terms of strength/stiffness development over 28 days at 55% RH when combined with GGBS, PFA and basic oxygen steel slag (BOSS). The RG–IBP ratios varied

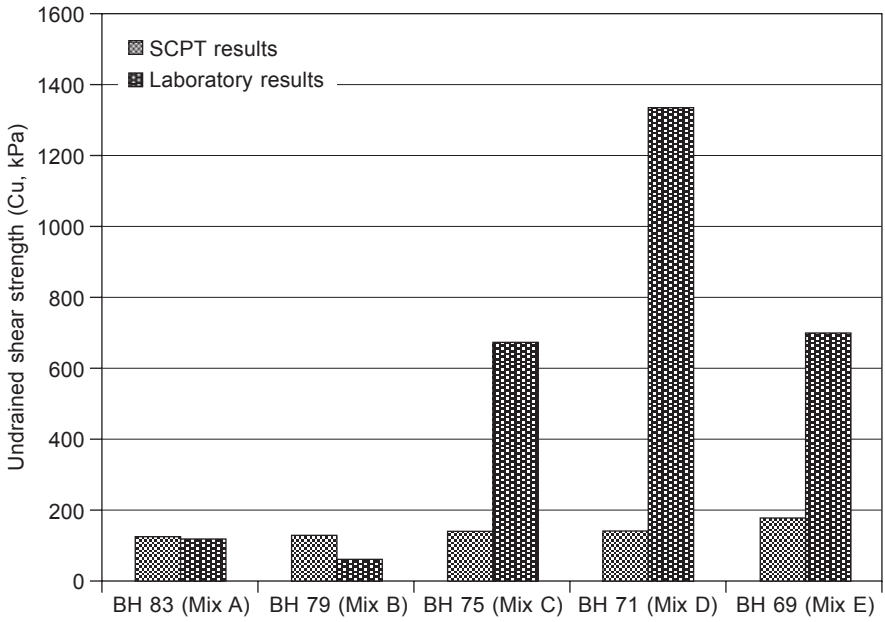

Figure 21.14 Variations in undrained shear strengths obtained for five GGBS-RG columns from *in-situ* SCPT and laboratory testing. Taken from Hughes and Glendinning (2004). Reproduced with permission from the Geological Society of London.

between 9:1 and 5:5; whereby 1% calcium hydroxide was also added to ensure pH was > 10.5. UCS results revealed that the most effective mixture was RG–GGBS at a ratio of 10:90 and moisture content of 35%, which produced strengths of 39.7 MPa. For the lower moisture contents tested by Hughes *et al.* (2011), RG–BOSS mixtures produced the highest UCS values, which produced highly brittle failures that could prove problematic when dynamically loaded. Although the highest strengths were achieved by RG–GGBS using a ratio of 10:90; Hughes *et al.* (2011) deemed the RG–GGBS ratio of 50:50 to be most favourable as it used as much IBP material as possible, whilst achieving high strengths.

Further to the above, Hughes *et al.* (2011) assessed RG–GGBS's performance in stabilising numerous UK soils, including an artificial alluvium, London Clay, Northumberland Glacial Till and Irish Moss Peat. For triaxial testing, confining pressures of 100 kPa and a strain rate of 1.23 mm/min were used. Samples were wet and dry cured for up to 112 days, whereby for the former an 18 kPa surcharge was exerted on top of samples to simulate realistic confining pressures beneath the water table.

For stabilised artificial alluvium samples, soak- and dry-cured samples achieved strengths of ~ 2.7 MPa and 5 MPa, respectively (Figure 21.15). Their rate of stiffness development was slower than that for CEM-I stabilised samples. For stabilised till samples, these developed lower undrained shear strengths (0.5 MPa) than those recorded for CEM-I-stabilised samples (3 MPa); any considerable strength developments were only observed after 28 days.

Significantly lower shear strength values were obtained for stabilised peat samples, even when additional lime was incorporated. However, such results were expected given the high water and organic contents and low pH levels, which inhibit pozzolanic

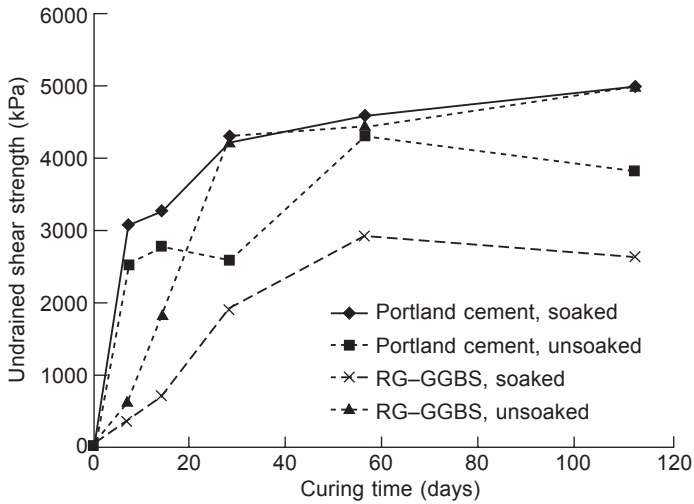

Figure 21.15 Undrained shear strength development of stabilised silty sand samples tested by Hughes *et al.* (2011). Taken from Hughes *et al.* (2011). Reproduced with permission from the Institution of Civil Engineers.

reactions. The highest undrained shear strength recorded after 14 days was 10 kPa for samples containing 30% lime. Similar to stabilised peat, negligible strength developments were observed for stabilised London Clay, reaching ≤150 kPa which was 10 times lower than that achieved by CEM-I samples. These results indicate that further work on binder chemistry and dosage is required for stabilising London Clay and soft organic peat soils.

21.8.3 Horpibulsuk et al. – Suranaree University of Technology, Thailand

Horpibulsuk *et al*. (2010) suggested that strength development within stabilised soils may be split into three zones (Figure 21.16(a)):

1. an active zone within which the volumes of pores < 0.1 μm decreased through incorporating a binder and the development of cementitious minerals;
2. an inert zone within which pore size distribution and volume of cementitious minerals undergo negligible change with increasing cement dosage and hence minimal strength enhancements; and
3. a deterioration zone where the amount of pore water present is insufficient for hydration given the relative excess of binder.

The cluster theory states that there are two pore types within stabilised soils: inter- (>0.01 μm) and intra-aggregate (<0.01 μm) (Horpibulsuk *et al*., 2010). Immediately post-mixing, the volume occupied by inter-aggregate pores decreases due to clay–cement agglomeration formation whilst the volume of larger inter-aggregate pores increases. With cementitious mineral growth, inter-aggregate pores become occupied and the soil's total pore volume decreases. Horpibulsuk *et al*. (2010) confirmed this after 7 days curing, where large pore volumes and total pore volumes within samples decreased as the volume of small pores (<0.01 μm) increased due to cementitious mineral growths (Figure 21.16(b)).

Horpibulsuk *et al*. (2011) investigated UCS development of PFA-biomass ash stabilised Bangkok clay, whereby the effects of various water contents (89, 119 and 149%), cement (0–30%) and PFA/biomass ash (0–60%) dosages were investigated for curing periods of up to 120 days at 20°C. An optimum PFA content of 25% produced the highest strengths (1900 kPa for 89% moisture content) after 28 days. Using this PFA dosage was also the most economic mixture, as it reduced the amount of binder required to stabilise the soil by 16% compared with using CEM-I. Horpibulsuk *et al*. (2011) observed that the relationship between sample strength, their clay-water/cement ratio and curing times was useful in estimating laboratory strengths and the required cement dosages within soils of different *in-situ* and field moisture contents (Figure 21.17).

PFA-stabilised soil mixes are expected to achieve strengths of 0.6–3.0 MPa after 28 days (Horpibulsuk *et al*., 2011). In relation to CEC, ash, silt and sand particles within such mixtures are non-interacting particles given their low specific surface areas and non-electrical nature, whereas cement and clay particles are able to undergo

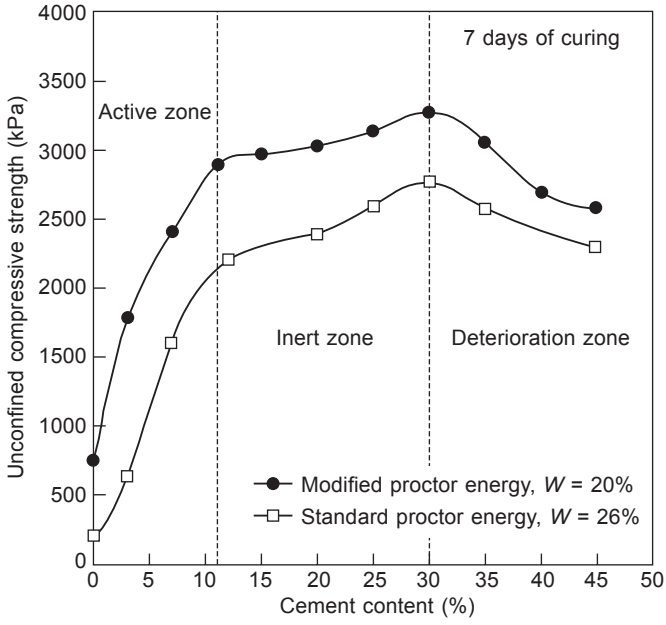

(a)

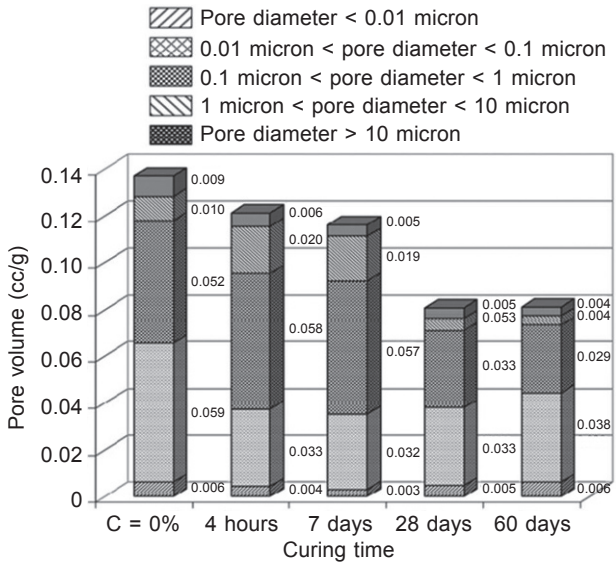

(b)

Figure 21.16 (a) Three zones of strength development within cemented soils; (b) chart showing pore size distribution for samples stabilised with 10% CEM-I. Reprinted from Horpibulsuk *et al.* (2010), Copyright © 2010, with permission from Elsevier.

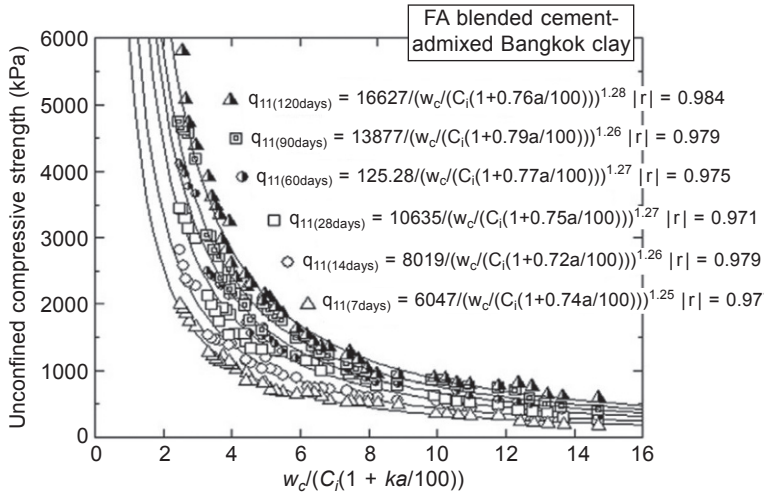

Figure 21.17 Relationship between unconfined compressive strength and clay-water/cement ratio for PFA-cement stabilised Bangkok clay. Reprinted from Horpibulsuk *et al.* (2011), Copyright © 2011, with permission from Elsevier.

physicochemical interactions with soil water. As a result of the clay's interactions, a micro-fabric develops which strengthens when cement is mixed into the soil, thereby creating large clay–cement agglomerations (Horpibulsuk *et al.* (2011).

Although PFA is silica and alumina rich, its pozzolanicity is very low. This contrasts with how many previous authors and industrial standards have characterised PFA as having good pozzolanicity levels (e.g. ASTM D5239-04). Rather than the conventional pozzolanic strength gain mechanism of $Ca(OH)_2$ produced via hydration by cements, PFA is only able to disperse large clay–cement agglomerations. This leads to increases in the reactive surface area of cement particles and subsequent strength enhancements. Horpibulsuk *et al.* (2011) confirmed this through the use of SEM, mercury intrusion porosimetry and thermal gravimetric analyses. Thus, Horpibulsuk *et al.* (2011) proposed a new hypothesis on how strength develops within blended cement–clay admixtures, whereby the strengths achieved depend solely on the clay-water/cement ratio. Hence, given PFA's poor pozzolanicity, the equivalent cement content within a stabilised soil depends on the dispersing potential of the material, which is controlled by the PFA content (Horpibulsuk *et al.*, 2011).

21.8.4 Ahnberg – Swedish Geotechnical Institute

Many previous laboratory studies which have examined the strength of stabilised soft soils have used UCS, due to its simplicity, low cost and usefulness in comparing the effects of different binders/other factors in influencing their strengths. However, Ahnberg (2007) amongst others believes that to develop a more detailed understanding of stabilised soil's mechanical behaviour, triaxial testing is more appropriate given that they fail in shear.

Little literature exists on yield stresses within stabilised soils and their effects on strength behaviour. Yield stresses within stabilised soils are largely influenced by cementation (Ahnberg, 2007). However, stresses acting on stabilised soils during curing also play a role. To examine the impact of these factors, effective stress path and shear strength behaviour of stabilised soils, Ahnberg (2007) carried out consolidated drained and undrained triaxial testing on two stabilised Swedish post-glacial clays, characterised by moisture contents of 80–90%, plastic and liquid limits of 24% and 68% respectively, high clay contents (>60%), low organic contents (1%), sensitivities of 20–25 and low undrained shear strengths (8–15 kPa).

The dry binder mixtures used by Ahnberg (2007) included CEM-II, quick lime, CEM-II+quick lime, CEM-II+GGBS, CEM-II+PFA and GGBS+quick lime, where the composite binders comprised a 50:50 ratio of each material. The binder dosage used for both soils was 100 kg/m^3. Ahnberg (2007) used two curing methods; most samples were stored within sealed plastic tubes and cured for 1, 28 and 360 days at 8°C according to Swedish testing standards. However, some CEM-II and quick lime-stabilised samples were cured within triaxial cells under numerous vertical stresses. Prior to shearing, Ahnberg (2007) mounted samples within the triaxial cells and subjected them to K_0 consolidation and curing under the same stresses for 28 days, where effective confining pressures of 20–60 kPa and vertical effective stresses of 40–120 kPa were applied. For comparison, Ahnberg (2007) also stored non-stressed stabilised samples for 28 days which were saturated from both ends. Given stabilised soil's high stiffnesses and low permeabilities, Ahnberg (2007) saturated samples by using back pressures of ≥400 kPa. Subsequently, samples were consolidated for 7.5 h to achieve a K_0 of 0.5. For shearing, a constant strain rate of 0.02%/min was used for all tests. A variation in shear strength was recorded for the different stabilised mixtures; ranging from 50 to 1500 kPa (Figure 21.18).

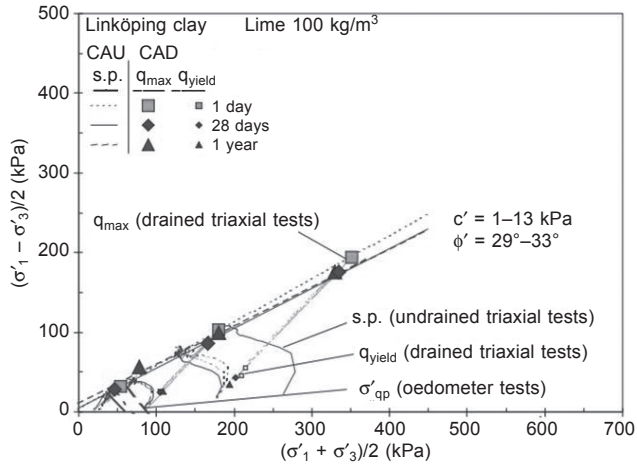

Figure 21.18 Measured effective stress paths in the *s–t* plane for stabilised Linköping clay mixtures. Taken from Ahnberg (2007). © 2008 Canadian Science Publishing or its licensors. Reproduced with permission.

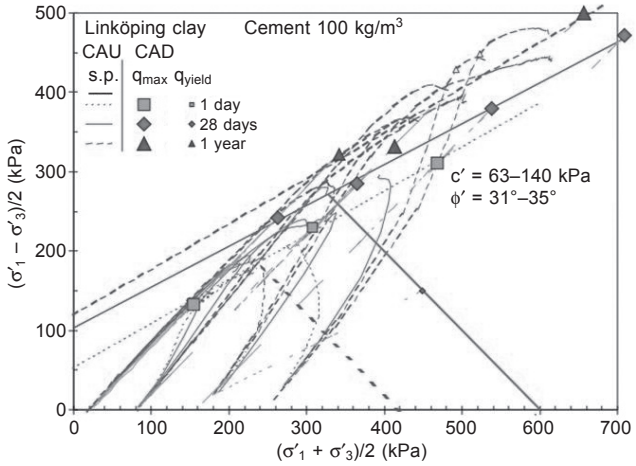

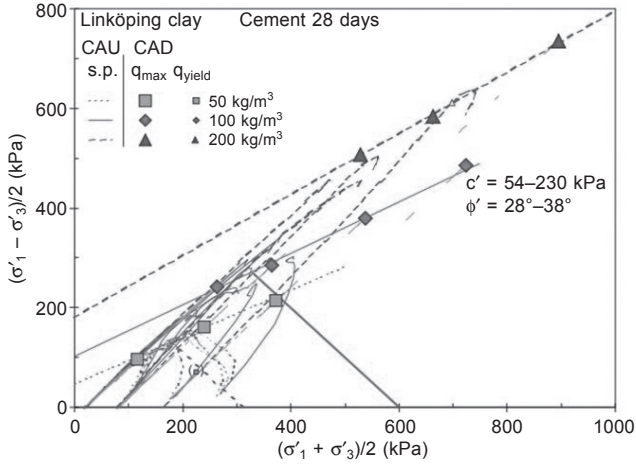

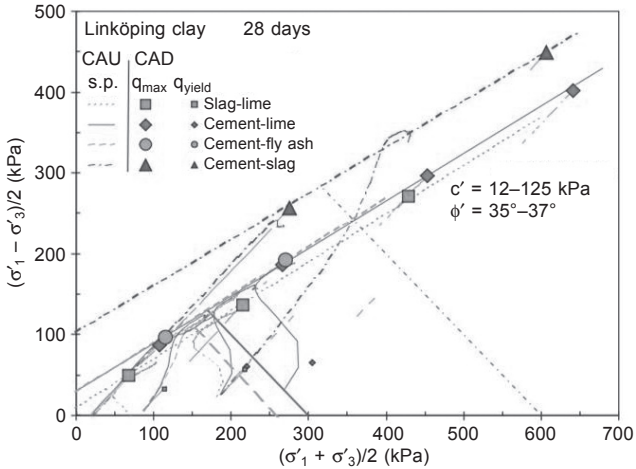

Figure 21.18 Continued

Samples which had been consolidated at stresses lower than their yield stresses behaved in an overconsolidated manner, whereas those which had been consolidated at stresses higher than their yield stresses behaved as normally consolidated soils. The majority of yield stress values were evaluated from oedometer tests, which depicted a stress dependency of stabilised soil's undrained shear strength behaviour.

Ahnberg (2007) recorded high effective friction angles (30–36°) and effective cohesion values (up to 175 kPa). Such increases in effective cohesion were attributed to simultaneous increases in undrained shear strength. However, Ahnberg (2007) noted this did not always apply, namely for lime-stabilised mixtures where the use of lime had negligible strengthening effects. Such poor performances are common when using high lime dosages within soils containing high moisture contents. Locat *et al*. (1990) confirmed that high lime dosages result in long-term strength increases only for soils with high moisture contents (Figure 21.19).

Drained triaxial tests revealed that yield points for lower strength samples were recorded at low strains, whereas failure occurred at much greater strains. However, Ahnberg (2007) noticed that yielding became less distinguishable within higher strength samples, where it occurred at stresses and strains close to failure.

Although significant variations in strength were seen by Ahnberg (2007) due to factors including soil type, binder type and curing period, relatively similar stress–strain behaviour was recorded for the different stabilised mixtures. This was linked to samples' degree of overconsolidation. For samples under drained conditions which failed at smaller strains, large reductions in shear strength with increasing strain post-failure were seen. Ahnberg (2007) noted this behaviour for samples that had been consolidated at lower stresses than their yield stresses.

Under undrained conditions, Ahnberg generally recorded little changes in deviator

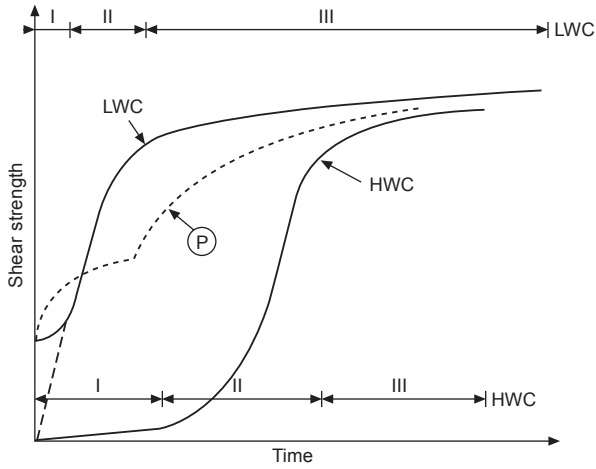

Figure 21.19 A mechanical conceptual model of shear strength development within lime-stabilised sensitive clays at both low and high moisture contents. (LWC: low water content; HWC: high water content; P: Perret model for silty soils.) Taken from Locat *et al*. (1990). © 2008 Canadian Science Publishing or its licensors. Reproduced with permission.

stress post-failure. The strains experienced at failure for normally consolidated untreated and stabilised samples were similar, as both experienced near-perfect plastic behaviour with no considerable strength degradations post-failure (Ahnberg, 2007). For highly overconsolidated samples, brittle behaviour was experienced at small strains, followed by significant strength degradation post-failure.

Ahnberg (2007) identified a 'phase-transformation' point during undrained tests where changes in pore pressure were zero and the stress paths of overconsolidated samples changed direction to follow the critical state line. Ahnberg interpreted this as depicting a yield surface and that Larsson's (1977) yielding model closely described this behaviour.

Ahnberg (2007) assumed that the effects of increased external stresses are related to the compression of the stabilised soil, inferring that increased stresses due to external loads ought to be applied shortly after stabilisation. This ensures that the material becomes compressed, allowing for cementation and increases in yield and overall shear strength to occur.

21.8.5 Wilkinson et al. – Department of Transport/Monash University, Australia

Wilkinson *et al*. (2010b) studied pH, plasticity and undrained shear strength development of various soil–binder mixtures with curing. Four soil types were stabilised; two high plasticity (Ginifer and Leeville), one low plasticity (Boambee) and one engineered clay soil (Table 21.4). The binders used included lime, lime-activated GGBS and lime activated PFA, which were added to the soils at a dosage of 10% by dry weight.

Table 21.4 Summary of the geotechnical, chemical, CEC and mineralogical characteristics of the soils stabilised by Wilkinson *et al.* (2010a,b)

Soil	Plasticity index (%)	Clay mineralogy	Cationic exchange capacity (meq/100 g)	pH at 1:3 soil/water ratio	Organic carbon content (%)
Ginifer	68.8 (high)	Smectite dominant	33.1	8.25	0.08 (low)
Leeville	47.9 (high)	Smectite dominant	18.1	5.38	1.22 (high)
Boambee	31.1(low)	Kaolinite dominant	6.0	4.45	0.35 (high)
Engineered soil	59.0 (high)	Kaolinite dominant	18.2	8.2	0

Source: Reproduced with permission from the Institution of Civil Engineers.

Davidson *et al.* (1965) determined that for pozzolanic reactions to occur within stabilised soils, a minimum pH of 10.5 was required. Based on the four soils' pH values in Table 21.4, each required alkali activation. Initial pH values post-stabilisation all exceeded 12 but degraded towards 11.5 over one year. Hence, pozzolanic reactions could occur within all samples and a relationship existed between decreasing soil pH with increasing strength as curing progressed. The mechanism by which this occurs involves calcium hydroxide acting as an electrolyte to fuel modification reactions and as a caustic agent, allowing stabilisation to occur through increasing pH for pozzolanic reactions (Rogers and Glendinning, 2000; Wilkinson *et al.*, 2010b). Pozzolanic reactions then consume hydroxyl ions from soil and binder particle surfaces, which combine with pore water to precipitate cementitious minerals.

Wilkinson *et al.*'s (2010b) results show that the most successful binder in the short and long term was lime-activated GGBS (Figure 21.20). Ginifer soil, which had been stabilised with this binder, produced the highest undrained shear strengths out of all twelve mixtures tested, where 388 kPa was achieved after 28 days.

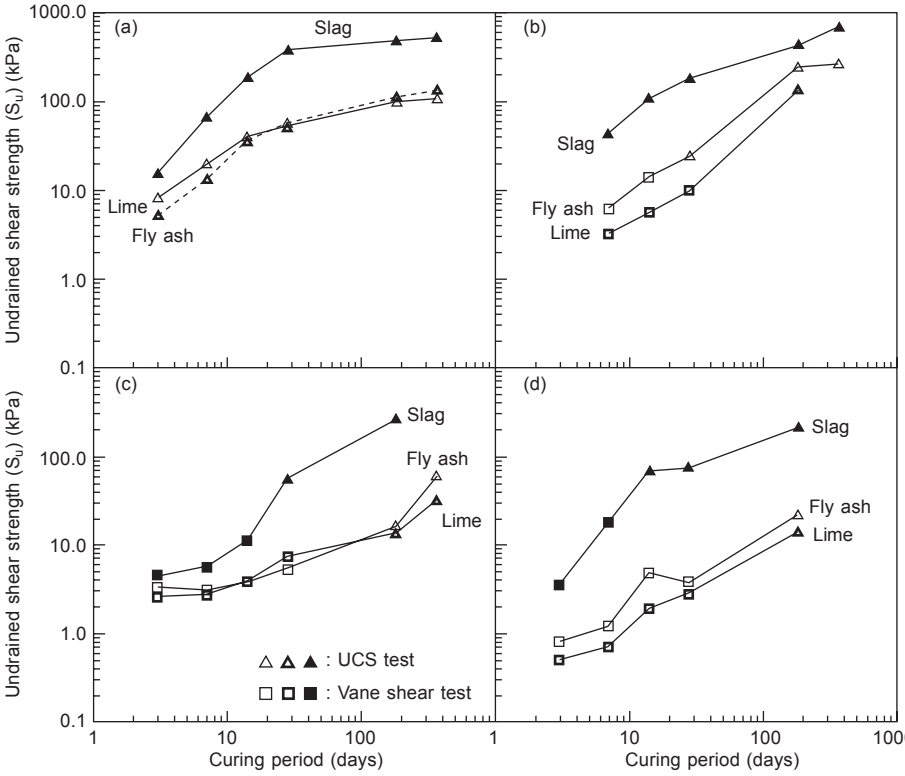

Figure 21.20 Undrained shear strength development of all stabilised soil mixtures tested by Wilkinon *et al.* (2010b): (a) Ginifer, (b) Engineered clay, (c) Leeville, (d) Boambee. Taken from Wilkinson *et al.* (2010b). Reproduced with permission from the Institution of Civil Engineers.

Activated PFA and lime binders exhibited similar performances within smectite-based clays, whereas activated PFA produced preferable performances over lime for the kaolinite-dominated soils. Work by Bell (1996) on the lime stabilisation of clay soils determined that smectite has higher short-term pozzolanicity compared with kaolinite, which can be attributed to smectite's higher surface area and CEC. These characteristics along with the higher organic carbon content of the Ginifer soil may be the root causes behind the GGBS-activated engineered soil producing higher strengths than the GGBS-activated Ginifer soil after 1 year curing.

Plasticity testing revealed that clay particles had been altered during cementation (as confirmed by SEM imagery), as the smectite-bearing soils demonstrated reductions in PI values due to smectite consumption. Contrastingly, kaolinite-bearing soils exhibited increases in PI values as cementation occurred.

21.8.6 Verástegui Flores et al. – Ghent University, Belgium

A triaxial study was conducted by Verástegui Flores and van Impe (2009) on artificially cemented kaolin clay samples, in order to distinguish between the material behaviour of stabilised and untreated kaolin. Untreated samples had a moisture content of 57.7% to simulate a very soft soil. Verástegui Flores and van Impe (2009) used a more advanced triaxial set-up than Ahnberg (2007), which involved the use of bender elements to gain insights into the small strain stiffness behaviour of cemented soils. The binder used was CEM-I at dosages of 5–20% by dry mass.

Once the samples were saturated, Verástegui Flores and van Impe (2009) isotropically consolidated untreated samples to an effective stress of 50 kPa prior to shearing. Treated samples containing binder dosages of 10% and 20% were isotropically consolidated under effective stresses of 100 kPa and 300 kPa, respectively. During consolidation, values of initial shear stiffness (G_0) were recorded through the use of bender elements; whereby shear waves were generated by 1 cycle of a sinusoidal electrical pulse at a frequency of 10 kHz (Verástegui Flores and van Impe, 2009). Initially high G_0 values were observed to decrease with increasing isotropic consolidation stresses to a minimum value, straight after which they increased. Verástegui Flores and van Impe (2009) stated that this behaviour is typical of non-cemented frictional soils, and that the transition from G_0 decreasing to increasing again denotes the point at which the material's structure degrades from cemented to non-cemented behaviour, defining the yield stress (p'_y) (Figure 21.21(a)).

At low confining pressures, shear strength behaviour was influenced by the level of cementation; whereas at higher confining pressures the behaviour was influenced by isotropic consolidation stresses. All treated samples produced a linear peak failure envelope, which was located above that defined for untreated samples (Figure 21.21(b)). Based on this observation, Verástegui Flores and van Impe (2009) interpreted that an unbound granular macrostructure existed within cemented samples. Verástegui Flores and van Impe's (2009) findings should therefore encourage the use of bender elements on soils stabilised with alkali-activated IBPs in the future, to gain further insights into their mechanical behaviour at small strains.

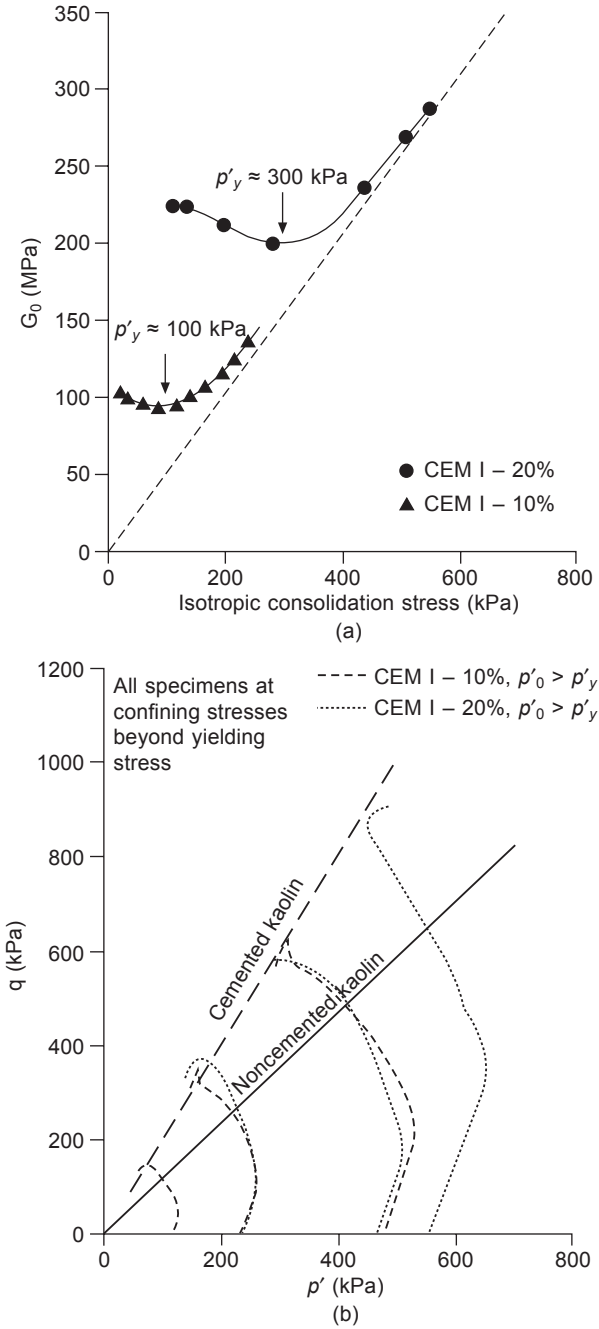

Figure 21.21 (a) Bender element measurement of G_0 for CEM-I stabilised kaolin mixtures; (b) Effective Cambridge stress path plot of treated and untreated kaolin samples. Reprinted from Verástegui Flores and van Impe (2009). Copyright © 2009, with permission from IOS Press.

21.8.7 Sargent et al. – Newcastle University, UK

Sargent *et al.* (2013) investigated the mechanical strength and durability of an artificial silty sand stabilised with various alkali-activated IBP binder mixtures. The artificial silty sand replicated alluvial soils typically found in the UK, which present difficult ground conditions for construction purposes. The soil was characterised by a gravimetric moisture content of 15%, PI of 12.02, CEC of 1.96 meq/100 g and a surface area of 2.275 m^2/g.

The IBPs used by Sargent *et al.* (2013) were PFA, GGBS and RG, where each was activated and tested individually and in combination with each other. Hughes *et al.* (2010, 2011) revealed that the use of lime as an alkali activator does not consistently result in improved engineering performance, due to insufficiently high pH values. Thus, based on work by Palomo *et al.* (1999) and Hughes *et al.* (2010, 2011), Sargent *et al.* (2013) used an alkali activator comprising NaOH flakes and Na_2SiO_3 solution.

UCS results presented in Figure 21.22 reveal that activated GGBS samples exhibited the highest and most rapid strength improvements of 6 MPa after 28 days curing, which was twice the strength of CEM-I. Other mixtures which showed encouraging strength results were activated GGBS–RG and GGBS–PFA with strengths of 5 and 3.5 MPa, respectively. The behaviour of the activated GGBS samples after each curing period upon failure was brittle, compared with the more ductile behaviour observed for other mixtures. Given that the soil had a low clay–high sand contents, this presented a limited number of sites for cation exchange and subsequent hydration/pozzolanic reactions to occur. Thus, activation within certain mixtures overcompensated for the lack of cation exchange surfaces available by increasing pH, which led to the dissolution of silica from the clay particles and subsequent formation of cementitious gels.

Sargent *et al.* (2013) also conducted oedometer testing on the aforementioned mixtures; whereby, according to Tomlinson (2001), results in Figure 21.23 show that each binder improved the soil's initial high level of compressibility to at least low to medium levels.

Alkali-activated specimens resulted in much greater improvements, particularly those containing GGBS–PFA due to high stiffness levels. Although the activated and non-activated PFA–RG samples produced lower M_v values than those achieved by the untreated soil after each loading stage, their compression index values were still comparable with that for the silty sand. Hence, rather than creating cementitious bonds, the PFA–RG binder acted as a bulking agent.

Durability testing revealed that the addition of activated GGBS or GGBS–PFA produced the most enhanced performances (Figures 21.24 and 21.25). These samples were dense and characterised by low porosities/permeabilities, which reduced the likelihood of water absorption and consequent sample degradation. RG and PFA–RG binders (activated or not) were the least durable, which was linked with RG's preparation technique, whereby a non-uniform coarse-grained powder was produced. The RG was less dense and more permeable than GGBS or PFA, which would have allowed water to permeate through samples and result in disintegration.

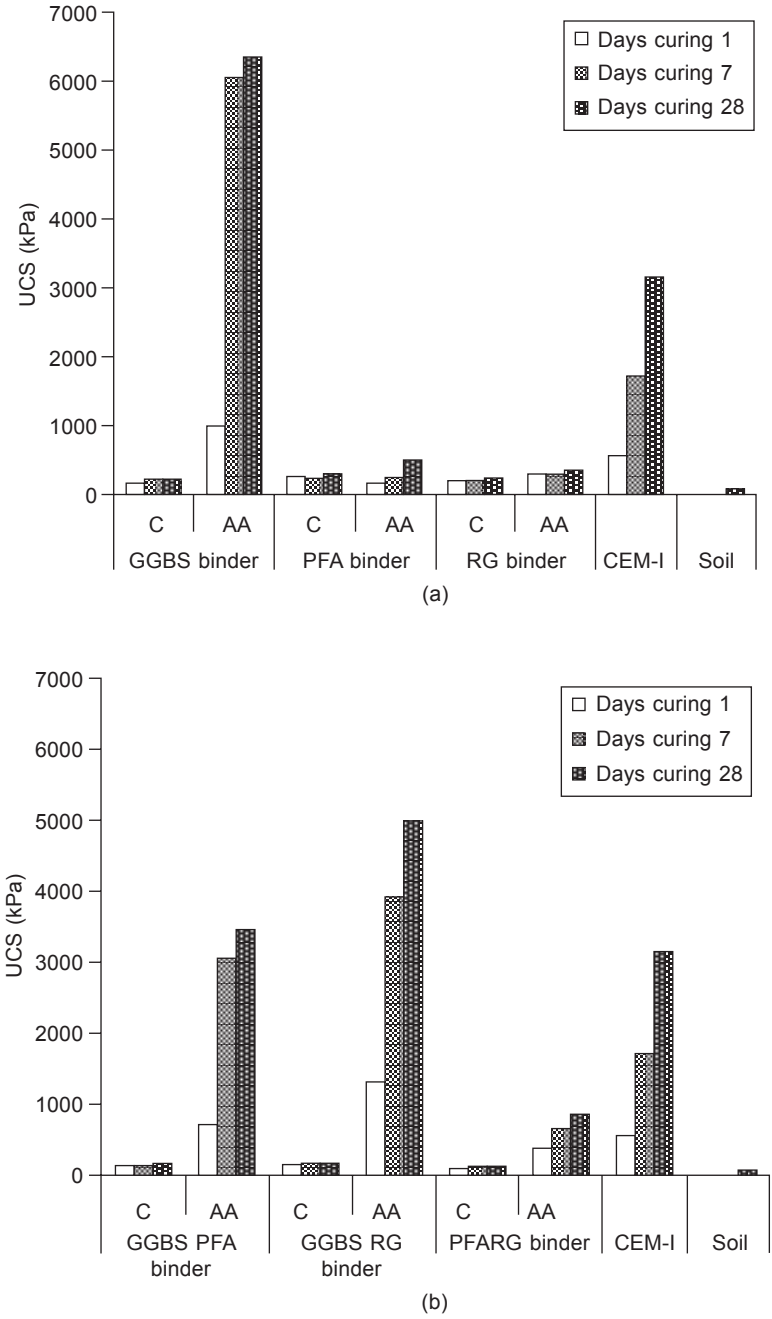

Figure 21.22 UCS development with increasing curing time for (a) individual and (b) combined IBP binders in both controlled (C) and alkali-activated (AA) states. Reprinted from Sargent *et al.* (2013), Copyright © 2013, with permission from Elsevier.

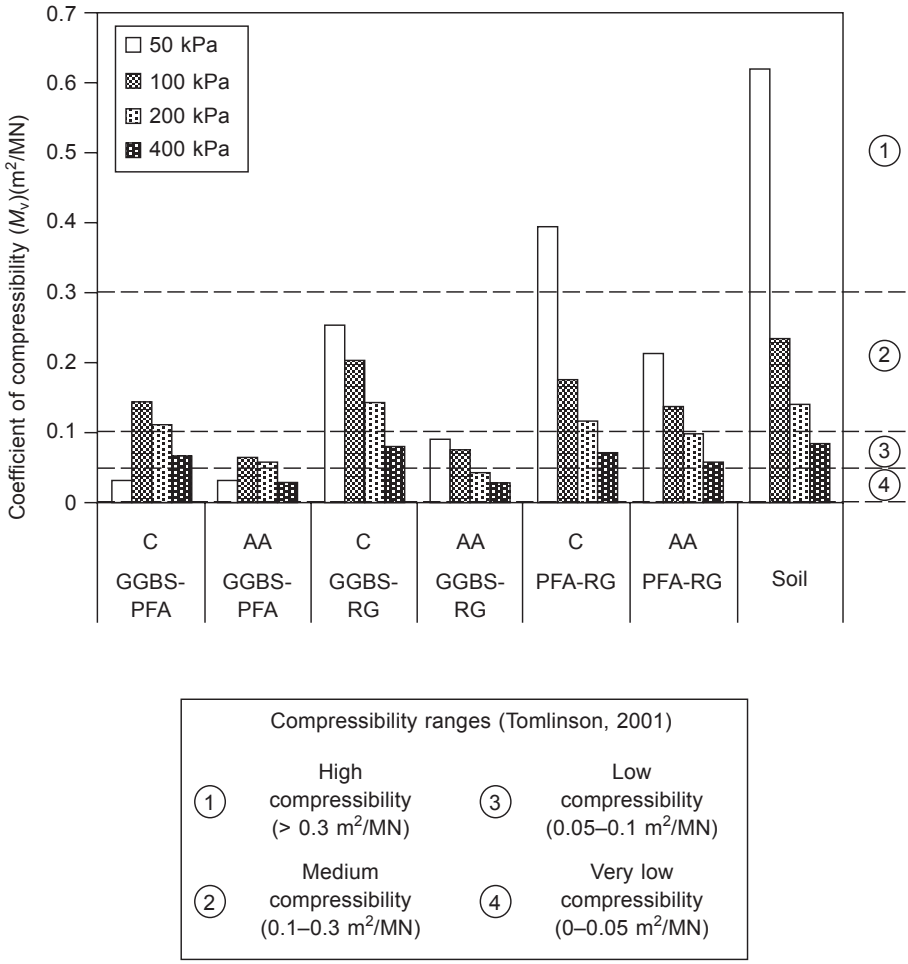

Figure 21.23 M_v values (m^2/MN) for alkali-activated IBP mixtures. Reprinted from Sargent *et al*. (2013), Copyright © 2013, with permission from Elsevier.

The addition of constituents including sodium hydroxide and sodium silicate to existing commercial binders would have an associated cost and add to the complexity of DSM processes. Given that the sodium silicate used by Sargent *et al*. (2013) was in liquid form, it would not be applicable to dry DSM. Hence, substituting this with an alternative high alkalinity waste-based powder would be preferable. Habert *et al*. (2011) suggest that sodic slags could be viable replacements.

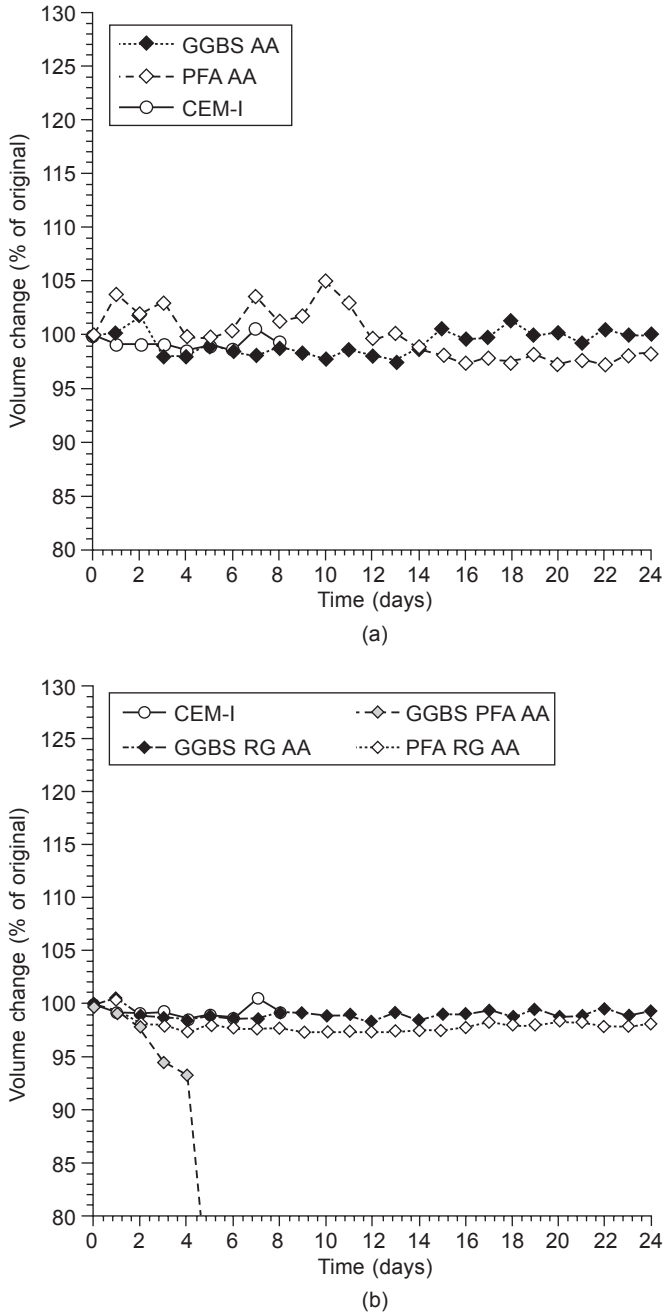

Figure 21.24 Volume changes recorded for samples containing (a) individual and (b) combination binders during wet-dry durability testing. Reprinted from Sargent *et al.* (2013), Copyright © 2013, with permission from Elsevier.

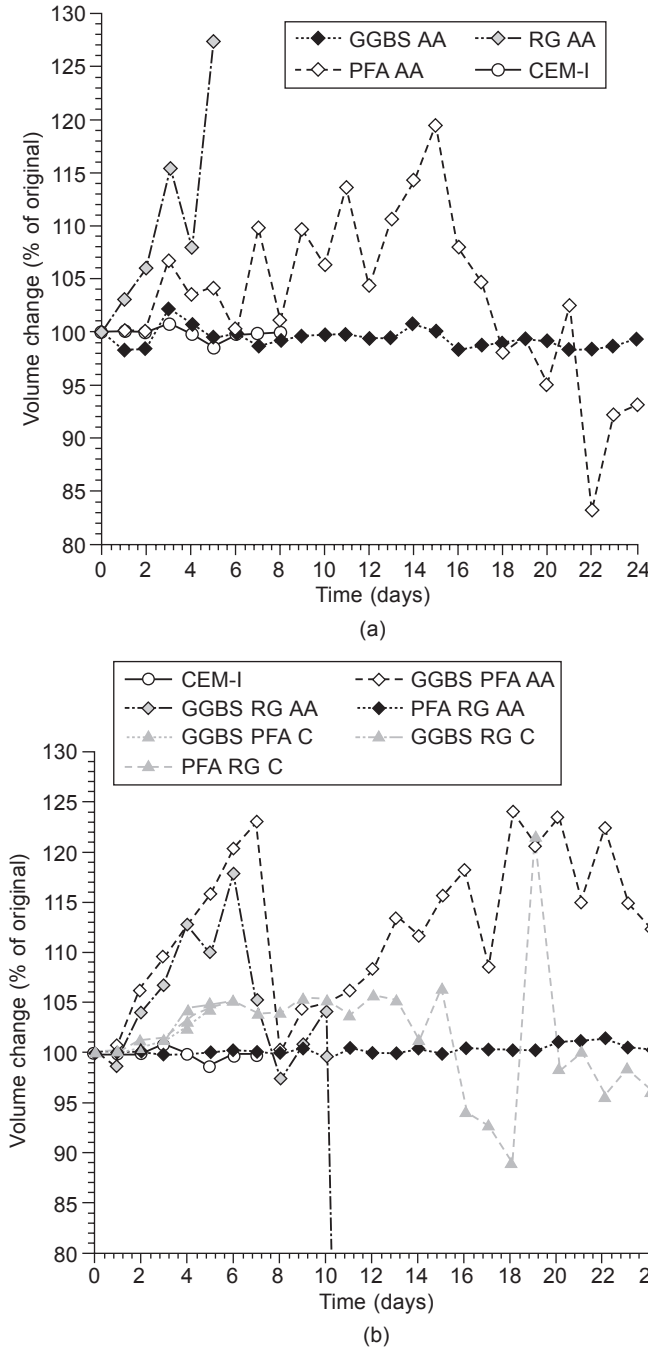

Figure 21.25 Volume changes recorded for samples containing (a) individual and (b) combination binders during freeze-thaw durability testing. Reprinted from Sargent *et al*. (2013), Copyright © 2013, with permission from Elsevier.

21.9 Recent research into the mineralogical and microstructural characteristics of alkali-activated binders for soil stabilisation

21.9.1 Al-Tabbaa et al. – Cambridge University, UK

Following their 1998 study, Al-Tabbaa and Evans (1999) used XRD and SEM techniques to examine the microstructural and physico-chemical characteristics of the same stabilised mixtures after 7 and 28 days curing.

XRD and SEM results (Figure 21.26) confirmed the presence of hydrating cementitious compounds, and that the presence of most contaminants within the soil–grout mixtures did not inhibit the development of cementitious minerals. However, the presence of lead nitrate appeared to inhibit cementitious mineral growth as much as mineral oil and lead nitrate combined (Al-Tabbaa and Evans, 1999).

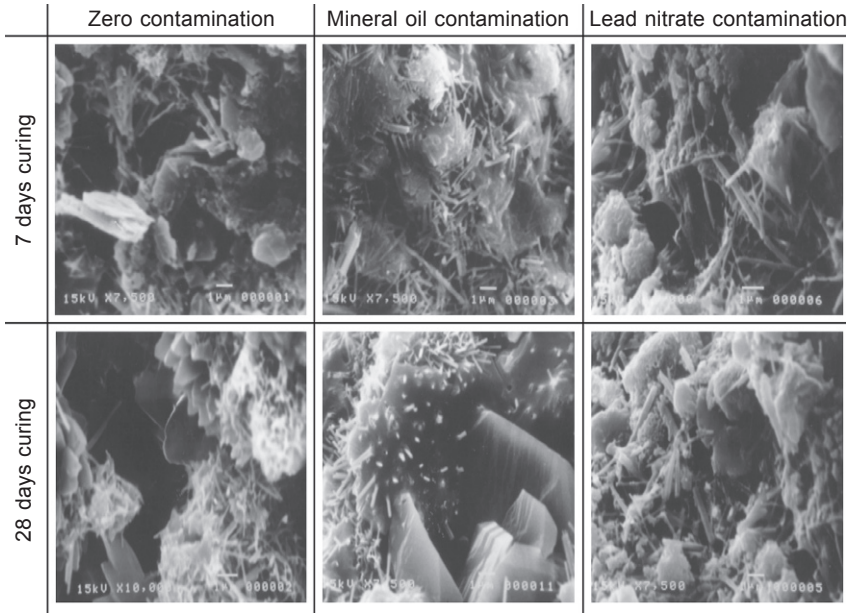

Figure 21.26 SEM micrographs of West Drayton soil in both uncontaminated and contaminated states after 7 and 28 days curing. Adapted from Al-Tabbaa and Evans (1999). Reproduced with permission from the Institution of Civil Engineers.

21.9.2 Hughes et al. – Newcastle University, UK

In addition to their geotechnical testing, Hughes and Glendinning (2004) conducted SEM and XRD analyses on samples recovered from the 27 DSM columns installed. XRD analyses revealed no evidence of ettringite or thaumasite within any of the samples, indicating that the GGBS–RG columns were not susceptible to sulphate attack

for up to 56 days post-treatment. However, the detection of hydrated cementitious minerals within samples was not possible by using XRD, due to their amorphous nature.

SEM techniques (including the EDS point elemental analysis tool) identified hydrated cementitious minerals infilling void spaces due to pozzolanic reactions. Some of the SEM micrographs taken showed the presence of a few needle-shaped minerals (Figure 21.27), which suggested the presence of ettringite/thaumasite. However, the SEM-EDS system determined these minerals as RG and posed no threat towards the soil's mechanical structure.

Hughes *et al.* (2011) also conducted XRD and SEM analyses on treated and untreated samples of artificial silty sand, Northumberland till, London Clay and Irish peat (Table 21.5). From Hughes *et al.*'s (2011) SEM-EDS analyses on polished sections of the mixtures in Table 21.5, little mineralogical differences existed between samples containing RG–GGBS or CEM-I. Hughes *et al.* (2011) did not recommend the use of the EDS tool, as it can only identify elements with atomic numbers > 5, and is thus unable to detect hydrogen.

The effectiveness of RG–GGBS in producing improved engineering performances was influenced by soil mineralogy and pH. For the artificial alluvium tested, the addition of lime was needed to raise the pH to > 10.5. In contrast, the mineralogy (specifically sulphate content) of the Northumberland glacial till, peat and London Clay caused pH levels to decrease with curing, where the lime added was insufficient

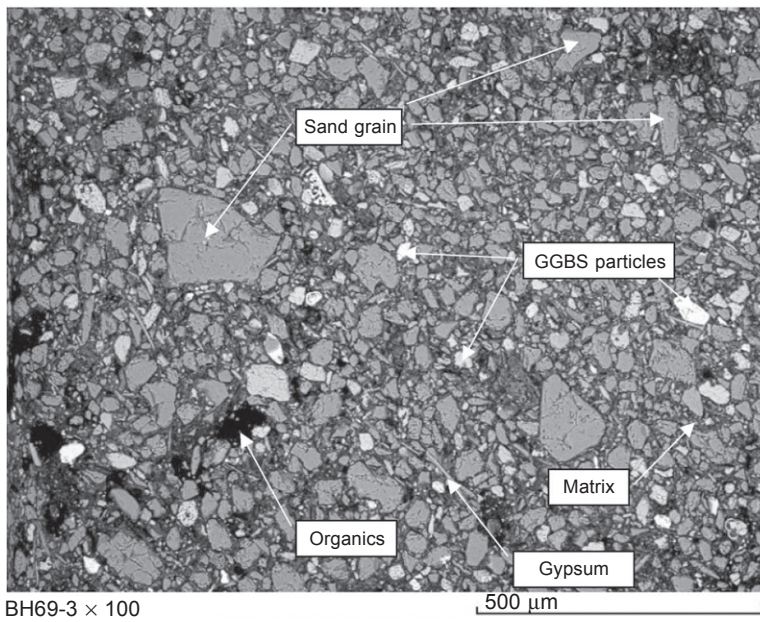

Figure 21.27 SEM micrograph of a polished sample section, which has been EDS analysed. Taken from Hughes and Glendinning (2004). Reproduced with permission from the Geological Society of London.

Table 21.5 Summary of mineral phases observed in each sample analysed by Hughes *et al.* (2011) using XRD

	RG-GGBS stabilised		CEM-I stabilised	
	Dry-cured	***Soak-cured***	***Dry-cured***	***Soak-cured***
Artificial alluvium	Kaolinite, Gypsum, Ettringite, Quartz and C-S-H	Kaolinite, Gypsum, Ettringite, Quartz and C-A-O-H	Kaolinite, Portlandite, Calcite, Quartz, C-S-H and C-A-O-H	Kaolinite, Portlandite, Calcite, Quartz, Calcium Silicate and C-A-O-H
London Clay	Gypsum, Ettringite, Quartz and Muscovite	–	Kaolinite, Calcite, Ettringite, Quartz, Muscovite and C-S-H	Ettringite, Quartz, Muscovite and Calcite
Northumberland Glacial Till	Kaolinite, Gypsum and Quartz	Kaolinite, Gypsum, Ettringite, Quartz and C-S-H	Kaolinite, Portlandite, Calcite, Quartz and C-S-H	Kaolinite, Portlandite, Calcite, Quartz and C-S-H

The symbol (–) denotes no sample was analysed.
Reproduced with permission from the Institution of Civil Engineers.

to raise pH levels, resulting in the unsuccessful activation of the RG–GGBS. Although the strengths achieved were lower compared with CEM-I, Hughes *et al.* (2011) believed that RG–GGBS should still be considered as a sustainable alternative to CEM-I which meets construction specifications.

Wax-sealing samples for curing was more effective in preventing sample evaporation compared with cling film wrapping samples, as adopted by Rahman *et al.* (2008). Hughes *et al.*'s (2011) RG preparation method was more effective than that adopted by Rahman *et al.* (2008) in producing higher strengths, which involved oven drying the moist RG filter cake at 40°C and then manually grinding it into a powder. The strengths of activated GGBS mixtures exceeded those achieved by CEM-I. Hence, the performance of the activated GGBS may conceal any effects due to the presence of RG.

21.9.3 Wilkinson et al. – Department of Transport/Monash University, Australia

Similar to Hughes *et al.* (2004, 2011), Wilkinson *et al.* (2010a,b) investigated the use of lime-activated PFA and GGBS to stabilise numerous Australian clayey soils. SEM and XRD were used to examine mineralogical changes within stabilised mixtures at various curing periods up to 1 year. SEM images revealed the occurrence

of flocculation and agglomeration once they had been stabilised. Wilkinson *et al.* (2010a) also observed the development of neoform products including AFt (aluminate ferro tri-) phases (ettringite and thaumasite; Figure 21.28), calcium hydroxide (Figure 21.28(b)), AFm (aluminate ferrite mono-) phases (i.e., strätlingite and calcium monosulphate hydrate; Figure 21.29(a)) and C-S-H (Figure 21.29(b)), where these products grew within pore spaces binding the soil structure together.

The abundance of AFt, AFm and C-S-H mineral phases increased with curing, where C-S-H minerals were most abundant after 182 days (Wilkinson *et al.*, 2010a). XRD analyses also confirmed the changing mineralogy of samples with time (Figure 21.30).

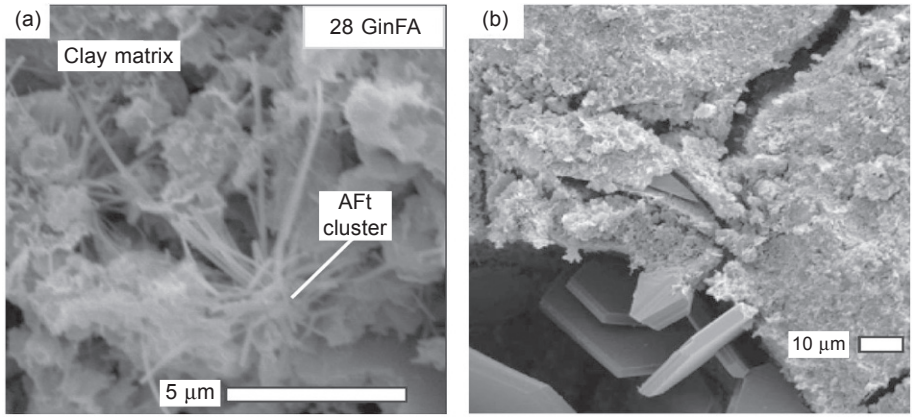

Figure 21.28 SEM images of (a) AFt phase ettringite and (b) CH minerals. Taken from Wilkinson *et al.* (2010a). Reproduced with permission from the Institution of Civil Engineers.

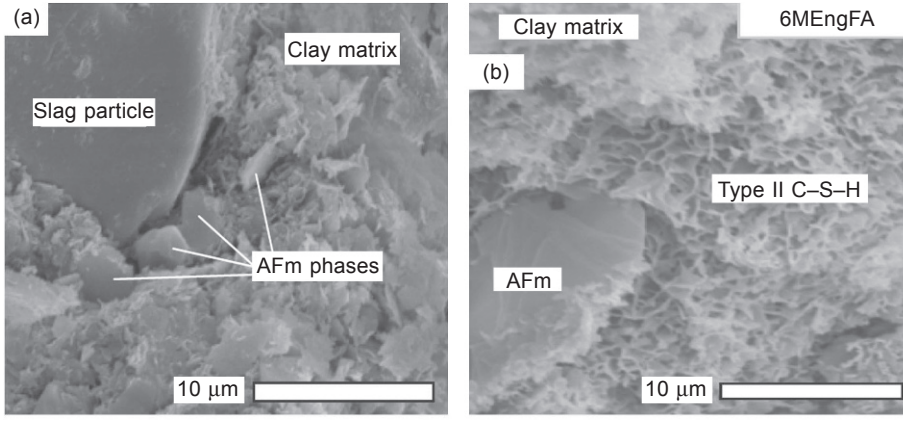

Figure 21.29 SEM images of (a) AFm phase and (b) type II C-S-H minerals. Taken from Wilkinson *et al.* (2010a). Reproduced with permission from the Institution of Civil Engineers.

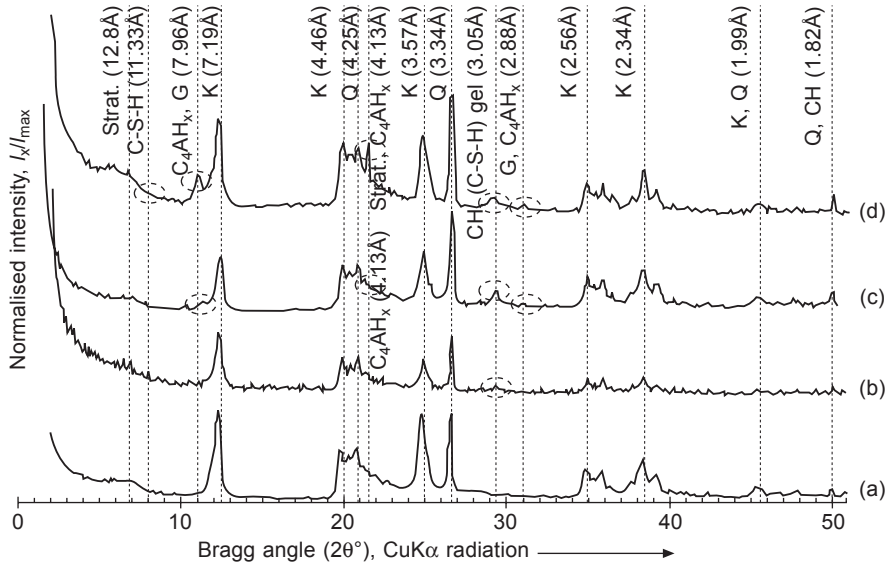

Figure 21.30 XRD traces of samples analysed by Wilkinson *et al*. after various curing periods: (a) untreated clay at 0 days, (b) with hydrated lime at 6 months, (c) activated PFA at 1 year and (d) activated GGBS at 6 months. (K = kaolinite, Q = quartz, G = gypsum, C_4AH_x = calcium aluminate oxide (carbonate) hydroxide.) Courtesy of Wilkinson *et al*. (2010a). Reproduced with permission from the Institution of Civil Engineers.

Overall, the activated PFA and GGBS were seen to influence the type and form of growing mineral phases. Finally, soil organic content was observed to hinder cementitious mineral growths and thus subsequent strength developments.

21.9.4 Sargent et al. – Newcastle University, UK

Previous studies have shown that a soil's pH may strongly influence its strength development, as higher UCS values (>1 MPa) are achieved by alkali-activated samples whose pH values are > 10.5. pH testing after 28 days showed that alkali activation was required to ensure that each mixture reached a minimum pH of 10.5 for pozzolanic reactions to occur. Whilst sufficiently high pH values were recorded for samples which achieved high UCS values (GGBS and GGBS–PFA), numerous samples with high pH levels did not achieve high strengths (RG–AA and PFA–RG–AA). Oxidising reactions and subsequent pH reductions can hinder pozzolanic reactions and strength gains. It is therefore necessary to fully assess the quantity of activator to be added to stabilised soil mixtures prior to treatment to ensure that pH remains > 10.5 for a sufficient curing period (Sargent *et al.*, 2013).

Mineralogically, XRD analyses from Sargent *et al.*'s (2013) study provided evidence for the existence of C-S-H and calcium aluminium oxide hydrate minerals within certain activated samples. Thenardite was observed within a PFA–RG–AA

sample, which can cause sulphate attack and strength degradations within concrete (Rodriguez-Navarro *et al*., 2000). No thaumasite was observed within any samples; however, ettringite was observed within one GGBS–RG–AA sample. The presence of ettringite/thaumasite within calcium-based stabilised sulphate-bearing clay soils can cause structural distress (Little *et al*., 2005). However, in the case of Sargent *et al*.'s (2013) study and that by Wild *et al*. (1998) for clay–lime–GGBS–gypsum systems with high lime–low GGBS compositions, Ettringite may strengthen soils.

21.9.5 Zhang et al. – Worcester Polytechnic Institute, USA/ Northwest A&F University, China

Similar to Sargent *et al*. (2013), Zhang *et al*. (2013) stabilised a low-plasticity synthetic clay soil in the laboratory and subjected it to UCS, volumetric strain, and mineralogical/microstructural testing; specifically XRD and SEM-EDX (energy dispersive X-ray spectroscopy). The stabiliser used for their study was metakaolin at dosages of 3–15%; whereby samples were cured for up to 28 days in cling film. For samples containing a Si/Al ratio of 1.7 and a 15% binder dosage, impressive 28-day UCS values of 31 MPa were achieved, even though cling-filming samples for curing is less desirable than wax-sealing and the fact that Duxson *et al*. (2007) believe that metakaolin should not be used in geopolymers due to the large volumes of water required and the consequent increase in the material's porosity.

The use of SEM-EDX was successful in qualitatively identifying the presence of cementitious gels within samples and that sample homogeneity (and thus strength) was enhanced through increasing binder dosage. As shown in Figure 21.31, sodium

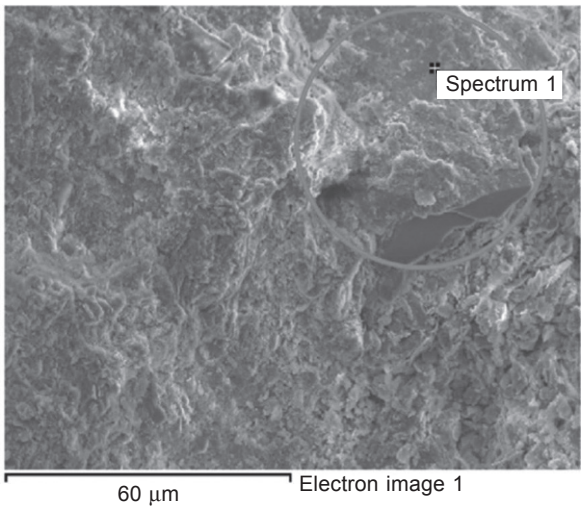

Element	Weight%	Atomic%
O K	52.62	67.21
Na K	6.37	5.66
Al K	9.57	7.25
Si K	25.03	18.21
Ca K	2.48	1.26
Au M	3.94	0.41
Totals	100.00	

Figure 21.31 EDX spectra of metakaolin geopolymers after 28 days curing. Reprinted from Zhang *et al*. (2013), Copyright © 2013, with permission from Elsevier.

was detected in all EDX analyses of metakaolin-stabilised samples, which is likely to be associated with the geopolymer gels (Zhang *et al*., 2013).

Upon blending the metakaolin with the soil, the reaction was observed to be rapid due to the metakaolin's fineness and high amorphous content (Zhang *et al*., 2013). Regarding XRD analyses, Zhang *et al*. (2013) recorded a negligible difference between stabilised and untreated samples, indicating that there was no reaction between the metakaolin and the soil minerals and that the strength enhancements were attributed solely to geopolymer gels. However, metakaolin is a costly material, which has been documented to be unsuitable for chemical stabilisation (Duxson *et al*., 2007) and must be used at high dosages (>11%) to produce comparable performances as using 5% CEM-I (Zhang *et al*., 2013). Hence, other alkalis ought to be used for activating IBP-based geopolymers.

21.10 Conclusions and future trends

This chapter has presented a detailed review of the processes and materials typically involved in chemical soil stabilisation, in addition to the development of new more sustainable alkali-activated mixtures as alternatives to lime and CEM-I. The key points to note are summarised below:

- Factors including high levels of versatility, low dust and noise emissions make DSM techniques ideal for improving ground conditions characterised by soft clayey and/or organic soils. This technique has been used successfully in stabilising local ground conditions for numerous major engineering projects, including the construction of the CTRL and the repair of levees in New Orleans after Hurricane Katrina in 2005.
- To ensure that the soil and binder react and that maximum engineering improvements will be achieved, a detailed understanding of the various binder materials available for use in chemical treatment is essential. Additionally, thorough assessments of the soil must be made in terms of particle size distribution, surface area/reactivity, mineralogical and chemical characteristics. Soils which are ideally suited to chemical treatment contain fines (>10% clays of smectite or montmorillonite composition), low organic and sulphate contents as organics can interfere with cementation reactions and sulphates can produce unfavourable minerals including ettringite and thaumasite.
- Although lime and CEM-I have been used in previous projects and produced high strengths and durabilities, there are numerous environmental and financial problems associated with their production and usage. The production of these materials incurs high costs due to their high levels of energy consumption and high greenhouse gas and carbon emissions. Hence, their continued use as binders is unsustainable and there becomes a need for identifying new sustainable binders; specifically in terms of lower energy consumption, greenhouse gas emissions, production and transport costs. To ensure that such materials are going to be competitive, they should provide engineering performances that are either comparable or surpass those of CEM-I and lime within similar curing times.
- Research into developing new alternative materials has been ongoing since the mid-1990s. One of the most preferred routes for selecting new binders has been recycling IBPs to form geopolymers. Such binders could be substituted for CEM-I and lime with only

minimal modification to existing plant and equipment or a reduction in the efficiency of the installation process.

- Recent laboratory and field-based research has demonstrated that IBPs have great potential as sustainable lime/CEM-I replacements. However, the inclusion of alkali activators is necessary to enhance the rates at which their mechanical properties are improved by increasing pH. This thereby promotes the conditions required for pozzolanic reactions and cementitious bonding to occur. Alkali-activated GGBS is known to produce excellent short- and long-term engineering performance, which comfortably surpass those exhibited by lime and CEM-I.
- For any chemical soil stabilisation project involving the use of alkali-activated mixtures, one should be aware that the cost of producing alkali activators is quite high. It is common for geopolymer components to come from various locations, meaning that the distances between sourcing plants and the stabilisation site can be considerable. Given that modern transportation costs are high, careful planning must be conducted to keep the aforementioned distances down to a minimum. This will ensure that the use of geopolymers remains more sustainable and competitive than lime or CEM-I.

References

Abu Bakar, B. H., Ramadhansyah, P. J. and Megat Azmi, M. J., 2011. Effect of rice husk ash fineness on the chemical and physical properties of concrete. *Magazine of Concrete Research* 65 (5), 313–320.

Ahnberg, H., 2007. On yield stresses and the influence of curing stresses on stress paths and strength measured in triaxial testing of stabilized soils. *Canadian Geotechnical Journal* 44, 54–66.

Al-Tabbaa, A., 2003. Soil mixing in the UK 1991–2000: state of practice report. *Ground Improvement* 7, 117–126.

Al-Tabbaa, A. and Evans, C. W., 1998. Pilot *in situ* auger mixing treatment of a contaminated site – Part 1: Treatability study. *Geotechnical Engineering* 131, 52–59.

Al-Tabbaa, A. and Evans, C. W., 1999. Laboratory-scale soil mixing of a contaminated site. *Journal of Ground Improvement* 3, 119–134.

Bell, F. G., 1996. Lime stabilisation of clay minerals and soils. *Engineering Geology* 42 (4), 223–237.

Bergado, D. T., Anderson, L. R., Miura, N. and Balasubramaniam, A. S., 1996, *Soft Ground Improvement in Lowland and Other Environments*, American Society of Civil Engineers – ASCE Press, Reston, VA.

Broms, B. B., 1984. Stabilization of soft clay with lime columns, Proc. Seminar on Soil Improvement and Construction Techniques in Soft Ground, Nanyang Technological Institute, Singapore.

Brunauer, S., Emmett, P. H. and Teller, E., 1938. Adsorption of gases in multimolecular layers. *Journal of the American Chemical Society* 60, 309–319.

Bye, G., 2011. *Portland Cement*, 3rd edn. Institution of Civil Engineers, London.

Christopher, B. R., Schwartz, C. and Boudreau, R., 2006. *Geotechnical Aspects of Pavements*. National Highway Institute, Federal Highway Administration, US Department of Transportation, Washington D.C. Publication No. FHWA NHI-05-037, May.

Cooper, T. H., 2009. Unit 12 Chapter 2 – Cation exchange and cation exchange capacity.

[online]. Available at <http://www.swac.umn.edu/classes/soil2125/doc/s12ch2.htm> (accessed 6 July 2014).

Davidson, L. K., Demirel, T. and Handy, R. I., 1965. Soil pulverization and lime migration in soil lime stabilisation. *Highway Research Record* 92, 103–126.

delle site, A., 2000. Factors affecting sorption of organic compounds in natural sorbent/water systems and sorption coefficients for selected pollutants: a review. *J. Hys. Chem. Ref. Data* 30 (1), 187–439.

Diamond, S. and Kinter, E. B., 1965. Mechanisms of soil-lime stabilization – an interpretative review, *Highway Research Record* 92, 83–102.

Duxson, P., Fernandez-Jimenez, A., Provis, J. L., Lukey, G. C., Palomo, A. and Deventer, J. S. J, 2007. Geopolymer technology: the current state of the art. *Journal of Materials Science, Advances in Geopolymer Science and Technology* 42, 2917–2933.

Ersahin, S., Gunal, H., Kutlu, T., Yetgin, B. and Coban, S., 2006. Estimating specific surface area and cation exchange capacity in soils using fractal dimension of particle-size distribution. *Geoderma* 136, 588–597.

EuroSoilStab, 2002. Development of design and construction methods to stabilise soft organic soils: design guide soft soil stabilisation. CT97-0351. Project No. BE 96-3177.

FHWA-RD-99-167, 2001. An introduction to the deep soil mixing methods as used in geotechnical applications: volume 3 – verification and properties of treated soil. Prepared by Geosystems (D. A. Bruce) for US Department of Transportation, Federal Highway Administration, p.163.

Gazquez, M. J., Bolivar, J. P., Vaca, F., Garcia-Tenorio, R. and Caparros, A., 2013. Evaluation of the use of TiO_2 industry red gypsum waste in cement production. *Cement & Concrete Composites* 37, 76–81.

Geo-Con., Inc., 1998. Promotional information.

Habert, G., d'Espinose de Lacaillerie, J. B. and Roussel, N., 2011. An environmental evaluation of geopolymer based concrete production: reviewing current research trends. *Journal of Cleaner Production* 19, 1229–1238.

Horpibulsuk, S., Rachan, R., Chinkulkijniwat, A., Raksachon, Y. and Suddeepong, A., 2010. Analysis of strength development in cement-stabilized silty clay from microstructural considerations. *Construction and Building Materials* 24, 2011–2021.

Horpibulsuk, S., Rachan, R. and Suddeepong, A., 2011. Assessment of strength development in blended cement admixed Bangkok clay. *Construction and Building Materials* 25, 1521–1531.

Hossain, K. M. A., 2010. Development of stabilised soils for construction applications. *Ground Improvement* 163, 173–185.

Hughes, P. N. and Glendinning, S., 2004. Deep dry mix ground improvement of a soft peaty clay using blast furnace slag and red gypsum. *Quarterly Journal of Engineering Geology and Hydrogeology* 37, 205–216.

Hughes, P. N., Glendinning, S., Manning, D. A. C. and Noble, B. C., 2010. Production of 'green' concrete using red gypsum and waste. *Engineering Sustainability* 163, 137–146.

Hughes, P. N., Glendinning, S., Manning, D. A. C. and White, M. L., 2011. Use of red gypsum in soil mixing engineering applications. *Geotechnical Engineering* 164, 223–234.

Jegandan, S., Liska, M., Osman, A. A-M. and Al-Tabbaa, A., 2010. Sustainable binders for soil stabilisation. *Ground Improvement* 163, 53–61.

Kurtis, K., 2007. Portland Cement Hydration; PowerPoint presentation from the School of Civil Engineering, Georgia Institute of Technology, Atlanta, Georgia. Available at <people.ce.gatech.edu/~kk92/hyd07.pdf> (accessed 10 December 2013).

Larsson, R., 1977. Basic behaviour of Scandinavian soft clays. Report 4, Swedish Geotechnical Institute, Linköping, Sweden.

Little, D. N. and Nair, S., 2009. NCHRP web-only document 145: Recommended Practice for Stabilization of Sulfate Rich Subgrade Soils. Contractor's Final Task Report for NCHRP Project 20-07. National Co-operative Highway Research Program, Transportation Research Board of the National Academies, Washington, DC.

Little, D. N., Herbert, B. and Kunagalli, S. N., 2005. Ettringite formation in lime-treated soils: establishing thermodynamic foundations for engineering practice. *Transportation Research Record: Journal of the Transportation Research Board* 1936, 51–59.

Locat, J., Berube, M. A. and Choquette, M., 1990. Laboratory investigations on the lime stabilization of sensitive clays: shear strength development. *Canadian Geotechnical Journal* 27, 294–304.

McCarthy, G. J., Swanson, K. D., Keller, L. P. and Blatter, W. C., 1984. Mineralogy of Western fly ashes. *Cement and Concrete Research* 14 (3), 471–478.

McLellan, B. C., Williams, R. P., Lay, J., van Riessen, A. and Corder, G. D., 2011. Costs and carbon emissions for geopolymer pastes in comparison to ordinary portland cement. *Journal of Cleaner Production* 19, 1080–1090.

Meunier, A., 2005. *Clays*, Springer Verlag, Berlin, Heidelberg.

Moranville-Regourd, M., 1998. Cements made from blast furnace slag. In Hewlett, P. (ed.) *Lea's Chemistry of Cement and Concrete* Arnold, London, 633–699.

Nair, S. and Little, D. N., 2009. Water as the key to expansion of ettringite in cementitious materials. *Transportation Research Record: Journal of the Transportation Research Board* 2104, 55–62.

Palomo, A., Grutzeck, M. W. and Blanco, M. T., 1999. Alkali-activated fly ashes: a cement for the future. *Cement and Concrete Research* 29, 1323–1329.

Puppala, A. J., Madhyannapu, R. S., Nazarian, S., Yuan, D. and Hoyos, L., 2008. Deep Soil Mixing Technology for Mitigation of Pavement Roughness. Texas Department of Transportation & Federal Highway Administration. Report No. FHWA/TX-08/0-5179-1.

Quasthoff, P., 2012. State of the art in 'dry soil mixing' – basics and case study. ISSMGE – TC 211 International Symposium on Ground Improvement, IS-GI, Brussels, 31 May – 1 June 2012, Vol. 3, 285–298.

Rahman, M. W., Ghataora, G. S., Chapman, D. N., Tyrer, M., Claisse, P. and Ganjian, E., 2008. Gypsum waste reduction through stabilization for trench backfill. Proceedings of GeoCongress 2008: Geotechnics of Waste Management and Remediation. ASCE, 320–327.

Rodriguez-Navarro, C., Doehne, E. and Sebastian, E., 2000. How does sodium sulphate crystallise? Implications for the decay and testing of building materials. *Cement and Concrete Research* 30, 1527–1534.

Rogers, C. D. F. and Glendinning, S., 1996. Modification of clay soils using lime. In Dixon, N., Glendinning, S. and Rogers, C. D. F. (eds), *Lime Stabilisation*. Thomas Telford, London, 99–114.

Rogers, C. D. F. and Glendinning, S., 2000. Lime requirement for stabilization. *Transportation Research Record* 1721. Paper No. 00-0604, 9–18.

Rogers, C. D. F., Glendinning, S. and Holt, C. C., 2000. Slope stabilisation using lime piles – a case study. *Ground Improvement* 4, 165–176.

Sargent, P., Hughes, P. N., Rouainia, M. and White, M., 2013. The use of alkali activated waste binders in enhancing the mechanical properties and durability of soft alluvial soils. *Engineering Geology* 152, 96–108.

Sherwood, P. T., 1993. *Soil Stabilisation with Cement and Lime – State of the Art Review*. Transport Research Laboratory, Department of Transport. HMSO publications, London.

Shi, C., Krivenko, P. V. and Roy, D., 2006. *Alkali-Activated Cements and Concretes*. Taylor & Francis, Abingdon.

Sumner, M. E. and Naidu, R., 1998. *Sodic Soils*. Oxford University Press, New York.

Supancic, K. and Obernberger, I., 2012. Wood ash utilization as a binder in soil stabilization for road construction – first results of large-scale tests. Proceedings of ASH 2012 conference, Stockholm, Sweden, 25–27 January.

Terzaghi, K., Peck, R. B. and Mesri, G., 1996. *Soil Mechanics in Engineering Practice*, 3rd edn. John Wiley & Sons, New York.

Tomlinson, M. J., 2001. *Foundation Design and Construction*, 7th edn, Pearson Education, Harlow.

Topolnicki, M., 2004. *In situ* soil mixing. In Moseley, M. P. and Kirsch, K. (eds) *Ground Improvement*, 2nd edition. Spon Press, London, 331–428.

Topolnicki, M. and Pandrea, P., 2012. Design of in-situ soil mixing. ISSMGE – TC 211 International Symposium on Ground Improvement, IS-GI, Brussels, 31 May – 1 June 2012, Vol. 3, 309–316.

Treviicos, 2013. Soil Mixing. Available at <http://www.treviicos.com/viewdoc.asp?co_id=1095> (accessed 6 July 2014).

Verástegui Flores, R. D. and van Impe, W. F., 2009. Stress–strain behaviour of artificially cemented kaolin clay. In Hanza, M. *et al*. (eds) Proceedings of the 17th International Conference on Soil Mechanics and Geotechnical Engineering, 283–286.

Weil, M., Dombrowski, K. and Buchwald, A., 2009. Life-cycle analysis of geopolymers. In Provis, J. L. and Van Deventer, J. S. J. (eds), *Geopolymers: Structures, Processing, Properties and Industrial Applications*. Woodhead Publishing Limited, Cambridge, 194–210.

Wild, S., Kinuthia, J. M., Jones, G. I. and Higgins, D. D., 1998. Effects of partial substitution of lime with ground granulated blast furnace slag (GGBS) on the strength properties of lime-stabilised sulphate bearing clay soils. *Engineering Geology* 51, 37–53.

Wilkinson, A., Haque, A. and Kodikara, J., 2010a. Stabilisation of clayey soils with industrial by-products: Part A. *Ground Improvement* 163, 149–163.

Wilkinson, A., Haque, A. and Kodikara, J., 2010b. Stabilisation of clayey soils with industrial by-products: Part B. *Ground Improvement* 163, 165–172.

Zain, M. F. M., Islam, M. N., Mahmud, F. and Jamil, M., 2011. Production of rice husk ash for use in concrete as a supplementary cementitious material. *Construction and Building Materials* 25, 798–805.

Zhang, M., Guo, H., El-Korchi, T., Zhang, G. and Tao, M., 2013. Experimental feasibility study of geopolymer as the next-generation soil stabilizer. *Construction and Building Materials* 47, 1468–1478.

Alkali-activated cements for protective coating of OPC concrete

22

Z. Zhang, H. Wang
University of Southern Queensland, Toowoomba, QLD, Australia

22.1 Introduction

Existing OPC concrete structures, particularly with steel reinforcements within the structures, can experience various problems under aggressive conditions. For example, almost all concrete structures suffer from alkalinity neutralization due to slow carbonation of hydrated cement in contact with wet air conditions. The concrete pipes in chemical engineering plants and waste treatment plants are suffering from chemical erosion and thermal attacks by high or low pH substance and high temperature. Marine concrete structures are suffering from salt water attacks, involving wave scouring, chloride and sulphate corrosion and carbonation at splash and tidal zones. Extending the service life of OPC concrete structures under rigorous conditions is an important aspect in support of the sustainable development of today's cement and concrete industry.

The improvement of durability of marine concrete structures, particularly their resistance to Cl^-, SO_4^{2-} and Mg^{2+}, has become the focus of civil engineering and material sciences due to the fast development of marine constitution (Binici *et al.*, 2008; Val and Stewart, 2003). Significant progress has been made in last decades to develop OPC concretes with low permeability and high corrosion resistance by optimizing the proportion of cement, secondary cementitious materials, such as slag and silica fume, and the packing of aggregates. The development of new water-reducing agents can reduce the water requirement of concrete by a large extent, consequently reducing the porosity and permeability of the concrete structures. However, these measures are only available for new structures. For existing structures, replacing the deteriorated concrete with new concrete or composites (mainly resin based) is the common option.

Applying a layer or several layers of coatings can be a cost-effective alternative to stop, or at least hinder, the immigration of corrosive fluids, so as to prolong the service life of existing OPC concretes. In general, there are three categories of protective surface treatments: (1) coating the surface with a thin or thick polymer film, (2) sealing the surface by blocking the front pores, and (3) impregnating the surface by water-repellent agent (Dai *et al.*, 2010). Currently many types of coatings are available for concrete: epoxy coatings and acrylic and polyurethane penetrating sealers. The durability of conventional organic coating materials, which are usually

Handbook of Alkali-activated Cements, Mortars and Concretes. http://dx.doi.org/10.1533/9781782422884.4.605

a thin layer of 100–400 μm placed on the concrete surface, is seriously questionable because of their quick ageing under UV and sea wave conditions, although it has been evaluated that their service life may reach up to 10 years (Huang *et al.*, 2002). It has been proved that silane-based surface impregnation agents (penetration depth >5 mm) are effective in reducing water absorption and prevent chloride penetration of uncracked concrete and reinforced concrete structures, while sodium silicate-based pore blockers are not effective (Dai *et al.*, 2010). The use of polymer impregnated permanent coating (thickness of 25 mm) has proved to be one of the effective solutions to protect and retrofit old and new concrete structures under aggressive conditions (Bhutta *et al.*, 2013).

Developing inorganic coating for OPC concretes has been reported by Balaguru (2002). The inorganic coatings by alkali-activated metakaolin incorporated with carbon and nylon fibres can be applied on various concrete surfaces in the ambient temperature range of 40–90°F (4.4–32.2°C), and were proven to be useful in improving the durability of concretes under outdoor conditions (Balaguru *et al.*, 2008). This chapter presents the development of alkali-activated metakaolin (AAM) as a new coating material to protect OPC concretes that are exposed to marine conditions – a common corrosive environment. Applying AAM on OPC concrete surfaces could be an alternative solution to provide a more durable and cost-effective coating layer. The study presented in this chapter includes laboratory investigations and on-site trial works, some of which have been reported by the authors (Zhang *et al.*, 2010a, 2010b, 2012; Zhu *et al.*, 2013). The laboratory investigations include the preparation of AAM pastes at different slag contents and liquid/solid ratios, accelerated corrosion tests using concentrated seawater, mechanical test and microstructure analysis of AAMs and concrete and their interfaces. On-site trials were performed at Hangzhou Bay (Shanghai, China), where severe degradation of OPC concretes is observed.

22.2 Basic properties of alkali-activated metakaolin (AAM) coating

As a coating material, particularly for existing OPC concrete structures in contact with corrosive fluids, AAM coatings must meet at least four requirements: suitable setting time, strong bonding with the substrate, low permeability and low shrinkage. For the purpose of application on marine concretes, the setting time needs to be shorter than 6 hours (approximately half of tidal time). The coating is expected to have sufficient bond strength after finally setting to resist the wave motions.

22.2.1 Setting time of AAM binders

The setting time of AAM depends on the nature of the solid precursor, the type and concentration of activator and curing temperature. When metakaolin is mixed with slag to form blend solid materials, the setting time is significantly affected by the slag

content. Figure 22.1 shows the initial and final setting time of AAM binders activated by a sodium silicate (modulus SiO_2/Na_2O M_s = 1.2) solution under 25°C ambient conditions. Without slag addition, the initial setting time of AAM paste is 75 min and the final setting is around 160 min. The substitution of slag shortens the setting time of AAM pastes. When slag content is up to 50%, the initial and final setting times are 35 and 55 min, respectively. The large reduction of setting time is due to the quick formation of calcium-containing aluminosilicate gels after the dissolution of slag in alkaline activation solution. The quick setting of alkali-activated slag (AAS) binders has been observed in many other conditions, such as high temperature (Zhu and Yao, 2013) and low M_s (Aydın and Baradan, 2014). It should be noted that setting too quickly can also be an issue for engineering applications (Pu, 2010). Therefore, it is suggested that if no additional setting control additive is used, the slag content should be controlled at a low ratio (<30% is recommended).

When fly ash is incorporated into the AAM systems, the setting time can also be changed. Being prolonged or shortened will depend on the substitution ratio and particularly the nature of fly ash. For example, when the fly ash is of low-Ca (usually Class F), the setting time will be prolonged (Zhang *et al.*, 2014); however, when a high-Ca fly ash is incorporated, the setting time might be shortened. This is observed in the manufacturing of alkali-activated fly ash-based concretes, the fly ash containing high calcium content, generating very quick setting (Diaz-Loya *et al.*, 2011).

The setting time of AAM binders is significantly affected by reaction temperature. Figure 22.2 shows the setting time of alkali-activated metakaolin/slag (90/10) binders at different temperatures. A small increase in temperature from 20 to 25°C significantly shortens the setting. At 35°C the binder will set within 1 h. The temperature range

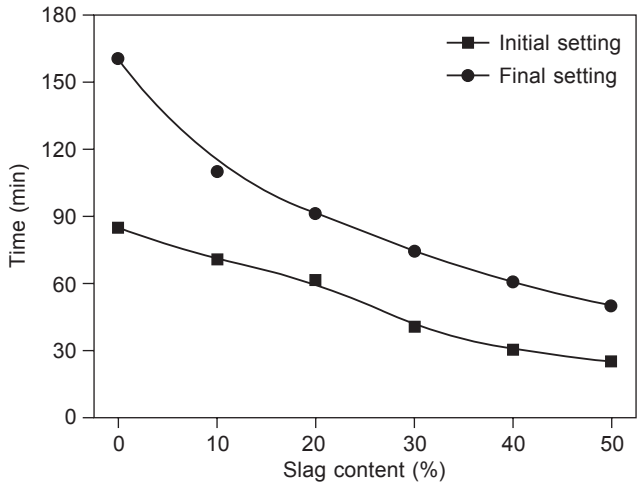

Figure 22.1 The effects of slag substitution on the setting time of AAM binders at 25°C. The activator is sodium silicate solution with M_s = 1.2 and concentration = 35% (reprinted from Zhang *et al.*, 2010a, Copyright © 2010, with permission from Elsevier).

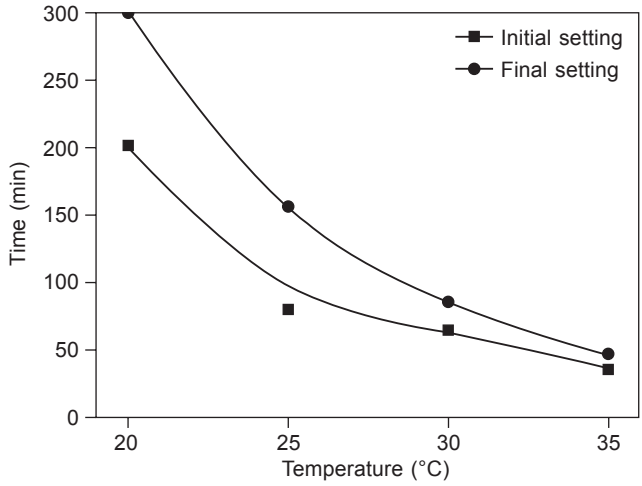

Figure 22.2 The effects of reaction temperature on the setting time of AAM binders. The activator is a sodium silicate solution with M_s = 1.2, concentration = 35%. The solid raw material is a blend of metakaolin/slag (90/10) (reprinted from Zhang *et al*., 2010a, Copyright © 2010, with permission from Elsevier).

chosen for study is very typical for subtropical areas, and the results suggest that this type of inorganic coating is applicable with relatively wide tolerance of temperature. However, slow setting of AAM coatings at temperatures lower than 20°C needs some attention for successful application, and might need to look at other alkali-activated binder alternatives.

Setting behaviour of fresh paste is an important engineering property for AAM to be used as protective coatings for marine concrete. On one hand, it needs a sufficient time for mixing and coating. Quick setting, at less than 30 min (Davidovits, 1996), or flash setting can result in difficulty for the coating layer wetting and penetrating into the OPC concrete substrate. On the other hand, the final setting time of the coating layer should not be longer than 6 h limited by the tide frequency if it is constructed in marine applications. For a certain outdoor temperature range, it is possible to adjust the setting time into this window by changing the slag content, alkali concentration and M_s (Aydın and Baradan, 2014; Hu *et al*., 2008).

22.2.2 Bond strength of AAM binders to cement substrates

The bond strength between AAM binder and OPC substrate is one of the key engineering properties. In particular, it requires the coating layer to be strongly adhesive to the substrate after final setting to resist the scrub of seawater waves.

Figure 22.3 shows the bond strength between AAM and OPC substrate as determined under laboratory simulation conditions. The bond strength is measured by pulling apart the 'dog-bone' specimens with half AAM binder and half OPC mortar or paste,

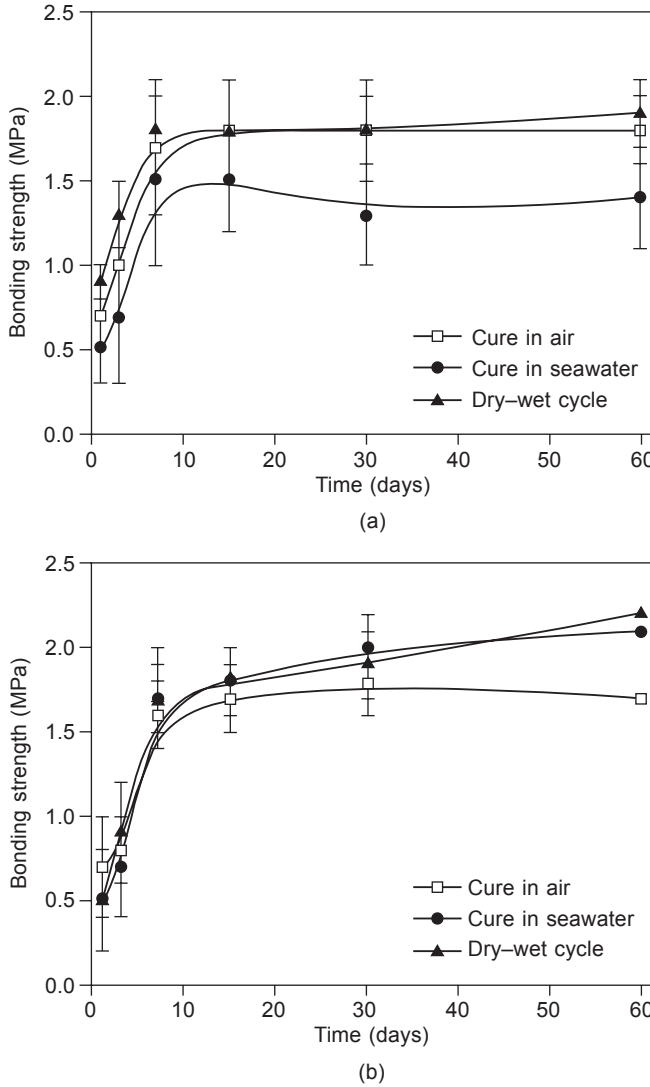

Figure 22.3 Bond strength of AAM binder to OPC mortar (a) and paste (b). The three curing conditions are in laboratory air at RH = 90 ± 5%, 20 ± 2°C, immersed in concentrated seawater and dry–wet cycle for 12 h in air and 12 h immersed in seawater (reprinted from Zhang *et al.*, 2010a, Copyright © 2010, with permission from Elsevier).

as shown in Figure 22.4(a). The bond strength is in the range of 0.5–1 MPa after 24 h of application of AAM binder on the OPC substrate. The final bond strength after 28 days of curing is 1.5–2.5 MPa, which is consistent with the results by other researchers who used a similar testing method (Hu *et al.*, 2008). Much lower bond strength (<0.2 MPa) has also been reported (Vasconcelos *et al.*, 2013). The bond

strength in the very early stage (<24 hours) has not been tested. However, on-site inspection (illustrated in Section 22.4.2) indicates that the AAM coating layer can strongly bond to OPC concrete within 6 h to resist the wave motions.

In fact, the force of seawater waves is in compression and shearing, rather than in tension. The assessments by compression testing may provide more useful information. It was reported that in compression mode (as shown in Figure 22.4(b)), the shear bond strength of slant prisms with geopolymer and concrete joints at a 60° angle of cross section is 10–20 MPa (Pacheco-Torgal *et al.*, 2008; Ueng *et al.*, 2012). Such a bonding is strong enough to resist wave impact in service.

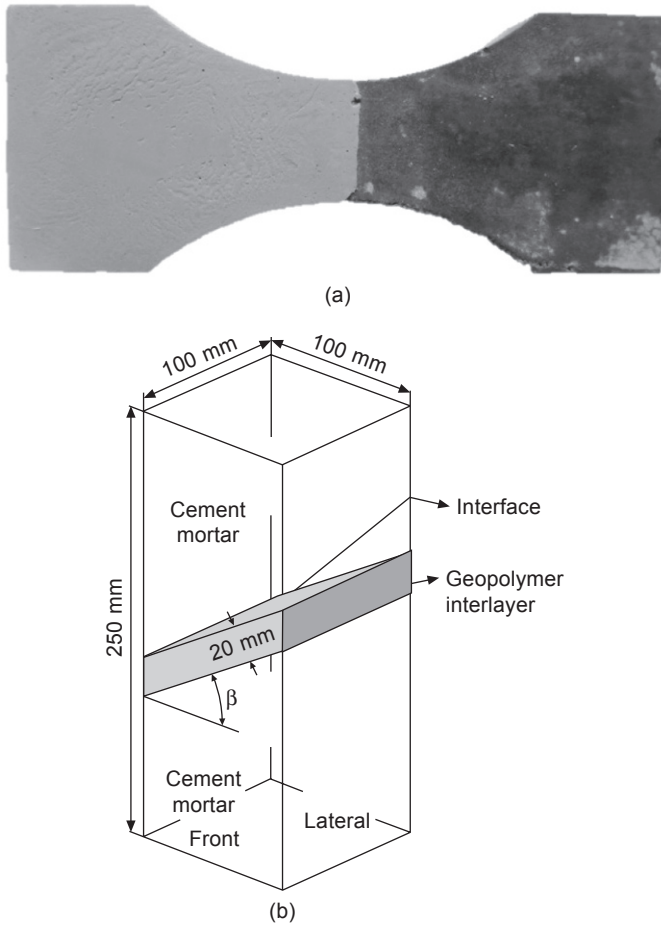

Figure 22.4 Patterns of bond strength testing: (a) the sample for tension testing (Zhu *et al.*, 2013); (b) sketch of sample for compression testing (Ueng *et al.* 2012); (c) the sample for compression testing (reprinted from Pacheco-Torgal *et al.*, 2008, Copyright © 2008, with permission from Elsevier).

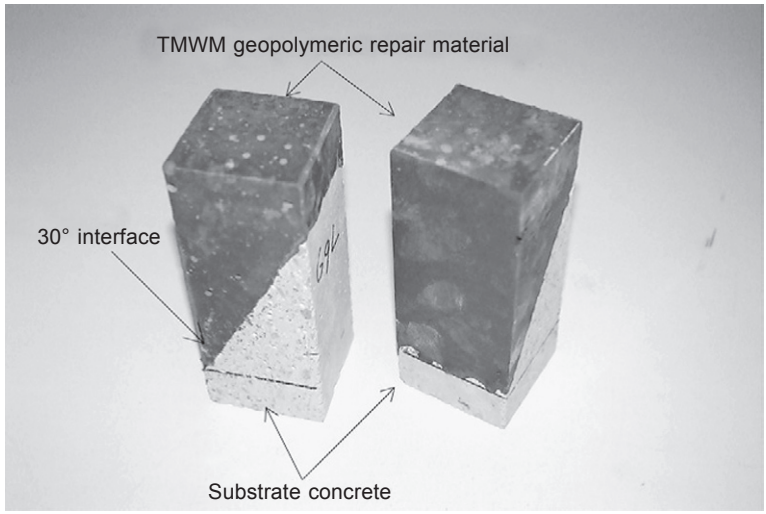

(c)

Figure 22.4 Continued

22.2.3 Permeability of AAM binders in comparison with hydrated OPC

The permeability of AAM binders depends on many factors, such as liquid/solid ratio, reaction/curing conditions and the nature of blended materials. Generally, AAM binders have extremely low permeability because of their dense matrix and complex pore structures (Zhang *et al*., 2010a). The permeability coefficient of binders by sodium silicate activation of metakaolin at room temperatures as determined by Darcy method under high hydrostatic pressure (20 MPa) is around 1×10^{-6} μm^2, which is only 1/100 to 1/10 of well-hydrated OPC binders. For those specimens cured by seawater, the permeability coefficient can be even lower, $0.8–0.9 \times 10^{-6}$ μm^2. More detailed information can be found in Chapter 9.

22.2.4 Shrinkage of AAM binders under laboratory conditions

Shrinkage could be one of the most challenging problems for the application of AAM binders and other alkali-activated materials. The total shrinkage of cement-based materials includes two parts, namely autogenous shrinkage and drying shrinkage. The autogenous shrinkage of AAM binders is not high, even at high reaction temperatures, as determined by measuring the length change of AAM specimens in water (Zhang *et al*., 2009). However, the drying shrinkage of AAM binders is large under low humidity conditions. This is because of the high liquid requirement (usually >0.5) and the continuous release of water molecules from aluminosilicate gel pores of hardened AAM binders. High temperature curing at 80°C without cover may even cause cracks on the surface of specimens (Zhang *et al*., 2009). Figure 22.5 shows

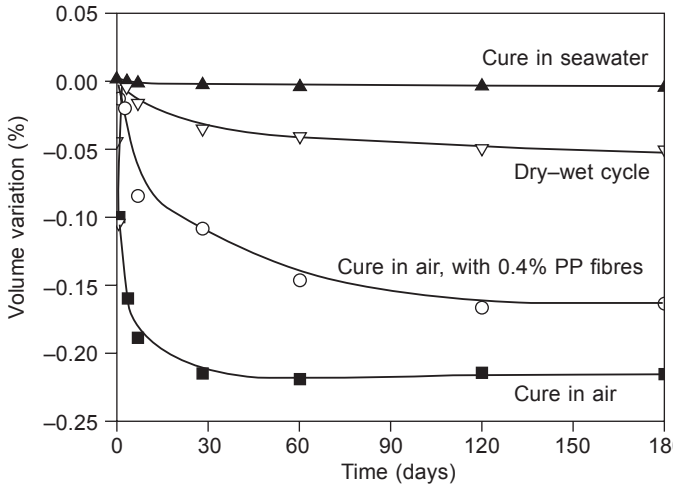

Figure 22.5 Shrinkage of AAM binder under different curing conditions. The AAM binder is formed by sodium silicate activation of a blend of metakaolin/slag (90/10) under room temperature (reprinted from Zhang *et al.*, 2010a, Copyright © 2010, with permission from Elsevier).

the shrinkage of AAM binders under different conditions. The volume shrinkage of binders ranges from 0 under seawater curing to 0.21% under air curing condition. Apparently environmental humidity is a key factor that affects the volume stability. By adding 0.4% polypropylene (PP) fibres and 1–2% MgO-based expansion agents, dry shrinkage can be successfully controlled, at least under the laboratory conditions (RH = 90 ± 5%) (Zhang *et al.*, 2010a).

22.3 Durability/stability of AAM coating

Durability is a comprehensive property for the material to meet its designed requirement in service. It can be evaluated using one or multiple parameters. For cement and concrete, durability is affected by chemical attacks, chloride penetration, alkali aggregate reaction, carbonation and some other property degradation under certain conditions. Durability is one of the most concerning issues for alkali-activated cements. Much of the published literature reports the excellent durability of alkali-activated fly ash (AAFA) and alkali-activated slag (AAS) products under extreme conditions, such as acid, sulphate and seawater (Bakharev *et al.*, 2003; Bakharev, 2005a, 2005b; Fernández-Jiménez *et al.*, 2007; Fernández-Jiménez and Palomo, 2009). The following sections present the durability of AAM binders under seawater and hydrothermal conditions.

22.3.1 Durability of AAM binders in contact with seawater

The durability of AAM binders is assessed using the change of the compressive strength after the material contact with concentrated seawater. As shown in Figure 22.6, AAM binders exhibit excellent corrosion resistance. The seawater cured specimens reach 25.9 MPa after 1 day of curing and the dry–wet cycle cured samples obtained 38.6 MPa. After 60 days of curing, the seawater cured specimens reached up to 74.6 MPa, which is only 4.8 MPa and 7.0 MPa lower than the dry–wet cycle cured and air cured specimens. Unlike under seawater curing conditions, the dry–wet cycle cured specimens show a similar trend in strength development as the air cured samples even after they experienced periodic immersion in concentrated seawater. It indicates that the dry–wet cycle, which simulates real seawater contact, has very limited influence on strength development. These data indicate that the AAM binders have excellent stability under seawater conditions.

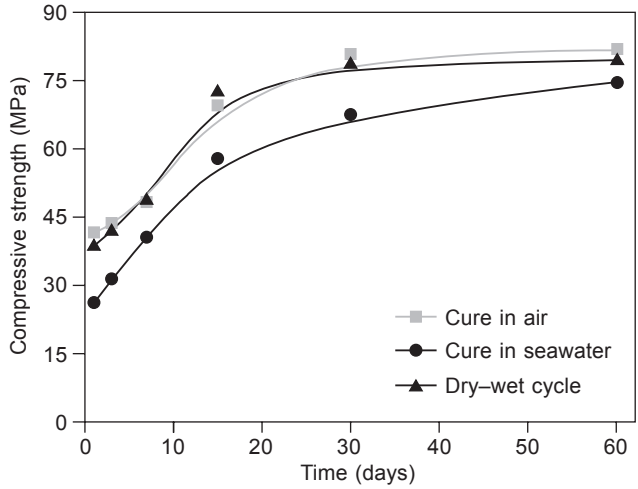

Figure 22.6 Compressive strength development of AAM binders in contact with seawater (reprinted from Zhang *et al.*, 2010a, Copyright © 2010, with permission from Elsevier).

22.3.2 Stability of AAM binders exposed to hydrothermal conditions

When AAM binders are exposed to hydrothermal conditions, the transformation of aluminosilicate gels to zeolites or other more ordered structure causes re-organization of the local structure. It has been noticed that such structural change has a negative effect on the mechanical properties (Lloyd, 2009). The compressive strength of AAM binders under different hydrothermal conditions is shown in Figure 22.7. The room temperature air cured specimens (AC) achieve 60 MPa after 7 days, 90% of the 28-day strength. When being cured at 80°C in steam, the specimens gain higher strength in the first 7 days but lose strength at 28 days. The elevated temperature

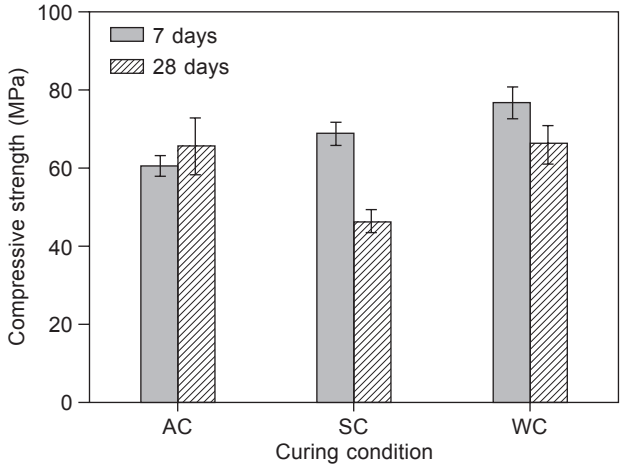

Figure 22.7 Compressive strength development of AAM binders under hydrothermal conditions. The specimens are formed by sodium silicate solution (M_s = 1.2, concentration = 35%) activation of metakaolin and set and harden at 20 ± 2°C, RH of 95 ± 5% for 1 day. The followed curing/aging conditions are AC = 20°C air curing at relative humidity of 95 ± 5%; SC = 80°C sealed curing in plastic bags; and WC = 80°C water curing in water bath (reprinted from Zhu *et al*., 2013, Copyright © 2013, with permission from Elsevier).

can accelerate the alkali activation in the first few days but has a negative influence on the mechanical properties if the samples are exposed to steam condition for too long (Zhang *et al*., 2009; Rovnanik, 2010). High temperature water bath cured specimens show higher strengths than the steam cured specimens. This suggests the importance of water in retaining the mechanical property. The strength degeneration is attributed to the loss of structural water (Zhang *et al*., 2009) and the increased porosity and pore size (Rovnanik, 2010; Muñiz-Villarreal *et al*., 2011). Testing on 95°C aged AAM binders shows that the phase change from amorphous to crystalline (zeolite Na-P1 and sodium chabazite) has a direct linkage to the compressive strength degradation (Lloyd, 2009).

The change of pore structure and phase transformation in AAM binder exposed to hydrothermal conditions has negative influences on its bonding behaviour to hydrated cement. Figure 22.8 shows the change of bond strength in tension of AAM binder and hydrated cement substrate. The binder composition and curing conditions are the same as described in Figure 22.7. Under the conditions of air curing (AC), the bond strength is 1.3 MPa at 7 days and increases to 1.5 MPa at 28 days. Under the conditions of steam curing and water bath curing at 80°C, the bond strength is 2.5 and 1.2 MPa at 7 days, and decreases by 31% and 37%, respectively, when the curing is extended to 28 days. The reduction of bond strength after hydrothermal curing indicates that special attention should be paid to the stability of metakaolin-based coatings when they are used as bonding and coating materials for OPC concrete at high temperatures or under hydrothermal conditions.

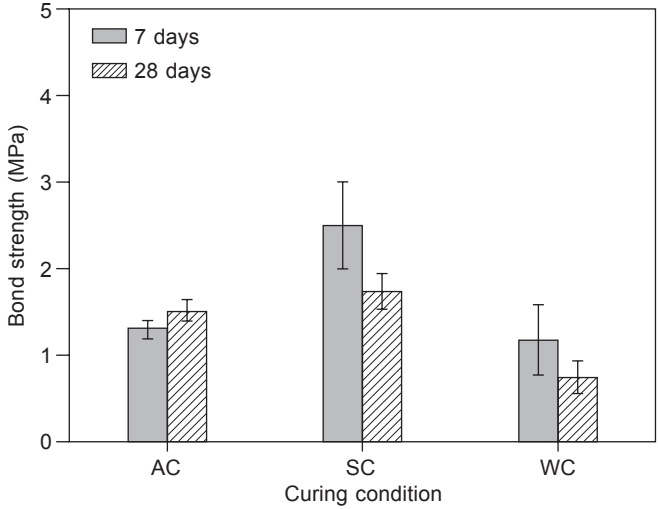

Figure 22.8 Bond strength of AAM binder to hydrated cement under hydrothermal conditions. Curing conditions as in Figure 22.7 (reprinted from Zhu *et al.*, 2013, Copyright © 2013, with permission from Elsevier).

22.4 On-site trials of AAM coatings

The following sections illustrate the working procedures and the coating inspection at on-site conditions. The reaction products after 6 months of service were examined.

22.4.1 AAM coating procedures

The outdoor trials using AAM binders as a coating material for OPC concrete were performed at Shanghai Jinshan coast (Hangzhou Bay, N30.705239, E121.334724). The large temperature change between summer and winter is the reason for selecting this location in order to examine the stability of the coating. The field experiment started from 20 August 2010 (middle of summer) and the observation lasted for 6 months till 20 February 2011 (middle of winter). During this period, the on-site temperature varied from 38°C (highest in summer) to –4°C (lowest in winter).

The OPC concrete sea wall and accropodes on the coast were built in 2004 and degraded very quickly due to salt water attack, as shown in Figure 22.9. Many cracks and peel off appear at the surface of the concrete due to the periodical corrosion by seawater in just 6 years. The accropodes have exposed coarse aggregates and the steel links in the accropodes have been badly rusted by seawater. Three typical accropodes on the coast were chosen as the concrete substrate for coating: the first one did not contact with seawater (dry condition), the second one was on the back to the wave shock, and the third was facing on the wave shock.

The composition of the AAM coating is shown in Table 22.1. The coating work

(a)

(b)

Figure 22.9 Field experiment location (a) and the deteriorated accropodes (b) on the coast.

Table 22.1 Composition of alkali-activated metakaolin coating

	Metakaolin	**Slag**	**Activator**	**PP fibre**	**MgO**
Mass%	42.97	7.52	47.17	0.39	0.95
Characteristics	14.1 m^2/g	0.65 m^2/g	$Na_2O{\cdot}1.2SiO_2$; concentration = 35%	Diameter = 35 μm; length = 19 mm	Reactivity = 87%

was performed in the afternoon of 20 August 2010, a cloudy and windy day. On the coast, the temperature was 26°C, the wind was Grade 7 (13.9–17.1 m/s) and the relative humidity was about 65%. After ebb tide, the second and third surfaces were scrubbed with a steel wire brush to remove the sea shells and the loose mortar (Figure 22.10(a)), and allowed to naturally dry for 30 min. The AAM slurry was manually coated on the surfaces to a thickness of 3–5 mm with a putty brush (Figure

(a)

(b)

Figure 22.10 Work procedures for placing AAM coating layer on OPC concrete exposed to marine conditions: (a) clean surface; (b) coat after 30 min of natural drying; (c) cover with wet straw mats after initial setting; (d) remove the cover after two tidal cycles.

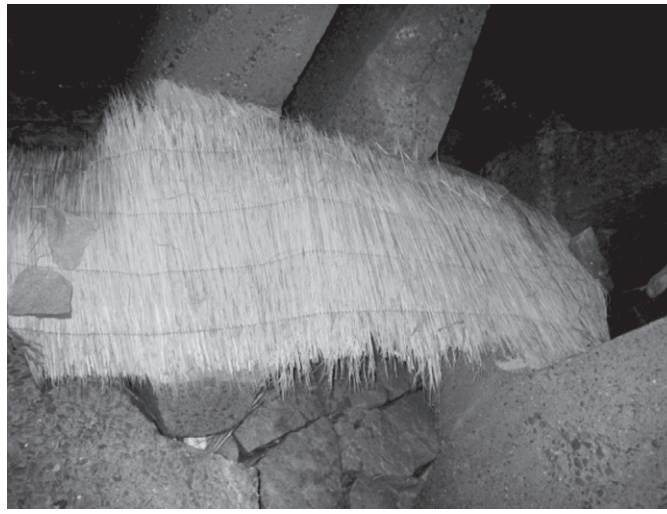

(c)

(d)

Figure 22.10 Continued

22.10(b)). After the initial setting (about 30 min), the coatings were covered with wet straw mats (Figure 22.10(c)). It was noted the final setting time under natural marine condition was within 4 h, which is shorter than the half tidal cycle of 6 h. After solidifying for two tidal cycles (Figure 22.10(d), the coating layers were immersed in seawater twice during the 12 h), the straw mats were removed to allow the coatings to be hardened under ambient conditions. The coatings were observed daily during the first month to record any changes in appearance.

22.4.2 The inspection and examination of the solidified coating layer

After 24 h of setting and hardening, the coating layers changed from soil-red to azury, which is the typical colour of alkali-activated slag. The slag fraction of the metakaolin/slag blend as the solid raw materials was 12%. The composition of the coating is shown in Table 22.1. Figure 22.11 shows that the solidified layers on surface II and surface III (at a position where immersed in seawater periodically) were smooth except for some impression from the straw. However, shrinkage caused micro-cracks to appear in the first 24 h for the two coatings with thickness of 3 mm

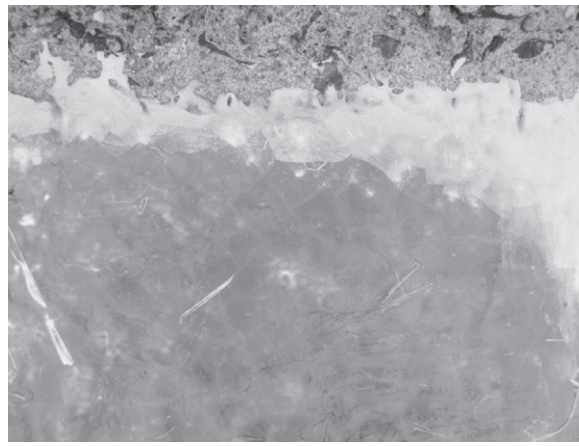

(a)

(b)

Figure 22.11 AAM coating layers with varied thickness on the three substrates after 24 h: (a) 3 mm on dry substrate I; (b) 5 mm on substrate II facing the wave shock; (c) 3 mm on substrate III back of wave shock.

(c)

Figure 22.11 Continued

on surface I (dry all the time) and surface III (periodically immersed in water but back to wave).

Figure 22.12 shows the solidified coatings on the three substrates after 24 h. After 7 days of exposure under the marine conditions, all of the three coatings turned back to the original soil-red of AAM slurry. After 180 days, many of the micro-cracks were observed on the 3 mm thick coatings that were applied on surface I and surface III. In contrast, there were fewer micro-cracks on the 5 mm thick coating applied on surface II and they were not in a crossing pattern. Small amounts of

Figure 22.12 Hardened coatings on OPC concrete substrates after 180 days.

white salt crystallized phases were observed on the surface of coatings in contact with seawater.

To test the bonding with concrete, the coating was tapped with a hammer. All coating chips scraped some mortar, as shown in Figure 22.13, which implied that the interface between the AAM coating and the concrete substrate was stronger than the substrate.

The strong bonding between AAM coating and OPC concrete substrate is due to the reaction of alkali activator and the hydrated cement. Figure 22.14 shows the

Figure 22.13 Examination of the bonding between AAM coating layer and OPC concrete after 180 days of exposure under marine tidal conditions.

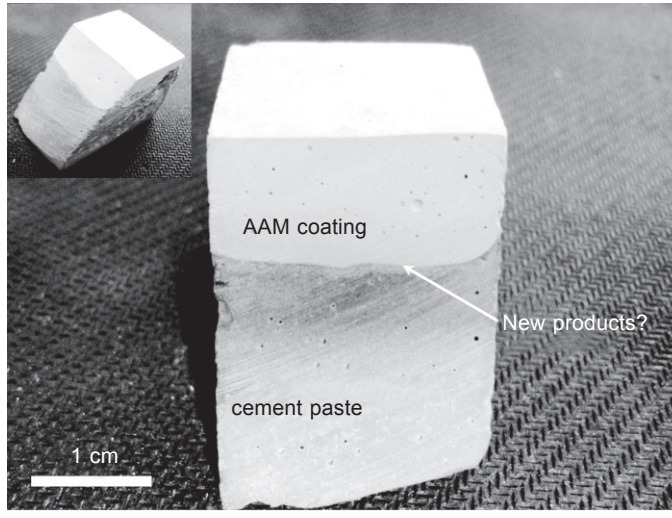

Figure 22.14 The oblique section of AAM coating on OPC paste substrate.

section of AAM coating on a hydrated cement paste substrate. A thin layer (~1 mm) of light grey products is observed on the surface of the cement paste. This thin layer could be formed due to the reaction of hydrated cement, or just a layer of carbonated cement paste, with alkali activator solution.

The backscattered electron (BSE) image of the interface (Figure 22.15) shows that the colour from AAM coating layer to cement paste changes gradually, which indicates the gradual change of elemental compositions and the chemical reaction that occurred between coating and substrate.

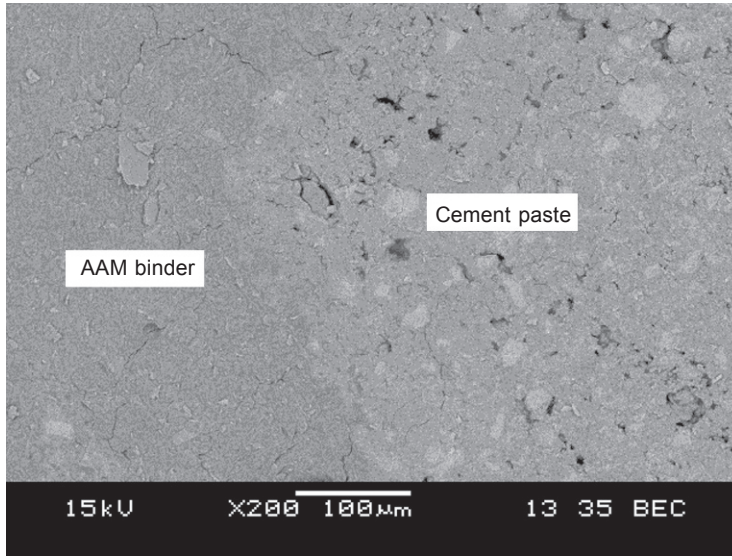

Figure 22.15 Backscattered electron (BSE) image of the interface between AAM coating and cement paste substrate (reprinted from Zhang *et al*., 2010b, Copyright © 2010, with permission from Elsevier).

22.5 The potential of developing other alkali-activated materials for OPC concrete coating

The development of alkali-activated cements for OPC concrete coating is still at a very early stage. The high viscosity of AAM coating can be an issue. In comparison, alkali-activated fly ash, slag or their blends have much better workability. High workability, in particular spreadability, enables easy application, either by manual or machinery coating methods.

For all alkali-activated coatings, setting time needs to be carefully considered. As discussed above, a suitable setting window is critical for successful application. The setting of alkali-activated low-Ca fly ash (AAFA) is usually very slow under room temperature conditions. It may take 24 h and in some cases several days, while high-Ca fly ash can give quick setting, from several minutes to a few hours (Diaz-

Loya *et al.*, 2011; Jumrat *et al.*, 2011). Increasing curing temperature can shorten the setting time of AAFA binders (Hardjito *et al.*, 2008), but it is not very practical for on-site work. Addition of chemical admixtures (Allahverdi and Ghorbani, 2006) could be more practical. The potential of developing AAFA-based coating is actually limited. This is because the AAFA binders are usually more porous and permeable than OPC paste (Ma *et al.*, 2013), which is not suitable as a protective layer. However, it has some potential for other applications, such as as a fire-resistant layer or for plain concretes (without steel reinforcement) where low permeability is not required.

It is also possible to develop alkali-activated slag (AAS) binders as coating materials for OPC concretes (Hu *et al.*, 2008). The control of setting behaviour of AAS binders is also critical for their applications (Aydın and Baradan, 2014; Pu, 2010; Zhu and Yao, 2013). Setting time of AAS binders depends on many factors, such as the reactivity of solid raw materials and the activators. Addition of low-Ca fly ash can delay the setting of AAS; however, it also increases the porosity and permeability (Provis *et al.*, 2012; Ismail *et al.*, 2013). A special setting-retarding agent was reported to be able to delay the setting of AAS systems without negative influences on their long-term mechanical properties (Pu, 2010). Alkali activator type and M_s were reported to have significant effects on the setting time of ASS pastes (Aydın and Baradan, 2014).

22.6 Conclusions and future trends

The laboratory research and small-scale on-site trials have shown that alkali-activated metakaolin (AAM) can be applied as an inorganic coating for the protection of existing marine concrete structures. The setting time of AAM coating can be adjusted by changing the slag substitution. The bonding between the coating and the aged OPC is very strong, 1–3 MPa in tension and >20 MPa in shearing/compression. The excellent corrosion resistance of AAM coatings against seawater and their extremely low permeability (only 1/10 to 1/100 of cement paste) provide durable effective protection of OPC concretes exposed to marine conditions, particularly at tidal zone.

The development of alkali-activated coating materials is still at a very early stage. There are several technical problems that need to be solved. One of the problems is the high viscosity of AAM coatings. Regardless of the low workability, high viscosity will cause immature wetting on substrate surface, particularly when the surface is coarse and porous. Other types of alkali-activated cements may have low viscosity, such as AAS; however, systematic research is lacking regarding other properties. Another problem is the high shrinkage. Using lower liquid/solid ratio, polymer fibres and MgO-based expansion agents can reduce the shrinkage effectively under laboratory conditions. However, under outdoor conditions shrinkage cracks may occur within the first 24 h. This is mainly due to the quick loss of water during setting and solidification at an early age. Increasing the thickness of coating is beneficial in

reducing shrinkage but is not cost-effective and is still not able to produce crack-free coatings. Therefore, in future R&D, works regarding setting and shrinkage control are both important. Developing new coating equipment and machinery is also an important aspect. Other works, including understanding of the interaction between coating layers and substrate, the coating resistance to thermal shock, and chemical attacks, are also interesting to industry.

References

Allahverdi A and Ghorbani J. Chemical activation and set acceleration of lime-natural pozzolan cement. *Ceramic – Silikáty*, 2006; 50: 193–199.

Aydın S and Baradan B. Effect of activator type and content on properties of alkali-activated slag mortars. *Composites B* 2014; 57: 166–172.

Bakharev T. Durability of geopolymer materials in sodium and magnesium sulfate solutions. *Cem Concr Res* 2005a; 35: 1233–1246.

Bakharev T. Resistance of geopolymer materials to acid attack. *Cem Concr Res* 2005b; 35: 658–670.

Bakharev T, Sanjayan J and Cheng YB. Resistance of alkali-activated slag concrete to acid attack. *Cem Concr Res* 2003; 33: 1607–1611.

Balaguru P. Geopolymer for protecting coating of transportation infrastructures. Project report of Center for Advanced Infrastructure and Transportation (CAIT). Civil and Environmental Engineering. Piscataway, NJ: Rutgers State University, 2002.

Balaguru P, Nazier M and Arafa M. Field implementation of geopolymer coatings. Project report of Center for Advanced Infrastructure and Transportation (CAIT). Civil and Environmental Engineering. Piscataway, NJ: Rutgers State University, 2008.

Bhutta MAR, Maruya T and Tsuruta K. Use of polymer-impregnated concrete permanent form in marine environment: 10-year outdoor exposure in Saudi Arabia. *Constr Build Mater* 2013; 43: 50–57.

Binici H, Aksogan O, Görür EB, Kaplan H and Bodur MN. Performance of ground blast furnace slag and ground basaltic pumice concrete against seawater attack. *Constr Build Mater* 2008; 22: 1515–1526.

Dai J, Akira Y, Wittmann FH, Yokota H and Zhang P. Water repellent surface impregnation for extension of service life of reinforced concrete structures in marine environments: the role of cracks. *Cem Concr Comp* 2010; 32: 101–109.

Davidovits J. Method for obtaining a geopolymeric binder allowing to stabilize, solidify and consolidate toxic or waste materials. 1996. US Patent No. 5,539,140.

Diaz-Loya EI, Allouche EN and Vaidya S. Mechanical properties of fly-ash-based geopolymer concrete. *ACI Mater J* 2011; 108: 300–306.

Fernández-Jiménez A and Palomo A. Chemical durability of geopolymers. In Provis JL and van Deventer JSJ (eds) *Geopolymers – Structure, Processing, Properties and Industrial Applications*. Woodhead Publishing Limited, Cambridge, 2009, pp. 167–193.

Fernández-Jiménez A, Garcia-Lodeiro I and Palomo A. Durability of alkali-activated fly ash cementitious materials. *J Mater Sci* 2007; 42: 3055–3065.

Hardjito D, Cheak CC and Ing CHL. Strength and setting times of low calcium fly ash-based geopolymer mortar. *Modern Appl Sci* 2008; 2: 3–11.

Hu S, Wang H, Zhang G and Ding Q. Bonding and abrasion resistance of geopolymeric repair material made with steel slag. *Cem Concr Com* 2008; 30: 239–244.

Huang J, Zhou Y, Wang S and Pan D. Analysis of exposure experiment and application of coatings for marine concrete structures. *China Harbour Eng* 2002; 6: 17–21 (in Chinese with English abstract).

Ismail I, Bernal SA, Provis JL, San Nicolas R, Brice DG, Kilcullen AR, Hamdan S and van Deventer JSJ. Influence of fly ash on the water and chloride permeability of alkali-activated slag mortars and concretes. *Constr Build Mater* 2013; 48: 1187–1201.

Jumrat S, Chatveera B and Rattanadecho P. Dielectric properties and temperature profile of fly ash-based geopolymer mortar. *Int Commun Heat Mass Transfer* 2011; 38: 242–248.

Lloyd RR. Accelerated ageing of geopolymers. In Provis JL and Van Deventer JSJ (eds) *Geopolymers – Structure, Processing, Properties and Industrial Applications*. Woodhead Publishing Limited, Cambridge, 2009, pp. 139–166.

Ma Y, Hua J and Ye G. The pore structure and permeability of alkali activated fly ash. *Fuel* 2013; 104: 771–780.

Muñiz-Villarreal MS, Manzano-Ramírez A, Sampieri-Bulbarela S, Gasca-Tirado JR, Reyes-Araiza, JL, Rubio-Ávalos JC, Pérez-Bueno JJ, Apatiga LM, Zaldivar-Cadena A and Amigó-Borrás V. The effect of temperature on the geopolymerization process of a metakaolin-based geopolymer. *Mater Letter* 2011; 65: 995–998.

Pacheco-Torgal F, Gomes JP and Jalali S. Adhesion characterization of tungsten mine waste geopolymeric binder: influence of OPC concrete substrate surface treatment. *Constr Build Mater* 2008; 22: 154–161.

Provis J L, Myers R J, White CE, Rose V and van Deventer JSJ. X-ray microtomography shows pore structure and tortuosity in alkali-activated binders. *Cem Concr Res* 2012; 42: 855–864.

Pu X. *Alkali Activated Slag Cements and Concretes*. Science Press, Beijing, 2010 (in Chinese).

Rovnanik P. Effect of curing temperature on the development of hard structure of metakaolin-based geopolymer. *Constr Build Mater* 2010; 24: 1176–1183.

Ueng T, Lyu S, Chu H, Lee H and Wang T. Adhesion at interface of geopolymer and cement mortar under compression: an experimental study. *Constr Build Mater* 2012; 35: 204–210.

Val DV and Stewart MG. Life-cycle cost analysis of reinforced concrete structures in marine environments. *Struct Saf* 2003; 25: 343–362.

Vasconcelos E, Fernandes S, de Aguiar B and Pacheco-Torgal F. Concrete retrofitting using CFRP and geopolymer mortars. *Mater Sci Forum* 2013; 730–732: 427–432.

Zhang Z, Yao X, Zhu H and Chen Y. Role of water in the synthesis of calcined kaolin-based geopolymer. *Appl Clay Sci* 2009; 43: 218–223.

Zhang Z, Yao X and Zhu H. Potential application of geopolymers as protection coatings for marine concrete I. Basic properties. *Appl Clay Sci* 2010a; 49: 1–6.

Zhang Z, Yao X and Zhu H. Potential application of geopolymers as protection coatings for marine concrete II. Microstructure and anticorrosion mechanism. *Appl Clay Sci* 2010b; 49: 7–12.

Zhang Z, Yao X and Wang H. Potential application of geopolymers as protection coatings for marine concrete III. Field experiment. *Appl Clay Sci* 2012; 67–68: 57–60.

Zhang Z, Wang H, Zhu Y, Reid A, Provis JL and Bullen F. Effects of fly ash on reaction process and microstructure of metakaolin-based geopolymer. *Appl Clay Sci* 2014; 88–89: 194–201.

Zhu H and Yao X. Effect of retarder on reaction process of metakaolin-slag-based geopolymer. *J Theor Appl Inform Techn* 2013; 48(3): 1384–1390.

Zhu H, Zhang Z, Deng F and Cao Y. The effects of phase changes on the bonding property of geopolymer to hydrated cement. *Constr Build Mater* 2013; 48: 124–130.

Performance of alkali-activated mortars for the repair and strengthening of OPC concrete

23

F. Pacheco-Torgal[1], J. Barroso de Aguiar[1], Y. Ding[2], W. Tahri[3], S. Baklouti[3]
[1]University of Minho, Guimarães, Portugal; [2]Dalian University of Technology, Dalian, China; [3]University of Sfax, Sfax, Tunisia

23.1 Introduction

Worldwide infrastructure rehabilitation costs are staggering. For example in the United States the needs are estimated to be over 1.6 trillion dollars over the next five years, where about 27% of all highway bridges are in need of repair or replacement, and the corrosion deterioration cost due to deicing and sea salt effects is estimated at over 150 billion dollars (Davalos, 2012). In the European Union nearly 84,000 reinforced and prestressed concrete bridges require maintenance, repair and strengthening with an annual budget of £215 million, and that estimate does not include traffic management costs (Yan and Chouw, 2012). In the US alone the costs in wasted fuel and lost time due to traffic congestion are as much as 50 billion dollars (Schlangen and Sangadji, 2013). However, others mention a much higher cost, as much as 100 billion dollars (Report, 2012). Many of the degraded concrete structures were built decades ago when little attention was given to durability issues (Hollaway, 2011). The importance of durability in the context of eco-efficiency of construction and building materials has been rightly put by Mora (2007), when he stated that increasing concrete durability from 50 to 500 years would mean a reduction in its environmental impact by a factor of 10. Materials with low durability require frequent maintenance and conservation operations or even its integral replacement, being associated with the consumption of raw materials and energy. The 'Law of Fives' cited by Delatte (2009) states that $1 spent on design and construction is equivalent to $5 spent as damage initiates and before it propagates, $25 once deterioration has begun to propagate, and $125 after extensive damage has occurred. This concept highlights the importance of acting as sooner as possible to prevent concrete structures from reaching that level when extensive damage has occurred and the rehabilitation costs grow exponentially. In that context, to assess if current repair materials are effective in addressing concrete infrastructure rehabilitation needs is of paramount importance. Very few studies in the alkali-activated field have addressed the rehabilitation of deteriorated concrete structures. One possible explanation for the aforementioned gap relates to the fact that most alkali-activated research groups belong to the field of materials science and not to the field of civil engineering. This shows the importance of a review paper that could highlight the importance of this area.

Handbook of Alkali-activated Cements, Mortars and Concretes. http://dx.doi.org/10.1533/9781782422884.4.627

23.2 Concrete patch repair

The patch repair method is widely used to restore the original conditions of concrete structures (Emmons and Vaysburd, 1994, 1996). In order to ensure the structural compatibility, Morgan (1996) states that repair mortar must meet the requirements defined in Table 23.1.

Figure 23.1 shows the disadvantages related to the use of composite materials with different modulus of elasticity. Still according to Morgan (1996), the repair mortars must comply with several requirements in order to ensure the compatibility with the concrete substrate (Figure 23.2).

Table 23.1 Structural compatibility – general requirements for repair mortars

Properties	Relation between the repair mortar (Rp) and the concrete substrate (Cs)
Strength in compression, tension and flexure	Rp ≥ Cs
Modulus in compression, tension and flexure	Rp ~ Cs
Poisson's ratio	Dependent on modulus and type of repair
Coefficient of thermal expansion	Rp ~ Cs
Adhesion in tension and in shear	Rp ≥ Cs
Curing and long-term shrinkage	Rp ≥ Cs
Strain capacity	Rp ≥ Cs
Creep	Dependent on whether creep causes desirable or undesirable effects
Fatigue performance	Rp ≥ Cs

Source: Morgan, 1996, Copyright © 1996, with permission from Elsevier.

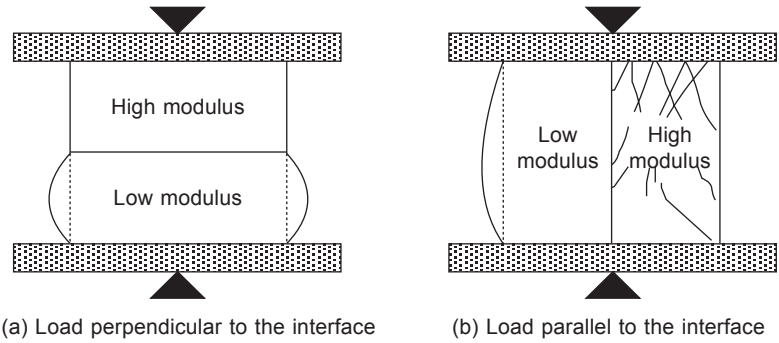

Figure 23.1 Mechanical behaviour of materials with different modulus of elasticity: (a) load perpendicular to the interface; (b) load parallel to the interface.

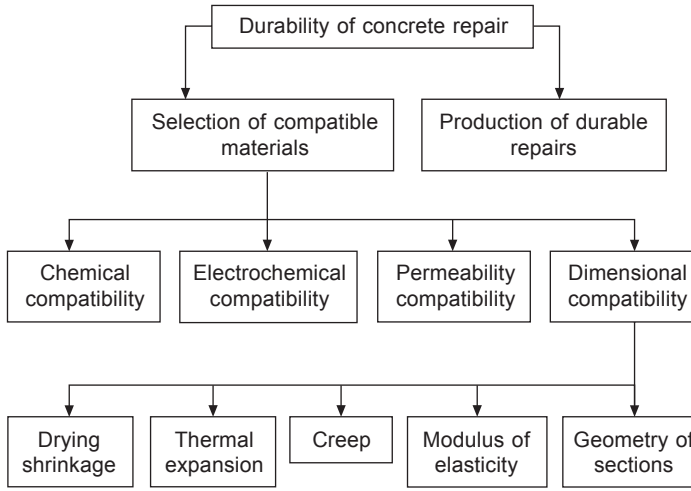

Figure 23.2 Factors that influence the durability of repair mortars (reprinted from Morgan, 1996, Copyright © 1996, with permission from Elsevier).

Several modes of repair failure were recently reported by Kristiawan (2012). The principal modes of repair failure were cracking (32%), debonding (25%), continued corrosion of embedded reinforcement (22%), alkali aggregate reaction (4%) and others (17%). Concerning cracking, which is the most important repair failure in most cases it could be due to restrained shrinkage (Pattnaik and Rangaraju, 2007). Figure 23.3 shows the cracking behaviour of repair mortars due to differential shrinkage between the reparation layer and the substrate concrete, which is a very heterogeneous and complex process.

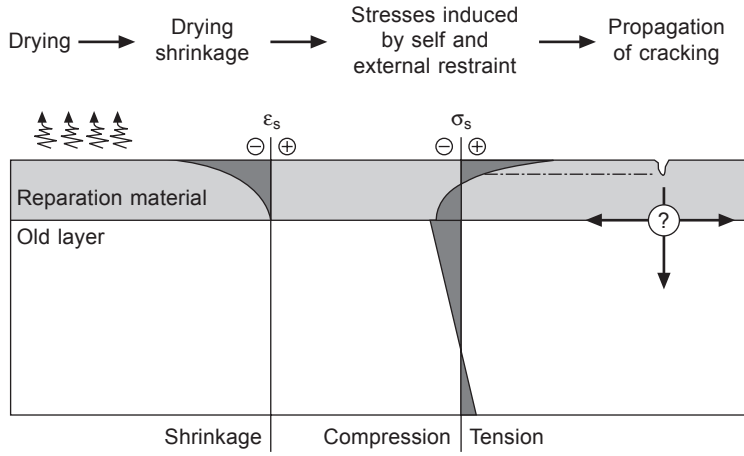

Figure 23.3 Development of cracking in a concrete reparation (reprinted from Sciumé *et al.*, 2013, Copyright © 2013, with permission from Elsevier).

ASTM C928 (2004) recommends that air shrinkage performance should not exceed 0.15% of the initial length. However, since cracking is also affected by creep and elastic modulus, a single shrinkage magnitude approach like the one previously mentioned in Table 23.1 is insufficient to prevent it. According to Kristiawan (2012) the most suitable way of reproducing the restraint of the patch repair system is by using the ring test. The ring test is commonly used to assess restrained shrinkage (Khan, 2013) and provides a useful qualitative comparison of the cracking performance of repair mortars (Beushausen and Chilwesa, 2013). This test is standardized by ASTM C1581 (2007) and its application encompasses the assessment of the time to first cracking, the number and the width of cracks. More information on the ring test can be found in the work by Hossain and Weiss (2006) who study restrained ring specimens tested using different geometries and boundary conditions. Mirza *et al*. (2014) analysed 40 different concrete repair mortars (15 cement-based, 11 polymer-modified cement-based, 14 epoxy-based) stating that freezing–heating cycle durability test is of paramount importance for the selection of the most suitable repair materials in severe climatic conditions, which means that thermal compatibility with the base concrete is also a very important parameter concerning the choice of repair mortars.

Rapid adhesion to the concrete substrate is a fundamental property of patch repair mortars, allowing the structure back into service. The adhesion in repair systems is a complex phenomenon resulting from a synergic effect of the surface roughness of concrete substrate, the presence of microcracks in the near-surface layer and deteriorated grains of aggregate as well as processing properties of repair materials, including interfacial tension between the bond coat and/or repair materials (Garbacz *et al*., 2005). The application of the patch repair mortar is therefore preceded by cleaning (with a wire brush) the concrete surface to remove pieces of degraded concrete. Moreover, as the roughness of the concrete substrate affects the performance of most patch repair mortars, it becomes necessary to artificially increase its roughness (most of the time using sand-blasting), regardless of the cleaning operation.

Most patch repair mortars fall into two categories, the mortars based on organic binders (epoxy resin or polyester) and those based on inorganic binders like Portland cement, which are available commercially as a pre-pack mixture of Portland cement, aggregates, silica fume, fibres and other additives. Cement-based repair mortars show improved adhesion when the surface of the concrete substrate was previously wetted. However, epoxy-based repair mortars show poor adhesion in moist surfaces. Murray (2009) mentioned that latex-modified patch repair mortars are used widely and successfully. However, the latter are more cost effective and less toxic. According to Pacheco-Torgal *et al*. (2012) the toxicity of building materials is a crucial issue under the recently approved Regulation (EU) 305/2011 related to the Construction Products Regulation (CPR) which has been in effect since 1 July 2013.

Recent investigations in the field of alkali-activated binders reveal a third category of mortars with high potential to be used in the field of concrete patch repair (Pacheco-Torgal *et al*., 2007, 2008). Since the adhesion to the concrete substrate is a crucial property of the repair mortars, some results related to the comparison between alkali-activated mortars and commercial products for the repair of concrete

structures are presented. The adhesion strength was evaluated using the slant shear test. The slant shear test uses square prisms made of two halves, one of the concrete substrate and one of the repair material, tested under axial compression. The adopted geometry for the slant shear specimens was a $50 \times 50 \times 125$ mm^3 prism with an interface line at 30º to the vertical. Bond strength was calculated by dividing the maximum load at failure by the bond area and was obtained from an average of four specimens determined at the ages of 1, 3, 7 and 28 days of curing. In order to increase the specific surface of the concrete substrate an etching procedure was carried out. The concrete surface was immersed in a 5% hydrochloric acid solution for 5 min and then carefully washed to ensure the removal of $CaCl_2$ which results from the reaction between HCl and $Ca(OH)_2$. The specimens were named after the repair materials and concrete substrate surface treatments. Specimens using concrete substrate repaired with commercial product R1 with and with no surface treatment were named respectively, R1-ES (etched surface) and R1-NTS (no treatment surface). Similarly, when the alkali-activated based binder was used to bond the two halves they were named GP-ES and GP-NTS, respectively. Slant specimens with substrate surface treatment as cast against metallic formwork, and as cast against wood formwork were also used with alkali-activated binder and were named GP-MF and GP-WF, respectively. The results of the effect of the several repair solutions on average adhesion strength are shown in Figure 23.4.

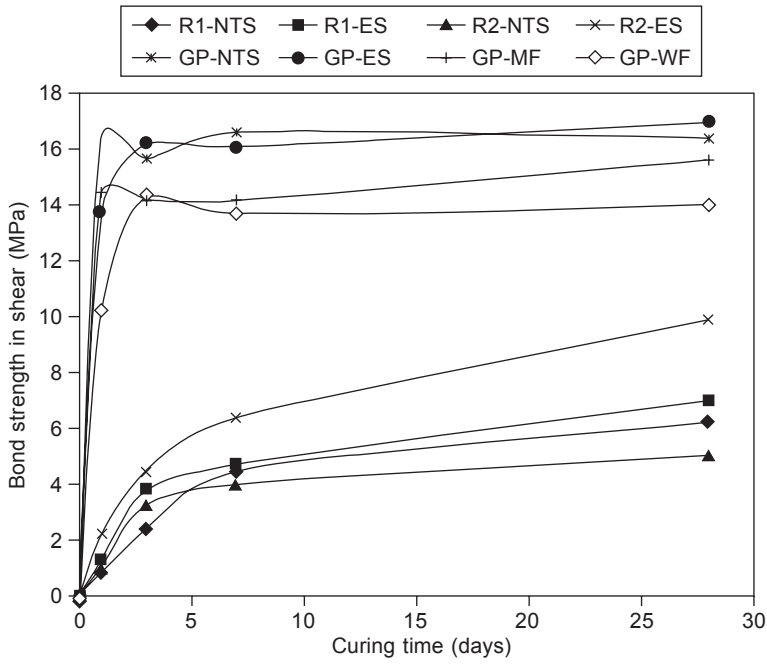

Figure 23.4 Adhesion strength using the 'slant-shear' test (reprinted from Pacheco-Torgal *et al.*, 2008, Copyright © 2008, with permission from Elsevier).

It can be seen that the specimens repaired with the alkali-activated mortar present high adhesion strengths even at early ages. Specimens repaired with alkali-activated mortar with 1 day curing have higher bond strength than specimens repaired with current commercial products after 28 days curing. Specimens repaired with the alkali-activated mortar appear to be influenced not by the chemical treatment in sawn concrete surface substrates, but by the use of concrete surfaces as cast against formwork. Those kinds of surfaces are rich in calcium hydroxide but lack exposed coarse aggregates which could contribute to improve bond strength due to silica dissolution from the aggregate surface. The strength performance of commercial repair products is very dependent on curing time and this constitutes a serious setback when early bond strength is required. The results show that bond strength using repair product R2 is clearly influenced by the surface treatment. Even if the current commercial repair materials had the same mechanical performance as the alkali-activated binder, the cost of the cheapest one (R1) is still 6.9 times higher than the alkali-activated binder.

When comparing the cost to bond strength ratio, the differences are even higher, with the cost of the cheapest solution with current commercial repair products (R1-ES) being 13.8 times higher than the alkali-activated repair mortar (see Figure 23.5). Still the assessment of the overall performance of the new mortars concerning structural compatibility and durability is yet to be fully investigated.

Other authors (Tahri *et al.*, 2013) studied the development of alkali-activated repair mortars based on calcined Tunisian clays, reporting a very low modulus of elasticity and an excessive unrestrained shrinkage. Further studies (Tahri *et al.*, 2014) show that an acceptable unrestrained shrinkage can be obtained (Figure 23.6) when calcined Tunisian clays are partially replaced by fly ash or metakaolin and most importantly when the alkali-activator/binder mass ratio is reduced to 80% of the initial ratio.

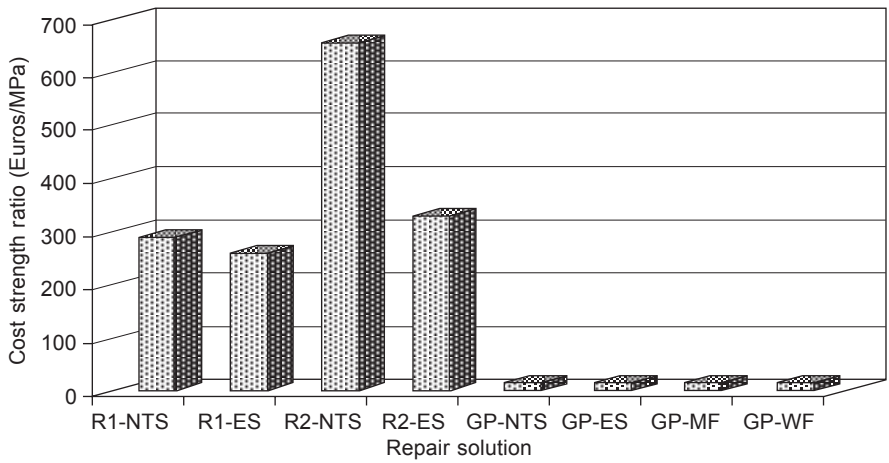

Figure 23.5 Cost-to-strength ratio after 28 days curing according to repair solution (reprinted from Pacheco-Torgal *et al.*, 2008, Copyright © 2008, with permission from Elsevier).

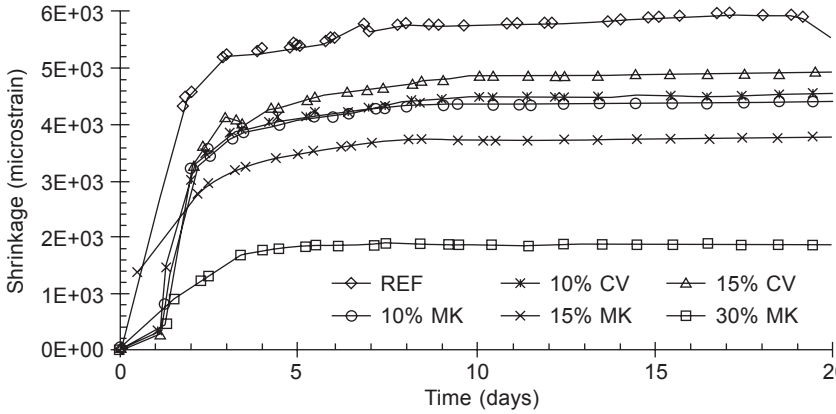

Figure 23.6 Unrestrained shrinkage as a function of curing time (Tahri *et al.*, 2014).

23.3 Strengthening concrete structures using fibre sheets

Different techniques can be used in strengthening of concrete structures. The most common are strengthening with fibre reinforced polymer (FRP) developed first in Japan (Fukuyama and Sugano, 2000; ACI, 2000; Badanoiu and Holmgren, 2003) and the increase of element sections with new concrete (ACI, 1997). The bond between the concretes, steel and FRP is usually made with epoxy adhesives. An important property of the epoxy adhesives is the glass transition temperature (T_g). It is the temperature above which polymers change from relatively hard and elastic to viscous, rubbery-like behaviour. Due to this, some recommendations have suggested that epoxy resins should not be used at temperatures above their T_g and further that the selected materials should have a T_g of at least 20°C above the maximum expected service temperature. According to Gamage *et al.* (2006) both experimental results and finite element calculations show that epoxy adhesives should not be exposed at temperatures above 70°C in order to maintain the integrity of the strengthened elements. Past investigations (Aguiar *et al.*, 2008) confirm that epoxy adhesives exhibit poor behaviour when subjected to increased temperatures, causing important bond deterioration. Epoxy resins also have low resistance to ultraviolet radiation (Bijen, 2000). This means that adhesive materials like alkali-activated binders known to possess high stability at high temperature, could be an alternative to epoxy resins. Balaguru *et al.* (2008) showed that concrete samples coated with carbon reinforced alkali-activated binder did not degrade even after 100 cycles of wetting and drying.

Probably the first experimental results related to the strengthening of concrete structures with alkali-activated binders were those published by Kurz *et al.* (1999). Those authors tested several OPC concrete beams reinforced by several carbon fabric layers reporting a 50% increase in the failure load. Unfortunately, absolutely no details on the composition of the alkali-activated binders were provided by the

authors. The only relevant details concern the use of heat cure at 80°C and the use of 94.8 kPa vacuum to enhance the adhesion.

Further details are disclosed in two US patents by Davidovits *et al.* (1998) and by Davidovits (1999). Accordingly the geopolymeric resin has the following composition: $yM_2O:Al_2O_3:xSiO_2$, where 'x' is 6.5–70, 'y' is 0.95–9.5 and M is Na, K or Na+K. The geopolymeric matrix uses silicious nanospheres with diameter less than 1 micron, preferably less than 500 nm and an alkaline poly(aluminosilicate) with the total formula of $M_4Si_2AlO_{10}$ to $M_2Si_4AlO_{16}$. The beams used a 43 MPa compressive strength concrete and the geopolymeric resin had a 15 MPa tensile strength. The bottom surface of the beams was roughened by grinding followed by sand blasting in order to remove the mortar layer. After preparation the resin was allowed to stand for 1–2 h before being used for the impregnation of carbon fabrics. The beams were primed with resin to avoid resin migration from fabric to concrete. After fabric placement the beams were allowed to dry for 24 h and heated to 80ºC (radiant heating) to cure the resin for 24 h (Davidovits, 1999).

Vasconcelos *et al.* (2011) studied the adhesion strength between CFRP sheets and metakaolin-based alkali-activated binders (Figures 23.7 and 23.8), reporting a much lower mechanical performance for alkali-activated binders when compared to the epoxy resin (Figure 23.9). The repair binders were a mixture of aggregates (three sand/binder mass ratio of 30%, 60% and 90%), metakaolin, calcium hydroxide and alkaline silicate solution. An activator with sodium hydroxide (14 M) and sodium silicate solution (Na_2O = 13.5%, SiO_2 = 58.7%, and water = 45.2%) was used with a mass ratio of 1:2.5. The authors mention that the low mechanical performance could be due to the fact that the CFRP sheet type was not prone to this kind of application.

Of course the results cannot be compared with the ones reported by Kurz *et al.* (1999) because of the absence of vacuum pressure. One may also add that the absence of heat curing could contribute to explaining the low mechanical performance of the beams strengthened with carbon fibres and alkali-activated metakaolin. It is well known that curing at elevated temperature has a remarkable influence on the setting and hardening of alkali-activated metakaolin. For a temperature of 10ºC Rovnanik (2010) reported a 4-day setting delay. More recent investigations confirm the importance of curing at elevated temperature to obtain a rapid setting and a high compressive strength (Muniz-Villarreal *et al.*, 2013; Lancellotti *et al.*, 2013). However, it is important to mention that Vasconcelos *et al.* (2011) decided not to use heating curing because it is a procedure that can hardly be replicated on *in-situ* conditions. Instead they used an alkali-activated mixture with a small amount of calcium hydroxide which is known to enhance the early mechanical strength of these materials (Yip *et al.*, 2005, 2008).

The low adhesion between alkali-activated mortars and carbon fibre reinforcement was also reported by other authors (Menna *et al.*, 2013). Those authors compared the flexural performance of 25 MPa reinforced concrete beams strengthened with high strength steel cord and carbon fibre (Figure 23.10) by using a metakaolin alkali-activated resin with a 98 MPa compressive strength after 28 days curing. No information on the tensile strength of the resin was provided. The solution

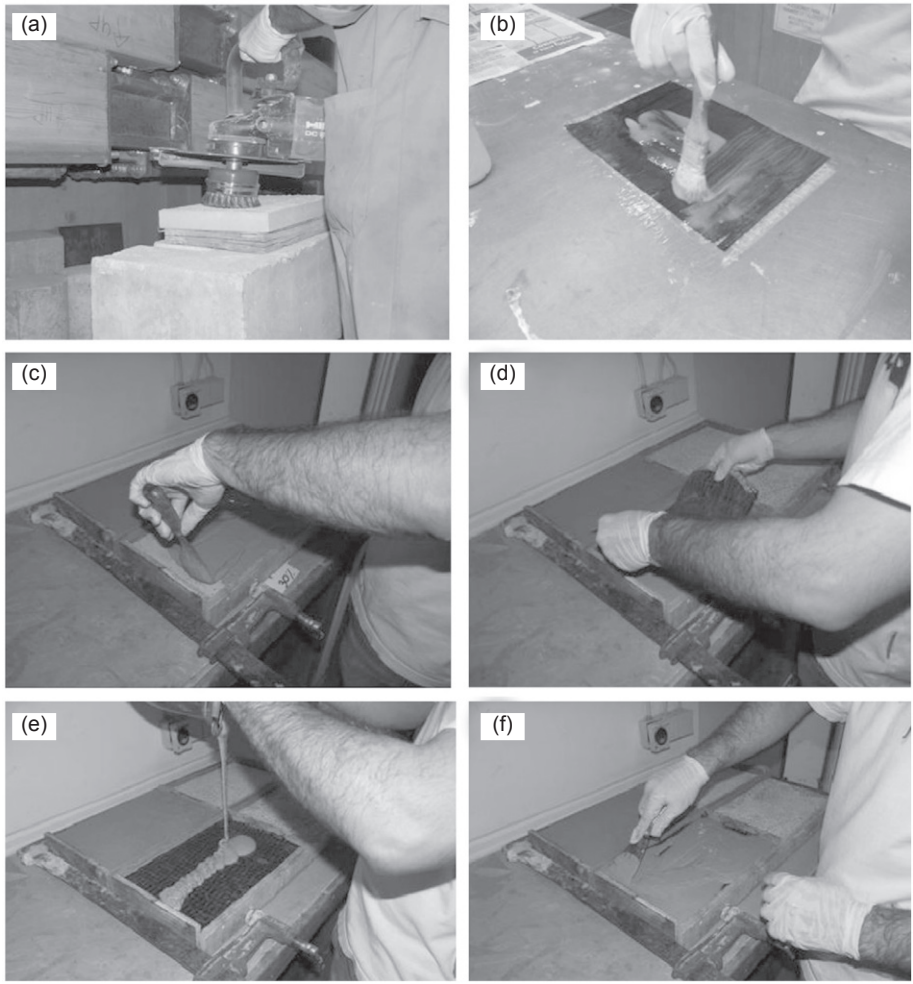

Figure 23.7 OPC concrete (20 MPa) slab preparation: (a) surface roughening; (b) CFRP sheet impregnation; (c) applying the alkali-activated mortar; (d) placing the CFRP sheet; (e and f) applying a second layer of alkali-activated mortar. (reprinted from Vasconcelos *et al*., 2011, Copyright © 2011, with permission from Elsevier).

composition was $Na_2O.1.34SiO_2.10.5H_2O$ while the whole resin matrix was $Na(SiO_2)_{1.40}AlO_25.2H_2O$. Instead of coarse aggregates, Menna *et al*. (2013) used a pure quartz powder (maximum particle diameter 63 μm) with the same weight as metakaolin. The several layers used to attach the steel reinforcement to the concrete beams are shown in Figure 23.11. First a fluid alkali-activated resin without quartz filler was applied to the beam. Only then was the first resin layer placed, followed by the steel fibre and by a second alkali-activated resin layer. Finally a PVC layer was used to avoid water evaporation. The flexural results show that steel fibres were

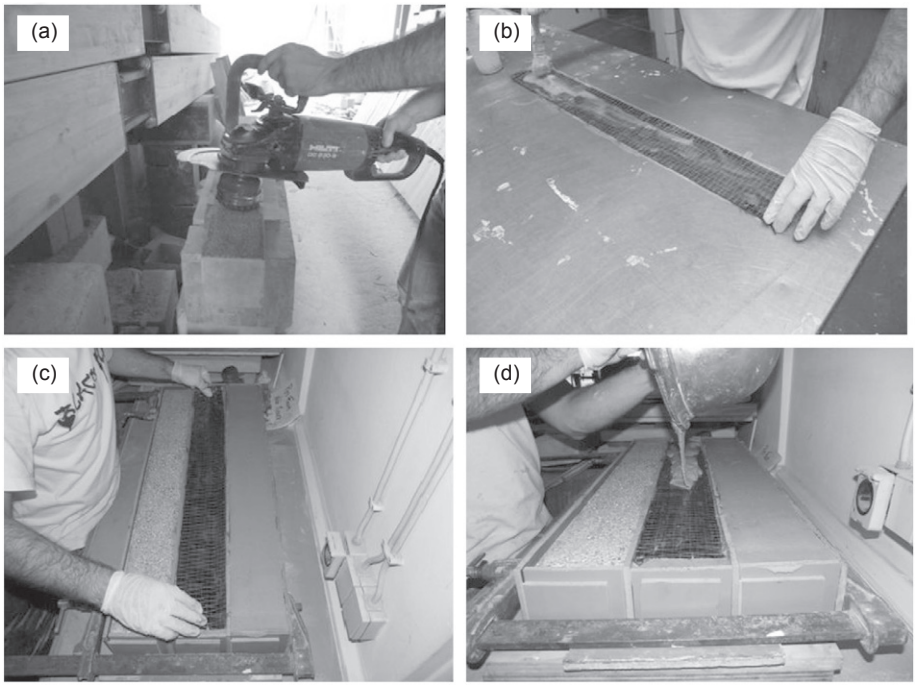

Figure 23.8 OPC concrete (20 MPa) beam preparation: (a) surface roughening; (b) CFRP sheet impregnation; (c) placing the CFRP sheet over the alkali-activated mortar; (d) applying a second layer of alkali-activated mortar (reprinted from Vasconcelos *et al*., 2011, Copyright © 2011, with permission from Elsevier).

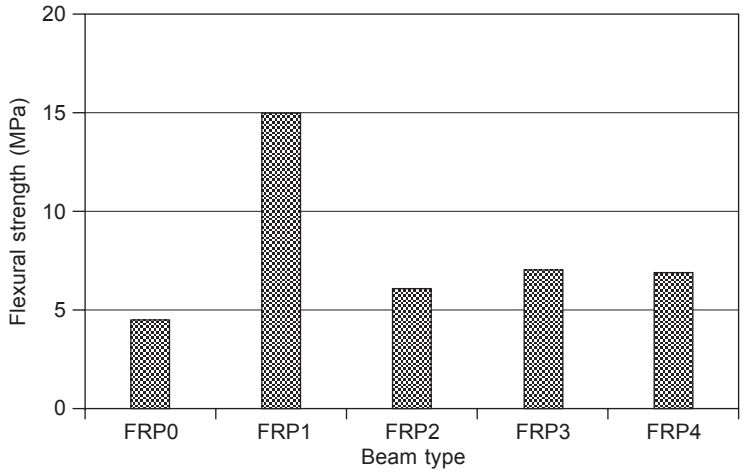

Figure 23.9 Flexural strength of OPC concrete beams reinforced with epoxy resin (FRP1) and with an alkali-activated binder (FRP2, FRP3, FRP4) (reprinted from Vasconcelos *et al*., 2011, Copyright © 2011, with permission from Elsevier).

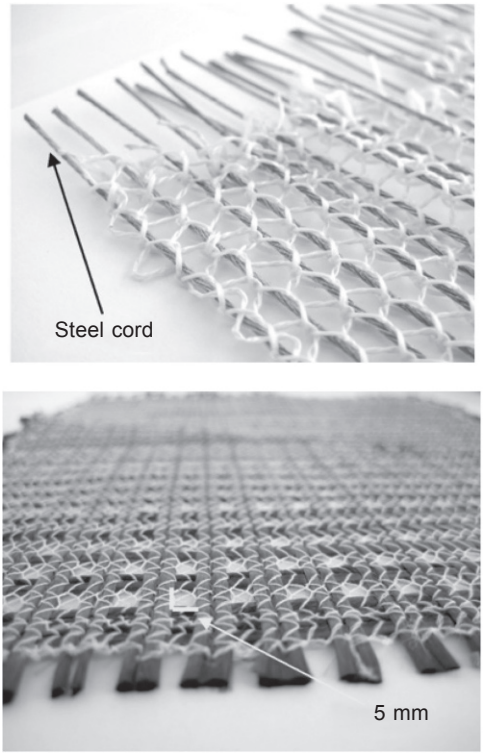

Figure 23.10 Top: steel reinforcement; bottom: carbon fibre reinforcement (reprinted from Menna *et al*., 2013, Copyright © 2013, with permission from Elsevier).

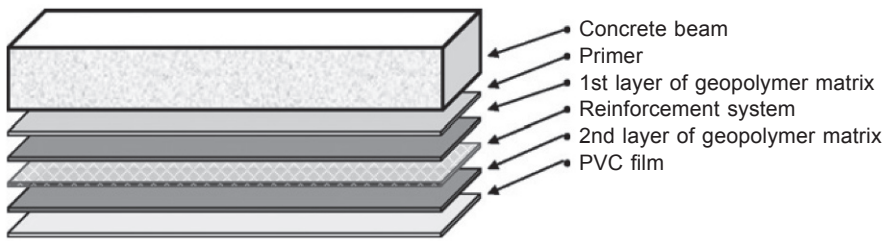

Figure 23.11 System layers (reprinted from Menna *et al*., 2013, Copyright © 2013, with permission from Elsevier).

able to increase the ultimate load capacity of the beams by about 100%. The beams reinforced with carbon fibres showed a load capacity not very different from the reference beam, thus meaning that the carbon fibres were useless.

SEM analysis (Figure 23.12) showed that the steel fibre is completely covered by the alkali-activated matrix, proving a strong interfacial interaction. It also shows a lack of impregnation of the carbon fibres, which explains the lower mechanical performance of the beams strengthened with those fibres. Still Menna *et al*. (2013)

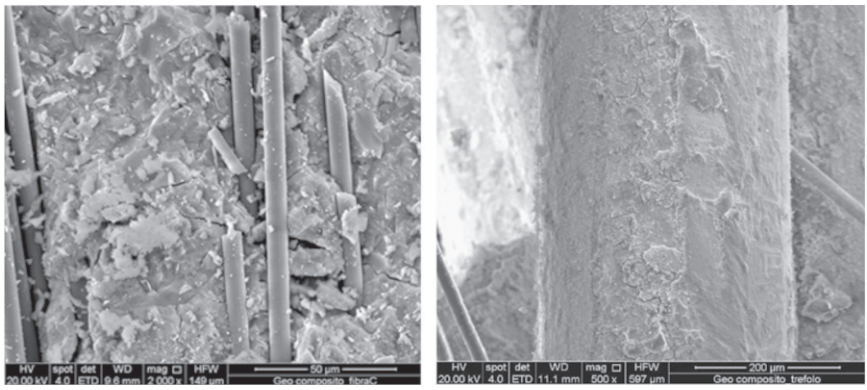

(a) (b)

Figure 23.12 SEM micrographs of a sample of fibre reinforced alkali-activated mortars taken after the flexural strength test: (a) carbon system and (b) steel cord system. (reprinted from Menna *et al.*, 2013, Copyright © 2013, with permission from Elsevier).

mentioned that a different carbon fibre sizing could have a better adhesion to the alkali-activated binders. Still it is yet to be explained why Davidovits reported such high performance when using carbon fabrics. Once again the heat curing hypothesis merits further study.

Despite the high flexural performance of concrete beams reinforced with steel fibre and metakaolin alkali-activated mortar, this parameter is insufficient to allow for conclusive statements on the overall repair and strengthening performance of that mortar mixture. Therefore, further tests regarding compatibility and durability issues (as per Table 23.1 and Figure 23.1) must be carried out in order to validate these repairing solutions.

23.4 Conclusions and future trends

Worldwide infrastructure rehabilitation costs are staggering. Since the majority of the existing infrastructure is concrete based, this means that concrete infrastructure rehabilitation is a hot issue to be dealt with. The patch repair method is widely used to restore the original conditions of the concrete structures. Most patch repair mortars fall into two categories, the mortars based on organic binders or those based on inorganic binders like Portland cement. The former allow for a rapid repair and have no shrinkage problems, while the latter are more cost effective and less toxic. Alkali-activated repair mortars seem to be even more cost effective and due to their stability at high temperature, they can be an alternative to epoxy resins for structural retrofitting using FRP. They can also be used as low toxicity, cost-efficient lining materials for trenchless rehabilitation of concrete sewage pipelines. However, new and future investigations are needed related to their use in the field of concrete

infrastructure rehabilitation. Investigations regarding compatibility and durability issues especbially concerning the assessment of restrained shrinkage, must be carried out in order to validate AA mortars as an effective repairing solution.

References

American Concrete Institute ACI (1997) Guide for application of epoxy adhesives for bonding freshly mixed and hardened concretes, ACI Committee 503. Farmington Hills, MI.

American Concrete Institute (ACI) (2000) Guide for design and construction of externally bonded FRP systems for strengthening concrete structures, ACI Committee 440. Farmington Hills, MI.

Aguiar, J., Camões A. and Vaz, N. (2008) Effect of temperature on RC elements strengthened with CFRP, *Materials and Structures*, 41, 1133–1142.

ASTM C928 (2004) Standard Specification for Packaged, Dry, Rapid-Hardening Cementitious Materials for Concrete Repairs. Annual Book of ASTM Standards, Philadelphia, PA.

ASTM C1581 (2007) Standard test method for determining age at cracking and induced tensile stress characteristics of mortar and concrete under restrained shrinkage. Annual Book of ASTM Standards, Philadelphia, AA.

Badanoiu, A. and Holmgren, J. (2003) Cementitious composites reinforced with continuous carbon fibres for strengthening of concrete structures. *Cement & Concrete Composites*, 25, 387–394.

Balaguru, P., Nazier, M. and Arafa, M. (2008) Field implementation of geopolymer coatings. Center for Advanced Infrastructure and Transportation (CAIT). Civil and Environmental Engineering, Rutgers State University, Piscataway, NJ.

Beushausen, H. and Chilwesa, M. (2013) Assessment and prediction of drying shrinkage in bonded mortar overlays. *Cement and Concrete Research* 53, 256–266.

Bijen, J. (2000) *Durability of Engineering Structures: Design, Repair and Maintenance*. Woodhead Publishing Limited, Cambridge

Davalos, J.F. (2012) Advanced materials for civil infrastructure rehabilitation and protection. Seminar at The City College of New York, New York.

Davidovits, J. (1999) Method for bonding fiber reinforcement on concrete and steel structures and resultant products. US Patent 5,925,449.

Davidovits, J., Davidovics, M. and Davidovits, N. (1998) Alkaline alumino-silicate geopolymeric matrix for composite materials with fiber reinforcement and method for obtaining same. US Patent 5,798,307.

Delatte, N. (2009) Introduction. In Delatte, N. (ed.), *Failure, Distress and Repair of Concrete Structure*, Woodhead Publishing Limited, Cambridge.

Emmons, P. and Vaysburd, A. (1994) Factors affecting the durability of concrete repair: the contractor's viewpoint. *Construction and Building Materials*, 8, 5–16.

Emmons, P. and Vaysburd, A. (1996) Total system concept – necessary for improving the performance of repaired structures. *Construction and Building Materials*, 10, 69–75.

Fukuyama, H. and Sugano, S. (2000) Japanese seismic rehabilitation of concrete building after the Hyogoken Nanbu earthquake. *Cement Concrete Composites*, 22(1), 59–79.

Gamage, J., Al-Mahaidi, R. and Wong, M. (2006) Bond characteristics of CFRP plated concrete members under elevated temperatures. *Compos Struct*, 75, 199–205.

Garbacz, A., Gorka, M. and Courard, L. (2005) Effect of concrete treatment on adhesions in repair systems. *Magazine of Concrete Research*, 57, 49–60.

Hollaway, L.C. (2011) Key issues in the use of fibre reinforced polymer (FRP) composites in the rehabilitation and retrofitting of concrete structure. In Karbhari, V.M. and Lee, L.S. (eds), *Service Life Estimation and Extension of Civil Engineering Structures*. Woodhead Publishing Limited, Cambridge.

Hossain, A. and Weiss, J. (2006) The role of specimen geometry and boundary conditions on stress development and cracking in the restrained ring test. *Cement and Concrete Research*, 36, 189–199.

Khan, M. (2013) Ring test for the measurement of restrained shrinkage of concrete. *Applied Mechanics and Materials*, 377, 86–91.

Kristiawan, S. (2012) Evaluation of models for estimating shrinkage stress in patch repair system. *International Journal of Concrete Structures and Materials*, 6(4), 221–230.

Kurz, S., Balaguru, P., Lyon, R. and Davidovits, J. (1999) Geopolymer composites layers for strengthening concrete structures. *1999 Géopolymère Conference Proceedings*, 173–180. Saint-Quentin.

Lancellotti, I., Catauro, M., Ponzoni, C., Bollino, F. and Leonelli, C. (2013) Inorganic polymers from alkali activation of metakaolin: effect of setting and curing on structure. *Journal of Solid State Chemestry*, 200, 341–348.

Menna, C., Asprone, D., Ferone, C., Colangelo, F., Balsamo, A., Prota, A., Cioffi, R. and Manfredi, G. (2013) Use of geopolymers for composite external reinforcement of RC members. *Composites: Part B*, 45, 1667–1676.

Mirza, J., Durand, B., Bhutta, A. and Tahir, M. (2014) Preferred test methods to select suitable surface repair materials in severe climates. *Construction and Building Materials*, 50, 692–698.

Mora, E. (2007) Life cycle, sustainability and the transcendent quality of building materials. *Building and Environment*, 42, 1329–1334.

Morgan, D. (1996) Compatibility of concrete repair materials and systems. *Construction and Building Materials*, 10, 57–67.

Muniz-Villarreal, M., Manzano-Ramirez, A., Sampieri-Bulbarela, S., Gasca-Tirado, J., Reyes-Araiza, J., Rubio-Avalos, J., Perez-Bueno, J., Apatiga, L., Zaldivar-Cadena, A. and Amigo-Borras, V. (2013) The effect of temperature on the geopolymerization process of a metakaolin-based geopolymer. *Materials Letters*, 65, 995–998.

Murray, M. (2009) Patching of deteriorated concrete structures. In Delatte, N. (ed.), *Failure, Distress and Repair of Concrete Structure*, Woodhead Publishing Limited, Cambridge, 282–295.

Pacheco-Torgal, F., Gomes, J. and Jalali, S. (2007) Investigations about the effect of aggregates on strength and microstructure of geopolymeric mine waste mud binders. *Cement and Concrete Research*, 37, 933–941.

Pacheco-Torgal, F., Gomes, J. and Jalali, S. (2008) Adhesion characterization of tungsten mine waste geopolymeric binder: influence of OPC concrete substrate surface treatment. *Construction and Building Materials*, 22, 154–161.

Pacheco-Torgal, F., Jalali, S. and Fucic, A. (2012) *Toxicity of Building Materials*. Woodhead Publishing Limited, Cambridge.

Pattnaik, R. and Rangaraju, P. (2007) Analysis of compatibility between repair material and substrate concrete using simple beam with third point loading. *Journal of Materials in Civil Engineering*, 19(12), 1060–1069.

Report (2012) A new economic analysis of infrastructure investment. Prepared by the Department of the Treasury with the Council of Economic Advisers. http://www.treasury.gov/resource-center/economic-policy/Documents/20120323InfrastructureReport.pdf

Rovnanik, P. (2010) Effect of curing temperature on the development of hard structure of metakaolin-based geopolymer. *Construction and Building Materials*, 24, 1176–1183.

Schlangen, E. and Sangadji, S. (2013) Adressing infrastructure durability and sustainability by self healing mechanisms and recent advances in self healing concrete and asphalt. *Procedia Engineering*, 54, 39–57.

Sciumé, G., Benboudjema, F., de Sa, C., Pesavento, Y., Berthaud, B. and Schrefler, B. (2013) A multiphysics model for concrete at early age applied to repairs problems. *Engineering Structures*, 57, 374–387.

Tahri, W., Samet, B., Pacheco-Torgal, F., Barroso de Aguiar, J., Jesus, C. and Baklouti, S. (2013) Shrinkage and mechanical performance of geopolymeric mortars based on Tunisian clay. *Chemistry and Materials Research*, Vol. 4, Special Issue for International Congress on Materials & Structural Stability, Rabat, Morocco, 27–30 November.

Tahri, W., Samet, B., Pacheco-Torgal, F., Barroso de Aguiar, J., Jesus, C. and Baklouti, S. (2014) Shrinkage and mechanical performance of geopolymeric mortars based on Tunisian clay. International Conference on Construction Materials and Structures (ICCMATS), South Africa.

Vasconcelos, E., Fernandes, D., Barroso de Aguiar, J.L. and Pacheco-Torgal, F. (2011) Concrete retrofitting using metakaolin geopolymers mortars and CFRP. *Construction and Building Materials*, 25, 3213–3221.

Yan, L. and Chouw, N. (2012) Behavior and analytical modeling of natural flax fibre reinforced polymer tube confined plain concrete and coir fibre reinforced concrete. *Journal of Composite Materials*, 47, 2133–2148.

Yip, C., Lukey, G. and van Deventer, J. (2005) The coexistence of geopolymeric gel and calcium silicate hydrate at the early stage of alkaline activation. *Cement and Concrete Research*, 35, 1688–1697.

Yip, C., Lukey, G., Provis, J. and van Deventer, J. (2008) Effect of calcium source on geopolymerization. *Cement and Concrete Research*, 38, 554–564.

This page intentionally left blank

The properties and durability of alkali-activated masonry units

24

S. Ahmari[1], *L. Zhang*[2]
[1]Cornerstone Engineering Inc., Louisville, KY, USA; [2]University of Arizona, Tucson, AZ, USA

24.1 Introduction

Masonry units (MU) are a widely used construction and building material. Clay bricks and concrete blocks are two main types of MU. Since clay bricks are produced from clay with high temperature kiln firing and concrete from ordinary Portland cement (OPC) concrete, they both contain high embodied energy and have large carbon footprint. The growing concerns about the environmental impacts of MU production and global warming and the modern civilization's need for sustainable development have urged scientists and engineers to develop alternative construction and building materials. Production of MU from waste materials has been studied by researchers (Chou *et al*., 2006; Morchhale *et al*., 2006; Roy *et al*., 2007; Liu *et al*., 2011). These methods to produce MU from waste materials either require high temperature kiln firing or use cement as the binder (Ahmari and Zhang, 2012; Zhang, 2013). Geopolymerization is a relatively new technology, which eliminates the need for extremely high temperatures.

Geopolymers have proven to be one of the potential replacements for OPC and have superior advantages. It is believed that geopolymer cement was used to build the Egyptian pyramids by the ancient Egyptians. However, it was first classically established and systematically studied only in the early 1980s by Davidovits (1982, 1991). Subsequently, geopolymers were studied by a number of researchers to reveal their physical, chemical, and mechanical properties (Alonso and Palomo, 2001; Xu and van Deventer, 2003; Duxson *et al*., 2005, 2007; van Deventer *et al*., 2006; Pacheco-*Torgal et al*., 2008; Dimas *et al*., 2009; Rattanasak and Chindaprasirt, 2009). Geopolymers are inorganic binders produced from aluminosilicate-containing material such as fly ash (FA) and metakaolin (MK) in a highly alkaline solution, usually sodium hydroxide (NaOH) or sodium silicate (SS). After dissolution of SiO_2 and Al_2O_3 from solid aluminosilicate phase, silica and alumina oligomers are formed and then polycondensed to form a polymeric binder with an amorphous structure consisting of silica and alumina units. Depending on the ratio between Si and Al, three types of oligomers can be formed: polysialate (PS) (-Si-O-Al-O-), polysialate-siloxo (PSS) (Si-O-Al-O-Si-O), and polysialate-disiloxo (PSDS) (Si-O-Al-O-Si-O-Si-O); PSDS has the highest density and the lowest porosity.

The physical and mechanical properties of geopolymer binders can be tailored by adjusting the synthesis condition to meet the requirements of a specific application. The most important factors that determine the properties of geopolymers are reactivity

Handbook of Alkali-activated Cements, Mortars and Concretes. http://dx.doi.org/10.1533/9781782422884.4.643

of initial materials, Si/Al and Na/Al ratios, type and concentration of alkali activator, and curing condition. The amorphous phase of the source material is primarily responsible for the generation of geopolymeric binders, although the crystalline phase may also partially participate in the reaction. Therefore, highly amorphous materials such as MK and FA are known as the most reactive materials for geopolymerization. Polycondensation at low Si/Al ratios primarily occurs between silica and alumina monomers leading to formation of PS, while at higher Si/Al ratios condensation initially happens between silica monomers followed by further condensation with alumina monomers (Silva *et al*., 2007). This results in PSS or PSD, which possesses more rigid microstructure. The optimum Si/Al ratio is between 2 and 3. Alkaline solution has two major functions in the geopolymerization process: dissolution of silica and alumina monomers and the cation acting as a charge-balancing agent for alumina units. As each alumina tetrahedral requires one Na^+ to balance its charge, a Na/Al ratio of about 1 is optimal. Too high a Na/Al ratio (i.e., too high a NaOH concentration) might be helpful in dissolving more silica and alumina, especially in less reactive materials such as mine tailings (MT). However, the extra NaOH remains unreacted and after exposure to water dissolves and results in porous microstructure. SS is commonly used as the activator due to the availability of soluble silicate in the activator. The optimum SiO_2/Na_2O_3 ratio in the activating solution varies from 1.0 to 1.5 depending on the solid materials (Duxson *et al*., 2005; Guo *et al*., 2010; Ahmari *et al*., 2012b). Elevated curing temperature essentially favors dissolution of silica and alumina species and polycondensation. There is an optimum curing temperature above which the geopolymerization process is decelerated. The optimum curing temperature depends on the reactivity of source material and the NaOH concentration (Ahmari *et al*., 2012b). Generally, the optimum curing temperature is lower for more reactive source materials.

One of the potential applications of geopolymers is the production of geopolymer masonry units (GMU) from waste materials. This is of particular importance for low reactive materials since heating is not feasible for the production of concrete in the field, but GMU can be easily produced in a factory under controlled conditions.

24.2 Alkali activation of industrial wastes to produce masonry units

GMU, both bricks and compressed blocks, can be produced from different types of wastes such as FA, MT, blast furnace slag (FS), and red mud (RM). A number of researchers have studied the properties of GMU from different types of wastes (Freidin, 2007; Arioz *et al*., 2010; Ahmari and Zhang, 2012, 2013a, 2013b; Chen *et al*., 2012; Kumar and Kumar, 2013). The production of conventional bricks includes the following steps:

1. Quarrying of clay or shale.
2. Processing and screening of the quarried material.

3. Mixing with water, forming/extruding, and cutting into standard-sized blocks.
4. Drying at room temperature (or in sunshine) for one to two days.
5. Kiln firing where the dried blocks are heated at extremely high temperatures up to 1300°C.
6. Packing and transportation.

In the production of GMU, steps 1 and 5 are not required because waste material instead of natural quarried material is used and the geopolymerization process can be completed at significantly lower temperatures ranging from room temperature to slightly elevated temperatures such as 90°C, depending on the phase composition and reactivity of the material. Sustainability in terms of conserving natural source material due to utilization of waste material and lowering energy usage due to low temperature curing is a remarkable advantage of GMU.

24.2.1 Fly ash (FA)

FA is one of the major potential waste materials for production of GMU due to its amorphous structure and fine particle size which yield high reactivity for geopolymerization. The amorphous structure of FA is due to the thermal history it has experienced in the power plant. High temperatures and subsequent sudden cooling break down the crystalline structures of coal minerals and lead to a disorderly structure.

Freidin (2007) produced geopolymer blocks from Class F FA or a mixture of FA and bottom ash by using SS solution as the alkali activator. He investigated the effect of SS content, forming pressure and hydrophobic additive under different conditions. The results indicated that the GMU produced from FA and bottom ash met the requirements of Israeli Standard for conventional cement concrete blocks. He also investigated the enhancement of water stability of the FA-based GMU using different methods and concluded that short-term impregnation by a hydrophobic liquid of the siloxane group results in the most durable GMU blocks in water.

Arioz *et al*. (2010) investigated the production of GMU using Class F fly ash, SS, and NaOH solution. The bricks were produced at a 30 MPa forming pressure and cured at various temperatures for different hours in oven and steam. The compressive strength of the produced GMU varied between 5 and 60 MPa. They did not observe any noticeable difference between the specimens cured under oven-dry and steam curing conditions. The curing temperature and duration showed a significant effect on the compressive strength, especially in short durations but not on the density. They reported that to produce a GMU with 25 MPa compressive strength at 40°C, 6 h curing is required.

24.2.2 Mine tailings (MT)

MT are waste materials generated from mineral processing operations. MT are fine particles and mainly constitute silica and alumina minerals and thus are suitable

for geopolymerization. Their phase and chemical compositions are variable and dependent on the properties of the mother rock and the mineral processing operations they have undergone. In general, MT are mainly crystalline material and thus it is relatively difficult to produce geopolymer binder from them. Pacheco-Torgal *et al.* (2008, 2010) and Pacheco-Torgal and Jalali (2010) conducted an extensive study on production of geopolymer concrete from tungsten mine waste. In order to improve the reactivity of tungsten mine waste, they dehydroxylated the mine waste by heating at 960°C during which the -OH- group is liberated from the chemical bonds and the molecular structure is transformed into a disordered one.

Ahmari and Zhang (2012, 2013a, 2013b) investigated the production of GMU from copper MT. They prepared small size cylindrical specimens of MT-based geopolymer brick activated by NaOH and cured at 60–120°C. The specimens were formed at varying pressures from 0 to 25 MPa and initial moisture contents from 10 to 18%. They reported 90°C as the optimum temperature for NaOH-activated MT and initial moisture content and forming pressure as the most important factors that affect the physical and mechanical properties of the MT-based GMU. The produced MT-based GMU produced met or exceeded the ASTM criteria for different applications of GMU. However, Ahmari and Zhang (2013b) reported substantial strength loss of MT-based GMU in water and nitric acid at pH 4. The durability of the MT-based GMU was enhanced by adding a small amount of cement kiln dust (CKD) (Ahmari and Zhang, 2013a). The physical and mechanical properties of MT-based GMU can also be enhanced by adding FS. Addition of other types of waste material to MT creates a hybrid geopolymer system, which can effectively improve the physical and mechanical properties and durability of MT-based GMU.

24.2.3 Furnace Slag (FS)

FS is another by-product of mining operations which results from the smelting or fire refining processes. It has been used as partial replacement for OPC, asphalt concrete aggregates, and construction bricks (Mobasher *et al.*, 1996; Kirillidi and Frogoudakis, 2005; Asmatulaev *et al.*, 2008; Arabani and Azarhoosh, 2012). FS can be used alone or mixed with other wastes such as MT to produce GMU. Studies in the authors' laboratory indicates that pure MT-based GMU specimens exhibit an unconfined compressive strength (UCS) of approximately 25 MPa while pure FS-based GMU specimens show a UCS of about 75 MPa. This indicates the high reactivity of FS with respect to MT. Therefore, FS can be added to MT to enhance the properties of MT-based GMU. Kim and Kim (2012) studied the production of geopolymer binder from a mixture of FA and FS and noted that the compressive strength of the binder increases with higher FS content.

Production of GMU based on a combination of FA and FS was studied by Mathew *et al.* (2013). A mixture of NaOH and SS was used as alkaline solution. Small cubic specimens were prepared by compaction at 13% water content and cured at ambient temperature for 28 days. Compressive strength up to approximately 5.0 MPa was reported. Radhakrishna *et al.* (2008) also studied GMU based on a combination of

FA and FS. NaOH and SS were used as alkali activator and water content was varied between 15 and 25%. Specimens were cured both at room temperature and 60°C. It was noted that with the increase in water content from 15% to 25%, the compressive strength decreased. They reported that the quality of FA, binder-to-aggregate ratio, molarity of the activator solution, fine aggregate type, and curing conditions are the important factors affecting the strength development in the geopolymer compressed blocks. Most FS contains substantial amount of calcium that can have an improving effect on the physical and mechanical properties of GMU due to the enhancement of geopolymerization and creation of C-S-H gel.

24.2.4 Metakaolin (MK)

MK is known as the most reactive material for the geopolymerization process due to its highly amorphous structure. It is obtained by heating kaolinite, a clay mineral, at high temperature and subsequent quick cooling. Although MK is favorable in comparison with different types of waste materials for geopolymer production, it originates from clay which needs to be quarried and produced through high temperature heating. Therefore, the sustainability of MK-based GMU is questionable. Mohsen and Mostafa (2010) studied the utilization of low kaolinitic clays (white clay, grey clay and red clay) to produce GMU. In order to produce MK, the raw clay materials were heated at 700°C for 2 h and ground before use. Both NaOH and mixture of NaOH and SS solutions were used as the alkali activator. The test specimens were formed at 15 MPa in a special steel mold and pre-cured at room temperature for 24 h and then cured at different temperatures for different times (room temperature for 3 days, 75°C for 24 h, or 150°C for 24 h) before testing. The results indicated that the alkali activator type and the curing temperature are two major factors that determine the behavior of GMU.

Zivica *et al*. (2011) also studied production of GMU from MK activated with only NaOH. Small cubic specimens were prepared at 8% water content and formed at 200 MPa pressure. Then they were cured at 20°C and relative humidity of 95% for 24 h. The densifying effect of forming pressure along with low water content resulted in a compressive strength up to 148.0 MPa. It can be seen that MK is the most suitable material in terms of reactivity and low temperature curing. To reduce the usage of natural kaolinite and the required high temperature heating, MK can be combined with different types of waste materials to produce GMU.

24.2.5 Other types of wastes

Production of GMU is not limited to the usage of waste materials described above. Other types of waste materials have also been studied by researchers. For example, Diop and Grutzeck (2008) investigated the feasibility of producing GMU from aluminosilicate-rich tuff. They used NaOH solution as the alkali activator and prepared cylindrical specimens with a forming pressure of about 10 MPa. They studied the effect of both the NaOH concentration (4, 8 and 12 M) and the curing temperature

(40, 80 and 120°C). The results showed that the strength increased with the NaOH concentration and the curing temperature. Kumar and Kumar (2013) added up to 40% RM to FA and noted that the reactivity of FA was intensified due to the addition of RM. However, the improvement in setting time and compressive strength was only observed at 5–20% addition. He *et al*. (2013) investigated production of geopolymer binder from a mixture of rice husk ash (RHA) and RM and reported compressive strengths ranging from 3.2 to 20.5 MPa, the higher compressive strength with higher RHA content. GMU can also be produced from waste concrete resulting from demolition of old concrete structures. Ahmari *et al*. (2012a) studied the feasibility of producing geopolymer binder from waste concrete fines (WCF) blended with FA and found that the half and half mix proportion is the optimal mixture in terms of compressive strength. They reported a compressive strength up to 35.0 MPa for the WCF/FA-based geopolymer paste.

24.3 Physical properties of alkali-activated masonry units

The physical properties that are used in most of the standards to quantify the suitability of GMU for construction purposes are bulk density, water absorption, and permeability. Lower bulk density and in the meantime higher compressive strength are the desired properties in order to minimize the dead load of, and maximize the strength of, masonry structures. The bulk density of GMU mainly depends on the forming pressure and the specific gravity of the constituting solid materials. FA has low specific gravity and is suitable for producing lightweight GMU. FA can be mixed with cenosphere (another by-product of coal burning in power plants) to even reduce the bulk density of GMU (Majrzak *et al*., 2007). On the other hand, FS has high specific gravity and thus it might not be a suitable source material if the weight of bricks is a concern. Mixing FS with other lower specific density wastes such as FA helps obtain a lower bulk density. Another alternative is to produce hollow core units. In this case, however, it would be difficult to provide forming pressure during the production of GMU.

Arioz *et al*. (2010) investigated the density of FA-based GMU cured at different temperatures for different periods of time. They did not find any remarkable influence of curing temperature and duration but reported that the density of specimens prepared under steam curing condition tend to be lower than those in oven-dry condition. The density for most of the specimens was 15 kN/m^3 or lower. Kishan and Radhakrishna (2013) studied the production of GMU from a mixture of FA and FS and compared the bulk densities of GMU and Portland cement masonry units (CMU). Both types of masonry units exhibited increase in density with time but the GMU was lighter than the CMU. Ahmari and Zhang (2012) measured the bulk density of MT-based GMU prepared at different water contents and forming pressures. They observed that the bulk unit weight increased with both the initial water content and the forming pressure (Figure 24.1). The unit weight increased with the forming pressure because

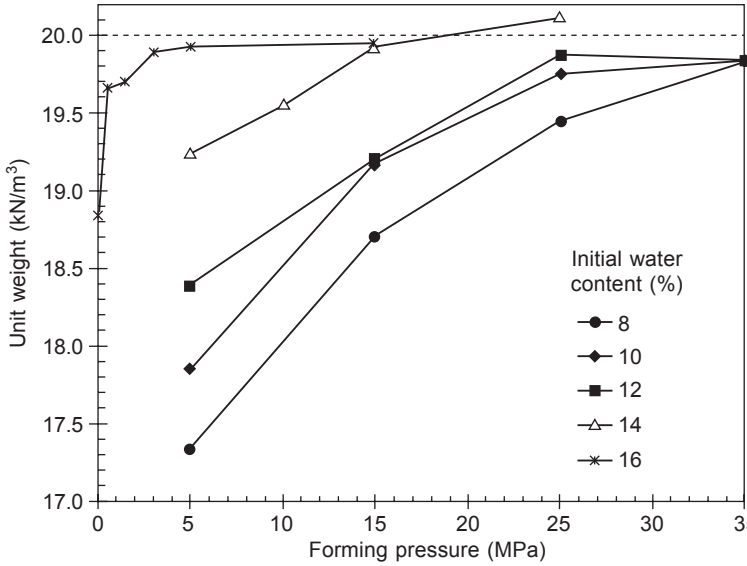

Figure 24.1 Bulk unit weight versus forming pressure for specimens prepared at different initial moisture contents and 15 M NaOH and cured at 90°C for 7 days (reprinted from Ahmari and Zhang, 2012, Copyright © 2012, with permission from Elsevier).

higher forming pressure resulted in denser structure of GMU. However, this was true only up to a certain level because at too high a forming pressure, the water (i.e., the alkaline solution) was squeezed out of the matrix. The unit weight increased with the initial water content because higher water content meant a larger amount of NaOH at the same NaOH concentration.

Water absorption is an important criterion in many standards and is dependent on the microstructure and permeability of GMU. It can also be an indicator of the degree of geopolymerization because higher degree of geopolymerization generates larger amount of geopolymer gel and leads to denser microstructure and consequently lower water absorption. GMUs with lower water absorption tend to be more durable in harsh environments because corrosive chemicals are less likely to penetrate into the material due to the smaller pore size. The ASTM standards present different maximum limits on water absorption for various applications of bricks, ranging from 8% for pedestrian and light traffic paving bricks to 25% for wall tiles. Ahmari and Zhang (2012) showed that the MT-based GMU prepared at 16% water content and different forming pressures exhibited water absorption of less than 5%. The increase in the GMU's weight due to water absorption continued for about 4 days and then became negligible (Figure 24.2).

Freidin (2007) found that FA-based GMU without hydrophobic additives exhibited water absorption of 25% within 1 day while the addition of hydrophobic agent decreased the ultimate water absorption to less than 10%, which was reached after about one week. Mohsen and Mostafa (2010) studied GMU produced from low kaolinitic clays which were calcined at 700°C for 2 h. They used NaOH and

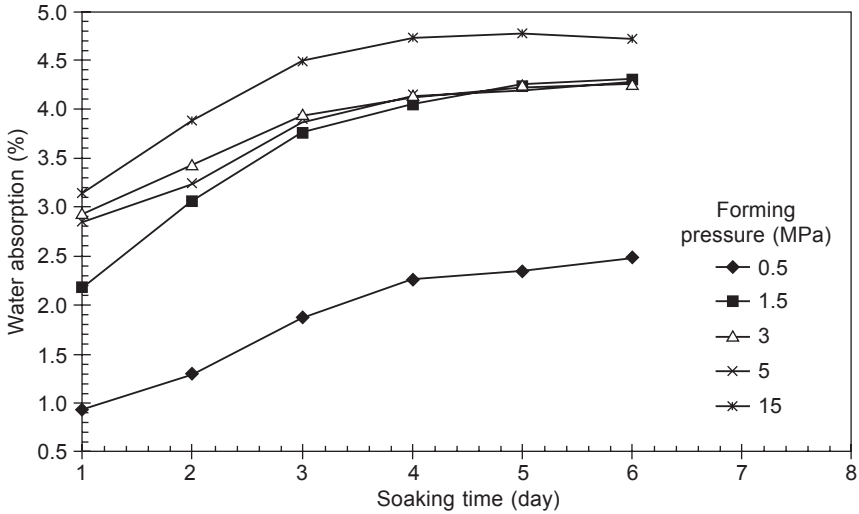

Figure 24.2 Water absorption versus soaking time for specimens prepared at 16% initial water content and different forming pressures and cured at 90°C for 7 days (reprinted from Ahmari and Zhang, 2012, Copyright © 2012, with permission from Elsevier).

a mixture of NaOH and SS as alkali activator. They reported that all specimens exhibited water absorption less than 17%, which is the minimum requirement for load-bearing masonry units according to ASTM C90. The specimens prepared with only NaOH exhibited higher water absorption than those prepared with NaOH and SS. This was because the specimens prepared with NaOH and SS showed a denser microstructure as indicated by SEM micrographs. The formation of a denser microstructure and thus the improvement of physical properties due to the addition of SS are because SS contains soluble silica species which facilitate the dissolution of alumina from the solid source material and thus promote the geopolymerization (Ahmari *et al.*, 2012b).

GMUs have higher humidity retention capacity than conventional MUs due to their pore size distribution. This makes GMU a good option for cooling applications in high temperature climates (Okada *et al.*, 2009; Obonoyo *et al.*, 2010). Excellent fire resistance, low shrinkage, low thermal expansion, and low thermal conductivity are other favorable characteristics of GMU. For example, GMUs have a thermal conductivity between 0.15 and 1 W/mK while conventional MUs have a thermal conductivity between 0.43 and 1.44 W/mK (Obonoyo *et al.*, 2011). Cheng and Chiu (2002) measured the physical properties of FS-based geopolymer prepared with potassium hydroxide (KOH) and SS. The results indicated that the porosity of the geopolymer binder varied between 28.3 and 35.6%. To measure the fire resistance, a 10 mm thick geopolymer panel was exposed to 1100°C on one side and the temperature on the other side was measured after 35 min. By adding metakaolin, the fire resistance of the FS-based geopolymer was improved, with the measured temperature decreased from 350°C to 250°C. So a combination of different source

materials is an effective way to improve the properties of geopolymer products by providing the favorable characteristics from each source material. This can be further seen from the improvement of mechanical properties and durability of GMU discussed in the next sections.

24.4 Mechanical properties of alkali-activated masonry units

Unconfined compressive strength (UCS) is the most commonly used mechanical property to describe the strength of GMU. It is a macro-scale property which is strongly dependent on the micro and nano-scale properties of geopolymer binders. The micro and nano-scale properties can be controlled by adjusting the factors that affect the geopolymerization process. The most important factors that affect the mechanical properties of geopolymers are degree of amorphicity of solid material, alkali type and concentration, Si/Al and Na/Al ratios, and curing time and temperature (Duxson *et al.*, 2007; Dimas *et al.*, 2009).

In the geopolymerization process, the amorphous phase of the source material mainly participates in the chemical reaction while the crystalline phase might only partially react to the activation solution. Quartz (SiO_2) is the most abundant mineral of silica, which exists in most of the earth materials. However, it is one of the most stable minerals and usually remains unreacted during geopolymerization. Many researchers use a mixture of NaOH and SS as the activation solution because SS contains soluble silica units that can be immediately available for reaction. Ahmari *et al.* (2012b) showed that the addition of SS to NaOH substantially increased the UCS of MT-based geopolymer. They argued that there is an optimum SiO_2/Na_2O ratio of about 1–1.2 at which the highest UCS can be obtained. Similarly, the optimum SiO_2/Na_2O ratio for other types of source materials such as FS, FA and MK, as stated earlier, is between 1 and 1.5 (Ahmari *et al.*, 2012b). Freidin (2007) showed that the UCS of FA-based GMU cured at room temperature increased from about 2 MPa to 16 MPa when the amount of SS increased from 10 to 30% (by weight of the solid phase). However, addition of SS beyond the optimum level will lead to decrease of UCS because it prevents evaporation of water and formation of geopolymeric binder by precipitation of the Si-Al phase in the contact between the solid material and the activating solution (Cheng and Chiu, 2002; Lee and van Deventer, 2002).

The concentration of activation solution is important because at higher NaOH or KOH concentration more silica and alumina can be dissolved from the surface of solid materials. Zhang *et al.* (2011) reported that the UCS of geopolymer based on 50% MT and 50% FA cured at 60°C for 7 days increased from approximately 3 MPa to over 12 MPa when the NaOH concentration went from 5 M to 15 M. Figure 24.3 shows the SEM micrographs of geopolymer prepared from a mixture of 50% FA and 50% MT at different NaOH concentrations. It is evident that a denser microstructure is created when the concentration is higher.

The Si/Al ratio also affects the mechanical properties of geopolymer. It is noted

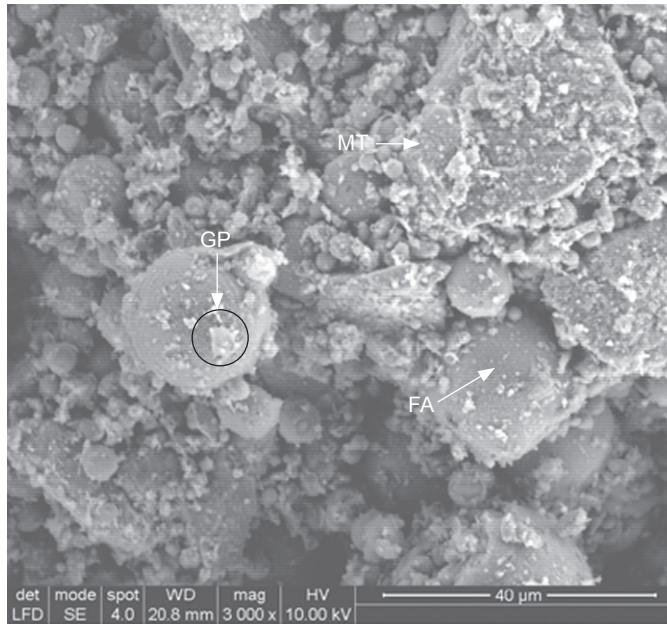

(a)

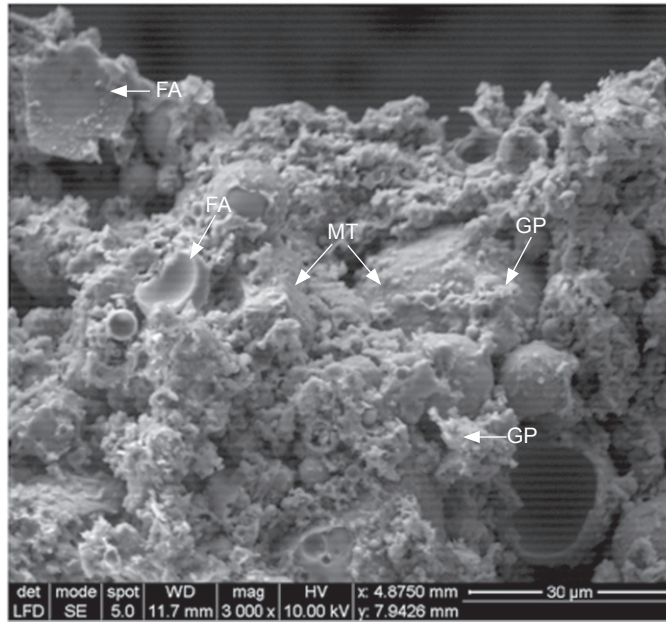

(b)

Figure 24.3 SEM micrographs of geopolymer prepared with 50% FA and 50% MT, after 7 days' curing, and at (a) 5 M and (b) 15 M NaOH (FA = fly ash, MT = mine tailings, and GP = geopolymer) (reprinted from Zhang *et al*., 2011, Copyright © 2011, with permission from Elsevier).

that the Si/Al ratio of geopolymer generated is not necessarily the same as the initial Si/Al ratio of the solid source material because some of the silicates such as quartz are crystalline and do not take part in the reaction. For example, Ahmari *et al*. (2012a) reported that the MT they used had a Si/Al ratio of 7.78 but the Si/Al ratio of the geopolymer binder after hardening was much lower. If the Si/Al ratio of the source material is far from the optimum one, it can be adjusted by adding other types of source materials. This is the reason that by adding FA to MT or WCF, the UCS of geopolymer increases (Zhang *et al*., 2011; Ahmari *et al*., 2012a). As for the Na/Al ratio, the optimum value is close to 1 because sodium cations serve as charge balancing for alumina species and extra sodium will remain un-reacted and increase the pH of pore water.

The curing temperature has a great effect on the mechanical properties of geopolymer. Table 24.1 indicates that optimum curing temperature depends on the concentration of the activation solution and the reactivity of the source material. For example, FA has a lower optimum curing temperature than MT. Figure 24.4 shows the relationship between UCS and curing temperature for MT-based GMU prepared at 12% initial water content and 25 MPa forming pressure and cured for 7 days. The optimum curing temperature for MT-based GMU is about 90°C. This temperature is considerably lower than the kiln firing temperature for regular bricks. The curing time is also important for GMU; but since geopolymer gains most of its ultimate strength much faster than OPC, the curing time beyond a certain limit becomes insignificant. For example, the MT/FA-based geopolymer prepared with only NaOH gains its ultimate strength within 7 days (Zhang *et al*., 2011). Mathew *et al*. (2013) studied GMU based on mixture of FA, granulated blast furnace slag, and bottom ash activated with NaOH and SS solution and cured at room temperature. Since curing at room temperature was relatively slow, the specimens kept gaining strength until 28 days.

The factors discussed above not only affect the mechanical properties of GMU but also other geopolymer products such as geopolymer concrete. The other two factors, initial water content and forming pressure, however, are more related to

Table 24.1 Summary of optimum curing temperature reported in the literature

Source material	Optimum curing temperature (°C)	NaOH concentration (M)	Reference
Metakaolin	35	4.3	Yao *et al*. (2009)
Natural zeolite	40	7	Villa *et al*. (2010)
Glass cullet	40	5–10	Cyr *et al*. (2012)
Class C fly ash	60	8.1	Guo *et al*. (2010)
Class F fly ash	75	7.5	Sindhunata *et al*. (2006)
Class F fly ash	80	7	Hou *et al*. (2009)
MT	75	5 and 10	Ahmari *et al*. (2012b)
MT	90	15	Ahmari *et al*. (2012b)

Source: Revised from Ahmari *et al*., 2012b, with kind permission from Springer Science and Business Media.

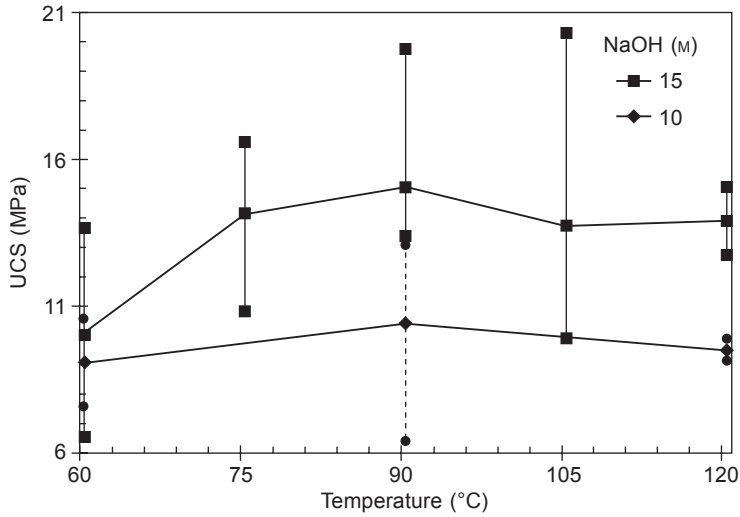

Figure 24.4 UCS versus curing temperature for GMU specimens prepared at 12% initial water content, 25 MPa forming pressure, and respectively 10 and 15 M NaOH concentrations (reprinted from Ahmari and Zhang, 2012, Copyright © 2012, with permission from Elsevier).

GMU. The mechanical (and also physical) properties of GMU can vary significantly if the water content and forming pressure change. With a higher forming pressure, a greater UCS value is expected since the higher forming pressure packs the particles into a denser matrix. However, the forming pressure alone is not enough to improve the strength of GMU because sufficient amount of binder must exist to bind the packed particles to each another. There is a limit on the level of forming pressure because too high a forming pressure may lead to a significantly heavy GMU and, more importantly, the activation solution will be squeezed out of the matrix and the geopolymerization will be adversely affected. As shown in Figure 24.5, the UCS increases with higher forming pressure but the rate of increase becomes lower as the forming pressure increases. When the forming pressure is high enough, the UCS of MT-based GMU with initial water content greater than 10% decreases. The studies by Freidin (2007) on FA-based GMU also indicate that the forming pressure increases the UCS but the effect becomes smaller at higher forming pressure (Figure 24.6). The effect of water content on the UCS of GMU seems more noticeable than that of forming pressure. Sufficient amount of water is required for the formation of geopolymer binder linking the un-reacted or partially reacted particles. However, too much water leads to porous structure and consequently lower UCS. Zivica *et al*. (2011) produced GMU from MK at 8% water content and 300 MPa forming pressure. A UCS of 146.6 MPa was obtained. They argued that the high densification and the low water content accounted for such a high compressive strength.

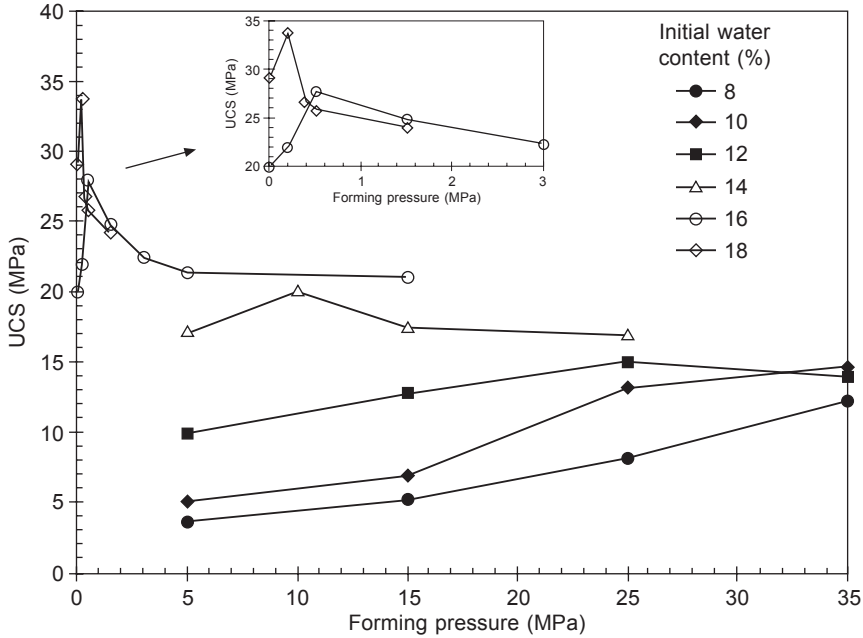

Figure 24.5 UCS versus forming pressure for MT-based GMU specimens prepared at different initial water contents and 15 M NaOH concentration and cured for 7 days at 90°C (reprinted from Ahmari and Zhang, 2012, Copyright © 2012, with permission from Elsevier).

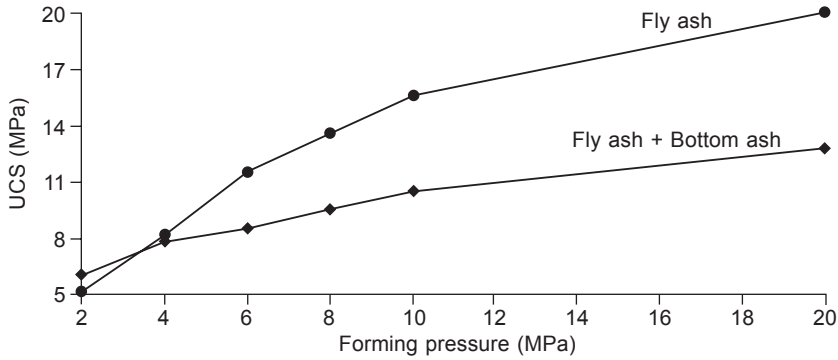

Figure 24.6 UCS versus forming pressure for GMU specimens based on fly ash or fly ash and bottom ash, prepared with SS and NaOH and cured at room temperature (reprinted from Freidin, 2007, Copyright © 2007, with permission from Elsevier).

24.5 Durability of alkali-activated masonry units

The durability of GMU consists of the performance and resistance against different environmental impacts including freeze-thaw resistance and resistance to aggressive environments, which are discussed below.

24.5.1 Freeze-thaw resistance

Freeze-thaw resistance is important in geographic locations where temperature may reach below zero. So far, however, very few researchers have studied the freeze-thaw resistance of GMU. Liu and van Engelenhoven (2009) modified the method in ASTM C67 specifically for evaluating the freeze-thaw resistance of fired clay bricks in order to study the freeze-thaw resistance of FA bricks. For example, ASTM C67 requires drying bricks at 110–115°C in the test, which does not affect fired clay bricks but it may change the properties of FA bricks. The tests indicated that the modified test yielded more meaningful and conservative results.

Liu *et al*. (2005) investigated different ways to enhance the freeze-thaw resistance of FA bricks, including using greater FA-to-water ratio, adding a small amount of fiber to FA before compaction, adding cement or lime to FA before compaction, using certain liquid sealants to coat the bricks, using higher forming pressure to produce denser bricks, increasing curing time, using a split mold in order to prevent tensile cracking when demolding with the regular process, and using air entrainment agent. They found that some of these methods, such as using optimum FA to water ratio, using higher forming pressure, increasing curing time, and adding Portland cement, increased the UCS of the bricks but were not effective in improving the freeze-thaw resistance. The reason is that these methods enhance the compressive strength of the FA bricks but the freeze-thaw resistance is closely related to the resistance to crack formation due to tensile stresses (Liu *et al*., 2005). Addition of air entrainment agent was the most effective method for enhancing the freeze-thaw resistance of FA bricks, which is the method commonly used for OPC concrete. The study showed that addition of only 0.2% air entrainment agent (by weight) increased the freeze-thaw cycles from less than 40 to more than 50. The most recent study in the senior author's lab also indicates that addition of air entrainment agent can enhance the freeze-thaw resistance of MT-based GMU.

Majrzak *et al*. (2007) tested different properties including durability of FA bricks after addition of cenosphere. Cenosphere is a powdered material derived from FA of coal-fired power plants. It has light weight and consists of small hollow spheres filled with inert gas. Its specific gravity ranges between 0.4 and 0.8. Bricks containing 0–20% cenosphere were tested to study the feasibility of reducing weight and improving freeze-thaw resistance of bricks. The results indicated that addition of 10% cenosphere increased the freeze-thaw resistance cycles from slightly less than 60 to over 120.

24.5.2 Water and chemical resistance

The acid resistance of geopolymer binder has been studied by a number of researchers (Sindhunata *et al*., 2006; Bakharev, 2005; Temuujin *et al*., 2011). The results show better performance of geopolymer binder than OPC in corrosive environment. Bakharev (2005) investigated the durability of geopolymer in acidic condition and reported strength loss due to depolymerization of geopolymer gel. He used FA-based geopolymer prepared with NaOH, SS, and mixture of NaOH and KOH,

respectively. The specimen activated with mixture of NaOH and KOH exhibited the best durability in 5% acetic acid after 6 months (38.3% strength loss) while OPC lost 90% of its strength. The specimen activated with only NaOH had the best durability in 5% sulfuric acid solution with only 17.5% strength loss while OPC deteriorated completely. Temuujin *et al.* (2011) reported approximately 80 and 90% weight loss and 20 and 30% reduction in UCS for FA-based geopolymer immersed respectively in 18% HCl and 14 M NaOH solutions for 5 days. It appears that the durability of geopolymer in harsh environment depends on the type of acid or base and the condition at which the geopolymer is prepared.

Durability of MT-based GMU was studied by Ahmari and Zhang (2013b). Their study indicated substantial strength loss after immersion in neutral water and nitric acid at pH 4.0. They reported respectively 59.3% and 53.3% strength loss at pH 4 and 7 for the GMU prepared with 12% water content and 25 MPa forming pressure while 78.4% and 75.2% strength loss at pH 4 and 7 for the specimen prepared at 16% water content and 0.5 MPa forming pressure. The durability of MT-based GMU can be enhanced by adding up to 10% CKD (Ahmari and Zhang, 2013a). This is mainly due to the formation of calcium carbonate which has very low solubility in water and alkaline condition. Freidin (2007) also reported substantial strength loss on NaOH and SS-activated FA-based GMU after immersion in water. Silva *et al.* (2012) studied the stability of calcined tungsten MT-based geopolymer immersed in water and reported disintegration after a certain period of time mainly due to partial geopolymerization.

24.6 Summary and future trends

Geopolymer binder has been proven to possess excellent physical and mechanical properties and durability. Different applications of geopolymer binders, such as concrete, coating material, and masonry units, have been studied. Study of GMU from different types of waste materials indicates that GMU is a superior replacement for regular MU, especially considering the environmental impacts of solid wastes and the sustainability issues related to usage of natural materials and energy. For wide application of GMU, the major issue is the transition from research stage to commercialization. GMU standardization and public education are the main steps to achieve this goal. Further research is also needed to study the long-term durability of GMU and the environmental and economic benefits of utilizing waste materials to produce GMU.

References

Ahmari, S. and Zhang, L. (2012) 'Production of eco-friendly bricks from copper mine tailings through geopolymerization', *Construction and Building Materials*, 29, 323–31.

Ahmari, S. and Zhang, L. (2013a) 'Utilization of cement kiln dust (CKD) to enhance mine tailings-based geopolymer bricks', *Construction and Building Materials*, 40, 1002–11.

Ahmari, S. and Zhang, L. (2013b) 'Durability and leaching behavior of mine tailings-based geopolymer bricks', *Construction and Building Materials*, 44, 743–50.

Ahmari, S., Ren, X., Toufigh V. and Zhang, L. (2012a) 'Production of geopolymeric binder from blended waste concrete powder and fly ash', *Construction and Building Materials*, 35, 718–29.

Ahmari, S., Zhang, L. and Zhang J. (2012b) 'Effects of activator type/concentration and curing temperature on alkali-activated binder based on copper mine tailings', *Journal of Materials Science*, 47, 5933–45.

Alonso, S. and Palomo, A. (2001) 'Calorimetric study of alkaline activation of calcium hydroxide-metakaolin solid mixtures', *Cement and Concrete Research*, 31, 25–30.

Arabani, M. and Azarhoosh, A.R. (2012) 'The effect of recycled concrete aggregate and steel slag on the dynamic properties of asphalt mixtures', *Construction and Building Materials*, 35, 1–7.

Arioz, O., Kilinc, K., Tuncan, M., Tuncan, A. and Kavas, T. (2010) 'Physical, mechanical and micro-structural properties of F type fly-ash based geopolymeric bricks produced by pressure forming process', *Advances in Science and Technology*, 69, 69–74.

Asmatulaev, B.A., Asmatulaev, R.B., Abdrasulova, A.S., Levintov, B.L., Vitushchenko, M.F. and Stolyarskiiv, O.A. (2008) 'Using blast-furnace slag in road construction', *Steel in Translation*, 38, 722–5.

Bakharev, T. (2005) 'Durability of geopolymer materials in sodium and magnesium sulfate solutions', *Cement and Concrete Research*, 35, 1233–46.

Chen, C., Li, Q., Shen, L. and Zhai, J. (2012) 'Feasibility of manufacturing geopolymer bricks using circulating fluidized bed combustion bottom ash', *Environmental Technology*, 33, 1313–21.

Cheng, T.W. and Chiu, J.P. (2002) 'Fire-resistant geopolymer produced by granulated blast furnace slag', *Mineral Engineering*, 16, 205–10.

Chou, M.I., Chou, S.F., Patel, V., Pickering, M.D. and Stucki, J.W. (2006) 'Manufacturing fired bricks with class F fly ash from Illinois Basin Coals. Combustion Byproduct Recycling Consortium', Project Number 02-CBRC-M12, Final Report.

Cyr, M., Idir, R. and Poinot, T. (2012) 'Properties of inorganic polymer (geopolymer) mortars made of glass cullet', *Journal of Materials Science*, 47, 2782–97.

Davidovits, J. (1982) 'Mineral polymers and methods of making them', US Patent 4349,386.

Davidovits, J. (1991) 'Geopolymers: inorganic polymeric new materials', *Journal of Thermal Analysis*, 37, 1633–56.

Dimas, D., Giannopoulou, I. and Panias, D. (2009) 'Polymerization in sodium silicate solutions: a fundamental process in geopolymerization technology', *Journal of Materials Science*, 44, 3719–30.

Diop, M.B. and Grutzeck, M.W. (2008) 'Low temperature process to create brick', *Construction and Building Materials*, 22, 1114–21.

Duxson, P., Provis, J.L., Lukey, G.C., Mallicoat, S.W., Kriven, W.M. and van Deventer, J.S.J. (2005) 'Understanding the relationship between geopolymer composition, microstructure and mechanical properties', *Colloids and Surfaces A: Physicochemical and Engineering Aspects*, 269, 47–58.

Duxson, P., Mallicoat, S.W., Lukey, G.C., Kriven, W.M. and van Deventer, J.S.J. (2007) 'The effect of alkali and Si/Al ratio on the development of mechanical properties of metakaolin-based geopolymers', *Colloids and Surfaces A: Physicochemical and Engineering Aspects*, 292, 8–20.

Freidin, C. (2007) 'Cementless pressed blocks from waste products of coal-firing power station', *Construction and Building Materials*, 21, 12–18.

Guo, X., Shi, H. and Dick, W.A. (2010) 'Compressive strength and microstructural characteristics of class C fly ash geopolymer', *Cement and Concrete Composites*, 32, 142–7.

He, J., Jie, Y., Zhang, J., Yu, Y. and Zhang, G. (2013) 'Synthesis and characterization of red mud and rice husk ash-based geopolymer composites', *Cement and Concrete Composites*, 37, 108–18.

Hou, Y., Wang, D., Zhou, W., Lu, H. and Wang, L. (2009) 'Effect of activator and curing mode on fly ash-based geopolymers', *Journal of Wuhan University of Technology – Mater. Sci. Ed.*, 24, 711–15.

Kim, H. and Kim, Y. (2012) 'Characteristics of the geopolymer using fly ash and blast furnace slag with alkali activators', *4th International Conference on Chemical, Biological and Environmental Engineering*, Singapore, 43, 154–9.

Kirillidi, Y. and Frogoudakis, E. (2005) 'Electric arc furnace slag utilization', *Proceedings of the 9th International Conference on Environmental Science and Technology*, Rhodes, Greece, 768–72.

Kishan, L.J. and Radhakrishna (2013) 'Comparative study of cement concrete and geopolymer masonry blocks', *International Journal of Research in Engineering and Technology*, *2,* 361–5.

Kumar, A. and Kumar, S. (2013) 'Development of paving blocks from synergistic use of red mud and FA using geopolymerization', *Construction and Building Materials*, 38, 865–71.

Lee, W.K.W. and van Deventer, J.S.J. (2002) 'The effects of inorganic salt contamination on the strength and durability of geopolymers', *Colloids and Surfaces A: Physicochemical and Engineering Aspects*, 21, 115–26.

Liu, H. and van Engelenhoven, J. (2009) 'Use of ASTM standards for testing freeze-thaw resistance of FA bricks', *World of Coal Ash (WOCA) Conference*, Lexington, KY.

Liu, H., Burkett, W. and Haynes, K. (2005) 'Improving freezing and thawing properties of fly ash bricks', *World of Coal Ash (WOCA)*, Lexington, KY.

Liu, Z., Chen, Q., Xie, X., Xue, G., Du, F., Ning, Q. and Huang, L. (2011) 'Utilization of the sludge derived from dyestuff-making wastewater coagulation for unfired bricks', *Construction and Building Materials*, 25, 1699–706.

Majrzak II, G.L., Watson, J.P., Bryant, M.M. and Clayton, K. (2007) 'Effect of cenospheres on fly ash brick properties', *World Coal Ash (WOCA)*, Covington, KY.

Mathew, B.J., Sudhakar, M. and Natarajan, C. (2013) 'Development of coal ash–GGBS based geopolymer bricks', *European International Journal of Science and Technology*, 2, 133–9.

Mobasher, B., Devaguptapu, R. and Arino, A.M. (1996) 'Effect of copper slag on the hydration of blended cementitious mixtures', *Proceedings*, *ASCE*, *Materials Engineering Conference*, *Materials for the New Millenium*, ed. K. Chong, pp. 1677–86.

Mohsen, Q. and Mostafa, N.Y. (2010) 'Investigating the possibility of utilizing low kaolinitic clays in production of geopolymer bricks', *Ceramics – Silikaty*, 54, 160–8.

Morchhale, R.K., Ramakrishnan, N. and Dindorkar, N. (2006) 'Utilization of copper mine tailings in production of bricks', *Journal of the Institution of Engineers*, Indian Civil Engineering Division, 87, 13–16.

Obonoyo, E., Kamseu, E., Melo, U.C. and Leonelli, C. (2011) 'Advancing the use of secondary inputs in geopolymer binders for sustainable cementitious composites: a review', *Sustainability*, 3, 410–23.

Okada, K., Ooyama, A., Isobe, T., Kameshima, Y., Nakajima, A. and Makenzie, K.J.D. (2009)

'Water retention properties of porous geopolymers for use in cooling applications', *Journal of the European Ceramic Society*, 29, 1917–23.

Pacheco-Torgal, F. and Jalali, S. (2010) 'Influence of sodium carbonate addition on the thermal reactivity of tungsten mine waste mud based binders', *Construction and Building Materials*, 24, 56–60.

Pacheco-Torgal, F., Castro-Gomes, J. and Jalali, S. (2008) 'Investigations of tungsten mine waste geopolymeric binder: strength and microstructure', *Construction and Building Materials*, 22, 2212–19.

Pacheo-Torgal, F., Castro-Gomes, J. and Jalali, S. (2010) 'Durability and environmental performance of alkali-activated tungsten mine waste mud mortars', *Journal of Materials in Civil Engineering*, 22, 897–904.

Radhakrishna, Shashishankar, A. and Udayashankar, B.C. (2008) 'Phenomenological model to re-proportion geopolymer compressed blocks', *33rd Conference on Our World in Concrete and Structures*, Singapore.

Rattanasak, U. and Chindaprasirt, P. (2009) 'Influence of NaOH solution on the synthesis of fly ash geopolymer', *Mineral Engineering*, 22, 1073–8.

Roy, S., Adhikari, G.R. and Gupta, R.N. (2007) 'Use of gold mill tailings in making bricks: a feasibility study', *Waste Management and Research*, 25, 475–82.

Silva, I., Castro-Gomes, J.P. and Albuquerque, A. (2012) 'Effect of immersion in water partially alkali-activated materials obtained of tungsten mine waste mud', *Construction and Building Materials*, 35, 117–24.

Silva, P.D., Sagoe-Crenstil, K. and Sirivivatnanon, V. (2007) 'Kinetics of geopolymerization: role of Al_2O_3 and SiO_2', *Cement and Concrete Research*, 37, 512–18.

Sindhunata, van Deventer, J.S.J., Lukey, G.C. and Xu, H. (2006) 'Effect of curing temperature and silicate concentration on fly-ash-based geopolymerization', *Industrial & Engineering Chemistry Research*, 45, 3559–68.

Temuujin, J., Minjigmaa, A., Lee, M., Chen-Tan, N. and van Riessen, A. (2011) 'Characterisation of class F fly ash geopolymer pastes immersed in acid and alkaline solutions', *Cement and Concrete Composites*, 33, 1086–91.

Van Deventer, J.S.J., Provis, J., Duxson, P. and Lukey, G.C. (2006) 'Technological, environmental and commercial drivers for the use of geopolymers in a sustainable material industry', *International Symposium of Advanced Processing of Metals and Materials*, 241–52.

Villa, C., Pecina, E.T., Torres, R. and Gómez, L. (2010) 'Geopolymer synthesis using alkaline activation of natural zeolite', *Construction and Building Materials*, 24, 2084–90.

Xu, H. and van Deventer, J.S.J. (2003) 'Effect of source materials on geopolymerization', *Industrial and Engineering Chemistry Research*, 42, 1698–706.

Yao, X., Zhang, Z., Zhua, H. and Chen, Y. (2009) 'Geopolymerization process of alkali–metakaolinite characterized by isothermal calorimetry', *Thermochimica Acta*, 493, 49–54.

Zhang, L. (2013) 'Production of bricks from waste material – a review', *Construction and Building Materials*, 47, 643–55.

Zhang, L., Ahmari, S. and Zhang, J. (2011) 'Synthesis and characterization of fly ash modified mine tailings-based geopolymers', *Construction and Building Materials*, 25, 3773–81.

Zivica, V., Balkovic, S. and Drabik, M. (2011) 'Properties of metakaolin geopolymer hardened paste prepared by high-pressure compaction', *Construction and Building Materials*, 25, 2206–13.

Part Five

Life cycle assessment (LCA) and innovative applications of alkali-activated cements and concretes

This page intentionally left blank

Life cycle assessment (LCA) of alkali-activated cements and concretes

25

C. Ouellet-Plamondon, G. Habert
Swiss Federal Institute of Technology Zurich (ETH Zurich), Zurich, Switzerland

25.1 Introduction

Concrete accounts for 5–8% of total anthropogenic CO_2 emissions and 95% of the CO_2 is produced during the fabrication of cement (Huntzinger and Eatmon, 2009; Worrell *et al.*, 2009). Half of it is released by the decarbonation of the limestone during cement fabrication. Furthermore, the rapid urban development in emerging countries will push forward the cement demand and recent studies estimate that cement production could represent 10–15% of global CO_2 emissions by 2020 (Szabó *et al.*, 2006). Thus there is an urgent need for more environmentally friendly, economically viable and socially relevant cement.

Since the 1980s and the development of superplasticizers (Flatt, 2004; Flatt *et al.*, 2012), and later with the detailed understanding of packing optimization, concrete mix design has changed drastically. Tailored concrete mix design allows for the appropriate amount of cement for the required strength and durability. A better understanding of colloidal interaction between particles (Kovler and Roussel, 2011) and knowledge transfer from the fundamental physics of grain and colloids to civil engineers (Yammine *et al.*, 2008) have permitted a further reduction in the amount of cement in concrete. These measures allow a significant reduction of CO_2 emissions. However, due to growth of consumption, especially in developing countries, it is difficult to imagine a CO_2 reduction in accordance with the Intergovernmental Panel on Climate Change (IPCC) recommendations. Overall, it can be expected that these technological improvements will reduce CO_2 emissions by a factor of two (Habert *et al.*, 2010), which is far from the fourfold reduction objectives of the IPCC. Alternative cements are therefore crucially needed.

Alkali-activated cements and concretes (AACC) are another promising alternative. As explained in more detail in the previous chapters, AACC are binders formed by the alkali activation of aluminosilicate sources which can be a natural or a synthetic material, or an industrial waste (Davidovits, 1991; Duxson *et al.*, 2007a). They are commonly called geopolymers. To evaluate the environmental impact of these alternatives on a standard concrete, life cycle assessment (LCA) is the best tool available. LCA, also known as the 'cradle to grave' approach, is an international normalized approach, used in universities, research centre and industries (ISO 14040, 2006). We have found five published life cycle assessments of AACC, and

Handbook of Alkali-activated Cements, Mortars and Concretes. http://dx.doi.org/10.1533/9781782422884.5.663

they give conflicting results. The objective of this chapter is then to provide an understanding of the current results of LCAs on AACC and highlight further points of research. After a brief presentation of the LCA methodology and the review of the recent papers published on this subject, we propose a methodology to more accurately compare geopolymeric products to cementitious materials. After reviewing an extensive number of publications, this method is applied to the set providing a reference standard concrete. We discuss the critical points to be resolved to improve the conclusions from LCA of AACC and finally the future trends are presented.

25.2 Literature review

25.2.1 LCA methodology

The LCA methodology evaluates the potential environmental impact of materials, products and technology. The LCA procedure was normalized in international standards in the series 14040. The life cycle is defined as the 'consecutive and interlinked stages of a product system, from raw materials acquisition or generation from natural resources to final disposition' (ISO 14040, 2006). The life cycle assessment is the 'compilation and evaluation of the inputs, outputs and the potential environmental impacts of a product system throughout its lifecycle'. It has four main stages: goal and scope definition, inventory analysis, impact assessment and interpretation (Figure 25.1) (DIN, 2006).

The LCA starts by defining the goal, scope, the needs and the targeted audience. Generally, the LCA method focuses either on describing the environmentally relevant physical flows to and from the studied system (attributional), or on describing how environmentally relevant flows will change in response to a future decision (consequential). To effectively achieve the goal of the study, the critical point is therefore to define accurately the boundaries of the system studied as well as the functions

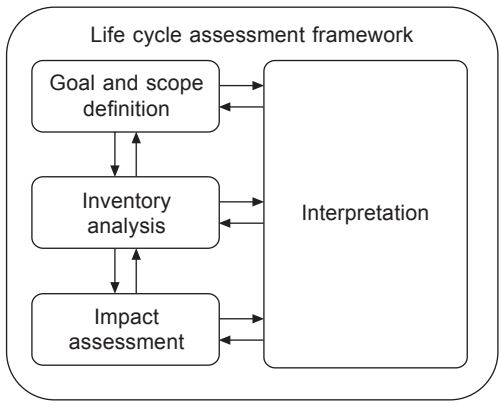

Figure 25.1 Life cycle assessment (LCA) framework.

that will be assessed. The functional unit refers to the 'quantified performance of a product system for use as a reference unit' (3.20, ISO 14040:2006). The quantitative description should include the service performance, or needs fulfilled, of the product studied (Rebitzer *et al.*, 2004). The functional unit is often a small unit that can be extended in time and space according to the emission inventory (Finnveden *et al.*, 2009). Although LCA originally aimed at considering every stage of the product's life cycle (cradle to grave), many studies terminate at an intermediate stage (cradle to gate, or gate to gate). Partial analyses are useful for civil engineering materials like concrete, because concrete can be included in end-products having different life cycles. As we know, 1 m^3 of concrete can be used in a structure, a wall, a bridge, or a road. Therefore, it is of definite interest to have quantified environmental impacts by providing results for 1 m^3 of concrete. The use of these data for the construction sector when compared to other materials such as wood or bricks has to be made with great care as the material with the lowest environmental impact per unit of volume (or mass) is not necessarily the one that will have the lowest environmental impact once integrated in a structure over its service life (Purnell, 2011).

Once the functional unit is defined, the second step is the inventory analysis. This means collecting and validating the data, calculating, and allocating the inputs and outputs. Collecting data is the most time-intensive stage of an LCA. The data quality depends on the access to manufacturer data, regional inventory databases, literature, estimates and judgments of the researchers. At the world level the Ecoinvent database is the largest and most complete database for life cycle inventory, but other databases such as the one integrated in the GaBi software are also often commonly used. Furthermore, a growing number of regional and national databases are emerging that can facilitate data collection (Finnveden *et al.*, 2009) even if very careful attention must be paid when combining databases (Lasvaux *et al.*, 2014).

The third step is the impact assessment which provides quantified information on the environmental impact of the studied products or process. While it is understood that an LCA cannot consider every impact, researchers from various domains have made huge efforts to develop indicators for the different impact categories. The reader is referred to Pennington *et al.* (2004) for background on the development of such indicators. In LCA, when a process produces more than one product, the environmental impact of this process needs to be allocated between the product and the by-product. If the by-product can be considered as waste, all impacts are allocated to the main product, but if this by-product can be considered a co-product of the process, then environmental impacts have to be shared between the main and co-products. Allocation can be done by mass or any other physical characteristic (e.g., energy). When no physical characteristic is relevant, then allocation can be done by a non-physical one (e.g., economic value).

The last step is the discussion of the implications of the life cycle assessment. This involves the identification of significant issues, their evaluation (check of completeness, sensitivity, consistency, etc.), conclusions, and limitations and recommendations. Finally, the uncertainty in an LCA can be tested by a large number of statistical methods: parameter variation and scenario analysis, classical frequentist theory-based hypothesis testing and parameter distributions, Monte Carlo simulations, analytical

methods based on first order propagation, non-parametric statistics (Bayesian and fuzzy set theory), and qualitative uncertainty methods based on quality indicators (Finnveden *et al*., 2009). However, most LCA studies do not explicitly describe the uncertainties.

25.2.2 Life cycle assessment of alkali-activated cements and concretes

The environmental impact of geopolymers remains a recent open debate, especially since they are presented as an alternative to conventional concrete. Initially, Duxson *et al*. (2007b) claimed that the CO_2 emissions from geopolymer production were much lower than ordinary Portland cement (OPC) production. However, in their analysis, they considered only geopolymers synthesized from ashes and slags, where the high temperature calcination step is not required. Such geopolymers are waste from the coal power or iron refining industries and therefore do not negatively impact the CO_2 balance. On the other hand, the calcination of the cement clinker consumes a large quantity of fossil fuel energy and releases additional CO_2 through the reaction. In geopolymers, the principal emitting component is the dissolved solids (Na_2O + SiO_2) in the activating solution. Thus, the first estimation of CO_2 equivalent emission reduction was presented as a function of the binder phase with the primary driver being derived from dissolved sodium and silica, and it showed that geopolymer production can reduce emissions by 80%. The two additional environmental benefits mentioned were the reduction of water usage and no requirement for superplasticizer admixtures. This first assessment did not discuss the impact of the production of the industrial waste, such as fly ash and ground blast furnace slag, which are also not accessible materials for all countries (e.g., Europe) (Habert, 2013). Furthermore recent publications contradict the conclusions of the first LCA of AACC. The methodology and conclusions of the more recent LCAs are summarized in Table 25.1.

The first LCA of geopolymers was published by Weil *et al*. in 2009. Comparison was made between 1 m^3 of freeze-thaw-resistant concrete of exposition class XF2 and XF4 according to DIN EN 206-1/DIN 1045-4 (CEM I 32.5R) and 1 m^3 of geopolymer with a slag/fly ash ratio of approximately 80:20 cured at room temperature. The LCA considered three impact categories: abiotic depletion potential (ADP), global warming potential (GWP) and cumulative energy demand (CED). Geopolymer outperformed CEM I concrete in the global warming potential by a factor 3, while it had a similar impact on the depletion of resources and energy use.

Habert *et al*. (2011) showed, however, that the production of geopolymer concrete has a higher environmental impact in other impact categories than global warming due to the production of sodium silicate solution. Ten environmental indicators were considered: abiotic depletion, global warming, ozone layer depletion, fresh and marine water ecotoxicity, terrestrial ecotoxicity, human toxicity, eutrophication, acidification and photochemical oxidation. Less sodium silicate solution is required in the activation of fly ash and ground blast furnace slag as compared to metakaolin-based geopolymers, but when the impacts are allocated as a by-product of production, the

Table 25.1 Comparison of recent articles on the life cycle assessment of geopolymers

References	Weil *et al.* 2009	Habert *et al.*, 2011	McLellan *et al.*, 2011	Turner and Collins, 2013	Yang *et al.*, 2013
Functional unit	1 m^3 of compliant concrete	1 m^3 of concrete with a mix design	1 m^3 concrete	1 m^3 concrete of 40 MPa	1 m^3 concrete of 24, 40, 70 MPa
System boundaries	Cradle to gate	Cradle to gate	Cradle to gate	Cradle to construction	Cradle to pre-construction
Reference OPC	Freeze-thaw-resistant concrete according to DIN EN 206-1/DIN 1045-4	Equivalent mechanical strength	100% OPC (2); OPC and slag (2); OPC and FA (2)	1 OPC	100% OPC (3); OPC + SCM (3)
Number of geopolymers	1 hybrid: slag/fly ash ratio 80:20 cured, room cure	FA (8 ref, 48 mixes), GBFS (4 ref, 12 mixes), MK (4 ref, 17 mixes)	FA (4)	FA (1)	AA GGBS (3), AA FA (3), AA MK (1)
Data source	Ecoinvent, literature, industry	Ecoinvent, literature, industry	Literature, calculation	Industry and Australia government	Korea LCI Database Information Network, Japanese database
Data quality	Very good to adequate	Good, but lack control for MK	Improvement needed on MK	Good	Good
Allocation		No, mass, economic			
Impact considered	3 indicators: ADP, GWP, CED	10 indicators	Energy, greenhouse emissions and cost	CO_2 footprint	CO_2 footprint
Conclusion	Improvement on GWP, but similar impact on ADP and CED	Higher impacts in other category than global warming	Results depend on the transport distance	Small improvement when taking into account the process	Favourable to geopolymers

Note: OPC: ordinary Portland cement; AA: alkali-activated; SCM: supplementary cementitious materials; FA: fly ash; GBFS: ground blast furnace slag; MK: metakaolin; ADP: abiotic depletion potential; GWP: global warming potential; CED: cumulative energy demand.

impact on global warming is comparable to that of standard concrete. The strength of this chapter is to maintain a broad definition of the functional unit of 1 m^3 of concrete with a given compressive strength in the hardened state, which allowed a comparison with a wide number of studies. The comparison between AACC is possible based on an equivalent mechanical strength taking into account the description in the Feret equation, explained in more detail in the next section. It was then possible to reanalyse a large number of published geopolymer mixes (fly ash (FA): 48 mixes; ground blast furnace slag (GBFS): 12 mixes; metakaolin (MK): 17 mixes).

McLellan *et al*. (2011) presented the variation in financial and environmental cost of geopolymers depending on the source of the materials and energy, and the mode and distance of transportation, especially for Australia. The three readily quantifiable metrics were energy (direct fuel and electricity usage), greenhouse gas emissions and cost. Transportation was taken into account at every stage of the life cycle. The functional unit was 1 kg/m^3 to compare the input of cement and geopolymer concrete. There was no information on the exact mechanical strength of the mixes and the selected ones were chosen from studies published in conference proceedings that are not necessarily easy to consult. The study highlighted the variability of the impact depending on the source of energy and the technology to produce the reagent. It provided good recommendations, which will be discussed later in this chapter.

Turner and Collins (2013) also showed that the CO_2 footprint reduction of geopolymer is less than expected when the mining, treatment and transport of raw materials and energy to manufacture the alkali activators and the curing temperature used to achieve reasonable strength are taken into account. The functional unit was defined as the CO_2 emitted to produce 1 m^3 of concrete. The calculation of the CO_2 emissions was based on the quantity of fuel combusted, the energy content and the GWP of the specific fuel, provided by Australian national guidelines. The assumptions of the study were the production of 1 m^3 of concrete with a compressive strength of 40 MPa, production of sodium hydroxide in Australia, use of sodium silicate with a weight ratio of less than 2.4 and no CO_2 offset due to carbonation. The CO_2 improvement of geopolymer as compared with OPC was only 9%. The main contributors were, in decreasing order: sodium silicate, curing, sodium hydroxide and fly ash.

Recently, based on their own CO_2 emissions procedure, Yang *et al*. (2013) found that the contribution of the binder is greater in OPC concrete, while the contribution of aggregate transportation is more critical in AAC concrete. The strength of this study is that they provided a reference OPC of three mechanical strengths (24, 40 and 70 MPa) and geopolymer mixes of the corresponding same strength, but the binder content was not consistent. They recognized that the increase of CO_2 emissions of the concrete with compressive strength was more significant in OPC concrete than AA concrete. This article supports the conclusion that the relative reduction of the CO_2 emissions by AAC as compared to OPC concrete ranged between 55 and 75%, depending on the type, concentration and dosage of the alkali activators. The CO_2 emissions were weighted according to the volume of the constituents in the mixture.

These recent LCA studies agree on the fact that the comparison between AACC

and OPC concrete requires a detailed approach. All studies were based on a functional unit of 1 m^3 of concrete. The main reference data on the sodium silicate solution referred to in the articles of Habert, McLellen and Turner remain those published in the study by Fawer *et al*. (1999). This dataset might not be representative of today's production technologies, since it is based on data provided 20 years ago. This is a critical point to resolve, because the impact of the sodium silicate solution has a significant impact on the final environmental assessment of AACC. New updated data on the environmental impact of the sodium silicate solution are therefore needed.

These recent studies also highlight different aspects: Habert shows the importance of other impact categories, Turner and Collins take into account the additional intermediate steps of processing, McLellan *et al*. consider the financial and environmental costs depending on the sources and the transport distance, and similarly Yang shows the impact of the aggregate transport. Most studies do not provide optimistic results on geopolymers as a viable alternative to cement concrete. Only the results by Yang are promising; the local transport distances are also reduced in South Korea, as compared to Australia. The alkaline activation is better optimized in its quantity in the Korean study, but the cement content of the concrete is high for the resulting compressive strength (i.e., 479 kg OPC in 1 m^3 of 40 MPa concrete). With these conflicting results, it is difficult to know how to compare concrete mixes. We must therefore go back to the theory of concrete to define a meaningful functional unit and revise the LCA methodology for alkali-activated cement and concrete.

25.3 Development of a unified method to compare alkali-activated binders with cementitious materials

A functional unit is required to compare two products. As the environmental impact of cement-based concrete is mainly by the amount of cement used, it is important to have a reliable method to calculate the amount of cement necessary to provide the same strength as the alkali-activated concrete. In this section, we will present a new method for a reliable comparison based on physical parameters controlling the concrete strength.

25.3.1 Theory on the compressive strength of cement-based concrete

In concrete technology and industry, it is known that the ingredients for a bad concrete are exactly the same as for a good concrete. It is the relative proportions that matter. Furthermore, since Feret, Bolomey or Abrams, it has been established that the compressive strength depends mainly on the water-to-cement ratio (w/c) and not so much on the specific amount of cement used in 1 m^3. The advantage of the Feret equation is that the mathematical form can be physically justified and can

be extrapolated (de Larrard, 1999). The Feret equation relates the cement content to the compressive strength:

$$f_c \approx K R_{c28} \left(\frac{V_{cement}}{V_{paste}} \right)^2 \tag{25.1}$$

where f_c is the compressive strength, K is a parameter that characterizes the aggregates quality, $R_{c_{28}}$ is the specific mechanical strength of cement (set to 52.5 MPa in this study), V_{cement} is the volume of cement and V_{paste} is the volume of paste which includes air, water and cement. Secondary order parameters have been established since then, such as the maximum paste thickness (de Larrard, 1999), but as a first approximation and due to the relative lack of detailed data on the concrete studied in the reviewed papers, this equation was selected to calculate the appropriate amount of cement needed.

25.3.2 Method description

We propose that in order to calculate the appropriate amount of cement needed to provide the same strength as the studied geopolymer, one needs to use the same amount of binder paste in both concretes (i.e., ordinary Portland cement and alkali-activated concrete). As a consequence, in Eq. (25.1), we use the compressive strength f_c and the paste volume of the geopolymer concrete. Furthermore, we need to calculate appropriate values for K relative to the standard OPC concrete formulation, preferably coming from the same studies as the alkali-activated binder. Once K is calculated, it is easy to calculate the OPC volume needed in an OPC concrete with the same amount of paste as well as the same compressive strength as the geopolymer concrete studied. Details of the procedure are given in four steps.

1. Calculate the K constant in the Feret equation according to the mix design:

$$K = \frac{f_c}{R_{c28} \left(\frac{V_c}{V_c + V_w + V_a} \right)^2} \tag{25.2}$$

where f_c is the compressive strength of the OPC concrete at 28 days, $R_{c_{28}}$ is the ISO strength of the cement at 28 days, V_c is the volume of the cement, V_w is the volume of the water and V_a is the volume of the air. The volumes are determined from the mass of the constituents and their respective density.

2. Calculate the volume of the cement equivalent to the geopolymer concrete according to:

$$V_{c_{\text{eq}}} = (1000 - V'ag) \sqrt{\frac{f'c}{K R_{c_{28}}}} \tag{25.3}$$

where $V_{c_{eq}}$ is the volume of the cement equivalent, V'_{ag} is the volume of the coarse and fine aggregates in the geopolymer concrete and f'_c is its compressive strength. K was

calculated in the previous step and $R_{c_{28}}$ is the known resistance of the cement. The term $(1000 - V_{ag})$ is actually the volume of the paste in the alkali-activated concrete.

3. Calculate the mass of cement. The mass of cement is determined according to the specific density, here taken to be 3.15.
4. Calculate the global warming potential of the equivalent concrete according to the relevant impact factors.

25.3.3 Impact factors

The Ecoinvent database v2 was the source of data for this analysis of the literature and the impact factors are given in Table 25.2. The ground blast furnace slag, fly ash and silica fume were considered as reused waste from other industries, thus the impacts were not allocated to these by-products of production and their impact was reduced to the impact of their treatment (see further details in Chen *et al.*, 2010).

Table 25.2 Global warming potential of the constituents of a standard concrete and alkali-activated concrete

Constituents of concrete	GWP (kg CO_2 eq)
Standard cement constituents	
Ordinary Portland cement (OPC)	8.44×10^{-1}
Superplasticizer	7.49×10^{-1}
Coarse aggregates	4.29×10^{-3}
Fine sand, aggregates	2.40×10^{-3}
Free water	1.55×10^{-4}
Supplementary cementitious materials	
Metakaolin	9.24×10^{-2}
Limestone filler	3.51×10^{-2}
Ground blast furnace slag	1.69×10^{-2}
Fly ash	5.26×10^{-3}
Kaolinite	2.93×10^{-3}
Silica fume	3.13×10^{-4}
Alkali-activators	
Soda powder (caustic soda)	2.24×10^{0}
Sodium silicate (2.0 WR, spray powder)	1.76×10^{0}
Sodium metasilicate pentahydrate	1.24×10^{0}
Sodium silicate (3.3 WR, 37% solids)	1.14×10^{0}
Phosphoric acid (1.2–1.6)	1.35×10^{0}
$Ca(OH)_2$ – hydraulic lime	4.16×10^{-1}

25.3.4 Results of the reanalysis of the published data

The alkali-activated concrete mixes referred to in the published LCA articles were recalculated for cement equivalent according to the Feret equation in order to test if the recalculation makes a difference to the global warming potential (GWP). The results are presented in Figure 25.2; the x-axis represents the comparison between the geopolymer concrete and the reference OPC used in the article, while the y-axis represents the comparison between the geopolymer concrete and the recalculated OPC concrete with the Feret equation. Furthermore, as a very large amount of cement used today is not 100% OPC, but rather blended cement, we draw lines representing the GWP of the current state of concrete mixes, where 30% of supplementary cementitious materials (SCM) are currently used instead of clinker (Schneider *et al*., 2011), and the GWP of the best available technology already have 50% SCM substitution for promising industrial applications, when considering that SCM have no impact (Habert and Roussel, 2009). With this figure, we see that the GWP potential calculated directly from the mix is highly correlated to the GWP calculated by our method based on cement equivalent. The choice of method does not change the results dramatically (Fig. 25.2), but our method ensures that the binder content in the mix has been optimized for its compressive strength. However, large variations between the CO_2 equivalent of the provided standard concrete mix

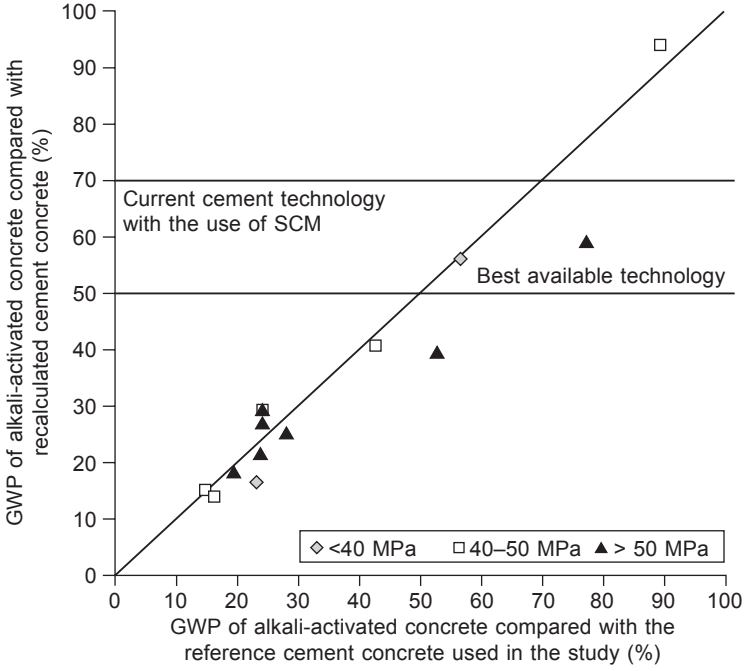

Figure 25.2 Global warming potential (GWP) according to the provided reference concrete and according to the cement equivalent calculated with the Feret equation for the geopolymer mixes referenced in the LCA articles.

and the recalculated mix according to the Feret equation can be seen in some cases, which highlights the difference between really innovative materials and a solution similar to current blended cements.

The comparison with a cement equivalent improves slightly the results published by Yang *et al*. (2013), which were already supportive of AACC. The improvement is more significant for the 40 MPa and 70 MPa concretes than for the concrete below 40 MPa. The reference 24 MPa concrete contained too much OPC. The results departed from the equivalence line and show that, using the new calculations, the geopolymer mixes are more comparable to the standard blended cement solution. The recalculation does not improve the geopolymer reported in Turner and Collins (2013), which is in fact from Sumajouw *et al*. (2007). Although Habert *et al*. (2011) reported many studies, only three had reference cements with a known mix and mechanical strength, one being Sumajouw *et al*. (2007). The comparison with cement equivalent slightly improves the results from the AACC studied in Yang *et al*. (2008). The comparison increases the impact of the AACC mixes in Collins and Sanjayan (1999).

A second part of the study consists of using this method to compare new studies on AAC that directly compare AAC with OPC, not necessarily for environmental reasons but for other scientific purposes. Over two hundred articles have been published since 2011, and we selected five recent studies because they provided the detail of the mix for the reference OPC concrete to compare with the geopolymer concrete. These studies were not specifically designed to compare the environmental performance of geopolymer and OPC concrete. The studies are first explained and then the GWP impact from the given reference and recalculated concrete are discussed.

Chi (2012) studied the effect of alkali-activated solution and curing conditions on ground blast furnace slag (GBFS). Curing room at 80% RH and temperature of 60°C improved the properties and the durability, but we considered only the curing in air because it has a lower impact and the properties were still better than a normal concrete. The paper by Law *et al*. (2012) focused on the durability of alkali-activated ground blast furnace slag (GGBS) concrete, blended concrete with GBFS as compared with OPC. The aggregates were kept constant for the total volume for all mixes. The alkali-activated slag concrete was prepared in terms of the activator modulus, $M_s = SiO_2/Na_2O$ and an activator modulus ratio of 1.0 was recommended. The article by Shi *et al*. (2012) aimed to bridge two major gaps: production of a fly ash geopolymer concrete with superior chemical and mechanical properties and recycling of aggregate (RA) to reduce the problem of construction and demolition waste disposal. The compressive strength of geopolymeric recycled concrete (GRC) was significantly higher than the corresponding recycled aggregate concrete (RAC). The addition of RA reduced the compressive strength of RAC and GRC, and the influence was greater on the GRC. Pan *et al*. (2014) studied the mechanical properties of geopolymer at and after the exposure at 550°C to test the claim that geopolymers are fire resistant. The strength of the geopolymer increases by 192% at high temperature, while the OPC shows little change. However, they both had the same residual strength after the exposure to high temperature. The article by Yusuf *et al*. (2014) investigated two locally available pozzolanic solid waste, ultrafine palm

oil fuel ash (UPOFA) and ground blast furnace slag (GBFS) to make high strength alkaline-activated strength concrete. The aggregate volume was constant.

The articles provided a detailed geopolymer concrete mix and a reference OPC concrete and it was thus possible to recalculate the cement equivalent according to the Feret equation. It was then possible to compare the geopolymer mix to the provided concrete reference and the recalculated standard concrete corresponding to the given AAC. The results, presented in Figure 25.3, show that it is possible to make geopolymer more efficient than the best available concrete technology, while a number are still competitive with the current alternatives and a few mixes would need further improvement. The scientific efforts must continue to reduce the level of alkali activation to ensure the environmental performance. We now comment on the five articles from the point of view of the GWP of the mixes to understand how to improve mix design.

The geopolymer concrete mixes presented in the article by Chi (2012) were all better than the best available technology and confirm the significant environmental improvement that can be provided by using GBFS. In the article by Law *et al.* (2012), the mix with an activator modulus of 1.0 represents an improvement, while the two others are comparable with the best technology available. This article is supportive

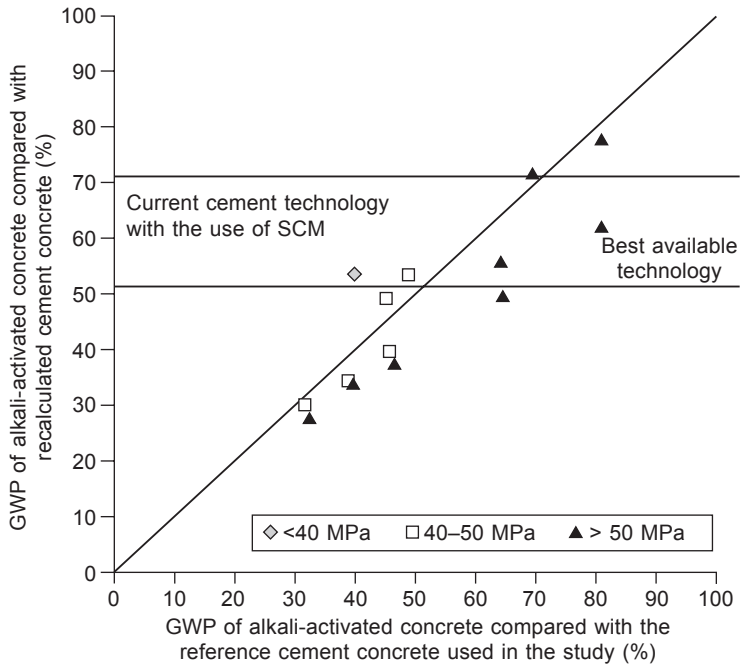

Figure 25.3 Global warming potential (GWP) according to the provided reference concrete and according to the cement equivalent calculated with the Feret equation for recent geopolymer mixes for research purposes.

of AACC and suggests that the activator modulus is effective at optimizing the activating solution. Regarding the study by Shi *et al*. (2012), the fly ash geopolymer was comparable with the current alternative available. Making the assumption that the impact of the recycled aggregate is the same as natural aggregate, the replacement did not represent an improvement. One would have to draw a system with larger boundaries including the construction industry to show the benefit of the recycled aggregate. In the study by Pan *et al*. (2014), the geopolymer was only an improvement of 30% to a traditional concrete, which is comparable to blended cement. The sodium silicate solution (spray powder) contributed to 80% of the impact. In the article by Yusuf *et al*. (2014), the higher strength alkali-activated concrete with both ultrafine palm fuel ash and ground blast furnace slag was in the range of the best alternative available. Using only the ultrafine palm fuel ash was in the range of the current blended cements. This article also shows the limit of the method proposed here. Ultrafine materials provide two improvements: compactability of granular skeleton as well as the facilitation of chemical reaction. The Feret equation (as used in our study) will be able to highlight only the chemical performance.

25.4 Discussion: implications for the life cycle assessment (LCA) methodology

With this current study and the few previous LCA studies made on geopolymer concrete, it seems clear that particular attention needs to be paid to the definition of the functional unit, the data quality and the impacts considered, in order to make an accurate environmental assessment of AACC.

25.4.1 Functional unit

This study highlights that focusing on a functional unit of 1 m^3 of concrete with a given compressive strength in the solid state is not enough to compare alkali-activated concrete to standard concrete. We show that the volume of the paste must also be the same. It does not drastically change the results, but some particular mix comparisons can appear to be much less or much more interesting than initially suggested. Another aspect that can influence the outcome of an LCA is the system boundary. Yang *et al*. (2013) provided a complete assessment considering the emissions of the materials, transport from cradle to the building site, production and curing phases. In other cases, studies have been reduced to cradle to gate. In some specific case, especially when dealing with waste valorization, a larger system boundary can be needed as one of the advantages of AAC is that inorganic waste, which would otherwise have to be landfilled, can be used. For example, while magnesium iron slags (Zosin *et al*., 1998), ferronickel slags (Komnitsas *et al*., 2007) or tungsten mine waste mud (Pacheco-Torgal *et al*., 2007) are of little or no benefit in blended cement technology, they can be used successfully as geopolymeric binders.

25.4.2 Data quality

The common result of all studies is that the sodium silicate solution is the greatest contributor to the CO_2 emissions, representing nearly half of the total emissions, while the clinker represents two-thirds of the impact for standard concrete (Figure 25.4). Furthermore, there is a consensus on the fact that the data on sodium silicate are hard to estimate. Turner and Collins (2013) found that manufacturers would not disclose the information on energy usage and emissions from their processes. Thus, most of the studies calculate the impact based on the comprehensive analysis summarized in a paper published by Fawer *et al.* (1999), which is based on the production year of 1995, 20 years ago. The process of production of sodium silicate must have improved since that time and the impacts are most probably reduced. The data on metakaolin also needs to be estimated, but it has less impact on the final result. The update on the sodium silicate data has the potential to change the outcome of the LCA of AACC.

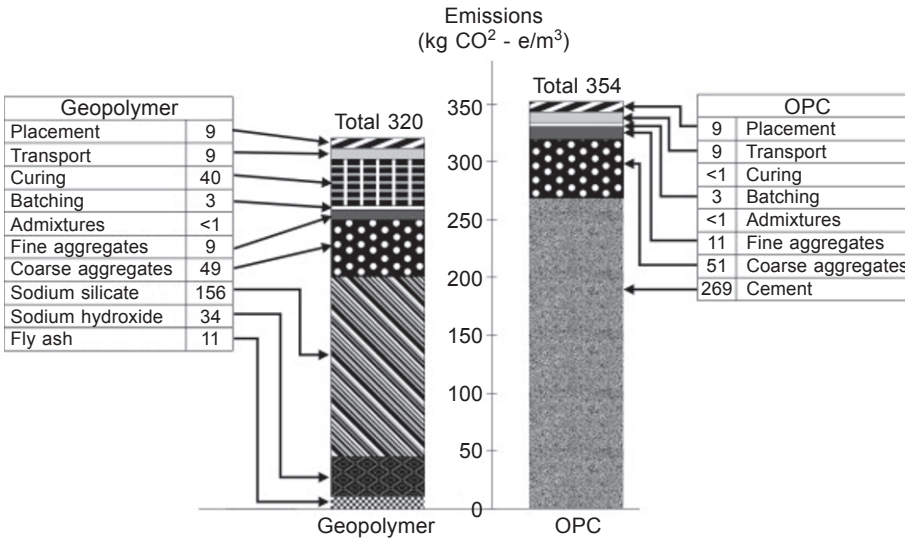

Figure 25.4 Comparison of the CO_2 emissions of concrete between a geopolymer and an OPC binder (reprinted from Turner and Collins, 2013, Copyright © 2013, with permission from Elsevier).

25.4.3 Environmental impacts

In most LCA of AACC, the only impact category is the equivalent CO_2 emissions. Comparing AACC and OPC concrete only on the basis of the equivalent carbon emission does not provide a representative picture of the global impacts. Figure 25.5 shows the environmental impact of geopolymers in the ten classic impact categories used in LCA, where 100% corresponds to the impact of OPC concrete. FA and GBFS geopolymers may be beneficial in term of GWP, but the impacts in the other

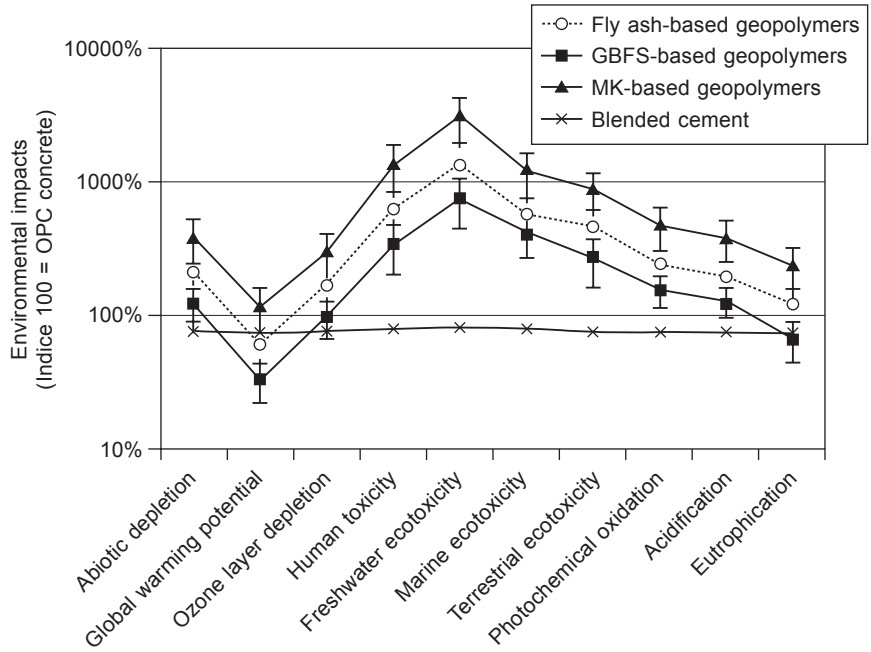

Figure 25.5 Eco-profile of different geopolymer concrete types compared to OPC-based concretes. The pure OPC concrete binder is made exclusively with CEM I, whereas current concrete binder is on average prepared with 70% CEM I and 30% mineral addition (reprinted from Habert *et al*., 2011, Copyright © 2011, with permission from Elsevier).

categories are clearly superior. It is, however, not easy with this calculation to know if the environmental impact for the other categories is of significant importance, even if it is higher than OPC concrete. For instance, we know that cement production represents more than 5% of the global anthropogenic CO_2 emissions, but what is the contribution of cement production to the acidification of the freshwater ecotoxocity? If we consider GWP as an important impact, we then need to know the impact in other categories relative to GWP.

One method used in LCA is normalization. In this method, the impacts for the different categories are normalized by dividing them by the yearly impact of an average citizen, here a European citizen. The results of this normalization are presented in Figure 25.6. For the sake of clarity, the normalized impacts are then all compared to the GWP. 100% in one impact category means, then, that the contribution of the cement production to this category is almost equal to its contribution to the GWP. Results show that geopolymers have greater impacts in the categories of abiotic depletion, freshwater toxicity and marine toxicity. So if CO_2 emissions is an important issue, these three categories of impact are even more sensitive and it becomes relevant to include them in the comparative assessment between OPC and geopolymer. It also shows that promoting geopolymers can induce a risk of pollution transfer. Since most of the impacts of the geopolymer are from the sodium silicate

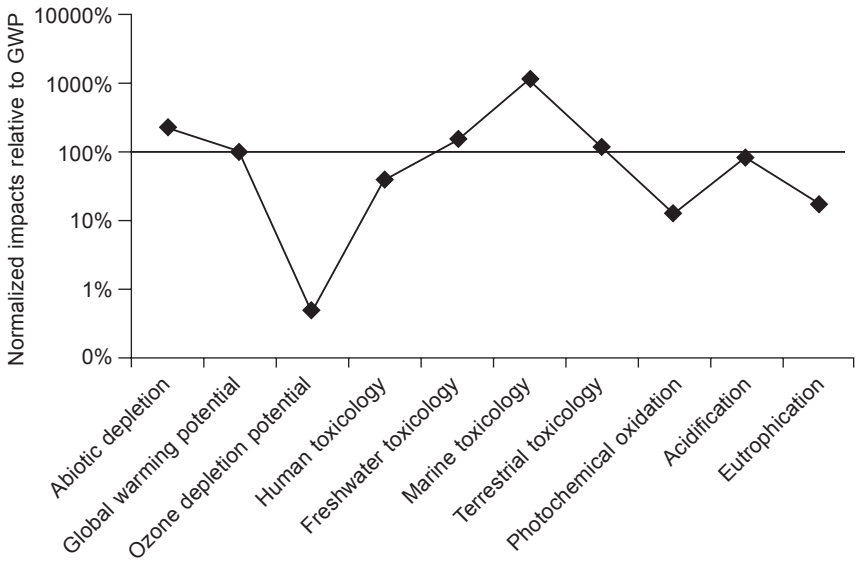

Figure 25.6 Comparative impact of geopolymers normalized by considering the impact of an average European citizen, relative to the GWP of FA geopolymer.

solution, revising the data on the sodium silicate is a priority in order to create a clear view on the life cycle assessment of alkali-activated cements and concretes.

25.5 Future trends in alkali-activated mixtures: considerations on global warming potential (GWP)

The environmental assessment could turn in favour of alkali-activated mixtures. The transport of conventional concrete is optimized, which is not yet true for geopolymers. In areas where the cement would need to be transported for a longer distance and in a future scenario where cement becomes a scarcer resource, alkali-activated mixtures can be potentially more environmentally and economically effective. As pointed out by McLellan *et al*. (2011), if more cement is imported from the production centres to the users, the debate will be in favour of geopolymers because of the reduction in greenhouse gas emissions. However, the alkali solution still needs to be optimized on a more consistent basis, as recent studies showed that it was not always the case. It is essential for the environmental performance of alkali-activated binders in other categories than global warming. The use of GBFS and FA is only interesting when waste is reused from other industries. These waste materials are not available everywhere and their production is declining in Europe and other countries.

In this section, we would like to assess in detail alkali-activated mixtures or innovations that are not considered to be mainstream and therefore do not receive

sufficient attention in many environmental impact studies, namely hybrid cements, one-part geopolymers and brick applications.

25.5.1 Hybrid cements

The first type of alternative to alkali-activated binders is the so-called hybrid cements. These cements are developed mainly by the Spanish group of Professor Palomo. The main underlying concept is that the clinker used in these binders provides a first and fast reaction that allows early strength but also provides heat to help the activation of fly ash and to quicken the polymerization reaction. To assess the environmental impact of these binders, we used the mixes detailed in Garcia-Lodeido *et al.* (2013). As they are not concrete or mortar mixes, but only paste, the proposed method developed earlier with the Feret equation cannot be applied and it needs to be adapted. Instead we used the general model for 28-day compressive strength of cement paste developed by de Larrard (1999):

$$f_{c_p} = 11.4\, R_{c_{28}} \left(\frac{V'c}{V_c + V_w + V_a} \right)^{2.85} \tag{25.4}$$

where f_{c_p} is the mechanical strength of the alkali-activated binder, $R_{c_{28}}$ is the ISO strength of the cement, V'_c is the volume of the equivalent OPC cement, V_c is the volume of the alternative alkali-activated cement, V_w is the volume of the water, V_a is the volume of the air. We solved for V'_c to find the cement equivalent. We find that the non-activated mix of OPC and fly ash represents 43% of an OPC binder. These mixes of cement and fly ash still have a 50% lower GWP than a standard cement. However, when taking into account the alkali activation, the GWP of the hybrid cement is 70% that of the OPC binder. This result is in the same range as the current blended cements. Clinker substitutions can be achieved by an improved packing optimization and a better adjuvantation, without activation. This technique of hybrid cement appears to be an interesting bridge between the classic clinker substitution technology and the still emerging alkali activation technology. It does not allow a complete breakthrough (which would be achieved with a 75% reduction rather than 50%), but it provides an opportunity for rapid practical implementation as norms can more easily be adapted for those binders than fully non-OPC binders. We note that a reduction of 75% relative to OPC is required to fulfil the objectives of the IPCC.

Ground granulated blast furnace slag (GGBFS) is the supplementary cementitious material with a lower environmental impact, as we saw in Figure 25.5. GGBFS and fly ash have been activated with a lower alkali activation. Other promising developments are the modification/improvement of an existing one such as an industrial glass waste that can be boosted in alkali activator (Kourti *et al.*, 2011) or by plasma induction (Harbec *et al.*, 2011). The next alternative is the one-part geopolymer, which involves the fabrication of an alkali activator in a solid form. It is an old project as it would considerably increase the speed of diffusion of the AAC at the construction site.

25.5.2 One-part geopolymer

This initiative is showing promising results to increase the alkali content of a feldspathic alumina-silicate melt. In fact, it is known that alkali alumina silicate melts have the lowest melting temperature, albite melt ($NaAlSi_3O_8$) being the lowest at only 700°C, compared to 1200°C for felsdpathic melt with Ca ($CaAl_2Si_2O_8$). As a consequence, making a slag of albite and sodium hydroxide in order to have a highly reactive solid product with a very high alkali content and Si and Al source fast released in the solution require much less energy than producing a Ca alumina silicate slag. This argument is proposed in a scientific paper (Feng *et al.*, 2012), but was patented earlier by nearly the same group. The patent provides very good examples of a one-part geopolymer (Zeobond Research Pty Ltd, 2007). The first example from the patent, where only 5% of alkali- and thermally activated polymerization aid was needed, is presented in Table 25.3. Aggregate is added to the binder to make concrete. To calculate the environmental impact associated with the production of this polymerization aid, we have converted the given mineral composition of the potash feldspar to 69.4% orthoclase, 29.6% albite and 1.0% anorthite. The specific heat capacities were then taken from Waples and Waples (2004), 628 J/kg/K for orthoclase, 730 J/kg/K for albite and 711 J/kg/K for anorthite and a latent heat between 250 and 450 kJ/kg was taken for the different feldspars (Tenner *et al.*, 2007). If we consider 20% heat loss in the process, our calculation shows that for 1 m^3 of one-part geopolymer, 38 MJ of energy would be needed. Using natural gas in the furnace would release 2.6 kg $CO_{2eq.}$ As a consequence, when making the calculation using Eq. (25.4), the one-part geopolymer cement contributes to less than 10% of the GWP of cement made with 100% OPC.

Table 25.3 Example of a one-part geopolymer and its cement equivalent

	Mass (kg)	GWP (kg CO_{2eq})
One part geopolymer		
Compressive strength at 28 days = 35.3 MPa		
Fly ash	621	3.3
GGBFS	621	10.5
Potash feldspar	41	0.1
Sodium hydroxide (NaOH)	25	56.0
Free water	476	0.1
Energy to activate the K-feldspar: 38 MJ		2.6
		72.6
Equivalent mix with Portland cement		
Portland cement	1167	985.0
Water	420	0.1
Fine aggregates	544	1.3
		986.4
GWP comparison with cement equivalent		7%

Since GGBFS may not be available in every country and OPC may be a reliable source of aluminosilicates for the production of alkali-activated binders, we simulated the GWP of the hybrid concrete in example 33 of the patent in Table 25.4. This is an example with the thermal activation of albite. The global warming potential of the hybrid concrete represents nearly 30% of an equivalent mix with only OPC. Recently the University of Queensland demonstrated that it was possible to build a four-storey-high building with three suspended floors made from structural geopolymer concrete (Figure 25.7). More examples with low alkali activation are needed to promote geopolymers for civil engineering applications.

Table 25.4 Example for 1 m^3 of concrete and its cement equivalent

	Mass (kg)	**GWP (kg CO_{2eq})**
Hybrid concrete		
Compressive strength at 28 days = 34.5 MPa		
OPC	243.9	205.9
Fly ash	544.8	2.9
Albite	16.3	0.0
Na_2CO_3	0.5	1.1
NaOH	4.4	9.8
Sand	813.1	2.0
Water	353.7	0.1
Energy to activate the albite: 14 MJ		1.0
		222.7
Equivalent mix with Portland cement		
OPC	905.1	763.9
Water	397.6	0.1
Sand	813.1	2.0
		766
GWP comparison with cement equivalent		29%

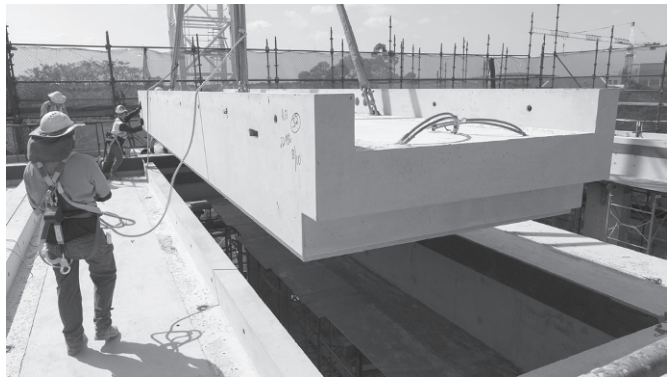

Figure 25.7 Precast slag/fly ash one-part geopolymer concrete floor part (www.wagner.com.au).

25.5.3 Brick applications

Finally, most of the studies compare AACC with conventional concrete due to its consistency and widespread use, but geopolymer could have a greater comparative advantage for other building materials. The concrete block is quite efficient since it represents only 16.0 kg CO_2 equivalent per 1 m^2 for its life cycle, while it can also reach a higher value of 76.9 kg per 1 m^2 CO_2 for self-compacting concrete floor (Base INIES, 2013; the database is in m^2). Traditional narrow-joint glued clay brick represents 26.4 kg CO_{2eq}/m^2 for its life span, while the Monomur structural brick with thermal properties represents 44.3 kg CO_{2eq}/m^2. Construction with fired brick is, however, widely used in housing construction. On this basis, we decided to assess whether alkali-activated binder mixes could be environmentally interesting for brick rather than concrete production. It is also based on the fact that early studies on geopolymer were initially proposed for brick production (Davidovics, 1983; Davidovits, 1982). To calculate the impact of a geopolymer mix for bricks, we took the mixes from Slaty *et al*. (2013) that focused on the development of alternative bricks with alkaline activation of clays instead of burning. We used the mix with lowest NaOH content reported in Slaty *et al*. (2013) (100 kg kaolinite, 50 kg sand, 8 kg NaOH and 22 kg water). We calculated the CO_2 equivalent using the impact factors in Table 25.2. We found out that the CO_2 equivalent of the mix was 234 kg CO_{2eq}/m^3, which represents 15.5 kg CO_{2eq}/m^2, when considering that 131 kg of bricks are needed per m^2. It is equivalent to the concrete block, but largely lower than the current environmental impact of fired brick (26–44 kg CO_{2eq}/m^2). Furthermore, the required strength of a brick for a wall is in the range of 5 MPa, but the evaluated geopolymer mix had a compressive strength of 13 MPa. Since the strength of the alkali activated clay is correlated with the NaOH content, it would be possible to reduce the alkali-activation and further improve the environmental assessment of geopolymer. Overall the alkali activation of clays is a good alternative to the clay burning process involved in fired brick production.

25.6 Conclusion

In this chapter, we have been able to show that a rigorous method for environmental comparison of cement and concrete mixes is needed to accurately compare emerging solutions. In fact, most of the studies compare not only the quality of the paste but also the efficiency of the granular packing which might some time lead to confusing results between studies. This is specifically the case for the LCA of geopolymers.

The method developed here, which uses the Feret equation, allows us to compare existing alkali-activated mixes as well as emerging alternatives. We have shown that the environmental impacts of the current mixes proposed in the literature are often better than cement or concrete made with 100% OPC but cannot be considered as groundbreaking techniques as they seldom achieve 75% savings.

However, we have identified so-called one-part geopolymer mixes, where the

polymerization aid represents a small part of the matrix. These binders, as well as hybrid cements, seem to have the potential to be game-changing technologies. Some mixes, even if data on their exact manufacturing process are difficult to access, seem to have only 10% of the global warming potential of cement or concrete made with 100% OPC.

25.7 Sources of further information and advice

A number of recommendations arise from this review of LCA of alkali-activated cement and concrete that are summarized in the following list.

- Think LCA to improve mix design technology, as we can see in the recent studies.
- Reduce the alkali activation of the mixes to prevent pollution transfer.
- Have a control with OPC specimen of the same volume of paste as the alkali-activated specimens to compare only the efficiency of the binder.
- Perform LCA locally, include the impact of transport, and make sure it will be possible to compare the result with other studies.
- Need objective functional comparison criteria, for example the equivalent mechanical strength and volume of binder paste.
- Compare geopolymers with other building materials than concrete, such as bricks.
- Improve the data quality at the local scale by accessing the producers as well as at the national and regional scale to improve the database inventory.
- When the data is confidential and sensitive, work with the industrial association to design procedure to collect data in a way that can benefit both the researchers and the contributing companies.

We can suggest a number of subsequent steps.

- Revise the data on the environmental impacts of the sodium silicate solution.
- Reduce the alkaline activation to improve the global environmental assessment of AACC beyond global warming potential.
- Design studies especially on the comparison between standard concrete and alkali-activated concrete with a constant volume of binder.
- Develop a rationale to include durability and service life of alkali-activated binders in the assessment.

References

Base INIES (2013) Base nationale française de référence sur les impacts environnementaux et sanitaires des produits, équipements et services pour l'évaluation de la performance des ouvrages, crée en 2004, propriétaire – gestionnaire: Association HQE. Available at: http://www.base-inies.fr/ (accessed on 15 December 2013)

Chen C, Habert G, Bouzidi Y, Jullien A, and Ventura A (2010) LCA allocation procedure used as an incitative method for waste recycling: an application to mineral additions in concrete. *Resources, Conservation and Recycling*, 54, 1231–1240.

Chi M (2012) Effects of dosage of alkali-activated solution and curing conditions on the properties and durability of alkali-activated slag concrete. *Construction and Building Materials*, 35, 240–245.

Collins F and Sanjayan JG (1999) Effects of ultra-fine materials on workability and strength of concrete containing alkali-activated slag as the binder. *Cement and Concrete Research*, 29(3), 459–462.

Davidovics M (1983) Method for manufacturing decorated, enamelled ceramic by monofiring with geopolymer silico-aluminates. International patent WO/1983/003093.

Davidovits J (1982) Utilisation des terres latéritiques dans les techniques de géopolymérisation. Actualité de la Construction de Terre en France, Plan Construction, Ministère du Logement, Paris.

Davidovits J (1991) Geopolymers. *Journal of Thermal Analysis*, 37(8), 1633–1656.

de Larrard F (1999) *Concrete Mixture Proportioning: a Scientific Approach*. London: Spon.

Deutsches Institut für Normung (DIN) (2006) Environmental management – Life cycle assessment – Requirements and guidelines (ISO 14044:2006). Deutsches Institut für Normung (DIN), Berlin.

Duxson P, Fernández-Jiménez A, Provis JL, Lukey GC, Palomo A and van Deventer JSJ (2007a) Geopolymer technology: the current state of the art. *Journal of Materials Science*, 42(9), 2917–2933.

Duxson P, Provis JL, Lukey GC and van Deventer JSJ (2007b) The role of inorganic polymer technology in the development of 'green concrete'. *Cement and Concrete Research*, 37(12), 1590–1597.

Fawer M, Concannon M and Rieber W (1999) Life cycle inventories for the production of sodium silicates. *International Journal of Life Cycle Assessment*, 4(4), 207–212.

Feng D, Provis JL and van Deventer JSJ (2012) Thermal activation of albite for the synthesis of one-part mix geopolymers. *Journal of the American Ceramic Society*, 95(2), 565–572.

Finnveden G, Hauschild MZ, Ekvall T, Guinée J, Heijungs R, Hellweg S, Koehler A, Pennington D and Suh S (2009) Recent developments in life cycle assessment. *Journal of Environmental Management*, 91(1), 1–21.

Flatt RJ (2004) Towards a prediction of superplasticized concrete rheology. *Materials and Structures*, 37(5), 289–300.

Flatt RJ, Roussel N and Cheeseman CR (2012) Concrete: an eco-material that needs to be improved. *Journal of the European Ceramic Society*, 32(11), 2787–2798.

García-Lodeiro I, Fernández-Jiménez A and Palomo A (2013) Variation in hybrid cements over time: alkaline activation of fly ash–Portland cement blends. *Cement and Concrete Research*, 52, 112–122.

Habert G (2013) A method for allocation according to the economic behaviour in the EU-ETS for by-products used in cement industry. *International Journal of Life Cycle Assessment*, 18, 113–126.

Habert G and Roussel N (2009) Study of two concrete mix-design strategies to reach carbon mitigation objectives. *Cement and Concrete Composites*, 31(6), 397–402.

Habert G, Billard C, Rossi P, Chen C and Roussel N (2010) Cement production technology improvement compared to factor 4 objectives. *Cement and Concrete Research*, 40(5), 820–826.

Habert G, d'Espinose de Lacaillerie JB and Roussel N (2011) An environmental evaluation of geopolymer based concrete production: reviewing current research trends. *Journal of Cleaner Production*, 19(11), 1229–1238.

Harbec D, Gitzhofer F and Tagnit-Hamou A (2011) Induction plasma synthesis of nanometric

spheroidized glass powder for use in cementitious materials. *Powder Technology*, 214(3), 356–364.

Huntzinger DN and Eatmon TD (2009) A life-cycle assessment of Portland cement manufacturing: comparing the traditional process with alternative technologies. *Journal of Cleaner Production*, 17(7), 668–675.

International Standard Organisation (2006) ISO 14040: Environmental management – Life cycle assessment – Principles and framework. Deutsches Institut für Normung (DIN), Berlin.

Komnitsas K, Zaharaki D and Perdikatsis V (2007) Geopolymerisation of low calcium ferronickel slags. *Journal of Materials Science*, 42, 3073–3082.

Kourti I, Devaraj AR, Guerrero Bustos A, Deegan D, Boccaccini AR and Cheeseman CR (2011) Geopolymers prepared from DC plasma treated air pollution control (APC) residues glass: properties and characterisation of the binder phase. *Journal of Hazardous Materials*, 196, 86–92.

Kovler K and Roussel N (2011) Properties of fresh and hardened concrete. *Cement and Concrete Research*, 41(7), 775–792.

Lasvaux S, Habert G, Schiopu N, Chevalier J and Peuportier B. (2014) Improvement potentials of simplified industry made EPDs database. *Journal of Cleaner Production*, accepted.

Law D, Adam A, Molyneaux T and Patnaikuni I (2012) Durability assessment of alkali activated slag (AAS) concrete. *Materials and Structures*, 45(9), 1425–1437.

McLellan BC, Williams RP, Lay J, van Riessen A and Corder GD (2011) Costs and carbon emissions for geopolymer pastes in comparison to ordinary Portland cement. *Journal of Cleaner Production*, 19(9–10), 1080–1090.

Pacheco-Torgal F, Castro-Gomes J and Jalali S (2007) Investigations about the effect of aggregates on strength and microstructure of geopolymeric mine waste mud binders. *Cement and Concrete Research*, 37, 933–941.

Pan Z, Sanjayan JG and Collins F (2014) Effect of transient creep on compressive strength of geopolymer concrete for elevated temperature exposure. *Cement and Concrete Research*, 56, 182–189.

Pennington DW, Potting J, Finnveden G, Lindeijer E, Jolliet O, Rydberg T and Rebitzer G (2004) Life cycle assessment Part 2: Current impact assessment practice. *Environment International*, 30(5), 721–739.

Purnell P (2011) Material nature versus structural nurture: the embodied carbon of fundamental structural elements. *Environmental Science & Technology*, 46(1), 454–461.

Rebitzer G, Ekvall T, Frischknecht R, Hunkeler D, Norris G, Rydberg T, Schmidt WP, Suh S, Weidema BP and Pennington DW (2004) Life cycle assessment: Part 1: Framework, goal and scope definition, inventory analysis, and applications. *Environment International*, 30(5), 701–720.

Schneider M, Romer M, Tschudin M and Bolio H (2011) Sustainable cement production – present and future. *Cement and Concrete Research*, 41(7), 642–650.

Shi XS, Collins FG, Zhao XL and Wang QY (2012) Mechanical properties and microstructure analysis of fly ash geopolymeric recycled concrete. *Journal of Hazardous Materials*, 237–238, 20–29.

Slaty F, Khoury H, Wastiels J and Rahier H (2013) Characterization of alkali activated kaolinitic clay. *Applied Clay Science* 75–76, 120–125.

Sumajouw DMJ, Hardjito D, Wallah SE and Rangan BV (2007) Fly ash-based geopolymer concrete: study of slender reinforced columns. *Journal of Materials Science*, 42(9), 3124–3130.

Szabó L, Hidalgo I, Ciscar JC and Soria A (2006) CO_2 emission trading within the

European Union and Annex B countries: the cement industry case. *Energy Policy*, 34(1), 72–87.

Tenner TJ, Lange RA and Downs RT (2007) The albite fusion curve re-examined: new experiments and the high-pressure density and compressibility of albite and NaAlSi 308 liquid. *American Mineralogist*, 92, 1573–1585.

Turner LK and Collins FG (2013) Carbon dioxide equivalent (CO_2-e) emissions: a comparison between geopolymer and OPC cement concrete. *Construction and Building Materials*, 43, 125–130.

Waples D and Waples J (2004) A review and evaluation of specific heat capacities of rocks, minerals, and subsurface fluids. Part 1: Minerals and nonporous rocks. *Natural Resources Research*, 13(2), 97–122.

Weil M, Dombrowski K and Buchwald A (2009) Life-cycle analysis of geopolymers. In Provis JL and van Deventer JSJ (eds), *Geopolymers: Structure, Processing, Properties and Industrial Applications* (pp. 194–210). Cambridge: Woodhead Publishing.

Worrell E, Bernstein L, Roy J, Price L and Harnisch J (2009) Industrial energy efficiency and climate change mitigation. *Energy Efficiency*, 2(2), 109–123.

Yammine J, Chaouche M, Guerinet M, Moranville M and Roussel N (2008) From ordinary rhelogy concrete to self-compacting concrete: a transition between frictional and hydrodynamic interactions. *Cement and Concrete Research*, 38(7), 890–896.

Yang K-H, Song J-K, Ashour AF and Lee E-T (2008) Properties of cementless mortars activated by sodium silicate. *Construction and Building Materials*, 22(9), 1981–1989.

Yang K-H, Song J-K and Song K-I (2013) Assessment of CO_2 reduction of alkali-activated concrete. *Journal of Cleaner Production*, 39, 265–272.

Yusuf MO, Megat Johari MA, Ahmad ZA and Maslehuddin M (2014) Evolution of alkaline activated ground blast furnace slag–ultrafine palm oil fuel ash based concrete. *Materials & Design*, 55, 387–393.

Zeobond Research Pty Ltd (2007) Dry mix cement composition, methods and systems involving same. European patent EP2010460 A4.

Zosin AP, Priimak TI and Avsaragov KB (1998) Geopolymer materials based on magnesia-iron slags for normalization and storage of radioactive wastes. *Atomic Energy*, 85, 510–514.

Alkali-activated concrete binders as inorganic thermal insulator materials

26

E. Prud'homme, E. Joussein, S. Rossignol
National School of Industrial Ceramics, Limoges, France

26.1 Introduction

26.1.1 Generality of porous materials

Currently, construction is subject to rising standards and increasing environmental constraints (UNSTATS, 2010) which require the development of new products, such as ecomaterials. These products are commonly used as building materials and must meet the technical criteria generally required in this area. One key driver in the development of ecomaterials is the desire to reduce greenhouse gas emissions from the manufacture of cementitious products (Allwood *et al.*, 2010). In recent years, a new class of materials known as 'geopolymers' has emerged in cement and concrete products (Khale and Chaudhary, 2007). Moreover, another field in construction is the development of insulating materials to decrease energy consumption for housing. The prohibition of certain insulators has led to the search for more efficient alternative materials. Air is a very efficient insulator with a thermal conductivity (λ) of approximately 0.026 $W.m^{-1}.K^{-1}$. The materials developed for thermal insulation are highly porous with minimal mechanical strength. Indeed, the presence of pores reduces the thermal conductivity, and thermal conductivity increases as the pore size decreases (Hinzelin, 1975) and a local structure is imposed.

There are two classes of insulators:

- conventional insulators with thermal conductivities between 10^{-3} and 10^{-1} $W.m^{-1}.K^{-1}$;
- super insulators with thermal conductivities between 10^{-5} and 10^{-3} $W.m^{-1}.K^{-1}$ (Hinzelin, 1975).

The thermal conductivities of different insulators conventionally used in construction are shown in Table 26.1 (Gallauziaux and Fedullo, 2009). Thus, the objective in the field of alkali-activated mineral materials is the development of a material with a greater thermal performance than conventional construction materials, such as aerated concrete or terracotta. That is to say, the thermal conductivity should be close to 0.070 $W.m^{-1}.K^{-1}$. This property can be obtained by the 'introduction' of a porous phase in dense materials. The combination of geopolymers and a porous phase can be very interesting for the ecofriendly production of an insulating material. The formation of porous materials based on a geopolymer matrix has already been

Handbook of Alkali-activated Cements, Mortars and Concretes. http://dx.doi.org/10.1533/9781782422884.5.687

Table 26.1 Thermal conductivity values for current insulators

Insulator	Thermal conductivity ($W.m^{-1}.K^{-1}$)
Cellular plastic materials	0.022–0.038
Mineral wool	0.032–0.040
Glass wool	0.030–0.040
Cotton wool	0.037–0.040
Wood wool	0.040–0.050
Aerated concrete	0.08–0.11
Clay brick	0.08–0.18

Source: Adapted from Gallauziaux and Fedullo, 2009.

investigated (Wu *et al.*, 2007; Barbosa and MacKenzie, 2003; Fletcher *et al.*, 2005; Bell and Kriven, 2009; Juettner *et al.*, 2007; Fernandes *et al.*, 2009) and will be discussed again later in the chapter.

26.1.2 Thermal phenomena in porous materials

According to the basic laws of thermodynamics (Meunier, 2004; Navarro, 1978), the transfer of energy can be explained by the interactions of a system with the surroundings. Three transfer modes exist within a material (Chaussin and Hilly, 1962), namely, conduction, convection and radiation. Radiation arises from the interaction between an electromagnetic wave and the material. This mode of transfer is primarily considered in solids at high temperature (Incropera and DeWitt, 2002). Convection occurs between a surface and a fluid; therefore, convection occurs in pores (Incropera and DeWitt, 2002). Finally, conduction occurs through the propagation of heat within the body under consideration. Static thermodynamics (Bruhat, 1968) also discusses the differences between macroscopic and microscopic phenomena. From a microscopic perspective, the thermal properties are related to the chemical structure of the solid and its possible porosity. From a macroscopic perspective, the organization of the pores plays a major role in thermal phenomena.

Thermal transfer principally depends on pore geometry and size but also depends on temperature. For a porous material, conduction is the primary type of thermal transfer because studies are performed at room temperature (no radiation) and convection phenomena are neglected. Indeed, convection can be considered if the thermal gradient and pores sizes are sufficient (> 4 mm) (Schulle and Schlegel, 1991; Hale, 1976). In an unsteady state and for a homogeneous and isotropic material, the equation for heat conduction is given by energy balance and Fourier's law (Eq. (26.1), with ρ, c, λ and P, respectively, as the density, specific heat, thermal conductivity and eventual formation of heat).

$$\rho c \frac{\partial T}{\partial t} - \lambda \Delta T = P \tag{26.1}$$

For a porous material, the thermal conductivity λ depends on the respective

conductivities of each phase and on the spatial organization of the phases. In fact, the influence of the pore distribution can only be neglected if there is at least a factor of 100 difference between the conductivities of the two phases (Hamilton and Crosser, 1962). Another phenomenon exists for a material with nanoscale pores, the Knudsen effect (Kennard, 1938). This effect is known for aerogel materials (Baetens *et al.*, 2011) and significantly decreases the thermal conductivity of the gas within the pores.

For alkali-activated porous materials, the pores are composed of dry air ($\lambda = 0.026$ $W.m^{-1}.K^{-1}$). Thus, the presence of pores tends to decrease the global conductivity of the material because the thermal conductivity of a dense geopolymer was estimated to be 1.0–1.2 $W.m^{-1}.K^{-1}$, depending on the alkali element used in the synthesis (Duxson *et al.*, 2006b).

26.1.3 Types of alkali-activated porous materials

The development of highly porous materials with minimal mechanical properties has become a challenge in the development of insulating materials. There are different ways to create a porous material (Studart *et al.*, 2006). Each process has a different cost and gives results with important variations in terms of the type and control of porosity. Generally speaking (Colombo, 2006), porosity results from the elimination of a compound introduced into the matrix, from the elimination of a gas introduced into a solution, or from the consolidation of a powder. In geopolymers, the second approach is generally used.

Little work has been devoted to the feasibility of producing geopolymer-synthesized foam without organic additives (Wu *et al.*, 2007; Barbosa and MacKenzie, 2003; Fletcher *et al.*, 2005). Davidovits previously mentioned the manufacture of porous materials with geopolymer skeletons through the use of blowing agents, such as hydrogen peroxide (H_2O_2) or sodium perborate ($NaBO_3$) (Davidovits, 2008a). This work led to the commercialization of foams with densities between 0.2 and 0.8 $g.cm^{-3}$, apparent thermal resistances of up to 1200°C and a minimum thermal conductivity of 0.037 $W.m^{-1}.K^{-1}$. On the same principle, Bell and Kriven (2009) explored the different ranges and types of foams obtained by the addition of H_2O_2 and aluminum powders. Recently, Vaou and Panias (2010) succeeded in reducing this value to 0.030 $W.m^{-1}.K^{-1}$ by using perlite and by making these inorganic foams competitive in terms of thermal insulation against the organic expanded polystyrene foams. Liu *et al.* (2010) synthesized aluminosilicate geopolymer foams from phosphoric acid through the addition of a small amount of aluminum metal (0.04–0.2%) as a blowing agent. These materials with varying porosities (40–85%) maintain their mechanical properties (6.5–10.5 MPa in compression) up to 1200°C. Aluminum was also used for the production of raw mineral-based, light-weight refractory materials (Juettner *et al.*, 2007). In the same way, glass foams were obtained from sheet glass cullet with dolomite or calcite as a foaming agent; the foams displayed efficient compressive strength (Fernandes *et al.*, 2009).

Among the sacrificial methods or inclusion methods, Wang *et al.* (2011) used hollow

ash cenospheres as inclusions; this approach allows the spheres to be embedded to prepare a composite at room temperature with closed spherical pores of varying sizes and with a very controllable porosity rate (15–40%). Finally, Okada *et al*. (2011) propose a novel method for the orientation of polylactic acid fibers of different sizes within a geopolymer mixture by extrusion. The fibers are then removed either by alkaline attack at pH 12, by thermal treatment (180–330°C) or by hydrothermal reaction (180°C) to create an oriented porosity. This type of porosity is interesting for its high capillarity.

Recently, interconnected ultra-macro-porosity was obtained in the alkaline-bonded matrices by exploiting the ability of pure silicon metal powder to generate H_2 in an aqueous medium (Medri *et al*., 2013; Landi *et al*., 2013). This possibility was already highlighted by Prud'homme *et al*. through the use of by-products containing free silicon from the manufacture process (Prud'homme *et al*., 2010a). The addition of silica fume to a geopolymer mixture involved modifications of the chemistry and the porosity of the sample through the formation of hydrogen during the synthesis. The inorganic foam was characteristic of a porous material in which the size could be controlled by drying and by the chemistry, in particular, the molar ratios of Si/Al and Si/K (Prud'homme *et al*., 2010a). Furthermore, this *in situ* inorganic foam was characterized as an insulating material. In this case, the foam can be synthesized from clays other than metakaolin, and potassium or sodium alkaline elements can be used to produce differences in the expansion volume and matrix network. The use of various clays (kaolin, illite or montmorillonite) for the synthesis has demonstrated similar features for all samples but has shown variability in their microstructures (Prud'homme *et al*., 2011a). This variability is caused by the possibility of the clay being altered in basic media, depending on the degree of crystallinity in the clay. Meanwhile, the use of various alkaline elements has demonstrated the formation of different networks (Prud'homme *et al*., 2011b), including a geopolymer network.

26.1.4 Primary goal of this chapter

The aim of this chapter is to highlight the fundamental role played by additives in geopolymer binders and to highlight the applicability of these binders through their intrinsic properties. The choice of different parameters (clay, blowing agents, quantities introduced and synthesis processes) allows the porosity to be controlled; therefore, the useful properties can be controlled to adapt the materials to the intended application.

This chapter will focus on the various ways to prepare foam-based alkali-activated binders, will evaluate the insulating properties of these binders, and will describe the foam formation, microstructure and porosity, and the evolution of the thermal properties as a function of the raw material and the synthesis process. Finally, this chapter will conclude with a focus on the possible use of porous geopolymer binders in wood construction.

26.2 The various ways to prepare foam-based alkali-activated binders

Porous geopolymers are generally formed through the introduction or formation of gas inside the reactive mixture. This chapter will primarily focus on the formation of foam through *in situ* gas generation.

26.2.1 Various precursors

Obtaining an alkali-activated binder with porosity is based on a geopolymer process. Thus, an alkaline solution and an aluminosilicate source are the major components to which a blowing agent is added. To control the porosity, a good knowledge of each precursor's composition, reactivity and microstructure is important.

26.2.1.1 Alkaline solution

The alkaline solution leads to siliceous species in solution, leads to alkali elements, and enables the pH value of the mixture to be controlled. Alkaline silicate solutions have already been extensively studied to determine their structure (Tognonvi *et al.*, 2010). Commercial or laboratory-made solutions (Autef *et al.*, 2012) can be used; however, commercial solutions are usually used with added hydroxide. This addition allows the solution reactivity and structure to be modified. Figure 26.1(a) presents the infrared spectrum of a commercial potassium silicate solution SiK ($3.4SiO_2;K_2O$, supplied by ChemLab (Zedelgem, Belgium), molar ratio Si/K = 1.7, density = 1.20 g.cm^{-3}, water content = 70 wt.%, and pH = 11.8). In this solution, the silicon environments are varied, and four of them can be detected by infrared spectroscopy. The bands at 1160, 1105 and 1015 cm^{-1} are attributed to the asymmetric stretching vibrations of Si-O-Si (Q^4), Si-O-Si (Q^3) and Si-O-Si (Q^2), respectively (Tognonvi *et al.*, 2010). The presence of potassium in the solution leads to the presence of a band from Si-O-K at 868 cm^{-1} (Tognonvi *et al.*, 2010) and to a solution that primarily consists of aggregated colloidal species. The addition of potassium hydroxide KOH (supplied by VWR (Leuven, Belgium), purity = 85 wt.%) to potassium silicate leads to a highly basic solution (SiK/KOH, 83.2 wt.% potassium silicate and 16.8 wt.% potassium hydroxide) and induces modifications in the ionic structure of the SiK solution because of the variation in the potassium and silicon concentrations. The comparison between the two solutions demonstrates the alteration of a significant portion of the colloids initially present in the potassium silicate and, therefore, the depolymerization of the oligomer into monomeric species. In fact, the absorbance relative to Q^4 and Q^3 is notably decreased by the addition of potassium hydroxide to the silicate solution. The band relative to Q^2 is shifted from 1015 to 980 cm^{-1}, which represents a shift of 35 cm^{-1}. Another feature is the appearance of bands at 920 and 820 cm^{-1}, which demonstrate the modification of the silicon environment by the addition of K^+ ions. These two bands can be attributed to the presence of symmetric stretches of Si-O-Si (Q^4, Q^3 or Q^2) and Si-O-M (Tognonvi *et al.*, 2010).

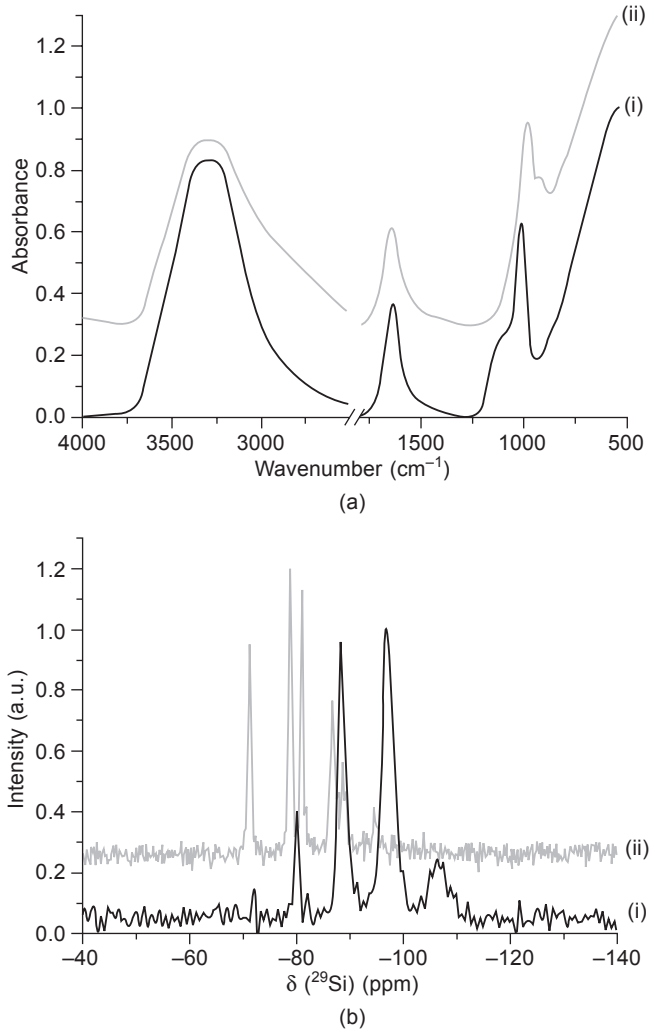

Figure 26.1 (a) Infrared spectra and (b) ^{29}Si MAS-NMR spectra of the alkaline solution (i) SiK (Si/K = 1.7) and (ii) SiK/KOH (Si/K = 0.6).

The increase of this last band is expected because of the large amount of potassium in the solution (37.1 mol.% in the SiK solution, 63.3 mol.% in the SiK/KOH solution). During the depolymerization of SiK, the number of non-bridging oxygen atoms increases, and consequently, the number of potassium ions and free silicate species is greater than that observed in SiK, which induces an increase of this band. The addition of potassium to the SiK solution induces the destruction of colloidal aggregates and the formation of monomers with a Si/K ratio of 0.6.

These results were confirmed by ^{29}Si NMR spectroscopy (Figure 26.1(b)). Only five signals (i.e., five species) were observed in the ^{29}Si NMR spectrum of the SiK

solution at –72, –80, –88, –97 and –106 ppm, which were attributed to the Q^0, Q^1, Q^2, Q^3 and Q^4 silicon species, respectively (Dietzel, 2000). The SiK solution was primarily composed of Q^2 and Q^3 species, which indicated that a condensed silicate species was present. Upon the addition of KOH pellets to form SiK/KOH, the silicate species were destabilized because of the change in pH from 11.8 to 14.0 (Dietzel, 2000). This destabilization led to increases in the intensities of bands related to the Q^0 and Q^1 species. The introduction of hydroxide yielded a solution that contained a higher amount of Q^0, which was the most reactive species (Liebau, 1985).

26.2.1.2 Silicate and aluminosilicate sources

Various silicate and aluminosilicate sources are used for the geopolymer synthesis. Commonly, the synthesis is performed from raw metakaolin material. This material is amorphous (Figure 26.2(b)) and displays easily available silicon and aluminum species. However, other studies have been devoted to geopolymer synthesis with crystalline clays. In most cases, the tests were performed with 1:1 or 2:1 types of clays, such as kaolinite, illite and montmorillonite (MacKenzie *et al.*, 2007, 2008;

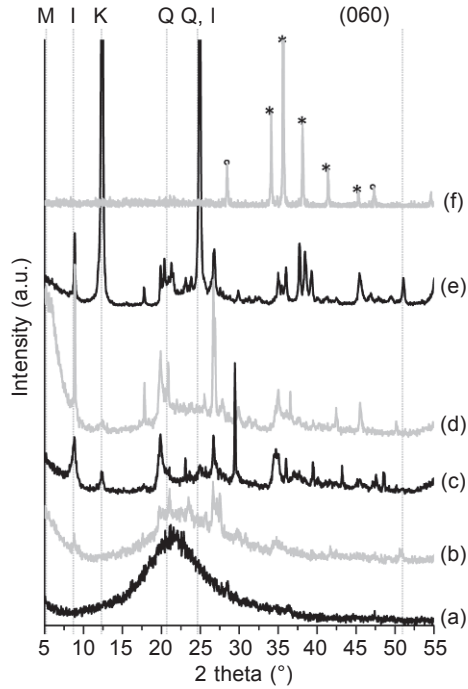

Figure 26.2 X-ray patterns of possible aluminosilicate sources for geopolymer foam synthesis: (a) silica fume, (b) metakaolin, (c) illite, (d) montmorillonite, (e) kaolinite and (f) silicon carbide (PDF files: Q: quartz (00-046-1045); I: illite (00-002-0056); M: montmorillonite (00-002-0239); K: kaolinite (01-089-6538); *: silicon carbide (04-010-5698); °: silicon (00-027-1402)).

Prud'homme *et al.*, 2011a). An example of the XRD patterns of these clays is given in Figure 26.2(b, c, d, e) and reflects the amorphous or crystalline character of each clay.

Clays are natural materials, so impurities are inevitable. For example, the mineralogical composition of the kaolin sample, determined by X-ray diffraction (Figure 26.2(e)), was kaolinite (7.14 Å peak) and illite (9.98 Å) with traces of quartz (4.26 and 3.33 Å) and feldspars (3.23–3.30 Å). The XRD data (not shown) further confirm that the kaolinite was well-crystallized according to Hinckley's criteria (Hinckley, 1963). The illite raw product (Figure 26.2(c)) was composed of illite (9.98 Å peak) with traces of kaolinite (7.14 Å) and quartz (3.33 Å).

The montmorillonite raw sample (Figure 26.2(d)) was essentially composed of montmorillonite clay, as shown by XRD (15 Å peak). Moreover, small amounts of quartz (3.33 Å) and feldspar (3.23–3.30 Å) were also observed, along with illite (9.98 Å). In each case, the (060) band at 1.49 Å is characteristic of dioctahedral clay minerals. As expected, none of the raw samples was pure. Because illite is an aluminosilicate that can react in alkaline conditions, its presence in the materials could affect the condensation reactions of the foam. However, the relative crystallinity of the illite varied from sample to sample, and illite in the montmorillonite raw sample had better crystallinity (evaluated from the FWMH/(001) peak ratio) than that in the kaolinite and illite raw samples.

The metakaolin was obtained by dehydroxylation at 700°C. The primary feature obtained by XRD measurements (Figure 26.2(b)) was from the very broad reflection between 15 and 35° (2θ), which is assigned to an amorphous phase, i.e., metakaolin here. Moreover, small amounts of quartz and feldspar were also observed, along with illite. Unfortunately, the impurities are not stable phases of metakaolin. Table 26.2 gives the chemical composition of various types of metakaolin, denoted M1, M2, and M3. All parameters are modified from one type to another, and the type and amount of impurities change, which leads to important modifications in the geopolymerization process (Prud'homme *et al.*, 2013).

Infrared spectroscopy is also an important source of information in the study of aluminosilicate materials. Figure 26.3 shows the infrared spectra of metakaolin M1, M2 and M3.

FTIR spectra are characteristic of a particular metakaolinite sample (Figure 26.3). These were previously deeply investigated by Autef *et al.* (2013). They demonstrate the presence of four νAl_2-OH vibration bands, in the OH-stretching region at 3692, 3670, 3651 and 3620 cm^{-1}, which are attributed to kaolinite and are observed for M1 and M2 (Farmer, 2000). In contrast, only two broad bands are present in the M3 samples; these bands are also attributed to a very small amount of kaolinite. This result is due to the high absorbance of kaolinite by FTIR, as reported by Joussein *et al.* (2001). These authors demonstrate the possibility of determining the amount of kaolinite in mixtures with other minerals from 8% by weight. If the metakaolin dehydroxylation process was efficient, there would be an absence of dehydroxylation phenomena near 500°C in the DTA data. The bands of SiO-stretching vibration at 1080 cm^{-1} (Figure 26.3) provide also important information on metakaolin structure (Fialips *et al.*, 2000; Frost and Vassallo, 1996). These bands are more or less defined

Table 26.2 Characteristics of the various powders used

Nature	Supplier	Characteristics			
		D_{50} (μm)	S_{BET} (m^2/g)	Chemical composition (wt%)	Si/Al
Metakaolin M1	AGS[a]	10.00	17.00	53.80 SiO_2 – 42.60 Al_2O_3 1.00 (K_2O + Na_2O) 0.90 Fe_2O_3 1.70 TiO_2	1.17
Metakaolin M2		6.09	21.50	56.10 SiO_2 – 39.60 Al_2O_3 1.00 (K_2O + Na_2O) 1.80 Fe_2O_3 1.50 TiO_2	1.19
Metakaolin M3		7.54	6.50	54.00 SiO_2 – 46.00 Al_2O_3	1.00
Silica fume	Ferropem[b]	0.40	25.00	99.00 SiO_2 – 0.72 Si^0 0.28 C^0	–
Silicon carbide waste	Rhodia[c]	1.00	–	85 SiC – 15 Si^0	–

Notes:
[a]AGS, F-17270 Clérac (France)
[b]Ferropem, 517 Avenue de la Boisse, 73025 Chambéry Cedex, France.
[c]Rhodia China, 3966 Jin Du Road, Xin Zhuang Industrial Zone, Shanghai 201108, China.

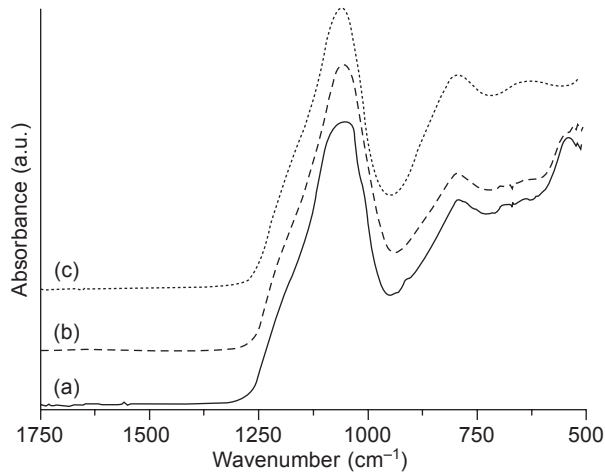

Figure 26.3 Infrared spectra from 1750 to 500 cm^{-1} of various metakaolin samples: (a) M1, (b) M2, and (c) M3.

as a function of the purity of the material. For the three examples given here, M1 metakaolin seems to be the less pure displaying a broad and less defined band at 1080 cm^{-1}. At the opposite, the M3 sample contains the lower amount of impurity

and presents well defined band, which highlights the quality of the bonds in the materials.

The most recent material used for geopolymer foam synthesis is a porogeneous agent. It can present very different natures. Two example materials will be presented for the production of foams. Indeed, these materials may either be prepared from silica fume, which is an amorphous material (Figure 26.2(a)) having free silicon (0.72 wt.%) or from sludge recovered from the silicon industry, which contains silicon carbide (85 wt.%) and silicon (15 wt.%). Unlike silica fume, this material is a crystalline material, as shown in the XRD pattern (Figure 26.2(f)). Unlike the geopolymeric matrix, which preferably forms in the presence of amorphous materials, the porosity may be obtained from materials with completely different structures.

26.2.2 Foam synthesis

Generally speaking, the formation of geopolymer foam is based on a geopolymer process (Figure 26.4). Three major types of potassium foams are investigated in more detail in this chapter. In each case, the synthesis of the silica foam begins with the formation of an alkaline solution, obtained by mixing a silicate solution and hydroxide pellets. The alkaline (denoted M) element is an important parameter in the formation of the matrix structure (Prud'homme *et al.*, 2011b, 2011c). Commonly, potassium and sodium elements are used alone or together.

The formation of this new basic solution (SiM/MOH), with a pH value of approximately 14, induces an increase in the mixture temperature. After cooling, clay and the following three ways of foam synthesis (Figure 26.4), silicon carbide

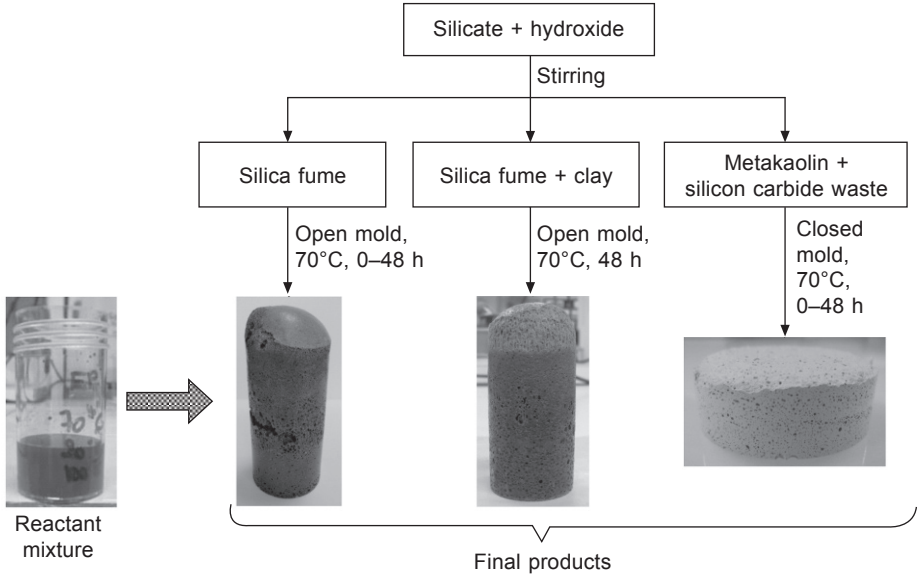

Figure 26.4 Synthesis protocol for the three types of foam.

and/or silica fume are added to this solution with the eventual additives. The mixture has a mole ratio between silicon and potassium Si/M from 1.90 to 3.30 and contains between 30 and 40 wt.% water. After stirring, this mixture is placed in a mold and in an oven at 70°C for various times from 0 to 48 hours. As shown in Figure 26.4, a significant volume expansion is observed in all the samples. Only the color changes because of the use of different raw materials in various amounts. After formation, the samples are kept at room temperature.

26.2.3 Evaluation of porosity

According to the International Glossary of Hydrology, the porosity can be defined as the property of a medium to contain pores, i.e., interstitial voids that are interconnected or not. Porosity can be expressed as the ratio of the volume of voids to the total volume of the medium. The porosity is defined both as a characteristic property of a porous medium and as a parameter that can be quantitatively expressed.

According to this definition, it is possible to represent the lack of porosity in a material as a very small cavity trapping *a priori* gaseous matter. Schoeller (1955) distinguishes two types of pores:

- open pores composed of intercommunicating voids connected to the exterior of the material;
- closed pores, isolated within the material and with no permeability.

Schoeller (1955) proposed a classification of porosity that defines a micropore (pore or matrix) to be a cavity with a diameter less than 0.1 μm and a macropore (pores or structural) to be a cavity with a diameter greater than 2.5 mm. Mesoporosities (or textural porosity or capillaries) of the interstices are of an intermediate diameter, between 0.1 μm and 2.5 mm.

The difficulty in the observation and quantification of porosity as a whole is one of the limiting factors in the study of pore formation and influence. The evaluation of open pores can be achieved through various techniques, such as mercury intrusion and helium picnometry correlated with apparent density measurements. However, only a few techniques can be used to quantify closed pores, i.e., those inaccessible to external agents (mercury, nitrogen, argon, etc.). The most common techniques are microtomography, ultrasound, chemical degradation, and image analysis.

Indeed, the microstructure of the material can be analyzed by optical or electron microscopy of raw or polished sections of the material followed by image processing. These measurements must be made on a planar surface. The preparation of samples is important in these measurements and becomes tricky for geopolymer materials. The pore size distribution is determined from the analysis of different sections of the sample at different heights by the software 'ImageJ' (National Institutes of Health, Bethesda, MD). The pore diameters are recorded based on their sizes to determine the mean diameter Γ_v (Cadle, 1965; Allen, 1981) of each section using Eq. (26.2). The average value is obtained from 300 measurements.

$$\Gamma_v = \frac{\sum_{i=0}^{n} n_i d_i^4}{\sum_{i=0}^{n} n_i d_i^3} \tag{26.2}$$

where d_i is the pore diameter of class i, and n_i/n is the ratio of the number of pores of class i to the total number of pores.

The pore diameter selected for a pore i in 2D corresponds to the equivalent diameter D_{equ} of a disc with same surface (Eq. (26.3)). The pores are circular or nearly circular 2D shapes, so this diameter is representative.

$$D_{equ} = 2 * \sqrt{\frac{S_{pi}}{\pi}} \tag{26.3}$$

where S_{pi} is the measured surface of pore i.

26.2.4 Evaluation of insulating properties

The insulating properties can be evaluated through various techniques based on the measurement of various thermal properties of the material (flash laser, hot wire, hot plan, hot tape, etc.). In this study, the focus is on measurement with a flowmeter, a flash laser and a Hot Disk.

26.2.4.1 Measurements with a flowmeter

The method here is based on Fourier's law under stable conditions:

$$\Phi = -\lambda S \frac{\mathrm{d}T}{\mathrm{d}x} \tag{26.4}$$

A thermal gradient is then imposed across a sample with a surface of 30 mm × 30 mm by applying a heat source to the top of the sample. Two heat flow sensors are used to obtain an average value of $\phi = \Phi / S$ in the sample. A thermocouple evaluates the temperature difference across the sample. The apparent thermal resistance per unit area of the sample is given by:

$$R^* = \frac{\Delta T}{\phi} \tag{26.5}$$

The thermal conductivity of the material is then given by:

$$\lambda = \frac{e_1 - e_2}{R_1^* - R_2^*} \tag{26.6}$$

where e_1 and e_2 are the thicknesses of samples 1 and 2, and R_1^* and R_2^* are the apparent thermal resistances of samples 1 and 2.

The measurements are performed with a Captec device (Captec SARL, Lille, France) on three samples to verify that the curve of R^* as a function of the thickness is approximately a straight line.

26.2.4.2 Measurements with the laser flash method

A cylindrical sample with a thickness d, which is considerably smaller than its diameter, is placed in a sample holder. One side is illuminated by pulses (on the order of one millisecond in duration) emitted by a laser, which ensures uniform heating of the sample front. The temperature of the back face is measured as a function of time with an infrared sensor. The time t needed to reach half the peak temperature at the back of the sample (relative to the oven temperature), allows the thermal diffusivity to be determined:

$$\alpha(T) = \lambda(T)/(\rho(T)*C_p\,(T)) \tag{26.7}$$

where $\lambda(T)$ is the thermal conductivity ($W.m^{-1}.K^{-1}$), $\alpha(T)$ is the thermal diffusivity ($cm^2.s^{-1}$), $\rho(T)$ is the specific weight ($g.cm^{-3}$), and $C_p(T)$ is the specific heat ($J.g^{-1}.K^{-1}$).

26.2.4.3 Measurements with a transient plane source

Thermal conductivity measurements of the foams can also be performed with the transient plane source (TPS) technique (Al-Ajlan, 2006; Gustafsson, 1991) at room temperature supplied by Hot Disk AB (Sweden). The disk-shaped TPS probe is composed of a nickel bifilar spiral sandwiched between two films of an insulating material. This probe is placed between two cylindrical samples with typical dimensions of 5 cm in diameter and 2 cm in height. The nickel wire is used to slightly heat the samples through the passage of an electrical current and to monitor the temperature increase by recording the variation of the voltage across the wire. The thermal conductivity is determined from the time-dependent temperature increase. During the experiment, the samples are considered to behave as an infinite medium. This assumption requires probing the heat penetration at a depth smaller than the available sample size. For these samples, a sensor radius of 3.189 mm and a measurement time of 20 s corresponded to a probe depth between 4 and 6 mm. A mean thermal conductivity value was determined from five measurements.

26.3 Investigation of the foam network

The synthesis of geomaterial foams relies on a geopolymer process, that is to say, on the dissolution of raw material and the restructuring of the network. The structural characteristics of the network formed will depend on the chemical elements available and, therefore, will depend on the raw materials selected. This section will therefore examine the impacts of the blowing agent when introduced in large quantities and of alkaline elements on the nature of the clays.

26.3.1 Influence of the blowing agent and alkaline element on the network

The formation of this geomaterial foam was the result of polycondensation reactions of silicon and aluminum atoms and involved the restructuring of the material. Geopolymer materials are generally amorphous, and their characterization by X-ray diffraction does not provide much information about their amorphous nature. Figure 26.5 shows the XRD pattern of the raw materials and the foam obtained from them. Here, the focus is on two geomaterial foams based on silica fume only or on silica fume and metakaolin. The two types of foams displayed an amorphous pattern with a maximum diffraction intensity of approximately 27 (°2θ). However, the diffraction pattern of metakaolin, which is an initial component of one of the synthesized geomaterials, shows some crystalline phases, such as quartz, illite and orthoclase ($KAlSi_3O_8$), which are not present in the diffraction patterns of the final products and reflect the dissolution of these raw materials. This alteration and restructuring of the materials are also demonstrated by an obvious shift in the scattering diffraction peak of each geomaterial relative to that of the raw materials. In fact, when the starting materials are activated with an alkaline solution, the scattering diffraction peak shifts from ~21 to ~27–28 (°2θ) (Figure 26.5), suggesting that the local bonding environment changes during the polymerization process and providing evidence for the dissolution of SiO_4 and AlO_4 species into the alkaline environment during the geopolymerization reaction. This mechanism could be observed in all the foam XRD patterns and corresponded to the change in composition with the introduction or lack of metakaolin. However, the maximum diffraction intensity is not the same for the different foams.

The dissolution of the raw materials can also be examined by infrared spectroscopy

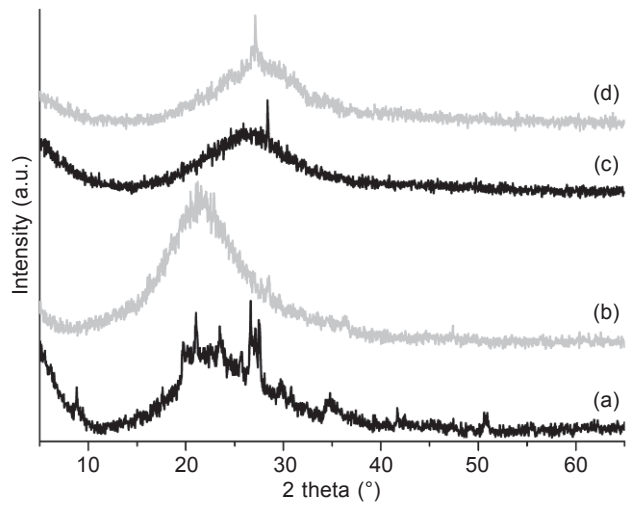

Figure 26.5 XRD patterns of (a) metakaolin and (b) silica fume and of the geomaterial foam based on (c) metakaolin and silica fume and (d) on silica fume only.

(FTIR). FTIR spectroscopy reveals the interactions of the silicate species in a material and enables the correlation of spectral variations with the variation in the alkaline elements used during the synthesis and with the use of silica fume in the initial mixture. The spectra shown in Figure 26.6 were acquired by an *in situ* technique during the formation of a potassium geopolymer and during the formation of a potassium geopolymer foam based on metakaolin and silica fume.

The bands at 3255 and 1620 cm^{-1}, respectively, were attributed to the Si-O-H bond and to the water bond (Innocenzi, 2003). The major band detected for the geomaterial was from Si-O-M bonds (Criado *et al.*, 2005; Davidovits, 2008b) (M= Si, Al, K), located in the 1100–950 cm^{-1} range. The specific positions of these peaks depend on the length and bending of the Si–O(M) bond, which explains the small shift in the main peak for the two samples after the formation process (940 cm^{-1} for geopolymer and 963 cm^{-1} for foam). The band at 1118 cm^{-1} in the foam spectra, relative to the Si-O-Si bond in the asymmetric stretching mode (Lee and van Deventer, 2003), is present as the main peak in the amorphous silica fume (Prud'homme *et al.*, 2011b). The intensity of this peak decreases during foam formation (Prud'homme *et al.*, 2010a) and becomes very weak after synthesis, reflecting local disorder and, consequently, the dissolution of the raw materials. Other peaks were located at 1200, 880, 800 and 670 cm^{-1}, corresponding to Si-O-Si in the asymmetric stretching mode (Tognonvi *et al.*, 2010; Rees *et al.*, 2007), Al-OH, Si-O-Si (Uchino *et al.*, 1989), Si-O-Al (Criado *et al.*, 2005), and O-Si-O (Koloušek *et al.*, 2007), respectively.

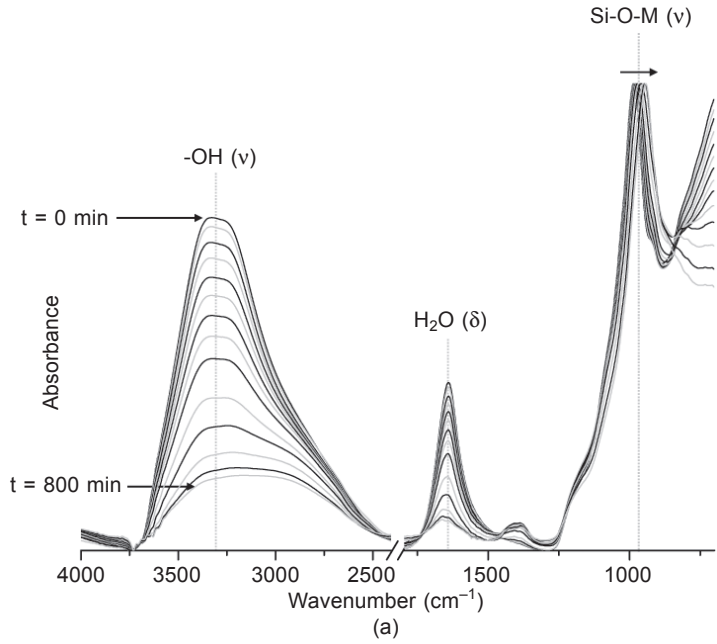

Figure 26.6 *In-situ* infrared spectroscopy (ATR mode) during the formation of (a) a potassium-based geopolymer and (b) a potassium-based foam synthesized with metakaolin and silica fume.

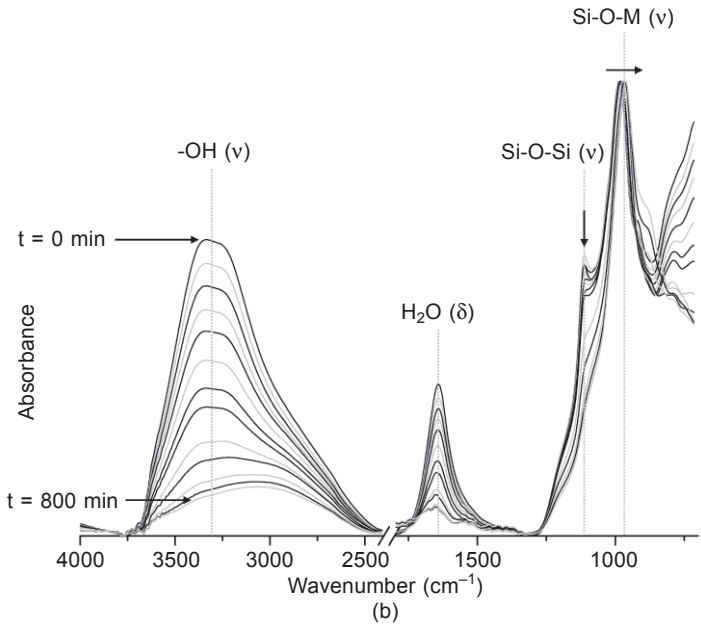

Figure 26.6 Continued

The decrease over time of the -OH bonds compared to the Si-O-Al bonds was from the increase in the polycondensation time and was characteristic of the formation of geomaterials. For geopolymer materials, the Si-O(M) (Lee and van Deventer, 2003) shifts from 979 to 946 cm^{-1}, also in agreement with the literature data, and gives evidence for the dissolution of the metakaolin species by the basic environment (Rees *et al*., 2007). For the potassium-based geopolymer, the band shifts from 986 to 943 cm^{-1} during the formation process and reflects the reorganization of the network. For the foam, the initial position of the bands is similar to that of the geopolymer. However, the magnitude of the shift is lower for the foam. This shift implies the development of two different types of networks. Moreover, the observed shift is caused by the geopolymerization process. Thus, the introduction of the silica fume may slightly inhibit geopolymerization by the creation of another network. *In situ* FTIR can reveal the competition between the development of these two skeletal frameworks.

Thus, although these foams are all based on the principle of geopolymer material formation, the introduction of a blowing agent disrupts the balance in question. Specific studies were conducted by Prud'homme *et al*. (2010a) to highlight the role of the blowing agent (silica fume) on the formation of the geopolymer network. The synthesis of such foams is derived from a geopolymer composition based on metakaolin, alkali hydroxide and an alkali silicate solution, with the addition of silica fume as the blowing agent. A quantity of gas (hydrogen gas) is produced during the chemical reaction of free silicon (as an impurity of silica fume) with water in a basic medium according to Eq. (26.8):

$$4H_2O + Si^0 \xrightarrow{\text{basic medium}} 2\overrightarrow{H_2} + Si(OH)_4 \quad (26.8)$$

The synthesized composition can be obtained with sodium or potassium. This composition was established through a stability study in solution at different pH values (Delair *et al*., 2012) that showed that the geopolymer foam does not exhibit 100% geopolymer composition. For the sodium foam, the solid skeleton is primarily made of geopolymer (56.7%) with other phases, such as SiO_2 (20.9%), $Na_2Si_2O_5$ (21.7%) and excess NaOH (0.7%). For the potassium foam, the solid skeleton consists of only 48.6% geopolymer, and the other phases present are SiO_2 (27.7%), $K_2Si_2O_5$ (18.9%), zeolite ($KAlSiO_4$, 1.5 H_2O, 4%) and excess KOH (0.8%). Based on the work of Prud'homme *et al*. (2012), the steps for the formation of the base of the geopolymer matrix M cation (K or Na) throughout the development protocol are as follows:

1. After the mixing of silicate and hydroxide: formation of monomers such as $Si(OH)_3O^-$ or $M_2Si_2O_5$ through Eq. (26.9).

$$K_4Si_7O_{18}H_4 \xrightarrow{K^+,OH^-,H_2O} 3[Si(OH)_3O^{-1}] + 2K_2Si_2O_5 \quad (26.9)$$

2. The reactive silica fume is then introduced to the mixture, and the obtained composition, based on potassium, consists of a mixture of the $K_2Si_2O_5$ compound and another nucleus of very reactive $K_2Si_4O_9$.
3. During the metakaolin addition: the dissolution of the mixture into reactive species $(Al(OH)_4^-$ and the formation of the last of the geopolymer based on the cation Na (Eq. (26.10)) and K (Eq. (26.11)) with, unlike the sodium foam, the additional creation of germs of zeolites in the foam containing potassium (Eq. (26.12)).

$$Na_2Si_2O_5 + 3[Al(OH)_4^-] \xrightarrow{K^+,OH^-,H_2O} 4[Na_{0.5}Si_{0.95}Al_{0.6}O_{4.5}H_{2.8}] \quad (26.10)$$

$$K_2Si_4O_9 + 3[Al(OH)_4^-] \xrightarrow{K^+,OH^-,H_2O} 4[K_{0.5}Si_1Al_{0.75}O_{6.85}H_{8.6}] \quad (26.11)$$

$$K_2Si_4O_9 + 3[Al(OH)_4^-] \xrightarrow{K^+,OH^-,H_2O} 2KAlSi_4, 1.5H_2O + 2Si(OH)_4 \quad (26.12)$$

4. In the specific case of the foam, an amorphous silica network is formed from excess silicate species.

The combination of all the studies of these foams can establish a pattern in the reaction mechanisms (Prud'homme *et al*., 2011b, 2011c, 2012). The formation of the *in situ* foam based on alkali-activated mixture can be divided into four separate stages. The example of the formation of a foam based on metakaolin is presented in Figure 26.7 (Prud'homme, 2011).

Initially (Zone 1), contact between the solution of potassium silicate and alkali hydroxide with the raw materials results in the dispersion of the silica fume. This material is then dissolved with metakaolin in basic medium to form free complexes of silicon and aluminum and to generate the hydrogen gas responsible for the porosity (Eq. 26.8) (Zone 2). Then, entities, which are gradually formed, are organized as small colloids. This material progressively coalesces to form a gel (Zone 3). The

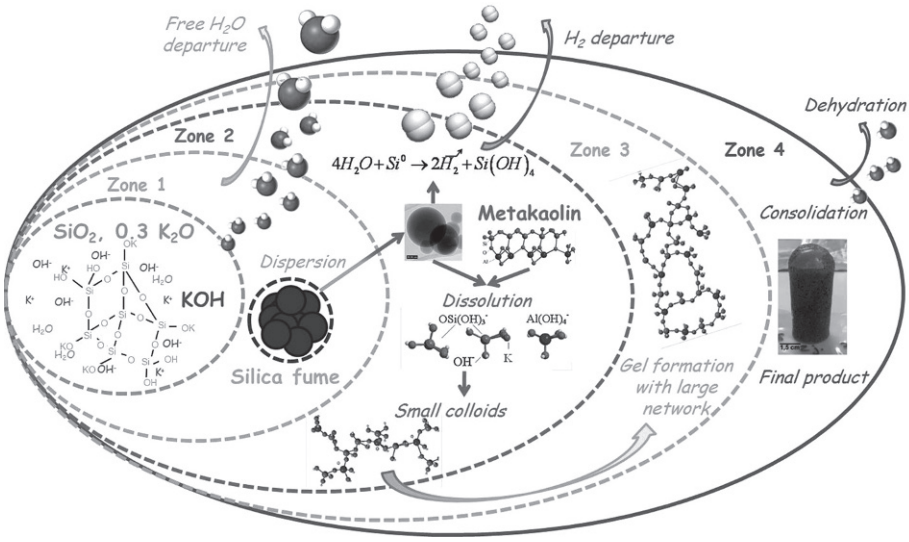

Figure 26.7 Diagram for foam formation.

viscosity of the mixture increases upon placement at 70°C, and this increase permits the retention of hydrogen in the sample and, thus, induces porosity. The excess water is finally removed by dehydration to obtain the final consolidated material (Zone 4).

26.3.2 Role of the ratio of aluminosilicate sources

Although geopolymers are considered to be eco-friendly materials, the use of metakaolin increases the energy balance. Indeed, the geopolymer synthesis is performed by calcining kaolin at temperatures of approximately 700°C. The synthesis of geopolymer-based raw clays would therefore reduce the energy balance. A large number of previous studies focused on making geopolymeric products obtained from kaolin or metakaolin as the main precursor (Barbosa and MacKenzie, 2003; Xu and van Deventer, 2002). Although 1:1 layer lattice aluminosilicates are typically used in the preparation of geopolymers, it is of interest to know if 2:1 clay minerals react similarly. In effect, the use and applications of geopolymers need to work with a large number of precursors that contain secondary minerals, which come from clay deposits. More recently, MacKenzie *et al.* (2008) have unsuccessfully tried to produce aluminosilicate inorganic polymers from a pyrophyllite, a 2:1 clay lattice, without first destroying the clay by grinding.

However, the synthesis of *in situ* inorganic foam prepared from mixtures containing K silicate, KOH solution, silica fume and various types of clays (kaolin, metakaolin, illite, and montmorillonite) can be achieved successfully (Prud'homme *et al.*, 2011a). These samples were prepared at a low temperature (60°C), and the reaction time

was very short, so only a small amount of energy was consumed. These consistent materials displayed similar features but showed variability in their microstructures. For example, Figure 26.8 shows the different microstructure that can be obtained with crystalline clays (metakaolin, kaolin, illite or montmorillonite).

No strength differences could be detected by handling the samples of the four foams formed from the various clays. All foams were cohesive and rigid solids with numerous small pores and small cracks (up to 2 mm in diameter). At first sight, all samples at low magnification appear to be similar, but more careful examination reveals significant differences in microstructure. The fracture surfaces were relatively heterogeneous and depended on the aggregate and the cementing phase, which were

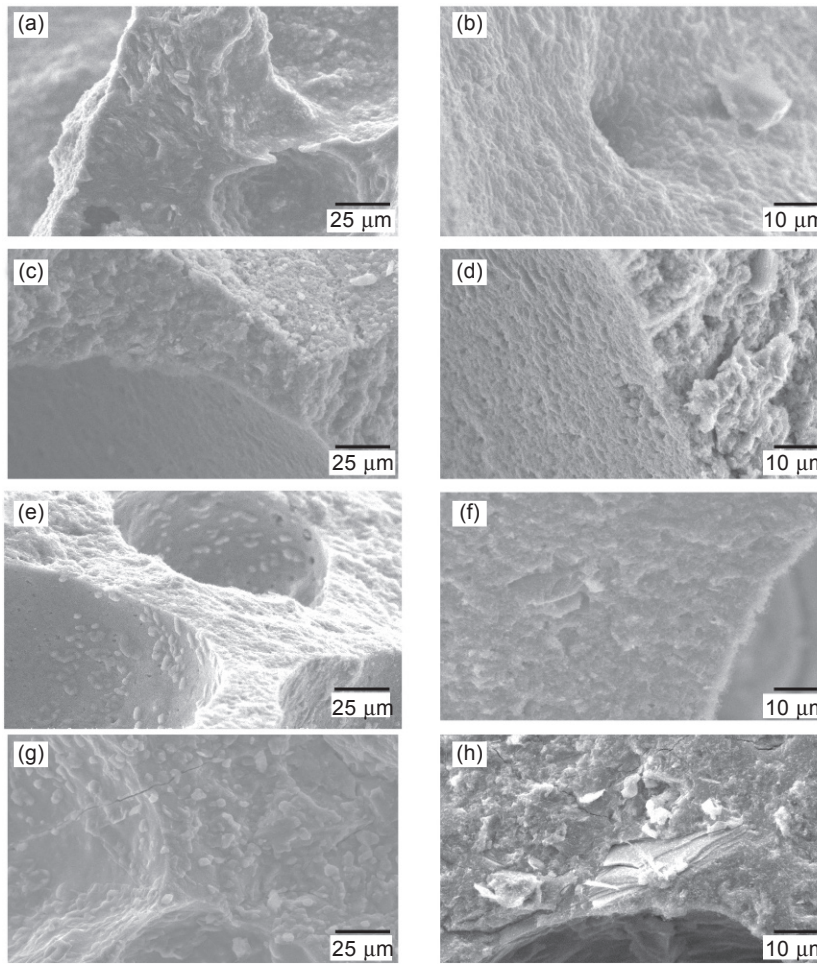

Figure 26.8 SEM observations of foam synthesized with various clays: (a, b) metakaolin, (c, d) kaolin, (e, f) illite and (g, h) montmorillonite. (reprinted from Prud'homme *et al.*, 2011a, Copyright © 2011, with permission from Elsevier).

clearly visible (Figure 26.8). For example, the surface fracture of the montmorillonite samples is clearly dominated by a large amount of aggregate. Moreover, the SEM images also clearly show textural modifications, notably on foam samples containing kaolinite, montmorillonite and illite, where blocky tactoids, which were most likely undissolved clays from their hexagonal or plate morphologies, were organized along the pores. At higher magnifications, the cementing phase and grains and/or aggregates are more visible. The presence of non-dissolved clays (e.g., Figure 26.8(h), montmorillonite micrographs) is evidenced by SEM-EDS (data not shown), as is the presence of the poorly reactive minerals, such as quartz and feldspars, in the raw products (Zibouche *et al.*, 2009). Even if secondary phases present in the raw product do not prevent a geopolymerization reaction, the reactivity of the clay used seems to play an important role in terms of the microstructure of the foams and, thus, most likely, in the mechanical behavior of each of the foams synthesized.

The alteration of the structure, which seems to be relative to the decrease in the stacking order (and then most likely to the degree of crystallinity of each clay studied), was partial for kaolinite and increased with illite, followed by montmorillonite. The results clearly showed the influence of the aluminosilicate sources, their crystallochemistry and their degree of crystallinity. Thus, the features of the materials depend on the nature of the clay types. Another parameter is the Si/Al ratio, which can influence the polycondensation reaction.

26.4 Microstructures and porosity

The thermal properties of a material are strongly dependent on the type of porosity. Indeed, the onset of the Knudsen effect or radiation phenomena depend entirely on the size of the pores (Incropera and DeWitt, 2002; Kennard, 1938). The thickness of the porous walls is also an important parameter in heat transfer phenomena. Thus, control of the size and shape of the porosity is important for the development of materials for insulation. In the case studied, porosity is obtained by gas generation, so control of porosity is principally obtained through a balance between rheology and hardening speed. Three approaches will be investigated by varying the setting time and chemical composition or by adding organic materials.

26.4.1 Setting time

To understand how porosity might be controlled by setting time, investigations were performed on samples based only on silica fume and silicate solution (Si/K = 0.6) during the drying of these samples at 70°C for 48 h. Samples were put in an oven at 70°C for different times and were then placed at ambient temperature to complete the drying time of 48 h. Nine experiments were performed by placing the silica foam mixture at 70°C for 1, 2, 3, 6, 8, 10, 16, 24 and 48 h. The density of the samples was then plotted as a function of the time at 70°C (Figure 26.9). Two types of sample can be distinguished. For a drying time less than 6 h, the density of the synthesized

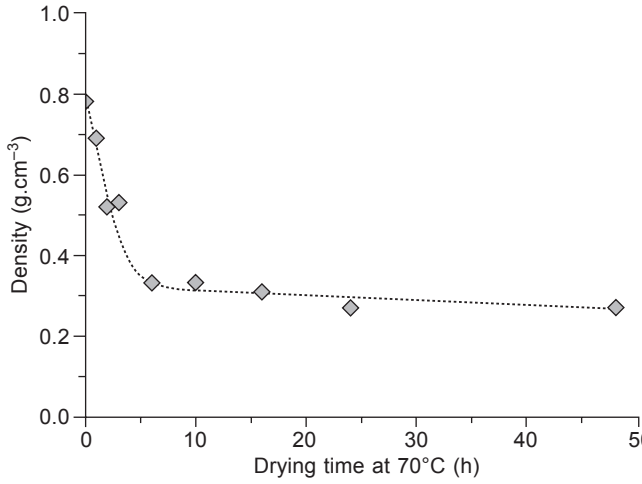

Figure 26.9 Evolution of sample density as a function of the drying time at 70°C.

sample is high, varying from 0.78 g.cm^{-3} to 0.53 g.cm^{-3}. The density of the sample evolves quickly to lower values. When the drying time at 70°C is greater than 6 h, the sample density is relatively stable with a value of 0.30 g.cm^{-3}.

Geopolymer foams show structural changes depending on the method of synthesis or on the raw materials used (Prud'homme *et al.*, 2010a; Delair *et al.*, 2012). To determine the influence of the decrease in drying time on the microstructure of materials, three samples were studied after drying times at 70°C of 1 h, 8 h or 48 h. Optical observations and electron microscope scans were made, and the pore size was measured with 'ImageJ' software to calculate the average value of the pore diameter Γ_v (see Section 26.2.3). SEM images of these samples are shown in Figure 26.10.

The sample with a time of 1 h at 70°C has a fine macroporosity (Γ_v = 0.75 mm) and homogeneous contrast to the samples with times of 8 h and 48 h at 70°C (Figure 26.10(a, c, e)), which have a wider pore distribution (Γ_v = 1.81 mm and Γ_v = 2.23 mm) and are completely heterogeneous. Indeed, the reaction kinetics is a key parameter for polycondensation reactions. The increase in the reaction time leads to a coalescence of the pores and makes them larger with heterogeneous sizes.

The thickness of the walls between the pores is also very different for the two groups of samples. This difference will have a significant impact on the thermal properties of the materials. In contrast, the samples with times of 8 h and 48 h at 70°C have many microcracks that are not visible in the photographs presented but are visually observed (Figure 26.10(d, f)). These microcracks can be explained by the presence of large stresses within the material during the removal of water.

In addition, the pore distribution is unique to each drying method. Figure 26.11 shows the different possible pore distributions. These changes will easily adapt the material to a particular application.

The example given here is for a foam synthesized from silica fume; however,

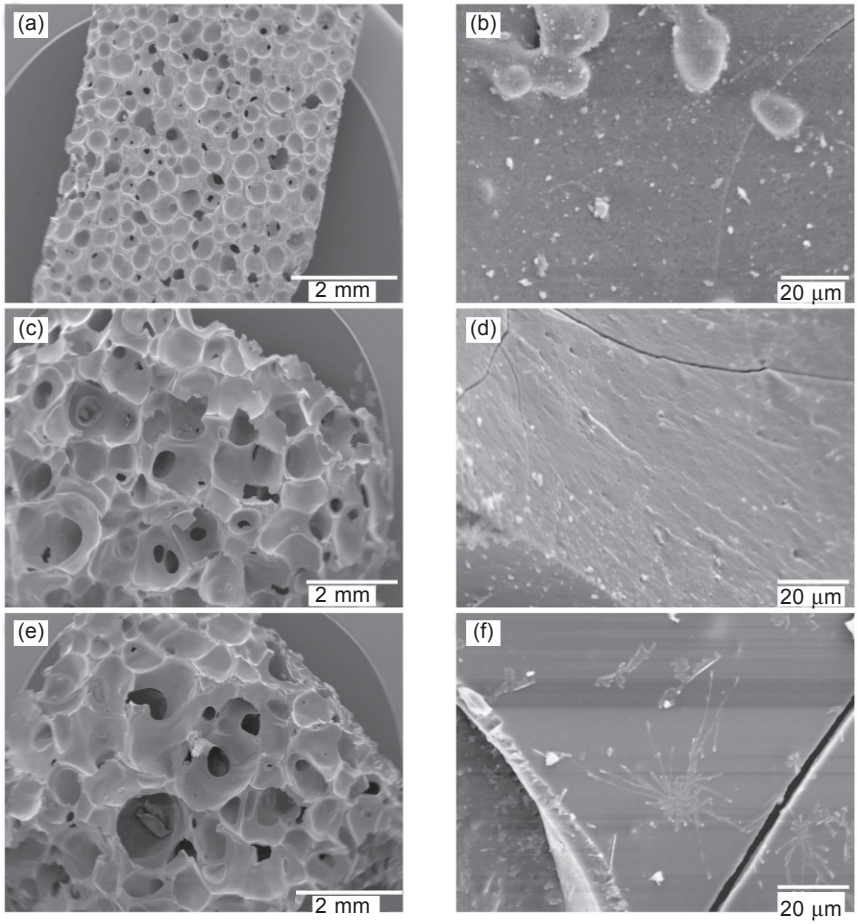

Figure 26.10 SEM images of dried samples for (a, b) 1 h, (c, d) 8 h, and (e, f) 48 h at 70°C.

control of the pore size distribution can also be obtained for geomaterial foams based on metakaolin and silica fume. Investigations here were performed for sample drying at 70°C for a period of 7 days. Only three experiments are shown in Figure 26.12, representing the removal of the sample from the mold after 6 h, 2 days and 7 days. The comparison of the pore sizes depends strongly on the time before removal from the mold. Without removal, the obtained foam displayed a large range of sizes with an average pore size of approximately 0.37 cm. Removal after 48 h involved a slight decrease in size, but the heterogeneous scale was displaced toward small pores. The smallest pore size, with a diameter of 0.13 cm, was achieved by removal of the mold after 6 h. This foam was characterized by some ladder-like structures with 0.02 cm diameter windows. We deduced that these drying conditions can be applied to some extent to control the pore size. The microstructure of the synthesized foam could be

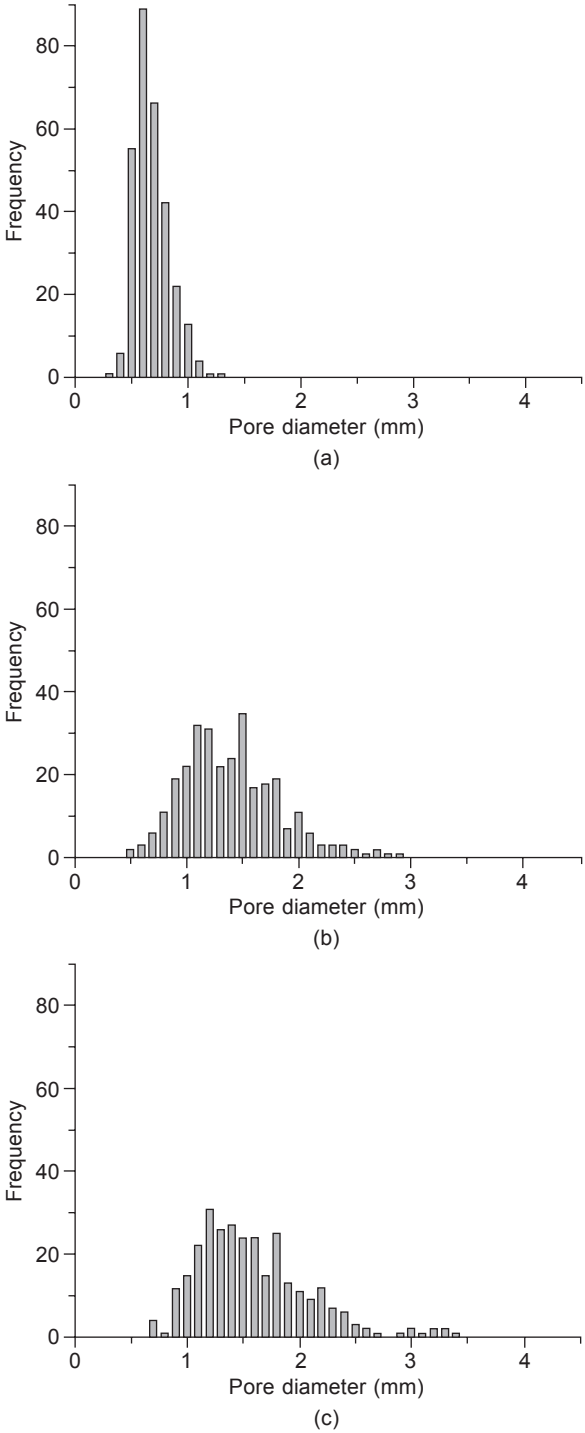

Figure 26.11 Pore size distributions for samples with a time of (a) 1 h, (b), 8 h, and (c) 48 h at 70°C.

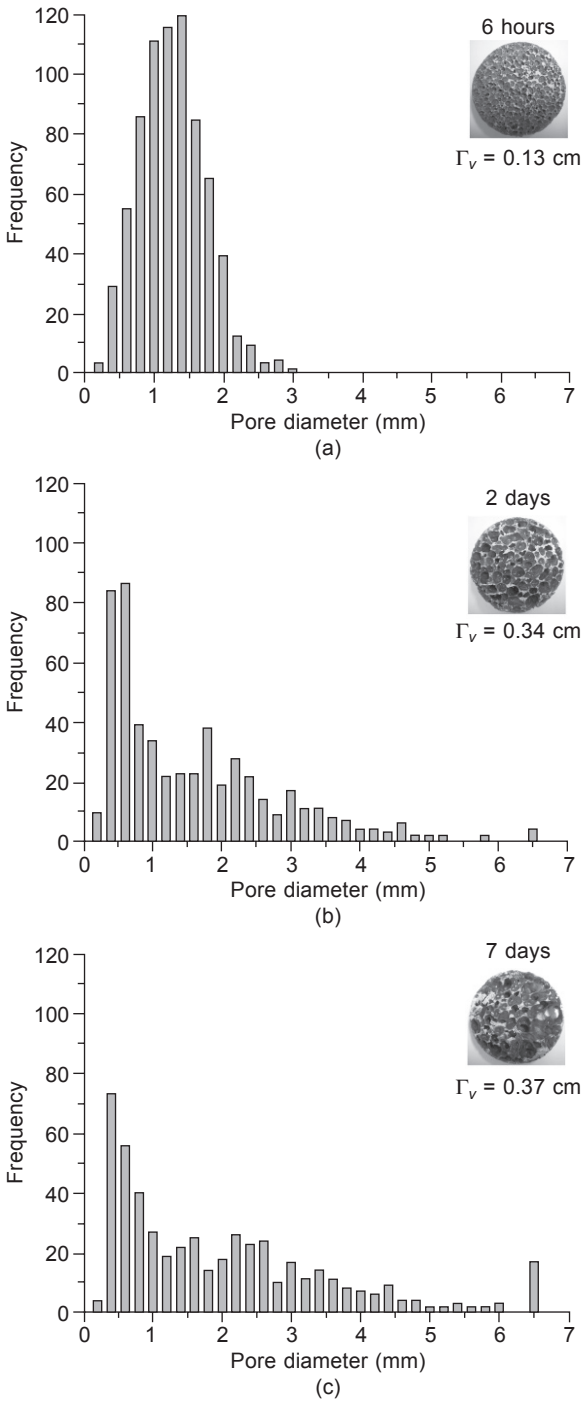

Figure 26.12 Evolution of porosity in the samples released after (a) 6 h, (b) 2 days, and (c) 7 days at 70°C.

compared to that of other metal foams (Binner *et al.*, 2009). The range in porosity from the removal at different times can also be explained by the production of a gas involving coalescence in a part of the foam, such as the foam center, as noted by Jim *et al.* (2009).

Finally, whatever the type of synthesized foams, control of the porosity is possible through the establishment of a special heat cycle during the formation of the foam. However, the parameters of these thermal cycles should be adapted to each type of product synthesized.

26.4.2 Modification of the chemical composition

26.4.2.1 Variation of the Si/Al ratio

The synthesis of the foam is highly sensitive to viscosity variation. Thus, of the various approaches to change the porosity of the material, rheological changes are one possible way. Before varying the amount of raw material, the first step is to choose a metakaolin with adequate properties. In fact, a large variety of metakaolins are available with various characteristics. The most important characteristic is the specific area, which will determine an important part of the mixture properties. For example, the use of metakaolin M1 or M2, which are mainly differentiated by their specific area (S_{BET} = 17.0 $cm^2.g^{-1}$ for M1 and S_{BET} = 21.5 $cm^2.g^{-1}$ for M2), leads to the formation of very different pastes and thus leads to the formation of very different products (Figure 26.13).

When the raw materials are fixed, a possible way to control porosity is to modify the ratio between powdered materials, i.e., metakaolin M2 here, and the blowing agent; SiC sludge is used as an example. The goal is usually to make insulation and lightweight materials. Different products can thus be initially evaluated in terms of density to be compared with each other.

The results of the density measurements of the different synthesized samples are shown in Figure 26.14 as a function of the amount of SiC sludge and metakaolin M2 introduced into the mixture. Four types of samples were synthesized with varying

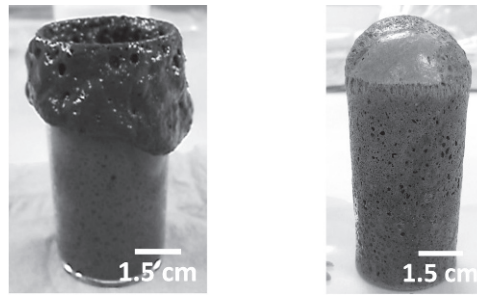

Figure 26.13 Images after the formation of foam synthesized with silica fume and (a) metakaolin M1 or (b) metakaolin M2.

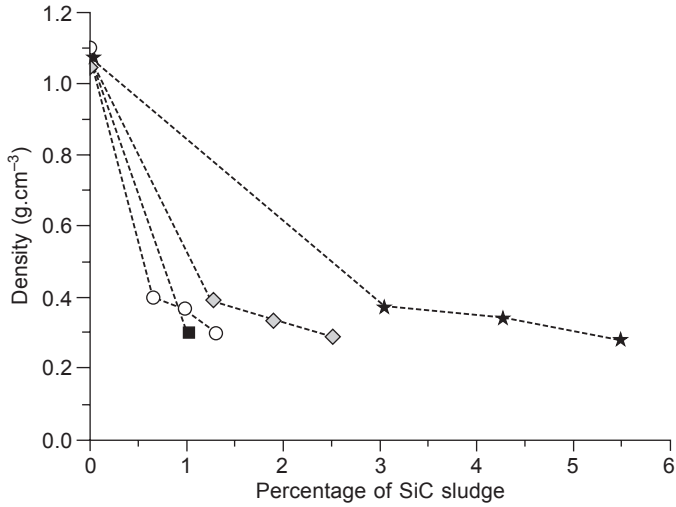

Figure 26.14 Evolution in density as a function of the amount of SiC in the mixture with (■) 37 wt.%, (○) 39 wt.%, (◇) 41 wt.%, and (★) 43 wt.% metakaolin M2.

metakaolin M2 amounts, 37 wt.%, 39 wt.%, 41 wt.% or 43 wt.%. The percentages of M2 are calculated for the global mixture composed of SiK/KOH solution (Si/K = 0.6) and metakaolin M2 and do not include the porogeneous agent. Different amounts of SiC sludge were added to the mixtures to adjust the pore volume and thus to vary the viscosity. The percentage of blowing agent added is calculated as a function of the amount of SiK/KOH and M2.

For samples containing the same amount of porogeneous agent, the sample density decreases with the amount of metakaolin. Indeed, the increase in the amount of metakaolin generates a decrease in the ratio of porogen amount/quantity of dry matter, so there is an increase in viscosity but no increase in the volume of gas produced. For a given mixture, the increase in the amount of SiC in the mixture (rich in silicon) causes a decrease in the density. For this study, the densities varied from 1.1 g.cm^{-3} to 0.27 g.cm^{-3}. This last value is low for a mineral material. Moreover, it is important to note that a density of approximately 0.3 g.cm^{-3} can be obtained for samples with various compositions. This density corresponds to samples with 37, 39, 41 and 43 wt.% metakaolin M2 added and with 1, 1.3, 2.5 and 4.5 wt.%, respectively, SiC sludge, denoted 37 wt.%(1%), 39 wt.%(1.3%), 41 wt.%(2.5%) and 43 wt.%(4.5%). Although these samples have the same density, changes in composition lead to changes in the viscosities of the mixtures and therefore cause variations in the porosity. To assess the influence of the amounts of metakaolin and sludge SiC on the microstructure, these four samples with the same density were imaged in a scanning electron microscope (Figure 26.15).

The microstructures are very different in the samples, both in terms of porosity and the appearance of the pore surfaces. The distribution in the number and size of pores seems random in the four samples. For an equivalent density, as the amount of metakaolin M2 increases, the smaller the pore size becomes (Table 26.3).

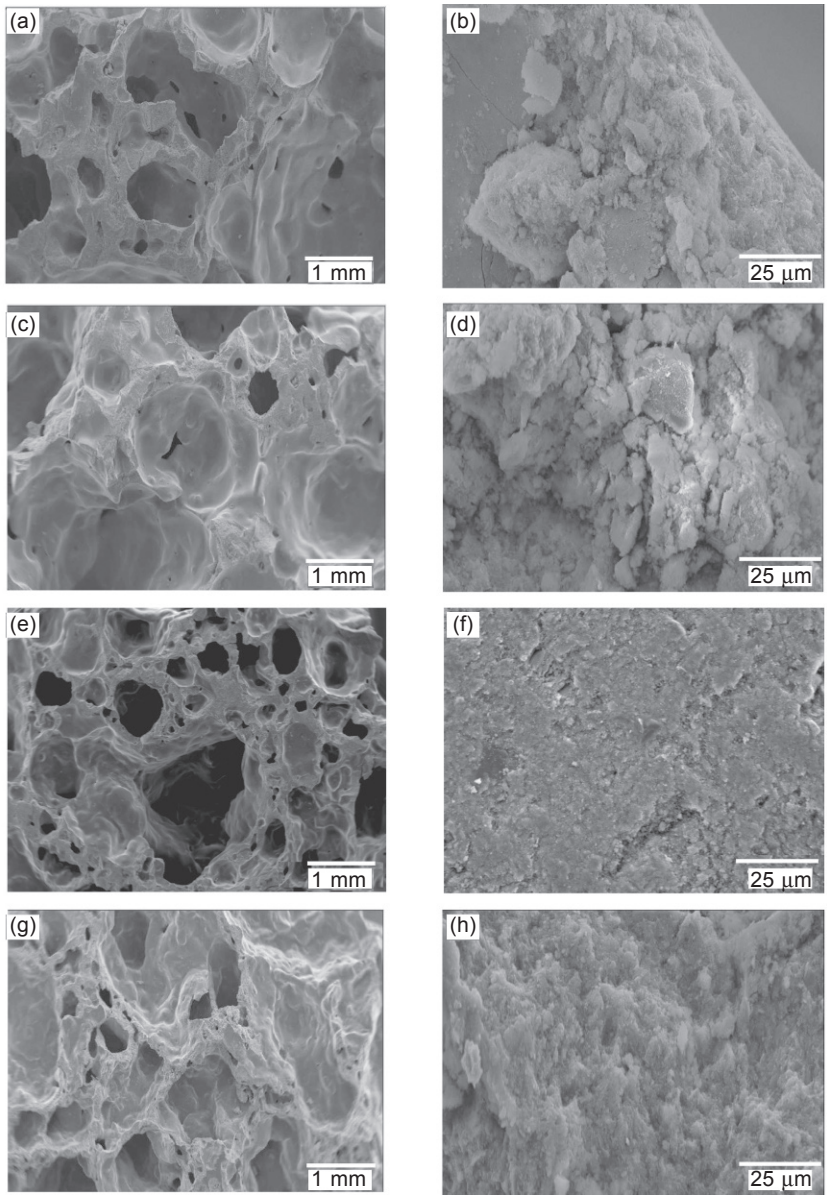

Figure 26.15 SEM images of samples with the same density based on (a, b) 37 wt.%(1%), (c, d) 39 wt.%(1.3%), (e, f) 41 wt.%(2.5%), and (g, h) 43 wt.%(4.5%) M2.

These variations in composition also affect the thickness of the walls between the pores. This parameter is important in the study of materials for insulation because the walls play a role in more or less active heat transfer. Based on these observations, the increased amount of metakaolin M2, and the simultaneous increase in the rheology

Table 26.3 Values of the mean diameter Γ_v for samples with the same density and different amounts of metakaolin (from 37 to 43 wt.%)

Sample name	37 wt.%(1%)	39 wt.%(1.3%)	41 wt.%(2.5%)	43 wt.%(4.5%)
Γ_v/mm	4.20	3.31	2.95	2.85

of the mixtures, induced the decrease in the thickness of the walls (Figure 26.15(a, c, e, g)). In a relatively fluid mixture, the bubbles will coalesce until they reach a size that is not critical and become stable. In more viscous mixtures, fewer bubbles will be able to coalesce. This effect explains the smaller pore size in mixtures with a high metakaolin content. The viscous mixture will therefore have a greater number of bubbles; thus, the distance between bubbles will be lower for an equivalent volume. The microstructure of these four materials is also very scalable. Although materials with a low intake of metakaolin have surfaces that appear powdery and poorly consolidated, materials with higher rates have a structure very similar to geopolymer materials (Figure 26.15(b, d, f, h)) (Hajimohammadi *et al.*, 2010).

26.4.2.2 Variation of the alkaline element

Geopolymer synthesis requires the use of an alkaline element, commonly sodium or potassium. This variation leads to differences in the mechanical properties (Duxson *et al.*, 2007), thermal properties (Duxson *et al.*, 2006a) and, particularly, the feasibility. This final aspect will vary significantly with the alkaline silicate solution used in the synthesis. Indeed, silicate solutions have very complex structures, which can contain dimers, linear trimers, and cyclic tetramers, among others, and their properties will depend strongly on the alkaline element used. The most striking difference between a sodium silicate solution and a potassium silicate solution is the disparity in their respective viscosities (Ingram *et al.*, 1981), which may be caused by the differing hydrations of Na^+ and K^+. This difference reflects the small concentration of free water in the sodium silicate solution relative to that in the potassium silicate solution. However, the viscosity of the initial mixture is a very important parameter for the foaming process, regardless of the foam type, and can influence the regularity, porosity, pore distribution, pores diameter, etc., of the foam structure (Song *et al.*, 2000). For *in situ* geopolymer foam formation, the viscosity increases during formation because of the reaction temperature, which causes a significant loss of water. Thus, there is a challenge in balancing foam formation, which requires a particular viscosity, with the departure of water, which increases the viscosity and hinders the development of bubbles. Investigations into the impact of the alkaline element on the microstructure have been performed by SEM (Figure 26.16). These images show significant differences in the size and porosity distribution in the three foam samples (Figure 26.16(a, c, e)).

In the presence of sodium, the porosity seems to be multiscale, whereas with potassium, this feature is less pronounced. This difference is most likely also caused by the difference in water content in each sample (30 wt.% for foam with sodium

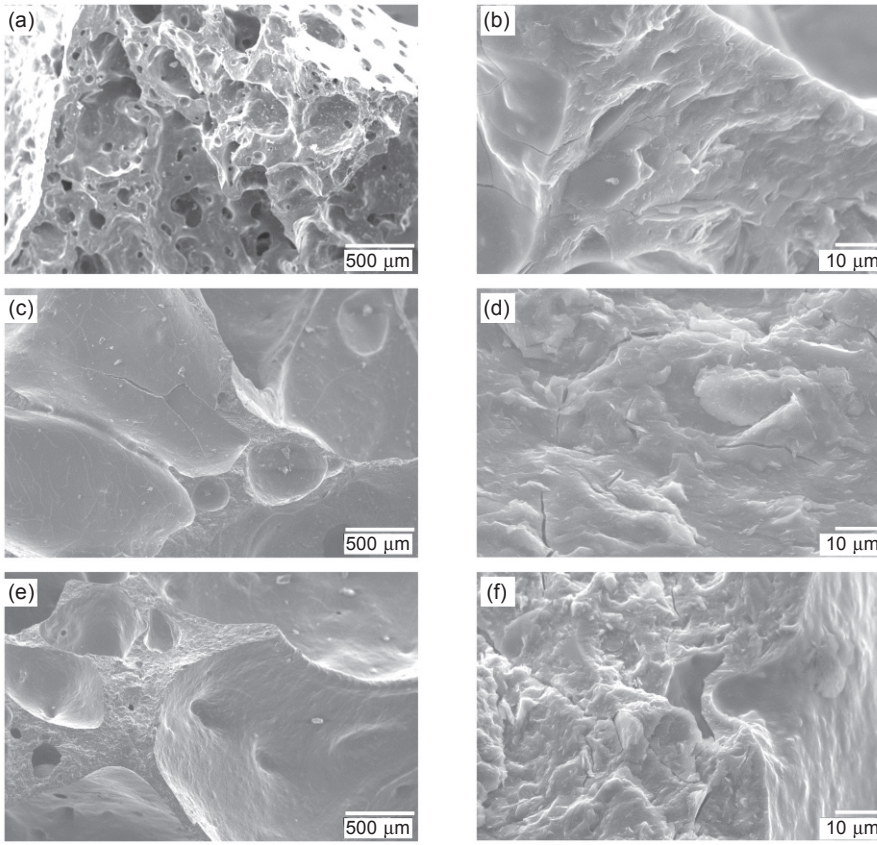

Figure 26.16 SEM images of foams with metakaolin and silica fume based on (a, b) sodium, (c, d) sodium and potassium, and (e, f) potassium (reprinted from Prud'homme *et al*., 2011b, Copyright © 2011, with permission from Elsevier).

against 37 wt.% for foam with potassium). An increase in the water content leads to a decrease in the viscosity through the dilution effect (Duxson *et al*., 2006a; Zhao *et al*., 2010), making it possible for pores to coalesce and leading to some differences in the dissolution mechanisms that create multiscale porosity. However, the bulk structure of each foam appears to be similar to that of the geopolymer material (Prud'homme *et al*., 2011b), which again provides evidence that foam formation is analogous to geopolymerization processing. Thus, the variation of the alkaline element used for the synthesis induces variations in the porosity (Duxson *et al*., 2007).

26.4.3 Ratio of porogent/aluminosilicate source

The stability of a two-phase system is a problem in many areas, ranging from the food industry to the stability of aggregates in self-compacting concrete. These areas

often respond to this problem by introducing a thickening agent. When introduced in very small quantities, these agents will increase the viscosity of the mixtures without changing the other properties, such as water reticulation, for example. Geopolymers are materials that can be modified in the same way with the added difficulty of their basicity. Indeed, organic additives are not very stable at high pH and lose their properties as thickening agents.

Different types of additives were tested in the composition of a porous geopolymer-based metakaolin and sludge SiC. For this test, three additives were selected: a rice starch, cellulose fibers and carbon fibers. The first two additives were chosen to compare elements with the same chemical compound (chain of D-glucose) but with different structures. The last additive is in the form of a fiber, such as cellulose fiber, but is rigid. The different morphologies of these three additives are presented in Figure 26.17.

These materials were added to the base reagent mixture to increase the viscosity of the mixture to obtain a finer porosity and thus a lower thermal conductivity. At first, the ability of the additives to alter the structure can be evaluated by measuring the densities of the samples obtained. Figure 26.18 illustrates the changes in the

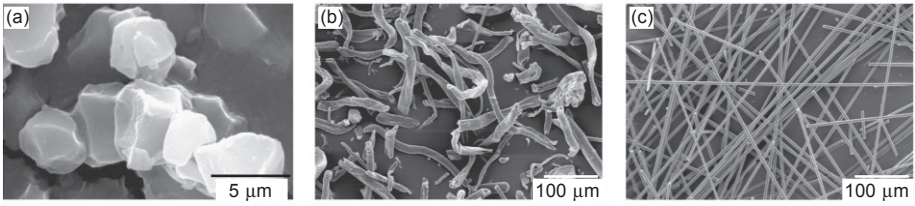

Figure 26.17 SEM images of (a) rice starch (adapted from Juste, 2008), (b) cellulose fibers, and (c) carbon fibers.

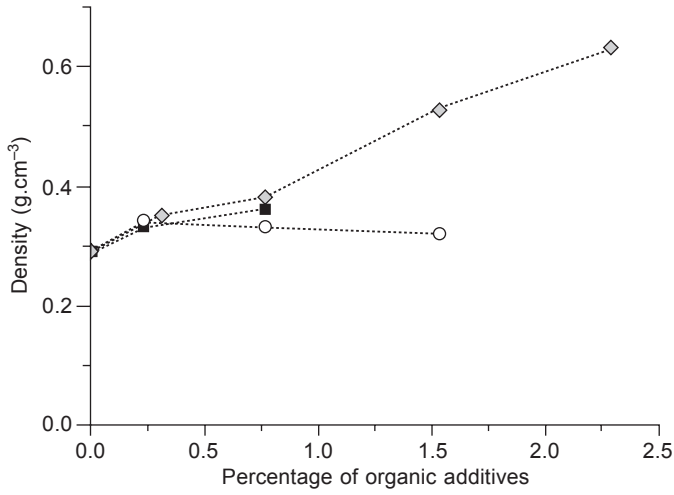

Figure 26.18 Density evolution of samples as a function of the amount of organic additives added (◇: rice starch, ○: cellulose fibers, and ■: carbon fibers).

density as a function of the amount of additive introduced. The percentage of the additives added is calculated as a function of the amount of SiK/KOH, M2 and SiC sludge.

In all cases, the maximum percentage value added corresponds to the limit for handling the mixtures. The introduction of a larger amount of additives leads to the formation of a heterogeneous dough and the formation of a completely heterogeneous material in terms of composition and porosity. The maximum input value is very low for materials based on carbon fibers because the rigid fibers quickly impede the flow of the material during mixing. Because they are small and almost spherical, rice starch particles are most easily introduced into the matrix. The introduction of rice starch and carbon fibers induces an increase in the density of the samples, whereas the introduction of cellulose fibers has little influence.

A study of the microstructure of the samples has been performed to assess the impact of this increase on the material microstructure (Figure 26.19). The foam without added aluminosilicate has less microporosity than the others (Figure 26.19(b, d, f, h)). In addition, the sample containing rice starch has the most developed microporosity (Figure 26.19(c, d)). This microporosity may be caused by the significant increase in the viscosity of the reaction mixture, which inhibits bubble coalescence and produces a fine porosity. Samples containing carbon fibers (Figure 26.19(e, f)) and cellulose fibers (Figure 26.19(g, h)) have a structure similar to that of the basic sample microstructure.

The addition of carbon fibers could have an effect on the mechanical properties of the samples based on the properties of the fibers.

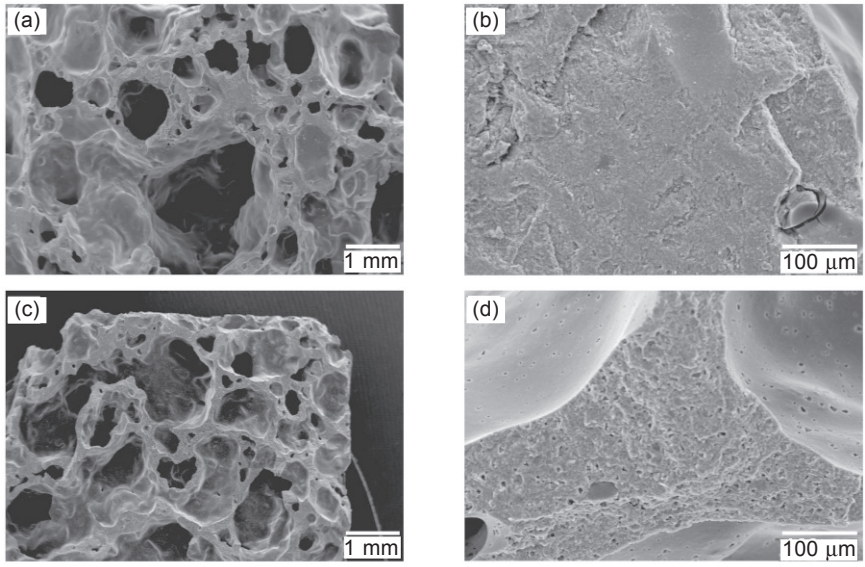

Figure 26.19 SEM images of porous materials (a, b) without additives, (c, d) with 0.77 wt.% rice starch, (e, f) with 0.77 wt.% carbon fibers, and (g, h) with 0.77 wt.% cellulose fibers.

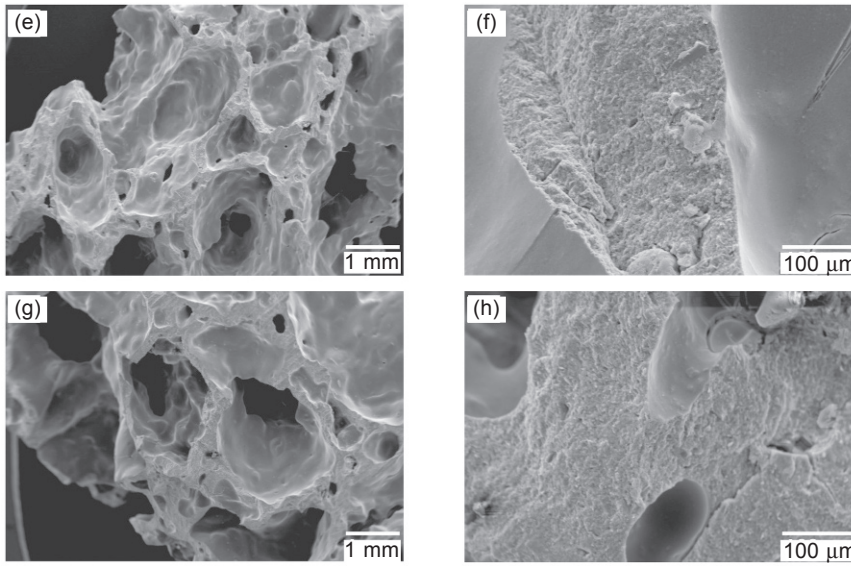

Figure 26.19 Continued

26.5 Thermal properties

Insulation plays a key role in reducing energy consumption and in creating a space for a healthy and comfortable life. Today, there are a large number of insulators. Each insulator is characterized by a set of well-defined physical properties that make it possible both to compare the insulators and determine their most appropriate application. We can describe two types of properties:

- static characteristics, such as thermal conductivity (λ), thermal resistance (R), the coefficient of surface transmittance (U), heat capacity (ρC) and permeability to water vapor (μ),
- dynamic thermal effusivity characteristics, such as thermal diffusivity (a) and (E) that characterize the behavior of a material based on its reaction time.

For thermal insulation, the primary parameter is the thermal conductivity. There are several techniques to measure this property. For example, the thermal conductivity of the samples was evaluated with a Hot Disk. The thermal conductivity of a material depends on the specific heat capacity and thus on the composition of the material. Figure 26.20 shows the change in the thermal conductivity of different materials based on metakaolin and SiC sludge as a function of the density of the material. This representation is valid because the aluminosilicate foams studied have very similar compositions. The value of the heat capacity is not expected to vary.

In general, the thermal conductivity of the samples increases with the density, which is normal because the pores act as thermal insulation (Henon *et al.*, 2012). For samples without additives and only composed of metakaolin, SiK/KOH solutions and a small amount of SiC sludge, the density of the material is a fundamental characteristic for its performance as thermal insulation. Indeed, as the density

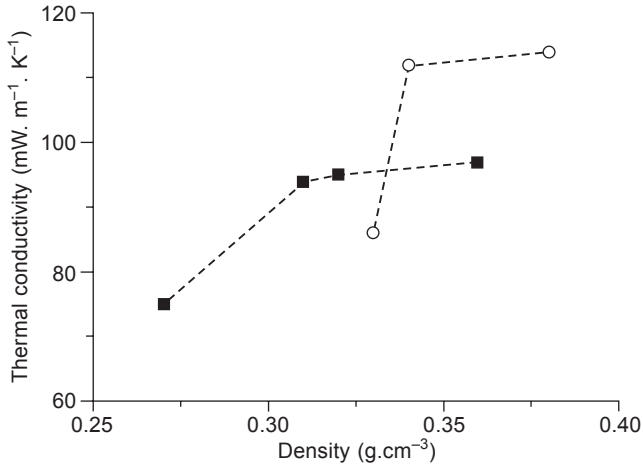

Figure 26.20 Thermal conductivity of samples based on metakaolin and sludge (○) with or (■) without additives.

increases, the conductivity increases. The conductivity even seems to move toward a value that could be attributed to the thermal conductivity of the solid skeleton. A lower value of 0.075 W.m^{-1}.K^{-1} can be reached for a material with a low density of 0.27 g.cm^{-3}. These characteristics are very good for a mineral material, which always displays non-negligible resistance to manipulation. The mechanical properties of the material have not been evaluated because of the high complexity of testing brittle porous materials. Samples containing additives are based on compositions with a lower value (density and thermal conductivity). Whatever the addition, there is an increase in the density, which is a disadvantage for thermal insulation. However, the addition of carbon fibers leads to a decrease in the thermal conductivity compared to sample with the same density.

These values ultimately show that different thermal conductivities can be obtained at similar densities. This difference can be explained by the variation in chemical composition and/or pore size distribution. Because of the H_2 production in the reaction mechanism involved in the formation of the materials, it is not possible to prepare monolithic materials with the same compositions as the foams. However, an estimate can be made with a model that includes the effect of porosity. A porous solid can be compared to a two-phase system composed of the solid skeleton and air. Collishaw and Evans (1994) have reviewed different analytical expressions describing the effective thermal conductivity of a porous solid as a function of pore volume fraction. In each case, there is a geometrical simplification of the microstructure based on the spatial distribution of the phases. Two standard models can be considered that describe the thermal conductivity of a porous solid (Bourret *et al.*, 2012). For open porosity, Landauer's effective medium expression has given close agreement to experimental data for alumina ceramics up to pore volume fractions of 0.6; however, significant differences between the theory and experiment are observed for higher pore volume fractions (Nait-Ali *et al.*, 2007; Kamseu *et al.*, 2012). For the present

set of samples, the approach would tend to overestimate the thermal conductivity of the solid phase. Given the cellular nature of the microstructures, shown in Figure 26.21, a model describing the effect of closed porosity on thermal conductivity seems more appropriate.

As a first approach, Maxwell–Eucken's expression can be used to predict the thermal conductivity of a solid containing unconnected spherical pores (Maxwell, 1892). This can be re-expressed in terms of λ_s, the calculated solid phase conductivity (Eq. (26.13)).

$$\lambda_s = \frac{\lambda_{eff}(2+v_p) - \lambda_p(1+2v_p)}{4(1-v_p)} + \frac{\sqrt{[\lambda_p(1+2v_p) - \lambda_{eff}(2+v_p)]^2 + 8\lambda_{eff}\lambda_p(1-v_p)^2}}{4(1-v_p)} \quad (26.13)$$

where λ_{eff} is the foam thermal conductivity, λ_p is the thermal conductivity of the pore phase, and v_p is the pore volume fraction. As a second approach, to include the pore size distribution, the thermal conductivity of the solid skeleton is calculated in two steps. The material is considered to be a system of two phases: large isolated pores (> 0.1 mm) and a pseudo-phase of the solid skeleton and a connected network of smaller pores (< 0.1 mm). The thermal conductivity of the pseudo phase (λ_2) is first calculated through the Maxwell–Eucken approach using Eq. (26.13). Then, to remove the influence of the interconnected smaller pores (< 0.1 mm) from the value of λ_2, a new value λ'_s corresponding to the thermal conductivity of the solid skeleton is determined from Landauer's expression (Hashin and Shtrikman, 1962). This approach is re-expressed in Eq. (26.14):

$$\lambda_{s'} = \frac{2\lambda_2^2 - \lambda_2\lambda_p(3v_{p'} - 1)}{\lambda_p + \lambda_2(2 - 3v_{p'})} \quad (26.14)$$

where λ_2 is the thermal conductivity of the pseudo phase and $v_{p'}$ is the relative pore volume fraction of the smaller pores (< 0.1 mm) in the pseudo-phase. The calculated values are generally larger than the single-step Maxwell–Eucken values. In fact, the

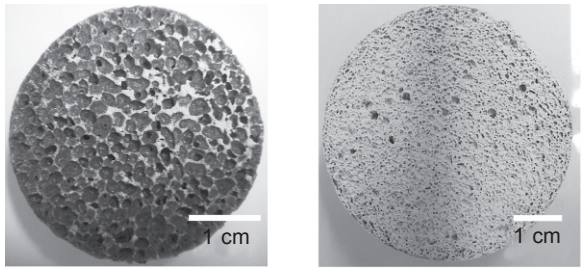

Figure 26.21 Images of macroporosity in (a) silica fume-based foam and (b) SiC sludge-based foam.

bimodal pore size distribution leads to a noticeable decrease in the effective thermal conductivity of these materials.

These theoretical models can be used to assess the potential and limits of different approaches for the preparation of thermal insulators. Knowledge of the solid phase thermal conductivity and the pore size distribution are therefore key input parameters (Nait-Ali *et al.*, 2006).

26.6 Possible use of a porous geopolymer binder

26.6.1 Formation of a composite with geopolymer foam and wood

Because of its insulating properties, foam application has been investigated as an interface (glue, mortar, etc.) in building construction. In this work, the preparation of various composite materials based on the junction of this geopolymer foam and wood was attempted (Prud'homme *et al.*, 2010b). First, the biocompatibility between wood and the mineral compound was investigated on a chemical basis through pH-dependent decomposition analysis, thermal analysis, and scanning electron microscopy (SEM). We subsequently examined the mechanical properties of the composite with embedding tests to observe interfacial shear behavior (Figure 26.22). Evidence from

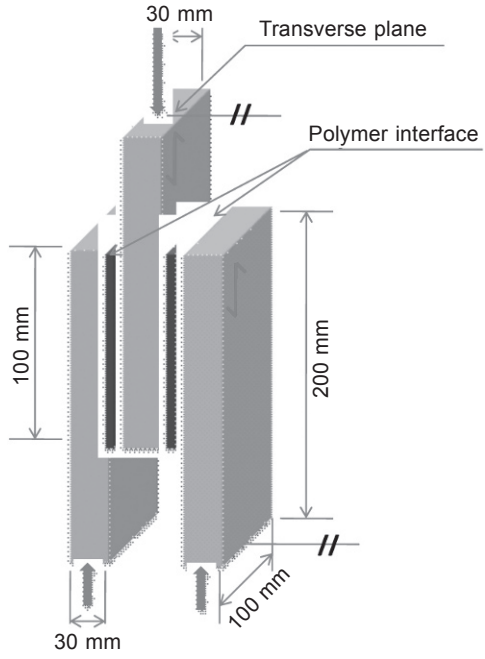

Figure 26.22 Composite specimen for testing mechanical properties in double shear (reprinted from Prud'homme *et al.*, 2010b, Copyright © 2010 The American Ceramic Society. All rights reserved).

the durability tests suggests hydric transfer occurs in the interfacial material. To identify possible chemical interactions between the wood and foam, X-ray mapping at the interface was performed (Figure 26.23).

Additionally, chemical analysis of the wood ash revealed the presence of K, Si, Na, O and C, as expected (Etiegni and Campbell, 1991). The X-ray mapping results revealed high levels of inorganic elements, such as Al, Si, O and K, in the foam. The strong signal corresponding to potassium observed from wood can be explained by the diffusion of these ions across the wood–foam interface. Indeed, we have previously observed that potassium can migrate easily as potassium hydrogen carbonate through hydration effects.

Figure 26.24(a) shows the load–displacement records from the embedding tests. Two types of sample were tested: one with a foam layer and another with an industrial glue layer. The shear failure stress is approximately 1.3 MPa for the wood/foam composite and 2.4 MPa for the industrial glue/wood composite. Although the foam/wood composite displays a lower shear failure stress, this mechanical strength is sufficient for composite-containing inorganic materials. In addition, the inorganic foam has interesting adherent properties. SEM measurements (Figure 26.24(b)) provide evidence that the mechanical failure from shear stress occurs in the foam itself and not at the interface. This result exemplifies both the brittle behavior of the foam and the strong adherence of the foam to the wood substrate.

We have demonstrated the development of an insulating geomaterial composite composed of wood and *in situ* inorganic foam that can be synthesized at low temperature and with low energy consumption. The interaction between foam and

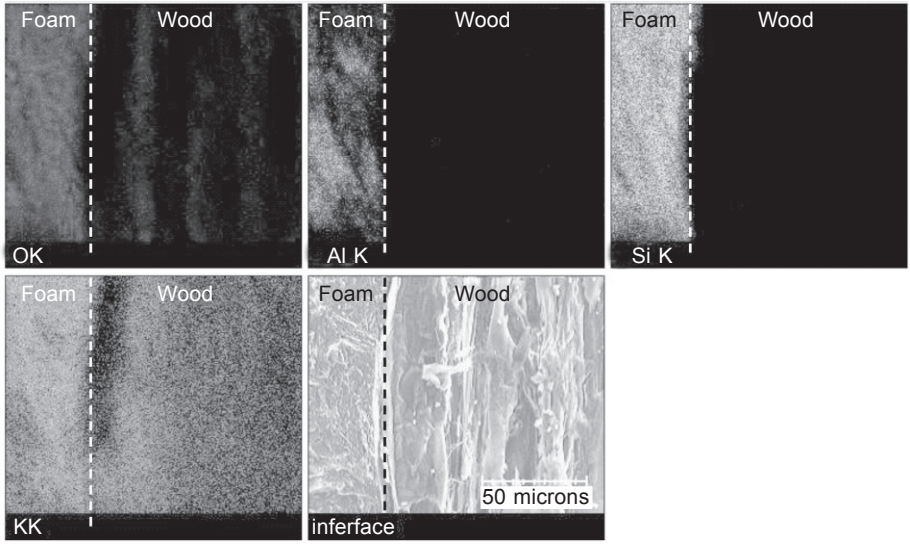

Figure 26.23 X-ray mapping of oxygen, aluminum, silicon, and potassium at the interface between wood and foam (reprinted from Prud'homme *et al*., 2010b, Copyright © 2010 The American Ceramic Society. All rights reserved).

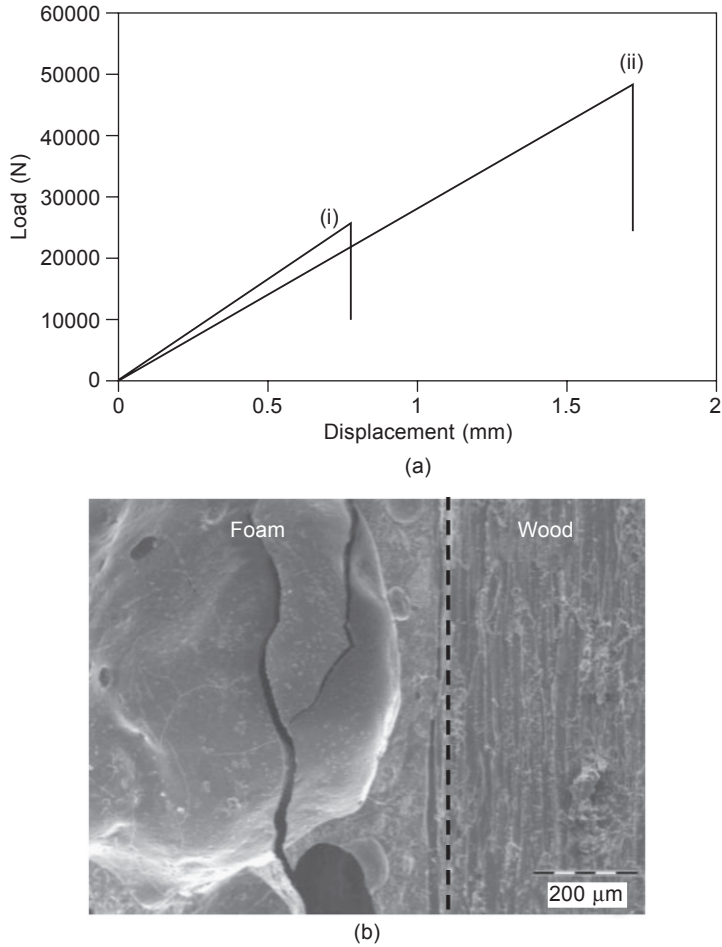

Figure 26.24 (a) Mechanical behavior of samples with (i) composite and (ii) wood glue layers tested in double-shear; (b) SEM image of the break (reprinted from Prud'homme *et al*., 2010b, Copyright © 2010 The American Ceramic Society. All rights reserved).

wood leads to the formation of an interface with desirable mechanical properties. The material also allowed us to consider its use in construction.

26.6.2 Use of a porous geopolymer binder: construction of a wall

To validate the feasibility of this building system, a wall was constructed. This full-scale test wall is exceptional and includes construction approaches based on composites of wood and mud brick. The construction of a wall, very different from a laboratory approach, was not easy and lasted three weeks. The test wall is an

internal wall timber frame; the filling is made of earth bricks. The wall consists of three compartments delimited by brick wood stiffeners.

First, the wooden frame enclosing the brick filling was built. The chamber is large, and the filling of the frame was performed at the time the frame was built. Two types of mortars were used, a geopolymer mortar with sand (Gouny *et al.*, 2012) to make the interface between the wood and the bricks and a traditional brick mortar between the bricks. The latter formulation was chosen to limit the shrinkage during drying. Figure 26.25 shows a picture of the wooden frame and the wall construction.

The porous geopolymer binder 'standard foam' shows strong adhesion with the mud brick and the wood, but its viscosity is too low to be easily implemented. A mortar was obtained by adding aggregates, such as sand, to increase the viscosity of the foam. From a reaction standpoint, the particle size and the nature of these aggregates influenced the kinetics of the reaction, the nature of the bonds formed and the compressive strength of the mortar. Regarding the performance of the wall, the tests showed that the wall was able to adsorb a large amount of water in a relatively short time, thereby controlling the relative humidity of the room. Moisture is initially quickly adsorbed on the surface and then gradually spreads throughout the thickness of the wall.

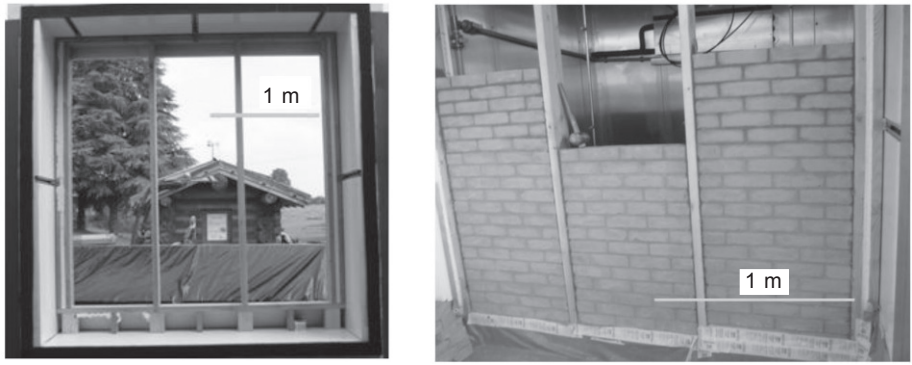

Figure 26.25 (a) Wood wall framing in carriage; (b) building wall placed in the double wall.

26.7 Summary

This work sought to determine the various geopolymeric materials by investigating various samples synthesized from various types of alkali silicate solutions and powders. Porous potassium-based geopolymers with a mutli-scale porosity were synthesized with efficient properties. An application of these porous materials permits us to describe and to understand the phenomena that occur between a geopolymer binder and structural materials, such as mud brick and wood, and also to identify the effect of siliceous species on the binder consolidation.

References

Al-Ajlan, S. (2006) 'Measurements of thermal properties of insulation materials by using transient plane source technique', *Appl Therm Eng*, 26 (17–18), 2184–2191.

Allen, T. (1981) *Particle Size Measurement*, London, Chapman and Hall.

Allwood, J.M., Cullen, J.M. and Milford, R.L. (2010) 'Options for achieving a 50% cut in industrial carbon emissions by 2050', *Environ Sci Technol*, 44 (6), 1888–1894.

Autef, A., Joussein, E., Gasgnier, G. and Rossignol, S. (2012) 'Role of the silica source on the geopolymerization rate', *J Non-Cryst Solids*, 358 (21), 2886–2893.

Autef, A., Joussein, E., Poulesquen, A., Gasgnier, G., Pronier, S., Sobrados, I., Sanz, J. and Rossignol, S. (2013) 'Influence of metakaolin purities on potassium geopolymer formulation: the existence of several networks', *J Colloids and Interface Sci*, 408, 43–53.

Baetens, R., Jelle, B.P. and Gustavsen, A. (2011) 'Aerogel insulation for building applications: a state of the art review', *Energy and Buildings*, 43 (4), 761–769.

Barbosa, V. and MacKenzie, K.J.D. (2003) 'Synthesis and thermal behaviour of potassium sialate geopolymers', *Mater Lett*, 57, 1477–1482.

Bell, J.L. and Kriven, W.M. (2009) 'Preparation of ceramic foams from metakaolin-based geopolymer gels', *Ceram Eng Sci Proc*, 29 (10), 97–112.

Binner, J., Chang, H. and Higginson, R. (2009) 'Processing of ceramic metal interpenetrating composites', *J Eur Ceram Soc*, 29, 837–842.

Bourret, J., Prud'homme, E., Rossignol, S. and Smith D.S. (2012) 'Thermal conductivity of geomaterial foams based on silica fume', *J Mater Sci*, 47 (1), 391–396.

Bruhat, G. (1968) *Thermodynamique-cours de physique générale à l'usage de l'enseignement supérieur scientifique et technique*, Paris, Masson & Cie.

Cadle, R.D. (1965) *Particle Size Theory and Industrial Applications*, New York, Reinhold Publishing Corp.

Chaussin, C. and Hilly, G. (1962) *Chaleur et thermodynamique*, Paris, Dunod.

Collishaw, P.G. and Evans, J.R.G. (1994) 'An assessment of expressions for the apparent thermal conductivity of cellular materials', *J Mater Sci*, 29 (9), 2261–2273.

Colombo, P. (2006) 'Conventional and novel processing methods for cellular ceramics', *Philos Trans R Soc, A*, 364 (1838), 109–124.

Criado, M., Palomo, A. and Fernández-Jiménez, A. (2005) 'Alkali activation of fly ashes. Part 1: Effect of curing conditions on the carbonation of the reaction products', *Fuel*, 84 (16), 2048–2054.

Davidovits, J. (2008a) *Geopolymer: Chemistry and Applications*, Saint-Quentin, Geopolymer Institute.

Davidovits, J. (2008b) 'Scientific tools, X-rays, FTIR, NMR', in Davidovits J, *Geopolymer: Chemistry and Applications*, Saint-Quentin, Geopolymer Institute, 61–76.

Delair, S., Prud'homme, E., Peyratout, C., Smith, A., Michaud, P., Eloy, L., Joussein, E. and Rossignol, R. (2012) 'Durability of inorganic foam in solution: the role of alkali elements in the geopolymer network', *Corros Sci*, 59, 213–221.

Dietzel, M. (2000) 'Dissolution of silicates and the stability of polysilicic acid', *Geochim Cosmochim Acta*, 64 (19), 3275–3281.

Duxson, P., Lukey, G.C. and van Deventer, J.S.J. (2006a) 'Thermal evolution of metakaolin geopolymers', *J Non-Cryst Solids*, 352, 5541–5555.

Duxson, P., Lukey, G.C. and van Deventer, J.S.J. (2006b) 'Thermal conductivity of metakaolin geopolymers used as a first approximation for determining gel interconnectivity', *Ind Eng Chem Res*, 45 (23), 7781–7788.

Duxson, P., Mallicoat, S.W., Lukey, G.C., Kriven, W.M. and van Deventer, J.S.J. (2007) 'Effect of alkali and Si/Al ratio on the development of mechanical properties of metakaolin-based geopolymers', *Colloids Surf, A*, 292, 8–20.

Etiegni, L. and Campbell, A.G. (1991) 'Physical and chemical characteristics of wood ash', *Bioresource Technology*, 37 (2), 173–178.

Farmer, V.C. (2000) 'Transverse and longitudinal crystal modes associated with OH stretching vibrations in single crystals of kaolinite and dickite', *Spectrochim Acta A Mol Biomol Spectrosc*, 56, 927–930.

Fernandes, H.R., Tulyaganov, D.U. and Ferreira, J.M.F. (2009) 'Preparation and characterization of foams from sheet glass and fly ash using carbonates as foaming agents', *Ceram Inter*, 35, 229–235.

Fialips, C.-I., Petit, S., Decareau, A. and Beaufort, D. (2000) 'Influence of synthesis pH on kaolinite "cristallinity" and surface properties', *Clays Clay Miner*, 48, 173–184.

Fletcher, R.A., MacKenzie, K.J.D., Nicholson, C.L. and Shimada, S. (2005) 'The composition range of aluminosilicate geopolymers', *J Eur Ceram Soc*, 25, 1471–1477.

Frost, R.L. and Vassallo, A.M. (1996) 'The dehydroxylation of kaolinite clay minerals using infrared emission spectroscopy', *Clays Clay Miner*, 44, 635–651.

Gallauziaux, T. and Fedullo, D. (2009) *Le grand livre de l'isolation*, Paris, Eyrolles.

Gouny, F., Fouchal, F., Maillard, P. and Rossignol, S. (2012) 'A geopolymer mortar for wood and earth structures', *Construction and Building Materials*, 36, 188–195.

Gustafsson, S. (1991) 'Transient plane source techniques for thermal conductivity and thermal diffusivity measurements of solid materials', *Rev Sci Instrum*, 62 (3), 797–804.

Hajimohammadi, A., Provis, J.L. and van Deventer, J.S.J. (2010) 'Effect of alumina release rate on the mechanism of geopolymer gel formation', *Chem Mat*, 22 (18), 5199–5208.

Hale, D.K. (1976) 'The physical properties of composite materials', *J Mater Sci*, 11 (11), 2105–2141.

Hamilton, R.L. and Crosser, O.K. (1962) 'Thermal conductivity of heterogeneous two component systems', *Ind Eng Chem Fundam*, 1 (3), 187–191.

Hashin, Z. and Shtrikman S. (1962) 'A variational approach to the theory of the effective magnetic permeability of multiphase materials', *J Appl Phys*, 33, 3125–3131.

Henon, J., Alzina, A., Absi, J., Smith, D. and Rossignol, S. (2012) 'Porosity control of cold consolidated geomaterial foam: temperature effect'. *Ceram Int*, 38, 77–84.

Hinckley, D.N. (1963) 'Variabilitiy in crystallinity values among the kaolin deposits of the coastal plain of Georgia and South Carolina', *Clays Clay Miner*, 11, 229–235.

Hinzelin, P. (1975) *Isolation thermique dans le bâtiment*, Lyon, Institut National des Sciences Appliquée Lyon.

Incropera, F.P. and DeWitt, D.P. (2002) *Fundamentals of Heat and Mass Transfer*, New York, John Wiley & Sons.

Ingram, M.D., King, K., Kranbuehl, D. and Adel-Hadabi, M. (1981) 'Mixed-alkali effect in aqueous silicate solutions', *J Phys Chem*, 85, 289–294.

Innocenzi, P. (2003) 'Infrared spectroscopy of sol–gel derived silica-based films: a spectra-microstructure overview', *J Non-Cryst Solids*, 316, 309–319.

Jim, H., Lee, S., Han, Y. and Park, J. (2009) 'Control of pore size in ceramic foams: influence of surfactant concentration', *Mater Chem Phys*, 113, 441–444.

Joussein, E., Petit, S. and Decarreau, A. (2001) 'Une nouvelle méthode de dosage des minéraux argileux en mélange par spectroscopie IRA [New method to determine the ratio of clay minerals in mixtures by IR spectroscopy]', *C.R. Acad Sci, Ser II: Sci Terre Planets*, 332, 83–89.

Juettner, T., Moertel, H., Svinka, V. and Svinka, R. (2007) 'Structure of kaoline-alumina based foam ceramics for high temperature applications', *J Eur Ceram Soc*, 27, 1435–1441.

Juste, E. (2008) Elaboration de réacteurs catalytiques membranaires à microstructures et architectures contrôlées, PhD Thesis, Limoges University.

Kamseu, E., Nait-Ali, B., Bignozzi, M.C., Leonelli, C., Rossignol, S. and Smith, D.S. (2012) 'Bulk composition and microstructure dependence of effective thermal conductivity of porous inorganic polymer cements', *J Eur Ceram Soc* 32 (8), 1593–1603.

Kennard, E.H. (1938) *Kinetic Theory of Gases*, New York, McGraw-Hill.

Khale, D. and Chaudhary, R. (2007) 'Mechanism of geopolymerization and factors influencing its development: a review', *J Mater Sci*, 42, 729–746.

Koloušek, D., Brus, J., Urbanova, M., Andertova, J., Hulinsky, V. and Vorel, J. (2007) 'Preparation, structure and hydrothermal stability of alternative (sodium silicate-free) geopolymers', *J Mater Sci*, 42, 9267–9275.

Landi, E., Medri, V., Papa, E., Dedecek, J., Klein, P., Benito, P. and Vaccari, A. (2013) 'Alkali-bonded ceramics with hierarchical tailored porosity', *Appl Clay Sci*, 73, 56–64.

Lee, W.K.W. and van Deventer, J.S.J. (2003) 'Use of infrared spectroscopy to study geopolymerization of heterogeneous amorphous aluminosilicate', *Langmuir*, 19, 8726–8734.

Liebau, F. (1985) *Structural Chemistry of Silicates*, Berlin, Springer-Verlag.

Liu, L.-P., Cui, X.-M., Qiu, S.-H., Yu, J.L. and Zhang, L. (2010) 'Preparation of phosphoric acid-based porous geopolymers', *Appl Clay Sci*, 50 (4), 600–603.

Maxwell, J.C. (1892) *A Treatise on Electricity and Magnetism*, Oxford, Clarendon Press.

MacKenzie, K.J.D., Brew, D.R.M., Fletcher, R.A. and Vagana, R. (2007) 'Formation of aluminosilicate geopolymers from 1:1 layer-lattice minerals pre-treated by various methods: a comparative study', *J Mater Sci*, 42 (12), 4667–4674.

MacKenzie, K.J.D., Komphanchai, S. and Vagana, R. (2008) 'Formation of inorganic polymers (geopolymers) from 2:1 layer lattice aluminosilicatés', *J Eur Ceram Soc*, 28 (1), 177–181.

Medri, V., Papa, E., Dedecek, J., Jirglova, H., Benito, P., Vaccari, A. and Landi, E. (2013) 'Effect of metallic Si addition on polymerization degree of *in situ* foamed alkali-aluminosilicates', *Ceram Int*, 39 (7), 7657–7668.

Meunier, F. (2004) *Thermodynamique de l'ingénieur: énergétique, environnement*, Paris, Dunod.

Nait-Ali, B., Haberko, K., Vesteghem, H., Absi, J. and Smith, D.S. (2006) 'Thermal conductivity of highly porous zirconia', *J Eur Ceram Soc*, 26 (16), 3567–3574.

Nait-Ali, B., Haberko, K., Vesteghem, H., Absi, J. and Smith, D.S. (2007) 'Preparation and thermal conductivity characterisation of highly porous ceramics: comparison between experimental results, analytical calculations and numerical simulations', *J Eur Ceram Soc*, 27 (2–3), 1345–1350.

Navarro, A. (1978) *Thermodynamique générale: cours fondamental – Tome I et II*, Lyon, Institut National des Sciences Appliquée Lyon.

Okada, K., Imase, A., Isobe, T. and Nakajima, A. (2011) 'Capillary rise properties of porous geopolymers prepared by an extrusion method using polylactic acid (PLA) fibers as the pore formers', *J Eur Ceram Soc*, 31 (4), 461–467.

Prud'homme, E. (2011) Rôles du cation alcalin et des renforts minéraux et végétaux sur les mécanismes de formation de géopolymères poreux ou denses, PhD Thesis, Limoges University.

Prud'homme, E., Michaud, P., Joussein, E., Peyratout, C., Smith, A., Arrii-Clacens, S., Clacens, J.M. and Rossignol, S. (2010a) 'Silica fume as porogent agent in geo-materials at low temperature', *J Eur Ceram Soc*, 30 (7), 1641–1648.

Prud'homme, E., Michaud, P., Peyratout, C., Smith, A., Rossignol, S., Joussein, E. and Sauvat,

N. (2010b) 'Geomaterial foam to reinforce wood', *Strategic Materials and Computational Design: Ceramic Engineering and Science Proceedings*, 31 (10), 3–10.

Prud'homme, E., Michaud, P., Joussein, E., Peyratout, C., Smith, A. and Rossignol, S. (2011a) '*In situ* inorganic foams prepared from various clays at low temperature', *Appl Clay Sci*, 51 (1–2), 15–22.

Prud'homme, E., Michaud, P., Joussein, E., Clacens, J.M. and Rossignol, S. (2011b) 'Role of alkaline cations and water content on geomaterial foams: Monitoring during formation', *J Non-Crystal Solids*, 357 (4), 1270–1278.

Prud'homme, E., Michaud, P., Joussein, E., Clacens, J.-M., Arrii-Clacens, S., Sobrados, I., Peyratout, C., Smith, A., Sanz, J. and Rossignol, S. (2011c) 'Structural characterization of geomaterial foams — thermal behavior', *J Non-Crystal Solids*, 357 (21), 3637–3647.

Prud'homme, E., Michaud, P., Joussein, E., Smith, A., Peyratout, C., Sobrados, I., Sanz, J. and Rossignol, S. (2012) 'Geomaterial foams: role assignment of raw materials in the network formation', *J Sol-Gel Sci Technol*, 61 (2), 436–448.

Prud'homme, E., Autef, A., Essaidi, N., Michaud, P., Samet, B., Joussein, E. and Rossignol, S. (2013) 'Defining existence domains in geopolymers through their physicochemical properties', *Appl Clay Sci*, 73, 26–34.

Rees, C.A., Provis, J.L., Lukey, G.C. and van Deventer, J.S.J. (2007) 'Attenuated total reflectance Fourier transform infrared analysis of fly ash geopolymer gel aging', *Langmuir*, 23, 8170–8179.

Schoeller, H. (1955) *Hydrogéologie*, Paris, Ecole Nationale Supérieure du Pétrole, Technip.

Schulle, W. and Schlegel, E. (1991) 'Fundamentals and properties of refractory thermal insulating materials', *Interceramics*, 40 (7), 1–12.

Song, Z.-L., Ma, L.-Q., Wu., Z.-J. and He, D.-P. (2000) 'Effects of viscosity on cellular structure of foamed aluminum in foaming process', *J Mater Sci*, 35, 15–20.

Studart, A.R., Gonzenbach, U.T., Tervoort, E. and Gauckler L.J. (2006) 'Processing routes to macroporous ceramics: a review', *J Am Ceram Soc*, 89 (6), 1771–1789.

Tognonvi, M.T., Rossignol, S. and Bonnet, J.P. (2010) 'Effect of alkali cation on irreversible gel formation in basic medium', *J Non-Cryst Solids*, 357 (1), 43–49.

Uchino, T., Sakka, T., Hotta, K. and Iwasaki, M. (1989) 'Attenuated total reflectance Fourier-transform infrared spectra of a hydrated sodium silicate glass', *J Am Ceram Soc*, 72 (11), 2173–2175.

UNSTATS (2010) *Greenhouse Gas Emissions by Sector (Absolute Values)*, New York, United Nations Statistical Division.

Vaou, V. and Panias, D. (2010) 'Thermal insulating foamy geopolymers from perlite', *Miner Eng*, 23 (14), 1146–1151.

Wang, M.R., Jia, D.C., He, P.G. and Zhou, Y. (2011) 'Microstructural and mechanical characterization of fly ash cenosphere/metakaolin-based geopolymeric composites', *Ceram Int*, 37 (5), 1661–1666.

Wu, J.P., Boccaccini, A.R., Lee, P.D. and Rawlings, R.D. (2007) 'Thermal and mechanical properties of a foamed glass-ceramic material produced from silicate wastes', *Eur J Glass Sci Technol A*, 48 (3), 133–141.

Xu, H. and van Deventer, J.S.J. (2002) 'Geopolymerisation of multiple minerals', *Miner Eng*, 15, 1131–1139.

Zhao, Y., Ye, J., Lu, X., Liu, M., Lin, Y., Gong, W. and Ning, G. (2010) 'Preparation of sintered foam materials by alkali-activated coal fly ash', *J Hazard Mater*, 174, 108–112.

Zibouche, F., Kerdjoudj, H., de Lacaillerie, J.-B. and van Damme, H. (2009) 'Geopolymers from Algerian metakaolin: influence of secondary minerals', *Appl Clay Sci*, 43, 453–458.

Alkali-activated cements for photocatalytic degradation of organic dyes

27

Y. J. Zhang, L. Kang, L. C. Liu
Xi'an University of Architecture and Technology, Xi'an, China

27.1 Introduction

Utilization of industrial by-products, such as fly ash (Pacheco-Torgal *et al*., 2008a; Temuujin *et al*., 2010; van Deventer *et al*., 2007), blast furnace slag (Khate and Chaudhary, 2007; Richardson and Cabrera, 2000; Richardson *et al*., 1989; Zhang *et al*., 2008) and steel slag (Belhadj *et al*., 2012; Hu *et al*., 2008; Lonescu *et al*., 2001) for preparation of alkali-activated solid waste-based cements have attracted considerable attention due to their excellent physical properties for potential applications in the building industry (Duxson *et al*., 2007; Habert *et al*., 2011; Pacheco-Torgal *et al*., 2008b; Songpiriyakij *et al*., 2011): encapsulation of radioactive material (Khalil and Merz, 1994), solidification of hazardous wastes (van Jaarsveld *et al*., 1997; Galiano *et al*., 2011), and fire-resistance (Kong and Sanjayan, 2010; Temuujin *et al*., 2011).

In recent years, some geopolymers with network structures have been used as adsorbents for removal of Pb^{2+}, Cu^{2+}, Cr^{3+} and Cd^{2+} ions from wastewater (Al-Zboon *et al*., 2011; Wang *et al*., 2007; Cheng *et al*., 2012), for adsorption of formaldehyde from indoor air (Huang and Han, 2011), and for removal of dye from wastewater (Li *et al*., 2006). It is suggested that the frameworks of geopolymers consist of $[SiO_4]^{4-}$ and $[AlO_4]^{5-}$ tetrahedra linked randomly by sharing all the oxygen atoms, and the negative charge of $[AlO_4]^{5-}$ tetrahedron is balanced by extra framework cations of Na^+, K^+ and Ca^{2+} ions (Davidovits, 1991; Komnitsas and Zaharaki, 2007). In general, the extra framework cations can be replaced by cations through ion exchange due to the porous structures of geopolymers (Bortnovsky *et al*., 2008; O'Connor *et al*., 2010). Sazama *et al*. (2011) reported that the geopolymer catalysts with Co^{2+} and Cu^{2+} cations were prepared by ion exchange reactions of metakaolin-based Na geopolymer and metakaolin-slag based K,Ca geopolymer, and were used as the selective catalytic reduction of nitrogen oxides using ammonia as reducing agent and the oxidation of decane using oxygen as oxidant. Gasca-Tirado *et al*. (2012) proposed that the incorporation of photoactive TiO_2 into a geopolymer by ion exchange was used for the degradation of methylene blue.

In this chapter, we introduce three kinds of alkali-activated granulated blast furnace slag-based (AGBFS), alkali-activated steel slag-based (ASS) and alkali-activated fly ash-based (AFA) cements coupled with Ni^{2+} ion and Fe_2O_3 by three-step polymerization, ion exchange and impregnation reactions, respectively. These alkali-

Handbook of Alkali-activated Cements, Mortars and Concretes. http://dx.doi.org/10.1533/9781782422884.5.729

activated solid waste-based cements were used as a new category of photocatalyst for degradation of methylene blue (MB) and Congo red (CR) dyes from wastewater. The hydration mechanism, the adsorption kinetics, the reaction kinetics and the degradation mechanism were investigated in detail.

27.2 Experimental technique

27.2.1 Materials

The granulated blast furnace slag (GBFS) with a Blaine specific surface area of 508 $m^2 \cdot kg^{-1}$ was provided by Long Steel Company, Shaanxi, China. The main chemical compositions in weight percent are shown in Table 27.1 (Zhang *et al*., 2013). The steel slag with a Blaine specific surface area of 450 $m^2 \cdot kg^{-1}$ and an average particle size of 17.49 μm was obtained from Laiwu Steel Company, Shandong, China. The main oxide components in weight percent are displayed in Table 27.2 (Zhang *et al*., 2012). The fly ash with a Blaine specific surface area of 500 $m^2 \cdot kg^{-1}$ and an average particle size of 11.16 μm was derived from the Hancheng thermal power plant, Shaanxi, China. The main chemical compositions in weight percent are shown in Table 27.3 (Zhang and Liu, 2013). The chemical reagents of $Na_2SiO_3 \cdot 9H_2O$ (A.R.), NaOH (A.R.), NH_4Ac (A.R.), $Fe(NO_3)_3 \cdot 9H_2O$ (A.R.), $Ni(NO_3)_2 \cdot 6H_2O$ (A.R.), Congo red (A.R.) and methylene blue (A.R.) were purchased from Xi'an Chemical Reagent Company, Shaanxi, China and were not purified prior to use.

27.2.2 Preparations of alkali-activated solid waste-based cements

27.2.2.1 Preparation of alkali-activated granulated blast furnace slag-based (AGBFS) cement

Three kinds of raw materials, activator ($Na_2SiO_3 \cdot 9H_2O$), GBFS and water, were blended in the ratio of 1 : 9 : 2.5 (by weight). The paste was cast into a triplicate iron mould measuring 50 (length) × 31.5 (width) × 31.5 (height) (mm^3). After demoulding, the samples were kept in a curing box at 20°C with 99% relative humidity and the curing time was 0.5 h, initial set, final set, 1 day (1 d), 3 days (3 d), 7 days (7 d) and 28 days (28 d), respectively. The compressive strengths of alkali-activated granulated blast furnace slag (AGBFS) cements are shown in Table 27.4 (Zhang *et al*., 2008) and the samples in different curing times were used to study the hydration mechanism.

27.2.2.2 Synthesis of NH_4 -alkali-activated slag-based cementitious material (NH_4-ASCM) cement

The GBFS, $Na_2SiO_3 \cdot 9H_2O$ and water were in the mass ratio of 1:0.11:0.30. In a typical synthesis, 1500 g of GBFS was put into a net paste stirrer and then the

Table 27.1 Chemical composition of AGBFS cements (wt.%)

Components	Na_2O	Fe_2O_3	Al_2O_3	SiO_2	CaO	MgO	K_2O	TiO_2	MnO	BaO	SO_3	Loss on ignition
GBFS	0.57	1.03	10.59	27.51	35.23	7.11	0.66	1.16	0.48	0.38	1.41	13.87
Na-ASCM	4.45	1.12	8.91	31.11	31.48	5.74	0.61	1.06	0.43	0.37	1.23	13.49
NH_4-ASCM	0.14	1.17	11.27	34.04	26.72	7.10	0.31	1.28	0.49	0.36	0.80	16.32
$0.5Fe_2O_3$/ASCM	0.16	1.77	11.19	33.83	27.16	7.04	0.31	1.26	0.49	0.36	0.73	15.70
$5Fe_2O_3$/ASCM	0.15	6.22	10.75	33.72	26.97	6.12	0.3	1.18	0.46	0.36	0.68	13.09
$10Fe_2O_3$/ASCM	0.14	11.39	9.34	32.24	26.46	5.19	0.24	1.07	0.4	0.33	0.58	12.62

Source: Reprinted from Zhang *et al.*, 2013, Copyright © 2013, with permission from Elsevier.

Table 27.2 Chemical composition of ASS cements (wt.%)

(wt.%)	Na_2O	K_2O	NiO	SiO_2	Al_2O_3	CaO	Fe_2O_3	TiO_2	MgO	V_2O_5	MnO	P_2O_5	Loss on ignition
Steel slag	0.15	0.12	0	19.13	4.87	37.42	18.77	1.62	5.55	0.98	3.63	0.65	7.11
Na,Ca-ASS	4.01	0.10	0	18.78	3.36	35.40	15.99	1.35	3.21	0.88	3.05	0.59	13.28
NH_4-ASS	0.09	0.05	0	23.08	3.84	33.38	17.92	1.57	3.71	1.00	3.42	0.66	11.28
Ni,Ca-ASS	0.06	0.04	6.95	22.47	3.73	28.09	17.62	1.56	3.61	1.02	3.38	0.62	10.85

Source: Reprinted from Zhang *et al.*, 2012, Copyright © 2012, with permission from Elsevier.

Table 27.3 Chemical composition of AFA cements (wt.%)

Specimen	Component (wt.%)								
	Na_2O	SiO_2	Al_2O_3	CaO	Fe_2O_3	TiO_2	K_2O	MgO	Loss on ignition
Fly ash	0.26	42.03	27.51	3.42	4.37	1.09	1.66	0.48	19.18
Na-geopolymer	4.70	51.15	28.23	3.37	4.78	0.94	1.67	0.53	4.63

Source: Reprinted from Zhang and Liu, 2013, Copyright © 2013, with permission from Elsevier.

Table 27.4 Compressive strength of AGBFS cements

Compressive strength (MPa)			
1 d	3 d	7 d	28 d
26.5	40.7	51.6	60.1

Source: Zhang *et al.*, 2008, with kind permission from Springer Science and Business Media.

aqueous solution of alkaline activator was poured into it. The slurry was poured into a triplicate iron mould measuring 160 mm × 40 mm × 40 mm to be compacted on the vibrating table, and then put into a standard curing box for 24 h. The samples were continuously cured at room temperature for an additional 7 days after demoulding, and then the samples, sealed in thin plastic bags respectively, were cured at 65°C for 24 h in a nitrogen atmosphere. The sample with compressive and flexural strengths of 86 MPa and 2 MPa respectively was crushed to obtain a Na-alkali-activated slag-based cementitious material (Na-ASCM) with particle size distribution from 0.125 to 0.315 mm.

160 g of Na-ASCM was placed into a 400 mL aqueous solution of 2.0 M NH_4Ac at room temperature for 24 h to carry out the ion exchange of Na^+ with NH_4^+. The sample was filtrated and washed adequately with deionized water, and then dried at 65°C for 4 h in a nitrogen atmosphere. As described above, the ion exchange was repeated once more to get NH_4-ASCM cement.

27.2.2.3 Synthesis of alkali-activated slag-based cementitious material (ASCM) loaded Fe_2O_3 cement

ASCM cements loaded with distinct Fe_2O_3 amounts were prepared by wetness impregnation. In a typical procedure for the fabrication of a 0.5 wt.% Fe_2O_3 loaded sample, 30 g of NH_4-ASCM was impregnated with 15 mL of aqueous solution which dissolves 0.7587 g of $Fe(NO_3)_3{\cdot}9H_2O$ overnight. The sample was dried at 65°C for

12 h in a nitrogen atmosphere and then calcinated at 300°C for 3 h. The sample was assigned as $0.5Fe_2O_3$/ASCM. Samples loaded with 5 wt.% and 10 wt.% Fe_2O_3 were designated as $5Fe_2O_3$/ASCM and $10Fe_2O_3$/ASCM, respectively. The precise Fe_2O_3 content in samples was determined by X-ray fluorescence (XRF) and is given in Table 27.1.

27.2.2.4 Preparation of alkali-activated steel slag-based (ASS) cement

The starting materials of steel slag and NaOH for respectively providing charge compensations of Ca^{2+} and Na^+ cations were mixed in the mass ratio of steel slag/activator/water = 1:0.11:0.28. A typical preparation procedure is described below. The steel slag was placed into a net paste stirrer containing an aqueous solution of alkaline activator and sufficiently mixed. The slurry was placed into a triplicate iron mould measuring 50 mm × 31.5 mm × 31.5 mm and then kept in a curing box at 20°C with 99% relative humidity for 1 day. The sample was continuously cured at room temperature for an additional 27 days (Zhang *et al.*, 2010). Subsequently, the sample with a compressive strength of 26 MPa was crushed and dried at 60°C for 3 h in a nitrogen atmosphere to obtain a Na,Ca-ASS specimen with particle size in the range of 120–425 μm.

27.2.2.5 Preparation of Ni,Ca-alkali-activated steel slag-based (Ni,Ca-ASS) cement

The Na,Ca-ASS specimen (10 g) was added to 100 mL aqueous solution of 0.3 M NH_4Ac at room temperature for 12 h to perform ion exchange of Na^+ with NH_4^+. The specimen was filtrated and washed sufficiently with distilled water and then dried at 60°C for 3 h in a nitrogen atmosphere. As mentioned above, the experimental procedure was repeated once more to get the NH_4-ASS cement. The NH_4-ASS specimen (10 g) was added to 100 mL aqueous solution of 0.1 M nickel nitrate to carry out ion exchange of NH_4^+ with Ni^{2+} at room temperature for 12 h. The specimen was filtrated and sufficiently washed with distilled water and then dried at 60°C for 3 h in a nitrogen atmosphere to acquire a Ni,Ca-ASS catalyst. The chemical compositions are shown in Table 27.2.

27.2.2.6 Preparation of alkali-activated fly ash-based (AFA) cement

The fly ash, $Na_2SiO_3 \cdot 9H_2O$ and water were mixed in the mass ratio of 1:0.11:0.32. The fly ash was added into a net paste stirrer containing an aqueous solution of $Na_2SiO_3 \cdot 9H_2O$ and was thoroughly mixed for several minutes. The slurry was put into a triplicate mould measuring 50 mm × 31.5 mm × 31.5 mm, which was put into a curing box at 20°C with 99% relative humidity for 24 h. The sample was continuously cured at room temperature for 27 days after being taken out from the mould. Subsequently, the sample with a compressive strength of 20 MPa was crushed and dried at 60°C for 3 h in a nitrogen atmosphere to obtain a fly ash-based

cement sample with particle size in the range of 120–425 μm. The main chemical compositions in weight percent are listed in Table 27.3.

27.2.3 Characterization of alkali-activated solid waste-based cements

The chemical composition analysis was performed on a Bruker S4 Pioneer X-ray fluorescence (XRF) analyzer. The morphology analysis was carried out using a Quanta 200 environmental scanning electron microscope (SEM) and a JSM-6700F field emission scanning electron microscope (FESEM). The microstructure image of samples was obtained on an H-600 transmission electron microscope (TEM). X-ray diffraction (XRD) patterns of samples were recorded on a D/MAX-2200 X-ray diffractometer equipped with a rotation anode using CuKα radiation with a 0.02° 2θ step interval in the working electric current of 40 mA and voltage of 40 kV. The Fourier transform infrared (FTIR) spectra of samples were measured using a Nicolet 5700 spectrometer with standard KBr technique. Diffuse reflectance UV-visible near infrared ray spectrum was recorded on a Hitachi UV-4100 spectrophotometer. The photoluminescence spectra were recorded on an F-4500 fluorescence spectrophotometer and a 150 W xenon lamp was used as excitation light source. Thermogravimetric analysis (TGA), differential thermogravimetry (DTG) and differential scanning calorimetry (DSC) were conducted on a Mettler Toledo TGA/DSC 1 Stare system. The pore size distribution of sample was determined using a Micromeritics AutoPore IV 9500 mercury intrusion porosimeter. The N_2 adsorption-desorption isotherms were measured on an ASAP 2020 instrument. The compressive strength of samples was tested on a YAW-300 automatic pressure testing machine at loading speed of 2.4 $kN \cdot s^{-1}$. The flexural strength of samples was carried out on a DKZ-5000 anti-rupture testing machine with a three-point bend device at loading speed of 50 $N \cdot s^{-1}$.

27.2.4 Evaluation of photocatalytic activities

A certain amount of sample was added to 100 mL of aqueous dye solution which was magnetically stirred and kept in the dark for a certain time to establish an adsorption-desorption equilibrium. The solution was irradiated by a UV-lamp (40 W) with a 254 nm output, and subsequently was centrifuged at 10–20 min intervals. The absorbance of the supernatant solution was monitored on a UV-visible spectrophotometer at the maximum absorption wavelength (500 nm for Congo red and 665 nm for methylene blue). The degradation efficiency (DE) was calculated by:

$$\text{DE}\ (\%) = [(A_0 - A_t)/A_0] \times 100 \tag{27.1}$$

where DE (%) represents the degradation efficiency by percent concentration. The A_0 and A_t are the absorbance of dye solution in the beginning and after t time under UV irradiation, respectively.

27.3 Microstructure and hydration mechanism of alkali-activated granulated blast furnace slag (AGBFS) cements

The granulated blast furnace slag (GBFS) is an industrial by-product from the manufacture of pig iron and predominately consists of calcium-magnesium aluminosilicate glass (Gartner and Macphee, 2011; Bakharev *et al.*, 1999). The slag in long-term stock not only occupies a great quantity of land, but gives rise to serious environmental pollution. In order to promote the recycling of resources and sustainable development of the steel industry, it is necessary to adopt an advanced method for the high value-added utilization of GBFS. In recent years, tremendous effort has focused on the utilization of GBFS for the synthesis of alkali-activated granulated blast furnace slag-based cementitious materials (ASCM) due to low energy consumption, high mechanical strength, low permeability and high stability in aggressive environments (Bernal *et al.*, 2011; Cheng and Chiu, 2003; Panagiotopoulou *et al.*, 2007; Roy, 1999; Yip *et al.*, 2004; Yip and van Deventer, 2003; Wang *et al.*, 1995). Under the effect of alkaline activator, the vitreous structure in GBFS initially depolymerizes and then forms amorphous calcium (aluminum) silicate hydrate (C(A)SH) gel. It is proposed that the skeleton of C(A)SH gel with negative charges is composed of SiO_4 and AlO_4 tetrahedra linked alternately by sharing all bridge oxygen atoms, and the negative charges are balanced by positive of Ca^{2+} and Na^+ (Duxson and Provis, 2008; Mozgawa and Deja, 2009). It is considered that calcium silicate hydrate (CSH) is the major amorphous phase in alkali-activated GBFS with a low Ca/Si ratio of 0.98–1.1 (Palomo *et al.*, 1999; Song and Jennings, 1999; Song *et al.*, 2000; Wang and Scrivener, 1995) and aluminum is present in CSH gel as four-coordination with an Al/Ca ratio of 0.16–0.25 (Yip *et al.*, 2005; Wang and Scrivener, 2003). Mercury intrusion porosimetry results revealed that the ASCM possesses porous structure of a higher mesopore pore volume and a lower capillary pore fraction (Qian *et al.*, 2003a; Roy *et al.*, 2000; Shi, 1996). Cho *et al.* (1999) reported that the micropore volume (< 5 nm) is about 78% of their total pore volume in alkali-activated slag pastes. In consideration of porosity, the matrix of ASCM has been successfully utilized in the incorporation and immobilization of radioactive wastes and toxic metals (Deja, 2002; Qian *et al.*, 2003b, 2003c). Moreover, the cations of Na^+, K^+ and Ca^{2+} in the charge-balancing sites of skeleton can be displaced by ion exchange. In a previous study, the Na^+ cation in alkali-activated steel slag-based Na,Ca-cementitious material was replaced by Ni^{2+} cation to generate Ni,Ca-cementitious material and was employed as a photocatalyst for degradation of methylene blue (Zhang *et al.*, 2012). Sazama *et al.* (2011) reported that Na^+ and K^+ cations in metakaolin-based Na geopolymer and metakaolin-slag based K,Ca geopolymer were replaced by Co^{2+} and Cu^{2+} cations to prepare the Co geopolymer and Cu geopolymer for the oxidation of decane and the selective catalytic reduction of NO_x.

27.3.1 Microstructure and mineral phases of AGBFS cement

Figure 27.1 shows the FESEM photomicrographs of samples at different curing times (Zhang *et al*., 2011). Figure 27.1(a) is the image of GBFS with distribution

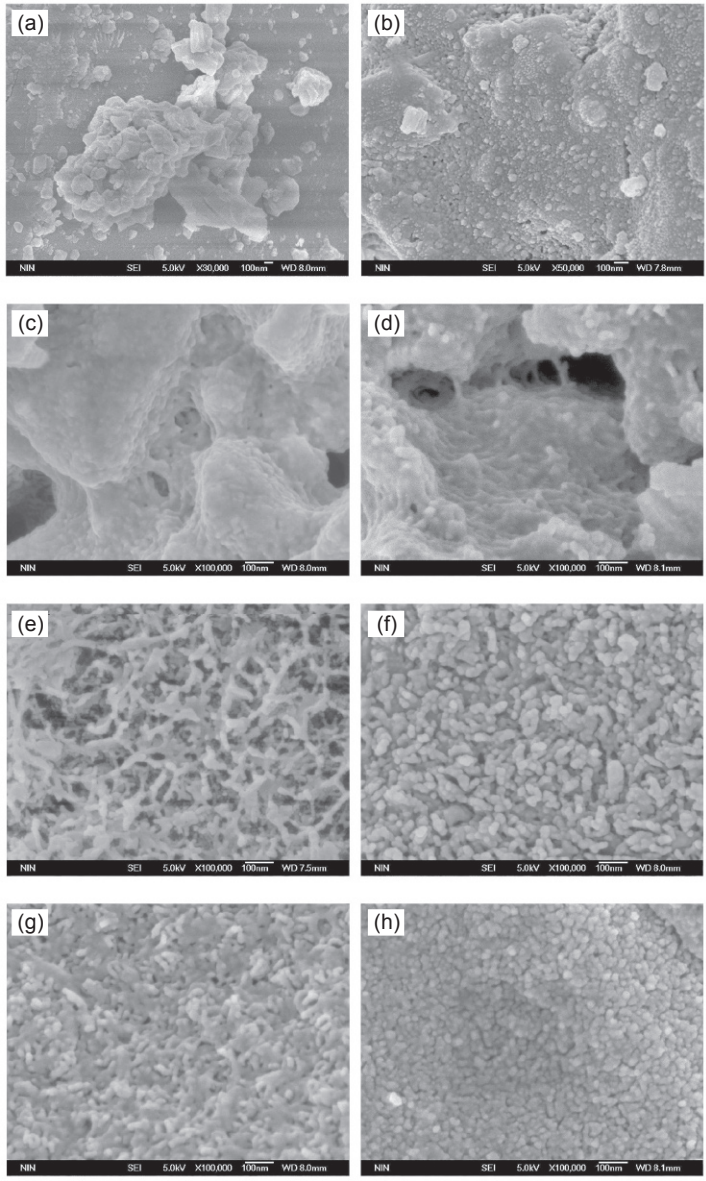

Figure 27.1 FESEM photomicrographs of samples: (a) slag powder, (b) seting time of 0.5 h, (c) initial setting time of 1.3 h, (d) final setting time of 4.2 h, (e) curing age of 1 day, (f) curing age of 3 days, (g) curing age of 7 days and (h) curing age of 28 days (Zhang *et al*., 2011).

of the mean particle size from 2 μm to 20 μm. The grain boundaries can be clearly distinguished after alkali-activated reactions have been carried out for 0.5 h in Figure 27.1(b). However, the obvious dissolution reaction takes place at granular boundaries of GBFS, indicating the vitreous structure of GBFS starts to disintegrate in alkaline media at the initial setting time of 1.3 h in Figure 27.1(c). A large quantity of gel-like hydration products are generated on the surface of granular boundaries as shown at the final setting time of 4.2 h in Figure 27.1(d). After the curing age of 1 day, it can be found that almost all of GBFS particles take part in the alkali-activated polycondensation reaction to form cementitious material which consists of -Si-O-Al- chains, and then those chains overlap one another to build up a network microstructure in Figure 27.1(e). With extending of curing time and development of compressive strength from 26.5 MPa after 1 day to 40.7 MPa after 3 days as shown in Table 27.4, the AGBFS rapidly develop into a dense material by further polycondensation reaction and the appearance shows worm-like microstructure as shown in Figure 27.1(f). Under the alkaline conditions, the polycondensation reactions occur continuously between different networks to constitute a criss-cross pattern at curing age of 7 days in Figure 27.1(g). It was surprising that the AGBFS cement materials are composed of the worm-like microstructure of quite dense nanoscale particles with an average diameter of 20 nm at curing age of 28 days as shown in Figure 27.1(h), and the compressive strength gradually increases from 51.6 MPa in 7 days to 60.1 MPa in 28 days as shown in Table 27.4 (Zhang *et al.*, 2008).

Energy dispersive X-ray analysis (EDXA) is used to monitor the variety of elemental compositions in the formation of AGBFS cement. As comparison with GBFS, the contents of elements, such as Si, Al, Ca and Mg, fluctuate to a certain extent between setting time of 0.5 h to final setting time of 4.2 h in Table 27.5. In particular, the content of calcium sharply increases in the period of initial setting time, indicating that a large amount of calcium was extracted from slag particles to gelatinous AGBFS cement. It is noteworthy that the content of element sodium increases dramatically, especially at the curing age of 1 day due to the hydrolysis of sodium silicate to produce NaOH which reacts with the silica-aluminum chain

Table 27.5 Elemental composition (wt.%) of AGBFS cement tested by EDXA

	Si	Al	Ca	Mg	Na	Na/(Si+Al)	Ca/(Si+Al)
GBFS	18.75	10.75	23.8	8.64	1.13	0.038	0.80
Curing 0.5 h[a]	16.35	8.79	42.00	6.00	2.85	0.11	1.67
Initial 1.3 h[a]	18.41	6.89	44.73	5.56	3.09	0.12	1.77
Final 4.2 h[a]	17.14	6.81	20.50	6.64	4.92	0.21	0.86
Curing 1 d[a]	18.07	5.70	29.53	4.83	6.72	0.28	1.24
Curing 3 d	18.22	6.26	25.06	5.11	6.24	0.25	1.02
Curing 7 d	17.65	6.11	22.15	4.89	6.91	0.29	0.93
Curing 28 d	17.33	6.23	24.58	5.11	7.31	0.31	1.04

[a] Setting time of 0.5 h, initial setting time of 1.3 h and final setting time of 4.2 h, curing age of 1 day.
Source: Zhang *et al.*, 2011.

so as to accelerate the cleavage of Si-O-Al, Si-O-Si and Al-O-Al bonds in GBFS. Quite significant changes take place in the ratios of Na to Si and Al, as well as Ca to Si and Al in Table 27.5 from initial setting time to final setting time. However, the content remains relatively steady in the range of 0.31–0.33 for the ratio of Na to Si and Al, and 0.98–1.01 for the ratio of Ca to Si and Al during the curing ages from 3 days to 28 days. This means that some Na-based and Ca-based cementitious materials were generated in the process of polycondensation reaction.

Figure 27.2 shows the XRD patterns of samples for the alkaline activation of GBFS cement. From the pattern of GBFS it can be observed that there is a broad diffuse hump peak in the region 20–38° 2θ suggesting that the GBFS predominantly consists of glassy phases (Khate and Chaudhary, 2007; Duxson *et al*., 2007; Komnitsas and Zaharaki, 2007). Besides, four kinds of mineral phases (akermanite, gehlenite, calcium silicate and merwinite) were identified. Their chemical composites as well as *d* values are listed in Table 27.6. In comparison to the pattern of GBFS, the relative intensities of diffraction peaks have no distinct changes and have no new peak appearance from setting time of 0.5 h to final setting time of 4.2 h in Figure 27.2, implying that the sodium hydroxide deriving from the hydrolysis of sodium metasilicate promotes some vitreous dissolution in the periods of curing.

The XRD patterns of samples for curing ages of 1–28 d and steam curing time of 28 d are displayed in Figure 27.3. After curing time of 1 d, the intensities of some

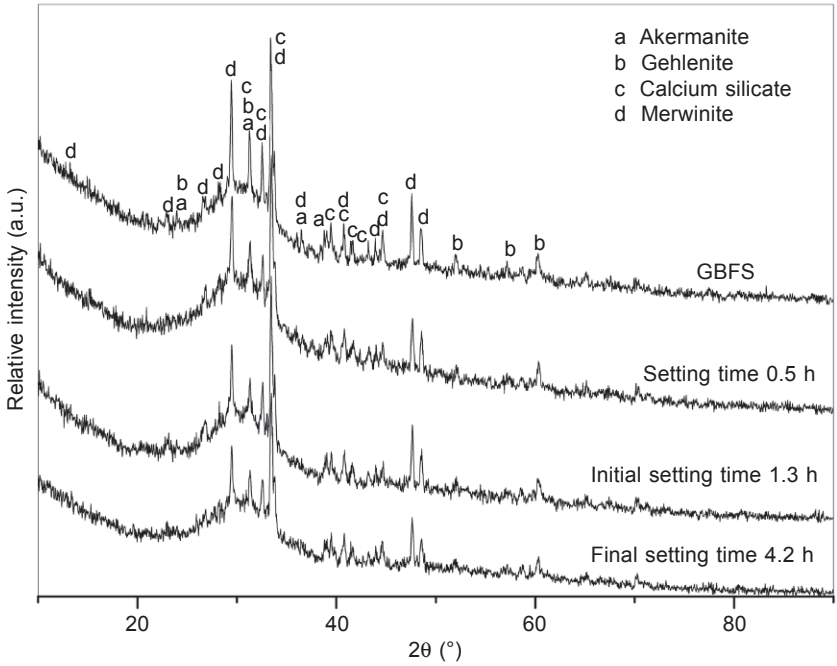

Figure 27.2 XRD patterns of AGBFS cement including the curves of GBFS, setting time for 0.5 h, initial set for 1.3 h and final set for 4.2 h, respectively (Zhang *et al*., 2008, with kind permission from Springer Science and Business Media).

Table 27.6 Mineral phases of AGBFS cement from initial setting time to final setting time

Mineral phase	Chemical formula	Number of JCPDS	*d* (nm)
Akermanite	$Ca_2MgSi_2O_7$	01-087-0049	0.37148, 0.28593, 0.24635, 0.23078
Gehlenite	$Ca_2Al_2SiO_7$	01-089-5917	0.37148, 0.28593, 0.17589, 0.16100, 0.15347
Calcium silicate	Ca_2SiO_4	00-033-0303	0.28593, 0.27520, 0.26840, 0.22836, 0.22140, 0.21772, 0.20913, 0.20282
Merwinite	$Ca_3Mg(SiO_4)_2$	00-026-1064	0.66288, 0.387703, 0.33578, 0.31639, 0.30332, 0.27520, 0.26840, 0.24635, 0.22140, 0.20596, 0.20282, 0.19094, 0.18774

Source: Zhang *et al.*, 2008, with kind permission from Springer Science and Business Media.

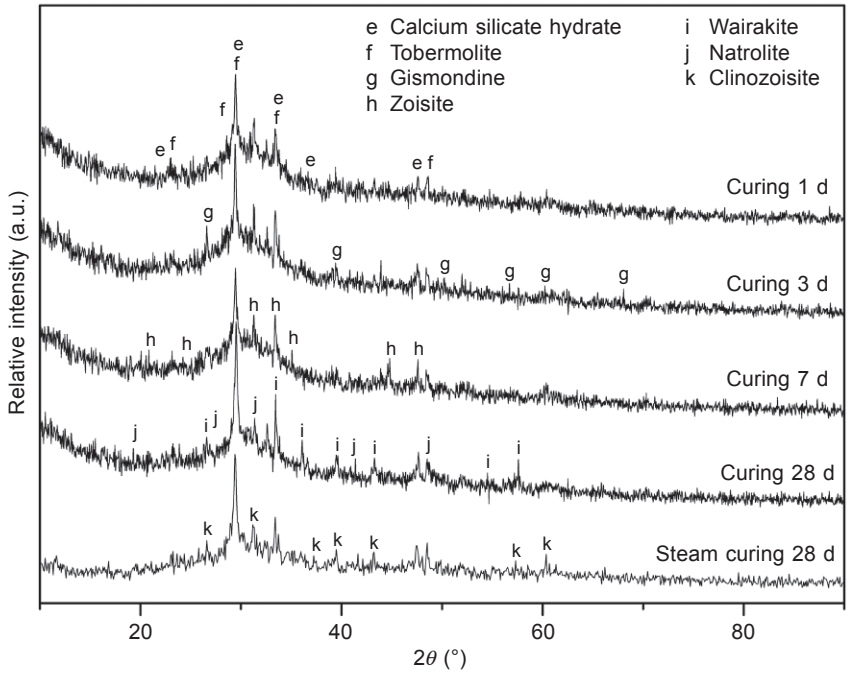

Figure 27.3 XRD patterns of AGBFS cement in the period of curing times 1–28 d (Zhang *et al.*, 2008, with kind permission from Springer Science and Business Media).

diffraction peaks remarkably decrease and some peaks disappear in comparison to final setting time in Figure 27.2, demonstrating that those crystal phases, either partial or whole, dissolve into aqueous sodium hydroxide solution derived from the hydrolysis of sodium metasilicate (Sagoe-Crentsil and Weng, 2007). It is noteworthy that some new phases, tobermolite and calcium silicate hydrate (CSH) gel, are generated during

curing time of 1 d. Schneider *et al*., reported that the CSH and other hydrated phases are present in hardened pastes of alkali-activated blast furnace slag (Schneider *et al*., 2001). Some new mineral phases are simultaneously produced at later curing times, for instance, gismondine at 3 d, zoisite at 7 d, wairakite and natrolite after 28 d, clinozoisite in steam curing time at 28 d. The chemical composites of these mineral phases and *d* values are listed in Table 27.7. Meanwhile, it can be observed that the hump peak in the range of 20–38° 2θ hardly changes in the period of curing time of 1 d to steam curing time of 28 d, suggesting that the geopolymer gel and the calcium silicate hydrate (CSH) gel produced coexist in the pastes (Yip and van Deventer, 2003). Indeed, once GBFS powder is mixed with the alkaline solution, geopolymer gel and CSH gel could be formed after shorter setting and hardening times. As there is insufficient time for the gel in pastes to grow into a well-crystallized structure, the hump peak was formed in the period of 1–28 d in Figure 27.3. The geopolymer exhibits increasing mechanical properties as shown in Table 27.4. Yip *et al*. (2005) described that the Na geopolymer gel, Ca geopolymer gel and CSH gel could be produced in a metakaolin/GGBFS system.

Figure 27.4 illustrates the FTIR spectra of samples by sodium metasilicate activation of GBFS in the period of initial to final setting times. The characteristic bands at around 947.3 cm^{-1} and 697 cm^{-1} are assigned to asymmetric Si-O-Al stretching mode and symmetric stretching vibrations of Si-O-Si and Si-O-Al bonds (Yip *et al*., 2004). The asymmetric Si-O-Al stretching vibration is shifted from 997 cm^{-1} at 0.5 h setting time in Figure 27.4(b) to 1017.2 cm^{-1} at 4.2 h final setting time for in

Table 27.7 Mineral phases of AGBFS cement in the period of curing times 1–28 d

Mineral phase	Chemical formula	Number of JCPDS	*d* (nm)
Calcium silicate hydrate	$Ca_2SiO_4{\cdot}0.3H_2O$	00-015-0584	0.36650, 0.30326(s), 0.26810, 0.24572, 0.19106
Tobermolite	$Ca_5(Si_6O_{16})(OH)_2$	01-089-6458	0.35642, 0.31152, 0.30326(s), 0.26810, 0.18760
Gismondine	$CaAl_2Si_2O_8{\cdot}4H_2O$	00-020-0452	0.33499(s), 0.13782, 0.18174, 0.16406, 0.15426, 0.13750
Zoisite	$Ca_2Al_3Si_3O_{12}OH$	01-078-1247	0.42538, 0.36951, 0.28585(s), 0.26836, 0.25602, 0.20277, 0.19110
Wairakite	$CaAl_2Si_4O_{12}{\cdot}2H_2O$	00-042-1451	0.33878(s), 0.26800, 0.24904, 0.22792, 0.20895, 0.16821, 0.16011
Natrolite	$Na_2Al_2Si_3O_{10}{\cdot}2H_2O$	00-022-1224	0.45987, 0.31576, 0.28506(s), 0.21835, 0.18769
Clinozoisite	$Ca_2Al_3Si_3O_{12}OH$	00-016-0705	0.34555, 0.28664(s), 0.24101, 0.22805, 0.20895, 0.1600, 0.15353

Source: Zhang *et al*., 2008, with kind permission from Springer Science and Business Media.

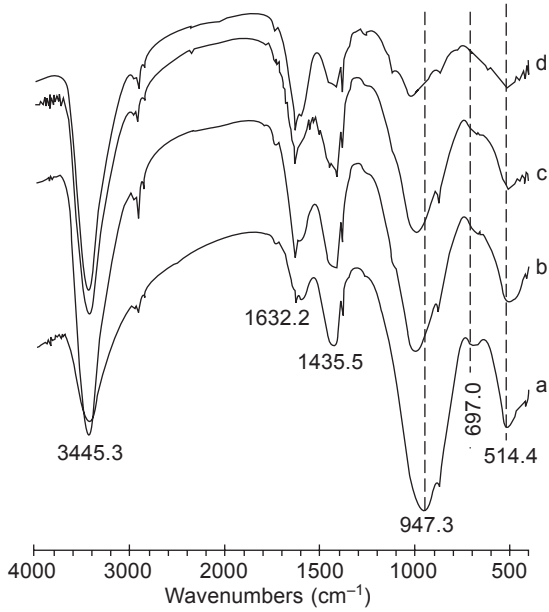

Figure 27.4 FTIR spectra of AGBFS cement from initial to final setting times: (a) GBFS, (b) AGBFS for 0.5 h, (c) initial setting time for 1.3 h; (d) final setting time for 4.2 h (Zhang *et al.*, 2008, with kind permission from Springer Science and Business Media).

Figure 27.4(d). The wavenumber of 1017.2 cm^{-1} is ascribed to asymmetric Si-O-Si stretching mode (Bakharev, 2005a) because of the hydrolysis of sodium silicate to produce different aggregates of silica gel which are composed of $[SiO_4]^{4-}$ monomers, $[Si_2O_7]^{6-}$ dimmer, $[Si_3O_{10}]^{8-}$ trimer and some oligomer species (Feng *et al.*, 2004). The band at around 1435 cm^{-1} in Figure 27.3(a)–(d) is attributed to the absorption of C-O stretching vibration due to carbonation formed in the atmosphere (Yousuf *et al.*, 1993). Both 1632 cm^{-1} and 3445 cm^{-1} are assigned to bending and stretching vibration of hydroxyl groups existing in various hydration products (Perera *et al.*, 2007b).

Figure 27.5 shows the FTIR spectra of the samples in the curing time from 1 d to 28 d. It can be clearly seen that the stretching vibration of Si-O-Al bonds is gradually shifted to a high wavenumber from 966.5 cm^{-1} at curing time of 1 d in Figure 27.5(a) to 981.5 cm^{-1} at steam curing time of 28 d in Figure 27.5(e), considering that the polymeric matrix is growing and accompanies the increase of the compressive strength shown in Table 27.4.

In comparison to final setting time in Figure 27.4(d), two new bands appear in the region 671.2 and 714.0 cm^{-1} belonging to the symmetric absorption of Si-O-Si and Al-O-Si bonds, and the relative intensities hardly change from Figure 27.5(a) to 27.5(d), It is demonstrated that some of the $[SiO_4]^{4-}$ units within the Si-O-Si skeleton are replaced by $[AlO_4]^{5-}$ to form geopolymer gel and have a relatively stable Si/Al ratio in the Si-O-Al network skeleton (Lee and van Deventer, 2002).

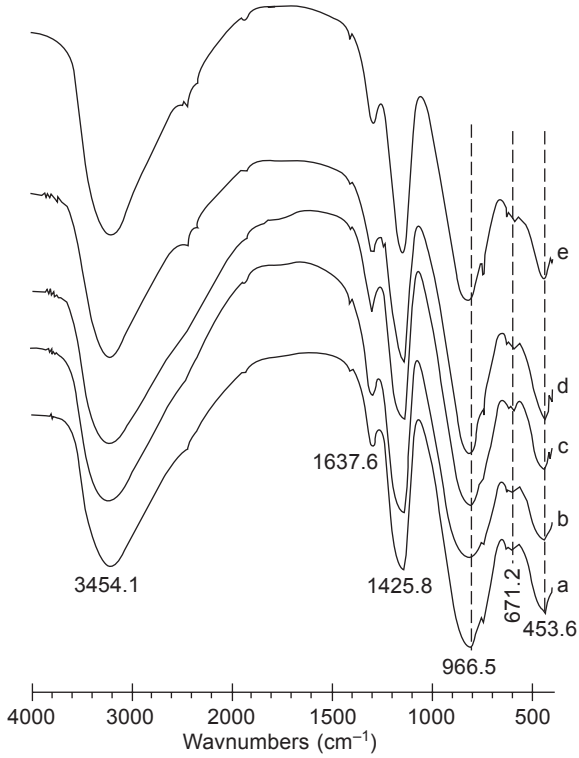

Figure 27.5 FTIR spectra of AGBFS cement in periods of curing times 1–28 d: (a) curing time of 1 d, (b) curing time of 3 d, (c) curing time of 7 d, (d) curing time of 28 d and (e) steam curing time of 28 d (Zhang *et al*., 2008, with kind permission from Springer Science and Business Media).

27.3.2 Hydration mechanism of AGBFS cement

From the XRD and FTIR results, the hydration mechanism for geopolymer formed by sodium metasilicate activation of GBFS can be schematically described as below.

27.3.2.1 Hydrolysis of sodium metasilicate

When solid sodium metasilicate is mixed with water, the hydrolysis takes place immediately and produces the orthosilicic acid and sodium hydroxide in the reaction:

$$2Na_2SiO_3 + 6H_2O \rightarrow 2Si(OH)_4 + 4NaOH \quad (27.2)$$

27.3.2.2 Disintegration of glassy network structure

Under alkaline conditions, the covalent Si-O-Si, Si-O-Al and Al-O-Al bonds in the vitreous phases of the GBFS are broken to form aluminum hydroxide and orthosilicic

acid as shown in Eq. (27.3). A higher concentration of hydroxyl ions facilitates the dissociation of different silicate and aluminate species, and then these species further react with NaOH to produce the basic sodium aluminate and basic sodium silicate in reactions shown by Eqs (27.4) and (27.5). The Al species consists of $[Al(OH)_4]^-$ and $[AlO(OH)_3]^{2-}$, while the Si species predominantly exists in the form of $Si(OH)_4$ and $[SiO(OH)_3]^-$ under alkaline conditions (Weng and Sagoe-Crentsil, 2007). In this reaction stage, the speed of monomer formation is greater than that of precipitation formation (Cho *et al.*, 1999).

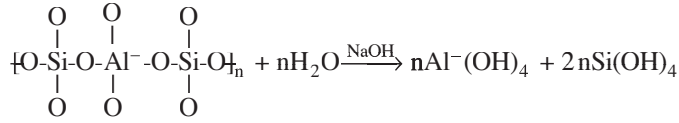

$$\text{nAl}^-(\text{OH})_4 + 2\,\text{nSi(OH)}_4 \tag{27.3}$$

$$^-\text{Al(OH)}_4 + \text{NaOH} \rightarrow \text{Na}^+[\text{OAl}^-(\text{OH})_3]^- + \text{H}_2\text{O} \tag{27.4}$$

$$\text{Si(OH)}_4 + \text{NaOH} \rightarrow \text{Na}^+[\text{OSi(OH)}_3]^- + \text{H}_2\text{O} \tag{27.5}$$

27.3.2.3 Production of geopolymers

The polymeric structure of Si-O-Al skeleton can be restructured by means of intermolecular polycondensation which is usually via nucleophilic addition-elimination reactions between $[OSi(OH)_3]^-$ and $[OAl(OH)_3]^{2-}$ species under alkaline conditions. The hydroxyl group of $[OSi(OH)_3]^-$ attacks the Al ion of $[OAl(OH)_3]^{2-}$ resulting in a nucleophilic addition reaction to produce an intermediate complex (Weng and Sagoe-Crentsil, 2007).

Two hydroxyl groups in the intermediate complex eliminate a H_2O molecule to form a chain-like geopolymer via an elimination reaction shown in Eq. (27.6). Further, an amorphous three-dimensional aluminosilicate network structure can be restructured through a polycondensation reaction that eliminates H_2O, as described in Eq. (27.7). Generally, it can be affirmed that the OH^- ion acts as a catalyst (Duxson *et al.*, 2007).

According to Davidovits' reports, the geopolymers having amorphous to semi-crystalline three-dimensional aluminosilicate structures were divided into the polysialate (Si-O-Al-O-), the polysialate-siloxo (Si-O-Al-O-Si-O-), and the polysialate-disiloxo (Si-O-Al-O-Si-O-Si-O-) (Davidovits, 1991).

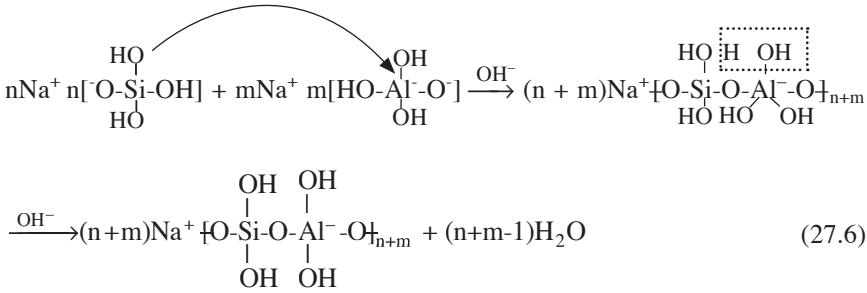

$$(n+m)\text{Na}^+ + (n+m-1)\text{H}_2\text{O} \tag{27.6}$$

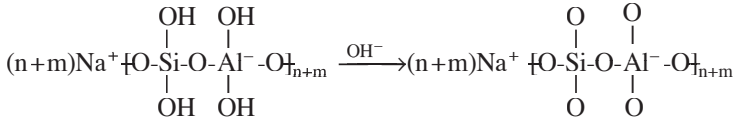

(27.7)

27.3.2.4 Generation of new mineral phases

The NaOH from the hydrolysis of sodium silicate increases the alkalinity in geopolymer paste. In such a case, the oligomers arising from the cleavages of glassy network structure consisting of SiO_4 and AlO_4 tetrahedron react with Ca^{2+} and Na^+ ions to produce the new mineral phases under the alkaline condition.

27.3.2.5 Generation of calcium silicate hydrate

The siliceous species could exist in the form of $[(HO)_2SiO_2]^{2-}$ and $[HOSiO_3]^{3-}$ under highly alkaline conditions so that the $[(HO)_3SiO]^-$ anions from the reaction shown by Eq. (27.5) further reacts with OH^- ion to produce the species in reactions described by Eqs (27.8) and (27.9) (Silva *et al.*, 2007). A new phase, calcium silicate hydrate (CSH), is generated by the reactions of Ca^{2+}, $HOSiO_3^{3-}$ and OH^- ions displayed in Eq. (27.10).

$$[(HO)_3SiO]^- + OH^- \rightarrow [(HO)_2SiO_2]^{2-} + H_2O \quad (27.8)$$

$$[(HO)_2SiO_2]^{2-} + OH^- \rightarrow [(HO)SiO_3]^{3-} + H_2O \quad (27.9)$$

$$Cd^{2+} + [(HO)SiO_3]^{3-} + OH^- \rightarrow CaSiO_4H_2O \quad (27.10)$$

27.3.2.6 Generation of tobermolite

Under alkaline catalytic conditions, two molecular $[(HO)_3SiO]^-$ and four molecular $[(HO)_2SiO_2]^{2-}$ groups undergo polycondensation to produce hexamer in Eq. (27.11), and then it further reacts with Ca^{2+} to generate tobermolite as shown in Eq. (27.12). Feng *et al.* (2004) reported that the glassy structure reacts with OH^- not only to produce $[(HO)_3SiO]^-$, $[(HO)_2SiO_2]^{2-}$ and $[HOSiO_3]^{3-}$ ionic groups, but also to generate distinct oligomers.

$$[(HO)_3SiO]^- + 4[(HO)_2SiO_2]^{2-} + [(HO)_3SiO]^-$$

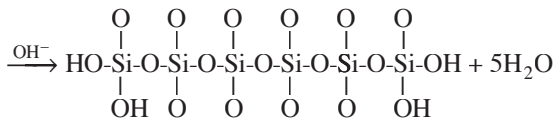

(27.11)

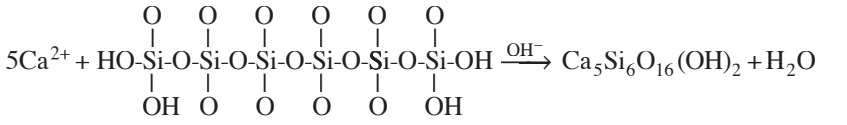

(27.12)

27.3.2.7 Generation of gismondine

Polycondensation of two molecular $Si(OH)_4$ and two molecular $Al^{-}(OH)_4$ groups involving H_2O loss will generate a tetramer containing silicon and aluminum under alkaline catalytic conditions depicted in Eq. (27.13), and then the tetramer reacts with Ca^{2+} to lose H_2O and produce gismondine in a reaction given by Eq. (27.14). Weng and Sagoe-Crentsil (2007) reported that the condensation reaction takes place between $Al^{-}(OH)_4$ and $[(HO)_3SiO]^{-}$ species.

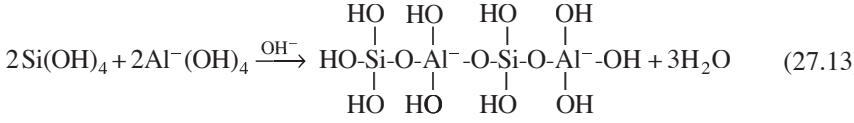

(27.13)

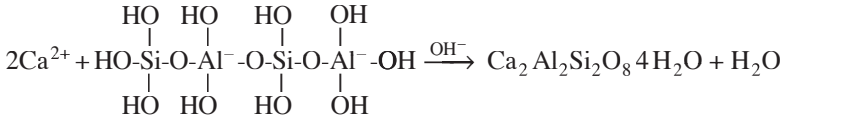

(27.14)

27.3.2.8 Generation of zoisite

One molecular $[(HO)_3SiO]^{-}$, one molecular $Al^{-}(OH)_4$ and two molecular $Si(OH)_4$ groups undergo polycondensation to eliminate water and generate hexamer as shown in Eq. (27.15). Then the hexamer reacts with Ca^{2+} to produce zoisite as shown in Eq. (27.16).

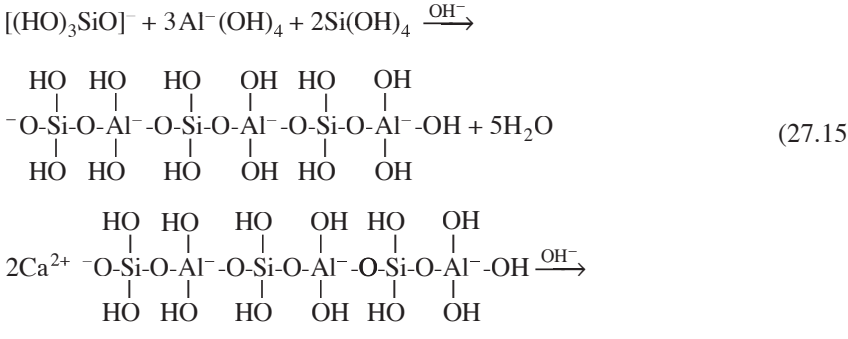

(27.15)

(27.16)

27.3.2.9 Generation of wairakite

Six molecules, four of $Si(OH)_4$ and two of $Al^-(OH)_4$, react to produce silicon and aluminum containing hexamers as shown by the reaction in Eq. (27.17), and then the hexamer sequentially reacts with Ca^{2+} to produce wairakite as shown in Eq. (27.18).

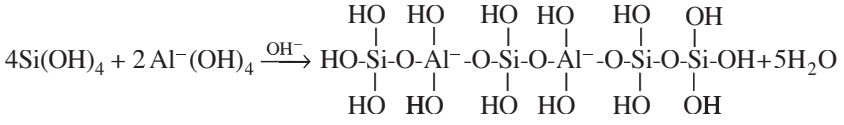

(27.17)

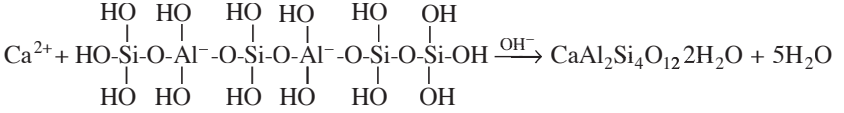

(27.18)

27.3.2.10 Generation of natrolite

The polycondensation takes place among three molecular $Si(OH)_4$ and two molecular $Al^-(OH)_4$ groups, to form the pentamer including three Si and two Al atoms, as shown in Eq. (27.19). Then the pentamer reacts with Na^+ to produce natrolite, as exhibited in Eq. (27.20).

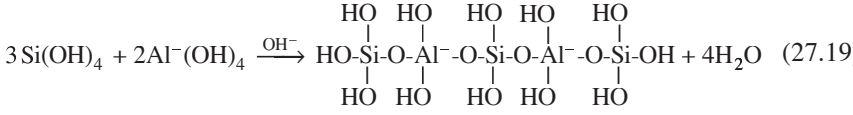

(27.19)

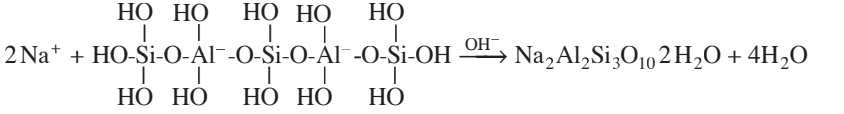

(27.20)

27.3.2.11 Generation of clinozoisite

Even if the chemical composition of clinozoisite is similar to zoisite, their crystal structures are different, that is, clinozoisite belongs to the monoclinic system while zoisite shows cubic structure. Anyway the reaction process for the formation of clinozoisite is similar to that of zoisite.

The hydration mechanism of geopolymer formed by sodium silicate activation of GBFS is via sodium metasilicate hydrolysis, cleavage of glassy network structure, formation of new gels of geopolymer and SCH, as well as generations of new mineral

phases through aluminosilicate oligomers reacting with Ca^{2+} and Na^{+} ions under OH^{-} catalysis.

27.4 Alkali-activated slag-based cementitious material (ASCM) coupled with Fe_2O_3 for photocatalytic degradation of Congo red (CR) dye

In this section, a novel alkali-activated granulated blast furnace slag-based cementitious material (ASCM) loaded with Fe_2O_3 was synthesized by a three-step reaction of polymerization, ion exchange and impregnation as mentioned above, and was used as a photocatalyst for the degradation of Congo red (CR) dye solution. The aims were: (i) to realize high value-added resource recycling of GBFS, (ii) to design a catalyst with low cost, environmentally friendly and energy-saving characteristics, (iii) to have excellent degradation efficiency for the wastewater of dye, and (iv) to make a catalyst with high compressive strength, which is easy to separate from suspension solution.

27.4.1 Structure characteristics of Fe_2O_3/ASCM catalysts

The chemical composition of samples is shown in Table 27.1. The contents of Na_2O and SiO_2 in GBFS are 0.57% and 27.51%, respectively, but those values in the Na-ASCM sample increase to 4.45% and 31.11%, respectively. After Na^{+} ions are replaced by NH^{4+} ions, the amount of Na_2O rapidly decreases to 0.14%, confirming the effectiveness of the ion exchange process at room temperature. Sazama *et al.* (2011) reported that the Na^{+} ions in the geopolymer network could be exchanged by Cu^{2+} or Co^{2+} ions at room temperature. The transformation of Na-ASCM into NH_4-ASCM attempts to reduce the alkalinity of ASCM and to prevent the generation of iron hydroxide precipitation in the process of wetness impregnation of Fe_2O_3.

Figure 27.6 shows TGA, DSC and DTG curves of the solid $Fe(NO_3)_3{\cdot}9H_2O$. The weight loss in the TGA curve can be divided into two steps. The weight loss in the first step, from room temperature to 108°C, reaches about 2.01% and the peak is observed at 87°C in DTG. The reaction heat given by the integral area (shaded area) approaches 3.80 $J{\cdot}g^{-1}$ in DSC. This reaction is then ascribed to the loss of free water. The weight loss in the second step from 108 to 314°C approaches 74.09% in TGA, and the peak is seen at 189°C in DTG. The reaction heat given by the integral area (shaded area) is up to 27.57 $J{\cdot}g^{-1}$ in DSC resulting from the thermal decomposition of solid $Fe(NO_3)_3{\cdot}9H_2O$. Therefore, this is the reason why the calcination temperature of the sample is selected to be 300°C.

Figure 27.7 displays the X-ray diffraction patterns of samples. From the pattern of GBFS it can be found that there is a broad diffuse hump in the region of 20–38 2θ, suggesting that the GBFS predominantly possesses glassy phase. In comparison with the pattern of GBFS, the amorphous hump has remarkably shifted towards

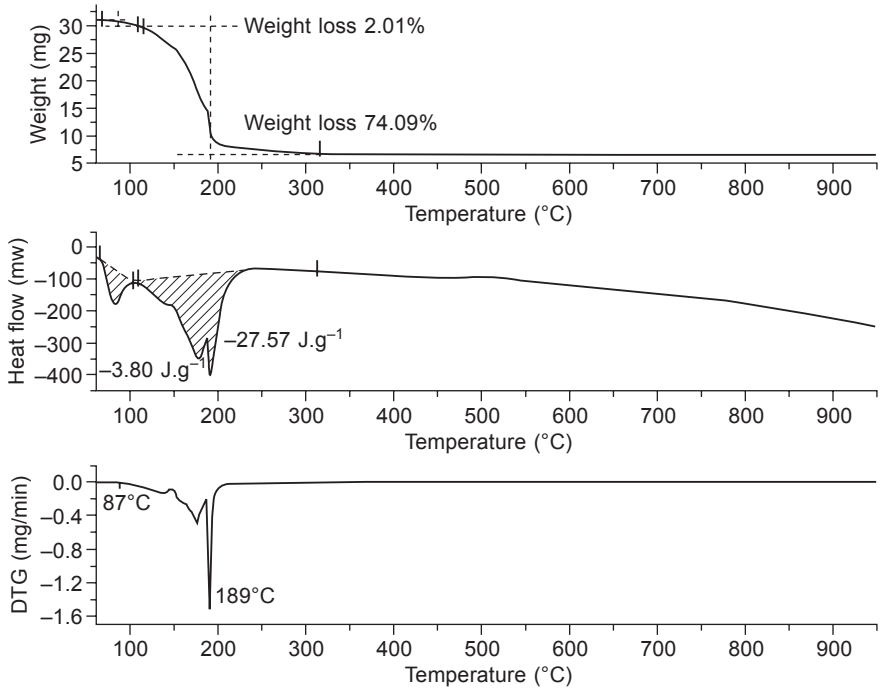

Figure 27.6 Thermogravimetric analysis (TGA), differential scanning calorimetry (DSC) and differential thermogravimetry (DTG) for the iron nitrate nonahydrate (reprinted from Zhang *et al.*, 2013, Copyright © 2013, with permission from Elsevier).

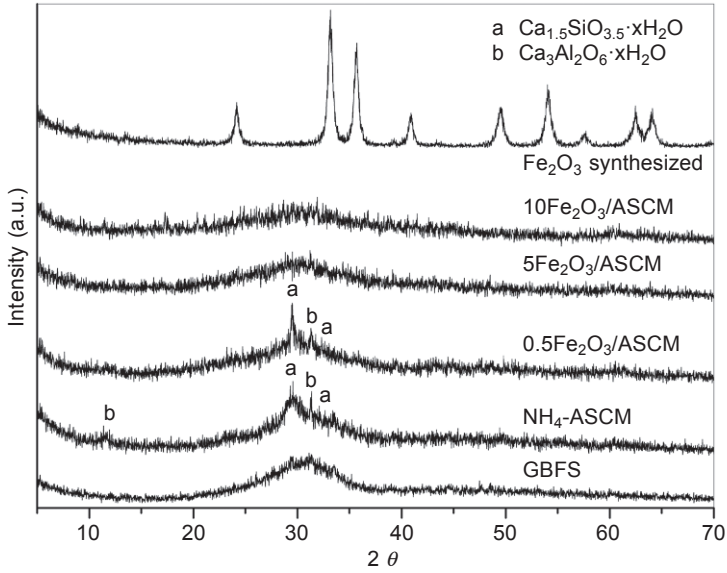

Figure 27.7 X-ray diffraction patterns of samples (reprinted from Zhang *et al.*, 2013, Copyright © 2013, with permission from Elsevier).

lower 2θ values in the pattern of NH_4-ASCM, indicating that the alkali-activated slag-based cementitious material is mainly constituted by amorphous phases (Duxson *et al*., 2007). Meanwhile, some small peaks superimposed on the amorphous hump at about 2θ = 29.4°, 32.1° are assigned to poorly crystalline phases of calcium silicate hydrate (CSH) (JCPDS No.00-033-0306), while the peaks at about 2θ = 11.4° and 31.3° are ascribed to the calcium aluminate hydrate (CAH) (JCPDS No.02-0083). Wang and Scrivener (1995) as well as Haha *et al*. (2011) reported that the CSH with low C/S ratio is the dominant hydration product, and Mozgawa and Deja (2009) confirmed that both CSH and CAH phases are present in alkali-activated GBFS. By looking to the XRD pattern of $0.5Fe_2O_3$/ASCM sample, no new peaks are visible, but the one observed in the Na-ASCM sample at 2θ = 11.4° disappeared. It is worth noting that the amorphous hump is further broadened and all peaks disappeared in samples containing increasing Fe_2O_3 amounts in the patterns of $5Fe_2O_3$/ASCM and $10Fe_2O_3$/ASCM. This suggests that Fe_2O_3 particles cover the surfaces of CSH and CAH phases forming well-dispersed clusters whose size is below the detection limit of XRD (Zhang *et al*., 2004). Perera *et al*. (2007a) reported the speciation of iron ions from octahedral coordination sites of MK-based geopolymer and no novel Fe-rich crystalline phases were detected.

Table 27.8 lists some physical parameters of samples, such as BET specific surface area, pore volume, average pore size and pore volume percentage. The GBFS sample shows the smallest S_{BET} (10.63 $m^2 \cdot g^{-1}$) and pore volume (0.034 $mL \cdot g^{-1}$) values. After the NH_4^+ for Na^+ ionic exchange treatment, with formation of NH_4-ASCM, values of S_{BET} (61.55 $m^2 \cdot g^{-1}$), pore volume (0.16 $mL \cdot g^{-1}$) and mesoporous volume percentage (73.69%) have significantly increased compared to the GBFS sample. This suggests that NH_4-ASCM with bigger mesoporous volume percentage is beneficial to adsorption of CR molecule having 3D size of 3 nm × 0.25 nm × 0.73 nm. Li *et al*. (2006) reported that synthesized alkali-activated fly ash binders exhibited much higher adsorption capacity than fly ash itself and natural zeolites.

Figure 27.8 shows the images of field emission scanning electron microscopy (FESEM) coupled with energy dispersive X-ray analysis (EDXA) for the $5Fe_2O_3$/ASCM sample. The morphology of the ASCM support denotes the presence of nanoparticle aggregates with mean particle size of about 50 nm. However, it is

Table 27.8 BET specific surface area, pore volume, average pore size and pore volume percentage

Sample	S_{BET} (m^2/g)	Pore volume (mL/g)	Average pore size (nm)	Pore volume (%)		
				< 5 nm	5-50 nm	> 50 nm
GBFS	10.63	0.034	12.71	33.08	51.41	15.51
NH_4-ASCM	61.55	0.16	10.44	21.14	73.69	5.17
$5Fe_2O_3$/ASCM	57.76	0.14	9.48	26.92	69.17	3.91
$10Fe_2O_3$/ASCM	60.42	0.10	6.79	38.37	58.08	3.55

Source: Reprinted from Zhang *et al*., 2013, Copyright © 2013, with permission from Elsevier.

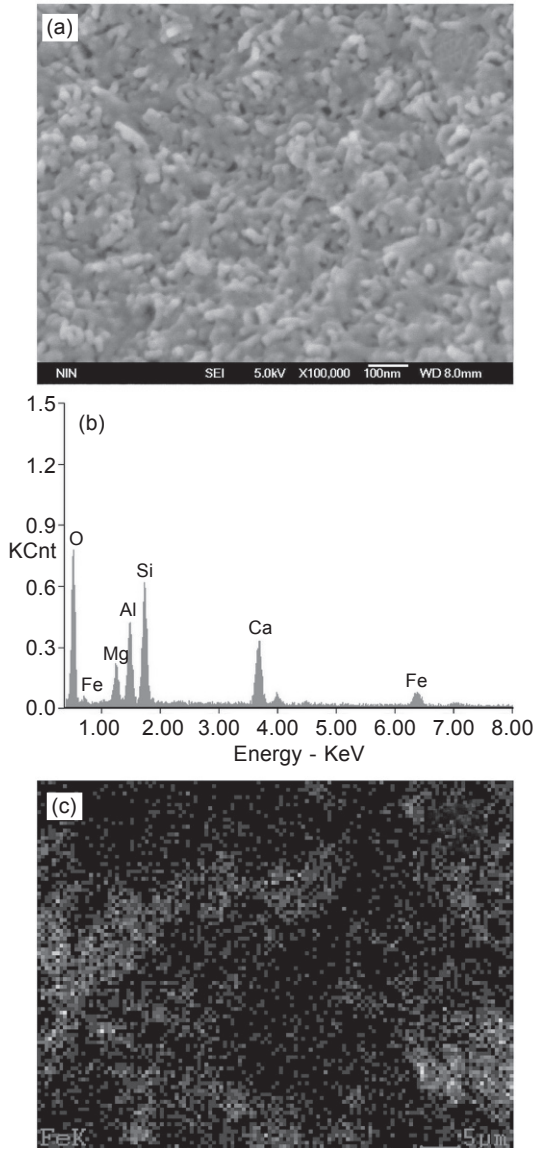

Figure 27.8 FESEM images coupled with EDXA for the $5Fe_2O_3$/ASCM sample: (a) FESEM image, (b) EDXA, and (c) Fe elemental map (reprinted from Zhang *et al.*, 2013, Copyright © 2013, with permission from Elsevier).

difficult to identify the particle size of Fe_2O_3 in Figure 27.8(a). By combining with XRD results in Figure 27.7 it can be suggested that the Fe_2O_3 particles are forming clusters. The EDXA result shows that the $5Fe_2O_3$/ASCM sample is mainly composed of Al, Ca, Fe, Mg, Si and O elements in Figure 27.8(b). The elemental map in Figure 27.8(c) shows that Fe particles or clusters are uniformly dispersed through the ASCM matrix.

Figure 27.9 presents the diffuse reflectance UV-vis near infrared ray spectra of samples. It can be observed that the absorption edges in the range of 250–700 nm are gradually blue-shifted with the decrease of Fe content due to the quantum size effect. But the spectrum intensity decreases in order of $5Fe_2O_3$/ASCM < $10Fe_2O_3$/ASCM < $0.5Fe_2O_3$/ASCM < Na-ASCM in the near infrared region, especially for the peaks located at 1424 and 2221 nm as a consequence of the strong interaction between Fe_2O_3 clusters and ASCM.

Figure 27.10 shows the photoluminescence spectra of samples excited by a 150

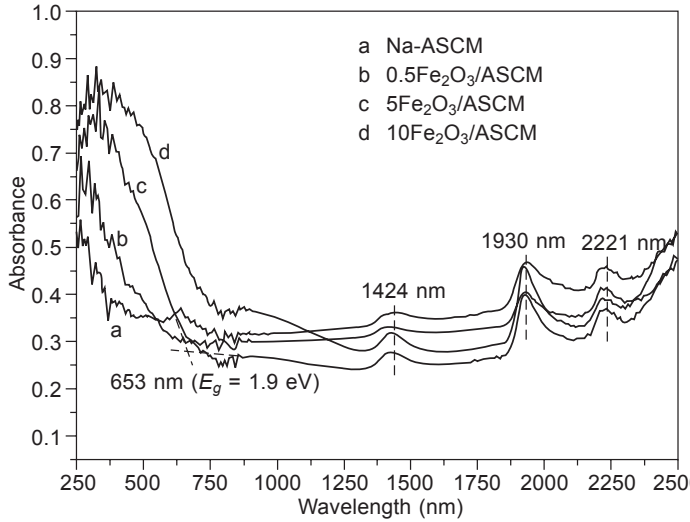

Figure 27.9 Diffuse reflectance UV-vis near infrared ray spectra of samples (reprinted from Zhang *et al.*, 2013, Copyright © 2013, with permission from Elsevier).

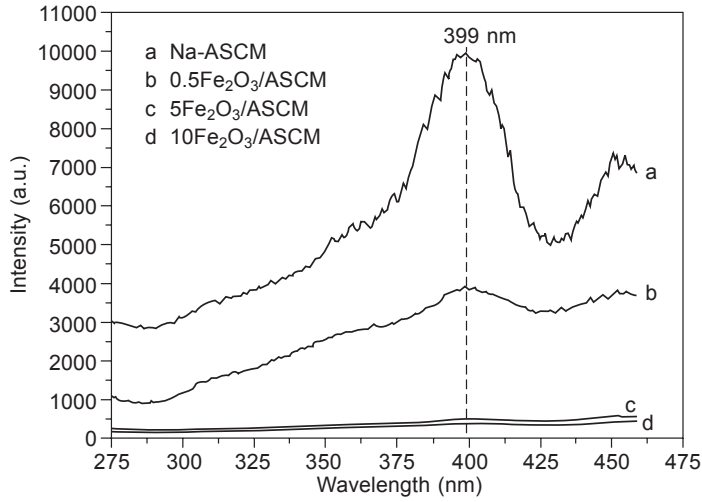

Figure 27.10 Photoluminescence spectra of specimens excited by a 150 W xenon lamp with an excitation wavelength of 250 nm (reprinted from Zhang *et al.*, 2013, Copyright © 2013, with permission from Elsevier).

W xenon lamp, emitting light of 250 nm wavelength. All samples show an emission peak at 399 nm, being highest for Na-ASCM. This suggests that recombination of photogenerated electron-hole pairs is faster in this material. The photoluminescence peak decreases sharply with increasing amount of Fe_2O_3, implying that the transition frequency of photogenerated electrons is quickened up and the recombination rate of electron-hole pairs largely diminishes in the interface of Fe_2O_3 clusters and porous ASCM (Chen *et al.*, 1998).

27.4.2 Photocatalytic degradation efficiency of CR dye

Figure 27.11 shows the degradation activities of different catalysts for CR. In order to know about the activities such as photocatalytic degradation, adsorption and photolysis, some experiments are designed as below. Both photocatalytic degradation for the Fe-immobilized catalysts and the removal of color tests for the Na-ASCM are carried out in an aqueous CR solution with suspending catalyst particles under UV irradiation in Figure 27.11(a)–(d). In the adsorption experiment, the aqueous CR solution with suspending catalyst is put in the dark as shown in Figure 27.11(e)–(g). The photolysis test involves that the aqueous CR solution is exposed to UV light in Figure 27.11(h). It can be found from Figure 27.11 that a series of Fe_2O_3/ASCM catalysts show excellent photocatalytic degradation rate in the following order: 100%

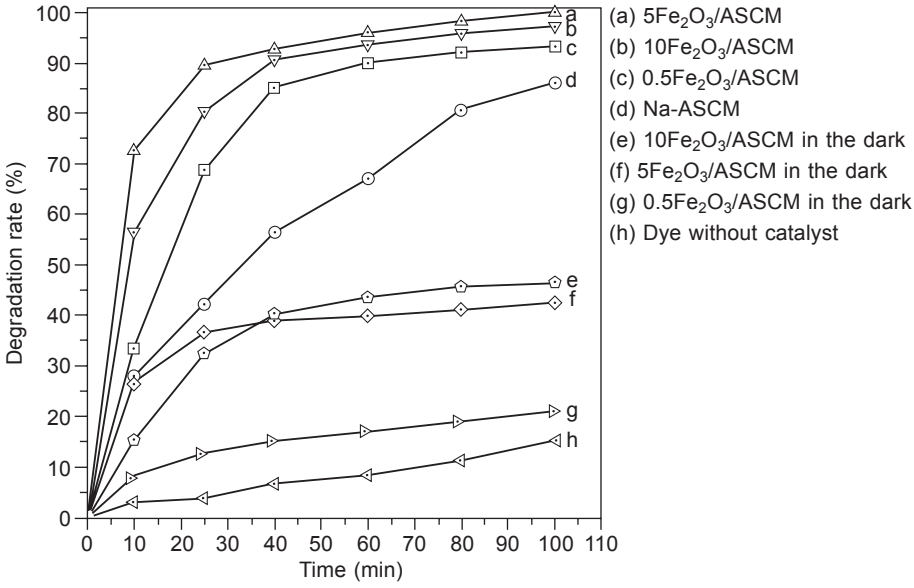

Figure 27.11 Degradation activities of different catalysts for CR dye under UV light irradiation (sample dosage: 0.4 g, initial concentration of CR: 6 mg·L^{-1}, solution: 100 mL, the maximum absorption wavelength of 500 nm) (reprinted from Zhang *et al.*, 2013, Copyright © 2013, with permission from Elsevier).

($5Fe_2O_3$/ASCM) > 97.3% ($10Fe_2O_3$/ASCM) > 93.2% ($0.5Fe_2O_3$/ASCM) > 86% (Na-ASCM). As compared with Na-ASCM, the higher activities for the Fe_2O_3/ASCM catalysts are considered to be the result of strong interaction between active species of Fe_2O_3 clusters and ASCM. The highest photocatalytic degradation rate for the $5Fe_2O_3$/ASCM catalyst is probably ascribed to the fact that the $5Fe_2O_3$/ASCM catalyst has the lowest absorption intensity in the near infrared region in Figure 27.9, and the active species of Fe_2O_3 clusters dispersed homogeneously on the ASCM surface provides much more effectively active sites to promote the photocatalytic degradation reaction. The lower removal efficiency for the Na-ASCM probably results from the fact that the CR dyes having sulfonate groups (CR-SO_3^-) with negative charges are strongly adsorbed on the Na^+ sites of the Na-ASCM via an electrostatic interaction. The adsorption results are as follows: 46.5% ($10Fe_2O_3$/ASCM) > 42.5% ($5Fe_2O_3$/ASCM) > 21.0% ($0.5Fe_2O_3$/ASCM), suggesting that the removal rate of CR is in proportion to the Fe_2O_3 loading. It can be observed that the aqueous CR solution shows the lowest photolysis rate of 15.3% due to an absence of catalyst.

Figure 27.12 shows the UV-vis absorption spectra of samples. The absorption spectrum of 6 $mg \cdot L^{-1}$ solution of CR shows two bands, one of which is in the visible region with maximum absorption at 500 nm and the other is in the ultraviolet region at 344 nm in Figure 27.12(a). It is assigned to be the band at 500 nm for azo bonds and the band at 344 nm for benzene and naphthalene rings in the CR molecule (Wang *et al.*, 2008). After the photocatalytic degradation of CR in the solutions suspending a solid Fe_2O_3/ASCM catalyst for 100 min, the absorption peaks of degradation

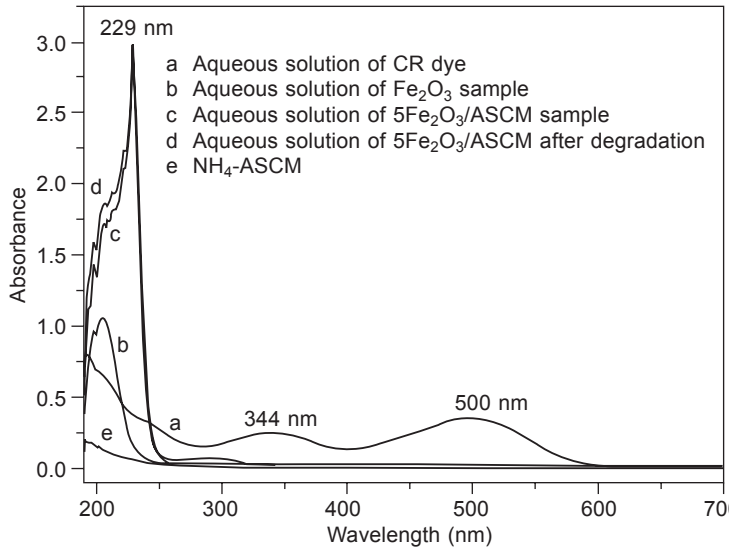

Figure 27.12 UV-vis spectra of samples: (a) aqueous solution of CR dye, (b) aqueous solution of Fe_2O_3 sample, (c) aqueous solution of $5Fe_2O_3$/ASCM sample, (d) aqueous solution of $5Fe_2O_3$/ASCM after degradation for 100 min, and (e) aqueous solution of ASCM sample (reprinted from Zhang *et al.*, 2013, Copyright © 2013, with permission from Elsevier).

products almost completely disappear in the range of 254–600 nm in Figure 27.12(d), demonstrating that the conjugated part, azo bond and some naphthalene rings in the molecule are destroyed. It is known that the hydroxyl radical (·OH) is the major oxidative intermediate to react with the azo bond in high rate coefficients (Flamigni and Monti, 1985).

To understand whether the sharp peak at 229 nm in Figure 27.12(d) originates from the residual fragment of dye or not, three kinds of contrast tests are performed, which involve $5Fe_2O_3$/ASCM, NH_4-ASCM and Fe_2O_3 samples being put into water for 100 min and then centrifugal separation is carried out, respectively. It can be found that the UV-vis spectrum of aqueous solution for the $5Fe_2O_3$/ASCM sample in Figure 27.12(c) is almost overlapping with the $5Fe_2O_3$/ASCM sample after degradation in Figure 27.12(d). There is a middle of peak for Fe_2O_3 sample in Figure 27.12(b) and no peak for NH_4-ASCM sample in Figure 27.12(e). Therefore, it can be taken into account that the peak at 229 nm in Figure 27.12(d) is closely associated with the strong interaction between Fe_2O and ASCM.

27.4.3 Photocatalytic degradation kinetics of CR dye

To know the kinetics of photocatalytic degradation of CR in solutions suspended on Fe_2O_3/ASCM particles, the experimental results were fitted in Figure 27.11 by equation transducing different kinetics reactions (different orders). The results are shown in Table 27.9. Each correlation coefficient was calculated from the kinetics equation, where R_0, R_1, R_2 and R_3 represent the correlation coefficient of zero, first, second and third order rate equations, respectively. Best fitting seems to be assured by R_2 (correlation ranges of 0.96232–0.99368) for the different catalysts. Therefore, it is suggested that the photocatalytic degradation of CR dye in the solutions suspended on solid Fe_2O_3/ASCM catalyst follows the second-order kinetics. From Table 27.9 it is seen that the k_2, the rate constant of the second-order reaction kinetics, follows the order: 0.06196 ($5Fe_2O_3$/ASCM) > 0.04678 ($10Fe_2O_3$/ASCM) > 0.02470 ($0.5Fe_2O_3$/ASCM) > 0.00986 (Na-ASCM), and also the $t_{1/2}$, half-life, has a negative order: 2.69 ($5Fe_2O_3$/ASCM) < 3.56 ($10Fe_2O_3$/ASCM) < 6.75 ($0.5Fe_2O_3$/ASCM) < 16.90 (Na-ASCM).

27.4.4 Photocatalytic oxidative degradation mechanism

A possible mechanism for photocatalytic oxidative degradation of CR is put forward in Figure 27.13. Congo red, 1-naphthalenesulfonic acid-3,3′-(4,4′-biphenylene bis (azo)) bis (4-amino-) disodium salt, is a benzidine-based anionic diazo dye. In the aqueous solution, this anionic diazo dye dissolves and ionizes out an anion of sulfonate group (for short CR-SO_3^-) as shown in Eq. (27.21).

$$\text{CR-SO}_3\text{Na} \xrightarrow{\text{H}_2\text{O}} \text{CR-SO}_3^- + \text{Na}^+ \tag{27.21}$$

Fe_2O_3 particles or clusters covering the surface of CSH and CAH phases have

Table 27.9 Kinetics equation of photocatalytic degradation of CR

Composite	Order (second)	k_2 ($L \cdot mg^{-1} \cdot min^{-1}$)	R_0	R_1	R_2	R_3	$t_{1/2}$(min)
Na-ASCM	$1/C_t = 0.00986t+0.07602$	0.00986	-0.95547	0.99628	0.96232	0.89781	16.90
$0.5Fe_2O_3$/ASCM	$1/C_t = 0.0247t+0.07292$	0.02470	-0.84493	0.95157	0.99361	0.97715	6.75
$5Fe_2O_3$/ASCM	$1/C_t = 0.06196t+0.04147$	0.06196	-0.70518	0.95592	0.99368	0.831	2.69
$10Fe_2O_3$/ASCM	$1/C_t = 0.04678t-0.05866$	0.04678	-0.77545	0.96232	0.99278	0.87989	3.56

Source: Reprinted from Zhang *et al*., 2013, Copyright © 2013, with permission from Elsevier.

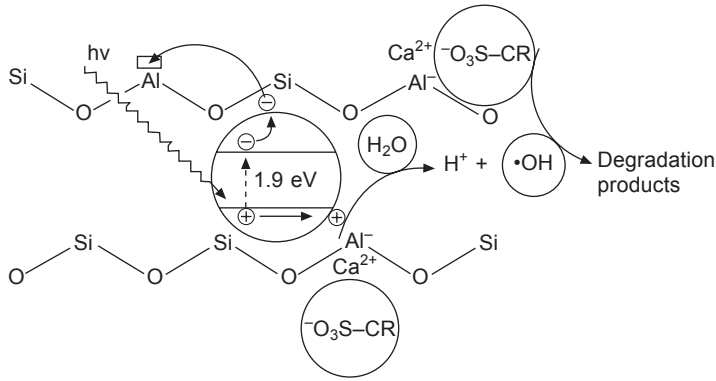

Figure 27.13 A mechanism of photocatalytic degradation of CR (reprinted from Zhang *et al*., 2013, Copyright © 2013, with permission from Elsevier).

semiconducting properties, having a narrow bandgap of about 1.9 eV as estimated from Figure 27.9(c). Gulshan *et al*. (2010) reported that the iron oxides of maghemite and hematite are semiconductors and thus are able to photodecompose methylene blue dye once irradiated by UV, visible and solar radiation. As the Fe_2O_3 particles are irradiated by a beam of UV light, an electron in the VB acquires the energy of a photon to become a photogenerated electron (e^-) which migrates to CB and simultaneously leaves behind a photogenerated hole (h^+) in the VB as shown in Eq. (27.22) and Figure 27.13.

$$Fe_2O_3 \xrightarrow{h\nu} Fe_2O_3(h^+) + e^- \tag{27.22}$$

The negative charges of AlO_4 tetrahedra located on the Si-O-Al framework of CSH gel are balanced by positive charges of Ca^{2+} ions (Duxson and Provis, 2008; Mozgawa and Deja, 2009). CR dye molecules are preferentially adsorbed on the surface-exposed Ca^{2+} sites due to stronger interaction between cationic Ca^{2+} and anionic sulfonate groups (CR-SO_3^-) as shown in Figure 27.13. In tetrahedral coordination, Al^{3+} and Si^{4+} have radii of 0.39 and 0.26 nm, respectively (Song and Jennings, 1999). In addition, Si^{4+} possesses a Z/r (charge density) more than twice that of Al^{3+}, and strongly polarizes the electron density on its neighboring oxygen atom (Gartner and Macphee, 2011) so that Al^{3+} ions in framework of CSH show a Lewis acidity which is able to ensnare photogenerated electrons (e^-) in Figure 27.13. The photogenerated hole (h^+) at the VB migrates to the surface of Fe_2O_3 clusters and reacts with H_2O molecules to produce hydroxyl radicals for the photocatalytic oxidation of dyes, as represented in Eq. (27.23) (Valenzuela *et al*., 2002; L. Zhang *et al*., 2011).

$$h^+ + H_2O \rightarrow H^+ + \bullet OH \tag{27.23}$$

The anionic sulfonate groups (CR-SO_3^-) adsorbed on the surface of catalyst particles are oxidized by hydroxyl radicals and generate the degradation products as shown in

Eq. (27.24). The hydroxyl radical (·OH) can successively participate in the oxidation reactions, until CR molecules are completely decomposed.

$$CR\text{-}SO_3^- + \bullet OH \rightarrow \text{Degradation products} \quad (27.24)$$

27.5 Alkali-activated steel slag-based (ASS) cement for photocatalytic degradation of methylene blue (MB) dye

The manufacture of ASS cement by utilization of steel slag is inexpensive and eco-friendly. The steel slag is a by-product from the conversion of pig iron to steel, and the methylene blue (MB) dye is one of the organic pollutants in wastewater disposed of by the dyeing and printing of textiles. In order to realize the dual purposes of the resource recycling of steel slag and to remove dye pollutants from the wastewater, a new type of Ni,Ca-ASS cement was synthesized by polymerization of alkali-activated steel slag and ion exchange.

27.5.1 Microstructure and absorption spectrum of Ni,Ca-ASS cement

Table 27.2 shows the chemical composition of specimens. The Na_2O content in steel slag powders is about 0.15 wt.% and dramatically increases to 4.01 wt.% in Na,Ca-cementitious material due to the polymerization of steel slag activated by sodium hydroxide. After Na^+ ions in turn are exchanged by NH^{4+} and Ni^{2+} ions, the amount of Na_2O rapidly drops to 0.06 wt.% and the content of NiO increases to 6.95 wt.%, which means almost all Na^+ ions in the matrix of Na,Ca-ASS cement were replaced by Ni^{2+} ions at room temperature. Sazama *et al.* (2011) reported that the Na^+ ions in the vicinity of all the Al atoms in the geopolymer network could be exchanged by Cu^{2+} or Co^{2+} ions at room temperature. The current study revealed a similar situation when Ni^{2+} ions are present.

Figure 27.14 shows the XRD patterns of specimens. The steel slag powders show some mineral phases, such as calcium iron oxide ($Ca_2Fe_2O_5$, JCPDS No. 19-0222), belite (Ca_2SiO_4, JCPDS No. 98-000-0275), alite (Ca_3SiO_5, JCPDS No. 98-000-0043), portlandite ($Ca(OH)_2$, JCPDS No. 98-000-0359) and wüstite (FeO, JCPDS No. 46-1312). The details about these mineral phases including chemical formula, serial number of JCPDS and 2θ are summarized in Table 27.10 (Zhang *et al.*, 2012). The intensities of some diffraction peaks decrease remarkably and some peaks disappear in the pattern of Na,Ca-ASS cement compared with the pattern of steel slag powders in Figure 27.14, suggesting that the mineral phases in the steel slag such as $Ca_2Fe_2O_5$, $Ca(OH)_2$, Ca_2SiO_4, and Ca_3SiO_5, partially react with sodium hydroxide solution to generate two types of new hydrated products, metahalloysite ($Si_2Al_2O_5(OH)_2$, JCPDS No. 01-074-1023) and calcium silicate hydrate (CSH) ($Ca_{1.5}SiO_{3.5}{\cdot}xH_2O$, JCPDS No. 33-0306) (Sagoe-Crentsil and Weng, 2007). Yip *et al.* (2005) reported the formation

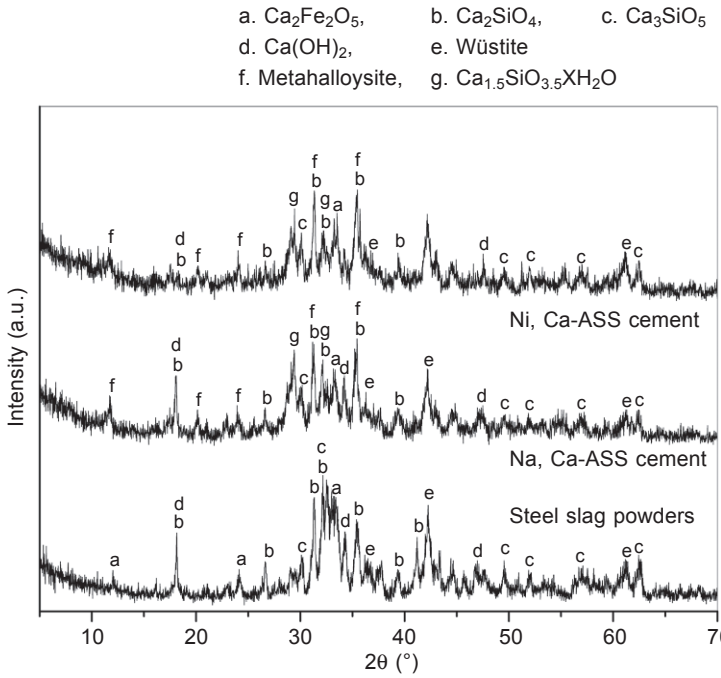

Figure 27.14 X-ray diffraction patterns of specimens (reprinted from Zhang *et al*., 2012, Copyright © 2012, with permission from Elsevier).

Table 27.10 Mineral phases of ASS cements

Mineral phase	Chemical formula	Number of JCPDS	2θ (°)
Calcium iron oxide	$Ca_2Fe_2O_5$	19-0222	12.00, 24.11, 33.35
Belite	Ca_2SiO_4	98-000-0275	18.08, 26.50, 31.19, 32.09, 35.36, 39.52, 41.28, 56.61
Alite	Ca_3SiO_5	98-000-0043	30.12, 32.24, 49.54, 51.92, 56.61, 62.45
Portlandite	$Ca(OH)_2$	98-000-0359	18.08, 34.11, 47.10
Wustite	FeO	46-1312	36.34, 42.15, 61.13
Metahalloysite	$Si_2Al_2O_5(OH)_4$	01-074-1023	11.48, 20.12, 23.85, 31.27, 35.36
Calcium silicate hydrate	$Ca_{1.5}SiO_{3.5}{\cdot}xH_2O$	33-0306	29.32, 32.09

Source: Reprinted from Zhang *et al*., 2012, Copyright © 2012, with permission from Elsevier.

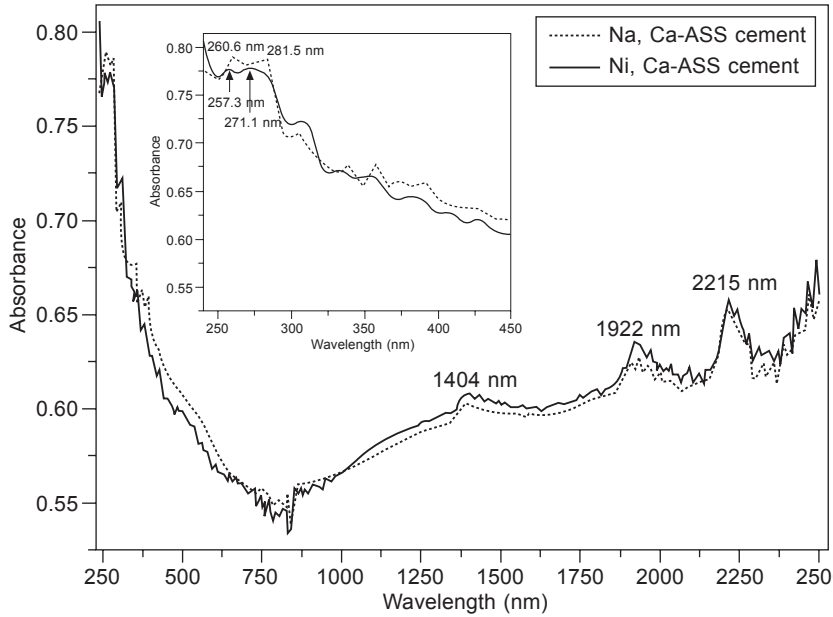

Figure 27.15 Diffuse reflectance UV-visible near infrared ray spectra of specimens (reprinted from Zhang *et al*., 2012, Copyright © 2012, with permission from Elsevier).

of Na geopolymer gel, Ca geopolymer gel and CSH gel in a metakaolin/GGBFS system. From Figure 27.14 it can be observed that the pattern of Ni,Ca-ASS cement is similar to that of Na,Ca-ASS cement except for the diminution of peak intensities of portlandite.

Figure 27.15 shows the diffuse reflectance UV-visible near infrared ray spectra of specimens. There are typical absorption bands in the range of 230–300 nm and they are much clearer after enlargement (top left of Figure 27.15). Absorption bands centered at 260.6 nm and 281.5 nm are observed in the Na,Ca-ASS cement sample, while these bands are slightly blue-shifted to 257.3 nm and 271.1 nm, respectively, in the Ni,Ca-ASS cement. The blue-shifted bands are probably attributed to the strong interaction of Ni^{2+} and negative charge of $[AlO_4]^{5-}$ tetrahedron in the framework of cementitious material as a result of Ni^{2+} ion (0.069 nm) with smaller ionic radius than Na^{+} ion (0.102 nm). In the near infrared ray region, three kinds of absorption bands are centred at 1404 nm, 1922 nm, and 2215 nm. They can be ascribed to the absorption of Si-OH bonds in the frameworks of Na,Ca-ASS and Ni,Ca-ASS cements. Elsherbiny *et al*. (2011) reported that the porous silica powders show a shielded complex $\equiv SiO–H(OH_2)$ absorption band at 1404 nm.

27.5.2 Photocatalytic degradation activities of MB dye

Figure 27.16 exhibits the photocatalytic degradation activities of samples for MB. The Ni,Ca-ASS catalyst shows the photocatalytic degradation rate of 94.39%, while

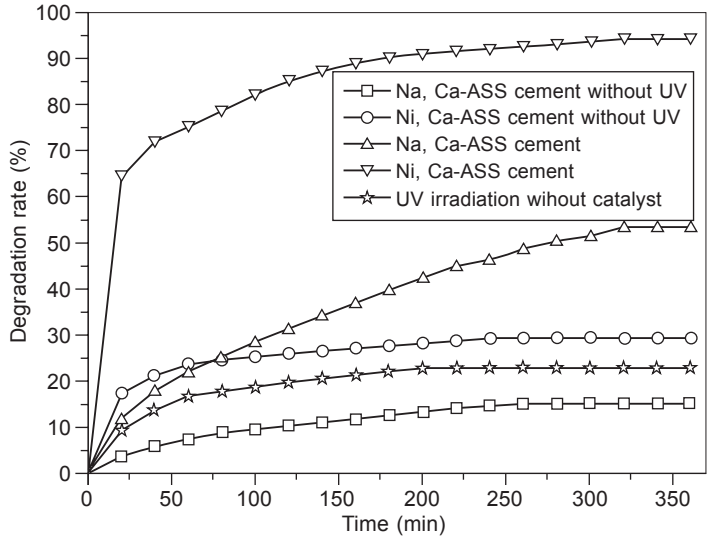

Figure 27.16 Photocatalytic degradation rate of MB dye under UV light irradiation (sample dosage: 0.2 g, initial concentration of MB: 4.01×10^{-6} M, solution: 100 mL, the maximum absorption wavelength of 665 nm) (reprinted from Zhang *et al.*, 2012, Copyright © 2012, with permission from Elsevier).

photocatalytic degradation rate for the Na,Ca-ASS catalyst is about 53.27% under UV irradiation. When the MB aqueous solution suspending catalyst was kept in the dark without UV irradiation, the catalytic degradation rate approaches 15.09% for the Na,Ca-ASS catalyst and 29.25% for the Ni,Ca-ASS catalyst. From Figure 27.16 it is also observed that the photolysis rate of MB is about 22.97%, as the MB solution is exposed to UV light without catalyst. For the Ni,Ca-ASS catalyst, the following conclusion can be drawn: photocatalytic degradation rate >> catalytic degradation rate (with catalyst and without UV) > photolysis rate (with UV and without catalyst). The highest photocatalytic degradation rate of MB for the Ni,Ca-ASS catalyst is considered to be the result of synergistic effects between the matrix of ASS cement and active Ni^{2+} species.

It is well known that the hydroxyl radical is the primary oxidant in the photocatalytic oxidation of organic compounds (Valenzuela *et al.*, 2002; L. Zhang *et al.*, 2011; Yang *et al.*, 2006). The electrode potential of hydroxyl radical (2.8 V) is much higher than that of MB (0.53 V) in aqueous solution. Thus, the MB cation adsorbed on the negatively charged $[AlO_4]^{5-}$ tetrahedron on the framework of the ASS cement can be photocatalytically oxidized by hydroxyl radical via demethylation, cleavage of chromophore ring and final degradation into CO_2, H_2O, NO_3^-, and SO_4^{2-} as shown in Eqs (27.25), (27.26), and (27.27), respectively (Houas *et al.*, 2001; Mozgawa and Deja, 2009; Zhang *et al.*, 2001):

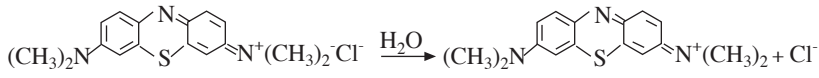

(27.25)

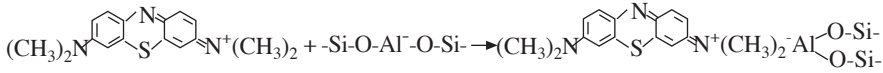

(27.26)

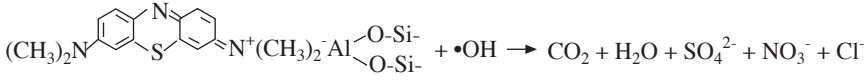

(27.27)

27.6 Alkali-activated fly ash-based (AFA) cement for photocatalytic degradation of MB dye

Fly ash is a solid waste generated from the combustion of coal in coal-fired power plants. It is estimated that the emission of fly ash is about 500 million tons per year worldwide (Ahmaruzzaman, 2010). It is considered that fly ash is a resource that has been put in the wrong place, and that has huge potential in applications in various new areas (Blissett and Rowson, 2012). It is recognized as one of the best ways to synthesize alkali-activated fly ash-based (AFA) cement due to its simple process, easy operation, reducing environmental pollution and turning waste into treasure (Bakharev, 2005b; Criado *et al*., 2005; Fernández-Jiménez and Palomo, 2005a, 2005b; Kovalchuk *et al*., 2007; Palomo *et al*., 2004; Rattanasak and Chindaprasirt, 2009; van Jaarsveld and van Deventer, 1999). AFA cements exhibit high mechanical properties, excellent encapsulation of radioactive wastes, solidification of hazardous wastes and fire-resistance (Bakharev, 2006; Phair *et al*., 2004; Temuujin *et al*., 2009). Corresponding to the different Si/Al ratios, the geopolymers are composed of network structures of polysialate (-O-Si-O-Al-O–), polysialate siloxo (-O-Si-O-Al-O-Si-O-), and polysialate disiloxo (-O-Si-O-Al-O-Si-O-Si-O-). The fly ash-based geopolymers with network structures can be used as adsorbents for removal of Pb^{2+} and Cu^{2+} ions from wastewater (Al-Zboon *et al*., 2011; Wang *et al*., 2007). They have also been employed as adsorbents to remove formaldehyde from indoor air (Wang *et al*., 2007) and to adsorb dye from aqueous solution (Huang and Han, 2011; Li *et al*., 2006). Even though fly ash-based geopolymers as adsorbents can remove the poisonous and harmful organic materials from the environment and aqueous solutions, the organic molecules adsorbed on the surface of geopolymers have not been degraded and easily cause secondary pollution. In order to explore a new approach for degradation of organic pollutants, the fly ash-based cement was prepared and then was used as a photocatalyst for the degradation of methylene blue (MB) dye from wastewater under UV irradiation, as described in this section.

27.6.1 Morphology, pore distribution and absorption spectrum of AFA cement

The chemical compositions of specimens are shown in Table 27.3. The fly ash with low calcium and rich in SiO_2 and Al_2O_3 is employed as a starting material for production of geopolymers with an amorphous or a zeolite-like structure by alkali-activated geopolymerization (Davidovits, 1991). The contents of Na_2O and SiO_2 in fly ash powders are 0.26 wt.% and 42.03 wt.%, respectively, and then dramatically increase to 4.70 wt.% and 51.15 wt.% in the fly ash-based geopolymer after the fly ash is activated by sodium silicate.

Mercury intrusion porosimetry is used to test the pore size distribution of geopolymer (Zhang *et al.*, 2010). Figure 27.17 shows the incremental intrusion and the differential intrusion of the AFA cement. It is observed that the cement displays a broad pore diameter distribution in the region of 3–10,000 nm and the differential pore size concentrates on 387 nm. The percentage of pores smaller than 17 nm and those greater than 700 nm in the total pore volumes are 4.8% and 3.0%, respectively. The dominant pore size fractions are centred at 17–170 nm and 170–700 nm corresponding to 29.1% and 63.1%, as shown in Figure 27.17 (Bernal *et al.*, 2011).

Figure 27.18 shows the diffuse reflectance UV-vis spectrum of the cement. A maximum absorption band occurs at the wavelength of 261 nm probably deriving from the absorption of transitional metal oxide TiO_2 in the matrix of fly ash. Three kinds of absorption bands located at 1390 nm, 1905 nm, and 2207 nm are explained as mentioned above.

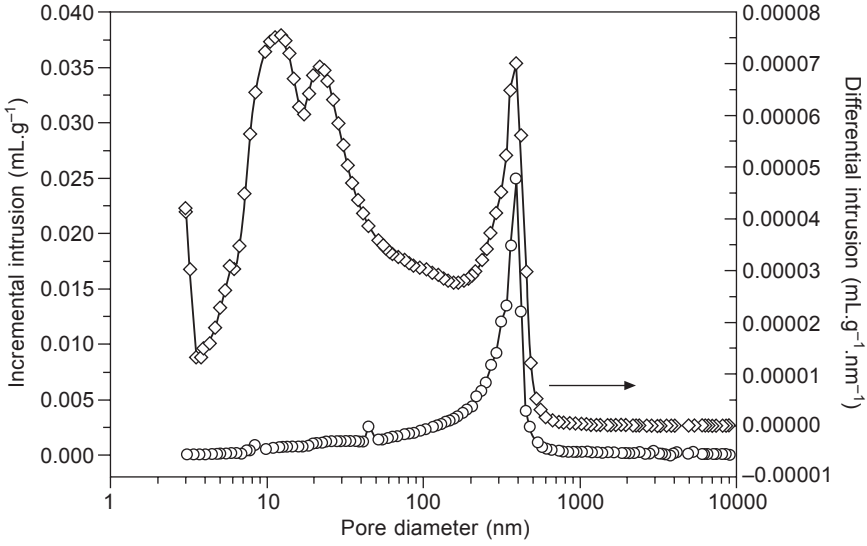

Figure 27.17 Pore diameter distributions of alkali-activated fly ash-based (AFA) cement (reprinted from Zhang and Liu, 2013, Copyright © 2013, with permission from Elsevier).

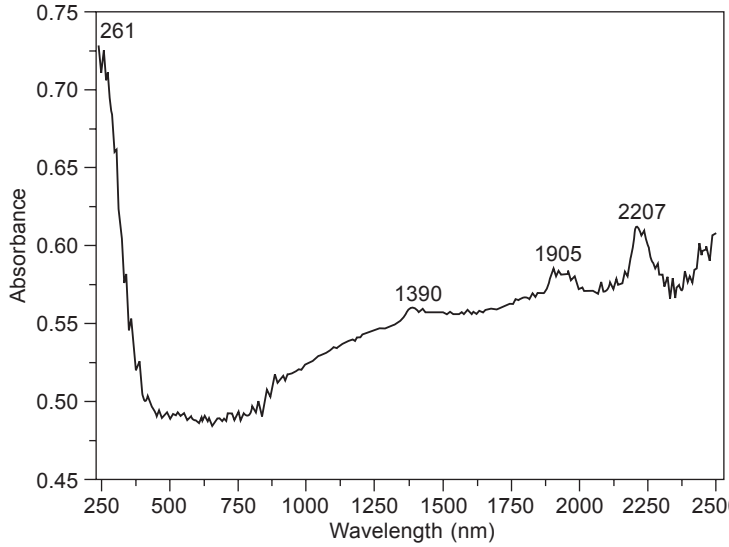

Figure 27.18 Diffuse reflectance UV-visible spectrum of alkali-activated fly ash-based (AFA) cement (reprinted from Zhang and Liu, 2013, Copyright © 2013, with permission from Elsevier).

27.6.2 Photocatalytic degradation activities of MB dye

Figure 27.19 shows the activities of removal of MB dye under different conditions. The lowest photolysis rate of 22.97% indicates that the partial MB molecules in

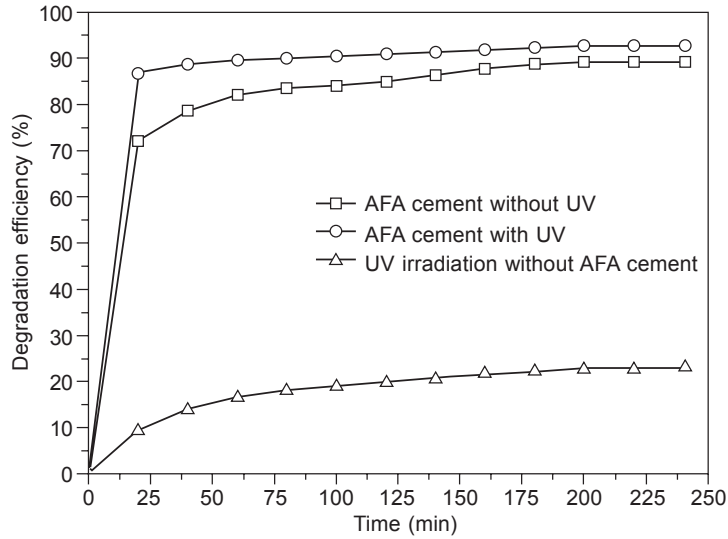

Figure 27.19 Photocatalytic degradation efficiency of MB under UV irradiation (sample dosage: 0.2 g, beginning concentration of MB: 4.01×10^{-6} M, solution: 100 mL, the maximum absorption wavelength of 665 nm) (reprinted from Zhang and Liu, 2013, Copyright © 2013, with permission from Elsevier).

solution can be directly decomposed by UV light without AFA catalyst. Higher removal efficiency of 89.15% manifests that AFA catalyst is a desirable adsorbent for removal of MB as described in Li *et al.* (2006). The highest photocatalytic degradation rate of 92.79% is simultaneously attributed to the combination of the adsorption of MB molecules and photocatalysis. Larger average pore diameter of 93.9 nm and bigger pore volume of 0.21 $mL \cdot g^{-1}$ in Figure 27.17 are beneficial to the adsorptions and diffusions of MB molecules (Pelekani and Snoeyink, 2000).

27.6.3 Adsorption kinetics of MB dye

In order to further study the adsorption kinetics of MB, the experimental data from Figure 27.19 were fitted by distinct functions that correspond to the pseudo-first-order, pseudo-second-order rate equations, and intra-particle diffusion mechanisms. Lagergren (1898) proposed a pseudo-first-order rate equation for the sorption of liquid–solid systems as described in Eq. (27.28).

$$\log (q_e - q_t) = \log q_e - \frac{k_1}{2.303} t \tag{27.28}$$

where q_e ($mg \cdot g^{-1}$) and q_t ($mg \cdot g^{-1}$) are the sorption capacities of MB dye at equilibrium and at a time t, respectively, and k_1 (min^{-1}) is the first-order rate constant. By plotting $\log (q_e - q_t)$ versus t, the first-order rate constant k_1 and the equilibrium capacity (q_e) can be estimated from the slope and intercept, respectively. Ho and McKay (1999) put forward a pseudo-second-order rate equation based on the amount of adsorbate on the adsorbent as displayed in Eq. (27.29).

$$\frac{t}{q_t} = \frac{1}{k_2 q_e^2} + \frac{1}{q_e} t \tag{27.29}$$

where q_e ($mg \cdot g^{-1}$) and q_t ($mg \cdot g^{-1}$) are the sorption capacities of MB at equilibrium and at a time t, respectively, and k_2 ($g \cdot mg^{-1} \cdot min^{-1}$) is the second-order rate constant. By plotting t/q_t versus t, the second-order rate constant (k_2) and the equilibrium capacity (q_e) are obtained from the intercept and slope, respectively. Crank (1933) established an intra-particle diffusion rate equation as expressed in Eq. (27.30).

$$q_t = k_p \times t^{1/2} + c \tag{27.30}$$

where q_t is the amount of adsorbed dye at t time, c is the intercept and k_p is the intra-particle diffusion rate constant ($mg/(g \cdot min^{1/2})$).

The fitting of experimental data from Figure 27.19 was carried out using Eqs (27.28)–(27.30). The values of correlation coefficients (R^2) estimated from the adjustment to a pseudo-first-order rate equation are 0.773 and 0.895 under and without UV irradiation, respectively. This indicates that the correlations do not fit quite well to the experimental results in Table 27.11. Moreover, the equilibrium adsorption capacity (q_e) calculated from the pseudo-first-order rate equation is much lower than the experimental value of q_{ec} in Table 27.11, which indicates that the

Table 27.11 Parameters of kinetics models for the adsorption of MB on AFA cement

Condition	q_{ec} ($mg \cdot g^{-1}$)	First-order kinetics parameter			Second-order kinetics parameter			Intra-particle diffusion parameter	
		k_1 (min^{-1})	q_e ($mg \cdot g^{-1}$)	R^2	k_2 ($g \cdot mg^{-1} min^{-1}$)	q_e ($mg \cdot g^{-1}$)	R^2	k_p $mg \cdot (g \cdot min^{1/2})^{-1}$	R^2
Without UV	0.669	0.022	0.30	0.895	0.202	0.687	0.999	0.012	0.933
With UV	0.696	0.021	0.14	0.773	0.576	0.701	0.999	0.004	0.982

Source: Reprinted from Zhang and Liu, 2013, Copyright © 2013, with permission from Elsevier.

model of the pseudo-first-order rate equation does not fit the adsorption of MB on the fly ash-based cement.

From Table 27.11, Figure 27.20(a and b) it can be found that correlation coefficients of MB absorbed on the fly ash-based cement by linear regression of the

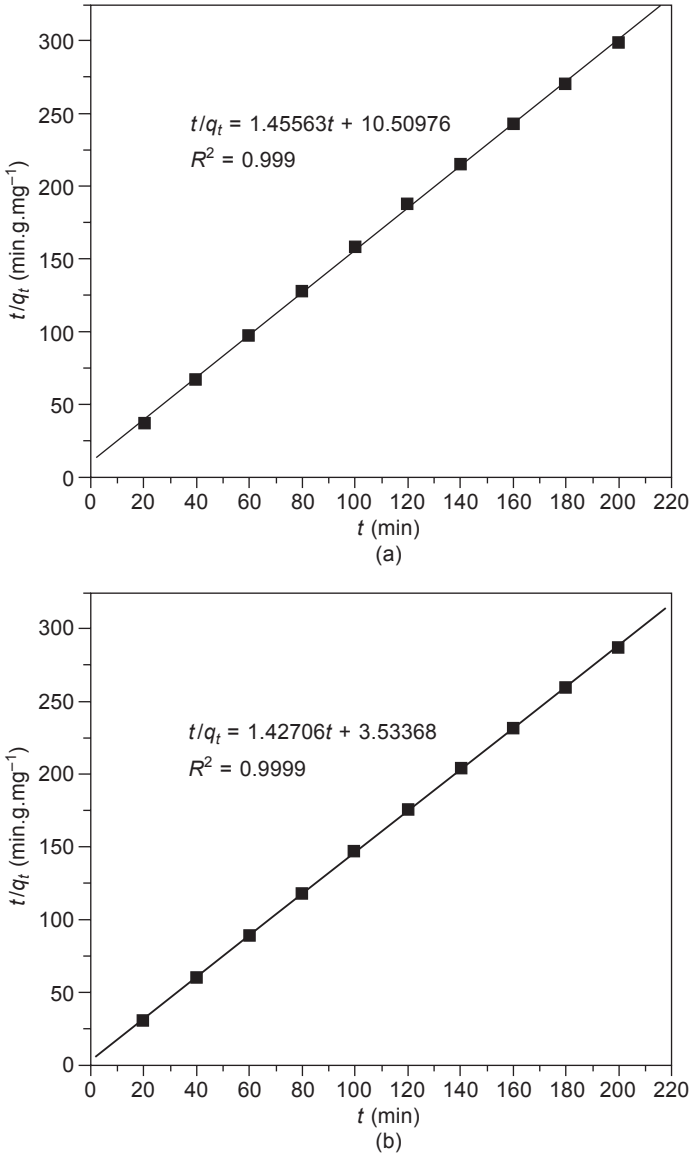

Figure 27.20 Plots of pseudo-second-order kinetics of MB adsorption on AFA cement: (a) without UV irradiation and (b) under UV irradiation (reprinted from Zhang and Liu, 2013, Copyright © 2013, with permission from Elsevier).

pseudo-second-order rate equation in both cases of with UV and without UV irradiations reach $R^2 = 0.999$, respectively, and the calculated values of q_e are surprisingly close to the experimental data of q_{ec} in both cases, respectively. So, the adsorption kinetics of MB on the AFA cement is considered to correspond to the pseudo-second-order

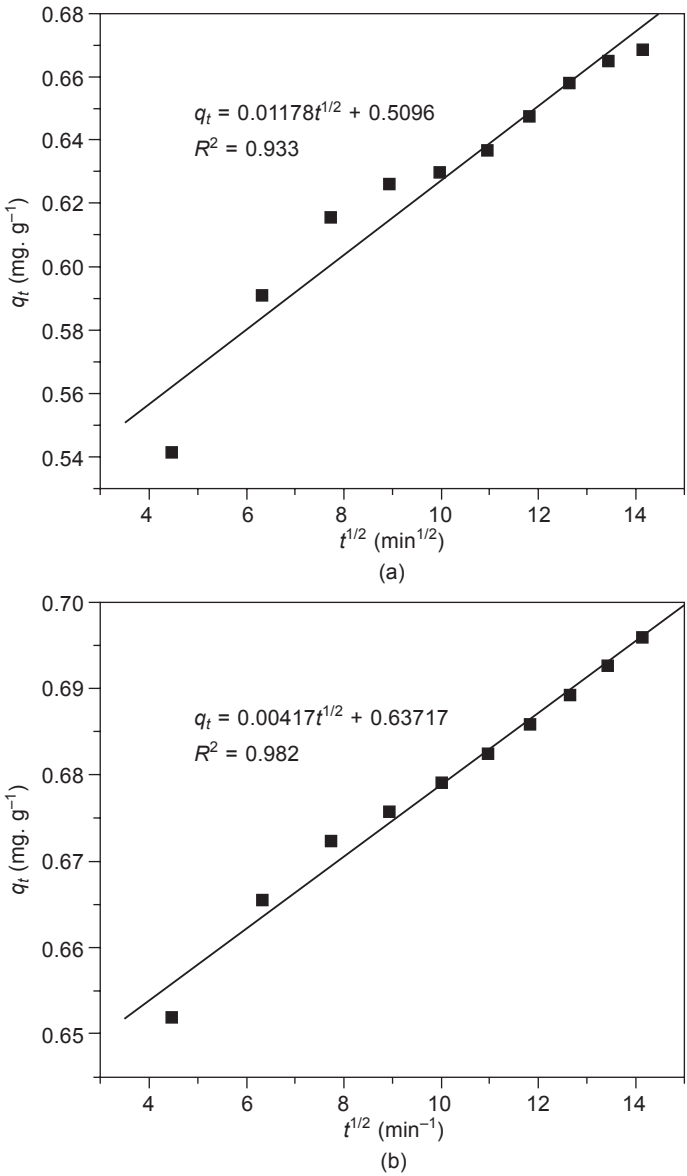

Figure 27.21 Plots of intra-particle diffusion kinetics of MB adsorption on AFA cement: (a) without UV irradiation and (b) under UV irradiation (reprinted from Zhang and Liu, 2013, Copyright © 2013, with permission from Elsevier).

rate equation. Li *et al*. (2006) reported that the MB adsorption on fly ash-based cement produced by solid fusion method also follows a pseudo-second-order rate kinetics. However, the adsorption rate constant of $k = 0.576$ ($g\cdot(mg\cdot min)^{-1}$) under UV irradiation is much bigger than the value estimated without light ($k = 0.202$ ($g\cdot(mg\cdot min)^{-1}$)), suggesting that the adsorption rate is photo-promoted.

The intra-particle diffusion plots are given in Figure 27.21(a) and 27.21(b). The values of q_t are found not to be linearly correlated with the values of $t^{1/2}$, which suggests that the intra-particle diffusion process is not the rate determining step. Therefore, the kinetic analysis indicates that the adsorption rate of MB dye on the AFA cement is simultaneously governed by liquid film diffusion, intra-particle diffusion, and surface sorption in the pseudo-second-order kinetics equation.

27.7 Conclusions

Three types of Fe_2O_3/ASCM, Ni,Ca-ASS and AFA cements were prepared and used as new photocatalysts for degradation of organic dye solution.

The hydration mechanism of GBFS is via hydrolysis of sodium metasilicate, cleavage of glassy network structure, generation of CSH and some mineral phases. The anion of CR dye (CR-SO_3^-) preferentially adsorbed on the Lewis acidity of Al^{3+} and Bronsted acidity of bridging hydroxyl group on the Si-O-Al framework of ASCM, and then was oxidized due to degradation by the hydroxyl radicals. High degradation activities for a set of Fe_2O_3/ASCM catalysts can be attributed to the strong interaction between ASCM and active Fe_2O_3 species.

There are two kinds of hydrated products, metahalloysite ($Si_2Al_2O_5(OH)_4$) and calcium silicate hydrate (CSH), in Ni,Ca-ASS cement. In the process of photocatalytic oxidative degradation of MB, the Ni^{2+} ions act as a critical role in transmission of photogenerated electrons so as to enhance separation efficiency of the electron-hole pairs and improve the photocatalytic degradation efficiency.

The differential pore size distribution centered on 387 nm in AFA cement is beneficial to adsorption and diffusion of MB molecules. The MB adsorption on AFA cement follows pseudo-second-order adsorption kinetics. The adsorption rate of MB dye is simultaneously controlled by liquid film diffusion, intra-particle diffusion and surface sorption.

27.8 Future trends

Even though the versatility of alkali-activated cements has been investigated for many years, there are many potential applications for us to exploit:

1. Learning from the applications of the photoactive TiO_2 in cement and mortar for air purification and photodegradation of NO_x (Pacheco-Torgal and Jalali, 2011; Chen and Poon, 2009; Diamanti *et al*., 2008; Maggos *et al*., 2008; Poon and Cheung, 2007; Matejka

et al., 2012; Cardenas *et al.*, 2012), the alkali-activated cement-based binary and multi-composites can be synthesized by combination of alkali-activated cement with transition oxide semiconductors for the application of photocatalytic degradation of wastewater.

2. For the global environmental and energy issues, production of hydrogen from photocatalytic water splitting is considered as a promising solar energy conversion method. The low cost and environmentally friendly alkali-activated cements can be employed as a novel catalyst for the production of hydrogen by photocatalytic water-splitting under solar irradiation (Zhang and Chai, 2014).

27.9 Sources of further information and advice

Many raw materials sources rich in alumina and silica, such as fly ash, steel slag, granulated blast furnace slag, kaolins, calcined clays, volcanic ash, titanium slag, red mud, magnesium slag and various kinds of tailing wastes, can be experimented with to fabricate the alkali-activated cements.

The available low cost and eco-friendly alkali-activated cements can be used as photocatalysts and adsorbents for the removal of hazardous dyes and heavy metal ions from various industrial, municipal and agricultural sewages, including textiles, leather, paper, printing, cosmetics, poultry and civil wastewater at the laboratory scale and pilot-plant scale.

Acknowledgements

The study was financially supported by National Natural Science Foundation of China (No. 21346011), Natural Science Basic Research Plan in Shaanxi Province (No. 2013JZ014), and Scientific Research Program Funded by Shaanxi Provincial Education Department (No. 12JK0579), respectively.

References

Ahmaruzzaman, M. (2010). A review on the utilization of fly ash. *Progress in Energy and Combustion Scien*ce, 36, 327–363.

Al-Zboon, K., Al-Harahsheh, M. S. and Hani, F. B. (2011). Fly ash-based geopolymer for Pb removal from aqueous solution. *Journal of Hazardous Materials*, 188, 414–421.

Bakharev, T. (2005a). Resistance of geopolymer materials to acid attack. *Cement and Concrete Research*, 35, 658–670.

Bakharev, T. (2005b). Geopolymeric materials prepared using class F fly ash and elevated temperature curing. *Cement and Concrete Research*, 35, 1224–1232.

Bakharev, T. (2006). Thermal behavior of geopolymers prepared using class F fly ash and elevated temperature curing. *Cement and Concrete Research*, 36, 1134–1147.

Bakharev, T., Sanjayan, J. G. and Cheng, Y. (1999). Alkali activation of Australian slag cements. *Cement and Concrete Research*, 29, 113–120.

Belhadj, E., Diliberto, C. and Lecomte, A. (2012). Characterization and activation of basic oxygen furnace slag. *Cement and Concrete Composites*, 34, 34–40.

Bernal, S. A., de Gutierrez, R. M., Pedraza, A. L., Provis, J. L., Rodriguez, E. D. and Delvasto, S. (2011). Effect of binder content on the performance of alkali-activated slag concretes. *Cement and Concrete Research*, 41, 1–8.

Blissett, R. S. and Rowson, N. A. (2012). A review of the multi-component utilization of coal fly ash. *Fuel*, 97, 1–23.

Bortnovsky, O., Dedecek, J., Tvaruzkova, Z., Sobalik, Z. and Subrt, J. (2008). Metal ions as probes for characterization of geopolymer materials. *Journal of the American Ceramic Society*, 91, 3052–3057.

Cardenas, C., Tobon, J. I., Garcia, C. and Vila, J. (2012). Functionalized building materials: photocatalytic abatement of NOx by cement pastes blended with TiO_2 nanoparticles. *Construction and Building Materials*, 36, 820–825.

Chen, J. and Poon, C. S. (2009). Photocatalytic construction and building materials: from fundamentals to applications. *Building and Environment*, 44, 1899–1906.

Chen, W., Xu, Y., Lin, Z., Wang, Z. and Lin, L. (1998). Formation, structure and fluorescence of CdS clusters in a mesoprous zeolite. *Solid State Communication*, 105, 129–134.

Cheng, T. W. and Chiu, J. P. (2003). Fire-resistant geopolymer produced by granulated blast furnace slag. *Minerals Engineering*, 16, 205–210.

Cheng, T. W., Lee, M. L., Ko, M. S., Ueng, T. H. and Yang, S. F. (2012). The heavy metal adsorption characteristics on metakaolin-based geopolymer. *Applied Clay Science*, 56, 90–96.

Cho, J. W., Ioku, K. and Goto, S. (1999). Effect of Pb^{II} and Cr^{VI} on the hydration of slag alkaline cement and the immobilization of these heavy metal ions. *Advances in Cement Research*, 11, 111–118.

Crank, G. (1933). *The Mathematics of Diffusion*. Oxford, Clarendon Press.

Criado, M., Palomo, A. and Fernández-Jiménez, A. (2005). Alkali activation of fly ashes. Part 1: Effect of curing conditions on the carbonation of the reaction products. *Fuel*, 84, 2048–2054.

Davidovits, J. (1991). Geopolymers: inorganic polymeric new materials. *Journal of Thermal Analysis*, 37, 1633–1656.

Deja, J. (2002). Immobilization of Cr^{6+}, Cd^{2+}, Zn^{2+} and Pb^{2+} in alkali-activated slag binders. *Cement and Concrete Research*, 32, 1971–1977.

Diamanti, V. M., Ormellese, M. and Pedeferri, M. P. (2008). Characterization of photocatalytic and superhydrophilic properties of mortars containing titanium dioxide. *Cement and Concrete Research*, 38, 1349–1353.

Duxson, P. and Provis, J. L. (2008). Designing precursors for geopolymer cements. *Journal of the American Ceramic Society*, 91, 3864–3869.

Duxson, P., Fernández-Jiménez, A., Provis, J. L., Lukey, G. C., Palomo, A. and van Deventer, J. S. J. (2007). Geopolymer technology: the current state of the art. *Journal of Material Science*, 42, 2917–2933.

Elsherbiny, A. S., Egelhaaf, H. J. and Oelkrug, D. (2011). Accessibility and shielding of silanol surface centers on porous silica beads; UV/vis absorption and fluorescence studies. *Journal of Photochemistry and Photobiology A*, 220, 39–46.

Feng, D., Tan, H. and van Deventer, J. S. J. (2004). Ultrasound enhanced geopolymerisation. *Journal of Materials Science*, 39, 571–580.

Fernández-Jiménez, A. and Palomo, A. (2005a). Composition and microstructure of alkali activated fly ash binder: effect of the activator. *Cement and Concrete Research*, 35, 1984–1992.

Fernández-Jiménez, A. and Palomo, A. (2005b). Mid-infrared spectroscopic studies of alkali-activated fly ash structure. *Microporous and Mesoporous Materials*, 86, 207–214.

Flamigni, L. and Monti, S. (1985). Primary processes in the reduction of azo dyes in alcohols studied by pulse radiolysis. *Journal of Physical Chemistry*, 89, 3702–3707.

Galiano, Y. L., Fernandez Pereira, C. and Vale, J. (2011). Stabilization/solidification of a municipal solid waste incineration residue using fly ash-based geopolymers. *Journal of Hazardous Materials*, 185, 373–381.

Gartner, E. M. and Macphee, D. E. (2011). A physico-chemical basis for novel cementitious binders. *Cement and Concrete Research*, 41, 736–749.

Gasca-Tirado, J. R., Manzano-Ramirez, A., Villasenor-Mora, C., Muniz-Villarreal, M. S., Zaldivar-Cadena, A. A., Rubio-Avalos, J. C., Borras, V. A. and Mendoza, R. N. (2012). Incorporation of photoactive TiO_2 in an aluminosilicate inorganic polymer by ion exchange. *Microporous and Mesoporous Materials*, 153, 282–287.

Gulshan, F., Yanagida, S., Kameshima, Y., Isobe, T., Nakajima, A. and Okada, K. (2010). Various factors affecting photodecomposition of methylene blue by iron-oxides in an oxalate solution. *Water Research*, 44, 2876–2884.

Habert, G., d'Espinose de Lacaillerie, J. B. and Roussel, N. (2011). An environmental evaluation of geopolymer based concrete production: reviewing current research trends. *Journal of Cleaner Production*, 19, 1229–1238.

Haha, M. B., Saout, G. L., Winnefeld, F. and Lothenbach, B. (2011). Influence of activator type on hydration kinetics, hydrate assemblage and microstructural development of alkali activated blast furnace slag. *Cement and Concrete Research*, 41, 301–310.

Ho, Y. S. and McKay, G. (1999). Pseudo-second order model for sorption processes. *Process Biochemistry*, 34, 451–465.

Houas, A., Lachheb, H., Ksibi, M., Elaloui, E., Guillard, C. and Herrmann, J. (2001). Photocatalytic degradation pathway of methylene blue in water. *Applied Catalysis B*, 31, 145–157.

Hu, S., Wang, H., Zhang, G. and Ding, Q. (2008). Bonding and abrasion resistance of geopolymeric repair material made with steel slag. *Cement and Concrete Composites*, 30, 239–244.

Huang, Y. and Han, M. (2011). The influence of α-Al_2O_3 addition on microstructure, mechanical and formaldehyde adsorption properties of fly ash-based geopolymer products. *Journal of Hazardous Materials*, 193, 90–94.

Khalil, M. Y. and Merz, E. (1994). Immobilization of intermediate-level wastes in geopolymers. *Journal of Nuclear Materials*, 211, 141–148.

Khate, D. and Chaudhary, R. (2007). Mechanism of geopolymerization and factors influencing its development: a review. *Journal of Material Science*, 42, 729–746.

Komnitsas, K. and Zaharaki, D. (2007). Geopolymerisation: A review and prospects for the minerals industry. *Minerals Engineering*, 20, 1261–1277.

Kong, D. L. Y. and Sanjayan, J. G. (2010). Effect of elevated temperatures on geopolymer paste, mortar and concrete. *Cement and Concrete Research*, 40, 334–339.

Kovalchuk, G., Fernández-Jiménez, A. and Palomo, A. (2007). Alkali-activated fly ash: effect of thermal curing conditions on mechanical and microstructural development – part II. *Fuel*, 86, 315–322.

Lagergren, S. (1898). Zur Theorie der sogenannten Adsorption geloster Stoffe. *Kungliga Svenska Vetenskapsakademiens Handlingar*, 24 (4), 1–39.

Lee, W. K. W. and van Deventer, J. S. J. (2002). The effects of inorganic salt contamination on the strength and durability of geopolymers. *Colloids and Surfaces A: Physicochem. Engineering Aspects*, 211, 115–126.

Li, L., Wang, S. and Zhu, Z. (2006). Geopolymeric adsorbents from fly ash for dye removal from aqueous solution. *Journal of Colloid and Interface Science*, 300, 52-59.

Lonescu, D., Meadowcroft, T. R. and Barr, P. V. (2001). Early-age hydration kinetics of steel slag. *Advances in Cement Research*, 13, 21–30.

Maggos, T. H., Plassais, A., Bartzis, J. G., Vasilakos, C. H., Moussiopoulos, N. and Bonafous, L. (2008). Photocatalytic degradation of NO_x in a pilot street canyon configuration using TiO_2-mortar panels. *Environmental Monitoring and Assessment*, 136, 35–44.

Matejka, V., Matejkova, P., Kovar, P., Vlcek, J., Prikryl, J., Cervenka, P., Lacny, Z. and Kukutschova, J. (2012). Metakaolinite/TiO_2 composite: photoactive admixture for building materials based on Portland cement binder. *Construction and Building Materials*, 35, 38–44.

Mozgawa, W. and Deja, J. (2009). Spectroscopic studies of alkaline activated slag geopolymers. *Journal of Molecular Structure*, 924–926, 434–441.

O'Connor, S. J., MacKenzie, K. J. D., Smith, M. E. and Hanna, J. V. (2010). Ion exchange in the charge-balancing sites of aluminosilicate inorganic polymers. *Journal of Materials Chemistry*, 20, 10234–10240.

Pacheco-Torgal, F. and Jalali, S. (2011). Nanotechnology: advantages and drawbacks in the field of construction and building materials. *Construction and Building Materials*, 25, 582–590.

Pacheco-Torgal, F., Castro-Gomes, J. and Jalali, S. (2008a). Alkali-activated binders: a review. Part 1. Historical background, terminology, reaction mechanisms and hydration products. *Construction and Building Materials*, 22, 1305–1314.

Pacheco-Torgal, F., Castro-Gomes, J. and Jalali, S. (2008b). Alkali-activated binders: a review. Part 2. About materials and binders manufacture. *Construction and Building Materials*, 22, 1315–1322.

Palomo, A., Grutzek, M. W. and Blanco, M. T. (1999). Alkali-activated fly ashes: a cement for the future. *Cement and Concrete Research*, 29, 1323–1329.

Palomo, A., Alonso, S., Fernández-Jiménez, A., Sobrados, I. and Sanz, J. (2004). Alkaline activation of fly ash: NMR study of the reaction products. *Journal of the American Ceramic Society*, 87, 1141–1145.

Panagiotopoulou, C., Kontori, E., Perraki, T. and Kakali, G. (2007). Dissolution of aluminosilicate minerals and by-products in alkaline media. *Journal of Materials Science*, 42, 2967–2973.

Pelekani, C. and Snoeyink, V. L. (2000). Competitive adsorption between atrazine and methylene blue on activated carbon: the importance of pore size distribution. *Carbon*, 38, 1423–1436.

Perera, D. S., Cashion, J. D., Blackford, M. G., Zhang, Z. and Vance, E. R. (2007a). Fe speciation in geopolymers with Si/Al molar ratio of 2. *Journal of European Ceramic Society*, 27, 2697–2703.

Perera, D. S., Uchida, O., Vance, E. R. and Finnie, K. S. (2007b). Influence of curing schedule on the integrity of geopolymers. *Journal of Materials Science*, 42, 3099–3106.

Phair, J. W., van Deventer, J. S. J. and Smith, J. D. (2004). Effect of Al source and alkali activation on Pb and Cu immobilisation in fly-ash based geopolymers. *Applied Geochemistry*, 19, 423–434.

Poon, C. S. and Cheung, E. (2007). NO removal efficiency of photocatalytic paving blocks prepared with recycled materials. *Construction and Building Materials*, 21, 1746–1753.

Qian, G., Sun, D. D. and Tay, J. H. (2003a). Immobilization of mercury and zinc in an alkali-activated slag matrix. *Journal of Hazardous Materials B*, 101, 65–77.

Qian, G., Sun, D. D. and Tay, J. H. (2003b). Characterization of mercury- and zinc-doped alkali-activated slag matrix, part I. Mercury. *Cement and Concrete Research*, 33, 1251–1256.

Qian, G., Sun, D. D. and Tay, J. H. (2003c). Characterization of mercury- and zinc-doped alkali-activated slag matrix, part II, Zinc. *Cement and Concrete Research*, 33, 1257–1262.

Rattanasak, U. and Chindaprasirt, P. (2009). Influence of NaOH solution on the synthesis of fly ash geopolymer. *Minerals Engineering*, 22, 1073–1078.

Richardson, I. G. and Cabrera, J. G. (2000). The nature of C-S-H in model slag-cements. *Cement and Concrete Composites*, 22, 259–266.

Richardson, I. G., Wilding, C. R. and Dickson, M. J. (1989). The hydration of blast-furnace slag cements. *Advances in Cement Research*, 2, 147–157.

Roy, D. M. (1999). Alkali-activated cements opportunities and challenges. *Cement and Concrete Research*, 29 (2), 249–254.

Roy, D. M., Jiang, W. and Silsbee, M. R. (2000). Chloride diffusion in ordinary, blended and alkali-activated cement pastes. *Cement and Concrete Research*, 30, 1879–1884.

Sagoe-Crentsil, K. and Weng, L. (2007). Dissolution processes, hydrolysis and condensation reactions during geopolymer synthesis: Part II. High Si/Al ratio systems. *Journal of Materials Science*, 42, 3007–3014.

Sazama, P., Bortnovsky, O., Dedecek, J., Tvaruzkova, Z. and Sobalik, Z. (2011). Geopolymer based catalysts – new group of catalytic materials. *Catalysis Today*, 164, 92–99.

Schneider, J., Cincotto, M. A. and Panepucci, H. (2001). ^{29}Si and ^{27}Al high-resolution NMR characterization of calcium silicate hydrate phase in activated blast-furance slag pastes. *Cement and Concrete Research*, 31, 993–1001.

Shi, C. (1996). Strength, pore structure and permeability of alkali-activated slag mortars. *Cement and Concrete Research*, 26, 1789–1799.

Silva, P. D., Sagoe-Crenstil, K. and Sirivivatnanon, V. (2007). Kinetics of geopolymerization: role of Al_2O_3 and SiO_2. *Cement and Concrete Research*, 37, 512–518.

Song, S. and Jennings, H. M. (1999). Pore solution chemistry of alkali-activated ground granulated blast-furnace slag. *Cement and Concrete Research*, 29, 159–170.

Song, S., Sohn, D., Jennings, H. M. and Mason, T. O. (2000). Hydration of alkali-activated ground granulated blast furnace slag. *Journal of Material Science*, 35, 249–257.

Songpiriyakij, S., Pulngern, T., Pungpremtrakul, P. and Jaturapitakkul, C. (2011). Anchorage of steel bars in concrete by geopolymer paste. *Materials and Design*, 32, 3021–3028.

Temuujin, J., van Riessen, A. and Williams, R. (2009). Influence of calcium compounds on the mechanical properties of fly ash geopolymer pastes. *Journal of Hazardous Materials*, 167, 82–88.

Temuujin, J., van Riessen, A. and MacKenzie, K. J. D. (2010). Preparation and characterization of fly ash based geopolymer mortars. *Construction and Building Materials*, 24, 1906–1910.

Temuujin, J., Rickard, W., Lee, M. and van Riessen, A. (2011). Preparation and thermal properties of fire resistant metakaolin-based geopolymer-type coatings. *Journal of Non-Crystalline Solids*, 357, 1399–1404.

Valenzuela, M. A., Bosch, P., Jimenez-Becerrill, J., Quiroz, O. and Paez, A. I. (2002). Preparation, characterization and photocatalytic activity of ZnO, Fe_2O_3 and $ZnFe_2O_4$. *Journal of Photochemistry and Photobiology A*, 148, 177–182.

van Deventer, J. S. J., Provis, J. L., Duxson, P. and Lukey, G. C. (2007). Reaction mechanisms in the geopolymeric conversion of inorganic waste to useful products. *Journal of Hazardous Materials*, 139, 506–513.

van Jaarsveld, J. G. S. and van Deventer, J. S. J. (1999). Effect of the alkali metal activator

on the properties of fly ash based geopolymers. *Industrial and Engineering Chemistry Research*, 38, 3932–3941.

van Jaarsveld, J. G. S., van Deventer, J. S. J. and Lorenzeni, L. (1997). The potential use of geopolymeric materials to immobilize toxic metals: part I. Theory and applications. *Minerals Engineering*, 10, 659–669.

Wang, J., Li, R. H., Zhang, Z. H., Sun, W., Xu, R., Xie, Y. P., Xing, Z. Q. and Zhang, X. D. (2008). Efficient photocatalytic degradation of organic dyes over titanium dioxide coating upconversion luminescence agent under visible and sunlight irradiation. *Applied Catalysis A*, 334, 227–233.

Wang, S. B., Li, L. and Zhu, Z. H. (2007). Solid-state conversion of fly ash to effective adsorbents for Cu removal from wastewater. *Journal of Hazardous Materials*, 139, 254–259.

Wang, S. D. and Scrivener, K. L. (1995). Hydration products of alkali activated slag cement. *Cement and Concrete Research*, 25, 561–571.

Wang, S. D. and Scrivener, K. L. (2003). ^{29}Si and ^{27}Al NMR study of alkali-activated slag. *Cement and Concrete Research*, 33, 769–774.

Wang, S. D., Pu, X. C., Scrivener, K. L. and Pratt, P. L. (1995). Alkali-activated slag cement and concrete: a review of properties and problems. *Advances in Cement Research*, 7, 93–102.

Weng, L. and Sagoe-Crentsil, K. (2007). Dissolution processes, hydrolysis and condensation reactions during geopolymer synthesis: Part I Low Si/Al ratio systems. *Journal of Materials Science*, 42, 2997–3006.

Yang, Y., Cao, Z., Jiang, Y., Liu, L. and Sun, Y. (2006). Photoinduced structural transformation of $SrFeO_3$ and $Ca_2Fe_2O_5$ during photodegradation of methyl orange. *Materials Science and Engineering B*, 132, 311–314.

Yip, C. K. and van Deventer, J. S. J. (2003). Microanalysis of calcium silicate hydrate gel formed within a geopolymeric binder. *Journal of Materials Science*, 38, 3851–3860.

Yip, C. K., Lukey, G. C. and van Deventer, J. S. J. (2004). Effect of blast furnace slag addition on microstructure and properties of metakaolinite geopolymeric materials. *Ceramic Transactions*, 153, 187–209.

Yip, C. K., Lukey, G. C. and van Deventer, J. S. J. (2005). The coexistence of geopolymeric gel and calcium silicate hydrate at the early stage of alkaline activation. *Cement and Concrete Research*, 35, 1688–1697.

Yousuf, M., Mollah, A., Hess, T. R., Tsai, Y. N. and Cocke, D. L. (1993). An FTIR and XPS investigations of the effects of carbonation on the solidification/stabilization of cement based systems – Portland type V with zinc. *Cement and Concrete Research*, 23, 773–784.

Zhang, L., Zhou, X., Guo, X., Song, X. and Liu, X. (2011). Investigation on the degradation of acid fuchsin induced oxidation by $MgFe_2O_4$ under microwave irradiation. *Journal of Molecular Catalysis A: Chemical*, 335, 31–37.

Zhang, T., Oyama, T., Aoshima, A., Hidaka, H., Zhao, J. and Serpone, N. (2001). Photooxidative *N*-demethylation of methylene blue in aqueous TiO_2 dispersions under UV irradiation. *Journal of Photochemistry and Photobiology A*, 140, 163–172.

Zhang, Y. J. and Chai, Q. (2014). Alkali-activated blast furnace slag-based nanomaterial as a novel catalyst for synthesis of hydrogen fuel. *Fuel*, 115, 84–87.

Zhang, Y. J. and Liu L. C. (2013). Fly ash-based geopolymer as a novel photocatalyst for degradation of dye from wastewater. *Particuology*, 11, 353–358.

Zhang, Y. J., Maroto-Valiente, A., Rodriguez-Ramos, I., Xin, Q. and Guerrero-Ruiz, A. (2004).

Synthesis and characterization of carbon black supported Pt-Ru alloy as a model catalyst for fuel cells. *Catalysis Today*, 93–95, 619–626.

Zhang, Y. J., Zhao, Y. L., Li, H. H. and Xu, D. L. (2008). Structure characterization of hydration products generated by alkaline activation of granulated blast furnace slag. *Journal of Material Science*, 43, 7141–7147.

Zhang, Y. J., Wang, Y. C., Xu, D. L. and Li, S. (2010). Mechanical performance and hydration mechanism of geopolymer composite reinforced by resin. *Materials Science and Engineering A*, 527, 6574–6580.

Zhang, Y. J., Li, H. H., Zhao, Y. L., Wang, Y. C. and Xu, D. L. (2011). Microstructure of alkali-activated granulated blast furnace slag-based geopolymer. *Advanced Materials Research*, 250–253, 528–531.

Zhang, Y. J., Liu, L. C., Xu, Y., Wang, Y. C. and Xu, D. L. (2012). A new alkali-activated steel slag-based cementitious material for photocatalytic degradation of organic pollutant from waste water. *Journal of Hazardous Materials*, 209–210, 146–150.

Zhang, Y. J., Liu, L. C., Ni, L. L. and Wang, B. L. (2013). A facile and low-cost synthesis of granulated blast furnace slag-based cementitious material coupled with Fe_2O_3 catalyst for treatment of dye wastewater. *Applied Catalysis B: Environmental*, 138–139, 9–16.

This page intentionally left blank

Innovative applications of inorganic polymers (geopolymers)

28

K. J. D. MacKenzie
MacDiarmid Institute for Advanced Materials and Nanotechnology, Wellington, New Zealand

28.1 Introduction

Inorganic polymers (geopolymers) are outstandingly versatile materials, by virtue of (i) their synthesis chemistry which allows them to be modified with additional chemical functionalities, (ii) their chemical structure and relationship to zeolites which confers ion exchange properties upon them, and (iii) their physical properties which allow them to function as supports for other chemical moities, or to be tailored to mimic natural materials. In addition to the better-known applications of geopolymers discussed in other chapters, these additional properties of inorganic polymers can be exploited to produce new materials with functionalities that are only now being recognised, and in many cases have yet to be fully implemented. These novel applications are the subject of the present chapter. Conventional geopolymers consist of randomly-arranged tetrahedral silicate and aluminate networks, with the inclusion of charge-balancing cations such as Na^+ or K^+ (Davidovits, 1991; Barbosa *et al.*, 2000). Apart from its randomness, which gives it the amorphous X-ray characteristics of a glass, this arrangement is not unlike that of zeolites, leading to the suggestion that inorganic polymers may be considered as incipient or nanometer-sized zeolites (Provis *et al.*, 2005). Further, it follows from these structural considerations that inorganic polymers might be formed from other elements which can form tetrahedral units with oxygen; this has been borne out by the formation of inorganic polymers containing tetrahedral BO_4 units (Nicholson *et al.*, 2005) or tetrahedral PO_4 units (MacKenzie *et al.*, 2005; Cao *et al.*, 2005). The chemical similarity between Al and Ga has also led to the synthesis of inorganic polymers in which some of the aluminium was substituted by gallium (Durant *et al.*, 2011), while the substitution of silicon by germanium has also been achieved (Durant and MacKenzie, 2011). The extreme alkalinity of inorganic polymers, which may be a drawback in some applications, can be offset by heating to about 600°C, thereby fixing the alkali within the structure (MacKenzie *et al.*, 2010), or by titrating with acid to pH 7 (Alzeer *et al.*, 2013). The charge-balancing cations in the inorganic polymer structure can also be exchanged for a range of other cations, further extending the potential applications of these materials (O'Connor *et al.*, 2010). This ability to manipulate the chemistry

Handbook of Alkali-activated Cements, Mortars and Concretes. http://dx.doi.org/10.1533/9781782422884.5.777

of inorganic polymers in such a variety of ways gives them an extreme degree of versatility that has yet to be fully exploited.

Likewise, the unique ability of inorganic polymers to cure and harden at ambient temperatures allows the physical properties of geopolymers to be manipulated. The introduction of unidirectional inorganic fibres (Welter, 2013) or organic fibres (Alzeer and MacKenzie, 2012, 2013) improves the mechanical properties, while unidirectional nanoporosity can also be introduced, allowing the inorganic polymer to mimic the ability of plants to draw up water by capillary action (Okada *et al.*, 2011a). The ability to manipulate the physical properties of inorganic polymers suggests a number of other potential new applications, some of which are discussed below. Since many of these materials are more suitable for higher-value lower-volume applications such as biomaterials, catalysts or electronic materials, they are typically based on metakaolinite, which is available in a purer and more reproducible form than fly ash or other raw materials often used to prepare geopolymers. If even purer inorganic polymers are required, for example in applications such as drug carriers for oral ingestion, synthetic aluminosilicate gels of sodium silicate and sodium aluminate can be used as starting materials (Brew and MacKenzie, 2007). The resulting chemosynthetic geopolymers, which can also be produced by hydrolysing a mixture of tetraethylorthosilicate (TEOS) and aluminium nitrate, have the additional advantage of providing a synthetic route to a wide range of geopolymer compositions, thereby allowing them to be tailored to suit a variety of applications.

28.2 Techniques for functionalising inorganic polymers

The simplest and most direct method for introducing other species or compounds into inorganic polymer is to incorporate the additional material at the mixing stage, before curing and hardening occurs. This technique can be used when the additional material can be homogeneously distributed in the inorganic polymer, and is not adversely affected by the alkalinity of the mixture. A surprisingly wide range of compounds can be incorporated in this way, ranging from carbon nanotubes (MacKenzie and Bolton, 2009), organic dyes (MacKenzie and O'Leary, 2008), to drugs (Jämstorp *et al.*, 2010, 2012; Forsgren *et al.*, 2011). Occasionally the morphology of the added material may interfere with the homogeneity of the sample prepared in this way, as has been found to be the case with the incorporation of plate-like graphite particles into geopolymers for the synthesis of SiAlON ceramics by carbothermal reduction and nitridation (O'Leary, 2012) (see Section 28.8.2). The high alkalinity of the geopolymer mixture may also decompose the added material, but this can be turned to advantage, as in the case of elemental silicon which may be deliberately added (Medri *et al.*, 2013), or which occurs as an impurity in some raw materials such as silica fume, and upon reaction with alkali, generates H_2 gas to produce a porous geopolymer (Prud'homme *et al.*, 2010). Other pore-generating reactions exploiting the alkaline conditions of geopolymerisation include the addition of

aluminium powder to a metakaolin-based geopolymer (Bell and Kriven, 2008) or a fly ash-based geopolymer (Brooks *et al.*, 2010) to produce H_2, the addition of H_2O_2 to form O_2 (Bell and Kriven, 2008), and the use of air as a pore-forming agent (Hung *et al.*, 2013).

The exchange of charge-compensating cations in Na-inorganic polymers by other cations in a similar manner to zeolites was achieved by Bortnovsky *et al.* (2008), who reported complete exchange of Na^+ by NH_4^+; this could then be completely exchanged by Co^{2+} or partially exchanged by Cs^+ (Bortnovsky *et al.*, 2008). This discovery has opened up new possibilities for inserting other functionalities into inorganic polymers by ion exchange. O'Connor *et al.* (2010) confirmed that complete exchange of Na^+ in sodium inorganic polymers can be achieved by washing with solutions of the chlorides or nitrates of K^+, Ag^+, NH_4^+ and Pb^{2+}, with less complete exchange of Li^+ (82%), Cd^{2+} (78%) and Mg^{2+} (57%), while Bortnovsky *et al.* (2010) have extended the ion exchange method to the preparation of Cu^{2+} and $Pt[NH_3]_4^{2+}$ geopolymers for catalyst applications (see Section 28.10). These methods for functionalising geopolymers are summarised schematically in Figure 28.1.

An alternative solid-state synthesis method for inorganic polymers originally proposed by Kolusek *et al.* (2007) involves the reaction at 800°C of undehydroxylated kaolinite with an alkali carbonate, followed by hydration of the solid product with a minimum amount of water. This synthetic method has been adapted as a convenient method to produce lithium inorganic polymers, which are difficult to prepare by the conventional route because of the limited solubility and relatively low alkalinity of LiOH (O'Connor and MacKenzie, 2010) and is also the method used to synthesise gallium or germanium aluminosilicate inorganic polymer analogues (Durant *et al.*, 2011; Durant and MacKenzie, 2011) with potential applications as luminescence materials.

28.3 Inorganic polymers with electronic properties

Being aluminosilicates, conventional geopolymers would be expected to be electrical insulators, but the presence of pore water and charge-balancing cations in their structure gives them a degree of electrical conductivity (Cui *et al.*, 2008). In a study of a series of chemosynthetic geopolymers with varying Na^+ contents with the aim of examining the possibility that these materials might act as fast ion conductors, the AC electrical conductivity measured from 25 Hz to 200 kHz was low (about 1.5×10^{-6} S cm^{-1} at room temperature) and relatively independent of the amount of pore water present; however, the latter determines the porosity of the samples, thereby providing a conduction path for any sodium ions in excess of those required for charge compensation (Cui *et al.*, 2008). When the residual water was removed by drying at 100°C, the sample conductivity increased with increasing sodium content, as would be expected, but these materials were prone to rehydrate, making it difficult to determine precisely the influence of the free sodium ions (Cui *et al.*, 2008).

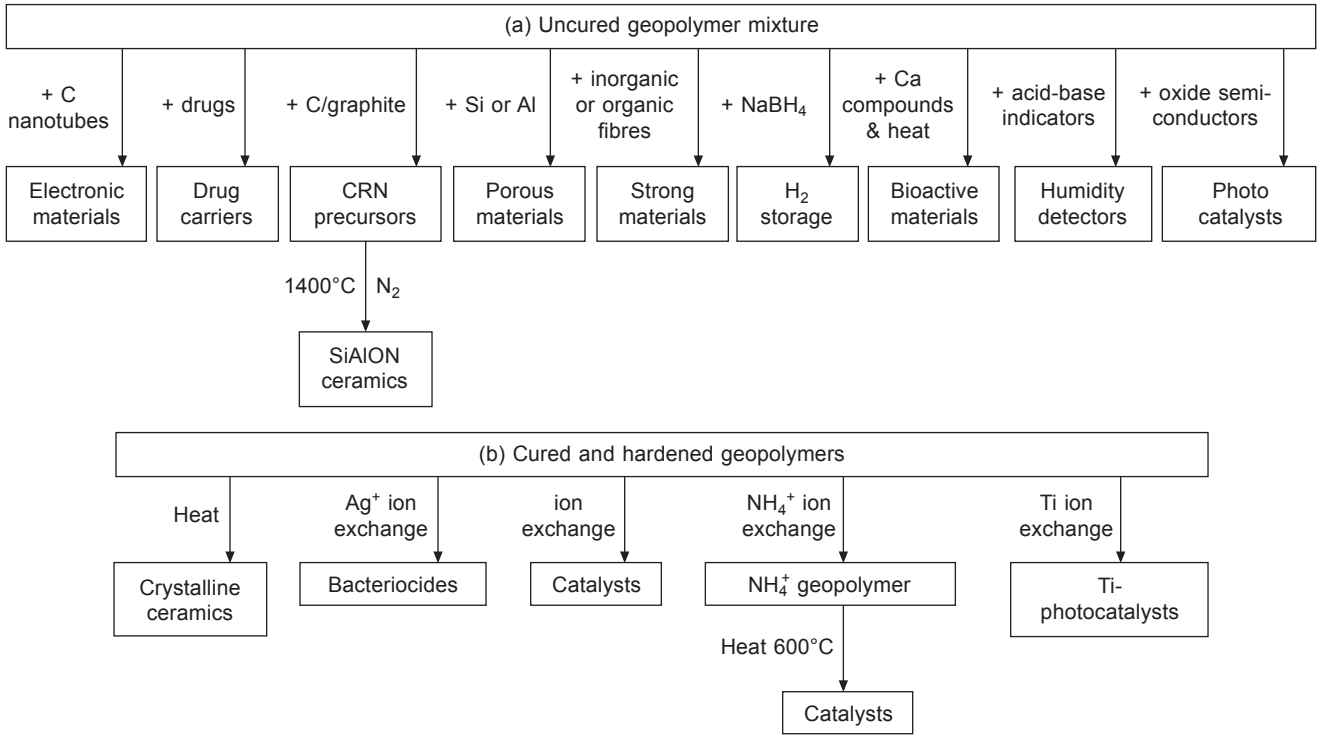

Figure 28.1 Schematic diagram of methods for preparing various functionalised products from inorganic polymers: (a) prior to curing, (b) after curing and hardening.

In another approach to increase the electrical conductivity of metakaolinite-based inorganic polymers, graphite or single-wall carbon nanotubes, which have high intrinsic electrical conductivity, were incorporated in a metakaolinite-based potassium-inorganic polymer (MacKenzie and Bolton, 2009). The DC conductivity of samples containing up to 6 wt.% nanotubes was measured as a function of temperature up to 340°C (the temperature at which the nanotubes begin to decompose). During the first heating cycle, the conductance of all the samples increased sharply as the water was removed, thereafter dropping with the depletion of the mobile charge carriers from the water. In subsequent heating cycles, the conductance more accurately reflected the contribution of the carbon additives; at 290°C the conductance of the sample containing 0.2 wt.% nanotubes (1.87×10^{-3} S m^{-1}) was greater than the sample containing the same amount of graphite (7.81×10^{-5} S m^{-1}), the latter being of a similar order to that of the carbon-free control sample (9.75×10^{-4} S m^{-1}) (MacKenzie and Bolton, 2009). The interpretation of these results is complicated by the possible operation of different conduction mechanisms in the nanotubes and graphite: both of these exhibit anisotropic conductance, but in addition, graphite may form conductive alkali intercalation compounds under the present alkaline synthesis conditions, whereas single-wall carbon nanotubes can take up water in their inner cavities, thereby increasing their electrical conductivity (MacKenzie and Bolton, 2009). Thus, although the DC conduction mechanisms in these two classes of carbon-containing inorganic polymers are difficult to compare, the incorporation of even a small amount of carbon nanotubes in geopolymers produces a significant increase in their DC conductance.

For some applications such as high-temperature packaging or encapsulation of electronic components, the dielectric behaviour of the material becomes an important parameter. In inorganic polymers, the dielectric loss is governed by movement of charge-balancing cations in the AC field, requiring low conductivities to obtain low dielectric losses. The dielectric losses of a series of chemosynthetic aluminosilicate geopolymers with a range of Na contents were found to be high in undried samples but decreased significantly in samples heated at 300 and 800°C, reflecting the reduction of electrical conductivity upon removal of water (Figure 28.2(a)). Heating at 800°C was slightly less effective in reducing the conductance, and thus the dielectric loss, due to shrinkage and structural transformations in the geopolymer (Cui *et al.*, 2011). These dielectric loss values could be reduced still further by changing the constitution of the inorganic polymer from a sodium-containing aluminosilicate to a phosphate geopolymer, prepared by treatment of the chemosynthetic aluminosilicate precursor with phosphoric acid (Cui *et al.*, 2011). Charge-compensation in these sodium-free geopolymers was suggested to occur by the presence of the tetrahedral phosphate units, resulting in a much lower dielectric loss, even in samples cured at ambient temperature for 72 h (Figure 28.2(b)). Thus, these phosphate-based inorganic polymers show considerable promise for electronic applications in which low dielectric loss is required.

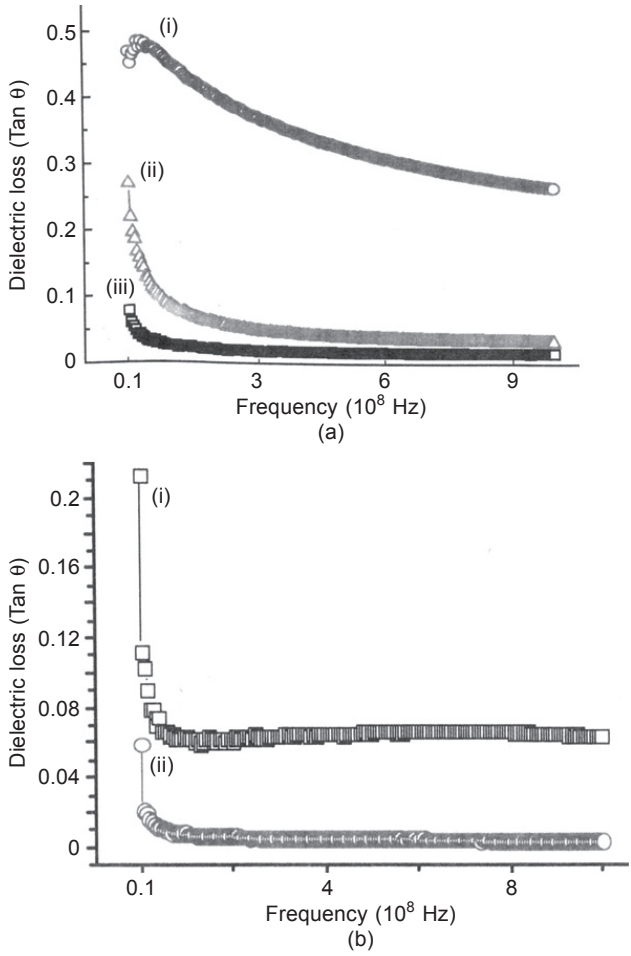

Figure 28.2 Dielectric loss as a function of frequency for (a) Na aluminosilicate geopolymers unheated and heated for 2 h, (i) unheated, (ii) 300°C, (iii) 800°C; (b) phosphate aluminosilicate geopolymers unheated and heated for 2 h (i) unheated, (ii) 300°C. Based on the data of Cui *et al.* (2011).

28.4 Photoactive composites with oxide nanoparticles

One of the most pressing problems of today is environmental pollution, which can occur in many forms, including increasing amounts of anthropomorphically generated greenhouse gases, vehicle emissions producing acid rain, halogenated hydrocarbon emissions which destroy the ozone layer of the atmosphere, and hazardous organic pesticides which pollute waterways. One method for converting many of these harmful substances into more benign products is by photodegradation using semiconductors with bandgaps of similar energy to the UV-visible region of the radiofrequency spectrum and preferably of nanoparticle size.

The most commonly used photoactive oxide is the anatase form of TiO_2, which for practical reasons of safety and ease of handling is usually encapsulated in an inorganic matrix. The use of a metakaolin-based geopolymer as the matrix has been reported by Gasca-Tirado *et al.* (2012), who introduced TiO_2 into the cured inorganic polymer by ion exchange with a solution of $(NH_4)_2TiO(C_2O_4)_2$, either of the as-prepared geopolymer or of a geopolymer that had been converted to the NH_4^+ form in a previous ion-exchange step (Gasca-Tirado *et al.*, 2012). This synthesis promoted the growth of anatase nanoparticles in the internal pore spaces of the geopolymer, resulting in a higher TiO_2 content and consequently better photocatalytic performance (judged by the photoluminescence spectrum and bleaching of methylene blue dye) than that shown by the material that had not previously been exchanged with NH_4^+ (Gasca-Tirado *et al.*, 2012).

The band gap of TiO_2 is 3.20 eV, but other semiconducting oxides have smaller bandgaps that should therefore couple more efficiently with light of visible wavelength. One such oxide is Cu_2O (bandgap 2.14 eV), which was incorporated into a metakaolin-based geopolymer matrix, both by a two-step synthesis in which the cubic Cu_2O nanoparticles were synthesised prior to being mixed with the uncured geopolymer, and in a single-step process in which the oxide and geopolymer were synthesised simultaneously (Fallah and MacKenzie, 2014). Preliminary studies on these nanoparticle composites have shown them to be effectively photocatalysts for the photodegradation of methylene blue dye (Fallah and MacKenzie, 2014).

28.5 Inorganic polymers with biological functionality

28.5.1 Bioactive inorganic polymers for bone repair

Inorganic materials used in biological applications as implants in the human body fall into two categories: bioinert materials such as engineering ceramics, typically used as wear-resistant joint replacement materials (alumina or toughened zirconia), and bioactive materials, which, when implanted into the human body, interact with the body fluids and bond to bone and soft tissue. One of the best known of the latter materials is Bioglass® (Hench, 1991), a sodium silicate glass with a typical composition $SiO_2 : Na_2O : CaO : P_2O_5 = 0.45 : 0.25 : 0.25 : 0.06$. The biological properties of materials of this type have proved outstandingly successful in repairing the effects of accident and disease (Hench, 1998). The possible use of inorganic polymers for the same purpose has the potential advantage that they can be shaped and hardened at ambient temperatures rather than at the temperature required to melt and shape a glass. Inorganic polymers can also accommodate phosphate and calcium moieties in their structure without compromising their properties (MacKenzie *et al.*, 2007), suggesting their possible bioactive behaviour. On the other hand, the alkalinity of inorganic polymers may prove toxic to the surrounding cells when transplanted into a living organism, and if <2 ppm of their aluminium content leaches the bloodstream,

brain disease could result (Hanston *et al.*, 1994; Geyer *et al.*, 1998; Yap *et al.*, 2002). Lower concentrations of aluminium could, however, prove beneficial in stimulating the proliferation of osteoblasts and new bone formation (Yap *et al.*, 2002).

One approach to overcoming the problem of leachable alkalinity from potassium inorganic polymers for biological applications has been to immobilise the alkali by heat-treating at 500°C; this lowered the pH from 11.5 to 7.1 and was also found to prevent leaching of the aluminium from the structure (Oudadesse *et al.*, 2007a). The release of pore water from the structure renders the inorganic polymer sufficiently porous to allow in ingress of bone-forming fluids, but although these materials were shown to be stable both *in vitro* and *in vivo*, the formation of bioactive compounds such as hydroxycarbonate apatite (HCA) upon exposure to simulated body fluid (SBF) was not demonstrated. To introduce bioactive functionality into these potassium inorganic polymers, known bone-forming compounds such as hydroxyapatite, $Ca_5(PO_4)_3(OH)$, (HA) or tricalcium phosphate, $Ca_3(PO_4)_2$, (TCP) were added prior to heat treatment to introduce porosity (Oudadesse *et al.*, 2007a,b).

Implantation of these inorganic polymers into rabbits revealed no toxicity after one month (Martin *et al.*, 2005), and longer-term stability of up to 6 months, with negligible leaching of aluminium into the blood after 750 h (Oudadesse *et al.*, 2007a,b). Since biomaterials for bone replacement should be strong as well as bioactive, the deliberate introduction of porosity into these materials raises the possibility that this may compromise their strength. Porosities of about 64% giving compressive strengths of about 5 MPa were reported to represent the best compromise in these materials (Oudadesse *et al.*, 2007b).

Other calcium-containing compounds including 10 wt.% each of $Ca(OH)_2$, nanostructured calcium silicate and $Ca_3(PO_4)_2$ have been added to induce bioactive functionality into metakaolinite-based potassium inorganic polymers which were subsequently heated to 600°C to lower their alkalinity (MacKenzie *et al.*, 2010). *In vitro* studies of these materials in SBF indicated that they all formed calcium phosphate biominerals by uptake of phosphorus from the SBF (Figure 28.3) (MacKenzie *et al.*, 2010). All the samples leached small amounts of aluminium into the SBF within acceptable levels for biomaterials applications, but the levels of calcium leached into the SBF were well in excess of the amount reported by Xynos *et al.* (2001) to be optimum for the stimulation of new bone growth by gene transcription in osteoblasts (6–8 ppm), and only the sample containing nanostructured calcium silicate released Si into the SBF, but in an amount that fell short of the optimum concentration (15–20 ppm, Xynos *et al.*, 2001). The compressive strength of the $Ca_3(PO_4)_2$ inorganic polymer was slightly higher than the other materials, making this a possible candidate as a bioactive inorganic polymer (MacKenzie *et al.*, 2010).

In an alternative approach, Catauro *et al.* (2012) studied the bioactivity of metakaolin-based Na geopolymers without the addition of bone-forming components. The possible leaching of aluminium was minimised by adjusting the composition of some samples to be silica-rich, by the addition of amorphous natural SiO_2. The formation of very small amounts of hydroxyapatite on the surface of these samples after exposure to SBF was found to depend on their Na/Al ratio; the sample with

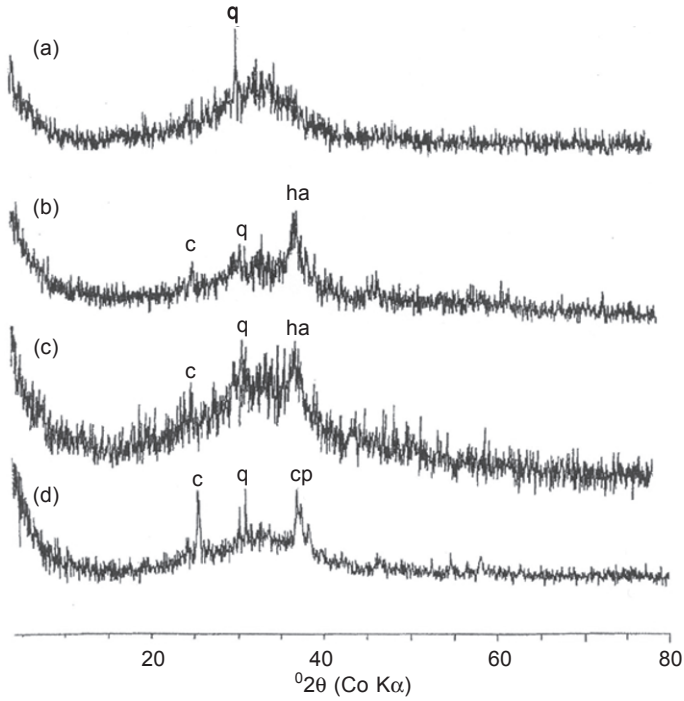

Figure 28.3 X-ray powder diffraction diagrams of calcium-containing potassium aluminosilicate inorganic polymers soaked *in vitro* in simulated body fluid for 7 weeks: (a) containing $Ca(OH)_2$, heated at 600°C, unsoaked, (b) containing $Ca(OH)_2$, heated at 600°C, soaked, (c) containing nano calcium silicate, heated at 600°C, soaked, (d) containing $Ca_3(PO_4)_2$, heated at 600°C, soaked. Peaks marked q and c (quartz and cristobalite) are impurities from the original clay, other peaks indicate the formation of bioactive compounds: ha = hydroxyapatite (PDF no. 9-432) and hydroxycarbonate apatite (PDF no. 19-272), cp = calcium hydrogen phosphate hydroxide (PDF no. 46-0905). Adapted from MacKenzie *et al.* (2010).

a ratio of 0.77 was not bioactive but when the ratio was increased to 1.05, apatite formation was observed by SEM/EDS (Catauro *et al.*, 2012).

28.5.2 Inorganic polymers as drug delivery agents

Inorganic materials are finding increased use as carriers for oral drug delivery. Several considerations must be taken into account when designing these carrier materials: they should be biocompatible and non-toxic, have good drug-loading capacity, have sufficient mechanical strength to survive the passage through the alimentary tract, be able to be tailored for the desired release rate and not interact with or degrade the drug. Desired drug release rates can vary; acute inflammation or chronic pain may necessitate a high release rate whereas other cases may require a more sustained release over a longer period.

Mesoporous silicas have been extensively investigated as drug carriers (Wang, 2009) but inorganic polymers have recently attracted attention for this application. Metakaolin-based Na geopolymers were reported to be suitable carriers for the powerful synthetic opioid analgesic drug Fentanyl and the structurally related sedative drug Zolpidem (Jämstorp *et al.*, 2010). The drug concentrations were 13 mg/g of metakaolinite, chosen to mimic a typical therapeutic dose of 2 mg of drug in a 200 mg pellet. The presence of the drugs did not adversely affect the mechanical strength of the geopolymer carrier, enabling it to withstand accidental or deliberate chewing, and the positive surface charge on these particular drugs facilitated their uptake by slight negative charge of the geopolymer pore surfaces. *In vitro* measurements indicated that the release kinetics of these drugs at pH 6.8 depended on the interconnected porosity of the geopolymers, which in turn depended on the amount of water used in their synthesis, suggesting a possible means of tailoring their release properties by adjusting their composition. At pH 1, mimicking the gastric juices of the stomach, 80% of both drugs was released within 5 h (Jämstorp *et al.*, 2010), possibly due to microstructural transformations in the geopolymer matrix at this pH, increasing the pore interconnectivity and facilitating the diffusion of the drug molecules from the structure. A further possibility at this low pH is that the increased proton concentration results in a positive charge on the geopolymer surfaces, releasing the electrostatically bound drug molecules (Jämstorp *et al.*, 2010).

In an extension of these studies to other model pharmaceutical compounds Sumatryptan, Theophylline and Saccharin, in addition to Fentanyl, the non-uniform concentration of the drug distribution in the geopolymer matrix was studied by a finite element method, indicating that the drug release behaviour at pH 6.8 was more influenced by the solubility of the drug in the geopolymer matrix than by the diffusion coefficient from the matrix (Jämstorp *et al.*, 2012).

The effect of the geopolymer pore size on the release of the opioid drug Oxycodone was studied in a series of geopolymers of differing Al/Si ratios synthesised by a sol-gel procedure rather than from metakaolinite (Forsgren *et al.*, 2011). The pore size decreased with increasing Al/Si ratio until a completely mesoporous geopolymer matrix with all pores in the range 2–35 nm was produced at an Al/Si ratio of 2:1; this composition produced a highly desirable drug release profile suitable for sustained release (Figure 28.4) (Forsgren *et al.*, 2011). These limited studies suggest that inorganic polymers are potentially very useful matrices for oral delivery of drugs, and would warrant further development.

28.5.3 Antimicrobial inorganic polymers

The well-known bacteriocidal properties of silver, in conjunction with ion-exchange properties of geopolymers have been exploited to produce bacteriocidal materials with potential applications for water purification in countries where a lack of clean drinking water is a problem. The charge-balancing sodium ions in metakaolin-based inorganic polymers can be completely replaced by silver ions by washing with a 0.1 M solution of $AgNO_3$ (O'Connor *et al.*, 2010). The resulting Ag-exchanged materials

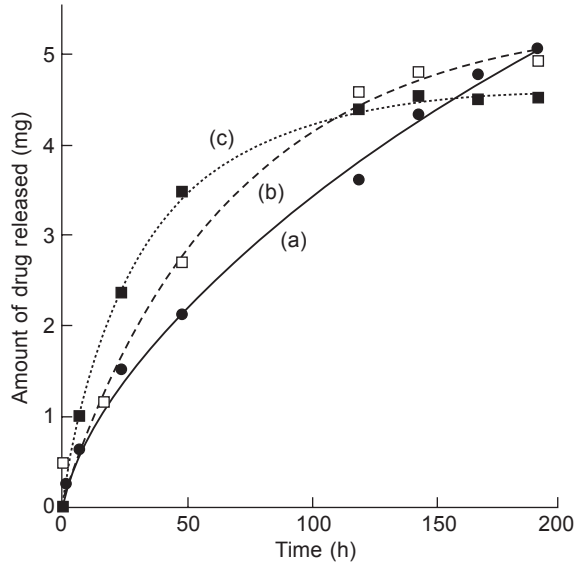

Figure 28.4 Release of the opioid pain-relieving drug oxycodone from synthetic aluminosilicate inorganic polymers of varying Al/Si ratios cured at 60°C, illustrating how the drug release kinetics can be tailored by adjusting the geopolymer composition: (a) Al/Si = 2:1, (b) Al/Si = 1:1, (c) Al/Si = 1:2. Adapted from Forsgren *et al.* (2011).

have been shown to be powerful antimicrobial agents against *Staphylococcus aureus*, this property being solely due to the presence of the silver, and not a result of the high alkalinity of the geopolymer (O'Connor *et al.*, 2010). Used as a packing for filter beds, these materials could potentially perform the dual purpose of removing both sediment and bacteria to produce a potable water supply.

28.6 Inorganic polymers as dye carrying media

The surface hydroxyl groups of a geopolymer can attract cationic organic dyes, leading to the suggested use of fly ash-based geopolymers to adsorb the dyestuffs methylene blue or crystal violet from wastewater streams (Li *et al.*, 2006). These geopolymers were reported to have a greater absorption capacity for the dyes than either the fly ash from which they were derived or natural zeolites which are often used for this purpose (Li *et al.*, 2006).

A different application for dye-containing inorganic polymers was suggested by the observation that the pH of geopolymers may vary reversibly with their degree of hydration, leading to the incorporation of several triphenylmethane and azo-dye acid-base indicators into a metakaolin-based Na inorganic polymer for use as a solid-state humidity indicator (MacKenzie and O'Leary, 2008). Since most of these indicators are soluble in alkaline solution and are stable at high pH, they could be

added at the geopolymer synthesis stage. Of the acid-base indicators bromothymol blue, thymol red, bromocresol green, phenolphthalein, thymolphthalein and methyl red, the most promising dye for use as a solid-state humidity indicator was thymol blue, which underwent a colour change from light tan in the dry state to dark blue in the damp state. At higher humidity, all these dyes began to fade on exposure to air, possibly due to oxidation of the sulphonic acid groups. Leaching of the dye from the inorganic polymer matrix was also noted in the presence of excess water (MacKenzie and O'Leary, 2008). Thus, for this application to be fully realised will require identifying an indicator that binds firmly to the inorganic polymer matrix, displays a distinct colour change in the desired pH range, and is chemically stable to bleaching and oxidation under humid conditions (MacKenzie and O'Leary, 2008).

28.7 Inorganic polymers as novel chromatography media

Chromatography is a widely used technique for separating mixtures of (usually organic) compounds by passing them in solution through a column packed with a solid stationary phase. The efficiency of the separation depends on a number of factors, including the chemical binding of the various components to the stationary phase and the morphology of the stationary phase particles, which determines the flow of the solvent through the column. The most ubiquitous stationary phase material for simple chromatography separations is silica, but alumina can also be used. One of the greatest difficulties with silica is its lack of chemical stability in strong organic solvents such as methanol or ethanol, causing the silicon to be stripped out and contaminate the eluted products, and rendering it unsuitable for multiple use. Methods for overcoming this problem include the use of silica-related compounds, but these require multi-step syntheses, and, being considerably more expensive to produce, are used in high-performance chromatography rather than for simpler open-column applications.

Inorganic polymers have been shown to provide a cost-effective, readily synthesised and efficient alternative for both silica and alumina chromatography stationary phases (Alzeer *et al.*, 2013). Three different compositions (high-silica, normal and high-alumina) were prepared and ground to give a particle size distribution comparable with chromatography-grade silica. Since the as-prepared materials are highly alkaline, they were titrated with acid to neutral pH, but this step subsequently proved to be unnecessary, since the alkaline materials performed equally well. The efficiency of the inorganic polymers as column chromatography stationary phase media was determined by separation of a mixture of three classes of organic compounds (a benzenoid, an ester and a pyrrole) and comparing the results with conventional chromatographic silica and two aluminas (Alzeer *et al.*, 2013). The as-prepared inorganic polymer of 'normal' composition ($SiO_2/Al_2O_3 = 3.54$, $Na_2O/SiO_2 = 0.36$, $H_2O/Na_2O = 10.76$) performed very comparably with chromatographic silica and alumina, on the basis of factors such as the number of plates per metre (a measure used by analysts to assess the efficiency of a chromatography column); this is significantly greater for

the normal geopolymer than for chromatography silica and alumina (Figure 28.5(a)). The peak area of the separated compounds is another parameter of interest since it reflects the degree of chemical absorption to the column stationary phase. In this respect silica performs better than all the geopolymers, which show an approximately similar degree of absorption to alumina (Figure 28.5(b)). The peak asymmetry of the separated compounds eluted from the column is a less important parameter since all the compounds are sufficiently separated that they are not interfered with

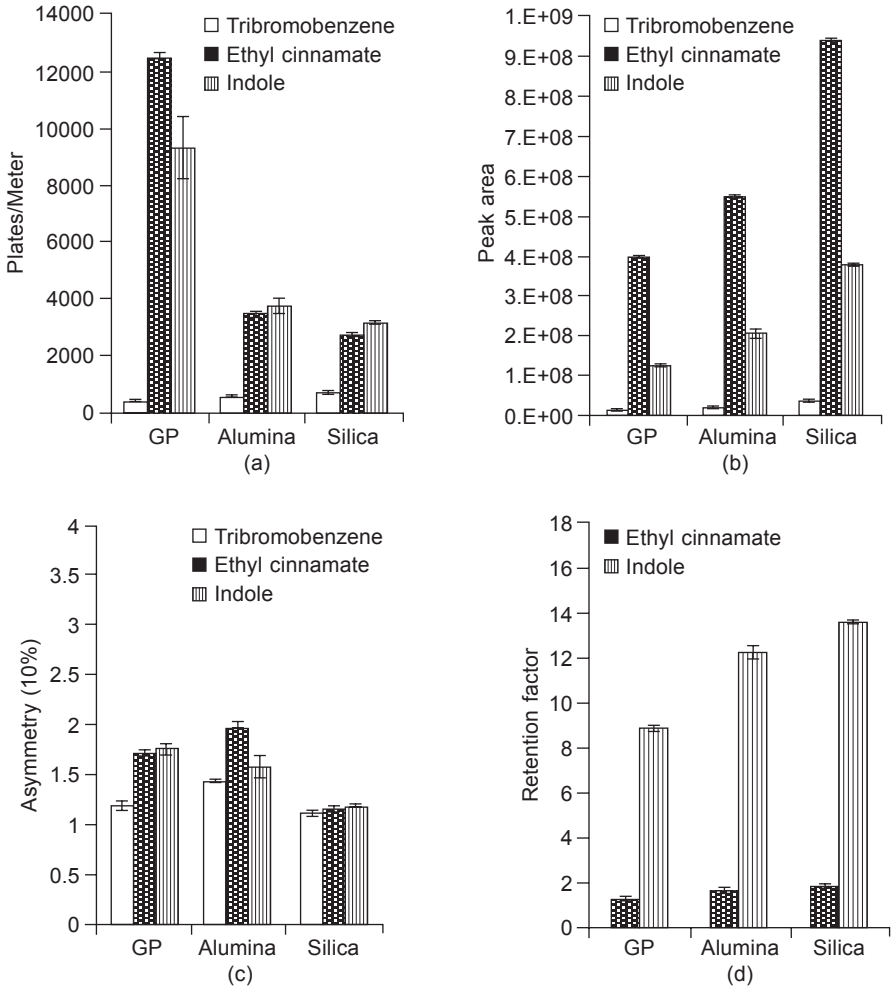

Figure 28.5 Chromatographic behaviour of an as-synthesised Na geopolymer compared with conventional chromatography-grade silica and alumina stationary phase column packing media: (a) number of plates per metre, (b) peak area of the separated organic compounds, (c) peak asymmetry of the separated compounds, (d) retention factor *k*. GP denotes the geopolymer of 'normal' composition. Adapted from Alzeer *et al.* (2013).

by this tailing effect (Figure 28.5(c)). A further parameter indicating the efficiency of the chromatography is the peak retention factor *k*, which takes into account a number of factors related to the column dimensions, packing density, etc., as well as the physical and chemical properties of the stationary phase. Values of *k* of 5–10 represent the best trade-off between time spent by the adsorbed compounds on the stationary phase and the length of time required for their complete separation; on this basis, the separation characteristics of all the geopolymers, together with silica and alumina, are comparable (Figure 28.5(d)) (Alzeer *et al*., 2013).

An important advantage of geopolymers over silica as the stationary phase for chromatography is their chemical resistance to attack by polar solvents such as ethanol, whereas significant leaching of Si from the silica occurs in these solvents. Thus, geopolymers are less likely than silica to contaminate the separated compounds, and are more suitable for re-use after cleaning with a strong solvent between runs (Alzeer *et al*., 2013).

28.8 Inorganic polymers as ceramic precursors

28.8.1 Oxide ceramics

Crystalline alkali aluminosilicates constitute a class of ceramic compounds with many practical applications. Although those which occur as natural minerals are often impure, they can be produced synthetically, for example, by solid state reaction between the constituent oxides or carbonates at high temperatures. Since inorganic polymers contain a homogeneous mixture of the appropriate elements and can be synthesised with a range of alkali cations from Li to Cs, they constitute excellent precursors which can be crystallised to the corresponding ceramics at relatively lower temperatures. The ability to form the precursors to some desired shape prior to heat treatment is another potential benefit of this approach. Lithium inorganic polymers, prepared either by conventional reaction of dehydroxylated 1:1 clay minerals with lithium silicate under alkaline conditions, or by a solid-state method, form crystalline $LiAlSiO_4$ (β-eucryptite) on heating at <800°C (O'Connor and MacKenzie, 2010). On further heating at 900°C, $LiAlSi_2O_6$ (β-spodumene) is formed, which at 1100°C decomposes to form further β-eucryptite (O'Connor and MacKenzie 2010). Ceramics containing these crystalline phases are of practical importance since they have excellent resistance to thermal shock arising from their near-zero or negative thermal expansion coefficients.

The products formed upon heating the more ubiquitous sodium inorganic polymers depend on their composition; in a series of metakaolin-based Na precursors, compositions which cured and hardened well remained X-ray amorphous up to 1100°C, forming a small amount of $Al_6Si_2O_{13}$ (mullite) at 1100–1300°C, whereas compositions richer in Na and Si, which did not cure and harden as well, formed crystalline $NaAlSiO_4$ (nepheline) at 800–1100°C, above which temperature it melted (Barbosa and MacKenzie, 2003a). In its natural form, nepheline is extensively used

as a fluxing agent to lower the melting temperature in the production of glasses and ceramics.

The thermal reactions of potassium inorganic polymers have been more extensively studied. As with the sodium compounds, the thermal stability of metakaolin-based potassium geopolymers was found to depend on the composition; samples with a lower SiO_2/Al_2O_3 ratio (4.13) were particularly thermally stable, but crystallised to a mixture of $KAlSiO_4$ (kalsilite) and $KAlSi_2O_6$ (leucite) at 1000–1400°C (Barbosa and MacKenzie, 2003b). By contrast, samples with a higher SiO_2/Al_2O_3 ratio (5.32) formed kalsilite at 1000°C, which transformed to a mixture of leucite and SiO_2 (cristobalite) on heating at 1200–1300°C (Barbosa and MacKenzie, 2003b). A study of the structural arrangement of a metakaolin-based potassium geopolymer with the composition $KAlSi_2O_6.5.5H_2O$ has been made using neutron pair distribution function (PDF) analysis, which allows the atomic ordering to be determined out to a distance of ~ 8Å (Bell *et al*., 2008a). The unheated geopolymer was found to be structurally similar to zeolitic leucite over that distance, but was disordered beyond 8Å. Heating to 300°C to remove chemically bound water resulted in changes in the short-to-medium range structural order, with the crystallisation of identifiable leucite beginning at >1050°C (Bell *et al*., 2008a, 2009a). A similar result was reported in a PDF study by White *et al*. (2010), which demonstrated that the tetrahedral aluminosilicate framework survived the loss of the pore and hydration water upon heating, and that medium-range structural order was retained upon heating (White *et al*., 2010). Crystallisation to leucite occurred at >1000°C, together with a small amount of amorphous mullite and glassy silica (White *et al*., 2010). By 1100°C shrinkage of the ceramic was complete, the density achieving 99.7% of the theoretical density of tetragonal leucite (Bell *et al*., 2009a). The formation of high-strength leucite glass-ceramics from potassium geopolymer precursors dried at 150°C, cold isostatically pressed and sintered at temperatures up to 1200°C was investigated by Xie *et al*. (2010) who reported the formation of materials with Vickers hardness up to 8.49 GPa, fracture toughness up to 2.36 $MPa.m^{1/2}$ and biaxial flexural strengths up to 139.63 MPa. The glassy phase was thought to form from the free alkali present in the pore water of the geopolymer precursor, which was not removed by drying (Xie *et al*., 2010).

A PDF study of a metakaolin-based caesium geopolymer of composition $Cs_2O.Al_2O_3.4SiO_2.11H_2O$ indicated that up to a distance of ~9Å the unheated material displayed structural ordering similar to $CsAlSi_2O_6$ (pollucite) into which it transformed upon heating >900°C (Bell *et al*., 2008b, 2009b). The atomic ordering of the crystallised pollucite product in the range 1–10 Å was a poorer fit with that of pure pollucite due to the presence of an additional amorphous phase in the heated Cs geopolymer (Bell *et al*., 2008b). Significant shrinkage occurred at >1200°C but heating at 1600°C was required for the ceramic to reach 98% of the theoretical density of pollucite (Bell *et al*., 2009b). Pollucite is of practical importance as an encapsulating material for radioactive ^{137}Cs, and its high melting point and low thermal expansion coefficient make it a good refractory ceramic.

28.8.2 Non-oxide ceramics

Non-oxide ceramics such as silicon nitride and the various silicon aluminium nitride (SiAlON) compounds are important high-technology materials with applications as wear-resistant engineering components and cutting tools because of their hardness and toughness. The SiAlONs are particularly important because they occur as several polymorphs with different crystal structures and a range of compositions, the most common being β-SiAlON ($Si_{6-z}Al_zO_zN_{8-z}$, isostructural with β-silicon nitride, where z can take values from 0 to about 4.2), O-SiAlON ($Si_{2-x}Al_xO_{1+x}N_{2-x}$, isostructural with silicon oxynitride, where x varies from 0 to 0.2) and X-SiAlON, $Si_3Al_6O_{12}N_2$, isostructural with mullite. A convenient method for synthesising the SiAlONs is by carbothermal reduction and nitridation (CRN), in which an aluminosilicate source such as a clay mineral is mixed with carbon powder and heated in a nitrogen atmosphere at >1400°C (O'Leary, 2012). The product is normally a powder, which requires further processing by shaping and high-temperature sintering, but if the precursor aluminosilicate + carbon can be formed to the desired shape prior to the CRN reaction, the second step of processing might be eliminated. The possibility of using a metakaolin-based geopolymer as the CRN precursor was investigated by O'Leary (2012), with particular attention to the nature of the SiAlON products formed and the fate of the alkali ion in the reaction. The reaction proceeds more readily when more reactive carbon of finer particle size is used, and K geopolymers were found to be more thermally stable CRN precursors than the corresponding Na geopolymers, which melt and sinter with the volatisation of the alkali at a lower temperature. The K geopolymers containing reactive carbon form an amorphous intermediate which then transforms to β-SiAlON with a high value of z via the intermediate formation of small amounts of other compounds (Figure 28.6(a)), whereas the Na geopolymers containing reactive carbon form β-SiAlON with a low value of z, via the reaction intermediates O-SiAlON, X-SiAlON and silicon carbide (Figure 28.6(b)) (O'Leary, 2012). The influence of the alkali ion was studied by carrying out CRN experiments on geopolymers in which the alkali was removed by ion-exchanging with NH_4^+; the reactions in these precursors were more like those of conventional clays, proceeding via the formation of mullite, cristobalite, X-phase SiAlON and silicon carbide, to produce β-SiAlON (Figure 28.6(c)). Thus, although the presence of the alkali influences the reaction path, and to some extent, the SiAlON products, it is not deleterious to the reaction, suggesting that geopolymers could be viable precursors for the formation of a range of SiAlONs (O'Leary, 2012).

28.9 Inorganic polymers with luminescent functionality

Luminescent materials find a number of present-day applications in television and computer monitor screens, oscilloscopes and radar screens, electron microscope screens and LEDs for general lighting and specialised applications. Some of the brightest luminescent activator ions are the trivalent rare-earth lanthanides Eu^{3+}, Gd^{3+} and Tb^{3+}

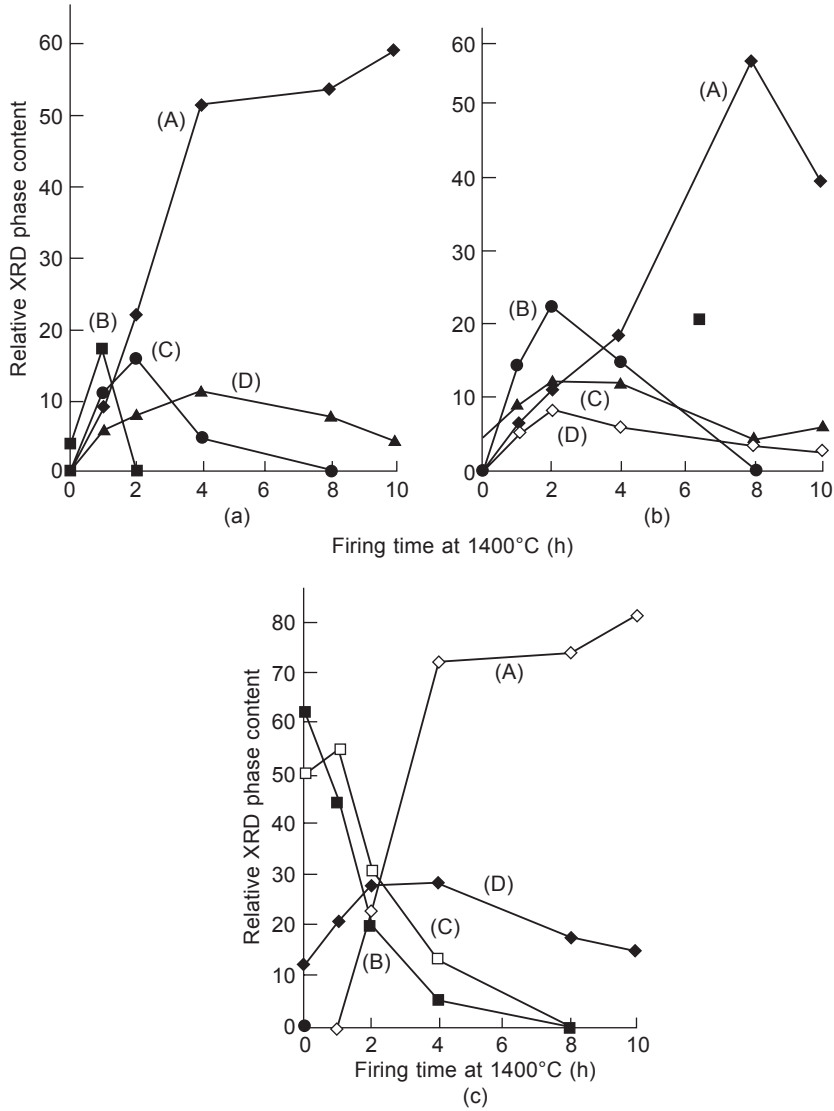

Figure 28.6 Semi-quantitative X-ray powder diffraction analyses of the high-technology SiAlON ceramic compounds formed from aluminosilicate geopolymer-carbon precursors by carbothermal reduction and nitridation (CRN) at 1400°C in flowing nitrogen gas: (a) potassium geopolymer precursor, (A) = β-SiAlON, (B) = leucite, (C) = O-SiAlON, (D) = silicon carbide. (b) sodium geopolymer precursor, (A) = β-SiAlON, (B) = O-SiAlON, (C) = silicon carbide, (D) = X-SiAlON. (c) ammonium geopolymer precursor, (A) = β-SiAlON, (B) = cristobalite, (C) = mullite, (D) = silicon carbide.

which have the largest energy gaps between their excited and ground states (Ropp, 2004). Practical luminescent systems require the activator luminescent ions to be incorporated into a stable host material which must also be transparent in the region of light absorption so as not to interfere with the luminescent centres. A number of these solid-state hosts have been proposed and investigated, but surprisingly little work has been done on the use of geopolymers as the host. The optical properties of undoped metakaolin-based sodium geopolymers, which will influence their performance as a host material, have been investigated by Gasca-Tirado *et al*. (2011) who reported a band in the absorption spectrum at 250–300 nm, with a similar trend in the transmission of a thin sample. This behaviour was found to depend on the curing temperature, which in turn correlated with the porosity of the geopolymer host (Gasca-Tirado *et al*., 2011). On this basis, an optimum curing temperature of 90°C was identified, and a viable photoluminescent geopolymer with a strong emission peak at 469 nm was synthesised by incorporating 20 wt.% of a commercial luminescent powder, $Sr_2MgSi_2O_7$:Eu^{2+} Dy^{3+} (Gasca-Tirado *et al*., 2011).

The interesting prospect of synthesising geopolymers with luminescence properties tailored into the structure has been investigated by Rogers and MacKenzie (2014) working with gallium aluminosilicate geopolymers synthesised by the method of Durant and MacKenzie (2011) and Durant *et al*. (2011). These hosts were activated by doping with Eu^{3+} or Sm^{3+}, incorporated both by solid-state reaction and ion exchange methods and preliminary studies indicate that they display interesting photoluminescence properties.

28.10 Inorganic polymers as novel catalysts

The structural similarity between metakaolin-based geopolymers and zeolites suggests that geopolymers should exhibit ion-exchange and catalytic properties (Bortnovsky *et al*., 2008; O'Connor *et al*., 2010). By exchanging the parent charge-compensating cation (Na^+ or K^+) for NH_4^+, followed by further ion-exchange with Co^{2+}, Cu^{2+} or $Pt(NH_3)_4^{2+}$, or by impregnating a K^+ geopolymer with a solution of $FeCl_3$ in acetyl acetone, Bortnovsky *et al*. (2010) produced a series of geopolymer-based catalysts which they tested using two model reactions. The NH_4^+ geopolymers and Cu-NH_4^+ geopolymers were tested on the selective catalytic reduction of NO_x and NH_3 to nitrogen, while the total oxidation of hydrocarbons to CO and CO_2 was tested using the $Pt(NH_4)$ geopolymer, the Fe-K geopolymer and the Co-NH_4^+ geopolymer (Bortnovsky *et al*., 2010). The Co^{2+} and Cu^{2+} were thought to be located predominantly in the cation exchange sites of these geopolymers, whereas the iron and platinum species are likely to occur in the respective geopolymers as highly dispersed clusters of undefined sizes (Bortnovsky *et al*., 2010).

The catalytic results show that conversion of NO_x to nitrogen (Figure 28.7(a)) over the Cu-NH_4^+ geopolymer (curve b) is already significant at <250°C, and the oxidation of NH_3 is complete by 230°C due to the presence of acid sites necessary for the absorption of basic molecules such as ammonia. These results in the temperature

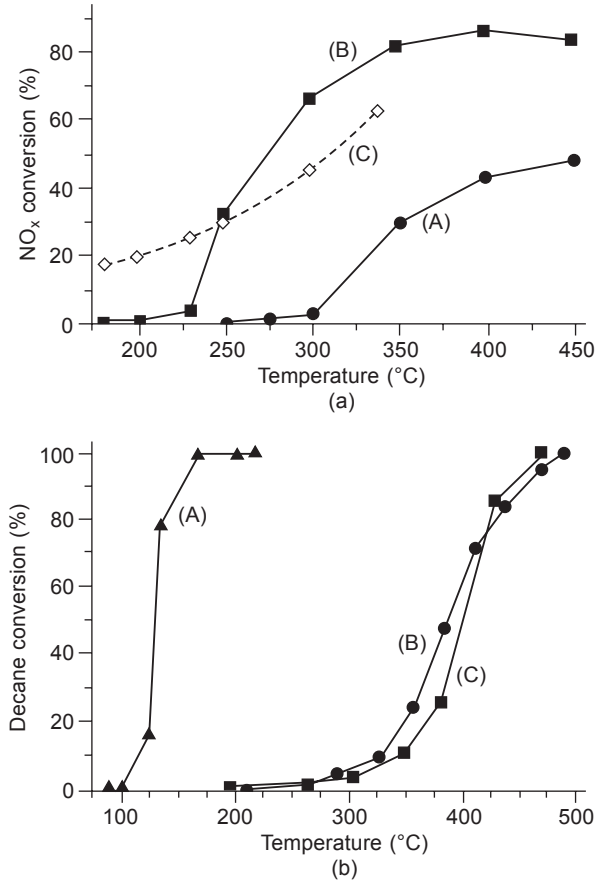

Figure 28.7 Catalytic activity of aluminosilicate geopolymer-based catalysts for (a) the conversion of nitrogen oxides to N_2 as a function of temperature: (A) NH_4 geopolymer, (B) NH_4Cu geopolymer, (C) conventional V_2O_5/Al_2O_3 catalyst; (b) the total oxidation of decane to CO_2 as a function of temperature: (A) $PtNH_4$ geopolymer, (B) Fe-K-Ca geopolymer, (C) $CoNH_4$ geopolymer (adapted from Sazama *et al.* (2011), Copyright © 2011, with permission from Elsevier).

range 250–350°C compare well with the performance of a V_2O_5/Al_2O_3 catalyst conventionally used for this reaction (curve c).

Oxidation of decane (Figure 28.7(b)) using the $Pt(NH_4)$ geopolymer was found to occur at low temperatures (curve a) producing CO_2 rather than CO, whereas the reaction over the Fe-K (curve b) and Co-NH_4^+ geopolymers (curve c) started at 260°C and was complete at 470–480°C (Bortnovsky *et al.*, 2010). The importance of this catalytic reaction lies in the fact that decane is a major component of transport fuel, and the high rate of conversion achieved by these compounds at moderate temperatures, coupled with their high thermal stability, ease of fabrication and cost-effectiveness, makes them of considerable interest for this application.

The effect of heating NH_4^+ exchanged geopolymers at 600°C has been reported by

O'Connor *et al*. (2010) to result in a change of aluminium coordination from four-fold to a significant proportion of five-fold coordination, signifying the formation of acid sites in the structure that should therefore be capable of acting as a catalyst for organic reactions such as the Friedel and Crafts acylation (Miller *et al*., 1997) and the Friedal and Crafts benzylation toluene (Alzeer and Mackenzie, 2014). Another organic reaction that could potentially be catalysed by the acid sites formed by thermally decomposing NH_4^+ exchanged geopolymers is the Beckmann rearrangement. The feasibility of using geopolymers to catalyse this reaction has been demonstrated in preliminary experiments in which 98% conversion of cyclohexanone oxime to ε-caprolactam was achieved using a NH_4^+ exchanged geopolymer heated at 450°C (Alzeer and MacKenzie, 2014). The presence of Lewis acid sites in addition to the acid sites responsible for the formation of ε-caprolactam was suggested by the formation of other by-products such as cyclohexanone, but these results indicate the potential application of geopolymers as catalysts for important organic reactions.

28.11 Inorganic polymers as hydrogen storage media

The emerging importance of hydrogen-based energy strategies has recently led to increased research on aspects of hydrogen generation, storage and utilisation. Problems of particular importance for transport applications are the safe storage of a maximum amount of hydrogen, its efficient retrieval from the storage medium and the possibility of re-hydrogenation of the spent material. A compound that has attracted attention for some time as a hydrogen storage medium is $NaBH_4$, which releases hydrogen by the following reaction:

$$BH_4^- + 2H_2O \leftrightarrow 4H_2 + BO_2^- \quad (28.1)$$

Problems associated with this material as an on-board hydrogen storage medium for automotive applications have been identified as a low gravimetric hydrogen storage capacity and the difficulty of securing the reverse reaction, but it may still be viable for other applications such as fuel cells (Demerci *et al*., 2009). Rüscher *et al*. (2014) have shown that possible problems associated with the supply of the necessary water for the forward reaction (Eq. 28.1) and the chemical and thermal instability of $NaBH_4$ can be mitigated to some extent by encapsulating the borohydride in a geopolymer matrix produced by mixing aqueous solutions of sodium aluminate and $NaBH_4$, followed by the dropwise addition of sodium silicate solution. The resulting geopolymer was cured at 80–110°C to form a typically X-ray amorphous compound containing the BH_4^- anion, and is thermally stable up to 300°C without significant degradation or release of hydrogen due to the protection of the anion by the geopolymer matrix (Rüscher *et al*., 2014). The high alkalinity of the system protects the borohydride from hydrolysis; below 40°C unencapsulated $NaBH_4$ forms the hydride $NaBH_4.2H_2O$ which decomposes spontaneously at about 40°C, whereas the geopolymer composite is stable in water up to at least 70°C (Rüscher *et al*., 2014). Hydrogen can be released controllably at room temperature from the $NaBH_4$–geopolymer composites by lowering the pH with hydrochloric acid. The amount of

hydrogen produced increases linearly with the amount of $NaBH_4$ in the composite (Figure 28.8(a)) up to about 72% of the hydrogen evolved from the pure borohydride (Rüscher *et al*., 2014). Hydrogen evolution also depends on the curing temperature of the geopolymer composite, the optimum temperature being about 80°C (Figure 28.8(b)) (Rüscher *et al*., 2014).The reverse reaction, the regeneration of $NaBH_4$ by hydrogenation of the $NaBO_2$ product, is more difficult, but several possibilities have been suggested, including reaction with hydrogen in the presence of a Pt catalyst at temperatures as low as 150°C (Rüscher *et al*., 2014). Thus, with improved handling and protection techniques afforded by encapsulation in a geopolymer matrix, $NaBH_4$ may yet prove a useful solid-state hydrogen storage material.

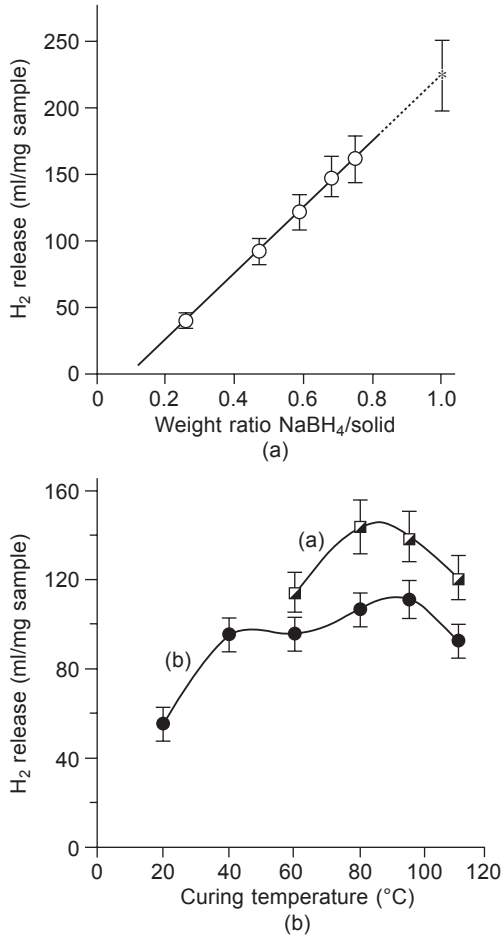

Figure 28.8 (a) Hydrogen release from aluminosilicate geopolymers as a function of their $NaBH_4$ content. The asterisk point represents pure $NaBH_4$. (b) Effect of the geopolymer curing temperature on hydrogen release from geopolymers with two different $NaBH_4$ contents: (a) $NaBH_4$/solid weight ratio = 0.59, (b) $NaBH_4$/solid weight ratio = 0.47. Adapted from Rüscher *et al*. (2014).

28.12 Inorganic polymers containing aligned nanopores

Depending on the method by which the pores in inorganic polymers are generated, materials with a very wide range of pore sizes and degrees of connectivity can be produced, ranging from nanopores up to pores a few mm in size such as required for building insulation. Porous geopolymers for the latter application are commonly synthesised by the *in-situ* generation of pore-forming gases (Bell and Kriven, 2008; Brooks *et al*., 2010, Medri *et al*., 2013; Hung *et al*., 2013).

A novel approach to the generation of continuous pores down to nanopore size is to incorporate fibres such as Nylon 66 or polylactic acid (PLA) fibres in an uncured metakaolinite-based geopolymer mixture. The fibres can then be removed after curing by gentle heating or treatment with alkali, or a combination of both (Okada *et al*., 2011a). The continuous nanopores introduced in this way can be unidirectionally aligned by extruding the mixture through an orifice prior to curing, thereby aligning the fibres parallel to the extrusion direction (Okada *et al*., 2011a) (Figure 28.9(a)). Depending on the fibre content and diameter, the resulting nanoporous geopolymers have proved capable of drawing up water to a height of at least 1125 mm by capillary action (Figure 28.9(b)), thus mimicking the mechanism occurring in the xylem of trees. The possible use of these materials for cladding buildings suggests a novel application for passively cooling the building by drawing up water on its surface and exploiting the latent heat of the water evaporation (Okada *et al*., 2009, 2011b).

28.13 Inorganic polymers reinforced with organic fibres

The mechanical behaviour of geopolymers is identical to that of other ceramics, which fail catastrophically under load in a brittle manner rather than in a ductile (graceful) mode. The considerable work that has been done on the use of short *inorganic* fibres or woven fibre cloth reinforcement to promote graceful failure in inorganic polymers is outside the scope of this chapter, as is the much more limited data on the use of *unidirectional* inorganic fibres, discussed by MacKenzie and Welter (2014).

By contrast with reinforcement of geopolymers with inorganic fibres, *organic* fibre reinforcement has received much less attention, despite their advantage of ready availability and cheapness, and their compatibility with the ambient temperature synthesis conditions. An additional advantage of inorganic polymer composites with natural organic fibrous materials should be the thermal protection of the fibres by the non-flammable inorganic matrix. Teixeira-Pinto *et al*. (2008) have reported that raw jute fibres can be used to improve the mechanical properties of a metakaolin-based geopolymer, while the addition of an optimum content of 0.5 wt.% of short cotton fibres has been reported to improve the flexural strength of a fly ash-based geopolymer from 10.4 to 11.7 MPa (Alomayri *et al*., 2013a). Reinforcement of the same fly ash-based geopolymer with woven cotton fabric has allowed a much higher fibre content to be achieved, resulting in an optimum enhancement of the mechanical properties at a fibre content of 2.1 wt.%, and enhanced thermal protection of the fibres

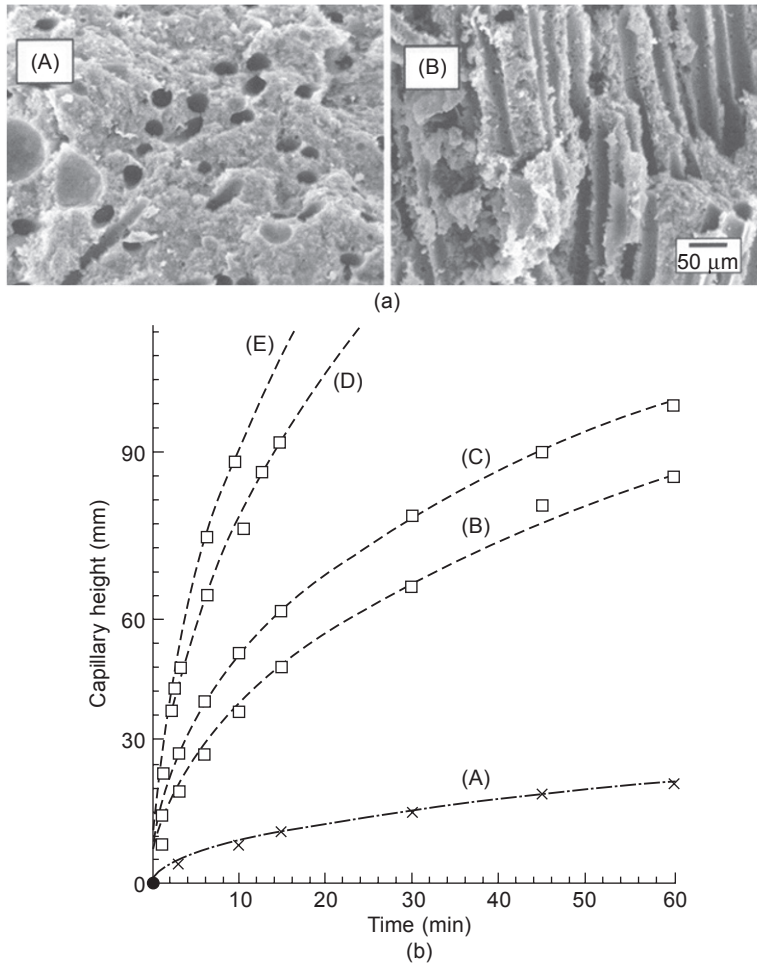

Figure 28.9 (a) Scanning electron micrographs of aligned nanopores introduced into a sodium aluminosilicate geopolymer by extrusion of a composite containing 13 vol.% of 12 µm polylactic acid (PLA) fibres as pore formers: (A) perpendicular to the extrusion direction, (B) parallel to the extrusion direction. (b) Capillary lift height of water for (A) the reference geopolymer without nanopores, (B) geopolymer prepared with 13 vol.% 12 µm PLA fibres, (C) 16 vol.%, (D) 19 vol.%, (E) 22 vol.%. Adapted from Okada *et al.* (2011a).

by the matrix up to 800°C (Alomayri *et al.*, 2013b). Short cellulose fibres derived from alkali-treated sorghum (the residue from ethanol production) have been used by Chen *et al.* (2014) to reinforce a geopolymer based on Class F fly ash. The optimum flexural strength of the composite (5.5 MPa) was obtained with a fibre content of 2 wt.%, after which the properties decreased (Chen *et al.*, 2014). A much greater improvement in the flexural strength of a sodium metakaolin-based geopolymer has been obtained by reinforcement with unidirectional fibres of another cellulose-

based fibre, New Zealand flax (*phormium tenax*), that is reported to improve the flexural strength from about 5.8 MPa in the unreinforced matrix to about 70 MPa, changing the fracture mode of the matrix from brittle to graceful failure (Alzeer and MacKenzie, 2013) (Figure 28.10(a)). The flexural strengths of the composites depends on the fibre content, being greatest at the highest concentration (curve a). The flax fibres were thermally protected by the inorganic matrix up to 400°C, and

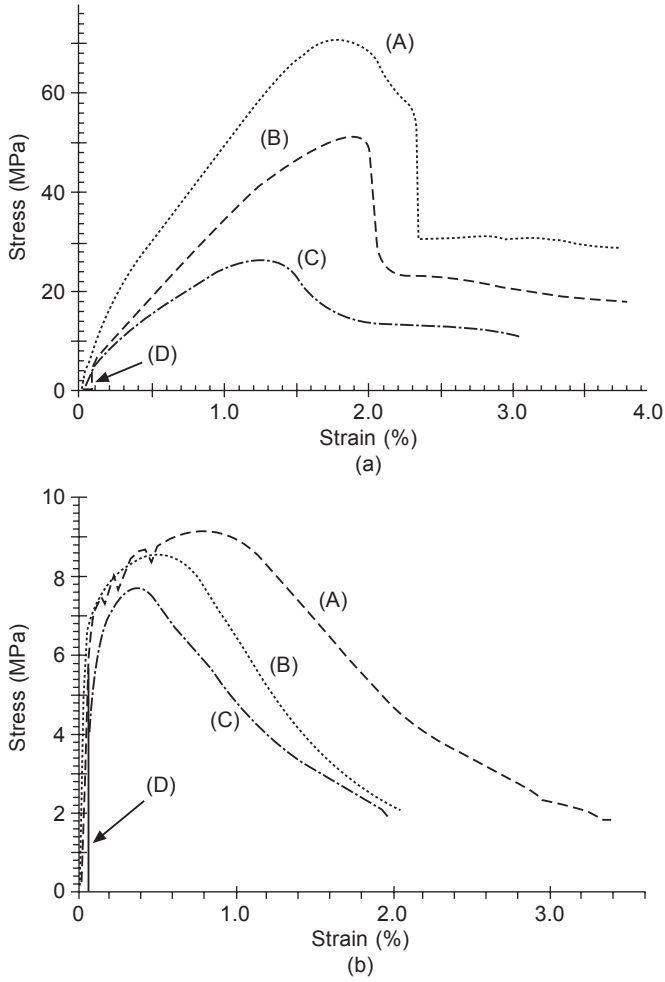

Figure 28.10 Stress–strain curves for sodium aluminosilicate geopolymer reinforced with (a) unidirectional cellulose (flax) fibres, (A) 10 wt.% fibre, (B) 7 wt.% fibre, (C) 4 wt.% fibre, (D) unreinforced geopolymer matrix (reprinted from Alzeer and MacKenzie (2013), Copyright © 2013, with permission from Elsevier). (b) 5 wt.% unidirectional protein (carpet wool) fibres, (A) treated with formaldehyde, (B) cleaned, (C) as-received, (D) unreinforced geopolymer matrix (from Alzeer and MacKenzie (2012), with kind permission from Springer Science and Business Media).

were not damaged by the alkaline environment of the matrix. Protein-based fibres (wool) have also been shown to produce an approximately 40% improvement in the flexural strength of metakaolin-based geopolymers and cause them to fail gracefully (Alzeer and MacKenzie, 2012) (Figure 28.10(b)). No significant difference was found between coarse carpet wool and finer (more expensive) Merino wool, but the flexural strength of the composites was improved by treatment of the wool with formaldehyde to increase the alkali resistance of the fibres (curve a). The occurrence of a chemical interaction between the wool fibres and the matrix was evidenced by the development of a blue colouration in the wool fibres due to the formation of a sodalite compound by reaction between the aluminosilicate matrix and the sulphide groups at the surface of the wool fibres (Alzeer and MacKenzie, 2012). These studies suggest that a combination of ecologically-friendly geopolymer matrices and abundant natural fibres producing strong and fire-resistant materials holds good promise for new and novel future applications of cost-effective fibre-reinforced geopolymer composites.

28.14 Future trends

Although all geopolymer-based materials discussed in this chapter have been developed and their properties demonstrated at the laboratory level, it remains for many of these applications to be taken up and exploited on a practical scale. This will involve overcoming further problems before these materials are fully utilised, but these examples show that geopolymers are capable of many more high-technology applications than are currently in use. Furthermore, the interesting chemistry and physical properties of geopolymers will continue to lead to the development of materials with new functionalities designed into their structure, or as scaffolds for other compounds. At the same time, the physical properties of the new geopolymer-based materials will continue to be developed and investigated, with the aid of cutting-edge electron optical and spectroscopic techniques, and the adoption of methodologies from other disciplines such as the innovative use of bright-field electron tomography to investigate the complex inner pore structures of porous coal ash-based geopolymers (Lee *et al.*, 2014). The future outlook for new geopolymer-based materials is bright, provided they are taken up and developed into usable products.

28.15 Sources of further information and advice

K.J.D. MacKenzie and M. Welter. Geopolymer matrix composites: new possibilities for CMC-like materials. Chapter 18 in *Advances in Ceramic Matrix Composites (CMCs)*, Ed. I.M. Low, Woodhead Publishing, Cambridge (2014), pp. 445–70.

K.J.D. MacKenzie. Utilization of non-thermally activated clays in the production of geopolymers. Chapter 14 in *Geopolymers: Structure, Processing, Properties and*

Industrial Applications, Ed. J. Provis and J. van Deventer, Woodhead Publishing, Cambridge (2009), pp. 294–314.

References

Alomayri, T., Shaikh, F.U.A. and Low, I.M. (2013a) 'Characterization of cotton fibre-reinforced geopolymer composites', *Compos. B* 50, 1–6.

Alomayri, T., Shaikh, F.U.A. and Low, I.M. (2013b) 'Thermal and mechanical properties of cotton fabric-reinforced geopolymer composites', *J. Mater. Sci.* 48, 6746–52.

Alzeer, M. and MacKenzie, K.J.D. (2012) 'Synthesis and mechanical properties of new fibre-reinforced composites of inorganic polymers with natural wool fibres', *J. Mater. Sci.* 47, 6958–65.

Alzeer, M. and Mackenzie, K.J.D. (2013) 'Synthesis and mechanical properties of novel composites of inorganic polymers (geopolymers) with unidirectional natural flax fibres (*phormium tenax*)', *Appl. Clay Sci.* 75–76, 148–52.

Alzeer, M. and MacKenzie, K.J.D. (2014) 'Inorganic polymers as catalysts for organic reactions'. To be published.

Alzeer, M., Keyzers, R.A. and MacKenzie, K.J.D. (2013) 'Inorganic polymers as novel chromatographic stationary phase media', *Ceram. Int.* 40, 3553–60.

Barbosa, V.F.F. and Mackenzie, K.J.D. (2003a) 'Thermal behaviour of inorganic geopolymers and composites derived from sodium polysialate', *Mater. Res. Bull.* 38, 319–31.

Barbosa, V.F.F. and Mackenzie, K.J.D. (2003b) 'Synthesis and thermal behaviour of potassium sialate geopolymers', *Mater. Lett.* 57, 1477–82.

Barbosa, V.F.F., MacKenzie, K.J.D. and Thaumaturgo, C. (2000) 'Synthesis and characterisation of materials based on inorganic polymers of alumina and silica: sodium polysialate polymers', *Int. J. Inorg. Mater*, 2, 309–17.

Bell, J.L. and Kriven, W.M. (2008) 'Preparation of ceramic foams from metakaolin-based geopolymers', *Ceram. Eng. Sci. Proc.* 29, 94–112.

Bell, J.L., Sarin, P., Driemeyer, P.E., Haggerty, R.P., Chupas, P.J. and Kriven, W.M. (2008a) 'X-ray pair distribution function analysis of a metakaolin-based $KAlSi_2O_6.5.5H_2O$ inorganic polymer (geopolymer)', *J. Mater. Chem.* 18, 5974–81.

Bell, J.L., Sarin, P., Provis, J.L., Haggerty, R.P., Driemeyer, P.E., Chupas, P.J., van Deventer, J.S.J. and Kriven, W.M. (2008b) 'Atomic structure of a cesium aluminosilicate geopolymer: a pair distribution function study', *Chem. Mater.* 20, 4768–76.

Bell, J.L., Dreimeyer, P.E. and Kriven, W.M. (2009a) 'Formation of ceramics from metakaolin-based geopolymers. Part II: K-based geopolymer', *J. Amer. Ceram. Soc.* 92, 607–15.

Bell, J.L., Dreimeyer, P.E. and Kriven, W.M. (2009b) 'Formation of ceramics from metakaolin-based geopolymers. Part I: Cs-based geopolymer', *J. Amer. Ceram. Soc.* 92, 1–8.

Bortnovsky, O., Dědeček, J., Tvarůžkovă, Z., Sobalik, Z. and Šubrt, J. (2008) 'Metal ions as probes for characterization of geopolymer materials', *J. Amer. Ceram. Soc*, 91, 3052–7.

Bortnovsky, O., Bezucha, P., Sazama, P., Dědeček, J., Tvarůžkovă, Z. and Sobalik, Z. (2010) 'Novel applications of metal-geopolymers', *Ceram. Eng. Sci. Proc*, 31, 69–82.

Brew, D.R.M. and MacKenzie, K.J.D. (2007) 'Geopolymer synthesis using silica fume and sodium aluminate', *J. Mater. Sci.* 42, 3990–3.

Brooks, R., Bahadory, M., Tovia F. and Rostami, H. (2010) 'Properties of alkali-activated fly ash: high performance to lightweight', *Int. J. Sust. Eng.* 3, 211–18.

Cao, D., Su, D., Lu, B. and Yang, Y. (2005) 'Synthesis and structure characterization of geopolymeric material based on metakaolinite and phosphoric acid', *J. Chinese Ceram. Soc*. 33, 1385–9.

Catauro, M., Bollino, F., Kansal, I., Kamesu, E., Lancellotti, I. and Leonelli, C. (2012) 'Mechanical and biological characterization of geopolymers for potential application as biomaterials' *AZojomo*, DOI: 10.2240/azojomo0322

Chen, R., Ahmari, S. and Zhang, L. (2014) 'Utilization of sweet sorghum fiber to reinforce fly ash-based geopolymer'. *J. Mater. Sci*. 49, 2548–58.

Cui, X.-M., Zheng, G.-J., Han, Y.-C., Su, F. and Zhou, J. (2008) 'A study on electrical conductivity of chemosynthetic Al_2O_3-SiO_2 geopolymer materials', *J. Power Sources* 184, 652–6.

Cui, X.-M., Liu, P.-P., He, Y., Chen, J.-Y. and Zhou, J. (2011) 'A novel aluminosilicate geopolymer material with low dielectric loss', *Mater. Chem. Phys*. 130, 1–4.

Davidovits, J. (1991) 'Geopolymers: inorganic polymeric new materials', *J. Thermal Anal*. 37, 1633–56.

Demerci, U.B., Akdim, O. and Miele, P. (2009) 'Ten-year efforts and a no-go recommendation for sodium borohydride for on-board automotive hydrogen storage', *Int. J. Hydrogen Energy*, 34, 2638–45.

Durant, A.T. and MacKenzie, K.J.D. (2011) 'Synthesis of sodium and potassium aluminogermanate inorganic polymers', *Mater. Lett*. 65, 2086–8.

Durant, A.T., MacKenzie, K.J.D. and Maekawa, H. (2011) 'Synthesis and thermal behaviour of gallium-substituted aluminosilicate inorganic polymers', *J. Chem. Soc. Dalton Trans*. 40, 4865–70.

Fallah, M. and MacKenzie, K.J.D. (2014) 'Novel inorganic polymer (geopolymer)composites with copper (I) oxide nanoparticles for photodegradation of organic pollutants'. To be published.

Forsgren, J., Pedersen, C., Strømme, M. and Engqvist, H. (2011) 'Synthetic geopolymers for controlled delivery of oxycodone: Adjustable and nanostructured porosity enables tunable and sustained drug release', *PLoS ONE*, 6, e17759.

Gasca-Tirado, J.R., Rubio-Avalos, J.C., Muniz-Villarreal, M.S., Manzano-Ramirez, A., Reyes-Araiza, J.L., Sampieri-Bulbarela, S., Villasenor-Mora, C., Perez-Bueno, J.J., Apatiga, L.M. and Amigo Borras, V. (2011) 'Effect of porosity on the absorbed, reemitted and transmitted light by a geopolymer metakaolin base' *Mater. Lett*. 65, 880–3.

Gasca-Tirado, J.R., Manzano-Ramirez, A., Villasenor-Mora, C., Muniz-Villarreal, M., Sampieri-Bulbarela, S., Rubio-Avalos, J., Amigo Borras, V. and Mendoza, R.N. (2012) 'Incorporation of photoactive TiO_2 in an aluminosilicate geopolymer by ion exchange' *Micro. Meso. Mater*. 153, 282–7.

Geyer, G., Baier, G. and Helms, J. (1998) 'Epidural application of ionomeric cement implants. Experimental and clinical results', *J. Laryn. Otol*. 112, 344-50.

Hanston, P., Mathieu, P., Gersdorff, M., Sindic, C.J.M. and Lauwerys, R. (1994) 'Encephalopathy with seizures after use of aluminium-containing bone cement', *Lancet* 344, 1647.

Hench, L.L. (1991) 'Bioceramics: from concept to clinic', *J. Amer. Ceram. Soc*. 74, 1487–510.

Hench, L.L. (1998) 'Biomaterials: a forecast for the future', *Biomater*. 19, 1419–23.

Hung, T.-C., Huang, J.-S., Wang, Y.-W. and Fan, Y.-C. (2013) 'Microstructure and properties of metakaolin-based inorganic polymer foams', *J. Mater. Sci*. 48, 7446–55.

Jämstorp, E., Fosgren, J., Bredenberg, S., Engqvist, H. and Strømme, M. (2010) 'Mechanically strong geopolymers offer new possibilities in treatment of chronic pain', *J. Contr. Rel*. 146, 370–7.

Jämstorp, E., Strømme, M. and Bredenberg, S. (2012) 'Influence of drug distribution and solubility on release from geopolymer pellets – a finite element method study', *J. Pharm. Sci.* 101, 1803–10.

Kolusek, D., Brus, J., Urbanova, M., Andertova, J., Hulinsky, V. and Vorel, J. (2007) 'Preparation, structure and hydrothermal stability of alternative (sodium silicate free) geopolymers', *J. Mater. Sci.* 42, 9267–78.

Lee, S., Jou, H-T., van Reissen, A., Rickard, W., Chon, C-M. and Kang, N-H. (2014) 'Three-dimensional quantification of pore structure in coal ash-based geopolymer using conventional electron tomography', *Constr. Build. Mater.* 52, 221–6.

Li, L., Wang, S. and Zhu, Z. (2006) 'Geopolymeric adsorbents from fly ash for dye removal from aqueous solution', *J. Colloid Interface Sci.* 300, 52–9.

Mackenzie, K.J.D. and Bolton, M.J. (2009) 'Electrical and mechanical properties of aluminosilicate inorganic polymer composites with carbon nanotubes', *J. Mater. Sci.* 44, 2851–7.

MacKenzie, K.J.D. and O'Leary, B.G. (2008) 'Inorganic polymers (geopolymers) containing acid-base indicators as possible colour-change humidity indicators', *Mater. Lett.* 63, 230–2.

MacKenzie, K.J.D. and Welter, M. (2014) 'Geopolymer (aluminosilicate) composites: synthesis, properties and applications', Chapter 18 in *Advances in Ceramic Matrix Composites*, Ed. Low, I.M. Woodhead Publishing, Cambridge, pp. 445–70.

MacKenzie, K.J.D., Brew, D.R.M., Fletcher, R.A., Nicholson, C.L., Vagana, R. and Schmücker, M. (2005) 'Towards an understanding of the synthesis mechanisms of geopolymeric materials', *Proc. World Geopolymer Conf., St. Quentin, Paris*, 41–4.

MacKenzie, K.J.D., Smith, M.E. and Wong, A. (2007) 'A multinuclear MAS NMR study of calcium-containing inorganic polymers', *Journal of Materials Chemistry*, 17, 5090–6.

MacKenzie, K.J.D., Rahner, N., Smith, M.E. and Wong, A. (2010) 'Calcium-containing inorganic polymers as potential bioactive materials', *J. Mater. Sci.* 45, 999–1007.

Martin, S., Derrien, A.C., Oudadesse, H., Chauvel-Lebret, D. and Cathelineau, G. (2005) 'Implantation of aluminosilicate/calcium phosphate materials: influence on bone formation in rabbit tibias', *Eur. Cell Mater.* 9, Suppl.1, 71–2.

Medri, V., Papa, E., Dedecek, J., Jirglova, H., Benito, P., Vaccari, A. and Landi, E. (2013) 'Effect of metallic Si addition on polymeric degree of *in situ* foamed alkali-aluminosilicates', *Ceram. Int.* 39, 7657–68.

Miller, J.M., Walls, D., Hartman, J.S. and Belelie, J.L. (1997) 'Friedel-Crafts catalysis using supported reagents: synthesis, characterization and catalytic applications of sol-gel derived aluminosilicates', *J. Chem. Soc. Farad. Trans.* 93, 2439–44.

Nicholson, C.L., MacKenzie, K.J.D., Murray, B.J., Fletcher, R.A., Brew, D.R.M. and Schmücker, M. (2005) 'Novel geopolymer materials containing borate structural units', *Proc. World Geopolymer Conf., St. Quentin, Paris*, 31–33.

O'Connor, S.J. and MacKenzie, K.J.D. (2010) 'Synthesis, characterization and thermal behaviour of lithium aluminosilicate inorganic polymers', *J. Mater. Sci.* 45, 3707–13.

O'Connor, S.J., MacKenzie, K.J.D., Smith, M.E. and Hanna, J.V. (2010) 'Ion exchange in the charge-balancing sites of aluminosilicate inorganic polymers', *J. Mater. Chem.* 20, 10234–40.

O'Leary, B.G. (2012) 'Carbothermal reduction and nitridation of geopolymer-carbon composites: a study of reaction mechanisms'. MSc thesis, Victoria University of Wellington, New Zealand.

Okada, K., Ooyama, A., Isobe, T., Kameshima, Y., Nakajima, A. and MacKenzie, K.J.D. (2009) 'Water retention of porous geopolymers for use in cooling applications', *J. Eur. Ceram. Soc.* 29, 1917–23.

Okada, K., Imase, A., Isobe, T. and Nakajima, A. (2011a) 'Capillary rise properties of porous geopolymers prepared by an extrusion method using polylactic acid (PLA) fibers as the pore formers', *J. Eur. Ceram. Soc.* 31, 461–7.

Okada, K., Isobe, T., Katsumata, K., Kameshima, Y., Nakajima, A. and MacKenzie, K.J.D. (2011b) 'Porous ceramics mimicking nature – preparation and properties of microstructures with unidirectionally oriented pores', *Sci. Technol. Adv. Mater.* 12.

Oudadesse, H., Derrien, A.C., Lefloch, M. and Davidovits, J. (2007a) 'MAS-NMR studies of geopolymers heat-treated for applications in biomaterials field', *J. Mater. Sci.* 42, 3092–8.

Oudadesse, H., Derrien, A.C., Mami, M., Martin, S., Cathlineau, G. and Yahia, L. (2007b) 'Alumino-silicates and biphasic HA-TCP composites: studies of properties for bony filling', *Biomed. Mater.* 2, S59–64.

Provis, J.L., Lukey, G.C. and van Deventer, J.S.J. (2005) 'Do geopolymers actually contain nanocrystalline zeolites? A re-examination of existing results', *Chem. Mater.* 17 3075–85.

Prud'homme, E., Michaud, P., Joussein, E., Peyratout, C., Smith, A., Arrii-Clacens, S., Clacens, J.M. and Rossignol, S. (2010) 'Silica fume as porogent agent in geo-materials at low temperature', *J. Eur. Ceram. Soc.* 30, 1641–8.

Rogers, J. and MacKenzie, K.J.D. (2014) 'Development of a new class of luminescent materials based on gallium aluminium silicate inorganic polymers'. To be published.

Ropp, S.C. (2004) *Luminescence and the Solid State*, 2nd edn, Elsevier Science, Burlington, VA.

Rüscher, C.H., Schomberg, L., Schulz, A. and Buhl, J.C., (2014) 'Basic research on geopolymer gels for production of green binders and hydrogen storage', *Ceram. Eng. Sci. Proc.* 34 (10), 97–114.

Sazama, P., Bortnovsky, O., Decedek, J., Tvaruzkova, Z. and Sobalik, Z. (2011) 'Geopolymer based catalysts – new group of catalytic materials', *Catal. Today* 164, 92–9.

Teixeira-Pinto, A., Varela, B., Shrotri, K., Panandiker, R.S.P. and Lawson, J. (2008) 'Geopolymer-jute composite: a novel environmentally friendly composite with fire resistant properties', *Ceram. Eng. Sci Proc.* 28, 337–46.

Wang, S. (2009) 'Ordered mesoporous materials for drug delivery', *Micropor. Mesopor. Mater.* 117, 1–9.

Welter, M. (2013) 'Fiber reinforced geopolymer matrix composites'. PhD thesis, Victoria University of Wellington, New Zealand.

White, C.E., Provis, J.L., Proffen, T. and van Deventer, J.S.J. (2010) 'The effects of temperature on the local structure of metakaolin-based geopolymer binder: a neutron pair distribution function investigation', *J. Amer. Ceram. Soc.* 93, 3486–92.

Xie, N., Bell, J.L. and Kriven, W.M. (2010) 'Fabrication of structural leucite glass-ceramics from potassium-based geopolymer precursors', *J. Amer. Ceram. Soc.* 93, 2644–9.

Xynos, I.D., Edgar, A.J., Buttery, L.D.K., Hench, L.L. and Polak, J.M. (2001) 'Gene-expression profiling of human osteoblasts following treatment with the ionic products of Bioglass® 45S5 dissolution', *J. Biomed Mater. Res.* 55, 151–7.

Yap, A.U.G., Pek, Y.S., Kumar, R.A., Cheang, P. and Khor, K.A. (2002) 'Experimental studies on bioactive material: HAlonomer cements', *Biomater.* 23, 955–62.

This page intentionally left blank

Index

S

This page intentionally left blank

This page intentionally left blank